FUNCTIONAL
Magnetic Resonance Imaging

SECOND EDITION

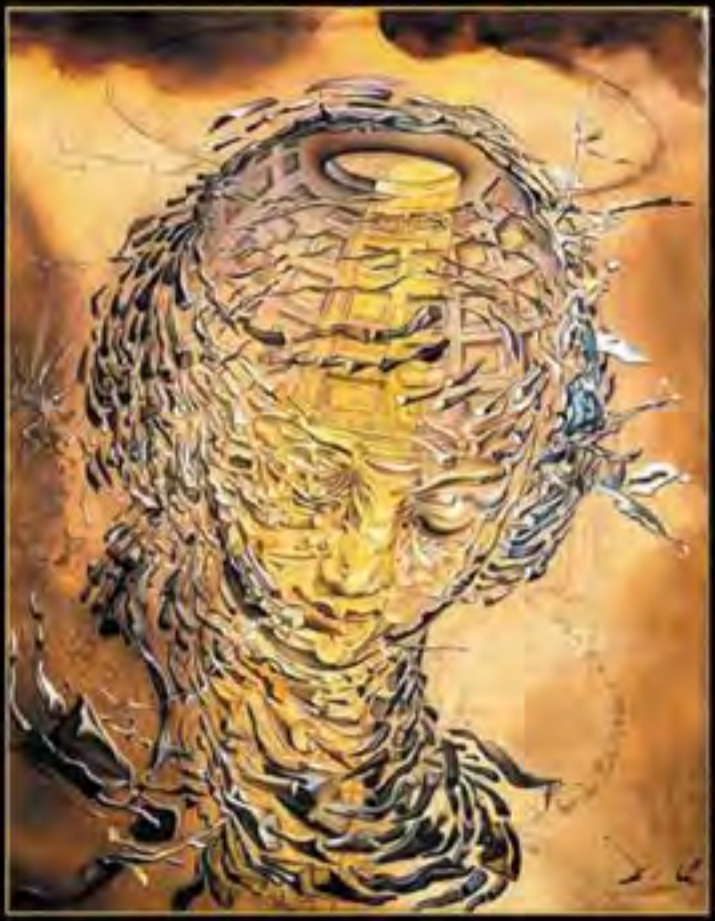

Scott A. Huettel • Allen W. Song • Gregory McCarthy

WN185
H871-2

FUNCTIONAL Magnetic Resonance Imaging

SECOND EDITION

Scott A. Huettel
Brain Imaging and Analysis Center, Duke University

Allen W. Song
Brain Imaging and Analysis Center, Duke University

Gregory McCarthy
Yale University

Sinauer Associates, Inc • Publishers
Sunderland, Massachusetts U.S.A.

1788096

Cover image: © 2008 Salvador Dali, Gala-Salvador Dali Foundation/Artists Rights Society (ARS), New York.

FUNCTIONAL MAGNETIC RESONANCE IMAGING, Second Edition.
Copyright © 2009 by Sinauer Associates, Inc. All rights reserved. This book may not be reproduced in whole or in part for any purpose. For information address: Sinauer Associates, Inc., 23 Plumtree Road, Sunderland, MA. 01375 U.S.A.

Fax: 413-549-1118
Email: publish@sinauer.com
www.sinauer.com

Library of Congress Cataloging-in-Publication Data

Huettel, Scott A., 1973-
Functional magnetic resonance imaging / Scott A. Huettel, Allen W. Song, Gregory McCarthy. — 2nd ed.
p. ; cm.
Includes bibliographical references and index.
ISBN 978-0-87893-286-3
1. Brain—Magnetic resonance imaging. 2. Cognitive neuroscience. I. Song, Allen W., 1971- II. McCarthy, Gregory, 1952- III. Title.
[DNLM: 1. Magnetic Resonance Imaging. 2. Brain Mapping—methods. WN 185 H888f 2009]
RC386.6.M34H84 2009
616.8'047548—dc22
2008054124

Printed in U.S.A.

6 5 4 3 2 1

We dedicate this book to our families,
especially Lisa, Nicholas, Elissa, Jan-Ru, and Paula,
for their patience and support during its development.

Brief Contents

1 *An Introduction to fMRI* 1

2 *MRI Scanners* 31

3 *Basic Principles of MR Signal Generation* 57

4 *Basic Principles of MR Image Formation* 89

5 *MR Contrast Mechanisms and Pulse Sequences* 121

6 *From Neuronal to Hemodynamic Activity* 159

7 *BOLD fMRI: Origins and Properties* 193

8 *Signal, Noise, and Preprocessing of fMRI Data* 243

9 *Experimental Design* 293

10 *Statistical Analysis: Basic Analyses* 331

11 *Statistical Analysis II: Advanced Approaches* 377

12 *Advanced fMRI Methods* 419

13 *Combining fMRI with other Techniques* 443

14 *The Future of fMRI: Practical and Ethical Issues* 485

Contents

Preface xiii

1 *An Introduction to fMRI* 1

What Is fMRI? 3
Measurement versus manipulation techniques 4
BOX 1.1 WHAT IS fMRI USED FOR? 6
Key concept: contrast 9
Key concept: resolution 11

History of fMRI 15
Early studies of magnetic resonance 15
NMR in bulk matter: Bloch and Purcell 17
The first MR images 18
Growth of MRI 21
BOX 1.2 THE NOBEL CONTROVERSY: SCANNERS OR IMAGES? 22

Organization of the Textbook 24
Physical bases of fMRI 25
Principles of BOLD fMRI 25
Design and analysis of fMRI experiments 26
Applications and future directions 27

Summary 28

Suggested Reading 28

Chapter References 29

2 *MRI Scanners* 31

How MRI Scanners Work 31
Static magnetic field 32
Radiofrequency coils 35
Gradient coils 38
Shimming coils 41
Computer hardware and software 41
Experimental control system 43
Physiological monitoring equipment 43

MRI Safety 44
Effects of static magnetic fields on human physiology 44
BOX 2.1 OUTLINE OF AN fMRI EXPERIMENT 45
Translation and torsion 49
Gradient magnetic field effects 50
Radiofrequency field effects 52
Claustrophobia 53
Acoustic noise 54

Summary 54

Suggested Reading 55

Chapter References 55

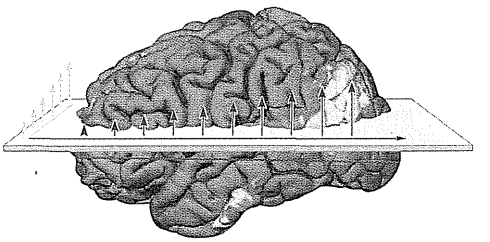

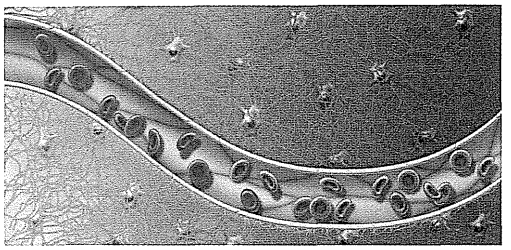

3 Basic Principles of MR Signal Generation 57

CONCEPTUAL PATH 57

Nuclear Spins 59

Spins in an External Magnetic Field 60

Magnetization of a Spin System 62

Excitation of a Spin System and Signal Reception 64

Relaxation Mechanisms of the MR Signal 65

Conceptual Summary of MR Signal Generation 67

QUANTITATIVE PATH 68

Common Terms and Notations 68

Nuclear Spins 69

Magnetic Moment 69

Angular Momentum 70

Spins in an External Magnetic Field 71

Spin precession 71

Energy Difference between Parallel and Antiparallel States 74

Magnetization of a Spin System 75

Excitation of a Spin System and Signal Reception 77

Spin excitation 78

BOX 3.1 A QUANTITATIVE CONSIDERATION OF THE ROTATING REFERENCE FRAME 80

Signal reception 83

Relaxation Mechanisms of a Spin System 85

The Bloch Equation for MR signal generation 87

Summary 87

Suggested Reading 88

4 Basic Principles of MR Image Formation 89

CONCEPTUAL PATH 90

Slice Selection 91

Frequency Encoding 93

Phase Encoding 95

Conceptual Path: Summary of Image Formation 96

QUANTITATIVE PATH 97

Analysis of the MR Signal 97

BOX 4.1 AN EXAMPLE OF SPATIAL ENCODING 98

Longitudinal magnetization (M_z) 101

Solution for transverse magnetization (M_{xy}) 102

The MR signal equation 105

Slice Selection, Spatial Encoding, and Image Reconstruction 106

Slice selection 106

Two-dimensional spatial encoding (frequency and phase encoding) 109

Relationship between image space and *k*-space 113

Converting from *k*-space to image space 114

3-D Imaging 117

Potential Problems in Image Formation 117

Summary 120

Suggested Reading 120

5 MR Contrast Mechanisms and Pulse Sequences 121

Static Contrasts and Related Pulse Sequences 122

Proton-density contrast 123

T_1 contrast 126

T_2 contrast 129

T_2^* contrast 131

Chemical contrast 132

Macromolecular contrast 133

Motion Contrasts 135

MR angiography 135

Diffusion-weighted contrast 138

BOX 5.1 DIFFUSION TENSOR IMAGING 140

Perfusion-weighted contrast 142

Fast Imaging Sequences for fMRI 147
Echo-planar imaging 147
Spiral imaging 148
Signal recovery and distortion correction for EPI and spiral images 152
Summary 154
Suggested Reading 156
Chapter References 157

6 *From Neuronal to Hemodynamic Activity 159*

Neuronal Activity 160
Ion channels in neurons 162
Neurotransmitters and action potentials 163
Cerebral Metabolism: Neuronal Energy Consumption 165
Adenosine triphosphate (ATP) 166
The Vascular System of the Brain 168
Arteries, capillaries, and veins 170
Arterial and venous anatomy of the human brain 171
Microcirculation 172
Blood Flow 174
Control of blood flow 175
Box 6.1 Neurovascular Coupling and Control of Blood Flow 176
Effects of increased blood flow on capillaries 179
Box 6.2 Primer on Neuroanatomy 182
Summary 190
Suggested Reading 190
Chapter References 191

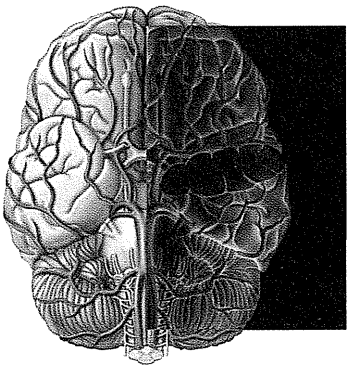

7 *BOLD fMRI: Origins and Properties 193*

History of BOLD fMRI 193
Discovery of BOLD contrast 194
The coupling of metabolism and blood flow 196
Box 7.1 PET Imaging 197
The Growth of BOLD fMRI 201
Contributing factors 201
Early fMRI studies 203
Box 7.2 Functional Studies Using Contrast Agents 204
The BOLD Hemodynamic Response 208
Box 7.3 Neuronal Activity and BOLD fMRI 209
The initial dip 211
Spatial Resolution 214
Spatial specificity in the vascular system 216
What spatial resolution is needed? 219
Temporal Resolution of fMRI 220
What temporal resolution is needed? 223
Effects of stimulus duration and timing 225
Linearity of the Hemodynamic Response 229
Properties of a linear system 230
Evidence for rough linearity 231
Challenges to linearity 233
fMRI-adaptation 235
Summary 237
Suggested Reading 238
Chapter References 239

8 *Signal, Noise, and Preprocessing of fMRI Data 243*

Understanding Signal and Noise 245
Signal and noise defined 245
Box 8.1 Terminology of fMRI 246
Functional SNR 248
Effects of Field Strength on fMRI Data 250
Field strength and raw SNR 251
Field strength and spatial properties of activation 252
Challenges of high-field fMRI 254

Sources of Noise in fMRI 255
Thermal noise 256
System noise 258
Motion and physiological noise 259
Non-task-related neural variability 262
Behavioral and cognitive variability in task performance 262
BOX 8.2 VARIABILITY IN THE HEMODYNAMIC RESPONSE OVER SUBJECTS AND SESSIONS 264
Preprocessing 267
Quality assurance 267
Slice acquisition time correction 269
Head motion: an overview 271
Prevention of head motion 274
Correction of head motion 276
Distortion correction 277
Functional–Structural Coregistration and Normalization 280
Functional–structural coregistration 280
Spatial normalization 281
Temporal and Spatial Filtering 284
Temporal filtering 285
Spatial filtering 287
Summary 289
Suggested Reading 289
Chapter References 290

9 *Experimental Design 293*

Basic Principles of Experimental Design 294
Setting Up a Good Research Hypothesis 296
Are fMRI data correlational? 298
Confounding factors 299
Good Practices in fMRI Experimental Design 302
Blocked Designs 303
Setting up a blocked design 304
BOX 9.1 BASELINE ACTIVATION IN fMRI 306
Advantages and disadvantages of blocked designs 310
Event-Related Designs 313
Principles of event-related fMRI 316
Advantages of event-related designs 319
BOX 9.2 EFFICIENT fMRI EXPERIMENTAL DESIGN 320
Mixed Designs 325
Summary 327
Suggested Reading 327
Chapter References 328

10 *Statistical Analysis: Basic Analyses 331*

Basic Statistical Tests 333
Contrasting experimental conditions: the *t*-test 334
Comparing experimental and predicted responses: correlation analyses 338
BOX 10.1 IDENTIFYING TASK-RELATED PERIODICITY: FOURIER ANALYSES 341
Regression Analyses 343
The general linear model: an overview 343
Constructing a design matrix: regressors of interest 345
Constructing a design matrix: nuisance regressors 349
Modeling neuronal activity 351
Modeling hemodynamic convolution 352
Contrasts 354
Assumptions of the general linear model 356
Corrections for Multiple Comparisons 357
Calculating the significance threshold 358
Thresholding based on clusters of activation 360
Estimating the number of independent tests 361
Region-of-Interest Analyses 362
Intersubject Analyses 365
Group and parametric effects 367
Displaying Statistical Results 369
Summary 373
Suggested Reading 373
Chapter References 374

11 Statistical Analysis II: Advanced Approaches 377

Data Exploration Approaches 378
Principal components analysis (PCA) 378
Independent components analysis (ICA) 380
Partial least squares (PLS) 382

Between-Subjects Correlations: Hyperscanning 384

Functional Connectivity Approaches 386
From coactivation to connectivity: a conceptual overview 386
BOX 11.1 INTERSUBJECT CORRELATIONS IN FREE VIEWING 387
Resting-state connectivity 391
Psychophysiological interactions 393
Inferring causality from fMRI data 394
Combining fMRI and DTI 399

Prediction Approaches 401
Predicting variation among individuals 402
BOX 11.2 REAL-TIME fMRI 403
Predicting variation in behavior 407
Pattern classification using machine learning algorithms 408
Capabilities and challenges of fMRI pattern classification 412

Summary 415

Suggested Reading 416

Chapter References 416

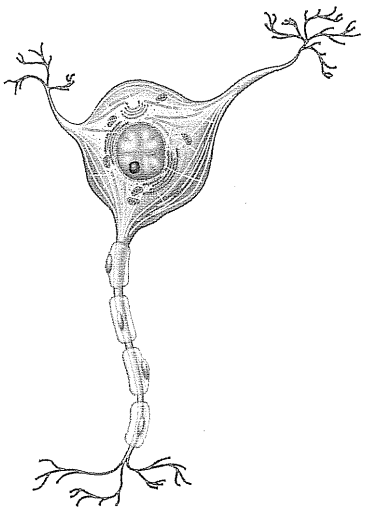

12 Advanced fMRI Methods 419

Improved Spatial Resolution 420
MR microscopy 420
Parallel imaging 423
Parallel imaging with massive coil arrays 425

Improved Temporal Resolution 426
Multiple-channel acquisition 427
Partial *k*-space imaging 427
Efficient *k*-space trajectories 430
Improved experimental designs 432

Improved Functional Resolution through New Contrast Mechanisms 433
Temperature-dependent contrast 434
pH-dependent contrast 435
Ion-gated contrast 437
Neuronal magnetic field contrast 438
Lorentz effect contrast 439

Summary 440

Suggested Reading 441

Chapter References 441

13 Combining fMRI with other Techniques 443

Cognitive Neuroscience 443
Strategies for research in cognitive neuroscience 445

Manipulating Brain Function 446
Direct cortical stimulation 446
Functional consequences of direct cortical stimulation 448
Transcranial magnetic stimulation (TMS) 450
Brain lesions 452
Combined lesion and fMRI studies 454
Probabilistic brain atlases 455
Brain imaging and genomics 457

Measuring Brain Function 458
Single-unit recording 458
BOX 13.1 ELECTROGENESIS 459
Limitations of single-unit recording 462
Properties of electrical field potentials 464
Localizing the neural generators of field potentials 465

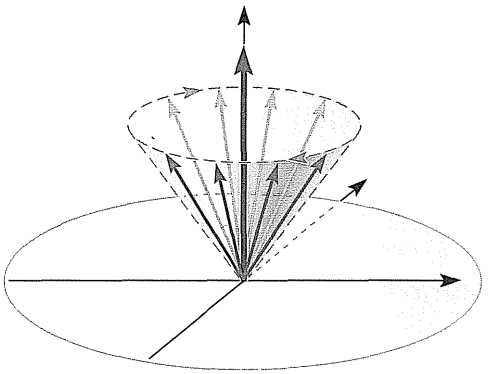

Intracranially recorded field potentials 466
Box 13.2 Localization of Function Using Field Potential Recordings 468
Scalp-recorded field potentials 470
Box 13.3 Combining fMRI and EEG/ERP techniques 472
Magnetoencephalography 474
Using fMRI with non-human primates 476

Summary 480

Suggested Reading 480

Chapter References 481

14 *The Future of fMRI: Practical and Ethical Issues 485*

Introduction 485

Interpreting and Presenting fMRI Data 486

Coverage of fMRI research in the popular media 487
Core principles for presenting fMRI research 489
Box 14.1 Reverse Inference 490

Conducting fMRI Research 494

Proposing and approving fMRI research 495
Ensuring the confidentiality of fMRI data 497
Box 14.2 Incidental Findings in fMRI Research 498
Safe conduct of fMRI studies 502
Pregnancy testing in fMRI research 504

Applying fMRI to New and Controversial Topics 505

Reading minds 506
Identifying traits 509

The Future of fMRI Research (and your role in it) 511

Summary 513

Suggested Reading 515

Chapter References 515

***Glossary* 517**

***Index* 533**

Preface

When we published the First Edition of *Functional Magnetic Resonance Imaging* in 2004, we marveled at the rapid growth of functional magnetic resonance imaging, which was becoming the dominant technique in cognitive neuroscience. Now, less than five years later, that growth shows no signs of abating. If anything, there has been a remarkable broadening of interest in fMRI, as researchers from a wide range of disciplines—from linguistics and biomedical engineering to political science and marketing—contribute to an ever-expanding literature on the functional properties of the human brain. This diversity, while positive in many ways, poses challenges for the field. A researcher who comes from a natural science or engineering background might be comfortable with the underlying MR physics, but have little prior experience with brain physiology or even cognitive function. A medical scientist might be well versed in neuroanatomy and practical uses of MRI, but not the theoretical basis for MR data acquisition or experimental design. Or, a social scientist, whether psychologist or economist, might have considerable experience with measuring cognitive phenomena using behavioral techniques, but little training in biophysics and physiology. Stated simply, the major challenge for explaining fMRI comes from its breadth.

The Second Edition, like its predecessor, seeks to provide a broad, comprehensive, and rigorous introduction to fMRI research. Because of the highly interdisciplinary nature of fMRI, a systematic review must necessarily encompass many topics. We begin the textbook by establishing strong foundations in the physics and biology of fMRI. Although these foundations rest on complex concepts, we believe that they can be described without unnecessary complication. We introduce physical concepts using both intuitive analogies and step-by-step explanations of theories, referring frequently to fMRI applications. We adopt a similarly functional approach to concepts in biology, progressing from the metabolic consequences of neuronal activity, through the supply of energy via the vascular system, to the changes in blood oxygenation that form the basis for fMRI. From these foundations, we extend upward

into fMRI experimentation, describing both the principles and practice of modern fMRI research. As examples of the diversity of topics advance, students will learn about proton spin, ions moving through membrane channels, neurovascular organization, experimental design, the general linear model, machine learning algorithms, signal processing, and the ethics of mindreading. Any student, regardless of background, will find much new material throughout the text.

Nevertheless, we do not sacrifice accuracy to gain this breadth of coverage. Without accurate, careful discussion of key concepts, any text (especially one on such a youthful field) risks mystifying its readers. The beginning student of fMRI faces a bewildering array of terms, often only operationally defined. Many of the most tantalizing ideas await empirical support and have not yet crystallized into guiding theory. Therefore, we introduce key concepts in a logical, straightforward manner, with clear definitions of research jargon. Throughout the book, we illustrate ideas by describing the primary research studies that support (or disconfirm) them. We present abstract ideas in the context of real-world fMRI studies, so that students can make informed decisions about research questions.

Finally, we present ideas in a format that can be easily understood by beginning researchers, whether undergraduate students, graduate students, postdoctoral fellows, or research faculty. We recognize that many aspects of fMRI seem very technical to those new to the field. It is easy to become daunted when faced with the physics of MR image formation, or the biological principles underlying neuroenergetics, or the statistical grounding of the general linear model. Yet these concepts are important and cannot be omitted simply to reduce the complexity of the book. Rather than simplifying the topical coverage, we instead simplify the explanations of these topics—for example, the chapters on MR physics include parallel quantitative and conceptual paths, so that students and instructors can select the format that best fits their pedagogical style.

We include features that, though designed for undergraduate and graduate courses, will benefit anyone learning fMRI for the first time. These include:

- *A course-oriented organization.* The textbook contains 14 chapters, each covering a discrete aspect of fMRI, with a clear progression across topics.
- *Boxes illustrating important examples or key topics.* Throughout the book, a large number of exciting concepts are set aside in boxes for special emphasis. These boxes make ideal stepping-off points for instructors to delve more deeply into the literature.
- *Copious use of color figures. More than 300 figures are included, many new to this edition.* The numerous figures within the chapters on physics and physiology complement the detailed discussions of those often-challenging topics.
- *A marginal glossary.* In addition to the standard glossary at the end of the book, key terms are defined in the margins at their first occurrence in a chapter.
- *Thought problems within the text.* Each chapter includes several thought problems to challenge the reader's understanding. These problems reinforce key ideas and promote critical evaluation of the material.

- *Comprehensive reference lists within each chapter.* Two types of references are included: *Suggested Readings* and *Chapter References*. The *Suggested Readings*, typically 6-8 per chapter, are selected for their comprehensiveness and accessibility. Annotations guide students to suggested readings of interest. All other primary source material is cited with full bibliographic information in the *Chapter References* section.
- *Clear summaries of equations.* When equations are introduced, their terms are systematically described and all variables are labeled explicitly. These annotations allow students with less mathematical background to work through the conceptual bases of the equations.
- *Discussions of the historical progression of ideas.* Within the textbook are descriptions of the physical and physiological discoveries that led to the development of fMRI. Students learn about the earliest fMRI studies and how those studies sparked future research. Conversely, we discuss many cutting-edge findings from cognitive neuroscience and MR physics, including many studies from 2007 and 2008.
- *A focus on primary source material.* We discuss the research of a large number of laboratories, many of which have graciously allowed use of images from their work.

Acknowledgments

We would like to thank the numerous colleagues, collaborators, and students who have contributed to this project. The many students in our fMRI courses have provided inestimable inspiration, criticism, and guidance, and our thinking has been greatly honed by their feedback. Thanks go to colleagues at Duke University and elsewhere, many of whom shaped specific sections of the text with their feedback: Alison Adcock, Geoff Aguirre, Greg Appelbaum, Michael Beauchamp, Aysenil Belger, Liz Brannon, Roberto Cabeza, Bin Chen, Nan-Kuei Chen, In-Young Choi, Michele Diaz, Ian Dobbins, Al Johnson, Ranga Krishnan, Kevin LaBar, James MacFall, Dave Madden, Joe McClernon, Martin McKeown, Kevin Pelphrey, Michael Platt, Russell Poldrack, Chris Rorden, Robert Savoy, Lihong Wang, and Daniel Weissman. We also thank Jim Voyvodic and Marty Woldorff for their contributions to boxes in Chapters 11 and 13, and Dale Purves and the other editors of *Neuroscience* and *Cognitive Neuroscience*; both texts provide important complementary material.

Production and technical assistance has been provided by many of our students and colleagues, including Alex Avram, Lindsay Carr, McKell Carter, John Clithero, Francis Favorini, Syam Gadde, Arnaud Guidon, Hua Guo, Todd Harshbarger, Debra Henninger, Justin Meyer, Charles Michelich, O'Dhaniel Mullette-Gillman, Brandi Newell, Chris Petty, Luke Pool, Ana Raposo, David Smith, Jon Smith, Dharol Tankersley, Trong-Kha Truong, Vinod Venkatraman, Bethany Weber, Amy Winecoff, and Richard Yaxley. We appreciate the many scientists who contributed figures from their work, and we recognize them individually with their provided figure(s).

A number of funding agencies have supported our teaching efforts, our research programs, and many of our studies discussed in this book. They include NCRR, NIA, NIDA, NIMH, NINDS, NSF, and the Department of Vet-

erans Affairs. We thank the Howard Hughes Medical Institute for support of the teaching laboratory used in our courses. We also appreciate the institutional support provided by the administration of Duke University and Duke University Medical School, including the Duke Institute for Brain Sciences.

Finally, we would like to thank our friends at Sinauer Associates for their guidance throughout this process. We thank Andy Sinauer for his support of this project since its inception, Chelsea Holabird for her tireless efforts during production, and Marie Scavotto for marketing the finished product. Under the guidance of Christopher Small, the production team at Sinauer Associates did excellent work, particularly Joan Gemme whose skill in design and layout are evident in this book. We also wish to thank Jane Murfett for her copyediting expertise, Grant Hackett for creating the index, and the talented artists at Imagineering Media Services, Inc. and Dragonfly Media Group for creating most of the figures in this text. Special thanks go to our editor, Graig Donini, for his continual enthusiasm and support.

Scott A. Huettel

Allen W. Song

Gregory McCarthy

Media & Supplements to accompany

Functional Magnetic Resonance Imaging

SECOND EDITION

For the Student

Companion Website (www.sinauer.com/fmri2e)
Available free of charge, the *Functional Magnetic Resonance Imaging*, Second Edition Companion Website provides students with study resources to help them master the material presented in the textbook. The site includes:

- Study questions for each chapter of the textbook, available both as Web pages and as downloadable Microsoft Word® files. These short-answer style questions are designed to test students' understanding of the material presented in each chapter. They can be used for student self-assessment or can be printed and submitted to the instructor as an assignment.
- A set of Web Links to a variety of online fMRI resources.
- A complete online Glossary of all the important terms introduced in the textbook.

For the Instructor

Instructor's Resource Library (ISBN 978-0-87893-353-2)
Available to qualified adopters, the Instructor's Resource Library includes electronic versions of all of the figures, photos, and tables from the textbook. Both line art and photographic images are included in high-resolution JPEG format, and all have been formatted and optimized for excellent legibility and projection quality. In addition, a ready-to-use PowerPoint® presentation of all figures and tables is provided for each chapter of the textbook. Also included are the study questions from the Companion Website.

國立成功大學圖書

Chapter 1

An Introduction to fMRI

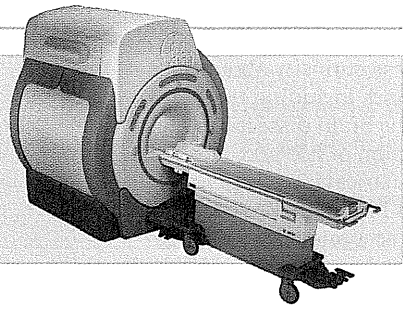

Few scientific developments have been more striking than the ability to make images of the functioning human brain. Why do these images evoke such wonder? To many, the human brain represents a barely-explored new world, with each image providing a glimpse of hidden structures. Like the navigational charts used by medieval explorers, our current maps of brain function are riddled with errors, inconsistencies, and puzzles deserving of solution. Yet the difficulty in understanding the brain has added to the excitement of the quest.

Renaissance and post-renaissance physicians and philosophers developed only very rough theories about brain function (Figure 1.1A and B). The philosopher Rene Descartes speculated in the mid-seventeenth century that mental activity arose through the influence of the pineal gland on the surrounding ventricles. Others of his contemporaries argued that the corpus callosum, whose fibers connect the two hemispheres of the brain, provided the basis for all cognition. Perhaps most prescient of all was Emanuel Swedenborg, who began his career as an engineer and ended as a theologian. Writing in the mid-eighteenth century, Swedenborg postulated that the cortex itself was responsible for higher cognition, and that different parts of the cortex were associated with different functions. He argued that the frontal lobes were associated with imagination, thought, and will; this was a surprisingly accurate description, given the complete lack of experimental evidence at that time. Even so, Swedenborg's ideas were completely ignored by his contemporaries—only to be rediscovered two centuries later, as a historical curiosity.

At the beginning of the nineteenth century, scientists began to think in new ways about brain function. There was popular interest in how body features related to behavior, and individuals known as physiognomists tried to predict personality from facial features. The time was right for the emergence of **localization of function**, the idea that different aspects of the human mind may be represented in different brain regions. The **phrenologists** added to this idea the concept that the amount of brain tissue devoted to a cognitive function determined its influence on behavior. Although phrenologists were unable to measure cortical volume directly, they assumed that increases in brain size would translate into measurable bumps on the skull. So, a devoted mother would have a protrusion over the brain area supporting "love for one's offspring," whereas a common thief would have a flattening of the skull above the area

localization of function The idea that the brain may have distinct regions that support particular mental processes.

phrenologists Adherents to the belief that bumps and indentations on the skull provided information about the magnitude of some trait supported by the underlying brain region.

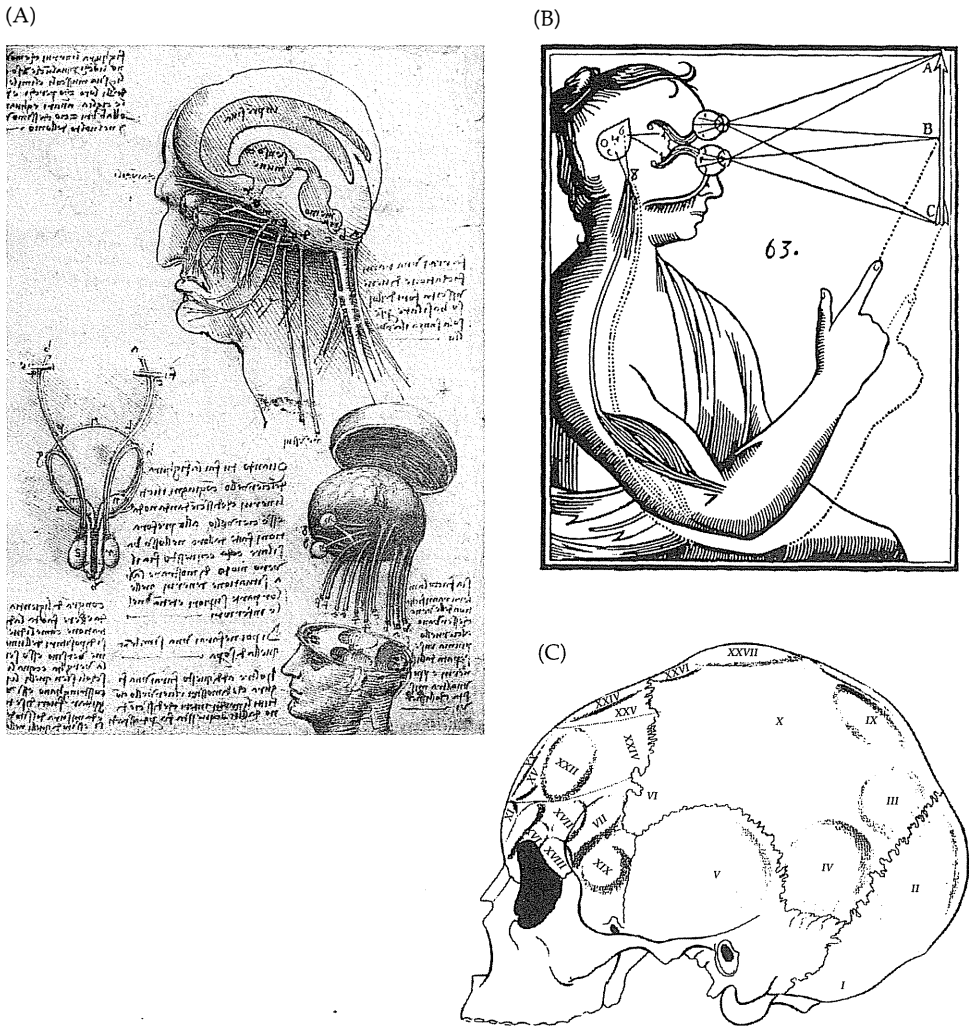

Figure 1.1 Some early views about brain function. (A) While the Italian genius Leonardo da Vinci is most famous for his paintings and inventions, he had boundless curiosity about the natural world, including the human form. His brain dissections included injection of hot wax into the ventricular cavities, which allowed him to make some of the earliest accurate maps of those fluid-filled structures. Consistent with the ideas of many of his contemporaries, he mapped different functions onto different parts of the ventricular system (drawings c. 1508). (B) Descartes likewise believed that the ventricles were critical for brain function, in that they contained psychic "spirits" that flowed from the pineal gland (shown here in a drawing from 1662). In his framework, the single pineal gland was the seat of the mind. (C) The phrenological mapping system created by Franz Joseph Gall (c. 1810). The phrenologists believed that people with an extreme trait (e.g., very wise, prone to thievery) would have an abundance of cortex devoted to that function. To find out which brain area was associated with the trait, researchers would examine the skulls of such people for bumps or protrusions. Each numbered region in this figure represents a different trait, from "reproductive instinct" (I) to "firmness of purpose" (XXVII).

supporting "honesty" (Figure 1.1C). The most prominent advocates, notably Franz Joseph Gall and Johann Spurzheim, lectured widely on the new maps of brain function that they had developed. Popular books used phrenology to explain differences among individuals, to provide self-improvement advice, and to advise employers on desirable qualities in workers.

As the initial novelty of the phrenologists' maps wore off, other scientists began to dispute their validity. To create their maps of the brain, the phrenologists relied heavily on anecdotal descriptions of individuals with extreme characteristics. Notably absent were experimentation and statistical validation of their maps. The phrenologists were not able to document the mechanisms by which cortex growth would lead to behavioral change, nor could they replicate their maps across individuals. Faced with these criticisms, the phrenologists changed their maps, adding more and more areas to already complex systems of bumps and valleys. In the most extreme cases, phrenological systems contained more than 150 distinct areas and used obscure terms such as "comicality" and "velocity" to describe brain organs. By the late 1830s, the idea of mapping the brain through bumps on the skull had collapsed on scientific grounds.

In the succeeding decades, scientists abandoned the approach of examining bumps on the skull and began looking at changes in brain physiology. Measurements of the effects of brain damage or of brain stimulation, usually obtained in animals, could be related directly to brain function and could be validated across many cases. Yet the invasive nature of these measures prevented the systematic study of the human brain, and many aspects of cognition remained inaccessible. Nearly 200 years later, a new group of modern-day explorers are mapping the human brain. These scientists use functional magnetic resonance imaging (fMRI) to take pictures of the active brain in both clinical and research settings. In barely 15 years, fMRI has grown from a theoretical concept to become the dominant technique in cognitive neuroscience.

functional magnetic resonance imaging (fMRI) A neuroimaging technique that uses standard MRI scanners to investigate changes in brain function over time.

static magnetic field The strong magnetic field at the center of the MRI scanner whose strength does not change over time. The strength of the static magnetic field is expressed in Tesla (T).

pulse sequence A series of changing magnetic field gradients and oscillating electromagnetic fields that allows the MRI scanner to create images sensitive to a particular physical property.

What Is fMRI?

As its name implies, magnetic resonance imaging (MRI) uses strong magnetic fields to create images of biological tissue. The strength of the static magnetic field created by an MRI scanner (Figure 1.2) is expressed in units of Tesla (one Tesla is equal to 10,000 Gauss). Scanners used for fMRI are typically at least 1.5 Tesla (1.5 T), and scanners with field strengths of 3 T or higher are now common. For comparison, the Earth's magnetic field is approximately 0.00005 Tesla. To create images, the scanner uses a series of changing magnetic gradients and oscillating electromagnetic fields, known as a pulse sequence. Depending on the frequency of the electromagnetic fields, energy may be absorbed by atomic nuclei. For MRI, scanners are tuned to the frequency of hydrogen nuclei, which are the most common in the human body due to their prevalence in water molecules. After it is absorbed, the electromagnetic energy is later emitted by the nuclei, and the amount of emitted energy depends on the numbers and types of nuclei present.

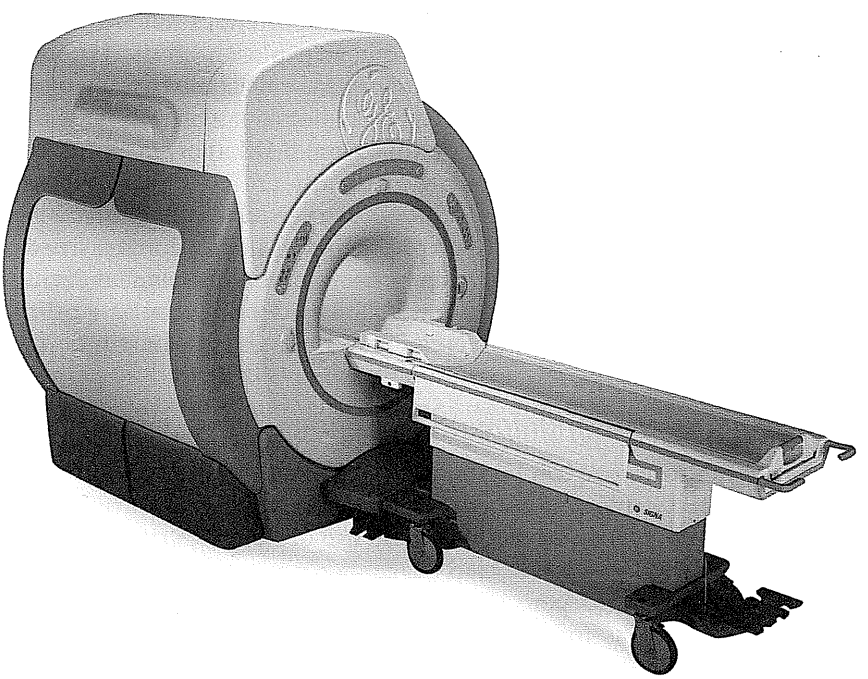

Figure 1.2 A modern MRI scanner. The main magnetic field of the scanner shown is 3.0 Tesla, or about 60,000 times the strength of the Earth's magnetic field. The subject lies down on the table at the front of the scanner, placing his or her head inside the volume coil at the center of the image. The table then moves back into the bore of the scanner until the head is positioned at the very center. (Courtesy of GE Healthcare, Waukesha, WI.)

functional neuroimaging A class of research techniques that create images of the functional organization of the brain. Common functional neuroimaging techniques include fMRI, PET, and optical imaging.

positron emission tomography (PET) A functional neuroimaging technique that creates images based on the movement of injected radioactive material.

Depending on the pulse sequence used, the MRI scanner can detect different tissue properties and distinguish between tissue types. For example, an MRI of the knee can reveal whether ligaments are intact or torn, and an MRI of the brain can detect the difference between gray and white matter. Different pulse sequences can be constructed that create images sensitive to tumors, abnormalities in blood vessels, bone damage, and many other conditions. The ability to examine multiple properties of biological tissue makes MRI an extraordinarily flexible and powerful clinical tool.

Much of our knowledge about the brain has come from the study of its structure, notably by relating neurological disorders to the patterns of brain injury that cause them. However, structural studies are limited in that they cannot reveal short-term physiological changes associated with the active functioning of the brain. Functional neuroimaging studies can help overcome this limitation both by identifying the different parts of the brain where particular mental processes occur and by characterizing the patterns of brain activation associated with those processes. In effect, successful functinal neuroimaging studies build maps that link brain activation to mental function. However, unlike the phrenologists, who believed that complex behaviors or personality traits were associated with discrete brain regions, modern researchers recognize that many functions rely on distributed networks, and that a single brain region may participate in more than one function.

Functional neuroimaging did not begin with fMRI, which has only reached prominence within the past decade. Before that time, the most commonly used functional neuroimaging technique was positron emission tomography (PET), which relies on the injection of radioactive tracers to measure changes in the brain, such as blood flow or glucose metabolism. Using PET, researchers can identify the parts of the brain that are metabolically associated with a given perceptual, motor, or cognitive function, like seeing faces, moving the right hand, or mentally reciting sentences. However, PET imaging suffers from several disadvantages. These include the invasiveness of the radioactive injections, the expense of generating radioactive isotopes, and the slow speed at which images are acquired. As we will discuss in Chapter 7, these limitations have slowed the growth of PET, although it still has important uses.

The development of fMRI has resulted in an explosion of interest in functional neuroimaging (Box 1.1). Most fMRI studies measure changes in blood oxygenation over time. Because blood oxygenation levels change rapidly following the activity of neurons in a brain region, fMRI allows researchers to localize brain activity on a second-by-second basis, and within millimeters of its origin. And, because changes in blood oxygenation occur intrinsically (endogenously) as part of normal brain physiology, fMRI is a noninvasive technique that can be repeated as many times as needed in the same individual. Because of these advantages, fMRI has been rapidly adopted as a primary investigative tool by thousands of researchers at hundreds of institutions.

Measurement versus manipulation techniques

Methods in neuroscience can be roughly divided into two classes based on how they relate brain function to behavior (Figure 1.3). One class, which we will call measurement techniques, involves the use of specialized equipment to measure brain function while subjects engage in one or more behaviors (e.g., performing motor actions, perceiving stimuli, or engaging in a specific form of thinking). Another class of methods, which we will call manipulation techniques, relies on changing the brain's structure or functioning and then exam-

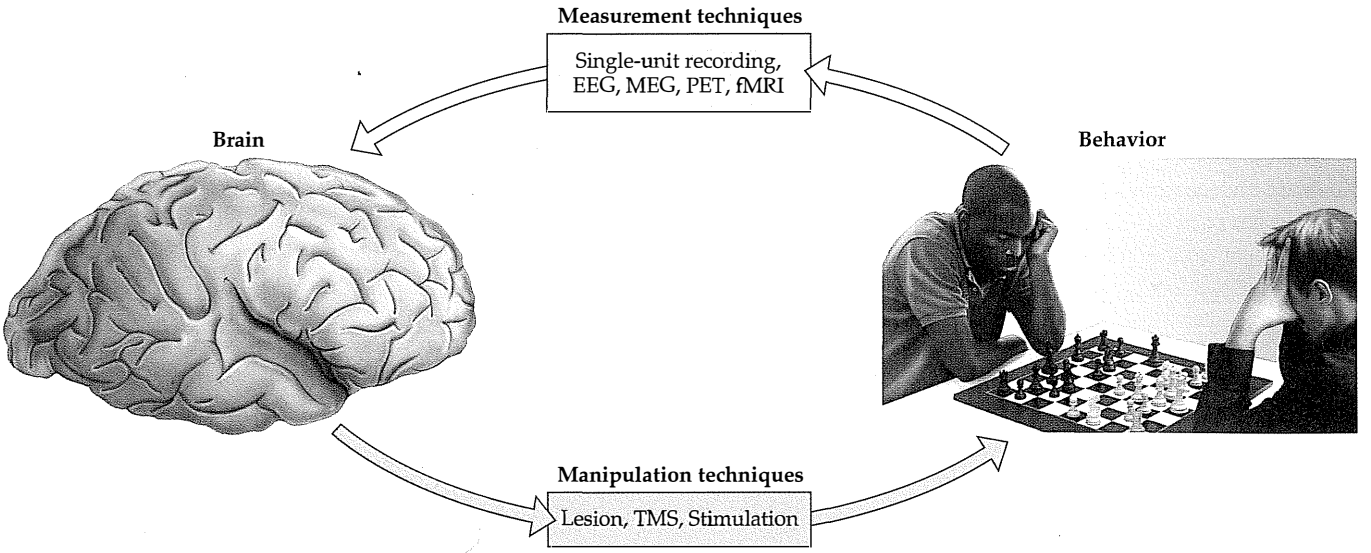

Figure 1.3 Manipulation techniques versus measurement techniques. Neuroscience techniques can be separated into two classes depending on whether they measure or manipulate brain function. When using a measurement technique, the researcher causes the subject to engage in some behavior and then measures how that behavior changes the physiological functioning of the brain. Functional MRI is a measurement technique: subjects engage in some experiment within the MRI scanner, while the experimenters measure changes in blood oxygenation within the brain. Manipulation techniques adopt the reverse approach. The researcher manipulates brain function, either directly (e.g., using transcranial magnetic stimulation [TMS]) or indirectly (e.g., by comparing patients with and without brain lesions), and then examines the effect of those manipulations on behavior.

ining the effects of those changes on behavior. Each has advantages and disadvantages, and many successful neuroscience research programs use both classes of techniques.

Functional MRI is a measurement technique: researchers measure changes in function, typically increases or decreases in blood oxygenation, while a subject performs an experimental task. The measurements provided by fMRI can include maps of how a particular function is represented within the brain, graphs of the relative timing of activation within a particular part of the brain, or even network diagrams that show functional relations among many different regions. Some of these different types of measurements are introduced in the next section, while others are described in later chapters. As noted briefly in the previous section and covered in much more detail in Chapter 3, the pulse sequences used in fMRI alter the properties of individual atomic nuclei within the brain. However, those changes are so slight that they have no effect on macroscopic functioning. For example, the pulse sequences used in MRI do not alter neuronal firing or blood flow.

It is critical to recognize that techniques differ in what they measure. The measures collected by fMRI and PET, for example, provide information about brain metabolism: how much energy is being used by a particular part of the brain, as indicated by changes in oxygen (fMRI, PET) or glucose (PET) levels. Information about metabolism can be used as an indirect indicator of the local neuronal activity. Other techniques, however, measure neuronal activity more

BOX 1.1 What Is fMRI Used For?

Over the past 15 years, fMRI has matured as a technique. Much of its maturation has been technical. MR scanners have become more powerful, while new hardware has facilitated improvements in the speed and quality of image acquisition. Similarly, an improved understanding of the physiological basis for fMRI has led to improved methods for data analysis. Yet, in our view, the most remarkable evidence for the maturation of fMRI can be seen in the creativity of its practitioners. Whereas early fMRI studies investigated simple perceptual and motor phenomena, researchers now apply fMRI to increasingly complex topics. In this box, we highlight two recent studies that used fMRI to study subjective and seemingly ineffable qualities of human experience, namely awareness and dread.

Following traumatic brain injury, stroke, or severe illness, some formerly comatose individuals may enter what is known as a "persistent vegetative state" (PVS): they may engage in autonomic (e.g., breathing) and reflexive behaviors (e.g., tracking objects with their eyes), but do not show any signs of conscious awareness. Some PVS patients recover spontaneously, while others remain in the state for years. A group of researchers led by Adrian Owen at the University of Cambridge hypothesized that fMRI could be used to determine whether or not a given PVS patient maintained conscious awareness, even in the absence of overt behavior.

Owen and colleagues brought a 23-year-old female PVS patient into their fMRI scanner. This patient had suffered severe brain damage in an automobile accident five months previously, and had been unresponsive to external stimulation ever since. When they spoke to her in complex sentences (e.g., "There was milk and sugar in his coffee"), they observed increased fMRI activation in brain regions associated with auditory processing and sentence comprehension. This provided evidence of sensory system function, albeit not of awareness itself. They then verbally instructed her to perform particular mental imagery tasks, namely playing tennis and walking through her home. Remarkably, following the tennis instructions, there was activation in the supplementary motor area, a region associated with the coordination and preparation of motor movements. In contrast, following the home exploration instructions, there was activation in the parahippocampal and parietal cortices, regions associated with spatial processing. The fMRI activations she exhibited were nearly identical to those of normal, healthy control subjects performing the same tasks (Figure 1). The authors argue that these results provide compelling evidence for aware, purposeful mental actions in a patient whose disorder precludes overt behavior.

Few of us will be so unfortunate as to experience PVS or another catastrophic disorder of consciousness. But we all experience short-term negative emotional states, many of which can be disturbing or even life altering. Imagine that you have one week until some impending, stressful event: an upcoming midterm

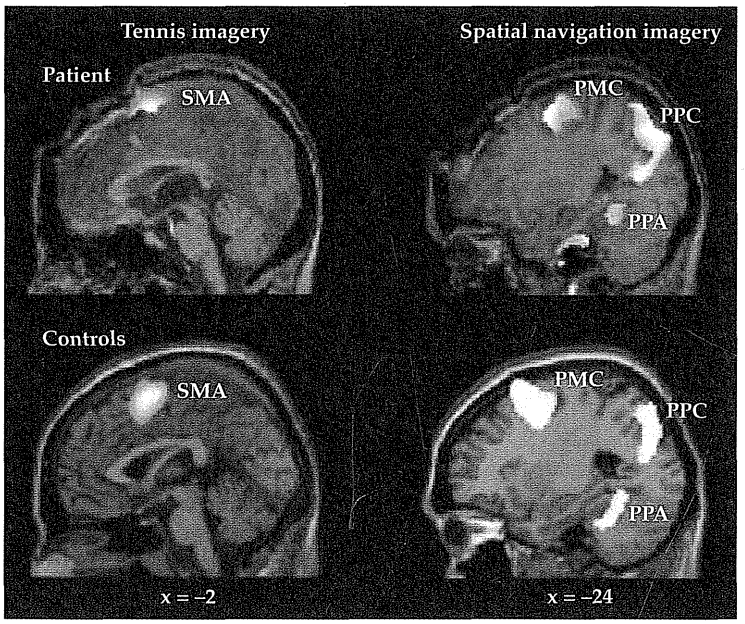

Figure 1 Functional MRI evidence for intact and purposeful brain function in a patient who was in a partial vegetative state. The researchers used fMRI to scan a patient who made no overt responses to external stimuli. When she was asked to imagine playing tennis, the patient's brain exhibited increased fMRI activation in the supplementary motor area (SMA), just like that found in a group of normal control subjects. Similarly, when asked to imagine walking around her house, the patient's brain showed activation in the premotor cortex (PMC), posterior parietal cortex (PPC), and the parahippocampal place area (PPA), again just like normal controls. (After Owen et al., 2006.)

BOX 1.1 *(continued)*

examination, a speech before a large audience, or a complicated surgery. You might feel anxious about the event, even to the point that you'd rather have the event occur now than continue waiting and worrying about it. In short, you are experiencing dread. To understand the potential neural basis for dread, Gregory Berns and his colleagues at Emory University brought subjects to the fMRI scanner and made them wait variable amounts of time for more- or less-painful shocks (Figure 2).

At the beginning of each trial of the experiment, an instruction screen told the subject how strong a shock he or she would receive (e.g., 80% of the voltage associated with their previously-determined pain threshold) and how long the subject would have to wait for the shock (e.g., 27 seconds). When the subject experienced the painful shock, there was increased activation in the somatosensory cortex, the cingulate cortex, and the insular cortex. Within these regions, which are together known as the "pain matrix," the magnitude of fMRI activation increased as the shock voltage increased. Interestingly, the activation at the time of the shock was not affected by how long the person had to wait, nor by whether the person tended to experience mild or extreme dread (Figure 2A). Instead, those individuals who most dreaded the upcoming shocks showed greater increase in fMRI activation as soon as the instruction screen was presented (Figure 2B). By using fMRI, Berns and colleagues could identify not only what brain regions respond to painful experience, but also how those regions are modulated by the accompanying subjective experience of dread.

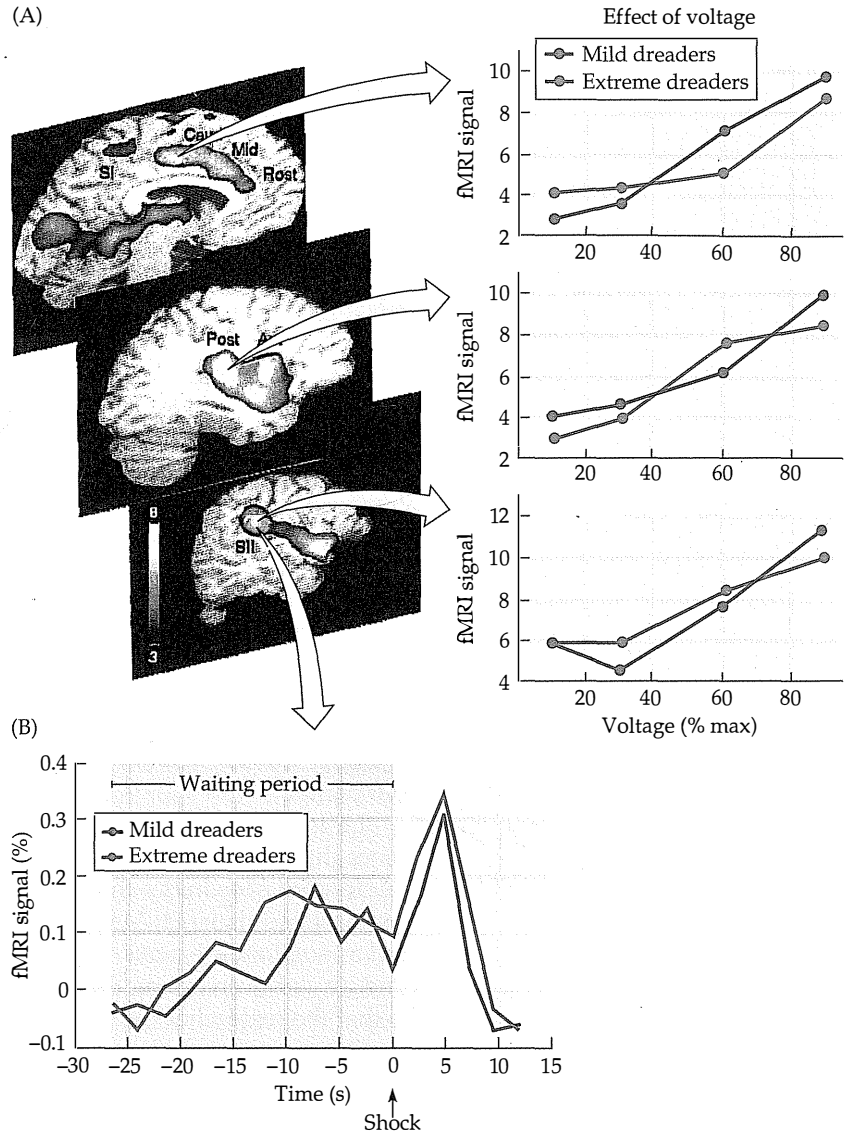

Figure 2 Using fMRI to study the neural basis of dread. (A) The experience of pain evokes activation in several brain regions associated with somatosensation and attention, including primary (SI) and secondary (SII) somatosensory cortices and the anterior cingulate cortex (ACC, labeled according to its caudal, middle, and rostral parts). When subjects are told to await a painful stimulus, activation within these regions increases over time, with (B) greater early activation found in those people who most dread the upcoming shock (blue lines) compared to people who experience the least dread (red lines). (After Berns et al., 2006.)

We call attention to these two studies not because they are the best or most prototypic fMRI experiments, but because they provide clear examples of how fMRI can be used to study increasingly abstract and complex aspects of human experience. Throughout the remainder of the book, we will highlight many more such cutting-edge studies.

directly. By placing an electrode near or within a single neuron, a researcher can record changes in electrical potential associated with the firing of that neuron. For example, if a monkey is trained to remember a picture over a delay of a few seconds, an electrode in one of its lateral frontal lobes will record increased activity during that delay interval. One cannot implant electrodes into healthy human subjects, although this is sometimes done in patients with severe epilepsy to help localize the source of their seizures. However, the electrical and magnetic activity generated inside the brain can be measured from outside the skull using techniques known as electroencephalography (EEG) and magnetoencephalography (MEG). These electromagnetic recording methods measure rapid changes in electrical potentials and magnetic flux, so these techniques are valuable for studying the timing of brain processes. Because the various techniques measure different aspects of brain function, they differ in their strengths and weaknesses.

Manipulation techniques evaluate the effects of brain changes on function. An early and landmark result was reported by the French physician Paul Broca regarding his examination of a single patient named Leborgne. This patient was effectively unable to speak, being only able to repeat the word "tan" in response to prompting. At Leborgne's autopsy in 1861, Broca demonstrated that the patient had damage to the brain that was largely restricted to the inferior frontal lobe in the left hemisphere. This demonstration provided conclusive evidence that language-production abilities are localized, at least in part, to the area of the brain that now bears Broca's name. During the following decades, many other nineteenth-century researchers created lesions in animals to test whether a brain region must be intact for expression of a behavior. And today, many laboratories collect data on groups of individuals who share damage to some brain region (e.g., people with lesions in their prefrontal cortex), so that researchers can evaluate which functions are impaired by damage to that region.

Lesion studies have unquestionable value: they provide compelling evidence that specific brain regions are *necessary* for specific functions. Yet lesion studies also pose many challenges. It is often difficult to find human patients with isolated damage. Many trauma or stroke patients have diffuse damage, and as such their lesions may encompass multiple functional brain regions. One way of overcoming this problem is to create lesions in a specific region, so that the researcher can control the spatial extent of the damage. The introduction of permanent lesions is limited to animal models, for obvious reasons. However, the temporary interruption of function within a brain region is possible using transcranial magnetic stimulation (TMS), which can be used in human subjects to disrupt neuronal activity for periods of seconds to minutes. An additional description of TMS, including how it is used in parallel with fMRI, will be provided in Chapter 13.

Interpreting deficits in function caused by brain damage, whether permanent from a lesion or temporary from TMS, can be problematic. The fact that damage to area X impairs behavior Y indicates necessity (i.e., the use of area X is necessary for behavior Y to occur), but not sufficiency (i.e., other areas may also be necessary). In an oft-cited analogy, damage to one part of a radio, such as the speakers, the tuner, or even the power switch, will result in its inability to play music. However, one could not damage one of those parts and then correctly claim that the damage knocked out the "music-playing" area of the radio. As an interconnected part of a complex system, a given brain region may contribute to more than one psychological process or behavior, and each process or behavior may be supported by multiple brain regions. The effects of a lesion

electroencephalogram/electroencephalography (EEG) The measurement of the electrical potential of the brain, usually through electrodes placed on the surface of the scalp.

magnetoencephalography (MEG) A noninvasive functional neuroimaging technique that measures very small changes in magnetic fields caused by the electrical activity of neurons, with potentially high spatial and temporal resolution.

transcranial magnetic stimulation (TMS) A technique for temporarily stimulating a brain region to disrupt its function. TMS uses an electromagnetic coil placed close to the scalp; when current passes through the coil, it generates a magnetic field in the nearby brain tissue, producing localized electric currents.

often change over time. As the brain heals, an injured region may once again be able to support processing, or other regions may change their processing to compensate for the damage. Furthermore, even a small lesion might result in damage to adjacent fiber pathways, impairing the connections between two distant regions. It is therefore critical to evaluate the effects of many different lesion locations and to track the effects of those lesions over time.

Brain function can also be manipulated through changes in brain chemistry. Neurons throughout the brain have receptors that are sensitive to particular neurotransmitters, such as acetylcholine or serotonin. Drugs or foods may change these neurotransmitters' concentrations or alter the ability of the brain to process them. Some chemical changes modify the activities of specific types of neurons, while others may alter how a wide variety of neurons fire and communicate. Drug studies are powerful, in that they allow the investigation of large-scale brain systems that are not associated with simple lesions, and they are clinically relevant, in that many drugs have well-understood effects on brain disorders (e.g., Parkinson's disease and drugs that manipulate the availability of the neurotransmitter dopamine). A central disadvantage, however, is the difficulty in identifying the functions of specific brain regions following the systemic application of a drug. If the motor skills of a patient with Parkinson's disease improve after administration of a drug that supplies dopamine to the brain, that improvement could be due to better functioning in the midbrain, the basal ganglia, the prefrontal cortex, or any number of regions responsive to that drug. In addition, many drug manipulations have relatively slow time courses, with functional changes that can take place over weeks, so that it is difficult or impossible to make inferences about short-term cognitive processes.

In conclusion, fMRI is one tool among many available to neuroscientists. It is a measurement technique that can provide information about brain metabolism in healthy human subjects. Measurement techniques provide one direction of causality: that a particular behavior (or perception or thought) causes a specific change (or changes) in brain function. Manipulation techniques provide the other causal direction, showing that particular changes in brain function cause specific changes in behavior. Typically, manipulation techniques damage the brain in some way, resulting in a disruptive change in behavior. Thus these two classes of techniques have complementary uses, and their combination provides a powerful approach to the study of human cognition. However, this complementarity is not absolute, as will be discussed later in this chapter. Chapter 13 provides more detailed information about the many techniques used to study brain function, with a focus on those techniques that are used in conjunction with fMRI.

Key concept: contrast

Any imaging technique, from X-rays to fMRI, can be evaluated by simple criteria: what quantity does it measure, how sensitively can it measure that quantity, how precisely in space does it measure that quantity, and how often can it make the measurement? Consider the simple imaging system formed by the sun, you, and a wall (Figure 1.4). If you stand between the bright sun and the wall, your shadow will appear. For opaque objects, like people, the shadow will be very dark compared with the wall around it. However, if the sun's rays pass through something insubstantial, like a cloud of steam or a sheer curtain, the shadow will be much lighter. In this imaging system, the quantity being measured is the number of photons of sunlight that strike the wall and, by

Figure 1.4 Images and contrast. In this very simple imaging system formed by the sun, two objects (the person and the steam), and a wall, the opacity of the objects can be estimated by the darkness of the shadows that are cast. This imaging system shows contrast based on opacity to visible light.

inference, the degree to which the intervening object absorbs photons. By comparing the shadows cast by different objects, like you or a cloud of steam, one can estimate the optical opacity of the objects. Here, the difference between dark and light on the wall indicates the opacity (i.e., light transmittance) of the object being imaged, with dark areas indicating opaque objects and bright areas indicating transparency. In fact, this simple system captures the essence of the familiar X-ray technique.

The difference between the lightest and darkest shadows is a measure of the contrast available in our imaging system. If the imaging technique is sensitive to small gradations in the quantity being measured, the resulting image will have good contrast and will enable us to discriminate between objects with only slight differences. Contrast, however, is not an absolute quantity. Because no imaging method is perfect, there will always be some amount of variation in the measured signal. For example, a plane passing overhead could momentarily block the sun and change the intensity of your shadow on the wall. Thus it is typical to express contrast in relation to the background variation, or noise, and to discuss the results in terms of the contrast-to-noise ratio (CNR). We will explore this topic in more detail in later chapters.

Depending on the pulse sequence used by the scanner, images can be created that differentiate between low and high proton densities, gray matter and white matter, or fluid and tissue. Thus, the quantity being measured is different for each of these image types. In this context, contrast has another special meaning that may be initially confusing. Shown in Figure 1.5 are images that have contrast based on the intrinsic tissue properties T_1 and T_2. We will describe these tissue properties and how these different types of images are created in Chapters 3 to 5. In T_1-weighted images, the difference, or contrast, between light and dark is a measure of the relative difference in the T_1 property of the tissues. Thus, we also refer to these images as T_1-contrast images. In T_1-contrast images, fluid appears as black, gray matter appears as dark gray, and white

contrast (1) The intensity difference between different quantities being measured by an imaging system. It also can refer to the physical quantity being measured (e.g., T_1 contrast). (2) A statistical comparison of the activation evoked by two (or more) experimental conditions, in order to test a research hypothesis.

contrast-to-noise ratio (CNR) The magnitude of the intensity difference between different quantities divided by the variability in their measurements.

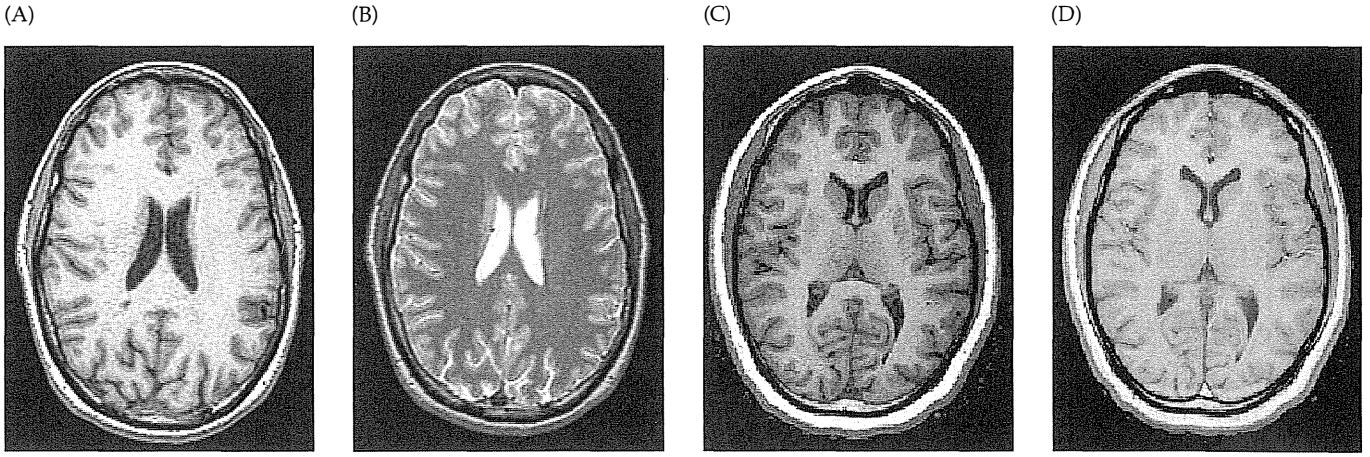

Figure 1.5 Contrast and contrast-to-noise in MR images. Shown in (A) and (B) are images sensitive to two different contrast types (T_1 and T_2, respectively). Note that although much of the same brain structure is present in both images, the relative intensities of different tissue types are very different. Shown in (C) and (D) are two images with the same contrast type but different contrast-to-noise ratios. (C) An image with very high contrast-to-noise; significant detail can be seen in the image. (D) An image with lower contrast-to-noise; some distinctions such as the boundary between gray and white matter are more difficult to identify.

matter appears as light gray. In T_2-contrast images, the contrast between light and dark measures a different tissue property called T_2, and in these images gray matter is light, white matter is dark, and fluid is very bright.

To map brain function, researchers must create images that distinguish between active and non-active areas of the brain (Figure 1.6). These images rely on functional contrast. In PET studies, functional contrast is based on the number of emitted radioactive decay particles. For researchers to say that one area of the brain is more active than another, there must be a statistically significant difference between the numbers of particles emitted by each of those regions. In fMRI studies, functional contrast is usually based on the total amount of deoxygenated hemoglobin in the blood, as will be discussed in detail in Chapter 7. Whether a region is classified as active or inactive depends on the change in the amount of deoxygenated hemoglobin measured in that region. We emphasize that the contrast-to-noise ratio, whether anatomical or functional, depends on both the *amount of signal change* and the *variability in the signal*. An image may have high contrast-to-noise despite small absolute intensity differences, if there is very little variability within each property being measured.

Key concept: resolution

The ability to distinguish different locations within an image is known as spatial resolution. Imagine a digital satellite photograph of a college campus and the surrounding countryside, such as that shown by Google Earth and similar programs. When that photograph covers many miles of terrain, even a large structure such as an enormous athletic stadium might appear as a single dot. But if you zoom in so that the photograph covers only a single street block, then much more detail can be appreciated; now you can see smaller buildings, walkways, and automobiles. In a digital photograph of a scene, the smallest elements that can be resolved are known as pixels, or picture elements. So, in a satellite photograph showing a broad area of countryside, each pixel might represent several hundred yards,

functional contrast A type of contrast that provides information about a physiological correlate of brain function, such as changes in blood oxygenation.

spatial resolution The ability to distinguish changes in an image (or map) across different spatial locations.

pixel A two-dimensional picture element.

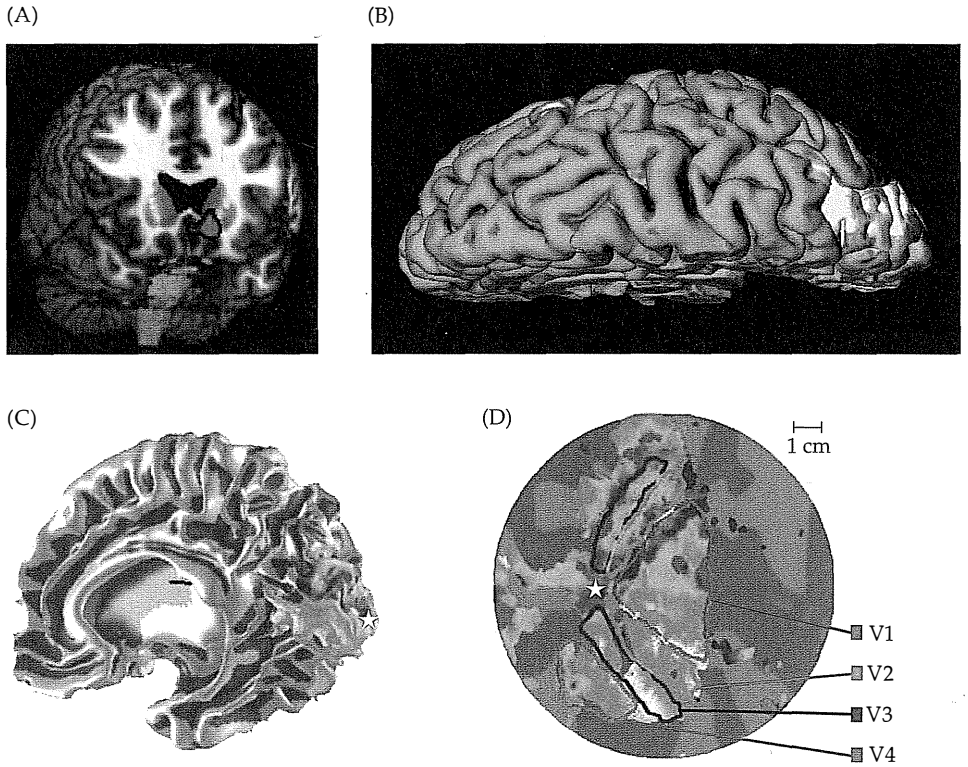

Figure 1.6 Functional maps of the brain produced by fMRI. Even though fMRI data are collected as a series of two-dimensional slices, these areas of activation they identify can be visualized in complex, three-dimensional figures. (A) Shown are areas of activation to the expectation of a monetary reward; the area colored red in the center of the image is the ventral striatum, an area important for reward and learning. (B) This image shows a reconstruction of the right hemisphere of the brain based on a high-resolution anatomical image. Areas of statistically significant activation are indicated in color. The experiment involved a visual search task, and thus areas in the occipital and parietal lobes (at right) are highly active. (C) The cerebral cortex consists of a thin (about 5mm) sheet of gray matter; its bumps and valleys are visible as the gyri and sulci of the brain. Shown on the reconstructed three-dimensional brain are areas important for visual processing, as identified using fMRI. Different parts of the visual system have been color-coded based upon how they responded to stimuli presented to different parts of the retina. (D) This information can be used to identify regions of visual cortex with distinct properties; shown here are the boundaries of four early regions (V1–V4), overlaid upon a flattened view of the cortex. For reference, the part of the visual cortex most sensitive to information presented at the center of gaze (i.e., the fovea) is indicated with a star on both images. (C,D courtesy of Dr. Greg Appelbaum, Duke University.)

while a photograph of a street block may contain pixels representing areas a few feet wide. Similarly, magnetic resonance (MR) images may be able to resolve relatively coarse or fine elements. Since all MR images sample the brain in three dimensions, the basic sampling units of MRI are known as voxels, or volume elements. As the voxel size decreases, the ability to identify fine structure in a brain image improves (Figure 1.7). In principle, the voxel size in MRI can be made arbitrarily small; high-spatial-resolution images of rodent brains (see Figure 12.1) may have voxels less than 0.05 mm on a side. But, as described in Chapter 7, the total signal recovered from a voxel is proportional to its size, and voxels that are too

voxel A three-dimensional volume element.

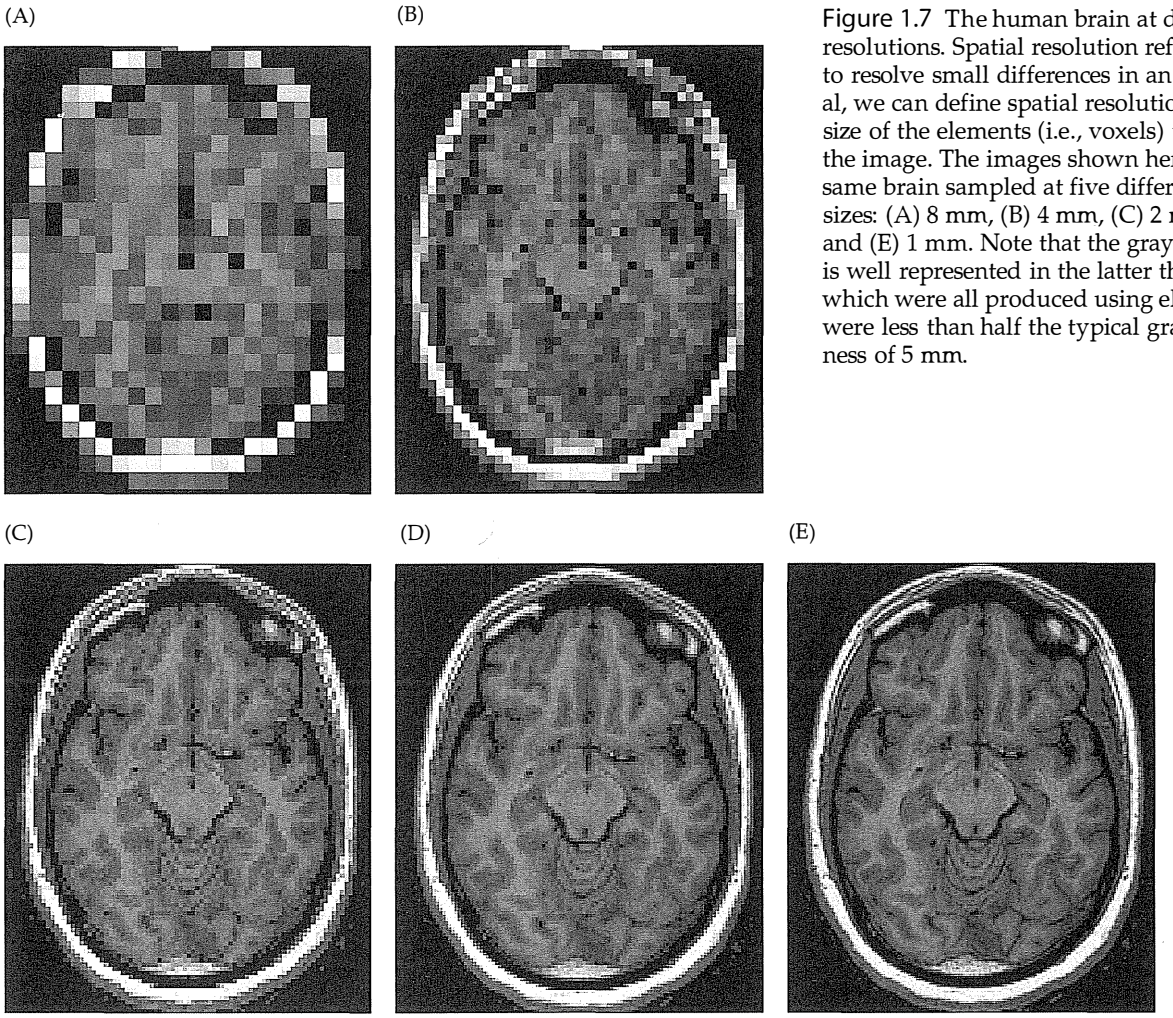

Figure 1.7 The human brain at different spatial resolutions. Spatial resolution refers to the ability to resolve small differences in an image. In general, we can define spatial resolution based on the size of the elements (i.e., voxels) used to construct the image. The images shown here present the same brain sampled at five different element sizes: (A) 8 mm, (B) 4 mm, (C) 2 mm, (D) 1.5 mm, and (E) 1 mm. Note that the gray–white structure is well represented in the latter three images, which were all produced using element sizes that were less than half the typical gray matter thickness of 5 mm.

small may have insufficient signal to create high-quality images. In structural MRI of the human brain, voxels are often about one to two mm in each dimension, while in fMRI, voxels are typically about three to five mm on a side.

Although structural MR images are considered to be static representations of the brain, fMRI is inherently dynamic, in that it measures changes in brain activity over time. The rate at which a technique acquires images, or its sampling rate, determines its temporal resolution. In a typical fMRI study, the sampling rate is often one image every few seconds, which is much faster than PET studies, which measure changes in brain activity over intervals of about a minute or even longer. Our ability to detect changes in functional activity over time is limited not only by the sampling rate, but also by the sluggishness of the physiological changes that we seek to measure. Most fMRI studies measure changes in blood oxygenation, which resolve over periods of a few seconds to a few tens of seconds. Even if we sample the brain very rapidly, the hemodynamic changes may occur too slowly for us to make inferences about the more rapid neuronal activity.

Together, spatial and temporal resolutions have been used to describe a "technique space" that shows how different experimental methods provide potentially complementary information about brain function (Figure 1.8). The

sampling rate The frequency in time with which a measurement is made.

temporal resolution The ability to distinguish changes in a signal (or map) across time.

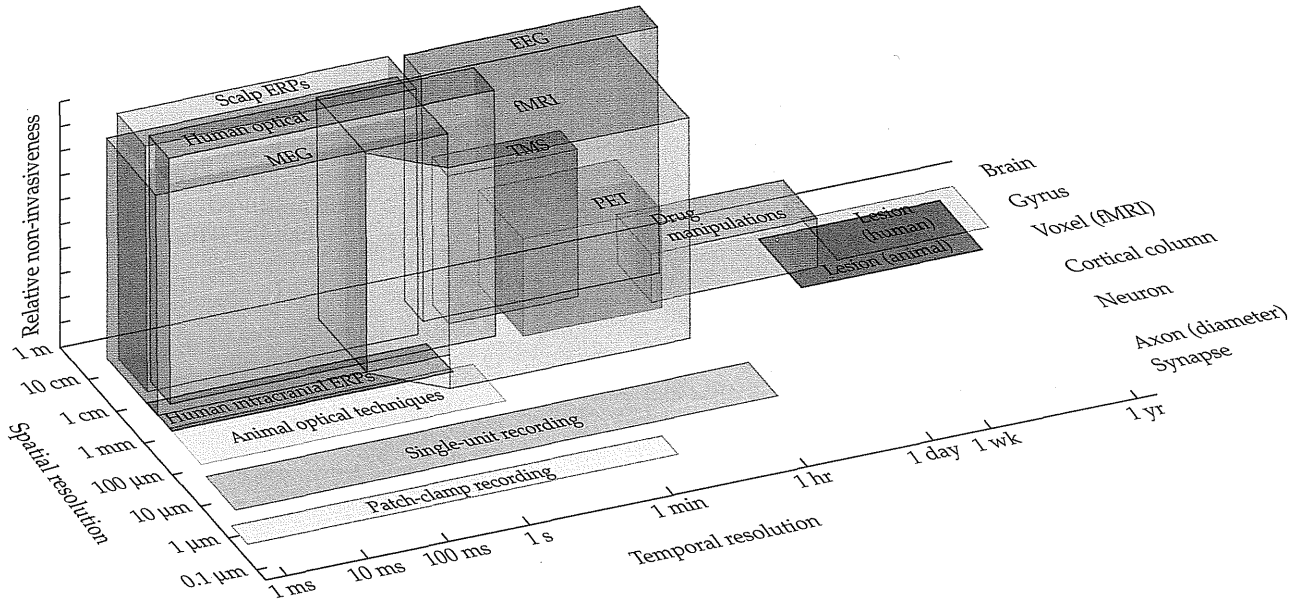

Figure 1.8 Neuroscience techniques differ in their spatial resolution, temporal resolution, and invasiveness. The vertical axes illustrate spatial resolution in terms of distance (left) and of the corresponding brain structures (right). The horizontal axis illustrates temporal resolution. The relative invasiveness (i.e., how much potential damage or risk it involves) is indicated in depth; relatively non-invasive techniques are shown as coming out of the page, while invasive techniques are recessed. Functional MRI provides a good balance of spatial and temporal resolution and thus is appropriate for a wide range of experimental questions. However, other approaches, including electrophysiology, lesion studies, and drug manipulations, can provide important complementary information. ERPs, event-related potentials; MEG, magnetoencephalography; TMS, transcranial magnetic stimulation; EEG, electroencephalography; PET, positron emission tomography.

canonical example of complementarity combines the measurement of brain hemodynamics by fMRI with the measurement of brain electrophysiology by EEG. Since fMRI has very good spatial resolution (millimeters) and EEG has very good temporal resolution (milliseconds), it is argued that combining them would apply the best aspects of each to a single research question. While seductive, this argument conceals a deeper issue that is introduced here and discussed in more detail in Chapter 13. Spatiotemporal graphs like the one in Figure 1.8 suggest that some fundamental quantity (i.e., brain activity) is a single variable that can be measured at different scales of time and space. However, no such fundamental quantity exists. Rather, each of the techniques measures a different aspect of brain physiology. These measures do not always correlate among themselves, and more importantly, they do not always correlate with the mental processes we study. Also, some techniques are appropriate for some subject populations but not others (e.g., animals vs. humans, adults vs. children). Even though spatial and temporal resolutions are important properties for comparing different techniques, they are insufficient and even misleading when exclusively used to decide whether a technique is appropriate for answering a specific research question.

functional resolution The ability to map measured physiological variation to underlying mental processes.

Instead, the value of a technique is determined by its functional resolution, or ability to map physiological variation to mental processes or behaviors. All of the above properties—contrast, spatial resolution, and temporal resolution—

contribute to functional resolution. Yet, other factors are also critical. The brain property being measured determines, in several ways, how well one can localize function in the brain. The changes in blood oxygenation measured by fMRI reflect the local vascular structure of the brain, with larger effects often measured around draining veins. In EEG studies using extracranial recording, the local vascular structure has little effect on activity, but the orientation and temporal synchrony of the active neurons have an enormous effect. So, while a given task might evoke significant activity in a particular brain region using one measurement technique, it might not evoke activity in the same region when a different technique is used. While fMRI is, in our view, the most promising technique for studying the intact human brain, it possesses many important limitations. We will return to this theme throughout the book.

Thought Question

As fMRI has become better established, researchers have become increasingly interested in applying it to clinical questions. What properties of fMRI might make it particularly well- (or poorly-) suited for studying disorders like schizophrenia, autism, or addiction?

History of fMRI

The scientific developments leading to modern fMRI can be divided into five main phases. Basic physics work in the 1920s to 1940s set forth the idea that atomic nuclei have magnetic properties and that these properties can be manipulated experimentally. Seminal studies reported by two laboratories in 1946 described the phenomenon of nuclear magnetic resonance (NMR) in solids, and ushered in several decades of non-biological studies. The first biological MR images were created in the 1970s after advances in image acquisition methods. By the 1980s, MR imaging became clinically prevalent, and structural scanning of the brain was commonplace. Finally, in the early 1990s, the discovery that changes in blood oxygenation could be measured using MRI ushered in a new era of functional studies of the brain. We provide in this section a brief overview of the history of MRI, and we will discuss specific physical principles in more detail in subsequent chapters.

Early studies of magnetic resonance

The beginnings of MRI can be traced to the work of the Austrian physicist Wolfgang Pauli in the 1920s. Noting some anomalies in the electromagnetic spectra emitted by excited atoms, Pauli postulated that atomic nuclei had two properties, called spin and magnetic moment, which could only take discrete values (or quanta). As an analogy, think of atomic nuclei as continually spinning tops. Pauli's suggestion in rough terms was that these tops could spin only at certain frequencies and exert only particular magnetic forces. At that time, nuclear properties were poorly understood (indeed, the neutron itself would not be identified until 1932, in a report by the English physicist James Chadwick), and Pauli's conjecture would not be tested for more than a decade.

An early technique for investigating whether different atomic nuclei spin at discrete frequencies was the molecular beam apparatus developed by Stern and Gerlach. A gaseous beam of a single element was passed through a strong

oscillating magnetic field A magnetic field whose intensity changes over time. Most such fields used in MRI oscillate at the frequency range of radio waves (megahertz, or MHz) and as such they are often called radiofrequency fields.

static magnetic field before hitting a detector plate. A static magnetic field is one whose intensity (ideally) does not change over space or time. If the spin frequencies of atomic nuclei could only take a number of discrete quantum states, then the static magnetic field would split the beam into some finite number of smaller beamlets before the beamlets hit the detector. On the other hand, if the spin frequencies of the atomic nuclei in the beam could take a continuous range of possible values, then there would be a similarly continuous distribution of intensity on the detector. The beams did split into discrete beamlets, as predicted by quantum theory.

These results proved that the spin frequency of an atomic nucleus can only take one of a number of discrete values. However, the spin frequency values for particular atomic nuclei remained to be measured. In 1933, the American physicist Isidor Rabi (Figure 1.9A) modified the Stern–Gerlach technique so that he could measure the spin frequencies of hydrogen and alkali metals. But Rabi felt that this beam technique was inelegant and sought a better method. The Dutch physicist Cornelis Gorter visited Rabi's laboratory in 1937 and described his recent experiments with oscillating magnetic fields. Stimulated by this discussion, Rabi realized that if the frequency of the oscillating magnetic

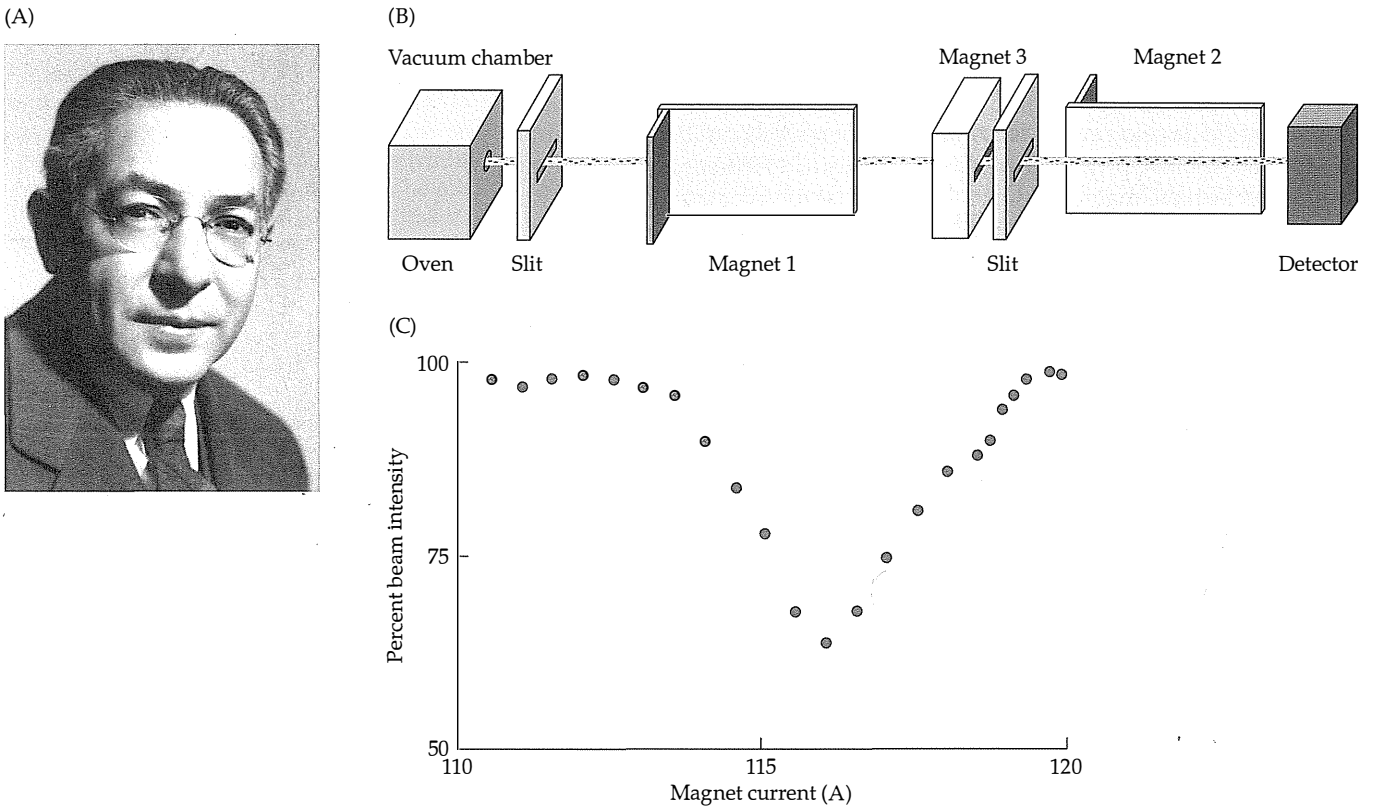

Figure 1.9 The determination of the magnetic moment of the lithium nucleus by Isidor Rabi (A). The beam technique devised by Rabi involved passing a beam of gaseous nuclei through several magnetic fields (B). The key innovation introduced by Rabi was an oscillating electromagnetic field (Magnet 3). If the oscillation rate was equal to the resonant frequency of an atomic nucleus (at the current strength of the static magnetic field), the spin of the atomic nuclei would change and then the subsequent magnetic field (Magnet 2) would deflect the nuclei away from the detector. (C) Data from Rabi's experiment, in which he kept the oscillation rate fixed and changed the current in the static field magnet to modify its magnetic field strength. He found a sharp reduction in beam intensity at about 116 amperes, allowing him to calculate the spin properties of the lithium nucleus. (A ©The Nobel Foundation.)

field could be matched to the spin frequency of the atomic nucleus, then the nucleus would absorb energy from the field. This concept is called magnetic resonance. To understand this idea, consider the analogy of a swing set, to which we will return in Chapter 3. If your friend is sitting on a swing set, you can help her swing back and forth by pushing her. A single hard push will have only a limited effect. But by pushing her gently, regularly, and in synchrony with her swinging, at each cycle she will swing a little higher. The frequency of pushing that has the most effect is known as the resonant frequency. Energy can be given to atomic nuclei in the same way, by a large number of small "pushes" from a magnetic field that oscillates at the resonant frequency of the nucleus.

magnetic resonance The absorption of energy from a magnetic field that oscillates at a particular frequency.

resonant frequency The frequency of oscillation that provides maximum energy transfer to the system.

This idea catalyzed work in Rabi's lab, and just days after Gorter's visit, the classic beam technique was modified to include an oscillating magnetic field. Rabi recognized that the resonant frequency needed for the oscillating field would depend on the strength of the static magnetic field, just as the speed at which someone swings would depend on the strength of the gravitational field. So, he held the frequency of the oscillating field constant and changed the strength of the static field by adjusting the current in the magnet. (Note that this approach is the opposite of that used by modern MR scanners, which keep the static field constant and vary the oscillating field to examine different atomic nuclei.) As the strength of the main field approached the resonant frequency of the lithium atoms in the beam, the atoms in the beam were deflected away from the detector (Figure 1.9B and C). This experiment represented the first demonstration of nuclear magnetic resonance effects, for which Rabi received the Nobel Prize in Physics in 1944.

NMR in bulk matter: Bloch and Purcell

During the early 1940s, much basic research in physics stopped because the top physicists of the day were working on military applications, such as the development of the atomic bomb and the improvement of radar and counter-radar measures. When the war ended in 1945, two physicists, Felix Bloch at Stanford (Figure 1.10A) and Edward Purcell at MIT/Harvard (Figure 1.10B), resumed their independent investigations of magnetic resonance in bulk matter (i.e., normal solid substances). The previous magnetic resonance experiments by Rabi and others had used beam methods that required purified gases; for magnetic resonance to become practical as a measurement technique, it would need to be applicable to normal substances, not just laboratory creations like beams of atoms.

On December 13, 1945, Purcell and his colleagues began their first experiment to demonstrate magnetic resonance in bulk matter. Borrowing a strong magnet that had originally been used for astronomical research, they placed paraffin wax into the center of the magnetic field. They reasoned that if they matched the resonance frequency of the wax to the oscillating magnetic field, the wax would absorb energy. This, in turn, would change the wax's electrical conductance, which could be detected by a simple circuit. Like Rabi, they recognized that the resonant frequency of the wax would depend on the static magnetic field strength, so they changed the current flowing through the coils of their electromagnet to change its field strength. Despite their careful planning, when they adjusted the current in the magnetic field no resonance was found!

At first, Purcell and colleagues suspected that they had not left their wax sample in the magnetic field for a long enough time before initiating their experiment. Scientists had previously theorized that it took some time before

(A)

(B)

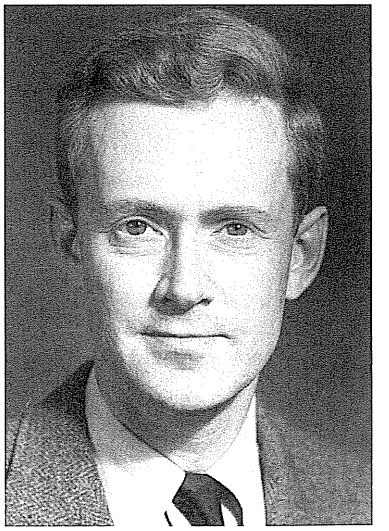

Figure 1.10 Nobel laureates Felix Bloch (A) and Edward Purcell (B) shared the 1952 Nobel Prize in Physics for their simultaneous but separate discoveries of magnetic resonance in bulk matter. (©The Nobel Foundation.)

transmitter coil An electromagnetic coil that generates an oscillating magnetic field at the resonant frequency of atomic nuclei within a sample.

detector coil An electromagnetic coil that measures energy emitted back to the environment after its initial absorption by the sample.

nuclear induction The initial term for nuclear magnetic resonance effects, as labeled by Bloch and colleagues.

nuclear magnetic resonance (NMR) The measurable changes in magnetic properties of atomic nuclei induced by the application of an oscillating magnetic field at the resonant frequency of the nuclei.

atomic nuclei became aligned with an external magnetic field, a concept known as relaxation time (discussed in detail in Chapter 3). However, Purcell and his colleagues did not know the relaxation time for the atomic nuclei in their sample—it could be as short as a few seconds or as long as a few years. On the chance that relaxation was a very slow process, they placed the wax in the magnetic field for several hours before repeating their experiment two days later. Even with this presaturation period, the second experiment failed; at the predicted current level of the magnet, there was no resonance effect. Finally, before ending the experiment, the researchers decided to test all possible magnetic field strengths, so they increased the magnet current to the maximum level and then slowly decreased it. To their surprise, they found a clear resonance effect at a near maximum value that was much higher than the one they had predicted; subsequent investigation revealed that they had simply miscalculated how much current was necessary to generate the appropriate magnetic field. Their discovery was reported in *Physical Review* in January 1946.

Almost simultaneously at Stanford, Bloch and his colleagues were also attempting to measure resonance effects in bulk matter, although they were using a very different apparatus. They placed a sample of water in a brass box between the poles of a strong magnet, whose field strength they could manipulate. An adjacent transmitter coil sent electromagnetic energy into the sample, while a second detector coil was used to measure changes in the energy absorbed by the water (as emitted back to the environment). As in the MIT/Harvard experiment, the sample was presaturated for 24 hours in the magnetic field to ensure that relaxation would take place. These long presaturation periods turned out to be excessive; for bulk substances like paraffin and water, relaxation times are only a few seconds rather than many hours.

In a striking parallel to Purcell's experiment, Bloch's group also detected magnetic resonance effects in their water sample. They labeled this phenomenon nuclear induction, and reported their findings in *Physical Review* two weeks after Purcell's report. Nuclear induction, now known as nuclear magnetic resonance (NMR), forms the basis for all modern MR imaging techniques, and all MR scanners share the basic design principles of Bloch's simple apparatus: a strong static magnetic field, a transmitter coil that sends electromagnetic energy to the sample, and a detector coil that measures energy emitted back from the sample. Purcell and Bloch were awarded a joint Nobel Prize in Physics in 1952 for their independent contributions to the discovery of nuclear magnetic resonance.

While the discoveries that enabled NMR were made by physicists, the first applications of the new technique came from chemistry. By the early 1950s, the Varian Associates Company had patented, with Felix Bloch's assistance, the basic ideas for using NMR to do chemical analyses of samples. NMR soon proved to be a very useful technique for understanding the chemical composition of a homogeneous substance, sharing both theory and methodology with modern MRI spectroscopy. Despite (or perhaps because of) the considerable commercial success of NMR, at least in fields like geology and organic chemistry, the primary uses of the new technique would remain chemical rather than biological for more than two decades.

The first MR images

By the late 1960s, NMR measurements had revealed differences between water molecules depending on whether or not they were within biological tissues. Specifically, the atomic nuclei contained in water molecules in biological tissues were constrained in their diffusion and orientation when compared with water

in other states, and these differences could be identified using NMR. The American physician Raymond Damadian hypothesized that similar differences might be observed between cancerous and non-cancerous cells; if so, NMR could become an extremely useful method for identifying cancerous tissue. Damadian tested this hypothesis in tissue samples taken from rats, and found that relaxation times were much longer in the cancerous tissue than in healthy tissue; this result was published in *Science* in 1971. Damadian's results were enormously influential in suggesting for the first time a clear medical application for NMR. Yet this application, assessing the properties of tissue samples, had limited value because it could not be used to create spatial images of the tissues. The advance that led to the explosion of interest in magnetic resonance was the ability to form such spatial images.

In a formal sense, an image provides information about how one or more quantities vary over space. As examples, standard photographs are images of the intensity (and frequency) of visible light and X-ray films are images indicating the density of intervening matter. The first NMR studies did not create images, because they measured the total energy absorbed and emitted by the entire sample. In fact, in order to improve the interpretation of their results, early NMR researchers strove to remove spatial information from their samples to ensure homogeneity. Without image formation, NMR remained a relatively obscure curiosity.

Having seen the results of NMR experiments like those conducted by Damadian, the American physicist Paul Lauterbur recognized that NMR had considerable potential for biological and physical applications, if a method for image formation could be developed. In 1972 Lauterbur had a novel idea: if the strength of the magnetic field were varied over space, the resonant frequencies of protons at different field locations would also vary. By measuring how much energy was emitted at different frequencies, one could identify how many protons were present at each spatial location. This idea, of inducing spatial gradients (G) in the magnetic field, proved to be the fundamental insight that led to the creation of MR images. Lauterbur also realized that a single gradient could only provide information about one spatial dimension; to recover two-dimensional structure, it would be necessary to use gradients at different orientations. By acquiring data using four gradients in succession, each turned 45° from its predecessor, Lauterbur created an image of a pair of water-filled test tubes (Figure 1.11). This picture, which was reported in *Nature* in 1973, was the very first MR image.

Lauterbur's method, though revolutionary, was inefficient because it essentially required a succession of one-dimensional projections through the object, and then combined the data into a two-dimensional image. Not only was there considerable redundancy in the data that were collected, but also the approach was quite time-consuming due to the need for many separate acquisitions. A more efficient technique, known eventually as echo-planar imaging (EPI), was proposed by the British physicist Peter Mansfield in 1976. Echo-planar imaging allowed the collection of data from an entire image slice at one time, by sending one electromagnetic pulse from a transmitter coil and then introducing rapidly changing magnetic field gradients while recording the MR signal. The resulting complex MR signal could be reconstructed into an image using Fourier analysis techniques, as will be discussed in Chapter 4. Echo-planar imaging reduced the time needed to collect a single image from minutes down to fractions of a second, which greatly improved the feasibility of clinical imaging. Concepts derived from echo-planar imaging underlie the most important approaches to MRI today, and they have been particularly important for fMRI studies, due to the need for

image A visual description of how one or more quantities vary over space.

spatial gradients (G) A magnetic field whose strength varies systematically over space. Note that since a given spatial location only experiences one magnetic field, which represents the sum of all fields present, spatial gradients in MRI act to change the effective strength of the main magnetic field over space.

echo-planar imaging (EPI) A technique that allows collection of an entire two-dimensional image by changing spatial gradients rapidly following a single electromagnetic pulse from a transmitter coil.

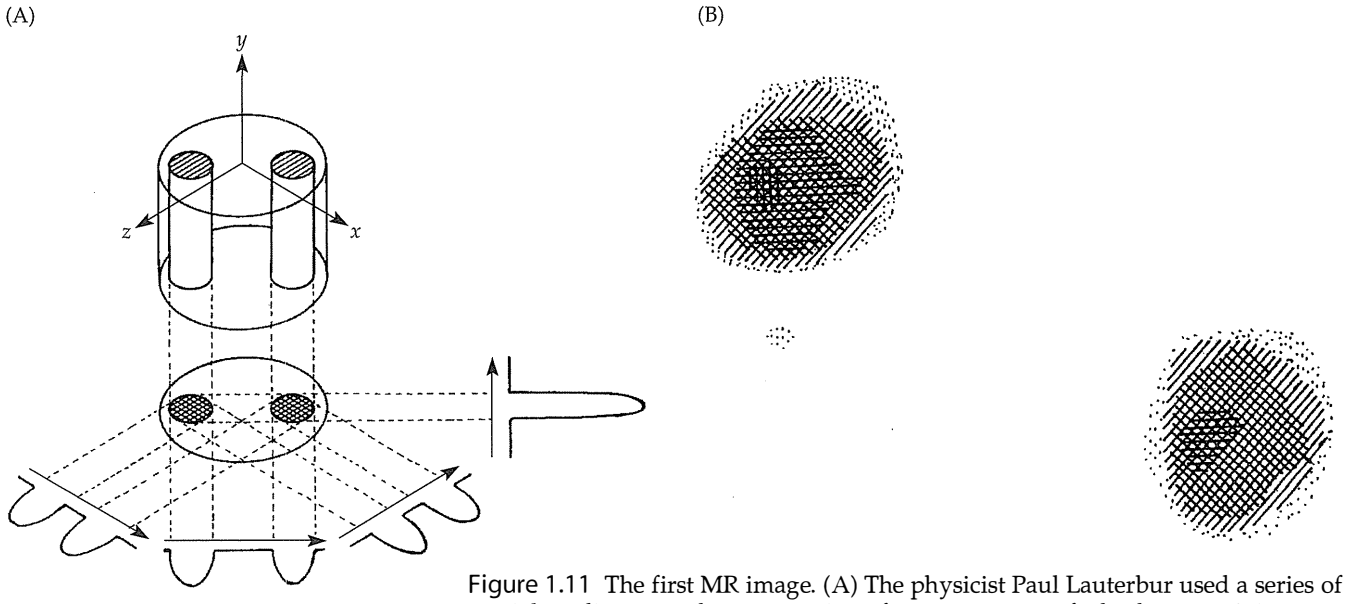

Figure 1.11 The first MR image. (A) The physicist Paul Lauterbur used a series of spatial gradients to take a succession of measurements of a beaker containing two water-filled test tubes. (B) Data collected under each gradient provided different information about the object. By combining these data using projection methods, Lauterbur was able to reconstruct the spatial organization of the object. The resulting picture was the first magnetic resonance image. The use of spatial variation in the magnetic field set the stage for modern MR imaging. (From Lauterbur, 1973.)

fast imaging to measure changes in brain function. Lauterbur and Mansfield were jointly awarded the Nobel Prize in Physiology and Medicine in 2003 for their independent contributions to image formation using MRI (Box 1.2).

While the theoretical underpinnings of MRI were largely in place, significant engineering problems were yet to be solved. In 1977, the first human NMR scanner was created by Damadian's FONAR Corporation, and christened "Indomitable" (Figure 1.12A). At that time it was difficult to create a strong, homogeneous magnetic field in a scanner large enough to fit an adult human. Therefore, the magnetic field in Damadian's scanner was weak (0.05 T) and homogeneous only within a small volume at its center. Data could be acquired from a single small part of the body at one time, whereupon the subject would have to be moved so that another part of the body could be located at the scanner center. This approach did not take advantage of the gradient methods developed by Lauterbur and Mansfield, but instead required the collection of each voxel as an independent NMR volume.

The first attempt to collect an NMR image using Indomitable failed, perhaps due to problems with adjusting the transmitter/receiver coil system to fit the large subject, Damadian himself (see the 1996 book by Mattson and Simon for a complete narrative). After several months of additional adjustment and preparation, they were ready for another attempt. On the morning of July 3, 1977, one of the postdoctoral fellows in Damadian's laboratory, Larry Minkoff, entered the scanner. They slowly collected data from one voxel at a time, changing Minkoff's position slightly after each acquisition. Each voxel in the image took more than 2 minutes to acquire, and the complete image of 106 voxels took nearly 4 hours. At the end of the marathon session, the researchers' patience was rewarded with the first full-body MR image, a single slice through

(A)

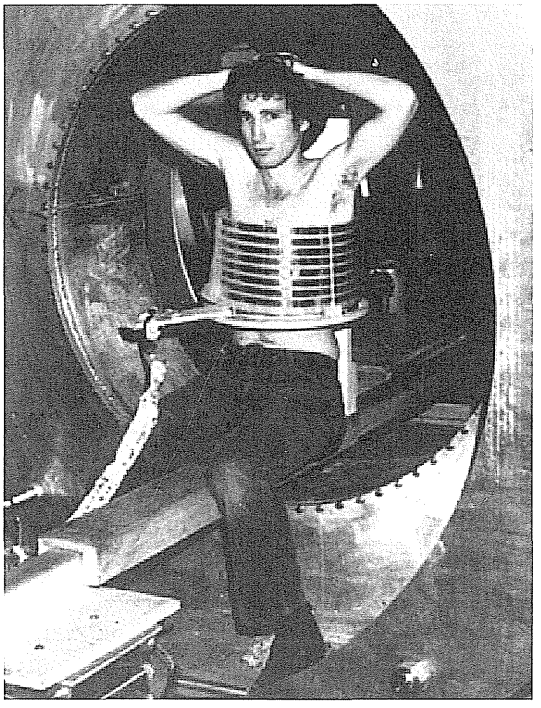

(B)

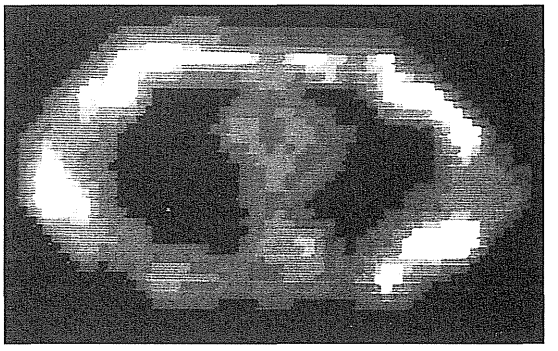

Figure 1.12 The first MR image of the human body. Raymond Damadian and colleagues constructed an early large-bore MRI scanner, which was called "Indomitable." (A) Larry Minkoff, a postdoctoral fellow in the laboratory, was the first subject from whom data were recorded. (B) The resulting image of his chest, while primitive by modern standards, shows the heart, lungs, and surrounding musculature. (A from Fonar Corporation; B from Damadian et al., 1977.)

Minkoff's torso (Figure 1.12B). Within 2 years, Damadian's group and other laboratories had created multiple images of the abdomen, upper torso, and head. In addition, researchers and clinicians could now acquire images of the brain from new orientations that were previously difficult to acquire using X-ray-based scanning.

With image formation using NMR a reality, many medical applications became evident. In the late 1970s, computerized tomography (or CT) imaging was commonly used to generate high-resolution images of the human body. CT uses a beam of X-rays that rotates around the body part of interest; the X-ray absorption at each angle is measured, and the resulting projections are combined to form a single picture representing one plane through the tissue. While CT is still commonly used today, it does require concentrated X-ray exposure. Because NMR images could provide similar information without X-ray exposure, there was substantial interest in NMR as a potential diagnostic tool. Around the same time, the term "nuclear magnetic resonance" fell into disfavor. It was abandoned partly because of the negative health connotations of the word "nuclear", and this change was justified because NMR does not use ionizing radiation. Also, hospital officials wanted to separate MR scanning departments from nuclear medicine departments. As a result of these factors, by the early 1980s, NMR became MRI: magnetic resonance imaging.

Growth of MRI

As we have seen, MRI had three primary advantages over other imaging techniques. It had the potential for very high spatial resolution of both bones and soft tissues. It did not require ionizing radiation, as did X-rays or CT scans. And it could obtain images in any plane through the body. However, the capital costs

BOX 1.2 The Nobel Controversy: Scanners or Images?

(A)

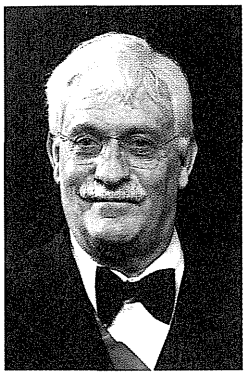

(B)

This Year's Nobel Prize in Medicine

The Shameful Wrong That Must Be Righted

This year the committee that awards The Nobel Prize for Physiology or Medicine did the one thing it has no right to do: it ignored the truth. Eminent scientists, leading medical textbooks and the international press are in disagreement with the decision of the committee. So is the U.S. Patent Office. Even Alfred Nobel's will is in disagreement. The committee is attempting to rewrite history.

The Nobel Prize Committee to Physiology or Medicine chose to award the prize, not to the medical doctor/research scientist who made the breakthrough discovery on which all MRI technology is based, but to two scientists who later made technological improvements based on his discovery.

Figure 1 Raymond Damadian, an early pioneer in MRI research, was passed over for the 2003 Nobel Prize. (A) Damadian was one of the first scientists to suggest a biological use for Nuclear Magnetic Resonance measurement and was also the first to build an MR scanner suitable for whole-body human imaging. (B) Upon learning of the Nobel Committee's award, Damadian's MRI company, FONAR Corporation, sponsored advertisements in several leading newspapers to protest Damadian's exclusion. Part of one of those advertisements is shown here. (A courtesy of Fonar Corporation.)

On October 9, 2003, readers of the *Washington Post* were greeted with a full-page advertisement titled "This Year's Nobel Prize in Medicine—The Shameful Wrong that Must Be Righted" (Figure 1). Similar advertisements appeared the next day in the *New York Times* and *Los Angeles Times*, all of which were paid for by the FONAR Corporation, founded by Raymond Damadian. They protested the announcement, made earlier that week, of the 2003 Nobel Prize in Physiology or Medicine, which was granted to the physicists Paul Lauterbur and Peter Mansfield (Figure 2).

The core argument in these advertisements rested on simple and compelling facts. Damadian demonstrated, in a 1971 *Science* article, that NMR measurements could distinguish between healthy and cancerous tissues. In 1972 he filed the first patent for an MR scanner. And, as recounted in this chapter, he and his colleagues built the first MR scanner that could create images of the entire human body. The rules of the Nobel Prizes allow the granting of each year's prize to up to three individuals, so the selection committee could have chosen to include Damadian (or any other MR pioneer) in addition to Lauterbur and Mansfield. As summarized in the advertisements: "The Nobel Prize Committee to Physiology or Medicine chose to award the prize, not to the medical doctor/research scientist who made the breakthrough discovery on which all MRI technology is based, but to two scientists who later made technological improvements based on his discovery."

These arguments have intuitive force. Damadian clearly played *some* role in the development and popularization of MRI—consider the photograph and scan in Figure 1.12, which document the first human MRI scanning. So, why was he not recognized by the Nobel Institute? The deliberations of its selection committee are sealed for 50 years, so the reasons underlying their decision will not be known for some time. Yet, some clues are evident in the press release, which is available for public review on the Nobel Prize website.

The press release begins by describing the basic principle of nuclear magnetic resonance—that atoms in a magnetic field will absorb, and later emit, energy if that energy is delivered at a particular resonant frequency (see Chapter 3). This discovery was the basis of the 1952 Nobel Prize in Physics. Lauterbur and Mansfield were cited not in Physics, but in Physiology or Medicine, because of the applications of their work to medical imaging. Lauterbur's citation reads in part: "introduction of gradients in the magnetic field made it possible to create two-dimensional images." Similarly, "Mansfield utilized gradients in the magnetic field in order to more precisely show differences in the resonance." The comments of the Nobel Institute indicate that the selection committee recognized Lauterbur and Mansfield for their development of methods for creating *images*. Each made a seminal discovery in the use of magnetic gradients. Lauterbur provided the first demonstration of image creation, and Mansfield developed the method of rapid image collection that is still used today.

What about the claim in the Washington Post advertisement that Damadian "made the breakthrough discovery on which all MRI technology is based"? While the first MRI scanner was indeed built by Damadian, it used a point-by-point collection process that was inefficient and quickly abandoned. Nor was the proposal that relaxation properties

BOX 1.2 *(continued)*

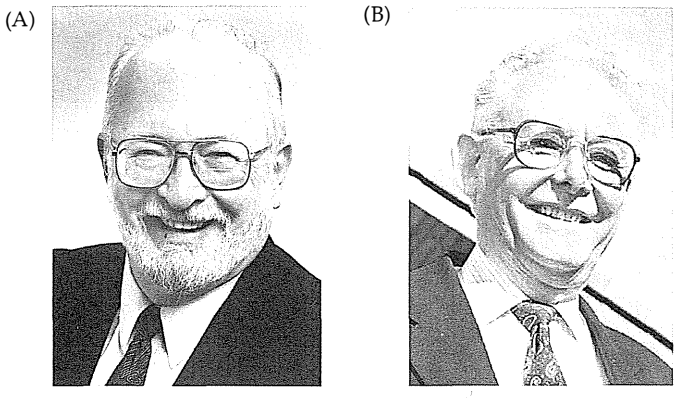

Figure 2 Nobel laureates Paul Lauterbur (A) and Peter Mansfield (B). Lauterbur and Mansfield shared the 2003 Nobel Prize in Physiology or Medicine for contributions to the development of MRI. Lauterbur was cited for his introduction of magnetic field gradients, which changed the spin frequencies of atomic nuclei over space and thus allowed the recovery of spatial information. Mansfield was recognized for his development of echo-planar imaging methods, which allowed rapid collection of images. (A ©The Nobel Foundation; B courtesy of Lisa Gilligan, University of Nottingham.)

would predict cancer supported by subsequent work. In short, neither current MRI practice nor its applications follow directly from Damadian's discoveries. Yet there may have been indirect influences. As Damadian and his supporters have argued, the idea of using NMR to study biological systems may have sparked Lauterbur to introduce magnetic gradients. (Lauterbur was familiar with Damadian's work and had seen a variant of the experiment, but dismissed it as a significant influence on his own work.)

Rarely has the selection of a Nobel award been as immediately controversial as the 2003 Prize in Physiology or Medicine. Some experts in the field believed that a deserving pioneer and inventor was unfairly excluded from recognition, perhaps because of his perceived brashness and ambition, or because he developed his inventions into a business. Many others argued that the Nobel Committee chose correctly by emphasizing image processing, rather than inventions. Consider these questions: Will a future Nobel Prize be awarded for functional MRI? And, if so, what discoveries will be recognized?

involved in setting up an MRI center were high, especially for hospitals facing budgetary constraints in the recessionary economy of the early 1980s. A typical MRI scanner could cost up to one million dollars to purchase, with maintenance, personnel, and supply contracts adding hundreds of thousands of dollars annually. Many hospitals had just invested heavily in expensive CT scanners and were loathe to commit more funds to an unproven technique. In addition, MRI was approved for research purposes only by the U.S. Food and Drug Administration (FDA). Therefore, insurance companies would not reimburse hospitals for the procedure. Nevertheless, there was enough appreciation of the potential of MRI that a number of companies, including FONAR, General Electric (GE), Philips, Siemens, and Varian, began developing MRI scanners for clinical use.

One consequence of the investment in MRI research and development was a substantial increase in scanner power. The standard resistive magnets were replaced by superconducting magnets, which had fewer limitations on field strength and homogeneity. However, expensive cooling agents were needed to maintain superconductivity. GE created the first commercial 1.5-T scanners for the human body in 1982, and began shipping them to hospitals shortly thereafter. While other companies focused on low- to medium-field scanners (0.1 to 1.0 T), GE's emphasis on high-field MRI resulted in considerable market success. As MRI grew, 1.5-T scanners would be the standard workhorses for clin-

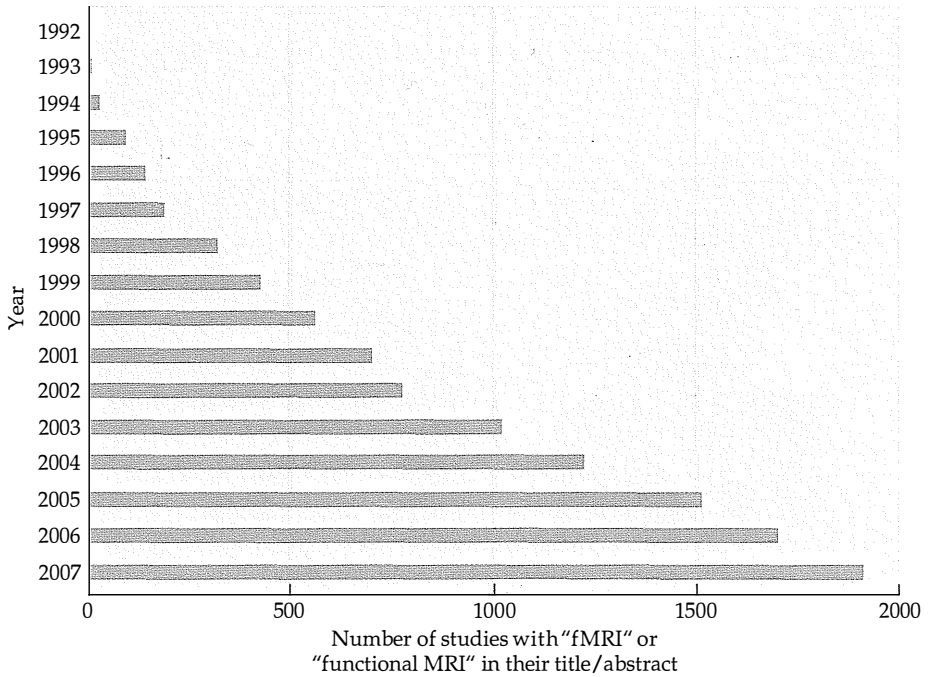

Figure 1.13 Growth in fMRI research over the past 15 years. Plotted for each year is the number of PubMed-indexed studies with the terms "fMRI" or "functional MRI" in their titles or abstracts. This necessarily underestimates the true volume of research, but provides a rough indicator of the change in research volume over the past 15 years. Note that of the more than 10,000 fMRI studies, well over half have been published since the first edition of this textbook in 2004.

ical imaging for more than two decades. Only in the mid-2000s would 1.5-T scanners be replaced by newer 3.0-T scanners, many of which also had updated electronics and multi-channel recording capabilities.

In 1985, the FDA approved MRI scanners for clinical use, opening the door for MRI scans to be prescribed by physicians and billed to insurance companies and Medicare. Rather than having to subsidize the enormous costs of scanners that were used for research purposes, hospitals now saw scanners as sources of profit, which could be obtained by both billing for the scans and attracting new patients. Over the following decade, thousands of MRI scanners were installed in North America alone, making structural MRI one of the most common diagnostic imaging procedures. This prevalence of MRI scanners was a necessary precondition for the explosion of interest in fMRI. Without the clinical need for MRI that led to the installation of many new scanners, the dramatic expansion in fMRI research (Figure 1.13) would not have occurred. We will return to this history in Chapter 7, by describing how the clinical MRI scanning of the 1980s led to the functional MRI scanning of the 1990s.

Organization of the Textbook

The history of fMRI outlined above suggests an incremental progression, beginning with basic physics (and biological principles), through improvements in image collection and hardware design, to the relatively recent onset of fMRI as a neuroscientific tool. The chapters in this textbook recapitulate this progression, by first establishing a foundation based on the physical and biological properties of fMRI and then describing how modern researchers use fMRI to study brain function.

We continue our introduction in Chapter 2, which describes how MRI scanners work. It is important to note that even the most modern MRI scanner has

the same basic components as those used in the experiments described above: a strong static magnetic field to reorient atomic nuclei, weaker but directionally oriented gradient magnetic fields to introduce spatial variation in nuclear magnetic properties, and oscillating radiofrequency fields to induce changes in the energy states of the atomic nuclei. While these three components are integral parts of all MRI scanners, their generators are not the only hardware needed for fMRI. In addition, researchers need equipment for ensuring the homogeneity of the magnetic field, for measuring physiological changes such as heart rate and respiration, and for presenting experimental stimuli. Even though MRI presents no dangers to research subjects if conducted correctly, the strong and rapidly changing magnetic fields used in scanning present a set of safety challenges. As safety should be the primary concern for all fMRI experimenters, Chapter 2 also discusses these challenges in detail.

Physical bases of fMRI

From this introduction, we turn to the physics of nuclear magnetic resonance. Chapter 3 introduces the basic principles of magnetic resonance using a combination of intuitive and mathematical descriptions. We describe how atomic nuclei behave in magnetic fields, and how the energy states of those nuclei can be changed by applying oscillating magnetic fields at particular frequencies. This discussion leads to the concept of relaxation, or the recovery and decay of magnetization over time, which provides the contrast we measure in MR imaging.

For "nuclear magnetic resonance" to become "magnetic resonance imaging," spatial information must be recovered from the raw MR signal. In Chapter 4 we discuss how the introduction of magnetic gradients allows the measurement of signal changes across space. This process is known as image formation. As discussed earlier in this chapter, the development of image formation technology sparked the explosive growth in the use of magnetic resonance for clinical purposes. We introduce the concept of *k*-space, which provides a useful metric for understanding the relationship between scanning hardware and the measured data.

Our final chapter in this section, Chapter 5, links biology and physics by describing the different approaches used by researchers to measure brain structure and function. The extraordinary power of MRI for biological imaging comes from its flexibility; by changing the properties of the gradient and the oscillating magnetic fields over time, images sensitive to many different types of contrast can be obtained. We discuss two major classes of contrasts, and the pulse sequences used to acquire them. Static contrasts provide information about the characteristics of the atomic nuclei at a spatial location, such as their density or tissue type. Motion contrasts provide information about how atomic nuclei, such as those within water molecules in axons or blood vessels, change position over time. We focus on how images can be made sensitive to changes in brain function, which will set the stage for the discoveries outlined in the following sections of the book.

Principles of BOLD fMRI

In the next section, we introduce the biological underpinnings of fMRI. For neuroimaging to be possible, there must be physiological markers of brain activity that can be measured. In general, there are two types of markers that are of interest to physiologists. Researchers can measure the direct consequences of neuronal activity, such as changes in electrical potentials or chem-

blood-oxygenation-level-dependent (BOLD) contrast The difference in signal on T_2*-weighted images as a function of the amount of deoxygenated hemoglobin.

ical gradients, or they can measure the metabolic correlates of neuronal activity (but not the activity itself). Functional MRI relies on the latter approach since it measures blood oxygenation level, which changes in response to the metabolic requirements of active neurons. In Chapter 6 we describe the metabolic demands of the brain and how they are met by vascular function. We also provide a primer for gross brain anatomy, as a background for subsequent discussions of fMRI research.

Even if the metabolic consequences of neuronal activity are understood, there remains the challenge of measuring how metabolic responses change using MRI. The technique that forms the basis for nearly all fMRI studies is blood-oxygenation-level-dependent (BOLD) contrast. Chapter 7 begins with a history of the developments that led to the discovery of BOLD contrast in the 1990s. This history both parallels that described earlier in this chapter, and picks up where it left off in the early 1990s. We discuss the early fMRI studies that first demonstrated the feasibility of this technique, and how those studies extended previous neuroimaging work with PET. We return to concepts like spatial and temporal resolution. Although the spatial resolution of fMRI is often claimed to be extremely good, there are many challenges to accurate mapping, notably that of translating between neuronal activity and measurable changes in the vascular system. Conversely, the temporal resolution of fMRI is often claimed to be rather poor, although there are approaches to improving temporal resolution, many of which have been used to identify sub-second changes in activity. Throughout the chapter we emphasize how the design choices made by researchers influence these properties.

In Chapter 8 we describe issues related to signal and noise in fMRI data. The central problem in fMRI research is that the signal we measure is very small compared with other sources of variability in the data. We provide definitions of experimental signal and noise and show how different signal-to-noise ratios influence the spatial and temporal patterns of activity measured by fMRI. We also discuss methods for improving the sensitivity of fMRI, such as improving experimental power through signal averaging, and the elimination of extraneous physiological variability. Many of the experimental procedures used to improve signal-to-noise ratios are described under the general term "preprocessing", which refers to the steps taken to reduce the variability in the data that is unrelated to the experimental task. Common preprocessing steps include correction for head motion, coregistration of functional images to higher-resolution anatomical images, and normalization of each subject's brain to match the shape, size, and orientation of a standard reference brain.

Design and analysis of fMRI experiments

In Chapter 9 we discuss the key concepts of experimental design. Most fMRI studies use either blocked or event-related designs. In a blocked design, subjects perform tasks for extended periods of time (e.g., 30 s), and brain activity while performing one task is compared with brain activity while performing another. In contrast, event-related designs examine activity associated with discrete events that could occur at any time point in the experiment. We describe the advantages and disadvantages of each type—as well as of new and increasingly common designs that combine features of each—for addressing different experimental questions.

It is essential to consider the methods of analysis that will be used to test the experimental hypotheses. Because of the increasing number of methods

used by researchers to conduct data analyses, we have partitioned this topic into two chapters in this new edition of the book. Chapter 10 considers the major statistical tests used for hypothesis testing in fMRI studies. These are discussed within the framework of the general linear model, which guides the analysis of most fMRI studies. While the statistical approaches used in fMRI research share many similarities with those of other domains of science, there are some challenges that are particularly relevant to fMRI. Chief among these is the problem of multiple comparisons: when tens of thousands of voxels are subjected to a statistical test, many effects may appear to be significant merely by chance. We discuss the various approaches to compensating for the multiple comparisons problem, including thresholding, smoothing, cluster analyses, and region-of-interest analyses.

Chapter 11 extends this discussion by introducing advanced methods for data analysis. Our primary focus is on "data-driven" methods. Broadly considered, such a method begins with the observed data, then creates a model for the pattern of brain activation (and thus, the types of cognitive processing) that could have generated those data. Common methods include the examination of functional connectivity, the estimation of causal relations between brain regions, and the use of fMRI data as a blind predictor for subjects' behavior. Although still only used in a minority of fMRI studies, data-driven analyses represent an increasingly important aspect of fMRI experimentation.

Applications and future directions

Perhaps nothing testifies to the pace of change in fMRI methodology more than this simple fact: most topics considered in our advanced fMRI methods chapter just four years ago are now commonplace in fMRI research. The continual development of new methods represents one of the most exciting aspects of the field. Researchers discover new ways to improve spatial resolution, temporal resolution, or signal-to-noise ratio, and those new methods quickly become part of the canon. In Chapter 12, we take on the difficult task of describing (and predicting) the next generation of fMRI methods.

Chapter 13 describes fMRI in the context of other neuroscientific techniques. Throughout the textbook, we emphasize that fMRI is just one of many techniques available to the neuroscientist. Although in our view it is one of the most flexible and powerful tools, fMRI nevertheless has many limitations that can be addressed by conducting studies that combine fMRI with other techniques. We discuss the theoretical basis for studies that combine multiple approaches, such as using fMRI to identify active brain regions that can then be temporarily disabled using magnetic stimulation, or comparing fMRI data from human and non-human primate subjects.

Finally, the new Chapter 14 outlines a set of ethical issues underlying fMRI research. Some ethical questions are rooted in practical considerations of MRI scanning. For example, how should researchers deal with the potential discovery of brain abnormalities in seemingly normal subjects? Others are more conceptual: how can we use fMRI to confirm, reject, or change models (or even thinking) of human behavior? Scientists within many fields, from economics to marketing, have begun to incorporate fMRI into their research programs. Yet, it often remains unclear whether fMRI data are even compatible with these other fields—with some skeptics taking the strong position that fMRI is irrelevant for modeling human behavior. We end by speculating on the future directions for fMRI research.

REFER TO THE
fMRI
COMPANION WEBSITE AT
www.sinauer.com/fmri2e
for study questions and Web links.

Summary

Functional magnetic resonance imaging, or fMRI, is one of the most important techniques for understanding the human brain in action. Although fMRI is a relatively new technique, the developments that led to its current stage span nearly a century. Many of the advances that made fMRI possible resulted from basic physics research, and the experimental apparatuses used in these early studies laid the groundwork for modern MRI equipment. Unlike most structural MRI, which measures differences between tissues, most functional MRI studies measure changes in the blood oxygenation of the brain over time. From these changes, researchers make inferences about the underlying neuronal activity and how different brain regions may support different perceptual, motor, or cognitive processes. The strengths of fMRI include that it is noninvasive, it can be used in a wide range of human subject populations, its spatial and temporal resolution are well matched to functional changes in the brain, and it is adaptable to many types of experimental paradigms. While fMRI cannot address every neuroscience question, it provides important measurements of brain function that complement the information obtained from other techniques.

Suggested Readings

*Bloch, F., Hansen, W. W., and Packard, M. (1946). Nuclear induction. *Phys. Rev.*, 69: 127. *This very short note describes the discovery of nuclear magnetic resonance in solid matter, for which Felix Bloch would share the 1952 Nobel Prize in Physics with Edward Purcell.*

Cabeza, R., and Kingstone, A. (eds.) (2006). *Handbook of Functional Neuroimaging of Cognition.* 2nd edition. MIT Press, Cambridge, MA. *This edited volume provides a broad introduction to the principles and applications of neuroimaging methods, with an emphasis on fMRI research.*

Finger, S. (2000). *Minds behind the Brain.* Oxford University Press, New York, NY. *This very accessible set of short biographies of neuroscience pioneers contains a description of the life and works of Franz Joseph Gall, who founded the discipline of phrenology.*

*Lauterbur, P. C. (1973). Image formation by induced local interactions: examples employing nuclear magnetic resonance. *Nature*, 242: 190–191. *This seminal article describes the first use of magnetic field gradients for the formation of images using magnetic resonance.*

*Mattson, J., and Simon, M. (1996). *The Pioneers of NMR and Magnetic Resonance in Medicine: The Story of MRI*. Dean Books, Jericho, NY. *This encyclopedic text describes in detail the histories of major twentieth-century figures in the discovery of MRI, providing both personal and scientific context for their work.*

*Purcell, E. M., Torrey, H. C., and Pound, R. V. (1945). Resonance absorption by nuclear magnetic moments in a solid. *Phys. Rev.*, 69: 37–38. *Published scant weeks before Bloch's similar report, this article describes the procedures and results from the very first study of nuclear magnetic resonance.*

*Indicates a reference that is a suggested reading in the field and is also cited in this chapter.

Chapter References

Berns, G. S., Chappelow, J., Cekic, M., Zink, C. F., Pagnoni, G., and Martin-Skurski, M. E. (2006). Neurobiological substrates of dread. *Science*, 312: 754–758.

Churchland, P. S., and Sejnowski, T. J. (1988). Perspectives on cognitive neuroscience. *Science*, 242: 741–745.

Damadian, R. V. (1971). Tumor detection by nuclear magnetic resonance. *Science*, 171: 1151–1153.

Damadian, R., Goldsmith, M., and Minkoff, L. (1977). NMR in cancer: XVI. FONAR image of the live human body. *Physiol. Chem. Phys.*, 9: 97–108.

Mansfield, P., and Maudsley, A. (1976). Line scan proton spin imaging in biological structures by NMR. *Physics in Medicine and Biology*, 21: 847–852.

Owen, A. M., Coleman, M. R., Boly, M., Davis, M. H., Laureys, S., and Pickard, J. D. (2006). Detecting awareness in the vegetative state. *Science*, 313: 1402.

Rabi, I. I., Zacharias, J. R., Millman, S., and Kusch, P. (1938). A new method of measuring nuclear magnetic moment. *Phys. Rev.*, 53: 318.

Chapter 2

MRI Scanners

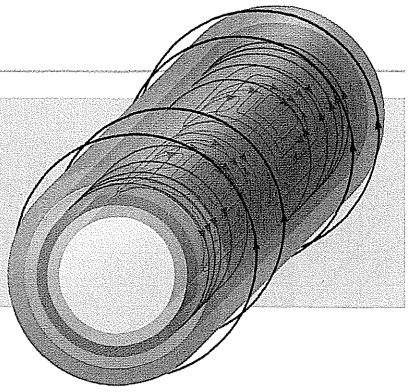

Modern MRI scanners do not resemble the devices used by Rabi, Bloch, Lauterbur, and other early pioneers. They are no longer blocky and kludgy masses of electronics that would be at home in a theoretical physics laboratory. Instead, as MRI has become an increasingly important—and standard—part of medical practice, MRI scanners have become more ergonomic and patient-friendly (Figure 2.1). Continual technological improvements make modern scanners far superior to their predecessors: in the ability to localize signals in space, in the rate of data acquisition, and in the flexibility with which they can acquire different types of images. Yet the fundamental principles underlying MRI have not changed. Just as Rabi used a strong magnetic field to measure spin properties of nuclei, today's MRI scanners use a strong magnetic field to induce changes in proton spin. Just as Bloch detected nuclear induction using transmitter and receiver coils, scanners now use similar coil systems to obtain MR signals. And just as Lauterbur manipulated the magnetic field strength using changing gradient fields to create an image, every current MRI study relies on magnetic gradients for image acquisition. In this chapter, we identify the major components of MRI scanners, describe their use in practice, and discuss their safety implications.

How MRI Scanners Work

An MRI scanner has three main components, as mentioned above, whose purposes can be easily remembered using the mnemonic M-R-I. The "M" represents the main static magnetic field, which is generated by a series of electromagnetic coils that carry very large currents around the bore of the scanner. The "R" refers to the delivery of energy at the resonance frequency of the targeted atomic nuclei. The "I" refers to image formation, which requires alteration of the magnetic field strength over space by turning on and off the magnetic gradient coils.

These are not the only components important for fMRI. Also necessary are the shimming coils, that ensure the homogeneity of the static magnetic field, specialized computer systems for controlling the scanner and the experimental task, and physiological monitoring equipment. This section introduces all of these components and their implementation in modern MRI scan-

(A)

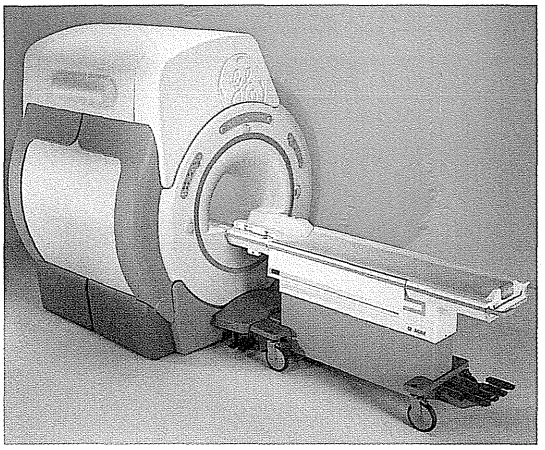

(B)

(C)

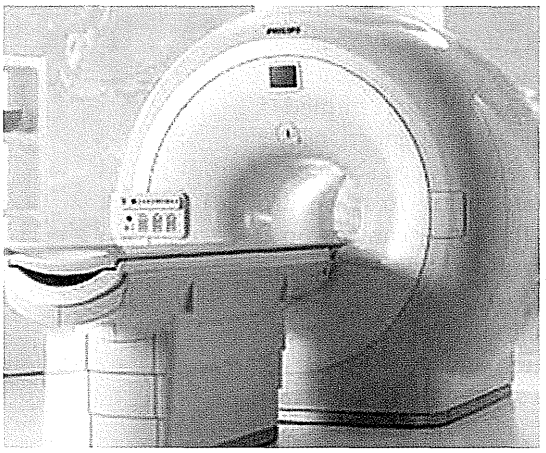

Figure 2.1 Examples of MRI scanners. Most MRI scanners use a closed-bore design, in which the patient or subject lies down on a table at the front of the scanner and then is moved back into the middle of the bore (i.e., central tube). Shown in (A) is a Signa series scanner from General Electric, in (B) is a MAGNETOM Avanto Scanner from Siemens, and in (C) is an Achieva scanner from Philips. (A courtesy of GE Healthcare, Waukesha, WI; B courtesy of Siemans Medical Solutions, Erlangen, Germany; C courtesy of Philips Medical Systems, Andover, MA.)

ners (Figure 2.2). We will return to a detailed discussion of how these hardware components are used to change the magnetic properties of atomic nuclei in Chapters 3 to 5.

Static magnetic field

The static magnetic field is an absolute necessity for MRI, providing the "magnetic" in magnetic resonance imaging. Magnetic fields were discovered in naturally occurring rocks, known as lodestones, in China almost 2000 years ago. By the eleventh century, the Chinese had recognized that the Earth itself has a magnetic field, so that a magnet suspended in water will orient itself along the Earth's magnetic field lines (i.e., from north to south). The rediscovery of magnetism centuries later by European scientists proved invaluable for subsequent nautical exploration, as ships adopted magnetic compasses for directional guidance. MRI scanners use strong static magnetic fields to align certain nuclei within the human body (most commonly, hydrogen within water molecules) to allow for the mapping of tissue properties.

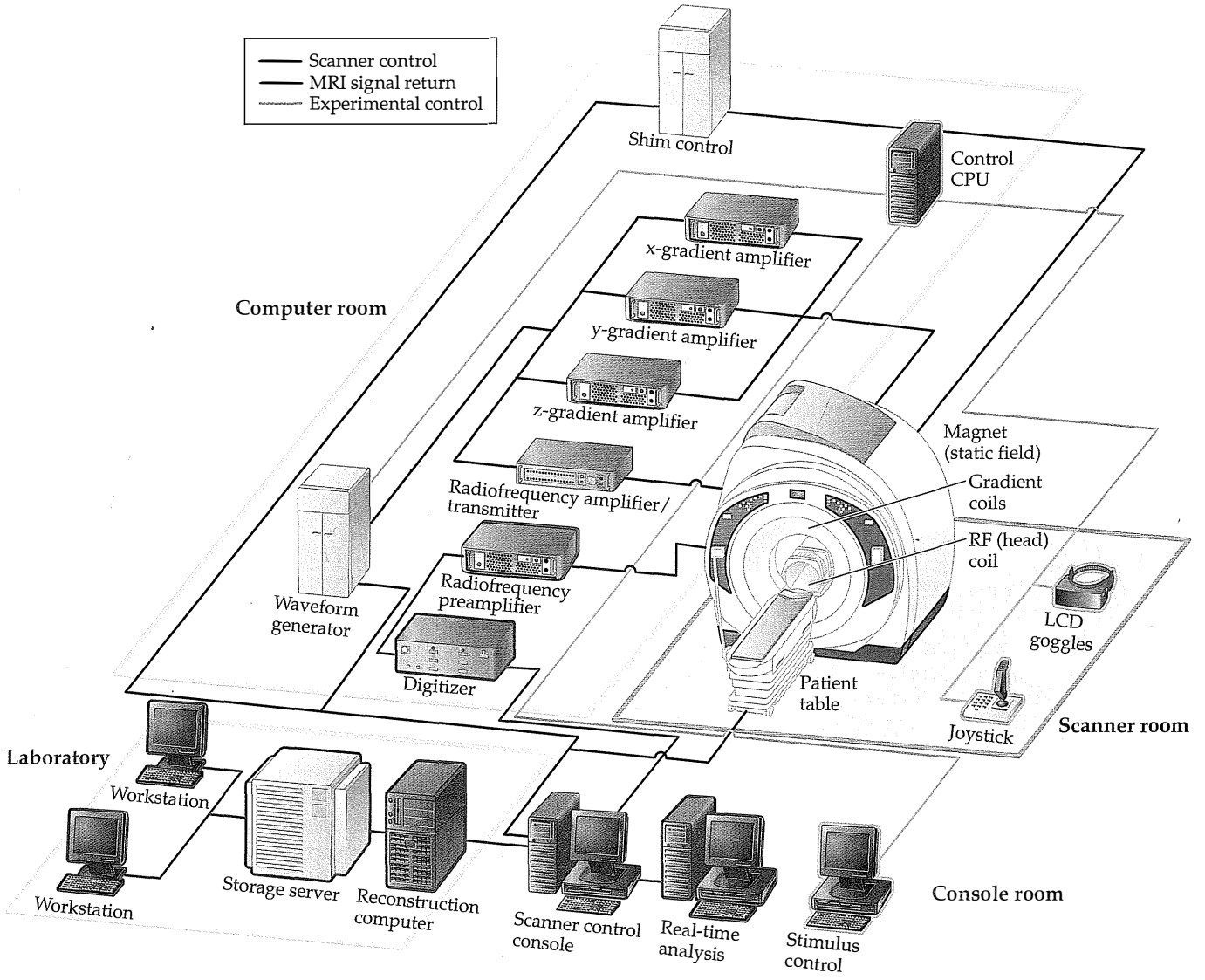

Figure 2.2 Schematic organization of the fMRI scanner and computer control systems. Two systems are important for fMRI studies. The first is the hardware used for image acquisition. In addition to the scanner itself, this hardware consists of a series of amplifiers and transmitters responsible for creating the gradients and pulse sequences (shown in black), and recorders of the MR signal from the head coil (shown in red). The second system is responsible for controlling the experiment in which the subject participates, and for recording behavioral and physiological data (shown in green).

Some early MRI scanners used permanent magnets to generate the static magnetic fields used for imaging. Permanent magnets typically generate weak magnetic fields that are fixed by their material composition, and it is difficult to ensure that the fields are not distorted over space. Another method of generating a magnetic field was discovered by the Danish physicist Hans Oersted in 1820, when he demonstrated that a current-carrying wire influenced the direction of a compass needle placed below the wire, redirecting it perpendicularly to the direction of the current. This relationship was quantified later that

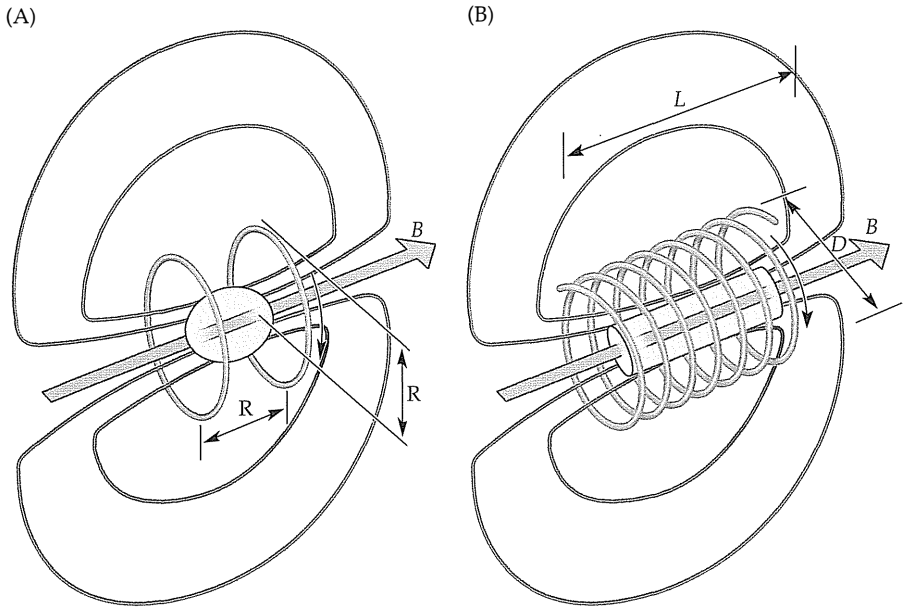

Figure 2.3 Generation of a static magnetic field. (A) The Helmholtz pair design can generate a homogeneous magnetic field. It consists of a pair of circular current loops that are separated by a distance equal to their radius (R); each loop carries the same current. (B) Modern MR scanners use a solenoid design, in which a coil of wire is wrapped tightly around a cylindrical frame. By optimizing the locations and density of the wire loops, a very strong and homogenous field (*B*) can be constructed. The green surfaces inside the coils indicate the approximate areas of maximum uniformity.

year by the French physicists Jean-Baptiste Biot and Félix Savart, who discovered that magnetic field strength is in fact proportional to current strength, so that by adjusting the current in a wire (or set of wires), one could precisely control the intensity of the magnetic field. These findings led to the development of electromagnets, which generate their fields by passing current through tight coils of wire. Nearly all MRI scanners today create their static magnetic fields through electromagnetism.

In general there are two criteria for a suitable magnetic field in MRI. The first is field uniformity (or homogeneity), and the second is field strength. Making the magnetic field uniform over both space and time is necessary so that we can create images of the body that do not depend on which MRI scanner we are using, or how the body is positioned in the field. If the magnetic field is not homogeneous, the signal measured from a given part of the body could change unexpectedly, depending on where it is located in the magnetic field. (In practice, MRI takes advantage of this effect by introducing controlled changes in the magnetic field to produce gradients.) A simple design for generating a homogeneous magnetic field is the Helmholtz pair (Figure 2.3A), which is a pair of circular wire loops of the same size that carry identical currents and are separated by a distance equal to the radius of each loop. An even more uniform magnetic field, however, can be generated by a solenoid, which is constructed by winding wire in a helix around the surface of a cylindrical form (Figure 2.3B). If the solenoid is long (*L*) compared with its cross-sectional diameter (*D*), the internal field near its center is highly homogeneous. Modern magnets are based on a combination of these classic designs, with the density of wires, and therefore the electrical current, optimized by computers to achieve a homogeneous magnetic field of the desired strength.

Whereas field uniformity requires finesse, field strength requires force. To generate an extremely large magnetic field, a huge electric current must be injected into the loops of wire. For example, the very large electromagnets used to lift cars in junkyards have magnetic fields on the order of 1 T, similar to that in the center of some MRI scanners. To generate these fields, the magnets require enormous

field uniformity In the context of MRI, a uniform magnetic field is one that has a constant strength throughout a wide region near the center of the scanner bore.

homogeneity Uniformity over space and time.

field strength The magnitude of the static magnetic field generated by a scanner, typically expressed in units of Tesla.

electrical power, and thus enormous expense. Modern MRI scanners use superconducting electromagnets whose wires are cooled to temperatures near absolute zero. Most MRI scanners use multiple cooling agents, or cryogens. The coil windings used to generate the static field are typically made of metal alloys such as niobium–titanium, which when immersed in liquid helium, reach temperatures of less than 12 K (–261°C). At these extremely low temperatures, the resistance in the wires disappears, thereby creating a strong, stable, and lasting electric current that can be maintained with no power requirements and at minimal cost. Liquid nitrogen is sometimes used as an insulator to minimize loss of the much more expensive helium.

By combining the precision derived from numerical optimization of the magnetic coil design with the strength afforded by superconductivity, modern MRI scanners can have homogeneous and stable field strengths in the range 1.5 to 11 T for human use, and up to 24 T for animal use. Since maintaining a field using superconductive wiring requires little electricity, the static fields used in MRI are always active, even when no images are being collected. For this reason, the static field presents significant safety challenges, as will be discussed later in this chapter.

Radiofrequency coils

While a strong static magnetic field is needed for MRI, the static field itself does not produce any MR signal. The MR signal is actually produced by the clever use of electromagnetic coils that generate and receive electromagnetic fields at the resonant frequencies of the atomic nuclei within the static magnetic field. This process gives the name "resonance" to magnetic resonance imaging. Because most atomic nuclei of interest for MRI studies have resonant frequencies in the radiofrequency portion of the electromagnetic spectrum (at typical field strengths for MRI), these coils are also called radiofrequency coils. Unlike the static magnetic field, the radiofrequency fields are turned on during small portions of the image acquisition process, and remain off the rest of the time. The radiofrequency fields are evaluated using similar criteria as the static field: uniformity (i.e., homogeneity over space and time) and sensitivity (i.e., the relative strength of the signal that can be emitted or detected).

After a human body is placed into a strong magnetic field, an equilibrium state is reached in which the magnetic moments of atomic nuclei (e.g., hydrogen) within the body become aligned with the magnetic field. The radiofrequency coils then send electromagnetic waves that resonate at a particular frequency (determined by the strength of the magnetic field) into the body, perturbing this equilibrium state. This process is known as excitation. When atomic nuclei are excited, they absorb the energy of the radiofrequency pulse. When the radiofrequency pulse ends, the atomic nuclei return to the equilibrium state and release the energy that was absorbed during excitation. The resulting release of energy can be detected by the radiofrequency coils in a process known as reception. This detected electromagnetic pulse defines the raw MR signal. The processes of excitation and reception will be covered in detail in Chapter 3.

One can think of the measurement of an MR signal through excitation and reception as analogous to the weighing of an object by lifting and releasing it in a gravitational field. If an object sits motionless on a supporting surface, so that it is in an equilibrium state with respect to the gravitational force, we have no information about its weight. To weigh it, we first lift the object to give it potential energy and then release it so that it transfers that energy back into the

superconducting electromagnets A set of wires made of metal alloys that have no resistance to electricity at very low temperatures. By cooling the electromagnet to near absolute zero, a strong magnetic field can be generated with minimal electrical power requirements.

cryogens Cooling agents used to reduce the temperature of the electromagnetic coils in an MRI scanner.

radiofrequency coils Electromagnetic coils used to generate and receive energy at the sample's resonant frequency, which for field strengths typical to MRI is in the radiofrequency range.

excitation The process of sending electromagnetic energy to a sample at its resonant frequency (also called transmission). The application of an excitation pulse to a spin system causes some of the spins to change from a low-energy state to a high-energy state.

reception The process of receiving electromagnetic energy emitted by a sample at its resonant frequency (also called detection). As nuclei return to a low-energy state following the cessation of the excitation pulse, they emit energy that can be measured by a receiver coil.

MR signal The current measured in a detector coil following excitation and reception.

surface coil A radiofrequency coil that is placed on the surface of the head, very close to the location of interest. Surface coils have excellent sensitivity to the signal from nearby regions but poor sensitivity to signal from distant regions.

volume coil A radiofrequency coil that surrounds the entire sample, with roughly similar sensitivity throughout.

phased array A method for arranging multiple surface detector coils to improve spatial coverage while maintaining high sensitivity.

environment. The amount of energy it releases, whether through impact against a surface or compression of a device like a spring (e.g., in a scale), provides an index of its weight. In the same way, we can perturb the magnetic properties of atomic nuclei (excitation) and then measure the amount of energy returned (reception) during their recovery to an equilibrium state. The amount of energy that can be transmitted or received by a radiofrequency coil depends on its distance from the sample being measured. In the case of fMRI, the radiofrequency coils are typically placed immediately around the head. There are three main ways to arrange radiofrequency coils: surface coils, volume coils, and phased arrays (Figure 2.4).

Surface coils are placed directly on the imaged sample; that is, adjacent to the surface of the scalp for functional imaging. The design of a surface coil is based on a single-loop inductor–capacitor (LC) circuit (Figure 2.4A). Within this circuit, the rapid charge and discharge of electricity between the inductor and

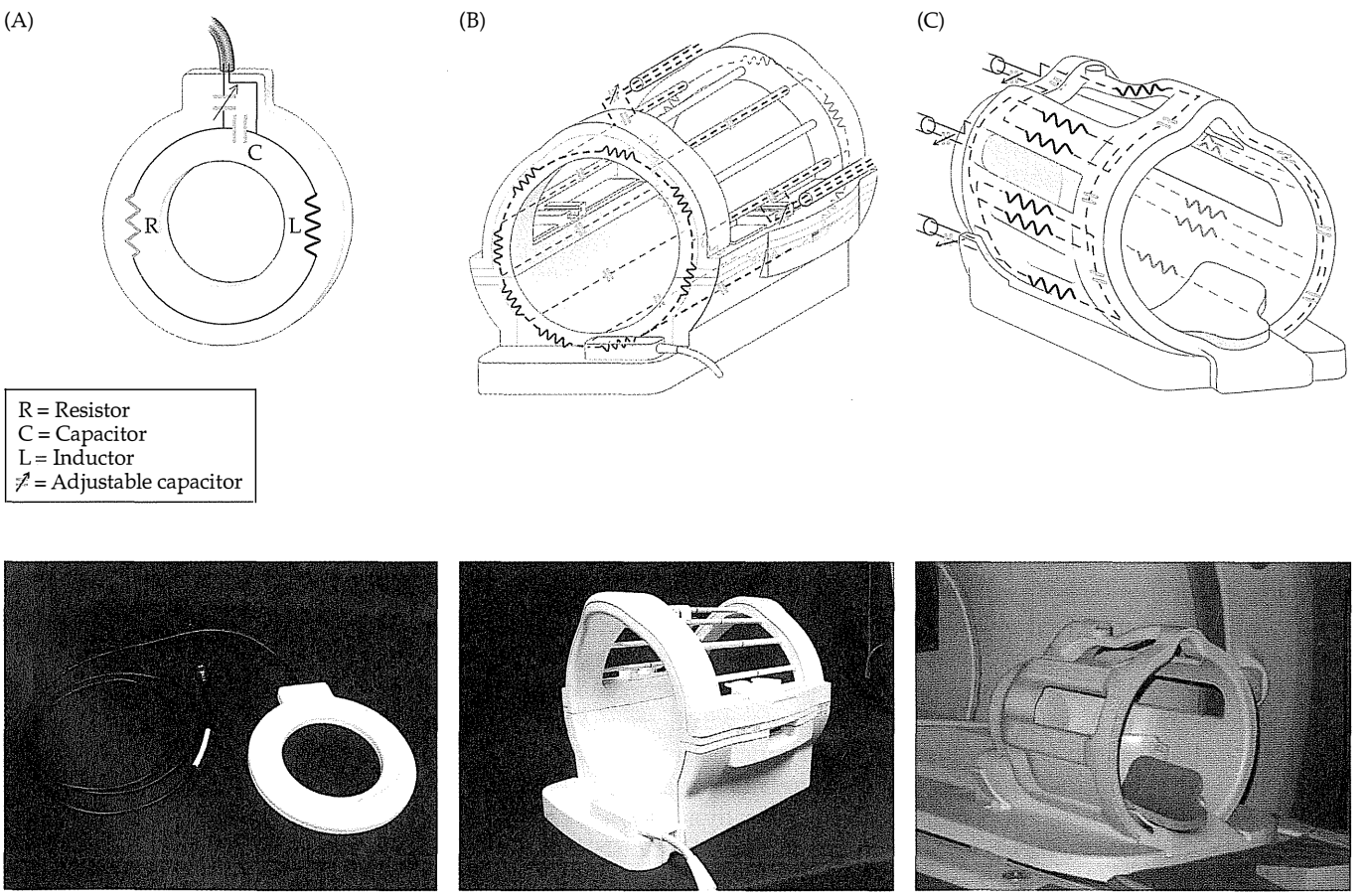

Figure 2.4 Surface, volume, and phased array coils. (A) Surface coils consist of a simple inductor (L) –capacitor (C) circuit, with additional resistance (R) also present. The rapid charging and discharging of energy between the inductor and capacitor generates an oscillating magnetic field. The signal from the surface coil is modulated by a variable capacitor (shown by the arrow). (B) Volume coils repeat the same LC circuit around the surface of a cylinder. This results in better spatial coverage than is provided by a surface coil, at the expense of reduced local sensitivity. (C) Phased-array coils combine multiple surface coils in an arrangement intended to give roughly equal spatial sensitivity. These can provide the best combination of spatial uniformity and signal strength.

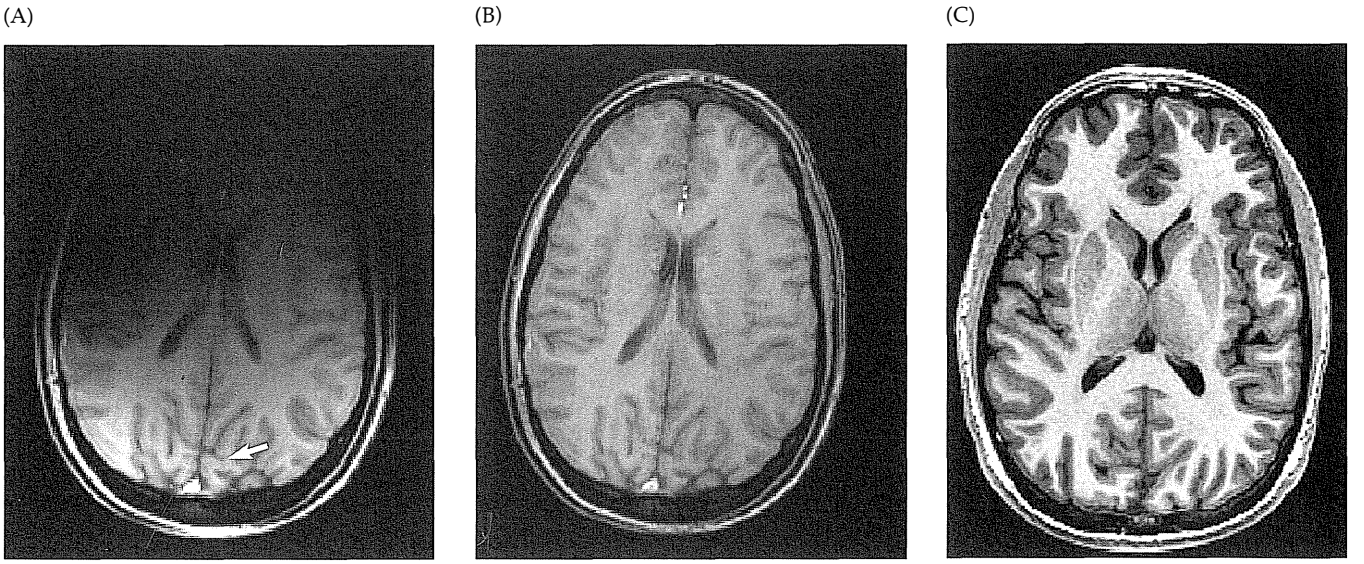

Figure 2.5 Signals recorded from surface, volume, and phased-array radiofrequency coils. (A) The use of a receiver coil adjacent to the surface of the skull can increase the signal-to-noise ratio in nearby brain regions (visible here as reduced graininess in the area indicated by the arrow), but the recorded signal will drop off in intensity as the distance from the coil increases. Thus, the use of a single surface coil is more appropriate for fMRI studies that are targeted toward a single brain region. (B) Volume coils have relatively similar signal sensitivity throughout the brain, so they are more appropriate for fMRI studies that need coverage of multiple brain regions. (C) Phased-array coils can be a good compromise between the sensitivity of a surface coil and the coverage of a volume coil.

capacitor generates an oscillating current that can be tuned to the frequency of interest. Because of their close spatial proximity to the brain, surface coils usually provide high imaging sensitivity and are often used for fMRI studies that are targeted toward one specific brain region, such as the visual cortex. The trade-off for high local sensitivity is poor global coverage. Since the amount of signal recovered from a given part of the brain depends on its distance from the surface coil, areas near the coil provide a great deal of signal but areas further away provide very little (Figure 2.5A). Thus, the signal recovered by a surface coil is spatially inhomogeneous, which makes a single surface coil inappropriate when whole-volume imaging is desired.

A second class of MR coil is the volume coil (Figure 2.4B), which provides uniform spatial coverage throughout a large volume. The basic element of the volume coil is the same LC circuit as is used in the surface coil. The LC circuit is replicated around a cylindrical surface to achieve a uniform distribution of energy within the enclosed volume. This arrangement resembles a birdcage, and thus a volume coil is sometimes referred to as a birdcage coil. Because the volume coil is farther from the head than a surface coil, it has less sensitivity to the MR signal, but a more even coverage across the brain (Figure 2.5B).

A compromise approach that combines the best features of both the surface and the volume coils is to use a volume coil for exciting the imaging volume and a set of surface coils for receiving the MR signal. If multiple receiver coils are arranged in an overlapping pattern known as a phased array (Figure 2.4C), the spatial coverage can be increased considerably while maintaining

gradient coils Electromagnetic coils that create controlled spatial variation in the strength of the magnetic field.

high sensitivity. Although the sensitivity does change somewhat across the image, the use of multiple receiver coils is an increasingly important technique in fMRI (Figure 2.5C).

The sensitivity of a radiofrequency coil is proportional to the strength of the magnetic field generated within the coil by the current. Thus, a coil that generates a strong magnetic field is also a sensitive receiver coil—an example of the principle of reciprocity. A stronger magnetic field can be generated by adding more wire loops to produce a higher current density. Assuming that the coil resistance is not zero, because radiofrequency coils are not typically superconducting, some energy will be lost in the generation of heat, which will reduce the coil's sensitivity. To obtain a quantitative measure of the coil sensitivity, a sensitivity factor (known as the *Q-value* to reflect "quality") is defined as the ratio of the maximum energy stored and total energy dissipated per time period. For an LC circuit, that quantity can be represented as:

$$Q = \frac{1}{R}\sqrt{\frac{L}{C}} \tag{2.1}$$

Thus, minimizing the resistance (R) boosts the coil sensitivity (Q).

Gradient coils

The ultimate goal of MRI is image formation. By placing an object in a strong static magnetic field and exciting its atomic nuclei using radiofrequency pulses, current can be detected in surrounding receiver coils. This current, which is the MR signal, has no spatial information and thus cannot be used to create an image by itself. By introducing magnetic gradients superimposed on the strong static magnetic field, gradient coils provide the final component necessary for imaging. The purpose of a gradient coil is to cause the MR signal to become spatially dependent in a controlled fashion, so that different locations in space contribute differently to the measured signal over time. Like the radiofrequency coils, the gradient coils are only used during image acquisition. They are typically turned on briefly after the excitation process to provide the spatial encoding needed to resolve an image.

To make the recovery of spatial information as simple as possible, separate gradient coils are used to modify the strength of the magnetic field so that it increases or decreases along specific directions. Three gradient coils are typically oriented along the cardinal directions relative to the static magnetic field. The direction represented by z is parallel to the main field, while x and y are perpendicular to the main field and to each other. Like the previously-discussed components of the scanner, gradient coils are evaluated based on two criteria: linearity (which is comparable to the uniformity measure used for the main magnet and the radiofrequency coils) and field strength.

The simplest example of a linear gradient coil is a pair of loops with opposite currents, known as a Maxwell pair (Figure 2.6A). A Maxwell pair generates opposing magnetic fields within two parallel loops, effectively producing a magnetic field gradient along the line between the two loops. This design is the basis for generating the z-gradients used today, although modern z-gradient coils have a more complicated design. The change in the magnetic field that is generated by the gradient coils is orders of magnitude smaller than that of the static magnetic field. The gradients used in modern scanners typically alter field strengths by a few tens of milliteslas per meter.

The x- and y-gradients, also known as transverse gradients, are both created in the same fashion, since the coils that wrap around the scanner are circular and

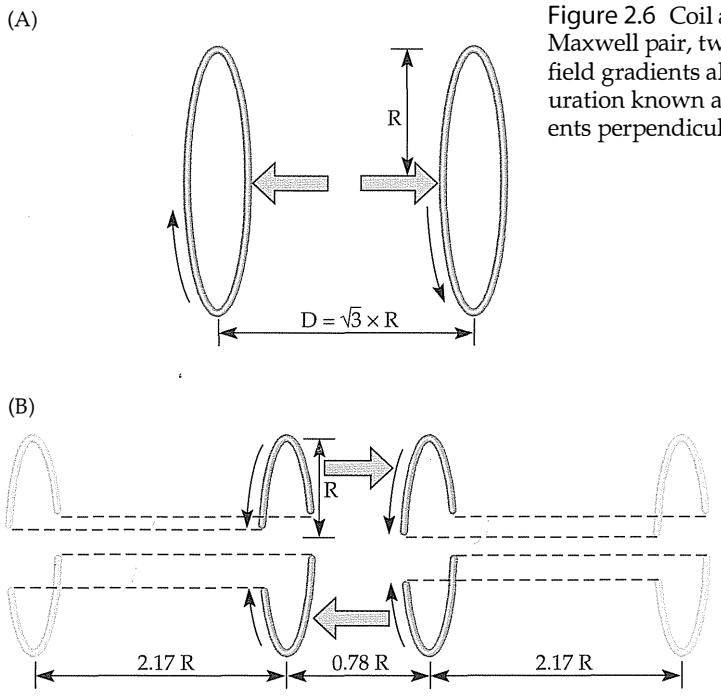

Figure 2.6 Coil arrangements for generating magnetic gradients. (A) A Maxwell pair, two loops with opposing currents, which generate magnetic field gradients along the direction of the main magnetic field. (B) The configuration known as a Golay pair. It allows generation of magnetic field gradients perpendicular to the main magnetic field.

thus symmetrical across those directions. It is important to understand that the transverse gradients change the intensity of the main magnetic field across space (i.e., along z); they do not introduce smaller magnetic fields along x and y, as one might suppose. That is, the introduction of a positive x-gradient, for example, makes the main magnetic field slightly weaker at negative values along x and slightly stronger at positive values along x. Therefore, to generate a transverse gradient, one cannot simply place the Maxwell pair along the x or y axis (which would generate a magnetic field perpendicular to the main field). Instead, scanners use a configuration similar to that shown in Figure 2.6B to generate these gradients. This slightly more complicated "double-saddle" geometry is known as a Golay pair. The final geometry that actually produces the x- or y-gradient field is numerically optimized and contains many more windings than the simple saddle coil shown here. Figure 2.7 illustrates the different patterns of coil windings used for the magnetic gradients and the static magnetic field. Note that the gradient coils are relatively small compared with those generating the main magnetic field. In a typical scanner, the gradient coils may weigh about 2 tons, while the main magnet coils could weigh between 10 and 30 tons.

The strength of a gradient coil is a function of both the current density and the bore size of the coil. Increasing the current density by increasing the electrical power supplied to the coil produces a stronger gradient field. Reducing the size of the coil, so that a given current travels through a smaller area, also produces a stronger gradient field. The trade-off between bore size and electrical power in generating field strength is not linear. In fact, as the bore size increases, the amount of power required for generating a gradient of the same strength increases with the fifth power of the bore size. The implications of this fact can be appreciated in a simple example. Consider that a physicist wants to increase the bore size of a scanner by a factor of two, while maintaining the same gradient strength. Although the bore size is only doubled, the

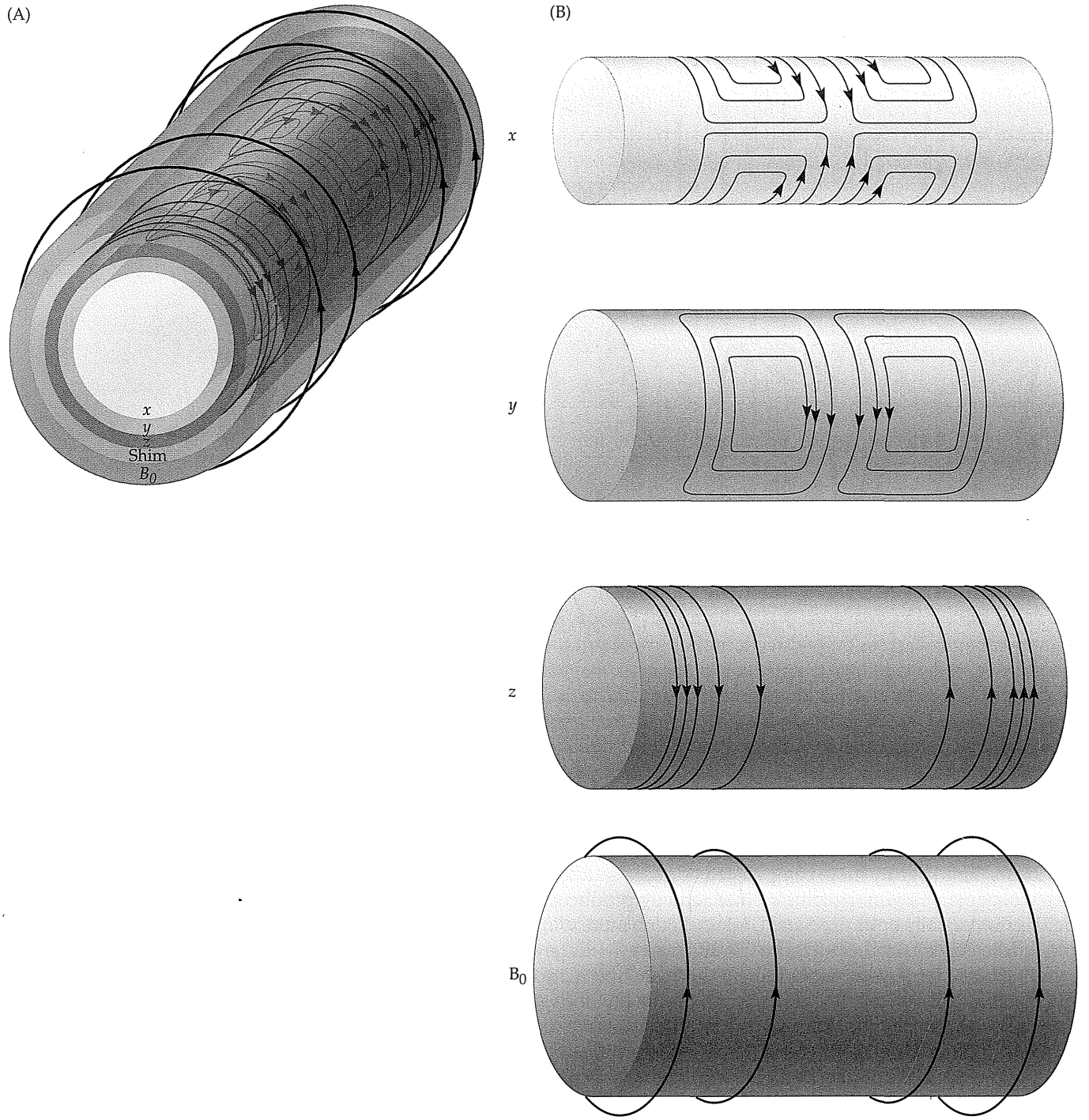

Figure 2.7 Generation of x-, y-, and z-gradients and the static magnetic field (B_0). (A) A number of different electromagnetic coils are used within a single MRI scanner. (B) The coils are arranged as a series of concentric circles, beginning with the gradient coils at the interior, followed by the shimming coils, and then the static field coils. The x- and y-gradients are generated using the Golay pair arrangement, and the only difference between them is that one is rotated 90° from the other. The z-gradient is generated using the Maxwell pair arrangement. The shimming coils are not shown here due to their complexity; as discussed in the text, there may be many different coil types depending on the scanner. Finally, the static field is generated using a series of Helmholtz pairs, with the distance between the pairs corresponding to their radius.

power requirements increase by a factor of 2^5, or 32. This constraint imposes a practical limitation on the bore size of an MRI scanner.

shimming coils Electromagnetic coils that compensate for inhomogeneities in the static magnetic field.

Shimming coils

In an ideal MR scanner, the main magnet would be perfectly homogeneous and the gradient coils would be perfectly linear. This is hardly the case in reality, as the authors (and anyone who has ever conducted an fMRI study) can attest. MRI scanners must correct for inhomogeneities in the static magnetic field. In some locations the field may be too strong; in others, too weak. This process of adjustment is analogous to what we do when a table is rocking because one leg is shorter than the others—we simply put a wedge under one of the uneven legs to make it stable. This wedge is called a shim. In a scanner, some shimming is done passively, when first setting up the scanner, by positioning pieces of iron or small magnets within the scanner itself. Other, active shimming uses additional coils that generate compensatory magnetic fields that correct for the inhomogeneity in the static magnetic field. These are aptly named shimming coils.

Typically, shimming coils can produce first-, second-, or even third-order magnetic fields. For example, an x-shimming coil would generate a magnetic field that depends on the position along the x-axis (first-order), while an x^3-shimming coil would generate a magnetic field that depends on the cube of the x position (third-order). These high-order magnetic fields are used in combination to correct for the inhomogeneities in the static magnetic field. Typically this results in a magnetic field that is uniform to roughly 0.1 part per million over a spherical volume with a diameter of 20 cm. For a 3.0 T magnet, this represents a deviation of only 0.0000003 Tesla.

Unlike the other magnetic fields, the shimming coils can be adjusted for each subject. In fMRI studies, each person's head distorts the magnetic field slightly differently. Thus, the shimming procedures used in fMRI account for the size and shape of the subject's head, so that the uniformity of the magnetic field can be optimized over the brain. Unlike the radiofrequency and gradient coils, which are turned on and off throughout the imaging session, the shimming coils are usually adjusted once and then left on for the duration of the session.

Thought Question

Some manufacturers have developed "head-only" MRI scanners for clinical and functional studies of the brain. Based on what you know so far, what would be the advantages of such scanners?

Computer hardware and software

Digitizing, decoding, and displaying MR images requires a considerable amount of computer processing power. All MRI scanners are equipped with at least one central computer to coordinate all hardware components (e.g., gradient coils, radiofrequency coils, digitizers), and often multiple computers are used to control separate hardware clusters. The computer type, processor, and operating system vary greatly among scanner manufacturers. In addition to the hardware requirements, two categories of specialized software are needed for fMRI. The first category sends a series of instructions to the scanner hardware so that

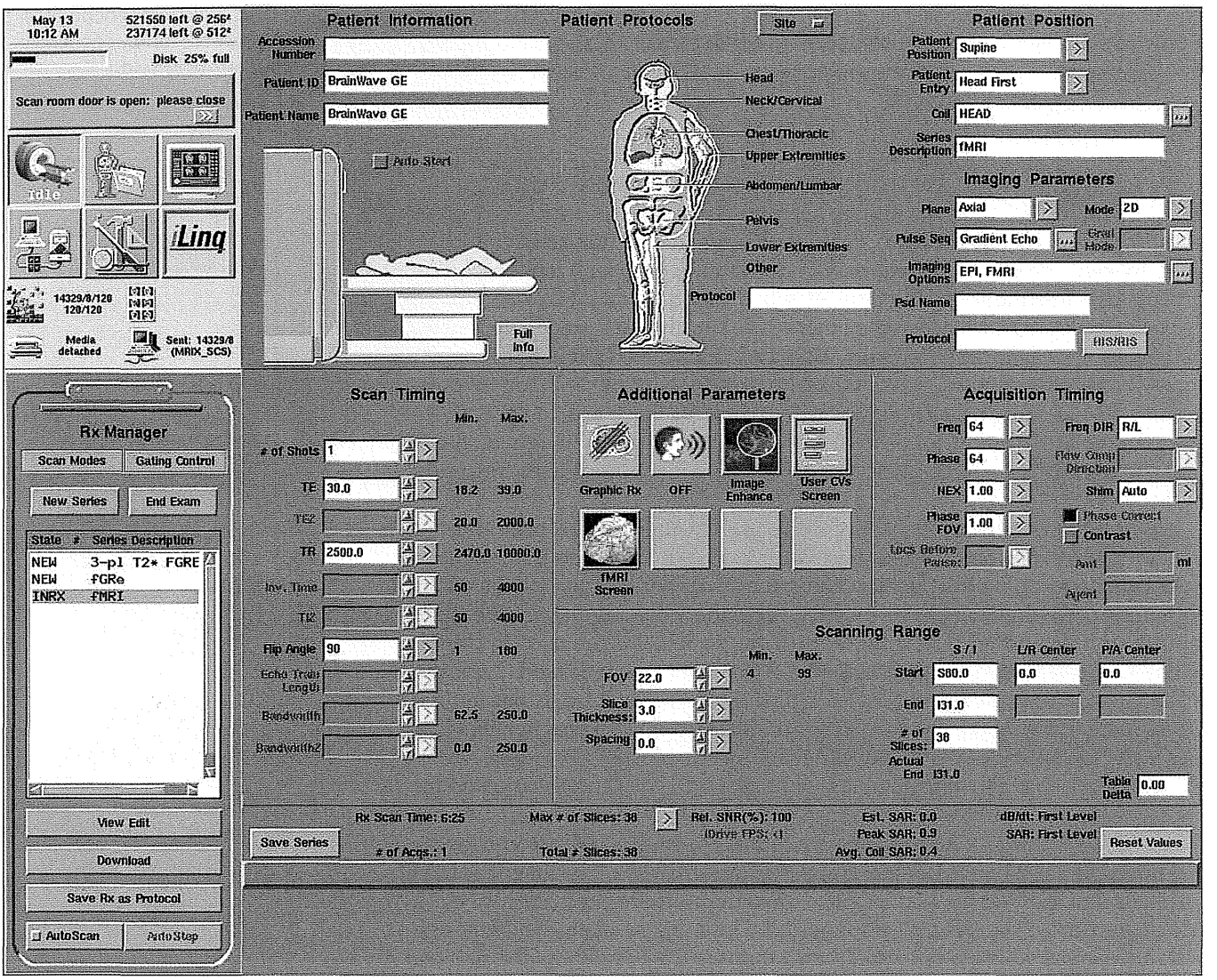

Figure 2.8 A graphic user interface used to control an MRI scanner. The operator of an fMRI scanner will use an interface similar to this one to select the pulse sequence parameters for a given study. (Courtesy of GE Healthcare, Waukesha, WI, and Dr. X. Joe Zhou, University of Illinois, Chicago.)

images can be acquired. These programs, often called pulse sequences, coordinate a series of commands to turn on or off certain hardware at certain times. The pulse sequence determines which kind of image is acquired. Usually the selection of parameters for a pulse sequence is done via a graphic user interface (Figure 2.8). The second category of software includes reconstruction and analysis packages that create, display, and analyze the images. Many types of images, especially those showing anatomical detail, are created online at the scanner. Often the large number of images collected, even in a short fMRI experiment, are sent to other more powerful computers for reconstruction and/or analysis. We will discuss the principles of image formation and pulse sequence selection in Chapters 4 and 5.

pulse sequence A series of changing magnetic field gradients and oscillating electromagnetic fields that allows the MRI scanner to create images sensitive to a particular physical property.

Experimental control system

To induce changes in brain function in response to task manipulations, researchers use computer systems to control their experiments. Although the particular hardware and software used will differ between laboratories, there are three basic components. First, the control system must generate the experimental stimuli, which may include pictures or words that subjects see, sounds that subjects hear, or even taps on the skin that subjects feel. Since normal computer monitors cannot go into the strong magnetic field of the scanner, visual stimuli are often shown to the subject using custom virtual-reality goggles that are MR compatible, or by projecting an image onto a screen in the bore of the scanner. Second, the control system must record behavioral responses made by the subject, such as pressing a button or moving a joystick. Usually, both the timing and the accuracy of the response are measured. Third, the presentation of stimuli and recording of responses must be synchronized to the timing of image acquisition, so that the experimental design can be matched with the fMRI data. This may be done through a direct electrical connection between the scanner hardware and the experimental control system, so that starting the scanner sends an electrical pulse to the control system, triggering the start of the experiment. The experimental control system often consists of specialized software packages designed for standard personal computers. The key challenge for any experimental setup is to ensure that the equipment used in the scanner room, such as a display device or joystick, is not attracted by the strong magnetic fields and does not interfere with imaging.

Physiological monitoring equipment

Many MRI scanners have equipment dedicated to recording physiological measures like heart rate, respiratory rate, exhaled CO_2, and skin conductance. In clinical studies, such equipment allows attending physicians to monitor patients' vital signs. If a patient has trouble breathing or has heart problems during the scanning session, a doctor may choose to remove the individual from the scanner. Physiological monitoring is especially important for patients who may be uncomfortable in the MRI environment, including the elderly, the severely ill, or young children. In functional MRI experiments, research subjects are often healthy young adults, and as such, they have little risk of clinical problems. Therefore, physiological monitoring in fMRI studies often has a different goal: to identify changes over time that may influence the quality of the functional images. Each time the heart beats or the lungs inhale, for example, the brain moves slightly. Also, changes in the air volume of the lungs can affect the stability of the magnetic field across the brain. By recording the pattern of physiological changes over time, researchers can later compensate, at least partially, for some of the variability in fMRI data (see Chapter 8).

A second reason to record physiological data during fMRI sessions is to better understand the relationship between physiology and cognition. Many physiological measures can be used as indicators of particular cognitive processes. For example, the diameter of the pupil can be used as an index of arousal, in terms of both alertness and the amount of cognitive processing. If the size of the pupil increases more in response to one photograph than to another, a researcher may conclude that the former picture is more arousing than the latter. Skin electrical conductance provides another indicator of arousal. The position of the eyes can be used to indicate the focus of a subject's attention. By examining the sequence of a subject's eye movements across a visual scene, a

projectile effect The movement of an untethered ferromagnetic object through the air toward the bore of the MRI scanner.

researcher may discover which objects are most important to the subject. The eyes would dwell on important objects, and skip over or ignore unimportant objects. Physiological monitoring thus has two primary purposes for fMRI studies: to improve the quality of the images, and to provide additional information about the subjects' mental states.

It is clear from the above discussion that the design of an fMRI experiment is complex, involving multiple components. Box 2.1 describes a typical fMRI experiment, and explains what the experience is like for both the researcher and the subject.

MRI Safety

Since the inception of clinical MRI testing in the early 1980s, more than 200 million MRI scans have been performed, with an additional 50,000 scans performed each day. The vast majority of these scans are performed without incident, confirming the safety of MRI as an imaging technique. However, the very serious exceptions to this generalization should give pause. The static magnetic field of an MRI scanner is strong enough to pick up even heavy ferromagnetic objects (i.e., objects containing iron, nickel, cobalt, or one of the rare earth elements chromium, gadolinium, and dysprosium), and pull them toward the scanner bore at great speed. Implanted metal objects, like aneurysm clips or pacemakers, may move or malfunction within the magnetic field. Only through constant vigilance and strict adherence to safety procedures can serious accidents be avoided.

Perhaps even more worrisome is that ignorance of the basic principles of MRI can lead to misconceptions about its effects on human tissue. This can influence policy makers and alter regulations. In 2005, the European Union proposed a new law, whose primary goal was to ensure that industrial workers were not exposed to excessive magnetic fields and electromagnetic radiation. One (perhaps unintended) consequence of the law was to preclude MR technologists (or other medical personnel) from remaining next to the scanner while images were being recorded. An estimated 30% of all MRI sessions, mainly those involving children or sedated patients, could be prohibited under this law. Reaction from the medical and scientific communities was swift and critical. Leading MRI experts, including Peter Mansfield (see Chapter 1), condemned the law as introducing unnecessary restrictions—and directly harming patients by restricting needed medical tests—without supporting scientific evidence. This debate has not yet been resolved, and demonstrates how scientific data—or the lack thereof—can influence public policy and, in turn, clinical applications.

Effects of static magnetic fields on human physiology

The overriding risks in any MRI study result from the use of extremely strong static magnetic fields. The magnetic field generated by an MRI scanner is sufficiently strong to pick up heavy objects and pull them toward the scanner at very high velocity. This is known as the **projectile effect**. Given the dramatic influence of the MRI static field on metal objects, it is not surprising that many people assume that magnetic fields themselves have substantial biological effects. However, this is a misconception. Static magnetic fields, even the extremely strong fields used in MRI, have no known long-term deleterious effects on biological tissues.

BOX 2.1 Outline of an fMRI Experiment

To some readers of this textbook, running an fMRI study may seem commonplace or routine. Yet all of us, even veteran researchers who have completed dozens of fMRI experiments, began as inexperienced novices who were nervous about their first fMRI sessions. One of the authors can remember several aspects of the first time he participated in an fMRI session: the noise and vibration, the confinement of the scanner bore, and (most vividly) his uncertainty about what fMRI actually measured. Can the experimenters see my thoughts? Will it be obvious when I'm distracted and not doing the task? What can the experimenters tell about my brain? Participating in an fMRI experiment is very different, in unexpected and important ways, from participating in other behavioral or even medical experiments. Here in this box (and in the textbook, more generally), we plan to give you a sense of what an fMRI experiment entails, from the viewpoint of both the experimenter and the participant.

Preparing for the Experiment

Ava came to the laboratory with a sense of excitement—today she was running her first subject in *her* fMRI experiment. As a second-year graduate student in the cognitive neuroscience program, she had previously tagged along with more senior graduate students to watch their studies. She had even helped with the data analysis on a study that would be presented at a conference next month. But now she was finally running a study that she had designed herself (with guidance from her advisor, of course).

Two weeks ago, she had placed advertisements for a "Functional neuroimaging study of decision making" around campus. The advertisements contained a short description of the study, details about the payment that subjects would receive, the Institutional Review Board protocol that covered the experiment, and Ava's contact information. While Ava knew that many potential participants would be most interested in the money they could earn, she was hopeful that others would be interested in helping science or seeing images of their own brain.

Her first potential participant, Owen, had called the laboratory the next day. He was very interested in the study—in part because he was a biology and psychology double major—but he was also a bit nervous because he did not know much about fMRI. To allay his concerns, Ava described what would happen in the study. The primary goal of this research, she said, was to investigate how activation of a particular brain region—something called the prefrontal cortex—differed depending on what information people used when making a decision. When he came in for the experiment, Owen would lie in the MRI scanner and read a series of ethical dilemmas. Ava emphasized that there was no right answer for any of these problems and that Owen could decide to agree or disagree with the proposed solution to each dilemma by pressing one of two buttons on a joystick. The MRI scanner would then measure the changes in his brain that occurred each time he made a decision. The experiment sounded interesting to Owen, and he agreed to participate. But, before he could be scheduled for a session, he needed to answer a series of MRI safety questions: whether he had any metal in his body, such as a pacemaker or aneurysm clip; whether he had any non-removable body piercings; and whether he was claustrophobic. Owen did not have these conditions, nor any other that would prevent him from participating, so he was scheduled for the fMRI session.

Now, Ava waited at the MR center entrance for her subject to arrive. She had tested the experimental protocol the night before; the computers, MR-compatible goggles, and joystick all worked fine. She had even sent a reminder to Owen the night before. A post-doc in the laboratory had joked with her that she was worrying too much about the study, before smiling and congratulating her on being organized. That reassured her, but she still knew that she'd feel better *after* the session ended successfully.

Setting Up the Subject

Owen arrived at the MRI center thirty minutes early, as instructed. He came prepared for going into the scanner: wearing no metal on his clothing nor any jewelry or watch, and leaving his book bag in his dorm room. Ava greeted him at the entrance and walked him to the MR console room. The only other person in the room was the MR technologist whose job was to run the MR scanner. The console room was large and contained several computers. Through an observation window, they could see the MR scanner, which was behind a locked door.

Ava pulled several forms from a folder she carried: a consent form that described the study, an instruction sheet for the experiment, and a screening form that asked questions about metal, medical conditions, and medications (Figure 1). Ava went over the consent form in detail, explaining that Owen was participating in this experiment as

(continued on next page)

BOX 2.1 *(continued)*

Brain Imaging and Analysis Center

Part I: For all individuals entering the scanner room

Name _____ Birth Date _____
Last name First name M.I.
Address _____ City _____
State ____ Zip Code _____ Phone (H)(____)_____ (W)(____)_____

1. Have you had any previous MRI studies or been in a MR scanner? ❑ No ❑ Yes
   If yes, please list (most recent first):
   Body part _____ Date _____ Facility Location _____
2. Have you ever worked with metal (grinding, fabricating, etc.) or ever had an injury to the eye involving a metallic object (e.g., metallic slivers, shavings, foreign body)? ❑ No ❑ Yes
   If yes, please describe: _____
3. Have you ever had surgery or other invasive medical procedure? ❑ No ❑ Yes

Some of the following items may be hazardous to your safety or may interfere with the MRI examination. Do you have any of the following:

❑ Yes ❑ No Cardiac pacemaker or defibrillator
❑ Yes ❑ No Insulin or infusion pump
❑ Yes ❑ No Cochlear, otologic, or ear implant
❑ Yes ❑ No Hearing aid
❑ Yes ❑ No Any implanted metal (e.g., clamps, valves, clips, shunts, catheters?)
❑ Yes ❑ No Body piercing(s)
❑ Yes ❑ No Tattoos or permanent makeup (e.g., eyeliner, lips)
❑ Yes ❑ No Artificial limb or prosthesis?
❑ Yes ❑ No Bone/joint pin, screw, nail, wire, plate
❑ Yes ❑ No Wire sutures or surgical staples
❑ Yes ❑ No Any implant held in place by a magnet (e.g., dental)
❑ Yes ❑ No Transdermal delivery system (Nitro)
❑ Yes ❑ No Tissue Expanders (plastic surgery)
❑ Yes ❑ No Colored contact lenses
❑ Yes ❑ No Any metal fragments (e.g., shrapnel)

Other, please explain: _____

Before you may enter the scanner room you must remove all metallic objects.

❑ All contents of pockets, including back pockets
❑ Wrist watch; any bracelets
❑ Hair pins, clips, weaves, fasteners
❑ Pins or badges on shirt
❑ Belt with metal (e.g., buckle)
❑ Shoes that contain any metal (e.g., steel-tipped)
❑ Hearing aids or other electonic devices
❑ Pagers, cell phones, PDAs
❑ Dentures or removable retainer
❑ Necklaces, chains

Note: You are required to wear earplugs or earphones during the MRI examination.

_____ ___/___/___
Signature of Person Completing Form Date

Form completed by: ❑ Self ❑ Parent/Guardian ❑ Other Relative ❑ Physician

Figure 1 A sample screening form used for fMRI studies. This form would be filled out by a prospective subject before a research study. The experimenter would then examine the form to make sure that the subject has no condition (e.g., ferrous metal in the body) that would preclude participation in the study.

a research volunteer, so he could quit the study at any time for any reason. One section of the consent form covered something called an "incidental finding." Even though the images were not the same as those used for clinical scanning, one of the scientists might see something abnormal in Owen's brain. If so, the MR images would be evaluated by a neuroradiologist who would then decide whether to contact Owen with more information. This seemed reasonable to Owen, so he signed the forms and was ready to begin the study.

As Owen walked to the scanner room door, the technologist asked him whether he had anything in his pockets or in his hair. At first, Owen thought that this was a strange question, but the technologist quickly explained that they wanted to make sure that people did not bring any metal with them into the scanner room. When Owen checked, he realized that he had his keys in his pocket, and he placed them on a table. Only then did the technologist unlock the scanner room and escort him inside. Owen hopped up onto a bed at the front of the scanner, and the technologist handed him some earplugs. As Owen put the earplugs in, the technologist explained that the scanner would be loud and that the earplugs would reduce the noise to a comfortable level. Owen then lay down on the table. The technologist handed him a joystick, a pair of goggles with tiny LCD screens inside, and a squeeze ball that was connected to an alarm in the console room. If Owen became uncomfortable or needed help immediately, he could squeeze the ball to summon the technologist.

Although he couldn't see the scanner room anymore, due to the goggles, Owen could feel a pillow being wrapped around the sides of his head. The technologist said that this was a vacuum pack that would support his head and keep it still during the experiment. After a few seconds, Owen heard a hissing sound and the pillow hardened to form a solid cushion. A plastic cylinder called a volume coil was then placed around his head (Figure 2). The technologist pressed a button on the scanner, and Owen found himself slowly moving back into the bore. The technologist returned to the control room and asked Owen over an intercom how he was feeling. Owen said that he was doing fine; any anxiety had worn off, and he was pretty comfortable in the scanner. This

BOX 2.1 *(continued)*

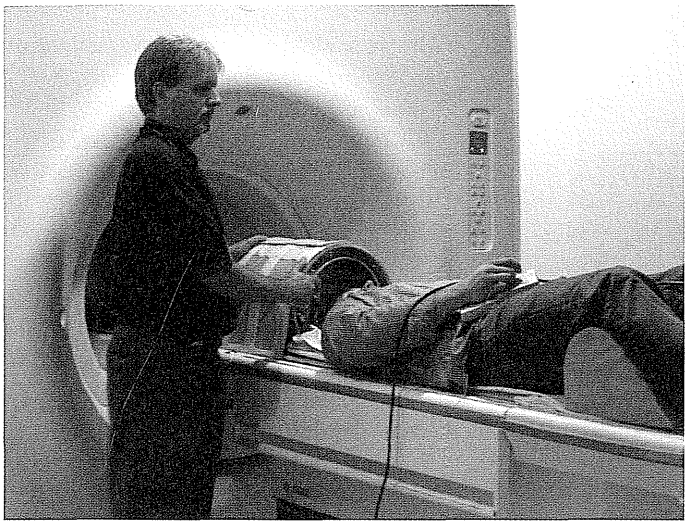

Figure 2 Setting up a subject in the scanner. The experimental subject is being positioned in the scanner before a research study. He is holding a joystick in his right hand that will be used for recording behavioral responses. The technologist standing next to the scanner is moving the table so that the subject's head is in a particular position. Once the subject is positioned properly, the technologist will move the volume radiofrequency coil forward so that it fits around the subject's head and then send him into the bore of the scanner.

reassured Ava greatly—she was more nervous than her subject, it seemed!

Structural and Functional Scanning

The first part of the session involved the collection of high-resolution anatomical images. Even though he had been warned (and had earplugs), Owen was still startled by that first knocking noise. He had expected the scanner to be quiet, like an X-ray machine. The structural images took about ten minutes, and then Ava came on the intercom to tell him that the experiment was about to begin. The experiment was broken into a series of six-minute runs. In each run, Owen read about many different ethical dilemmas. Some of the solutions seemed completely obvious, allowing him to press the joystick button right away. Others were much more challenging—it took him a few seconds to deliberate and respond, and even then he sometimes regretted his choice.

Ava followed the experiment and Owen's choices on the computers in the console room. His decisions in the first few experimental trials matched those of pilot subjects she had recently tested outside the scanner. In these trials, where the solution was made completely obvious, Owen always responded quickly and accurately. Ava could even get a rough idea of Owen's head movements using the real-time tracking program on the scanner's reconstruction computer. So far, he was performing the task well. Between the runs, Ava used the intercom to ask Owen how he was doing, and each time he reported that he was doing well. Forty-five minutes (and six runs) later, the experiment was finished and the technologist brought Owen out of the scanner. He was a little tired from concentrating for an hour, but had still enjoyed the experiment and wanted to see the pictures of his brain.

After the Experiment

Owen re-entered the MR console room and sat down in front of a computer monitor. Ava gave him a short document called a debriefing statement; it explained the basic goals of the experiment and what Ava and her colleagues were hoping to discover. The basic idea, as Ava explained it, seemed simple. Previous researchers in Ava's laboratory had identified areas in the brain associated with making specific types of ethical decisions, but those researchers had only used one type of ethical decision. Ava and her advisor had hypothesized that a slightly different set of regions in the medial prefrontal cortex, would be involved when the ethical decisions were about specified individuals. This made sense to Owen because, in thinking back to the experiment he'd just completed, he remembered having the most difficulty making decisions when the dilemmas concerned a particular person. Owen asked if those areas were active in his brain during the experiment, but Ava told him they would not know anything about his brain function until the data were analyzed by computer programs back in the laboratory.

She could, however, show him the structural images they had collected (Figure 3): a set of sagittal images that showed a side view of his brain, and two sets of horizontal images that showed bottom-up views of his brain. Owen immediately asked whether his brain looked normal. Ava reminded him that this was only a research study and that the images were optimized for research purposes, but not for clinical evaluation. Owen told Ava that she or others in her

(continued on next page)

BOX 2.1 *(continued)*

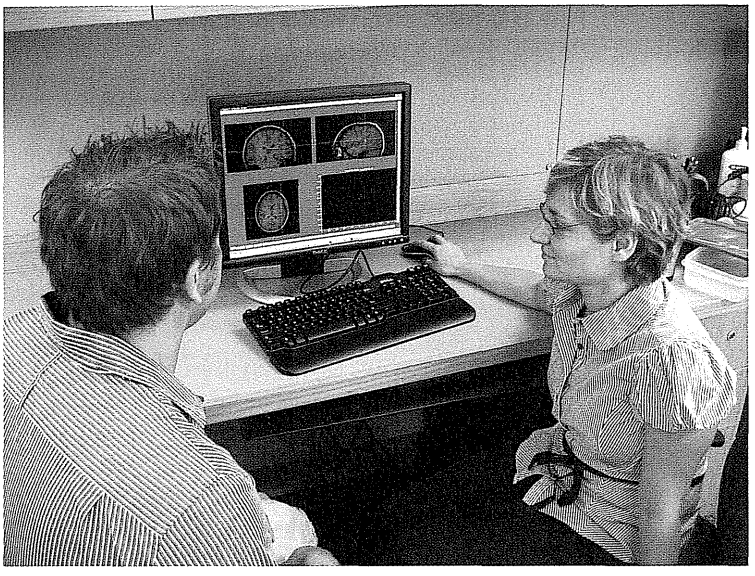

Figure 3 Reviewing the anatomical MR images after the experiment. The graduate student who ran the experiment explains the nature and purpose of the experiment. She shows the subject pictures of his brain and discusses the goals of the research.

center were welcome to contact him for more studies, especially if they involved interesting questions like this one. Then he went back to his dorm to rest.

Ava returned to the console room and flopped down in a chair next to the technologist. The session had gone as well as she had hoped. The subject had finished the entire experiment, had kept his head reasonably still, and had answered all of the questions without any problems. No technical problems with the scanner had affected the data collection; in fact, the data were already being transferred back to her laboratory. All in all, everything had gone smoothly and safely.

Thought Question

Why do you think that a belief in the biological effects of magnetic fields has persisted, in the absence of strong evidence in support of such effects?

The study of the health effects of magnetic fields long predates MRI. In the 1920s, the prevalence of large industrial magnets in factories prompted the physiologists Drinker and Thompson to study the effects of magnetic fields on both cells and animals. No health effects were found. Yet by the 1980s and 1990s, concerns about magnetic fields (sometimes confused with concern about electromagnetic radiation) reemerged into public awareness, as people worried about exposure to power lines, cellular telephones, and MRI scanners. A full discussion of the history of magnetic field safety is beyond the scope of this book. However, the outcome of a century of research can be summarized as follows: no replicable experiment has ever demonstrated a long-term negative effect of magnetic fields on human or animal tissue. Where plausible mechanisms for biological effects of magnetic fields have been postulated, they involve very high magnetic field strengths that are greater than those typically used in MRI—and orders of magnitude greater than those generated by power lines, cellular telephones, or other common sources.

There have been anecdotal reports of minor and short-lived effects associated with static field strengths greater than 2 T. These include reports of visual

disturbances known as phosphenes, metallic taste sensations, sensations in teeth fillings, vertigo, nausea, and headaches. These sensations happen infrequently, but appear to occur when the subject's head is moved quickly within the static field. It is believed that some of these effects—particularly vertigo, nausea, and phosphenes—may be related to "magnetohydrodynamic" phenomena. When an electrically conductive fluid such as blood flows within a magnetic field, an electric current is produced, as a force opposing the flow. In the case of blood flow, magnetohydrodynamic forces are resisted by an increase in blood pressure. However, this effect is negligible, requiring a field strength of 18 T to generate a change of 1 mm Hg in blood pressure. These resistive forces could, however, impose torque upon the hair cells in the semicircular canals of the inner ear, causing vertigo and nausea, or upon the rods or cones in the retina, causing the sensation of phosphenes. We emphasize that these effects are likely to occur only during quick movements of the head within the field. Moving the subject slowly in and out of the scanner, and restricting head movement, should eliminate these sensations.

Given the lack of evidence for magnetism-induced health risks, as well as the absence of any plausible mechanism for such effects, why have magnetic fields generated such concern? We speculate that the issue of magnetic field safety is symptomatic of two larger problems in the public understanding and evaluation of scientific findings. First, magnetic fields and electric currents are mysterious to most non-physicists, acting invisibly and over large distances. Surely a force powerful enough to lift a car or pull an oxygen canister across the room must have some effect upon the human body! The mysterious nature of magnetic fields makes any effect seem plausible, from the threat of cancer by prolonged exposure to power lines to the promised health benefits of magnetic bracelets, even if those effects are contradictory. Indeed, some data suggest that the experiences related to magnetic field exposure may, at least partially, result from psychological suggestion. For example, a group of researchers at the University of Minnesota put subjects into the bore of a 4-T scanner and found that 45% of the subjects reported unusual sensations. This high rate of self-reported effects was interesting, given that the magnet had been powered down and there was no magnetic field present at the time of the study.

A second problem with the public evaluation of scientific findings is that many people (including many scientists) tend to select evidence in support of a preconceived viewpoint, and reject evidence that refutes their ideas. While the vast majority of studies (and all the studies whose findings have been replicated) show absolutely no health risks for magnetic fields of less than 2 T, there remain a few studies that have claimed specific effects of exposure. Even though attempts to replicate these results have failed, the results can be used as evidence by people who believe that magnetic fields must have some effect on health. The efforts to demonstrate health consequences, either positive or negative, from magnetic fields fall perilously close to what has been called "pathological" or "voodoo" science. Despite increasing numbers of these studies, the evidence for long-term health effects has not become stronger. For more information on this issue, see the references at the end of this chapter.

Translation and torsion

The primary risk of the static field used in MRI results from the field's effect on metal objects. Objects that are constructed in part or wholly from ferromagnetic materials are strongly influenced by magnetic fields. Steel objects, and even some medical grades of stainless steel are ferromagnetic. Metals such as

translation The movement of an object along an axis in space (in the absence of rotation).

torsion A rotation (twisting) of an object. Even if the motion of an object is restricted so that it cannot translate, a strong magnetic field will still exert a torque that may cause it to rotate so that it becomes aligned with the magnetic field.

aluminum, tin, titanium, and lead are not ferromagnetic, but objects are rarely made of a single metal. For example, ferromagnetic steel screws may be used to secure titanium frames for eyeglasses.

The most dramatic risk in a strong magnetic field is the projectile effect that results in the translation, or movement, of a ferromagnetic object toward the scanner bore. The magnetic pull on an object can increase dramatically as it nears the scanner, causing its movement to accelerate. A movement of just a few inches toward the bore of the magnet can exponentially increase the magnetic pull, making it impossible for a person to hold on to a ferromagnetic object such as a wrench or screwdriver. Similarly, a pager may stay clipped to a belt at the doorway to the magnet room, but become propelled into the magnet bore at 20 to 40 mph if the wearer takes a few steps forward. Projectile injuries have resulted from a number of metal objects, including scissors, IV-drip poles, and oxygen canisters, that were brought too close to an MRI scanner (Figure 2.9). In a tragic example of the danger of projectile effects, a six-year-old boy was killed in 2001 when a ferromagnetic oxygen canister was brought into the MRI scanner room to compensate for a defective oxygen supply system.

Even if they are unable to translate toward the scanner center, ferromagnetic devices and debris will be subject to a force that will cause them to re-align so that they are parallel with the static magnetic field. This alignment process is known as torsion. Torsion poses an enormous risk for individuals with implanted metal in their bodies. In 1992 a patient with an implanted aneurysm clip died when the clip rotated in the magnetic field, resulting in severe internal bleeding. Another potential problem is metal within the eyes, which may be present in someone who suffered an injury while working with metal shavings. If lodged in the vitreous portion of the eye, the metal may have no ill effects upon vision. But exposure to a strong magnetic field may dislodge the fragments, blinding the patient. Torsion effects may also explain the swelling and/or irritation that have been reported for some subjects with tattoos or wearing certain makeup—particularly mascara and eyeliner. The pigments in tattoos and makeup may contain iron oxide particles with sharp edges or irregular shapes. If these particles move in an attempt to align with the magnetic field, they may produce local tissue irritation.

The cardinal rule of MRI safety is that no ferromagnetic metal should enter the scanner room. All participants and medical personnel should remove any objects that contain metal, such as pagers, PDAs, cell phones, stethoscopes, pens, watches, paper clips, and hairpins, prior to entering the room. Once the scanner is ramped to its full field strength, the magnetic field is always present, even if no one is in the scanner and no images are being acquired. For this reason, it is the responsibility of all MRI researchers and technicians to be constantly vigilant to prevent metal from entering the scanner room.

Gradient magnetic field effects

The main safety risk from the gradient magnetic fields is the generation of electric currents within the body. The gradient magnetic fields are much weaker than the static magnetic field, typically changing the overall strength of the field by only a few thousandths of a Tesla (mT) per meter. Therefore, they do not alter the translation or torsion effects on objects. However, the gradient magnetic fields change rapidly over time. The effect of a gradient is calculated by dividing the change in magnetic field strength (ΔB, or dB) by the time

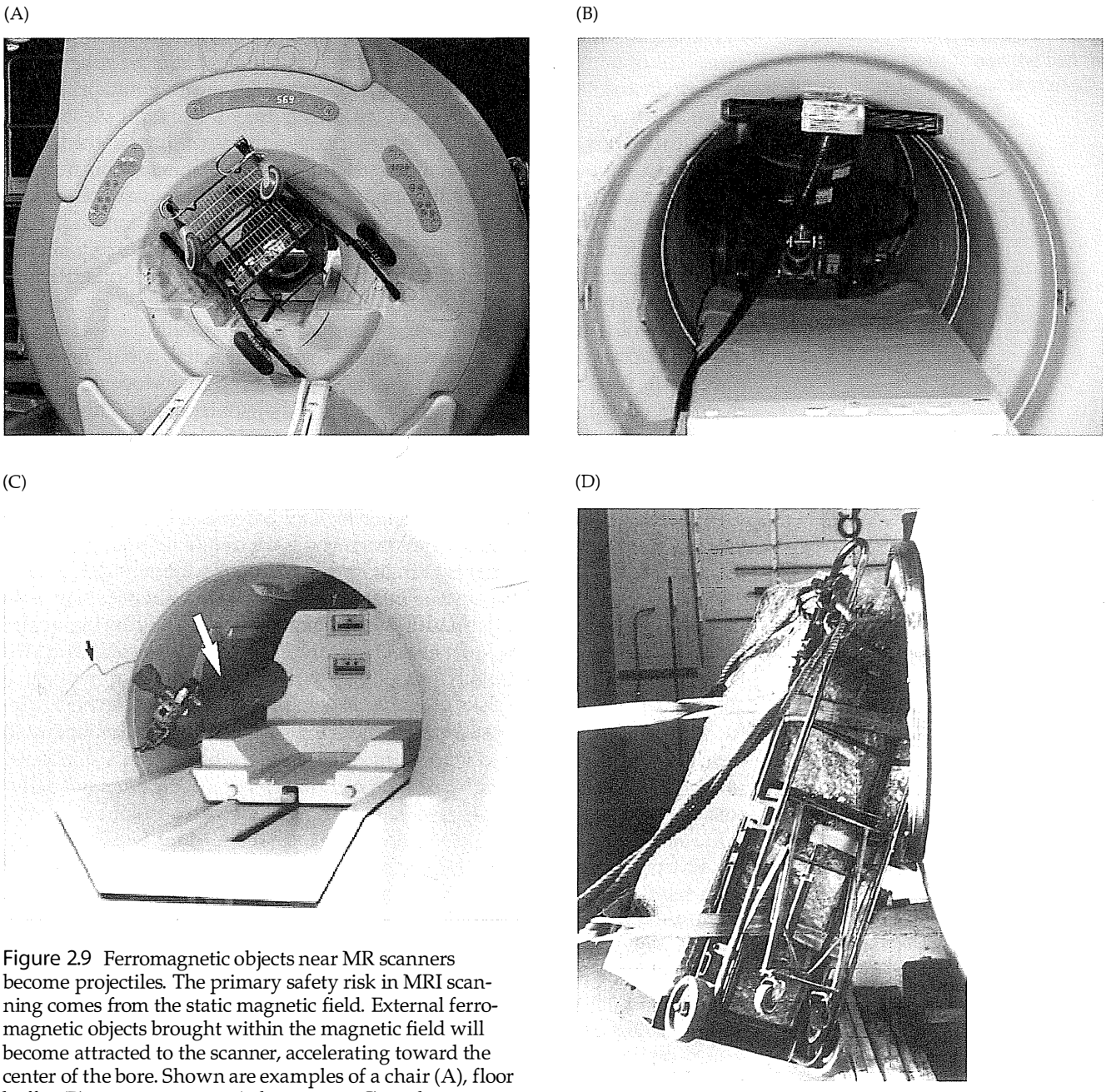

Figure 2.9 Ferromagnetic objects near MR scanners become projectiles. The primary safety risk in MRI scanning comes from the static magnetic field. External ferromagnetic objects brought within the magnetic field will become attracted to the scanner, accelerating toward the center of the bore. Shown are examples of a chair (A), floor buffer (B), oxygen canister (white arrow; C), and power supply (D), all lodged in the bores of MRI scanners. Projectiles present a severe risk to subjects within the scanner bore. (A,B courtesy of Dr. Moriel NessAiver; C from Chaljub et al., 2001; D from Schenck, 2000.)

required for that change (Δt, or dt), resulting in the quantity dB/dt. Since the human body is a conductor, gradient switching can generate small electric currents that have the potential to stimulate nerves and muscles, or to alter the functions of implanted medical devices.

dB/dt The change in magnetic field strength (dB) over time (dt).

specific absorption rate (SAR) A quantity that describes how much electromagnetic energy is absorbed by the body over time.

Currents induced in the body by gradient switching can cause peripheral nerve or muscle stimulation. This stimulation may result in a slight tingling sensation or a brief muscle twitch. Although this may startle the subject, it is not recognized as a significant health risk. Threshold sensations such as these should not be ignored, however, because they may become unpleasant or painful at higher levels of dB/dt. The current operating guidelines in the United States are based on the threshold for sensation, rather than a specific numerical value for dB/dt. To prevent peripheral nerve stimulation, subjects should be instructed not to clasp their hands or cross their legs during scanning; these actions create conductive loops that may enhance dB/dt effects. Subjects should also be instructed to report any tingling, muscle twitching, or painful sensations that occur during scanning.

Gradient field changes can also induce currents in medical devices or in implanted control wires that remain after device removal. If a patient with a pacemaker were to be scanned, gradient field effects might induce voltages in the pacemaker that could cause rapid myocardial contractions. This type of electrical malfunction, rather than the translation or torsion of the pacemaker, appears to be the primary cause of pacemaker-related fatalities in the MRI setting. At least six individuals with pacemakers have died as a result of MRI, and clinical or research centers no longer allow patients with pacemakers to enter MRI scanners. Recent studies, however, have demonstrated that under appropriate conditions patients with pacemakers can be scanned safely at field strengths of up to 1.5 T. Because of the increasing prevalence of pacemakers in an aging population, further studies of pacemaker safety will be necessary. Other implanted devices, such as cochlear implants, also pose risks for MRI participation, and patients with those devices should be excluded from research studies. To minimize the risks of gradient field effects, fMRI researchers carefully screen potential subjects and exclude any subject who has an implanted medical device.

Radiofrequency field effects

Recall from our discussion of the scanner hardware that the radiofrequency coils send energy, in the form of electromagnetic radiation, into the body. Because the energy is in the radiofrequency range, the radiation is not ionizing (i.e., it does not break molecular bonds). Yet it still can influence biological tissue. While the re-emission of some of the radiofrequency energy forms the basis for MRI, not all of the energy is re-emitted. Excess energy is absorbed by the body's tissues and dissipated in the form of heat—through convection, conduction, radiation, or evaporation. Thus, a potential concern in MRI is the heating of the body during image acquisition.

The specific absorption rate (SAR) determines how much electromagnetic energy is absorbed by the body, and is typically expressed in units of watts per kilogram, or W/kg. SAR depends on the pulse sequence and the size, geometry, and conductivity of the absorbing object. Because the difference between low- and high-energy states increases with increasing field strength, there is a corresponding increase in the resonant frequency of the energy required to change atomic nuclei between those states. Furthermore, those higher frequencies are more energetic than lower frequencies, resulting in a greater potential for heating at higher static field strengths. As will be discussed in Chapter 5, larger-flip-angle pulses (180°) deposit more energy than smaller-flip-angle pulses (90°), and SAR is greater for pulse sequences that employ many pulses per unit time (such as fast spin echo) than those that employ fewer (such as

gradient-echo or echo-planar imaging). Also, SAR increases with scanner field strength, making it more of a concern for high-field fMRI studies.

To ensure participant safety, SAR in MRI studies is limited to minimize body temperature increases. Accurately determining SAR is difficult; it depends on heat conduction and body geometry as well as upon the weight of the subject. Subjects regulate heat dissipation through perspiration and blood flow changes, so researchers should attend to patient comfort throughout a session. Thermoregulation is impaired in patients with fevers, cardiocirculatory problems, cerebral vascular disease, or diabetes, and thus SAR thresholds should also be lowered for these individuals.

Metal devices and wires also absorb radiofrequency energy and may become hotter than the surrounding tissue. The most common source of heating results from looped wires, such as electroencephalogram or electrocardiogram leads, that act as antennae and focus energy to small areas. Metal necklaces, other jewelry, and even some tattoos can also focus radiofrequency energy and cause irritation or burning. Thus, the most significant safety risk caused by the radiofrequency fields used in MRI is local burning. Note that the induced currents caused by gradient field effects can also result in heating, through a different mechanism (described in the previous section).

To prevent radiofrequency heating, researchers should (1) exclude subjects who have metal devices or wires implanted within their bodies; (2) ensure that subjects remove all metal prior to entering the scanner—including non-ferromagnetic jewelry such as necklaces and earrings; and (3) make certain that any wire leads are not looped, and that wires are not run over bare skin.

mock scanner A device that simulates a real MRI scanner, usually by reproducing the scanner bore, the bed that the subjects lie on, and the sounds made during scanning.

Claustrophobia

The most common risk from participation in an fMRI study is claustrophobia. Most participants find the physical confinement of the MRI bore only somewhat uncomfortable, and any concern passes within a few moments. However for some subjects, confinement results in persistent anxiety, and in extreme cases, panic. Roughly ten percent of all patients experience claustrophobia during clinical MRI scans. This percentage is much lower for research studies, because research subjects are generally younger and healthier than their clinical counterparts, and people who know that they are claustrophobic are unlikely to volunteer for research studies. In our experience, only about one to three percent of research subjects suffer from claustrophobia during fMRI experiments.

There is no simple solution to the problem of claustrophobia. Subjects who state that they are claustrophobic during a pre-experiment screening should be excluded from study. Researchers with access to a **mock scanner**, which is a simulated scanner without a static magnetic field, can put prospective subjects in that device before the real fMRI sessions. Anxiety in the scanner can be reduced by talking with subjects frequently throughout the scan (particularly at its onset), by directing air flow through the bore to reduce heat and eliminate any fear of suffocation, and by providing the subjects with an emergency panic device. If subjects know that assistance is immediately available and that they can quit the study at any time, they will feel in control of the session. For first-time subjects, an experimenter should explain that the sounds they will hear are a normal part of scanning. Subjects should also be told that mild apprehension in enclosed spaces is a normal reaction, but if they feel increasingly anxious, they can ask to stop the scan. An experimenter must listen for telltale signs of growing anxiety or discomfort, such as the subject repeatedly asking how much longer the scan will last. Taking a few minutes to enter the scanner room and reassure a

subject may help avoid an escalation of anxiety. However, if a subject appears to be more than mildly anxious or declares himself or herself to be anxious, then the experimenter must remove the subject from the scanner immediately.

Thought Question

Under some conditions, clinical patients may have MRI scans even if they have some contraindications (e.g., implanted devices, claustrophobia) that would preclude their participation in a research study. Why should there be different standards for clinical patients and research subjects?

Acoustic noise

The rapid changes of current in the gradient coils induce Lorentz forces, or physical displacement of the wires, which in turn cause vibrations in the coils and their mountings. To the subject, the vibrations sound like knocking or tapping noises. The quality of the noise depends on the particular pulse sequence used, but during functional scanning sequences, which make up the bulk of any fMRI session, the noises are often very loud (greater than 95 dB) and of high frequency (1000 to 4000 Hz). In general, fast sequences, such as in echo-planar imaging, and sequences that tax the gradient coils, like diffusion-weighted imaging, are louder than conventional sequences. Without some protection, temporary hearing loss could result from the extended one- to two-hour exposure of a typical fMRI study. To reduce acoustic noise, fMRI participants should always wear ear protection in the form of earplugs and/or headphones. Researchers should check the fit of the protective devices to ensure their effectiveness.

Summary

REFER TO THE
fMRI
COMPANION WEBSITE AT
www.sinauer.com/fmri2e
for study questions and Web links.

The basic parts of most MRI scanners include a superconducting magnet to generate the static field, radiofrequency coils (transmitter and receiver) to collect the MR signal, gradient coils to provide spatial information in the MR signal, and shimming coils to ensure the uniformity of the magnetic field. Additional computer systems control the hardware and software of the scanner, present experimental stimuli and record behavioral responses, and monitor physiological changes.

Although fMRI is a noninvasive imaging technique, these hardware components do have associated safety concerns. Most important are issues related to the very strong static field, which can cause translation or torsion effects in ferromagnetic objects near the scanner. The changing gradients and radiofrequency pulses can also cause problems if researchers do not follow standard safety precautions. Some subjects report brief claustrophobic reactions upon entering the scanner, although for most people these feelings fade within a few minutes. Since these risks can be minimized for most subjects, fMRI has become an extraordinarily important research technique for modern cognitive neuroscience.

Suggested Readings

Kanal, E., Borgstede, J. P., Barkovich, A. J., Bell, C., Bradley, W. G., Felmlee, J. P., Froelich, J. W., Kaminski, E. M., Keeler, E. K., Lester, J. W., Scoumis, E. A., Zaremba, L. A., and Zinninger, M. D. (2002). American College of Radiology White Paper on MR safety. *Am. J. Radiol.*, 178: 1333–1347. *A report from leading experts on MR safety about recommended procedures in the MRI environment.*

Schenck, J. F. (2000). Safety of strong, static magnetic fields. *J. Magn. Reson. Imaging*, 12: 2–19. *This journal article provides a scholarly and comprehensive introduction to the effects of magnetic fields on biological tissue.*

Shellock, F. G., and Crues, J. V. (2002). Commentary: MR safety and the American College of Radiology White Paper. *Am. J. Radiol.*, 178: 1349–1352. *This short commentary provides additional interpretation, and in some cases rebuttal, of the report authored by Kanal and colleagues.*

Chapter References

Chaljub, G., Kramer, L. A., Johnson, R. F., Johnson, R. F., Singh, H., and Crow, W. N. (2001). Projectile cylinder accidents resulting from the presence of ferromagnetic nitrous oxide or oxygen tanks in the MR suite. *Am. J. Roentgen.*, 177: 27–30.

Drinker, C. K., and Thomson, R. M. (1921). Does the magnetic field constitute an industrial hazard? *J. Ind. Hug.*, 3: 117–129.

Guidance for Industry and FDA Staff: Criteria for Significant Risk Investigations of Magnetic Resonance Diagnostic Devices. (2003). U.S. Food and Drug Administration. www.fda.gov/cdrh/ode/guidance/793.pdf

Reilly, J. P. (1998). Maximum pulsed electromagnetic field limits based on peripheral nerve stimulation. *IEEE Trans. Boomed. Eng.*, 45: 137–141.

Shellock, F. G. (2000). Radiofrequency energy-induced heating during MR procedures: a review. *J. Magn. Reson. Imaging*, 12: 30–36.

Chapter 3

Basic Principles of MR Signal Generation

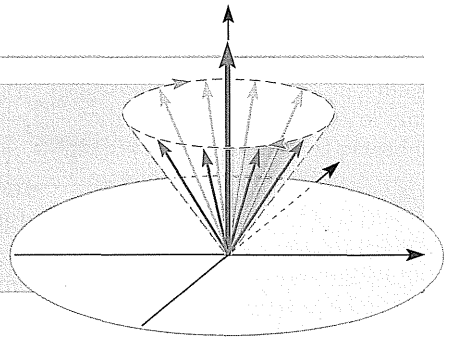

All magnetic resonance imaging, including fMRI, relies on a core set of physical principles that were discovered by Rabi, Bloch, Purcell, and other pioneers during the first half of the twentieth century. These principles are elegant in their simplicity. They begin with the properties of single atomic nuclei and progress, step-by-step, to the signal measured using MRI. Yet, they are also rigorous and quantitative.

The greatest challenge faced by teachers of MRI is to do justice to both the elegance and the rigor of signal generation. Some students prefer to learn by intuition and analogy, while others are most comfortable when working through the underlying equations. To accommodate both groups while maintaining completeness of scope, we will discuss the principles of signal generation in two sections of the chapter, which follow independent but corresponding paths through the material (Figure 3.1). We begin the chapter with a *conceptual path* that uses textual descriptions and analogies to illustrate and reinforce the key concepts of signal generation. This is followed by the *quantitative path*, which covers the same basic principles using equations and mathematical notation, allowing interested students to understand the exact contributions of different components to the measured MR signal.

Both paths cover the same topics in the same order; so either one can provide the background necessary for reading subsequent chapters in the book. Thus, instructors and students can choose to either take one path or go back and forth between them, using the concepts to simplify the equations, and the equations to elaborate and give more specific meaning to the key concepts.

Conceptual Path

To provide students with an intuitive understanding of key concepts like spin, precession, and relaxation, this overview emphasizes the underlying principles rather than the mathematical formulas. Although individual concepts might seem complex, they build on each other in a step-by-step fashion. First we consider individual spins (i.e., atomic nuclei), then we discuss how those spins are influenced by magnetic fields and the delivery of electromagnetic energy. We end by describing how spins subsequently release energy over time to generate the signal measured by MRI.

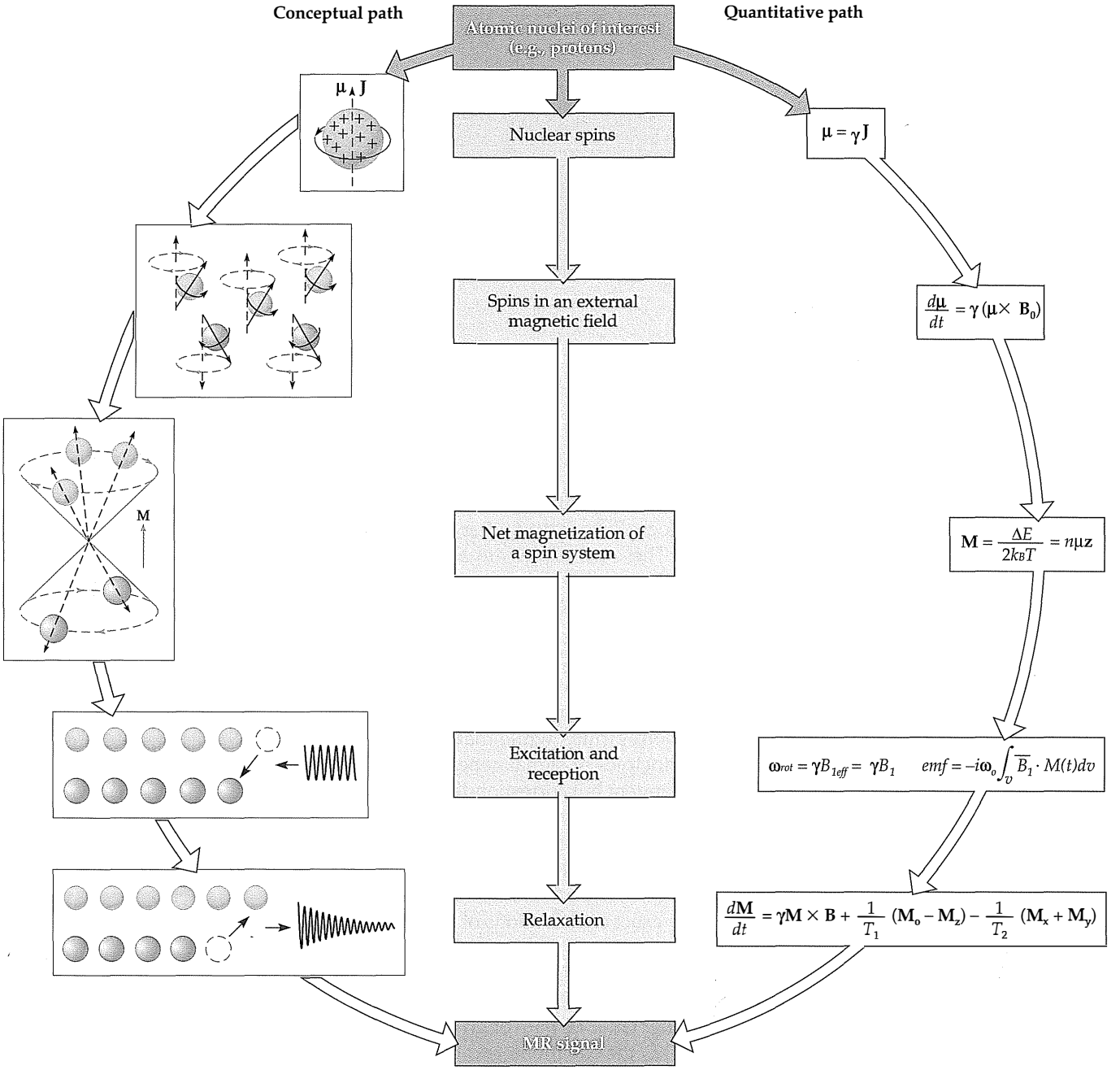

Figure 3.1 Overview of the chapter. We have structured this chapter (and Chapter 4) along two parallel paths, each covering the basic principles of MR signal generation: from proton spins to magnetic resonance to excitation and reception. The initial *conceptual path* uses physical models and analogies to cover these principles in a straightforward and intuitive manner, with the minimally necessary jargon, and using no equations. Then, for the benefit of technically curious readers, the subsequent *quantitative path* moves systematically through the equations that govern the generation and reception of the MR signal. Although the quantitative path contains many equations, we have worked to make those equations as accessible as possible, by defining terms and labeling quantities throughout.

Nuclear Spins

All matter is composed of atoms, which contain three types of particles: protons, neutrons, and electrons. The protons and neutrons are bound together in the atomic nucleus. Different atoms have different nuclear compositions; hydrogen nuclei, which are by far the most abundant in the human body, consist of single protons. Because of their abundance, hydrogen atoms are the most commonly-imaged nuclei in MRI, and we will focus on the properties of single protons throughout this discussion.

Consider a single proton of hydrogen. Under normal conditions, thermal energy causes the proton to spin about its axis (Figure 3.2A). This spin motion has two effects. First, because the proton carries a positive charge, its spin generates an electrical current on its surface, just as a moving electrical charge in a looped wire generates current. This current on the surface of the proton creates a small magnetic source and a torque when it is placed within a magnetic field. The strength of this magnetic source, or the maximum torque (i.e., the torque generated when an external magnetic field is at a right angle to the axis of the proton's spin) per unit of magnetic field strength is called the **magnetic moment** (μ). Second, because the proton has an odd-numbered atomic mass (i.e., a mass of one), its spin results in an **angular momentum**, or J. Both $\boldsymbol{\mu}$ and J are vectors pointing in the same direction, given by the **right-hand rule**, along the spin axis. To remember the difference between the magnetic moment and angular momentum, think of the proton as a spinning bar magnet. As the magnet spins, the changing magnetic field generates a magnetic moment and the moving mass results in angular momentum (Figure 3.2B).

For a nucleus to be useful for MRI, it must have both a magnetic moment and an angular momentum. If both are present, the nucleus is said to possess the **nuclear magnetic resonance (NMR) property**. A few nuclei that are used often in NMR include ^{1}H, ^{13}C, ^{19}F, ^{23}Na, and ^{31}P. A nucleus with the NMR property can be referred to as a **spin** and a collection of such nuclei at one spatial location is known as a **spin system**. If a nucleus does not have both characteristics, it cannot be studied using magnetic resonance. For example, in a nucleus that has an even number of protons and an even number of neutrons, its magnetic moment can be cancelled by distributing the same amount of charges in opposite directions, and thus it would be invisible to magnetic resonance imaging.

An average person who weighs 150 pounds contains approximately 5×10^{27} hydrogen protons (because of the high water content in our bodies) and much smaller numbers of other

magnetic moment (μ) The torque (i.e., turning force) exerted on a magnet, moving electrical charge, or current-carrying coil when it is placed in a magnetic field.

angular momentum (J) A quantity given by multiplying the mass of a spinning body by its angular velocity.

right-hand rule A method used to determine the direction of a magnetic moment generated by a moving charge or electrical current. If the fingers of the right hand are curled around the direction of spin, then the magnetic moment will be in the direction indicated by the thumb.

NMR property A label for atomic nuclei that have both a magnetic moment and angular momentum, which together allow them to exhibit nuclear magnetic resonance effects.

spins Atomic nuclei that possess the NMR property; that is, they have both a magnetic moment and angular momentum.

spin system A collection of atomic nuclei that possess the NMR property within a spatial location.

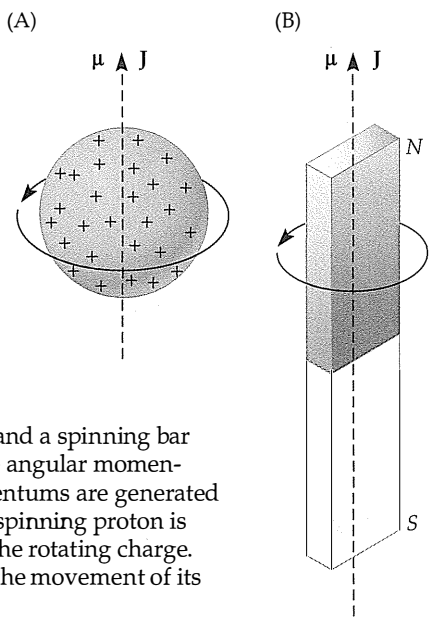

Figure 3.2 Similarities between a spinning proton (A) and a spinning bar magnet (B; north and south poles indicated). Both have angular momentums (J) and magnetic moments (μ). The angular momentums are generated by the spinning masses. The magnetic moment for the spinning proton is generated by the electric current, which is induced by the rotating charge. The magnetic moment for the bar magnet comes from the movement of its internal magnetic field.

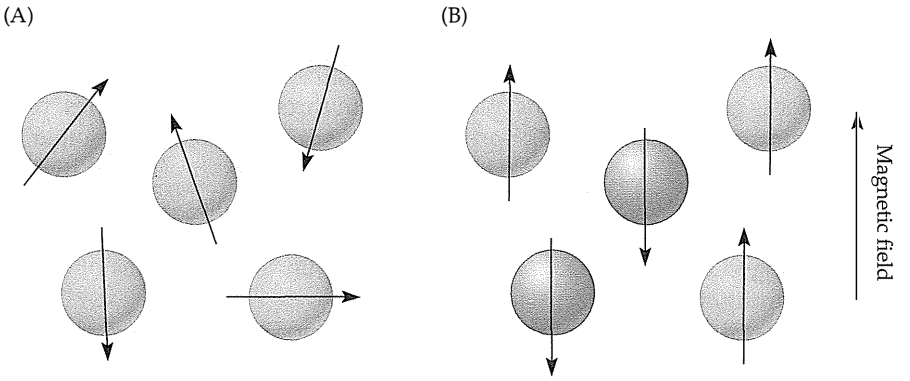

Figure 3.3 Magnetic fields cause the alignment of nuclei that have the NMR property. (A) In the absence of an external magnetic field, protons in free space will have their spin axes aligned randomly. (B) When an external magnetic field is introduced, each proton's axis of spin will tend to take one of two states: either aligned along (parallel to) or against (antiparallel to) the magnetic field. More of the spins will enter the parallel state, resulting in a net magnetization that is parallel to the scanner's magnetic field.

net magnetization (M) The sum of the magnetic moments of all spins within a spin system.

NMR-property nuclei. Each proton possesses a magnetic moment and angular momentum and is thus a potential contributor to the MR signal. However, in the absence of a strong external magnetic field, the spin axes of the protons are oriented randomly (Figure 3.3A) and tend to cancel each other out. Thus, the sum of all magnetic moments from spins of different orientations, or the **net magnetization (M)**, is infinitesimally small under normal conditions. To increase the net magnetization of the protons, a strong magnetic field must be applied to align the axes of spin of the protons (Figure 3.3B).

Spins in an External Magnetic Field

A classic demonstration of magnetism can be created by sprinkling some iron filings around a standard bar magnet. The filings clump most densely around the poles of the magnet but also form a series of arcs between the poles (Figure 3.4A). These arcs run along the field lines of the magnet and result from the

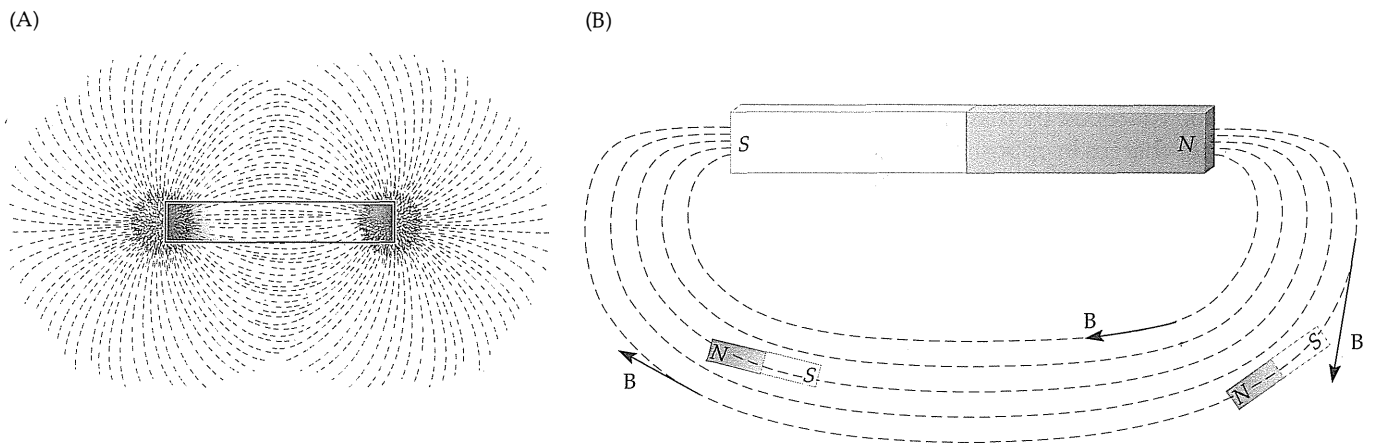

Figure 3.4 Lines of flux in a magnetic field. (A) The alignment of iron shavings in the magnetic field surrounding a bar magnet. (B) A schematic illustration of alignment along the flux lines near a bar magnet. By convention, lines of flux extend from the north (N) to south (S) poles of the magnet. At each point in space, however, the experienced magnetic field is a vector (indicated by the arrows labeled B). Magnetic objects, such as the small bar magnets shown, would align along the flux lines.

tendency of individual iron filings to align with the external field. Figure 3.4B presents a schematic illustration of this alignment, which is driven by the principle of energy minimization. Just as massive objects in a gravitational field tend to lower their energy by falling rather than remaining suspended in midair, magnetically susceptible objects in a magnetic field will orient along the field lines rather than across them. For macroscopic objects like oxygen canisters or iron filings, the alignment process is known as torsion, and it presents safety issues, as discussed in Chapter 2. Note that the magnetic field is still present between the field lines. The pattern of field lines can be interpreted as a mathematical description of the contours of the magnetic field. The density of lines at a particular location indicates the local strength, or **flux**, of the magnetic field. In magnetic resonance imaging, the main magnetic field of the scanner is often indicated by the symbol B_0.

Protons, like iron filings, change their orientations when placed within an external magnetic field. However, instead of turning to align with the magnetic field, the spinning protons initiate a gyroscopic motion known as **precession** (Figure 3.5A). Because the precession frequency is determined by the type of nucleus, to a first approximation all protons precess at the same frequency when experiencing the same external magnetic field strength. This characteristic frequency is called the **Larmor frequency**. To understand precession, imagine a spinning top on a desk (Figure 3.5B). The top does not remain perfectly upright; instead its axis of rotation traces a circle perpendicular to the earth's gravitational field. At any moment in time the top is tilted from the vertical, but it does not fall. Why does the top spin at an angle? A spinning object responds to an applied force by moving its axis in a direction perpendicular to the applied force. A bicycle, for example, is very stable and resists falling over when it is moving at high speeds, due to the gyroscopic effects of its spinning wheels. When a rider leans to one side, the moving bicycle will not fall but will instead turn in that direction. Similarly, a spinning top turns its axis of rotation at an angle perpendicular to the force exerted by gravity, so that the top precesses in a circle around a vertical axis.

The behavior of a proton in a magnetic field is analogous to that of a spinning top in a gravitational field. Specifically, protons precess around an axis parallel to the main magnetic field. The angle between a proton's axis of spin and the direction of the main magnetic field is determined by the proton's angular momentum. There are two states for precessing protons: one parallel to the magnetic field and the other antiparallel (Figure 3.6). Protons in the

flux A measure of the strength of a magnetic field over an area of space.

B_0 The strong static magnetic field generated by an MRI scanner.

precession The gyroscopic motion of a spinning object, in which the axis of the spin itself rotates around a central axis, like a spinning top.

Larmor frequency The resonant frequency of a spin within a magnetic field of a given strength. It defines the frequency of electromagnetic radiation needed during excitation to make spins change to a high-energy state, as well as the frequency emitted by spins when they return to the low-energy state.

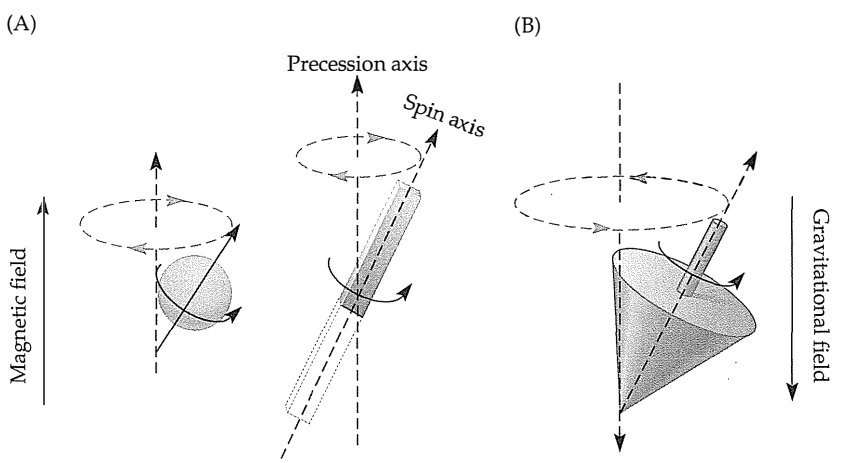

Figure 3.5 Precession. The movement of a rotating proton or magnet within a magnetic field (A) is similar to the movement of a top in the earth's gravitational field (B). In addition to the spinning motion, the axis of spin itself (spin axis) wobbles around the main axis of the magnetic or gravitational field (precession axis). This latter motion is known as precession.

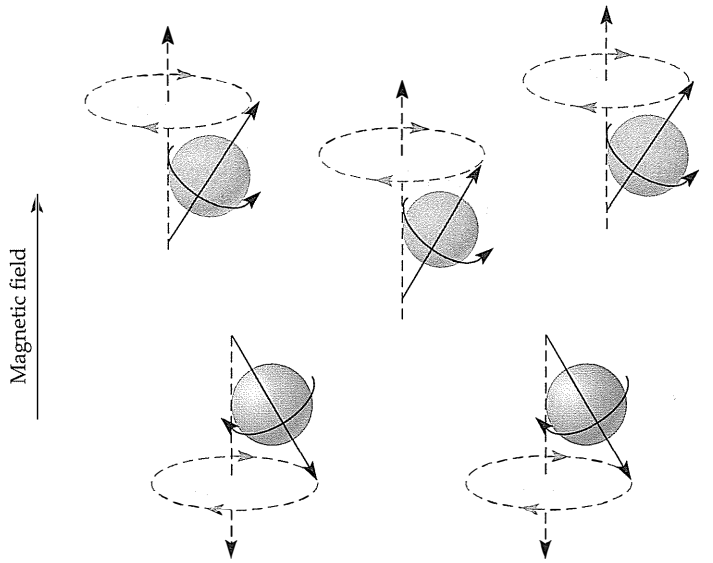

Figure 3.6 High- and low-energy states. Protons in an external magnetic field assume one of two possible states: the parallel state (shown in orange), which has a lower energy level, and the antiparallel state (shown in blue), which has a higher energy level. In the absence of spin excitation, note that there always will be more protons in the parallel state than in the antiparallel state.

parallel state The low-energy state in which an atomic spin precesses around an axis that is parallel to that of the main magnetic field.

antiparallel state The high-energy state in which an atomic spin precesses around an axis that is antiparallel (i.e., opposite) to that of the main magnetic field.

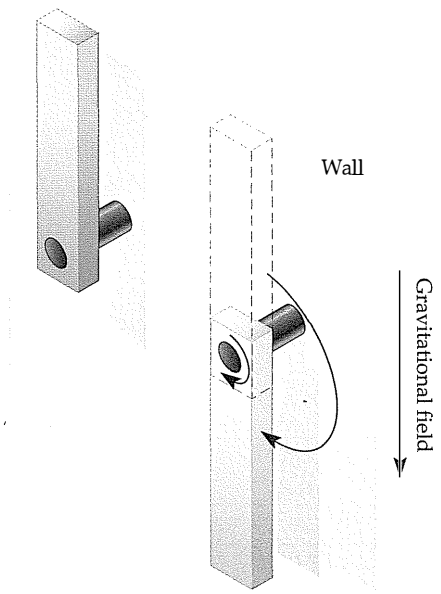

Figure 3.7 High- and low-stability states. Just like a proton in a magnetic field, a bar within the earth's gravitational field can assume two states: the antiparallel state against gravity (blue), which has a higher energy level but is less stable, and the parallel state with gravity, which has a lower energy level but is more stable (orange). Energy must be applied to keep the bar in the high-energy state.

parallel state have a lower energy level than protons in the antiparallel state. The idea of two energy states can be understood by imagining a bar that can rotate around one end (Figure 3.7). There are two vertical positions for the bar: in one it is balanced above the pivot point and in the other it hangs down from the pivot point. The balanced position is a high-energy state and is not very stable; even a small perturbation may tip the bar over and cause it to fall to the hanging position. The only way to keep the bar in a balanced position is to apply an external force that can counteract gravity. That is, energy must be applied to keep the bar in the high-energy state. The hanging position is much more stable, since it is at the minimum energy level for this system. For protons, the parallel (low-energy) state is slightly more stable than the antiparallel state, so there will always be more protons in the parallel state (in the absence of externally delivered energy), with the exact proportions depending on the temperature and the strength of the magnetic field. In Earth's magnetic field at room temperature, roughly equal numbers of protons are in the two energy states, with only slightly more in the parallel state. If the temperature increases, some protons will acquire more energy and jump to the antiparallel state, diminishing but never reversing the already small difference in numbers between the two levels. Conversely, if the temperature decreases, spins will possess less energy and even more protons will remain at the lower energy level.

The discrete energy difference between the two states can be measured experimentally. Interestingly, this energy difference is equal to the energy possessed by a photon at the same frequency as the precession frequency of the proton (i.e., the Larmor frequency). This coincidence provides a basis for unifying quantum mechanics and classical mechanics concepts in the context of spin excitation.

Magnetization of a Spin System

It is important to emphasize that MR techniques do not measure the magnetization of a single atomic nucleus, but instead measure the net magnetization

of all nuclei in a volume. We can think of the net magnetization as a vector with two components: a longitudinal component that is either parallel or antiparallel to the magnetic field and a transverse component that is perpendicular to the magnetic field. Because of the enormous number of spins within even the smallest volume, their transverse components will tend to cancel out, and there will be no net magnetization perpendicular to the main magnetic field. The net magnetization **M** is thus a vector whose orientation is along the longitudinal direction and whose magnitude is proportional to the difference between the number of the spins in the parallel and antiparallel states. The more spins at the parallel state, the bigger the **M** (Figure 3.8).

Because the proportion of parallel spins increases with decreasing temperature, one way to increase the net magnetization is to reduce the temperature. While theoretically possible, this approach is impractical because the temperature would need to be lowered by many degrees to observe a noticeable increase in net magnetization. A more feasible approach, based on the Zeeman effect, is to increase the strength of the external field (Figure 3.9). Just as it would require more energy to lift an object in a stronger gravitational field than in a weaker gravitational field, it takes more energy to shift from a low-energy state to a high-energy state when the external magnetic field is stronger. Therefore, to increase the net magnetization in a sample (i.e., the proportion of parallel spins), one can place that sample in a very strong magnetic field.

Both the increase in net magnetization and the energy difference between the two states are linearly proportional to the strength of the magnetic field. The combination of these two factors means that the theoretical amplitude of the measured MR signal increases quadratically with field strength (e.g., the raw MR signal in a 3-T scanner is four times larger than the signal in a 1.5-T scanner). However, other factors (discussed more extensively in Chapter 8) temper this advantage of high field scanning. Thermal noise in the MR scanner increases approximately linearly with field strength, while some aspects of physiological noise have more complex relationships with field strength. Nevertheless, increasing the strength of the static magnetic field provides significant improvements in the signal-to-noise ratio. For this reason, scanners used for fMRI in humans have increased in field strength, from 1.5 T in the early years, to current standards of 3 T and 4 T. Some scanners used for human fMRI have even stronger magnetic fields of up to 7 T.

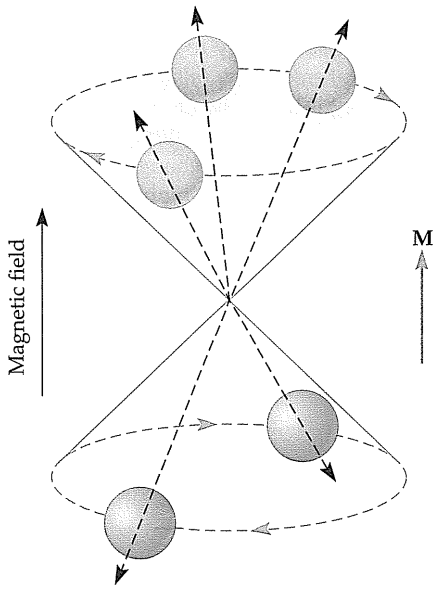

Figure 3.8 Net magnetization. The net magnetization (**M**) is determined by the difference between the number of spins in the parallel state and the number of spins in the antiparallel state. The net magnetization is also called the bulk magnetization.

longitudinal Parallel to the main magnetic field, or the *z*-direction, of the scanner (i.e., into the bore).

transverse Perpendicular to the main magnetic field of the scanner, in the *x*–*y* plane.

Thought Question

What would happen to the relative proportions of parallel and antiparallel spins in a spin system if we reduced its temperature to near absolute zero?

The net magnetization of spins within a volume provides the basis for MR signal generation, but net magnetization itself cannot be measured directly under equilibrium conditions. To understand this principle, think of an object whose weight you are trying to estimate. You cannot know the object's weight just by looking at it; instead, you have to lift it. By lifting the object, you perturb its equilibrium state in the gravitational field, and the force observed in reaction to that perturbation allows you to estimate its weight. Measuring the net magnetization of spins in a magnetic field is analogous to measuring the weight of an object; you must perturb the equilibrium state of the spins and then observe how they react to the perturbation. Just as lifting perturbs the position of an object, excitation perturbs the orientation of the net magnetiza-

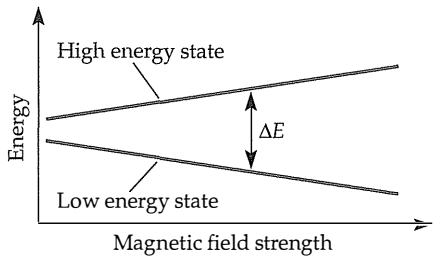

Figure 3.9 The Zeeman effect. The energy difference (ΔE) between the parallel and antiparallel states increases linearly with the strength of the static magnetic field. As the energy difference between the states increases, spins are more likely to remain in the lower-energy state.

excitation The process of sending electromagnetic energy to a sample at its resonant frequency (also called transmission). The application of an excitation pulse to a spin system causes some of the spins to change from a low-energy state to a high-energy state.

tion, which allows the precession of the spins within the volume to be visible. Because the net magnetization is the sum of the magnetic moments of all the individual spins, the net magnetization will naturally precess at the same characteristic frequency as that of the individual spins, the Larmor frequency.

Excitation of a Spin System and Signal Reception

Remember that any spin can take either a high-energy state or a low-energy state within a magnetic field (Figure 3.10A). A spin in the low-energy state can jump to the high-energy state by absorbing an amount of energy equivalent to the energy difference between the two states. So transitions between these two states can be triggered by the delivery of energy to the spin system. In MRI, that energy is delivered in the form of radiofrequency pulses. Radiofrequency coils within the MRI scanner bombard spins in the magnetic field with photons, which are actually electromagnetic waves that are adjusted to oscillate at the resonant frequency of the nucleus of interest (e.g., for hydrogen nuclei, the resonant frequency is around 42 MHz per Tesla of static magnet field). The delivery of this energy changes the distribution of spins between the high-energy and low-energy states, with the net effect of favoring transitions from the more abundant state to the less abundant state (i.e., typically, from low to high energy). The process of providing radiofrequency energy to atomic nuclei, so that some spins change from low- to high-energy states, is known as **excitation** (Figure 3.10B).

If the electromagnetic waves are delivered continuously, an increasing proportion of the spins will have jumped to the higher energy state, eventually reaching a point where there are equal numbers of spins in each state. Once that occurs, there is no net magnetization along the longitudinal direction: the original longitudinal magnetization (and the associated energy) has been fully transferred into the transverse plane. The amount of electromagnetic energy that is exactly sufficient to generate equal numbers of nuclei in each energy

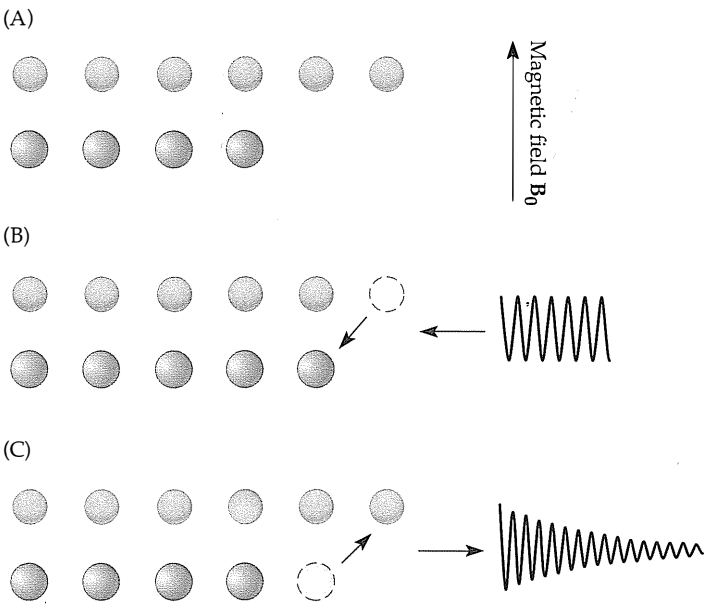

Figure 3.10 Change between states due to absorption or transmission of energy. (A) When spins are placed in an external magnetic field, more will be at the low-energy state (orange) than at the high-energy state (blue). (B) If an excitation pulse (represented in the figure by a wavy black line) with the right amount of energy is applied, some spins will absorb that energy and jump to the high-energy state. (C) After the excitation pulse ceases, some of the spins in the high-energy state will return to the low-energy state, releasing the absorbed energy as a radiofrequency wave with the same frequency as the excitation pulse (i.e., the resonant frequency). The amount of released energy diminishes over time, as indicated by the black line in the figure.

state is known as the 90-degree excitation pulse. This term reflects the classical mechanics perspective of tipping the net magnetization from the longitudinal axis over into the transverse plane, or rotating the vector through 90 degrees. As will be discussed later in this chapter, the measurable MR signal is greatest (and thus imaging is most efficient) when the net magnetization precesses within the transverse plane.

If the electromagnetic waves are left on even longer, beyond the duration needed for a 90-degree excitation pulse, the rate of the spin transitions will slow down as more spins accumulate at the higher energy state. Even so, the number of higher energy spins will continue to grow until the proportions of energy states within the system reach the exact opposites of the original proportions. At this point there are as many high-energy nuclei following excitation as there were low-energy nuclei before excitation. The amount of electromagnetic energy that is exactly sufficient to reverse the numbers of high- and low-energy nuclei, and thus flip the net magnetization vector, is known as the 180-degree excitation pulse. While not typically used to measure fMRI signals, 180-degree excitation pulses are important for increasing contrast on some types of anatomical MR images (see Chapter 5).

Delivering still more electromagnetic energy will cause the spin system to reverse its behavior, such that the proportion of high-energy nuclei will again become lower. If the electromagnetic pulse is left on long enough, enough nuclei will change to the low-energy state that the spin system will return to its original character. Thus, as long as electromagnetic energy is delivered to a spin system, the relative proportions of high- and low-energy spins will change in a predictable, if not always intuitive, manner.

When the electromagnetic waves (radiofrequency pulses) are turned off, the excitation of the atomic nuclei stops. Since excitation has disrupted the thermal equilibrium by creating more high-energy spins than would normally be present, the excess spins at the higher-energy level must return to the lower level (Figure 3.10C), so that equilibrium can be restored. When these high-energy spins fall back to the low-energy state, they emit photons whose energy is equal to the energy difference between the two states (i.e., energy corresponding to the Larmor frequency). Considered from a classical mechanics perspective, the precession of the net magnetization in the transverse plane leads to an electromagnetic oscillation at the Larmor frequency. During this reception period, the changes in transverse magnetization can be detected using a radiofrequency coil tuned to the Larmor frequency. Because the frequencies of excitation and reception are identical (i.e., both at the Larmor frequency), the same radiofrequency coil is often used for both processes. The changing current in these detector coils constitutes the MR signal.

The critical concept underlying excitation and reception is that of the change in net magnetization from the longitudinal axis to the transverse plane. When the net magnetization is along the longitudinal axis, the individual spins' precession cannot be measured in detector coils. But when the net magnetization is tipped into the transverse plane via excitation, its precession can generate an oscillating electric current in reception coils within the scanner.

Relaxation Mechanisms of the MR Signal

The MR signal detected through receiver coils does not remain stable forever. It changes in two ways during signal reception: the transverse magnetization quickly loses coherence, and the longitudinal magnetization slowly recovers.

90-degree excitation pulse A quantity of electromagnetic energy that, when applied to a spin system during MR excitation, results in equal numbers of nuclei in the low- and high-energy states.

180-degree excitation pulse A quantity of electromagnetic energy that, when applied to a spin system during MR excitation, results in a flipping of the usual net magnetization, such that there are now more nuclei in the high-energy state than in the low-energy state.

reception The process of receiving electromagnetic energy emitted by a sample at its resonant frequency (also called detection). As spins return to a low-energy state following the cessation of the excitation pulse, they emit energy that can be measured by a receiver coil.

MR signal The current measured in a detector coil following excitation and reception.

relaxation A change in net magnetization over time.

transverse relaxation (or spin–lattice relaxation) The loss of net magnetization within the transverse plane due to the loss of phase coherence of the spins.

longitudinal relaxation (or spin–spin relaxation) The recovery of the net magnetization along the longitudinal direction as spins return to the parallel state.

T_2 (decay) The time constant that describes the decay of the transverse component of net magnetization due to accumulated phase differences caused by spin–spin interactions.

T_2* (decay) The time constant that describes the decay of the transverse component of net magnetization due to both accumulated phase differences and local magnetic field inhomogeneities. T_2* is always shorter than T_2. BOLD-contrast fMRI relies on T_2* contrast.

T_1 (recovery) The time constant that describes the recovery of the longitudinal component of net magnetization over time.

Together, these changes in the MR signal are called **relaxation**. The change in transverse magnetization is termed **transverse relaxation** (or transverse decay), while the longitudinal change is known as **longitudinal relaxation** (or longitudinal recovery). The parameters governing these two types of relaxation differ across tissues, and this allows a single MRI scanner to collect many types of images.

After spin excitation, the net magnetization is tipped from the longitudinal axis into the transverse plane. Because the net magnetization reflects the vector sum of many individual spins, its amplitude depends on the coherence between those spins, being greatest when they all precess at the same phase and with the same frequency. But over time, the spins lose coherence. Spatially proximate spins may interact like bumper cars on a track, causing some spins to precess at higher frequencies, and some lower. The differences in precession frequencies cause spins to get out of phase with each other, which lead to an exponential decay in the MR signal that is described by a time constant called T_2. Furthermore, any spatial inhomogeneities in the magnetic field will cause different spins to experience different magnetic fields over time, again causing some to precess more rapidly than others. This effect is additive to that of T_2 decay, and the combined effects of spin–spin interactions and magnetic field inhomogeneities is described by the time constant T_2*. As a result of T_2* decay, spins lose coherence relatively quickly (typically within a few tens of milliseconds), resulting in a diminishing net magnetization in the transverse plane (Figure 3.11).

Following excitation, some of the energy of the spin system is emitted as radiofrequency waves that can be detected by receiver coils or antennae as the MR signal. As the spin system loses energy, it recovers back to the same state it was in before the excitation—with the net magnetization aligned along the longitudinal axis (Figure 3.12). The longitudinal recovery is relatively slow, typically on the order of a few hundreds of milliseconds to a few seconds, and is described by the time constant T_1 recovery.

While the T_1 and T_2 relaxations begin simultaneously, their time constants are often very different (T_1 is usually about one order of magnitude larger than T_2) and vary according to the type of tissue that is present. For practical purposes, they can be considered to contribute independently to the MR signal. Depending on when an image is acquired during the relaxation process, either

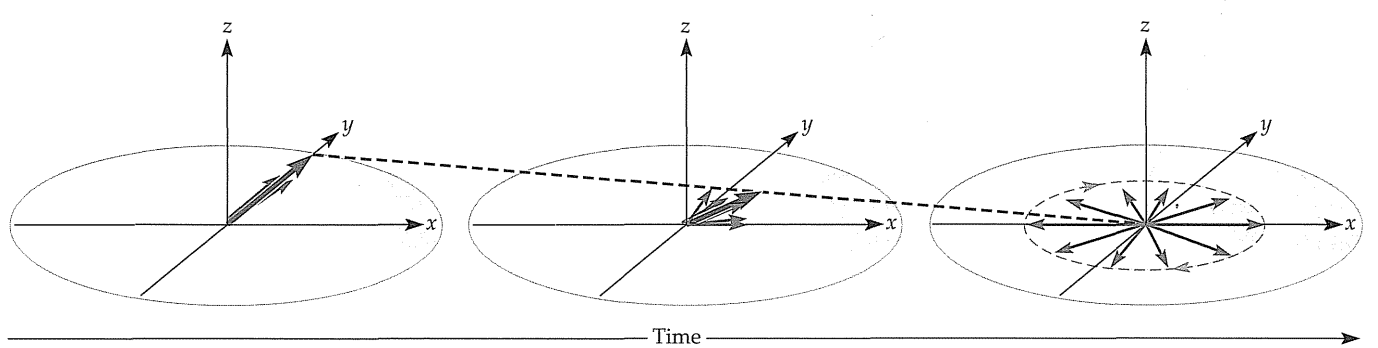

Figure 3.11 A conceptual overview of T_2 decay. After the net magnetization has been tipped into the transverse plane, it rapidly decays because of a loss of coherence among the spins. For most types of tissue, the net magnetization available to generate the MR signal decays to near zero within a few hundred milliseconds (red dashed line).

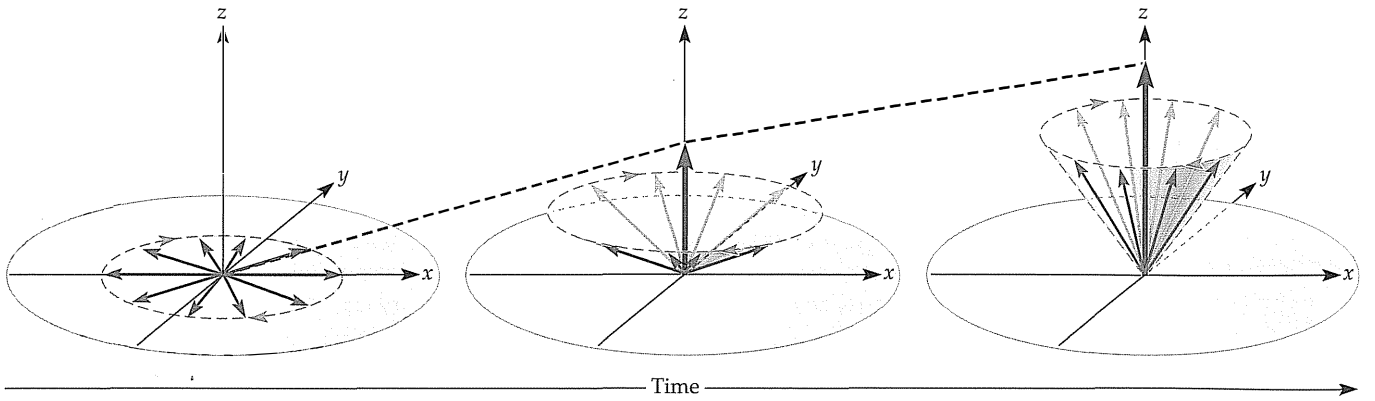

Figure 3.12 A conceptual overview of T_1 recovery. The net magnetization tips into the transverse plane as a result of the absorption of energy by some spins (i.e., those that have changed from low- to high-energy states). Once the excitation pulse ceases, spins begin to release energy back into the surrounding environment. This causes the net magnetization to recover along the longitudinal axis, often returning to near its original amplitude within a few seconds (red dashed line).

T_1 or T_2 (or a combination) will determine the amplitude of the recovered MR signal, and thus the intensity of the image. By choosing appropriate imaging parameters, different tissues (e.g., gray or white matter) will correspond to different intensities, so that investigators can differentiate between them for diagnostic or research purposes. In addition, the speed of T_1 recovery influences the rate at which images can be collected, because T_1 recovery renews the longitudinal magnetization so that it can be excited again.

Conceptual Summary of MR Signal Generation

MR signal generation depends on very simple physical principles. Because of thermal energy, atomic nuclei with the NMR property have an intrinsic characteristic called spin. When placed in a strong magnetic field, these nuclei precess (or wobble) around an axis that is either parallel to the magnetic field (low-energy) or antiparallel to the magnetic field (high-energy). Usually, more nuclei (or spins) take the low-energy state, resulting in a net magnetization parallel to the magnetic field (i.e., longitudinal magnetization). If energy is applied to the nuclei at a particular frequency known as the resonant frequency, some low-energy nuclei will absorb energy from the system and change to the high-energy state, effectively converting the longitudinal magnetization into transverse magnetization. This is known as excitation. Once the energy source is removed, some nuclei will return to the low-energy state by releasing that energy, which restores the longitudinal magnetization. The emitted energy provides the MR signal data that go into our images. The recording of the MR signal is known as reception. The changes in the MR signal over time are known as relaxation, of which there are two types: recovery of the longitudinal magnetization (T_1*) and decay of the transverse magnetization (T_2). By specifying a pulse sequence that targets one of these relaxation parameters, images can be collected that are sensitive to specific properties of the underlying tissue.

Quantitative Path

For those who are mathematically inclined or who simply want to become more informed users of fMRI, this path elaborates the details of MR signal generation with the necessary equations. These equations are helpful for clarifying the key concepts and providing a quantitative analysis of the amount of MR signal measured under different conditions. Most of the discussion relies on simple algebra, and where calculus is necessary we have included additional explanations.

The concepts presented here can be described in terms of either quantum or classical mechanics. However, for macroscopic phenomena, these two views are fundamentally equivalent. Because the quantitative aspects of MR signal generation can be better visualized using concepts from classical mechanics, we will use the notation and descriptions from classical mechanics in this section.

Common Terms and Notations

To ground our description of the MR signal generation process, we first introduce a few common terms and their notations. A scalar is a quantity representing the magnitude of some property. Properties like mass, charge, length, and area are represented by scalars. Scalars may have units; for example, the mass of a person may be 70 kg. Scalars are indicated in italicized type (e.g., M is the amount of net magnetization). A vector is a quantity or phenomenon in which both magnitude and direction are stated. Examples of vectors include force, velocity, momentum, and electromagnetic fields. Vectors are denoted by boldface type (e.g., $\mathbf{M}$ is the net magnetization vector). Because vectors are directional, the rules for manipulation of vectors are different from those for adding and multiplying scalar numbers.

The dot product, also called the scalar product, of two vectors is a scalar quantity obtained by summing the products of the corresponding components. Consider the two-dimensional vectors $\mathbf{A}$ and $\mathbf{B}$, which can each be represented by the sum of vectors along the x- and y-dimensions. The dot product of A and B is given by $\mathbf{A} \bullet \mathbf{B} = |\mathbf{A}|\ |\mathbf{B}| \cos\theta$, where $|\mathbf{A}|$ and $|\mathbf{B}|$ are the magnitudes of $\mathbf{A}$ and $\mathbf{B}$ and θ is the angle between the two vectors when they are placed tail to tail. The dot product may only be performed for pairs of vectors that have the same number of dimensions.

The cross product, or vector product, of two vectors produces a third vector that is perpendicular to the plane in which the first two lie. The value of the cross product of vectors A and B may be defined by $|\mathbf{A} \times \mathbf{B}| = |\mathbf{A}|\ |\mathbf{B}| \sin\theta$, where $|\mathbf{A}|$ and $|\mathbf{B}|$ are the magnitudes of $\mathbf{A}$ and $\mathbf{B}$ and θ is the angle between the two vectors. The orientation of the cross product may be determined using the right-hand rule. As one's fingers curl through an angle θ from $\mathbf{A}$ to $\mathbf{B}$, the cross product, or the thumb, points toward the vector perpendicular to the plane defined by $\mathbf{A}$ and $\mathbf{B}$. The magnitude of the cross product is equal to the area of the parallelogram defined by the two vectors. If the components of vectors $\mathbf{A}$ and $\mathbf{B}$ are known, then the components of their cross product, $\mathbf{C} = \mathbf{A} \times \mathbf{B}$, may be expressed as:

$$\mathbf{C}_x = \mathbf{A}_y\mathbf{B}_z - \mathbf{A}_z\mathbf{B}_y$$
$$\mathbf{C}_y = \mathbf{A}_z\mathbf{B}_x - \mathbf{A}_x\mathbf{B}_z$$
$$\mathbf{C}_z = \mathbf{A}_x\mathbf{B}_y - \mathbf{A}_y\mathbf{B}_x$$

scalar A quantity that has magnitude but not direction. Scalars are italicized in this text.

vector A quantity with both magnitude and direction. Vectors are in boldface in this text.

dot product The scalar product of two vectors. It is created by summing the products along each dimension.

cross product The vector product of two vectors. Its direction is perpendicular to the plane defined by those vectors and its magnitude is given by multiplying their product times the sine of the angle between them.

Nuclear Spins

Not all nuclei can be used to generate MR signals. For a nucleus to be useful for MRI, it must have both a magnetic moment and an angular momentum. In nuclei with odd numbers of protons (or sometimes odd numbers of neutrons), it is not possible to distribute either the electric charge or the atomic mass evenly. As such, these nuclei have the NMR property and can be detected using MRI. A few nuclei that are often used for MRI include ^{1}H, ^{13}C, ^{19}F, ^{23}Na, and ^{31}P. All these NMR-property nuclei are generally referred to as spins, and a collection of nuclei in a particular spatial location is known as a spin system. Because of the natural abundance of water and therefore hydrogen nuclei (^{1}H) in biological systems, hydrogen is the most commonly used nucleus for MRI. Hence, we will use the hydrogen nucleus, which is a single proton, in the following discussion of spins.

NMR property A label for atomic nuclei that have both a magnetic moment and angular momentum, which together allow them to exhibit nuclear magnetic resonance effects.

spins Atomic nuclei that possess the NMR property; that is, they have both a magnetic moment and angular momentum.

spin system A collection of atomic nuclei that possess the NMR property within a spatial location.

magnetic moment (μ) The torque (i.e., turning force) exerted on a magnet, moving electrical charge, or current-carrying coil when it is placed in a magnetic field.

torque A force that induces rotational motion.

Magnetic Moment

A proton can be visualized as a small sphere with a positive charge distributed over its surface. Because of thermal energy, the proton rotates at a high speed about its axis. The proton's rotation produces a current that in turn generates a small magnetic field, whose strength is known as the magnetic moment and is denoted as $\boldsymbol{\mu}$. Any moving magnet, current-carrying coil, or moving charge has a magnetic moment, which can be quantified as the ratio between the maximum torque on the magnet, coil, or charge exerted by an external magnetic field and the strength of the external field (B). Magnetic moments are measured in "Amperes times meters squared", or Am^2. To provide a visual representation of magnetic moment, we consider a simple rectangular current loop [length (L), width (W), and current level ($\mathbf{I}$)] within a magnetic field (Figure 3.13). Note that a spin will trace a circular loop through the magnetic field, so the rectangular loop is just a convenient simplification. The force ($\mathbf{F}$) exerted on the segment of wire with length (L) within the magnetic field ($\mathbf{B}$) is defined by Equation 3.1a:

$$\mathbf{F} = \mathbf{I} \times \mathbf{B}\, L \tag{3.1a}$$

The maximum force (F_{max}) exerted on the segment of wire occurs when it is perpendicular to the magnetic field, with its quantity given as:

$$F_{max} = IBL \tag{3.1b}$$

Put simply, force is proportional to the strength of the magnetic field (B) and the strength of the current (I). If the magnetic field strength increases, the force will also increase. The effect of this force on objects in the field is to cause them to rotate; the rotational force is known as torque. Thus, torque can be thought of as the change in rotational momentum over time. The maximum torque (τ_{max}) exerted by the magnetic field is given by multiplying the maximum force exerted on the current element by its width. We can account for all wire segments in the current element, or loop, by replacing the length of one segment with the length and width of the loop, which effectively can be replaced by the area (A) of the loop:

$$\tau_{max} = IBLW = IBA \tag{3.2}$$

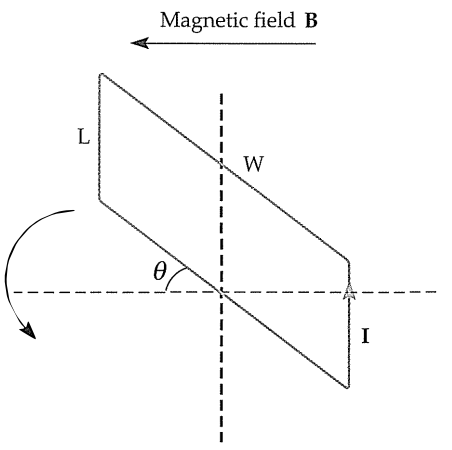

Figure 3.13 Torque on a current loop. A rectangular current loop ($W \times L$) with electric current ($\mathbf{I}$) would experience a torque if placed within a magnetic field $\mathbf{B}$ at an angle θ.

Since the magnetic moment $\boldsymbol{\mu}$ is defined as the maximum torque divided by the magnetic field strength (B), its magnitude μ can now be represented as the product of the current and the area of the current loop:

$$\mu = \frac{\tau_{\max}}{B} = IA \tag{3.3}$$

Note that the direction of the magnetic moment vector is defined by the right-hand rule based on the flow direction of the current. For a single proton in a strong magnetic field, this direction is generally parallel to the main axis of the magnetic field.

Angular Momentum

Because the proton also has mass, its rotation produces an angular momentum, often denoted as **J**. Angular momentum is a vector that defines the direction and amount of angular motion of an object. It changes in the presence of an external torque, but is conserved in the absence of external torques. Quantitatively, the angular momentum is defined as the product of the mass (m), the angular velocity ($\boldsymbol{\omega}$), and the radius (r) squared:

$$\mathbf{J} = \mathrm{m}\,\boldsymbol{\omega} r^2 \tag{3.4}$$

Since angular momentum is also a vector, its direction is defined by the right-hand rule based on the direction of rotation. The vectors defining the current flow and rotation have the same direction, so there should exist a scalar factor between the magnetic moment and angular momentum. This scalar factor is denoted as γ, such that:

$$\boldsymbol{\mu} = \gamma \mathbf{J} \tag{3.5}$$

It is important to recognize that Equation 3.5 merely states that the magnetic moment (from the rotating charge of the proton) and the angular momentum (from the rotating mass of the proton) have the same direction, with one larger than the other by an unknown factor γ.

To understand what γ represents, let's consider the simplest atomic nucleus, a single proton. First we must make some assumptions, namely that the charge (q) of the proton is an infinitely small point source, the proton rotates about a radius (r), and its rotation has a period (T). From Equation 3.3, we know that the amount of magnetic moment of a moving charge is given by multiplying two properties, the size of the current and the area of the loop it traverses. The former is simply the charge of the proton divided by the time it takes to move around the loop, while the latter is the area of the circle given by its radius r, or πr^2:

$$\mu = IA = \frac{q}{T}\pi r^2 \tag{3.6}$$

We also know that the angular velocity of the proton is equal to the radians of a circle (2π) divided by the time it takes to go around the circle (T). Substituting these values into Equation 3.4, we get the equation for the amount of J:

$$J = m\omega r^2 = m\frac{2\pi r^2}{T} \tag{3.7}$$

Substituting Equations 3.6 and 3.7 into Equation 3.5, it can be derived that:

$$\gamma = \frac{\mu}{J} = \frac{\frac{q}{T}\pi r^2}{m\frac{2\pi r^2}{T}} = \frac{q\pi r^2}{2m\pi r^2} = \frac{q}{2m} \tag{3.8}$$

The final form of this equation is elegant in its simplicity. What Equation 3.8 demonstrates is that the scaling factor (γ) depends only on the charge (q) and mass (m) of the proton. Since the charge and mass of the proton (or any other atomic nucleus) never change, the scaling factor (γ) is a constant for a given nucleus, regardless of the magnetic field strength, temperature, or any other factor. The constant (γ) is known as the gyromagnetic ratio, and is critical for MRI.

In reality, the magnetic moment and angular momentum of a proton cannot be modeled by assuming a simple point charge engaged in circular motion. A proton has a mass of about 1.67×10^{-27} kg and a charge of about 1.60×10^{-19} coulombs so the estimated value of γ is 4.79×10^7 radian/T. However, researchers have determined by experimentation that the real value of γ for a proton is closer to 2.67×10^8 radian/T. Nevertheless, while Equation 3.8 provides only a very rough estimate of the gyromagnetic ratio, it does demonstrate that γ is a unique quantity for a given nucleus. The gyromagnetic ratio has also been measured for other common nuclei; it is 6.73×10^7 for ^{13}C, 2.52×10^8 for ^{19}F, 7.08×10^7 for ^{23}Na, and 1.08×10^8 for ^{31}P (all units in radians per Tesla).

gyromagnetic ratio (γ) The ratio between the charge and mass of a spin. The gyromagnetic ratio is a constant for a given type of nucleus.

parallel state The low-energy state in which an atomic spin precesses around an axis that is parallel to that of the main magnetic field.

antiparallel state The high-energy state in which an atomic spin precesses around an axis that is antiparallel (i.e., opposite) to that of the main magnetic field.

Spins in an External Magnetic Field

If a uniform external magnetic field is applied to proton spins (Figure 3.6), those protons will assume one of the two equilibrium positions: the parallel state (aligned with the magnetic field) or the antiparallel state (opposite to the magnetic field). In MRI, the convention is to refer to the direction along the main magnetic field $\mathbf{B}_0$ as the parallel state. Both states are at equilibrium, although the energy level of the spin in the parallel state is lower than its energy level in the antiparallel state, and hence the spin is more stable in the parallel state. Because the proton spin possesses both a magnetic moment and an angular momentum, it will wobble (or precess) about the direction of the external magnetic field, whether it is in the parallel or the antiparallel state.

Spin precession

Before we examine the effect of an external magnetic field on spin motion in any more detail, let's consider a simple analogy. If we place a magnetic bar that is not spinning into a static magnetic field at an angle θ, it will oscillate back and forth across the main field (Figure 3.14A). However, if the magnetic bar is spinning about its axis, it will wobble around this field instead of oscillating back and forth. This is what happens to atomic nuclei. Because a proton has both magnetic moment and angular momentum, it will wobble around the direction of the external magnetic field (Figure 3.14B). This motion, which we described earlier in the chapter, is known as precession. It is useful to determine the frequency of such precession for any spin used in MRI. In this section, we will derive the precession frequency for hydrogen nuclei in a magnetic field.

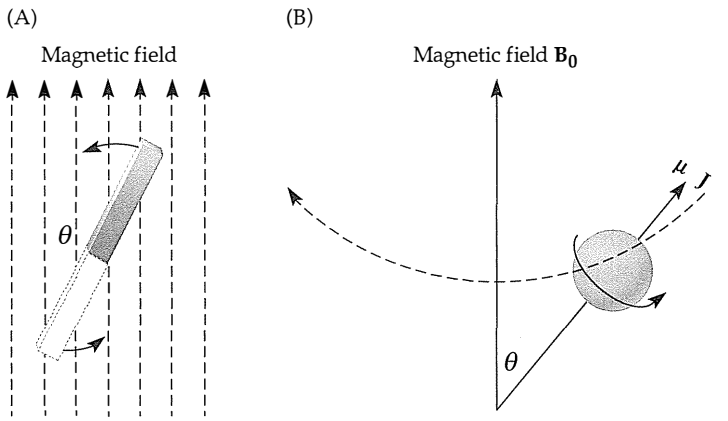

Figure 3.14 Movement within a magnetic field. (A) If a magnetic bar is placed in an external magnetic field, it will oscillate back and forth across the main axis of the field. (B) A spin within an external magnetic field ($\mathbf{B_0}$) has a magnetic moment (μ) and angular momentum (J) and thus will precess around the magnetic field. The cross product of μ and B_0 determines the precession direction. The symbol θ indicates the angle between the axis of spin and the direction of the external field.

A moving charge experiences maximum torque (τ_{max}) equal to the product of its magnetic moment (μ) and field strength (B), when its motion is perpendicular to the main magnetic field:

$$\tau_{\text{max}} = \mu B \tag{3.9}$$

However, if the moving charge is not perpendicular to the main magnetic field, but at some angle θ, then the amount of torque on that charge will be lessened. Specifically, only the component of the magnetic moment vector that is perpendicular to the static field contributes to the torque. Consistent with Figure 3.14B, the perpendicular component of the magnetic moment vector $\boldsymbol{\mu}$ is just $\mu \sin \theta$, since in a right-angled triangle, the sine of a given angle represents the length of the opposite side (the perpendicular component) divided by the length of the hypotenuse (the vector):

$$\tau = \mu B \sin \theta \tag{3.10a}$$

or, in vector form:

$$\boldsymbol{\tau} = \boldsymbol{\mu} \times \mathbf{B} \tag{3.10b}$$

As we use $\mathbf{B_0}$ to denote the main external magnetic field used for MRI, we get:

$$\boldsymbol{\tau} = \boldsymbol{\mu} \times \mathbf{B_0} \tag{3.10c}$$

This means that the torque on the spin's magnetic moment is given by the cross product of the magnetic moment and the main field. Recall also that since torque indicates the change in angular momentum over time, it can be defined as the derivative of angular momentum over the derivative of time:

$$\boldsymbol{\tau} = \frac{d\mathbf{J}}{dt} \tag{3.11}$$

where d is the mathematical symbol indicating change such that $d\theta$ represents the change of θ. Replacing $\boldsymbol{\tau}$ in Equation 3.10c with its value from Equation 3.11, we obtain the following equation:

$$\frac{d\mathbf{J}}{dt} = \boldsymbol{\mu} \times \mathbf{B}_0 \tag{3.12}$$

From Equation 3.5 we learned that angular momentum **J** is equivalent to $\boldsymbol{\mu}/\gamma$, where the constant γ is the gyromagnetic ratio. Thus, there must be a similar generalized expression for how the magnetic moment changes under the main magnetic field, $\mathbf{B}_0$:

$$\frac{d\boldsymbol{\mu}}{dt} = \gamma(\boldsymbol{\mu} \times \mathrm{B}_0) \tag{3.13}$$

Equations 3.12 and 3.13 express in mathematical terms that the torque ($\boldsymbol{\mu} \times \mathbf{B}_0$) on a spin induces changes in the angular momentum and the magnetic moment of that spin over time.

Thought Question

Why does the torque on a spin cause precession? More generally, why does a spinning object precess around a central axis?

To solve for the precession frequency, we need to simplify the vector structure of Equation 3.13. We can do this by breaking down the magnetic moment $\boldsymbol{\mu}$, which is a vector, into its scalar components in three spatial dimensions. At time zero, the components along the three directions can be defined as μ_{x0}, μ_{y0}, and μ_{z0}. The total magnetic moment, $\boldsymbol{\mu}(0)$, is simply the sum of the three components. Here, **x**, **y**, and **z** are unit vectors along the three cardinal directions:

$$\boldsymbol{\mu}(0) = \mu_{x0}\mathbf{x} + \mu_{y0}\mathbf{y} + \mu_{z0}\mathbf{z} \tag{3.14}$$

So, we can transform Equation 3.13 into three separate scalar equations, representing three different dimensions:

$$\frac{d\mu_x}{dt} = \gamma\mu_y B_0 \tag{3.15a}$$

$$\frac{d\mu_y}{dt} = -\gamma\mu_x B_0 \tag{3.15b}$$

$$\frac{d\mu_z}{dt} = 0 \tag{3.15c}$$

We do not go through the entire derivation here, but the result can be summarized simply as follows. The change in the x-component of the magnetic moment at any point in time depends on the current y-component value; at extreme y-values, x changes quickly. The change in the y-component over time depends on the x-component in a similar way. The z-component of the magnetic moment never changes. While this set of equations may seem complex, it merely specifies that the magnetic moment will trace a circular path around the z-axis. As we have already learned, this circular motion is known as precession.

Solving the set of differential equations (3.15) is beyond the scope of this introduction and is left as an exercise for the interested student. The solution, given the initial conditions at time zero (i.e., $\mu_{x0}, \mu_{y0}, \mu_{z0}$), is given by the following equation:

$$\boldsymbol{\mu}(t) = (\mu_{x0}\cos\omega t + \mu_{y0}\sin\omega t)\mathbf{x} + (\mu_{y0}\cos\omega t - \mu_{x0}\sin\omega t)\mathbf{y} + \mu_{z0}\mathbf{z} \tag{3.16}$$

Larmor frequency The resonant frequency of a spin within a magnetic field of a given strength. It defines the frequency of electromagnetic radiation needed during excitation to make spins change to a high-energy state, as well as the frequency emitted by spins when they return to the low-energy state.

where **x**, **y**, and **z** are unit vectors along three spatial dimensions. The terms $\cos \omega t$ and $\sin \omega t$ indicate that magnetic moment precesses at angular velocity ω. Importantly, the angular velocity ω is given by γB_0, which is the Larmor frequency.

Energy Difference between Parallel and Antiparallel States

The net magnetization of a spin system is determined by the relative proportions of spins precessing in the parallel and, antiparallel states. Changing the energy states of some of the spins, therefore, will manipulate the net magnetization. To understand how this change can be effected, three concepts must be discussed: the energy difference between spin states, spin excitation, and signal reception.

To flip a spin from a low-energy (parallel) state to a high-energy (antiparallel) state, we must apply energy. The required energy, or work (W), can be calculated by integrating the torque over the 180-degree rotation angle during this flip:

$$W = -\int_0^{\pi} \tau d\theta = -\int_0^{\pi} \mu B sin\theta d\theta = -\mu B_0 \cos\theta \,|_0^{\pi} = 2\mu B_0 \tag{3.17}$$

where d is the mathematical symbol indicating change such that $d\theta$ represents the change of θ. In our analogy of a bar that can rotate around a pivot point, in order to rotate the bar from the hanging position to the balanced position we must exert a force (torque) for the entire rotation angle. Likewise, to change the spin state of a proton, we must apply enough torque to complete the total amount of work W. Note that W depends only on the magnetic moment μ and the magnetic field B_0. So if the field strength increases, more work will be required to change a spin from one state to another.

We can think of W as being equivalent to the energy difference between the states (ΔE). Remember that when a spin changes states it will either emit or absorb energy in the form of an electromagnetic pulse. The frequency v of this electromagnetic pulse is determined by the energy difference between the states, as given by the Bohr relation:

$$\Delta E = hv \tag{3.18}$$

where h is called Planck's constant. Combining Equations 3.17 and 3.18, we obtain:

$$v = \frac{\Delta E}{h} = \frac{2\mu}{h} B_0 \tag{3.19}$$

It was shown experimentally that the longitudinal component (i.e., along the magnetic field) of the angular momentum **J** of a proton is $\hbar/2$; where $\hbar = h/2\pi$. Thus the longitudinal magnetic moment can be calculated using Equation 3.5 to be:

$$\mu = \gamma \frac{\hbar}{2} = \gamma \frac{h}{4\pi} \tag{3.20}$$

Substituting the result of Equation 3.20 into Equation 3.19, we find that the frequency v of the electromagnetic pulse is equal to the gyromagnetic ratio divided by 2π and multiplied by the magnetic field strength:

$$\nu = \frac{2\mu}{h} B_0 = \mu \frac{2B_0}{h} = \gamma \frac{h}{4\pi} \frac{2B_0}{h} = \frac{\gamma}{2\pi} B_0 \tag{3.21}$$

Let us pause at this point to review what we know so far. First, a nuclear spin can be characterized by its magnetic moment and angular momentum, both of which are expressed as vectors with the same direction. The magnetic moment is larger than the angular momentum vector by a factor γ, which is known as the gyromagnetic ratio. Second, spins in a magnetic field can take one of two possible states, either a low-energy state parallel to the magnetic field or a high-energy state antiparallel to the magnetic field. To change from the low-energy state to the high-energy state, a spin must absorb electromagnetic energy. Conversely, when changing from a high- to a low-energy state, a spin emits electromagnetic energy. Third, Equation 3.21 demonstrates that the frequency of the absorbed or emitted electromagnetic energy depends only on the gyromagnetic ratio of the spin and the magnetic field strength. So, for any atomic nucleus in a magnetic field with a known field strength, we can calculate the frequency of electromagnetic radiation that is needed to make spins change from one state to another. This frequency ν is also quantitatively equal to the Larmor frequency. Note that although the quantities for angular velocity ω and frequency ν are directly related to each other, they are expressed in different units and differ by a constant factor of 2π : ω is measured in radians per second, while ν is measured in Hertz (Hz), or cycles per second.

You should recognize that $\gamma/2\pi$ in Equation 3.21 is a constant for a given nucleus, expressed in units of frequency divided by field strength. For hydrogen, its numerical value is 42.58 MHz/Tesla. So, for common MR scanners with field strengths of 1.5 T, the Larmor frequency for hydrogen is approximately 63.87 MHz. This frequency is within the radiofrequency band of the electromagnetic spectrum. If we place a human brain into a 1.5-T MR scanner and apply electromagnetic energy at 63.87 MHz, some of the hydrogen nuclei within that brain will change from a low-energy state to a high-energy state. This idea, that energy at a given frequency is needed for changing particular nuclei from one state to another, represents the cardinal principle of magnetic resonance.

The correspondence between ω and ν means that a single quantity, the Larmor frequency, governs two aspects of a spin within a magnetic field: the energy that the spin emits or absorbs when changing energy states and the frequency at which it precesses around the axis of the external magnetic field. This correspondence has important consequences for understanding MR signal generation. The change in energy state is a concept from quantum mechanics, in that spins can only take discrete energy levels with a fixed energy difference between them. The frequency of precession is a concept from classical mechanics, in that it describes the motion of a particle (e.g., proton) through space. Yet, because ω and ν represent the same quantity, these two perspectives, quantum and classical mechanics, are unified in describing MR phenomena. This unification allows us to visualize the quantum behavior of spins using classical mechanics, to derive the basic equations for MR signal generation.

Magnetization of a Spin System

We now have a fundamental and quantitative analysis of the spin properties of individual atomic nuclei in an external magnetic field. Using the equations

introduced so far, we can characterize the magnetic moment and angular momentum of a spin, quantify how spins change from a high-energy state to a low-energy state, and predict how spins precess through a magnetic field. However, while the properties of individual nuclei were of interest to Rabi and other early MR physicists, fMRI researchers are not interested in the behavior of a single atomic nucleus. Instead, we are interested in the characteristics of bulk matter within the human brain, which consists of many protons with potentially different properties. Again, because the most abundant nuclei in the human body are hydrogen nuclei, principally within water molecules, we will focus the subsequent discussion on hydrogen.

In the absence of a magnetic field, the spin axes of the nuclei in bulk matter are oriented in random directions, so that the net magnetization (i.e., the sum of all individual magnetic moments) is zero. Once the bulk matter is moved into a magnetic field, each magnetic moment must align itself in either the parallel or antiparallel state. We will refer to the parallel state as p and the antiparallel state as a, and denote the probability for a given nucleus to be found in the parallel state as P_p and the probability for it to be found in the antiparallel state as P_a. Each spin must be in one state or the other, with the sum of the probabilities being one. That is,

$$P_p + P_a = 1 \tag{3.22}$$

If the spins are evenly distributed between these two states, such that there are as many parallel spins as antiparallel spins, there will be no net magnetization. Fortunately for MRI, under normal conditions there are more parallel spins (in the more stable low-energy state) than antiparallel spins (in the high-energy state), and thus there will always be a net magnetization. The relative proportion of the two spin states depends on their energy difference (ΔE) and the temperature (T). This proportion can be determined using Boltzmann's constant, k_B (1.3806×10^{-23} J/K), which governs the probabilities of spin distribution under thermal equilibrium.

$$\frac{P_p}{P_a} = e^{\frac{\Delta E}{k_B T}} \tag{3.23}$$

Note that given the very small value of Boltzmann's constant, $\Delta E / k_B T$ will be much less than one under normal conditions. For very small exponents x, the exponential e^x can be approximated by $1 + x$. Thus, Equation 3.23 can be replaced by:

$$\frac{P_p}{P_a} \approx 1 + \frac{\Delta E}{k_B T} \tag{3.24}$$

Equation 3.24 is called the high-temperature approximation. By algebraically solving Equations 3.22 and 3.24, we obtain:

$$P_p - P_a = \frac{1 + \frac{\Delta E}{k_B T}}{2 + \frac{\Delta E}{k_B T}} - \frac{1}{2 + \frac{\Delta E}{k_B T}} = \frac{\frac{\Delta E}{k_B T}}{2 + \frac{\Delta E}{k_B T}} \approx \frac{\Delta E}{2 k_B T} \tag{3.25}$$

The quantity $P_p - P_a$ indicates how many more spins are parallel to the magnetic field than are antiparallel. Each of these spins contributes a magnetic moment with magnitude μ along the z-direction. Thus, the total magnetic moment, which is called the bulk magnetization or net magnetization, is simply this proportion multiplied by the number of protons per unit volume (n) times the magnetic

moment of each spin in the z-direction. The net magnetization is represented by the symbol **M**. (Here **z** is a unit vector in the z-direction.)

$$\mathbf{M} = (P_p - P_a)n\mu_z\mathbf{z} = \frac{\Delta E}{2k_B T} n\mu_z\mathbf{z} \tag{3.26}$$

At room temperature, the proportional difference between the numbers of hydrogen spins in the parallel and antiparallel states is 0.003% per Tesla, which is a very small amount. Note that the net magnetization is parallel to the main field (i.e., the z-direction) and that as long as the temperature remains unchanged it will not vary in amplitude. If the temperature increases, the net magnetization will decrease. Also, and more importantly, since the difference between the energy states, ΔE, increases proportionally with the strength of the main field, the net magnetization is also proportional to the main field strength. This is why using a strong magnetic field increases the amount of MR signal recorded.

While the net magnetization is initially aligned with the main magnetic field, its precession angle is 0° at equilibrium. When tipped away from this starting position by an excitation pulse, the net magnetization will precess around the main axis of the field, just like a single magnetic moment. We can describe the motion of the net magnetization, following an excitation pulse at time point $t = 0$, in three scalar equations as follows:

$$\frac{dM_x}{dt} = \gamma M_y B_0 \tag{3.27a}$$

$$\frac{dM_y}{dt} = -\gamma M_x B_0 \tag{3.27b}$$

$$\frac{dM_z}{dt} = 0 \tag{3.27c}$$

This equation group is nearly identical to Equation group 3.15, with the only difference being that here we are quantifying the net magnetization of a spin system (M) rather than the magnetic moment of a single spin (μ). The solution to this equation group, for net magnetization at a given point in time, is similar to that given in Equation 3.16:

$$\mathbf{M}(t) = M_{x0}(\mathbf{x}\cos\omega t - \mathbf{y}\sin\omega t) + M_{y0}(\mathbf{x}\sin\omega t + \mathbf{y}\cos\omega t) + M_{z0}\mathbf{z} \tag{3.28}$$

Here, M_{x0}, M_{y0}, and M_{z0} are initial conditions for the net magnetization. In summary, the net magnetization of bulk matter behaves similarly to the magnetic moment of a single spin, in that it precesses at the Larmor frequency around the axis of the main field. This suggests that we may be able to affect the motion of the net magnetization vector in the same way that we can affect the energy state of a single spin: by applying electromagnetic energy at the Larmor frequency. We demonstrate this in the next section.

Excitation of a Spin System and Signal Reception

Now we are ready to explore the concepts governing MR signal generation. To help visualize and subsequently quantify the generated signal, we will adopt a classical mechanics perspective that builds on the equations introduced so far.

Spin excitation

excitation The process of sending electromagnetic energy to a sample at its resonant frequency (also called transmission). The application of an excitation pulse to a spin system causes some of the spins to change from a low-energy state to a high-energy state.

laboratory frame The normal reference frame that is aligned with the magnetic field of the scanner.

By measuring the precession of the net magnetization of a spin system, we can discover some of its properties. For example, based on Equation 3.26 above, we can estimate the number of protons within a unit volume (i.e., proton density) based on the quantity n. But we cannot measure the net magnetization of a spin system directly. Therefore, we need to find an indirect approach that perturbs the spin system away from equilibrium and then measures the response of the system to that perturbation, as in the earlier analogy of lifting an unknown object to estimate its weight. This process is called spin excitation.

In a typical MRI experiment, the object sample to be imaged is placed within a strong, uniform magnetic field at the center of the scanner. We now know that the net magnetization of the sample precesses at the Larmor frequency. For hydrogen, the net magnetization oscillates around the main field vector approximately 64 million times per second, if the magnetic field of the scanner is 1.5 T. Because the magnetization rotates so rapidly, it is extremely difficult to change the magnetization with a single pulse of electromagnetic energy. Instead, energy is applied at a given frequency for an extended period of time. To understand the effect of frequency on an oscillating system, consider the example of a backyard swing set. If you apply energy at the swing's natural frequency by pushing each time the swing is in the same place, even very small pushes will help increase the velocity of the swing, and thereby increase the energy in the system. This phenomenon, where small applications of energy at a particular frequency can induce large changes in a system, is known as resonance. For similar reasons, MRI scanners use specialized radiofrequency coils to transmit an electromagnetic excitation pulse (B_1) at the spin precession (i.e., the Larmor) frequency, in order to exert torque on the spins and perturb them (Figure 3.15).

$$\mathbf{B}_1 = B_1\mathbf{x}\ \cos\omega t - B_1\mathbf{y}\sin\omega t \tag{3.29}$$

We are now ready to examine the effect of this electromagnetic pulse on the sample. Because both the spins and the field generated by the excitation pulse are rotating at the Larmor frequency, we can adopt a reference coordinate system that is also rotating at that frequency. For clarity, we will refer to the normal frame of reference that is aligned with the magnetic field of the scanner as the laboratory frame (Figure 3.16A) and the frame of reference rotat-

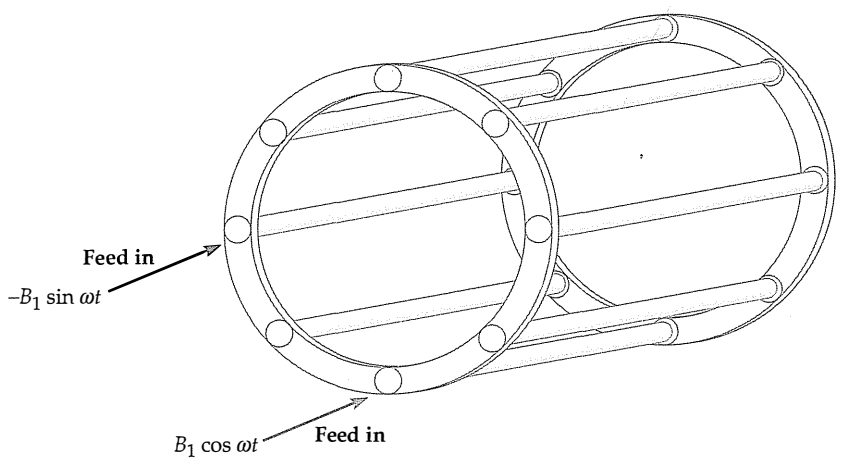

Figure 3.15 Generation of a rotating magnetic field. By driving the volume headcoil using two currents that are out of phase with each other, each fed into a separate part of the circuit, the MR scanner generates a rotating electromagnetic field that allows for efficient excitation at the resonant frequency (i.e., in the radiofrequency range).

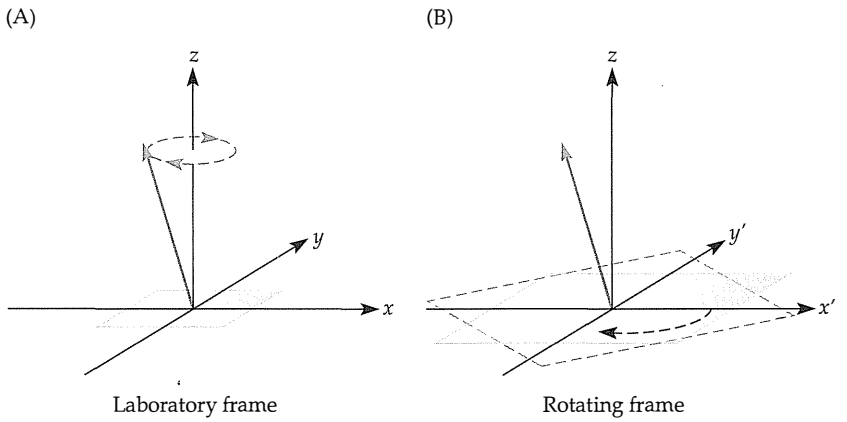

Figure 3.16 Laboratory and rotating reference frames. (A) In the laboratory frame, the magnetization rotates at a given frequency about the main axis (oriented in the z-direction). (B) If a rotating frame ($x' - y'$) is adopted, that spins the transverse plane (the $x - y$ plane) at the same frequency as the magnetization, the magnetization will appear stationary.

ing at the Larmor frequency as the rotating frame (Figure 3.16B). Imagine that you are watching some children ride on a carousel. The laboratory frame is analogous to the situation in which you stand on the ground outside the carousel, watching the children ride around. The rotating frame corresponds to the situation if you get on the carousel and watch the children as you spin around with them. In the latter case, the children will appear stationary, since your rotation speed matches theirs. The unit vectors in the transverse plane within the rotating frame are represented by $\mathbf{x}'$ and $\mathbf{y}'$ and correspond to the following unit vectors in the laboratory frame:

rotating frame A reference frame that rotates at the Larmor frequency of the spin of interest. The rotating frame is adopted to simplify mathematical descriptions of the effects of excitation.

on-resonance excitation The presentation of an excitation pulse at the resonant frequency of the sample, resulting in maximum efficiency.

$$\mathbf{x}' = \mathbf{x} \cos \omega t - \mathbf{y} \sin \omega t \tag{3.30}$$

$$\mathbf{y}' = \mathbf{x} \sin \omega t + \mathbf{y} \cos \omega t \tag{3.31}$$

Within the rotating frame, both the spins and the excitation pulse become stationary, making subsequent formulas much simpler. The net magnetization ($\mathbf{M}$) becomes a stationary quantity along the z-direction, while the excitation pulse ($\mathbf{B}_1$) can now be thought of as a stationary vector along the new x'-direction. We therefore would have:

$$\mathbf{M} = M_0\mathbf{z} \tag{3.32a}$$

$$\mathbf{B}_1 = B_1\mathbf{x}' \tag{3.32b}$$

To assess combined magnetization, Equation 3.13 can be rewritten as Equation 3.33, which states that the change in net magnetization over time is the vector product of the net magnetization and the excitation pulse. Similarly to Equation 3.13, this new equation implies that applying a torque ($\gamma \mathbf{M} \times \mathbf{B}$) to the net magnetization will rotate its direction over time:

$$\frac{d\mathbf{M}}{dt} = \gamma \mathbf{M} \times \mathbf{B} \tag{3.33}$$

Note that here the torque on the net magnetization depends on the total magnetic field $\mathbf{B}$ experienced by the spin system. However, this field is the sum of two magnetic fields, the static magnetic field $\mathbf{B}_0$ and the excitation pulse $\mathbf{B}_1$. The effect of the excitation pulse, when it is presented at the resonant frequency of the sample, or on-resonance, is a simple rotation of the net magnetization vector from the z-direction toward the transverse ($x - y$) plane. But if the pulse is

BOX 3.1 A Quantitative Consideration of the Rotating Reference Frame

The use of a rotating reference frame simplifies our interpretations of the change in net magnetization over time. However, this simplification masks some complex mathematical derivations. Here, we demonstrate the mathematical underpinnings of how net magnetization changes over time, so that readers can appreciate what is gained by changing to a rotating reference frame.

Expanding Equation 3.33 in the rotating frame results in the following equation, which illustrates how the magnetization vector changes over time in each direction:

$$\begin{aligned}\frac{d\mathbf{M}}{dt} &= \frac{d(\mathbf{x}'M_{x'} + \mathbf{y}'M_{y'} + \mathbf{z}'M_{z'})}{dt} \\ &= M_{x'}\frac{d\mathbf{x}'}{dt} + M_{y'}\frac{d\mathbf{y}'}{dt} + \mathbf{x}'\frac{dM_{x'}}{dt} + \mathbf{y}'\frac{dM_{y'}}{dt} + \mathbf{z}'\frac{dM_{z'}}{dt}\end{aligned} \tag{3.34}$$

Since it can be derived that:

$$\frac{d}{dt}\begin{pmatrix}\mathbf{x}' \\ \mathbf{y}'\end{pmatrix} = \begin{pmatrix}\omega\cdot(-\mathbf{x}\sin\omega t - \mathbf{y}\cos\omega t \\ \omega\cdot(\mathbf{x}\cos\omega t - \mathbf{y}\sin\omega t)\end{pmatrix} = \begin{pmatrix}\omega\cdot(-\mathbf{y}') \\ \omega\cdot(\mathbf{x}')\end{pmatrix} = -\omega\mathbf{z}\times\begin{pmatrix}\mathbf{x}' \\ \mathbf{y}'\end{pmatrix} \tag{3.35}$$

where $\omega\mathbf{z}$ indicates ω as a vector pointing along the z-direction. If we define the changing magnetization in the rotating frame as $\delta\mathbf{M}/\delta t$, in addition to the changing magnetization in the laboratory frame, $d\mathbf{M}/dt$, Equation 3.33 can be rewritten in the following form (Equation 3.36). It indicates that the net magnetization (in the laboratory frame) has two independent components: precession around the z-direction with frequency ω, and a rotation from the longitudinal to the transverse plane (within the rotating frame):

$$\frac{d\mathbf{M}}{dt} = -\omega\mathbf{z}\times\mathbf{M} + \frac{\delta\mathbf{M}}{\delta t} \tag{3.36}$$

By reorganizing Equation 3.36 and substituting Equation 3.33, we can describe a new quantity, $\mathbf{B}_{1\text{eff}}$, which depends on the frequency and amplitude of the applied $\mathbf{B}_1$ field. This quantity is the magnetic field that the spin system actually experiences, and it governs the behavior of the net magnetization within the rotating frame of reference:

$$\begin{aligned}\frac{\delta\mathbf{M}}{\delta t} &= \frac{d\mathbf{M}}{dt} + \omega\mathbf{z}\times\mathbf{M} = \gamma\mathbf{M}\times\mathbf{B} + \omega\mathbf{z}\times\mathbf{M} \\ &= \gamma\mathbf{M}\times(\mathbf{B} - \frac{\omega\mathbf{z}}{\gamma}) = \gamma\mathbf{M}\times\mathbf{B}_{1\text{eff}}\end{aligned} \tag{3.37}$$

off-resonance excitation The presentation of an excitation pulse at a frequency other than the resonant frequency of the sample, resulting in reduced efficiency.

$B_{1\text{eff}}$ The effective magnetic field experienced by a spin system during excitation.

presented at a slightly different frequency, so that it is off-resonance, its efficiency greatly decreases. While this loss of efficiency makes intuitive sense, its mathematical derivation is complex. The effective magnetic field experienced by the spin system is not just $\mathbf{B}_1$ but a new field called $B_{1\text{eff}}$ that is influenced by

both $\mathbf{B_1}$ and $\mathbf{B_0}$. For interested students, we have included the derivation of $\mathbf{B_{1eff}}$ within Box 3.1, and the conclusion is given in Equation 3.37.

Within the rotating frame, the change in the net magnetization over time, notated as $\delta\mathbf{M}/\delta t$, is determined by the quantity $\mathbf{B_{1eff}}$, not by $\mathbf{B_1}$ alone. The net magnetization rotates around the vector $\mathbf{B_{1eff}}$ during excitation:

$$\frac{\delta \mathbf{M}}{\delta t} = \gamma \mathbf{M} \times \mathbf{B}_{1\text{eff}} \tag{3.38}$$

The value of the effective excitation pulse ($\mathbf{B_{1eff}}$) is given by the following equation (derived from Equation 3.37), which has both longitudinal ($\mathbf{z}$) and transverse ($\mathbf{x'}$) components:

$$\mathbf{B}_{1\text{eff}} = \mathbf{z}(B_0 - \frac{\omega}{\gamma}) + \mathbf{x}' B_1 \tag{3.39}$$

If the excitation pulse ($\mathbf{B_1}$) is at the resonant frequency of the spin system, so that $\omega = \gamma B_0$, the term $(B_0 - \omega/\gamma)$ will be equal to zero. This means that if the excitation pulse is on-resonance, the net magnetization vector (in the rotating frame) will simply rotate around the $\mathbf{x'}$-component (Figure 3.17A) with an angular velocity ω_{rot} (Equation 3.40). Note that this equation nicely illustrates why γ is known as the gyromagnetic ratio, in that γ determines the rate at which an introduced magnetic field, in this case $\mathbf{B_1}$, causes a gyroscopic rotation of the net magnetization:

$$\omega_{rot} = \gamma B_{1\text{eff}} = \gamma B_1 \tag{3.40}$$

At this point, we want to pause and emphasize the critical importance of Equation 3.40. This equation tells us that the application of an electromagnetic field at the Larmor frequency will induce a rotation within the rotating frame of reference. This double rotation sounds complicated, but it is actually very simple (see Figure 3.17A). We can think of the rotation within the rotating frame as tipping the net magnetization vector downward from the longitudinal or z-direction into the transverse or $x' - y'$ plane. Within the laboratory frame, the net magnetization vector will follow a spiral path that combines the tipping motion from the rotating frame with precession at the Larmor frequency. This spiral motion in the laboratory frame is known as nutation (Figure 3.17B). The angle θ around which the net magnetization rotates following excitation is determined by the duration T of the applied electromagnetic pulse:

nutation The spiraling change in the precession angle of the net magnetization during an excitation pulse.

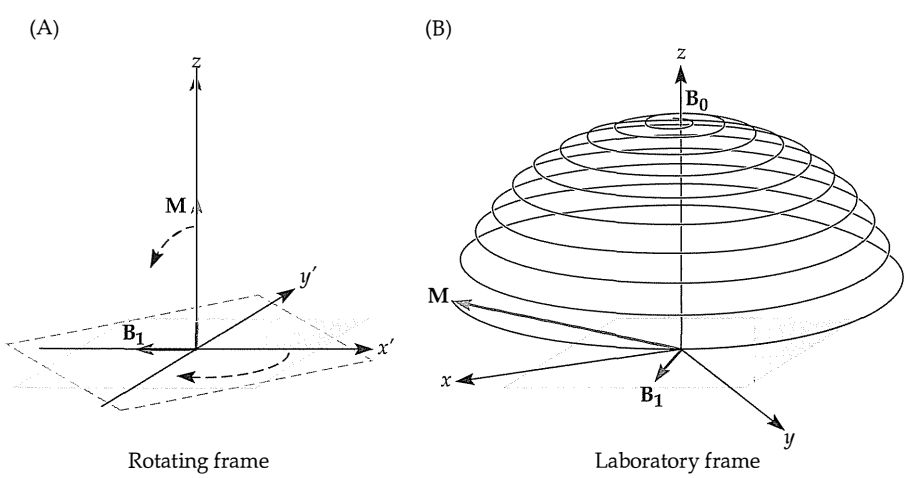

Figure 3.17 Spin nutation. The delivery of an excitation pulse ($\mathbf{B_1}$) causes the longitudinal magnetization ($\mathbf{M}$) to be tipped into the transverse plane. (A) In the rotating frame of reference, whose directions are represented by x' and y', this would look like a simple rotation downward (i.e., the longitudinal magnetization falls smoothly down to the transverse plane). (B) However, in the laboratory frame of reference, the longitudinal magnetization would trace out a complex wobbling path as it rotates downward to the transverse plane. This wobbling motion is known as nutation.

flip angle The change in the precession angle of the net magnetization following excitation.

$$\theta = \gamma B_1 T \tag{3.41}$$

This simple equation determines how long we must apply an electromagnetic field to change the net magnetization vector by an angle θ, called the **flip angle**. To change the net magnetization by 90 degrees, from along the main field to perpendicular with the main field, the excitation pulse should be presented for a brief period, on the order of milliseconds. Remember that when the net magnetization is entirely in the longitudinal direction, it is stable and does not change over time. Therefore, its amplitude is impossible to measure. But if we tip the net magnetization into the transverse plane with an excitation pulse, there will be large changes in its direction as it rotates. This changing magnetic field can be detected by external receiver coils. In short, by tipping the net magnetization we can create measurable MR signal.

Thought Question

What are the relative proportions of low-energy spins and high-energy spins following application of a 90-degree excitation pulse?

The concept of the $\mathbf{B}_{1\text{eff}}$ (see Equation 3.39) is also very important in understanding off-resonance excitation due to the application of an inhomogeneous field, which results in an actual rotation frequency that does not match the Larmor frequency for a spin system. As such, the difference between B_0 and ω/γ is not zero, which means that the excitation pulse would have a longitudinal component. Because the spins always rotate about the axis of $\mathbf{B}_{1\text{eff}}$, the effectiveness of the excitation pulse will be compromised. To understand the effects of off-resonance excitation, think of an extreme situation in which the excitation pulse has a **z**-component approaching the size of the main field, $\mathbf{B}_0$. As a result, the $\mathbf{B}_{1\text{eff}}$ would be aligned along the *z*-direction. In this case the $\mathbf{B}_{1\text{eff}}$ would have the same direction as the spins themselves, and would exert no torque on the spins. Thus, their angle of rotation would not change. In mathematical terms, the cross product between two vectors with the same direction is equal to zero. Consequently, an excitation pulse along the same direction as $\mathbf{B}_0$ would have absolutely no effect. If hardware problems with the scanner make the **z**-component of $\mathbf{B}_{1\text{eff}}$ sufficiently large, then full excitation may be impossible to achieve.

But what if $\mathbf{B}_{1\text{eff}}$ is only slightly off-resonance? The rotational trajectories of a perfectly on-resonance pulse and a slightly off-resonance pulse are illustrated in Figure 3.18. The on-resonance pulse has a more efficient trajectory, which reduces the duration of the pulse needed to tip the magnetization into the transverse plane. However, it is still possible to achieve full excitation using the off-resonance pulse. This full excitation comes at the cost of additional time (required to traverse the longer path to the transverse plane), and if the duration of the pulse is held constant, the excitation will be incomplete.

Thought Question

If the excitation pulse is only slightly off-resonance, it is still possible to reach full excitation, but if the pulse is considerably off-resonance, then full excitation cannot be reached. Based on what you have learned (and Figure 3.18), what is the threshold angle of $\mathbf{B}_{1\text{eff}}$ beyond which full excitation cannot be achieved?

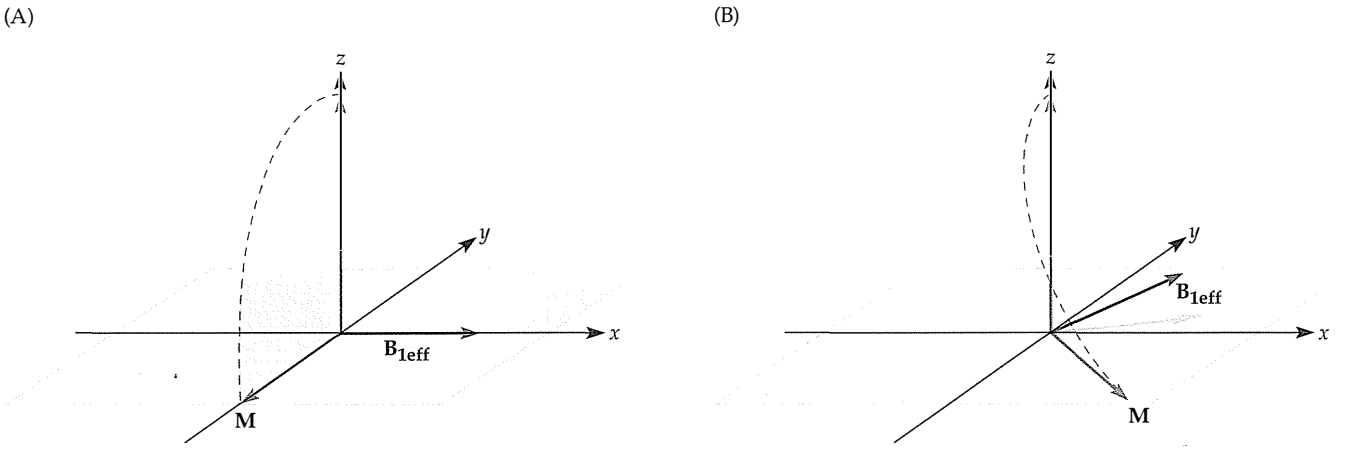

Figure 3.18 On-resonance and off-resonance excitation. (A) Application of an on-resonance excitation pulse will efficiently tip the longitudinal magnetization into the transverse plane (orange trajectory). (B) Application of an off-resonance excitation pulse will result in an inefficient trajectory that takes longer to completely tip the magnetization. The goal of excitation is to achieve full rotation of the magnetization from the longitudinal axis to the transverse plane.

Signal reception

So far, we have shown that an electromagnetic excitation pulse applied by a transmitter coil can change the net magnetization of a spin system. To measure this change, we need another receiver coil (or detector coil). Receiver coils acquire signal through the mechanism of electromagnetic coupling, as governed by Faraday's law of induction. After the magnetization of the sample is tipped to the transverse plane, its precession at the Larmor frequency sweeps across the receiver coil, causing the density of magnetic flux (Φ) experienced by the receiver coil to change over time (Figure 3.19). This change of flux, $d\Phi/dt$, in turn induces an electromotive force (emf) in the coil. By definition,

$$emf = -\frac{d\Phi}{dt} \tag{3.42}$$

where the magnetic flux penetrating the coil area is given by $\Phi = \int_S B \cdot dS$.

The measurement of electromotive force in a receiver coil is known as reception.

The excitation–reception process simulates the mutual coupling of two coils. Just as a current change in one coil induces a similar current change in another nearby coil through mutual inductance, magnetic field changes in a sample (e.g., the brain) induce magnetic field changes in the receiver coil. The volume magnetic flux generated by the sample and penetrating through the receiver coil can be represented as:

$$\Phi(t) = \int_S \overline{B}_1 \cdot M(t) dv \tag{3.43}$$

where $\overline{B}_1$ is the magnetic field per unit current of the receiver coil and $M(t)$ is the magnetization created by the sample.

electromotive force (emf) A difference in electrical potential that can be used to drive a current through a circuit. The MR signal is the electromotive force caused by the changing magnetic field across the detector coil.

reception The process of receiving electromagnetic energy emitted by a sample at its resonant frequency (also called detection). As spins return to a low-energy state following the cessation of the excitation pulse, they emit energy that can be measured by a receiver coil.

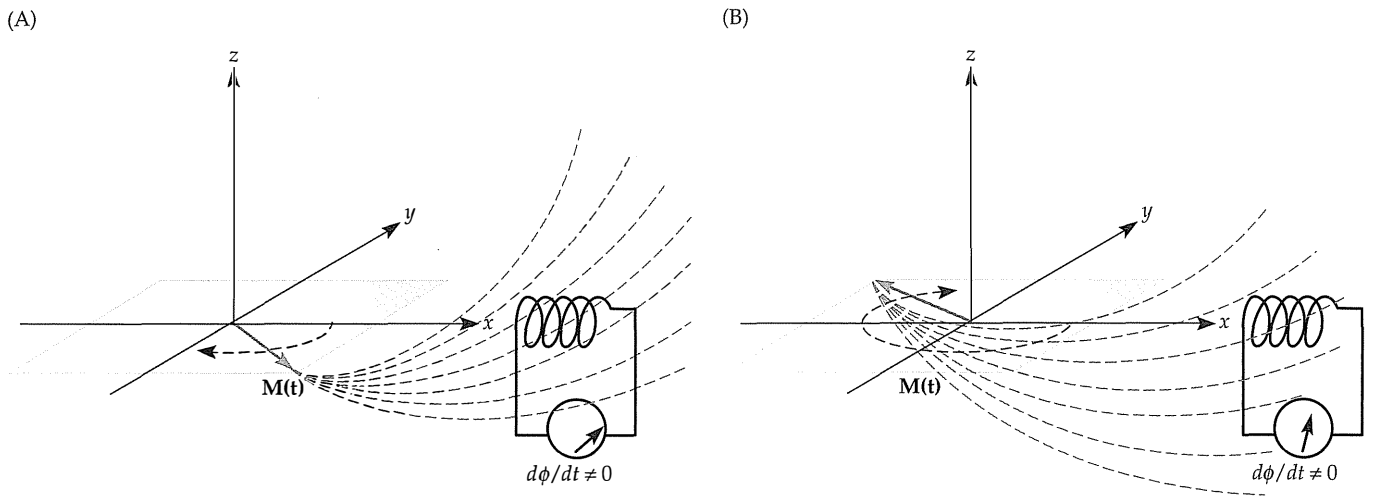

Figure 3.19 MR signal reception. As the net magnetization rotates through the transverse plane, the amount of magnetic flux experienced by the receiver coil changes over time (A and B). The changing flux generates an electromotive force, which provides the basis for the MR signal.

This relationship shows that the magnetic flux through the receiver coil actually depends on the magnetic field that could be produced by the coil. That is, the stronger the magnetic field that can be generated by a coil, the better its reception. Likewise, if a radiofrequency coil can generate a homogeneous magnetic field within a sample, it can also receive signals uniformly from the sample. This relationship is known as the principle of reciprocity.

Substituting Equation 3.43 into Equation 3.42, we get:

$$emf = -i\omega_0 \int_v \bar{B}_1 \cdot M(t)dv \tag{3.44}$$

The additional scaling factor ω_0 comes from taking the time derivative of $M(t)$, which contains the term $\omega_0 t$ (consult Equation 3.28).

Note that the electromotive force oscillates at the Larmor frequency, as do the excitation pulses, so that the receiver coil must be tuned to the resonant frequency to best measure the changes in MR signal. Since both M and ω_0 are proportional to the main field strength B_0, the measured electromotive force is proportional to B_0^2. Stated simply, the amount of MR signal received by the detector coil increases with the square of the magnetic field strength. Unfortunately, the amplitude of noise in the MR signal is proportional to the strength of the magnetic field, so the signal-to-noise ratio increases only linearly with B_0. The effects of field strength on signal and noise will be discussed in detail in Chapter 8.

principle of reciprocity The rule stating that the quality of an electromagnetic coil for transmission is equivalent to its quality for reception (i.e., if it can generate a homogeneous magnetic field at excitation, it can also receive signals uniformly).

Equation 3.44 also confirms that before the excitation pulse tips the net magnetization into the transverse plane, there is no detectable electromotive force and thus no MR signal. This is because when the net magnetization is in its original longitudinal direction, its amplitude and direction do not change, so there is no signal to be measured by the receiver coil (Figure 3.20). We emphasize that only changes in the transverse plane contribute to the MR signal.

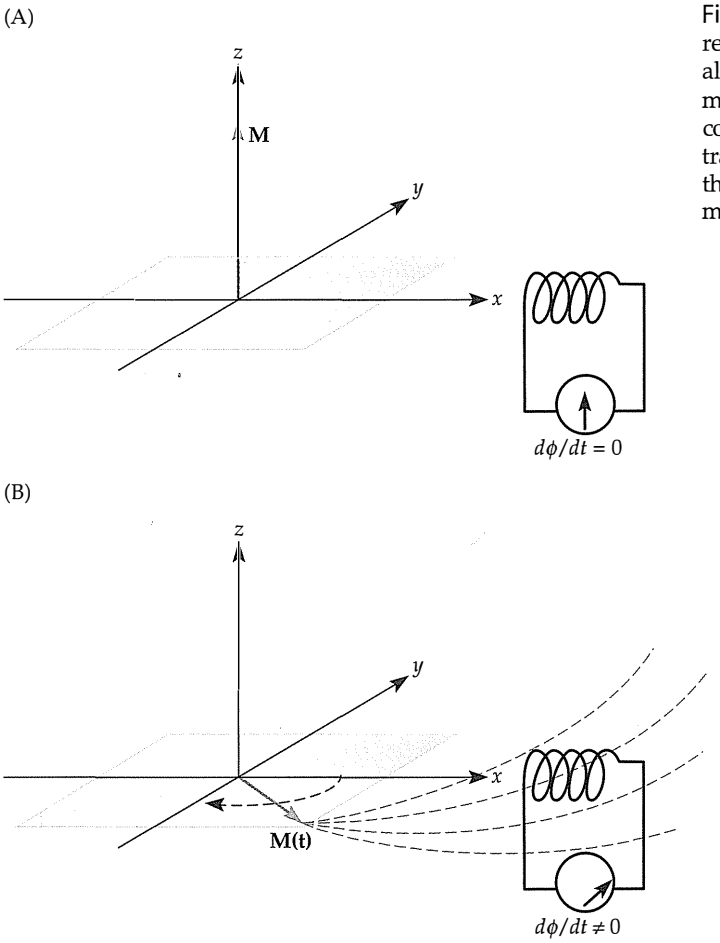

Figure 3.20 Effects of net magnetization orientation on the recorded MR signal. (A) When the net magnetization, **M**, is along the longitudinal axis, there is no detectable change in the magnetic field and thus no electromotive force in the detector coil. (B) After the net magnetization has been tipped into the transverse plane, its motion over time, **M(t)**, causes changes in the measured current within the detector coil. Magnetization must be in the transverse plane for detection using MR.

Relaxation Mechanisms of a Spin System

The MR signal that follows an excitation pulse does not last indefinitely; it decays over time, generally within a few seconds. This phenomenon is called spin relaxation. Two primary mechanisms contribute to the loss of the MR signal: longitudinal relaxation (Figure 3.21A) and transverse relaxation (Figure

relaxation A change in net magnetization over time.

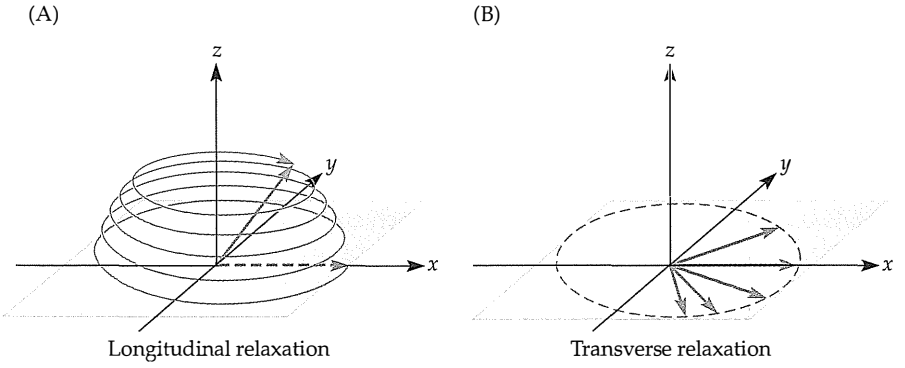

Figure 3.21 T_1 and T_2 relaxation. Schematic illustration of longitudinal relaxation, or T_1 recovery (A), and of transverse relaxation, or T_2 decay (B). The time constant T_1 governs the rate at which longitudinal magnetization recovers, while the time constant T_2 governs the rate at which transverse magnetization decays. Note that T_2* decay is similar to T_2 decay, except that it accounts for both spin–spin interactions (as in T_2) and local field inhomogeneities.

longitudinal relaxation (or spin–lattice relaxation) The recovery of the net magnetization along the longitudinal direction as spins return to the parallel state.

T_1 (recovery) The time constant that describes the recovery of the longitudinal component of net magnetization over time.

transverse relaxation (or spin–spin relaxation) The loss of net magnetization within the transverse plane due to the loss of phase coherence of the spins.

T_2 (decay) The time constant that describes the decay of the transverse component of net magnetization due to accumulated phase differences caused by spin–spin interactions.

3.21B). For a particular substance (e.g., water, fat, or bone) in a magnetic field of a given strength, the rates of longitudinal and transverse relaxation are determined by time constants that we introduce in this section. (We provide the mathematical derivation of these equations and its impact on MR signal in the next two chapters.)

When the excitation pulse is taken away, the spin system gradually loses the energy absorbed during the excitation. The simplest way to think about this energy loss is by using the quantum mechanics perspective. As they lose energy, spins in the high-energy (antiparallel) state go back to their original low-energy (parallel) state. This phenomenon is known as longitudinal relaxation, or spin–lattice relaxation, because the individual spins are losing energy to the surrounding environment, or lattice of nuclei. As increasing numbers of individual spins return to their low-energy state, the net magnetization returns to a direction that is parallel with the main field. From a classical mechanics point of view, the transverse magnetization gradually resumes the longitudinal direction, which it had before the excitation pulse. Because the total magnetization is constant, the growth in the longitudinal magnetization corresponds with a reduction in transverse magnetization and a smaller MR signal. The time constant associated with this longitudinal relaxation process is called T_1, and the relaxation process is called T_1 recovery. The amount of longitudinal magnetization, M_z, present at time t following an excitation pulse is given by Equation 3.45, where M_0 is the original magnetization.

$$\mathbf{M}_z = \mathbf{M}_0(1 - e^{-t/T_1}) \tag{3.45}$$

After the net magnetization is tipped into the transverse plane by an excitation pulse, it is initially coherent, in that all of the spins in the sample are precessing around the main field vector at about the same phase. That is, they begin their precession within the transverse plane at the same starting point. Over time, the coherence between the spins is gradually lost and they fall out of phase. This phenomenon is known as transverse relaxation. In general, there are two main causes for transverse relaxation, one intrinsic and the other extrinsic. The intrinsic cause is from spin–spin interaction: when many spins are excited at once, there is a loss of coherence due to their effects on one another. As an analogy, consider a single racing car driving rapidly around a track; the driver can adopt a high and constant speed because no other cars are present. But in a pack of many cars, the movement of one car influences the speed of the others, making it impossible for all the cars to maintain a constant high speed. Likewise, interactions among spins cause some to precess faster and some slower, causing the relative phases of the precessing spins to become increasingly dispersed over time. The signal loss by this intrinsic mechanism, which is irreversible, is called T_2 decay (Equation 3.46) and is characterized by the time constant T_2.

$$\mathbf{M}_{xy} = \mathbf{M}_0 e^{-t/T_2} \tag{3.46}$$

An extrinsic source of differential spin effects is the external magnetic field, which is usually inhomogeneous. Because each spin precesses at a frequency proportional to its local field strength, spatial variations in field strength cause spatial differences in precession frequencies. This also leads to a loss of coherence. Note that the loss of coherence caused by the lack of field homogeneity can be reversed with specialized pulse sequences, as will be discussed further in Chapter 5. The combined effects of spin–spin interaction and field inhomo-

geneity lead to signal loss known as T_2* decay, characterized by the time constant T_2*. Note that T_2* decay is always faster than T_2 decay alone, since it includes the additional factor of field inhomogeneity, and thus for any substance the time constant T_2* is always smaller than T_2. The equation for T_2* decay is similar to that for T_2 decay. We will discuss T_2* decay again in Chapters 5 and 7, because it plays a critical role in the BOLD contrast that we use for fMRI.

These relaxation processes constrain how much MR signal can be acquired following a single excitation pulse. Since transverse magnetization decays over a short period of time, there is a limited window within which MRI data can be collected. To acquire a very complex, high-resolution anatomical image, a sample must often receive a sequence of many excitation pulses to allow collection of all data points. The trade-offs between MR signal and acquisition time are discussed further in Chapter 5. It is important to realize that relaxation processes are not a problem for MRI, but instead they provide the capability for measuring different properties of matter. The versatility of MRI as an imaging tool results from its sensitivity to the different relaxation properties of tissues.

T_2* (decay) The time constant that describes the decay of the transverse component of net magnetization due to both accumulated phase differences and local magnetic field inhomogeneities. T_2* is always shorter than T_2. BOLD-contrast fMRI relies on T_2* contrast.

Bloch equation An equation that describes how the net magnetization of a spin system changes over time in the presence of a time-varying magnetic field.

The Bloch Equation for MR signal generation

The physical principles introduced in this chapter provide an overview of MR signal generation, including the establishment of net magnetization of a spin system within a magnetic field, excitation of those spins using electromagnetic pulses, reception of MR signal in detector coils, and relaxation of magnetization over time. Because these components are related, we can describe MR phenomena in a single equation, which is a modification of Equation 3.33 that includes the T_1 and T_2 effects:

$$\frac{d\mathbf{M}}{dt} = \gamma \mathbf{M} \times \mathbf{B} + \frac{1}{T_1}(\mathbf{M}_0 - \mathbf{M}_z) - \frac{1}{T_2}(\mathbf{M}_x + \mathbf{M}_y) \qquad (3.47)$$

Stated generally, the net magnetization vector of a spin system precesses around the main magnetic field axis at the Larmor frequency, with its change in the longitudinal or z-direction governed by T_1 and its change in the transverse plane governed by T_2. This equation is called the Bloch equation, after the physicist Felix Bloch (see Chapter 1), and it describes the behavior of the net magnetization of a spin system in the presence of a magnetic field that varies over time. As we will learn in the following chapters, solutions to this equation provide mathematical representations of magnetization during the steady state, excitation, and relaxation. Thus, the Bloch equation provides the theoretical foundation for all MRI experiments.

Summary

A set of physical principles underlies the generation of the MR signal. The primary concepts are those of nuclear spin and net magnetization. Atomic nuclei with a magnetic moment and angular momentum are known as spins, and they exhibit rapid gyroscopic precession in an external magnetic field. The axis around which they precess is known as the longitudinal direction, and the plane in which they precess is known as the transverse plane. Each spin adopts either a low- or a high-energy state. These low- and high-

REFER TO THE
fMRI
COMPANION WEBSITE AT
www.sinauer.com/fmri2e
for study questions and Web links.

energy states are parallel and antiparallel to the magnetic field, respectively. Under normal conditions, the net magnetization from all spins is a vector parallel to the static magnetic field. By applying an electromagnetic pulse that oscillates at the resonant (Larmor) frequency of the spins, in a process known as excitation, one can tip the net magnetization vector from the longitudinal direction into the transverse plane. This causes the net magnetization to change over time in the transverse plane, generating the MR signal that can be measured using an external detector coil. A single formula, known as the Bloch equation, forms the basis for the quantitative description of magnetic resonance phenomena.

Suggested Readings

Haacke, E. M., Brown, R. W., Thompson, M. R., and Venkatesan, R. (1999). *Magnetic Resonance Imaging: Physical Principles and Sequence Design.* John Wiley & Sons, New York. *A comprehensive encyclopedia of the theoretical principles of MRI.*

Jin, J. (1999). *Electromagnetic Analysis and Design in Magnetic Resonance Imaging.* CRC Press, Boca Raton, FL. *This book describes the basic theory and design underlying the radiofrequency hardware for MR signal excitation and reception.*

Slichter, C. P. (1996). *Principles of Magnetic Resonance* (3rd ed.). Springer-Verlag, New York. *This book provides a detailed mathematical treatment of the physics of MRI.*

Chapter 4

Basic Principles of MR Image Formation

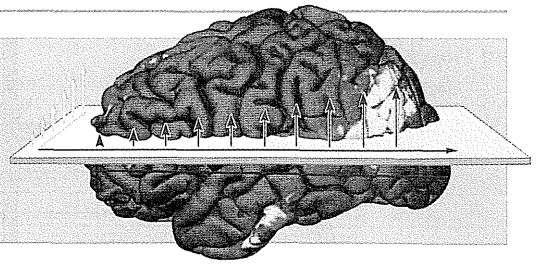

As its name implies, the goal of magnetic resonance imaging is the formation of an image. It is important to recognize that in the context of MRI, an image is not simply a photograph of the object being scanned. It is a map that depicts the spatial distribution of some property of the atomic nuclei (or spins) within the sample. That property might reflect the density of the spins, their mobility, or the T_1 or T_2 relaxation times of the tissues in which the spins reside.

Creating an image from MR signals may now seem commonplace, but more than 25 years passed between the first NMR experiment (1945) and the first MR image (1972). In the intervening period, researchers actively strove to make their samples as homogeneous as possible so that no spatial variability could corrupt the data, and therefore, no images were made. Remember that the 2003 Nobel Prize in Physiology or Medicine was awarded not for the discovery of the medical applications of magnetic resonance, but for the development of techniques for image formation. In this chapter, we describe the concepts of image formation by illustrating how spatial information is encoded and decoded by MRI scanners. Specific topics include slice excitation, frequency encoding, phase encoding, and the representation of MRI data in *k*-space.

The fundamental concept underlying image formation in MRI is that of the magnetic gradient, or spatially varying magnetic field, introduced by Lauterbur in 1972 (for which he won the Nobel Prize in 2003). In the first NMR experiments conducted by Purcell, Bloch, and other early researchers, the magnetic fields were uniform, so that all spins in the entire sample experienced the same magnetic field. But as Lauterbur later demonstrated, superimposing a second magnetic field that varies in strength across space will cause spins at different locations to precess at different frequencies in a controlled fashion. By measuring changes in magnetization as a function of precession frequency, the total MR signal can be separated into components associated with different frequencies, thus providing information about the spatial distribution of the targeted atomic nuclei.

As we did in Chapter 3, we have constructed two independent paths for understanding the principles of image formation. The *conceptual path* includes descriptions and analogies that do not depend heavily on equations, and the *quantitative path* includes mathematical equations that elaborate on the image formation principles (Figure 4.1).

image A visual description of how one or more quantities vary over space.

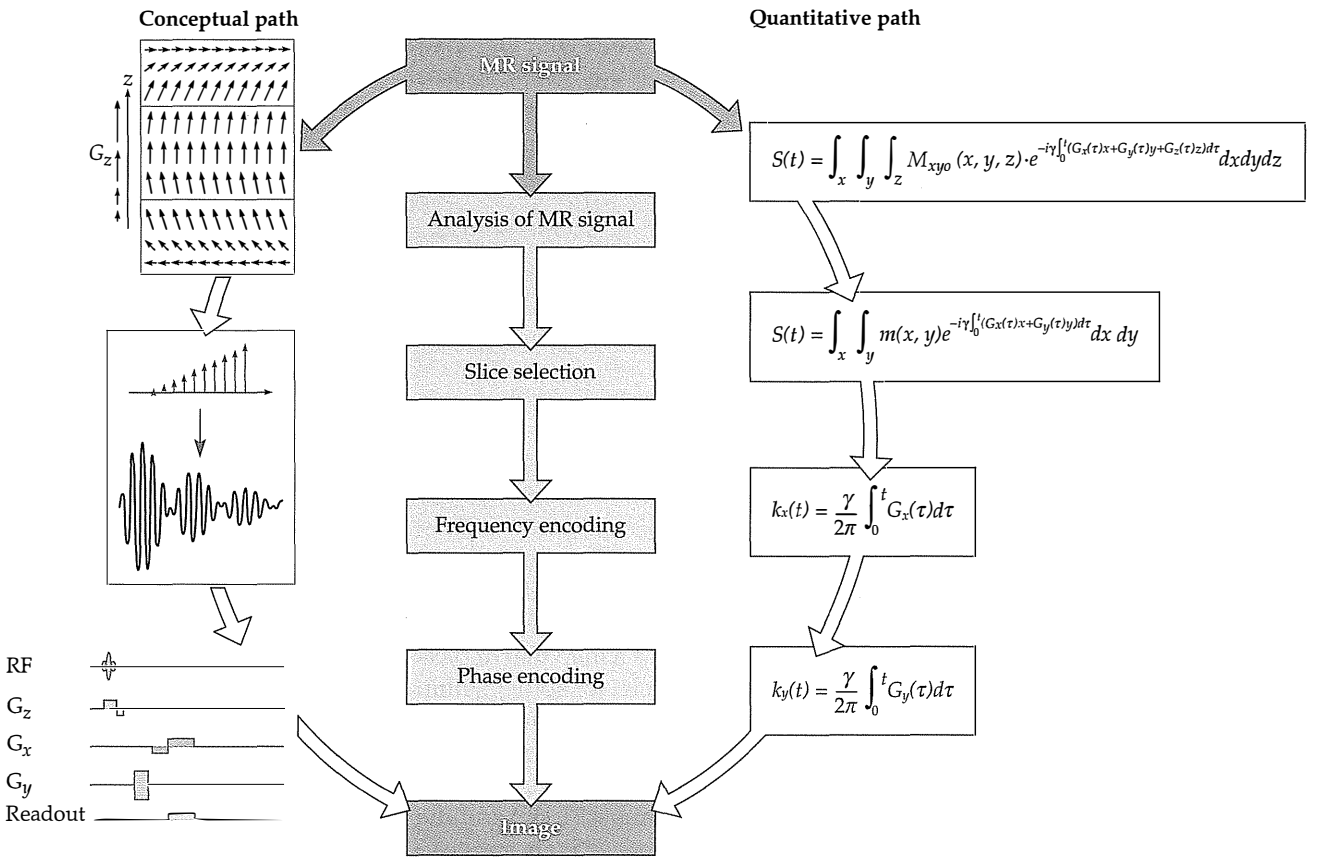

Figure 4.1 Overview of the chapter. We have structured this chapter (and Chapter 3) along two parallel paths, each covering the basic principles of MR image formation. The conceptual path uses physical models and analogies to cover these principles in a straightforward and intuitive manner, while the second quantitative path introduces the relevant equations. While the two paths cover the same principles in different ways, the figures throughout the chapter are intended to be accessible to all readers.

Conceptual Path

The central innovation that made MR imaging possible was the introduction of superimposed gradient (spatially varying) magnetic fields. Because the precession frequency is proportional to the strength of the magnetic field, gradient magnetic fields cause atomic nuclei in different spatial locations to precess at different rates. By dividing the MR signal into components with different frequencies, we can generate maps (or images) that provide information about the characteristics of those atomic nuclei.

To resolve spatial information in three dimensions, we need at least three gradient fields. In MRI, the static magnetic field is always oriented along the longitudinal direction (commonly known as the z-direction), which is parallel with the scanner bore. The gradient magnetic fields along the x, y, and z directions indicate how the strength of that static magnetic field changes in each of the three directions, as shown in Figure 4.2. It is critical to remember that the

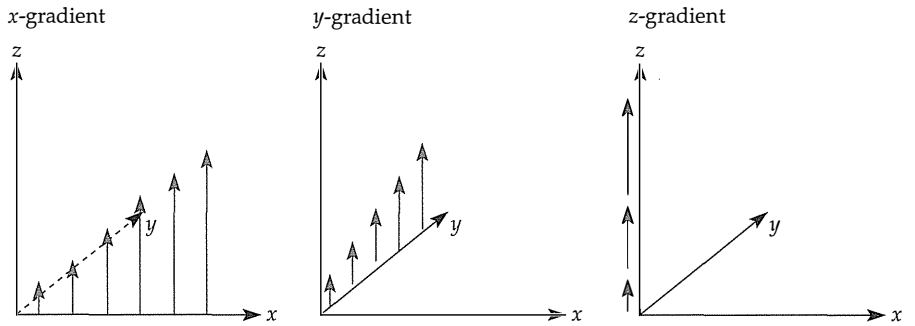

Figure 4.2 A schematic illustration of the spatial distributions of the x-, y-, and z-gradient magnetic fields. Note that each of these gradients only changes the strength of the magnetic field along the relevant axis; they do not alter the direction of the magnetic field.

direction of the magnetic field is *always* along the longitudinal direction; gradient fields change the *strength* of the static magnetic field at a given spatial location, but not its direction.

Since gradient fields along any direction will modulate the spin precession frequencies, one cannot turn on all gradient fields at the same time and hope to resolve spatial information. Instead, a sequence of gradient field changes, along with radiofrequency pulses, is used to create an MR image. We break down MR image formation into three steps, which often occur in a consistent sequence. First, we use a process called slice selection to select a two-dimensional slice of the object to be imaged, and then we systematically resolve the remaining two dimensions within this slice, by frequency encoding and phase encoding, to obtain a final image.

Slice Selection

Most structural MRI and all functional MRI involve the construction of three-dimensional images from sets of two-dimensional slices. Direct three-dimensional imaging is used for some structural MRI, however it is a much slower process, and is therefore inappropriate for measurements of brain function. Thus, a common first step in producing an MR image is dimensional reduction: restricting the MR signal to one two-dimensional slice at a time. This is termed slice selection.

As we introduced in the previous chapter, the MR signal recorded in the detector coils contains contributions from all the atomic nuclei that received an on-resonance excitation pulse. Thus, selection of any particular slice requires the excitation of spins within that slice, but not of any other spins in the sample. So, the key element of slice selection is to ensure that there is a match between the precession frequency of the spins within the desired slice and the radiofrequency (RF) excitation pulse, but no such match elsewhere. Imagine that the MR scanner introduced a positive gradient along the z direction, often given the label G_z. Spins toward the back of the scanner (i.e., at the top of the brain) would precess more rapidly and spins toward the front of the scanner would precess more slowly. This scenario is represented in highly stylized form in Figure 4.3A. To select the middle slab, we set the frequency of the RF excitation pulse to match that of the middle slab. This ensures that the spins in the middle slab are on resonance with the excitation pulse, whereupon many will absorb energy and change from low- to high-energy states. Then the MR signal will only be emitted by spins in the middle slab following the cessation of the excitation pulse.

slice selection The combined use of a spatial magnetic field gradient and an electromagnetic pulse to excite spins within a slice.

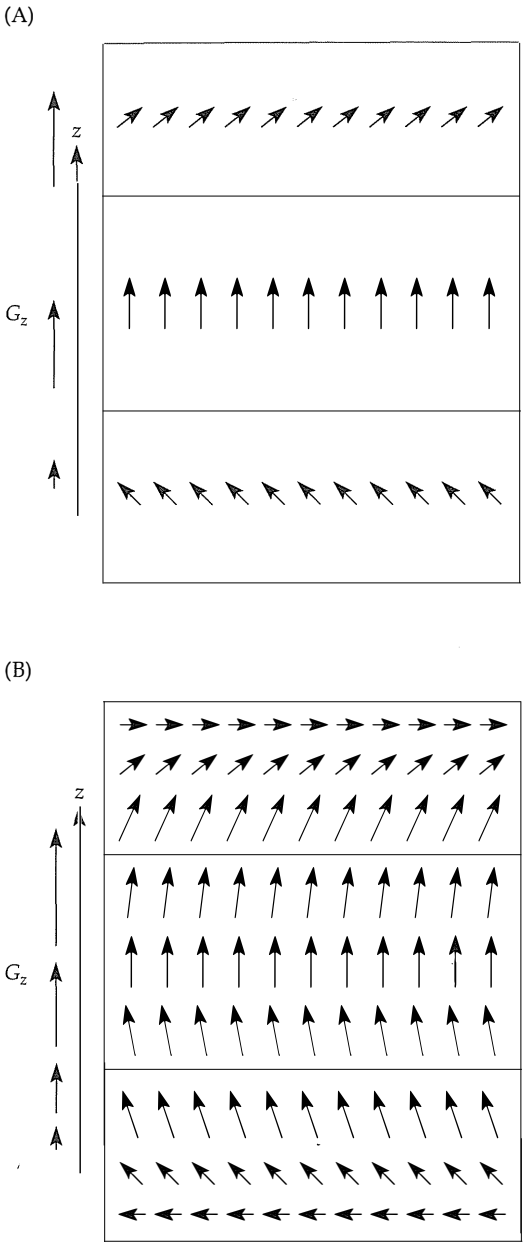

Figure 4.3 A schematic illustration of slice selection. Before excitation, a spatial gradient is introduced (by convention, along the z direction) that causes the precession frequencies of the atomic nuclei of interest to differ along that gradient. If all nuclei in the desired slice had the same precession frequency, as shown in (A), then an excitation pulse at that precession frequency would excite all spins in that slice. However, because precession frequency changes continuously along the slice-selection direction, as shown in (B), an excitation pulse contains a band of frequencies whose spectrum is matched to those of nuclei within the desired slice.

In reality, no magnetic gradient can create discrete bands of precession frequencies across space. Instead, if a spatial gradient (*G*) field is turned on along the slice direction (e.g., the *z*-direction), it will cause a continuous change in the strength of the magnetic field, as illustrated by the continuous change in the directions of the arrows in Figure 4.3B. This means that a band within the gradient field, such as the green band in Figure 4.3B, will contain spins with a range of precession frequencies. To match this frequency band, the excitation radiofrequency (RF) pulse will need to contain the same frequency range. Fortunately, if we know the characteristics of the static magnetic field and of the gradient along the direction of slice selection, as well as the desired slice location, we can determine the center frequency needed for our excitation pulse. Moreover, from the desired slice thickness, we can calculate the necessary bandwidth for the excitation pulse (i.e., the range of frequencies it needs to include). Because slice selection usually involves the generation of one gradient across space and a single excitation pulse, it can be completed very rapidly, usually within a few milliseconds.

Immediately after the excitation pulse, the affected spins begin to undergo T_1 and T_2 relaxation processes, as described in Chapter 3. T_2 relaxation causes a loss of spin coherence in the transverse plane and T_1 relaxation leads to an exponential recovery of the longitudinal magnetization—both resulting in the decay of the MR signal. Because of these relaxation effects, especially the very rapid T_2 decay, slice selection must be immediately followed by the application of other gradients that provide information about the distribution of atomic nuclei within the slice itself.

The pattern of radiofrequency pulses and magnetic gradients used to collect a given type of MR image is known as a pulse sequence. Over the course of this chapter, we will introduce the basic elements of pulse sequences in a conventional graphical format, so that readers can become familiar with their representation. The basic format of a pulse sequence diagram consists of a series of horizontal lines, each representing how a different component of the MR scanner changes over time. The elements that we have introduced so far, as part of slice selection, constitute two parts of the MR scanner: the radiofrequency coil and the *z*-gradient (Figure 4.4). The excitation pulse will be represented throughout this book as a set of three ovals; these schematically convey the idea of a band of frequencies within a sinc function (see Figure 4.13 for an example). The slice-selection gradient is shown, by convention, on the *z*-gradient line; it consists of an initial positive gradient, followed by a second negative gradient. (This second negative gradient is applied to coun-

spatial gradient (*G*) A magnetic field whose strength varies systematically over space. Note that since a given spatial location only experiences one magnetic field, which represents the sum of all fields present, spatial gradients in MRI act to change the effective strength of the main magnetic field over space.

pulse sequence A series of changing magnetic field gradients and oscillating electromagnetic fields that allows the MRI scanner to create images sensitive to a particular physical property.

teract the effects of the excitation pulse on the portion of the slice selection gradient within the selected slice).

Note that the pulse sequence diagram should be considered a schematic, not literal, representation of what the scanner is doing. If the slice selection is along the x-axis, for example, then an x-gradient will be necessary; if the slice is tilted slightly, as is common, then some combination of two or three gradients will be necessary. For the remainder of this book, we will simplify the pulse sequence diagrams by assuming that the slice-selection gradient is purely along the z-direction, and that the x- and y-gradients are used to localize the distribution of atomic nuclei within that slice.

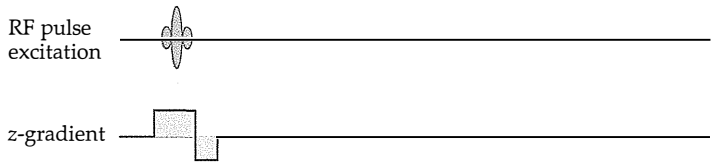

Figure 4.4 Elements of a pulse sequence necessary for slice selection. To select a slice, an excitation pulse is delivered through the radiofrequency coil (i.e., head coil in fMRI). Simultaneously, a magnetic gradient is introduced within the sample. By convention, we will indicate the slice-selection gradient along the z-direction. Each line of a pulse sequence diagram indicates a separate component of the scanner hardware, with the x-axis indicating time and the y-axis indicating the strength of that component at that point in time.

Frequency Encoding

Once a slice is selected, all excited spins contribute to the MR signal. Thus, the next step is to apply additional gradients that cause spins at different spatial locations to precess at different rates, so that their individual contributions can be measured. For reasons that will become apparent in this and the following section, the application of magnetic gradients within a slice involves two intertwined processes known as frequency encoding and phase encoding. We consider these processes in separate sections, both for clarity, and because they are often conducted in a particular sequence.

Let's begin by considering a very simple task: creating a one-dimensional image that identifies the locations of two thin vials of water (Figure 4.5). Note that this example is not arbitrarily chosen; Paul Lauterbur used a similar setup when creating the very first MR image (see Figure 1.11). Suppose that we have just completed the slice selection step, as described above, by exciting the spins within a single two-dimensional slice, but that we have not introduced any other spatial gradients (Figure 4.5A). All of the protons in the water molecules within the slice would therefore be precessing at the same rate. Our detector coils would measure an emitted MR signal that oscillated at that precession frequency, and that decayed over time based on the T_2 value of hydrogen in water. However, we would not be able to tell from this MR signal whether there were one, two, or many vials of water within our slice. In fact, all we can tell from this MR signal is that there are protons somewhere within our slice, but we have no idea where.

Suppose that we repeat our experiment while introducing a magnetic gradient from left to right, so that the magnetic field is relatively weaker near the left vial and relatively stronger near the right vial (Figure 4.5B). Now, the protons within the two vials will have distinct precession frequencies: slower in the left vial, and faster in the right vial. Because of this effect, the first step of gradient application is often called frequency encoding. The resulting MR signal will still have high-frequency oscillations and transverse relaxation, as it did before the gradients were introduced. But now there are slower oscillations, superimposed on the faster oscillations at the resonant frequency that provide information about the width and spacing of the two vials. (These reflect constructive and destructive interference between signals with slightly different frequencies, akin to beat frequencies in music.) By using signal processing tools,

frequency-encoding gradient A gradient that is applied during the data acquisition period, so that the spin precession frequencies change over space.

phase-encoding gradient A gradient that is applied before the data acquisition period, so that spins can accumulate differential phase offsets over space.

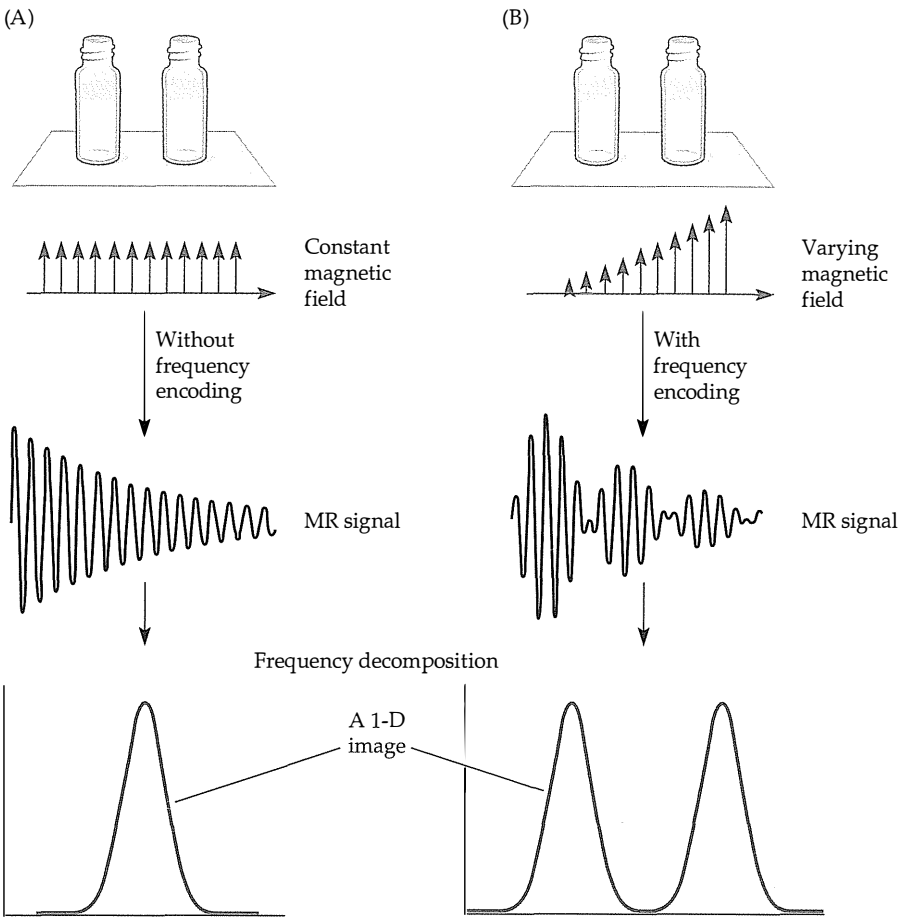

Figure 4.5 The use of a magnetic gradient to resolve the spatial locations of two vials of water. (A) If both water vials experience the same, constant magnetic field (i.e., there is no frequency encoding), then the measured MR signal reflects the total contributions of all protons within those vials. Thus, the resulting image (at bottom) would provide information about how much water was present, but would not provide information about where the vials were located. (B) By introducing variation in the magnetic field strength over space (i.e., including frequency encoding), the resulting MR signal will have multiple frequency components whose strength depends on the relative locations of the vials. The MR signal could thus be decomposed into a one-dimensional image of the vials.

we can resolve the different resonance frequencies that led to the different oscillations in the MR signal; this information can, in turn, be used to map the physical distance between the two vials. In summary, the introduction of a single gradient makes it possible to construct a map of proton density along the direction of that gradient; effectively, this map is a one-dimensional image.

To indicate the steps of frequency encoding on our pulse sequence diagrams, we can introduce two more lines (Figure 4.6): one for the frequency-encoding gradient (often indicated as G_x), and one for the receiver coil, indicating the period of data acquisition (sometimes called the "readout period"). Note that the readout period is sometimes omitted from pulse sequence diagrams, especially those with complex gradient patterns, like the ones we will intro-

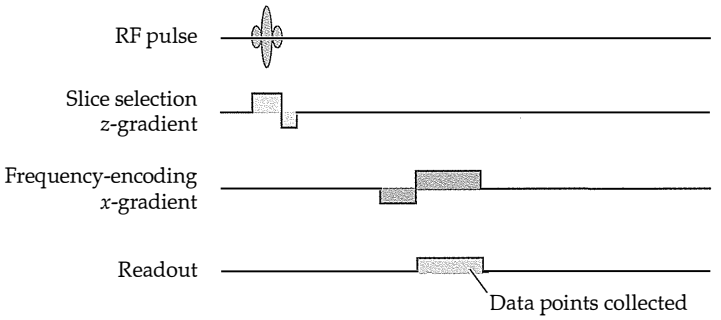

Figure 4.6 Elements of a pulse sequence necessary for frequency encoding within a slice. To create a one-dimensional map within a slice, a second magnetic gradient must be applied during data acquisition. Note that data acquisition usually occurs with some delay after excitation for T_1- or T_2-sensitive images. By convention, this frequency-encoding gradient is usually indicated as G_x.

duce in the next chapter. In general, data acquisition can be assumed to occur simultaneously with the manipulation of the frequency and phase gradients.

Phase Encoding

How can we move from one-dimensional data of the type illustrated in Figure 4.5B to a complex two-dimensional image? One intuitive approach is to collect a large number of one-dimensional projections, each oriented differently within the slice, and then superimpose them to construct a two-dimensional image. This sort of strategy could be used for image creation; indeed, an analogous approach underlies tomographic techniques like CAT scanning, but it has some severe disadvantages. Most notably, the construction of even a simple image would require a large number of sequential excitations, and the collection of much redundant data, making this strategy very slow and inefficient. A much better approach would involve collecting minimal but sufficient data to uniformly cover one part of the image (or even the entire two-dimensional image) following a single excitation pulse. To do this, we must introduce another spatial gradient, in a step known as phase encoding.

The key concept of phase encoding is the *sequential* application of a second gradient within the slice that alters spin precession frequencies in a spatially controlled manner. Why must we apply the frequency-encoding and phase-encoding gradients sequentially, rather than simultaneously? Suppose that we applied positive x- and y-gradients at the same time and with the same strengths. Spins in the top right of the slice would experience the strongest magnetic field (remember that spatial gradients alter the strength of the magnetic field but not its direction), while spins in the lower left of the slice would experience the weakest field strength. Thus, the simultaneous application of both x- and y-gradients would simply introduce a linear change in precession frequency along a diagonal axis between the x and y directions. We would be no better able to resolve the two-dimensional spatial information than if we had applied only one gradient.

Thus, in the simplest form of phase encoding, we first apply one gradient (say the y-gradient) before the other and before any MR signal is acquired. This causes spins along the first gradient to precess at different rates depending on their positions, so that by the time the second gradient is introduced, these spins already differ in their phase (i.e., the current angle of precession). The characteristic of the recorded MR signal will depend on the combination of phase- and frequency-gradients that were applied. If a strong positive y-gra-

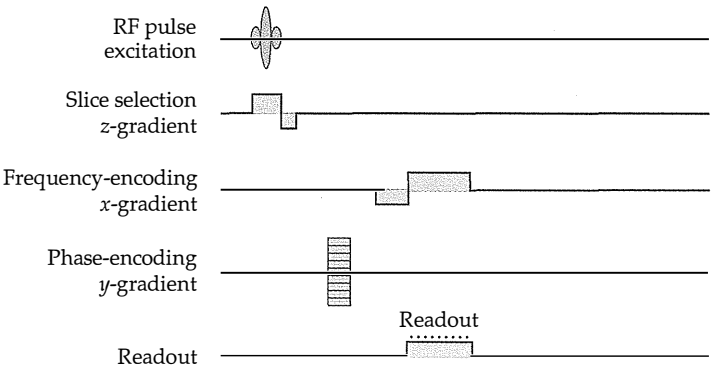

Figure 4.7 Elements of a pulse sequence necessary for frequency and phase encoding within a slice. To create a two-dimensional image of a given slice, two independent magnetic gradients must be used within that slice. In many cases, a phase-encoding gradient is applied before the frequency-encoding gradient (as shown in this simple schematic), so that there is time for phase differences among spins to accumulate along that direction. However, the frequency- and phase-encoding gradients can also be acquired simultaneously (see Figure 5.32). By convention, the phase-encoding gradient is usually indicated as G_y.

dient is applied during phase encoding, then the application of an x-gradient will cause the kind of diagonal change in precession frequency that was described in the previous paragraph. But if a very weak y-gradient is applied, then the precession frequency would change across the x-direction, with minimal changes in the y-direction. If a negative y-gradient is applied, then the precession frequency will again change along a diagonal axis, but along the opposite diagonal as the one before. The key concept is that these different patterns of precession frequencies will lead to different recorded MR signals, depending on the distribution of spins over space. This means that by recording the MR signal many times, following many different combinations of gradients, we can effectively estimate the characteristics (i.e., the density and distribution of specific atomic nuclei) of the object we are imaging. We will explore further the use of two magnetic gradients for changing the pattern of recorded MR signal, in the discussion of k-space, later in this chapter.

If frequency and phase encoding are separated, as in this example (and as illustrated in Figure 4.7), then the resolution along the phase-encoding direction determines the number of repeated excitations (and thus the total time) required to collect the entire image. For example, if we want to collect an image with 256×256 resolution, we would need 256 separate excitations, each with a different phase-encoding gradient. Many anatomical images are collected in this way, taking a few tens of seconds. However, images can be collected much more rapidly if we allow frequency and phase encoding to occur simultaneously. Functional MRI almost always uses very fast pulse sequences in which two gradients alternate rapidly over the period of data acquisition. For such sequences, the distinction between *frequency-* and *phase*-encoding gradients can be less obvious. In Chapter 5, we introduce those types of sequences that are most commonly used for fMRI.

Conceptual Path: Summary of Image Formation

We can now construct a sequence of events (Figure 4.8) that underlies the formation of a three-dimensional MR image: first, the selection of a slice in which spins will be excited at a particular resonant frequency (in blue); then the pre-application of one spatial gradient during phase encoding (in yellow), and the simultaneous application of another gradient for frequency encoding during acquisition of the MR signal (in red).

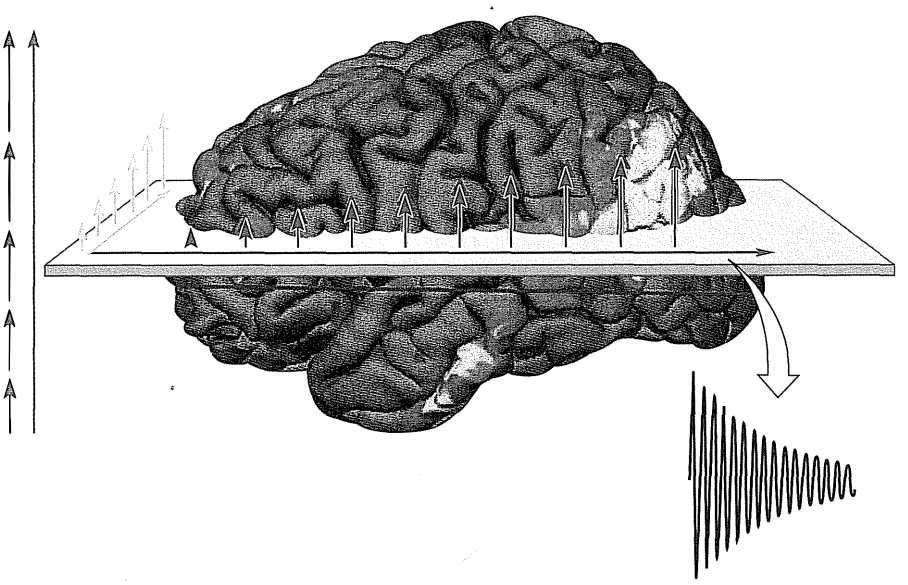

Figure 4.8 Summary of image formation. For most images acquired during fMRI experiments, three steps are used: initial selection of a two-dimensional slice (blue), and combined phase encoding (yellow) and frequency encoding (red). Data acquisition is typically done concurrently with encoding.

These steps are conceptually straightforward, however, our discussion so far has over-simplified some of the complex mathematical issues. In particular, using the algebraic approach (see Box. 4.1) to reconstruct the MR signal into an image would be very computationally intensive, especially for high-resolution images. For example, anatomical images are frequently acquired with a matrix size of 256 × 256 voxels (i.e., 65,536 total voxels in a single slice). To resolve such complex images, the information recorded during data acquisition is subjected to a computationally efficient mathematical process called a Fourier transform. We discuss the mathematical foundations of image formation, including the application of the Fourier Transform, in the following quantitative path.

Quantitative Path

Spatial encoding results from the effects of gradient magnetic fields on the detected MR signal. In order to understand the process of image formation quantitatively, we will need to characterize how the MR signal changes as a function of the particular magnetic field gradients that are applied. Thus, we will begin this section by analyzing the MR signal under magnetic gradients using the Bloch equation. This is followed by theoretical and experimental descriptions of the various spatial encoding steps such as slice selection, frequency and phase encoding, and image reconstruction.

Analysis of the MR Signal

Recall that the precession frequency of a spin within a magnetic field (i.e., the Larmor frequency) is determined by two factors: the gyromagnetic ratio, which is a constant for a given atomic nucleus, and the magnetic field strength (see Equation 3.21). Likewise, the net magnetization of a spin system precesses around the main field axis at the Larmor frequency when tipped toward the

Fourier transform A mathematical technique for converting a signal (i.e., changes in intensity over time) into its power spectrum.

Larmor frequency The resonant frequency of a spin within a magnetic field of a given strength. It defines the frequency of electromagnetic radiation needed during excitation to make spins change to a high-energy state, as well as the frequency emitted by spins when they return to the low-energy state.

BOX 4.1 An Example of Spatial Encoding

In this box, we provide an integrative perspective on spatial encoding of the MR signal, using a graphical representation that involves basic algebra and geometry. We begin by emphasizing one core concept of MR data acquisition: that the scanner records the MR signal at discrete points in time. Suppose that we again want to create an MR image of two small vials containing different liquids (e.g., arterial and venous blood). As will be covered in much more detail in Chapter 5, we could select pulse sequence parameters such that the amount of MR signal generated would differ between these vials (e.g., by using a sequence with an intermediate echo time, TE), but we would still face the challenge of identifying which vial was which.

If we excited a slice containing both vials, the total MR signal emitted would contain the contributions from all spins in the slice (Figure 1, left), as given by the sum S_1 of the vectors **A** and **B**. There would be no way to tell how much of that signal came from Vial 1 and how much from Vial 2. Next, we can apply a magnetic gradient whose amplitude G is along the direction separating the two vials, here shown as going from left-to-right (i.e., the x-direction). After that gradient is left on for a short while, spins that experienced a stronger gradient (i.e., those to the right in this figure) would precess relatively faster than spins that experienced a weaker gradient. Thus, the received signal will have a new intensity S_2 that is governed by the sum of the vectors **A** and **B**. To make solving for **A** and **B** simplest, we can arrange to acquire data at a specific time point such that the rotation angles of vectors **A** and **B** are 180 degrees out of phase (Figure 1, right). By knowing how much MR signal was measured at each time point (0 and t), we can calculate the MR signal associated with each of the two vials, using the algebraic equations shown in the figure.

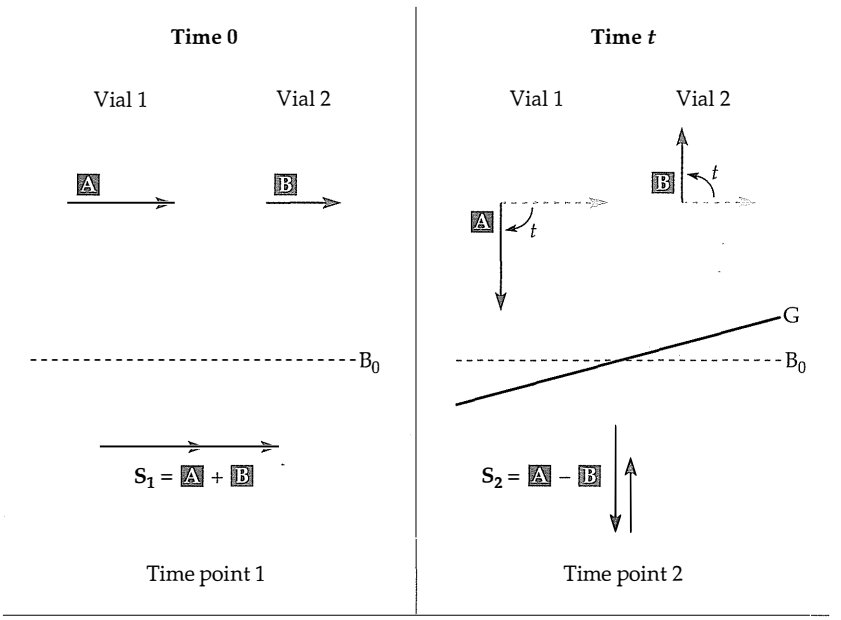

Resulting in A = $(S_1 + S_2)/2$, and B = $(S_1 - S_2)/2$

Figure 1 Resolving two spatial locations using a single gradient. If there are two vials, each with an unknown signal intensity, then the total MR signal recorded following excitation will be the sum of the signals from both vials (as shown at left). However, if a spatial gradient is introduced and left on long enough for the spin precessions in each vial to become 180 degrees out of phase, then the total MR signal recorded would equal the difference in signals between the vials (as shown at right). By using information collected at these two time points, one could calculate the signal emitted by spins within each of the two vials, effectively creating a two-voxel image.

We can use a similar approach to expand our analysis of these two vials to more complex examples. Suppose that we wanted to identify the MR signal associated with not two, but 64 different spatial locations along one dimension. We would have to collect data at 64 different points in time, each corresponding to a different x-gradient. (Technically considered, this could be accomplished by turning on a single gradient and measuring the MR signal amplitude at 64 times that reflect phase differences evenly spaced from 0 to 360 degrees.) In essence, the use of a single spatial gradient generates differences in precession frequencies that in turn allow the separation of MR signals coming from different spatial locations. To resolve more locations along a spatial dimension, the scanner must collect information about the MR signal at more points in time.

Two-dimensional spatial encoding, as introduced in the main text, leads to additional complexities. If we simply turned on the x- and y-gradients simultaneously and with equal strengths, both gradients would cause similar changes in the MR signal, and we would

BOX 4.1 *(continued)*

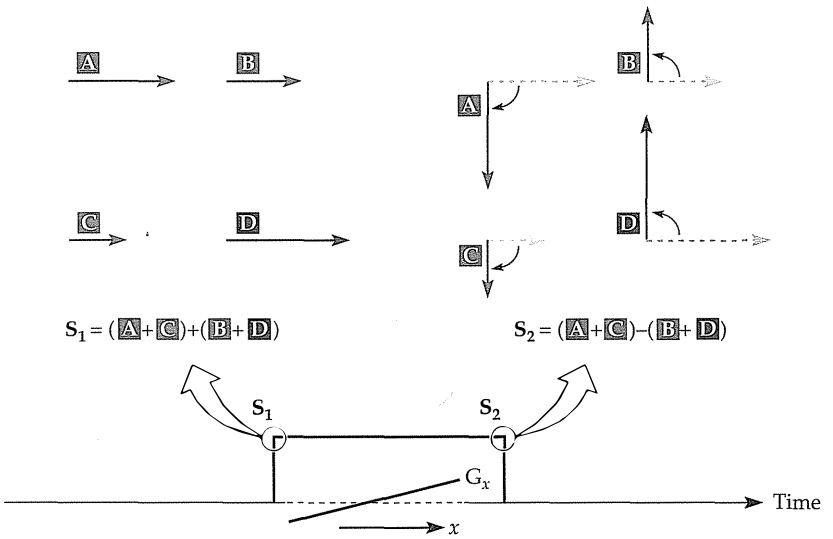

Figure 2 Resolving a two-by-two image using two gradients. To create a simple two-dimensional image, two magnetic gradients are required. First, data can be collected before and after application of the frequency-encoding gradient (as shown at top). This provides two data points, which are insufficient to distinguish the four spatial locations. Then, data collection can be repeated following a phase-encoding step, providing two new data points that include the accumulated phase from the first gradient. This provides two more data points. By using information from all four data points, reflecting two different phase-encoding steps, one could determine the amount of MR signal generated at each of the four spatial locations.

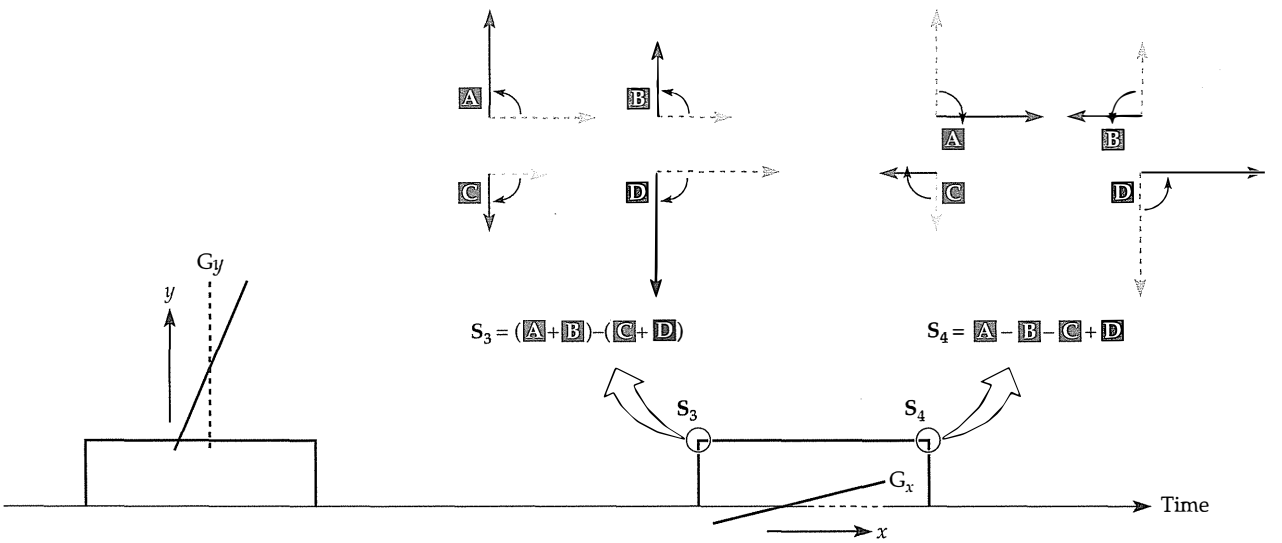

Resulting in $A = (S_1 + S_2 + S_3 + S_4)/4$, $B = (S_1 - S_2 + S_3 - S_4)/4$, $C = (S_1 + S_2 - S_3 - S_4)$, $D = (S_1 - S_2 - S_3 + S_4)/4$

be unable to identify unique locations in space. Instead, we use sequential combinations of both gradients. As shown at the top of Figure 2, acquisition of the MR signal before and after the application of an x-gradient (by itself) gives us two equations, while the introduction of a y-gradient beforehand would give us two more. The four equations shown in the figure are independent, and thus they could be used to calculate the individual intensities at the four spatial locations of interest. Real MR image formation is much more complex (e.g., a 64*64 image is made up of 4096 intensity values) and so different analytic approaches are required for identifying what signal comes from what spatial location. Nevertheless, the core principle of data acquisition remains the same: by using multiple magnetic gradients, applied in a controlled sequence, we can resolve the contributions of individual spatial locations to the total MR signal.

B The sum of all magnetic fields experienced by a spin.

Bloch equation An equation that describes how the net magnetization of a spin system changes over time in the presence of a time-varying magnetic field.

transverse plane (see Equation 3.28). Since the Larmor frequency depends on the strength of the magnetic field, changes in the strength of the magnetic field will also change the Larmor frequency. Keep in mind that during MR imaging, a spin experiences only one magnetic field, B, which represents the sum of all magnetic fields at its location.

In the previous chapter, we described two types of magnetic fields that are important for the generation of the MR signal: the static (or main) field, $\mathbf{B}_0$, and the electromagnetic (or radiofrequency) field, $\mathbf{B}_1$. The static magnetic field aligns the precession axes of the nuclei and generates the net magnetization, **M**, and the electromagnetic field excites the nuclei by applying energy that, when subsequently released, can be measured in detector coils. The combined effects of these fields on the net magnetization of a spin system are described by the Bloch equation (see Equation 3.47). We now introduce a third kind of magnetic field, the spatial gradient **G**, which alters the precession frequencies of spins depending on their spatial locations. With the addition of gradient fields as components of **B**, we will solve the Bloch equation later to account for all external magnetic fields, including gradient fields that vary over space. This will allow us to understand the essence of image formation using the spatial gradients. We repeat the Bloch equation here as Equation 4.1 for ease of reference:

$$\frac{d\mathbf{M}}{dt} = \gamma \mathbf{M} \times \mathbf{B} + \frac{1}{T_1}(\mathbf{M}_0 - \mathbf{M}_z) - \frac{1}{T_2}(\mathbf{M}_x + \mathbf{M}_y) \tag{4.1}$$

The Bloch equation describes the changes in net magnetization as the sum of three terms. As given by the precession term, the MR signal precesses around the main axis of the magnetic field at a rate given by the gyromagnetic ratio and the field strength (see Figure 3.14). The T_1 term indicates that the longitudinal component of the net magnetization recovers at a rate given by T_1 (see Figure 3.21A), and the T_2 term indicates that the transverse component of the net magnetization decays at a rate given by T_2 (see Figure 3.21B). Remember that in MR, the term longitudinal refers to the axis parallel to the main magnetic field, and the term transverse refers to the plane perpendicular to the main magnetic field.

We next solve the Bloch equation to determine the MR signal at each point in time, $M(t)$. First we break down the Bloch equation, which describes the MR signal in a three-dimensional vector format, into a simplified scalar form along each axis. Figure 4.9 illustrates that the net magnetization vector can be thought of either as a single vector in three dimensions or as a set of three vectors along each of the three cardinal axes. To represent the Bloch equation in scalar form, we need to isolate changes along each axis. Note that the change in the net magnetization in the x- and y-directions depends on both the precession term and the T_2 term. In contrast, the change in magnetization in the z-axis depends only on the T_1 term. Considering the axes separately, we can rearrange Equation 4.1:

$$\frac{dM_x}{dt} = M_y \cdot \gamma B - \frac{M_x}{T_2} \tag{4.2a}$$

$$\frac{dM_y}{dt} = -M_x \cdot \gamma B - \frac{M_y}{T_2} \tag{4.2b}$$

$$\frac{dM_z}{dt} = -\frac{(M_z - M_0)}{T_1} \tag{4.2c}$$

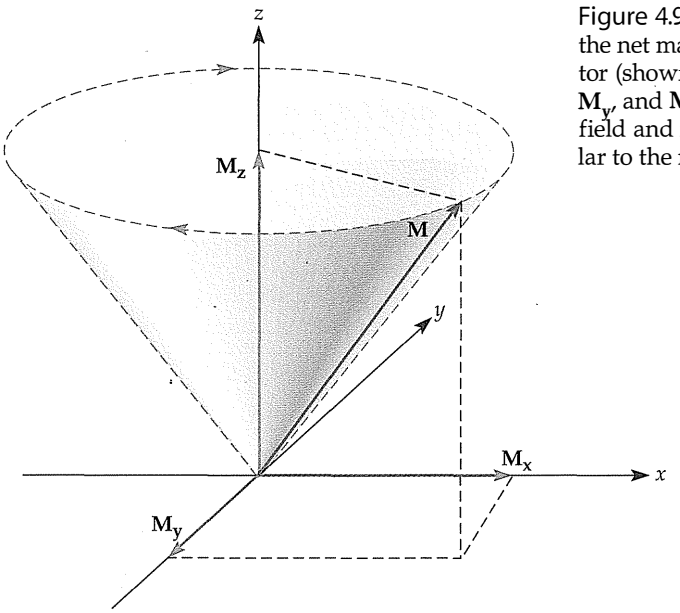

Figure 4.9 The net magnetization vector and its axis projections. While the net magnetization, **M**, of a sample can be represented as a single vector (shown in blue), it can also be described by a set of three vectors: $\mathbf{M}_x$, $\mathbf{M}_y$, and $\mathbf{M}_z$. By convention, the *z*-axis is parallel to the main magnetic field and is known as the longitudinal axis. The *x*–*y* plane is perpendicular to the main magnetic field and is known as the transverse plane.

So, Equations 4.2a and 4.2b describe the changes in magnetization over time, along the *x*- and *y*-directions, as the spins precess about the main axis. The time constant T_2 specifies the rate of decay of magnetization in the transverse plane, but it has no effect on the longitudinal magnetization along the *z*-axis. Equation 4.2c describes the change in the longitudinal magnetization over time, as it recovers at a rate specified by T_1.

Longitudinal magnetization (M_z)

The longitudinal magnetization depends only on a single equation (4.2c), which is an ordinary first-order differential equation. Thus, its solution is an exponential recovery function that describes the return of the main magnetization to the original state. Equation 4.3 replaces dM_z/dt with a mathematical equivalent, $d(M_z - M_0)/dt$, that represents the change in longitudinal magnetization from the fully relaxed state, M_0:

$$\frac{d(M_z - M_0)}{dt} = -\frac{M_z - M_0}{T_1} \tag{4.3}$$

Swapping sides for dt and $M_z - M_0$, we get:

$$\frac{d(M_z - M_0)}{M_z - M_0} = -\frac{dt}{T_1} \tag{4.4}$$

By integrating both sides of this equation, we obtain Equation 4.5. This equation states that the natural log of the change in longitudinal magnetization over time (0 to t') is equal to the change in time divided by the constant T_1:

$$ln(M_z(t) - M_0)\Big|_0^{t'} = -\frac{t}{T_1}\Big|_0^{t'} \tag{4.5}$$

If we assume that the initial magnetization at time zero is given by M_{z0}, the solution for M_z at a later time point (t) is given by Equation 4.6. This equation states that the longitudinal magnetization (M_z) is equal to the fully relaxed magnetization, plus the difference between the initial and fully relaxed magnetization states, multiplied by an exponential time constant. Note that since

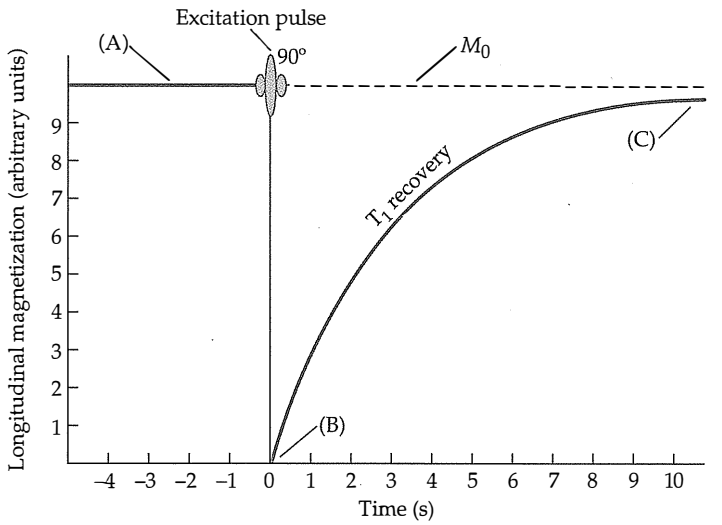

Figure 4.10 The change in longitudinal magnetization over time is known as T_1 recovery. When fully recovered (A), the longitudinal magnetization is at its maximum value, as shown by the horizontal blue and dotted lines, and does not change over time. However, following an excitation pulse that tips the net magnetization into the transverse plane, there will be zero longitudinal magnetization (B). As time passes following excitation, the longitudinal magnetization recovers toward its maximum value (C). The time constant T_1 governs this recovery process.

M_{z0} is always less than M_0, the exponential term describes how much longitudinal magnetization is lost at a given point in time. As t increases, more longitudinal magnetization is recovered and the signal M_z approaches the fully relaxed signal M_0:

$$M_z = M_0 + (M_{z0} - M_0) \cdot e^{-t/T_1} \tag{4.6}$$

To illustrate T_1 recovery, let us consider some extreme values for the initial magnetization, M_{z0}. Consider the situation when the net magnetization is fully relaxed (Figure 4.10A). Here, M_{z0} is equal to M_0, and the term $(M_{z0} - M_0)$ will be zero. Once the net magnetization is fully relaxed, it does not change over time, as indicated by the horizontal line segment. However, after an excitation pulse is applied (Figure 4.10B), the net magnetization is tipped entirely into the transverse plane and the net longitudinal magnetization is zero. The subsequent recovery of longitudinal magnetization is given by:

$$M_z = M_0(1 - e^{-t/T_1}) \tag{4.7}$$

as shown in Figure 4.10C. This equation is important for determining the imaging parameters for T_1-contrast images. For example, by choosing when to acquire an image, we can make that image more or less sensitive to T_1 differences between tissues. The details of pulse sequences used for T_1 contrast generation are discussed further in Chapter 5.

Solution for transverse magnetization (M_{xy})

The solution for the transverse magnetization is complicated by the fact that we must now consider the plane defined by two axes, x and y. Equations 4.2a and 4.2b reorganize the Bloch equation, treating the precession term as separate one-dimensional projections, along the x- and y-axes, of an object undergoing circular motion, and the T_2 term as a decay factor (Figure 4.11). Solving for M_x and M_y, given an initial magnetization of $(-M_0, 0)$, we get the following equation pair:

$$M_x = (M_{x0} \cos \omega t + M_{y0} \sin \omega t) e^{-t/T_2} \tag{4.8a}$$

$$M_y = (-M_{x0} \sin \omega t + M_{y0} \cos \omega t) e^{-t/T_2} \tag{4.8b}$$

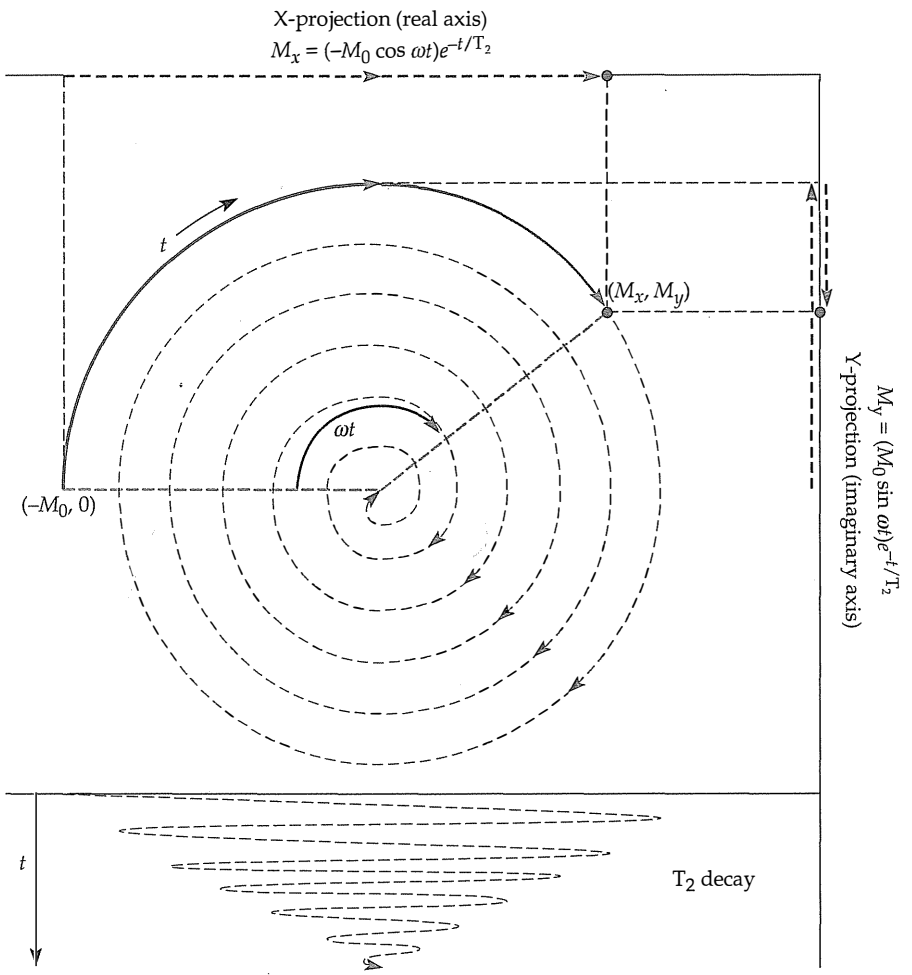

Figure 4.11 The change in transverse magnetization over time (t). The magnetization in the transverse plane is a vector defined by its angle and magnitude. As time passes, its angle follows a circular motion with constant angular velocity ω, while its magnitude decays with time constant T_2. These two components combine to form the inward spiral path shown (dashed lines). Shown at the top and right sides of the spiral path are its projections onto the x- and y-axes, respectively. Within each axis, the projection of the transverse magnetization is a one-dimensional oscillation, as illustrated by the blue and green lines. This oscillation is shown over time at the bottom of the figure, which illustrates the decaying MR signal.

Although these equations appear complex, each describes two components that are illustrated in Figure 4.11. The parenthetical terms (e.g., $M_0 \cos \omega t$) describe one-dimensional projections of circular motion with constant velocity. The exponential term (e^{-t/T_2}) describes the decay of the circle over time. Together, they form an inward spiral pattern. As time (t) increases, the transverse magnetization will spiral farther inward, and transverse signal will be lost at an increasing rate. The constant T_2 determines the rate at which the spiral shrinks. The quantity ωt is the angle of the net magnetization within the transverse plane, and thus determines how fast the spiral turns.

We can combine the x- and y-components of the net magnetization into a more generalized single quantity, M_{xy}, which represents the transverse magnetization. The quantity M_{xy} is traditionally represented as a complex number, with one dimension represented using a real component and another represented using an imaginary component (Equation 4.9).

$$M_{xy} = M_x + iM_y \tag{4.9}$$

This equation depends on a specific initial condition for (M_x, M_y) at ($-M_0$, 0). For an arbitrary initial magnitude of the transverse magnetization $M_{xy0} = M_{x0} + iM_{y0}$, the transverse magnetization can be represented as:

$$M_{xy} = (M_{x0} + iM_{y0})e^{-t/T_2}(\cos \omega t - i \sin \omega t)$$
$$= M_{xy0}e^{-t/T_2}e^{-i\omega t} \tag{4.10}$$

phase Accumulated change in angle.

Here we use the term $e^{-i\omega t}$, which is identical to the term $(\cos \omega t - i \sin \omega t)$, to simplify the later derivation of the MR signal equation. The solution shown in Equation 4.10 states that the transverse magnetization depends on three factors: the initial magnitude of the transverse magnetization (M_{xy0}), a loss of transverse magnetization over time due to T_2 effects (e^{-t/T_2}), and the accumulated phase, or change in angle ($e^{-i\omega t}$). The phase term can be dropped during synchronized detection by having the receiver antenna oscillate at the same frequency as the RF coils, as seen in the previous chapter's discussion of rotating frames of reference. Note that at $t = 0$, the exponential terms e^{-t/T_2} and $e^{-i\omega t}$ both reduce to $e^0 = 1$, so that the transverse magnetization is given by M_{xy0}. But after a long period of time (i.e., $t = \infty$), the term e^{-t/T_2} will become exceedingly small, and thus the transverse MR signal will be zero. Thus, Equation 4.10 is important for determining the imaging parameters for T_2-contrast images. As with T_1, by choosing when to acquire an image, we can make that image more or less sensitive to T_2 differences between tissues. To obtain contrast that is based on the T_2 relaxation parameter, an intermediate delay before image acquisition must be introduced, as will be discussed in the next chapter. The decay of the transverse magnetization, visualized in one dimension, is illustrated at the bottom of Figure 4.11. The details of pulse sequences used for T_2 contrast generation will be discussed further in Chapter 5.

Thought Question

Why does the transverse magnetization vector take a spiraling path rather than a circular path? How does the amplitude of the measured MR signal change over time?

After the spin excitation, the magnetic field, **B**, experienced by spins at a given spatial location, will depend on the large static field, $\mathbf{B_0}$, and the smaller gradient field, **G**. The static field is oriented along the main axis of the scanner, and the gradient field modulates the strength of the main static field along the x-, y-, and z-axes. Note that while the magnitude of **B** varies depending on the spatial location (x, y, z), its direction is always aligned with the main field. Therefore, we can describe the magnitude of the total magnetic field, **B**, experienced by a spin system at a given spatial location (x, y, z) and time point (τ) as a linear combination of the static field and the gradient fields, which are direction-specific and vary over time:

$$B(\tau) = B_0 + G_x(\tau)x + G_y(\tau)y + G_z(\tau)z \tag{4.11}$$

Knowing that $\omega = \gamma B$, we can substitute the ω term in Equation 4.10 using the magnitude of the total magnetic field described in Equation 4.11 and get the following rather intimidating equation. Here we have split the exponential $e^{-i\omega t}$ into separate terms that describe the accumulated phase over time t, caused by the strength of the static magnetic field (B_0) and by the time-varying gradient fields ($G_x(\tau)$, $G_y(\tau)$, $G_z(\tau)$) at any given instant τ:

$$M_{xy}(x,y,z,t) = M_{xy0}(x,y,z)e^{-t/T_2}e^{-i\gamma B_0 t}e^{-i\gamma\int_0^t (G_x(\tau)x + G_y(\tau)y + G_z(\tau)z)d\tau} \tag{4.12}$$

Again, although this equation has many components and seems complex, it can be broken down into simpler and more understandable parts. It states that the transverse magnetization for a given spatial location and time point,

$M_{xy}(x, y, z, t)$, is governed by four factors: (1) the original magnetization at that spatial location, $M_{xy0}(x, y, z)$; (2) the signal loss due to T_2 effects, $e^{-t/T2}$; (3) the accumulated phase due to the main magnetic field, $e^{-i\gamma Bot}$; and (4) the accumulated phase due to the gradient fields:

$$e^{-i\gamma\int_0^t (G_x(\tau)x+G_y(\tau)y+G_z(\tau)z)d\tau}$$

Note that this last factor is indicated as an integral over time because gradients may change over time in some forms of MRI. If a constant gradient along one direction were used (e.g., G along the x-direction), the accumulated phase over time t could be more simply described as $\gamma G_x t$.

Let us pause for a moment to review what we have covered so far. We know that the net magnetization of a sample within a magnetic field can be thought of as a vector with magnitude and direction. The net magnetization vector can be broken down into longitudinal (along the static magnetic field) and transverse (perpendicular to the static magnetic field) components. After the net magnetization is tipped toward the transverse plane by an excitation pulse, it precesses around the longitudinal axis at the Larmor frequency. The precession of the net magnetization in the transverse plane allows for measurement of the MR signal. We have just learned that the introduction of a spatial magnetic gradient alters the transverse magnetization over time, because the frequency of precession depends on the local magnetic field strength. This last point suggests that spatial gradients may allow encoding of spatial information within the MR signal. We explore this possibility in the next section.

MR signal The current measured in a detector coil following excitation and reception.

MR signal equation A single equation that describes the MR signal as a function of the properties of the object being imaged under a spatially varying magnetic field.

The MR signal equation

MRI typically does not use separate receiving antennae for individual voxels. Indeed, such a setup would be impossible given that there may be 100,000 or more voxels within a single imaging volume. Often we use a single antenna (e.g., a volume coil) that covers a large region. The **MR signal** measured by the antenna reflects the sum of the transverse magnetizations of all voxels within the excited sample. We re-emphasize this important point because it underlies all of the principles of image formation: again, the total signal measured in MRI combines the changes in net magnetization generated at every excited voxel. This can be restated in the formal mathematical terms of Equation 4.13, which expresses the MR signal at a given point in time, $S(t)$, as the spatial summation of the MR signal from every voxel:

$$S(t) = \int_x \int_y \int_z M_{xy}(x, y, z, t)dx\,dy\,dz \tag{4.13}$$

Combining Equations 4.12 and 4.13 results in Equation 4.14:

$$S(t)=\int_x \int_y \int_z M_{xy0}(x,y,z)e^{-t/T_2}e^{-i\omega_0 t}e^{-i\gamma\int_0^t (G_x(\tau)x+G_y(\tau)y+G_z(\tau)z)d\tau}dxdydz \tag{4.14}$$

Equation 4.14 can be read as stating that the total MR signal measured at any point in time reflects the sum across all voxels of the net magnetization at time point zero, multiplied by a decay factor based on T_2, with the accumulated phase given by the combined strength of the static magnetic field and of the gradient field at that point in space. This vastly important equation is known as the **MR signal equation**, because it reveals the relationship between the acquired signal, $S(t)$, and the properties of the object being imaged, $M(x,y,z)$. It is important to recognize that this equation is sufficiently general to describe the MR signal in virtually all imaging methods.

slice A single slab of an imaging volume. The thickness of the slice is defined by the strength of the gradient and the bandwidth of the electromagnetic pulse used to select it.

In practice, the term $e^{-i\omega_0 t}$ is not necessary for calculation of the MR signal, because modern MRI scanners demodulate the detected signal with the resonance frequency ω_0. That is, they synchronize data acquisition to the resonance frequency. This demodulation process is analogous to the idea of transforming from laboratory to rotating reference frames, as introduced in Chapter 3. Imagine that you were watching the precession of the transverse magnetization from the laboratory (i.e., normal) reference frame. You would see the transverse magnetization spinning around the longitudinal axis at the Larmor frequency. Now imagine that you were rotating around the longitudinal axis at the same speed as the precessing magnetization. The magnetization vector would now appear to be still.

The T_2 decay term, e^{-t/T_2}, affects the magnitude of the signal but not its spatial location. Because it does not contain any spatial information, we can ignore it for the moment. By removing these two terms, we arrive at a simpler version of the MR signal equation:

$$S(t) = \int_x \int_y \int_z M_{xy0}(x,y,z) e^{-i\gamma \int_0^t (G_x(\tau)x + G_y(\tau)y + G_z(\tau)z)d\tau} dxdydz \tag{4.15}$$

This equation illustrates the profound importance of the gradient fields for encoding spatial information within an MR image. In principle, we can collect a single three-dimensional (3-D) MR image by systematically turning on gradient fields along the x, y, and z-axes. However, because 3-D imaging sequences present additional technical challenges and are less tolerant of hardware imperfections, most forms of imaging relevant to fMRI studies use two-dimensional (2-D) imaging sequences. For the sake of simplicity, we will next discuss the principles underlying common 2-D imaging techniques. We will return to the less common 3-D imaging techniques at the end of the chapter.

Slice Selection, Spatial Encoding, and Image Reconstruction

Note that the simplified MR signal equation (see Equation 4.15) is still in 3-D form, in that the signal contribution from each spatial location depends on all three spatial gradients. In order to reduce this signal equation to two dimensions, there must be some way to eliminate variation over one spatial dimension. This can be accomplished by separating the signal-acquisition process into two steps. First we select a particular slice within the total imaging volume using a one-dimensional excitation pulse. Then we use a two-dimensional spatial encoding scheme within the slice to resolve the spatial distribution of the spin magnetizations. This two-step process forms the basis for most pulse sequences used in MRI, including those used for nearly all fMRI images. We will discuss the theoretical bases for these steps in this section, and describe their practical implementation in the following sections.

Slice selection

The first step in an imaging sequence is slice selection. Remember that the goal of slice selection is to excite only a particular thin slab of the sample so that the signal within that slab can be spatially encoded. From Chapter 3 we know that an electromagnetic field ($\mathbf{B}_1$) at the Larmor frequency, when applied in the transverse plane, tips the longitudinal magnetization. If the duration and strength of the electromagnetic field are appropriately calibrated, the longitudinal magnetization will rotate exactly into the transverse plane. Such a cali-

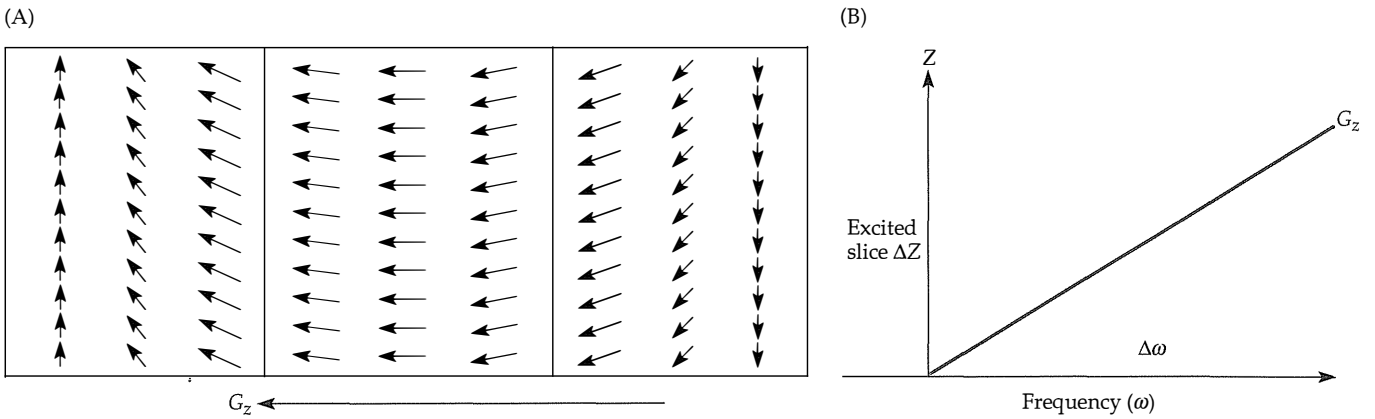

Figure 4.12 Slice selection. As shown in (A), application of a slice selection gradient (G_z) changes the Larmor frequency of spins within the sample. The gradient is chosen so that spins within the slice of interest (shading) will precess at the desired frequency. Following the application of the gradient, a subsequent excitation pulse at a given frequency (ω) and bandwidth (Δω) is applied. As shown in (B), the excitation frequency and the frequency bandwidth determine the slice location (Z) and slice thickness (ΔZ).

brated electromagnetic field is known as an excitation pulse. But if the magnetic field were uniform, the applied excitation pulse would affect all of the spins within the volume. However, by introducing a static gradient along the slice selection axis (e.g., G_z), we can tune the Larmor frequencies of all spins in the slice (and only those spins) to match the frequency of the excitation pulse (Figure 4.12).

Ideally, we would like to excite a perfectly rectangular slice along the z-direction; for example, we might excite all spins from $z = +10$ mm to $z = +15$ mm and no spins outside of that range. One might think that this could be achieved by a rectangular slice selection pulse, as shown in Figure 4.13A. How-

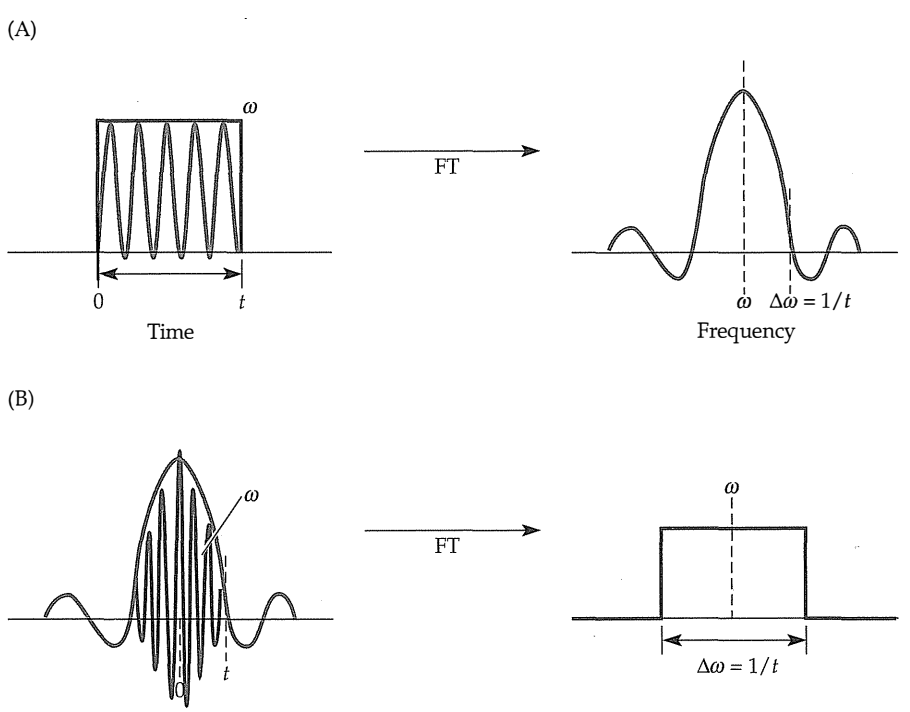

Figure 4.13 Possible slice selection pulses. (A) A rectangular slice selection pulse that consists of a constant application of a radiofrequency field at frequency ω_0 for a time t. The slice selection profile of this pulse is given by its Fourier transform (FT) and shown at right as a sinc function with fundamental frequency ω_0. This profile is not ideal for selection of a rectangular slice. However, (B) shows the use of a pulse with time amplitude given by a sinc function. This pulse gives a rectangular frequency profile and allows excitation of spins within a rectangular slice.

interleaved slice acquisition The collection of data in an alternating order, to minimize the influence of excitation pulses on adjacent slices.

ever, a rectangular pulse actually contains a distribution of frequencies shaped like a sinc function, so it does not excite a rectangular slice. Instead, we must use a sinc-modulated electromagnetic pulse (Figure 4.13B). Since the Fourier transform of a sinc function is a rectangular function, a sinc-modulated pulse has a rectangular frequency response; thus it contains all frequencies within a band and no frequencies outside that band.

Although a perfectly rectangular slice profile would be optimal, it is difficult to achieve because of off-resonance excitation. As discussed in the previous chapter, off-resonance effects may excite spins to some intermediate stage, as they rotate about the $\mathbf{B}_{1\mathrm{eff}}$ field. The primary consequence for MRI is cross-slice excitation, or the bleeding of excitation from one slice to the next. If we excite adjacent slices sequentially, each slice will have been pre-excited by the previous excitation pulse, leading to saturation of the MR signal. To minimize this problem, most excitation schemes use interleaved slice acquisition. For example, if we are to excite ten contiguous slices, we will excite in order the first, third, fifth, seventh, ninth, second, fourth, sixth, eighth, and tenth slices. The use of interleaved slice acquisition effectively eliminates excitation overlap problems.

Slice location and thickness are determined by three factors: the center frequency of the excitation pulse (ω), the bandwidth of the excitation field ($\Delta\omega$), and the strength of the gradient field (G_z), as illustrated in Figure 4.14. Together, the center frequency and the gradient field determine the slice location, while the bandwidth and the gradient field determine the slice thickness. This relationship can be described by $\omega \pm \Delta\omega/2 = \gamma G_z (z \pm \Delta z/2)$. By sliding the center frequency up and down over successive acquisitions, the MR signal from different slices along the z-axis can be acquired selectively. Likewise, by choosing a wide or narrow excitation bandwidth, thick or thin slices can be collected. Note that the use of a stronger gradient, in principle, means that spins at nearby spatial locations will have greater differences in their Larmor frequencies, allowing for more selective excitation by a given electromagnetic pulse. Thus, stronger gradients increase spatial resolution across slices.

Thought Question

Assume that we doubled the strength of the gradient fields in our scanner. How would the frequency and bandwidth of the excitation pulse need to change to keep the same slice selection?

In summary, slice selection involves the application of an electromagnetic pulse that excites spins within one slice but has no effect on spins outside that slice. The slice chosen by the selection process is defined by its location, orientation, and thickness. For example, let us assume that we want to create an image of a plane centered at $z = z_0$. For a given location (x, y) within that slice, the total magnetization summed along the z-direction, $M(x,y)$, for a thickness Δz is given by Equation 4.16. This equation describes the bulk magnetization of an individual voxel, or x–y coordinate pair, within the slice.

$$M(x,y) = \int_{z_0-\frac{\Delta z}{2}}^{z_0+\frac{\Delta z}{2}} M_{xy0}(x,y,z)dz \tag{4.16}$$

After slice selection, all signals along the z-direction are integrated, therefore, the magnetization, M, is dependent only on x and y, but not on z. Thus, by first

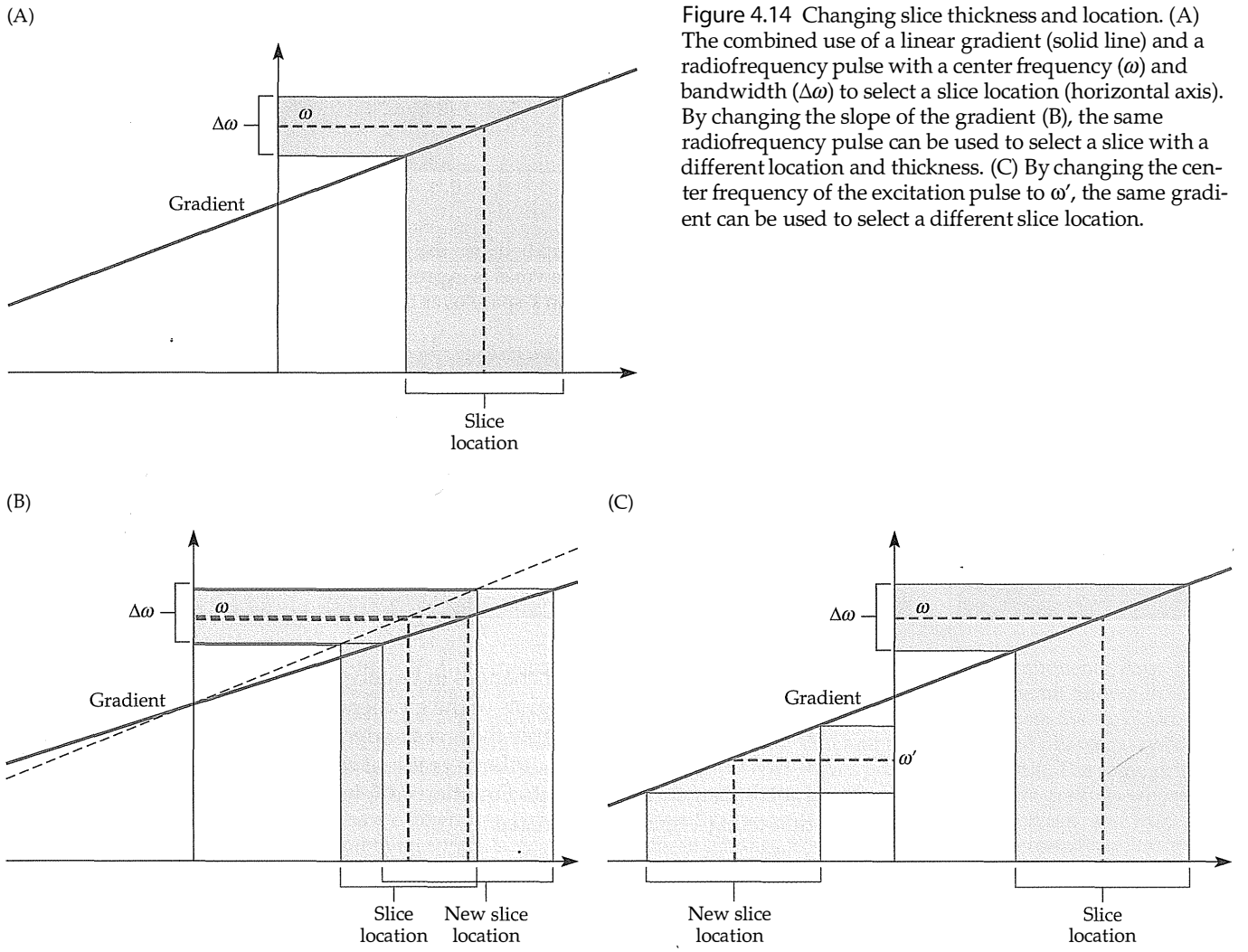

Figure 4.14 Changing slice thickness and location. (A) The combined use of a linear gradient (solid line) and a radiofrequency pulse with a center frequency (ω) and bandwidth ($\Delta\omega$) to select a slice location (horizontal axis). By changing the slope of the gradient (B), the same radiofrequency pulse can be used to select a slice with a different location and thickness. (C) By changing the center frequency of the excitation pulse to ω', the same gradient can be used to select a different slice location.

selecting an imaging slice, the simplified MR signal equation (see Equation 4.15) can be further reduced into a 2-D form, as follows:

$$S(t) = \int_x \int_y M(x,y) e^{-i\gamma \int_0^t (G_x(\tau)x + G_y(\tau)y)d\tau} \, dx dy \qquad (4.17)$$

Two-dimensional spatial encoding (frequency and phase encoding)

Equation 4.17 states that the total signal recorded from a slice depends on the net magnetization at every (x, y) location within that slice, and that the phases of individual voxels in the slice depend on the strengths of the gradient fields at that location. Although the parts of Equation 4.17 are individually understandable, this equation is difficult to visualize and solve in its present form. To facilitate a better understanding of the relation between the MR signal, $S(t)$, and the object to be imaged, $M(x,y)$, MR researchers have adopted a different notation scheme known as *k*-space. Recognize that *k*-space differs in an impor-

k-space A notation scheme used to describe MRI data acquisition. The use of *k*-space provides mathematical and conceptual advantages for describing the acquired MR signal in image form.

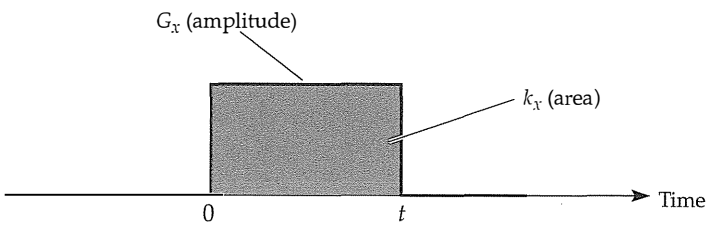

Figure 4.15 The relationship between the gradient waveform and k-space. The effect of a gradient, G_x, on a given voxel is expressed as the amplitude of the gradient signal over time. The change in k-space over time is given by the blue area of the graph.

k-space trajectory A path through k-space. Different pulse sequences adopt different k-space trajectories.

image reconstruction The process by which the raw MR signal, as acquired in k-space form, is converted into spatially informative images.

tant way from the normal space, in which the object resides. Consider the terms k_x and k_y in Equation 4.18. Each equation represents the time integral of the appropriate gradient multiplied by the gyromagnetic ratio:

$$k_x(t) = \frac{\gamma}{2\pi}\int_0^t G_x(\tau)d\tau \tag{4.18a}$$

$$k_y(t) = \frac{\gamma}{2\pi}\int_0^t G_y(\tau)d\tau \tag{4.18b}$$

These equations state that changes in k-space over time, or **k-space trajectories**, are given by the time integrals of the gradient waveforms. In other words, the k-space trajectories are simply the areas under the gradient waveforms, as illustrated in Figure 4.15 for a uniform gradient change over a time interval (t). By substituting these terms into Equation 4.17, we can restate the MR signal equation using k-space coordinates:

$$S(t) = \int_x \int_y M(x,y)e^{-i2\pi k_x(t)x}e^{-i2\pi k_y(t)y}dxdy \tag{4.19}$$

Equation 4.19 is remarkable because it indicates that k-space and image space have a straightforward relationship: they are 2-D Fourier transforms of each other. Just as any signal that changes over time, no matter how complex (e.g., a musical composition), can be constructed from a series of simpler frequencies, any image can be constructed from a series of simpler components in what is called the spatial-frequency domain (Figure 4.16). The Fourier transform is one mathematical tool for this construction process. The mathematics of the Fourier transform are well established, so we can take advantage of those mathematics to decode the k-space representation of the MR signal, $S(t)$, into the magnetization at each spatial location, $M(x,y)$, creating a spatially informative image. Equation 4.19 suggests that an inverse Fourier transform can convert k-space data into an image, a process known as **image reconstruction**. Conversely, a forward Fourier transform can convert image-space data into k-space data.

To collect the k-space data needed for image formation, we apply additional magnetic gradients known as frequency- and phase-encoding gradients. These gradients influence the individual spin phases for different voxels, as illustrated in Figure 4.17, which in turn alters the total MR signal that is recorded from the sample. As we learned earlier in this chapter, if we reorganize signal $S(t)$ to $S(k_x(t), k_y(t))$ as indicated in Equation 4.19, then the MR signal can be represented by a 2-D function in a coordinate system where k_x and k_y are the two axes. This coordinate system defines k-space and has units in

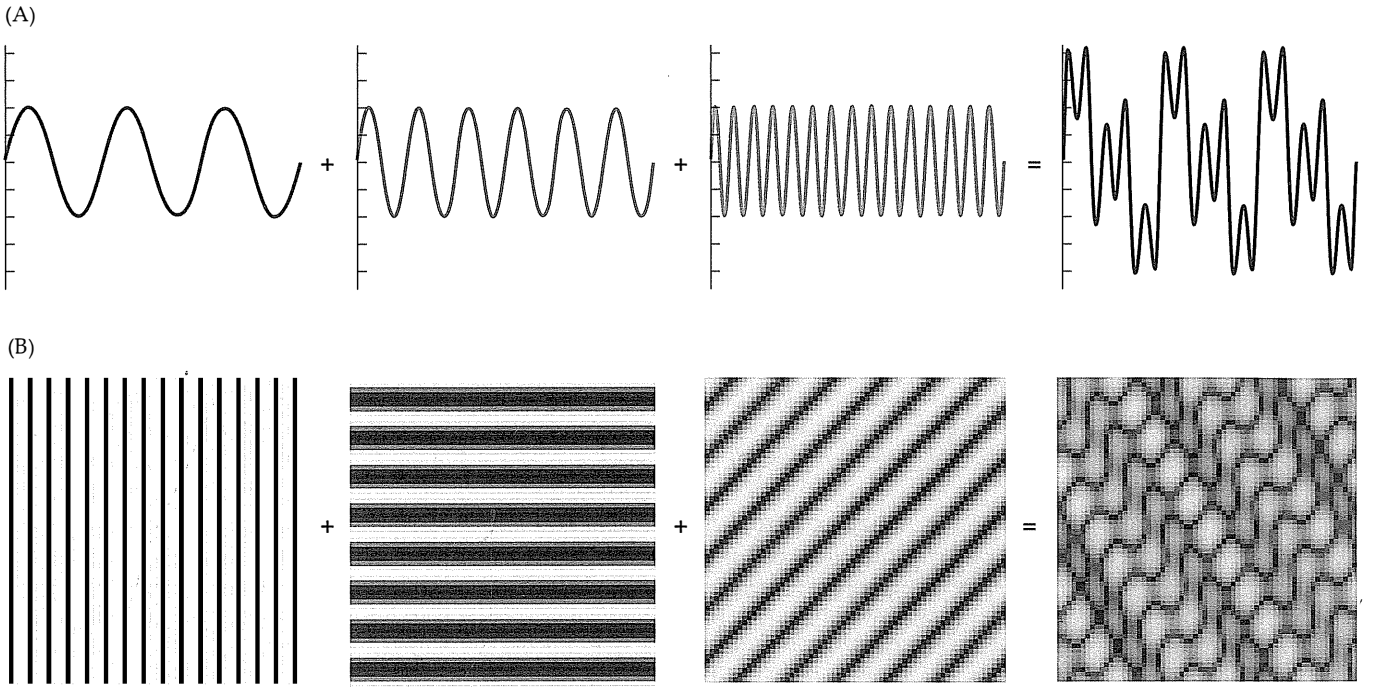

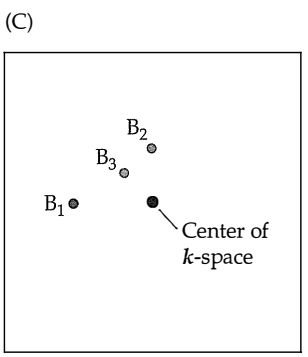

Figure 4.16 Constructing a complex waveform or image from simpler components. Any dataset, no matter how complex, can be constructed from simpler components. Shown in (A) are three sine waves, each with a different frequency. When combined, they form the waveform at right. By combining more and more sine waves of different frequencies and phases, very complex waveforms can be created, such as the sound waves produced by music. The same principle holds for two-dimensional data (B), except that here the components are gratings whose patterns are determined by spatial frequencies (i.e., distances between bars), phases, and angles. By combining a very large number of these gratings, complex images can be created, such as those used in MRI. Shown in (C) is the k-space plot of the summed image; the individual gratings shown in (B) each correspond to one of these three points (B_1, B_2, and B_3, respectively) in k-space.

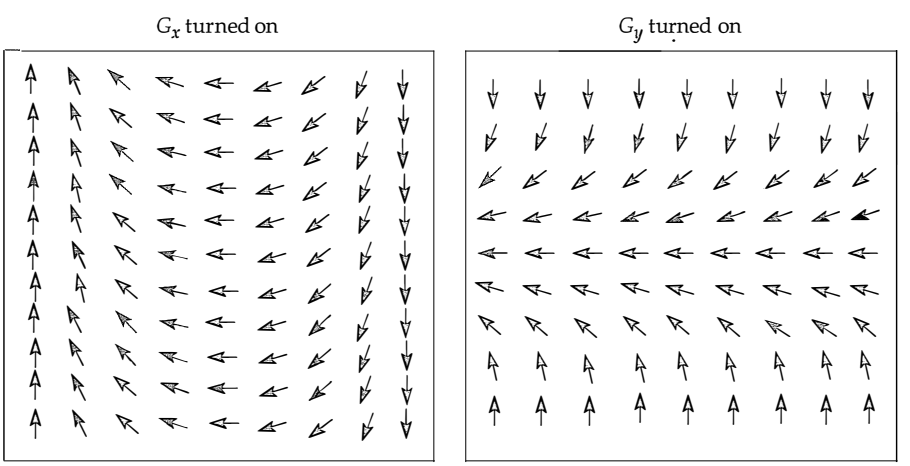

Figure 4.17 A schematic illustration of the effects of magnetic field gradients on spin phase. Each arrow shows the phase of spins at a given location in space, following the application of either a x-gradient (A) or y-gradient (B). For example, a stronger magnetic field from left to right (x-gradient) would cause spins at the right side of image space to precess faster than those on the left side. Thus, the spins on the right would accumulate phase (i.e., angle of their spin axis, relative to the main magnetic field) over time.

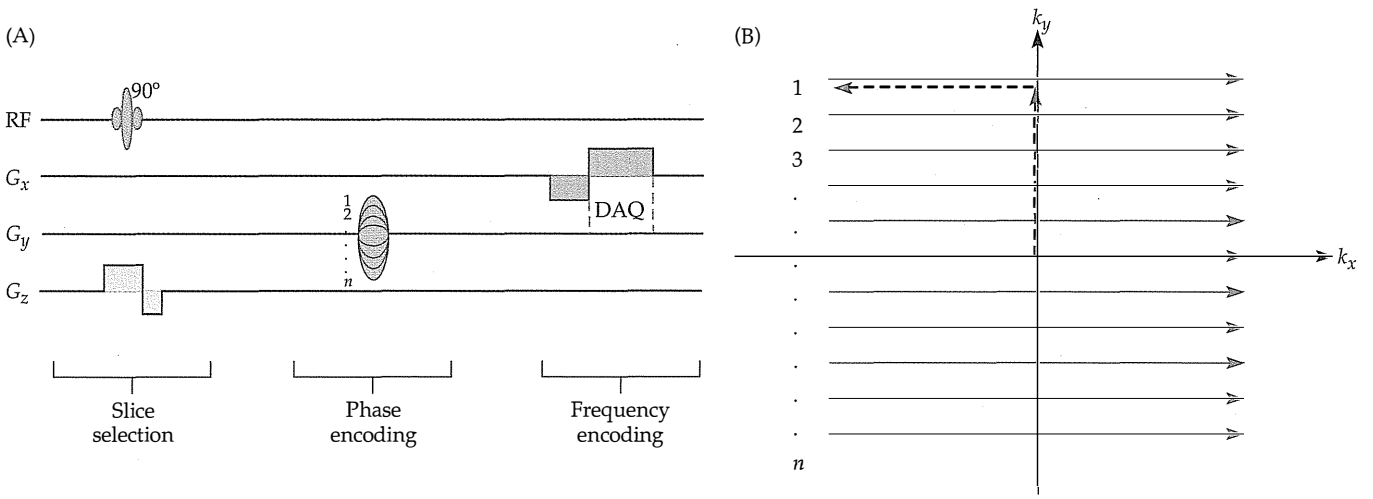

Figure 4.18 A typical two-dimensional gradient-echo pulse sequence. Shown in (A) are lines representing the activities of the radiofrequency field (RF) and the three spatial gradients. The pulse sequence begins with a combined slice selection gradient (G_z) and excitation pulse. The G_y gradient is used for selecting one line of *k*-space following each excitation pulse, while the G_x gradient is turned on during data acquisition (DAQ). The sequence then repeats with a G_y of different strength for each of the *n* lines of the image. (B) Shown here is the pattern that this sequence traverses in *k*-space. Each line of *k*-space is acquired following a separate excitation, then the application of the G_y at a particular strength (causing an upward or downward motion in *k*-space), then the application of the G_x at a constant strength and duration (causing a rightward motion in *k*-space). Following *n* excitations, all of *k*-space is filled and image acquisition is complete.

filling *k*-space The process of collecting samples from throughout *k*-space in order to collect data sufficient for image formation.

gradient-echo (GRE) imaging One of the two primary types of pulse sequences used in MRI; it uses gradients to generate the MR signal changes that are measured at data acquisition.

spatial frequency (1/distance). Because a complete sample of the *k*-space is usually required to construct an image, collecting the MR signal is often referred to as filling *k*-space.

Remember from Figure 4.15 that k_x and k_y are actually time integrals of the gradient waveform. Thus, by manipulating the gradient waveforms, we can control the sampling path within *k*-space during MR signal acquisition. For example, by altering the strength of different gradients over time, we could first collect data from the upper-left point in *k*-space, and then move rightward, and then downward, and then leftward, etc., tracing a snakelike path through the image. While any path that covers all of *k*-space can be used to collect the *k*-space data, in practice, regular paths that include straight lines or smooth curves are preferred.

In typical anatomical imaging sequences, like the gradient-echo sequence shown in Figure 4.18A, *k*-space is filled one line at a time, following a succession of individual excitation pulses. During each excitation the combination of the electromagnetic pulse and the G_z gradient selects the desired slice. Then, one gradient (e.g., G_y) is turned on before the data acquisition period. This accumulates a certain amount of phase offset before the activation of the other (e.g., G_x) gradient is applied. This results in the movement of the effective location of data acquisition in *k*-space along the *y*-direction, as shown by the blue arrow in Figure 4.18B. In this example, G_y can be considered to be the phase-encoding gradient, as it was used to generate a certain amount of phase before the acquisition. During data acquisition, the G_x gradient is turned on, changing the frequency of the spins during signal readout, so by convention G_x is named the

frequency-encoding gradient. Note, however, that both gradients act similarly in driving the position of data acquisition within *k*-space, because k_x and k_y both reflect the time integrals of the gradient waveforms.

Sampling of *k*-space occurs in a discrete fashion. Along the k_y direction, each line represents a separate amplitude of the G_y gradient (shown as 1...*n* steps in Figure 4.18B). While the trajectory along the k_x direction is continuous, the MR signal is sampled digitally with a specific interval, so that each row consists of a number of discrete data points.

spatial frequency The frequency with which some pattern occurs over space.

Relationship between image space and k-*space*

To illustrate the relationship between image space and *k*-space, Figure 4.19 shows some sample images and the resulting Fourier transforms. Think of each pair as showing an object and the acquired MR signal in its raw form within *k*-space. An image with a single circle at its center corresponds to a pattern of alternating light and dark circles throughout *k*-space (Figure 4.19A). (This pattern is equivalent to a 2-D Bessel sinc function.) Note that the center of *k*-space represents the point in time when the signals from all voxels are at the same phase, so it represents the total transverse magnetization within that slice. Thus, the center always has the highest signal of any point in *k*-space.

We can add a second circle to the image to illustrate another concept, that *k*-space reflects the spatial frequency of the object(s) in the image space. Spatial frequency defines how often some pattern occurs in space, just as temporal frequency (e.g., the pitch of a piano note) defines how often something occurs in time (e.g., the vibration rate of one string of that piano). Shown in Figure 4.19B are two circles, one offset from the center. If we trace a line from the top left to the bottom right of the image, it will encounter two circles separated by a distance between their centers. The *k*-space data will thus have a spatial-frequency component along that line, with the frequency equal to the inverse of that distance. This is visible as a grating running from top left to bottom right in the *k*-space image, on top of the concentric pattern that results from the shapes of the circles.

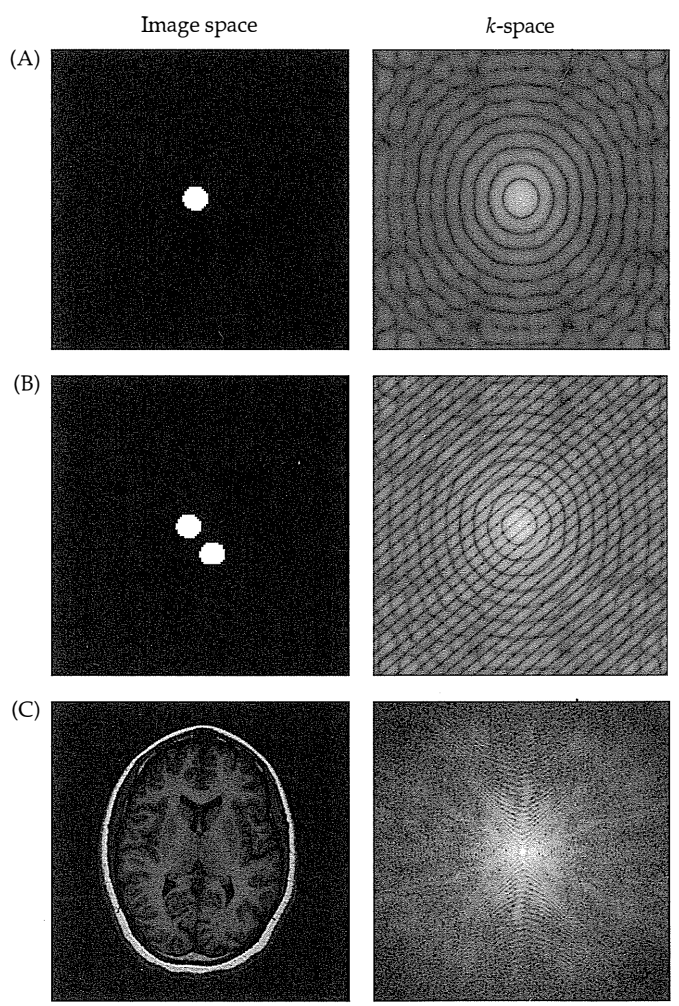

Figure 4.19 Images and their Fourier transforms. (A) A single circle at the center of the image space and the representation of the circle in *k*-space. Note that the *k*-space representation follows a sinc function, with greatest intensity at the center and intensity bands of decreasing amplitude toward the edges of the *k*-space. Addition of a second circle to the image space (B) introduces a grating pattern to the *k*-space. An image of the brain (C) contains much more spatial information, and thus its representation in *k*-space is similarly more complex.

Thought Question

How would the *k*-space data in Figure 4.19B change if the lower circle were moved to the bottom-left quadrant of the image? How would the *k*-space data change if it were moved farther toward the bottom-right corner?

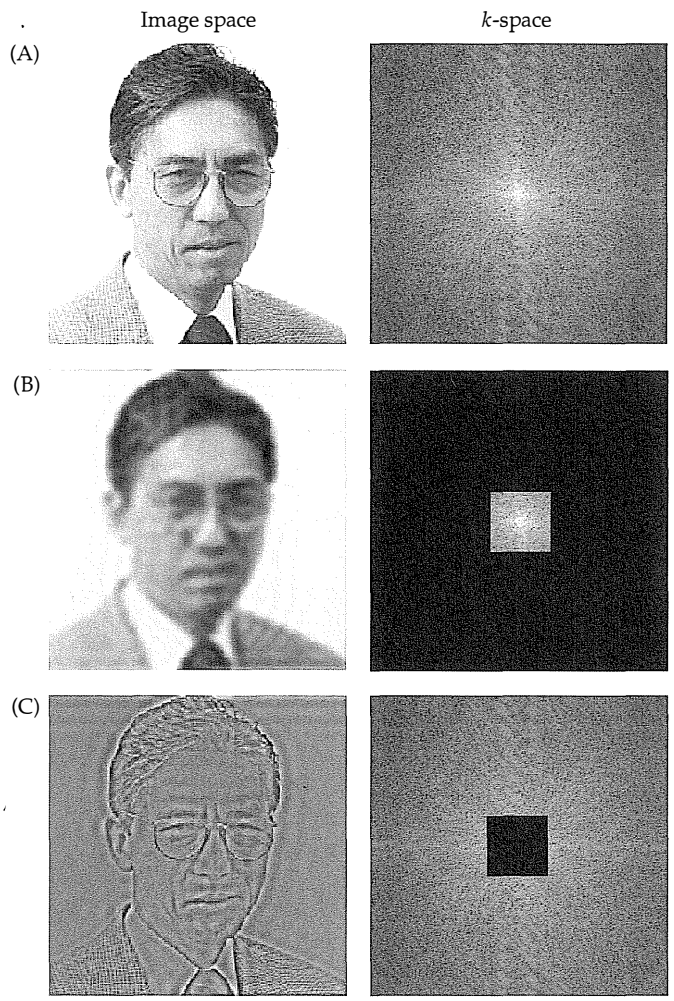

Figure 4.20 How the different parts of *k*-space contribute to image space. Images such as this photograph of Dr. Seiji Ogawa can be converted using a Fourier transform into *k*-space data (A). Different parts of the *k*-space data correspond to different spatial-frequency components of the image. The center of *k*-space (B) provides low-spatial-frequency information, retaining most of the signal but not fine details. The periphery of *k*-space (C) provides high-spatial-frequency information, and thus more image detail, but it contributes relatively little signal to the image.

Any image, no matter how complex, can be represented as an assembly of spatial-frequency components. The *k*-space representation of an anatomical image is shown in Figure 4.19C. The *k*-space image is brightest in the center and darkest near the edges. This illustrates that low-spatial-frequency data (i.e., grating patterns with thick lines) from near the center of *k*-space are most important for determining the signal-to-noise ratio of the image. In comparison, high-spatial-frequency data collected at the periphery of *k*-space (i.e., grating patterns with thin lines) help to increase the spatial resolution of the image. Figure 4.20 illustrates this important distinction between the low-spatial-frequency and high-spatial-frequency regions of *k*-space. If we take from a normal photograph (Figure 4.20A) only the low-spatial-frequency region of its *k*-space data, the image would have most of the signal but would lack good spatial resolution (Figure 4.20B). But if we take only the high-spatial-frequency region of its *k*-space data, the image would have a low signal level, and would lack overall brightness differences between areas of the image, but the spatial detail would be preserved (Figure 4.20C).

Contrary to intuition, there is *not* a one-to-one relationship between points in *k*-space and voxels in image space. For an illustration of what each point in *k*-space represents, consider Figure 4.21. The center plot shows the *k*-space data (or raw MR signal). Each point in the *k*-space data is acquired at a different point in time and has contributions from all voxels within the slice. We have highlighted four sample *k*-space points, each showing the net magnetization vectors within each voxel (in image space) at the moment in time when that point in *k*-space was acquired. For the point at the center of *k*-space (Figure 4.21A), all of the magnetization vectors are at the same phase, and thus the total signal is at its maximum. At other *k*-space points (Figure 4.21B–D), the magnetization vectors differ across voxels, and the intensity of the *k*-space point represents the sum of those vectors.

Converting from k-*space to image space*

After *k*-space is filled, a 2-D inverse Fourier transform, is necessary for conversion of the raw data from *k*-space

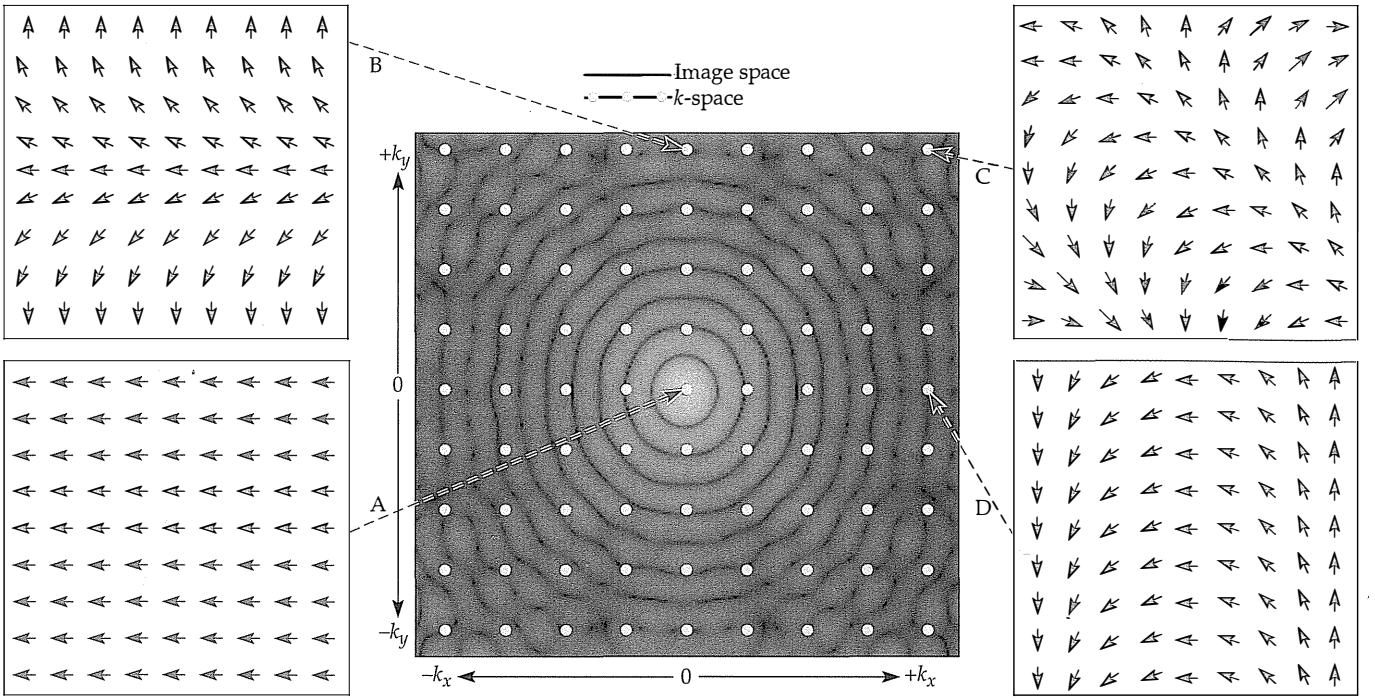

Figure 4.21 Contributions of different image locations to the raw k-space data. Each data point in k-space (shown in yellow) consists of the summation of the MR signal from all voxels in the image space, based on the x- and y-gradients that have been applied so far. For four k-space points (A–D), the side plots indicate the relative phases of the magnetization vectors for sample voxels in image space. For the center of k-space, the phases for all voxels in the respective image space are identical (A), therefore leading to the maximum signal in k-space. For a data point where k_y is at the maximum and k_x is at zero (B), the precession frequency of the magnetization vectors changes rapidly along the y-direction but remain the same along the x-direction. Thus, there will be an accumulated phase differential along the y-direction. For a data point where both k_x and k_y are large (C), the relative phases change rapidly along the combined diagonal direction. And finally, where k_y is zero and k_x is at its maximum (D), the relative phases change rapidly only along the x-direction.

to image space, $M(x,y)$. It is important to recognize that the sampling parameters in these two spaces are inversely proportional to each other. In image space, the basic sampling unit is distance, while in k-space, the basic sampling unit is spatial frequency (1/distance). Qualitatively speaking, this means that a wider range of coverage in k-space results in higher spatial resolution in image space (i.e., smaller voxels). This concept can be appreciated by the photographs shown in Figure 4.20, which demonstrate that the periphery of k-space contributes to the fine details of the image (i.e., the spatial resolution). Conversely, finer sampling in k-space results in a greater extent of coverage, or a larger field of view, in the image domain. This relationship is illustrated graphically in Figure 4.22 and quantitatively in Equation 4.20a,b. Here, field of view (FOV) is defined as the total distance along a dimension of image space (i.e., how large the image is). Typical fields of view in fMRI experiments are about 20 to 24 cm.

field of view (FOV) The total extent of an image along a spatial dimension.

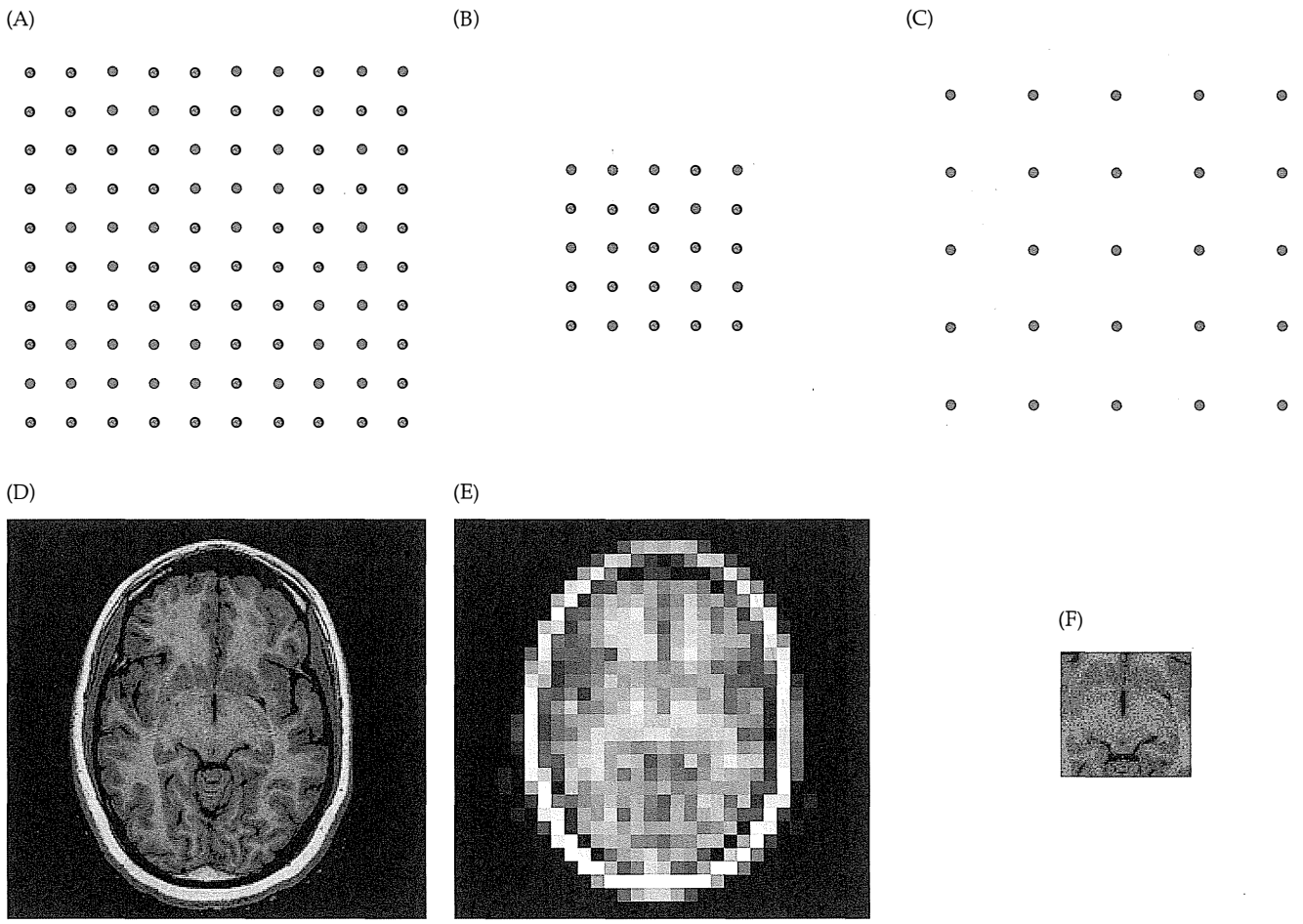

Figure 4.22 Effects of sampling in k-space on the resulting images. The field of view and resolution have an inverse relationship when applied to image space and k-space. (A) A schematic representation of densely sampled k-space with a wide field of view, resulting in the high-resolution image (D). (B) If only the center of k-space is sampled, albeit with the same sampling density, then the resulting image (E) has the same field of view but lower spatial resolution. (C) Conversely, if k-space is sampled across a wide field of view but with a limited sampling rate, the resulting image will have a small field of view but high resolution (F).

$$\mathrm{FOV}_x = \frac{1}{\Delta k_x} = \text{sampling rate along } k_x = \frac{1}{\frac{\gamma}{2\pi}(G_x \Delta t)} \tag{4.20a}$$

$$\mathrm{FOV}_y = \frac{1}{\Delta k_y} = \text{sampling rate along } k_y = \frac{1}{\frac{\gamma}{2\pi}(\Delta G_y \mathrm{t})} \tag{4.20b}$$

These equations can be reorganized (Equation 4.21a,b) to give the voxel size, which is just the FOV divided by the number of samples. Note that the quantities $2k_{\mathrm{xmax}}$ and $2k_{\mathrm{ymax}}$ refer to the total extent of k-space along each of the cardinal directions. If k_{max} is large, then the voxel size will be small.

$$\frac{\mathrm{FOV}_x}{M_x} = \frac{1}{M_x \Delta k_x} = \frac{1}{2k_{x\mathrm{max}}} \tag{4.21a}$$

$$\frac{\mathrm{FOV}_x}{M_y} = \frac{1}{M_y \Delta k_y} = \frac{1}{2k_{y\mathrm{max}}} \tag{4.21b}$$

In summary, the raw MR signal, $S(t)$, is a one-dimensional string of data points through k-space that has been sampled at a very high rate. This signal can be broken into two dimensions, according to k_x and k_y, to facilitate a 2-D inverse Fourier transform. Decreasing the separation between adjacent data points in k-space increases the FOV in image space. Likewise, increasing the extent of k-space decreases the voxel size in image space. Note also that if we want to collect data from $N \times N$ voxels in our image, then we need an equal number of k-space data points ($N \times N$).

3-D Imaging

While 2-D imaging methods are common for most applications, not all MR imaging techniques are based on 2-D principles. Pulse sequences that collect k-space data in three dimensions are often used, especially for high-resolution anatomical images. Compared with 2-D imaging, 3-D sequences provide the primary advantage of a high signal-to-noise ratio, due to the fact that the 3-D volume can be larger than a single slice, and therefore, more excited spins can contribute to the MR signal. The principles of 3-D imaging can be extrapolated from those of 2-D imaging, so in theory, any 2-D imaging sequence can be converted to a 3-D sequence. Since slice selection is unnecessary, the traditional slice excitation step is replaced by a volume excitation step that uses a very small z-gradient to select a thick slab. To resolve spatial information along the z-direction, another phase-encoding gradient is presented along that dimension during the data acquisition phase. Therefore, within a typical 3-D pulse sequence, there are two phase-encoding gradients and one frequency-encoding gradient. The concept of k-space can also be expanded to three dimensions by adding k_z, defined by the time integral of the G_z gradient. To reconstruct the 3-D image, an inverse Fourier transform in three dimensions is executed.

Unfortunately, the advantages of 3-D sequences are accompanied by several disadvantages. For example, phase encoding is usually more vulnerable to field inhomogeneities and motion artifacts than frequency encoding. Because 3-D imaging methods have two phase-encoding dimensions, they are more vulnerable to these artifacts. Also, more time is required to fill k-space when an entire volume is excited than when only a single slice is excited. Thus, movement of the head at any point within the acquisition window will cause distortions throughout the entire imaging volume. In fMRI studies, 3-D imaging is typically restricted to anatomical scans, while most fMRI pulse sequences create 2-D images.

Potential Problems in Image Formation

The goal of any image formation method is to achieve a true representation of the imaged object. Of course, in an ideal scanning environment with a perfectly uniform main magnetic field, perfectly linear gradient fields, an absolutely square excitation profile, and optimized image acquisition software, there would be no problems! Under such perfect conditions, the acquired image would exactly match the scanned object in every way. It would have the same size and shape, with local intensities dependent on the appropriate proton densities and relaxation characteristics. However, as anyone with substantial MRI experience will attest, the images acquired under normal laboratory conditions are not always faithful to the original objects. We next discuss some of the typical problems encountered in forming MR images.

The first problem to consider is inhomogeneity of the static magnetic field, which means that the actual strength of the field at one or more spatial locations is not the same as the theoretically desired value. Note that inhomogeneity in the static magnetic field becomes increasingly problematic at higher field strengths, because it becomes more difficult to adequately shim the field to correct for local distortions. The imperfection in the static field can be mathematically represented by a difference quantity, ΔB_0, representing the increased or decreased field strength at a given location. Equation 4.22 is a modified version of the MR signal equation that contains the new term ΔB_0:

$$S(t) = \int_x \int_y m(x,y) e^{-i2\pi(k_x(t)x + k_y(t)y + \Delta B_0 t)} dx dy \tag{4.22}$$

We usually do not know the exact nature of static field inhomogeneities, but if present they will introduce artifacts in images, following conventional inverse Fourier transformations. In practice, ΔB_0 can lead to two distinct types of artifacts: geometric distortions and variations in signal intensity. We can think of these artifact types, taken roughly, as macroscopic and microscopic effects.

Large-scale inhomogeneities cause geometric distortions due to the spatial shifting of voxels. Because the frequency of spins depends upon the magnetic field strength, magnetic field inhomogeneities will lead to changes in spin frequencies. Remember that the position of a voxel is encoded by its spin frequency. Thus, a voxel with the incorrect spin frequency will be displaced to an incorrect spatial location. Small-scale inhomogeneities cause spins within a voxel to lose coherence due to T_2^* effects. This reduces the total magnetization available within a voxel and thus reduces its signal intensity. These two effects may be present within the same image (Figure 4.23).

A second problem results from nonlinearities in the gradient fields. Because the spatial gradients control the *k*-space trajectories, we use *k*-space to evaluate their artifacts. We use for this example a typical gradient-echo pulse

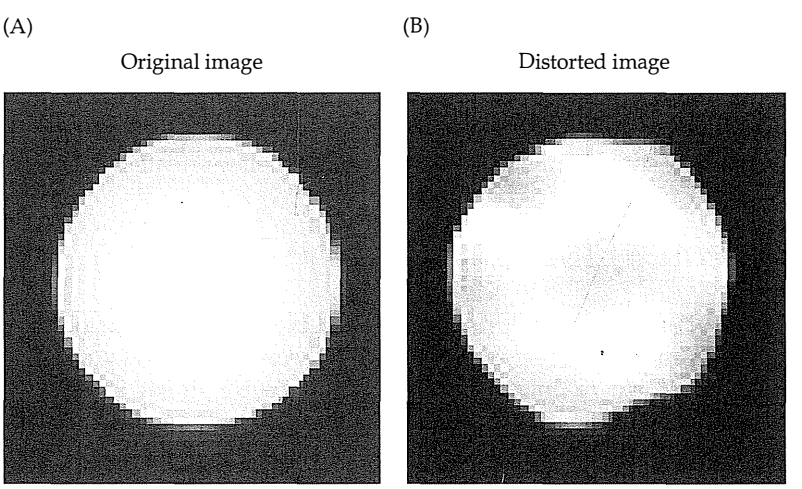

Figure 4.23 Spatial and intensity distortions due to magnetic field inhomogeneities. Under a homogeneous magnetic field, the image of a circular phantom (e.g., a liquid-filled ball) is itself circular and of relatively similar intensity throughout (A). Local magnetic field inhomogeneities cause two types of distortions, geometric distortions and signal losses, both of which are visible on the distorted image (B).

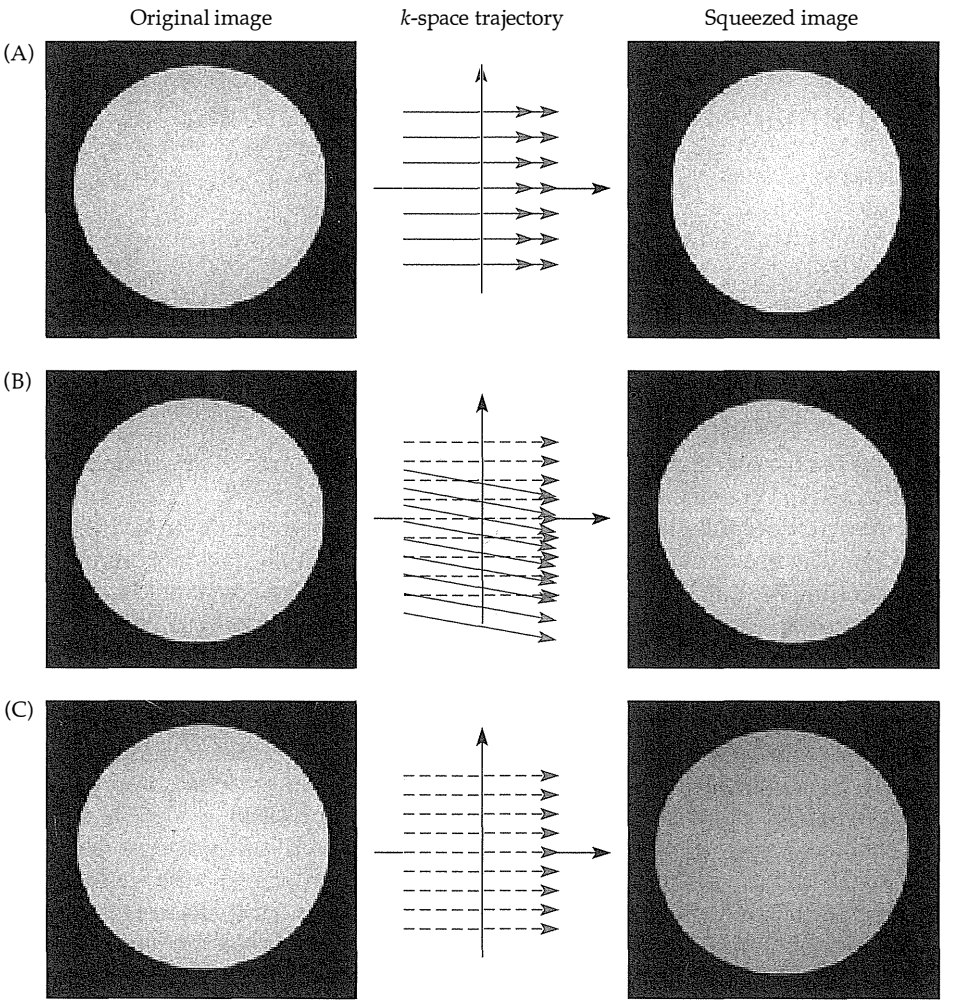

Figure 4.24 Image distortions caused by gradient problems. Each row shows the ideal image (left), the problem with acquisition in k-space, and the resulting distorted image (right). (A) Problems with the x-gradient will affect the length of the trajectory along the x-dimension in k-space, resulting in an image that appears compressed. (B) Problems with the y-gradient will affect the path taken through k-space over time, resulting in a skewed image. (C) Problems with the z-gradient will affect the match of excitation pulse and slice selection gradient, here resulting in a thinner slice and reduced signal intensity.

sequence, a type that will be discussed more extensively in the following chapter. First, if the x-gradient G_x is off by a small amount, as shown in Figure 4.24A, the resulting k-space trajectories will have an error along the k_x direction. Second, if the y-gradient G_y is off, the k-space trajectories will be skewed along the k_y direction (Figure 4.24B). Note that this skew affects both the onset of each line in k-space as well as the path taken through k-space. The magnitude of this skew depends on the time integral of the gradient amount. Third, if the z-gradient G_z is off, the slope of the excitation gradient will be altered. Altering the slope of the slice-selection gradient can cause a mismatch between the gradient-induced changes in spin frequency and the excitation pulse. However, because the k-space trajectory in the x–y plane would not change, the

shape of the object would not be distorted. Thus, problems with the G_z gradient can lead to changes in slice thickness and signal intensity (Figure 4.24C).

Summary

REFER TO THE
fMRI
COMPANION WEBSITE AT
www.sinauer.com/fmri2e
for study questions and Web links.

The net magnetization of a spin system, as described by the Bloch equation, can be broken down into separate spatial components along the *x*-, *y*-, and *z*-axes. By convention, the longitudinal magnetization is defined as M_z and the transverse magnetization is defined as M_{xy}. The recovery of the longitudinal magnetization following excitation is governed by the time constant T_1, while the decay of the transverse magnetization following excitation is governed by the time constant T_2. The total measured MR signal is the combination of the transverse magnetization from all voxels in the sample and can be described using a single equation. The use of spatial gradients is necessary for the measurement of spatial properties of a sample, in essence allowing MR to become MRI. The simultaneous application of a G_z gradient and an excitation pulse allows selection of a defined slice within the imaging volume. The use of two additional gradients within the slice allows unique encoding of spatial locations. Image acquisition can be considered using the concept of *k*-space, which reflects the Fourier transform of image space. Different pulse sequences sample *k*-space differently, and the inverse relationship between *k*-space sampling and image space sampling is important to understand. Inhomogeneities in the net magnetic field can cause systematic artifacts in the reconstructed images, in the form of geometric distortions and/or signal loss.

Suggested Readings

Bracewell, R. N. (1986). *The Fourier Transform and Its Applications.* McGraw-Hill, New York. *A textbook for everything you want to know (and more) about the Fourier transform.*

Haacke, E. M., Brown, R. W., Thompson, M. R., and Venkatesan, R. (1999). *Magnetic Resonance Imaging: Physical Principles and Sequence Design.* John Wiley & Sons, New York. *A comprehensive encyclopedia of the theoretical principles of MRI.*

Twieg, D. B. (1983). The *k*-trajectory formulation of the NMR imaging process with applications in analysis and synthesis of imaging methods. *Med. Phys.*, 10(5): 610–621. *An original description of the* k*-space trajectory formulation.*

Chapter 5

MR Contrast Mechanisms and Pulse Sequences

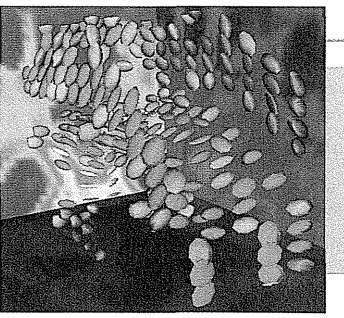

Compared with other neuroimaging methods, MRI has extraordinary versatility for generating images of a wide range of different tissues. In this chapter, we consider the approaches used to create these different types of contrast. Static contrasts are sensitive to the type, number, relaxation, and resonance properties of atomic nuclei within a voxel. Typical static contrasts are based on density (e.g., proton density), relaxation time (e.g., T_1, T_2, T_2*), chemical concentration (e.g., lactate or acetylcholine), and even content of a particular molecular type (e.g., macromolecules). We use images influenced by static contrast to determine brain anatomy in fMRI experiments. Motion contrasts are sensitive to the movement of atomic nuclei. Typical motion contrasts provide information about the dynamic characteristics of the protons in the brain, such as blood flow in MR angiography, water diffusion in diffusion-weighted imaging, or capillary irrigation in perfusion-weighted imaging. We will also discuss some of the most common techniques for collecting images rapidly, at the time scale needed for fMRI, and their associated pulse sequences.

A further distinction can be drawn depending on whether the contrast is derived from intrinsic properties of the biological tissues (i.e., endogenous contrast) or from the presence of foreign substances that have been introduced into the body (i.e., exogenous contrast). Nearly all fMRI experiments result in images that are derived from an endogenous contrast mechanism: the amount of deoxygenated hemoglobin within a brain region. An example of an exogenous contrast mechanism is the injection of gadolinium-DTPA, a rare earth compound that has extremely high magnetic susceptibility, and which greatly distorts the surrounding magnetic field. The use of exogenous agents is a common practice in clinical MRI for enhancing both static and motion contrasts, but it is less prevalent in functional studies due to the obvious safety issues associated with any injections. In the following sections, we will focus on endogenous contrast measures, especially those commonly used in structural and functional brain imaging. Potentially valuable advances in the application of exogenous contrast to fMRI are considered in Chapter 12, which covers advanced MRI techniques.

static contrasts Contrast mechanisms that are sensitive to the type, number, relaxation properties, and local environment of spins (e.g., T_1, T_2, proton density).

motion contrasts Contrast mechanisms that are sensitive to the movement of spins through space (e.g., diffusion, perfusion).

endogenous contrast Contrast that depends on an intrinsic property of biological tissue.

exogenous contrast Contrast that requires the injection of a foreign substance into the body.

Static Contrasts and Related Pulse Sequences

Static contrast mechanisms have been widely used in MRI due to their ability to illustrate basic tissue characteristics. To understand how static contrast can be generated, we consider first the simple cases of T_1 and T_2 contrast. As derived in the previous chapters, there are two equations for magnetization after an initial excitation of a fully recovered spin system (Figure 5.1). Equation 5.1 describes the longitudinal magnetization:

$$M_z(t) = M_0(1 - e^{-t/T_1}) \tag{5.1}$$

Equation 5.2 describes the transverse magnetization:

$$M_{xy}(t) = M_0 e^{-t/T_2} \tag{5.2}$$

There are two important factors that govern the time at which MR images are collected. The first factor is the time interval between successive excitation pulses, which is known as the repetition time, or TR. Often, consecutive excitations occur at time intervals not long enough to allow full recovery of the longitudinal magnetization. Under such short TRs, the subsequent transverse magnetization, which translates to detectable MR signal, should be described as

$$M_{xy}(t) = M_0(1 - e^{-TR/T_1})e^{-t/T_2} \tag{5.3}$$

repetition time (TR) The time interval between successive excitation pulses, usually expressed in seconds.

This equation illustrates that the MR signal depends not only on the original magnetization (which in turn depends on proton density) but also on the properties of the tissue being imaged, as expressed through both the T_1 and T_2 constants (Table 5.1). Shown in this table are rough values for the time constants T_1 and T_2 at a field strength of 1.5 T. Another value of interest is the T_2* value

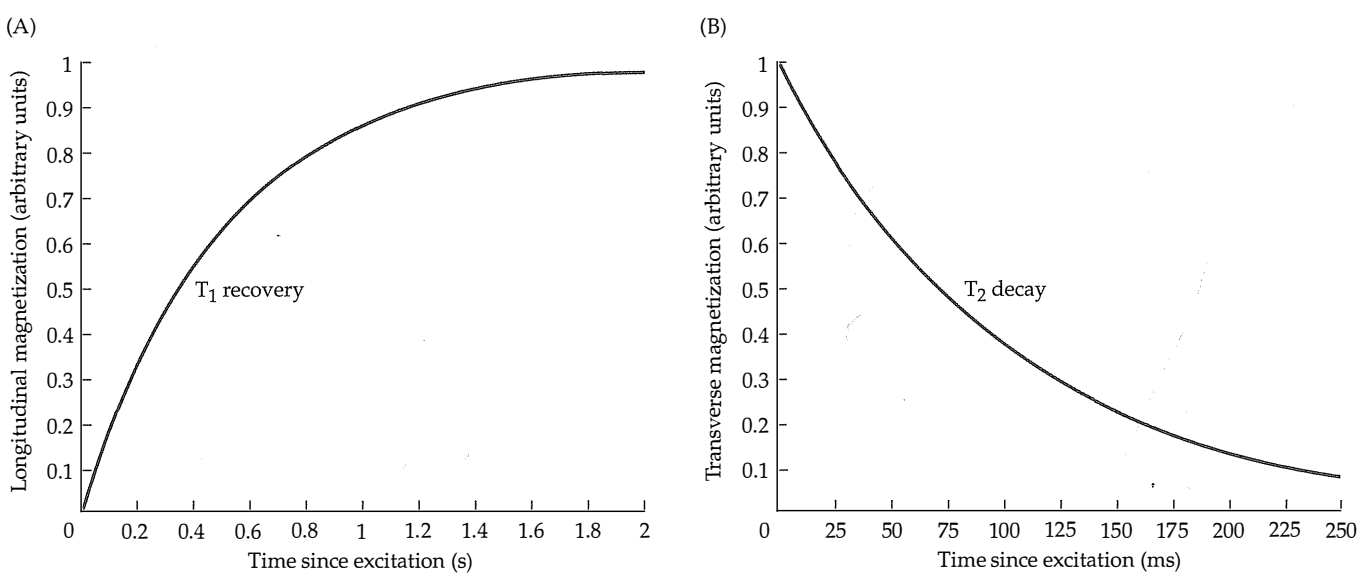

Figure 5.1 Changes in longitudinal and transverse components of magnetization. (A) The time constant T_1 is usually on the order of 1 s, so recovery of longitudinal magnetization (T_1 recovery) occurs over a period of several seconds. (B) The time constant T_2 is typically on the order of a few tens of milliseconds, so decay of transverse magnetization occurs over a period of about 100 ms. The values used for T_1 and T_2 in these plots are similar to those for gray matter at field strengths used for fMRI studies.

TABLE 5.1 Rough Values for the Time Constants T_1 and T_2 at Field Strength of 1.5 T

	Gray Matter	White Matter	Cerebrospinal Fluid
T_1	900 ms	600 ms	>2000 ms
T_2	100 ms	80 ms	2000 ms

for gray matter, about 40 ms at 1.5 T, which determines the echo time (TE; see definition below) used for BOLD-contrast fMRI images. Note that the values given in the table are only approximate, as these constants will vary according to field homogeneity and other factors. Moreover, each constant changes with field strength: as field strength increases, T_1 gets longer, while T_2 and T_2^* get shorter. We provide these approximate values as a guideline for thinking about the contrast mechanisms discussed in this chapter. In Equation 5.3, the term $(1-e^{-TR/T_1})$ accounts for the incomplete recovery of the longitudinal magnetization, which will reach a steady state after repetitive excitations. If the TR is much longer than T_1, then this term approaches one (i.e., full recovery) and can be removed from the equation.

The second factor that governs the timing of MR image collection is the echo time (TE), which is the time interval between excitation and data acquisition (from the center of *k*-space). Remember that the MR signal received at the center of *k*-space has the greatest amplitude, as described in the previous chapter, so at that point it resembles an echo of the initial transmission. For simplicity, we can replace the term t with TE to give the MR signal for an image with a given TE.

$$M_{xy}(t) = M_0(1-e^{-TR/T_1})e^{-TE/T_2} \tag{5.4}$$

Equation 5.4 provides the foundation for manipulating the signal from a particular tissue type by controlling TR and TE. However, in MRI we are interested in comparing MR signals from multiple tissue types. The signal difference between any two types of tissue is known as contrast. For tissue types A and B, the contrast between them, C_{AB}, is simply the difference between the MR signals associated with each (Equation 5.5). The terms M_{0A} and M_{0B} are the original magnetization values for tissues A and B, T_{1A} and T_{1B} are the T_1 values of A and B, and T_{2A} and T_{2B} are the T_2 values of A and B.

$$C_{AB} = M_{0A}(1-e^{-TR/T_{1A}})e^{-TE/T_{2A}} - M_{0B}(1-e^{-TR/T_{1B}})e^{-TE/T_{2B}} \tag{5.5}$$

Proton-density contrast

One of the simplest forms of MR contrast is proton-density imaging. The net magnetization of each voxel reflects the total contribution from all of that voxel's spins, most of which are hydrogen atoms (i.e., protons). Proton-density images, as the name implies, provide contrast based on the sheer number of protons in a voxel, which of course differs in different tissue types. To maximize proton-density contrast, researchers use pulse sequences that minimize T_1 and T_2 contrasts. To minimize T_1 contrast, a pulse sequence must use either a very short or very long TR, and to minimize T_2 contrast, a pulse sequence must use either a very short or very long TE. Logically, either long or short values for either parameter would work for proton-density-weighted images (i.e., images whose intensity depends primarily on relative proton density). In

contrast (1) The intensity difference between different quantities being measured by an imaging system. It also can refer to the physical quantity being measured (e.g., T_1 contrast). (2) A statistical comparison of the activation evoked by two (or more) experimental conditions, in order to test a research hypothesis.

echo time (TE) The time interval between an excitation pulse and data acquisition (defined as the collection of data from the center of *k*-space), usually expressed in milliseconds.

proton-density imaging The creation of MR images that are sensitive to the number of protons present within each voxel.

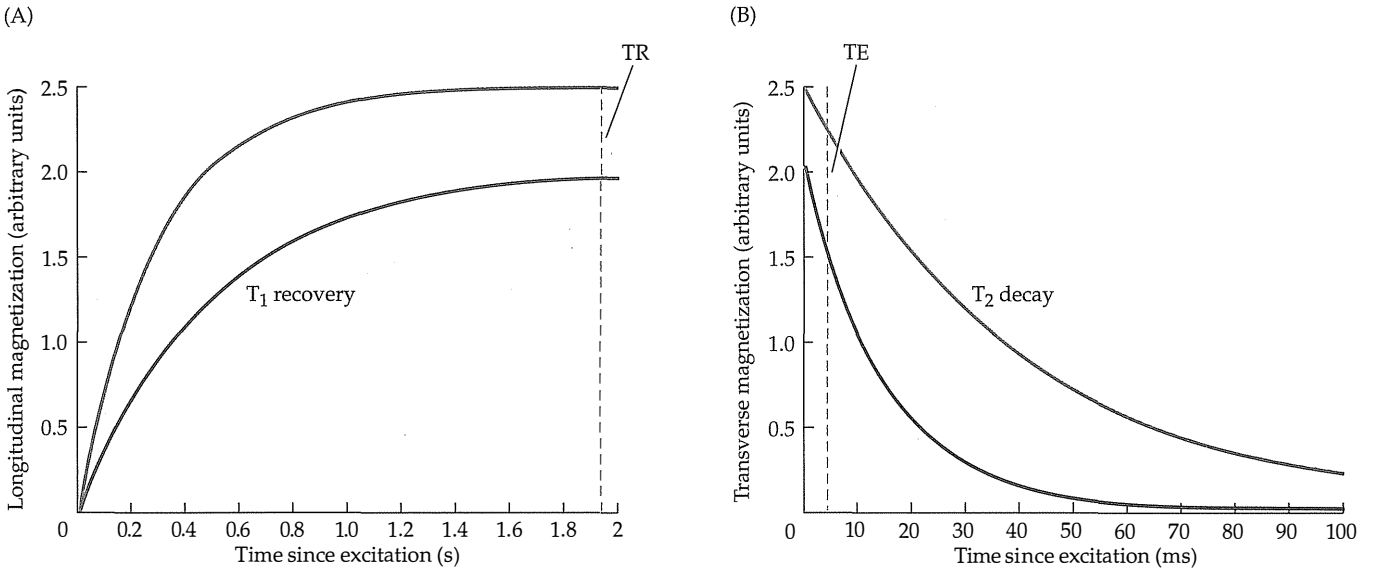

Figure 5.2 Selection of TR and TE values for proton-density contrast. The use of long TR (A) and short TE (B), shown as vertical dashed orange lines on two different tissues (red and blue), will minimize T_1 and T_2 effects, leaving only differences in overall signal intensity due to proton density.

practice, however, the use of extremely short TR or long TE values results in low MR signal. To maximize proton-density weighting while still recovering sufficient MR signal, pulse sequences are used that have very long TR values (Figure 5.2A) and very short TE values (Figure 5.2B). In practice, a TR greater than T_1 and a TE less than T_2 satisfy the criteria. If the TR used is much greater than the T_1 value of the tissue being imaged (e.g., two to three times as long), the protons will be nearly fully recovered after each excitation. Likewise, if the TE value is much less than the T_2 value (e.g., one tenth as long), there will be minimal decay before image acquisition.

Thought Question

How does the concept of proton density relate to the concept of net magnetization?

One disadvantage of using a very long TR is that it greatly increases imaging time. In many situations, such as when scanning patients who have difficulty tolerating lengthy MRI sessions, slow imaging sequences may not be feasible. To reduce acquisition time while still maintaining proton-density contrast, a smaller flip angle (less than 90°) may be used for excitation, to only partially tip the longitudinal magnetization toward the transverse plane. This will require less time to achieve full longitudinal recovery. The effect of using a smaller flip angle for partial excitation is illustrated in Figure 5.3, where it can be seen that a shorter TR can be used without introducing significant T_1 weighting (see below for the definition of a T_1-weighted image), effectively reducing the imaging time. In summary, to generate images sensitive to proton density, we must collect those images using a pulse sequence with a long TR and a short TE.

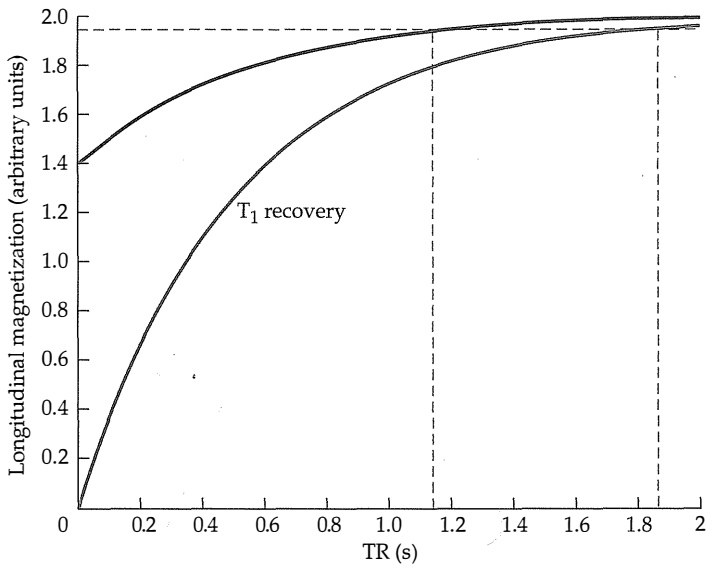

Figure 5.3 The use of a smaller flip angle in proton-density imaging. One approach for minimizing the acquisition time necessary for proton-density imaging is to reduce the flip angle of the excitation pulse. With a typical 90° excitation pulse the net magnetization (blue solid line) takes a long time to reach a near maximal level, as indicated by the blue dashed line. But if the flip angle of the excitation pulse is reduced, there is only partial excitation. In this latter case, the net magnetization (red solid line) reaches the same near maximal level much more rapidly, as indicated by the orange dashed line.

As long as there is sufficient T_1 recovery and minimal T_2 decay, any type of pulse sequence, including common gradient-echo (GRE) imaging and spin-echo (SE) imaging sequences, can acquire proton-density images. A gradient-echo sequence uses only gradients to generate the signal echo in the center of *k*-space. A spin-echo sequence, on the other hand, uses a second 180° electromagnetic pulse, called a refocusing pulse, to generate the signal echo. We will discuss examples of these types of sequences throughout this chapter.

An example of a proton-density gradient-echo sequence, which is often used due to its very fast acquisition rate, is shown in Figure 5.4A. Here, the excitation pulse is immediately followed by the data acquisition period (indicated by DAQ in the figure), so that there is little signal decay due to transverse relaxation. In addition, the very long repetition time allows the excited magnetization to fully recover before the subsequent excitation. A sample proton-density-weighted image is shown in Figure 5.4B. The highest signal is evident in the cerebrospinal fluid (CSF) and ventricles (e.g., at the center of the image), with less signal in the gray matter, even less signal in white matter, and the lowest signal in air. These intensity values are consistent with the relative densities of the tissues. The greatest tissue density, and hence the most protons, in the brain will be found in fluid-filled regions like the ventricles. Gray matter, which is composed of both cell bodies and the supporting vasculature, weighs proportionally less, and white matter, which is mostly axonal projections across the brain, weighs even less.

Proton-density images can be used as high-resolution reference images for determining anatomical structure in the brain. For this reason, they are often an important part of fMRI studies. In addition, the intensity values they provide can be used to improve algorithms for labeling different parts of the brain according to the types of tissue they contain (e.g., gray matter vs. white matter). Such segmentation approaches are often important when understanding how damage or atrophy in a region alters its functional properties, such as in the study of disease or aging. To facilitate tissue segmentation, proton-density images are frequently acquired at the same slice locations as T_1- or T_2-weighted images (see below) so that complementary anatomical information can be acquired.

gradient-echo (GRE) imaging One of the two primary types of pulse sequences used in MRI; it uses gradients to generate the MR signal changes that are measured at data acquisition.

spin-echo (SE) imaging One of the two primary types of pulse sequences used in MRI; it uses a second 180° electromagnetic pulse to generate the MR signal changes that are measured at data acquisition.

refocusing pulse A 180° electromagnetic pulse that compensates for the gradual loss of phase coherence following initial excitation.

segmentation The process of partitioning an image into constituent parts, typically types of tissue (e.g., gray matter, white matter) or topographical divisions (e.g., different structural regions like Brodmann areas).

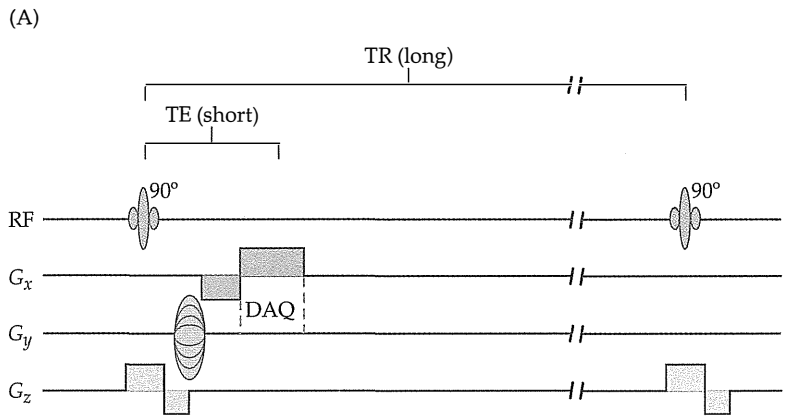

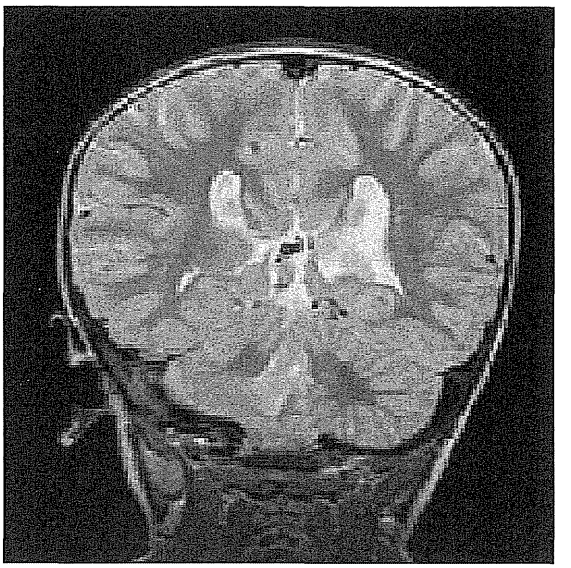

Figure 5.4 A pulse sequence used for proton-density imaging. The primary requirements for proton-density imaging are a very short TE and a very long TR, such as those used in this gradient-echo sequence (A). The resulting image (B) is brightest in voxels with high density (e.g., CSF within ventricles) intermediate in gray matter, and darkest in areas of low density (e.g., air, white matter). The data acquisition period is indicated by DAQ. In this and subsequent pulse sequence diagrams, the line labeled RF describes the signals sent via the radiofrequency head coil, while the lines labeled G_x, G_y, and G_z describe the direction and strength of the gradients along each of the three cardinal axes.

T_1 contrast

While proton-density images have many uses, other forms of contrast emphasize differences in the relaxation properties of atomic nuclei. The most commonly used structural contrast for anatomical images of the brain is T_1 weighting. Images are called **T_1-weighted**, or **T_1-dependent**, if the relative signal intensity of voxels within the image depends on the T_1 value of the tissue. Figure 5.5 provides an example of the TR and TE values necessary to generate T_1 contrast. At very short TRs, there is no time for longitudinal magnetization to recover and thus no MR signal is recorded for either tissue. Conversely, at very long TRs, all longitudinal magnetization recovers for both tissues. So, at short and long TR values, the amount of longitudinal magnetization will be similar between the tissues. At intermediate TRs, however, there are clear differences between them (Figure 5.5A). The tissue that has a shorter T_1 value recovers more rapidly and thus has greater MR signal. For any two tissues that differ in T_1, there is an optimal TR value that maximally differentiates between them. To have exclusive T_1 contrast, we must also have a very short TE, to minimize T_2 contrast. When TE is much less than T_2, the term e^{-TE/T_2} from Equation 5.4 becomes approximately equal to 1 (Figure 5.5B). Equation 5.5 then reduces to

$$C_{AB} = M_{0A}(1-e^{-TR/T_{1A}}) - M_{0B}(1-e^{-TR/T_{1B}}) \tag{5.6}$$

In this case, C_{AB} depends on TR but not TE. Note that the proton density of the tissues always contributes to the contrast, because the number of spins in the imaging volume determines the original net magnetization. In summary, to generate images sensitive to T_1 contrast, we must collect those images using a pulse sequence with intermediate TRs and short TEs.

T_1-weighted (T_1-dependent) Images that provide information about the relative T_1 values of tissue; also known as T_1 images.

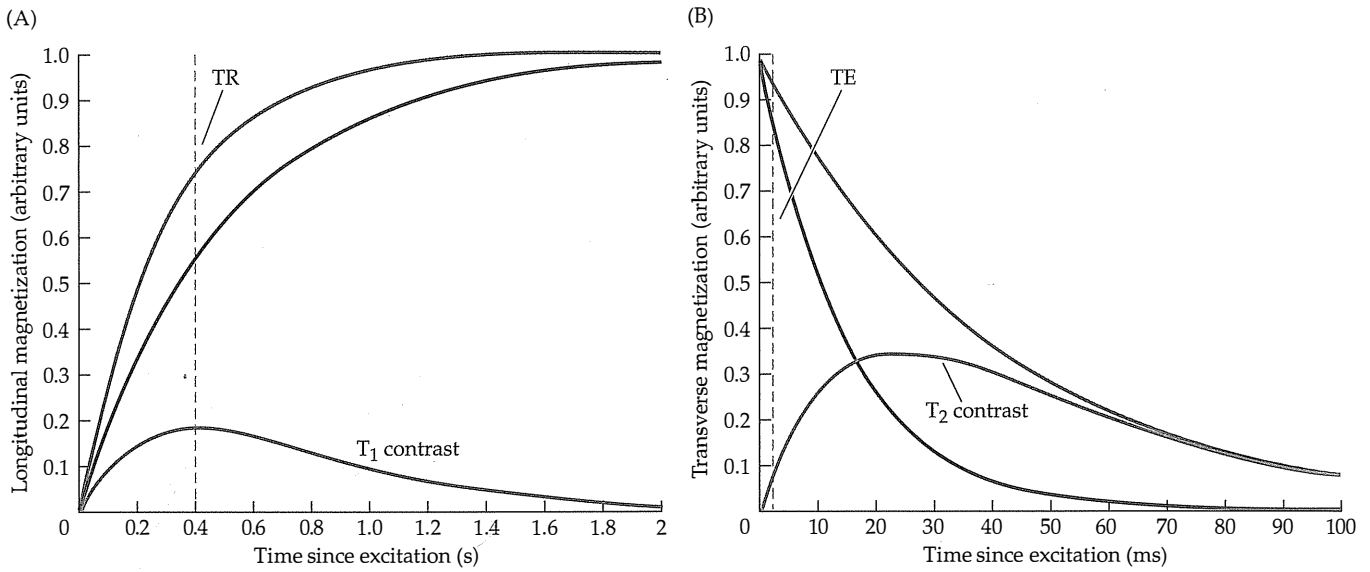

Figure 5.5 Selection of TR and TE values for T_1 contrast. The use of intermediate TR (A) and short TE (B), shown as vertical, dashed orange lines, on two tissues (red and blue lines), will maximize the T_1 differences between tissues and minimize the T_2 differences between tissues. This combination provides T_1 contrast. The green lines show the relative contrast associated with different TR (A) and TE (B) values.

Just as proton-density contrast can be generated with any type of pulse sequence, T_1 contrast will be evident using any pulse sequence that meets the above criteria (i.e., medium TR and short TE). In practice, both gradient-echo and spin-echo sequences are commonly used. Since a gradient-echo pulse sequence was used in the previous example, we show a spin-echo pulse sequence in Figure 5.6A. The hallmark of spin-echo sequences is the 180° refocusing pulse that is applied shortly after the initial 90° excitation pulse. The refocusing pulse corrects for phase dispersion due to T_2 effects, so that all spins are approximately in phase during the data acquisition period. This sequence elicits the most signal from white matter and bone marrow, due to their short T_1 values, and an intermediate amount of signal from gray matter. Since water has a very long T_1 value, very little signal is recovered from cerebrospinal fluid, which becomes nearly indistinguishable from air (Figure 5.6B).

To boost T_1 contrast, researchers often use a technique called **inversion recovery**, which begins the sequence with a 180° inversion pulse rather than the more common 90° pulse (Figure 5.7A). Because the inversion pulse flips the net magnetization to the negative state, it effectively doubles the dynamic range of the signal. To understand the advantage of inversion recovery, consider Figure 5.7B. Shown in red are typical effects of TRs from two different tissues on MR signal. By introducing an inversion recovery pulse, the range over which the signals must recover becomes twice as large (blue curves). This in turn increases the maximal T_1 difference that can be measured between the tissues. Inversion recovery is also useful for selectively eliminating the MR signal of a single tissue type. For example, by collecting images using a TR at which the longitudinal magnetization from CSF is zero (the "zero crossing," see arrow in Figure 5.7B), there will be no signal from CSF in any voxel. The suppression of CSF allows better assessment of other tissue types, such as gray and white matter.

inversion recovery A technique for increasing T_1 contrast by adding a 180° inversion pulse before a standard pulse sequence.

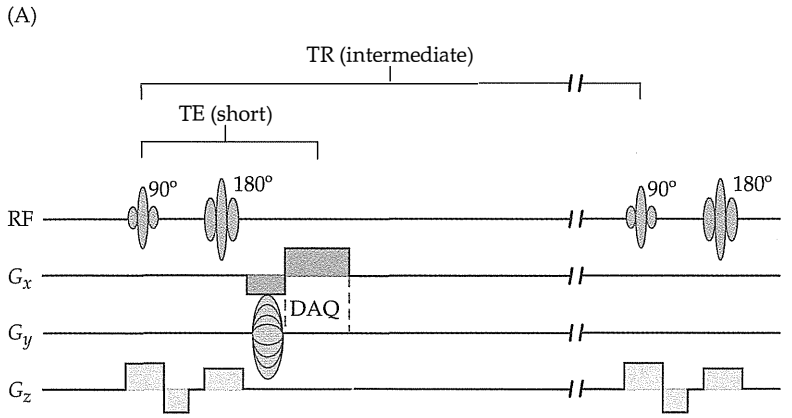

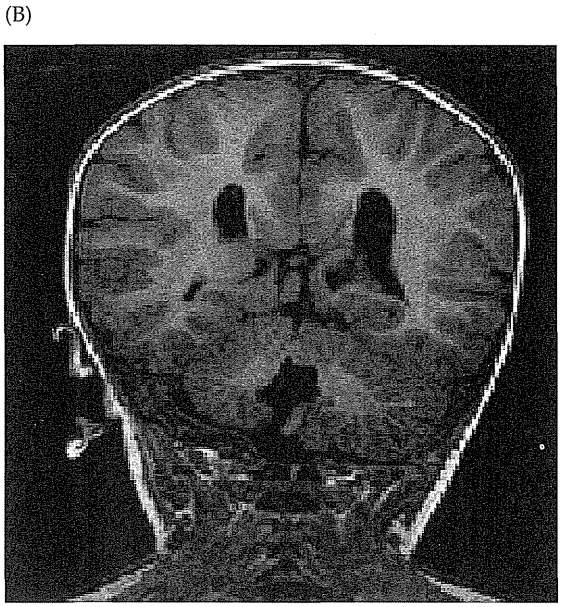

Figure 5.6 A pulse sequence used for T_1-weighted images. The primary requirements for T_1 imaging are a short TE and an intermediate TR. Either gradient-echo or spin-echo sequences can be used. Shown in (A) is a spin-echo sequence. The resulting image (B) is brightest in voxels with short T_1 values (e.g., white matter and bone marrow), intermediate in gray matter, and darkest in areas with long T_1 values (e.g., CSF). DAQ, data acquisition period.

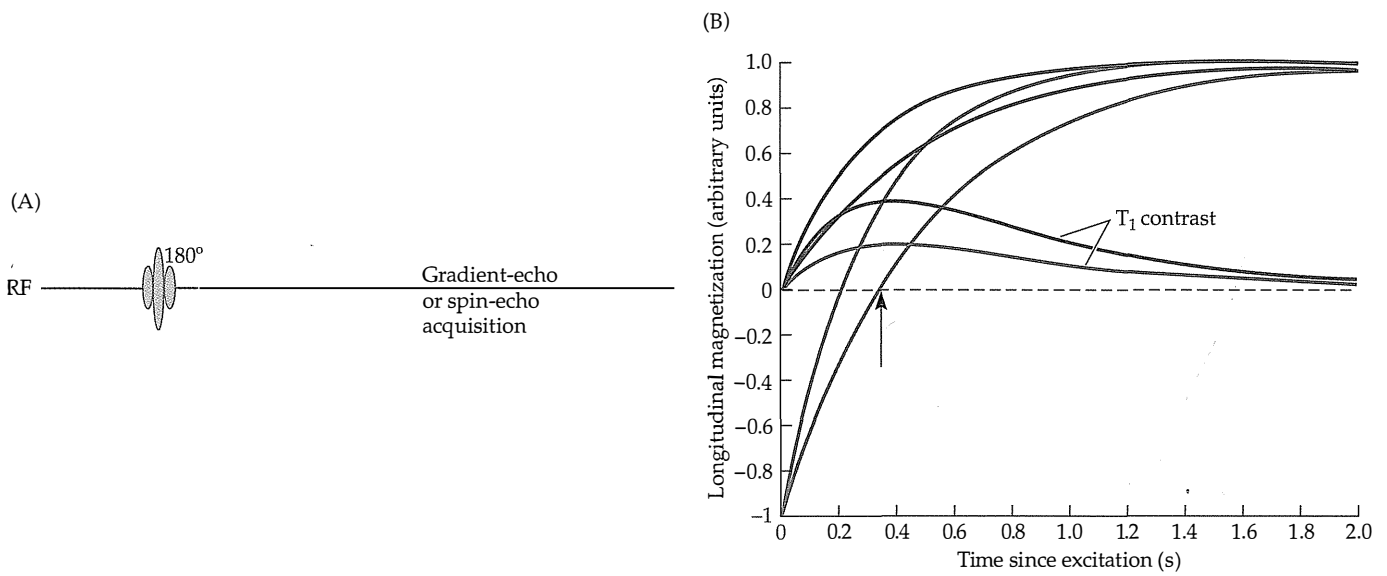

Figure 5.7 Use of inversion recovery to increase T_1 contrast. By including a 180° inversion pulse before a typical gradient-echo or spin-echo sequence (A), the net magnetization can be flipped to the negative state. As a result, the net magnetization must recover over twice the dynamic range, and thus the relative difference in T_1 recovery between the tissues is increased. As illustrated in (B), the T_1 contrast is much greater for the same pair of tissues following an inversion pulse (blue curves) than under normal conditions (red curves). The green and purple lines indicate the differences between red curves and blue curves, respectively. Inversion recovery sequences can also used to eliminate MR signal from a tissue of a particular type, by collecting images at a TR that corresponds to the zero crossing for that tissue (arrow).

T_2 contrast

T_2-contrast images have maximal signal in fluid-filled regions, which is important for many clinical applications. Many tumors, arteriovenous malformations, and other pathological conditions show up most readily under T_2 contrast. High-resolution T_2 images are also used as anatomical references in fMRI studies, either in isolation or in conjunction with proton-density or T_1 images in a multi-contrast tissue segmentation algorithm. Thus, common clinical protocols include both T_1- and T_2-weighted images.

T_2-weighted (T_2-dependent) Images that provide information about the relative T_2 values of tissue; also known simply as T_2 images.

For T_2-weighted, or T_2-dependent images, the amount of signal loss depends on the time between excitation and data acquisition, or echo time (TE). Again, an optimal combination of TR and TE exists for any two tissues to maximize the T_2 contrast between them (Figure 5.8). If an image is acquired immediately after excitation, such that the TE is very short, then little transverse magnetization will be lost regardless of T_2, and thus there will be no T_2 contrast. If the TE is too long, then nearly all transverse magnetization will be lost and still the image will have no T_2 contrast. But at an intermediate TE, the difference in transverse magnetization can be maximized (Figure 5.8B).

To have exclusive T_2 contrast, we must have a very long TR, so that the longitudinal recovery is almost complete and T_1 contrast is minimal (Figure 5.8A). When the TR is much 1greater than T_1, the term e^{-TR/T_1} from Equation 5.4 approaches 0 and thus can be eliminated. The resulting formula for contrast is completely T_2-weighted and depends highly on the TE:

$$C_{AB} = M_{0A}e^{-TE/T_{2A}} - M_{0B}e^{-TE/T_{2B}} \tag{5.7}$$

In summary, to generate images sensitive to T_2 contrast, we must collect those images using a pulse sequence with a long TR and an intermediate TE.

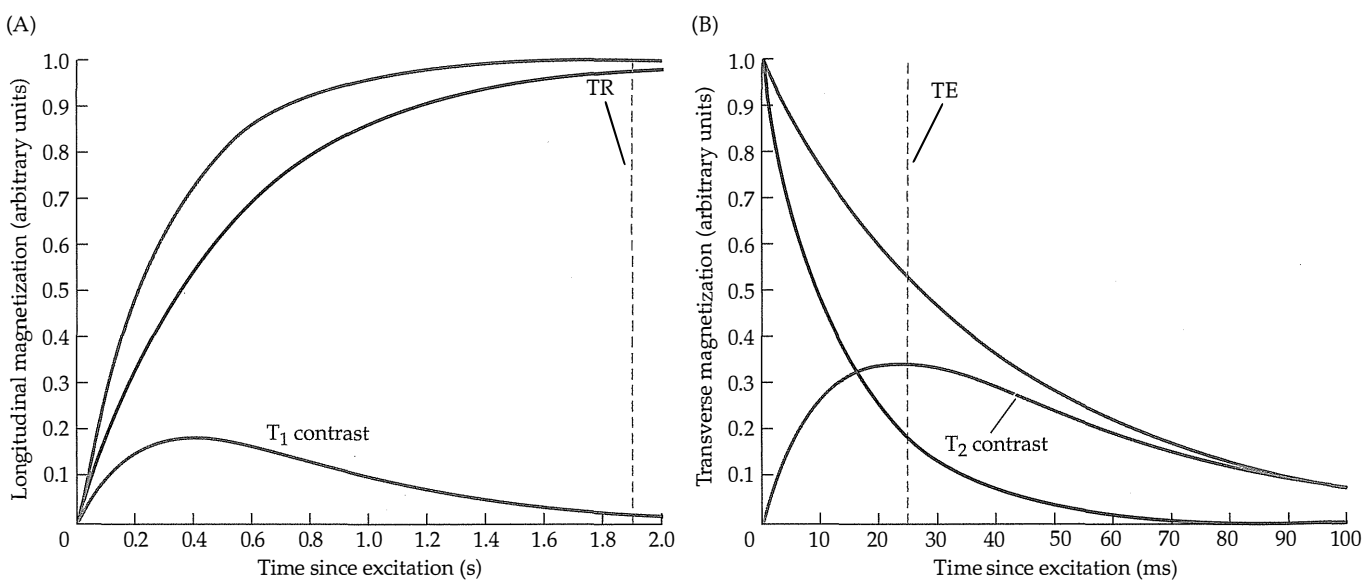

Figure 5.8 Selection of TR and TE values for T_2 contrast. The use of long TR (A) and intermediate TE (B), shown as vertical, dashed orange lines, on two tissues (red and blue) will maximize the T_2 differences between tissues and minimize the T_1 differences between tissues. This combination provides T_2 contrast. The green lines show the relative contrast associated with different TR (A) and TE (B) values.

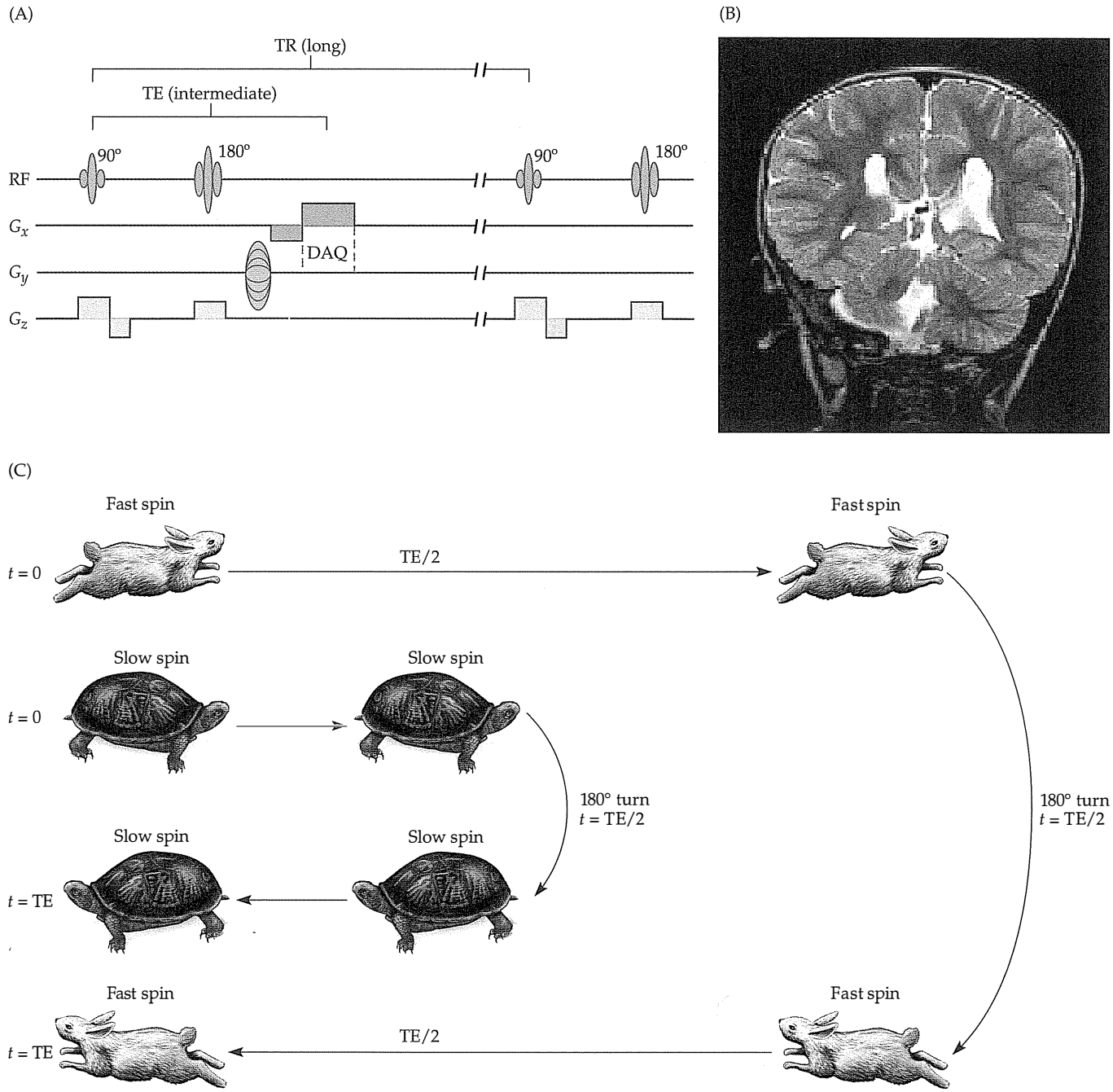

Figure 5.9 Creating T_2-weighted images. The primary requirements for T_2 imaging are an intermediate TE and a long TR. (A) Only spin-echo sequences (i.e., those containing a 180° refocusing pulse) can be used. The resulting image (B) is brightest in voxels with long T_2 values (e.g., CSF in ventricles) and darkest in areas with short T_2 values (e.g., white matter). (C) Restoring phase coherence using a 180° pulse. As time progresses following excitation, magnetic field inhomogeneities will cause a loss of phase coherence over time, as some spins (represented by rabbits) have fast precession frequencies and some (represented by turtles) have slow precession frequencies. If a 180° refocusing pulse is presented at time TE/2, the precession direction will be flipped. At the precise time TE, all of the spins will have their original phases (as indicated here by the return of the rabbits and turtles to their original locations).

Unlike proton-density or T_1-weighted images, T_2-weighted images can only be generated using spin-echo-based pulse sequences. Only spin-echo sequences allow true spin–spin relaxation that does not depend on the field inhomogeneity. A typical pulse sequence is shown in Figure 5.9A. The resulting brain image will be brightest in fluid-filled regions such as the CSF and ventricles, of medium brightness in gray matter, and darkest within white matter (Figure 5.9B). These intensity values are consistent with the relative T_2 values of the regions. Remember from the previous chapter that T_2 values depend on spin–spin interactions, and thus homogeneous tissues tend to have longer T_2 relaxation periods. For example, CSF has the longest T_2 value due to its high water content, gray matter has an intermediate T_2 value from its rich blood supply, and white matter has the lowest T_2 value (see Table 5.1).

susceptibility artifacts Signal losses on T_2*-dependent images due to magnetic field inhomogeneities in regions where air and tissue are adjacent.

T_2*-weighted (T_2*-dependent) Images that provide information about the relative T_2* values of tissue. T_2*-weighted images are commonly used for BOLD-contrast fMRI.

Thought Question

Often, proton-density and T_2-weighted images are acquired within the same pulse sequence. What aspects of their pulse sequences make this possible?

Because the 180° pulse reverses the loss of phase coherence experienced by spins, spin-echo imaging has little sensitivity to static magnetic field inhomogeneities (e.g., T_2* effects). As shown in Figure 5.9C, differences in the magnetic field strength experienced by different spins cause loss of phase coherence over time, as some spins will precess faster and some slower. By introducing the 180° pulse at a time point exactly halfway between excitation and TE, the relative phase difference between the spins can be reversed. Therefore, the spins that precess faster will now be behind the spins that precess more slowly, so the faster spins will catch up at time TE. Spin-echo imaging can thus help eliminate the effects of magnetic field inhomogeneities around large blood vessels, minimizing the contaminating effects of those vessels. Another advantage of spin-echo imaging lies in its resistance to susceptibility artifacts, which are caused by magnetic field inhomogeneities near air–tissue interfaces in the brain, as found in the ventral frontal and temporal lobes.

T_2 contrast*

Recall from Chapter 3 that there are two causes for transverse relaxation: spin–spin interaction (T_2) and changes in spin precession frequencies due to inhomogeneities in the magnetic field. The combined effect of these two factors on the decay of transverse magnetization is given by the time constant T_2*. Although T_2 and T_2* are related, the former constant is always greater than the latter, so T_2 decay is always slower than T_2* decay. Quantitatively, the relationship between T_2 and T_2* is given by $1/T_2^* = (1/T_2) + (1/T_2')$, where T_2' reflects the dephasing effect caused by field inhomogeneity. Because it forms the basis for BOLD-contrast fMRI, there has been a rapid increase in use of T_2*-based imaging protocols since 1990. As will be discussed further in Chapter 7, T_2*-weighted (or T_2*-dependent) images are sensitive to the amount of deoxygenated hemoglobin present, which changes according to the metabolic demands of active neurons. T_2*-weighted imaging is therefore the contrast basis for fMRI. Anatomical imaging using T_2*-weighted contrast can be used to generate images of the brain's venous system (i.e., venograms; Figure 5.10), because of the high concentration of deoxygenated hemoglobin in venous blood.

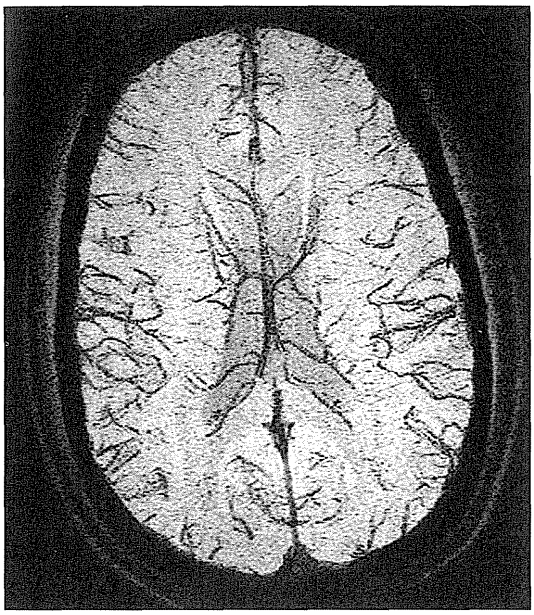

Figure 5.10 An application of T_2*-weighted image in generating a vein image, known as a venogram. This image illustrates the pattern of large and small veins present within a single horizontal slice. Venograms use phase discrepancies caused by local susceptibility (T_2*) effects to map out the venous system. (Courtesy of Dr. Todd Parrish, Northwestern University, and Dr. E. Mark Haacke, Wayne State University.)

Like T_2 contrast, T_2* contrast is provided by pulse sequences with long TR and medium TE values. An additional requirement is that the pulse sequence must use magnetic field gradients to generate the signal echo, because refocusing pulses will eliminate field inhomogeneity effects. Most commonly used are gradient-echo sequences, as illustrated in Figure 5.11. Note the similarity to the proton-density sequence shown in Figure 5.4, which differs only in its TE value. Here, an intermediate TE is used so that the image is sensitive to local field inhomogeneity and not just to the number of protons present. The pulse sequence shown can provide information about factors that decrease magnetic field homogeneity, such as the presence of deoxygenated hemoglobin. Because spin-echo pulse sequences have reduced T_2* sensitivity, they are less frequently used for BOLD-contrast fMRI.

Chemical contrast

The MR signal can be made sensitive to the concentrations of particular tissue chemicals. For neuroimaging, important brain chemicals include N-acetyl aspartate (NAA), creatine, glucose, and lactate, which play critical roles in regulating brain function, energetics, and metabolism. An important technique used to measure these substances is called chemical shift imaging. Because protons experience different shielding effects from the surrounding electrons in different molecules, their resonance frequencies vary slightly from one type of molecule to another. For example, the resonance frequencies of protons in NAA and water differ by about 2 parts per million (ppm), or roughly ~250 Hz in a typical 3.0 T scanner. The chemical shift therefore reflects the difference in proton resonance frequencies in different molecules. By quantifying the magnitude of MR signal at individual frequencies and resolving their spatial locations by spatial encoding, maps can be generated that reflect the concentrations of individual chemicals of interest (Figure 5.12). In practice, the pulse sequences used for chemical shift imaging

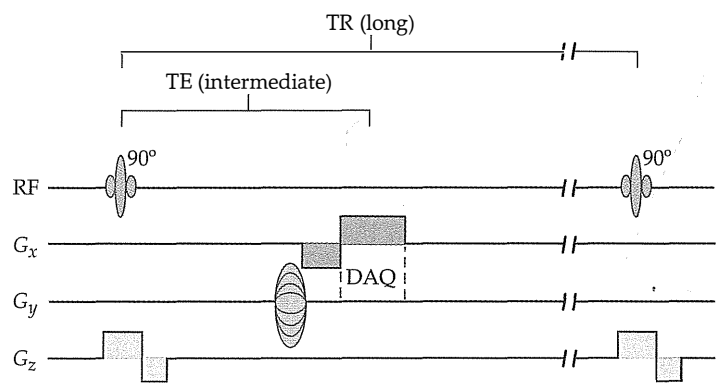

chemical shift imaging A technique for measuring the concentration of particular chemicals, based on subtle differences in the resonance of the protons they contain.

Figure 5.11 A pulse sequence used for T_2*-weighted images. Like T_2-weighted images, T_2*-weighted images require an intermediate TE and a long TR. Gradient-echo sequences are most commonly used, because the refocusing pulses used in spin-echo images will eliminate the field inhomogeneity effects that form the basis of the T_2* effect.

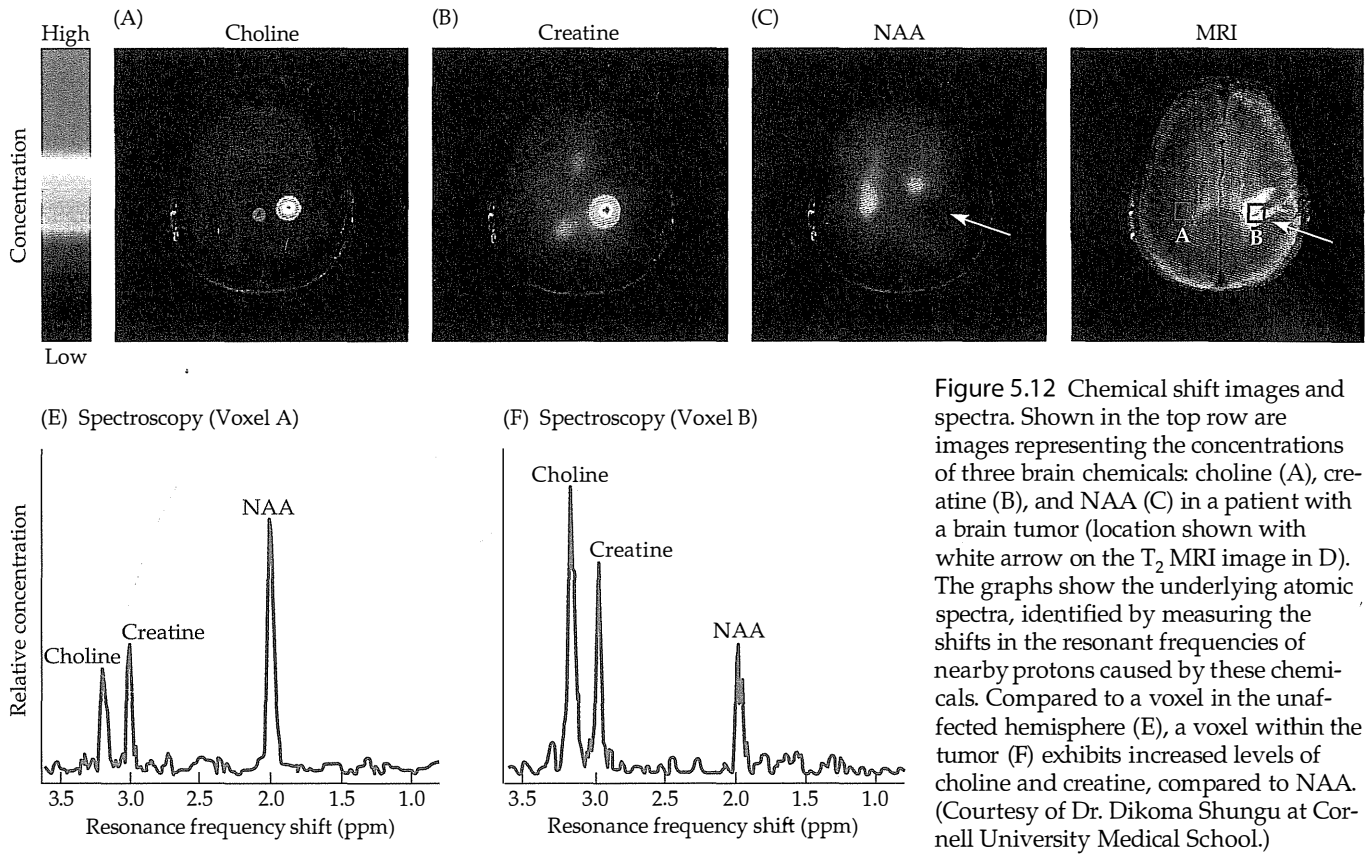

Figure 5.12 Chemical shift images and spectra. Shown in the top row are images representing the concentrations of three brain chemicals: choline (A), creatine (B), and NAA (C) in a patient with a brain tumor (location shown with white arrow on the T_2 MRI image in D). The graphs show the underlying atomic spectra, identified by measuring the shifts in the resonant frequencies of nearby protons caused by these chemicals. Compared to a voxel in the unaffected hemisphere (E), a voxel within the tumor (F) exhibits increased levels of choline and creatine, compared to NAA. (Courtesy of Dr. Dikoma Shungu at Cornell University Medical School.)

involve the acquisition of hundreds or thousands of data points within each excitation, on top of the normal requirements for spatial encoding discussed in the previous chapter (Figure 5.13). Thus, acquisition of high-resolution chemical shift images can very be time-consuming and is not commonly combined with standard fMRI studies.

Thought Question

Why can a conventional combination of frequency encoding and phase encoding not be used for chemical shift imaging?

Macromolecular contrast

So far in this chapter we have discussed the generation of images with contrast based on the properties of individual atomic nuclei or small molecules. Contrast can also be based on the interactions between molecules. For example, the magnetization of the protons in macromolecules (e.g., proteins) can

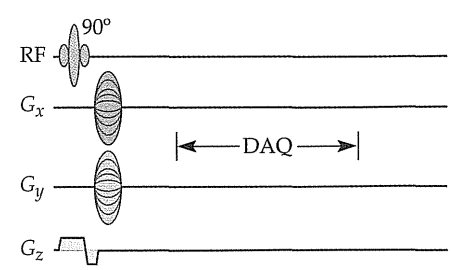

Figure 5.13 A chemical shift imaging sequence. Instead of sequentially applied frequency and phase encoding gradients, chemical shift imaging employs simultaneous phase encoding gradients along both G_x and G_y to resolve spatial locations. During the data acquisition window (DAQ), the scanner acquires a large number of data points over an extended period of time to resolve spectral frequency changes (i.e., changes in the resonant frequencies of protons caused by local chemical concentrations).

magnetization transfer An MR imaging technique that uses an off-resonance excitation pulse to saturate the MR signal from large molecules; the subsequent influence of that pulse upon free protons in water indicates the concentration of those large molecules.

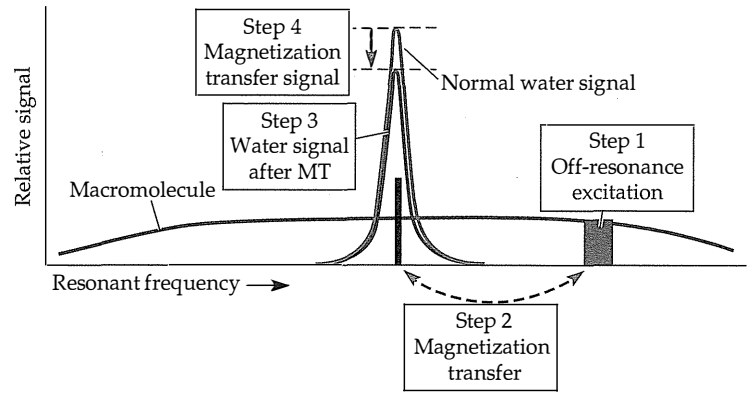

Figure 5.14 Conceptual illustration of the generation of magnetization transfer contrast. Protons in macromolecules have a wide range of resonant frequencies (purple distribution), reflecting the varied local magnetic environments experienced by protons in different parts of the molecules. In contrast, the resonant frequencies of protons in water have a much tighter distribution (blue) around the Larmor frequency (black line). Here, we illustrate the process of magnetization transfer in four steps. An off-resonance excitation pulse (Step 1, red) will provide energy to protons in some of the macromolecules, while not affecting the protons in normal water. Over a short period of time, some of the magnetization of those macromolecules will be transferred to the surrounding water molecules (Step 2, green), reducing the MR signal obtained from protons in those water molecules in a subsequent image (Step 3, red). By determining the magnitude of signal loss in a particular voxel, researchers can estimate the concentration of the targeted macromolecules (Step 4, orange).

Figure 5.15 An image sensitive to magnetization transfer contrast. Here, the brightness of the voxels provides a measure of the concentration of myelin, a lipid/protein layer that surrounds axons to increase the velocity of their signaling. Shown are areas of high myelin content that correspond to major fiber tracts in the brain.

influence that of nearby water molecules, a phenomenon known as magnetization transfer.

Like chemical shift imaging, magnetization transfer depends on differences between molecule types, specifically differences in the proton resonance frequencies due to various shielding effects. In particular, the resonance frequencies of protons within water molecules have a fairly narrow range, typically about 100 Hz. However, protons in macromolecules can have resonance frequency ranges of several thousand Hz. These two distinctly different frequency distributions allow the selective excitation of some protons within macromolecules without exciting those in water, through the use of specialized pulse sequences (Figure 5.14). The first step in this process is the delivery of an off-resonance excitation pulse that provides energy to protons in some of the macromolecules while not affecting the protons in normal water. After a short time interval (e.g., a few tens of milliseconds), some of the magnetization will transfer into protons in the water surrounding the macromolecule. If a second excitation pulse is delivered after this magnetization transfer occurs, the overall MR signal will be lower than it would be without the magnetization transfer. Because the amount of magnetization transfer is directly proportional to the concentration of the targeted macromolecule, the reduction in MR signal provides a measure of macromolecule concentration.

Many years after its first demonstration, magnetization transfer is now widely used to generate contrast based on the macromolecular properties of brain tissues. The resulting images often have significant clinical impact. For example, magnetization transfer can be used to detect changes in the myelination of the brain's white matter (Figure 5.15), since myelin is composed of specific macromolecules (i.e., lipids and proteins). Magnetization transfer has been used to study

the maturation of myelin in pediatric brains and to investigate myelin disorders such as multiple sclerosis (which is associated with demyelination).

Motion Contrasts

The human body is inherently dynamic. Within the vascular system, for example, water molecules are in constant motion, flowing as rapidly as one meter per second in large arteries. Water also diffuses within and among cells, such as along axons in white matter. Pulse sequences sensitive to motion provide important information about the brain, including both structural and functional information. Structural techniques include MR angiography and diffusion tensor imaging, which are often used for mapping the neurovascular system and white-matter tracts, respectively. Functional techniques include diffusion imaging, which maps the motion of water molecules over time, and perfusion imaging, which maps blood flow through capillaries. These techniques are collectively known as motion-weighted contrasts.

MR angiography

Magnetic resonance angiography, or MRA, provides images of the structure of blood vessels through noninvasive MRI (Figure 5.16). In classic angiography, a contrast agent is injected into the bloodstream through an inserted catheter. X-ray images are then collected with and without the contrast agent present to generate a difference image (i.e., angiogram) that maps the vascular system. Although angiography provides good vascular images, it is a very invasive procedure, requiring both the insertion of a foreign substance and exposure to ionizing radiation. Because MRA does not require ionizing radiation, it can be used to noninvasively detect, diagnose, and aid in the treatment of many types of medical problems, including cardiac disorders, stroke, and vascular disease.

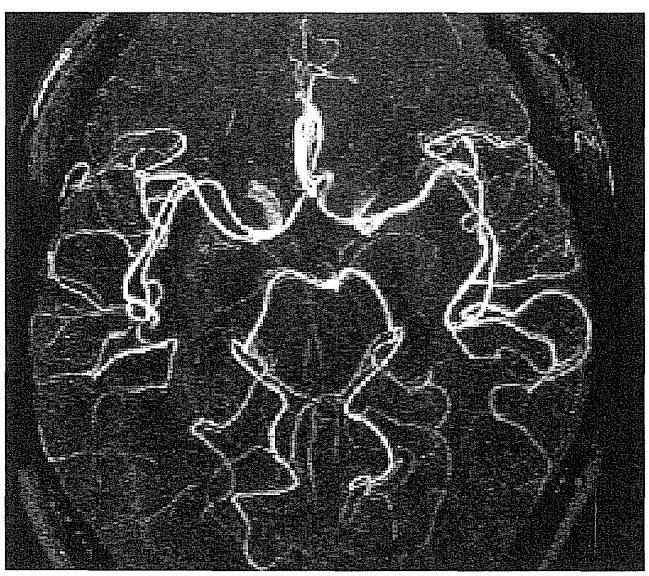

Figure 5.16 A sample magnetic resonance angiography (MRA) image.

magnetic resonance angiography (MRA) The creation of images of the vascular system using MRI.

bolus A quantity of a substance that is introduced into a system and then progresses through that system over time.

time-of-flight (TOF) MRA A type of MR angiography that generates contrast by suppressing signal from spins within an imaging plane so that voxels with inflowing spins (i.e., those with blood vessels) have high signal.

MRA also complements fMRI studies by identifying major blood vessels that may confound experimental results. If identified, the data from these vessels can be removed from analyses to improve the localization of activity to the capillary bed.

MRA can be performed using either exogenous or endogenous contrast. In some clinical settings, exogenous contrast-enhancing agents are used to increase the vessel signal. For a typical contrast-enhanced MRA, a small quantity (or bolus) of a gadolinium-based contrast agent is injected into the patient's bloodstream. The gadolinium itself is not visible on MR images, but it radically shortens the T_1 recovery period for nearby blood, allowing the use of specialized pulse sequences with extremely short TRs (three to seven milliseconds) and TEs (one to three milliseconds). The short TR saturates the signal from stationary tissues but not from the gadolinium-enhanced blood, while the short TE minimizes T_2 decay. Depending on the delay between bolus injection and image acquisition, the contrast agent may travel through different components of the vascular system, so the images can be calibrated to provide information about arterial or venous networks.

In research settings, MRA is usually performed using noninvasive endogenous contrast. There are two primary techniques for endogenous contrast MRA. The most common is **time-of-flight (TOF) MRA**, which involves the generation of signal based on blood displacement. The underlying principle of the TOF technique is spin saturation. By repeatedly and frequently applying excitation pulses or gradient pulses to a single imaging plane, the signal within that plane can be suppressed. Thus, tissues whose spins remain within the plane, such as gray or white matter, will produce little MR signal and will appear to be very dark on TOF images. Blood vessels, however, are constantly replenished with new spins from outside the plane. These spins have not experienced the excitation or gradient pulses, and thus they contribute normal levels of MR signal. TOF images are typically acquired in the axial (i.e., horizontal, relative to the brain itself) plane and can be reformatted to other planes for ease of viewing.

The TOF signal is proportional to the amount of blood that enters the slice (Figure 5.17). If a completely new column of blood enters the slice every TR, the TOF signal will be at its maximum. But if blood flow is weak or absent, then the TOF signal will be much reduced. Consequently, TOF MRA is a flow-dependent imaging technique. Because of this, the TR and slice thickness of a TOF image must be chosen based on the expected flow.

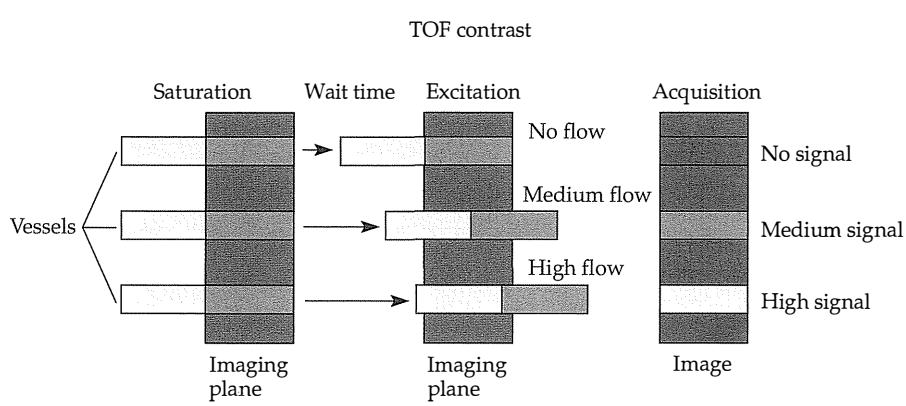

Figure 5.17 Schematic illustration of the signal-generation mechanism for TOF magnetic resonance angiography. In TOF MRA, repeated excitation pulses saturate the MR signal from spins within a plane, as shown by the blue rectangle at left. Then there is a waiting period during which voxels with flow (e.g., blood vessels) have new spins introduced, while voxels without flow (e.g., white matter) do not. The amount of MR signal recorded following excitation and acquisition is greatest for voxels that had the most new spins enter during the waiting period.

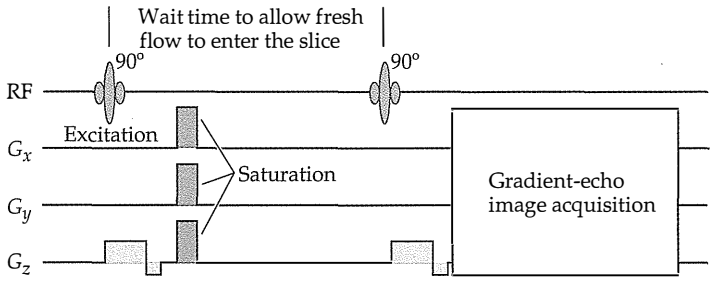

Figure 5.18 Pulse sequence used for TOF MRA. The TOF technique requires the initial saturation of a slice, followed by a wait time to allow blood to enter the slice. Then a standard gradient-echo sequence can be used to acquire the images.

To acquire MRAs with TOF contrast, a specialized pulse sequence is required (Figure 5.18). As described in the preceding paragraphs, the imaging plane is presaturated by the electromagnetic excitation pulse and gradient saturation pulses. After a brief waiting period during which fresh blood can enter the plane, the MR signals are acquired by a gradient-echo acquisition technique, so that only the signal from this new blood will be present.

A second technique is velocity-encoded phase contrast (VENC-PC) MRA, which uses gradient fields to produce a difference in precession phase between the vasculature and the surrounding tissue. The amount of the phase difference that accumulates depends on the relative velocities of the moving spins and the strength and duration of the applied gradient. That is, spins changing positions rapidly over time will precess more rapidly, and thus gain precession phase, relative to spins that stay in roughly the same place. By measuring phase differences in each of three orthogonal directions, a map of three-dimensional flow can be created. Typical VENC-PC protocols involve the acquisition of two sets of images: one with a strong gradient and the other with either no gradient or a gradient in the opposite direction. The difference between these images indicates the magnitude of the phase difference at each voxel, and thus the brightness at each voxel is proportional to flow. Voxels with stationary spins will not give signals, since there are no phase differences between the images, whereas voxels with rapidly moving spins will produce bright signals due to the large phase differences. The VENC-PC technique, unlike TOF, does not depend on TR or slice thickness, because it acts on the blood already present in the imaging slice.

Since the VENC-PC technique relies on relative phase, it is sensitive to the strength and duration of the gradients used. Imagine that the gradients are set up so that a flow velocity of 20 cm/s corresponds with a phase change of 180°. If a given vessel, such as a large artery, has a very fast flow rate of 40 cm/s, the resulting phase angle change will be 360°. As in basic geometry, an angle of 360° cannot be distinguished from one of 0°, so this fast-flowing artery would appear to have no flow whatsoever! This problem, known as velocity aliasing, demonstrates the importance of choosing appropriate velocity-encoding parameters. If the gradient is too strong, as in the above example, fast-flowing vessels may not be identified. But if the gradient is too small, the ability to resolve differences between slow-flowing vessels will be compromised. If the choice of gradient strength is matched to the expected velocities of blood in the different vessel types, then selective imaging of different parts of the vascular system is possible.

To acquire MRAs with VENC-PC contrast, a pulse sequence like the one in Figure 5.19 is necessary. Here, the velocity-encoding gradients are inserted

velocity-encoded phase contrast (VENC-PC) MRA A type of MR angiography that uses gradient fields to induce phase differences associated with vascular flow so that the flow velocity of vessels can be measured.

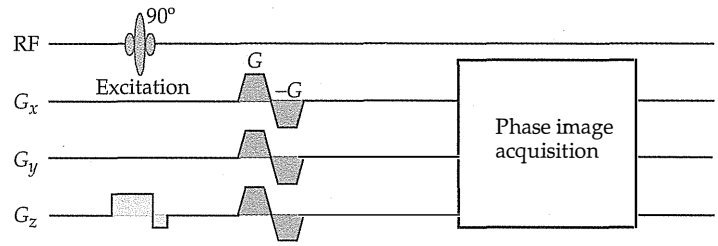

Figure 5.19 Pulse sequence used for VENC-PC MRA. This technique uses spatial gradients to induce changes in spin phase. The magnitude of the phase difference between a pair of images (e.g., one with gradients versus one without) provides information about the velocity of spins within each voxel.

after the excitation pulse but before the phase image acquisition. Note that they are bipolar in shape, which has no effect on static tissue. When this pulse sequence is repeated twice, once with velocity-encoding gradients and once without (or with opposite gradients), flow-dependent phase contrast will be generated.

Diffusion-weighted contrast

At all temperatures above absolute zero, thermodynamic effects cause molecules to move randomly. The motion of molecules due to thermodynamic effects is known as **diffusion** (Figure 5.20). In gases and liquids, molecules can move relatively freely, as when a dye spreads through a glass of water or when the smell of freshly baked bread wafts through a house. In solids, however, the motion of molecules is restricted, and thus diffusion is much slower. The abundance of water molecules in the human body makes it possible to perform diffusion-weighted imaging using MRI. And, because of the different cellular environments experienced by different water molecules, diffusion-weighted MRI can provide a new dimension of image contrast based on the mobility of those molecules, in terms of both the magnitude and direction of their diffusion.

If the magnetic field were perfectly homogeneous, the effect of diffusion would be hardly visible, as the water molecules would experience the same

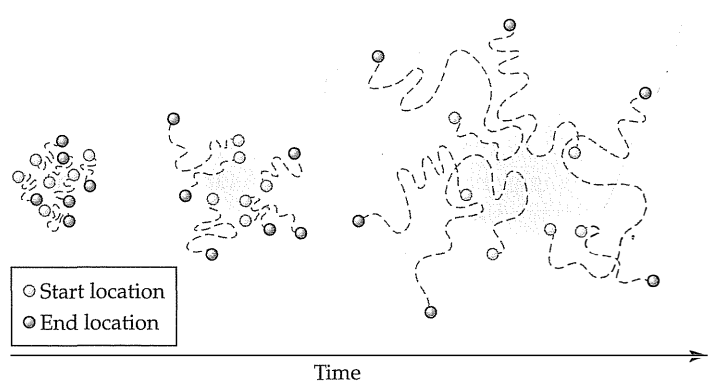

Figure 5.20 Diffusion. Over time, molecules within gases or liquids will move freely through the medium. This motion is known as diffusion. Shown here are sample random paths that could be taken by molecules within a medium that allows isotropic (i.e., the same in every direction) diffusion. As time passes, molecules become increasingly distant from their starting location.

diffusion The random motion of molecules through a medium over time.

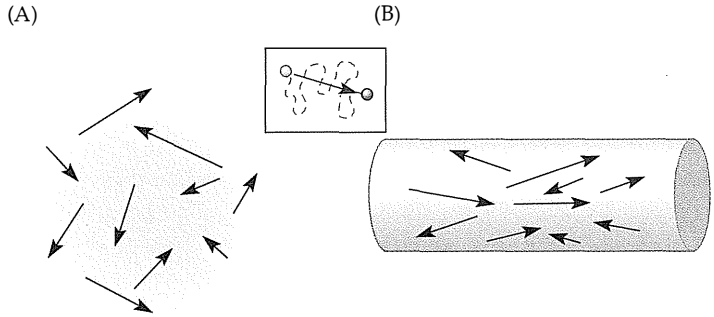

Figure 5.21 Isotropic and anisotropic diffusion. If there are no restrictions on diffusion, molecules will diffuse equally in all directions (A). This is known as isotropic diffusion. However, if there are restrictions on diffusion, as is the case within long neuronal axons, diffusion may occur primarily along one axis (B). This is an example of anisotropic diffusion. Note that the vector representations here are simplified versions of the random-walk paths taken by molecules, as indicated in the inset figure at upper center.

magnetic field regardless of their position over time. However, when magnetic fields are inhomogeneous, due to either intrinsic non-uniformity or to externally applied gradients, water molecules experience different magnetic fields as they diffuse. This causes a loss of phase coherence, which in turn attenuates the MRI signal. Unlike the loss of phase coherence due to static magnetic field inhomogeneity (i.e., T_2* effects), this loss cannot be recovered even with spin-echo pulse sequences. Because diffusion is random, the path taken by each molecule cannot be reversed. Thus, the refocusing pulse of a spin-echo sequence cannot recover signal lost to diffusion.

Diffusion weighting is the application of controlled gradient magnetic fields to quantify the amplitude and direction of diffusion. The presence of diffusion-weighting gradients further attenuates the MR signal beyond that caused by common T_2 relaxation. Assuming equal, or isotropic, diffusion along all directions (Figure 5.21A), the attenuation effect (A) due to diffusion weighting is given by the exponential

$$A = e^{-\int_0^T D(\gamma G(t)t)^2 dt} \tag{5.8}$$

In this equation, D is the apparent diffusion coefficient, or ADC (i.e., the measured value of the diffusion coefficient), G the strength of the external diffusion-weighting gradient, and T the duration of the diffusion-weighting gradient. We can define the degree of diffusion weighting as the b factor:

$$b = \int_0^T (\gamma G(t)t)^2 dt \tag{5.9}$$

To further simplify Equation 5.8:

$$A = e^{-bD} \tag{5.10}$$

Equation 5.12 quantifies the mean diffusivity within a voxel without providing directional information. But water molecules in the brain do not diffuse equally in all directions. Most water is contained within tissues that have considerable structure, such as the long processes of axons or the narrow walls of blood vessels. Unequal, or anisotropic, diffusion (Figure 5.21B) refers to the preference in some tissues for water molecules to diffuse in one direction or another. In anisotropic diffusion, the motion of molecules over time does not resemble a sphere, in which molecules move equally in every direction, but instead resembles an ellipsoid whose long axis indicates the fastest axis of diffusion. The diffusion ellipsoid is mathematically described as a three-dimensional tensor, which is a collection of vector fields governed by three principal axes (Box 5.1).

The ability of diffusion weighting to attenuate a signal based on its ADC can be very useful in fMRI for understanding the origins of the detected brain

diffusion weighting The application of magnetic gradients to cause changes in the MR signal that are dependent on the amplitude and/or direction of diffusion.

isotropic Having similar properties in all directions.

apparent diffusion coefficient (ADC) The quantification of diffusivity assuming isotropic diffusion.

b factor The degree of diffusion weighting applied within a pulse sequence.

anisotropic Having different properties in different directions; often referenced in the context of anisotropic diffusion, where molecules tend to diffuse along one axis but not others.

tensor A collection of vector fields governed by three principal axes.

BOX 5.1 Diffusion Tensor Imaging

A particularly important form of diffusion-weighted imaging is **diffusion tensor imaging (DTI)**, which quantifies the relative diffusivity of water in a voxel into directional components. For example, white matter, which is composed mostly of nerve fibers, shows prominent anisotropy, such that water molecules diffuse most quickly along the length of the fiber and most slowly across the width of the fiber. A scalar quantity known as the **fractional anisotropy (FA)** can be computed for each voxel to express the preference of water to diffuse in an isotropic or anisotropic manner. FA values are bounded by 0 and 1 and are calculated using equation below, where Dx, Dy, and Dz represent the three principal axes of the diffusion tensor:

$$FA = \frac{\sqrt{(Dx-Dy)^2+(Dy-Dz)^2+(Dz-Dx)^2}}{\sqrt{2(Dx^2+Dy^2+Dz^2)}}$$

FA values approaching the maximum of 1 indicate that nearly all of the water molecules in the voxel are diffusing along the same preferred axis, while FA values approaching the minimum of 0 indicate that the water molecules are equally likely to diffuse in any direction. Fractional anisotropy provides important information about the composition of the tissue within a voxel. Notably, some neurological diseases, such as multiple sclerosis and vascular dementia, are characterized by potentially severe white-matter pathology. The resulting axonal damage can be identified as decreased FA values in affected voxels.

To determine the coefficients of diffusion along different directions (i.e., axes of a diffusion tensor), we need to apply controlled gradients in a pulse sequence. These gradients must be balanced in time to preserve the MR signal. In spin-echo sequences (Figure 1A), this balance is achieved by presenting the gradients before and after the refocusing pulse. In gradient-echo sequences (Figure 1B), successive positive and negative gradients are applied. In an ideal isotropic medium, application of a gradient along any axis would be sufficient for measuring the ADC. However, the brain contains many tissues that constrain diffusion, and thus diffusion-weighting gradients must be applied in many directions to quantify the diffusion tensor. In practice, at least six different directions are needed to account for the six degrees of freedom in spatial coordinates and angles for any given tensor. Many new DTI sequences collect data from diffusion-weighted gradients in 15, 32, or even more directions.

Thought Question

Why are the gradients used in the spin-echo pulse sequence of the same sign, while the gradients used in the gradient-echo sequence are of opposite signs?

Tractography is an advanced application of DTI. Based on the estimated diffusion tensors, the longest axis of the diffusion ellipsoid (e.g., the most preferred direction of diffusion) can be used to guide the tracking of nerve fibers as they travel between functionally associated brain regions (Figure 2A). By following these directions and continuously connecting the long axes in space, we can construct images of complete nerve fibers and form maps of structural connectivity (Figure 2B). A high-resolution example of the major fiber tracts is shown in Figure 2C. More advanced acquisition techniques, such as diffusion spectrum imaging (DSI)

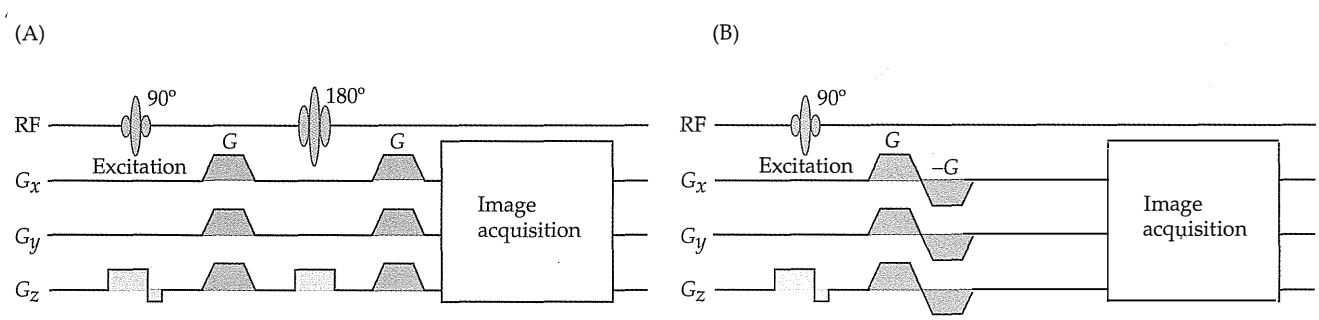

Figure 1 Pulse sequences used for diffusion-weighted imaging. Shown are sample pulse sequences used for diffusion-weighted spin-echo imaging (A) and diffusion-weighted gradient-echo imaging (B). Note that the spin-echo sequence has a refocusing pulse between two gradients of similar sign, while the gradient-echo sequence alternates gradients of opposite sign.

BOX 5.1 *(continued)*

(A)

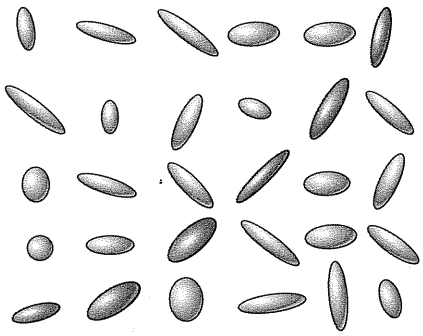

(B)

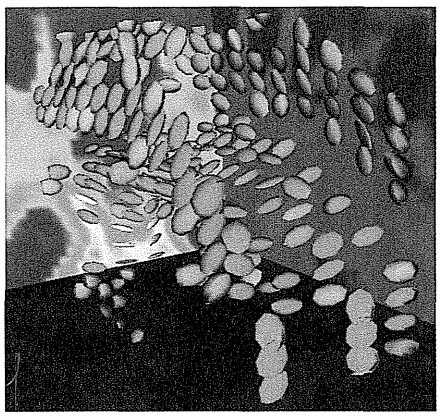

(C)

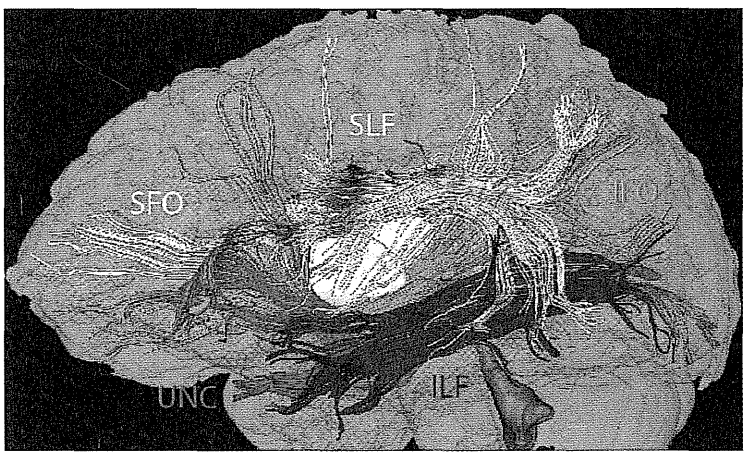

(D)

Figure 2 Fiber tracking using diffusion tensor imaging. DTI allows the measurement of the relative motion of water molecules within a voxel. (A) Each voxel is represented by an ellipsoid whose dimensions reflect the rate of diffusion, with spheres reflecting isotropic diffusion and narrow ellipses showing diffusion along a preferred axis. White-matter tracts can be reconstructed from these data using algorithms that find continuous tracks of diffusion across voxels, as indicated schematically for a hypothetical five-by-six set of voxels. Visible in red is a curve obtained by tracing diffusion axes across adjacent voxels. (B) An image showing, in three dimensions, a sample set of oval diffusion tensors used to generate maps of fiber tracts. (C) An image of DTI tractography that illustrates major fibers. Shown here are the superior longitudinal fasciculus (SLF), the superior fronto-occipital tract (SFO), the inferior fronto-occipital tract (IFO), the uncinate fasciculus (UNC), and the inferior longitudinal fasciculus (ILF). (D) An image created using diffusion spectrum imaging to improve the fine separation of crossing fiber tracts. Shown are the distortions in the normal pattern of white matter caused by a large brain tumor (yellow), compared with the pattern in the healthy side. (B courtesy of Dr. Guido Gerig, University of Utah; C courtesy of Dr. Susumu Mori, Johns Hopkins Medical School; D courtesy of Dr. Isaac Tseng, National Taiwan University Hospital.)

and high angular resolution diffusion imaging (HARDI), can resolve multiple tensors to improve fiber tracking at regions with complex, crossing sets of white-matter tracts. DSI can be used to resolve detailed white-matter structure, as shown in Figure 2D. In this image the normal pattern of the genu and splenium of the corpus callosum are altered by a large brain tumor.

In the context of fMRI, DTI can aid in determining the connectivity between various activated regions, to help infer their potential hierarchy in functional pathways. To date, DTI has been used most commonly in studies of memory and of visual function (e.g., see Figure 3). The development of DTI tractography is still at an early stage. New technical developments may lead to improvements in the quantitative assessment of white-matter integrity (and volume). This will greatly broaden its application for fMRI researchers.

(continued on next page)

BOX 5.1 *(continued)*

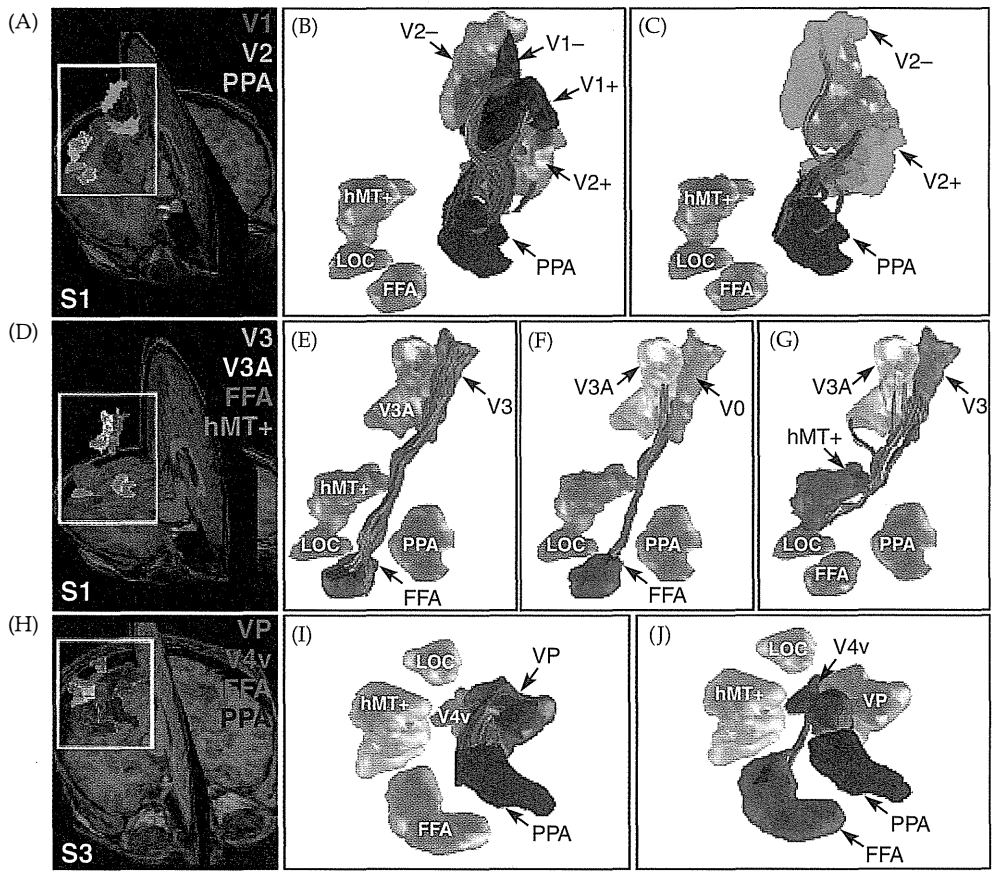

Figure 3 DTI tractography guided by areas of BOLD fMRI activation. Shown in the left column (panels A–C) are 3-D representations of the core regions of the human visual system, all functionally defined using fMRI. Some of these regions process basic features like line edges and their position (V1, V2) and more complex features like form, color, and motion (V3, V3A/VP, V4v, V5/hMT+). Other regions are selective for particular types of object processing (FFA: faces; PPA: places). Panels D–J provide examples of the fiber tracts, measured using DTI, that connect pairs of these regions (blue lines). (From Kim et al., 2006.)

diffusion tensor imaging (DTI) The collection of images that provide information about the magnitude and direction of molecular diffusion. It is often used to create maps of fractional anisotropy.

fractional anisotropy (FA) The preference for molecules to diffuse in an anisotropic manner. An FA value of 1 indicates that diffusion occurs along a single preferred axis, while a value of 0 indicates that diffusion is similar in all directions.

tractography The identification and measurement, often using diffusion tensor imaging, of white matter tracts that connect distant brain regions.

signals. Figure 5.22 illustrates the spatial distribution of ADCs within brain activations, with large vessels that have large ADCs distributed along the surface of the brain, while low ADC values are located in deep brain regions.

Perfusion-weighted contrast

The human brain requires oxygen for metabolism (see Chapter 6). To ensure a constant supply, hemoglobin molecules carry oxygen through the bloodstream to all parts of the brain. The irrigation of tissues via blood delivery is known as perfusion, and the family of imaging procedures that measure this process are

perfusion Blood flow through tissue.

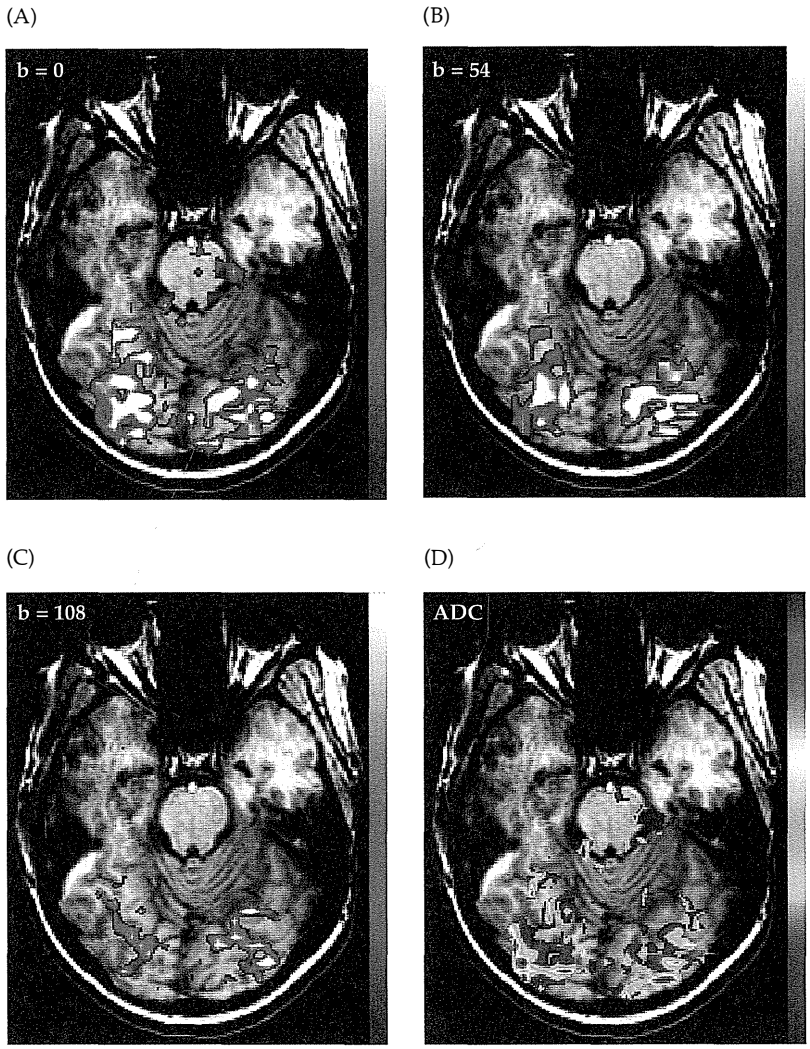

Figure 5.22 BOLD maps acquired at different b factors and the resulting ADC map. A single subject passively viewed objects presented in a blocked design, while BOLD contrast was measured at 4 T using different values of diffusion weighting. Shown in (A) is a map of BOLD activity with no diffusion weighting (b = 0); this is equivalent to the normal BOLD contrast measured in most fMRI studies. As diffusion weighting increases to b factors of 54 (B) and 108 s/mm^2 (C), the region of significant activity reduces in extent due to the elimination of signal from large blood vessels. The data from the three different diffusion-weighting values can be combined into a single map of static ADC contrast (D). The color scales for (A–C) reflect statistical values of a *t*-test of 3.6 to 8.0 (and greater), while the color scale for (D) reflects ADC values of 0.4 to 4.0×10^{-3} mm^2/s. Thus in the ADC map, red indicates voxels with high spin mobilities due to the presence of large vessels, and blue indicates voxels with low spin mobilities, such as areas containing largely capillaries.

known as perfusion MRI. Perfusion is expressed as the volume of blood that travels through a tissue mass over time. In the human brain, gray-matter perfusion is approximately 60 mL/100 g/min, and white-matter perfusion is lower, about 20 mL/100 g/min. Unlike the MRA techniques described in the section on MR angiography, (which are often used to measure the properties of large blood vessels for clinical reasons), perfusion MRI is used most frequently to generate images of blood flow in capillaries and other small vessels.

Perfusion MRI may use either exogenous or endogenous contrast. Exogenous contrast approaches use intravascular contrast agents that freely perfuse through the vascular system. The attenuation of the MR signal in each voxel is proportional to the amount of the contrast agent present. Thus, signal changes can be interpreted as a function of perfusion, and images can be created that depict different perfusion properties, such as the relative cerebral blood flow (rCBF), relative cerebral blood volume (rCBV), and mean transit time (mTT). As their names imply, relative blood flow and relative blood volume express changes in how much blood comes into a voxel, and how much blood is contained within a voxel, respectively. The mean transit time measures how quickly blood passes through a particular voxel and can indicate brain regions with

arterial spin labeling (ASL) A family of perfusion imaging techniques that measure blood flow by labeling spins with excitation pulses and then waiting for the labeled spins to enter the imaging plane before data acquisition.

continuous ASL A type of perfusion imaging that uses a second transmitter coil to label spins within an upstream artery while collecting images.

pulsed ASL A type of perfusion imaging that uses a single coil both to label spins in one plane and to record MR signal in another plane, separated by a brief delay period.

labeling plane The plane in which initial excitation pulse(s) are applied during perfusion imaging.

imaging plane The plane in which changes in MR signal are recorded during perfusion imaging.

delayed blood flow. The use of exogenous contrast agents provides very high signal changes but has limited use for research because of its invasiveness.

Endogeneous contrast perfusion imaging is noninvasive and is therefore used in fMRI research. Contrast is generated through the clever use of radiofrequency pulses to magnetically label, or tag, protons in blood water molecules before they reach the tissue of interest. This approach is known as **arterial spin labeling**, or **ASL**, of which there are two types: continuous and pulsed. **Continuous ASL** typically uses additional hardware, like a labeling coil, to saturate spins in upstream blood, such as in the carotid arteries of the neck (Figure 5.23A). Following this labeling process, the blood travels to the brain and enters the imaging slice. The brain images are then acquired in the presence of the labeled blood. Next, the labeling coil is turned off and a second set of images is acquired without the presence of the labeled blood. The difference between the two sets of images reflects only the blood flow, as any tissue that does not contain flow will be similar in the two conditions. A drawback of the continuous ASL technique is the requirement for a second transmitter coil to label the inflowing blood.

An alternative approach, **pulsed ASL**, uses a single coil both to label blood in the **labeling plane** and to record the MR signal change in the **imaging plane** (Figure 5.23B and C). Labeling pulses are broadcast for a brief period, followed by a delay and then image acquisition. The delay period must be calibrated to account for the distance between the labeling plane and imaging plane, so the labeled bolus of blood water will enter the imaging plane during image acquisition.

Regardless of the ASL method used, labeling blood only alters the longitudinal magnetization. Thus, we can describe the endogenous perfusion signal quantitatively by modifying the T_1 term of the Bloch equation (Equation 4.1). To do so, we introduce an additional term, $f(\mathbf{M}'(t) - \mathbf{M}_0)$, that accounts for the effects of blood flow:

$$\frac{d\mathbf{M}(t)}{dt} = \frac{\mathbf{M}_0 - \mathbf{M}_z(t)}{T_{1\text{app}}} + f(\mathbf{M}'(t) - \mathbf{M}_0) \tag{5.11}$$

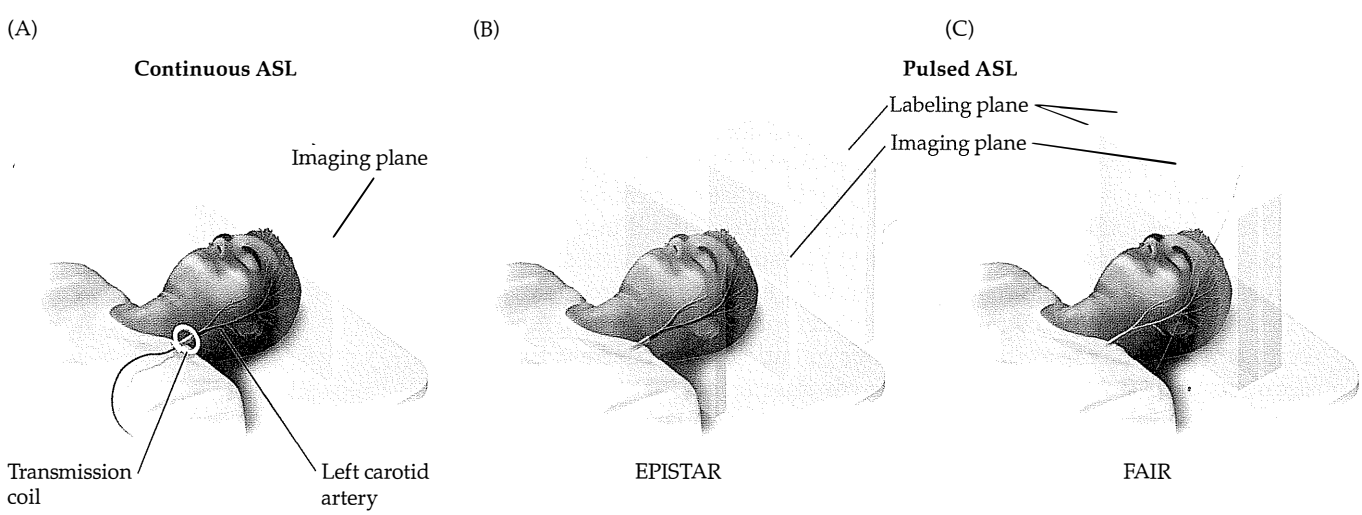

Figure 5.23 Perfusion imaging mechanisms. (A) Continuous ASL techniques use an upstream transmission coil to saturate spins in an artery that feeds the brain. Images collected following spin saturation can be compared with images in the absence of saturation to determine flow into the imaging plane. There are two primary types of pulsed ASL techniques, EPISTAR (B) and FAIR (C). EPISTAR relies on alternating two labeling planes that are equidistant from the imaging plane, one below the plane that includes feeding arteries and one above the plane that does not include any feeding vessels (i.e., is outside the head). FAIR alternates between labeling the entire brain and just the imaging plane. For either of the pulsed ASL techniques, differences between the two sets of images can be attributed to flow into the imaging plane.

In this equation, f is the blood flow in mL/g/sec and T_{1app} is the apparent T_1 value in the presence of blood flow. T_{1app} can be calculated from $1/T_{1app} = 1/T_1 + f/\lambda$, where λ is the blood–brain partition coefficient. This coefficient describes the movement of some substance between the vascular system and the brain, within a standardized time interval; its typical value for water is about 0.9 mL/g. Because the blood is labeled with an inversion pulse, its magnetization, $\mathbf{M}'(t)$, is given by $-\mathbf{M}_0$, so that the difference between the two conditions becomes:

$$\frac{d\mathbf{M}(t)^{\text{label}}}{dt} - \frac{d\mathbf{M}(t)^{\text{control}}}{dt} = -\frac{\mathbf{M}(t)^{\text{label}} - \mathbf{M}(t)^{\text{control}}}{T_{1\text{app}}} + f(-2\mathbf{M}_0) \quad (5.12)$$

and thus the signal remaining in the final perfusion image would be:

$$\mathbf{M}(t)^{\text{label}} - \mathbf{M}(t)^{\text{control}} = -2T_{1\text{app}} f \mathbf{M}_0 / \lambda \quad (5.13)$$

This equation defines the relationship between the measured perfusion signal and blood flow in the brain.

Because the continuous ASL method uses a second transmitter coil to label blood, the images can be acquired with any standard spin- or gradient-echo pulse sequence. To achieve the maximal signal difference, the echo time (TE) must be kept as short as possible, which minimizes signal loss due to T_2^* or T_2 relaxation effects.

Pulsed ASL techniques require specialized pulse sequences to label the blood. One type of pulsed ASL is called EPISTAR (echo-planar imaging at steady state with alternating inversion recovery). In EPISTAR, alternating off-center inversion pulses are used to select labeling planes below and above the imaging plane (Figure 5.24A). For odd-numbered scans, the labeling plane is in the neck, below and upstream from the imaging plane. For even-numbered scans, the labeling

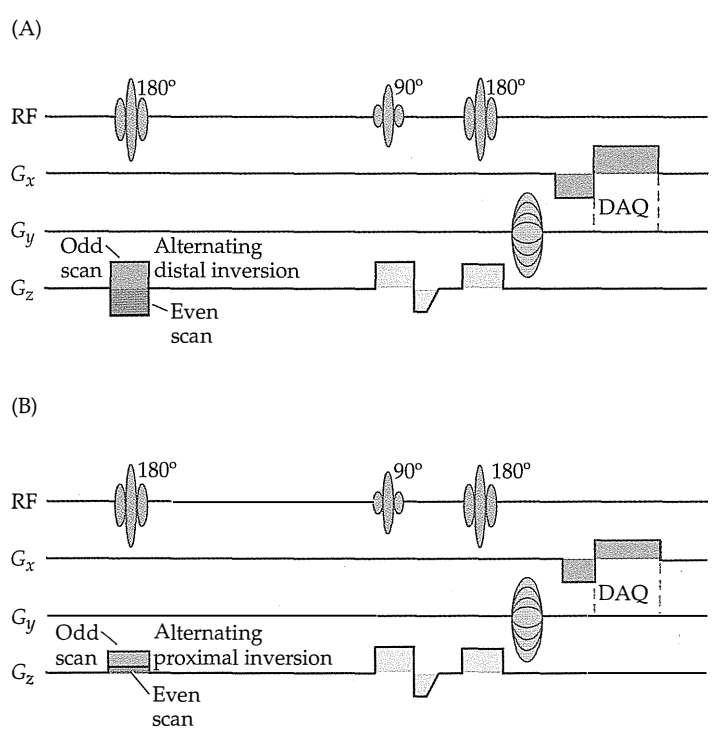

Figure 5.24 Pulse sequences for pulsed ASL imaging. Shown are typical pulse sequences used for the EPISTAR technique (A) and the FAIR technique (B). Both techniques require alternating between different labeling planes, as shown for the G_z gradient at left.

plane is at an equal distance above the imaging plane, and can actually be outside of the brain. This is necessary to ensure that the inversion pulse has a similar effect on the spin system in both the odd and even scans.

EPISTAR is directionally specific, in that it is only sensitive to spins flowing from the labeling plane to the imaging plane. A second type of pulsed ASL, FAIR (flow-sensitive alternating inversion recovery), is not directionally specific (Figure 5.24B). For odd scans, the entire brain is labeled. For even scans, only the imaging plane is labeled. The difference between the odd and even scans reflects those spins that flow into the imaging plane from anywhere else in the brain; thus FAIR is insensitive to the direction of flow. However, flow within the plane will be similar between scans and does not contribute to the image. Because the inversion pulse is present for both acquisitions, its effect within the imaging plane is identical.

Like the diffusion imaging techniques described in the previous section, perfusion imaging can be used to create images of brain function (Figure 5.25), providing potentially complementary information to standard BOLD contrast.

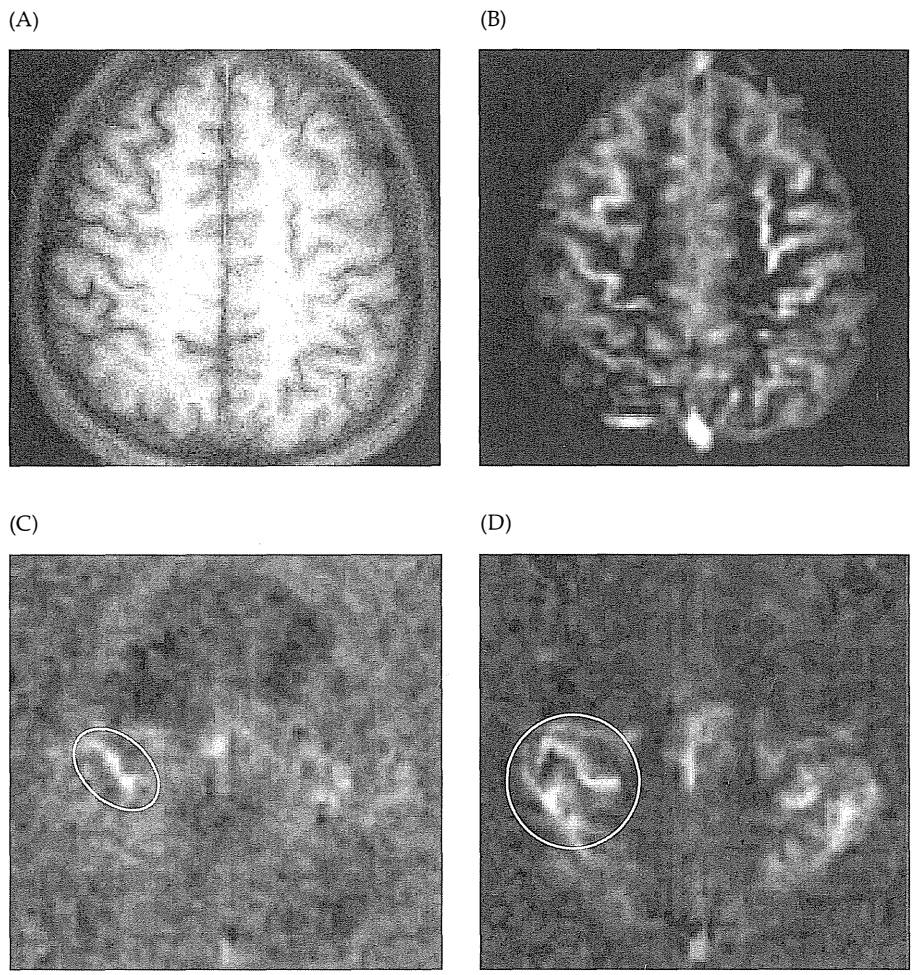

Figure 5.25 Comparison of perfusion and BOLD contrasts. Shown are an anatomical reference image (A), and a resting-state perfusion map from the same slice (B). During a simple motor task, there were significant increases in perfusion within the primary motor cortex (C, oval highlight). These perfusion-related increases generally were similar to those obtained using BOLD contrast (D, circle highlight), but were more spatially specific. In all images, absolute signal intensity is shown using a grayscale color map. (From Luh et al., 2000.)

Fast Imaging Sequences for fMRI

For anatomical images of the brain, contrast is more important than speed of acquisition, since structural parameters such as size and shape change little over the course of a single scanning session. However, understanding the function of the brain requires images to be acquired very rapidly, at approximately the same rate as the physiological changes of interest. Fast pulse sequences have been developed that can be used to acquire very large numbers of images within short periods of time; for example, state-of-the art sequences may allow the acquisition of 20 or more images per second. These sequences typically use variants of the gradient-echo approach described in Chapter 4 and are sensitive to T_2* contrast. The basic principles underlying these sequences are described in the remainder of this chapter.

echo-planar imaging (EPI) A technique that allows collection of an entire two-dimensional image by changing spatial gradients rapidly following a single electromagnetic pulse from a transmitter coil.

Echo-planar imaging

The first human MR images were acquired using a laborious voxel-by-voxel procedure. The image shown in Figure 1.12 took about 4 hours to acquire, and was collected at the slothlike pace of about two minutes per voxel. To put the current methods in perspective, a modern pulse sequence that results in the acquisition of 20 image slices per second, collects data at a rate that is approximately 10,000,000 times faster than the rate of acquisition of the first MR image. The development of fast MR imaging can be traced to the work of Peter Mansfield and colleagues at the University of Nottingham. At that time, the traditional method for acquiring images was to fill up *k*-space in a line-by-line fashion, which necessitated a large number of separate excitations for even a moderate-resolution image. In 1977, Mansfield proposed a new method, known as echo-planar imaging (EPI), in which the entire *k*-space is filled using rapid gradient switching, following a single excitation. For this technique, Mansfield shared the Nobel Prize in Physiology or Medicine in 2003.

Early MRI scanners were very limited in terms of the strength of the gradients that they could produce and the slow rate with which they could change the gradients. While high-static-magnetic field scanners were available by the early 1980s, advanced gradient technology was not common until the late 1980s and early 1990s. The maturation of gradient technology has made EPI the most commonly used fast imaging method in functional MRI. The basic EPI pulse sequence has changed little since its development by Mansfield (Figure 5.26A). Since all of *k*-space must be filled following a single excitation pulse, the data must be acquired before significant T_2* or T_2 decay can occur. However, to

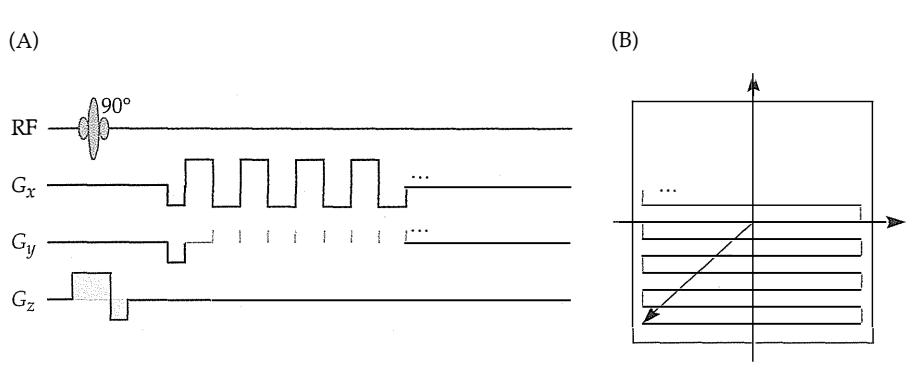

Figure 5.26 An EPI pulse sequence (A) and its *k*-space trajectory (B). The black arrow in the *k*-space trajectory represents the initial negative G_x and G_y gradients used to move to the bottom left of *k*-space. The subsequent gradient changes are highlighted in different colors for easy comparison between the pulse sequence and its *k*-space representation. Note that the directions of the gradients are changed rapidly over time to allow the back-and-forth trajectory through *k*-space.

achieve reasonable spatial resolution, a relatively large k-space must be sampled, which takes time. To meet these constraints, the k-space must be filled very rapidly. This requires a very strong gradient system. For EPI to be practical, gradients of about 2.5 Gauss/cm are sufficient, but stronger whole-body systems now exist that can produce gradients of up to 5 Gauss/cm. The use of very strong gradients can shorten the scan time required for one image to less than 20 ms.

To fill k-space, EPI uses an unconventional pattern in which alternating lines are scanned in opposite directions. This switchback approach taxes the gradient hardware heavily, since different sets of gradients must be cycled to enable the 90° turns in the k-space pattern. This pattern is also inefficient in that data collected while transitioning from one line of k-space to another (i.e., the vertical lines in Figure 5.26B) are not used in the image-creation process. Furthermore, the raw data obtained from the EPI acquisition must be sorted and realigned to remove the influence of the zigzag trajectory before being reconstructed using a Fourier transform. Without such realignment, serious artifacts can arise (Figure 5.27).

The most common EPI artifacts result from imperfections in the magnetic fields, either static or gradient, used to collect the images. Small- and large-scale static field inhomogeneities can result in signal losses and geometric distortions, respectively, and are discussed in Chapter 4. Figure 5.28 shows a set of typical EPI images, each a single axial (i.e., horizontal) slice, with the lowest parts of the brain in the upper left of the figure. Visible are significant losses in MR signal in the ventral frontal lobes and inferior medial temporal lobes, due to magnetic susceptibility artifacts resulting from the field inhomogeneities present at the boundaries between brain tissues and nearby, air-filled cavities. The signal loss in the ventral frontal region results from the nasal and oral cavities, which sit just under the frontal lobe, and the loss in the inferior medial temporal region results from the auditory canals below.

Geometric distortion is also present in EPI images, due to the long time spent acquiring the data from k-space after each excitation. In anatomical images, which have short data acquisition intervals, small field variations in the image plane may cause only sub-pixel distortions. But in EPI images with long readout periods, there can be noticeable distortions of up to several pixels. A long readout time makes the system more prone to geometric distortions due to both the reduced sampling frequency and the reduced strength of the gradients used during data acquisition. Variation in the magnetic field along a single in-plane direction (e.g., x or y) causes stretching and shearing of the otherwise circular phantom image (Figure 5.29A–C). Rarely, however, will geometric distortion be in a single direction; instead, gradient variation usually changes across the image in a complex fashion, resulting in more-complex patterns of distortion. A further problem results from small field variations along the z (i.e., slice-selective, or through-plane) direction, which cause off-resonance excitation and thus severe signal losses (Figure 5.29D).

Spiral imaging

While EPI enables fast image acquisition, its speed is constrained by the physical limitations of the MR scanner gradient hardware. A new family of fast imaging sequences, called spiral imaging, utilizes a very different trajectory in k-space from that of EPI. Spiral imaging sequences use sinusoidal changes in the gradients (Figure 5.30A) to trace a corkscrew path through k-space that typically begins at the center and winds its way to the perimeter (Figure

spiral imaging A technique for fast image acquisition that uses sinusoidally changing gradients to trace a corkscrew trajectory through k-space.

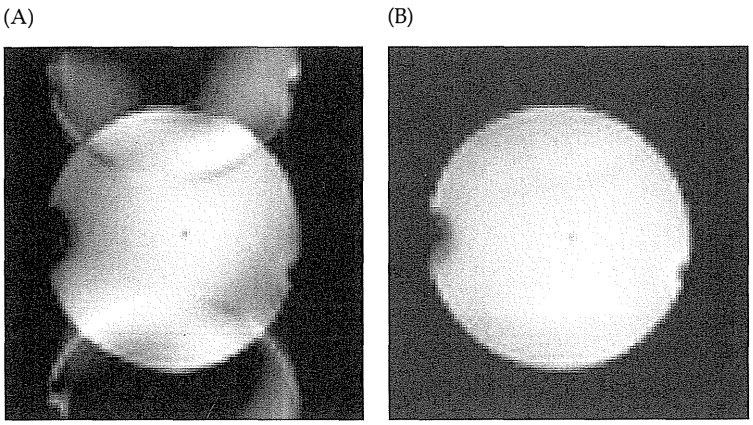

Figure 5.27 Artifacts due to the misalignment of EPI images. If the raw *k*-space data from an EPI acquisition are not realigned to remove the influence of the back-and-forth trajectory, significant image distortions can arise (A). (B) The corrected image of a phantom.

5.30B). This can be much less taxing on a gradient system compared with EPI sequences, and can reduce the time needed to collect an image. An additional advantage is that all points sampled along the spiral trajectory are used for reconstructing the final image, improving the efficiency of the acquisition. A disadvantage of spiral imaging is that the *k*-space data do not follow a Cartesian grid. This necessitates an additional step in which the acquired data points are interpolated back onto a Cartesian grid so that a Fourier transform can be used to reconstruct the image. While this consumes additional

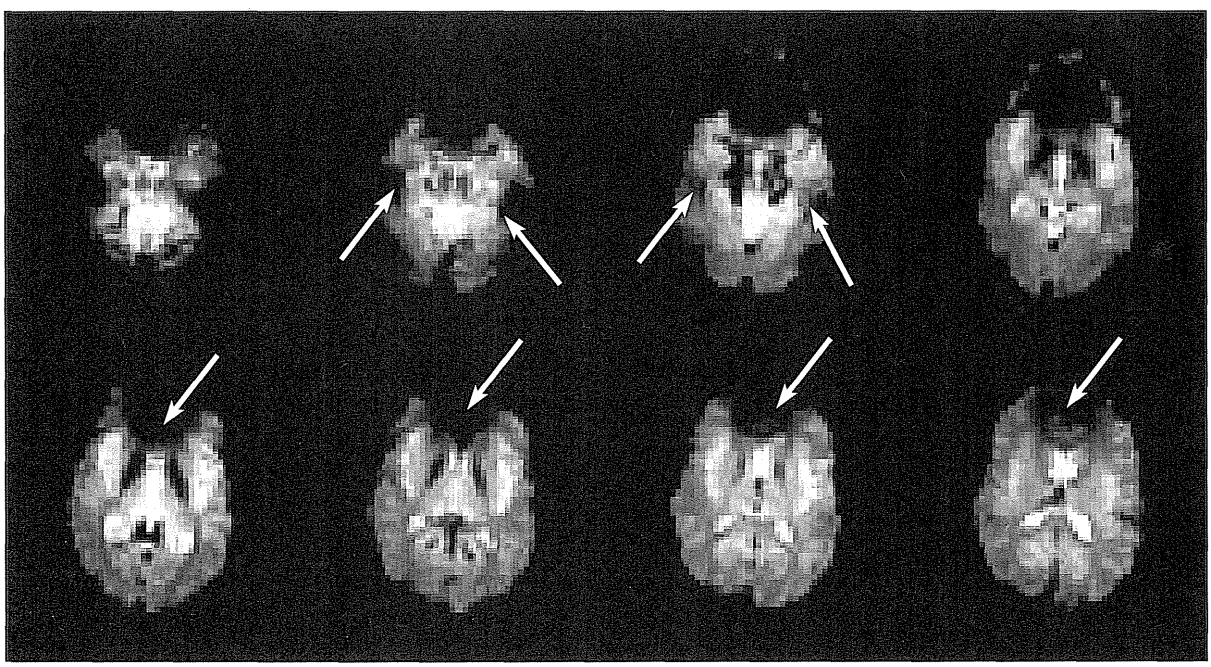

Figure 5.28 Signal loss due to susceptibility artifacts in EPI images. Shown here is a series of slices within an EPI image volume collected using a 4-T scanner (TE: 40 ms). In areas of the brain near interfaces between air and tissue, such as near the sinuses and auditory canals (arrows), there is significant signal loss due to magnetic field inhomogeneities.

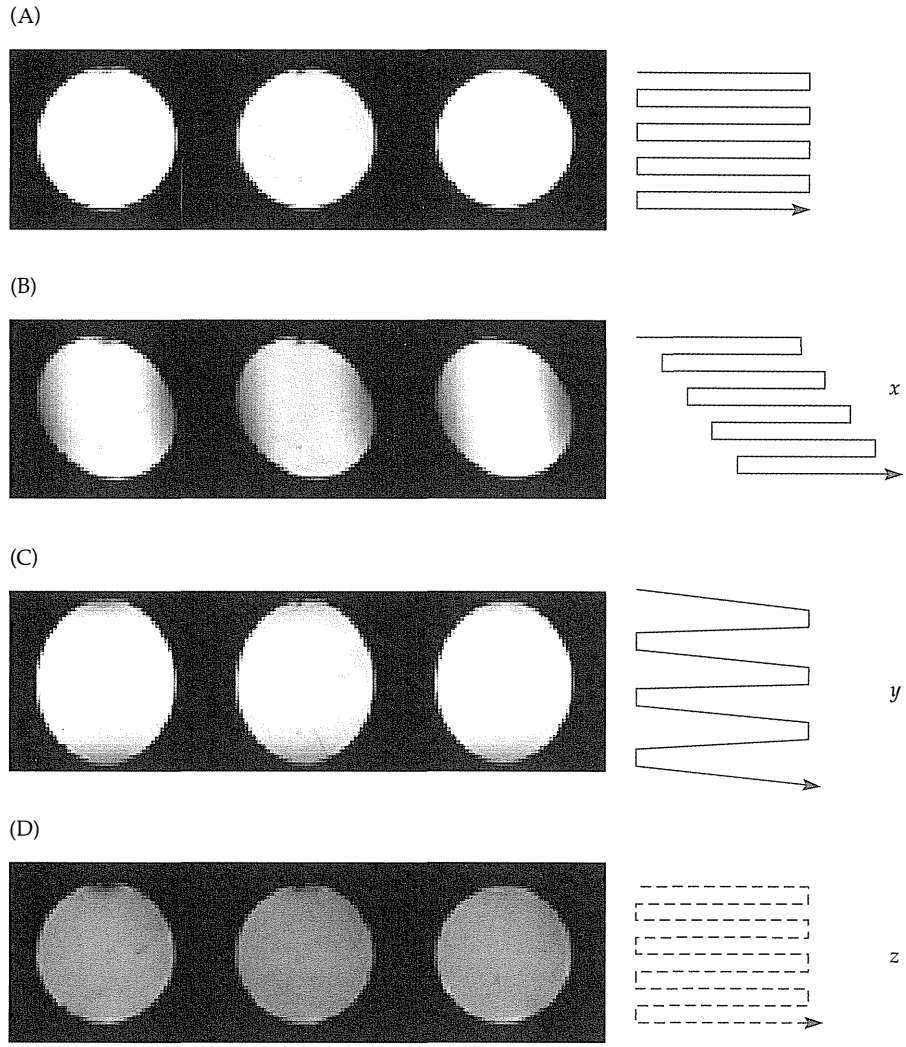

Figure 5.29 Effects of small field variations on EPI images. A normal EPI image (A) will be distorted by small variations in magnetic field strength along a single direction. If the variation is along x (B) or y (C), the image is systematically stretched or sheared. If the variation is along the slice selection axis z (D), the excitation is off-resonance and the MR signal intensity is reduced.

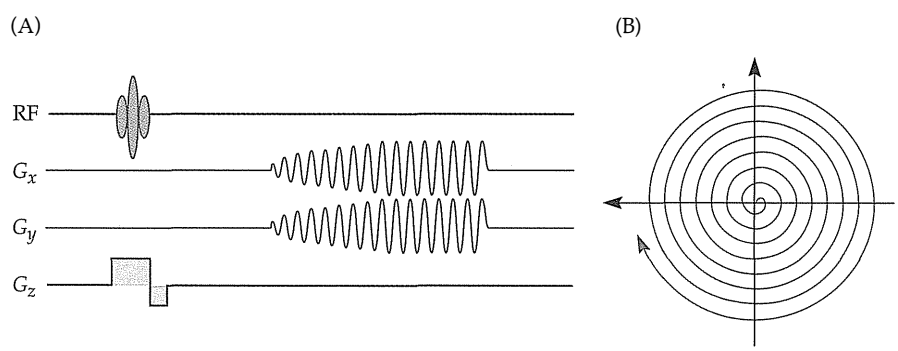

Figure 5.30 Spiral imaging. As illustrated here, spiral imaging pulse sequences use sinusoidally changing gradients (A) to generate a curving path through k-space (B).

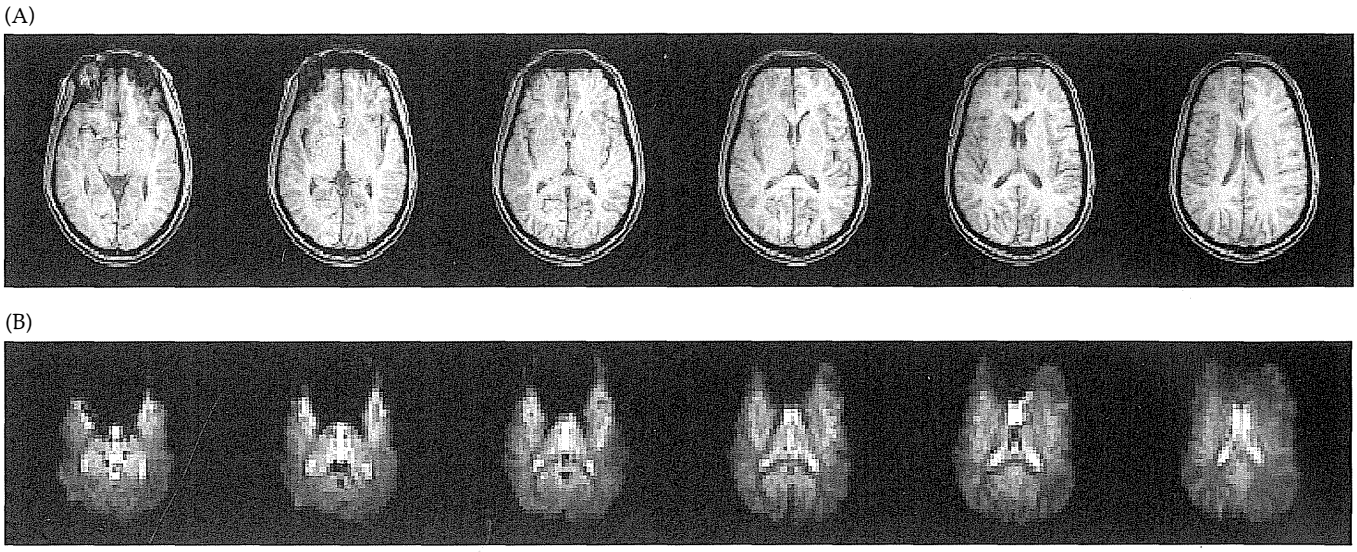

Figure 5.31 Signal losses due to susceptibility artifacts in spiral images. Compared with anatomical images (A), spiral images (B) exhibit regions of signal loss similar to those of EPI images (compare with Figure 5.28).

time during data processing, it is a small price to pay for the (often considerable) increase in acquisition rate.

Thought Question

The echo time (TE) is defined as the interval between excitation and the collection of the center of *k*-space. How do EPI and spiral sequences differ in where the TE falls within the duration of the data acquisition window?

Spiral images have the same vulnerability as EPI to signal losses in inhomogeneous regions, as shown in Figure 5.31. In addition, even though the spiral readout is more efficient than EPI in filling up *k*-space, it is still considerably longer than that used in conventional anatomical imaging methods, and thus spatial distortions are also present. The types of spatial distortion, however, are quite different from those found in EPI. Because of the non-Cartesian *k*-space sampling scheme, the regular distortion pattern seen in EPI images is usually not present in spiral images (Figure 5.32). For example, linear field variations in the x- or y-direction commonly shear and stretch entire EPI images. These same linear field variations would cause asymmetric compression in one dimension in spiral images. Due to the rotational symmetry between the x- and y-coordinates in spiral imaging, the artifact caused by the field variation along x (Figure 5.32B) is simply a 90°-rotated version of that caused by the field variation along y (Figure 5.32C). Another potential problem is that the spatial re-sampling necessitated by the spiral trajectory may blur the image. Like EPI, spiral imaging is also influenced by field inhomogeneities along the z-direction, resulting in severe signal losses (Figure 5.32D).

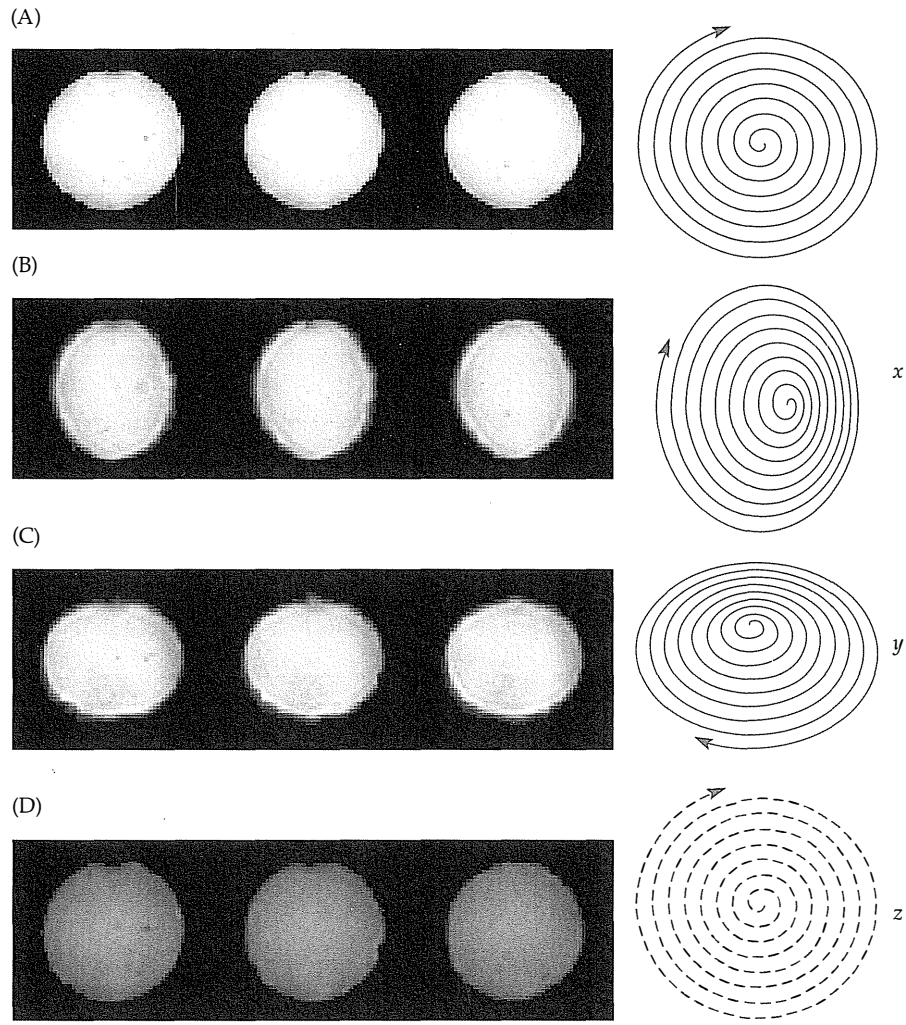

Figure 5.32 Effects of small field variation on spiral images. A normal spiral image (A) is distorted by small variations in magnetic field strength along a single direction, although the pattern of distortion is different from that of EPI. If the variation is along x (B) or y (C), the image is systematically compressed along the y-direction or x-direction, respectively. As with EPI, however, variation along the slice selection direction (D) causes a reduction in overall MR signal intensity.

Signal recovery and distortion correction for EPI and spiral images

As discussed above, a central weakness of BOLD fMRI, whether using EPI or spiral sequences, is its vulnerability toward magnetic field inhomogeneities. The air and bones in the sinuses and auditory canals have distinctly different magnetic susceptibilities compared with nearby brain tissues, leading to large magnetic field inhomogeneities and thus image artifacts. Specifically, in gradient-echo acquisitions, marked signal loss will be observed in EPI or spiral images; while in spin-echo acquisitions, significant geometric distortions will be seen. Since gradient echo imaging techniques are widely used in fMRI experiments, the resulting inability to measure fMRI signal in ventral brain regions

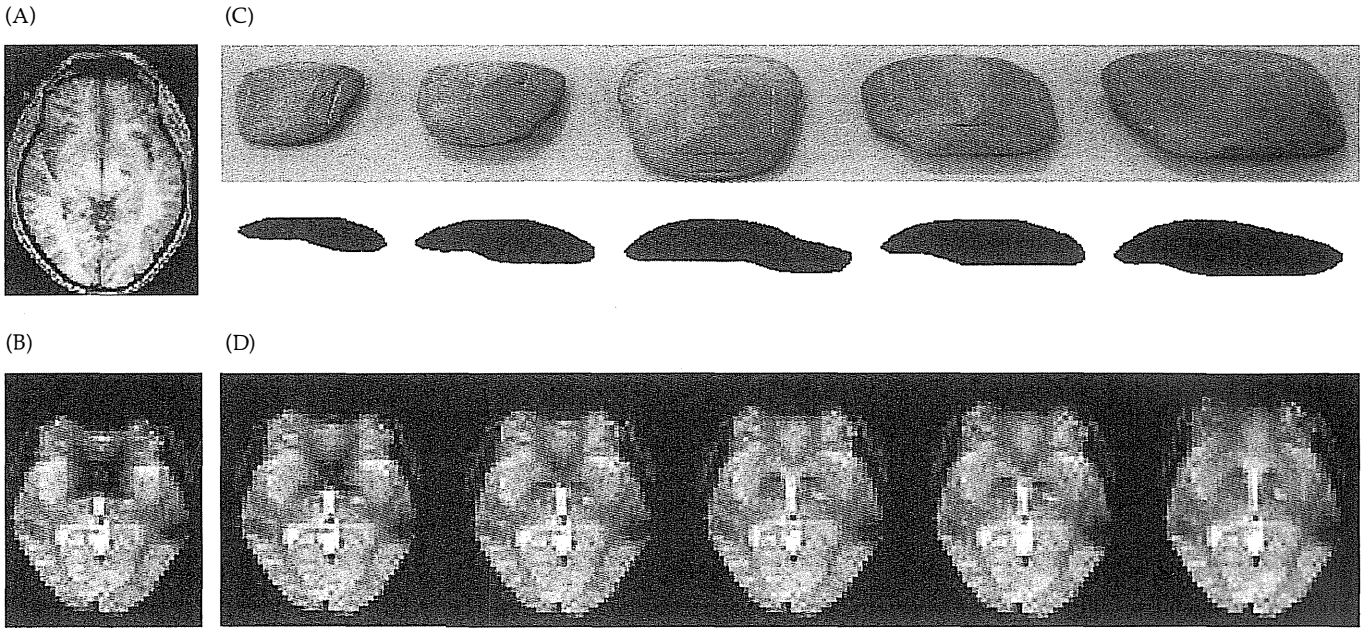

Figure 5.33 Use of a passive local shim (intra-oral graphite) to reduce susceptibility artifacts. Whereas images sensitive to T_1 contrast (A) can provide relatively good signal from throughout the ventral brain, images sensitive to T_2* contrast (B) show marked signal reductions in the ventral frontal lobe and ventral temporal lobe, due to susceptibility artifacts caused by the different magnetic properties of neighboring air and tissue. One approach for dealing with these signal losses is the introduction of a passive shim, such as a specially constructed mouth insert containing diamagnetic graphite (C, showing sample shims of different sizes and profiles). When placed in the mouth, these shims minimize susceptibility differences and thus ameliorate loss of signal in the ventral frontal lobes (D). Note that signal loss in the ventral temporal lobes (i.e., that caused by the auditory canals) is unaffected. (From Wilson et al., 2003.)

has been of significant concern. So, how can fMRI researchers who are interested in those regions compensate for these problems?

To prevent MR signal loss, we need to find effective means to compensate for the field inhomogeneities at boundaries between air and tissues. There are three types of compensation methods, all involving the shimming of the magnetic field (see Chapter 2 for an introduction to shimming). A relatively straightforward and effective approach is to introduce materials (e.g., pieces of graphite placed in the mouth) to provide passive local shims (Figure 5.33). However, the associated discomfort and inconvenience can make this a less-than-desirable option for many fMRI participants. A second option is the addition of active local shims, often using looped electrical circuits, to compensate for field inhomogeneities (shown in Figure 5.34). Yet, these can cause imaging artifacts and safety concerns. Third, since many of these intrinsic inhomogeneities induce gradient fields along the z-direction (i.e., inferior to superior), the pulse sequence can incorporate a z-shim gradient. Because this approach relies on the existing scanner hardware, it can provide good recovery of signal without consequences for the subject (Figure 5.35).

For spin-echo sequences that use a refocusing 180° pulse to generate MRI signal, magnetic field homogeneity is less critical for image quality, and thus there is much less signal loss due to inhomogeneities when using these

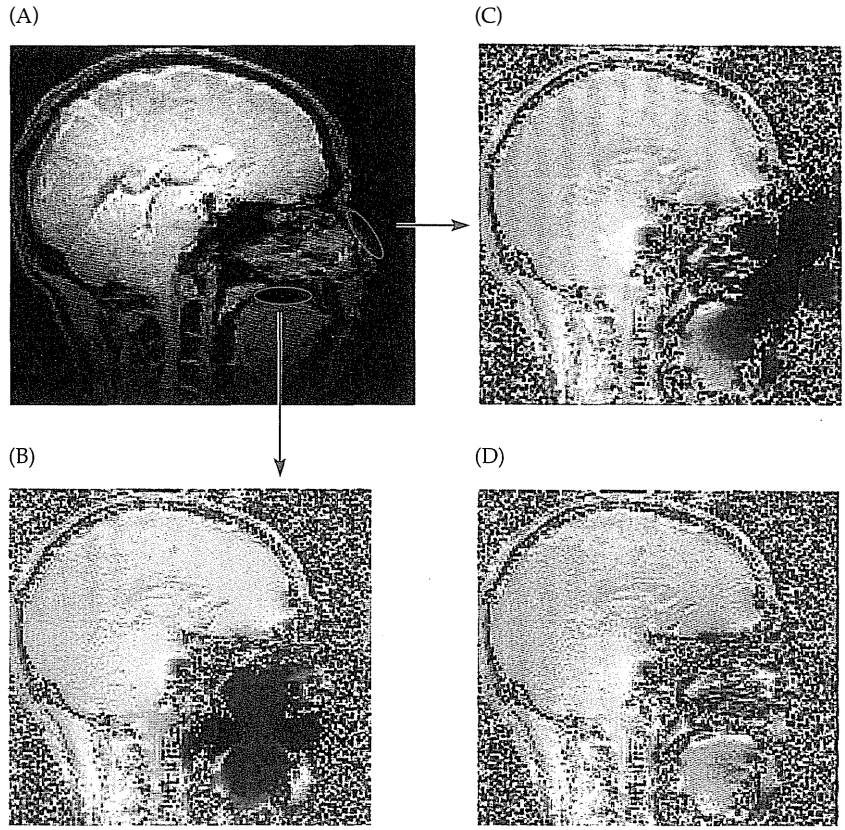

Figure 5.34 Use of an active local shim (magnetic field compensation) to reduce susceptibility artifacts. Electromagnetic coils positioned in the mouth and outside the nose (A) can generate compensatory magnetic field gradients with different orientations, resulting in the images shown in (B) and (C), respectively. Areas of similar color in these images reflect relative magnetic field homogeneity; areas with different colors indicate local inhomogeneities. The combined use of these coils recovers signal from the ventral frontal lobe, minimizing susceptibility artifacts (D). (Images courtesy of Dr. Eric Wong, University of California, San Diego.)

sequences. But because the spatial encoding is still achieved through gradient fields, magnetic field inhomogeneities can still shift the voxels in space and introduce large geometric distortions in the image. One important method for correcting such spatial shifts involves the use of a magnetic field map. The map is derived from two images acquired at slightly different TEs, and can be used subsequently to remove distortions from the images (Figure 5.36).

Summary

REFER TO THE
fMRI
COMPANION WEBSITE AT
www.sinauer.com/fmri2e
for study questions and Web links.

There are two general types of contrast for magnetic resonance imaging of the brain. Static contrast provides information about the number or content of atomic nuclei, while motion contrast describes how atomic nuclei move within a region of interest. Each basic type may use either endogenous mechanisms that rely on naturally occurring properties of biological tissue or exogenous mechanisms that typically involve the injection of compounds to greatly distort the magnetic field. Every contrast mechanism has associ-

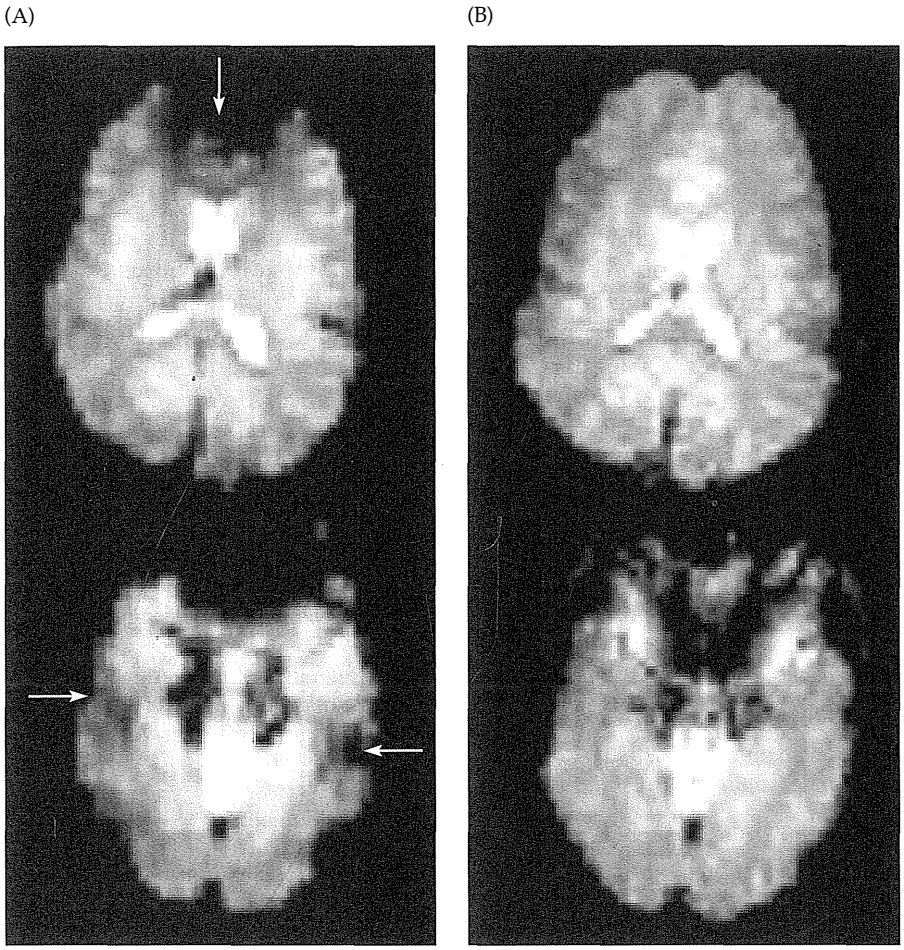

Figure 5.35 Use of a pulse sequence with a compensatory z-gradient to reduce susceptibility artifacts. Shown in (A) are two representative axial slices acquired using gradient-echo echo-planar imaging. Visible is the typical pattern of susceptibility-induced signal losses in frontal and inferior temporal regions (indicated by arrows). (B) The same slices, here acquired using a single-shot susceptibility compensation sequence. Much greater signal is present in the regions of susceptibility artifact, and anatomical details are clearly visible within those regions. Both pairs of images were collected at 4.0 T from the same subject.

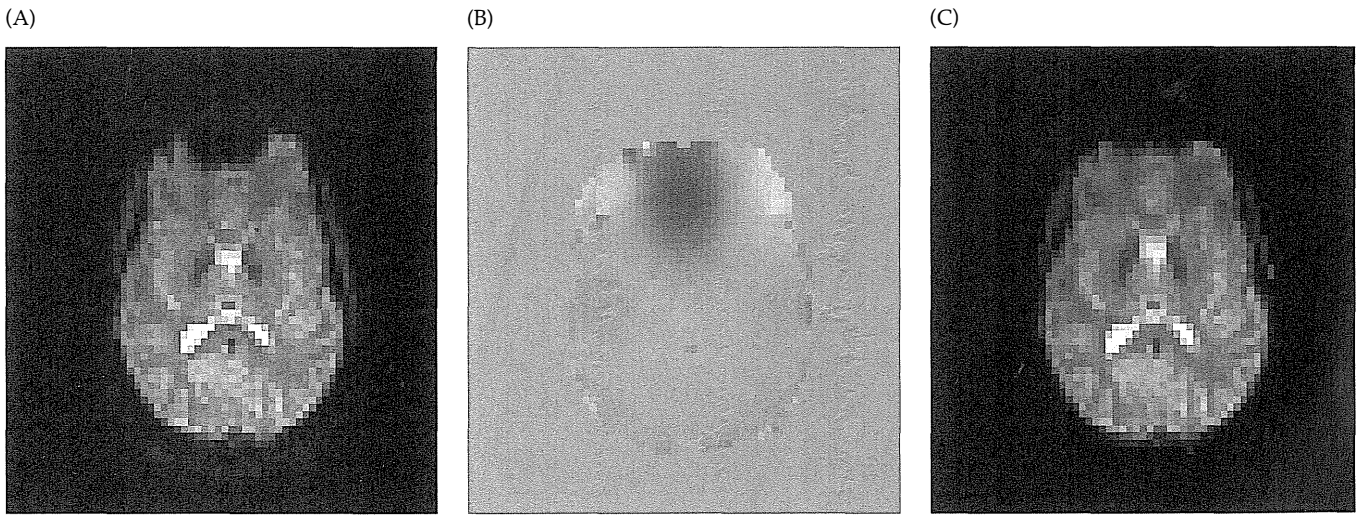

Figure 5.36 Use of a map of magnetic field strength to correct for image distortion. (A) One frequent consequence of magnetic field inhomogeneity is image distortion, shown here as skewing of the frontal lobes because of the underlying susceptibility artifact. By recording a map of magnetic field strength (B), correction algorithms can be applied to minimize that distortion (C).

ated pulse sequences describing the gradient changes and radiofrequency pulses that are used to collect the MR signal. By varying the parameters of a given pulse sequence, images can be collected that are sensitive to one form of contrast or another. Common static contrasts include proton-density, T_1-weighted, T_2-weighted, and T_2*-weighted. In fMRI experiments, these static contrasts are typically used for the collection of high-resolution images that provide anatomical detail. The use of T_2*-weighted contrast also provides the foundation for high-temporal-resolution studies of functional changes in the human brain. Motion contrasts include MR angiography, diffusion weighting, and perfusion imaging. Diffusion and perfusion imaging, in particular, have potential for providing information about brain physiology that can be complementary to that gained with BOLD fMRI. Gradient-echo imaging is the most common form of fMRI pulse sequence, for which both echo-planar and spiral imaging are used.

Suggested Readings

Buxton, R. (2001). *Introduction to Functional Magnetic Resonance Imaging: Principles and Techniques.* Cambridge University Press, Cambridge, U.K. *Provides an advanced overview of many facets of MRI, including a detailed discussion of perfusion imaging.*

Haacke, E. M., Brown, R. W., Thompson, M. R., and Venkatesan, R. (1999). *Magnetic Resonance Imaging: Physical Principles and Sequence Design.* John Wiley & Sons, New York. *A comprehensive encyclopedia of the theoretical principles of MRI.*

Slichter, C. P. (1990). *Principles of Magnetic Resonance* (3rd ed.). Springer-Verlag, New York. *Provides a detailed mathematical treatment of the physics of MRI.*

Chapter References

Arlart, I. P., Bongartz, G. M., and Marchal, G. (eds.) (1995). *Magnetic Resonance Angiography*. Springer-Verlag, New York.

Brown, T. R., Kincaid, B. M., and Ugurbil, K. (1982). NMR chemical shift imaging in three dimensions. *Proc. Natl. Acad. Sci. U.S.A.*, 79(11): 3523–3526.

Feynman, R. P., Leighton, R. B., and Sands, M. (1964). *Lectures on Physics*, Vol. II. Addison-Wesley Publishing Company, New York.

Grossman, R. I. (1999). Application of magnetization transfer imaging to multiple sclerosis. *Neurology*, 53: S8–11.

Hsu, J. J. and Glover, G. H. (2005). Mitigation of susceptibility-induced signal loss in neuroimaging using localized shim coils. *Magn. Reson. Med.*, 53: 243–248.

Kim, M., Ducros, M., Carlson, T., Ronen, I., He, S., Ugurbil, K., and Kim, D. S. (2006) Anatomical correlates of the functional organization in the human occipitotemporal cortex. *Magn. Reson. Imaging*, 24: 583–590.

Le Bihan, D. (ed.) (1995). *Diffusion and Perfusion Magnetic Resonance Imaging: Application to Functional MRI*. Raven Press, New York.

Luh, W. M., Wong, E. C., Bandettini, P. A., Ward, B. D., and Hyde, J. S. (2000). Comparison of simultaneously measured perfusion and BOLD signal increases during brain activation with T_1-based tissue identification. *Magn. Reson. Med.*, 44(1): 137–143.

Mansfield, P., and Maudsley, A. (1976). Line scan proton spin imaging in biological structures by NMR. *Physics in Medicine and Biology*, 21: 847–852.

Moonen, C. T. W. and Bandettini, P. A. (eds.) (1999). *Functional Magnetic Resonance Imaging*. Springer-Verlag, New York.

Wilson, J. L., Jenkinson, M., and Jezzard, P. (2003). Protocol to determine the optimal intraoral passive shim for minimisation of susceptibility artifact in human inferior frontal cortex. *NeuroImage*, 19: 1802–1811.

Wolff, S. D. and Balaban, R. S. (1989). Magnetization transfer contrast (MTC) and tissue water proton relaxation in vivo. *Magn. Reson. Med.*, 10: 135–144.

Chapter 6

From Neuronal to Hemodynamic Activity

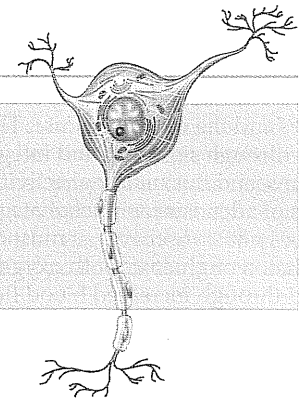

In the previous chapters, we explained how the principles of magnetic resonance can be used to create images of the brain. We have further shown that by changing how electromagnetic pulses and gradient magnetic fields are applied, we can create MR images that have contrast based on any number of different biophysical properties, including proton density, relaxation constants like T_1 or T_2*, diffusion, or perfusion. However, another step is necessary for MRI to become fMRI. We must identify a biophysical property—some quantity that is altered by information processing—that can be used as a marker of brain function.

Because information processing results from the activity of assemblages of neurons, some neuroscience techniques directly measure neuronal activity. Invasive electrophysiological methods like single-unit recording measure the changes in membrane potential and ionic currents caused by the transfer of information by neurons. However, to make a whole-brain image of neuronal activity using electrophysiological methods, one would need to have closely spaced electrodes placed throughout the brain—a prospect that is neither practical nor ethical in humans. Electroencephalography (EEG) and magnetoencephalography (MEG) measure neuronal activity using sensors located outside of the brain, and thus these non-invasive techniques can be used in humans, but even these valuable approaches have many limitations, especially in their spatial resolution. Some optical imaging techniques measure neuronal activity using voltage-sensitive dyes that change their transmissive properties in response to changes in neuronal membrane potential, potentially within milliseconds of neuronal activity. However, the invasiveness of deep-tissue optical measurements and the toxicity of the dyes used preclude this approach for the study of the intact human brain.

How does fMRI create images of neuronal activity? The short answer is that it does not! Instead, fMRI creates images of physiological changes that are *correlated* with neuronal activity. To presage the key concepts: the information-processing activity of neurons increases their metabolic requirements. The vascular system provides energy to meet these requirements in the form of two fuel sources, glucose and oxygen, the latter bound to hemoglobin molecules. And, because deoxygenated hemoglobin has magnetic properties that distort

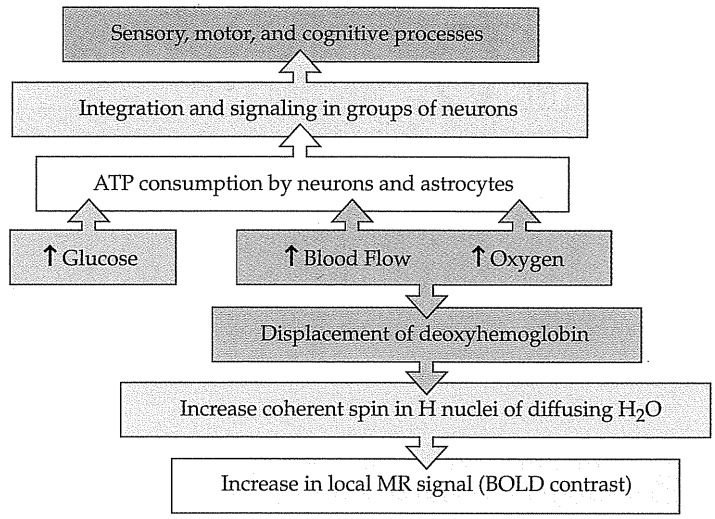

Figure 6.1 An overview of the physiological changes leading to fMRI data. In fMRI studies, researchers draw conclusions about sensory, motor, and cognitive processes based on changes in the MR signal within specific parts of the brain. Yet, many links intervene between these mental processes and the measured data. These processes are realized through signaling and integration within groups of neurons, and this neuronal activity requires energy in the form of adenosine triphosphate, or ATP. Because the brain does not store energy, it must create ATP through the oxidation of glucose. Both oxygen and glucose are supplied through increased blood flow to active neurons. The increase in blood flow replaces deoxyhemoglobin in the capillaries, venules, and small veins of the active area with oxygenated hemoglobin. Since deoxyhemoglobin molecules have magnetic field gradients that alter the spins of nearby diffusing hydrogen nuclei, the presence of deoxyhemoglobin reduces their MR signal intensity. By displacing deoxyhemoglobin with oxygenated hemoglobin, the increase in blood flow results in a local increase in the MR signal.

some types of MR images, changes in its concentration provide a measure of brain function based on blood-oxygenation-level dependent (BOLD) contrast.

It is important to recognize that BOLD contrast is a consequence of a series of indirect effects. It is a measure of changes in the magnetic properties of water molecules, which in turn reflect changes in the concentration of paramagnetic deoxyhemoglobin. The deoxyhemoglobin concentration is a physiological indicator of oxygen consumption, which reflects changes in neuronal activity evoked by sensory, motor, and/or cognitive processes (Figure 6.1). Through investigation of this chain of processes, a number of important questions have arisen. How direct is the link between neuronal activity and the BOLD signal? How well is the spatial distribution of neuronal activity reflected in the spatial distribution of blood flow? How well does the relative timing of vascular, or hemodynamic, events reflect neuronal activity in different groups of neurons comprising a functional network? Understanding the answers to these questions is critical to being an informed user of fMRI methods and an informed consumer of fMRI results. In this chapter and the next, we consider the links between neuronal activity, energy consumption, cerebral metabolism, blood flow, and the MR signal.

blood-oxygenation-level dependent (BOLD) contrast The difference in signal on T_2*-weighted images as a function of the amount of deoxygenated hemoglobin.

hemodynamic Having to do with changes in blood flow or other blood properties.

neuron A cell that is the basic information-processing unit of the nervous system.

cortex (neocortex) The thin wrapping of cell bodies around the outer surface of the brain.

soma The body of the cell; it contains cytoplasm, the cell nucleus, and organelles.

dendrite A neuronal process that receives signals from other cells, performing a primarily integrative function.

axon A neuronal process that transmits an electrical impulse from the cell body to the synapse, performing a primarily signaling function.

Neuronal Activity

We begin this inquiry with the neuron (Figure 6.2), which is the basic information-processing unit of the central nervous system. We will focus on the relationship between information processing in the neuron and the resulting energy requirements. Modern stereological evidence has estimated that the human brain contains about 100 billion neurons. Of these, about 20 billion are contained within the cortex, or neocortex, a thin wrapping of cell bodies around the outer surface of the brain. Each cell body, or soma, of a neuron, as in other cells of the body, contains cytoplasm, organelles such as the Golgi apparatus and mitochondria, and a nucleus containing DNA. In a typical neuron, the cell body gives rise to branching protoplasmic processes called dendrites that vary greatly in number and spatial extent. Neurons also usually have one or more protoplasmic processes called axons that transmit information to other neurons, via projections to their dendrites and cell bodies.

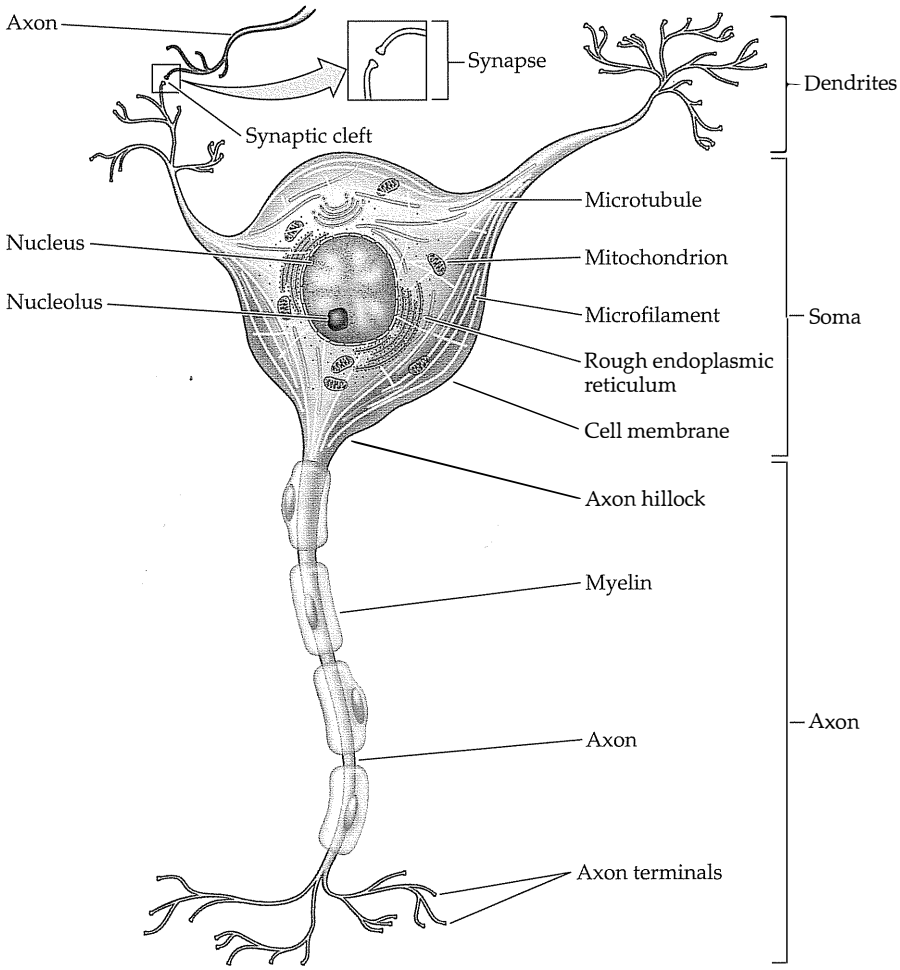

Figure 6.2 The neuron. Neurons are organized into three basic parts. Dendrites integrate signals coming from other neurons via small gaps known as synapses. The soma, or cell body, of the neuron contains the nucleus and organelles that support metabolic and structural properties of the neuron. Changes in the membrane potential of the neuron are signaled to other neurons by action potentials that travel along its axon.

Neurons come in many varieties, some with dense dendritic arbors and some without any dendrites. Some neurons have long axons that travel great distances in the nervous system, others have short axons that terminate locally, and still others have no axons at all. In addition to neurons, the human brain contains other types of supporting cells, known as **glial cells (glia)**, including astrocytes, oligodendrocytes, and microglial cells. Glial cells are not thought to be directly involved in information processing within the brain, but they do participate indirectly by helping with synapse formation and regulation of the chemical environment surrounding neurons.

A useful generalization is that neuronal activity can be characterized as either integrative or signaling. **Integrative activity** collects inputs from other neurons through connections on both the dendrites and the cell body. **Signaling activity** transmits the outcome of integrative processes to other neurons. The transfer of information between neurons occurs at specialized junctions called **synapses**, where an axon terminal process from one neuron (i.e., the presynaptic terminal) is located adjacent to the postsynaptic membrane of the dendrite or soma of another neuron. In most synapses, the presynaptic and postsynaptic elements are separated by a small gap, the **synaptic cleft**, in which chemicals released from the presynaptic element influence activity in the postsynaptic membrane. In a relatively small number of specialized synapses, the presynaptic and postsynaptic membranes are in physical contact and electri-

glial cells (glia) Brain cells that support the activities of neurons but are not primarily involved with information transmission.

integrative activity The collection of inputs from other neurons through dendritic or somatic connections.

signaling activity The transmission of the outcome of an integrative process from one neuron to another.

synapse A junction between neurons where the presynaptic process of an axon is apposed to the postsynaptic process of a dendrite or cell body.

synaptic cleft A gap between presynaptic and postsynaptic membranes.

concentration gradient A difference in the density of a substance across space. Substances diffuse along concentration gradients from areas of high concentration to areas of low concentration.

ion A charged atom.

ion channel A pore in the membrane of a cell that allows passage of particular ions under certain conditions.

pump A transport system that moves ions across a cell membrane against their concentration gradients.

sodium–potassium pump A transport system that removes three sodium ions from within a cell while bringing two potassium ions into the cell.

cal signaling events cross the membranes without intervening chemical messengers. A neuron may have hundreds or even thousands of synapses on its dendrites and soma, and it has been estimated that there are 100 trillion synapses in the human brain.

Ion channels in neurons

Both neuronal integration and signaling depend on the properties of neuronal membranes, which are lipid bilayers that separate the internal contents of the neuron from the external milieu. An important role of neuronal membranes is to restrict the flow of chemical substances into and out of the neurons. When substances are allowed to diffuse freely, they tend to diffuse from areas of high concentration to areas of low concentration. That is, they move along a concentration gradient until equilibrium is reached. However, neuronal membranes prevent free diffusion. They do, however, have embedded proteins that form pores or channels through which some ions, such as sodium (Na^+), chloride (Cl^-), potassium (K^+), and calcium (Ca^{2+}), can diffuse (Figure 6.3). (Note that an ion is an atom that has either a negative charge from having gained one or more electrons, or a positive charge from having lost one or more electrons.) These ion channels are selective, such that some ions can pass and others cannot. Furthermore, channels have gating mechanisms that can close or open them to ion traffic. While some gating mechanisms depend on the actions of specific molecules, others are also voltage-dependent and open when the electrical potential difference across the membrane has reached a particular threshold.

While an open channel can allow ions to diffuse passively down their concentration gradients, membranes also contain transporters, or pumps, that can move ions across the membrane against their concentration gradients and thereby create or maintain an unequal distribution of some ions (see Figure 6.3). One of the most important pumps is the sodium–potassium pump. The sodium–potassium pump uses a transporter molecule that forces three sodium ions (Na^+) out of the cell and then picks up and brings two potassium ions (K^+) into the cell on the return trip. Due to the action of the sodium–potassium pump and other transporters, along with the selective permeability of the membrane channels to different ions, a neuron at rest has a greater concentration of K^+ inside its membrane and a greater concentration of Na^+, Ca^{2+}, and Cl^- outside its membrane. Any transient change in the permeability of the membrane

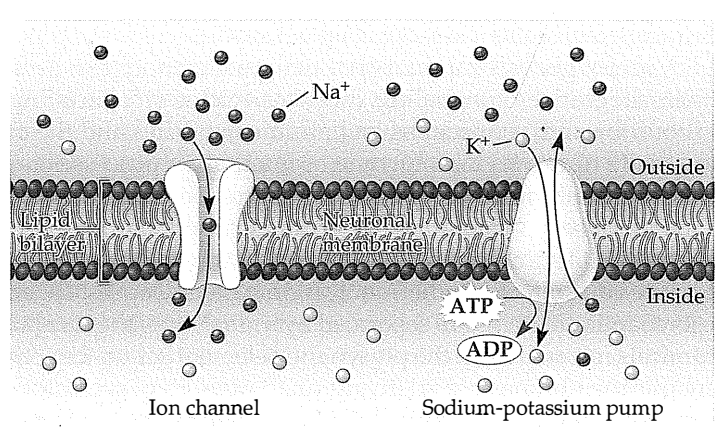

Figure 6.3 Ion channels and pumps. Ion channels allow particular ions to diffuse across membranes along concentration gradients. They may be opened by the actions of particular molecules, or they may open when the voltage difference across the membrane reaches a threshold. Pumps move ions across membranes against their concentration gradients, usually at a cost of energy supplied by ATP. A very important pump transports sodium out of the cell while bringing potassium into the cell.

will cause an influx (movement into the cell) or an efflux (movement out of the cell) of these ions as the system attempts to eliminate the concentration gradient and establish equilibrium.

The diffusion of substances through channels down their concentration gradients requires only kinetic energy from heat, but the operation of pumps requires cellular sources of energy. For example, one turn of the sodium–potassium pump requires the energy of one molecule of adenosine triphosphate, or ATP, which is converted to adenosine diphosphate, or ADP. (We will have more to say about ATP later in this chapter in the section on cerebral metabolism.) Consider the analogy of a water tower where holes in the bottom of the water reservoir allow passage of the water into descending pipes below. Here the gravity gradient is analogous to the concentration gradient and the holes are analogous to open ion channels. The water will move through the holes and run through the pipes down the gravity gradient without additional energy. The situation is quite different, however, if we want to return the escaping water to the water tower. Active pumping against the gravity gradient is now required, and the pump requires energy to operate. Note that while this analogy is instructive, it is incomplete with respect to ions. Because ions have electrical charge, their unequal distribution also results in an electrical potential (about –40 to –70 mV) between the inside and outside of the membrane. Thus, the movement of ions across a membrane is governed by both chemical and electrical gradients.

Neurotransmitters and action potentials

The primary location for communication between neurons is the synapse (Figure 6.4). The presynaptic process of the axon releases neurotransmitters, which are chemicals that diffuse across the synaptic cleft and interact with receptors on the postsynaptic membrane that gate (i.e. control the opening and closing of) ion channels. For example, the neurotransmitter glutamate opens normally blocked ion channels that allow Na^+ to move down its concentration gradient and through the postsynaptic membrane into the target neuron. This influx of Na^+ ions decreases the electrical potential between the inside and outside of the membrane at the channel location. Another type of glutamate receptor called the NMDA (N-methyl-D-aspartate) receptor admits Ca^{2+} through its channel when a threshold membrane potential is reached. This local depolarization of the postsynaptic cell membrane is referred to as an excitatory postsynaptic potential, or EPSP, and thus glutamate is known as an excitatory neurotransmitter. Glutamate is the most common excitatory neurotransmitter in the brain, and it is released by about 90% of all neurons.

Other neurotransmitters, such as γ-aminobutyric acid (GABA), interact with other receptors to open chlorine or potassium channels. Either the influx of the negatively charged Cl^- into the neuron or the efflux of the positively charged K^+ out of the neuron results in a net increase in the resting potential in the vicinity of these newly opened channels. This local hyperpolarization of the neuronal membrane is referred to as an inhibitory postsynaptic potential, or IPSP, and thus GABA is known as an inhibitory neurotransmitter.

A single EPSP or IPSP is a transitory event. Afterward, the neurotransmitter will be deactivated or removed from the synaptic cleft and from the receptor, the channel that was opened by the neurotransmitter will close, and ion pumps will restore both the unequal distribution of ions across the membrane and the resting membrane potential. However, because a neuron may have thousands of synapses, it may experience a barrage of individual EPSPs and IPSPs simultaneously progressing throughout its dendritic trees and soma.

neurotransmitters Chemicals released by presynaptic neurons that travel across the synaptic cleft to influence receptors on postsynaptic neurons.

glutamate One of the most important excitatory neurotransmitters.

excitatory postsynaptic potential (EPSP) A depolarization of the postsynaptic cell membrane.

γ-aminobutyric acid (GABA) One of the most important inhibitory neurotransmitters.

inhibitory postsynaptic potential (IPSP) A hyperpolarization of the postsynaptic cell membrane.

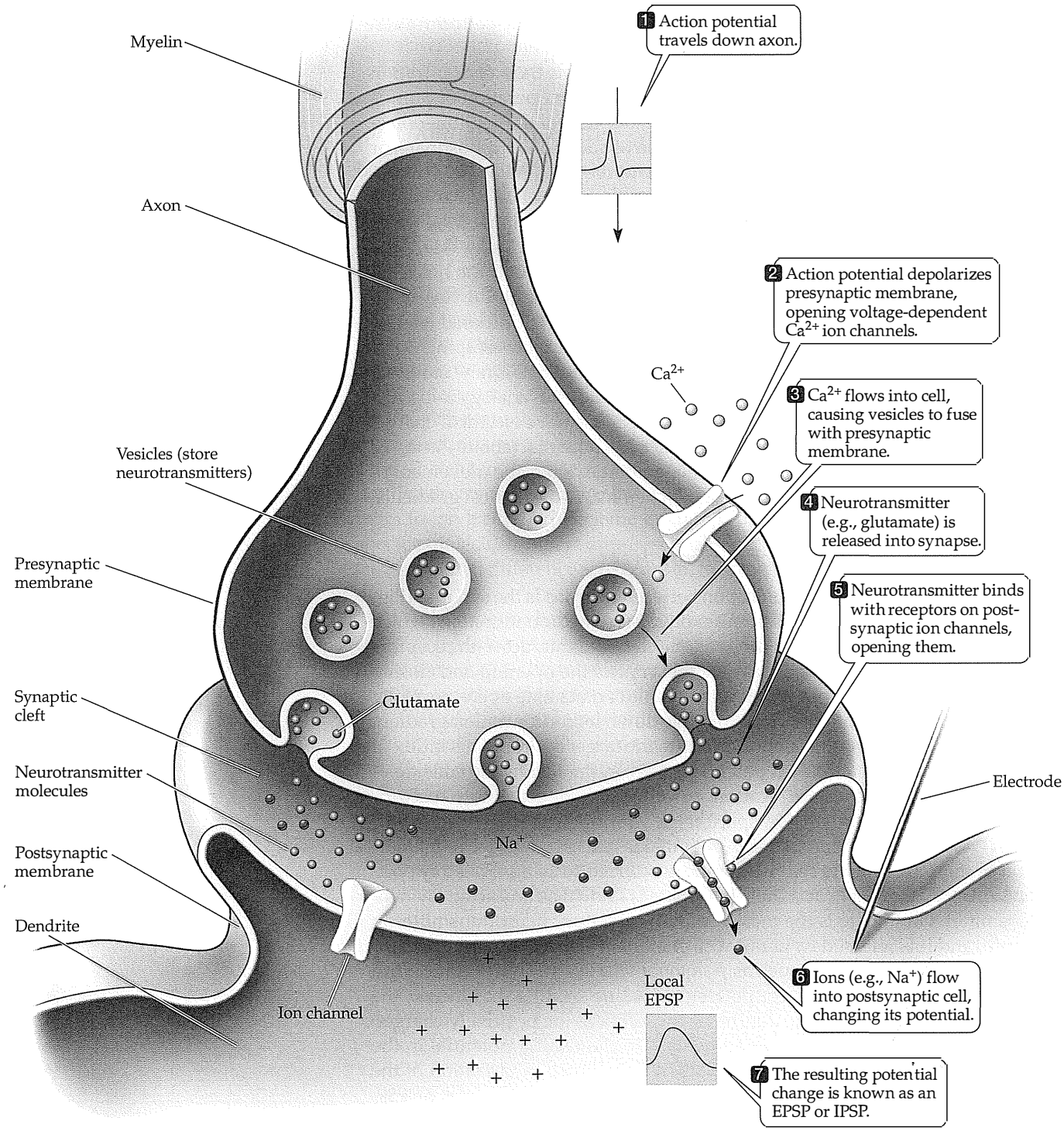

Figure 6.4 Synapses and the release of neurotransmitters.

axon hillock A region of the cell body located at the emergence of the axon. Changes in its electrical potential lead to the generation of action potentials.

These depolarizing and hyperpolarizing membrane potentials are integrated by the neuron. Both their timing and spatial pattern influence the net polarization of a specialized region of the soma called the **axon hillock**, which is located where the axon emerges from the cell body.

If, over a brief time interval, the net depolarization experienced at the axon hillock (i.e., the sum of the depolarizing signals minus the sum of the hyperpolarizing signals) decreases below a threshold voltage, large numbers of voltage-gated sodium channels will open and there will be a concomitant large influx of Na^+ into the cell. This large depolarization spreads down the axon, opening more voltage-gated sodium channels farther and farther down the membrane. The wave of depolarization, known as a nerve impulse or action potential, sweeps down the axon in a self-propagating manner, independently of the EPSPs that triggered it. Eventually, the nerve impulse will reach the end of the axon, where a presynaptic terminal forms a synapse with another neuron. Here the wave of depolarization will open voltage-dependent channels in the presynaptic membrane that allow Ca^{2+} influx into the presynaptic terminal. This influx of Ca^{2+} initiates a cascade of events that causes the release of neurotransmitters into the synaptic cleft, which interact with receptors that gate postsynaptic ion channels on the target neuron. This initiates either an IPSP or EPSP on the postsynaptic membrane of the target neuron, thus propagating the signal to another neuron elsewhere in the brain.

action potential A wave of depolarization that travels down a neuronal axon.

One can think of information processing by neurons as the combination of their integrative and signaling roles. Integration reflects the total spatiotemporal pattern of EPSPs and IPSPs, each generated at a synapse from another cell, which collectively determines the relative polarization of the neuron. Note that only EPSPs can trigger action potentials. Hyperpolarizing IPSPs, in contrast, make action potentials less likely by making the membrane potential more negative. An EPSP that might have sufficient strength to depolarize the axon hillock below threshold when this region is at its normal resting potential may not be able to do so if the axon hillock was hyperpolarized by a preceding IPSP. Signaling reflects the binary output—that is, whether or not an action potential was generated—of the integration process within a neuron.

Neither form of information processing, whether postsynaptic or action potential, itself requires an external source of energy, because the associated movements of ions are along concentration gradients. However, both sorts of potentials cause changes in ion concentration that require energy to restore. For example, the influx of Na^+ during an action potential causes a change in the local membrane potential of the neuron, so electrical gradients now oppose the reentry of the positively charged K^+ into the cell. To restore the asymmetric distribution of Na^+ and K^+ across the cell membrane and return the membrane to its resting potential, the sodium–potassium pump removes three Na^+ ions from within the cell for every two K^+ ions it brings into the cell. The energy necessary for restoring these potentials, so that the neuron becomes ready for its next contribution to information processing, is discussed in the next section.

Cerebral Metabolism: Neuronal Energy Consumption

Why are the energy demands of neurons important for fMRI? To help answer this question, imagine that neurons stored energy to buffer moderate changes in their neuronal firing rates. Could we then construct meaningful theories of brain function based on energy delivery by the blood supply? Or imagine that it were known that energy consumption following neuronal firing served to increase the synthesis of protein, in support of structural changes in the neurons initiated by learning. How would this change the interpretation of neuroimaging results? Finally, imagine that we learned (as was once thought true) that information processing accounted for a tiny fraction of the brain's energy

budget. How then would one account for the enormous metabolic demands of the active brain?

Thought Question

Assume that the brain did indeed have large local stores of energy that could support neuronal activity. Based on what you know so far, would fMRI be possible?

We now know that these hypothetical situations are not true. Local brain regions require external sources of energy to support metabolic processes, and much of this energy facilitates the restoration of concentration gradients following changes in membrane potential. Thus, measurements of brain metabolism can be used to make inferences about brain activity. So although our interests as neuroscientists may be in the relationships between mind and brain (where in this context "brain" refers to the activity of neurons), we can draw inferences about brain activity by measuring its energy supply. Here, we delve more deeply into the energy needs of neurons and how those needs are met by the vascular system.

Adenosine triphosphate (ATP)

The principal energy currency for cells in the human body is adenosine triphosphate, or ATP. ATP is a nucleotide that contains three phosphate groups. Free energy is released when the third phosphate group of ATP is removed by the insertion of a water molecule, in a reaction called hydrolysis. In body tissues, ATP can be produced from many substrates, including the sugar glucose, fatty acids, ketone bodies, and even proteins. Glucose is stored throughout the body in the form of glycogen. However, there is little glycogen in the brain, and thus, to maintain function, the brain requires a continuous supply of glucose and oxygen via the vascular system. Under normal circumstances, the brain extracts about 10% of the approximately 90 mg/dL of glucose in arterial blood. If the glucose concentration in blood falls below about 30 mg/dL, a coma may ensue.

The generation of ATP from glucose has three primary steps: glycolysis, the TCA cycle, and the electron transport chain (Figure 6.5). Glucose transporter molecules move glucose through the interstitial space from capillaries to neurons. Once in the cytoplasm of brain cells, glucose is broken down through a reaction called glycolysis, in which the six-carbon glucose is cleaved into two three-carbon sugars, which are then catabolized through a series of steps into a compound called pyruvate. Glycolysis consumes two ATP molecules but produces four, thus providing a net gain of two ATPs. If oxygen is present, the process is called aerobic glycolysis and the pyruvate product then enters a reaction called the tricarboxylic (TCA) cycle, also known as the citric acid cycle or the Krebs cycle. The TCA cycle uses oxygen extracted from hemoglobin in the blood to oxidize pyruvate, and a network of proteins in the cell mitochondria, known as the electron transport chain, passes electrons across a series of compounds to release energy, which in turn is used by an enzyme known as ATP synthase to generate an additional 34 ATP molecules. So, while glycolysis itself produces only 2 ATP molecules from each glucose molecule, the addition of oxygen allows the production of a total of 36 ATP molecules from each molecule of glucose.

If oxygen is not present, the pyruvate is reduced to an end product, lactate, in a process called anaerobic glycolysis. During strenuous exercise when the sup-

adenosine triphosphate (ATP) A nucleotide containing three phosphate groups that is the primary energy source for cells in the human body.

glucose A sugar made by the human body whose stored energy is used to produce ATP.

glycolysis The process of breaking down glucose into other compounds to produce ATP.

aerobic glycolysis The process, consisting of glycolysis, the TCA cycle, and the electron transport chain, that breaks down glucose in the presence of oxygen, resulting in a gain of 36 ATP molecules.

TCA cycle The second step in aerobic glycolysis; it involves the oxidation of pyruvate.

electron transport chain The third step in aerobic glycolysis; it generates an additional 34 ATP molecules.

anaerobic glycolysis The conversion of glucose to lactate in the absence of oxygen.

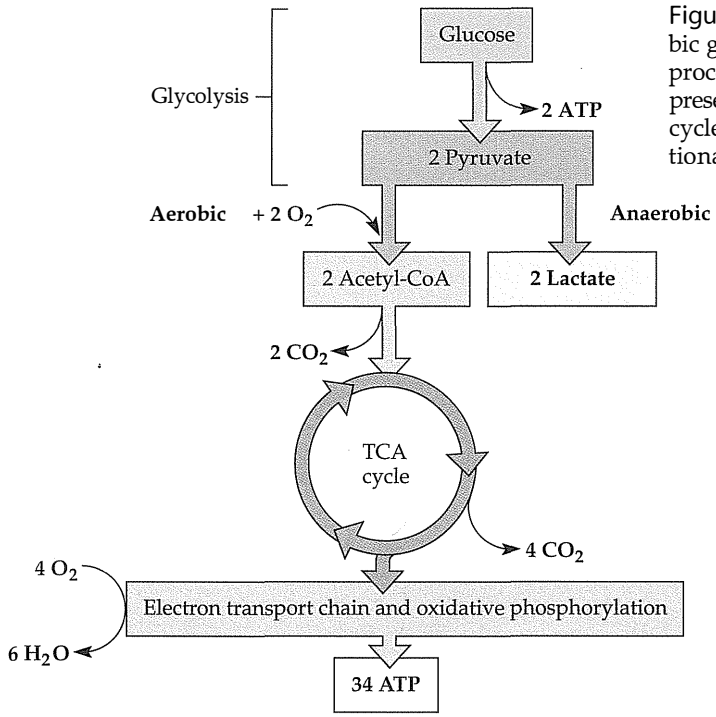

Figure 6.5 Anaerobic and aerobic glycolysis. In anaerobic glycolysis, glucose is converted to lactate via a fast process that produces two ATP molecules. If oxygen is present, then the resulting aerobic processes of the TCA cycle and the electron transport chain produce an additional 34 ATP molecules.

ply of oxygen from the lungs is insufficient, anaerobic glycolysis occurs in muscles, and it is the buildup of lactate that can cause pain and fatigue. Lactate is removed from the muscles by the vascular system. While anaerobic glycolysis is a relatively inefficient source of ATP, it is quite fast; it can occur at a rate about 100 times faster than the oxidation of pyruvate into ATP through the TCA cycle and the electron transport chain. In addition, some cells can convert lactate back into pyruvate and use it in the TCA cycle to produce more ATP.

The energy provided by ATP supports many aspects of brain physiology: housekeeping functions related to the synthesis of proteins, the maintenance and turnover of membranes, axoplasmic transport, and the synthesis, packaging, and breakdown of neurotransmitters. Yet, the lion's share of energy goes to restoring unequal distributions of ions following EPSPs, IPSPs, and action potentials. The gray matter of the brain consumes about 30 to 50 μmol of ATP every minute for each gram of tissue (i.e., 30 to 50 μmol/g/min of ATP), while a brain in coma consumes only about 10 μmol/g/min of ATP. Thus, integrative and signaling activities in neurons should account for about 75% of the energy expenditure in gray matter, while housekeeping functions account for only about 25%.

Moreover, because the chemical reactions associated with neuronal integration and signaling are well known, researchers can determine how much of the brain's energy budget supports different processes. In a 2001 study based on data from the rodent brain, Attwell and Laughlin estimated that the restoration of membrane concentration gradients following the passage of an action potential consumes 47% of the energy expenditure, while restoring postsynaptic membrane concentration gradients following IPSPs and EPSPs consumes 34% (Figure 6.6). The authors commented that the energy cost of IPSPs is probably less than that of EPSPs for two reasons: Cl^- ions move down a smaller electrochemical gradient than the Na^+ ions, and inhibitory synapses are out-

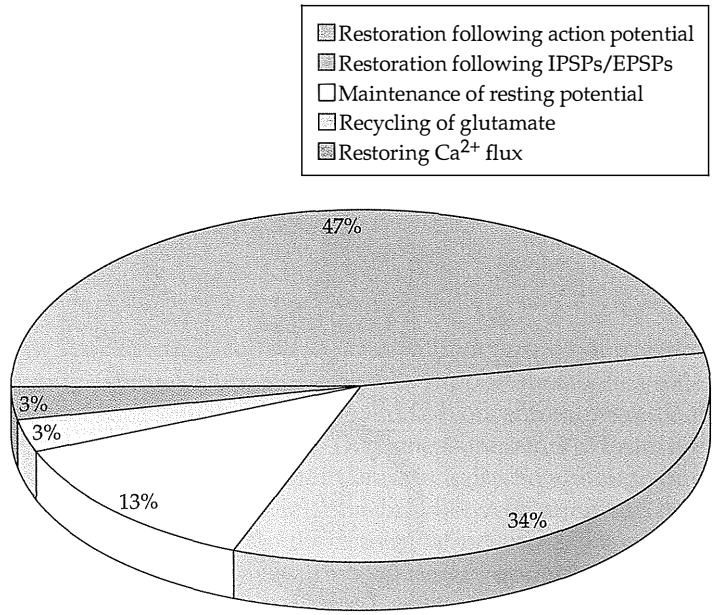

Figure 6.6 The energy budget of the (rodent) brain. Data from the rodent brain, shown here, indicates that the vast majority of energy is required to support the restoration of concentration gradients following action potentials and postsynaptic potentials. While human data are not available for these categories, the differences in brain structure between humans and rodents suggests that the proportion of energy needed for restoring gradients after postsynaptic potentials is even greater in humans. These results indicate that the primary energy expenditure of the brain supports the integrative and signaling roles of neurons. (Data from Atwell and Laughlin, 2001.)

numbered by excitatory synapses in the brain by about one order of magnitude. The maintenance of the resting potential in neurons and glia was estimated to consume 13% of the energy expenditure. Note that the consumption of energy in each of these processes principally involves the operation of the sodium–potassium pump. Furthermore, given that glutamate is by far the dominant excitatory neurotransmitter in the brain, most of the energy budget associated with signaling and integration involves this single neurotransmitter. The uptake, breakdown, and repackaging of glutamate was estimated to consume 3% of the energy budget, and restoring Ca^{2+} fluxes in presynaptic membranes accounted for the remaining 3%.

In extrapolating their results to primates, these authors argued that the greater number of synapses per neuron in primates would cause a greater proportion of the energy budget to be spent on restoring postsynaptic concentration gradients, perhaps as much as 74%. They concluded, therefore, that the metabolic demands of the integrative and signaling activities of neurons form the bulk of the energy requirements of the human brain. To meet these energy demands, the vascular system must ensure a continuous supply of glucose and oxygen.

The Vascular System of the Brain

The idea that changes within the vascular system of the brain reflect changes in brain function is not new. The nineteenth-century British physiologists Roy and Sherrington postulated that changes in activity associated with specific brain functions might result in locally increased blood flow:

> These facts seem to us to indicate the existence of an automatic mechanism by which the blood supply of any part of the cerebral tissue is varied in accordance with the activity of the chemical changes which underlie the functional action of that part. Bearing in mind that strong evidence exists of localisation of function in the brain, we are of the opinion that an automatic mechanism, of the kind just referred to, is well fitted to provide for a local variation of the blood supply in accordance with local variations of the functional activity. (1890, p.105)

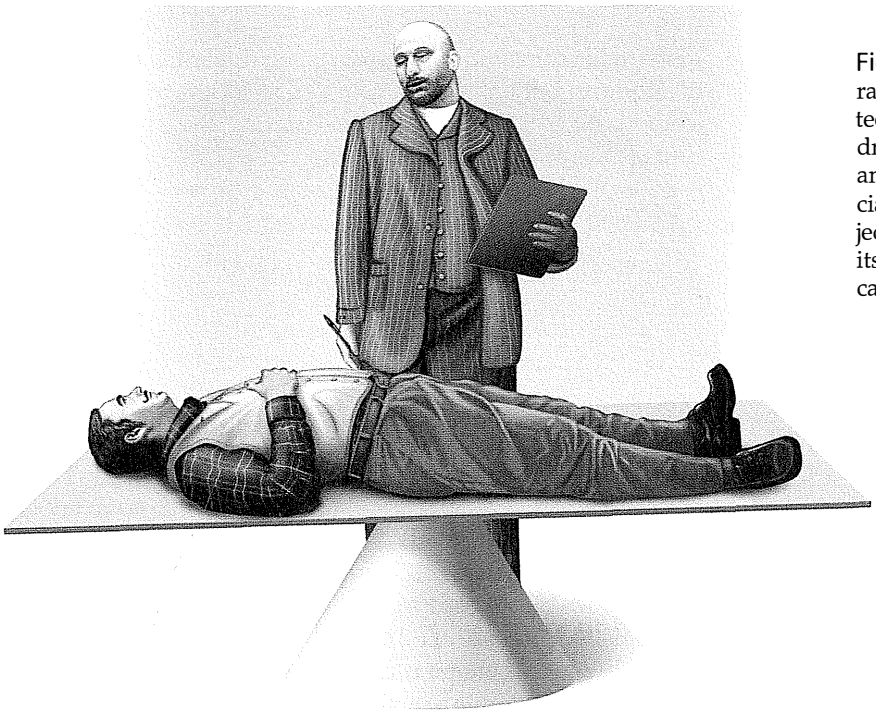

Figure 6.7 The crude brain-measurement apparatus used by Angelo Mosso in the late nineteenth century. Mosso theorized that thinking drew blood to the brain, and constructed a balance device to measure changes in weight associated with this increased blood flow. The subject lay down on a large table with a fulcrum at its center, so that any change in weight would cause the table to tip.

A variant of this idea, that activity could cause changes in blood flow, was tested in an experiment conducted by the Italian physiologist Angelo Mosso around that same time. Mosso had pioneered the measurement of comparative blood volume in the brain and extremities, and he was interested in whether thinking resulted in increased blood flow to the brain. His earlier studies had revealed that blood flow to the brain decreases during sleep and increases with waking, consistent with the idea that brain activity requires a greater blood supply than inactivity. To directly test the hypothesis that active thought requires increased blood volume in the brain, Mosso constructed an ingenious apparatus (Figure 6.7), as reported by William James in his *Principles of Psychology*:

> The subject to be observed lay on a delicately balanced table which could tip downward either at the head or at the foot if the weight of either end were increased. The moment emotional or intellectual activity began in the subject, down went the balance at the head end, in consequence of the redistribution of blood in his system. (1890, p. 98)

Such a result, if observed, would have provided strong evidence for a relationship between vascular changes and cognitive function. Yet, the reported results were almost certainly overstated. For the table to tip downward, the brain's total blood *volume*, not local blood *flow*, would need to increase by an appreciable amount. But overall blood volume is relatively constant over time, even if local blood flow changes in response to metabolic demands. To use a hydraulic analogy, if pipes are filled with water, they will weigh essentially the same regardless of whether the water is flowing quickly or slowly. Nevertheless, the idea that changes in blood flow may result from local functional changes in the brain was a remarkable insight. The discussion of this issue in James's *Principles*, especially the difference between causal and correlational roles for blood flow, is highly recommended to the interested student. We explore the relationship between blood flow and brain function in the following sections, leading to the idea that the functional activity of neurons may evoke changes in blood flow and thus changes in the local concentrations of metabolites.

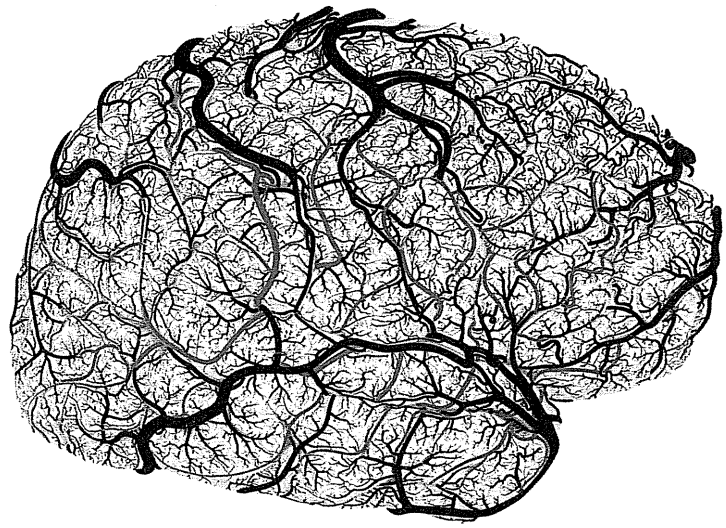

Figure 6.8 Blood supply to the human cerebrum. As illustrated here, the surface pattern of blood supply to the human cerebrum is highly complex. The red vessels are tributaries of the middle cerebral artery, the yellow vessels are tributaries of the anterior cerebral artery, and the blue vessels are tributaries of the posterior cerebral artery. The veins are shown in black. (After Duvernoy, Delon, and Vannson, 1981.)

Arteries, capillaries, and veins

From our discussion earlier in this chapter, we know that the integrative and signaling activities of neurons constitute a large proportion of the brain's energy budget, and we also know that there is little energy stored in the brain. The energy needs of neurons and glia are met by the ATP created during glycolysis and during the subsequent oxidation of pyruvate. The oxygen and glucose fuel required for those reactions is delivered through the vascular system (Figure 6.8). In the adult human brain, about 54 mL of blood flows through each 100 g of tissue every minute. This adds up to about 800 mL/min for the average 1400 g brain, and represents about 15 to 20% of the blood flow in the entire human body. Thus, although the brain constitutes a mere 2 to 3% of total body weight, it consumes about 20% of blood oxygen.

The lungs are the source of the oxygen carried by the blood. Oxygen diffuses from the alveoli of the lungs, via small blood vessels, into red blood cells, where it binds to hemoglobin. Four oxygen molecules are attached to each hemoglobin molecule, and there are about 280 million hemoglobin molecules in each red blood cell. The oxygen-rich blood returns to the heart from the lungs, where it enters the left atrium, moves to the left ventricle, and is pumped from the left ventricle through the aorta. The aorta gives rise to several large **arteries**: thick-walled vessels that carry blood away from the heart. Each artery branches into smaller arteries and then to even smaller **arterioles** that eventually terminate in capillaries. The change in scale as these vessels branch is remarkable. The diameter of the aorta in an adult human is about 2.5 cm (about one inch); typical large arteries can be 4 to 10 mm in diameter; while the diameters of arterioles are in the range of 10 to 50 μm. Thus, the largest artery has a diameter about 2500 times that of the smallest arteriole!

The extraction of oxygen and glucose from the blood and the removal of waste carbon dioxide occurs at the surfaces of the capillaries. **Capillaries** are thin-walled vessels comparable in diameter (5 to 10 μm) to the width of a red blood cell (about 7.5 μm), which actually deform as they move through the narrowest capillaries. The small sizes of individual capillaries is more than made up for by their number and density (Figure 6.9). It has been estimated that any cell in the body is, on average, less than 50 μm from a capillary. If lined up end to end, the capillary network in the human body would stretch 60,000 miles and have a total surface area of 800 to 1000 m^2. Capillary density in a particular part of the body roughly indicates its cellular metabolism in that

arteries Blood vessels that carry oxygenated blood from the heart to the rest of the body.

arterioles Small arteries.

capillaries Small and thin-walled blood vessels. The extraction of oxygen and glucose from the blood and the removal of waste carbon dioxide occur in the capillaries.

area. Areas with high metabolism have higher capillary densities than those with lower metabolic rates. For example, in the cat brain, gray matter, composed of neural cell bodies, has twice the capillary density of white matter, which is composed largely of axonal processes.

Thought Question

Many techniques in fMRI attempt to localize hemodynamic activity to the capillaries. Why is this desirable for studies of brain function?

Following oxygen extraction, the deoxygenated hemoglobin molecules, which now bind waste carbon dioxide, are carried from the capillaries to small venules that are comparable in size to arterioles. The venules collect into larger and larger veins that eventually return the oxygen-poor blood through the vena cava to the heart. The deoxygenated blood then travels to the lungs, where the waste carbon dioxide is released and where oxygen binds to the hemoglobin to start the cycle again.

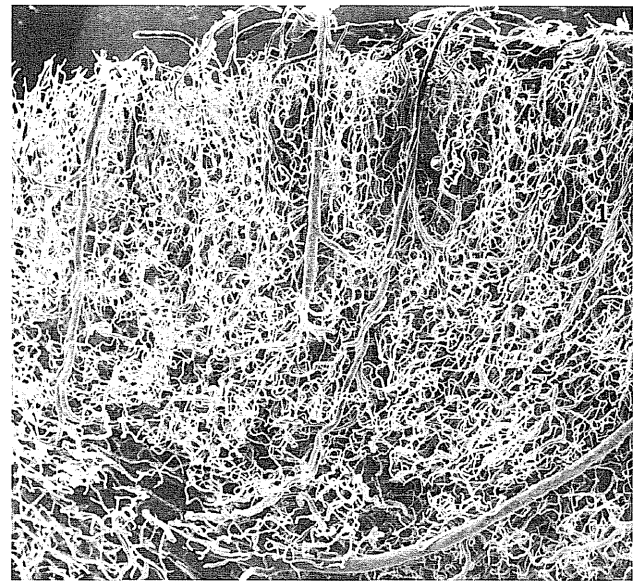

Figure 6.9 Capillary structure. This electron microscope image shows the density of capillary beds within the cortex. (From Duvernoy, Delon, and Vannson, 1981.)

Arterial and venous anatomy of the human brain

The flow of blood to the brain is supplied by two major arterial systems: the left and right internal carotid arteries and the vertebral/basilar arteries (Figure 6.10). A short distance from the heart, the aortic arch gives rise to the right

venules Small veins.

veins Blood vessels that carry blood from the body to the heart. Blood in the veins (except for the pulmonary vein) is partially deoxygenated.

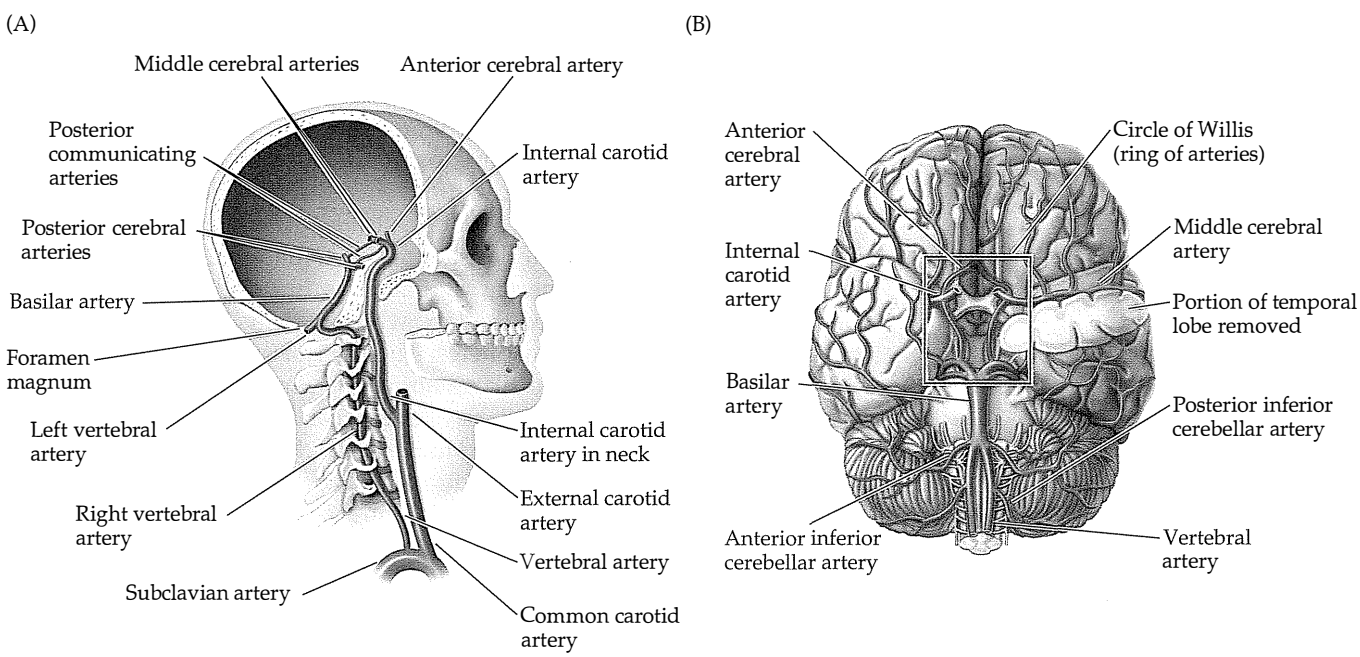

Figure 6.10 The arterial system of the human brain. The arterial distribution of blood to the human brain is shown in cross-section (A), and in a ventral view of the base of the brain (B). The box highlights the anastomoses of the basilar artery and internal carotid arteries that form the circle of Willis.

circle of Willis The interconnection between the basilar artery and the carotid arteries at the base of the cranial vault.

sinuses The term sinus has two primary meanings in neuroanatomy: (1) long venous channels formed by meningeal coverings that form the primary draining system for the brain, and (2) air-filled cavities in the skull.

and left common carotid arteries, which ascend in the neck before each divides into the external and internal carotid arteries. The external carotid arteries supply the external head and face with blood, while the internal carotid arteries enter the skull through an opening in the base called the foramen lacerum and supply blood to the brain. The aortic arch also gives rise to the right and left subclavian arteries, which, in turn, give rise to the left and right vertebral arteries, which run along the anterior surface of the spinal cord and enter the brain through the foramen magnum. The vertebral arteries give rise to the descending arterial branches, which provide blood to the brain stem, medulla, and spinal cord. As the vertebral arteries ascend to the level of the pons, they fuse into the single basilar artery, which gives rise to arterial branches that perfuse the pons and cerebellum.

The basilar artery interconnects, or forms an anastomosis, with the left and right internal carotid arteries to form the circle of Willis, named for the celebrated English physician Thomas Willis, who first illustrated this vascular structure in 1664. The circle of Willis sits on the floor of the cranial vault, surrounding the brainstem. Supplied by blood from both arterial systems, it gives rise bilaterally to the anterior, middle, and posterior cerebral arteries (Figure 6.11A and B). Each of these major cerebral arteries supplies blood to a distinct region of the brain. The anterior cerebral artery primarily supplies the medial surface of the brain and the head of the caudate, branches of the middle cerebral artery supply much of the lateral and superior cerebral cortex as well as the remainder of the basal ganglia, and the posterior cerebral artery supplies the posterior temporal and occipital cortex. This specificity has important implications for neurology, in that strokes within particular arteries tend to affect particular regions of the cortex and thus have functionally distinct cognitive consequences.

The venous drainage of the brain's circulation (Figure 6.11C and D) is accomplished through the left and right jugular veins, which exit the skull base through the jugular foramen, then join with the subclavian vein and eventually the superior vena cava, progressing to the right atrium and ventricle of the heart, which pumps blood to the lungs for reoxygenation. The jugular veins themselves are fed by the sinus system of the brain. Sinuses are long venous channels that are formed by the meningeal covering of the brain. The superior sagittal sinus runs along the superior midline of the entire brain, where the two hemispheres meet. Large cerebral veins on the cortical surface drain into the superior sagittal sinus, and blood is transported back along the sinus to the back of the brain. The inferior sagittal sinus follows a similar midline path to that followed by the superior sagittal sinus, but deeper in the brain in the part of the dura mater called the falx, which extends down into the midline separating the cerebral hemispheres. The inferior sagittal sinus empties into the straight sinus, which runs back above the cerebellum and joins with the superior sagittal sinus at the back of the brain to form the transverse sinus. The transverse sinus wraps around to the left and right of the base of the brain, terminating in the left and right internal jugular veins.

Microcirculation

The blood supply to the cerebral and cerebellar cortices is derived from meningeal arteries that traverse the cortical surface (Figure 6.12). A distinction can be drawn between conducting and distributing arteries. Conducting arteries run for long distances along the pial surface and are about 700 μm in diameter (i.e., narrower than the 4 to 5 mm diameters of the internal carotid and basilar arteries). In the cerebral cortex, many conducting arteries run along the

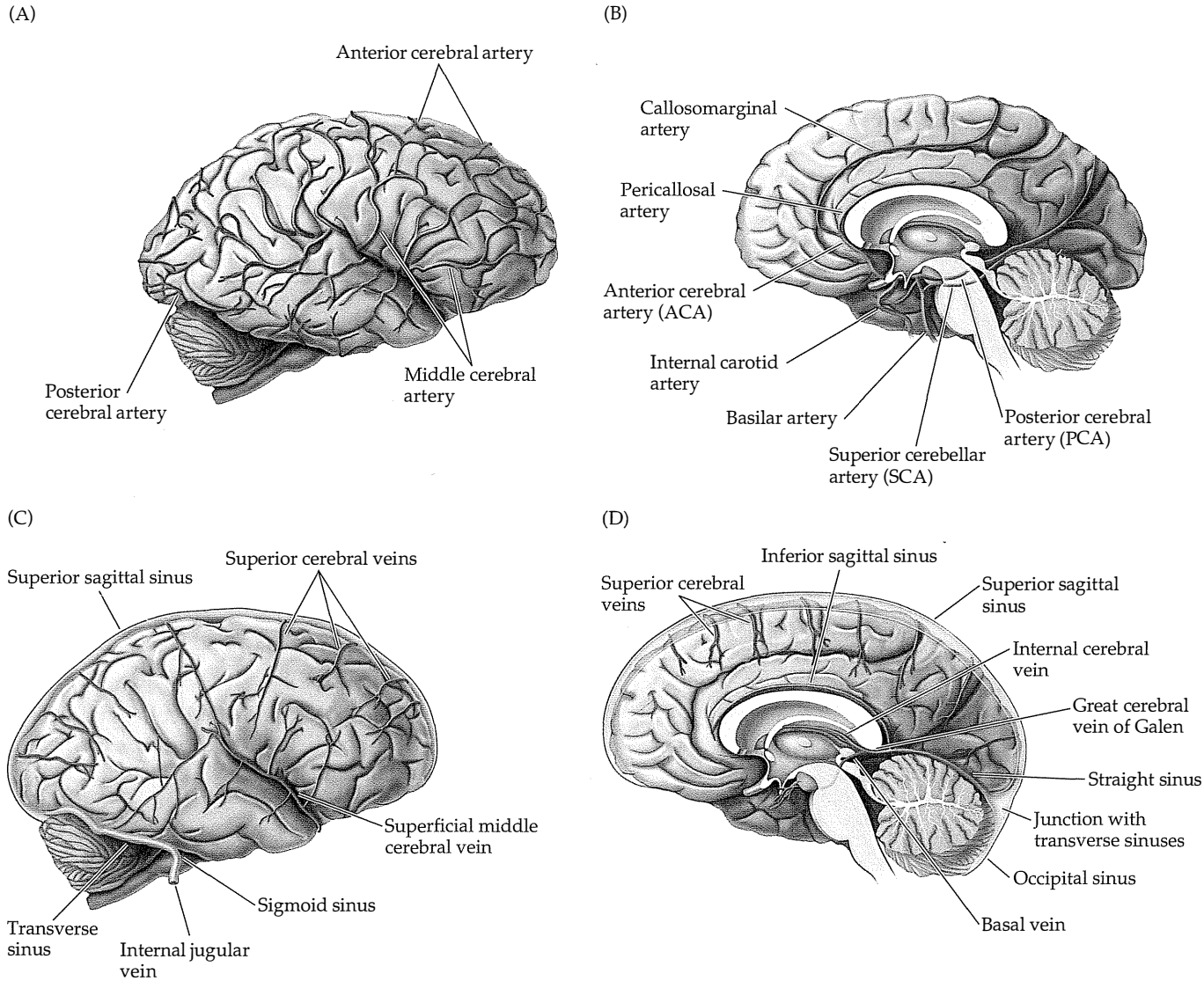

Figure 6.11 The arterial (red) and venous (blue) organization of the cerebral vasculature. Shown are lateral (A) and medial (B) views of the major arterial systems of the human brain. Blood is drained by a system of sinuses and veins, shown here in lateral (C) and medial (D) views.

sulci that demarcate adjacent gyri, while others run directly across the gyral surface. Many shorter and smaller distributing arteries, each about 150 to 200 μm in diameter, branch from the conducting arteries. Many researchers have noted constrictions where the distributing arteries branch from larger arteries, suggesting the presence of muscular sphincters that could control blood flow. The distributing arteries continue to ramify on (or branch over) the cortical surface into yet smaller precortical arteriole of about 50 to 70 μm in diameter. Anastomoses, or branches and reconnections, between arterioles have been observed in several studies. According to Nonaka and colleagues, a distributing artery supplies a 3.5-by-2-mm area on the cortical surface, while each precortical artery supplies an approximately 1-by-1-mm area of cortical surface. Each precortical artery then ramifies into smaller arterioles of about 30 to 40 μm diameter that penetrate the cortical surface at right angles.

(A)

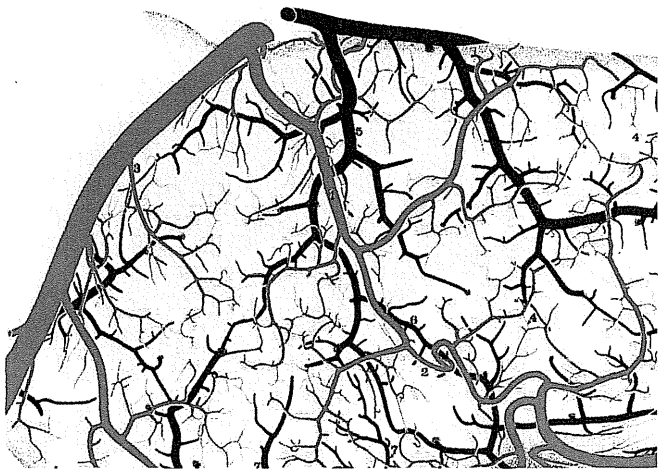

(B)

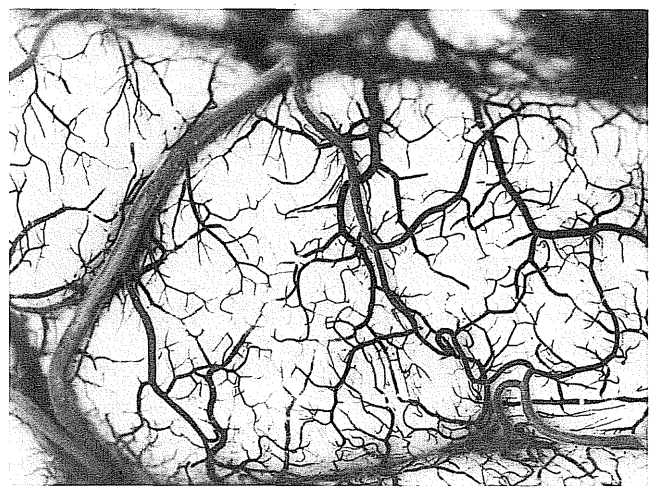

Figure 6.12 Microcirculation in the human brain. The distributions of arteries (red) and veins (black) on the medial orbital gyrus of the human brain are illustrated in (A). A photograph of the same region is provided in (B). (From Duvernoy, Delon, and Vannson, 1986.)

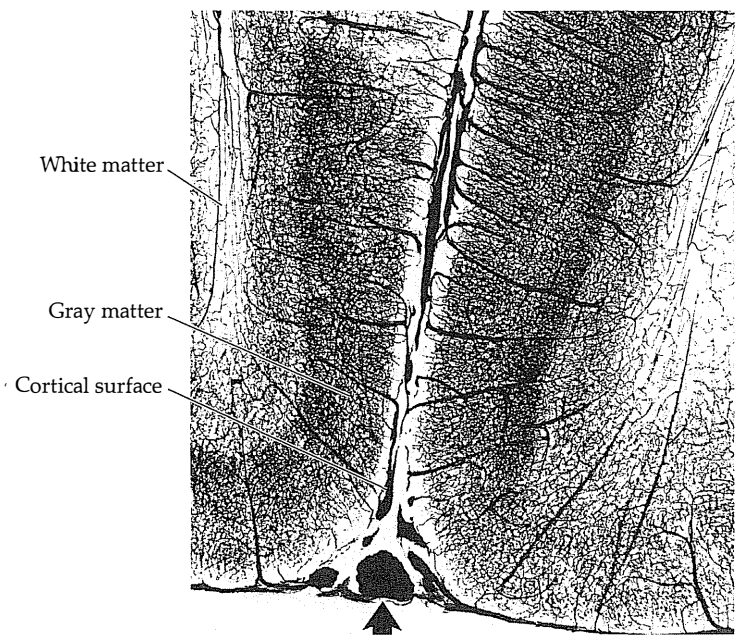

Figure 6.13 Distribution of vascularization across cortical layers. This figure shows the distribution of blood vessels in the cortical layers of the calcarine sulcus. The penetrating arteries enter the cortical layers in a direction that is perpendicular to the cortical surface. The density of the vascular ramifications varies across the cortical layers and is greatest where cell density is greatest. The deep white matter beneath the cortical layers has the lowest vascular density. The arrow points to the superior sagittal sinus. (From Duvernoy, Delon, and Vannson, 1981.)

As part of their seminal studies of the brain's vascular system, Duvernoy and colleagues documented the properties of these intracortical arterioles. Most small arterioles vascularize the gray matter, with increasing vessel diameters in those that vascularize deeper layers. The density of vascularization is not uniform across cortical layers; noticeably denser vascularization is observed where the highest concentrations of neural cell bodies are located (Figure 6.13). Some intracortical vessels have been described as resembling a fountain or candelabra, with dense ramifications ascending into more superficial layers. Still other intracortical arterioles, those with the largest diameters, appear to penetrate straight though the cortex to vascularize the white matter below. Vascularization in the white matter is considerably less dense than in the gray matter.

Blood Flow

Neuronal activity evokes changes in blood flow (i.e., the volume of moving blood per unit time) by changing both the volumes of blood vessels and the velocity with which blood moves through those vessels. These quantities vary considerably within the vascular system due to many physical and physiological factors: blood pressure; the

diameter of the blood vessel; the density of the red blood cells; the amount of oxygen and carbon dioxide in the blood; and the age, health, and activity level of the subject. Peak flow velocity in the aorta can exceed 90 cm/s. Using a technique called transcranial Doppler, researchers have measured the mean blood flow velocity in the basilar and internal carotid arteries at about 40 cm/s. Blood flow through the smaller arteries and arterioles is considerably slower, ranging from 10 to 250 mm/s, and blood flow through the capillaries can be less than 1 mm/s. As the blood collects in venules and travels to larger veins, the velocity once again increases to a range of 10 to 250 mm/s, which is still considerably slower than within the arterial system. These values are approximate, because the estimated velocity of blood flow depends on how it is measured.

Holding other factors constant, blood flow is proportional to the pressure difference from one end of the vessel to the other, divided by the resistance of the vessel to flow. As a result, flow is proportional to vessel radius expressed to the fourth power, so very small changes in vessel diameter can produce large changes in resistance and flow. For example, doubling the size of the vessel would increase flow by a factor of 16. In large arteries, blood flow is pulsatile due to the pumping of the heart, and flow velocity can vary greatly between the peak flow measures obtained during systole and the lower velocities measured during diastole.

The small arteries on the pial surface have high resistance and thus oppose flow. These resistance vessels help convert the pulsatile ejection of blood from the heart into a steady flow through the capillaries. Indeed, if no resistance were present and high blood pressure persisted into the capillaries, blood plasma would be pushed through the thin capillary walls, leading to a considerable loss of blood volume and concomitant damage. Thus, small resistance vessels are an important component in the control of blood flow through the capillary bed.

Control of blood flow

Functionally specific changes in blood flow are believed to be initiated when active neurons release substances that diffuse through the extracellular space and reach nearby blood vessels. These vasoactive substances cause the vessels to dilate, and because the increase in diameter reduces the vessels' resistance, flow increases. However, this local change is not sufficient by itself to regulate blood flow, because flow is also influenced by the higher-resistance arterioles located on the pial surface, which can be well upstream and distant from the active neurons. Thus, there needs to be coordination between the local blood flow changes induced by neural activity and upstream control mechanisms.

Several candidate mechanisms have been identified for the local control of blood flow (see Box 6.1). These include potassium ions (K^+), which enter the extracellular space as a result of synaptic activity, and adenosine, which is created during the dephosphorylation of ATP, and which increases in concentration during times of high metabolic activity. Other research has focused on nitric oxide, which is released by the activation of both local and distant neurons. Nitric oxide mediates both local and distal vasodilation (or increase in the size of blood vessels) by causing the smooth muscle cells surrounding arterioles to relax. Gap junctions between endothelial cells in arteries propagate the vasodilatory response upstream, causing increased blood flow to larger arteries. This propagated action initiated by nitric oxide along the arterioles shares conceptual similarities with the propagation of neuronal action potentials. Even more exciting,

resistance vessels Arterioles that control the flow of blood through the capillary bed.

vasoactive substances Substances that change the diameter of blood vessels.

BOX 6.1 Neurovascular Coupling and Control of Blood Flow

Many cortical vessels are surrounded by intertwining processes arising from neurons and glial cells, raising the possibility that some aspects of blood flow may be controlled by neurons themselves, either directly or indirectly. For example, some large pial arteries receive projections from cranial nerves and sensory ganglia, and these projections surround the smooth muscles that encase the vessel. Studies have shown that the neurotransmitters released by these projections can dilate or constrict the vessel. However, the relationship between neurogenic control of blood flow and local brain function remains unclear. Given that these large vessels supply extensive regions of cortex, changes in their flow must be shaped by local resistance vessels to direct the blood flow to the active neuronal region.

Substantial research has implicated specific neurotransmitters in the local control of blood flow. As one example, Krimer and colleagues examined the role of dopamine, which is produced centrally by small clusters of midbrain neurons that project broadly to the striatum and cerebral cortex. Using histological staining techniques, light microscopy, and electron microscopy, these investigators demonstrated that dopamine terminals are found in apposition to small intracortical arterioles and capillaries. Moreover, at capillaries, the dopamine terminals are apposed to pericytes, contractile elements that can constrict or dilate the capillary and thus influence local flow patterns (Figure 1). The direct application of dopamine onto small cortical arterioles caused a constriction of the diameter of the vessels that started about 18 to 40 s after application onset and reached a maximum constriction of 18 to 24%. Full recovery occurred after several minutes. The time course of these changes is slower than the change in the BOLD-contrast fMRI signal, which can peak 4 to 5 s after the onset of a stimulus. However, these data raise the interesting possibility that neurons could influence blood flow *independently* of local neuronal activity, perhaps in anticipation of upcoming needs. Such centrally stimulated blood flow changes might be associated with long-duration changes in MRI signal that are maintained over many minutes. If true, this would require a refinement of our idea that the BOLD signal is strictly related to the energy needs of active neurons. Addition-

dopamine An important neurotransmitter that is part of the family known as biogenic amines. Dopamine is produced within cells in the brainstem that project broadly to the striatum and cortex (especially the frontal lobe).

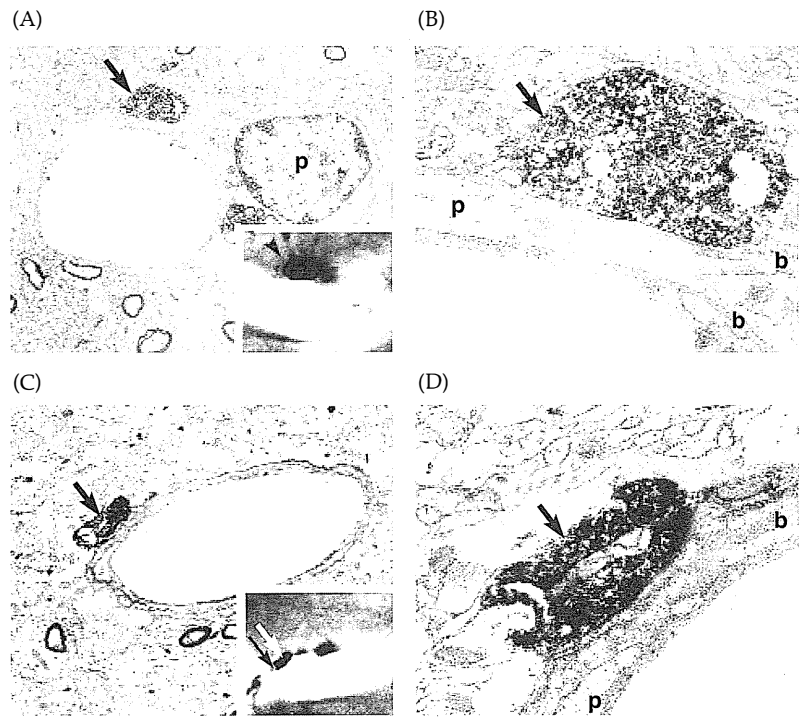

Figure 1 Evidence of direct innervation of capillaries by dopaminergic neurons. (A) An electron micrograph that shows a large dopamine terminal (arrow) adjacent to a capillary. As can be seen in the light-microscopic inset, which shows a cross section of the same spatial location, the terminal lies along this capillary over a large spatial extent. (B) An enlargement of this dopamine terminal. The terminal is separated from the basal lamina (b) of the blood vessel by only a process from an adjacent pericyte (p), a cell with contractile properties. The inset in (C) shows a light-microscopic image depicting a string of three terminals adjacent to a capillary. The electron micrograph in (C), enlarged in (D), shows that one of the terminals is directly apposed to the basal lamina of the capillary. (From Krimer et al., 1998.)

BOX 6.1 *(continued)*

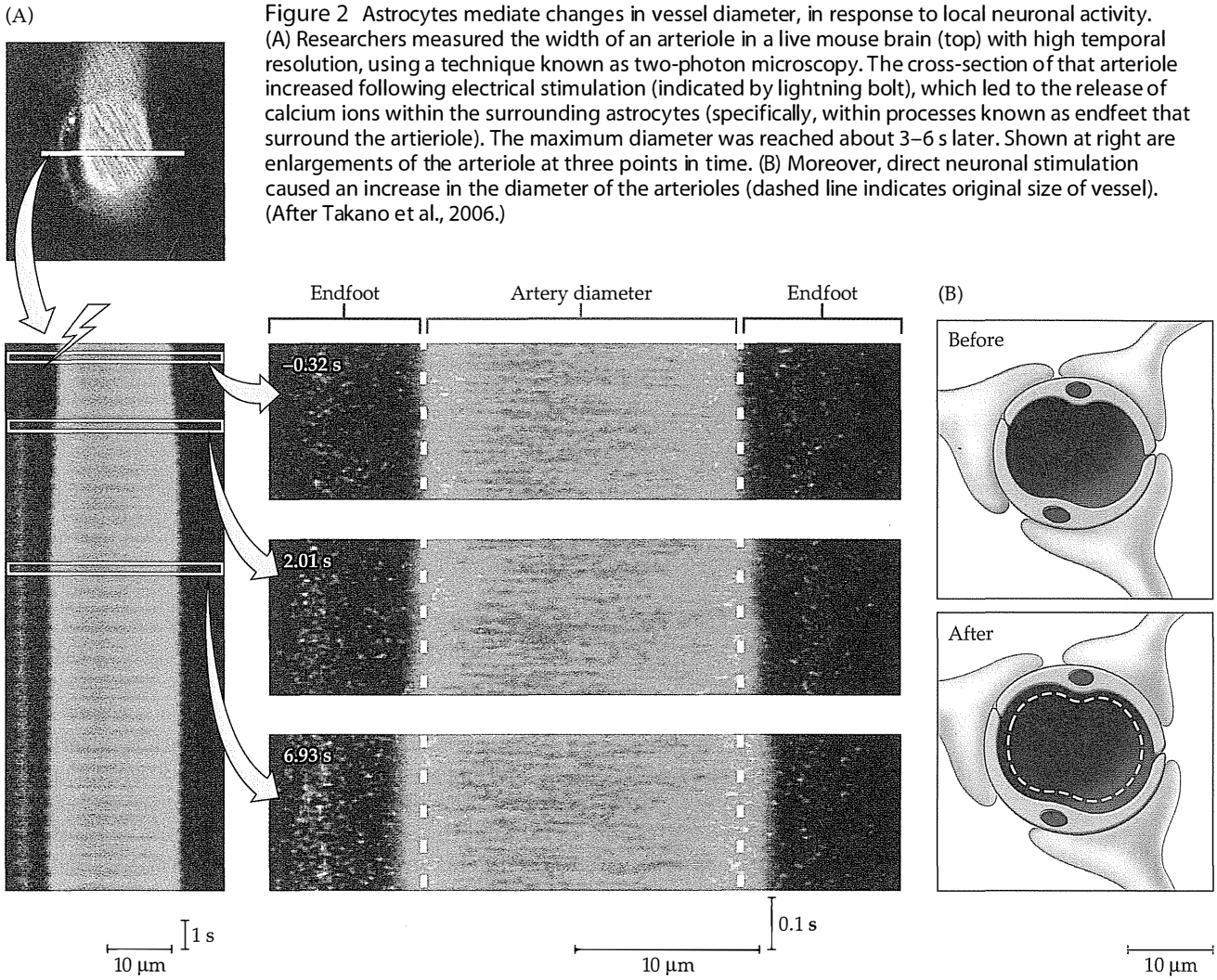

Figure 2 Astrocytes mediate changes in vessel diameter, in response to local neuronal activity. (A) Researchers measured the width of an arteriole in a live mouse brain (top) with high temporal resolution, using a technique known as two-photon microscopy. The cross-section of that arteriole increased following electrical stimulation (indicated by lightning bolt), which led to the release of calcium ions within the surrounding astrocytes (specifically, within processes known as endfeet that surround the artieriole). The maximum diameter was reached about 3–6 s later. Shown at right are enlargements of the arteriole at three points in time. (B) Moreover, direct neuronal stimulation caused an increase in the diameter of the arterioles (dashed line indicates original size of vessel). (After Takano et al., 2006.)

al studies have provided evidence that blood flow is influenced by other neurotransmitters, including serotonin, acetylcholine, and norepinephrine.

Also possible are less direct effects: neuronal activity may trigger changes in nearby glial cells, which in turn cause dilation in nearby blood vessels. In a compelling 2006 study, Takano and colleagues used a high-resolution technique known as two-photon imaging to identify the role of one type of glial cell, the astrocyte, in the local control of blood flow in anesthetized mice. The authors labeled astrocytes with a chemical that was sensitive to changes in local calcium, and then selectively released calcium (Ca^{2+}) to visualize rapid changes in the astrocytes and in the blood vessels they were in contact with. They found that release of Ca^{2+} triggered vasodilation. Local arterioles increased in cross-sectional area by about 18%, while blood flow increased by 37%. The timing of these changes were consistent with known hemodynamic properties (Figure 2A), in that increases in calcium concentration preceded changes in vessel diameter by only about 500 ms, and full dilation followed within a few seconds. Then, they stimulated the brain directly using an electrode, and found increases in astrocytic calcium concentrations, dilation of blood vessels, and increased blood flow (Figure 2B). Through

(continued on next page)

BOX 6.1 *(continued)*

a series of tests, they showed that specific chemicals could selectively suppress the increase in blood flow through their effects on the astrocytes, without altering the neuronal activity. They concluded that local changes in blood flow are mediated, at least in part, by chemical signals from active neurons (likely via the synaptic release of glutamate) that lead to increases in Ca^{2+} in astrocytes, which in turn increase the diameters of nearby vessels.

This study, among several others, points to an important new direction for understanding how neuronal activity leads to changes in blood flow. There now exists substantial evidence that local changes in blood flow reflect neurovascular coupling, likely through intervening glial cells that can influence the diameter of nearby arterioles. While the work of Takano and colleagues focused on rapid dilation associated with increased activity, other studies have illustrated other aspects of what seems to be a complex system for dilating and constricting blood vessels based on metabolic demands. As noted in a 2004 in vitro study by Mulligan and MacVicar, the effects of calcium may be mediated by the neurotransmitter noradrenaline, through broad neuronal projections from a midbrain structure known as the locus coeruleus that targets the astrocytes. This brain structure supports, among other capacities, changes in the overall arousal and alertness of an organism. Thus, the changes in blood flow measured in fMRI likely reflect the complex interactions among neuronal activity, neurotransmitter release, nearby glial cells, the response properties of the local vasculature, and even systemic changes that may predict future metabolic demands. Given these effects, researchers are exploring ways of calibrating fMRI data by accounting for baseline blood flow when estimating task-related changes in cerebral energy metabolism, as advanced by Hyder and colleagues. Clearly, given the rapid pace of discovery in this area, these experimental manipulations along with future studies will clarify this picture and may suggest unexpected new contributors to the control of blood flow.

some recent studies have demonstrated that changes in calcium concentration, triggered by neuronal activation, may lead to dilation of nearby blood vessels.

Animal studies by many investigators have demonstrated the effects of neuronal activity on local blood flow. Ngai and colleagues applied low-intensity somatosensory stimulation to the sciatic nerve of the rat while monitoring the pial vasculature through a window cut into the skull. The time courses of vascular diameter and blood flow were measured in response to 20 s periods of stimulation. Vascular diameter increased rapidly with the onset of stimulation, reaching a peak 5.5 s later. The diameter of the artery increased from a mean of 33 μm at baseline to a peak of about 44 μm, an increase of about 33%. After reaching its early peak, the diameter contracted to a plateau about 10% above baseline until the stimulation ended. The blood flow measures showed a very similar time course (Figure 6.14). Thus, in response to a sensory stimulus, the pial arteries dilate and blood flow increases. The authors also investigated the issue of the spatial extent, or coarseness, of these flow-related changes. Localizing the active neurons by measuring evoked field potentials, the authors noted that the vasodilatory response was remarkably discrete in its anatomic distribution, and that other arterioles branching from the same distribution artery, but that perfused other parts of somatosensory cortex, did not dilate (Figure 6.15).

Similar findings were obtained by Iadecola and colleagues. Electrical stimulation of parallel fibers in the rat's cerebellum produced focal neuronal stimulation that was exquisitely localized using evoked field potential mapping. The authors found that the arterioles supplying the activated neurons dilated

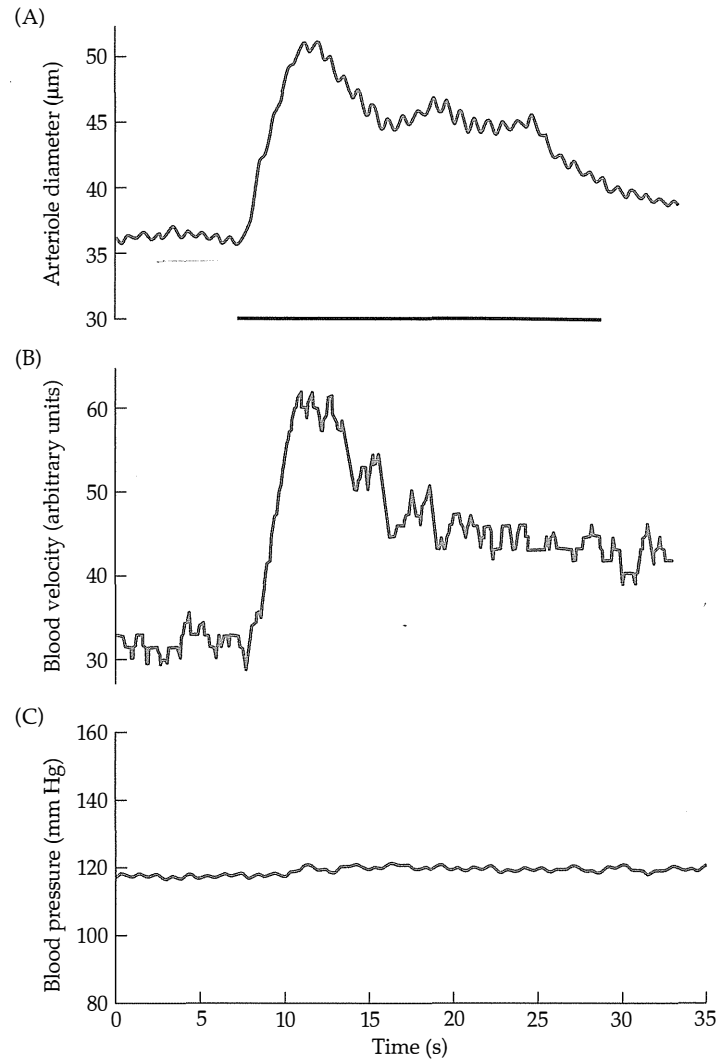

Figure 6.14 The relationship between sensory stimulation and local blood flow changes. The sciatic nerve of the rat was stimulated (solid horizontal line below graph in part A) and the time course of arteriole dilation (A) and blood velocity (B) were measured in the somatosensory cortex. The neuronal stimulation increased both diameter and flow. No change in mean arterial blood pressure (C) accompanied these functional vascular changes. (Data from Ngai, Morii, and Winn, 1988.)

by up to 26%. Larger arterioles upstream from the activated site showed smaller diameter increases of about 8%. No field potentials were recorded in the vicinity of these larger arterioles, which were about 2 to 3 mm distant (Figure 6.16). This result demonstrated that blood flow can increase in vessels that are upstream of the local neuronal activity. In subsequent studies, these upstream responses were found to be highly attenuated in mice that were genetically deficient in an enzyme responsible for the production of nitric oxide. Thus, these data support the role of nitric oxide in triggering blood flow increases through the control of upstream resistance vessels.

These data also put limits on the spatial specificity of hemodynamic changes as an indicator of neuronal activity. While the epicenter of the blood flow response was in the region of synaptic activity, arteriolar dilation and increased blood flow were also observed a few millimeters distant, where there was no synaptic activity. Iadecola and colleagues noted that neuronal activity produces a hemodynamic change over an area that is larger than the area of increased neuronal activity. This emphasizes that the distribution of hemodynamic responses measured using functional neuroimaging techniques will be ultimately determined by the local architecture of the microvascular blood supply.

Thought Question

Why do the results of Iadecola and colleagues limit the spatial resolution of neuroimaging techniques that depend on hemodynamic changes?

Effects of increased blood flow on capillaries

As we have reviewed, increased neuronal activity leads to increased blood flow in the arterioles that supply those neurons, and such increases in flow can occur in vessels up to several millimeters distant from the epicenter of neuronal activity. The effects of this increased blood flow on capillaries, venules,

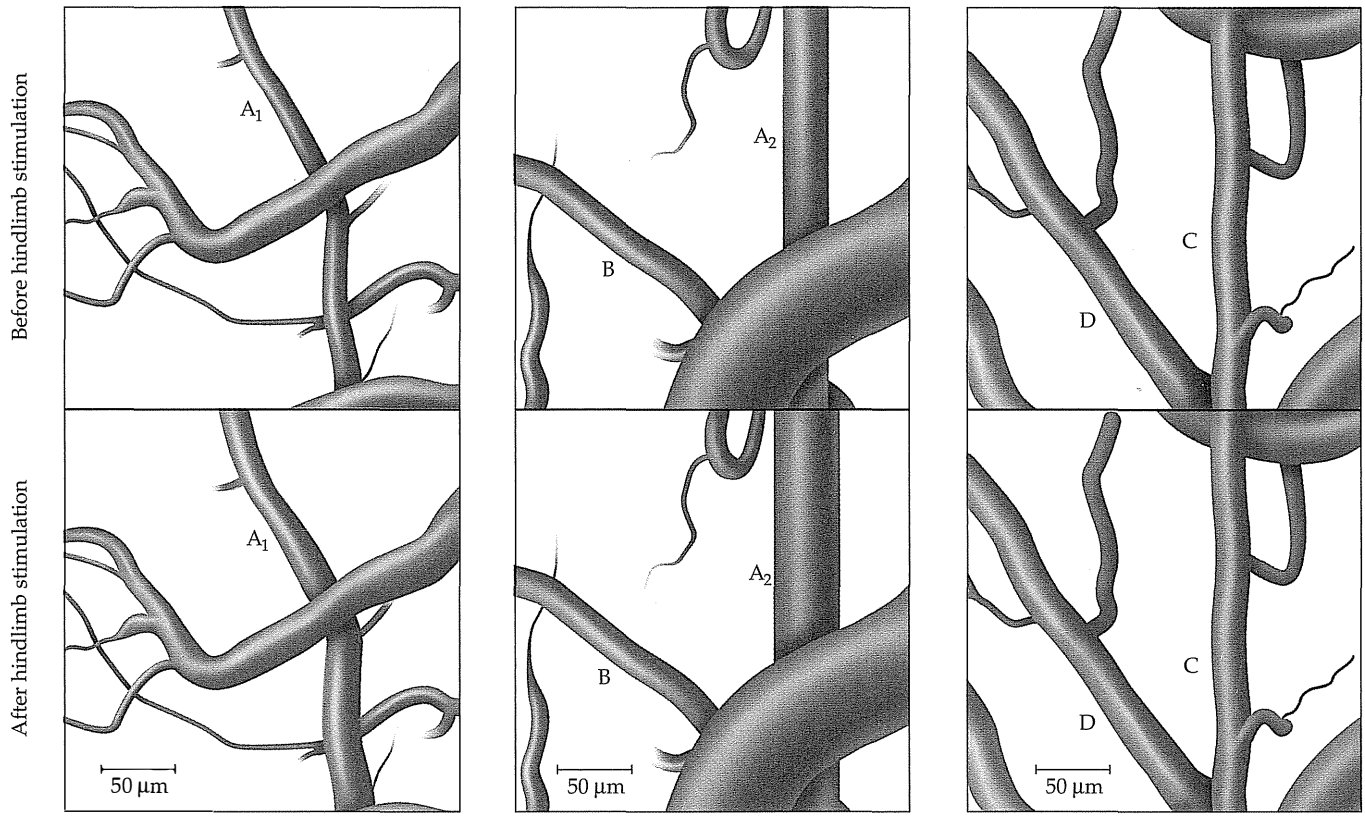

Figure 6.15 The change in diameter of arterioles following sciatic (hindlimb) stimulation. Arterioles that perfuse the cortical region corresponding to the hindlimb of the rat (A_1 and A_2), increase in diameter. Nearby vessels (B) and those that perfuse the forepaw region (C and D) do not increase in diameter. (After Ngai, Morii, and Winn, 1988.)

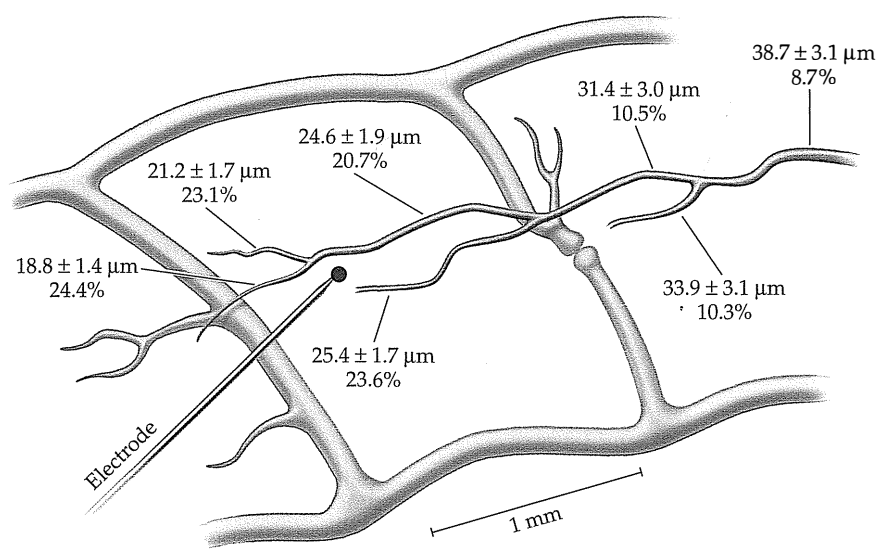

Figure 6.16 Change in arteriole dilation as a function of distance from active neurons. Changes in the diameter of blood vessels on the surface of the rat's cerebellum during parallel fiber stimulation were measured. Neuronal field potential activity was recorded at the black dot. Shown in this schematic diagram is an arteriole (center) passing over larger draining veins. Numbers indicate the mean diameter (± standard error) of the arteriole, and percentages indicate the change in that diameter with stimulation, at different points along its branches. As might be expected, the largest dilations occurred in the immediate vicinity of the neuronal stimulation. However, upstream vessels 2 to 3 mm from the site of activity (i.e., to the right on this figure) also showed modest dilation, even though there was no evoked activity nearby. (After Iadecola et al., 1997.)

and veins is less well understood. In the studies discussed in the previous section, the diameters of both arterioles and venules were measured in response to stimulation, and while arterioles dilated, no such effect was observed for venules. Many other studies have measured relative dilation of both arterioles and venules in response to physiological manipulations, such as hypocapnia (low levels of CO_2 in the blood), hypercapnia (excessive CO_2 in the blood), and pharmacological manipulations in which drugs were locally injected in the vessel. In general, these studies have shown that while venules do dilate, they do to a much lesser extent than arterioles. For example, under hypercapnia, the diameters of arterioles that were normally 10 to 30 μm in diameter increased by 50%, while similarly sized venules increased in diameter by only 10%.

What are the consequences in the capillary bed for this increased blood flow from the arterioles? One popular hypothesis is that a large reserve of unperfused (i.e., unfilled) capillaries is available to accept this increased flow, leading to an increase in total blood volume within the capillaries. This hypothetical phenomenon, known as capillary recruitment, may seem plausible. Yet in vivo studies with capillary staining and high-resolution microscopic techniques provide contradictory evidence: nearly all capillaries in the brain are perfused, the proportion of perfused capillaries does not change according to arousal state (e.g., sleeping vs. wakefulness), and increased blood flow has minimal effects on capillary perfusion. Thus, capillary recruitment can be rejected as a model for hemodynamic changes following neuronal activity. Another possibility is that individual capillaries distend slightly and thus decrease their resistance to flow, leading to increased flow within those capillaries and, again, increased overall blood volume within the capillary bed. Studies that have manipulated the amount of CO_2 dissolved in the blood to stimulate vessel contraction and dilation have reported that capillaries can, in fact, alter their diameters by about 20% between the physiologically extreme conditions of hypocapnia and hypercapnia. This capillary distension would increase the surface areas of individual capillaries, which could increase the area available for the transfer of oxygen and glucose to active neurons. The degree to which this occurs during normal physiological conditions, however, is not known.

The most likely result of increased flow into the capillaries is the regularization of flow velocity. Individual capillaries exhibit remarkable heterogeneity in their flow velocities. Some capillaries have very high rates of flow, while others have very low rates. With increased flow, the distribution of flow velocities increases and becomes more uniform. This process bears conceptual similarities to capillary recruitment, as discussed in the previous paragraph. However, unlike models of capillary recruitment, this scenario presumes that all vessels are perfused at some baseline level. Thus, the principal response of the capillary bed to increased blood flow appears to be an increase in overall flow velocity, with an unknown contribution from capillary distension. One consequence of this increased rate of flow is that the transit time of hemoglobin molecules through the capillaries decreases, which might affect the likelihood that an individual hemoglobin molecule would exchange its oxygen with an active neuron. We resume this story in Chapter 7, where we discuss how the properties of oxygenated and deoxygenated hemoglobin can be measured by MRI, to allow mapping of brain function onto brain structure (see Box 6.2 for an overview).

capillary recruitment The idea that increased blood flow through the capillary bed results in perfusion of previously unperfused capillaries.

BOX 6.2 Primer on Neuroanatomy

Throughout this book, we will be making frequent reference to neuroanatomical structures, and frequent use of neuroanatomical terms. After all, our subject is functional *brain* imaging! While a detailed treatment of human neuroanatomy is beyond the scope of this book, here we present a brief overview sufficient for the discussions in this text.

Taken together, the brain and spinal cord form the central nervous system, or CNS. Special, sometimes confusing terms are often used to describe the relative locations of anatomical structures. Imagine that the CNS is a long cylinder that rises as a vertical column from the beginning of your spinal cord near your tailbone into your skull, and then bends 90° toward your nose. Along this axis, the term caudal, from the Latin term for "tail," refers to the direction of the tail or hind limbs. The term rostral, derived from the Latin term for "beak," refers to the direction of the nose. Again relative to this axis, dorsal refers to the back while ventral refers to the front. So your chest is ventral to your back, and your back is dorsal to your chest (cf., the dorsal fin of sharks). Once inside the brain, where the axis of the CNS bends 90°, dorsal structures are now superior and ventral structures are inferior. So the top of your brain is dorsal to the bottom of your brain, and the bottom of your brain is ventral to the top of your brain. Structures that are closer to the midline of the brain are medial, and structures that are closer to the edge of the brain are lateral.

The CNS is composed of a number of cellular elements. The principal information-processing cells of the CNS are called neurons, which have cell bodies and protoplasmic processes called dendrites and axons (see the main text for a more complete description). Areas within the CNS composed primarily of cell bodies are sometimes called gray matter, while areas composed primarily of large axon bundles are called white matter. The white matter is so named due to the color of myelin, the fatty sheath that encases the axons of many neurons and speeds the propagation of action potentials. The myelin sheath is constructed by a support cell called the oligodendrocyte. Another type of support cell found in the CNS is the astrocyte, which helps regulate the extracellular environment within the CNS, including changes in blood flow (see Box 6.1). The supporting oligodendrocytes and astrocytes are known collectively as glial cells, or glia (from the Greek for "glue").

Neurons come in different sizes, shapes, and typical patterns of connectivity. Two common neuron types are pyramidal cells, named for the triangular shape of their cell bodies, and stellate cells, which have more spherical cell bodies. Pyramidal cells have long axons that can travel great distances within the brain, while stellate cells appear to play a primary role in local processing.

Three membranes, or meninges, cover the outside surface of the brain and spinal cord. The outermost covering is called the dura, which is quite thick and tough. The middle layer is called the arachnoid, its weblike appearance being the source of its name. The innermost layer is called the pia, which is a delicate membrane that closely adheres to the contours of the brain. The pia is highly vascularized and, as discussed in the main text, is the source of the small arteries that supply the cortex. The space between the arachnoid and pia is filled with cerebrospinal fluid, or CSF, a colorless liquid that bathes the brain and spinal cord. CSF is produced in the choroid plexus, an invagination of the pia into the ventricles of the brain. The ventricles are a continuous series of cavities within the brain that are filled with CSF. The CSF flows down from the two lateral ventricles, through the midline third ventricle, into the fourth ventricle in the

central nervous system (CNS) The brain and spinal cord.

caudal Toward the back of the brain.

rostral Toward the front of the brain.

dorsal Toward the top of the brain.

ventral Toward the bottom of the brain.

medial Toward the middle of the brain.

lateral Toward the side of the brain.

myelin A fatty substance that forms sheaths surrounding axons that serve to speed the transmission of action potentials.

oligodendrocyte A type of glial cell that constructs the myelin sheaths around axons.

astrocyte A type of glial cell that regulates the extracellular environment.

dura The outermost membrane covering the brain; its name comes from its thickness and toughness.

arachnoid The middle membrane covering the brain; its name comes from its weblike appearance.

pia The innermost membrane covering the brain; it closely adheres to the brain's contours.

cerebrospinal fluid (CSF) A colorless liquid that surrounds the brain and spinal cord and fills the ventricles within the brain.

ventricles Fluid-filled cavities within the brain.

BOX 6.2 *(continued)*

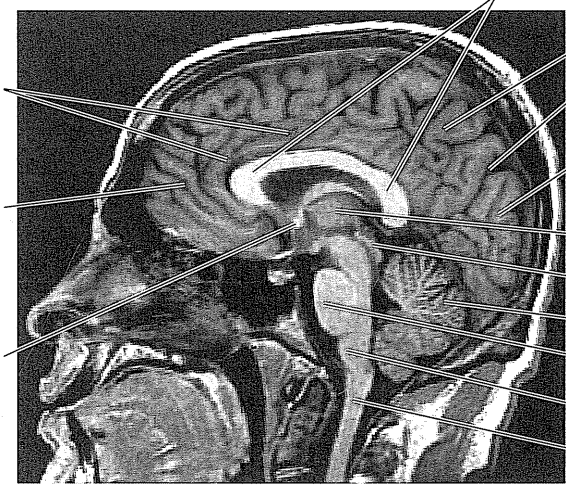

Figure 1 A mid-sagittal MRI of the human head.

region of the brain stem (see the next section), and then into the cisterns, where it flows both upward to bathe the surfaces of the cerebrum and downward into the spinal cord. The CSF is eventually absorbed into the vascular system in the superior sagittal sinus, part of the venous drainage system of the brain found between layers of the dura. The CSF forms a fluid cushion that protects the brain, particularly from its bony encasement. It also serves to maintain a consistent external environment for the cells of the CNS and helps remove metabolic wastes.

Major Components of the CNS

Figure 1 shows an MRI of the head taken along the midline and thus bisecting the brain. A view of the brain in any parallel plane is called a **sagittal** view and this specific slice is known as a mid-sagittal view. The position of the brain within the head and skull can be well appreciated in this view, which also provides a convenient starting place for describing the major subdivisions of the CNS.

The most caudal aspect of the CNS visible in Figure 1 is the spinal cord, which can be seen entering the brain through an opening within the base of the skull called the foramen magnum (unlabeled, but located just above the line indicating the position of the spinal cord). The spinal cord contains ascending sensory fiber tracts that transmit somatosensory information to the brain from sensors throughout the body, and descending motor fiber tracts that transmit control information to the muscles from the brain. Just rostral to the foramen magnum is a continuation of the spinal cord called the **medulla oblongata**. The medulla contains the cell bodies for several major cranial nerves, some of which are involved in the control of respiration, circulation, and vegetative functions. In many texts, the medulla is also referred to as the myelencephalon (in Greek, *enkephalos* means "in the head or brain"), one of the five major subdivisions of the brain.

The **pons** is a prominent structure just rostral to the medulla. Like the medulla, the pons is a thoroughfare that is traversed by many ascending sensory and descending motor fiber tracts. The pons also contains the cell bodies that are the source of cranial nerves that innervate the face and eye muscles.

Just posterior and intimately connected through thick fiber bundles to the pons is the **cerebellum**, which is a large structure important in the coordination of walking and posture, motor learning, and even complex cognitive functions. The cerebellum is located within a part of the skull called the posterior fossa, which is separated from the remainder of the brain by a tough membrane called the tentorium. Together, the pons and cerebellum comprise the metencephalon. Collectively, the metencephalon and myelencephalon are sometimes called the hindbrain.

Rostral to the pons is the **midbrain**, or mesencephalon (see Figure 6). The midbrain gives rise to two major cranial nerves and also contains several impor-

sagittal A side view of the brain (along the y–z plane in MRI).

medulla oblongata A continuation of the spinal cord at the base of the brain that is important for the control of basic physiological functions.

pons Part of the brain stem; it serves as a relay system for motor and sensory nerves.

cerebellum A large cortical structure at the caudal base of the brain that plays an important role in motor function.

midbrain A section of the brain rostral to the pons; it includes a number of important nuclei.

(continued on next page)

BOX 6.2 *(continued)*

tant cell clusters or nuclei, including the red nucleus and substantia nigra. The latter is a major source of dopamine in the brain; loss of cells in the substantia nigra can cause Parkinson's disease, a serious affliction of aging that is associated with tremor and a progressive deterioration of motor control. The superior and inferior colliculi are paired structures located on the posterior aspect of the midbrain (they appear as small bumps on the back of the midbrain in Figure 1). The superior colliculi are part of the visual system, while the inferior colliculi are part of the auditory system.

The midbrain, pons, and medulla contain clusters of neurons that comprise the ascending reticular formation, which is important in regulating sleep, arousal, and levels of consciousness. Many neuroanatomists refer collectively to the midbrain, pons, and medulla as the **brain stem**, as it appears to support the more rostral brain as a stem supports a flower.

Rostral to the midbrain are the **hypothalamus** and **thalamus**, which together with the epithalamus and pineal gland constitute the diencephalon. The hypothalamus is involved in autonomic functions and somatic functions, including the regulation of temperature, water intake, and hunger. The hypothalamus is also an important structure in the regulation of endocrine functions—particularly in its control of the pituitary gland.

The thalamus is a paired structure connected at the midline by the massa intermedia. The thalamus is composed of a large number of nuclei that are sometimes referred to as relay nuclei because they receive information from sensory, motor, and other regions of the brain, organize or process this information, and then project the information to specific regions of cortex. For example, the lateral geniculate is a nucleus of the thalamus that receives and processes visual information from the eyes before projecting that information to the visual cortex. Similar functions are carried out by the medial geniculate for auditory information and by the ventral posterolateral nucleus for the somatosensory system. Some thalamic nuclei are involved in relaying motor information in the brain. For example, the ventral lateral nuclei receive motor information from the cerebellum and project it to the motor cortex. Other thalamic nuclei appear to integrate information from other brain regions that are neither motor nor sensory. For example, the dorsomedial nucleus receives information from the amygdala, hypothalamus, and other thalamic nuclei and projects this information to the frontal lobes.

Rostral to the diencephalon is the telencephalon, or forebrain. The telencephalon is the largest, most complex, and most evolutionarily advanced part of the brain. It is composed of the cerebral cortical hemispheres (the cerebrum), older layered structures like the hippocampus, and large subcortical nuclei such as the amygdala and the **basal ganglia** (itself composed of the caudate, putamen, and globus pallidus). Interconnecting these brain regions are extensive white-matter tracts, which can be seen in Figure 2.

brain stem The midbrain, pons, and medulla.

hypothalamus A brain nucleus that supports homeostatic functions, including the regulation of food and water intake.

thalamus A brain nucleus that is important for many aspects of perception and cognition; it is highly interconnected with many regions of the cerebral cortex.

basal ganglia A set of nuclei in the forebrain that includes the caudate, putamen, and globus pallidus.

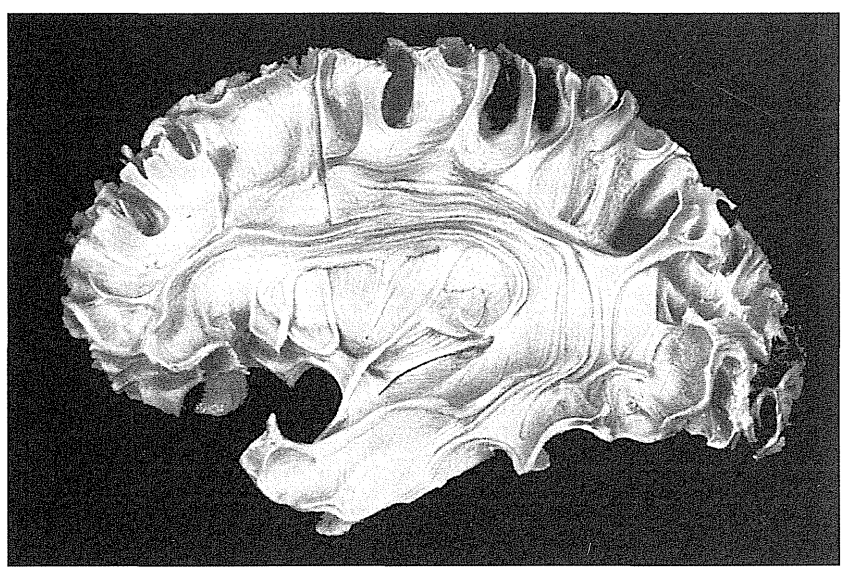

Figure 2 A sagittal drawing of the white-matter tracts of the human cerebral cortex. (From Ludwig and Klionger, 1956.)

BOX 6.2 *(continued)*

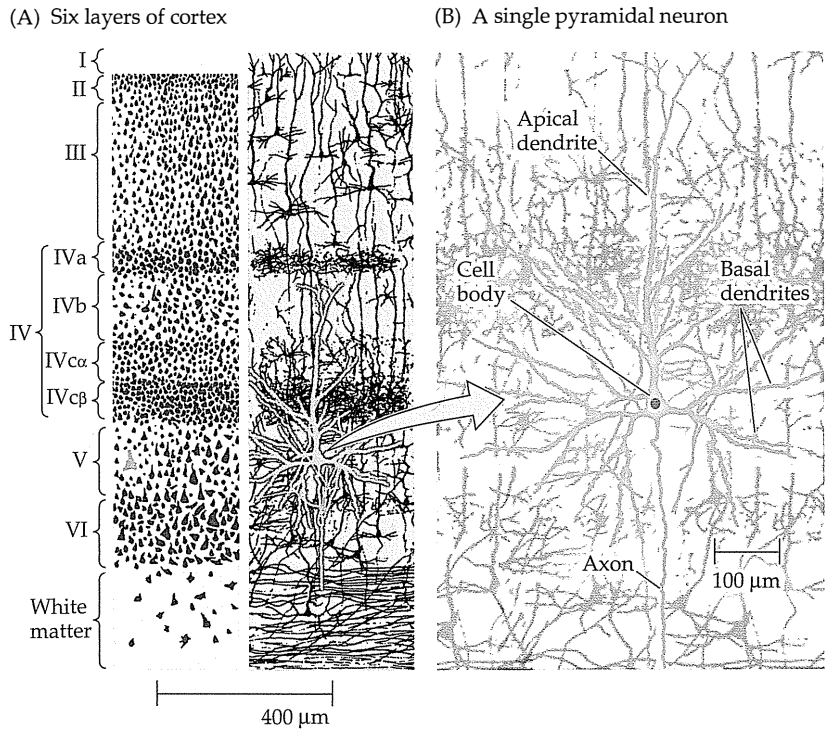

Figure 3 (A) The six-layer structure of the neocortex, showing the relative density of cell bodies (at left) and sample neurons and their projections within and across layers (at right). Note that within some brain regions, one or more of the six primary layers may be divisible into sub-layers, as here for Layer IV. (B) A enlarged view of a single neuron in the context of the surrounding cortical layers.

The Cortex

The cerebral hemispheres (cerebrum) are composed of a continuous sheet of cerebral cortex that has been folded into an undulating pattern of gyri and sulci. Gyri are rises of cortex that are separated by infolded troughs, or sulci. If unfolded and laid out as a sheet, the cortex of the average human brain would have an area of 2500 cm^2. The most evolutionarily recent region of the cortex is called the neocortex, which is about 5 mm thick and composed of six layers, or lamina (Figure 3). Layer I is the closest to the pial surface and is composed primarily of axonal and dendritic processes with few neurons. Layers II and III are composed primarily of pyramidal cells, and the cells in Layer II have smaller cell bodies than those of Layer III. Layer IV is relatively devoid of pyramidal cells but is densely packed with stellate cells. Layer IV contains projections from other cortical regions and thus appears to be the primary input layer of the cortex. Layer IV appears to project primarily to Layers I, II, and III, which appear to comprise the intracortical processing layers. Layers V and VI contain large pyramidal cells that project their axons to other brain regions and thus appear to represent the output layers of the neocortex. Note that although few fMRI studies distinguish between these layers given that the typical voxel size is on the order of several millimeters, other techniques like electrophysiologic single cell recording are able to do so. (See Chapter 8 for a few intriguing examples in which fMRI is used to distinguish between cortical layers.)

Cortical thickness, packing density, and composition and size of constituent cells differ across the various regions of the cortex. Anatomists have developed detailed maps of the cortex based on these differences in cytoarchitecture, with the hope of differentiating function on the basis of structure. One popular cytoarchitectonic map published by Korbinian Brodmann in 1909 divides the cerebral cortex into 47 different regions (Figure 4). These regions, or Brodmann areas, are used today in many studies to communicate the locations of brain activation measured by fMRI or by positron emission tomography (PET). Although no non-invasive neuroscience method can measure the cytoarchitecture of the brain directly, sufficient similarities exist between individuals to permit the use of spatial transformations

cerebrum The two hemispheres forming the major part of the brain.

gyri Rises in the cortical surface.

sulci Troughs in the cortical surface.

cytoarchitecture The organization of the brain on the basis of cell structure.

Brodmann areas Divisions of the brain based on the influential cytoarchitectonic criteria of Korbinian Brodmann.

(continued on next page)

BOX 6.2 *(continued)*

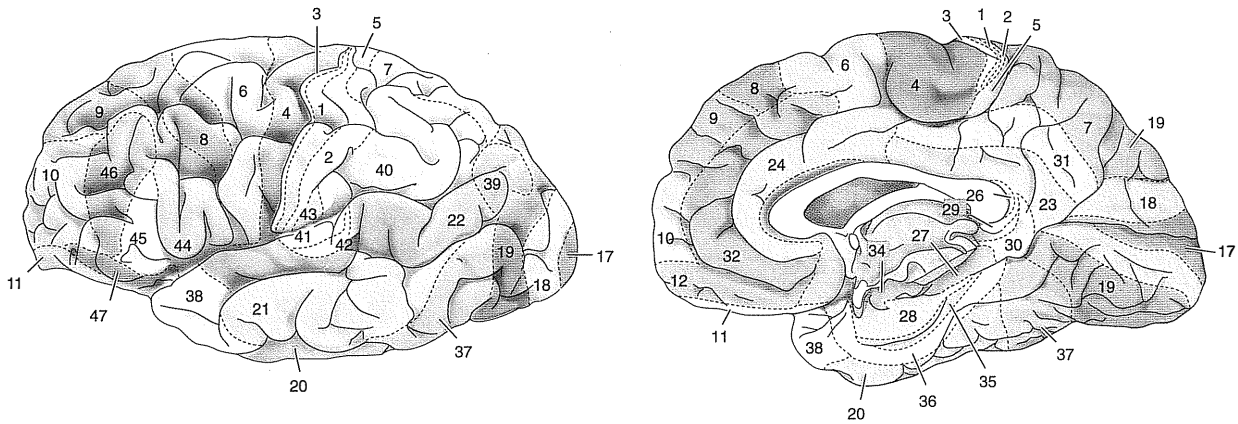

Figure 4 The cytoarchitectonic map of Brodmann (1909).

that warp an individual's brain into a common atlas space (such as the atlas of Talairach and Tournoux) that has been annotated with Brodmann areas.

Although the cortical sheet is continuous, the presence of several deep fissures in the typical brain has resulted in the subdivision of the brain into four major lobes: the frontal, parietal, temporal, and occipital lobes—so named for the skull bones that cover them. A fifth lobe, the insula, is hidden behind part of the anterior temporal lobe and inferior frontal lobe. Some neuroanatomists also describe a limbic lobe that is composed of midline structures including the cingulate cortex, hippocampus, and amygdala. The cerebral hemispheres and their constituent lobes and nuclei are paired structures. Although the two hemispheres appear roughly similar in shape, there are subtle anatomical differences between them that most likely form the basis for such lateralized functions as language and spatial skills.

The left lateral surface of the cerebral hemisphere with meninges and blood vessels removed is shown in Figure 5. The locations of the frontal, parietal, occipital, and temporal lobes are shown. The precentral and postcentral gyri are separated by the **central sulcus**, a deep fissure that separates the frontal and parietal lobes. The gyrus anterior to the central sulcus—the precentral gyrus—is often described as the primary motor cortex. Along its medial to lateral extent is a somatotopic representation of the body, or homunculus, with the lower extremities represented near the midline, the hands in the middle, and the mouth and tongue near its most lateral extent. Electrical stimulation of this gyrus causes involuntary movement of the represented limb. The gyrus posterior to the central sulcus—the postcentral gyrus—has a sensory representation of

central sulcus A deep fissure that separates the frontal and parietal lobes of the brain.

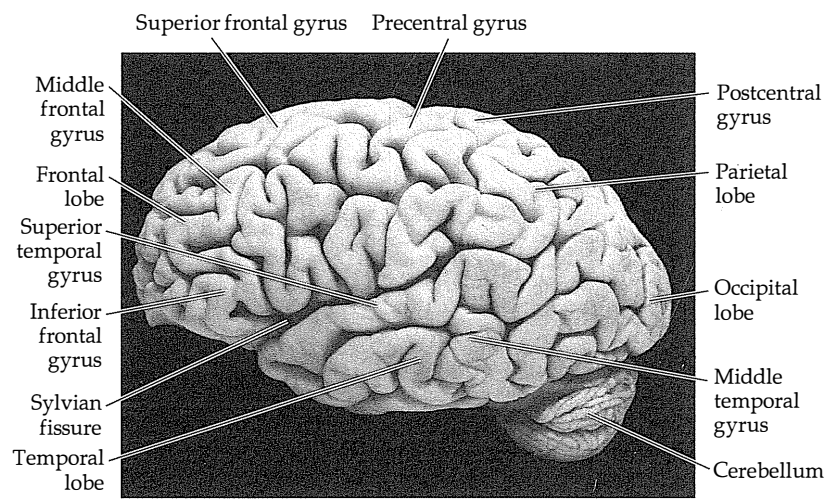

Figure 5 Surface view of the left hemisphere of the human brain. (Courtesy of S. Mark Williams and Dale Purves, Duke University Medical Center.)

BOX 6.2 *(continued)*

the body that is closely aligned to the motor representation just described. Electrical stimulation of the postcentral gyrus causes a tingling sensation in a particular body part.

The **temporal lobe** is separated from the frontal and parietal lobes by the deep **Sylvian fissure**. The lateral part of the temporal lobe plays an important role in auditory and visual processing, and the temporal lobe in the left hemisphere is particularly important for language processing. The **occipital lobe** at the posterior end of the brain is the primary region of the brain for visual processing. It is separated from the parietal lobe by the parieto-occipital fissure, which is best seen in the medial view presented in Figure 6. The **parietal lobe** plays an important role in spatial processing, among many other functions. The **frontal lobes** are quite large and have many functions. The dorsal lateral frontal lobe plays an important role in complex cognitive processing including executive functions like reasoning and decision making. Within the left frontal lobe in most individuals is a region supporting language production known as Broca's area. The more ventral and medial parts of the frontal lobe appear to play a role in emotional processing. The **insula**, not visible in Figure 5 (see Figure 8), is hidden deep within the anterior part of the Sylvian fissure and inferior frontal lobe. The insula is important for the chemical senses such as olfaction and gestation, but also plays an important role in a wide range of affective processes from evaluating fear and pain to avoiding risky situations.

The **corpus callosum** is a large white-matter bundle that connects the hemispheres of the brain (it can be easily seen in Figure 6). The most anterior part of the corpus callosum is known as the genu, while the posterior enlargement is called the splenium.

Figure 7 presents two views of the ventral surface of the brain. The photographed brain in Figure 7A has the cerebellum attached, but the surface blood vessels have been removed. The drawing in Figure 7B has omitted the cerebellum so that the gyri and sulci on the ventral surface of the temporal lobe can be identified. Many regions in the inferior temporal lobe play an important role in higher visual processes, including the perception of complex objects. The entorhinal cortex and parahippocampal gyrus, along with the adjacent hippocampus (not shown), are

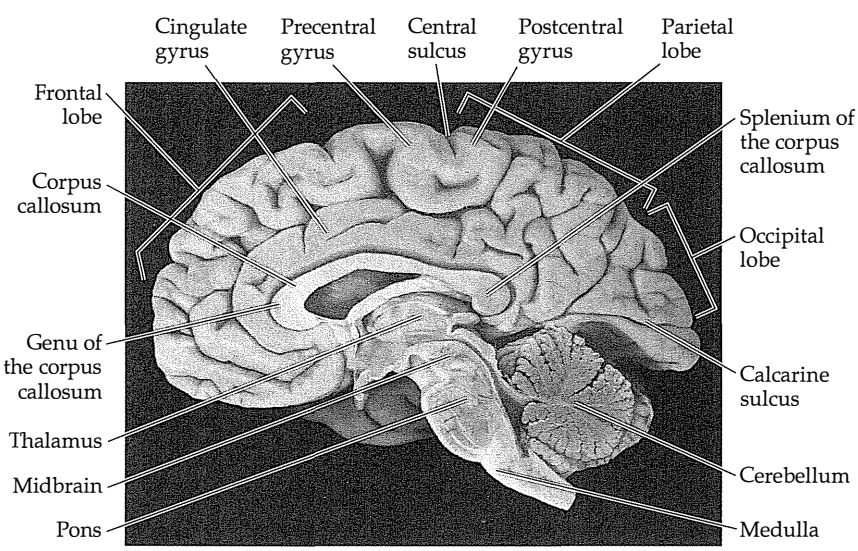

Figure 6 Midsagittal view of the human brain. (Courtesy of S. Mark Williams and Dale Purves, Duke University Medical Center.)

temporal lobe The lobe on the ventral surface of the cerebrum; it is important for auditory and visual processing, language, memory, and many other functions.

Sylvian fissure The deep sulcus separating the temporal lobe from the frontal and parietal lobes.

occipital lobe The most posterior lobe of the brain; it is primarily associated with visual processing.

parietal lobe The lobe on the posterior and dorsal surfaces of the cerebrum; it is important for spatial processing, cognitive processing, and many other functions.

frontal lobe The most anterior lobe of the cerebrum; it is important for executive processing, motor control, memory, and many other functions.

insula The "island" cortex hidden inside the anterior part of the Sylvian fissure; it is important for emotional processing and for the chemical senses.

corpus callosum The large white-matter bundle that is the primary connection between the cerebral hemispheres. The anterior portion is known as the genu and the posterior portion is known as the splenium.

(continued on next page)

BOX 6.2 *(continued)*

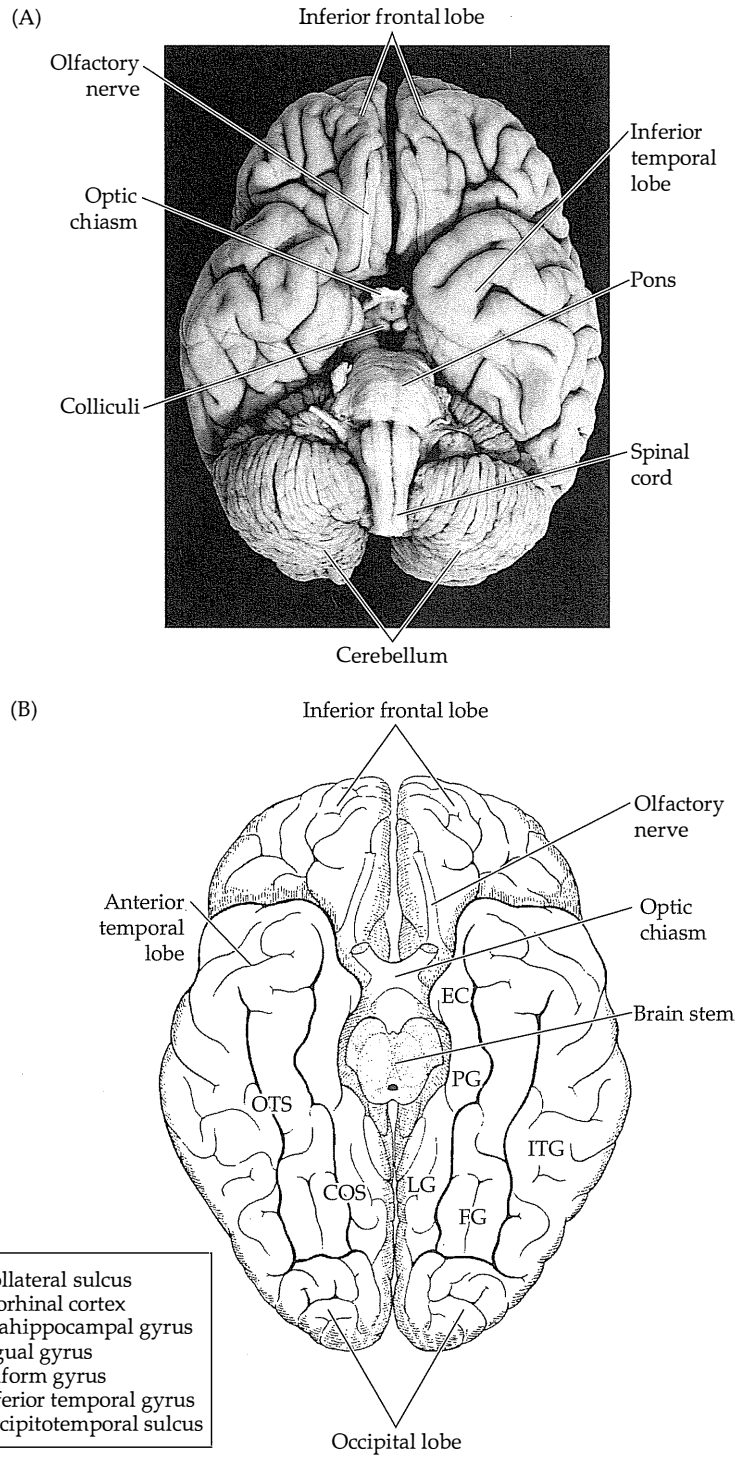

collectively referred to as the medial temporal lobe and support memory processes.

Figure 8 and Figure 9 present two brain slices that have orthogonal orientations frequently used in MRI. Figure 8 is an **axial** view taken at one slice within the dorsal–ventral plane, in which rostral is at the top of the image and caudal is at the bottom of the image. Figure 9 is a **coronal** view taken at one slice within the rostral–caudal plane, in which the dorsal is up and the ventral is down. In both the coronal and axial views, the midline of the brain is the midline of the view. Visible is a clear distinction between the thin layer of cortical gray matter and the deep white-matter tracts; it is clear that the cortex in the deep sulci is continuous with the cortex of the gyri. The insula is visible as an island of cortex hidden behind the outer surfaces of the temporal and frontal lobes. Also visible are the basal ganglia (caudate and putamen), which are important for motor control and play key roles in many cognitive processes associated with learning.

The lateral ventricles are clearly visible in Figure 9 near the center of the brain. Also visible is the anterior end of

axial A horizontal view of the brain (along the x–y plane in MRI).

coronal A frontal view of the brain (along the x–z plane in MRI).

Figure 7 Ventral view of the human brain. Shown in (A) is a photograph of the ventral surface, with the cerebellum and brain stem visible. The drawing in (B) has the cerebellum removed, so that gyri can be identified. (A courtesy of S. Mark Williams and Dale Purves, Duke University Medical Center.)

BOX 6.2 *(continued)*

the amygdala, which supports emotional processing and is an important component of the limbic lobe. Notable in this coronal view are the interhemispheric white matter tracts. The corpus callosum forms by far the largest such connection, with the anterior commissure a secondary but still important source of communication between the hemispheres.

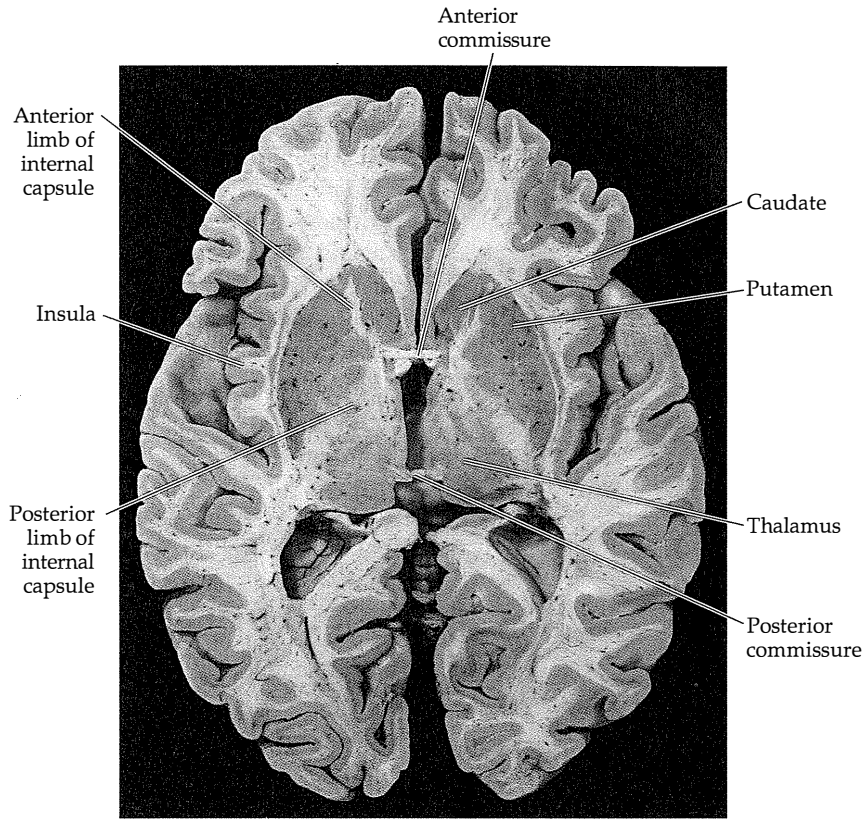

Figure 8 Axial view of the human brain at the level of the anterior commissure. (Courtesy of S. Mark Williams and Dale Purves, Duke University Medical Center.)

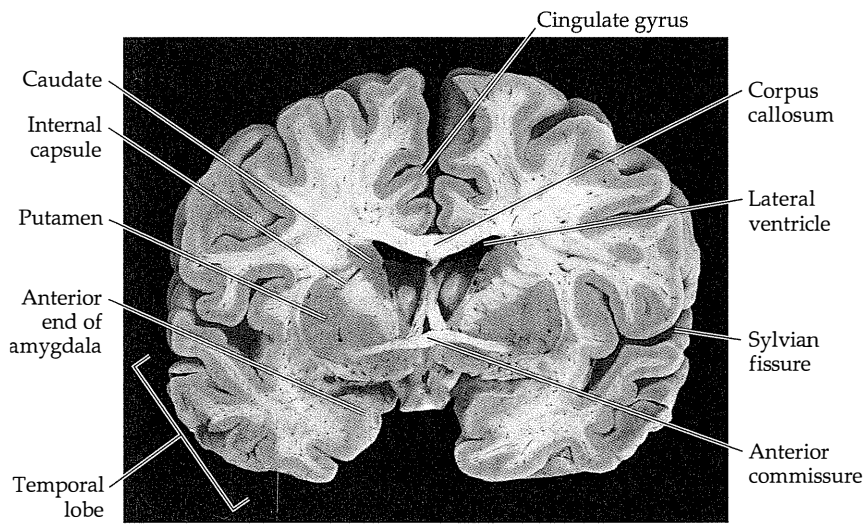

Figure 9 Coronal view of the human brain at the level of the anterior commissure. (Courtesy of S. Mark Williams and Dale Purves, Duke University Medical Center.)

REFER TO THE
fMRI
COMPANION WEBSITE AT
www.sinauer.com/fmri2e
for study questions and Web links.

Summary

The fundamental element of information processing in the human brain is the neuron. Neurons have two primary roles, integration and signaling, which rely on changes in cell membrane potential and the release of neurotransmitters. While the integrative and signaling activities themselves do not require external sources of energy, the restoration of ionic concentration gradients following these activities does require an energy supply. The primary metabolites supplied to active neurons are glucose and oxygen, which together are important for the synthesis of ATP. These metabolites are supplied via the vascular system. The main components of the vascular system are arteries, capillaries, and veins, each present at different spatial scales. Changes within the vascular system in response to neuronal activity may occur in brain areas far from the neuronal activity, initiated in part by flow-controlling substances released by neurons into the extracellular space, or by direct influences from neurons or nearby glial cells. Neurons may directly alter flow in pial arteries, arterioles, and capillaries, but it is unknown whether such effects have consequences for fMRI measurements. A major consequence of the vascular response to neuronal activity is the arterial supply of oxygenated hemoglobin, from which oxygen is extracted in the capillaries. These changes in the local concentration of deoxygenated hemoglobin provide the basis for fMRI.

Suggested Readings

Attwell, D., and Iadecola, C. (2002). The neural basis of functional brain imaging signals. *Trends Neurosci.*, 25(12): 621–625. *This article provides a succinct review of the energy budget of the brain and how it may relate to functional neuroimaging.*

*Duvernoy, H. M., Delon, S., and Vannson, J. L. (1981). Cortical blood vessels of the human brain. *Brain Res. Bull.*, 7(5): 519–579. *This paper provides a thorough exploration of the blood supply to the human brain with numerous and spectacularly detailed photographs.*

*James, W. (1890). *The Principles of Psychology.* Dover, New York. *The masterwork of a scientist who integrated brilliant introspections with a keen experimental sense, this classic compendium still provides useful insights on a wide range of topics. The chapter on brain physiology is highly recommended.*

Lauritzen, M. (2005). Reading vascular changes in brain imaging: is dendritic calcium the key? *Nat. Rev. Neurosci.*, 6: 77–85. *A comprehensive overview of the cellular and neurotransmitter contributions to local control of the vascular system.*

Purves, D., Augustine, G., Fitzpatrick, D., Hall, W. C., LaMantia, A., McNamara, J. O., and White, L. E. (eds.) (2008). *Neuroscience* (4th ed.). Sinauer Associates, Sunderland, MA. *This well-illustrated textbook provides detailed discussions of all aspects of neuroscience, including neuroanatomy, neuronal signaling and integration, and membrane channels and transporters.*

*Roy, C. S., and Sherrington, C. S. (1890). On the regulation of the blood-supply of the brain. *J. Physiol.*, (11): 85–108. *A comprehensive and engaging description of the vascular system in the brain, it includes speculations in its final pages about the possible functional implications of blood flow.*

*Indicates a reference that is a suggested reading in the field and is also cited in this chapter.

Chapter References

Attwell, D., and Laughlin, S. B. (2001). An energy budget for signaling in the grey matter of the brain. *J. Cereb. Blood Flow Metab.*, 21(10): 1133–1145.

Branston, N. M. (1995). Neurogenic control of the cerebral circulation. *Cerebrovasc. Brain Metab. Rev.*, 7(4): 338–349.

Brodmann, K. (1909). *Vergleichende Localisationslehre der Grosshirnrinde in ihren Prinzipien dargestellt auf Grund des Zellenbaues.* Barth, Leipzig.

Duelli, R., and Kuschinsky, W. (1993). Changes in brain capillary diameter during hypocapnia and hypercapnia. *J. Cereb. Blood Flow Metab.*, 13(6): 1025–1028.

Friedland, R. P., and Iadecola, C. (1991). A centennial reexamination of "On the regulation of the blood-supply of the brain." *Neurology*, 41(1): 10–14.

Gobel, U., Klein, B., Schrock, H., and Kuschinsky, W. (1989). Lack of capillary recruitment in the brains of awake rats during hypercapnia. *J. Cereb. Blood Flow Metab.*, 9: 491–499.

Hudetz, A. G. (1997). Blood flow in the cerebral capillary network: A review emphasizing observations with intravital microscopy. *Microcirculation*, 4(2): 233–252.

Hyder F., Rothman, D. L., and Shulman, R. G. (2002).Total neuroenergetics support localized brain activity: Implications for the interpretation of fMRI. *Proc. Natl. Acad. Sci. U. S .A.*, 99: 10771–10776.

Iadecola, C. (1998). Neurogenic control of the cerebral microcirculation: Is dopamine minding the store? *Nat. Neurosci.*, 1(4): 263–265.

Iadecola, C. (2002). Intrinsic signals and functional brain mapping: Caution, blood vessels at work. *Cereb. Cortex*, 12(3): 223–224.

Iadecola, C., Yang, G., Ebner, T. J., and Chen, G. (1997). Local and propagated vascular responses evoked by focal synaptic activity in cerebellar cortex. *J. Neurophysiol.*, 78(2): 651–659.

Krimer, L. S., Muly, E. C., III, Williams, G. V., and Goldman-Rakic, P. S. (1998). Dopaminergic regulation of cerebral cortical microcirculation. *Nat. Neurosci.*, 1(4): 286–289.

Lee, S. P., Duong, T. Q., Yang, G., Iadecola, C., and Kim, S. G. (2001). Relative changes of cerebral arterial and venous blood volumes during increased cerebral blood flow: Implications for BOLD fMRI. *Magn. Reson. Med.*, 45(5): 791–800.

Ludwig, E., and Klionger, J. (1956). *Atlas Cerebri Humani.* Little, Brown and Co., Boston, MA.

McHedlishvili, G., and Kuridze, N. (1984). The modular organization of the pial arterial system in phylogeny. *J. Cereb. Blood Flow Metab.*, 4(3): 391–396.

Menon, R. S., and Goodyear, B. G. (1999). Submillimeter functional localization in human striate cortex using BOLD contrast at 4 Tesla: Implications for the vascular point-spread function. *Magn. Reson. Med.*, 41(2): 230–235.

Metea, M. R. and Newman, E. A. (2006). Glial cells dilate and constrict blood vessels: a mechanism of neurovascular coupling. *J. Neurosci.*, 26: 2862–2870.

Mulligan, S. J. and MacVicar, B. A. (2004). Calcium transients in astrocyte endfeet cause cerebrovascular constrictions. *Nature*, 431: 195–199.

Ngai, A. C., Ko, K. R., Morii, S., and Winn, H. R. (1988). Effect of sciatic nerve stimulation on pial arterioles in rats. *Am. J. Physiol.*, 254(1 Pt 2): H133–H139.

Ngai, A. C., Meno, J. R., and Winn, H. R. (1995). Simultaneous measurements of pial arteriolar diameter and laser-Doppler flow during somatosensory stimulation. *J. Cereb. Blood Flow Metab.*, 15(1): 124–127.

Nonaka, H., Akima, M., Hatori, T., Nagayama, T., Zhang, Z., and Ihara, F. (2002). The microvasculature of the human cerebellar meninges. *Acta Neuropathologica*, 104(6): 608–614.

Nonaka, H., Akima, M., Nagayama, T., Hatori, T., Zhang, Z., and Ihara, F. (2003). Microvasculature of the human cerebral meninges. *Neuropathology*, 23(2): 129–135.

Raichle, M. E., and Gusnard, D. A. (2002). Appraising the brain's energy budget. *Proc. Natl. Acad. Sci. U. S. A.*, 99(16): 10237–10239.

Rodriguez-Baeza, A., Reina-De La Torre, F., Ortega-Sanchez, M., and Sahuquillo-Barris, J. (1998). Perivascular structures in corrosion casts of the human central nervous system: A confocal laser and scanning electron microscope study. *Anat. Rec.*, 252(2): 176–184.

Segebarth, C., Belle, V., Delon, C., Massarelli, R., Decety, J., Le Bas, J. F., Decorps, M., and Benabid, A. L. (1994). Functional MRI of the human brain: Predominance of signals from extracerebral veins. *NeuroReport*, 5(7): 813–816.

Sibson, N. R., Dhankhar, A., Mason, G. F., Rothman, D. L., Behar, K. L., and Shulman, R. G. (1998). Stoichiometric coupling of brain glucose metabolism and glutamatergic neuronal activity. *Proc. Natl. Acad. Sci. U. S. A.*, 95(1): 316–321.

Takano, T., Tian, G. F., Peng, W., Lou, N., Libionka, W., Han, X., and Nedergaard, M. (2006). Astrocyte-mediated control of cerebral blood flow. *Nat. Neurosci.*, 9: 260–267.

Talairach, J., and Tournoux, P. (1988). *Co-Planar Stereotactic Atlas of the Human Brain.* Stuttgart, Germany, Thieme.

Vafaee, M. S., and Gjedde, A. (2000). Model of blood–brain transfer of oxygen explains nonlinear flow-metabolism coupling during stimulation of visual cortex. *J. Cereb. Blood Flow Metab.*, 20(4): 747–754.

Villringer, A., Them, A., Lindauer, U., Einhaupl, K., and Dirnagl, U. (1994). Capillary perfusion of the rat brain cortex. An in vivo confocal microscopy study. *Circ. Res.*, 75: 55–62.

Williams, S. M., White, L. E., and Mace, A. C. (2007). *Sylvius 4: An Interactive Atlas and Visual Glossary of Human Neuroanatomy.* Sinauer Associates, Sunderland, MA.

Yang, G., Zhang, Y., Ross, M. E., and Iadecola, C. (2003). Attenuation of activity-induced increases in cerebellar blood flow in mice lacking neuronal nitric oxide synthase. *Am. J. Physiol. Heart Circ. Physiol.*, 285(1): H298–H304.

Zoccoli, G., Lucchi, M. L., Andreoli, E., Bach, V., Cianci, T., Lenzi, P., and Franzini, C. (1996). Brain capillary perfusion during sleep. *J. Cereb. Blood Flow Metab.*, 16: 1312–1318.

Chapter 7

BOLD fMRI: Origins and Properties

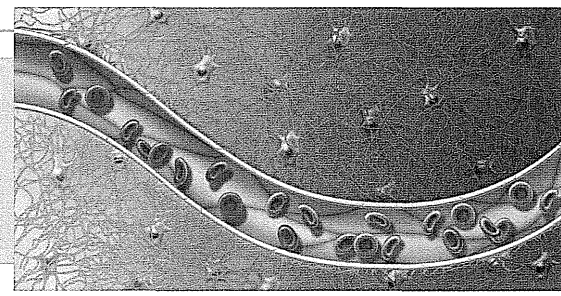

Neuronal activity has metabolic consequences. Specifically, energy is required for the maintenance and restoration of neuronal membrane potentials. That energy is not stored within the brain, but must be continuously supplied by the vascular system through the delivery of glucose and oxygen. How can this delivery of oxygen and glucose to active neurons lead to a signal that can be measured by MRI? In this chapter, we will answer this question by describing blood-oxygenation-level dependent (BOLD) fMRI. We consider, in more detail, the changes in the vascular system that are triggered by neuronal activity, and how those changes can (somewhat counterintuitively) alter certain types of MR images. Then, we consider the spatial and temporal properties of BOLD fMRI. Some recent studies have provided striking examples of fMRI's power: mapping activation to specific cellular layers within the cortex, or determining the direction of information flow between active regions. These advances have been made possible both by improvements in scanner hardware and by new approaches to fMRI analysis. Yet, our measurements in fMRI will be ultimately limited by the spatial and temporal concordance of the BOLD signal with the underlying neuronal activity. Thus, researchers using fMRI should understand both its capabilities and its limitations.

History of BOLD fMRI

While investigating the molecular structure of hemoglobin in 1936, the American chemist and Nobel laureate Linus Pauling and his student Charles Coryell discovered a remarkable and (for our purposes) fortuitous fact of nature: the hemoglobin molecule has magnetic properties that differ depending on whether or not it is bound to oxygen. Oxygenated hemoglobin (Hb) is diamagnetic; that is, it has no unpaired electrons and zero magnetic moment. In contrast, deoxygenated hemoglobin (dHb) is paramagnetic; it has both unpaired electrons and a significant magnetic moment. Completely deoxygenated blood has a magnetic susceptibility about 20% greater than fully oxygenated blood. Pauling and Coryell noted wryly that this fact had eluded previous researchers, including the great nineteenth-century physicist Michael Faraday, only because they had not separated arterial blood (which contains only oxygenated hemoglobin) from venous blood (which contains both oxygenated and deoxygenated hemoglobin).

blood-oxygenation-level dependent (BOLD) contrast The difference in signal on T_2*-weighted images as a function of the amount of deoxygenated hemoglobin.

oxygenated hemoglobin (Hb) Hemoglobin with attached oxygen; it is diamagnetic.

diamagnetic Having the property of a weak repulsion from a magnetic field.

deoxygenated hemoglobin (dHb) Hemoglobin without attached oxygen; it is paramagnetic.

paramagnetic Having the property of being attracted to a magnetic field, though with less concentration of magnetic flux than ferromagnetic objects.

magnetic susceptibility The intensity of magnetization of a substance when placed within a magnetic field.

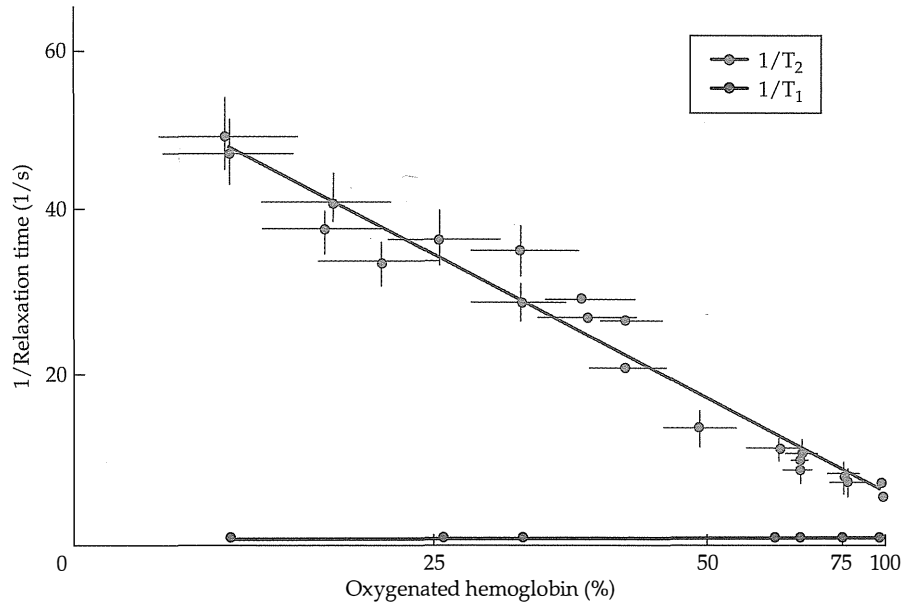

Figure 7.1 Effects of blood deoxygenation on MR relaxation constants. Shown are the differential effects of blood deoxygenation on transverse and longitudinal relaxation times, as expressed by the constants $1/T_2$ (blue circles) and $1/T_1$ (red circles). The *x*-axis indicates the square of the proportion of deoxygenated blood. Note that oxygenation increases from left to right. Clearly evident is the decrease in $1/T_2$ with increasing oxygenation; that is, the more deoxygenated hemoglobin that is present, the shorter the T_2 (which here represents loss of phase due to both spin-spin interactions and local field inhomogeneities). Note that T_1 is not affected by blood oxygenation level. (After Thulborn et al., 1982.)

Because paramagnetic substances distort the surrounding magnetic field, nearby protons will experience different field strengths and will thus precess at different frequencies, resulting in the more rapid decay of transverse magnetization (i.e., a shorter T_2*). Thus, MR pulse sequences sensitive to T_2* should show more MR signal where blood is highly oxygenated and less MR signal where blood is highly deoxygenated. This prediction was verified experimentally in the early 1980s by Thulborn and colleagues, who found that the decay of transverse magnetization depended on the proportion of oxygenated hemoglobin within a test tube of blood (Figure 7.1). They noted that the magnitude of this effect increased with the square of the strength of the static magnetic field. At a low field strength (i.e., less than 0.5 T), there was little difference between the transverse relaxation values for oxygenated and deoxygenated blood, but in higher fields (i.e., 1.5 T or greater), their values differed significantly. So, strong static magnetic fields are necessary for MR imaging of T_2*-weighted contrast in blood. These results showed that changes in blood oxygenation could, in principle, be measured using MRI.

Discovery of BOLD contrast

During the late 1980s, Seiji Ogawa, a research scientist at Bell Laboratories, investigated the possibility of examining brain physiology using MRI. Ogawa and his colleagues recognized that MRI was ill-suited for examining physiological processes directly. Since standard MRI contrasts are based on properties of hydrogen, the ubiquity of hydrogen in water throughout the body precludes the detection of the very subtle changes in concentration associated with most metabolic reactions. For MRI to be useful in measuring physiology, it would need to be sensitive to some indirect measure of metabolism. One possibility was blood flow, since metabolic processes require oxygen that is supplied through hemoglobin within red blood cells. Based on the earlier work by Thulborn and colleagues, Ogawa hypothesized that manipulating the proportion of blood oxygen would affect the visibility of blood vessels on T_2*-weighted images.

In a seminal 1990 study, Ogawa and colleagues tested this hypothesis by scanning anesthetized rodents using high-field (7.0 T and greater) MRI. To

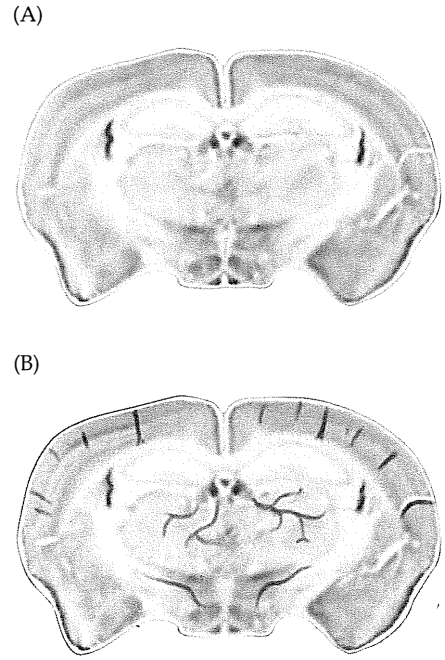

Figure 7.2 A schematic illustration of blood-oxygenation-level dependent (BOLD) contrast. Ogawa and colleagues manipulated the amount of oxygen in the blood of rats by adjusting the contents of the air that the rats breathed. (A) When the rats breathed pure oxygen, the cortical surface had a uniform texture on images sensitive to T_2* contrast. (B) But when the rats breathed normal air, there were areas of signal loss, shown as lines corresponding to blood vessels within the cortex. These lines indicated areas with increased amounts of deoxygenated hemoglobin. This forms the basis for BOLD contrast. (After Ogawa et al., 1990.)

manipulate blood oxygenation, they changed the proportion of oxygen that the animals breathed. When the rodents breathed pure oxygen, gradient-echo images of their brains showed only structural differences between tissues (Figure 7.2A). But when the rodents breathed normal air (21% oxygen), the images took on a very different character. Thin dark lines became visible throughout the cerebral cortex, usually perpendicular to its surface (Figure 7.2B), and if the oxygen content was further reduced to 0%, the lines became even more prominent. They attributed these thin lines to the magnetic susceptibility effects of paramagnetic deoxygenated hemoglobin in blood vessels. Conversely, when the hemoglobin was bound to oxygen, it was diamagnetic and had little effect on the surrounding magnetic field.

To verify this interpretation, they placed test tubes with oxygenated or deoxygenated blood into a saline-filled container and created images using both spin-echo and gradient-echo pulse sequences. Recall from Chapter 5 that spin-echo images are largely insensitive to T_2* effects, whereas gradient-echo images are distorted by T_2* decay. The tubes containing oxygenated blood appeared as black circles on both types of images, since the blood had shorter T_2* values than the surrounding saline (Figure 7.3A and B). The spin-echo image of the deoxygenated blood was likewise nearly normal (Figure 7.3C). The largest effect by far was observed for gradient-echo images of the deoxygenated blood, which exhibited a dramatic signal loss that extended well beyond the test tube (Figure 7.3D). These results demonstrated unequivocally that deoxygenated blood decreases the measured MR signal in T_2* images.

Ogawa and colleagues speculated that this blood-oxygenation-level dependent contrast could identify areas of increased brain activity. They

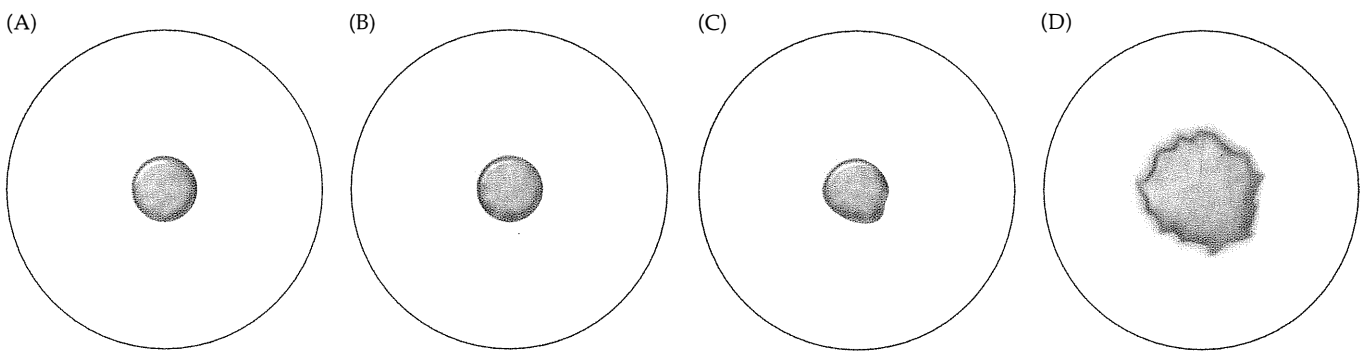

Figure 7.3 Magnetic properties of oxygenated and deoxygenated hemoglobin. To verify that the effects illustrated in Figure 7.2 resulted from changes in blood oxygen level, Ogawa and colleagues compared images of oxygenated and deoxygenated blood collected using both spin- and gradient-echo imaging. The images of oxygenated blood were not distorted, regardless of whether spin-echo (A) or gradient-echo (B) images were acquired. The spin-echo image of the deoxygenated blood (C) was slightly distorted, but the distortion did not extend to the area surrounding the test tube. However, there was substantial signal loss surrounding the gradient-echo image of the deoxygenated blood (D), showing that the presence of deoxygenated hemoglobin reduces the MR signal from water molecules outside of the test tube in adjacent space. (After Ogawa et al., 1990b.)

hypothesized two possible nonexclusive mechanisms. First, neuronal activity might increase oxygen consumption, which would increase the amount of deoxygenated hemoglobin, given a constant blood flow. Alternatively, increased blood flow in the absence of increased metabolic demand might decrease the amount of deoxygenated hemoglobin.

To evaluate the contribution of oxygen consumption to BOLD contrast, Ogawa and colleagues manipulated the gases inhaled by anesthetized rats while collecting T_2* images and measuring brain activity using concurrent EEG. At a relatively high anesthesia level (3.0% halothane), there was reduced spontaneous brain activity and relatively little BOLD contrast, but at a low anesthesia level (0.75% halothane) there was both increased brain activity and greater BOLD contrast. These results indicated that the reduction in the BOLD signal depended on the metabolic demand for oxygen. To evaluate the effect of blood flow on BOLD contrast, they compared two inhalant conditions: pure (100%) oxygen and a mixture of 90% oxygen and 10% carbon dioxide. Carbon dioxide in the blood does not have significant paramagnetic effects, but it does increase overall blood flow (e.g., it increased velocity in the sagittal sinus by about 300%). While significant BOLD contrast was observed in the pure oxygen condition, the contrast disappeared when the animals breathed the CO_2 mixture. The researchers inferred that with greater blood flow in the absence of increased metabolic demand, the deoxygenated hemoglobin is essentially flushed from the venous system, leaving only oxygenated hemoglobin that does not reduce the BOLD signal.

In summary, BOLD contrast depends on the total amount of deoxygenated hemoglobin present in a brain region, which in turn depends on the balance between oxygen consumption and oxygen supply. When neuronal activity increases, one might predict that oxygen consumption will also increase, leading to more deoxygenated hemoglobin and a darker MR image, as Ogawa and colleagues originally hypothesized. Yet, increased neuronal activity actually *increases* the signal of T_2* images! How can this be? The answer requires a more complete exploration of the relationships between cerebral blood flow, blood oxygenation level, and metabolism.

The coupling of metabolism and blood flow

Glucose is the major energy source for the brain, and oxygen facilitates the most efficient conversion of glucose to ATP. In the 1970s, Sokoloff and colleagues used an invasive imaging technque known as autoradiography to establish that regional brain changes in the rate of glucose metabolism were coupled with an increase in blood flow to that same region. The overall accounting of glucose and oxygen consumption during oxidative metabolism is given by Equation 7.1:

$$C_6H_{12}O_6 + 6O_2 = 6CO_2 + 6H_2O \tag{7.1}$$

Each glucose molecule to be oxidized requires the consumption of six oxygen molecules, which together lead to six carbon dioxide and six water molecules as products. Thus, the ideal oxygen-to-glucose index (OGI) would be 6:1 if all of the glucose that entered the brain were oxidatively (i.e., aerobically) metabolized. Brain measurements performed under resting conditions have established an OGI of approximately 5.5:1, indicating that while the vast majority of glucose metabolism in the brain is oxidative, a small but significant glucose fraction may be metabolized nonoxidatively (i.e., anaerobically). The rates of oxygen and glucose consumption during local neuronal activity may differ, however, and this fact has engendered considerable controversy that persists today.

In an influential series of PET experiments (see Box 7.1) conducted in 1988 by Fox, Raichle, and their colleagues, cerebral blood flow (CBF), cerebral meta-

autoradiography An invasive imaging technique that labels molecules using radioactive isotopes and then measures the concentration of those molecules by exposing slices of tissue to photographic emulsions.

BOX 7.1 PET Imaging

Positron emission tomography, or PET, is a powerful functional imaging technique. At the beginning of a PET study, the researcher uses a particle accelerator called a cyclotron to create a radioactive isotope, or tracer, that can be attached to a molecule to enter a biological pathway of interest. For example, ^{18}F, a radioactive isotope of fluorine, can be attached to glucose, creating the molecule fluoro-2-deoxy-D-glucose, or FDG. The fluorine tracer does not prevent FDG from entering into the normal pathways for glucose metabolism. Thus, researchers can inject a bolus of FDG into a vein and then use imaging to determine where it is taken up by cells.

As the radioactive isotope decays, it emits a positron (the antimatter counterpart of an electron). When the emitted positron collides with a nearby electron (Figure 1A), they are mutually annihilated and produce two gamma rays that travel in opposite directions. The gamma rays are subsequently detected by their near-simultaneous impact on opposite sides of a ring of scintillation crystals that surround the subject's head (Figure 1B). A computer algorithm then evaluates the number and timing of impacts at all of the crystals surrounding the head and traces the paths taken by the gamma rays back to their origins. Through this method, the distribution of the radioactive isotope in the brain can be measured, and changes in glucose uptake in different brain regions caused by sensory, motor, or cognitive activity can be determined (Figure 1C). PET imaging can also be used to study oxygen metabolism or blood flow using ^{15}O, a radioactive isotope of oxygen. Certain neurotransmitters can be similarly labeled. For example, ^{18}F can be attached to dopamine to study its distribution in the human brain.

PET scanning provides a relatively direct and easily interpretable measure of brain metabolism, and for many years it was the mainstay of human functional neuroimaging. However, its dependence on high-energy gamma ra-

(continued on next page)

positron emission tomography (PET) A functional neuroimaging technique that creates images based on the movement of injected radioactive material.

Figure 1 Positron emission tomography (PET) imaging. Until the mid-1990s, the most common functional neuroimaging technique was PET, which relies on the injection of a radioactive tracer into the bloodstream. As the tracer decays, it emits positrons, which travel a short distance before colliding with an electron (A). The collision results in a pair of emitted gamma rays that travel in opposite directions. The PET scanner (B) consists of a series of coincidence detectors that record the simultaneous arrival of these gamma rays. Depending on the tracer used, PET can be sensitive to several aspects of brain metabolism, including blood flow or oxygen consumption. The output of a PET scan indicates the number of events measured from each voxel during a long time period. (C) These numbers can be converted to statistical maps, which can then be overlaid on anatomical images, often from MRI. (C courtesy of Dr. David Madden, Duke University.)

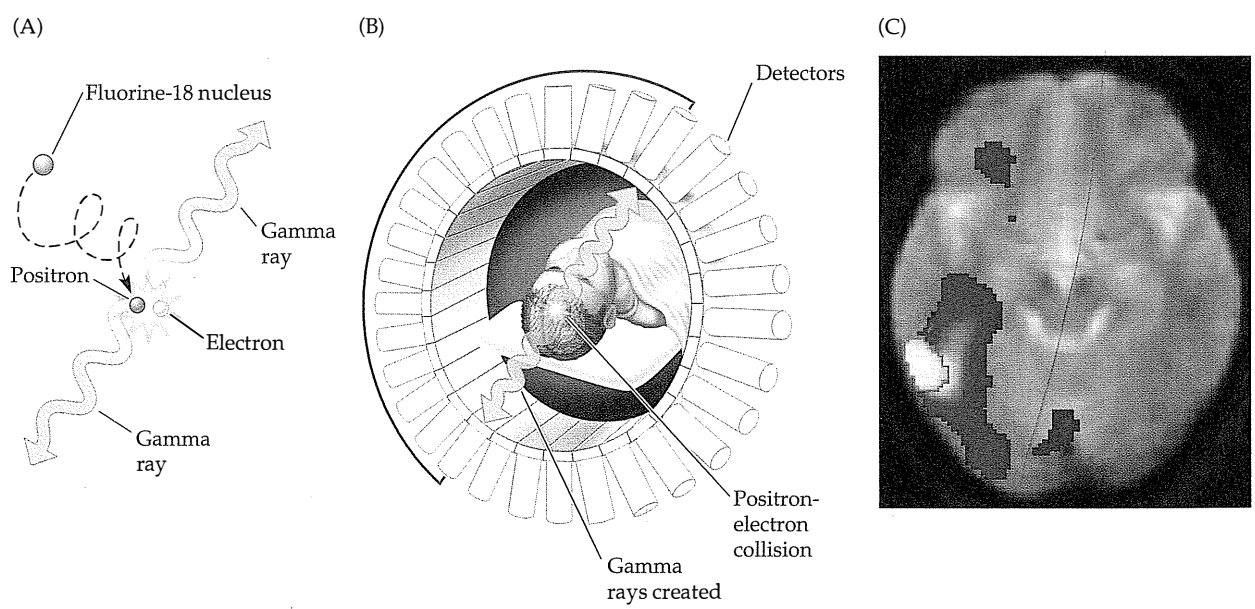

BOX 7.1 *(continued)*

diation (or **ionizing radiation**, as named for its potential to break chemical bonds) presents problems for human studies. Radiation exposure in human research is carefully regulated, and subjects can participate in only a few PET scans. There are other drawbacks to PET imaging. Its spatial resolution is limited by the distance the positron travels away from the labeled molecule before it collides with an electron. This is dependent on the particular isotope used; for example, positrons emitted by ^{18}F will travel about 2.6 mm before encountering an electron. Recall that it is the location of the gamma ray emission that is localized and not the location of the molecule of interest. More limiting, however, is the very poor temporal resolution of PET imaging. Many emissions must be detected to produce an image with sufficient signal-to-noise ratio, requiring the collection of data over a long period of time. For example, an image of blood flow based on ^{15}O may take 90 seconds to acquire, while an image of glucose metabolism based on ^{18}F may take 30 to 40 minutes to acquire. These acquisition times severely limit the temporal resolution of PET imaging and restrict the types of experimental designs that can be used.

When compared with PET imaging, MRI has several advantages. Because MRI does not involve ionizing radiation, subjects can participate repeatedly without the cumulative health risks of radiation exposure. Images with high signal-to-noise ratios can be acquired in less than a second, and spatial resolution is limited primarily by the motion of the sample and by the signal-to-noise ratios, not by the inherent uncertainty in the measurement technique. And, fMRI can be used in event-related designs to identify processes specific to one phase of a complex experiment, to understand changes in functional connectivity, or to classify data on a trial-by-trial basis. But these advantages should not lead to the incorrect assumption that PET imaging has no relevance for modern neuroscience. Even with the caveats described above, PET can be used to image glucose or oxygen consumption directly. In comparison, BOLD fMRI does not provide any direct information about metabolic processes, but instead measures an indirect correlate of those processes. Moreover, only PET can be used to create images specifically sensitive to a single metabolite or neurotransmitter. Thus, for many important questions about brain physiology and function, PET imaging remains the technology of choice.

ionizing radiation Electromagnetic radiation that has sufficient energy to separate electrons from electrically neutral atoms, turning them into ions.

bolic rate for glucose (CMR_{glu}), and cerebral metabolic rate for oxygen ($CMRO_2$) were measured during rest and during visual stimulation. When subjects were exposed to prolonged visual stimulation, CBF in the visual cortex increased by 50% and CMR_{glu} increased by 51%, consistent with Sokoloff's autoradiographic findings in animals. However, $CMRO_2$ increased by only 5%. The authors concluded that most of the increased uptake of glucose during stimulation was not oxidized but rather was metabolized nonoxidatively through anaerobic glycolysis. Recalling our discussion from the previous chapter, anaerobic glycolysis is relatively inefficient (but fast), yielding only two ATP molecules for each glucose molecule consumed, and thus the energy produced from the increased glucose uptake would be relatively small. Corroborating evidence has come from studies by Prichard and colleagues, who demonstrated that extended visual stimulation results in increased lactate production, which would be expected, since lactate is the primary end product of anaerobic glycolysis.

Not all investigators accepted the apparent uncoupling of $CMRO_2$ and CMR_{glu} during stimulation as indicative of anaerobic metabolism. In 1996 Malonek and Grinvald used a high-resolution optical imaging method in which the surface of the visual cortex of a cat was exposed to a light source and the reflected light was analyzed. Because different molecules (e.g., oxygenated and deoxygenated hemoglobin) absorb light of different wavelengths, the spec-

trum of the reflected light can be used to determine the presence of different molecules at any given location in the cortex. The authors selectively activated small, spatially segregated populations of neurons in the visual cortex by presenting the cat with images of line gratings at particular orientations. The expected spatial pattern of neuronal activation across the visual cortex could then be compared with the spatial patterns of oxygenated and deoxygenated hemoglobin accumulation, and the optical imaging method allowed for measurements with high spatial and temporal resolution.

The results of the experiment showed that the evoked changes in hemoglobin and deoxygenated hemoglobin were quite distinct (Figure 7.4). The deoxygenated hemoglobin–time curve showed a rapid increase that peaked about 2 s after the onset of the stimulus and then rapidly declined. By 6 s after the onset of the stimulus, the deoxygenated hemoglobin signal had declined to well below the prestimulus baseline level. In contrast, the oxygenated hemoglobin signal had a slightly delayed onset and then a much slower rise to a peak at about 5 to 6 s after stimulus onset. It was also much greater in amplitude than the deoxygenated hemoglobin signal. Moreover, unlike the weak deoxygenated hemoglobin signal, the spatial pattern of the oxygenated hemoglobin signal did not reflect the expected pattern of neuronal activity. Indeed, it extended into regions where there should have been no neuronal activity.

Several conclusions can be drawn from this experiment. First, the active neurons utilized whatever oxygen was already present to support their initial activity. This suggests that increased metabolism at the onset of activation is oxidative. Second, there is an exquisite spatial correspondence between the initial neuronal activity and the initial increase in the deoxygenated hemoglobin signal. Third, the poor correspondence and greater spatial extent of the later oxygenated hemoglobin response indicates that the regulation of blood flow and oxygen delivery to the cortex is on a coarse spatial scale and mismatches metabolic needs. As Malonek and Grinvald put it, this is analogous to "watering the entire garden for the sake of one thirsty flower." These data suggest that the uncoupling reported by Fox and Raichle results not from an increase in anaerobic glycolysis but instead from a superfluous perfusion of oxygenated blood that exceeds metabolic need. However, CMR_{glu} was not measured in this experiment, so whether the spatial pattern of the OGI matched the pattern of neuronal activity could not be determined.

Recent studies have indicated that changes in coupling between metabolism and flow may have functional consequences. Neuronal activity may lead to prolonged reductions in glucose metabolism compared with flow, and those changes may persist even after activity ceases. Moreover, the coupling between CBF and CMR_{glu} differs across regions, as shown by an intriguing 2008 paper by Gur and colleagues. These authors found that brain regions differed in whether they exhibited CBF-CMR_{glu} coupling, were hyperperfused (i.e., had greater flow than glucose metabolism), or were hypoperfused (i.e., had reduced flow compared with glucose metabolism). Those regions that were hyperperfused—including the amygdala, basal ganglia, thalamus, and cingulate cortex—might be necessary for rapid action, like detecting and responding to unexpected and important environmental events. In contrast, the hypoperfused regions might be parts of the cortex associated with complex cognition, such as much of the lateral frontal and parietal lobes. These results, though still requiring further elaboration, argue that the function supported by a region may influence its vascular properties. Note that differential coupling between regions may have consequences for BOLD sensitivity; see the 2008 paper by Ances and colleagues for such evidence.

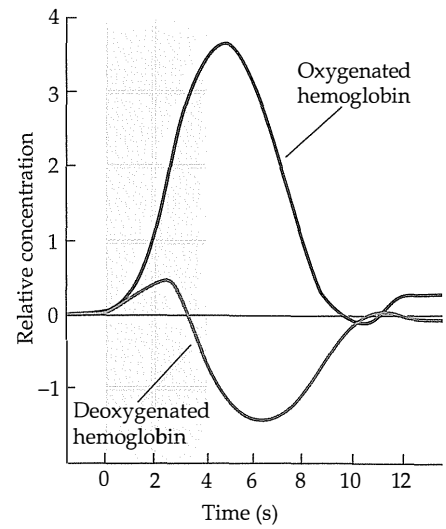

Figure 7.4 Changes in oxygenated and deoxygenated hemoglobin following neuronal stimulation. The concentration of deoxygenated hemoglobin increases rapidly at stimulus onset, peaking at about 2 s, and then declines to a minimum value about 6 s after onset, before returning to baseline at about 10 s. Note that this curve defines the BOLD hemodynamic response. The oxygenated hemoglobin concentration shows no decline, but begins rising shortly after stimulus onset and reaches a peak at about 5 to 6 s, with a slow decline to about 10 s. (After Malonek and Grinvald, 1996.)

Thought Question

Why might the brain supply blood to a larger region than that immediately surrounding neuronal activity?

Collectively, these studies help explain the paradox we noted previously, namely that the MR signal increases during neuronal activity even though deoxygenated hemoglobin decreases the MR signal. The disparity between oxygen utilization and oxygen delivery means that more oxygen is supplied to a brain region than is consumed. Fox and Raichle note that this is consistent with the experience of neurosurgeons, who have long observed that the cortex becomes more pink in color when it becomes active. As the excess oxygenated blood flows through active regions, it flushes the deoxygenated hemoglobin from the capillaries supporting the active neural tissue and from the downstream venules. So the BOLD contrast following neuronal activity occurs not because the oxygenated hemoglobin increases the MR signal but because it displaces the deoxygenated hemoglobin that had been suppressing the MR signal intensity (Figure 7.5).

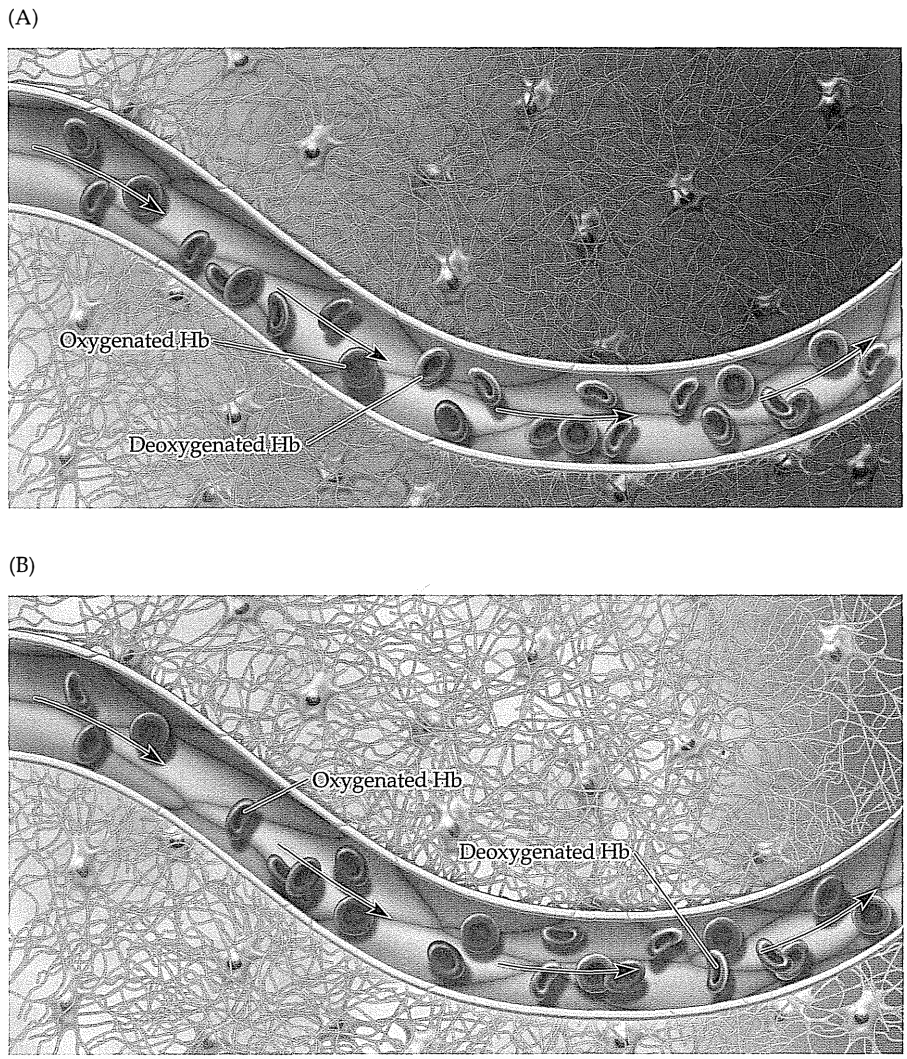

Figure 7.5 Summary of BOLD signal generation. (A) Under normal conditions, oxygenated hemoglobin (Hb) is converted to deoxygenated hemoglobin at a constant rate within the capillary bed. (B) But when neurons become active, the vascular system supplies more oxygenated hemoglobin than is needed by the neurons, through an overcompensatory increase in blood flow. This results in a decrease in the amount of deoxygenated hemoglobin and a corresponding decrease in the signal loss due to T_2^* effects, leading to a brighter MR image. (After Mosley and Glover, 1995.)

The Growth of BOLD fMRI

From the work of Ogawa and colleagues, it was clear that changes in blood oxygenation could be measured using MRI. The next step was to demonstrate that BOLD contrast could be used to localize different functions in the human brain. The first functional studies used simple visual and motor tasks, such as watching a flashing checkerboard or squeezing one's hand repeatedly. Such simple tasks were not intended to provide new information about the organization of the brain; indeed, the locations of the visual and sensorimotor cortices had been known since the end of the nineteenth century! Instead, the first fMRI studies strived to replicate well-established findings, thus validating the capabilities of the new technique. Before describing these early studies, we must resume our historical discussion from Chapter 1 so that the early fMRI studies can be considered in the context of their times.

Contributing factors

Few scientific discoveries are made in isolation. Most result from a combination of factors, often including external societal influences, that together allow a nascent idea to flourish. The birth of fMRI was no exception (Figure 7.6). Consider that the paramagnetism of hemoglobin had been known for almost a half century before Thulborn and colleagues examined oxygenated and deoxygenated blood using MRI, and even then it would be another decade before the first fMRI studies were published. This slow pace of progress did not

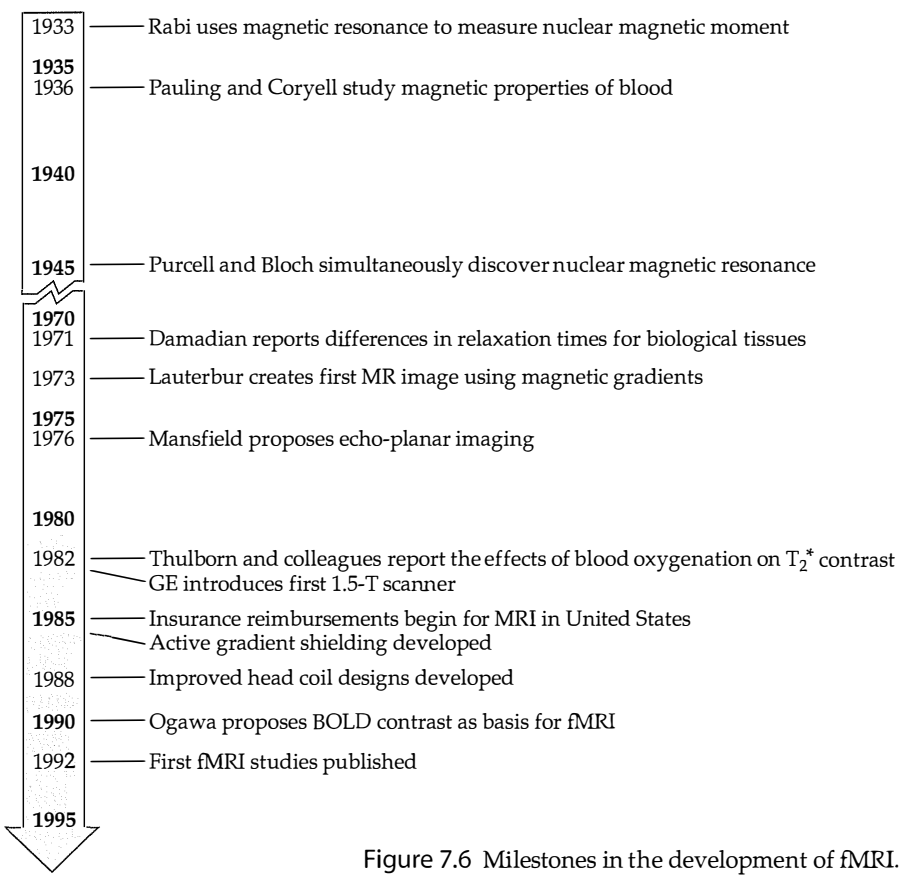

Figure 7.6 Milestones in the development of fMRI.

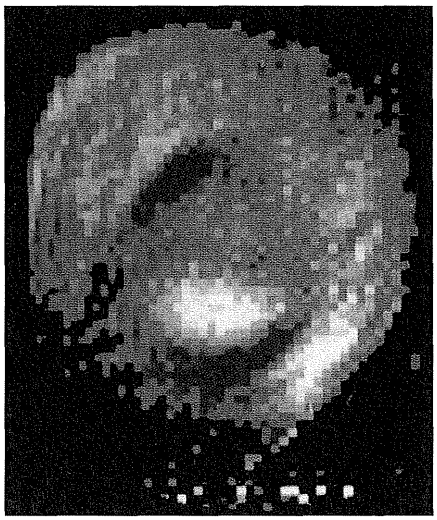

Figure 7.7 One of the earliest EPI images. This cross section of a human finger represents one of the first uses of echo-planar imaging to scan living human tissue. (From Mansfield and Maudsley, 1977.)

reflect a lack of interest in the brain—there was considerable interest in scalp recordings of electrical potentials during the 1960s and 1970s and in PET imaging during the 1980s. The extended gestation and subsequent rapid growth of fMRI shown in the timeline resulted in a large part from two external factors, both related to the clinical use of MRI.

First, improvements in pulse sequence design and scanner hardware reduced image collection time from many seconds to a few tens of milliseconds. Early MR imaging was a slow process. The first MR image, for example, was acquired at a rate of more than two minutes per voxel. In modern imaging, in which the brain may consist of many thousands of voxels, such a slow acquisition rate would correspond to approximately one volume per month! As discussed in Chapter 1, the development of echo-planar imaging (EPI), largely through the work of Peter Mansfield in the late 1970s, allowed an entire image to be collected following a single excitation pulse (Figure 7.7). Yet, limitations in the scanning hardware delayed the practical implementation of EPI. Rapid changes in gradient fields, as required by EPI, could induce currents in metal parts within the scanner hardware, introducing artifacts in recorded images. Rather than change scanner hardware to ameliorate this problem, manufacturers adopted other approaches, such as fast low (flip) angle shot, or FLASH, sequences, that did not tax scanner hardware as significantly as EPI. Not until about 1985 were active gradient-shielding techniques developed, largely through the work of Mansfield and colleagues, that incorporated an outer gradient winding in the opposite direction. The outer winding reduced currents in the scanner hardware but added complexity and increased power requirements. Major manufacturers began adding actively shielded gradients to their standard scanner platforms over the following years. By the early 1990s, fast switching gradient technology proposed by Turner, and high linearity developed by Wong and colleagues, together provided the advances needed for EPI to be practical.

The second key factor that contributed to the growth in fMRI was the increasing *clinical* applicability of structural MRI. Most of the relatively few MR scanners used in the 1970s were devoted to industrial applications, and almost none were being used in hospital settings. The workhorses of diagnostic imaging were computerized tomography (CT) scanners, which allowed clinicians to assess damage to soft-tissue structures (Figure 7.8). The three-dimensional scans were demanded by doctors and patients alike, serving both to draw new patients to hospitals that possessed the latest equipment and to generate new income from the expensive procedures. Despite the capital commitment required (typically more than $300,000), by the early 1980s more than 5000 CT scanners were in use worldwide.

Around the same time, hospitals began considering the use of MRI as a complement to CT scanning, in part due to the enthusiasm of pioneers like Raymond Damadian (see Chapter 1). Several medical device companies, including Damadian's FONAR Corporation, General Electric (GE), and Varian, developed high-field MRI scanners that promised image resolution that would far surpass that of CT. The first clinical 1.5-T scanner was installed at Duke University by GE in 1982, and this would remain the most common field strength for both clinical and research purposes for more than two decades.

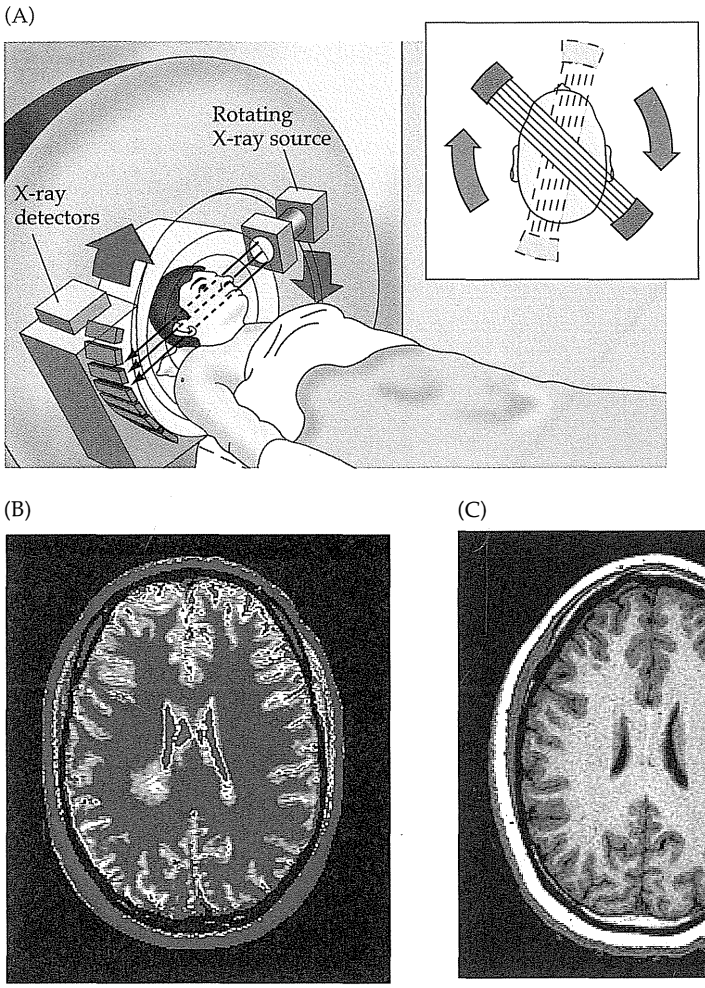

Figure 7.8 Computerized tomography (CT) imaging. (A) CT uses a moving X-ray source to create a three-dimensional map of underlying tissue. While CT imaging can distinguish tissue types, such as gray/white matter from CSF within the brain (B), it is sensitive to the same limitations on resolution and contrast as conventional X-rays. For comparison, a structural MRI image (C) provides much better contrast between many types of tissue.

By 1985, MR scanning was sufficiently well established that insurance companies in the United States began reimbursing for MRI procedures. The cost of MRI scanners was still very high, often as much as $2 million, but hospitals were now able to recoup those costs through many procedures. As had happened previously with CT, this new clinical demand sparked an explosion in the number of MRI scanners. Just 20 years after the introduction of the first high-field scanner, there were more than 10,000 such scanners worldwide. Although most were devoted to patient care during normal business hours, researchers at many institutions were able to use the scanners at night and on weekends for research into brain function. These research studies were often facilitated by supplemental hardware, such as gradient insert coils, that improved on the hardware provided by the clinical manufacturers. The advances that facilitated the first fMRI studies, therefore, were developed largely to meet the clinical demand for structural MRI.

Early fMRI studies

In the early 1990s, many research laboratories were competing to create the first images of brain function using MRI. Some explored the use of exogenous contrast agents (see Box 7.2). Others investigated the new endogenous BOLD

BOX 7.2 Functional Studies Using Contrast Agents

BOLD contrast depends on the paramagnetic properties of deoxygenated hemoglobin, which causes a loss of phase coherence in nearby protons, and is measurable using T_2* imaging. Yet, the effects of hemoglobin on nearby protons are tiny: even large BOLD effects result in signal changes of only about one percent. Another method for increasing image contrast is to use exogenous contrast agents, highly paramagnetic substances that can be injected into the bloodstream but do not cross the intact blood–brain barrier. Common contrast agents like gadolinium diethylenetriaminepentaacetic acid (Gd-DTPA) are well tolerated by most people, with mild headache and nausea as the most common side effects. Contrast agents have great importance for clinical imaging, especially in the detection of pathological tissue, including brain tumors. Under normal conditions, the diffusion of a contrast agent like Gd-DTPA through the bloodstream will reduce T_1 values of hydrogen protons in the blood, increasing signal within blood vessels but not elsewhere. But if there is damage to the blood–brain barrier due to brain pathology, the contrast agent may escape from the bloodstream and enter the surrounding tissue, resulting in increased signal on T_1-weighted images.

This effect on T_1 relaxation, though clinically important, provides no information about brain function. Rather, it is the effect of contrast agents on local magnetic field homogeneity that enables functional studies. Because the injected contrast agent is highly paramagnetic and has a very strong magnetic moment, it causes a considerable inhomogeneity between the tissue outside the blood vessel and the contrast-enhanced blood within. Remember from Chapter 5 that sharp gradients in magnetic field homogeneity can cause signal losses known as susceptibility artifacts, due to differential effects of the magnetic gradient on spin precession. Pulse sequences sensitive to T_2* effects can measure the local concentration of the contrast agent over time. Unlike BOLD contrast, which depends on both blood flow and oxygen extraction, exogenous contrast methods generally rely only on blood volume changes associated with functional activity. In addition, they have a limited lifetime due to their passage through the brain and subsequent dispersal through the vascular system. But, because the exogenous contrast agent is much more paramagnetic than deoxygenated hemoglobin, it causes much larger signal changes that can be extracted from a single pass of the agent through the brain.

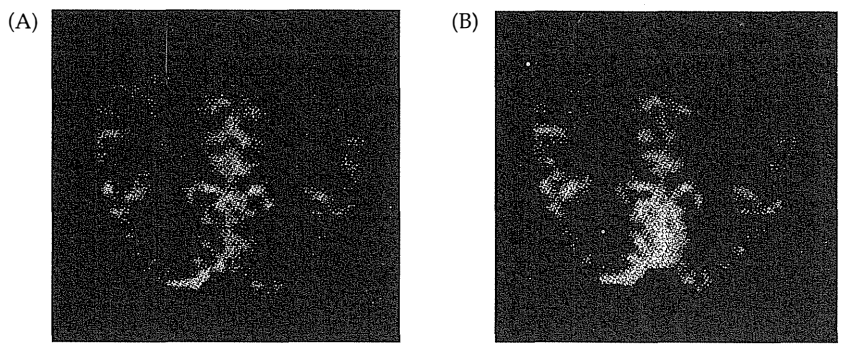

Figure 1 Functional MRI using exogenous contrast. This figure provides the first example of functional mapping of the human brain using MRI. Subjects were injected with the contrast agent Gd-DTPA and exposed to darkness or rapidly flashing lights. Compared with darkness (A), there was a significant increase in cerebral blood volume when the flashing lights were presented (B), as shown on these axial slices (visual cortex at bottom of images).

The first fMRI study to use exogenous contrast (and the first fMRI study of any form) was reported by Belliveau and colleagues in 1991. They measured visual cortex activation using spin-echo EPI at 1.5 T following injection of a bolus of Gd-DTPA. In the test condition, subjects viewed a visual pattern that flashed at a rate of about 8 Hz, and in the control condition there was no visual stimulus. Based on electrophysiological data, this rate was known to robustly activate the primary visual cortex. The authors hypothesized that, following injection of the contrast agent, the raw MR signal would decrease due to increased magnetic susceptibility. Furthermore, the magnitude of this decrease should be greater for active brain regions due to local increases in blood volume. As shown in Figure 1, there was a transient decrease in MR signal associated with passage of the contrast agent through the primary visual cortex. There was a delay of about 8 to 10 s between the injection of Gd-DTPA and the onset of the signal decrease. This delay reflects the time required for the contrast agent to travel from the injec-

contrast agent A substance injected into the body to increase image contrast.

bolus A quantity of a substance that is introduced into a system and then progresses through that system over time.

BOX 7.2 *(continued)*

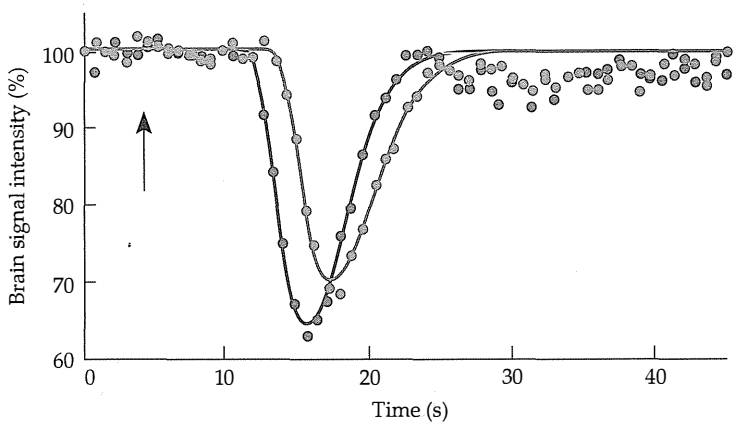

Figure 2 The plot shows the passage of the contrast agent through the visual cortex, in conditions of visual stimulation (red circles) and darkness (blue circles), following injection (black arrow). In both cases there are significant decreases in the MR signal due to the magnetic susceptibility effects of the contrast agent. However, the decrease occurs earlier and is larger in the activated condition. (After Belliveau et al., 1991.)

tion site, which was the antecubital vein in the arm, through the heart to the primary visual cortex. Although decreases in signal intensity in the visual cortex were present in both the test and control conditions, the decrease was larger and occurred earlier for the flashing pattern than for darkness (Figure 2). From this result, the researchers concluded that blood volume had increased in the calcarine cortex and thus that neurons in that part of the brain are associated with visual perception.

The power of exogenous contrast agents comes from the enormous signal changes they induce. Even in this early experiment, the signal change observed due to the contrast injection was about 30%. The difference between the test and control conditions was on the order of 5%. To appreciate the magnitude of such changes, compare them to the much smaller signal changes observed in BOLD fMRI. Furthermore, the clear differences shown in Figure 2 represent two trials, one test and one control, from a single subject. In comparison, modern BOLD studies usually represent data combined from many subjects with many trials per condition.

Despite this power, exogenous contrast agents are rarely used for fMRI research. One limitation can be seen in the time course of signal change. Because of the substantial transit delay of the agent, it is challenging to accurately measure the timing of brain activity. And since a single bolus is used, one measurement of signal change is obtained per trial. If one wants to study two types of trials, like Belliveau and colleagues, two injections are required. In general, as more conditions are added, more injections are needed. These requirements preclude some types of analyses that are possible with endogenous BOLD contrast, such as the sorting of many trials based on accuracy or reaction time, fast event-related designs, evaluation of brain response as a function of stimulus sequence, and complex parametric studies. In addition, many subjects are less likely to participate in studies that require intravenous injection. So, while a number of researchers are actively investigating the use of contrast agents for fMRI (see Chapter 12), especially for studies in animals, nearly all current fMRI studies use endogenous BOLD contrast.

contrast mechanism developed by Ogawa and colleagues, culminating in three studies published in 1992. The first study, by Kwong and colleagues, used a gradient-echo EPI sequence at 1.5 T to study activation in the visual cortex. They evoked visual cortex activation by alternating 60 s periods of visual stimulation (e.g., the flashing of an LED pattern) with 60 s baseline periods of darkness. At the onset of the stimulation period, there was a sharp increase in MR signal around the calcarine fissure, increasing by about 3% within 10 s (Figure 7.9). The activation increase was sustained for the duration of the visual stimulation period, then receded to the baseline level once darkness returned. Despite its crudeness in both timing and spatial resolution by today's standards, this study provided the very first example of BOLD fMRI.

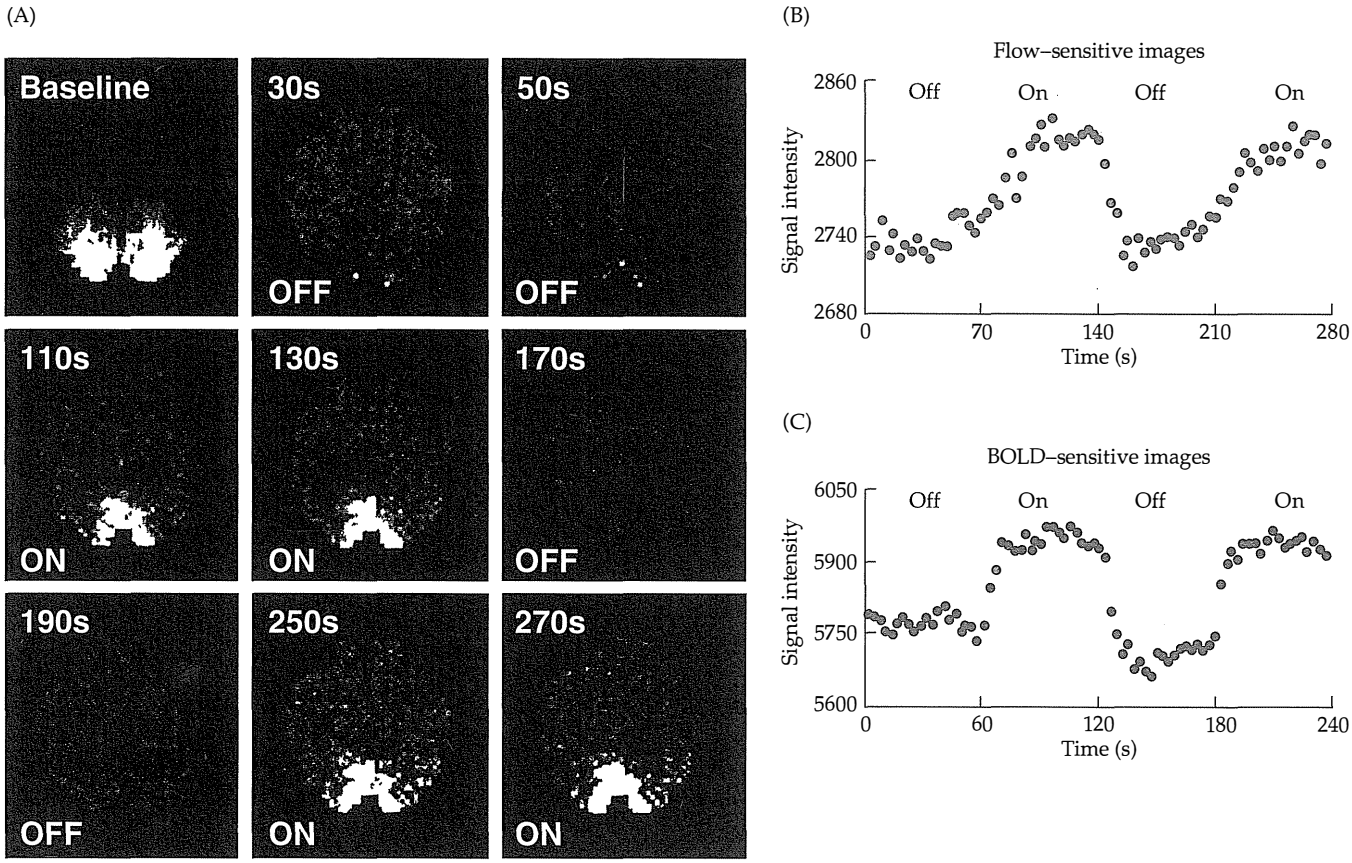

Figure 7.9 The first use of BOLD fMRI for functional mapping of the human brain. In this study, fMRI data were collected that were sensitive to two forms of contrast: spin-echo inversion recovery (IR) images were sensitive to changes in blood flow, and gradient-echo images were sensitive to BOLD contrast. (A) The area of activation for the flow-sensitive IR sequence, which revealed changes in the occipital lobe (bottom of the images) during periods of visual stimulation (ON), compared to periods with no visual stimulation (OFF), with representative time points indicated in seconds. (B, C) The time courses of activation measured using each technique. Note the use of a long-interval blocked design, consistent with PET studies of that time. (After Kwong et al., 1992.)

These findings were replicated in a similar study published the following month by Ogawa and colleagues, who also evaluated changes in fMRI gradient-echo signals resulting from long-duration (e.g., 100 s) presentations of visual stimuli. Unlike the Kwong study, however, they used a pulse sequence that was limited to an effective TR of about 10 s, and collected data on a high-field (4.0 T) scanner. They also manipulated the TE to show that the BOLD signal depends on T_2* effects, and not T_1, which should be independent of the TE. At a TE of 40 ms, the stimuli caused changes in the BOLD intensity, whereas at a very short TE of 8 ms, the stimulus-related effects disappeared. Almost simultaneously, a third paper was published by Bandettini and colleagues, describing the use of a motor task in which subjects repeatedly touched their fingers to their thumbs for long blocks of time. Data recorded using gradient-echo EPI at 1.5 T showed significant activation in the primary motor cortex.

While most early fMRI studies used long stimulus durations, work reported later in 1992 by Blamire and colleagues examined responses to individual visual stimuli using a spin-echo EPI sequence at 2.1 T. They found that lengthy visual stimuli (10 s to 90 s) generated long-duration and large (about 10%) increases in signal in the visual cortex, similar to the findings of Kwong and colleagues. More remarkable were the results from much shorter-duration stimuli. Even the shortest stimulus (2 s) evoked a significant signal change within the visual cortex (Figure 7.10). The authors noted that there was a short but measurable delay between the stimulus presentation and the MR signal change. On average, the first observable fMRI change in the primary visual

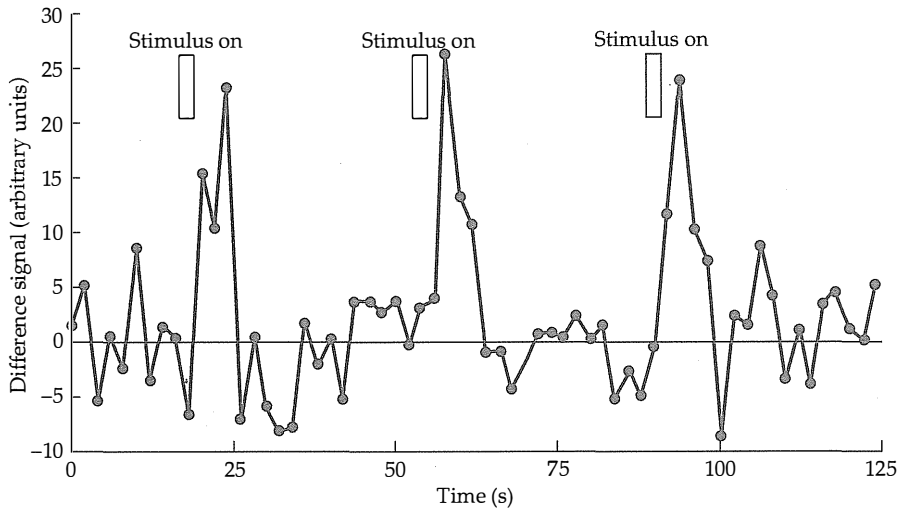

Figure 7.10 Changes in BOLD activation associated with presentations of single events. This graph provides the first example of increased BOLD response to single events. While event-related methods are extremely common in contemporary fMRI studies, their use did not become widespread until the late 1990s. (After Blamire et al., 1992.)

cortex occurred about 3.5 s after the onset of the stimulus. This was the first demonstration of the time course of the BOLD hemodynamic response evoked by a single stimulus event.

Thought Question

Why was it critical to observe measurable BOLD activation to short-duration stimuli? What implications does this have for fMRI experimentation?

It is instructive to compare these early studies with current fMRI practices. At first glance, the procedures and equipments seem very similar. The field strengths reported above (i.e., 1.5 T, 2.1 T, 4.0 T) are similar to those of MRI scanners used now, more than fifteen years later. EPI pulse sequences are also still used commonly, though other sequences such as spiral imaging have grown in popularity. Yet, there are subtle differences between the studies described above and modern studies. The gradient coils on early scanners generated only weak magnetic gradients that could not be changed rapidly, constraining the rate of data acquisition (i.e., early studies collected data from only one or a few slices, despite having relatively long TRs). Now, the collection of 20 or more slices per second is commonplace. Even more important are differences in the approach to data analysis. None of these early studies used preprocessing techniques, which will be introduced in Chapter 8, to correct for head motion or physiological variability. (Blamire and colleagues did note that voxels on the edge of the brain showed systematic oscillations in signal intensity, which they attributed to pulsatile motion of the brain associated with the cardiac cycle.) Nor did they use modern statistical approaches based on the general linear model, which will be introduced in Chapter 10. Instead, they used simple statistics to evaluate whether activation in a region of interest was greater during a task condition than during a control condition. While this approach provided adequate power for evaluating very simple visual or motor tasks, answering more complex experimental questions would require more complex approaches. Nevertheless, the basic elements of modern fMRI practice can be traced back to these early studies. They hinted at the future capabilities of fMRI, setting the stage for later research.

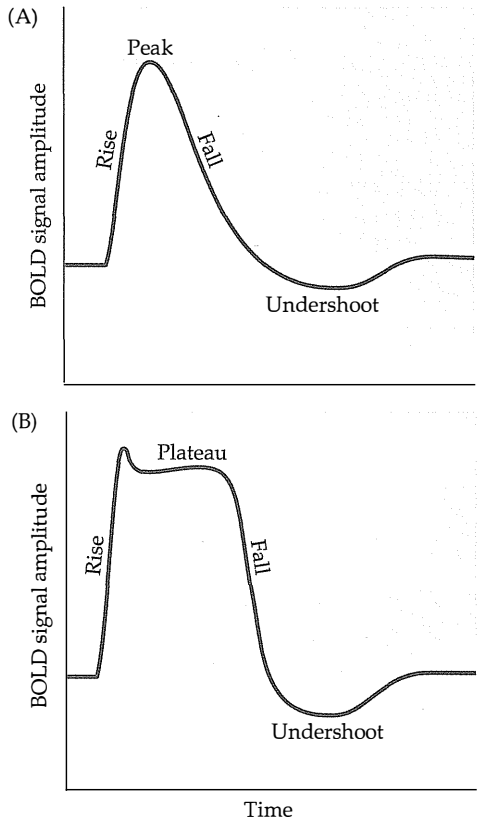

Figure 7.11 Schematic representations of the BOLD hemodynamic response. Shown are representative waveforms for the hemodynamic response to a single short-duration event (A) and to a block of multiple consecutive events (B).

The BOLD Hemodynamic Response

The change in the MR signal triggered by neuronal activity is known as the hemodynamic response, or HDR (Figure 7.11). Referring to *the* hemodynamic response is, however, a bit misleading, as its shape varies with the properties of the stimulus and, presumably, with the underlying neuronal activity. We might expect, therefore, that increasing the rate of neuronal activity would increase the amplitude of a hemodynamic response, whereas increasing the duration of neuronal activity would increase the width of the hemodynamic response. Determining the exact relationship between neuronal activity and fMRI activation, however, is complicated by the different dynamics of the two processes (Box 7.3). Cortical neuronal responses occur within tens of milliseconds following a sensory stimulus, but the first observable hemodynamic changes do not occur until 1 s to 2 s later. Thus, the hemodynamic response is said to lag the neuronal events that initiate it. Throughout the remainder of the book, we will make frequent references to different aspects of the hemodynamic response waveform, and so here we define some terms.

Remember that BOLD fMRI, defined simply, measures changes in the total amount of deoxygenated hemoglobin in a voxel over time. Yet, the quantity of deoxygenated hemoglobin depends not just on the extraction of oxygen by active neurons, but also (and more importantly) on changes in blood flow and blood volume that together shape the BOLD hemodynamic response (Figure 7.12). We can summarize the BOLD response as a series of phases. As described below, some studies have reported an initial dip of 1 to 2 s duration that has been attributed to a transient increase in the amount of deoxygenated hemoglobin in the voxel. After a short latency, the metabolic demands due to the increased neuronal activity over baseline levels

hemodynamic response (HDR) The change in MR signal on T_2* images following local neuronal activity. The hemodynamic response results from a decrease in the amount of deoxygenated hemoglobin present within a voxel.

initial dip The short-term decrease in MR signal immediately following the onset of neuronal activity, before the main positive component of the hemodynamic response. The initial dip may result from initial oxygen extraction before the later overcompensatory response.

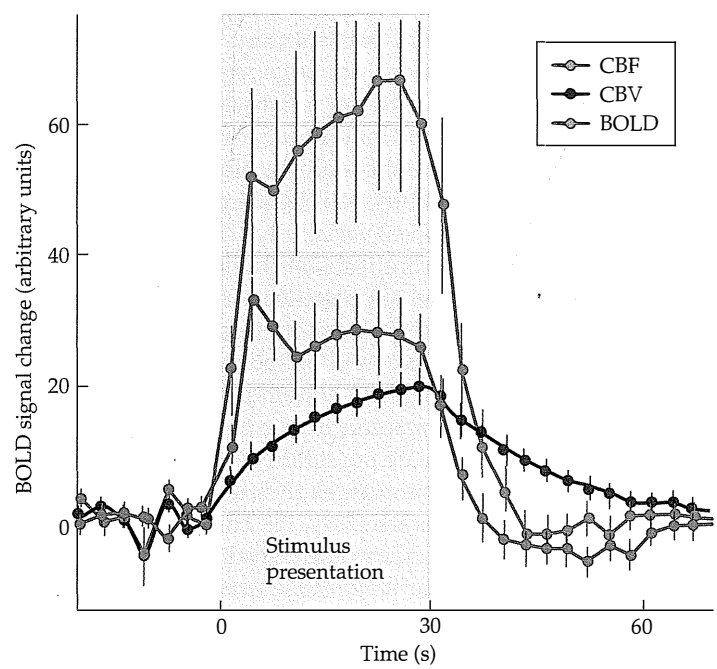

Figure 7.12 Relative changes in cerebral blood flow and cerebral blood volume following neuronal activity. This figure shows data from an experiment in which the forepaw of a rat was stimulated for a period of 30 s and the resulting changes in cerebral blood flow (CBF) and cerebral blood volume (CBV) were measured. Note that following the stimulus offset, CBF returns quickly to baseline levels but CBV returns slowly. Elevated CBV relative to CBF causes an increase in the total amount of deoxyhemoglobin that is present, which may lead to the poststimulus undershoot in the BOLD signal. (After from Mandeville et al., 1999.)

BOX 7.3 Neuronal Activity and BOLD fMRI

Both single-unit firing and field potentials provide direct, albeit different, measures of the informational transactions of neurons. While we have emphasized so far in this chapter that these measures complement fMRI data, it is important to recognize that the relationship between neuronal activity and the BOLD response remains unclear. Is there a strong correlation between BOLD fMRI measurements and these direct measures of neuronal activity? How might the integrative and signaling aspects of neuronal activity individually contribute to the BOLD signal? One might expect that both electrophysiological measures would have similar influences on the BOLD response, since the EPSPs that trigger action potentials also generate field potentials. However, summated IPSPs generate field potentials as well, but inhibit the firing of action potentials, so there are clear circumstances in which different electrophysiological measures could have different contributions. We will thus consider signaling and integrative aspects of neuronal activity separately.

Few studies have directly compared electrophysiological and BOLD fMRI measurements. In a landmark 2001 report, Logothetis and colleagues simultaneously recorded fMRI and electrophysiological data from the primary visual cortex. Anesthetized monkeys viewed a rotating visual checkerboard pattern while being scanned in a 4.7-T scanner using gradient-echo echo-planar imaging. The authors simultaneously recorded three types of electrophysiological activity: single-unit (firing of an individual neuron close to the electrode), multi-unit (the collective firing rate of neurons, particularly large pyramidal cells, within a few hundred microns), and local field potentials (synchronous changes in integrative activity from cells within a few millimeters). The results are shown in Figure 1. Single-unit and multi-unit activity occurred transiently at the onset of the stimulus and did not persist over time, while the local field potentials showed both transient and persistent activity. The local field potential activity—which includes both post-synaptic potentials and integrative activity occurring at the soma—better predicted the BOLD signal change than did the multi-unit activity, although the latter

(continued on next page)

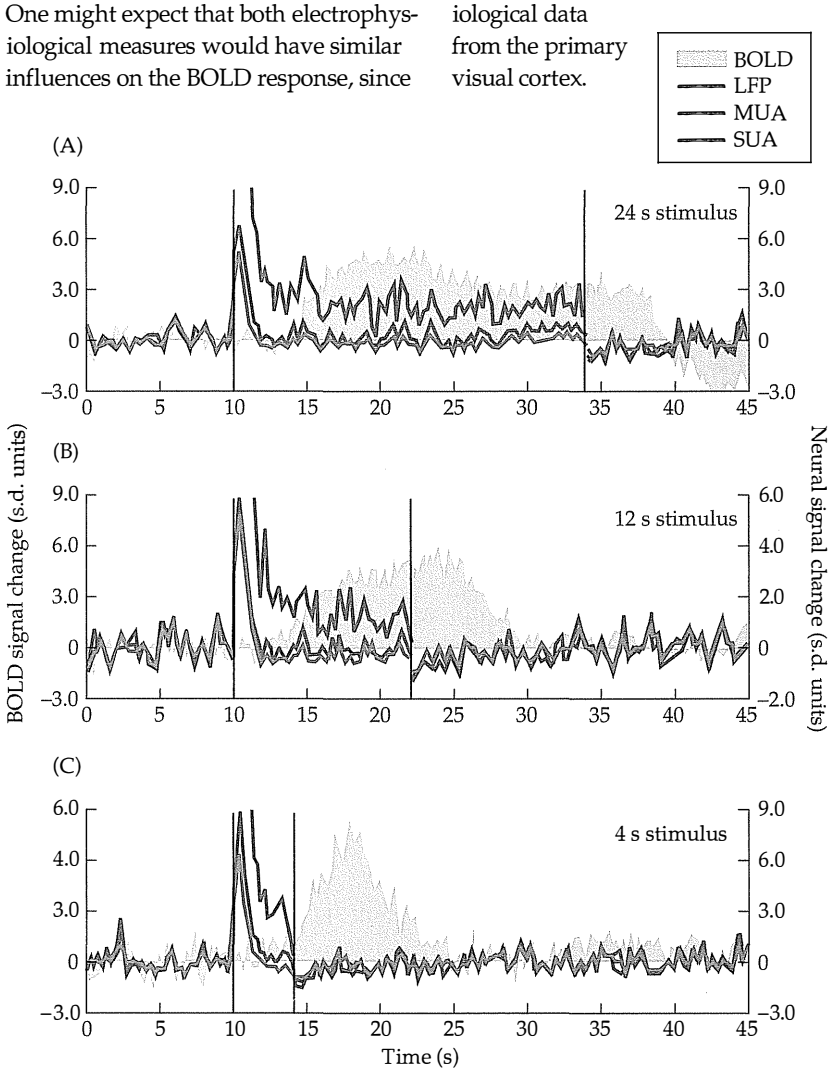

Figure 1 The relationship between BOLD activation and neuronal activity. Simultaneous electrophysiological and fMRI data were recorded in monkeys during the presentation of visual stimuli. The time course of BOLD activation evoked by visual stimulation is shown as a solid green histogram, while the time course of multi-unit activity (MUA) is shown in purple, the time course of single-unit activity (SUA) is shown in blue, and the time course of local field potentials (LFP) is shown in red. The duration of visual stimulation, indicated by vertical black bars, varied from 24 to 12 to 4 s, shown in the top, middle, and bottom panels, respectively. Note that the BOLD activation and the local field potential activity are extended in time throughout stimulus presentation, while the single- and multi-unit activities rapidly return to baseline. These results suggest that postsynaptic activity that generates local field potentials may be a primary contributor to the BOLD response. (After Logothetis et al., 2001.)

BOX 7.3 *(continued)*

still provided some predictive information. Moreover, as shown in a 2008 study by Goense and Logothetis, these results hold when measured in awake monkeys viewing simple visual stimuli: measured hemodynamic responses tracked the sustained changes in local field potentials, but not the more transient changes in single- and multi-unit activity. Data from several studies indicate that local field potential activity in the frequency range of about 20–60Hz best predicts the BOLD signal.

These and other results have led to a simple conclusion: the BOLD contrast mechanism reflects primarily the input and intracortical processing in a given area, that which we have characterized as the integrative aspect of neuronal processing, rather than the output reflected in action potential firing. Given this result, recall from the previous chapter our discussion of Attwell and Laughlin's energy budget for the brain. On the basis of the large number of synapses per neuron in primates, they hypothesized that compared with lower animals, a greater proportion of the brain's energy budget would be required to restore postsynaptic concentration gradients. Integrative activity may be the best predictor of the current and future metabolic demands of a region. However, it must be emphasized that post-synaptic activity may represent, to a large extent, the inputs to a given brain region. Thus, its amplitude may depend on computations elsewhere in the brain, not necessarily local information processing.

Due to technical limitations, notably the invasiveness of electrode recording, relatively little data of this type has been collected from human subjects. One notable exception comes from a 2005 paper by Mukamel and colleagues, who recorded single-unit activity from patients with implanted electrodes and fMRI data from neurologically normal subjects, while each individual watched and listened to an extended clip from a movie (see Box 11.1 for a discussion of this approach). From the electrode recordings, the authors measured changes in local field potentials and firing rate over time in the primary auditory cortex. (Note that because of the complexity of their auditory stimulus, the firing rate and the local field potentials were highly correlated, precluding the authors from separating these as individual contributors to the BOLD response.) Then, they convolved the neuronal activity with a standard hemodynamic response function to obtain a predicted BOLD timecourse, which they used as a regressor in the analysis of their fMRI data from the normal subject group. The resulting activation map revealed activation localized to the primary auditory cortex, exactly replicating the location of electrophysiological activity in the other subject group. Another study, reported in 2004 by Huettel and colleagues, examined simpler visual stimuli that varied in duration, also in separate groups of subjects: samples of patients with implanted electrodes, and neurologically normal fMRI subjects. Their results suggested that stimulus duration had corresponding effects on electrophysiological and fMRI signals, at least within the primary visual cortex, although somewhat different effects were reported for other brain regions.

Despite the data showing the remarkable correspondence between neuronal activity and BOLD fMRI, largely from simultaneous recordings in monkeys, some key challenges remain for future work. The slow temporal resolution of the BOLD response precludes the separation of feed-forward and feedback processing within a region. If the BOLD signal is indeed most sensitive to input-related activity, then complex and temporally sustained feed-back processing could contribute more to the signal than initial first-pass information processing. Moreover, both excitatory and inhibitory post-synaptic activity can contribute to the BOLD signal. In principle, a large BOLD signal could be observed in a region in which these two types of activity are relatively balanced, such that the region's output (and thus its contribution to thought and behavior) remains unchanged. Finally, there are likely to be situations where the amount of information processing might not be correlated with metabolic demand. Suppose that you observe that BOLD activation in a region (e.g., the prefrontal cortex) is evoked by a complex cognitive task (e.g., maintaining information in working memory), and furthermore the amplitude of that activation correlates positively with task performance. You might then conclude that individuals have good working memory if they engage the prefrontal cortex. But, what if the opposite relationship were observed: *less* activation in individuals with the best performance? At first consideration, this may seem implausible, given the concepts raised throughout this chapter. Yet, strong support exists for this possibility; for example, activation within a brain region tends to decrease with task practice, while the practice results in improvements in performance. One plausible hypothesis for such effects is that the brain represents the needed computations more efficiently, requiring fewer neurons to accomplish the same processing. Future research will be necessary to extend the results obtained so far, in order to clarify our understanding of the relationships between BOLD fMRI and neuronal activity in different brain regions, forms of information processing, and subject populations.

result in an increased inflow of oxygenated blood. More oxygen is supplied to the area than is extracted, and this results in a decrease in the amount of deoxygenated hemoglobin within the voxel. If we monitor the voxel's activation using BOLD fMRI, we find that its signal increases above baseline at about 2 s following the onset of neuronal activity, rising to a maximum value at about 5 s after a short-duration stimulus. This maximum is known as the peak of the hemodynamic response. If the neuronal activity is extended in time, the peak may be similarly extended into a plateau, typically maintained at a slightly lower amplitude than the peak (see Figure 7.12B for a typical example).

After the neuronal activity has ceased, the BOLD signal decreases in amplitude to a below-baseline level and remains below baseline for an extended interval. This effect, known as the poststimulus undershoot, has been attributed to both biophysical and metabolic effects. Some biophysical models, such as the balloon model advanced by Buxton and colleagues, postulate that neuronal activation evokes an inflow of blood that is initially greater than its outflow. The result is an increase in blood volume so that the venous system expands like a balloon. Then, following cessation of neuronal activity, blood flow decreases more rapidly than blood volume. While volume remains elevated but flow has returned to baseline, a greater amount of deoxygenated hemoglobin will be present. This reduces the overall fMRI signal below baseline levels. As blood volume slowly returns to normal levels, the fMRI signal will similarly increase to baseline, ending the undershoot. However, other data indicate that changes in oxygen metabolism play a key role. For example, Lu, van Zijl, and their colleagues have hypothesized that a continuously elevated cerebral metabolism would lead to the poststimulus undershoot. Supporting this perspective, a study published in 2008 by Harshbarger and Song investigated whether the application of diffusion weighting, which should minimize large-vessel contributions, influenced the amplitude of the BOLD undershoot. Targeting voxels in the visual cortex that were activated by a flashing visual stimulus, they found that diffusion weighting modulated the undershoot amplitude in some voxels, but not others. Still other voxels, primarily those in higher-order visual regions, exhibited no undershoot at all. These results, along with similar data from other groups, are difficult to reconcile with a purely vascular explanation, but instead suggest that sustained metabolic demand is an important contributor to the poststimulus undershoot.

To illustrate a sample hemodynamic response, Figure 7.13A provides data from a single voxel showing its change in MR signal over time, or its time course. In this experiment, the subject squeezed both hands whenever a brief flashing checkerboard was presented. There were long intervals between the stimuli so that there would be time for the hemodynamic response to return to baseline. Each line in Figure 7.13B presents the change in MR signal within a single voxel over a 21 s epoch, beginning 3 s before the stimulus through to 18 s after. Immediately apparent is the variability in the response over time. Even for very robust responses, the noise in the data has an amplitude similar to that of the hemodynamic response, making it difficult to identify the exact response evoked by each presentation of the stimulus (see Chapter 8 for an extended discussion of this problem). However, as data are combined from many evoked responses, a pattern similar to that shown in Figure 7.11A emerges.

The initial dip

Thus far, we have emphasized that neuronal activity leads to an increase in the BOLD signal. However, some research suggests that this positive change is preceded by a smaller decrease in the MR signal, which is often called the initial dip. Data from several studies using optical spectroscopy in animals

peak The maximal amplitude of the hemodynamic response, occurring typically about 4 to 6 s following a short-duration event.

undershoot The decrease in MR signal amplitude below baseline due to the combination of reduced blood flow and increased blood volume.

balloon model A model of the interaction between changes in blood volume and changes in blood flow associated with neuronal activity.

time course The change in MR signal over a series of fMRI images.

epoch A time segment extracted from a larger series of images, usually corresponding to the period in time surrounding an event of interest.

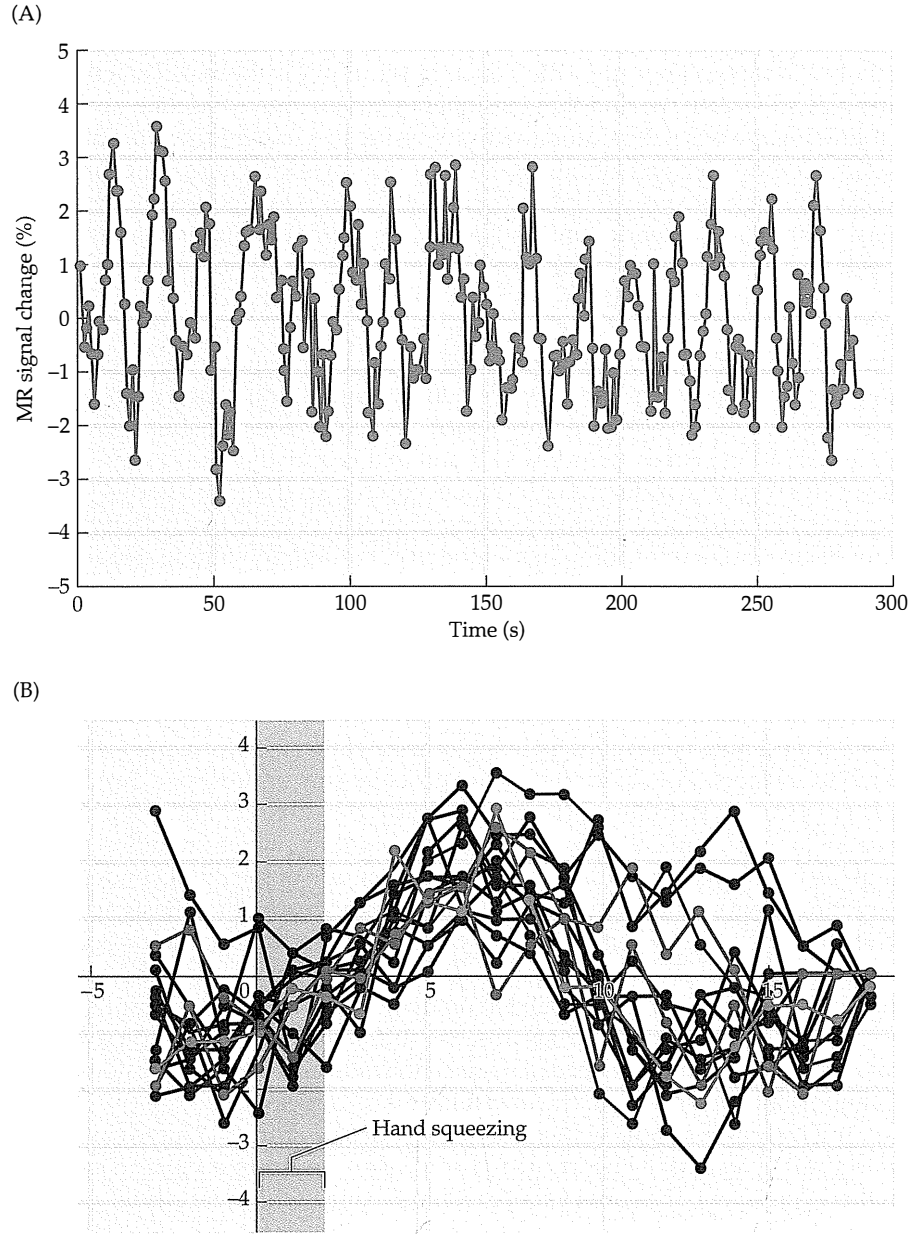

Figure 7.13 Examples of the BOLD hemodynamic response. (A) A sample fMRI time course from a single voxel in the motor cortex during a task in which the subject squeezed her hand for 2 s every 16 to 18 s. Even though this is a very high signal-to-noise task with clear responses present following every stimulus event, there remains substantial variability in the amplitude and form of the hemodynamic response over events. (B) Data from the individual events that make up (A). Note the variability from event to event, although all have generally similar hemodynamic responses that peak about 5 to 6 s following the hand squeezing. Three randomly selected individual trials are highlighted in color for clarity.

found a rapid increase in deoxygenated hemoglobin that had good spatial correspondence with active neurons, at least initially. In 1995 Menon and colleagues attempted to identify a similar phenomenon within the fMRI hemodynamic response. They presented a visual pattern that flashed for 10 s while collecting data using high-field (4.0 T) and fast-rate (TR of 100 ms) echo-planar imaging, with a local surface coil to increase detection power in the visual cortex. They found that some activated voxels showed an initial reduction in signal that had less than half the amplitude of the positive hemodynamic response (Figure 7.14). Those voxels were found within gray matter along the calcarine sulcus, which corresponds to the primary visual cortex. However, the activated region associated with the later positive response was more spatially diffuse and extended into neighboring veins and white matter.

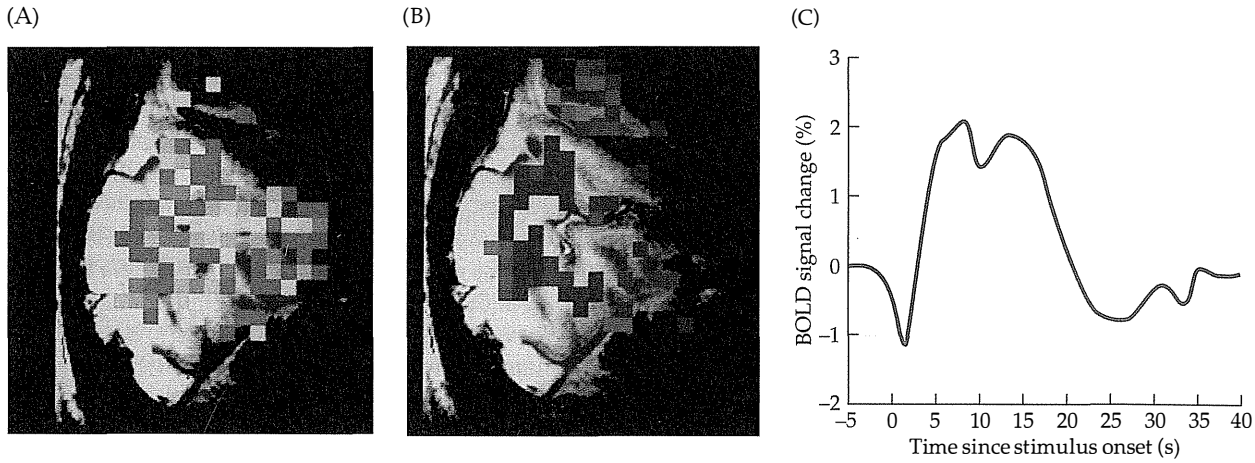

Figure 7.14 Spatial specificity of the BOLD initial dip. (A) On this sagittal slice, the statistical map that shows all voxels around the calcarine fissure (i.e., primary visual cortex) that had significant late positive hemodynamic responses to visual stimulation. (B) The map of voxels that showed significant early negative responses (i.e., displayed the "initial dip") has fewer voxels, suggesting that the initial dip may be more spatially specific. (C) The BOLD hemodynamic response across all voxels with an early negative response is shown. (From Menon et al., 1995.)

To demonstrate the spatial specificity of the initial dip, other investigators have used experimental designs that evoke highly specific activation patterns. In a study conducted in 2001, Duong and colleagues examined the BOLD response in the primary visual cortex of anesthetized cats using high-field (4.7 T and 9.4 T) fMRI. They targeted orientation columns, which are small, vertically organized collections of neurons that respond preferentially to stimuli of a particular orientation (e.g., lines). By collecting data at very high spatial resolution (about 150 μm^2), the researchers could identify individual orientation columns, which they expected would be differentially activated by stimuli with perpendicular orientations (e.g., 45° and 135°). They found that the initial dip showed good spatial specificity, in that voxels with an initial dip in response to one orientation did not show an initial dip in response to the stimuli in the perpendicular orientation. In contrast, the later positive BOLD response was blurred over the columns, such that most voxels showed positive BOLD activation in response to both orientations. The authors noted that the spatial specificity of the BOLD response was greatest over the first 2 s and decreased over time. This result suggests that the initial dip may reflect decreased oxygenation in nearby capillaries, while the positive response reflects overcompensatory delivery of oxygenated blood within the surrounding venous drainage system.

Despite these intriguing results, the initial dip is a controversial topic for a simple reason: despite many examples of its existence, including several dozen well-controlled studies in anesthetized animals, it is not reported in the vast majority of fMRI studies. (See the 2004 review article by Ances for an extended discussion.) So what could explain its infrequent observation? One likely factor is the rarity of high-field MR scanners for functional studies. The amplitude of the initial dip seems to scale dramatically with field strength. When measured at 1.5 T, the initial dip was only 12% of the magnitude of the positive response, which is only one-third of the proportion measured at 4.0 T. This result is consistent with the idea that the initial dip has a microvascular origin, since signals recorded from small blood vessels should scale more dramatically with field strength than signals recorded from large blood vessels. Another possible factor is that averaging over a large spatial region or over an extended time period obscures the smaller-scale effects of the initial dip. Highly specialized image acquisition methods, like those reported in a 2008 article by Lindquist and colleagues, may be useful for isolating the rapid but small-scale negative BOLD changes.

While the evidence in support of the initial dip has strengthened in recent years, its underlying mechanisms still require further investigation. For example, even though the oxygen extraction hypothesis remains the best theoretical interpretation, a transient decrease in flow or increase in volume would also result in a decrease in the BOLD signal. Furthermore, the specific relationships between neuronal activity and metabolic changes also require further elucidation. As suggested in a 2007 experiment by Li and Freeman, the increase in deoxygenated hemoglobin that may underlie the initial dip may exhibit different patterns of non-linearity than those of the positive response. We emphasize that the physiological changes that underlie the initial dip are themselves well-supported by a wealth of evidence from multiple imaging and optical recording techniques. What remains (somewhat) controversial is whether those physiological changes affect the BOLD signal and, assuming they do, under what conditions an initial BOLD decrease would be observed.

Spatial Resolution

The spatial resolution of an fMRI study, or its ability to distinguish differences between nearby spatial locations, depends on several factors. One straightforward influence is the voxel size. Voxels are three-dimensional rectangular prisms whose dimensions are specified by three scanner parameters: field of view, matrix size, and slice thickness. The field of view describes the extent of the imaging volume within a slice and is generally expressed in centimeters. The matrix size determines how many voxels are acquired in each dimension, within that slice. Most studies use matrix sizes that are symmetric powers of two, such as 64×64 or 256×256, to facilitate the use of the fast Fourier transform for image reconstruction. So, for a field of view of 24 by 24 cm and a matrix size of 64×64, the resulting within-slice (in-plane) voxel size would be 3.75 mm by 3.75 mm. Slice thickness provides the third dimension (through-plane) and is generally the same or larger than the in-plane voxel size (e.g., 5 mm). When the slice thickness is equal to the in-plane resolution, the voxels are cubic and the spatial resolution is said to be isotropic.

The size of the voxel used in a study may depend on the research question. Studies that examine the entire brain will use relatively large voxels, often around 4 to 5 mm on each side. In contrast, studies that examine a single brain region, such as the visual cortex, may use smaller voxels of 1 to 2 mm. For comparison, the letters making up this sentence are each about 2 to 3 mm in size. It is common to acquire anatomical images with smaller voxel dimensions (e.g., 1 mm by 1 mm in-plane), and functional data are often displayed on these high-resolution anatomical images. Note that the actual spatial resolution of the fMRI data is not affected by the resolution of the images on which it is displayed.

It seems obvious that increased spatial resolution would carry advantages for fMRI studies: more voxels within a brain region should improve the ability to distinguish boundaries between neighboring functional areas. So if fMRI data can be collected at any voxel size, why do researchers not always use the smallest possible size? There are two primary challenges for using small voxels in fMRI: reduced signal compared with noise and increased acquisition time.

First, variation in the BOLD signal depends on the change in the total amount of deoxygenated hemoglobin within a voxel. So, if we reduce the voxel volume by a factor of two, the BOLD signal changes will be half as large, resulting in a smaller signal-to-noise ratio. In some brain regions, such as the primary motor or visual cortex, a finger flexion or a visual flash may evoke a very

spatial resolution The ability to distinguish changes in an image (or map) across different spatial locations.

isotropic Having similar properties in all directions.

large brain response, and thus the reduced signal amplitude generated from small voxels may not be a problem. But in other brain regions, like the frontal lobe, a complex cognitive task may evoke much smaller changes in neuronal activity, and larger voxels may improve the ability to detect those changes in the presence of noise. We will discuss the concepts of signal and noise in more detail in the next chapter.

Second, as voxel size decreases, the time needed to acquire a given volume of the brain increases. While slice acquisition rates will vary between scanners and pulse sequences, increasing the within-image resolution can double or even quadruple acquisition time. Increasing the through-plane resolution also increases acquisition time, in this case exactly in proportion with the resolution change. If one halves the slice thickness, then twice as many slices will be needed to cover the same volume, and twice the acquisition time will be required. For example, a typical scanner might acquire 16 slices per second at $4 \times 4 \times 4$ mm resolution, but only 1 slice per second at $1 \times 1 \times 1$ mm resolution. The vertical extent of the cerebrum is about 110 mm, so 27 4-mm slices that cover most of the brain could be acquired in less than 2 s. At 1 mm resolution, that same volume would take nearly 110 slices and two minutes to acquire. Though extreme, this example points out the difficulty in using high spatial resolution for full-brain functional imaging. And, even if possible in theory, the long data acquisition periods needed for high-resolution images can cause **T_2* blurring**. Remember from Chapter 4 that data acquisition (e.g., filling *k*-space) takes time; this can be only a few tens of milliseconds for a typical 64×64 image but is much longer for very-high-resolution images. During this acquisition period, the spins are continuously undergoing T_2* decay, so if the acquisition period is very long compared with the T_2* value of the tissues being imaged, there will be virtually no signal for *k*-space locations collected toward the end of the acquisition period, which results in blurred BOLD images.

Conversely, using voxels that are too large can also reduce detection power. All fMRI studies, especially those using relatively large voxels, suffer from **partial volume effects**. Even the smallest voxel may contain multiple tissue types, each contributing differently to the total MR signal from that voxel. Figure 7.15

T_2* blurring Distortions in T_2* images that result from having a data acquisition window that is sufficiently long that significant T_2* decay occurs over that interval.

partial volume effects The combination, within a single voxel, of signal contributions from two or more distinct tissue types or functional regions.

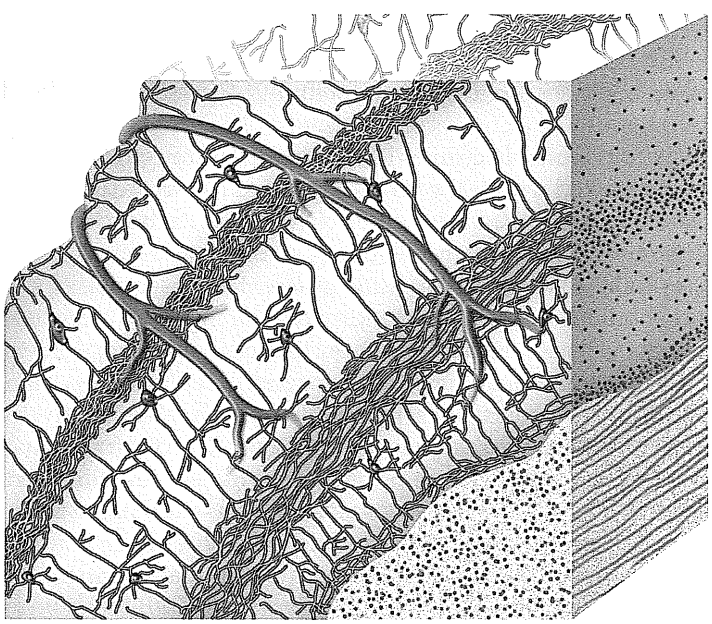

Figure 7.15 Partial volume effects. A single voxel may contain many different types of tissue, including gray matter, white matter, cerebrospinal fluid, or blood vessels. The MR signal recorded from that voxel is the sum of signals recorded from all of these different tissue types. So, if a voxel on a T_1 image contains 25% cerebrospinal fluid (with low signal), 50% gray matter (with medium signal) and 25% white matter (with high signal), the MR signal recorded from the voxel will contain contributions from all three, potentially taking an intermediate value.

shows the possible contents of a single 4 × 4 × 5 mm voxel. A typical voxel within the brain consists mostly of neurons (and their processes, like axons) and glia, with only about 3% of the volume made up of blood vessels. That voxel could include a few million neurons and some tens of billions of synapses, all of which contribute to the combined metabolic demand and thus the total BOLD signal from the voxel. See the 2008 article by Logothetis in the Suggested Readings for further calculations and discussions. In addition to the active neurons of interest and the local capillary bed, there may be other brain tissue that does not contribute to the measured activation. For example, voxels on the edge of the brain can contain gray matter, white matter, and cerebrospinal fluid. Only the gray matter will contribute to the BOLD signal, but protons in the other tissue types may contribute to the noise.

Spatial specificity in the vascular system

The functional resolution of fMRI depends on more than voxel size; it also depends on the concordance of neuronal activity and vascular responses to that activity (see Box 7.3). In an important study conducted in 2001, Logothetis and colleagues investigated the correspondence between the BOLD signal and electrophysiological measures, using simultaneous recordings in the primary visual cortex of monkeys. They found good spatial correspondence between BOLD changes and local field potentials that reflect summated EPSPs and IPSPs. Similarly, a 2000 study by Disbrow and colleagues used both fMRI and separate microelectrode recordings to map hand and face representations in the somatosensory cortex of the monkey. The maps of activation produced by the two methods largely overlapped, although the areas of activation were somewhat larger for fMRI compared with the more precise electrode recordings (Figure 7.16). This discrepancy was attributed to the filtering effects of the vascular system. These and related studies demonstrate the limitations in the spatial resolution of BOLD fMRI: in the best case, it can provide information about the capillaries closest to active neurons, but in the worst cases, its signal can come from larger and more distant blood vessels.

How might different parts of the vascular system contribute to the BOLD effect? Recall that the BOLD signal depends on the amount of deoxygenated hemoglobin, which is present in capillaries and veins but absent in fully oxygenated arterial blood. Because deoxygenated hemoglobin molecules are paramagnetic, they create magnetic field gradients within the vessel that extend into the surrounding tissue. The primary mechanism for the BOLD signal is the dephasing of spins within water molecules as they diffuse through these gradient fields. The spins located within the vessel itself give rise to the intravascular component of the BOLD signal, while the spins located in the surrounding tissue (i.e., parenchyma) give rise to the extravascular component of the BOLD signal. In a typical fMRI experiment using gradient-echo sequences, the BOLD signal reflects both intravascular and extravascular signal sources.

Both of these signal sources can arise from capillaries that are adjacent to and perfuse the active neurons. Capillaries are very small, typically less than a millimeter in length, and are generally separated from each other by tens to hundreds of microns. This suggests that the absolute lower limit for functional resolution of any hemodynamic measure of brain activity is a few hundred microns. Even if the brain were sampled at a finer spatial resolution, the functional resolution would not improve. Nevertheless, given the much coarser resolution of most current fMRI research, improving the spatial specificity of BOLD contrast would be of considerable value.

excitatory postsynaptic potential (EPSP) A depolarization of the postsynaptic cell membrane.

inhibitory postsynaptic potential (IPSP) A hyperpolarization of the postsynaptic cell membrane.

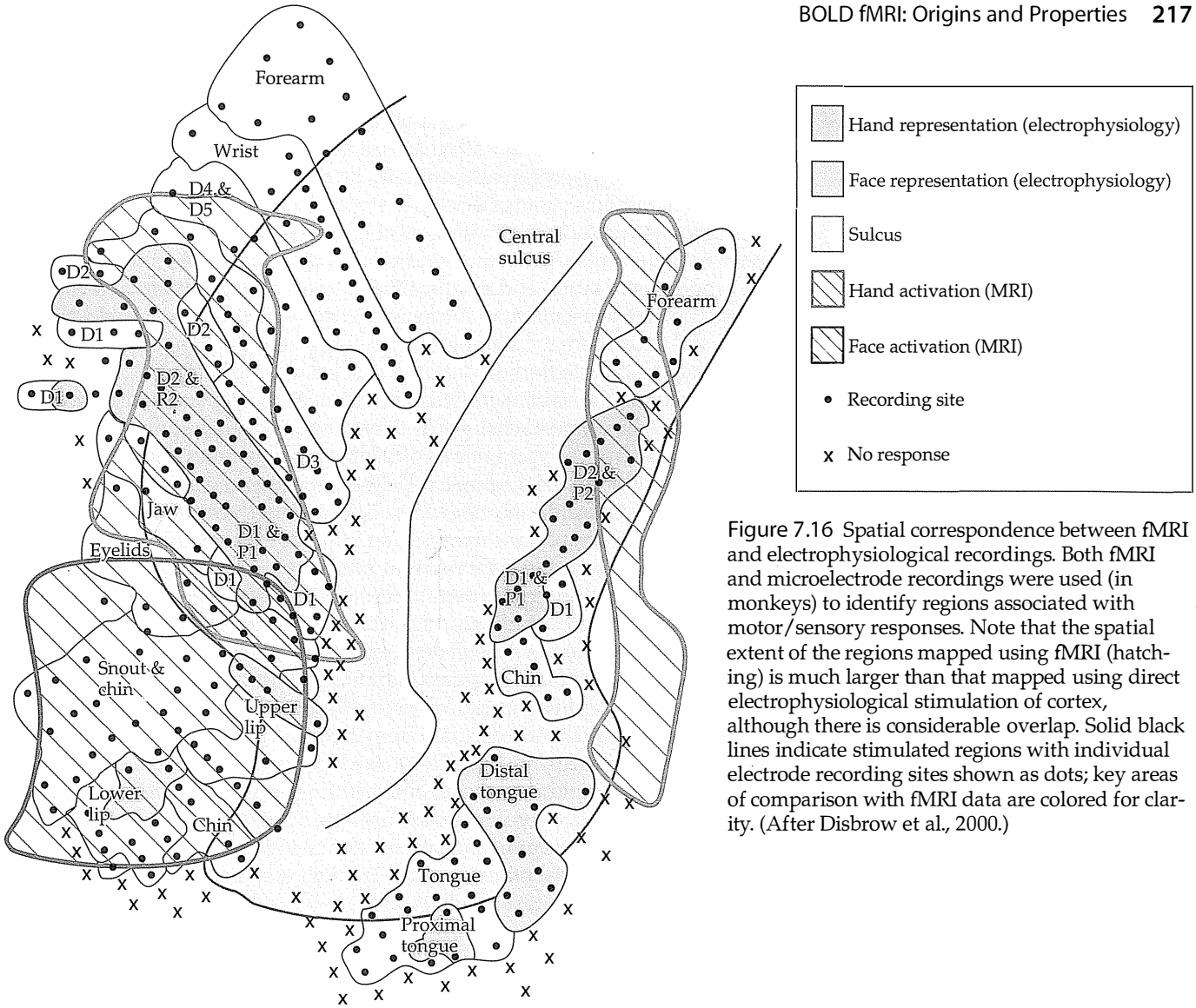

Figure 7.16 Spatial correspondence between fMRI and electrophysiological recordings. Both fMRI and microelectrode recordings were used (in monkeys) to identify regions associated with motor/sensory responses. Note that the spatial extent of the regions mapped using fMRI (hatching) is much larger than that mapped using direct electrophysiological stimulation of cortex, although there is considerable overlap. Solid black lines indicate stimulated regions with individual electrode recording sites shown as dots; key areas of comparison with fMRI data are colored for clarity. (After Disbrow et al., 2000.)

Yet, the BOLD signal is not restricted to nearby capillaries. As described earlier in the chapter, as the flow of oxygen-rich blood increases dramatically in response to neuronal activity, a smaller proportion of oxygen molecules are extracted as fuel. The remaining hemoglobin-rich blood enters the venous system, displacing deoxygenated hemoglobin and increasing the BOLD signal downstream from the active neurons. This effect led to the question "Brain or vein?" that was posed by Frahm and colleagues in 1994, and is a vitally important issue for fMRI studies. Many reported areas of activation may be a consequence of venous drainage, not local neuronal activation, as any researcher who has found significant activation in the superior sagittal sinus will attest. Large-vessel effects associated with large draining veins can compromise studies that require high functional resolution.

Several characteristics are indicative of large-vessel effects. The simplest is magnitude of signal change. Veins have much greater volume, and thus larger potential BOLD changes, than capillaries. Systematic changes in the phase of the MR signal may also indicate large-vessel effects, since large vessels have specific orientations within a voxel, unlike capillaries, which are randomly oriented (see the 2002 article by Menon for an approach to overcoming this prob-

large-vessel effects Signal changes in veins that drain a functionally active region but are distant from the neuronal activity of interest.

spin-echo (SE) imaging One of the two primary types of pulse sequences used in MRI; it uses a second 180° electromagnetic pulse to generate the MR signal changes that are measured at data acquisition.

diffusion weighting The application of magnetic gradients to cause changes in the MR signal that are dependent upon the amplitude and/or direction of diffusion.

lem). Voxels containing draining veins will have reduced functional specificity, since they may be downstream from multiple functionally distinct populations of neurons. Finally, the initial dip that is sometimes observed at high field is thought to represent oxygen extraction in the capillaries, so it will not be seen within voxels containing large vessels that are distant from the active neurons.

Advanced acquisition techniques can minimize the BOLD signal originating from large vessels. These techniques take advantage of the different magnetic properties of large- and small-caliber vessels and the different diffusion properties of extravascular and intravascular spins. The magnetic field generated by the deoxygenated hemoglobin in large vessels changes slowly over space as it extends into the surrounding tissue and fluid (Figure 7.17A). Thus, nearby extravascular spins within diffusing water molecules experience relatively small magnetic field changes as they travel. Indeed, within the few tens of milliseconds that are typical for a BOLD fMRI acquisition period, the deoxygenated hemoglobin within large vessels can be approximated as having a constant pattern of field inhomogeneity. Spin-echo sequences (see Chapter 5) can reverse the loss of phase coherence, and therefore can eliminate the BOLD signal that arises from the extravascular compartments of large vessels. The situation is quite different for small vessels (Figure 7.17B). They generate steeper magnetic field gradients, compared with the diffusion distance of nearby water molecules, in the surrounding parenchyma. The lost phase coherence caused by these magnetic field inhomogeneities cannot be completely refocused by a 180° pulse, and thus spin-echo sequences retain their sensitivity to the small-vessel extravascular component of the BOLD signal.

Spins within diffusing intravascular water molecules also experience dynamic magnetic field inhomogeneities, because their diffusion distance is large compared with the local magnetic field gradient, for both large and small vessels. For this reason, spin-echo sequences are still sensitive to the intravascular BOLD signal, and another approach must be employed to eliminate those effects. Because these intravascular spins are in flowing blood, they have a higher mobility (especially within large vessels), and thus motion-weighted image acquisition techniques like diffusion-weighted imaging (see Chapter 5)

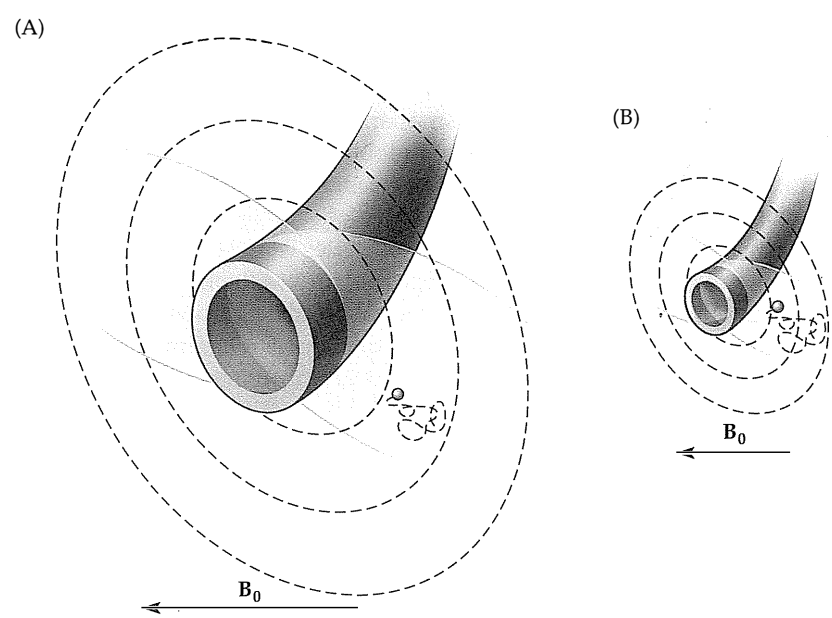

Figure 7.17 Different effects of large and small vessels on extravascular spins. The magnetic field gradient created by deoxygenated hemoglobin within a blood vessel depends on the diameter of the vessel. For large vessels (A), the gradient changes slowly over space, so diffusing extravascular spins experience a relatively constant magnetic field over time. Spin-echo imaging can be used to refocus the loss of phase coherence and eliminate the large-vessel signal. For small vessels (B), the gradient changes rapidly over space relative to a water molecule's diffusion distance, so extravascular spins experience different magnetic fields as they diffuse. Loss of phase coherence cannot be recovered by spin-echo imaging, and thus spin-echo imaging is sensitive to the small-vessel extravascular component of the BOLD signal.

can selectively suppress the intravascular component of large vessels. The combined use of spin-echo and diffusion-weighted sequences can eliminate the signals from large vessels while preserving the small-vessel signals most critical for functional resolution. Yet, this approach is hardly a panacea: it leads to greatly reduced BOLD sensitivity. For this reason, the introduction of refocusing pulses to eliminate large-vessel effects may be practical only at very high fields, where the increased overall signal can overcome the lost sensitivity to functional changes.

TABLE 7.1 Different Spatial Scales in the Human Brain

Structure	Scale
Brain	100 mm
Gyri	10 mm
Dominance column	1 mm
Neuron	0.01 mm
Synapse	0.001 mm
Ion channel	0.00001 mm

What spatial resolution is needed?

The right spatial resolution for an experiment depends on the question being asked. If you are a neurologist examining the effects of frontal lobe damage on intelligence tests, you may examine lesions that span 5 centimeters or more. If you are an electrophysiologist recording the firing of layer 4 neurons within the parietal lobe, you may need to localize the tip of your microelectrode within a few hundred microns of the area of interest. As shown in Table 7.1 (see also Figure 1.8), the properties of the human brain span about seven orders of magnitude from large-scale anatomy to small-scale microbiology. The spatial resolution of fMRI is intermediate between these extremes, and fMRI is most suited for examining a spatial range from millimeters to centimeters. Many aspects of brain function vary over this spatial range. Brain regions identified by cytoarchitectonic features, such as those identified by Brodmann in 1909, generally are several centimeters in size. Individual functional regions within the visual cortex extend from a few millimeters to a centimeter or more, although the entire visual pathways span several centimeters. Subcortical nuclei such as the caudate, putamen, and thalamus are all sufficiently large to encompass multiple fMRI voxels. Nevertheless, many brain structures, including the horizontal cortical layers and the vertical cortical columns (see the ocular dominance columns illustrated in Figure 7.18), exist on a much smaller scale and are difficult (but not impossible) to elucidate functionally using fMRI.

ocular dominance The degree to which a given neuron in the visual cortex responds more to stimuli presented to one eye than to stimuli presented to the other eye.

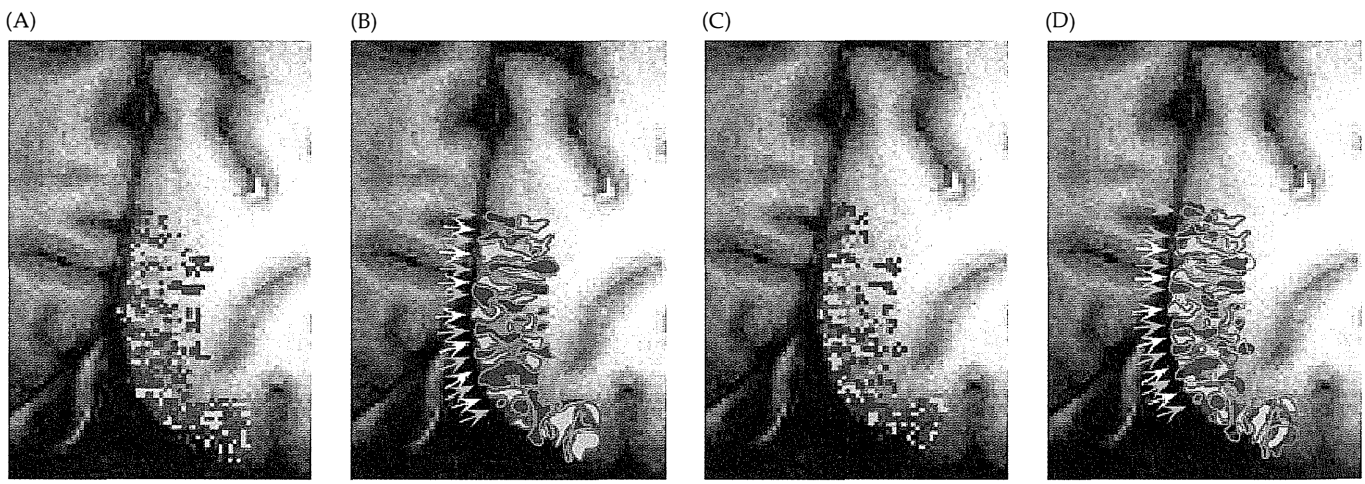

Figure 7.18 Ocular dominance columns in the visual cortex. Neurons in the primary visual cortex are organized into very small (~1 mm) columns that are sensitive to information coming from one eye. The same subject participated in two fMRI sessions, shown in panels A and C, that mapped the relative sensitivity of each visual cortex voxel to stimulation from each eye. Note that the outlines of the areas of ocular dominance from the first session (B) correspond well to the results from the second session (D). (From Cheng et al., 2001.)

spatial smoothing The blurring of fMRI data across adjacent voxels to improve the validity of statistical testing and maximize functional SNR, at a cost of spatial resolution.

normalization The transformation of MRI data from an individual subject to match the spatial properties of a standardized image, such as an averaged brain derived from a sample of many individuals.

region-of-interest (ROI) analyses Evaluations of hypotheses about the functional properties of brain regions (i.e., aggregated over a pre-determined set of voxels), often chosen to reflect a priori anatomical distinctions within the brain.

temporal resolution The ability to distinguish changes in a signal (or map) across time.

While this discussion has focused on the effects of data acquisition methods on spatial resolution, choices made in experimental analysis are also important. A common preprocessing step explicitly reduces spatial resolution by smoothing fMRI data using a three-dimensional Gaussian filter of several voxels in width (see Chapter 8). Typical smoothing parameters can increase the effective voxel size to $6 \times 6 \times 6$ mm or greater. Note that such a voxel contains more than three times the volume of a voxel 4 mm on each side, and 27 times the volume of a voxel that is 2 mm per side. While smoothing can reduce spatial resolution, it can improve the validity of statistical tests and comparisons between subjects. Other analysis steps also reduce spatial resolution, through more subtle effects. Algorithms for transforming subjects to a common stereotaxic space, a process known as normalization, further reduce spatial resolution due to the difficulty in matching a person's individual anatomy to a stereotaxic template. Moreover, combining data from multiple subjects introduces spatial blurring associated with functional differences between the subjects. Using anatomically based region-of-interest analyses changes the basic spatial unit from a single voxel to a region containing many voxels, greatly reducing spatial resolution. However, if the chosen regions accurately map onto functional divisions within the brain, the functional resolution of the data may be greatly increased by averaging many similar voxels. For example, the putamen is a relatively small structure within the basal ganglia that is associated with motor preparation, interval timing, learning, and some cognitive processes. Since there are clear anatomical divisions between the putamen and the surrounding white matter, it is simple to create a region of interest that includes the entire structure. This will prevent the identification of functionally distinct subregions (e.g., medial vs. lateral), but may increase the ability to detect changes in the putamen as a whole. As a general rule, many analysis steps sacrifice spatial resolution in order to increase functional resolution.

Temporal Resolution of fMRI

For many experimental questions, it is important to measure the timing of brain activity with accuracy, or with high temporal resolution. Neuroscience techniques differ dramatically in their ability to assess the relative timing of events (see also Figure 1.8). Recordings from microelectrodes within the brain can identify the firing of a single neuron as it occurs, resolving activity in time to the millisecond level, but these can only be made in nonhuman animals or (rarely) in humans who are undergoing special tests associated with neurosurgical procedures. Lesion studies, drug manipulations, and even some imaging techniques like PET provide almost no information about the timing of brain activity. Functional MRI has an intermediate level of temporal resolution, because it can discriminate events that are separated by a few seconds. Just as the basic sampling unit for spatial resolution is the voxel, the basic sampling unit for temporal resolution is repetition time, or TR. Depending on the experiment, the TR may vary from very short (e.g., 500 ms) to very long (e.g., 3000 ms), with even more extreme values used in specialized experiments. While the duration of the TR contributes to the temporal resolution of an experiment, it is not the only factor.

The fMRI BOLD hemodynamic response rises and falls over a period of more than 10 seconds, even if the duration of neuronal activity is very short (e.g., less than a second). So, when we collect fMRI data, we do not take snapshots of neuronal activity, but estimate that activity based on slower changes

in the vascular system. Decreasing the TR to better sample the fMRI hemodynamic response improves our estimate of these vascular changes, which in turn improves the inferences we can make about neuronal activity.

We emphasize this framework because it suggests that there may be a preferred temporal resolution for a given experimental question. Consider the very simple event-related design in which a subject squeezes her hand whenever she sees a visual stimulus. To determine whether an area of the brain becomes active due to hand motion (i.e., detection of the active region), a relatively slow sampling rate will suffice. At a 3-s TR, the hemodynamic response may be easily identified when compared with the prestimulus baseline, but its exact shape may be difficult to estimate (Figure 7.19A). Halving the TR to 1500 ms improves our estimates of the shape and timing of the hemodynamic response but does not substantially change the measured amplitude (Figure 7.19B). Something very interesting becomes evident if we shorten the TR, to 750 or even 375 ms (Figure 7.19C and D): the measured hemodynamic response, though sampled much more often, does not appreciably change.

Figure 7.19 Effects of sampling rate (TR) on the measured hemodynamic response. In each figure, an idealized hemodynamic response is sampled at a different rate.

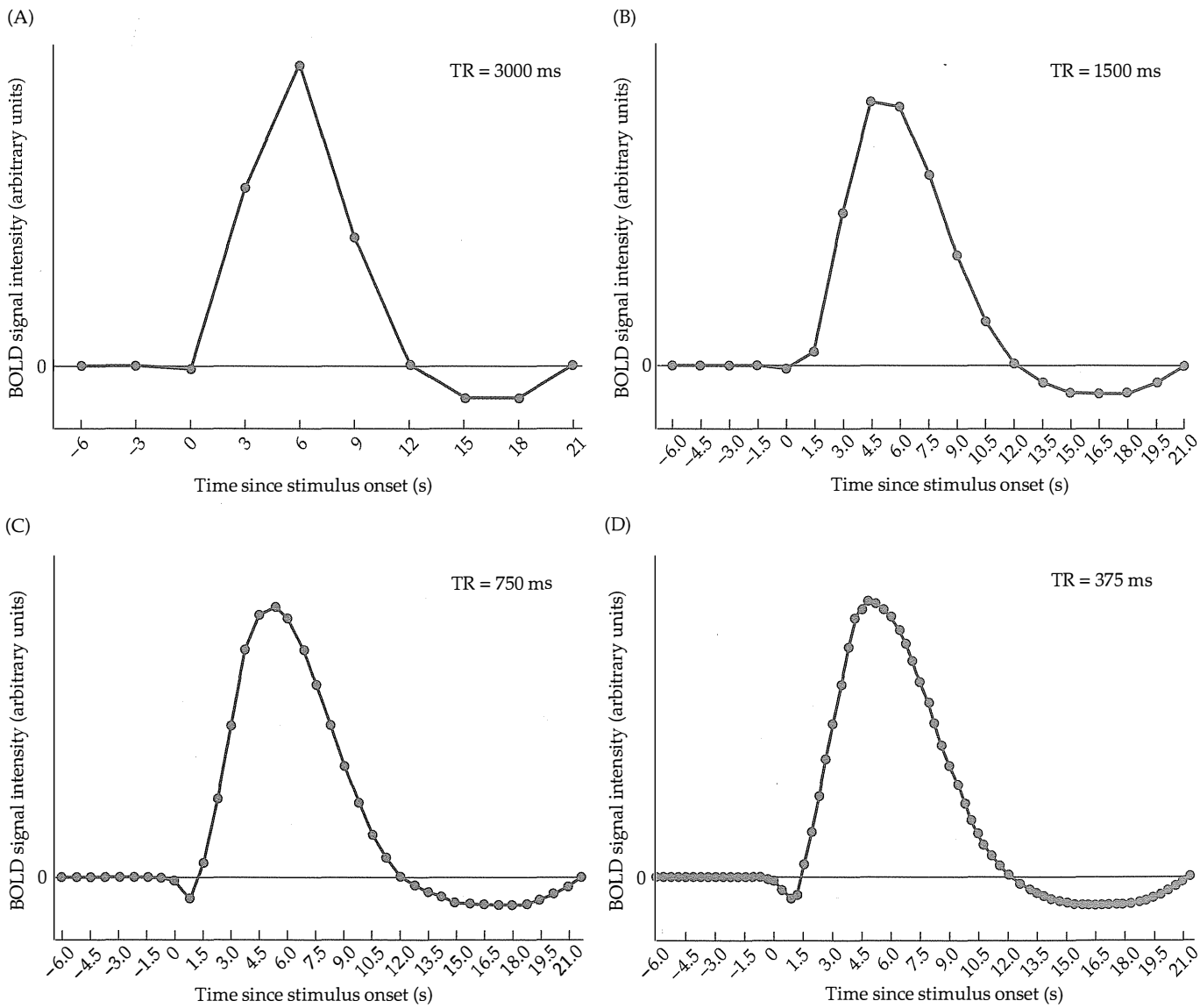

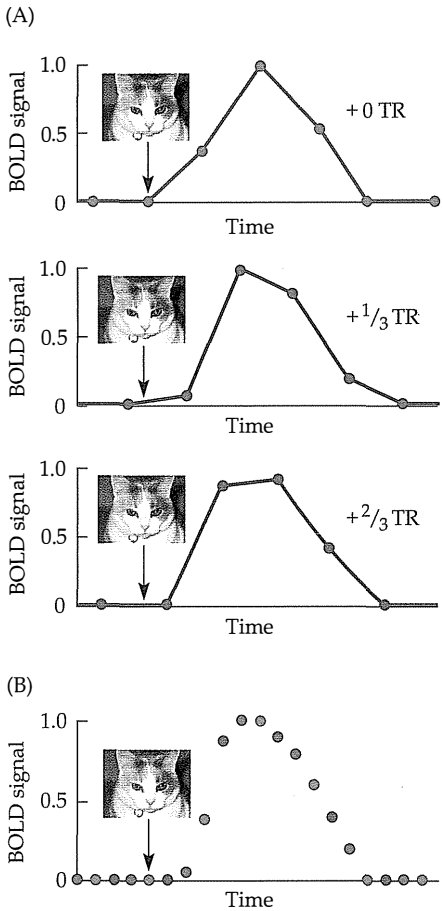

Figure 7.20 Use of interleaved stimulus presentation. In an experimental design with interleaved presentation, the experimental stimulus is presented at different points relative to the TR in different trials (A). Although the hemodynamic response may be sampled coarsely in each trial, the sampling occurs at different phases within the TR. Thus, combining data from all trials (B) fills in the intermediate points, improving the effective temporal resolution, at a cost of increased experiment length.

flip angle The change in the precession angle of the net magnetization following excitation.

interleaved stimulus presentation The presentation of events of interest at different points within a TR over trials (e.g., one-quarter, one-half, and three-quarters of TR in addition to TR onset), increasing the effective sampling rate of an experiment at the expense of fewer trials per condition.

Thought Question

How does the temporal resolution that is needed to detect significant activation change for long-interval blocked designs? Is the required TR larger or smaller than for event-related designs?

It seems counterintuitive that dramatic increases in sampling rate would have little effect on temporal resolution. However, think about how additional samples might change our estimate of the hemodynamic response. In the case of a 3-s TR, what do we know about the time points between samples (i.e., 1.5 s, 4.5 s, etc.)? Although they are not measured directly, a reasonable assumption might be that the hemodynamic amplitude at these points would be intermediate between those of the recorded samples. For now, we can consider simple linear interpolation, such that the midpoint would be given by the average of the two adjacent samples. At TRs greater than about 2 s, linear interpolation does not provide a good estimate of the values that would have been recorded from the intervening points. But as we shorten the TR to 1.5 s or less, even simple linear interpolation will accurately reproduce intermediate values, because the hemodynamic response has reproducible structure. The changes in blood flow and oxygen extraction that form the basis of BOLD contrast occur as a result of slow physiological processes. Only if these processes varied wildly within short intervals, say 100 ms, would increasing the sampling rate be critical. Note that this example shows the results of an event-related design, so that the hemodynamic response evolves over about 10 to 15 s. If a long-interval blocked design were used, then the changes in the hemodynamic response would be much slower and an even longer TR would be adequate. In summary, the temporal resolution of fMRI is determined both by the repetition time, TR, and by the limitations of the vascular system. For many experimental questions, TRs of about 1 to 2 s are sufficient.

Moreover, using very short TRs introduces some problems. In Chapter 3 we learned that one parameter of an MR pulse sequence is the flip angle, which reflects how far the net longitudinal magnetization is tipped toward the transverse plane by an excitation pulse. Since the amount of MR signal is proportional to the projection of the magnetization vector on the transverse plane, large flip angles provide greater MR signals. For typical gradient-echo sequences with long TRs (i.e., greater than about 2 s), a flip angle of 90° can be used to recover maximal MR signal. But at shorter TRs, a smaller flip angle is required so that the magnetization will reach a steady state over repeated excitations. As a result, the amplitude of the transverse magnetization following excitation will be reduced, and less MR signal will be measured. Short repetition times also reduce spatial coverage. If a scanner can acquire 14 slices per second with a given pulse sequence, then only 7 slices could be acquired with a 500-ms TR, while 28 could be acquired with a 2000-ms TR.

Temporal resolution can be improved by using an interleaved stimulus presentation, in which the experimental stimuli are presented at different points within a TR during different trials. Note that this should not be confused with interleaved slice acquisition, which refers to the order of slice excitation within a TR. Figure 7.20 illustrates the basic approach of interleaved stimulus presentation. In a typical experiment with a 3-s TR, the experimental stimuli might be presented at TR onset, so the hemodynamic response is sampled at 3 s, 6 s, 9 s, etc., following stimulus presentation. In an interleaved design with three presentation times, the stimuli could be presented either at TR onset, one sec-

ond into the TR, or two seconds into the TR. Thus, one-third of the trials would be sampled normally, one-third would be sampled at 1 s, 4 s, 7 s, etc., and one-third would be sampled at 2 s, 5 s, 8 s, etc. By combining data from all three sets of trials, the hemodynamic response can be estimated with a temporal resolution of 1 s. Interleaved presentation can therefore provide improved temporal resolution without limiting spatial coverage or reducing signal amplitude, and is thus an attractive option for many studies. Its primary disadvantage, however, lies in the reduction in the number of trials conducted for each delay condition, which reduces the precision of the estimated hemodynamic response. Researchers must always balance improvements in temporal resolution against possibly diminished spatial coverage, spatial resolution, or experimental power.

reaction time The time required for someone to make a simple motor response to the presentation of a visual stimulus. Note that this is distinct from response time, which applies to situations in which someone must choose between two or more possible responses.

What temporal resolution is needed?

To understand the use of fMRI in studying the timing of mental processes, it is necessary to appreciate the different time scales over which such events occur. Imagine that you are driving a car and must quickly swerve to avoid an obstacle in the road (Figure 7.21). Within a millisecond or so after the image of the obstacle hits your eye, photoreceptors in the retina begin to release neurotransmitters. Over the next few milliseconds, those neurotransmitters influence the activity in adjacent bipolar neurons, which in turn evoke action potentials in retinal ganglion cells that project to the lateral geniculate nucleus of the thalamus (as well as to a few other targets). Transmission of visual information through the thalamus to the primary visual cortex requires a few tens of milliseconds, and significant changes in neuronal activity can be detected in secondary visual areas after about 100 ms. Yet, the reaction time before you move the steering wheel has a lower limit of about 200 ms. (For comparison, in Olympic track events, runners who leave the starting blocks within 100 ms of the starter's pistol are penalized, because there has not been enough time for them to react to the stimulus.) By about 500 ms, you become aware of the obstacle and begin reflecting on the near accident. More complex processes, like retrieving the memory of a similar event, may take several seconds, and changes in your emotional or physiological state may last for minutes or hours.

Figure 7.21 Timing of mental events. When a person makes a simple motor response, like turning a steering wheel to avoid an obstacle (A), a large number of different brain regions will become increasingly active. However, across these regions, the timing of activation may vary considerably (B). Neuronal activation may be present within about 100 ms of stimulus presentation, in regions that support basic sensory processing (e.g., the lateral geniculate nucleus, LGN; primary visual cortex, V1; motion-sensitive cortex, V5; parietal cortex, PC; motor regions, SMA/M1), But in regions supporting more complex cognitive functions (i.e., the prefrontal cortex), activation may persist for tens of seconds.

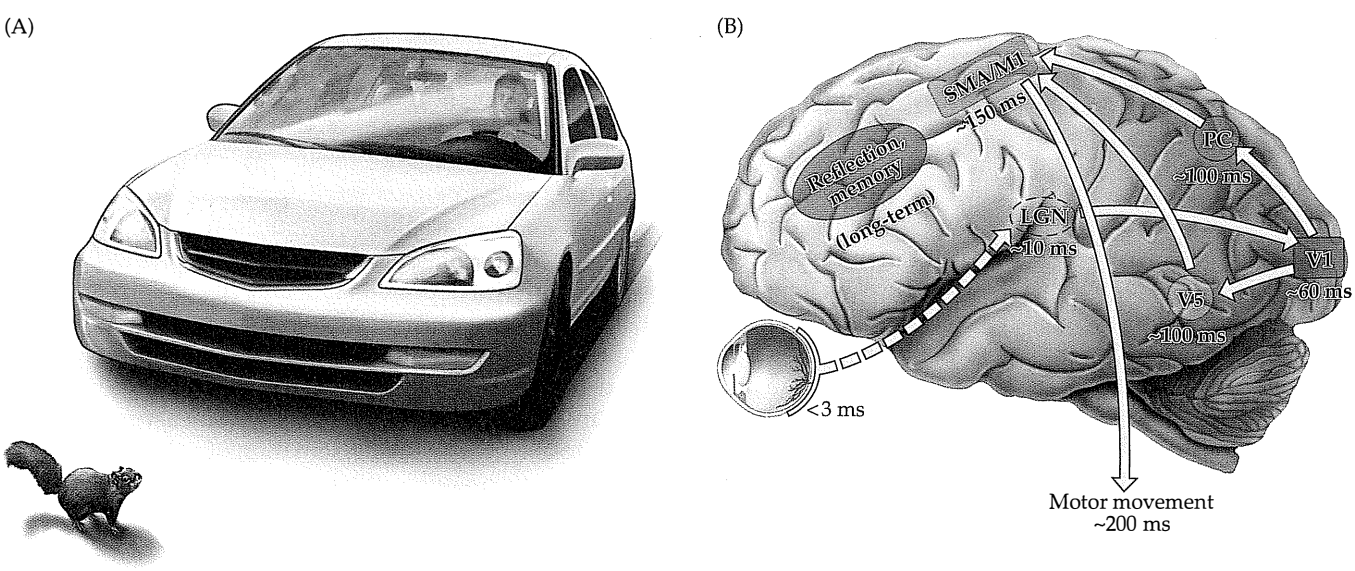

Finally, there may be long-term effects, such as learned changes in your driving patterns, that persist for days, months, or even indefinitely.

A single stimulus can thus evoke changes in the brain that span more than eight orders of magnitude in time, from milliseconds to days. While this range is very large, most psychological experiments manipulate cognitive processes that occur over periods of a few seconds, well within the range of fMRI. For example, studies examining executive processing, long-term memory, or decision making typically present stimuli every few seconds, while experiments of working memory may require the subject to maintain a stimulus in memory for about 10 s. It is more difficult to use fMRI to study topics involving very small or very large time scales. A rough estimate of the lower limit of fMRI's temporal resolution for most conditions is a few hundred milliseconds. For example, there are well-known reentrant circuits running from higher visual processing regions back to the primary visual cortex. Attending to a visual stimulus has been shown to increase fMRI activation in the primary visual cortex, but that activation might be attributed to the initial neuronal activity or to feedback from other brain regions that occurs hundreds of milliseconds later.

Thought Question

How could experiments be designed to investigate feedback circuits in the brain using fMRI?

While there is no limit, in principle, on the length of long-term fMRI studies, practical factors make very long studies unrealistic. One common manipulation is to change experimental instructions between runs, so that the participant does one task for several minutes and then another during the next run. This approach is necessary for many types of experimental questions, such as memory studies that separate stimulus learning from memory retrieval. When using such an approach, the researcher must monitor for problems like head motion and scanner drift that can cause systematic signal changes during and between runs. If the time scale needed is longer than an hour or two, such as when examining the encoding and retrieval of long-term memories, then multiple scanner sessions will be necessary. Comparisons of data from different sessions raises many additional problems, since there may be differences in head position, fatigue level, and practice with the task. Nevertheless, it is important to emphasize that while the lower and upper limits discussed here apply to most fMRI BOLD studies, it is possible to overcome them with careful selection of imaging parameters and clever experimental design.

The relationship between timing and hemodynamic amplitude is critical for models of fMRI activation. Because of the constraints of the vascular system, one might expect a larger response to reach its peak more slowly than a smaller response. Alternatively, a large-amplitude response might reflect greater neuronal activity, and thus greater metabolic demand, which could cause an earlier supply of oxygen and an earlier peak. While both arguments are plausible, neither is correct. For a given stimulus and brain region, the amplitude of the fMRI hemodynamic response appears to be independent of the timing of the response in both latency to onset (i.e., time before an initial rise above baseline) and latency to peak (Figure 7.22). This means that if you measure the fMRI BOLD response in the auditory cortex to the presentation of a 2-s music video clip, there will be no correlation across subjects between its amplitude and timing. However, if you measure the activation in that region in response to several different stimulus durations, the response at longer durations will be of

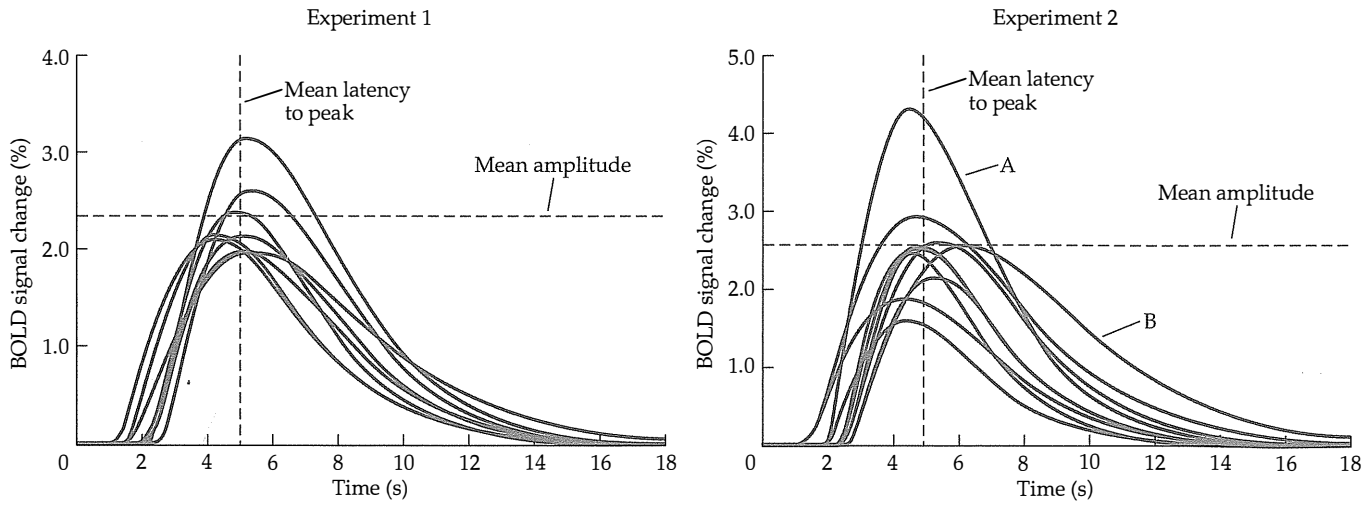

Figure 7.22 The amplitude and timing of the event-related fMRI hemodynamic response are uncorrelated. Two experiments were conducted in which hemodynamic responses in the visual cortex to a short-duration visual stimulus were measured. In both experiments, there was no correlation across subjects between the amplitude of the response and its time to peak. Note that in Experiment 2, the subject with the largest response (A) had a relatively short latency to peak, while the subject with the longest latency response (B) had an average peak amplitude. (After Miezen et al., 2000.)

both greater amplitude and increased latency to peak. Likewise, if you compare activation in the auditory cortex with activation in another brain region (e.g., the visual cortex), the two brain regions may differ in both amplitude and latency. These differences could reflect differences in neuronal processing as a function of stimulus duration or brain region, or differences in the hemodynamic response itself. In summary, changes in the amplitude of the fMRI hemodynamic response do not appear to cause changes in the timing of the response, or vice versa, although external factors may affect both measures similarly.

Effects of stimulus duration and timing

Over intervals from a few seconds to a few tens of seconds, the duration of the fMRI hemodynamic response provides a reasonable estimate of the duration of neuronal activity. A good example of this was reported in 1997 by Richter, Kim, and their colleagues, who investigated the role of the superior parietal lobe in the mental rotation of complex objects. Decades of cognitive psychology studies have shown that the time needed to judge whether or not two similar objects are identical depends on the rotation angle between them. Thus, response time is twice as long for pairs that differ by 90° compared with pairs that differ by 45°. Richter and colleagues hypothesized that since the superior parietal lobe is critical for spatial processing, including mental rotation, its activation should extend in time for the entire rotation process. To test this idea, they measured the duration of the BOLD response in this region during each of 16 different trials that required objects to be rotated through different angles. They found that for each trial, the duration of the BOLD response matched well with the subject's response time (Figure 7.23). The onset of the BOLD response did not differ across trials, suggesting that neuronal activity began at the start of the mental rotation process and stopped when mental rotation was complete.

Recognize, however, that the duration of the *stimulus* or *behavior* does not necessarily correspond with the duration of the *neuronal activity*. Imagine seeing a photograph of a familiar face that is presented for 5 s. Neurons in the primary visual cortex will have their largest response over the first 100 ms or so, then become much less active. Neurons within face-sensitive regions in the inferior temporal lobe will be active at stimulus onset, as well as throughout the 5 s period, due to feedback from other brain regions. Some neurons within

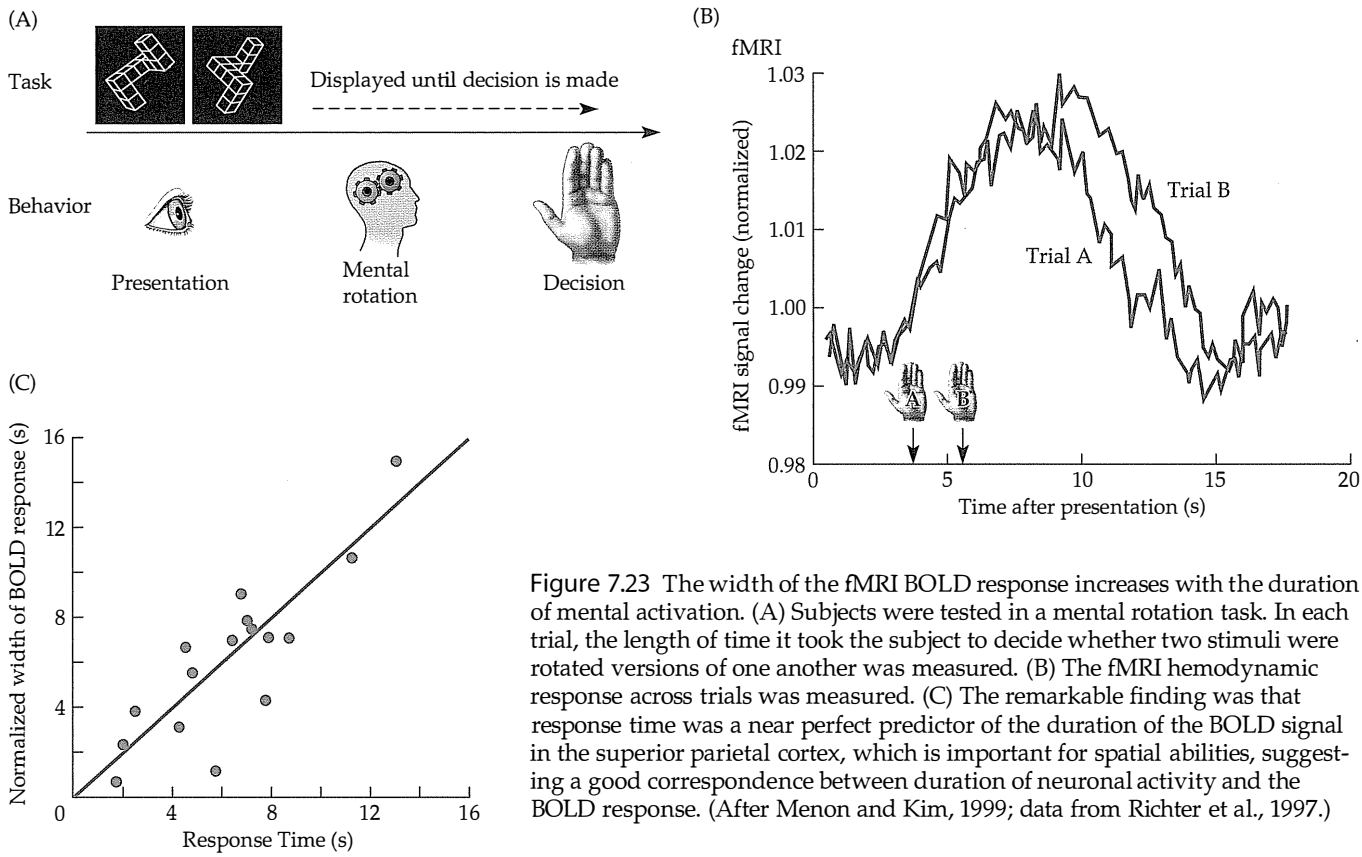

Figure 7.23 The width of the fMRI BOLD response increases with the duration of mental activation. (A) Subjects were tested in a mental rotation task. In each trial, the length of time it took the subject to decide whether two stimuli were rotated versions of one another was measured. (B) The fMRI hemodynamic response across trials was measured. (C) The remarkable finding was that response time was a near perfect predictor of the duration of the BOLD signal in the superior parietal cortex, which is important for spatial abilities, suggesting a good correspondence between duration of neuronal activity and the BOLD response. (After Menon and Kim, 1999; data from Richter et al., 1997.)

the frontal and parietal lobes may become active after the face disappears, as you reflect on what you just saw. For these reasons, researchers construct their fMRI analysis models based on estimated neuronal activity, not necessarily stimulus duration.

Even though it is difficult to determine the absolute timing of neuronal activity based on the fMRI BOLD signal, the relative timing of activation can be identified with great precision. In 1998 this was demonstrated in an elegant study by Menon and colleagues, who investigated relative timing in two fMRI experiments at high field (4.0 T) and high temporal resolution (TR of 100 ms). Their first experiment used a visual checkerboard stimulus that was split into left and right hemifields, each presented for 2 s. The left hemifield was presented either before the right with a delay interval ranging from 125 to 1000 ms, or at the same time. When they measured the difference in hemodynamic latency between the two hemispheres in the visual cortex, they found a near perfect correspondence with the presentation delay.

Thought Question

How is it possible that researchers can identify timing differences of a few hundred milliseconds using fMRI if the hemodynamic response is delayed by a few seconds following the neuronal activity?

hemifield One half of a visual display, usually referring to the left or right half.

The second experiment extended this result by introducing a motor reaction-time task. Each trial began with the subjects watching a fixation cross at the center of a screen for 6 s. When the screen flashed bright yellow, the sub-

ject used a joystick to move a cursor to a target as quickly as possible. One second after the cursor was successfully moved, the screen returned to gray and the subjects returned the joystick back to its center. The authors investigated the timing of activation in three cortical regions: the primary visual cortex (V1), the primary motor cortex (M1), and the supplementary motor area (SMA). Activation in V1 was observed, on average, about 200 ms before activation in SMA, which in turn was activated about 30 ms before M1. Especially remarkable were the effects of reaction time on these differences. Reaction times varied between subjects in a range from about 200 to 300 ms. The time differences between activation in V1 and SMA were proportional to the differences in reaction times, suggesting that the pathway between them may be associated with preparatory processes that differ between subjects (Figure 7.24A). However, the delay between SMA and M1 activation was constant across reaction times, suggesting that the link between these regions supports more basic response-execution processes. The timing differences found between these regions using fMRI were larger than those calculated from electrophysiological studies, where a latency of around 100 ms between V1 and M1 is more typical. This discrepancy illustrates the basic problem with comparing the timing of neuronal activity between brain regions based on fMRI data: differences in vascular properties also contribute to the timing of activity. This caveat, however, does not call into question the results of Menon and colleagues, because they demonstrated that the timing differences between regions depended on reaction time. To cognitive neuroscientists, these sorts of results suggest that variability in behavior, such as reaction time, the most commonly used measure in psychological experiments, can provide important information about the functions and connectivity between brain regions. We return to this theme in Chapter 11.

Within a single region, however, any vascular properties will be similar across timing conditions, allowing for accurate estimations of small timing differences. In 2000, Miezin and colleagues investigated the issue of relative timing using a clever visuomotor task. They presented checkerboard stimuli in a rapid event-related design. Each stimulus was presented for 1.5 s, and the time

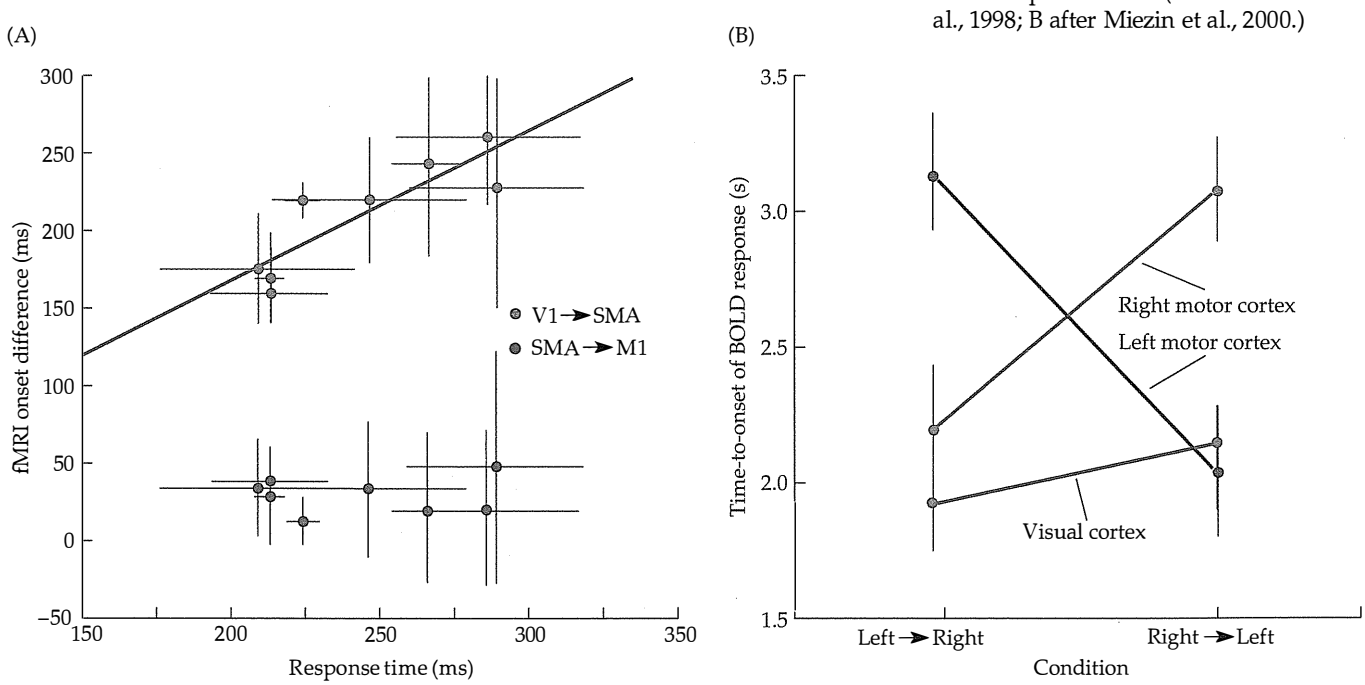

Figure 7.24 Using fMRI to identify the relative timing of activation across brain regions. (A) After the presentation of a visual cue, subjects moved a target square across the display with a joystick. The relative latency of the fMRI signal in different brain regions as a function of the subject's reaction time (RT) on the task was measured. The latency between BOLD activation in the primary visual cortex (V1) and in the supplementary motor area (SMA) increased roughly linearly with RT, while the latency between SMA and the primary motor cortex (M1) was unchanged with RT. This result suggests that processes influencing the speed of a response occur between V1 and SMA but not between SMA and M1. (B) In an experiment with a similar approach, subjects pressed a button with one hand when a stimulus of 1.5 s duration appeared and another button with the other hand when that stimulus disappeared. The order of activation between motor cortex regions depended on the order of responses, while activation in the visual cortex was independent of response order. (A after Menon et al., 1998; B after Miezin et al., 2000.)

jittering Randomizing the intervals between successive stimulus events over some range.

between stimuli was randomly varied, in a technique called jittering, with a mean of about 5 s between stimuli. The subjects' task was to press a button with one hand when the stimulus appeared and press another button with the other hand when the stimulus disappeared. In half of the trials, the right hand was used first, and in the other half, the left hand was used first. They found that the BOLD response in the motor cortex corresponding to the hand used at the onset of the stimulus was shifted earlier in time by about 0.75 to 1.0 s, compared with the response in the motor cortex corresponding to stimulus offset (Figure 7.24B). The fact that this shift was slightly less than the stimulus duration likely reflected preparation processes, since the subjects knew when the stimulus would disappear and could prepare for that button press. A subsequent power analysis suggested that timing differences as small as 100 ms could be reliably detected using this type of experimental design.

In summary, fMRI can measure small latency differences between brain regions, under appropriate task conditions (Figure 7.25). These differences may reflect the timing of neuronal activity and the form of the hemodynamic response. To draw inferences that are specific to neuronal activity, researchers

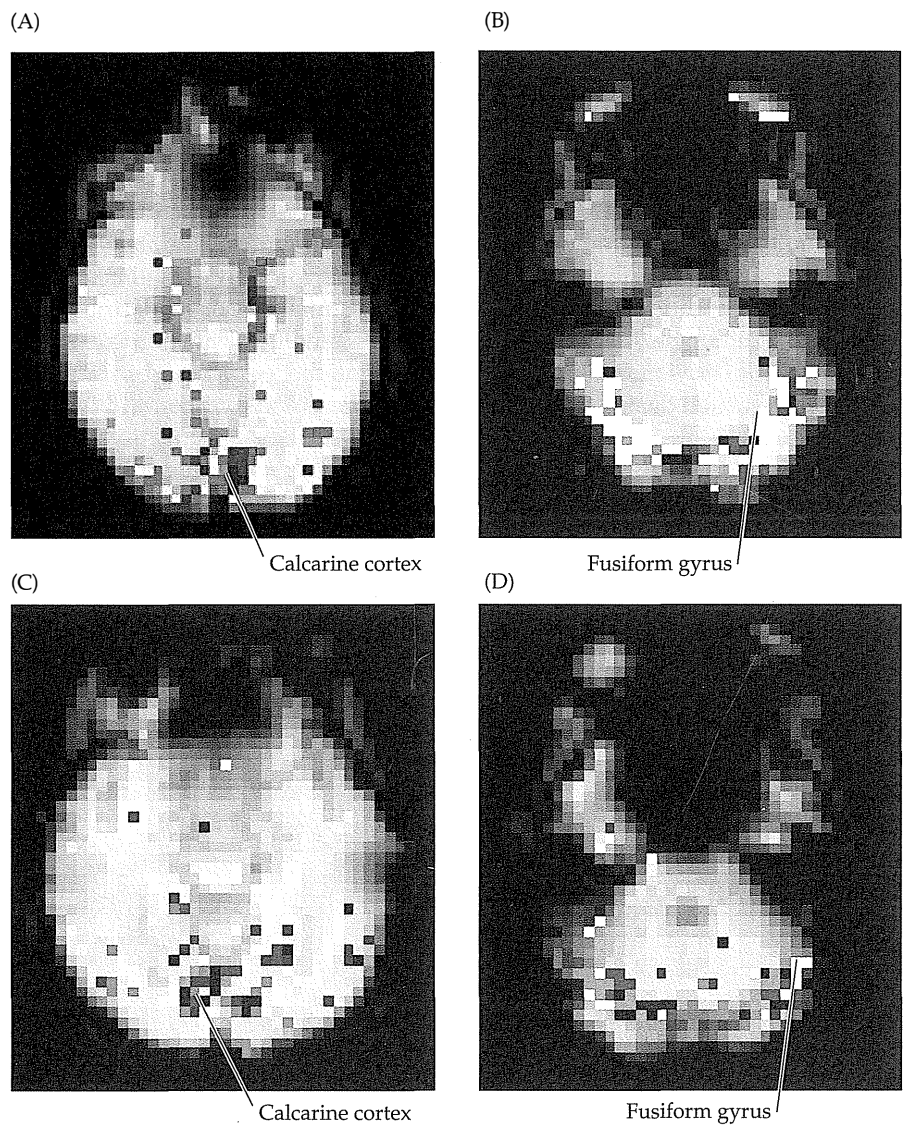

Figure 7.25 Maps of BOLD latency to peak in visual cortical regions. A 500 ms visual stimulus was presented and the latency to peak in voxels with significant BOLD activation was measured. Data are shown for two subjects [one subject shown in panels (A) and (B), and the other shown in (C) and (D)]. The colormap indicates the latency to peak of each voxel, with blue colors indicating more rapid hemodynamic responses, red colors indicating intermediate responses, and yellow colors indicating the slowest responses. Peak latency was shortest in voxels near the calcarine cortex (A, C), and was longest in the fusiform gyrus (B, D). (From Huettel et al., 2001.)

must selectively manipulate or measure one mental process while holding another constant. For example, decision processes may be proportional to response time, while low-level perceptual processes may be independent of response time, as in the study by Menon and colleagues. Comparisons within the same region do not suffer from the problem of neuronal vs hemodynamic activity, and thus very small within-region timing differences can be identified.

linear system A system that obeys the principles of scaling and superposition.

refractory effects Changes in the amplitude and timing of a response based on the characteristics of preceding responses.

Linearity of the Hemodynamic Response

So far we have considered the properties of the hemodynamic response to a single isolated stimulus. What happens when multiple stimuli are presented in succession, as is necessary for most experiments? One possibility is that the same hemodynamic response is evoked for every stimulus, independently of the other stimuli presented, as shown in Figure 7.26A. If so, stimuli delivered sufficiently close together that their hemodynamic responses overlap would generate a total change in MR signal equivalent to the sum of the individual responses (Figure 7.26B). This is known as a **linear system**, and its properties are discussed in the following section. Another possibility is that the hemodynamic response to a given stimulus depends on what other stimuli are presented (Figure 7.26C and D). If two stimuli are presented very close together, the combined response might be less than the sum of the two individual responses. Reductions in hemodynamic amplitude as a function of interstimulus interval are known as BOLD **refractory effects**. If refractory effects are present, then a linear model will overestimate the hemodynamic response to closely spaced stimuli, potentially reducing the effectiveness of experimental analy-

Figure 7.26 Linear and nonlinear addition of hemodynamic responses. If the same fMRI hemodynamic response were evoked by every stimulus (A), then the combined hemodynamic response to two stimuli would be a linear combination of two identical responses (B). But if the hemodynamic response were attenuated when stimuli were presented in rapid succession (C), then the combined response would be reduced in amplitude (D).

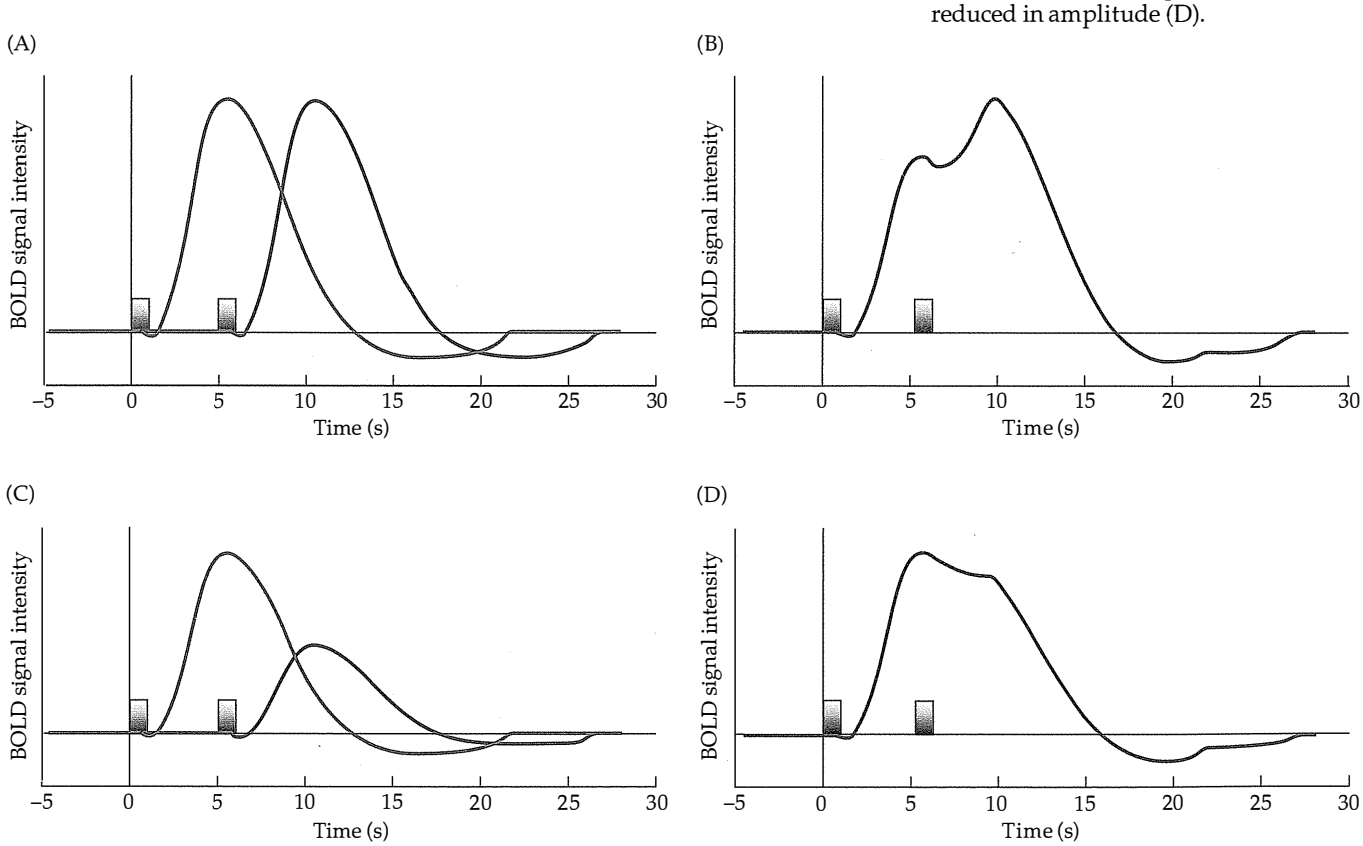

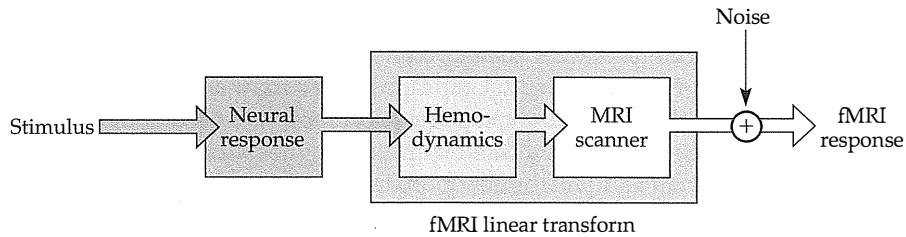

Figure 7.27 The linear systems framework for fMRI. Boynton and colleagues investigated whether the fMRI hemodynamic response might be a linear transformation of neuronal input, combined with additive Gaussian noise. (After Boynton et al., 1996.)

ses. It is critical, therefore, to consider the evidence for and against the linearity of the fMRI hemodynamic response.

Properties of a linear system

impulse A single input to a system. Impulses are assumed to be of infinitely short duration.

scaling A principle of linear systems that states that the magnitude of the system output must be proportional to the system input.

superposition A principle of linear systems that states that the total response to a set of inputs is equivalent to the summation of the independent responses to the inputs.

A basic framework for measurement of signal in fMRI is shown in Figure 7.27. Under this framework, when a stimulus is presented, it induces neuronal activity within a particular region of the brain. Since the neuronal activity requires oxygen delivered via the vascular system, there are resulting flow and volume changes in that brain region, as discussed earlier in this chapter. The reduction in magnetic susceptibility associated with increased blood oxygenation then becomes measurable as BOLD contrast using fMRI. To reformulate this framework in terms of a linear system, we can consider the neuronal activity as a short-duration input, or impulse, to the hemodynamic system, whose output is measured as an MR signal. For a given impulse, the hemodynamic system is assumed to always respond in the same manner. From this assumption follow two basic principles of a linear system: scaling and superposition.

The principle of scaling states that the output of a linear system is proportional to the magnitude of its input (Figure 7.28A). If the input is doubled, then the output is likewise doubled; if the input is halved, then so is the output. For fMRI data, this principle would predict that changes in the relative amplitude of neuronal activity should lead to similar changes in the amplitude of the hemodynamic response. Why is this principle important? Remember that the goal of fMRI is to determine changes in neuronal activity, which must be inferred from the amplitude changes in the hemodynamic response. So, a study may involve a test condition and a control condition, find that activation in the brain region of interest was twice as large in the test condition, and then infer that neuronal activity was also twice as large in that condition. If the hemodynamic amplitude were independent of the amplitude of neuronal activity, then no such inferences would be possible.

Whereas scaling refers to the amplitude of activation, the principle of superposition refers to the timing of activation (Figure 7.28B). Stated simply, superposition means that the total response to two or more events is the summation of the individual responses. If a single event generates a hemodynamic response, then two events presented in succession will generate a combined response equal to two individual responses added together. To understand the importance of superposition, consider a very simple experiment. You are interested in studying the brain activation associated with short-term memory for verbal stimuli, so you devise an experiment in which a word is presented, followed by a 2 s delay and then another word. The subject's task is to indicate whether or not the two words are the same. Since the two stimuli are both words, they will likely activate many of the same brain regions, and since they are presented so close together in time, their hemodynamic responses will overlap. How can you determine whether an area is active in response to the first word, the second word, or both? By assuming superposition, you can create

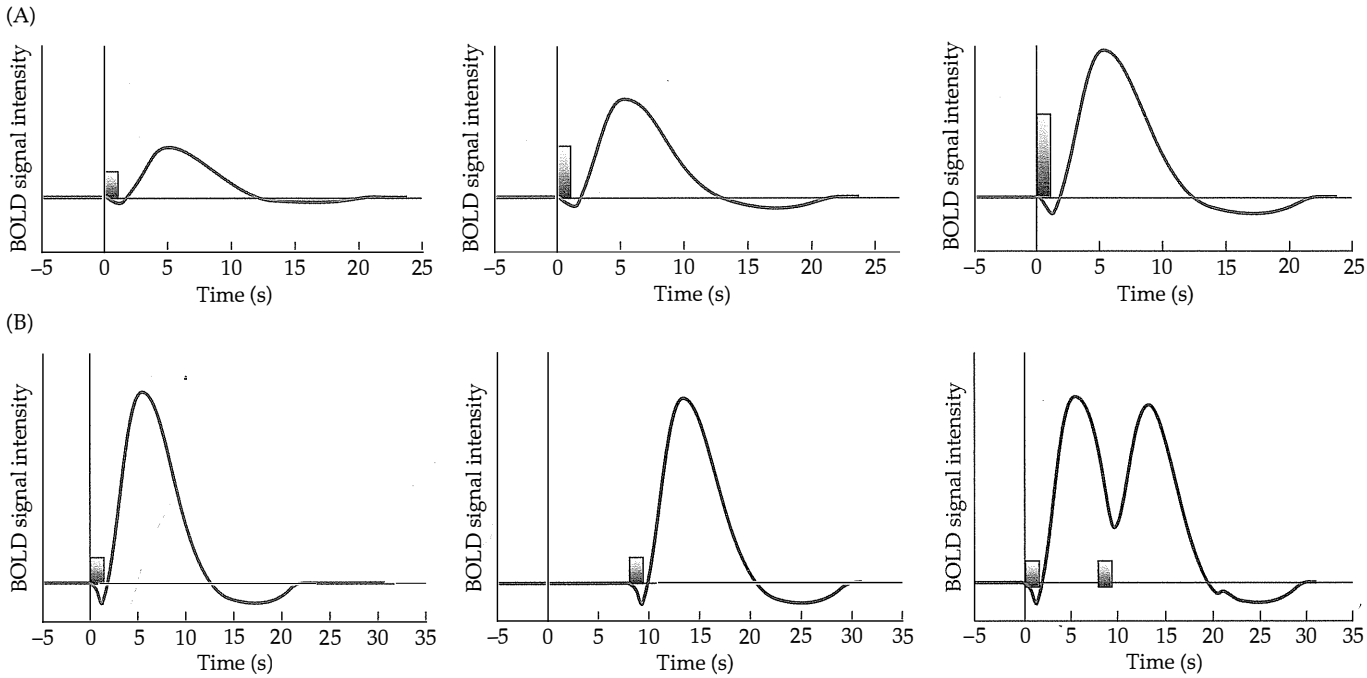

Figure 7.28 Scaling and superposition. (A) The principle of scaling states that the output of a linear system is proportional to the magnitude of the input. For fMRI, this implies that the amplitude of the hemodynamic response reflects the amount of underlying neuronal activity. (B) The principle of superposition states that the output of a linear system with more than one input is the sum of the responses to the individual inputs.

models for what combined hemodynamic response would be expected in each condition. If an area is active in response to the first word but not the second, it will show an early rise to a peak at about 5 s, whereas if it is active only in response to the second word, the rise will occur 2 s later. If it is active in response to both words, there will be an intermediate but larger peak. Without assuming superposition, or using approaches to correct for deviations from superposition, analysis of complex designs would be very challenging.

Evidence for rough linearity

The first study of the linearity of the fMRI BOLD response was reported by Boynton and colleagues in 1996. They investigated the effects of duration of visual stimulation, from 3 to 24 s, on activation in the primary visual cortex, using an EPI gradient-echo sequence at 1.5 T. The visual stimuli were checkerboard patterns that moved from right to left while flickering at a high rate (8 Hz). The contrast between dark and light squares on the checkerboard was manipulated over trials. The authors hypothesized that the duration and contrast of the stimuli should have independent and additive effects on the BOLD signal if the hemodynamic response behaved as a linear system. They found that, for all stimulus durations, the amplitude of activation was greater at higher visual contrast levels, but the hemodynamic response had the same basic shape. This was consistent with the scaling principle. To test whether the superposition principle also held for the BOLD data, they investigated whether the response to a longer stimulus could be predicted by the sum of multiple shorter stimuli. Their results indicated linear superposition for most stimulus durations, so the response to a 24-s stimulus could be approximated by the addition of two sequential responses to the 12-s stimuli or four sequential responses to the 6-s stimuli (Figure 7.29). The one exception they noted was that using the response to a 3-s stimulus led to an overestimation of the responses to longer stimuli, and this discrepancy was attributed to neuronal

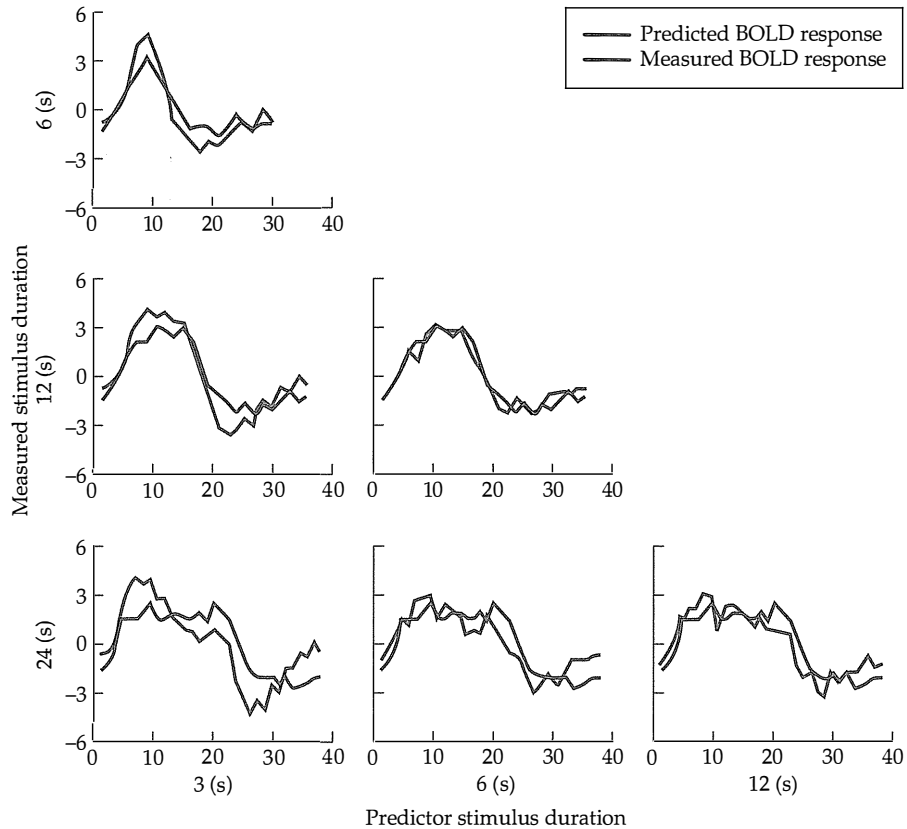

Figure 7.29 Evidence for the linearity of the fMRI hemodynamic response. Boynton and colleagues investigated whether the addition of the fMRI responses to several short-duration stimuli (blue lines) predicted the fMRI response to a longer-duration stimulus (red lines). The prediction fit the observed data well, apart from the overestimation of longer duration responses by addition of the 3 s stimuli. (After Boynton et al., 1996.)

adaptation effects (i.e., the neurons themselves decrease in activation over the first few seconds of a stimulus). In total, these results provided strong evidence for the linearity of the hemodynamic response over stimulus durations ranging from a few seconds to a few tens of seconds.

Building on the results of Boynton and colleagues, in 1997 Dale and Buckner investigated the linearity of the hemodynamic response to individual stimulus events, rather than extended stimulus blocks. They reasoned that neuronal adaptation effects could be eliminated by separating stimuli in time by an interval sufficiently long to allow complete neuronal recovery. To test whether complete linearity would be observed under such conditions, they presented clusters of one, two, or three stimuli at interstimulus intervals of either 2 or 5 s. The hemodynamic response to a second stimulus in a cluster was determined by subtracting the single-stimulus response from the response to a pair of stimuli. Likewise, the response to the third stimulus was determined by subtracting the two-stimulus response from the three-stimulus response. If the principle of superposition holds for fMRI BOLD data, then all responses should have the same amplitude and shape regardless of where they occur in the cluster. Dale and Buckner's evidence supported this interpretation, in that the responses to the second and third trials in each set were generally similar to that of the first trial, (Figure 7.30) especially for pairs of trials at a 5-s interval. They concluded that the fMRI BOLD response increases with additional stimuli in a "roughly linear" fashion at intervals typical of experimental testing (e.g., a few seconds).

This finding, that individual trials evoke recognizable hemodynamic responses even when separated by relatively short intervals, has become

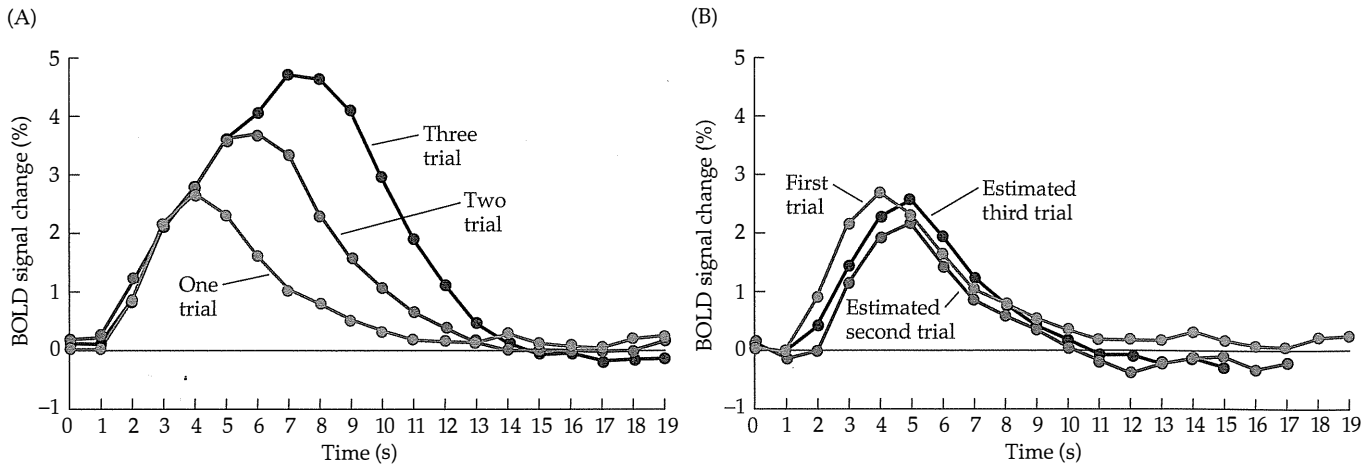

Figure 7.30 Linear addition of hemodynamic responses to individual stimulus events. (A) The hemodynamic responses evoked by presentation of one, two, or three identical stimuli (short-duration visual flashes) at short interstimulus intervals were measured. Shown here are data from a 2-s interval. The total hemodynamic response increased in a regular fashion as the number of stimuli in a trial increased. (B) By subtracting the one-stimulus trial from the two-stimulus trial, and the two-stimulus from the three-stimulus, the contributions of the second and third stimuli in a trial were estimated. The responses to the second and third stimuli were generally similar to the response to the first stimulus, suggesting that the BOLD response scales in a roughly linear fashion. (From Dale and Buckner, 1997.)

extremely influential in the design and analysis of fMRI studies. At first interpretation, it suggests that individual trials can be closely spaced to increase the number of trials presented and thus the experimental power, without loss of response amplitude. But, as the authors themselves note, there might be significant limitations in such fast-rate studies. The most important of these are the deviations from linearity at short intervals. Close examination of the data from 2-s interstimulus intervals (see Figure 7.30B) reveals that the responses to the second and third stimuli in a cluster are reduced in amplitude and increased in latency compared with the response to a single stimulus. In the best case, such nonlinearities would reduce the power of experimental analyses but would have little additional effect. But in the worst case, large nonlinearities could preclude the use of very short intervals (e.g., 1 s) between experimental stimuli. As shown in a 2005 article by Wager and colleagues, accounting for nonlinearities within fMRI analysis models can dramatically improve their sensitivity.

Challenges to linearity

Subsequent work on nonlinearities in the fMRI hemodynamic response investigated whether there is a refractory period following stimulus presentation during which subsequent stimuli evoke smaller hemodynamic responses. A preliminary suggestion based on the results described above is that the fMRI hemodynamic response may be nonlinear at intervals of less than 6 s but linear at longer intervals, since superposition was found at durations of 6 s but not 3 s, and better scaling was observed at intervals of 5 s than 2 s. Tests of refractory periods have been conducted using both blocked and event-related designs. Blocked designs (e.g., the 1996 Boynton and colleagues study) usually manipulated stimulus duration, and event-related designs (e.g., the 1997 Dale and Buckner study) usually manipulated interstimulus interval. The issues investigated by the researchers included the timing of refractory effects, whether such effects differ across subject groups, and whether different brain regions have different refractory properties.

Blocked-design studies have verified that substantial refractory effects are present after short stimulus durations. In 1998 Robson and colleagues examined whether the response to a long-duration auditory stimulus could be predicted by the addition of multiple short-duration stimuli, testing durations from

nonlinearity The property whereby the combined response to two or more events is not equivalent to the summation of the responses to the individual events in isolation.

refractory period A time period following the presentation of a stimulus during which subsequent stimuli evoke a reduced response. For BOLD fMRI, the refractory periods for many types of stimuli last approximately 6 s.

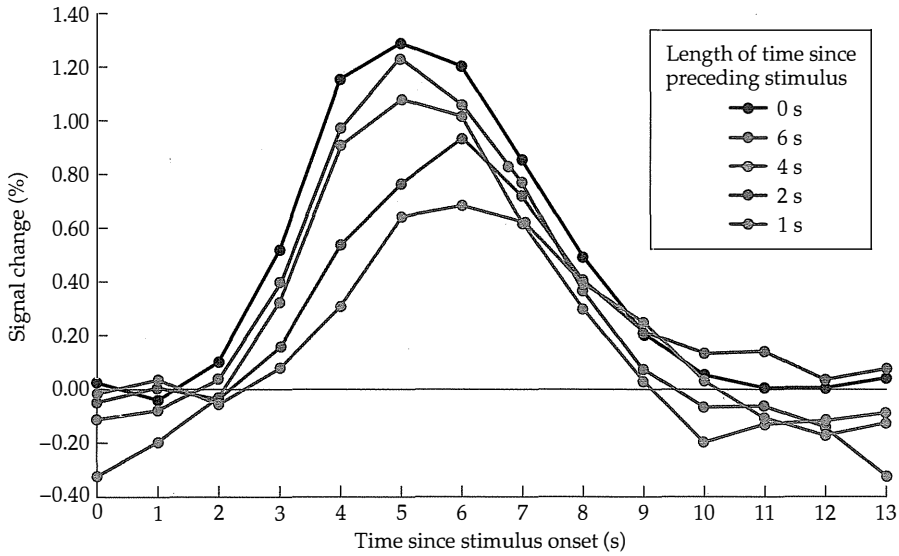

Figure 7.31 Nonlinearity of the hemodynamic response at short interstimulus intervals. Each trial consisted of a single visual stimulus or a pair of visual stimuli separated by a short interval. Single stimuli evoked a robust hemodynamic response (black line). At short interstimulus intervals (e.g., 1 to 2 s), the hemodynamic response was reduced in amplitude and increased in latency. These changes reflect the presence of refractory effects in the hemodynamic response. (After Huettel and McCarthy, 2000.)

100 ms to 25.5 s. As for the previous study by Boynton and colleagues, superposition held for stimuli of 6 s or more in duration, but not for shorter-duration stimuli. Furthermore, as the stimuli became shorter, the deviations from superposition became greater. Similar results were reported by Vazquez and Noll in 1998 for visual stimuli, with significant nonlinearities found for stimuli shorter than 4 s. Event-related studies also support the idea of a refractory period. Huettel and McCarthy presented short-duration visual checkerboard stimuli either singly or in pairs separated by a 1-s to 6-s interstimulus interval (Figure 7.31). Within the primary visual cortex, the response to a second stimulus in a pair separated by 1 s was reduced by more than 40% compared with the single-stimulus response and was delayed in time by nearly 1 s. By 6 s, both the amplitude and latency of the hemodynamic response to the second stimulus in a pair had returned to near normal values. The finding of both amplitude and latency changes is consistent with the earlier work of Dale and Buckner, as well as with computational simulations of the hemodynamic response.

The existence of refractory effects in the BOLD signal is now well-supported by many studies. As a result, the focus of research has shifted toward examining differences in refractory effects between individuals or brain regions. One of the first subject group comparisons was between young adults and healthy elderly adults. Given the many structural changes in the brain that accompany aging, including possible impairments in blood flow, it was predicted that refractory effects would be greater in elderly adults. This prediction, though sensible, turns out to be wrong. The magnitude of the refractory effect is similar for older and younger adults, as is the amplitude of the hemodynamic response itself. Another area of research is whether, in some patient groups, nonlinearities might be diagnostic of neurological or psychiatric deficits. Patients with schizophrenia, for example, exhibit abnormal sensory habituation, as indicated by electrophysiological measures. While neurologically normal adults show a significant decrease in electrophysiological responses when a stimulus is presented twice in rapid succession, a phenomenon known as sensory gating, schizophrenic adults show a much smaller decrease. While there are now many fMRI studies of sensory gating, whether these effects have consequences for the BOLD response remains unknown. For example, in a 2003 study by Barch and colleagues, individuals with schizo-

phrenia showed normal BOLD linearity with an interstimulus interval of 5 s. Future research that combines electrophysiological and fMRI data will provide important insights into these and other individual differences.

A number of studies have shown that refractory effects can also differ in different brain regions. Primary sensory or motor regions appear to have smaller refractory effects (i.e., are more linear) than other regions of the cortex. In 2001, Birn and colleagues measured activity in the motor regions M1 and SMA while subjects tapped their fingers for different durations. The hemodynamic response in M1 increased in amplitude with increasing duration, although there were deviations from superposition for stimuli shorter than about 4 s. But in the SMA, which is involved with the planning of motor behavior, activation amplitude was similar across all stimulus durations. Huettel and colleagues showed in 2004 that a similar relationship holds for visual stimuli: activation in the primary visual cortex scaled with duration of a visual stimulus, but activation in the motion-sensitive region V5 was independent of duration. However, comparisons of refractory effects between brain regions may be confounded by differences in neuronal activity. In both of the studies described above, the secondary regions examined (SMA and V5) may be transiently active at the beginning of the stimulus, while the primary cortex may show sustained activation throughout stimulus presentation. Thus, it is worth reemphasizing that refractory effects measured using fMRI may result from neuronal adaptation or from changes in vascular responsiveness, either of which could differ in different brain regions.

fMRI-adaptation

Although refractory effects are often seen as impediments to fMRI research, they can be used to understand brain function in cleverly designed experiments. The basic idea comes from physiological studies of adaptation. If one repeatedly presents the same stimulus to a subject, such as repeatedly exposing a rat to a loud noise or showing a bright red balloon to a human infant, the response to that stimulus will diminish over time. After a number of presentations, the rat will stop flinching at the noise and the infant will become bored with the balloon. When the response to a stimulus decreases with repeated presentation, the subject is said to have adapted to that stimulus. By changing the stimulus slightly, we can discover to which aspects of the stimulus the subject has adapted. If we replace the red balloon with a red fire truck and the infant is still bored, then we can infer that she adapted to the color red. But if she is now very interested in the fire truck, then she must have adapted to some other property of the balloon, such as its shape. Many neurons in the visual system will preferentially fire for one type of visual stimulus, due to its particular shape, color, or way of movement. But with repeated presentations of that stimulus, the neuron's firing rate will decrease dramatically.

Given the presence of fMRI refractory effects, we can apply similar principles to experimental designs in an approach known as fMRI-adaptation (Figure 7.32). First, we present a stimulus that evokes activation in a particular brain region. After a short time period, we then present another stimulus that differs in some fashion. If the region being investigated contains neurons that respond differently to the new stimulus, it will show an increase in fMRI activation. But if the neurons do not distinguish between the old and new stimuli, fMRI activation will be at a low level because of refractory effects. For example, refractory effects in the secondary (but not primary) visual cortex depend on the orientation of visual line gratings; refractory effects in face-sen-

adaptation A change in the response to a stimulus following its repeated presentation.

fMRI-adaptation Reduction in the BOLD response to the repeated presentation of a set of stimuli that differ in some attribute, indicating that the brain region being studied is insensitive (as measured by fMRI) to the stimulus attribute being varied.

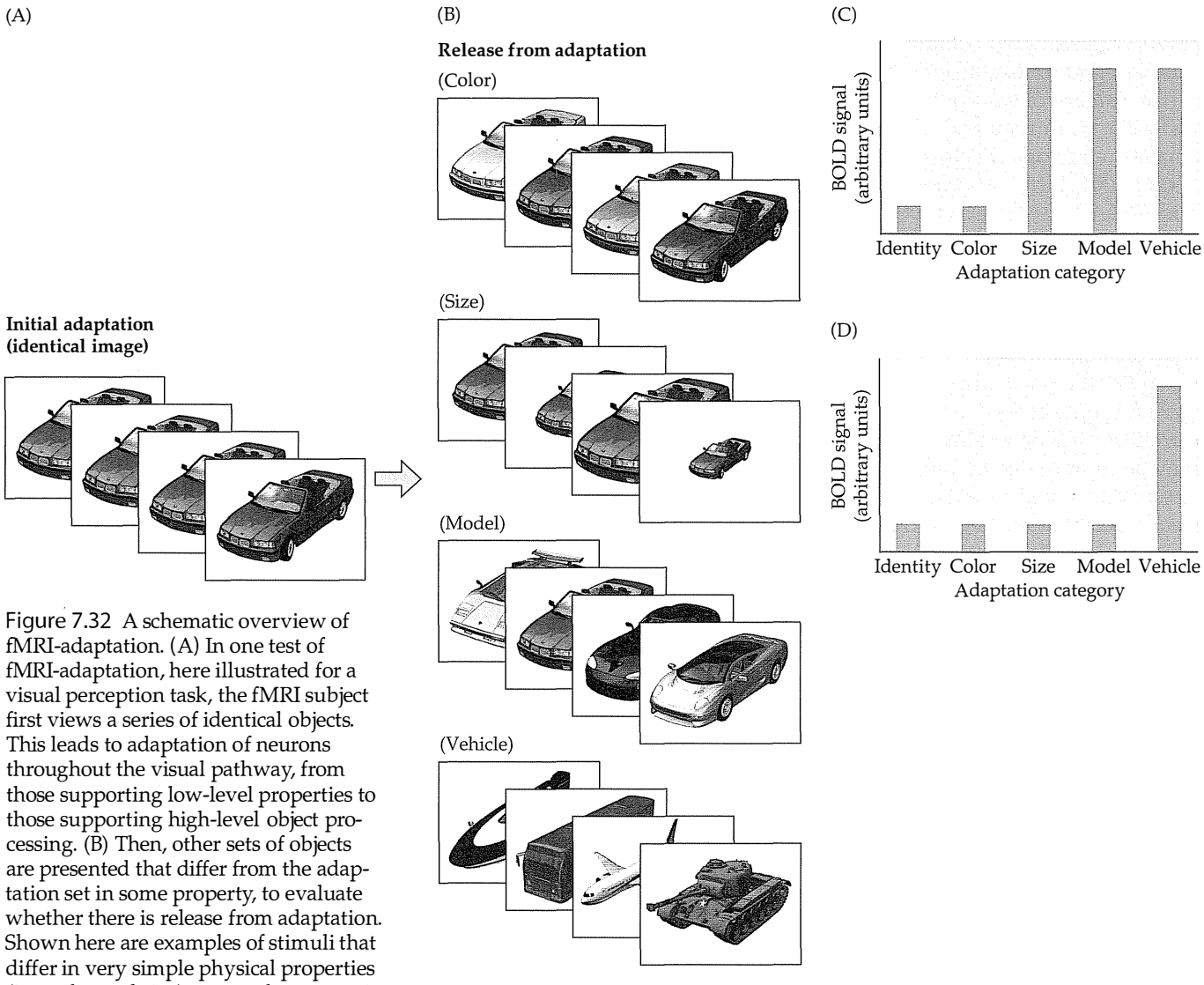

Figure 7.32 A schematic overview of fMRI-adaptation. (A) In one test of fMRI-adaptation, here illustrated for a visual perception task, the fMRI subject first views a series of identical objects. This leads to adaptation of neurons throughout the visual pathway, from those supporting low-level properties to those supporting high-level object processing. (B) Then, other sets of objects are presented that differ from the adaptation set in some property, to evaluate whether there is release from adaptation. Shown here are examples of stimuli that differ in very simple physical properties (i.e., color and size) or complex categorical properties (i.e., car model and vehicle type). By comparing which stimulus sets lead to the greatest fMRI activation in a given brain region, the researcher can identify properties that the neurons in that region are sensitive to. Shown here are hypothetical BOLD responses in (C) a region whose neurons are sensitive to any physical change in a stimulus other than color and (D) a region whose neurons code complex object categories, like cars, but do not generalize to all vehicles.

sitive cortical regions are greater for pairs of identical faces than for pairs of different faces; and refractory effects in the motion-sensitive area V5 depend on the direction of motion.

While these and other findings provided insight into the functional specificity of BOLD effects in these regions, other studies have explored fMRI-adaption in more complex forms of processing. In an elegant series of experiments published in 2001, Grill-Spector and Malach investigated whether neurons in the lateral occipital complex, which contains the lateral occipital lobe and the posterior fusiform gyrus, are sensitive to changes in higher-order properties of objects. For one of their experiments, they presented the same face repeatedly within a 10-s block. They compared the activation in this "identical face" condition with the activation measured in conditions where some property of the face was manipulated, such as position on the screen, viewpoint from left to right, illumination, size, or identity (i.e., different faces presented). Only one condition was varied within each block. In these brain regions, roughly similar activation would be observed in response to any of the faces presented in isolation, so differential activation in the blocks would indicate refractory effects

associated with some aspect of the stimulus presentation. The researchers found that activation in the fusiform gyrus, for example, was greatly reduced in response to repeated presentations of identical, size-varying, or position-varying faces, compared with repeated presentations of entirely different faces. In contrast, variation in direction of illumination or viewpoint caused a recovery from adaptation. From these results, the researchers concluded that the fusiform gyrus recognizes facial identity despite size or position manipulations, but does treat illumination or viewpoint manipulations as new stimuli.

The power of the fMRI-adaptation approach comes from its flexibility. In principle, any stimulus property that can evoke activation within a region can be manipulated to evaluate adaptation effects. For example, two independent but simultaneously published 2007 studies by Piazza and colleagues and by Cohen Kadosh and colleagues used fMRI-adaptation to study number processing in the posterior parietal cortex. With a number of manipulations, both groups found clear evidence that voxels in this region coded for numerosity regardless of whether the stimulus was presented as a numeral, word, or dot pattern. That is, if the numeral "4" was followed by the word "four," the response to that word was attenuated. (Note that there was also some evidence that at least some parts of the parietal cortex may code separately for numeral and word representations of a number.) Moreover, the amount of recovery from adaptation depended on the magnitude difference between successive stimuli: a larger response was observed when the new number was very different from the adaptation number (e.g., from 17 to 39) compared with when the numbers were only slightly different (e.g., from 17 to 20). Other domains to which fMRI-adaptation has been applied include commonalities between visual and motor processing, properties of word processing, and many other aspects of sensation and perception. Yet, there are limitations to these types of studies: effects attributed to adaptation within a region could also arise from adaptation within neurons elsewhere that project to the target region. For a broad overview of the strengths and limitations of fMRI-adaptation, see the 2006 review article by Krekelberg and colleagues in the Chapter References.

Summary

Nearly all fMRI studies rely on an endogenous measure known as blood-oxygenation-level dependent (BOLD) contrast. The idea of using blood properties as indices of brain functions is more than a century old. Early research found that deoxygenated hemoglobin is paramagnetic and altered the T_2^* properties of nearby tissue. Important studies demonstrating the feasibility of BOLD contrast were conducted by Ogawa and colleagues using both test tube and animal models. These results, in conjunction with the increased prevalence of MRI scanners and the development of high-speed pulse sequences, set the stage for the growth of fMRI in the early 1990s. The BOLD response to brief neuronal activity (i.e., the hemodynamic response) consists of a short onset delay, a rise to a peak after a few seconds, a return to baseline, and a prolonged undershoot. Some researchers report the presence of an initial dip in the BOLD signal due to oxygen extraction before the large increase in blood flow, but this effect is not always seen. The spatial resolution of an fMRI study determines our ability to separate adjacent brain regions with different functional properties. It can be improved by collecting data using smaller voxels, at a cost of reduced BOLD signal. However, the organization and response properties of the vascular system introduce spatial constraints. The temporal resolution of fMRI refers to the ability to esti-

REFER TO THE
fMRI
COMPANION WEBSITE AT
www.sinauer.com/fmri2e
for study questions and Web links.

mate the timing of neuronal activity from the measured hemodynamic changes. While using a short repetition time can improve temporal resolution, the sluggishness of the hemodynamic response limits researchers' ability to make precise temporal measurements. Nonlinearities in the fMRI hemodynamic response reflect the temporal dynamics of activation in a single spatial location. If the same brain region becomes active twice in rapid succession, within an interval of about 6 s, the hemodynamic response to the second event is reduced in amplitude compared with that evoked by a single event. While refractory effects present an analysis challenge for most studies, some researchers have taken advantage of these effects to study functional adaptation within a brain region.

Suggested Readings

*Blamire A. M., Ogawa S., Ugurbil K., Rothman D., McCarthy G., Ellermann J. M., Hyder F., Rattner Z., and Shulman R. G. (1992). Dynamic mapping of the human visual cortex by high-speed magnetic resonance imaging. *Proc. Natl. Acad. Sci. U. S. A.*, 89(22): 11069–11073. *This early study describes the first use of event-related designs in fMRI.*

*Boynton, G. M., Engel, S. A., Glover, G. H., and Heeger, D. J. (1996). Linear systems analysis of functional magnetic resonance imaging in human V1. *J. Neurosci.*, 16(13): 4207–4221. *This early and influential study provides evidence supporting the idea that the fMRI BOLD signal results from a linear transformation of neuronal activity.*

*Fox, P. T., Raichle, M. E., Mintun, M. A., and Dence, C. (1988). Nonoxidative glucose consumption during focal physiologic neural activity. *Science*, 241(4864): 462–464. *This classic paper details the relationship between blood flow, glucose metabolism, and oxygen utilization in the human brain, studied by PET.*

*Krekelberg, B., Boynton, G. M., and van Wezel, R. J. (2006). Adaptation: from single cells to BOLD signals. *Trends Neurosci.*, 29: 250–256. *An overview of how refractory effects in the fMRI signal can be used to draw inferences about brain function.*

*Kwong K. K., Belliveau J. W., Chesler D. A., Goldberg I. E., Weisskoff R. M., Poncelet B. P., Kennedy D. N., Hoppel B. E., Cohen M. S., and Turner R. (1992). Dynamic magnetic resonance imaging of human brain activity during primary sensory stimulation. *Proc. Natl. Acad. Sci. U. S. A.*, 89(12): 5675–5679. *This manuscript describes the first BOLD fMRI study.*

*Logothetis, N. K. (2008). What we can do and what we cannot do with fMRI. *Nature*, 453: 869–878. *A comprehensive and engaging summary of how the biological underpinnings of fMRI shape its strengths and limitations.*

*Menon, R. S., Luknowsky, D. C., and Gati, J. S. (1998). Mental chronometry using latency-resolved functional MRI. *Proc. Natl. Acad. Sci. U. S. A.*, 95(18): 10902–10907. *This article provides striking early demonstrations of the power of fMRI to detect very small differences in timing between successive events.*

*Ogawa S., Lee T. M., Kay A. R., and Tank D. W. (1990a). Brain magnetic resonance imaging with contrast dependent on blood oxygenation. *Proc. Natl. Acad. Sci. U. S. A.*, 87(24): 9868–9872. *This report provided the initial demonstration of the effects of blood oxygenation on T_2* contrast, through studies of rats at high magnetic field strengths.*

*Pauling, L., and Coryell, C. D. (1936). The magnetic properties and structure of hemoglobin, oxygenated hemoglobin, and carbonmonoxygenated hemoglobin. *Proc. Natl. Acad. Sci. U.S.A.*, 22(4): 210–236. *This accessible manuscript from a future Nobel laureate describes the basic chemical and physical properties of hemoglobin.*

*Indicates a reference that is a suggested reading in the field and is also cited in this chapter.

Chapter References

Ances, B. M. (2004). Coupling of changes in cerebral blood flow with neural activity: what must initially dip must come back up. *J. Cereb. Blood Flow Metab.*, 24: 1–6.

Ances, B. M., Leontiev, O., Perthen, J. E., Liang, C., Lansing, A. E., and Buxton, R. B. (2008). Regional differences in the coupling of cerebral blood flow and oxygen metabolism changes in response to activation: implications for BOLD-fMRI. *NeuroImage*, 39, 1510–1521.

Bandettini, P. A., Wong, E. C., Hinks, R. S., Tikofsky, R. S., and Hyde, J. S. (1992). Time course EPI of human brain function during task activation. *Magn. Reson. Med.*, 25: 390–397.

Barch, D. M., Mathews, J. R., Buckner, R. L., Maccotta, L., Csernansky, J. G., and Snyder, A. Z. (2003). Hemodynamic responses in visual, motor, and somatosensory cortices in schizophrenia. *NeuroImage*, 20: 1884–1893.

Belliveau J. W., Kennedy D. N., Jr., McKinstry R. C., Buchbinder B. R., Weisskoff R. M., Cohen M. S., Vevea J. M., Brady T. J., and Rosen B. R. (1991). Functional mapping of the human visual cortex by magnetic resonance imaging. *Science*, 254(5032): 716–719.

Birn, R. M., Saad, Z. S., and Bandettini, P. A. (2001). Spatial heterogeneity of the nonlinear dynamics in the fMRI BOLD response. *NeuroImage*, 14(4): 817–826.

Blamire A. M., Ogawa S., Ugurbil K., Rothman D., McCarthy G., Ellermann J. M., Hyder F., Rattner Z., and Shulman R. G. (1992). Dynamic mapping of the human visual cortex by high-speed magnetic resonance imaging. *Proc. Natl. Acad. Sci. U. S. A.*, 89(22): 11069–11073.

Boynton, G. M., and Finney, E. M. (2003). Orientation-specific adaptation in human visual cortex. *J. Neurosci.*, 23: 8781–8787.

Brodmann, K. (1909). *Vergleichende Lokalisationslehre der Grosshirnrinde in ihren Prinzipien dargestellt auf Grund des Zellenbaues.* Barth, Leipzig, Germany.

Buxton, R. B., and Frank, L. R. (1997). A model for the coupling between cerebral blood flow and oxygen metabolism during neural stimulation. *J. Cereb. Blood Flow Metab.*, 17(1): 64–72.

Buxton, R. B., Wong, E. C., and Frank, L. R. (1998). Dynamics of blood flow and oxygen metabolism during brain activation: the balloon model. *Magn. Reson. Med.*, 39: 855–864.

Cheng, K., Waggoner, R. A., and Tanaka, K. (2001). Human ocular dominance columns as revealed by high-field functional magnetic resonance imaging. *Neuron*, 32(2): 359–374.

Cohen Kadosh, R., Cohen Kadosh, K., Kaas, A., Henik, A., and Goebel, R. (2007). Notation-dependent and -independent representations of numbers in the parietal lobes. *Neuron*, 53: 307–314.

Dale, A. M., and Buckner, R. L. (1997). Selective averaging of rapidly presented individual trials using fMRI. *Hum. Brain Mapping*, 5: 329–340.

D'Esposito, M., Zarahn, E., Aguirre, G. K., and Rypma, B. (1999). The effect of normal aging on the coupling of neural activity to the BOLD HDR. *NeuroImage*, 10: 6–14.

Disbrow, E. A., Slutsky, D. A., Roberts, T. P., and Krubitzer, L. A. (2000). Functional MRI at 1.5 Tesla: A comparison of the blood oxygenation level-dependent signal and electrophysiology. *Proc. Natl. Acad. Sci. U. S. A.*, 97(17): 9718–9723.

Duong T. Q., Kim D. S., Ugurbil K., and Kim S. G. (2001). Localized cerebral blood flow response at submillimeter columnar resolution. *Proc. Natl. Acad. Sci. U. S. A.*, 98(19): 10904–10909.

Fox, P. T., and Raichle, M. E. (1986). Focal physiological uncoupling of cerebral blood flow and oxidative metabolism during somatosensory stimulation in human subjects. *Proc. Natl. Acad. Sci. U. S. A.*, 83(4): 1140–1144.

Frahm, J., Merboldt, K. D., Hanicke, W., Kleinschmidt, A., and Boecker, H. (1994). Brain or vein—oxygenation or flow? On signal physiology in functional MRI of human brain activation. *NMR Biomed.*, 7(1–2): 45–53.

Gjedde, A., Marrett, S., and Vafaee, M. (2002). Oxidative and nonoxidative metabolism of excited neurons and astrocytes. *J. Cereb. Blood Flow Metab.*, 22(1): 1–14.

Goense, J. B., and Logothetis, N. K. (2008). Neurophysiology of the BOLD fMRI signal in awake monkeys. *Curr. Biol.*, 18: 631–640.

Grill-Spector, K., and Malach, R. (2001). fMR-adaptation: A tool for studying the functional properties of human cortical neurons. *Acta Psychologica*, 107(1–3): 293–321.

Gur, R. C., Ragland, J. D., Reivich, M., Greenberg, J. H., Alavi, A., and Gur, R. E. (2008). Regional differences in the coupling between resting cerebral blood flow and metabolism may indicate action preparedness as a default state. *Cereb. Cortex*, doi:10.1093/cercor/bhn087

Harel, N., Lee, S. P., Nagaoka, T., Kim, D. S., and Kim, S. G. (2002). Origin of negative blood oxygenation level-dependent fMRI signals. *J. Cereb. Blood Flow Metabol.*, 22(8): 908–917.

Harshbarger, T. B., and Song, A. W. (2008). Differentiating sensitivity of post-stimulus undershoot under diffusion weighting: implication of vascular and neuronal hierarchy. *PLoS ONE* 3, e2914.

Huettel, S. A., and McCarthy, G. (2000). Evidence for a refractory period in the hemodynamic response to visual stimuli as measured by MRI. *NeuroImage*, 11(5): 547–553.

Huettel, S. A., McKeown, M. J., Song, A. W., Hart, S., Spencer, D. D., Allison, T., and McCarthy, G. (2004). Linking hemodynamic and electrophysiological measures of brain activity: Evidence from functional MRI and intracranial field potentials. *Cereb. Cortex*, 14: 165–173.

Huettel, S. A., Obembe, J., Song, A., and Woldorff, M. (2004). The BOLD fMRI refractory effect is specific to stimulus attributes: Evidence from a visual motion paradigm. *NeuroImage*, 21: 402–408.

Huettel, S. A., Singerman, J., and McCarthy, G. (2001). The effects of aging upon the hemodynamic response measured by functional MRI. *NeuroImage*, 13(1): 161–175.

Hyder, F., Rothman, D. L., and Shulman, R. G. (2002). Total neuroenergetics support localized brain activity: Implications for the interpretation of fMRI. *Proc. Natl. Acad. Sci. U. S. A.*, 99(16): 10771–10776.

Jones M., Berwick J., Johnston D., and Mayhew J. (2001). Concurrent optical imaging spectroscopy and laser-Doppler flowmetry: The relationship between blood flow, oxygenation, and volume in rodent barrel cortex. *NeuroImage*, 13(6 Pt. 1): 1002–1015.

Kim, S. G., and Ogawa, S. (2002). Insights into new techniques for high resolution functional MRI. *Curr. Opinion Neurobiol.*, 12(5): 607–615.

Li, B., and Freeman, R. D. (2007). High-resolution neurometabolic coupling in the lateral geniculate nucleus. *J. Neurosci*, 27: 10223–10229.

Lu, H., Golay, X., Pekar, J. J., and Van Zijl, P. C. (2004). Sustained poststimulus elevation in cerebral oxygen utilization after vascular recovery. *J. Cereb. Blood Flow Metab.*, 24: 764–770.

Lindquist, M. A., Zhang, C. H., Glover, G., and Shepp, L. (2008). Rapid three-dimensional functional magnetic resonance imaging of the initial negative BOLD response. *J. Magn. Reson.* 191: 100–111.

Logothetis, N. K., Pauls, J., Augath, M., Trinath, T., and Oeltermann, A. (2001). Neurophysiological investigation of the basis of the fMRI signal. *Nature*, 412(6843): 150–157.

Madsen, P. L., Linde, R., Hasselbalch, S. G., Paulson, O. B., and Lassen, N. A. (1998). Activation-induced resetting of cerebral oxygen and glucose uptake in the rat. *J. Cereb. Blood Flow Metab.*, 18: 742–748.

Madsen, P. L., Hasselbalch, S. G., Hagemann, L. P., Olsen, K. S., Bulow, J., Holm, S., Wildschiodtz, G., Paulson, O. B., and Lassen, N. A. (1995). Persistent resetting of

the cerebral oxygen/glucose uptake ratio by brain activation: evidence obtained with the Kety-Schmidt technique. *J. Cereb. Blood Flow Metab.*, 15: 485–491.

Magistretti, P. J., and Pellerin, L. (1999). Cellular mechanisms of brain energy metabolism and their relevance to functional brain imaging. *Philos. Trans. Royal Soc. London Ser. B Biol. Sci.*, 354(1387): 1155–1163.

Malonek, D., and Grinvald, A. (1996). Interactions between electrical activity and cortical microcirculation revealed by imaging spectroscopy: Implications for functional brain mapping. *Science*, 272(5261): 551–554.

Mandeville J. B., Marota J. J., Ayata C., Moskowitz M. A., Weisskoff R. M., and Rosen B. R. (1998). Dynamic functional imaging of relative cerebral blood volume during rat forepaw stimulation. *Magn. Reson. Med.*, 39(4): 615–624.

Mandeville J. B., Marota J. J., Kosofsky B. E., Keltner J. R., Weissleder R., Rosen B. R., and Weisskoff R. M. (1999). MRI measurement of the temporal evolution of relative CMRO(2) during rat forepaw stimulation. *Magn. Reson. Med.*, 42(5): 944–951.

Mansfield, P., and Maudsley, A. A. (1977). Medical imaging by NMR. *Br. J. Radiol.*, 50(591): 188–194.

Menon, R. S. (2002). Postacquisition suppression of large-vessel BOLD signals in high-resolution fMRI. *Magn. Reson. Med.*, 47: 1–9.

Menon, R. S., and Kim, S. G. (1999). Spatial and temporal limits in cognitive neuroimaging with fMRI. *Trends Cogn. Sci.*, 3(6): 207–216.

Menon R. S., Ogawa S., Hu X., Strupp J. P., Anderson P., and Ugurbil K. (1995). BOLD based functional MRI at 4 Tesla includes a capillary bed contribution: Echo-planar imaging correlates with previous optical imaging using intrinsic signals. *Magn. Reson. Med.*, 33(3): 453–459.

Miezin, F. M., Maccotta, L., Ollinger, J. M., Petersen, S. E., and Buckner, R. L. (2000). Characterizing the hemodynamic response: Effects of presentation rate, sampling procedure, and the possibility of ordering brain activity based on relative timing. *NeuroImage*, 11(6 Pt. 1): 735–759.

Moseley, M. E., and Glover, G. H. Functional MR imaging: capabilities and limitations. In: Kucharczyk, J., Moseley, M. E., Roberts, T., and Orrison, W. U. (eds) (1995). *Functional Neuroimaging*. W. B. Saunders Company, Philadelphia, p. 161–191.

Mukamel, R., Gelbard, H., Arieli, A., Hasson, U., Fried, I., and Malach, R. (2005). Coupling between neuronal firing, field potentials, and FMRI in human auditory cortex. *Science*, 309: 951–954.

Ogawa, S., and Lee, T. M. (1990). Magnetic resonance imaging of blood vessels at high fields: In vivo and in vitro measurements and image simulation. *Magn. Reson. Med.*, 16(1): 9–18.

Ogawa S., Lee T. M., Nayak A. S., and Glynn P. (1990b). Oxygenation-sensitive contrast in magnetic resonance image of rodent brain at high magnetic fields. *Magn. Reson. Med.*, 14(1): 68–78.

Ogawa S., Tank D. W., Menon R., Ellermann J. M., Kim S. G., Merkle H., and Ugurbil K. (1992). Intrinsic signal changes accompanying sensory stimulation: Functional brain mapping with magnetic resonance imaging. *Proc. Natl. Acad. Sci. U. S. A.*, 89(13): 5951–5955.

Parri, R., and Crunelli, V. (2003). An astrocyte bridge from synapse to blood flow. *Nat. Neurosci.*, 6(1): 5–6.

Piazza, M., Pinel, P., Le Bihan, D., and Dehaene, S. (2007). A magnitude code common to numerosities and number symbols in human intraparietal cortex. *Neuron*, 53: 293–305.

Richter, W., Ugurbil, K., Georgopoulos, A., and Kim, S. G. (1997). Time-resolved fMRI of mental rotation. *NeuroReport*, 8: 3697–3702.

Robson, M. D., Dorosz, J. L., and Gore, J. C. (1998). Measurements of the temporal fMRI response of the human auditory cortex to trains of tones. *NeuroImage*, 7: 185–198.

Shulman, R. G., Hyder, F., and Rothman, D. L. (2002). Biophysical basis of brain activity: Implications for neuroimaging. *Q. Rev. Biophys.*, 35(3): 287–325.

Silva, A. C., Lee, S. P., Iadecola, C., and Kim, S. G. (2000). Early temporal characteristics of cerebral blood flow and deoxyhemoglobin changes during somatosensory stimulation. *J. Cereb. Blood Flow Metab.*, 20(1): 201–206.

Smith, A. J., Blumenfeld, H., Behar, K. L., Rothman, D. L., Shulman, R. G., and Hyder, F. (2002). Cerebral energetics and spiking frequency: The neurophysiological basis of fMRI. *Proc. Natl. Acad. Sci. U. S. A.*, 99(16): 10765–10770.

Sokoloff, L., Reivich, M., Kennedy, C., Des Rosiers, M. H., Patlak, C. S., Pettigrew, K. D., Sakurada, O., and Shinohara, M. (1977). The ^{14}C-2-deoxyglucose method for the measurement of local cerebral glucose utilization. Theory, procedure, and normal values in the conscious and anaesthetized rat. *J. Neurochem.*, 28: 897–916.

Soon, C.-S., Venkatraman, V., and Chee, M. W. L. (2003). Stimulus repetition and hemodynamic response refractoriness in event-related fMRI. *Hum. Brain Mapping*, 20: 1–12.

Thulborn K. R., Waterton J. C., Matthews P. M., and Radda G. K. (1982). Oxygenation dependence of the transverse relaxation time of water protons in whole blood at high field. *Biochim. Biophys. Acta*, 714(2): 265–270.

Turner, R. (1988). Minimum inductance coils. *J. Phys. E Sci. Instrum.*, (21): 948–952.

Vanzetta, I., and Grinvald, A. (1999). Increased cortical oxidative metabolism due to sensory stimulation: Implications for functional brain imaging. *Science*, 286(5444): 1555–1558.

Vazquez, A. L., and Noll, D. C. (1998). Nonlinear aspects of the BOLD response in functional MRI. *NeuroImage*, 7: 108–118.

Wager, T. D., Vazquez, A., Hernandez, L., and Noll, D. C. (2005). Accounting for nonlinear BOLD effects in fMRI: parameter estimates and a model for prediction in rapid event-related studies. *NeuroImage*, 25: 206–218.

Wong, E. C., Jesmanowicz, A., and Hyde, J. S. (1991). Coil optimization for MRI by conjugate gradient descent. *Magn. Reson. Med.*, 21: 39–48.

Yacoub, E., and Hu, X. (2001). Detection of the early decrease in fMRI signal in the motor area. *Magn. Reson. Med.*, 45(2): 184–190.

Chapter 8

Signal, Noise, and Preprocessing of fMRI Data

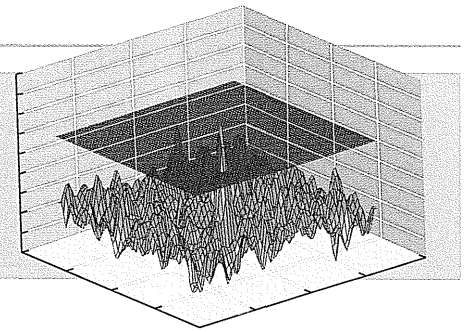

In fMRI experiments, small but meaningful changes in brain activity lie buried within highly variable measurements. To understand how small fMRI signal changes are, even in the very best cases, consider the two brain images shown in Figure 8.1A and B. Both are T_2*-weighted images taken from the same subject while the subject performed a hand-squeezing task, which is one of the most reliable and robust ways of evoking large BOLD signal changes. One image (Figure 8.1A) was taken while the subject was resting, while the other (Figure 8.1B) was acquired at the maximum of the BOLD hemodynamic response. These images appear nearly identical to the naked eye, despite an intensity change of about 5% in voxels within the primary motor cortex (Figure 8.1C and D). Figure 8.1E shows a plot of these signal changes over time. This discrepancy illustrates the first fundamental problem of fMRI data analysis: *the measured BOLD signal change is very small compared with the total intensity of the MR signal.*

Small absolute effects are not necessarily difficult to measure. Thermometers can reliably identify temperature changes of small fractions of a degree, while stopwatches can identify timing changes of a few milliseconds. Nor are they unimportant: a one percent increase in body temperature from absolute zero (approximately 3 K, 3°C, or 6°F) could have fatal consequences. However, there is a second fundamental problem for fMRI data analysis: *the task-related change in the BOLD signal is very small compared with other sources of spatial and temporal variability across and within images.* Figure 8.1D shows a map of the percent signal change between two brain images. The large variability across the image is readily apparent, especially in areas outside the brain or near its edges. Based on a single pair of images alone, it would be impossible to tell which increases in activity are due to the experimental task, and therefore meaningful, and which are due to other non-task-related sources.

In this chapter, we describe the sources of variability in fMRI data that can potentially mask the BOLD effect. Some variability results from temperature fluctuations in the MR scanner or the subject's body, which can cause artifactual changes in the recorded signal. While a potential problem, thermal variability tends to be highly random and independent of the experimental task. More problematic are physiological effects like head motion or changes in heart rate or respiration, which can be temporally correlated with an experimental

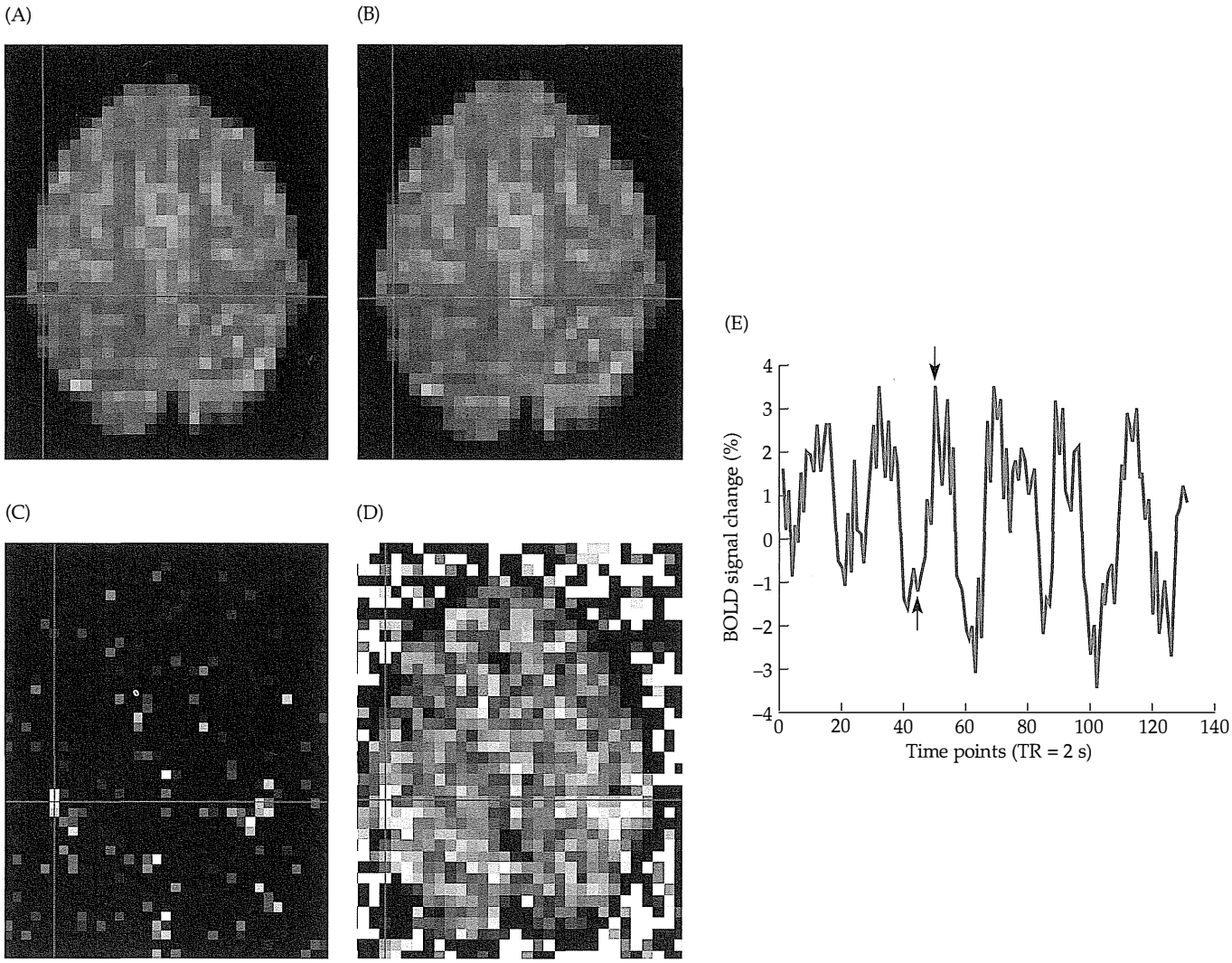

Figure 8.1 Changes in fMRI activity over time. Shown here are two BOLD fMRI images, one taken at time point 45, while the subject was resting (A), and the other taken at time point 50, while the subject was squeezing both hands (B). Even though this slice contains the hand regions of the primary motor cortex, the images appear nearly identical. The numerical difference between these images is shown in (C), and the percent signal change is shown in (D), scaled with white representing a +5% change and black representing a −5% change. The time course of the voxel indicated by the crosshairs is shown in (E), with arrows indicating the time points of (A) and (B). TR = repetition time.

preprocessing Computational procedures that are applied to fMRI data following image reconstruction but before statistical analysis. Preprocessing steps are intended to reduce the variability in the data that is not associated with the experimental task, and to prepare the data for statistical testing.

manipulation. For example, the subject may move her head a small distance each time a visual stimulus is presented, due to the alerting or arousing properties of the image. Even if these problems are overcome, there may still be variation in the brain regions that are active during performance of the task due to strategic, practice, or fatigue effects. Given these many sources of variability, it often seems a wonder that we can identify any significant effects at all!

To minimize the effects of unwanted variability in the BOLD signal, nearly all fMRI studies incorporate preprocessing algorithms that compensate for specific sources of variability (e.g., head motion). Preprocessing steps can be considered separately from other aspects of data analysis because they are generally applied to all fMRI data in a similar manner, independent of the particular

experimental design. It is important to understand the causes of noise in fMRI data, along with the potential strategies for reducing that noise, so that fMRI researchers can improve the quality of their data and the validity of the inferences they draw from their results.

Understanding Signal and Noise

Consider the following analogy. You are at a party and a friend speaks to you. While straining to hear your friend, you also hear many other sounds, such as other conversations, loud music, or the hum of the air conditioner. What you understand depends not just on the loudness of your friend's voice, but also on the loudness and character of these other sounds. In this analogy, we can refer to your companion's speech as the signal and the other sounds that interfere with your ability to hear him as noise. Note that what constitutes signal or noise depends on your current interest. If you wanted to eavesdrop on an adjacent conversation, you may stop listening to your friend. The new conversation would become the signal, and your friend's words would become noise. However, some sounds, like an air conditioner's hum, are unlikely to ever become signals.

We can use this analogy to think about fMRI. When we present a stimulus, we hope to measure a response in the brain, just as you expected to hear your companion's speech. However, in both cases the signal we hope to detect is mixed with other irrelevant sources of variability. We can improve our ability to detect the signal by increasing its amplitude or by decreasing the noise, that is, by increasing the signal-to-noise ratio (SNR). In fMRI studies, the definition of the signal also depends on our interests, as will be discussed in the next section. And, just like in the party environment, noise can come from multiple sources, each with different spatial and temporal properties. For these reasons, terms like *signal-to-noise ratio* can have different meanings in different contexts. We will begin by carefully defining important terms to minimize such confusion (Box 8.1).

Signal and noise defined

Recall that in an fMRI experiment, only one physical quantity is measured: the magnitude of the current in a detector coil. Thus far we have referred to this quantity as the MR signal. This quantity reflects both the change in net magnetization caused by the excitation pulse (signal) and fluctuations caused by thermal energy in the sample and the imaging hardware (noise). Because thermal noise tends to be evenly distributed throughout the image, MR physicists and engineers quantify a raw signal-to-noise ratio (raw SNR) by dividing the intensity of the image in a region that contains the object being imaged (the signal) by the intensity of the image in a region that is outside of the sample (the noise). Raw SNR is used to evaluate the performance of the scanner hardware, and institutions compare such measures of SNR when deciding which MRI scanner to purchase and when monitoring the quality of a MRI scanner over time. Engineers strive to maximize raw SNR by using more efficient detector coils and pulse sequences, and by shielding the scanner from outside interference.

While raw SNR is useful for evaluating scanner quality, other measures are more important for MRI and fMRI. Since we want to create maps of brain anatomy or function, we need to be able to characterize differences in MR signal within different regions of the brain, and not just between the inside and outside of the brain. For this purpose, we introduce a new measure, the con-

signal Meaningful changes in some quantity. For fMRI, an important class of signals includes changes in intensity associated with the BOLD response across a series of T_2^* images.

noise Non-meaningful changes in some quantity. There are many sources of noise in fMRI studies, and some changes may be classified as either noise or signal, depending on the goals of the study.

signal-to-noise ratio (SNR) The relative strength of a signal compared with other sources of variability in the data.

raw signal-to-noise ratio (raw SNR) The ratio between the MR signal intensity associated with a sample (e.g., the brain) and the thermal noise that is measured outside the sample.

BOX 8.1 Terminology of fMRI

The remainder of this book focuses on the design, analysis, and interpretation of BOLD fMRI experiments, along with the relation of fMRI to other neuroscience techniques. It is therefore necessary to introduce key concepts that recur throughout the following chapters.

Data Acquisition

Functional and structural MRI differ in more than just contrast sensitivity. The goal of structural MRI is to distinguish different types of tissue. Each structural image collected provides a snapshot of the underlying tissue, so a single image may be sufficient for mapping brain structure if contrast-to-noise is sufficiently high. Functional MRI has a very different goal: to relate changes in brain physiology *over time* to an experimental manipulation. A single functional image provides no information about brain activity. Only by examining changes across images over time can we infer that our experimental manipulation has an effect. For this reason, fMRI data are collected as a time series that can then be examined for changes associated with the experimental task, such as voxels that increased (or decreased) their activation following the presentation of a stimulus. Unlike structural imaging, which attempts to minimize noise within an image, functional imaging benefits from minimizing noise across successive images. Functional MRI analyses attempt to detect small task-related changes in BOLD signal while ignoring signal fluctuations due to other factors.

Functional MRI data are generally organized in a hierarchical fashion (Figure 1). It is common in fMRI studies to run 12–20 subjects (sometimes called participants) in an experiment, with complex cognitive tasks running more subjects and simpler perceptual tasks running fewer. The number of subjects depends upon the power of the experimental design and the size of the expected BOLD effect. Usually each subject participates in a single experimental session lasting 1 to 2 hours, but some experiments, such as those testing memory or drug effects, may require multiple sessions separated by days or weeks. Each session includes collection of anatomical images and one or more runs of functional images. Depending on the experiment, each run may last from a few minutes to a few tens of minutes. Breaking the session into runs can minimize subjects' fatigue, improve subjects' compliance with task instructions, and provide opportunities to identify and correct problems.

Within each run, the functional data are acquired as a time series of volumes. In an experiment with a 1-second TR, there might be 600 volumes acquired during a 10-minute run and several times that number for the entire experiment. Note that the overall MR signal is elevated in the first few volumes in each run, because the net magnetization has not yet reached a steady state (Figure 2). Therefore, the first few volumes are often excluded from further analysis. Each volume comprises a variable number of slices, ranging from 1 to 4 in an experiment targeting a particular region, to 25 or more in a study designed to cover the entire brain. Each slice is acquired at a different point in time within the TR, but all data *within* the slice are effectively acquired at the same time. Slices contain thousands of voxels that together form an image of the brain. Due to the Fourier approaches used for reconstructing MR data, slices usually consist of a 2^n-by-2^n matrix of voxels, such as 64×64 or 128×128. Data for an fMRI experiment constitute a four-dimensional matrix: x by y by slice (z) by time point (e.g., $64 \times 64 \times 25 \times 1200$).

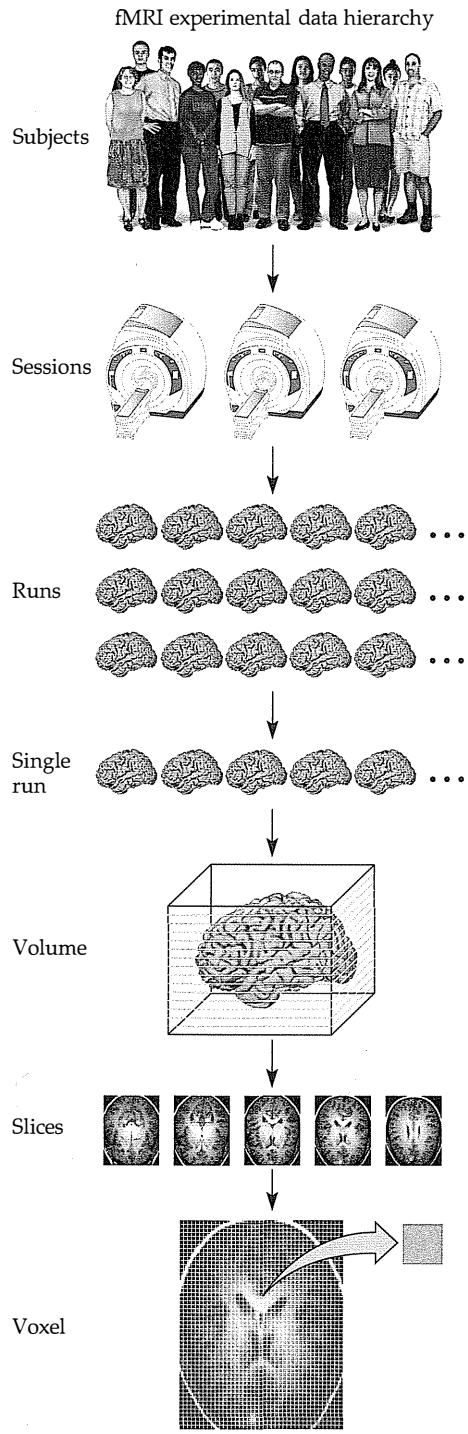

Figure 1 How fMRI data are organized.

BOX 8.1 *(continued)*

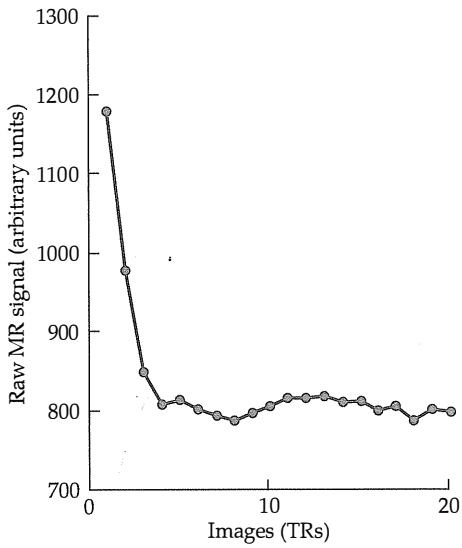

Figure 2 MR signal is elevated early in runs, before longitudinal magnetization reaches a steady state. Shown is a sample time course of activation in a single voxel for the first 20 images in a single run. Because of this increased activation, fMRI researchers often discard the first few images in a run, before they are even saved to disk. Note that although the steady-state activation looks very flat at this scale, there is about a 4% variation across time points, much greater than the typical BOLD response.

Experimental Design and Analysis

There are two basic types of experimental designs for fMRI: blocked designs and event-related designs. A blocked design presents two or more conditions in an alternating pattern (see the work of Kwong and colleagues described in the previous chapter). Most early fMRI studies used blocked designs. Blocks are typically about 10 to 30 s in duration, and there may be many alternations between different block types in a single run. An event-related design presents stimuli as individual events, or trials. The study by Blamire and colleagues in 1992 was the first to use an event-related design. If the interval between stimuli is sufficiently long (i.e., greater than about 10 s), the hemodynamic response decays to baseline after each stimulus. But, if events are sufficiently close together, special analysis procedures are required to separate their hemodynamic responses. There are also mixed designs that combine features from both types. The goal of some experiments is detection, or the determination of which brain regions are active during a task. In general, blocked designs have high detection power. Another goal is estimation, knowing how activation within brain regions changes over time. Event-related designs, especially those that use fast stimulus rates, have high estimation power. Issues related to experimental design are discussed in detail in Chapter 9.

With regard to the analysis of fMRI experiments, the key division is between voxelwise analysis and anatomical region-of-interest (ROI) analysis. In a voxelwise analysis, statistical tests are conducted on each voxel to evaluate its significance relative to the experimental hypothesis. Most fMRI studies use voxelwise approaches, and a number of software packages have been created to facilitate such analyses. In contrast, ROI analyses partition the brain into a smaller set of discrete regions, which are then individually analyzed for significance. ROI analyses can answer questions about the function of particular brain regions at a potential cost of spatial specificity. The core concepts of fMRI data analysis are introduced in Chapter 10.

time series A large number of fMRI images collected at different points in time.

subject A participant in a research study. Some journals and scientific societies prefer the term "participant," to emphasize the voluntary nature of research.

session A single visit to the scanner by a subject. For fMRI studies, each session usually includes both structural and functional scans.

run An uninterrupted presentation of an experimental task, usually lasting 5 to 10 minutes for fMRI studies. It also refers to the set of functional images collected during that task presentation.

volume A single image of the brain, itself consisting of multiple slices and voxels.

slice A single slab of an imaging volume. The thickness of the slice is defined by the strength of the gradient and the bandwidth of the electromagnetic pulse used to select it.

voxel A three-dimensional volume element.

blocked design The separation of experimental conditions into distinct blocks, so that each condition is presented for an extended period of time.

event-related design The presentation of discrete, short-duration events whose timing and order may be randomized.

trial A single instance of the experimental manipulation.

mixed design A design that contains features of both blocked and event-related approaches.

detection Determination of whether activation of a given voxel changes in response to the experimental manipulation.

estimation Measurement of the pattern of change over time within an active voxel in response to the experimental manipulation.

voxelwise analysis The evaluation of statistical tests at the level of individual voxels.

region-of-interest (ROI) analysis Evaluations of hypotheses about the functional properties of brain regions (i.e., aggregated over a pre-determined set of voxels), often chosen to reflect a priori anatomical distinctions within the brain.

contrast-to-noise ratio (CNR) The magnitude of the intensity difference between different quantities divided by the variability in their measurements.

contrast (1) The intensity difference between different quantities being measured by an imaging system. It also can refer to the physical quantity being measured (e.g., T_1 contrast). (2) A statistical comparison of the activation evoked by two (or more) experimental conditions, in order to test a research hypothesis.

functional signal-to-noise ratio (functional SNR) The ratio between the intensity of a signal associated with changes in brain function and the variability in the data due to all sources of noise. Functional SNR is sometimes called dynamic CNR or functional CNR.

effect size The numerical difference between means divided by the standard deviation.

trast-to-noise ratio (CNR). Two properties of CNR are important to understand. First, CNR is always relative to some comparison within an image. As introduced in Chapter 1, the contrast of an MRI image refers to the physical property to which it is sensitive. An image sensitive to T_1 contrast will be bright for voxels with short T_1 values (like white matter) and dark for voxels with long T_1 values (like gray matter or cerebrospinal fluid). Thus, T_1-weighted pulse sequences have a very good ability to distinguish between gray and white matter (high CNR), but only a limited ability to distinguish between cerebrospinal fluid and air (low CNR). Second, CNR depends on the absolute difference in intensity divided by the shared variability. For example, for high CNR between gray and white matter not only must the mean voxel intensity be much higher for one tissue type (e.g., white matter for T_1 images), but also the signal should be relatively constant within each tissue type (see Figure 1.5 for examples).

For most fMRI experiments, however, CNR is unimportant. Typical T_2*-weighted images have intrinsically low contrast (see Figure 8.1A and B), making it hard to identify boundaries between different types of tissue. Instead, the important quantity for fMRI studies is functional signal-to-noise ratio (functional SNR). Some authors refer to this quantity as dynamic CNR or functional CNR. Here, we use the term "signal" to describe the difference in BOLD activation between two states of the brain caused by an experimental manipulation. Likewise, the term "noise" refers to the variability in those states *over time.* The concept of functional SNR is closely related to that of effect size in statistics, which refers to the difference between two conditions in units of standard deviation.

In summary, just as CNR reflects how easily we can see differences between tissues, functional SNR reflects how easily we can see differences between experimental conditions. For the remainder of this book, we will focus our discussion on the ability of fMRI experiments to detect meaningful changes in brain activity. We will use "SNR" to denote functional SNR, and "raw SNR" to describe the signal and noise directly measured by the detector coil. We will use "CNR" to refer to the contrast sensitivity of anatomical images.

Functional SNR

The functional SNR measured in an fMRI experiment depends on the amplitude of the task-related BOLD signal compared with non-task-related variability. As shown in Figure 8.2, a simple motor or visual task, like squeezing one's hand or watching a flashing checkerboard image, may generate BOLD changes of several percent in the primary motor cortex, even with scanners at 1.5 T. However, if the hand is squeezed less frequently and less vigorously, or if the checkerboard is blurred and flashed at a slower rate, BOLD activity may decrease dramatically. In addition, signal magnitude also depends on the area being measured. Many experimental tasks evoke activity in a set of related brain regions, such as areas associated with perceptual and motor processing and those associated with working memory and decision-making. As a rule of thumb, task-evoked fMRI signal changes are largest in primary motor or sensory areas, and generally decrease in amplitude in regions associated with higher cognitive function.

Thought Question

Why might the amplitude of the BOLD response typically be larger in primary sensory and motor cortices than in brain regions associated with complex cognitive processes?

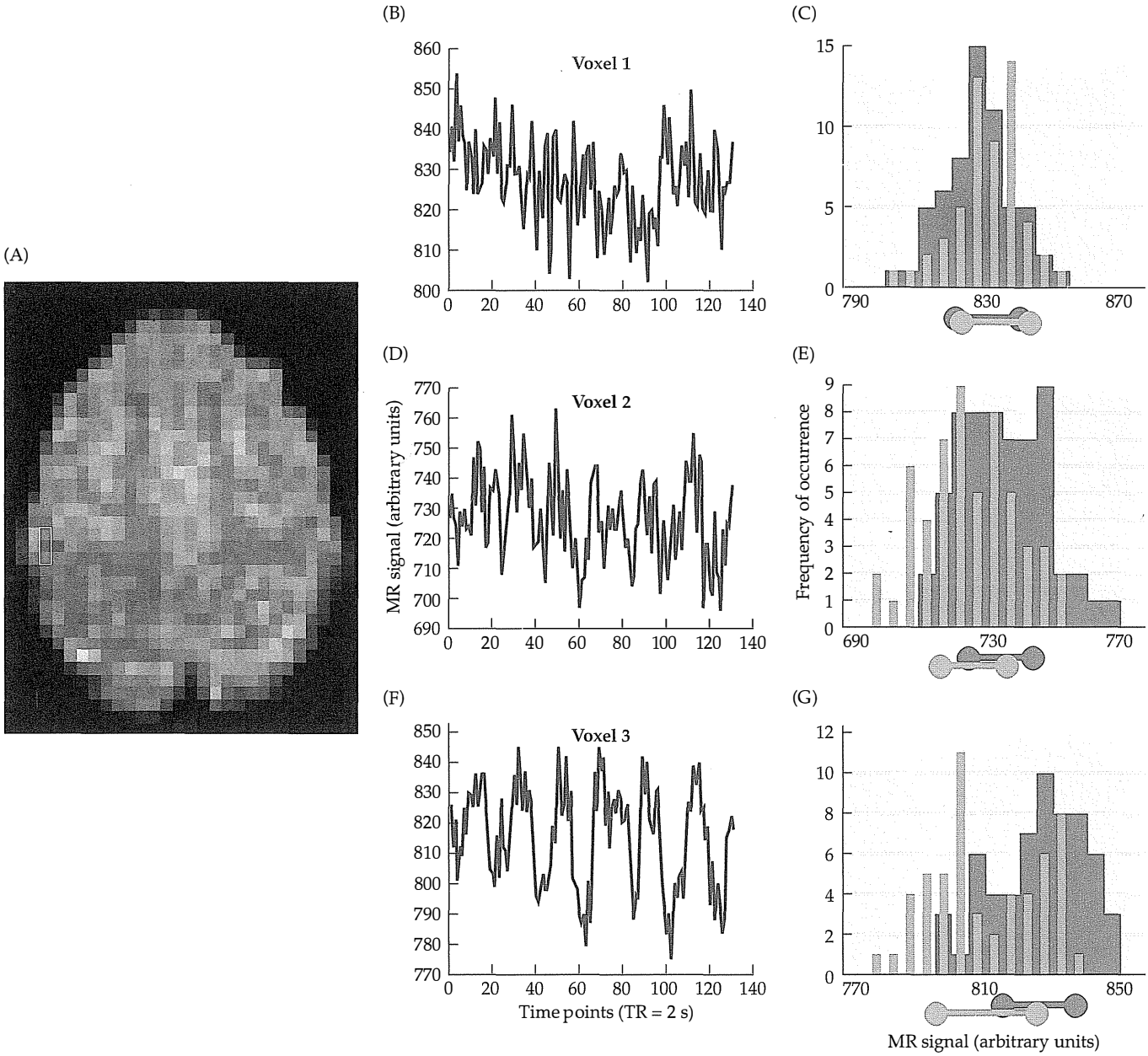

Figure 8.2 Effects of increasing functional SNR from relatively low to high levels. (A) shown within the yellow box are three voxels in and adjacent to the primary motor cortex, during performance of a blocked-design hand-squeezing task. (B) The uppermost voxel has little to no task-related signal change (low SNR). Plotted at right are histograms comparing the frequency of occurrence of each MR signal range during the hand squeezing blocks (in red) and during resting blocks (in blue). (C) The distributions of activation during task and non-task periods are highly overlapping for this voxel. (D) The middle voxel has a medium SNR, but there is still substantial overlap between the distributions (E). However, the lowermost voxel (F) has a very high SNR, and the distributions have much less overlap (G). The red and blue lines below each graph indicate the means +/– one standard deviation of each histogram. If the difference between the means is large enough compared with the standard deviation, as in the bottom graph, we can identify significant activation.

If a study compares two experimental conditions, such as a memory test comparing remembered and forgotten words, the difference in signals between conditions (for which the term "contrast" is also used) is almost always much smaller than the difference between the signal associated with each condition

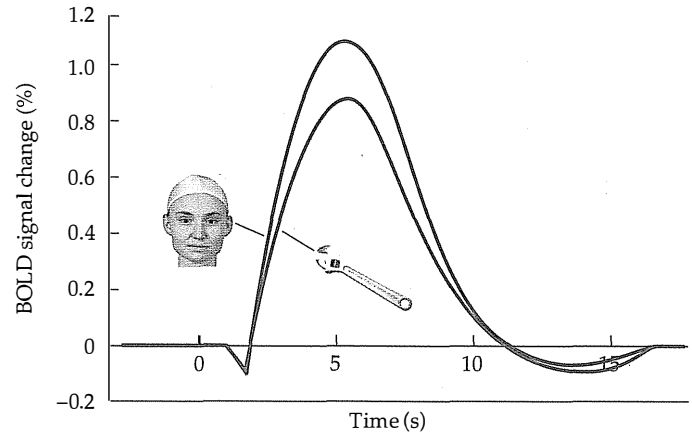

Figure 8.3 Using fMRI to examine relative activation. Signal changes in fMRI are rarely all or none, but are often a matter of degree. Shown are the hypothetical responses of a face-sensitive region of the brain to images of a face (red line) and a wrench (blue line). The responses to both stimuli are large compared with the difference between the two responses. The difference between two conditions is often called an experimental contrast.

and baseline (Figure 8.3). Consider the fusiform gyrus in the temporal lobe, which plays an important role in the perception of objects, including faces. If an fMRI subject views a single face presented in isolation, activity in the fusiform gyrus might increase by about 1.1% over baseline. Other stimuli, such as images of tools, may evoke lower-amplitude activation in this region. For example, an image of a wrench might evoke a 0.8% increase in signal. Thus, the difference in signal between the conditions would be 0.3%. The more similar the conditions are, the smaller the functional SNR for detecting a difference between them.

Researchers can improve functional SNR in two ways. First, one can increase the signal (i.e., improve the experimental power) by using a higher-field scanner or by collecting more data. These carry costs, however, by requiring a more expensive machine or longer scanning time. And, using a high-field scanner introduces some important disadvantages, like increased signal loss in ventral brain regions. Conversely, one can take steps to reduce noise. The most important factor is creating a good experimental design (see Chapter 9) that distinguishes task-related signal from task-unrelated noise. Researchers also strive to eliminate some of the many sources of noise in fMRI data through the application of corrective algorithms before the data are analyzed (i.e., preprocessing). We consider both approaches—increasing signal and minimizing noise—in the remainder of this chapter.

Effects of Field Strength on fMRI Data

In any MRI scan, the amount of net magnetization is proportional to the strength of the static magnetic field (see Chapter 3). Remember, however, that the signal we measure in fMRI does not depend solely on the net magnetization. Because the net magnetization must be tipped into the transverse plane to become measurable, other effects come into play, including T_1 and T_2 relaxation, pulse sequence parameters, motion-related contrast preparations (e.g., perfusion, diffusion), and susceptibility effects, all of which were discussed in

power The probability of detecting an effect of the experimental manipulation.

Chapters 4 and 5. These latter factors temper the gains associated with strong magnetic fields, with important consequences for BOLD fMRI.

Field strength and raw SNR

One solution for increasing the amplitude of the BOLD signal is to increase the scanner field strength. With increasing field strength, the energy difference between high- and low-energy states increases, causing more spins to align parallel with the static field and increasing net magnetization. The theoretical relationship between field strength and MR signal is simple: as static field strength increases linearly, raw signal increases quadratically (i.e., with the square of the field strength). Thus, a 3.0-T scanner measures four times as much raw signal as a 1.5-T scanner. For comparison, thermal noise increases linearly with the field strength, so a 3.0-T scanner measures twice as much thermal noise as a 1.5-T scanner. When we divide the quadratic increase in signal by the linear increase in noise, we find that the raw SNR only increases linearly with the field strength. Recall from Chapter 1 the first whole-body MRI scanner, used by Damadian and colleagues in 1977, and named "Indomitable." The field strength of that scanner was only 0.05 T, resulting in a theoretical raw signal and a raw SNR that were only about one thirty-six hundredth and one sixtieth, respectively, as strong as in a modern 3.0-T scanner!

Indeed, researchers have demonstrated that both fMRI BOLD signal amplitude and functional SNR increase with increasing field strength. A very early fMRI study was reported in 1993 by Turner and colleagues, who compared visual cortex activation at 1.5 T and 4.0 T. Using a simple design that alternated blocks of flashing lights and darkness every 30 s, they found that the evoked MR signal within the visual cortex was much larger at 4.0 T than at 1.5 T, with signal changes of approximately 15% and 5%, respectively (Figure 8.4). These results suggested that raw SNR increases roughly linearly with field strength. There are now numerous more recent examples of parallel fMRI data acquired at two or more field strengths, often 1.5 T and 3.0 T. The general findings are that signal amplitude increases with field strength, but that the relationship is usually less than linear (e.g., doubling the field strength might result in a 50% increase in amplitude). And, as we will discuss further below, increases in field

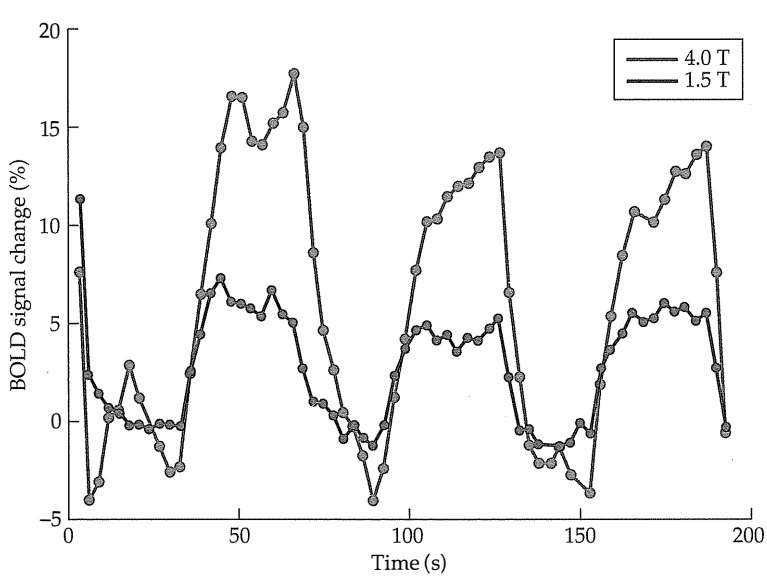

Figure 8.4 An early study of field strength effects in fMRI. Turner and colleagues measured changes in visual cortex activity at 1.5 T and 4.0 T. Approximately 2–3 times as much signal was recorded at the higher field strength.

spatial extent The number of active voxels within a cluster of activation (i.e., the size of the active region).

partial volume effects The combination, within a single voxel, of signal contributions from two or more distinct tissue types or functional regions.

strength have consequences for physiological variability, which further temper the advantages of higher field strengths. In many cases, the advantages of newer MRI scanners for fMRI imaging come mainly from the ability to do parallel imaging with high-performance gradients rather than from higher field strengths (see Chapter 5 for examples).

Field strength and spatial properties of activation

Greater field strength has two main effects on the spatial distribution of activation: improved spatial specificity and increased spatial extent of activation. Improvements in spatial specificity are critical for many applications of fMRI. Many phenomena of interest have small spatial scale and thus are more identifiable at higher fields. Recently, Yacoub and colleagues used a 7.0 T scanner to reproducibly identify spatial patterns of activation that likely reflect ocular dominance columns (Figure 8.5), thus building on prior work at lower field strengths. Another intriguing example of spatial specificity comes from a 2007 study by Ress and colleagues of cortical layering. By collecting fMRI data at 3.0 T in very small voxels (less than 1 cubic millimeter), they found that the amplitude of the BOLD signal in a given voxel depended on its position within the gray matter, with the largest signal changes observed about 3 mm from the gray–white boundary. These advances come in part because these very small voxels are highly specific; they minimize partial volume effects (see Figure 7.15). If a small voxel is primarily composed of active neural tissue that is responsive to the experimental task, it will generate a larger BOLD signal change than the same amount of active neural tissue located within a larger voxel. For this reason, decreasing voxel sizes can result in larger BOLD signal changes from active voxels.

Increasing spatial specificity can result in better sensitivity to signal changes from small blood vessels. Because the T_2^* value of blood decreases significantly with increasing field strength, the intravascular contribution, especially from the large vessels, drops out at high field strengths. Conversely, the extravascu-

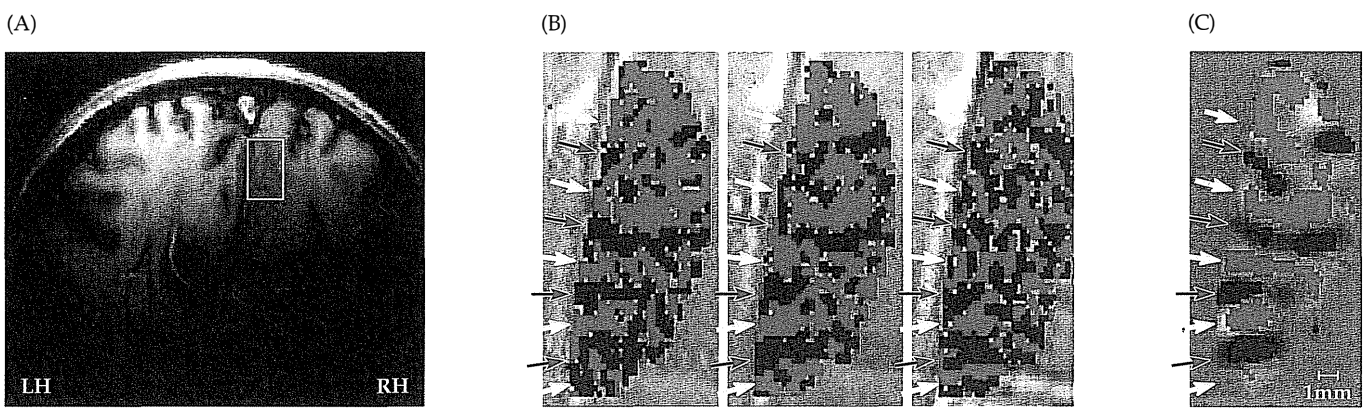

Figure 8.5 Identification of ocular dominance columns using high-field (7.0-T) fMRI. Visual input from each eye is represented within the primary visual cortex in small (~1mm) columns that are organized in a roughly alternating pattern along the cortex. (A) To maximize the chances of identifying reliable ocular dominance patterns, Yacoub and colleagues selected thin slices that ran along the interhemispheric fissure, targeting a small area within the primary visual cortex (white box). (B) Shown are maps of voxels that responded most to stimulation of the left eye (blue) or right eye (red), in each of three separate fMRI sessions. (C) A substantial fraction of the voxels passed significance thresholds in all three sessions (same color scheme as in B), providing good evidence for the robustness of the measurements. (After Yacoub et al., 2007.)

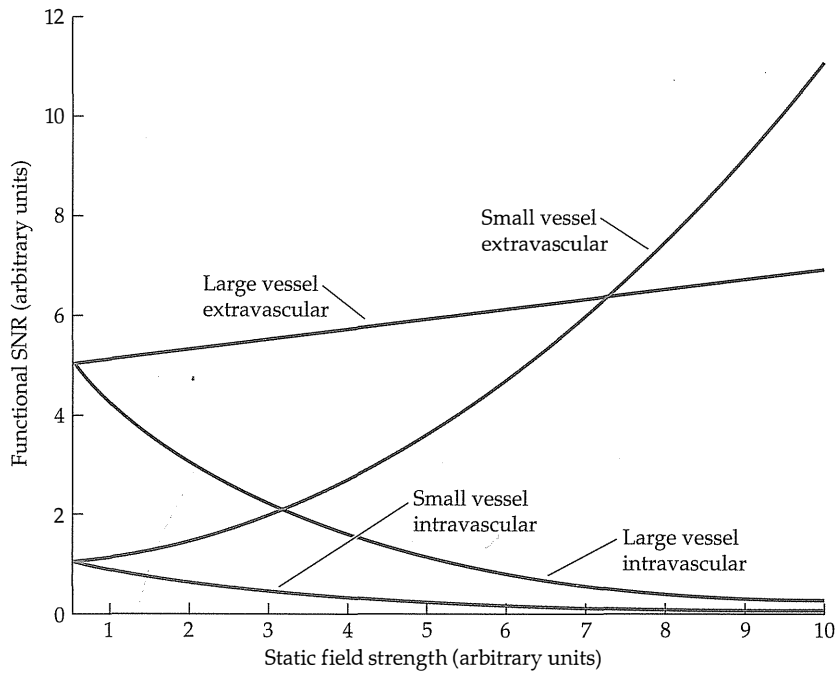

Figure 8.6 Effects of field strength on the contributions of different vascular components to functional SNR. As field strength increases, the intravascular component of the functional SNR falls and becomes negligible, leaving only the extravascular component. The small-vessel extravascular component of the functional SNR increases more rapidly than that of the large vessels, suggesting that at high field strengths BOLD fMRI may be more spatially specific to signal changes in small vessels.

lar signal from spins near large blood vessels increases linearly with field strength, while the signal from spins near small vessels increases quadratically (i.e., with the square of the field). Therefore, as field strength increases, the small-vessel extravascular component of the BOLD response increases faster than the large-vessel extravascular component. A schematic illustration of the different effects of field strength on these various BOLD signal components is given in Figure 8.6. This scheme suggests that the extravascular component of small vessels would prevail at very high magnetic fields.

Small vessels are more likely to be located near the neuronal activity of interest, and thus the BOLD response may be more spatially specific at higher field strengths. In 2001, Kruger and colleagues investigated the effects of field strength (1.5 T vs. 3.0 T) on functional SNR in different types of voxels during a combined visual and motor task. In addition to an overall increase in functional SNR, they found that functional SNR increased by a factor of about 1.8 in small regions of activation that may correspond to large blood vessels, and by a factor of about 2.2 in larger regions of active gray matter. This work demonstrated the tendency toward improved signal specificity near small vessels at high field strengths. Note, however, that the extravascular component originating around large vessels would still be present, despite its relatively reduced proportion in the overall BOLD signal (Figure 8.6). This will partially compromise spatial specificity.

A second consequence of increased functional SNR is the increased spatial extent of activation (i.e., number of active voxels within a region). In their 1999 study, Yang and colleagues measured activity within the sensorimotor cortex while subjects performed a blocked-design finger tapping task at either 1.5 T or 4.0 T. Under optimum TR and TE parameters, there were approximately 70% more active voxels within the sensorimotor region at the higher field strength. Kruger and colleagues also found that spatial extent depends on field strength, with about 40% more voxels active across the motor and visual cortices at 3.0

T compared with 1.5 T. While these studies used simple visual and motor tasks, a 2003 study by Krasnow and colleagues examined the effects of field strength on several more complex tasks, including perceptual, memory, and emotional processing paradigms. They compared activity at field strengths of 1.5 T and 3.0 T and found that there were substantial increases in the number of activated voxels with increasing field strength. Increases of 35 to 83% were observed across multiple brain regions during a cognitive task, suggesting that detection power throughout the brain improves with increasing field strength.

These two consequences may appear contradictory: how can we gain spatial specificity at the same time as spatial extent increases? However, no true contradiction exists. The gain in spatial specificity comes from changes in the weighting of different vascular components. The large-vessel extravascular component does increase with field strength, but it does not increase as rapidly as the small-vessel extravascular component. The gain in spatial extent is an effect of increasing functional SNR, which in turn improves our estimates of whether a voxel's activation matches our experimental hypotheses. We can use increased functional SNR in two ways. First, we can identify more voxels as active at the same statistical threshold. Or, by increasing our statistical threshold, we can improve our estimates of which voxels are active, without changing the spatial extent of activation.

Thought Question

What do the effects illustrated in Figure 8.6 predict for studies of the fMRI initial dip (see Chapter 7)?

Challenges of high-field fMRI

It is also important to realize that as field strength increases, the MR properties of spin systems change. For example, the relaxation parameters T_1 and T_2*, which both affect signal recorded in fMRI experiments, change with increasing field strength. The parameter T_1 increases with field strength (by about 30% from 1.5 T to 3.0 T), and this could reduce the effective signal recovery for short TR values. The parameter T_2* decreases with increasing field strength, and this could reduce the time available to acquire a signal. Detailed measurements were reported in 2007 by Peters and colleagues, who found that T_2* values in gray matter were 22% shorter at 3.0 T and 60% shorter at 7.0 T, compared with values at 1.5 T. A more significant challenge comes from susceptibility artifacts that distort the uniformity of the magnetic field. Just as BOLD susceptibility effects increase with field strength, so too do signal losses in regions of the brain near air–tissue boundaries (Figure 8.7). These regions include the ventral frontal and temporal lobes, which are adjacent to air-filled sinuses. Without the use of specialized pulse sequences or equipment that can partially compensate for susceptibility-induced signal loss (see Chapter 5), imaging of these regions becomes more difficult or impossible at higher field strengths. Field inhomogeneity can also lead to geometric distortions that require specialized software and hardware for their correction.

At the time of publication of this Second Edition, the current standard for static field strength in fMRI studies is 3.0 T, although many institutions use scanners with lower (e.g., 1.5 T) or higher (e.g., 4.0 T or 7.0 T) field strengths. It is critical to emphasize that, while field strength is the most salient characteristic of an fMRI scanner, the quality of a scanner depends on many other factors.

susceptibility artifacts Signal losses on T_2*-dependent images due to magnetic field inhomogeneities in regions where air and tissue are adjacent.

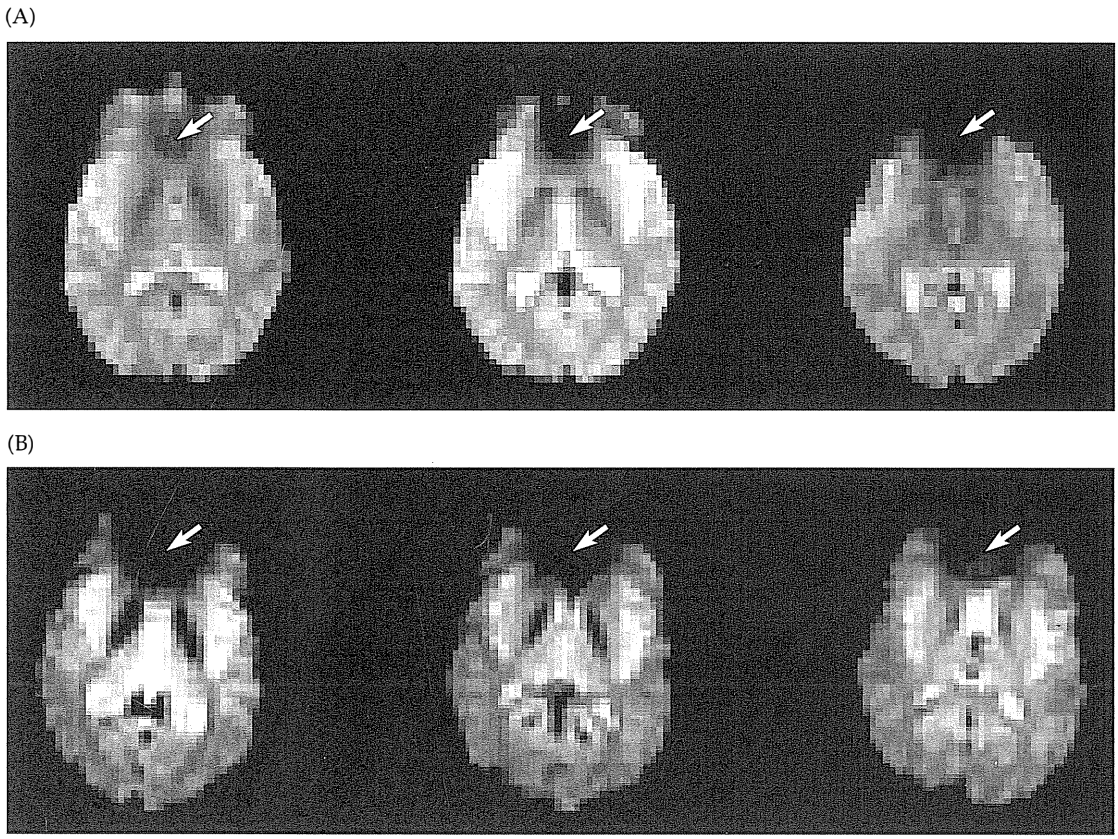

Figure 8.7 Susceptibility artifacts increase at higher field strengths. While susceptibility artifacts at air–tissue boundaries are present on gradient-echo images at all field strengths, they increase in spatial extent at higher field strengths. Shown are images from three subjects, each scanned at both 1.5 T (A) and 4.0 T (B). Visible in all images are areas of signal loss in the ventral frontal lobe, which is indicated by the arrows. Note that the areas of signal loss are more extensive in the 4.0-T images.

Sources of Noise in fMRI

At a given field strength, the overall signal is mainly determined by the amount of net magnetization, which in turn reflects the number of atomic nuclei and their relaxation properties. However, the sources of noise are numerous and complex, varying over both time and space. Some sources of noise involve regular temporal variation, as can be seen in Figure 8.8, which presents the power spectrum of a single experimental run. A power spectrum shows what frequencies are present in a time series of data, and is created using the Fourier transform. Peaks within a power spectrum can be thought of as regular oscillations in the intensity of the given voxel, reflecting changes over time due to the respiratory cycle, cardiac pulsations, or BOLD activity. Spatial features of fMRI noise can be seen in Figure 8.9. The most striking feature of this set of images is that much of the anatomical structure of the brain was recovered, indicating that the variability inside the brain is much higher than the variability outside the brain. If noise were evenly distributed across the image, the image would be a uniform gray.

There are five main causes of temporal and spatial noise in fMRI: intrinsic thermal noise within the subject and the scanner electronics; system noise

power spectrum A representation of the strength of different frequency components within a signal. The Fourier transform converts a signal (i.e., changes in intensity over time) into its power spectrum.

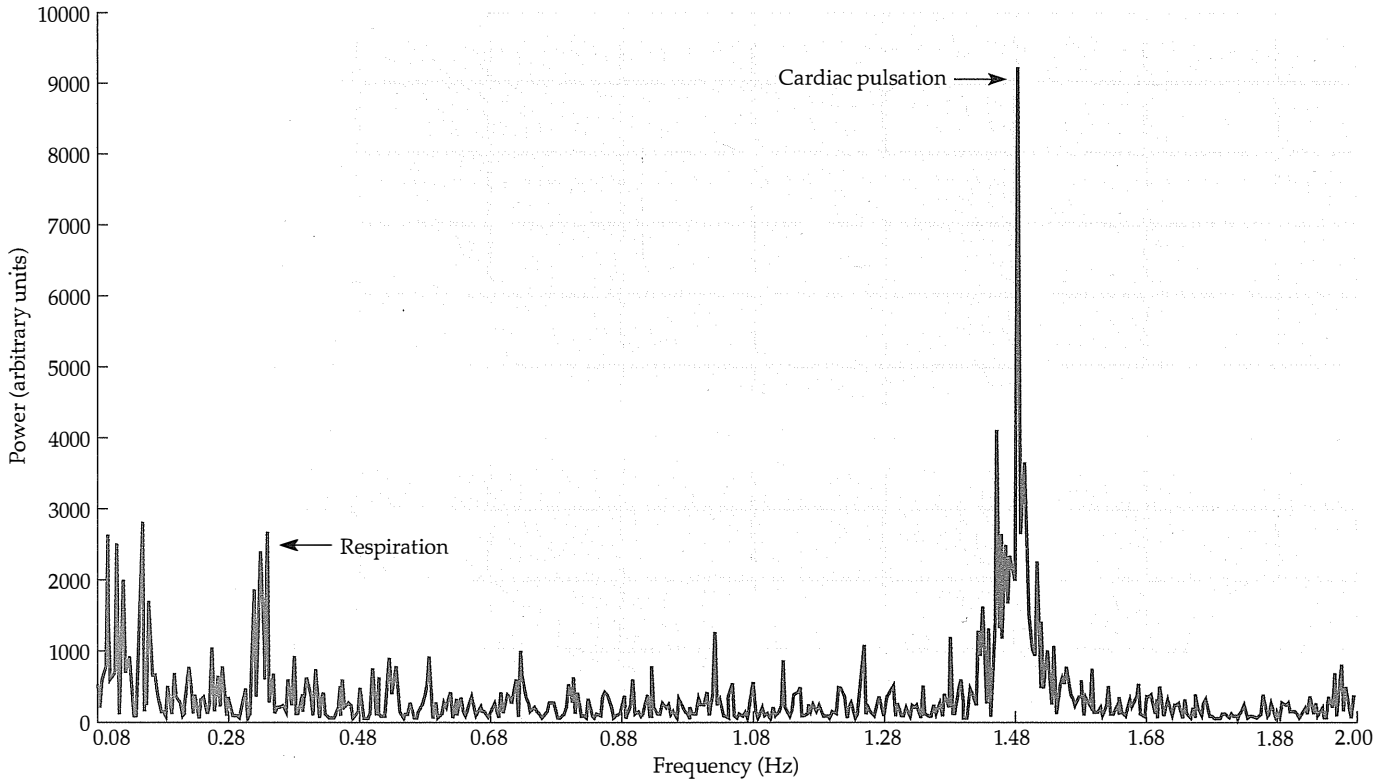

Figure 8.8 The power spectrum of an experimental voxel over a single run. The experimental task used an event-related design in which visual stimuli of 1-s duration were separated by intervals of 9 s. Plotted on the *y*-axis is the power at each frequency; i.e., how much did regular changes at that frequency contribute to the overall BOLD time course. Visible are clear peaks at the respiratory and cardiac frequencies. The accuracy of these peaks was verified by physiological monitoring. To detect such high-frequency changes, a single slice was sampled at a TR of 250 ms. Note that the lowest frequencies are excluded from this plot because the very high power at low frequencies obscures the effects shown. A small peak is evident near the task frequency of 0.1 Hz.

associated with imperfections in the scanner hardware; artifacts resulting from head motion, respiration, heart rate, and other physiological processes; variability in neuronal activity associated with non-task-related brain processes; and changes in behavioral performance and cognitive strategy. We discuss each of these sources of noise in the following sections.

Thermal noise

thermal noise Fluctuations in MR signal intensity over space or time that are caused by the thermal motion of electrons within the sample or scanner hardware.

All MR imaging, whether anatomical or functional, is subject to **thermal noise** (also called intrinsic noise), which reflects the heat-related motion of electrons within the subject and within the scanner electronics. To understand the possible sources of thermal noise, recall from Chapter 2 the hardware that underlies the acquisition of MRI data. Following its excitation, the sample (e.g., the brain) emits a radiofrequency signal that is detected by the receiver coil. The signal then becomes an electric current that passes through a series of electronics hardware, replete with many conductors, resistors, and power amplifiers.

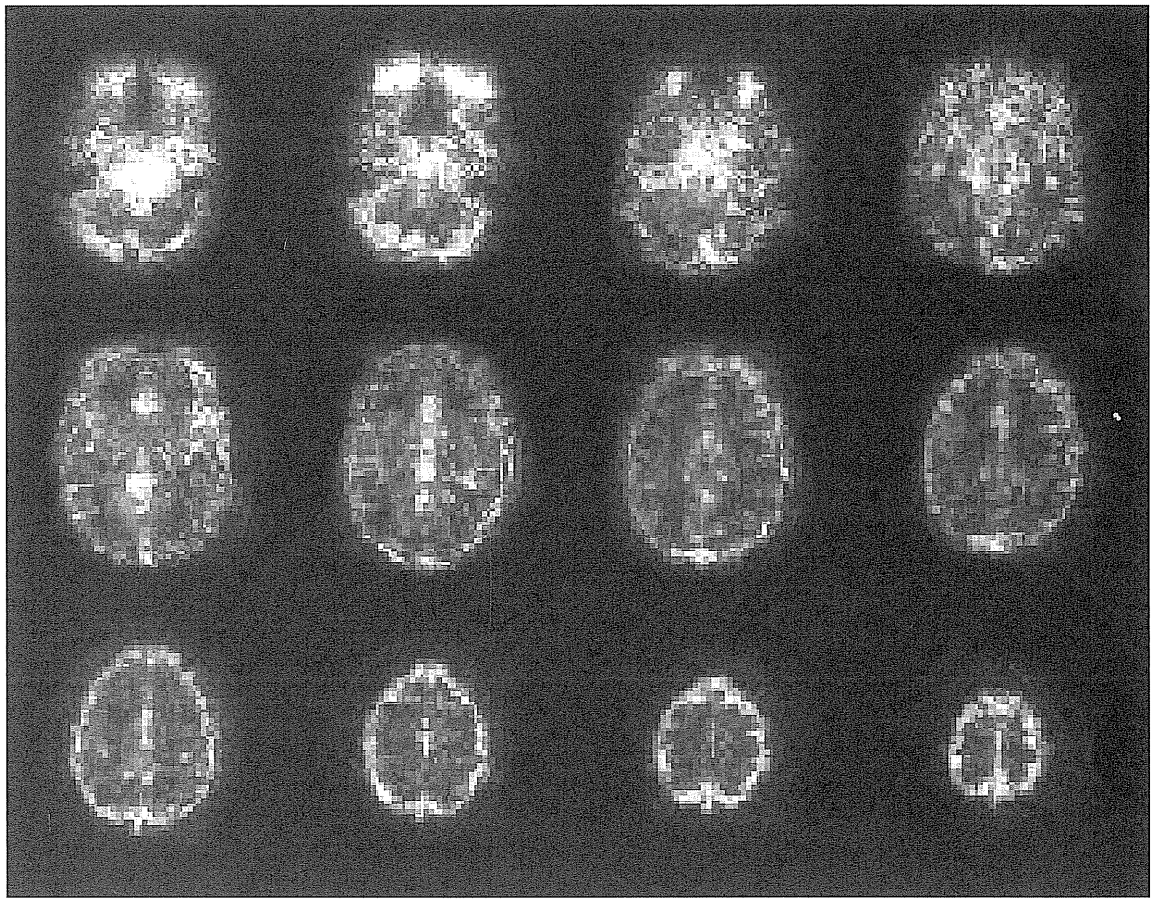

Figure 8.9 A map of noise across the brain. Shown are maps of the standard deviation over time during a single experimental run while the subject performed a simultaneous motor/visual task. Voxels with high standard deviation (i.e., high levels of noise) are shown in white, while voxels with low standard deviation are shown in black. Note that the standard deviation is not uniform across the image. Instead, it is greatest around the edges of the brain.

Within each component of the hardware, free electrons collide with atoms, resulting in an exchange of energy. The higher the temperature of the system, the more frequent the collisions and the more the current becomes distorted. Thermal noise also depends on the frequency bandwidth of the receiver and the resistance in the detector coil. Theoretical formulations of thermal noise by Edelstein and colleagues in 1986 showed that thermal noise increases linearly with field strength. So thermal noise will be approximately twice as large at 3.0 T as at 1.5 T.

Because the magnitude of thermal contributions to the MR signal varies randomly over time, thermal noise has no spatial structure. That is, the magnitude of thermal noise within a voxel is independent of its spatial location. However, the *effect* of thermal noise depends on the voxel's signal amplitude. Consider a voxel within the brain that has very high raw signal (i.e., it appears bright on images). Thermal noise during image acquisition may add or subtract from the measured intensity values, resulting in a Gaussian distribution of intensity values over time. Now consider a voxel in air outside the brain;

system noise Fluctuations in MR signal intensity over space or time that are caused by imperfect functioning of the scanner hardware.

scanner drift Slow changes in voxel intensity over time.

that voxel has negligible raw signal (i.e., it appears dark on images). Thermal noise can only have an additive effect on that voxel. The resulting distribution will have a lower bound at zero and will be positively skewed (i.e., it will have a Rayleigh rather than a Gaussian distribution). A book published in 2002 by Buxton is listed in the chapter references, and gives a good discussion of the relationship between raw signal and thermal noise effects.

System noise

A second factor that contributes to variability in the measured fMRI signal is system noise, which generally describes variations or discrepancies in the functioning of the imaging hardware. Some common causes of system noise are static field inhomogeneities due to imperfect shimming, nonlinearities and instabilities in the gradient fields, and off-resonance or loading effects in the radiofrequency transmitter and receiver coils. One particularly important form of system noise is scanner drift (Figure 8.10). Although drift can result from any of several different sources, a common cause is changes in the resonant frequency of hydrogen protons associated with subtle changes in the strength of the static field. Even though it is powered by superconducting currents, the static field strength of the main magnet still drifts slowly over time, often on the order of a few tenths of a part per million per day. Expressed in terms of field strength and resonant frequency, such drifts might reflect an alteration in the main field strength on the order of 0.005 of a Gauss and variation in the resonant frequency by a few Hertz. This can lead to changes in global or local signal intensity over time. Similarly, instability in the gradient coils can cause the shape and location of the recorded images to change over time (see Chapter 4).

Problems with the radiofrequency coils can introduce several types of system noise. If the frequency of the excitation pulse does not match the resonant frequency of the sample, excitation will be inefficient and intensity variation may be introduced, causing the MR signal to fluctuate over time. Another

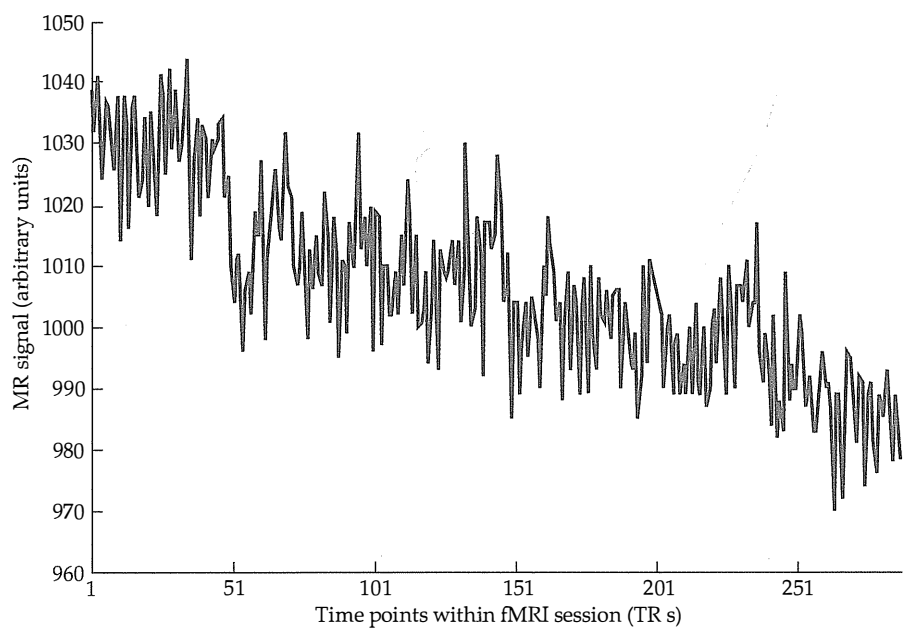

Figure 8.10 Scanner drift. Low-frequency changes in MR signal are collectively known as drift. Shown here is a roughly linear decrease in activation throughout a single run (each time point collected with TR of 1.5 s).

potential problem results from the fact that the receiver coil is coupled to the sample via mutual inductance, meaning that changes in the current or voltage distribution in the sample will induce corresponding changes in the current or voltage carried by the receiver coil. Thus, noise in the brain effectively reduces the sensitivity of the receiver coil. To minimize this problem, scanners match the impedance in the sample and the receiver coil. This matching process is referred to as achieving the dominant loading factor for the object being imaged (i.e., a particular subject's brain) so that optimal mutual coupling can be reached.

Some aspects of system noise are the responsibility of the MR center, because they affect all researchers who use a scanner. By ensuring that the MR scanner electronics are as stable as possible and by preventing extraneous radiofrequency signals from entering the scanner room, the research center can improve the consistency of fMRI data, both within and between sessions. Researchers should become familiar with the quality assurance procedures at their MRI center so that they can recognize problems as they arise and, in turn, provide feedback to the technical staff running the scanner.

physiological noise Fluctuations in MR signal intensity over space and time due to physiological activity of the human body. Sources of physiological noise include motion, respiration, cardiac activity, and metabolic reactions.

aliasing The sampling of a signal at a rate insufficient to resolve the highest frequencies that are present. The energy at those frequencies becomes artifactually expressed at lower frequencies, distorting the measured signal.

Motion and physiological noise

So far we have considered thermal and system noise, which result from intrinsic properties of the scanning system. If we scan an inert object (e.g., a plastic ball filled with fluid or gel), we will still measure significant thermal and system noise. The human brain, on the other hand, is hardly inert. Muscles contract with each breath or heartbeat. Blood pulses through arteries and veins. The metabolic demands of neurons drive chemical reactions. This activity results in variations in fMRI signal due to motion artifacts and physiological noise.

Signal variability due to subject motion is common and extremely disruptive for fMRI studies. Throughout an experiment, a subject may shift the position of his head; move his shoulders, arms, or legs to become more comfortable; or swallow because of nervousness. In the best cases, small head motions can be partially corrected during data preprocessing, while in the worst cases, large motions may render data completely un-interpretable. In addition, small-scale motions result from the regular oscillatory activity of the heart and lungs. This activity is much faster and more periodic than large-scale head motion, introducing a different set of challenges. If the rate of sampling is fast enough, it may be possible to characterize and minimize motion due to heart and lung activity during preprocessing. But in most fMRI studies, motion due to cardiac activity, in particular, is too fast to be sampled effectively (i.e., for TRs >500 ms), and if the TR is long enough (i.e., >2500 ms), respiratory activity may likewise be under-sampled. Under those circumstances, the signal changes associated with these sources of motion are still present, but become distributed throughout the fMRI time series in a manner that may be difficult to identify or correct; this phenomenon is known as aliasing. Respiration also introduces variability in the fMRI signal through systematic distortions in the magnetic field. As the subject breathes, the expansion of the lungs casts a magnetic susceptibility "shadow," influencing field strength and homogeneity of the magnetic field, and altering signal intensity throughout the image (including areas outside the brain). This phenomenon was demonstrated by Raj and colleagues in 2001.

The effects of motion in fMRI are usually not due to motion during image acquisition, which would reduce the raw SNR. Recall from Chapter 5 that typical fMRI pulse sequences (e.g., spiral or echo-planar gradient-echo imaging)

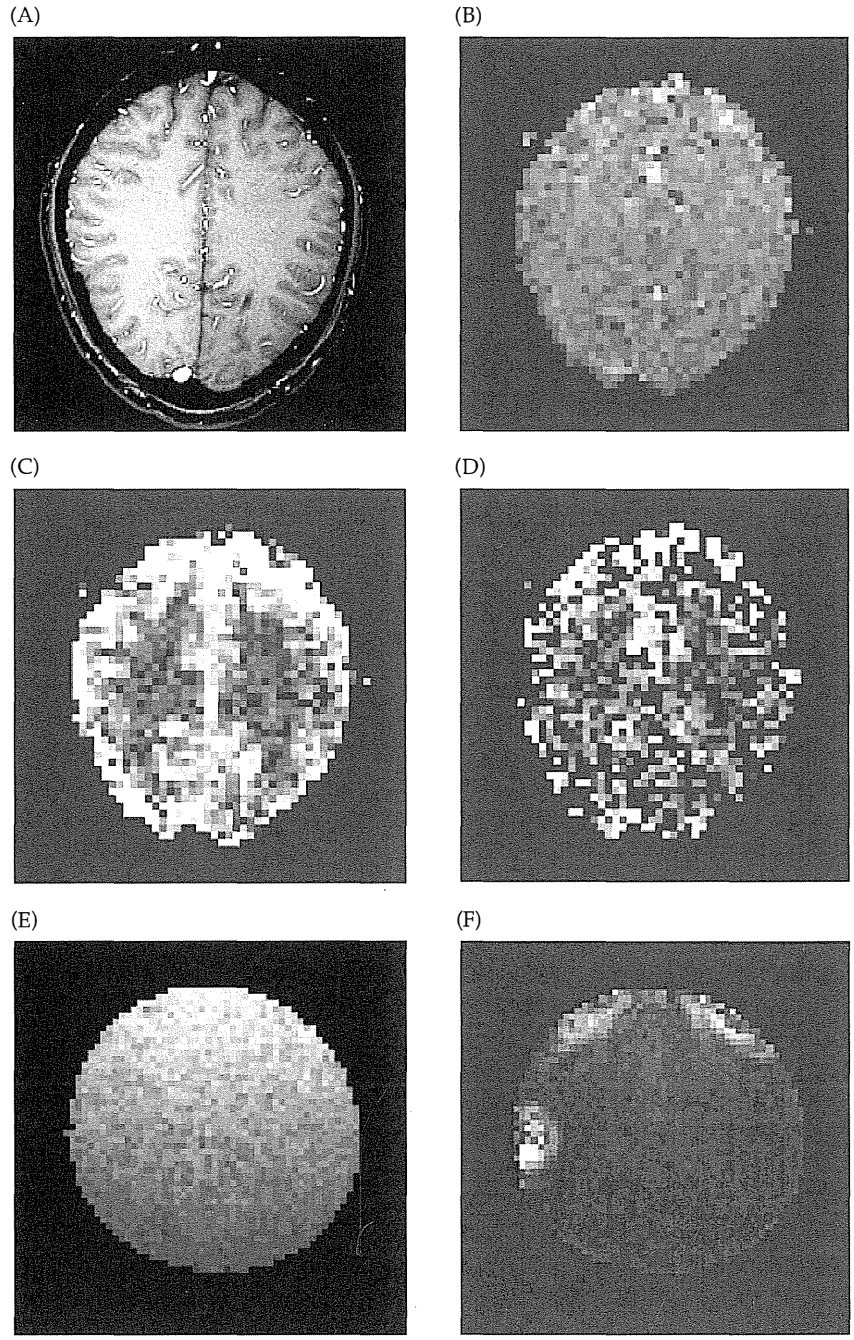

Figure 8.11 Distribution of physiological noise. For one subject, images show brain anatomy (A), noise from all sources (B), physiological noise due to variation in blood flow and metabolic processes (C), and noise due to bulk head motion and cardiac and respiratory pulsations (D). Note that the noise in (C) is concentrated within gray matter, while that in (D) is more uniform, save for effects around the edge of the brain. (E, F) For comparison, the authors also collected data from a fluid-filled ball (i.e., a phantom). Overall noise levels are generally uniform throughout the phantom (E) and there is negligible physiological noise (F). (From Kruger and Glover, 2001.)

have very short TEs, often about 30 to 40 ms. There is little opportunity for motion to occur during such a short acquisition window. Motion causes problems because of variability across the time series of images, which is critical for functional SNR. A voxel near the edge of the brain, for example, may begin by containing mostly gray matter but end up, after motion, containing mostly cerebrospinal fluid. Note that if motion were completely random, the resulting reduction in SNR could be ameliorated by additional data collection. Motion is rarely random, however. It is often correlated with the experimen-

tal task; for example, when subjects catch their breath each time they press a response button. Motion also introduces both spatial correlations, since adjacent voxels move together, and temporal correlations, since movements are extended over time.

Other physiological sources of noise include fluctuations in blood flow, blood volume, and oxygen metabolism. In 2001, Kruger and Glover investigated the spatial distribution of physiological noise, separating it into one component (σ_B) associated with variability in the transverse relaxation rate and another component (σ_{NB}) associated with cardiac and respiratory motion. Since the former component, like BOLD contrast itself, results from susceptibility-related signal changes, its magnitude depends on TE. The latter component, in contrast, is independent of TE. Kruger and Glover found that the spatial distribution of these two components differed (Figure 8.11). The former was much greater in gray matter than in white matter, while the latter was equally distributed throughout the brain. Furthermore, σ_B was typically about twice as large as σ_{NB}. Furthermore, they found that at 1.5 T, physiological noise makes up about 40% of the total noise, but at 3.0 T, physiological noise constitutes more than 52% of total noise.

These results suggest that physiological noise, rather than thermal or system noise, is the dominant source of variability in fMRI studies, especially at higher field strengths. Theoretical formulations suggest that thermal noise increases linearly with increasing field strength, but physiological noise increases quadratically with field strength. So, as field strength increases from 1.5 T to 3.0 T, raw signal will quadruple, thermal noise will double, and physiological noise will quadruple. These relations suggest that at very high field strengths, physiological noise may become dominant, and thus the improvement of functional SNR with increasing field strength may be considerably less than linear (Figure 8.12). More recent data from Triantafyllou and colleagues support this notion, indicating that at 7.0 T, the ratio of physiological to thermal noise becomes more than two to one. This suggests that, at high

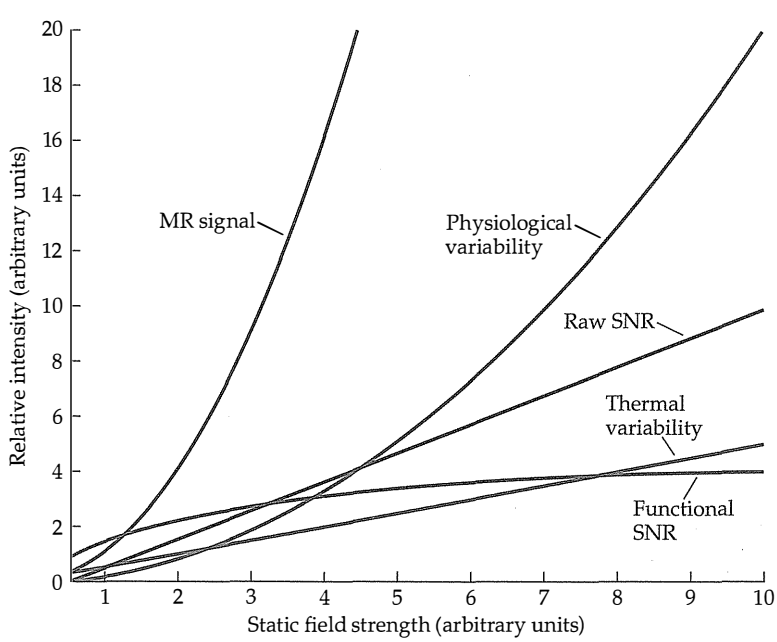

Figure 8.12 Changes in signal and noise with increasing static field strength. MR signal increases with the square of the field strength, while thermal noise increases linearly with field strength. The ratio of these quantities, raw SNR, thus increases linearly with field strength. However, because physiological noise increases with the square of field strength, functional SNR (which is dependent on both thermal and physiological noise) may reach an asymptote at high fields. Note that here the field strength is indicated in arbitrary units; the field strength beyond which such an asymptote would occur is not yet established.

reaction time The time required for someone to make a simple motor response to the presentation of a stimulus. Note that this is distinct from response time, which applies to situations in which someone must choose between two or more possible responses.

response time The time required for someone to execute a choice between two or more possible responses. Note that this is distinct from reaction time, which applies to situations when only one possible response is present.

intersubject variability Variability in fMRI data across a set of subjects; it includes the factors associated with intrasubject variability, along with between-subjects differences in task performance and physiology.

intrasubject variability Variability in the fMRI data from a single subject associated with thermal, system, and physiological noise, as well as with variability in the pattern of brain activity during task performance.

fields, increases in physiological noise may counteract gains in signal, setting an asymptotic upper limit for functional SNR. Note that data indicate that this limit increases for small voxel sizes, for which there is still an improvement in functional SNR as field strength increases. Thus, high-field fMRI might be most useful for research that requires very good spatial resolution. For an example, see the article by Bodurka and colleagues in the Chapter References.

Non-task-related neural variability

In the party analogy described at the beginning of this chapter, we noted that other nearby conversations could make it difficult to hear your friend's speech. However, unlike the other sources of noise discussed thus far, the words spoken in these other conversations represent legitimate signals that could, in principle, be of interest to you. Similarly, during any fMRI experiment there will be a surfeit of ongoing cognitive processes, most of which are not anticipated by the experimenters.

Let us consider an fMRI experiment in which we stroke the thumb with a brush to investigate which brain areas are activated by somatosensory stimuli. At the same time that the subject's brain experiences this discrete task-related sensory stimulus, the subject may also be hearing the sounds of the scanner gradients, receiving varying visual stimuli as he or she looks around within the scanner, recalling memories, or planning events as he or she thinks about appointments for later that day. All of these stimuli—internal and external—activate neural processes that incur metabolic demands and thus influence BOLD contrast. We only label these other processes as noise because they are unrelated to the stimulus of interest. However, under a different experimental design or analysis they could provide important information about brain function. This illustrates that the task-related responses in which we are interested occur within a highly active brain where routine neural processes are altering BOLD contrast at every moment.

Behavioral and cognitive variability in task performance

An additional source of noise in fMRI data comes from variability in how subjects perform the experimental task. (Box 8.2 considers other sources of interindividual variability, including potential differences in the form of the hemodynamic response.) In general, the more complex the task, the more performance will vary across time and across subjects. Performance is often measured by the time it takes to generate a response, known as reaction time or response time, depending on the experimental task. If the task simply requires the detection of a stimulus, the behavioral measure is known as reaction time and is typically around a few hundred milliseconds. But if the task requires the subjects to make some judgment about a stimulus, such as whether or not they remember it from earlier in the experiment, then the behavioral measure is known as response time. Since response times require additional cognitive processes, they are longer than reaction times. Depending on the experiment, response time may be as short as 300 ms or as long as several seconds. In any experiment, there will be both intersubject and intrasubject variability in reaction or response time (Figure 8.13). Variability in response time may have important consequences for the timing and amplitude of the BOLD signal. For examples, see the work of Menon and colleagues (Figure 7.24A) and Richter and colleagues (Figure 7.23), introduced in Chapter 7. To deal with this issue, many fMRI studies include reaction time, or some other behavioral measure, as a covariate in their analyses.

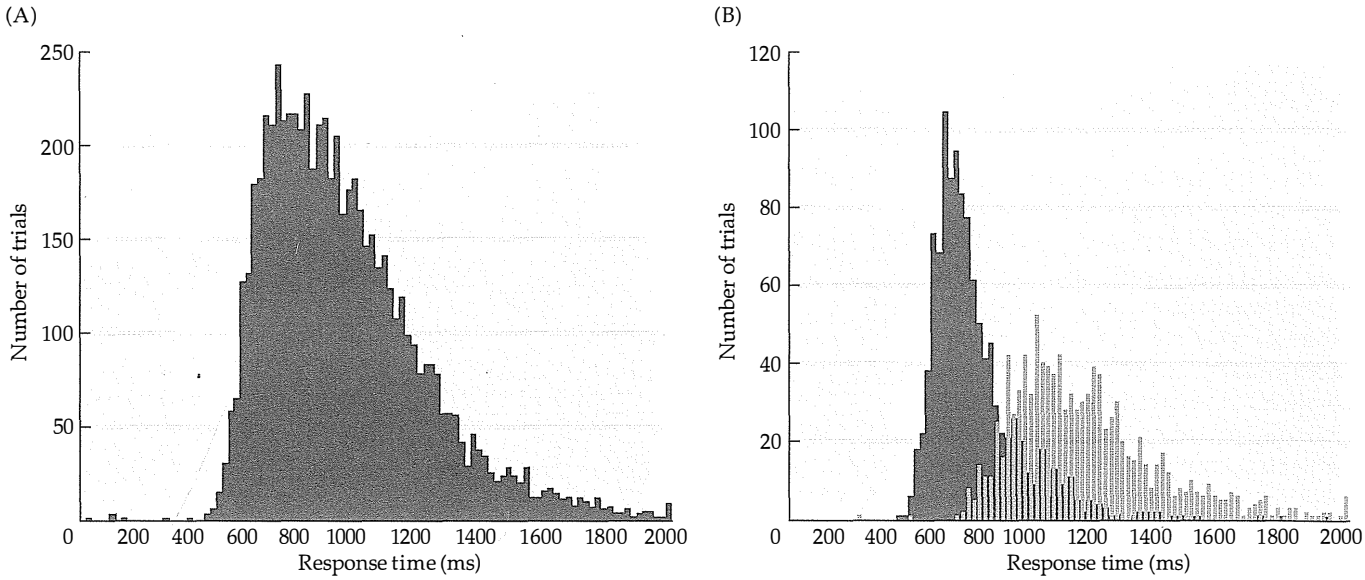

Figure 8.13 Variability in response time. Shown are histograms of response time data obtained during a target detection task conducted as part of an fMRI experiment. While the input stimulus was similar on every trial, the behavior differed dramatically from trial to trial. (A) The distribution of response times across approximately 10,000 trials collected from many subjects. Note that the distribution is highly positively skewed, with the shortest response times at about 400 ms and the mean at about 800 ms. (B) Distributions from two individual subjects. Note that even though these subjects were performing the same task, their patterns of performance were very different.

Performance can also be measured by examining the accuracy of responses. However, accuracy is frequently related to response time: subjects can perform most tasks more accurately when doing them more slowly. This relation is known as a speed–accuracy trade-off. Imagine that you are shown a series of photographs of faces and are asked to judge the emotion they are expressing. If you try to guess the emotion as quickly as possible, you will make many mistakes, especially on more complex emotions like disgust. Conversely, if you spend more time considering each face carefully, your accuracy will increase but your response times will slow. Because of these trade-offs, it is often reasonable to emphasize one factor as a constraint on behavior: "Respond as quickly as you can while maintaining a low error rate." This reduces variability in error rates across subjects, especially if you provide feedback about errors and the target error rate. Accuracy should be emphasized when the characteristics of the response are critical (e.g., when classifying stimuli as correctly remembered or forgotten). Speed should be emphasized when the processes of interest would change if the subject is allowed unlimited time to respond. Experiments on attention often emphasize speed, because the effects of attention on behavior may change if subjects are allowed a long time to respond.

Thought Question

How could differences in task performance confound fMRI studies that compare different subject groups, such as young and elderly adults?

speed–accuracy trade-off The improvement in the speed of a response at the expense of accuracy, or vice versa, within an experimental task.

BOX 8.2 Variability in the Hemodynamic Response over Subjects and Sessions

In most fMRI experiments, it is assumed that the measured signal has similar temporal and spatial properties between subjects (and across brain regions), allowing researchers to apply a single analysis model throughout an experiment. Yet, the fMRI hemodynamic response might vary in different subjects because of differences in local vasculature, neuronal activity, or even the functional organization of small areas of cortex. If there is substantial intersubject variability in the hemodynamic response, then an analysis model that is appropriate for one subject (e.g., who has a hemodynamic response peak at 5 s) might be inappropriate for another (e.g., who has a hemodynamic response peak at 7 s). This could potentially lead to erroneous conclusions about brain function. While intersubject variability in fMRI data has been studied for more than a decade, clear conclusions about its sources have been surprisingly difficult to draw. For an extended discussion of how experimental limitations can lead to unwarranted conclusions about variability, refer to the article by Savoy, cited in the chapter references.

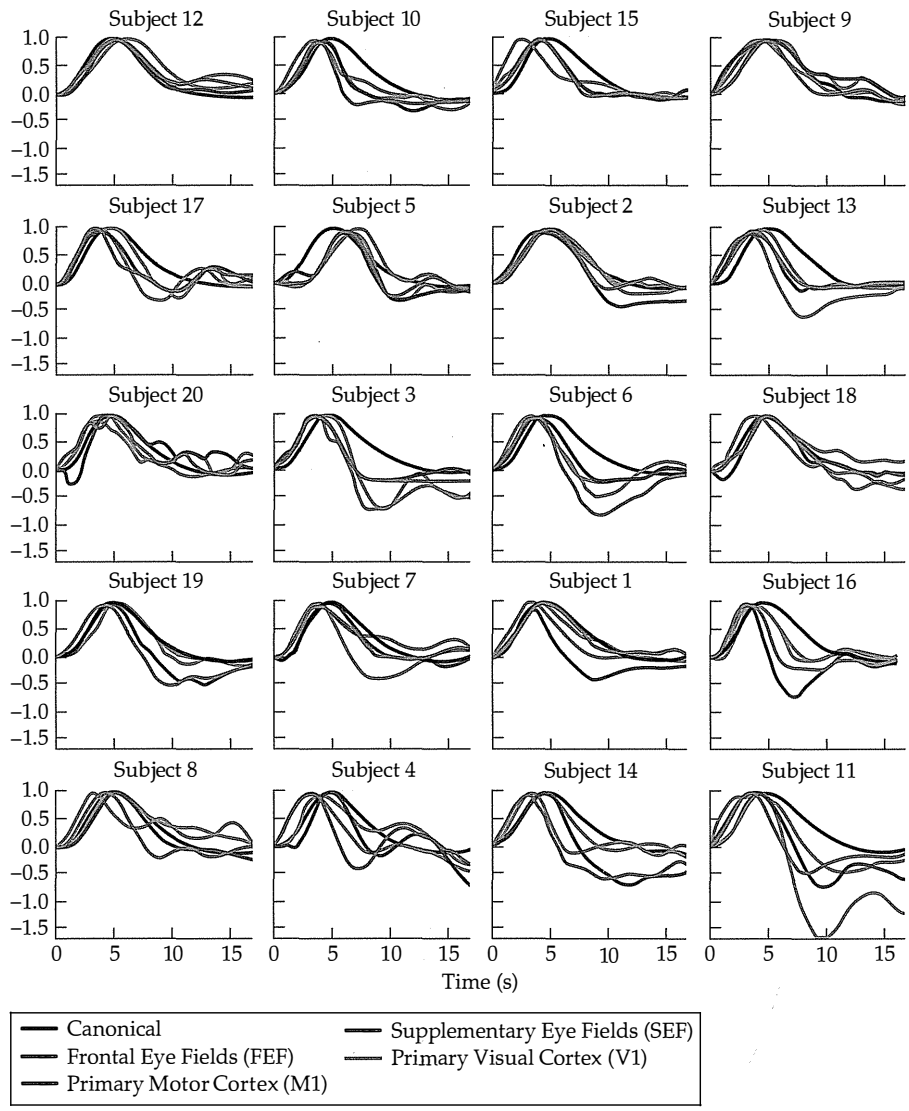

A good example of both the extent and implications of intersubject variability is found in a 2004 report by Handwerker and colleagues (which builds on earlier work by Aguirre and colleagues). Their subjects watched for infrequent, unexpected presentations of a flickering checkerboard, whereupon they would simultaneously press buttons on a response box and move their eyes to the location of the checkerboard. This design allowed the authors to compare hemodynamic responses in multiple anatomically defined regions of interest: the primary visual cortex, the primary motor cortex, and the frontal eye fields, which are important for the control of eye movements. They found that within a given individual, the hemodynamic responses in each region tended to be rather similar in onset, shape, and peak latency. However, striking differences were found in different individuals, with some individuals' responses peaking as early as 3–4 s, while those of other individuals peaked as late as 6–7s (see Figure 1 for examples). These measured hemodynamic responses allowed the authors to simulate how intersubject differences could influence analyses.

BOX 8.2 *(continued)*

◀ Figure 1 Intrasubject consistency and intersubject variability in the BOLD hemodynamic response. The reproducibility of the fMRI hemodynamic response has been examined in several experiments. Here, hemodynamic responses derived from four different brain regions are plotted for 20 subjects, within the same experiment. The task involved moving eyes and pressing buttons in response to an unexpected stimulus. Subjects are arranged according to the consistency of their BOLD responses across brain regions, from most consistent (upper left) to least consistent (lower right). All responses are normalized to a maximum amplitude of 1.0. Although there are substantial differences between individuals in the timing of their hemodynamic responses, with some peaking earlier and some later than the canonical hemodynamic response (lines), there is relatively good consistency in the timing of the hemodynamic response across regions within the same individual. (After Handwerker et al., 2004.)

They found that the detection of activated voxels was not dramatically influenced by the choice of hemodynamic response function (e.g., whether the function was derived from canonical data or from the subject's own data). However, the amplitude of the estimated activation was greatly reduced by a poor-fitting function. Thus, the authors concluded that using subject-specific functions may be beneficial, especially when conclusions are derived from the distribution of activation amplitudes across subjects. This may be especially important in cases where individual differences are of particular interest, such as when examining within-subject effects of a specific treatment.

A considerable number of studies have documented three aspects of temporal variability: (1) the same experimental task will evoke different hemodynamic responses in different subjects, (2) some of this variability reflects intersubject differences in task performance, and (3) residual variability in the shape and timing of the hemodynamic response is partially consistent across brain regions within a subject. Handwerker and colleagues showed that functions derived from subject-specific hemodynamic responses can improve analysis sensitivity compared with canonical functions derived from large numbers of subjects. However, what task should be used to develop the function is an open and important question, given that there will be intersubject variability in even simple motor and visual tasks. One intriguing possibility is calibrating the hemodynamic response using data from a breath-holding task, which evokes a state of hypercapnia (i.e., increased carbon dioxide) associated with large increases in BOLD signal. In a 2007 report, Thomason and colleagues reported that using the magnitude of the breath-holding response to normalize the evoked BOLD responses both reduced inter-individual variability and increased the number of activated voxels in a working memory task.

While the discussion so far has focused on temporal variability in fMRI data, it is also important to consider spatial variability. How much does the pattern of activation across regions differ from session to session? When different individuals perform complex cognitive tasks, differences in strategy may contribute to differences in measured activation, as outlined in the main text. Indeed, such individual differences are an important part of many fMRI studies. But, strategic differences should be relatively minimal when the same subject repeatedly performs a relatively simple task.

In a study reported by McGonigle and colleagues in 2000, a single subject participated in 33 separate scanner sessions, each containing three blocked-design tasks: finger tapping, passive visual stimulation, and random-number generation. Every session was identically run on the same scanner, with the same room lighting and ambient sounds, with the same operator giving the same instructions. Indeed, the authors note that the subject had the same "I've done this before" thoughts before every session! When the activation maps were examined at standard significance thresholds, there were apparent differences in the pattern of activation, even in the passive visual task (Figure 2A). In some sessions, there was very robust activation along the calcarine sulcus, which encompasses the primary visual cortex. However, other sessions had almost no activated voxels. A natural interpretation of these results is that the spatial pattern of activation is highly variable from session to session, even under conditions most likely to lead to reproducible activation.

Yet, this interpretation was challenged by the authors themselves in a 2005 reanalysis of their original data. Two conclusions of this new study are especially important. First, inter-session variability was of similar magnitude to intra-session variability, and this conclusion held across a range of different statistical packages and analysis approaches. If inter-session variability were of much greater magnitude, for comparison, it would pose problems for

(continued on next page)

BOX 8.2 *(continued)*

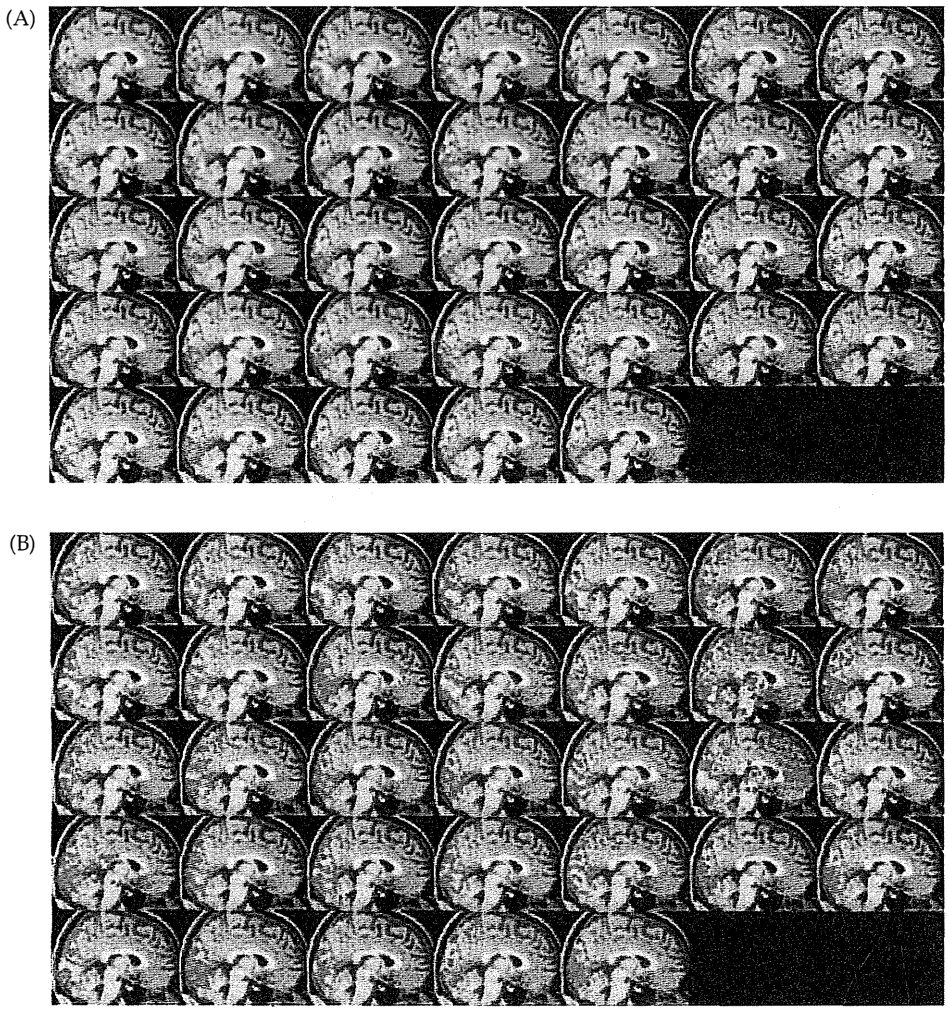

Figure 2 Reproducibility of fMRI activity across sessions. In what is likely a record, a single subject participated in 33 fMRI sessions, each containing simple motor, visual, and cognitive tasks. The experimental procedures were repeated in exactly the same manner at every session, right down to repeating the quite familiar experimental instructions. (A) Initial analyses suggested that there were different patterns of activation evoked in different sessions, based on the voxels passing conventional significance criteria. Shown here are data from the 33 visual-task sessions, each thresholded at a level of $p < 0.05$ and corrected for full-brain cluster significance. (B) A subsequent reanalysis by the same authors demonstrated that the activation differences that were found between sessions were largely an effect of using a relatively conservative threshold. When the significance threshold was relaxed by 33%, the patterns of activation became much more similar across sessions. (From Smith et al., 2005; data in A initially published by McGonigle et al., 2000.)

studies that involve repeated scanning of the same subject (e.g., before and after treatment). Second, they found that the apparent variability across sessions was largely an artifact of statistical thresholding. When using a slightly reduced threshold, the pattern of activation seemed much more similar across sessions (Figure 2B). It is important to emphasize that these two figures display the same activation map; they differ only in what parts of that map are shown in color and what are omitted. Considered in this new light, the authors make a compelling case that fMRI data can be highly reproducible across many sessions. In summary, data from the same subject may show significant temporal and spatial variability. However, much of that variability results from the same sources—scanner noise, physiological noise, and strategic variation—as intra-session variability.

Strategy changes are another source of task-induced variability. In many cognitive tasks, there may be more than one strategy that can be used to solve a task. When making decisions, some subjects may use specific heuristics (e.g., selecting the option that seems most familiar to them), whereas others may

adopt a more analytic approach (e.g., comparing the costs and benefits of every option). Such individual differences in strategy may be identifiable based on differences in the pattern of fMRI activation. (Evidence in support of this has come from several studies showing both inter-individual variability and intra-individual consistency across a number of fMRI tasks.) When planning an experiment, fMRI researchers should consider what strategies a subject might use to solve the task. If multiple strategies are possible, then there should be some way of identifying when different subjects (or even the same subject, at different times) employ particular strategies. To gain insight into how subjects may approach a task, researchers should always use themselves as pilot participants (in the behavioral task) before recruiting fMRI subjects.

Good training of research subjects can also reduce unwanted behavioral variability. Providing clear instructions improves the subjects' understanding of the experimental task, while practice before the fMRI session allows subjects to attain a steady-state performance level before entering the scanner session. These practice sessions ahead of time—or even during anatomical imaging—minimize the learning effects or strategy changes that typically occur at the beginning of an experiment.

Preprocessing

As described in the previous chapters, one can consider fMRI data as consisting of a 3-D matrix of volume elements (voxels) that is repeatedly sampled over time. A single experiment might have an imaging volume of $64 \times 64 \times 30$ voxels that is sampled every 2 seconds for a total of 10 minutes, resulting in 300 time points per voxel. A straightforward way of analyzing such a data set would be to extract the raw time course for each voxel and compare each of these time courses to some hypothesis using a test of significance. While this approach does indeed form the basis of much fMRI data analysis, it contains some hidden assumptions, which we will discuss in more detail in Chapter 10. Notably, it assumes that each voxel represents a unique and unchanging location in the brain and that the sampling of that voxel occurs at a regular known rate. These assumptions, though seemingly plausible, are always rendered incorrect by the sources of variability described earlier in this chapter.

Here, we discuss a series of computational procedures, collectively known as preprocessing, that operate on fMRI data following image reconstruction but prior to statistical analysis. Similar preprocessing algorithms are generally applied, regardless of the experimental design (e.g., the same procedures would be used for a blocked design study of language and an event-related study of memory). Preprocessing has two principal goals: to remove uninteresting variability from the data and to prepare the data for statistical analysis. If done correctly, preprocessing steps can greatly increase the functional resolution of an fMRI experiment.

Quality assurance

An important and often underutilized aspect of preprocessing is quality assurance (QA) testing. Quality problems can (and will) arise on even the best-maintained scanner. If a subject's data are corrupted by extreme scanner noise, or by some problem with data acquisition, that subject may have to be excluded from further analyses, incurring both scientific and financial cost. Even more worrisome are hidden quality problems. The prevalence of automated statis-

quality assurance (QA) A set of procedures designed to identify problems with fMRI data so that they do not compromise experimental analyses.

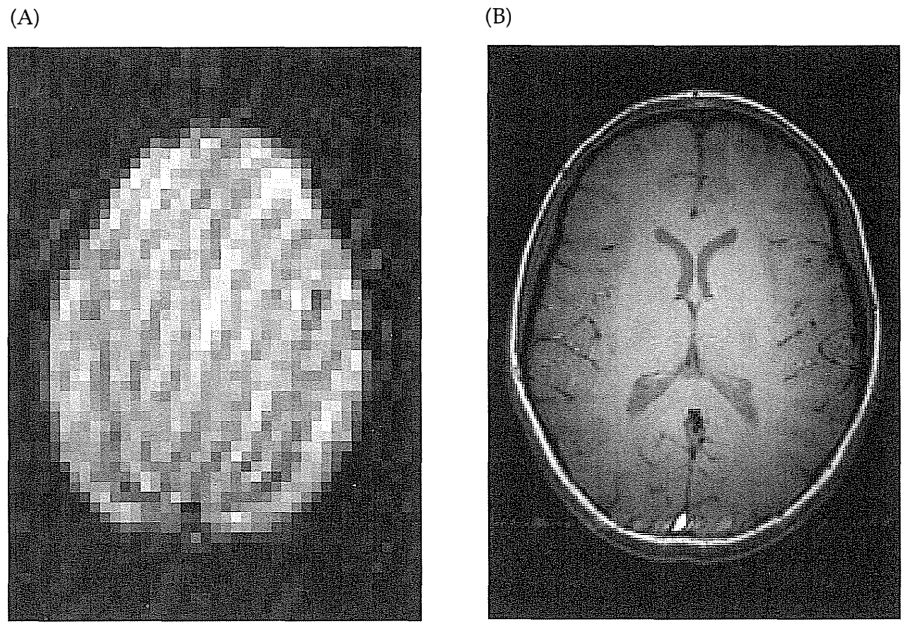

Figure 8.14 Common artifacts found in MR images. An important goal for quality assurance programs is the identification of image artifacts that can corrupt MR data. (A) Radiofrequency leakage resulting from an ungrounded electrical connection can cause "white pixels" in *k*-space, resulting in grating patterns on reconstructed images. (B) Variations in the local properties of the field can cause intensity variations across an image, such as the brightening of the center of the image compared with the periphery.

tical packages has made it possible for investigators to preprocess, analyze, and combine data across subjects without ever examining an individual subject's data. Without QA testing, unnoticed problems might propagate into the final results of an experiment, with potentially disastrous consequences.

The first rule of QA is simple: examine your data. Many common artifacts are readily visible in the raw images, even under a cursory examination (Figure 8.14). An effective way of viewing experimental data is as a time-series movie, in which an entire experimental run is shown, one volume after another, in a rapid sequence. Because our visual system is very good at picking up changes between successive images, many types of problems will appear as we view the sequence. Radiofrequency noise, for example, can show up as repeating patterns on top of the data, while head motion can appear as rapid jerks. Although visual inspection of fMRI data should be a regular part of any QA procedure, it is not in itself sufficient for ensuring data quality. Researchers should also apply statistical tests that evaluate the quality of collected fMRI data. These can include calculations of the mean image intensity, the raw SNR (over space), or the image intensity divided by the standard deviation over time (as a rough approximation of functional SNR). Some analysis packages and many imaging centers have developed quality assurance testing, some of which can be run automatically and in real time during fMRI sessions.

Though not strictly part of preprocessing, frequent tests of a single object, often called a **phantom**, are important for ensuring data quality. Phantoms (Figure 8.15) are typically balls or cylinders filled with a homogeneous fluid or gel, although they can have internal structure (including some that roughly mimic brain anatomy). Daily scanning of the same phantom with the same pulse sequences will indicate changes in the scanning environment, since the data should look identical across sessions. Imaging centers should regularly scan phantoms so that they will identify problems with scanner hardware as soon as possible.

phantom An object used for testing MR systems. Most phantoms are filled with liquids or gels with known properties, so that problems with the scanner system can be readily identified.

Finally, while we emphasize quality assurance in the context of data acquisition, that concept should pervade all aspects of fMRI research. Problems or

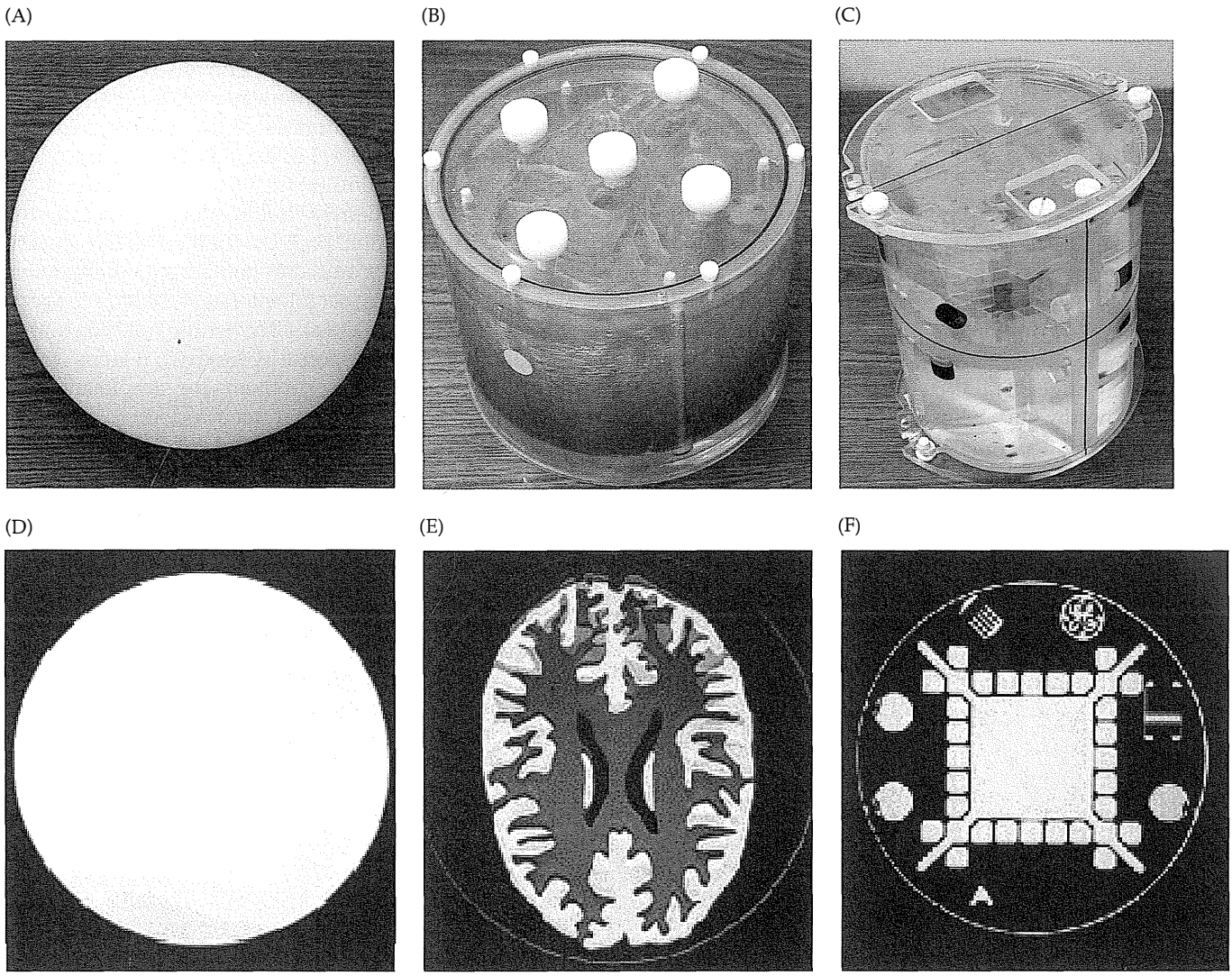

Figure 8.15 Examples of phantoms and their appearance on MR images. Phantoms are fluid- or gel-filled shapes that are used for testing MR scanners. They may be homogeneous (A), or have internal structure (B, C). Shown below each phantom in (D, E, F) are structural MR images collected using each of these phantoms. (Phantoms courtesy of General Electric Corporation.)

mistakes can appear during any stage of fMRI experimentation: at data collection, following preprocessing, during final analyses, or even when preparing results for publication. Without a diligent QA program, problems with data quality will corrupt experimental results and frustrate investigators.

Slice acquisition time correction

Most fMRI data are acquired using pulse sequences of the form described in Chapter 4: slice selection using radiofrequency excitation, followed by simultaneous data collection from throughout that slice (i.e., using echoplanar or spiral techniques). To collect data from the entire brain, a typical pulse sequence might acquire 30 or more slices within a TR of 1.5 to 3.0 s, depending on the

ascending/descending slice acquisition The collection of data in consecutive order, so that slices are acquired sequentially from one end of the imaging volume to the other.

interleaved slice acquisition The collection of data in an alternating order, so that data are first acquired from the odd-numbered slices and then from the even-numbered slices, to minimize the influence of excitation pulses upon adjacent slices.

temporal interpolation The estimation of the value of a signal at a time point that was not originally collected, using data from nearby time points.

capabilities of the scanner. In virtually all fMRI scanning, the slices are acquired with equal spacing across the TR. One approach is to use ascending/descending slice acquisition, in which the slices are collected consecutively (e.g., 1-2-3-4-5-6-7-8-9-10-11-12). Most fMRI studies now use interleaved slice acquisition, in which the scanner first collects all of the odd-numbered slices and then collects all of the even-numbered slices to avoid cross-slice excitation. If there were 12 slices in the imaging volume, numbered from 1 at the bottom of the brain to 12 at the top, an interleaved acquisition sequence would collect the slices in the order 1-3-5-7-9-11-2-4-6-8-10-12. One potential problem for interleaved acquisition is that adjacent parts of the brain are acquired at non-adjacent time points within the TR (Figure 8.16). Thus, assuming that the interleaved example above had a TR of 3 s and that slice 1 was acquired at 0 s, slice 2 would not be acquired until 1.5 s later. In effect, an identical BOLD response in these two regions would seem to occur earlier in the latter slice, posing problems for simple analyses (especially in event-related experimental designs) if uncorrected.

Thought Question

In most fMRI pulse sequences, the slices are equally spaced throughout a TR. Can you think of a type of experiment in which researchers might concentrate all of the slices at the beginning of the TR, so that there is a period of time in which no acquisition takes place? (Hint: Refer to Chapter 2 to consider what the subject experiences each time a slice is acquired.)

The most common approach for dealing with slice-timing discrepancies is correction via temporal interpolation during preprocessing. Interpolation uses

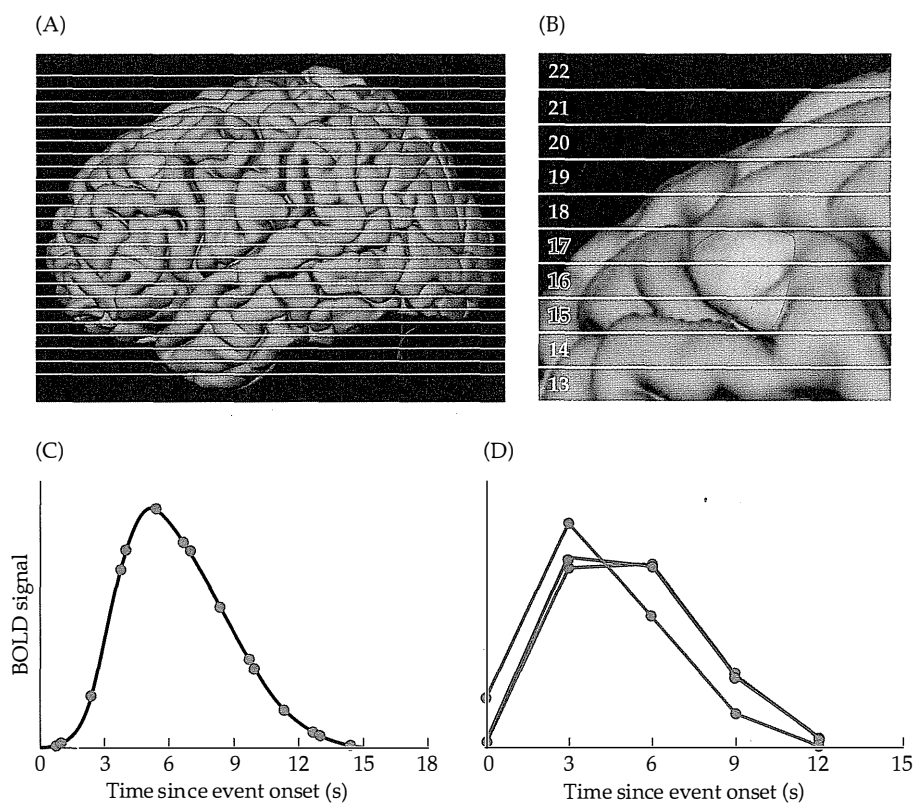

Figure 8.16 Effects of slice acquisition time on the hemodynamic response. Imagine that a single brain region, shown in red (A), is uniformly active following presentation of a stimulus. This region spans three slices, 15 to 17, within the imaging volume, which is acquired with a standard interleaved sequence (i.e., that first acquires the odd-numbered slices and then acquires the even-numbered slices) (B). Because the slices within this region are acquired at different times within the 3 s TR, the hemodynamic response within the slices will have different time courses. The signal recorded from the different slices is plotted against the time each slice was acquired in (C). Yet, without correcting for the time of acquisition of each slice, the time courses would seem to differ dramatically across slices (D). The hemodynamic response in slice 16 (acquired late in the TR) appears to peak earlier than those in the surrounding slices (acquired early in the TR), even though the underlying activity is identical.

information from nearby time points to estimate the amplitude of the MR signal, for every slice, at a single point within the TR (e.g., the onset or middle). Sinc interpolation is most often used, because it accounts best for noise-related variability in fMRI data (see Chapter 4 for a discussion of this function). It is important to emphasize that interpolation techniques are intrinsically imperfect; any attempt to recover the missing information will be limited by the variability in the experimental data, particularly variability that is not associated with the task. Another approach is to create separate analysis models for each slice, effectively moving slice-acquisition correction from preprocessing to data analysis. This latter approach may be preferable if the experiment targets specific brain regions, but it can make some forms of post hoc analyses (e.g., extracting a mean time course from a region that spans slices) more challenging.

Head motion: an overview

Probably the most damaging (and frustrating) problem for fMRI studies is head motion. To appreciate how little head motion is required to render data meaningless, examine the data shown in Figure 8.17. Note the large intensity difference between adjacent voxels in panel B. Now imagine that the subject moves his head almost imperceptibly, shifting by only 5 mm (i.e., the width of a single voxel) to the right. Even such a tiny movement has a drastic effect on the data, as shown in panel C. Because the scanner acquires images at absolute spatial locations, not relative to the brain's position, head motion can cause a given voxel to contain signal from two very different types of tissue (e.g., gray matter and ventricle). This can cause very large apparent changes in raw signal over time, leading to spurious motion-related activations that often form a distinctive ring pattern around the edges of the brain (Figure 8.18). Moreover, head motion can cause a loss of data at the edges of the imaging volume. Most fMRI protocols use fields of view that are substantially larger than the brain, such as 20 or 24 cm, so movements within the plane of data acquisition do not move the brain outside of the imaging volume. But large through-plane movements can cause a portion of the brain (e.g., portions of the superior frontal and parietal lobes) to move out of the imaging volume, with an irreversible loss of data from the affected regions. Researchers often acquire additional slices around the edges of the area of interest, whether

(A)

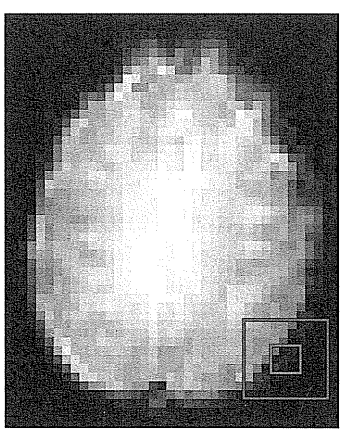

(B)

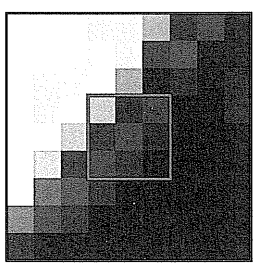

507	89	154
119	171	83
179	117	53

(C)

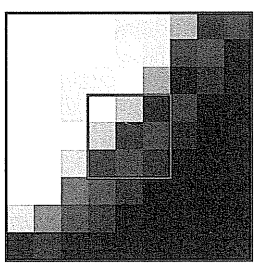

663	507	89
520	119	171
137	179	117

Figure 8.17 Effects of head motion on fMRI data. Large intensity transitions exist at tissue boundaries, including the edges of the brain (A). Here we demonstrate the effects of head motion on voxel intensity. The magnified views show the position of the brain before head motion (B) and after a movement of one voxel to the right (C). The numerical intensity values for the voxels within the blue square are shown below. Note that the intensity in a given voxel may change by more than a factor of 5 due solely to head motion. This compares to a change of only 1 to 2% for real brain activity.

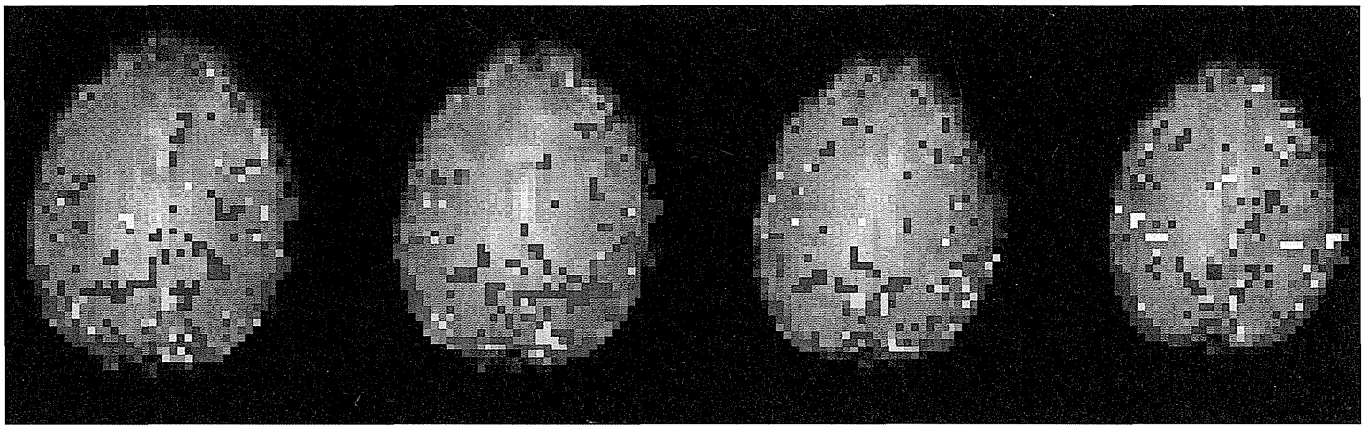

Figure 8.18 Edge effects of head motion in fMRI analyses. Because the intensity transitions in the brain are greatest at its edges, head motion often results in systematic rings of artifactual activation around the edges of the brain. Shown are activation maps, in four axial slices, derived from the analysis of a motor task generally similar to that described in Figure 8.1. Here, however, the brain moved forward by two voxels at the beginning of one stimulus onset, and remained forward for 4 s. This causes large changes in signal intensity around the edges in the brain; for example, voxels at the back of the brain changed from high intensity to low intensity as a result of the movement. Thus, these voxels had a significant decrease in activation (plotted in a blue-to-white colormap) due entirely to the movement, and these movement-related effects dwarf the significant task-related increases in activation (plotted in a red-to-yellow colormap) within motor cortex.

the full brain or just a single region, so that small through-plane movements can be corrected.

There are several characteristic forms of head motion (see Figure 8.19 for examples). Many fMRI experiments are partitioned into multiple runs to reduce subject fatigue and, in some cases, to overcome hardware constraints on data acquisition. During the breaks between runs, subjects typically relax and talk to the experimenters, often resulting in considerable head motion. When different experimental conditions are separated in different runs (e.g., in studies of memory encoding and retrieval), motion can have differential effects across conditions. Within runs, subjects often make numerous small movements of the head. During a one- to two-hour session, while the subject lies in a small space, he or she will become increasingly tired and restless. Experimental stimuli themselves may cause head motion. Many experimental tasks require subjects to make motor responses, usually by moving a joystick or pressing a button, which may in turn lead to head motion. Anyone who has been a subject in an MRI study has experienced momentary drowsiness, only to be startled into alertness by the next stimulus. Motion effects that co-occur with stimulus presentation pose challenges for analysis and preprocessing techniques, because in these cases it is difficult to separate real brain activation from artifacts of motion. Within-run and between-runs movements are sometimes corrected separately because of their different spatial properties.

Even though head motion is an inherently spatial problem, it can have consequences for activation timing. Motion through the slice plane (i.e., along the z-dimension for most fMRI studies) will change the pattern of excitation across the brain. Recall that for functional pulse sequences, like gradient-echo

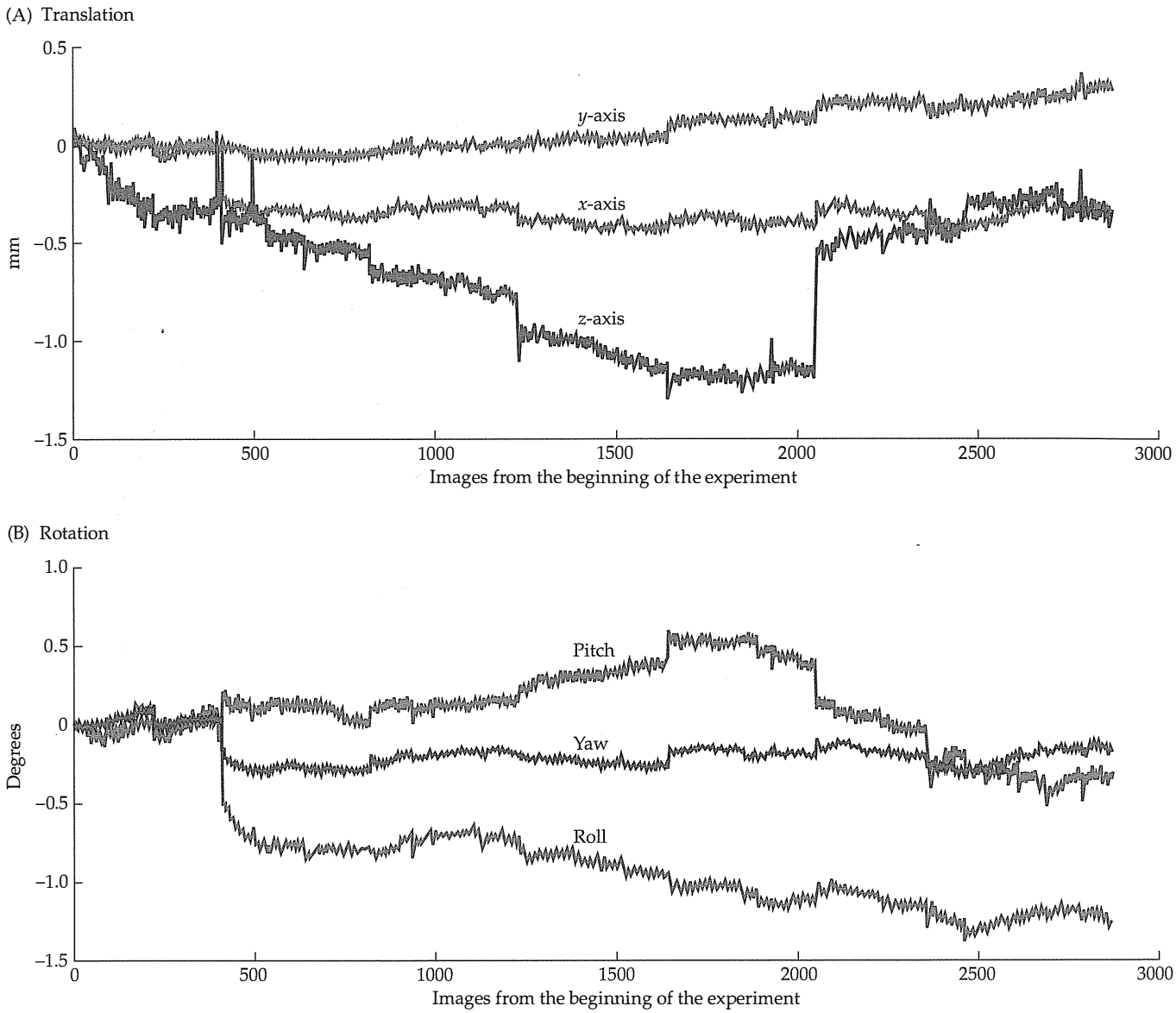

Figure 8.19 Plots of head motion over an experimental session. Shown are plots of translational (A) and rotational (B) head motion from a single fMRI session. By convention, translational effects comprise movements from left-to-right (x-axis), forward-to-back (y-axis), and top-to-bottom (i.e., in the slice acquisition direction; *z-axis).* Rotational effects comprise turns around the x-axis (pitch), around the y-axis (roll), and around the z-axis (yaw). This experiment consisted of seven runs, each of 410 images, with a TR of 1500 ms. Large motions between runs are visible as vertical lines on the plot; for example, see the vertical line near image 2050 that reflects an upward through-plane movement. Note that these are the *estimated* motion values at each point in time, and thus can be influenced by a number of factors besides head motion itself, as indicated in the text.

EPI, each excitation pulse is targeted to one slice at a time. But if the head moves during the acquisition of a single volume, then some of the slices may miss the excitation pulse, whereas others will experience two (or more) excitation pulses in rapid succession. The former will experience more T_1 recovery than expected,

whereas the latter will experience less T_1 recovery, changing the relative BOLD signal recorded from each. Motion also influences the timing of activation, potentially by a second or more in a typical interleaved slice acquisition.

Prevention of head motion

Like many other problems, head motion is more easily prevented than corrected. Most laboratories use head restraints of some form (Figure 8.20). The most effective but difficult-to-use option is the bite bar (Figure 8.20A and B). As its name implies, a bite bar immobilizes the head by requiring the subject to clamp his or her teeth firmly on a dental mold, which in turn is solidly attached to the scanning hardware. With the jaw immobilized, potential head movement becomes very limited. Some subjects dislike using bite bars, and this both increases the likelihood that a participant will end a session prematurely, and discourages participation in the first place. Systems that use mold-

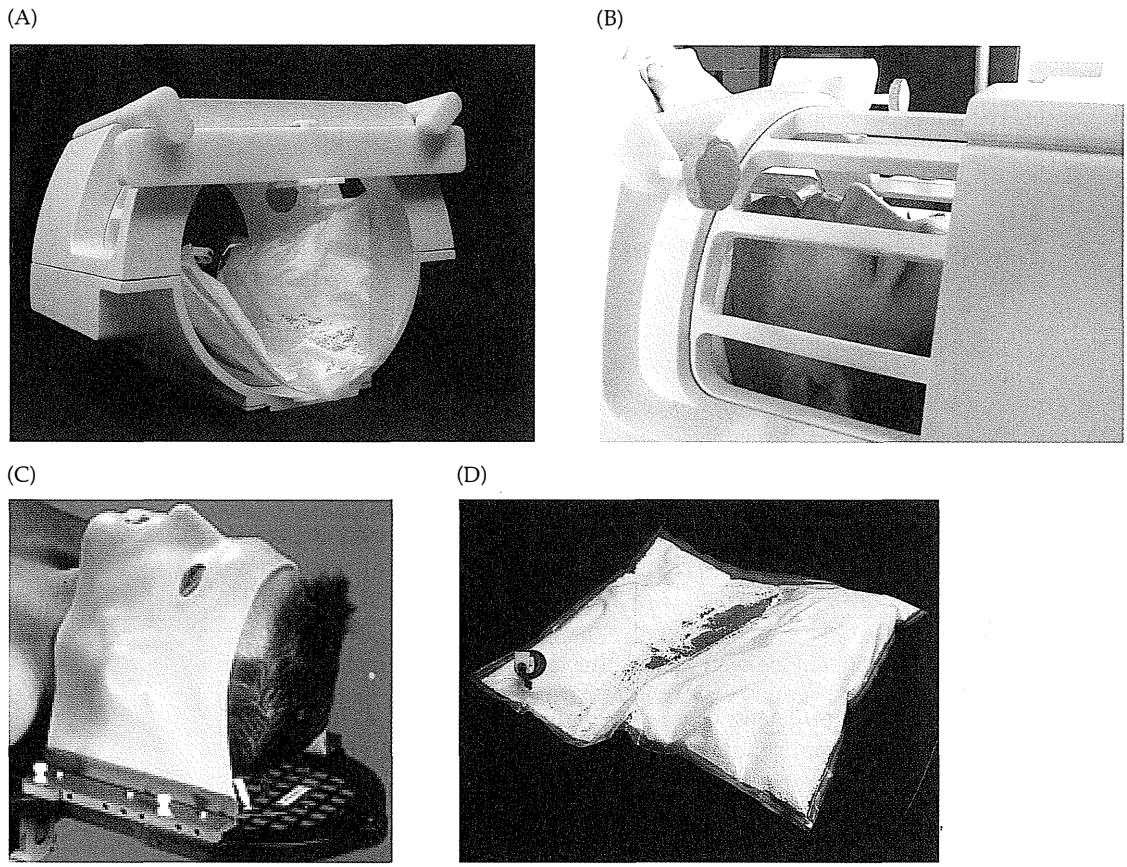

Figure 8.20 Head restraint systems. Because severe head motion can render fMRI data useless, several systems for head-immobilization exist. Shown in (A) is a standard volume head coil with two motion-restraint systems. Attached to the top of the head coil is a bite bar, while at the bottom is a vacuum pack. When the bite bar is used (B), the subject clenches his teeth on a dental mold that has been customized to his bite pattern. This greatly restricts the effective motion of the head. Thermoplastic masks (C) mold to the subject's face, and are anchored to a static support. Vacuum packs (D) contain many soft foam beads within a plastic casing. When air is pumped out, the pack hardens to form a shell around the contours of the subject's head. (C from Med-Tec.)

able plastic or mesh to create a mask around the subject's head (Figure 8.20C) are usually tolerated better. Such masks passively restrict head motion without requiring jaw clenching and are individually molded to each participant's physiognomy. Mask systems take time to customize for each subject, especially thermoplastic devices that must be heated and cooled before scanning. Another disadvantage is that some subjects may feel claustrophobic due to the high degree of immobilization.

Vacuum-pack systems combine good motion prevention with improved patient comfort (Figure 8.20D). The vacuum pack consists of a large number of soft beads within a flexible plastic casing. Once the subject is positioned in the scanner, the pack is fitted around the sides of the head and its air is pumped out, which hardens the vacuum pack into a form-fitting shell molded to the contours of the skull. Since the face is left open, the risk of claustrophobia is not increased significantly. In fact, many subjects report that they prefer the vacuum system to no restraint at all, because its head support allows them to relax their neck muscles. Vacuum packs, and similar systems that use static padding, provide a reasonable compromise between restriction and comfort.

While restraint systems play an essential role in preventing head motion, probably the most important factor is subject compliance. When subjects become uncomfortable, they may terminate the session or move to relieve soreness or pain. Working to maximize the subjects' comfort and interest in the study greatly improves the chances of acquiring a complete data set that is not corrupted by excessive motion. Researchers should regularly talk to their subjects; even a simple "How are you doing?" after each run will help prevent anxiety and the accompanying motion. We have also found that taping down the subjects' foreheads will help to reduce head motion. Although a single piece of tape cannot prevent a subject from moving his or her head, it provides the subject with feedback (in the form of changes in tension) when he or she moves.

Head motion can also be minimized through subject training. At many centers, subjects participate in training sessions within an MRI simulator, or mock scanner, that is constructed from the parts of a decommissioned scanner (Figure 8.21A). Recorded scanner noises can be played within the bore of the simulator for added realism, and (at some centers) head position can be mon-

mock scanner A device that simulates a real MRI scanner, usually by reproducing the scanner bore, the bed that the subjects lie on, and the sounds made during scanning

(A)

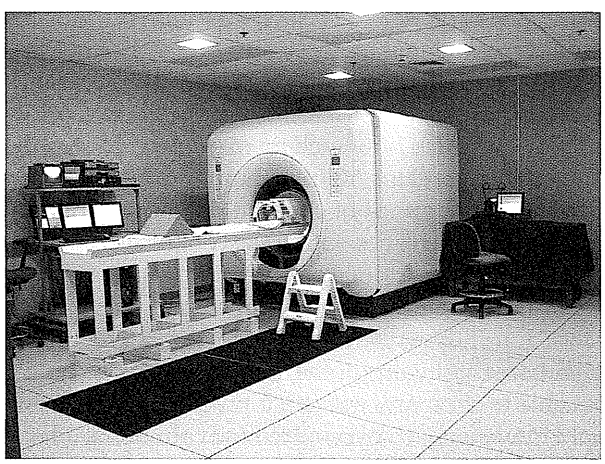

(B)

Figure 8.21 Use of a mock scanner system for prevention of head motion. By acclimating potential subjects to the MRI environment in a simulated or mock scanner (A), head motion and other subject compliance problems can be greatly reduced. (B) An adolescent subject with a head-tracking system around her forehead. If she moves her head beyond a threshold amount, the movie that she is watching through the mirrored glasses will stop playing.

coregistration The spatial alignment of two images or image volumes.

reference volume A target image volume to which other image volumes are to be aligned.

rigid-body transformation A spatial transformation that does not change the size or shape of an object; it has three translational parameters and three rotational parameters.

translation The movement of an object along an axis in space (in the absence of rotation).

rotation The turning of an object around an axis in space (in the absence of translation).

cost function A quantity that determines the amount of residual error in a comparison.

mutual information In the context of MRI, the amount of information about one image that is provided by knowledge of another image.

itored (Figure 8.21B). Mock-scanner training can make subjects more relaxed and comfortable during their real scanning sessions. Subjects who cannot tolerate confinement in the mock scanner, or who cannot avoid moving their heads over the course of the mock scanning session, can be excused from further participation.

Correction of head motion

When the head moves during an experiment, some of the images will be acquired with the brain in the wrong location. The goal of motion correction is to adjust the series of images so that the brain is always in the same position. The general process for spatially aligning two image volumes is called coregistration. For motion correction, successive image volumes in the time series are coregistered to a single reference volume. Because the brain's size and shape do not change, a rigid-body transformation is often used. Rigid-body transformations assume that the size and shape of the two objects to be coregistered are identical, and that one can be superimposed exactly upon the other by a combination of three translations (i.e., moving the entire image volume along the x-, y-, and z-axes) and three rotations (rotating the entire image volume through the x–y, x–z, and y–z planes). The assumption of rigid-body movements is generally plausible in fMRI studies, although inhomogeneities in the magnetic field may lead to differential scaling of images depending on their position in the scanner.

To determine the likely amount of head motion, computer algorithms identify the set of translation and rotation parameters that provides the best match to a reference volume, such as the first image acquired in the session (Figure 8.19). The mathematical measure of how well one image matches another is determined by a similarity measure, or cost function. In the ideal case of perfect coregistration between the corrected volume and the reference volume, a voxel-by-voxel subtraction would yield a difference of zero. A simple cost function, then, could be the sum of absolute intensity differences between voxels in the corrected and reference volumes. Since large differences are much more problematic than small differences, other cost functions weight large movements more heavily. Different cost functions are sensitive to different aspects of the data. For example, in 2001 Freire and Mangin reported that using the sum of squared differences as a cost function can sensitize the coregistration to the presence of large task-related BOLD activations, and this can shift the images and introduce spurious activations at high contrast borders. Other cost functions that minimize the mutual information between volumes are less sensitive to such task-related effects. Mutual information is a measure roughly analogous to correlation, which considers how well a voxel's intensity in the reference volume predicts, or reduces the uncertainty about, the intensity of a voxel in the corrected image. Unlike the sum of squared deviations, mutual information does not assume that the intensities within the coregistered images must match. Motion correction is sometimes done on smoothed images to minimize the effects of noise within the image on the cost function.

Regardless of the cost function chosen, the goal of coregistration is to find the transformation at which the smallest value of the cost function is obtained. It is not computationally feasible to compare, with high precision, all possible ways in which the head could move for each of hundreds of volumes acquired during an experiment. Thus, to minimize computational costs, realignment algorithms use iterative approaches that include an initial rough estimation followed by more precise refinement. While faster than testing all possible

movements, these algorithms have the minor disadvantage of potentially identifying a local minimum in the cost function, rather than the global minimum corresponding to the true motion.

Once a set of realignment parameters is determined, the next step is to resample the original data to estimate the values that would have been obtained had there been no head motion. This process is called **spatial interpolation** and is similar to the temporal interpolation described earlier in the chapter. However, whereas temporal interpolation only considers the single dimension of time, spatial interpolation considers the three dimensions of space. Simple trilinear interpolation assumes that each interpolated point should be a weighted average of all adjacent points. More complex sinc interpolation is optimal for well-sampled images, but may introduce artifacts if the data are not band-limited; that is, if there are important spatial frequencies in the brain that are not represented in the image.

spatial interpolation The estimation of the intensity of an image at a spatial location that was not originally sampled, using data from nearby locations.

Most researchers minimize the effects of head motion during preprocessing by using coregistration algorithms or, less frequently, by removing motion-related components from the data with filtering techniques (e.g., independent components analysis). It is also possible to isolate motion effects within experimental analyses. Including the calculated motion parameters as regressors reduces the amount of error (i.e., unaccounted-for variability) in the analysis model, which can increase the experimental power for detecting effects of interest. In a 2005 study, Johnstone and colleagues demonstrated that the inclusion of motion parameters in the experimental model can have a positive effect on the sensitivity of the analysis to true activations, especially within event-related designs. However, as already noted, head motion is often correlated with the experimental task, so including motion parameters in analysis models can also remove task-related activity.

Motion correction has become a standard part of fMRI preprocessing and is now used in nearly all published fMRI studies. The major software packages for fMRI analysis all include some form of motion correction, although the algorithms differ from package to package. When different motion correction approaches have been systematically compared, both on simulated and real fMRI data, the results have been equivocal. To a first approximation, all major packages do a creditable job correcting for motion, in that they all provide significant and measurable increases in the amplitude and specificity of BOLD activation. However, no one approach seems demonstrably superior to the rest. This suggests that the current approaches to motion correction provide robust and effective methods for improving fMRI data quality, although future advances remain possible. One target for future study will be using motion parameters to estimate the history of excitation of each voxel, potentially leading to changes in the predicted BOLD signal changes. While not part of most current approaches, the inclusion of spin history effects may become a standard part of preprocessing in the coming years.

Distortion correction

As we learned in Chapter 5, functional images often suffer from geometric or intensity distortions that preclude simple matching to the high-resolution structural images. The most common cause of such distortions is field inhomogeneities. Static field inhomogeneities usually cause geometric distortions, although they can also lead to signal losses under severe conditions. Excitation field inhomogeneities (i.e., uneven excitation or reception across space) usually cause intensity variations within the image. To ensure that images pro-

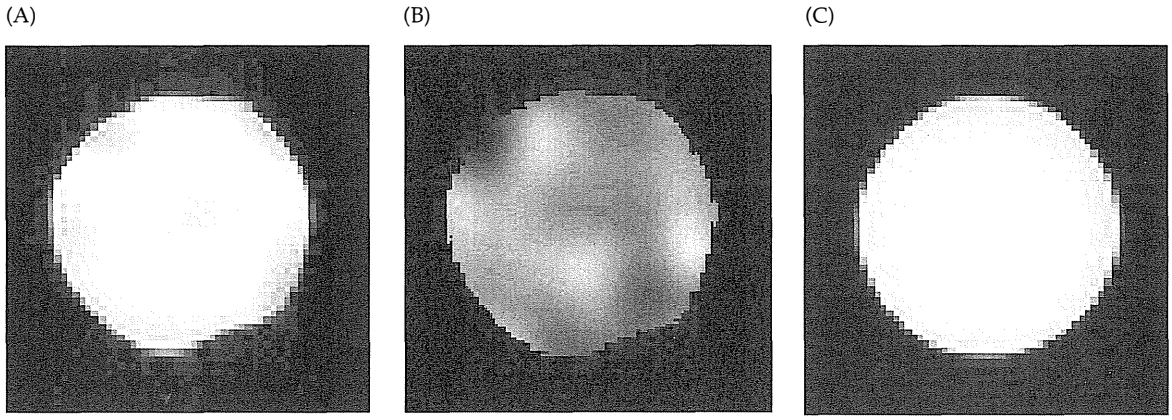

Figure 8.22 Correction of geometric distortions in functional images. In this image of a spherical phantom (A), there is obvious geometric distortion. To correct for the distortion, a map of magnetic field intensity is acquired (B). The intensity map can be used to generate a corrected image (C).

vide a true and undistorted representation of the functional neuroanatomy, researchers use specialized acquisition techniques and computational algorithms that correct the acquired images to account for these distortions.

A common method to prevent non-uniformity within the static magnetic field is magnetic field shimming. By adjusting many first-, second-, and higher-order magnetic field gradients generated by shimming coils (see Chapter 2), most field distortions can be corrected and a reasonably homogeneous field can be created. However, when shimming conditions cannot be optimized, especially at very high magnetic field strengths, residual magnetic field inhomogeneities may remain significant enough to induce noticeable geometric distortions (Figure 8.22). An alternative approach, called magnetic field mapping, can be adopted to provide explicit knowledge of the static magnetic field. A field map of the main magnetic field can be created by acquiring two images of the signal phase with slightly different echo times. The difference between the phase images is proportional to the strength of the field at any given location. If the field is completely uniform, then the phase difference induced by the different echo times will be the same in all voxels, and the resulting image will be a uniform gray. Field maps can be determined for a phantom or human brain and can be incorporated into the image reconstruction routine to correct for any geometric distortions.

Thought Question

Why does acquiring images of the spin phase at two different echo times provide a measure of local magnetic field strength?

shimming coils Electromagnetic coils that compensate for inhomogeneities in the static magnetic field.

magnetic field mapping The collection of explicit information about the strength of the magnetic field at different spatial locations.

field map An image of the intensity of the magnetic field across space.

A common method to prevent non-uniformity in the excitation field is to construct very homogeneous volume transmitter and receiver coils. While the physical principles for producing such coils are well worked out (see Chapters 2 and 3 for additional discussion), in practice, even the best-constructed volume coils have residual intensity variations across space. This problem is exacerbated by the use of high-sensitivity surface coils, which by design intro-

duce large, spatially dependent intensity variations. Thus, it would be useful to have explicit knowledge of the excitation field, so intensity compensation algorithms can be applied post hoc, based on such knowledge. To create a map of the excitation field, a large uniform object (e.g., a water-filled phantom) is placed in the center of the magnetic field. For each voxel in the phantom, the recorded signal depends on two factors: the number of spins (e.g., hydrogen nuclei in a proton-density scan) and the strength of the excitation field at that location. The number of spins should be approximately constant across the phantom, since it is homogeneous; thus, any differences in intensity across the image will be due to variations in the strength of the excitation field.

New techniques can correct for intensity variations even when the user does not have explicit knowledge of the imperfections in the static or excitation fields. These techniques can be especially useful when field maps are not available (i.e., for previously acquired images). One promising technique is based on **bias field estimation**. This technique is used to estimate a map of intensity variations across space (i.e., the bias field) using the distorted image itself. Because the image reflects a combination of the true data (e.g., the actual number of protons or the real changes in blood oxygenation) and the distorting effects of the bias field, researchers must estimate the bias field by making assumptions about the properties of the noise and the smoothness of the signal. This determines the most likely pattern of distortions and thus recovers an estimate of the true data. An example of bias field correction is shown in Figure 8.23. Common methods rely on Markov random field models and their associated expectation-maximization algorithms to create a map of global and local signal gradients. While a detailed explanation of these methods is beyond the scope of this book, we refer interested readers to the Guillemaud and Brady reference listed at the end of the chapter.

bias field estimation A technique for estimating inhomogeneities in the magnetic field based on intensity variations in collected images.

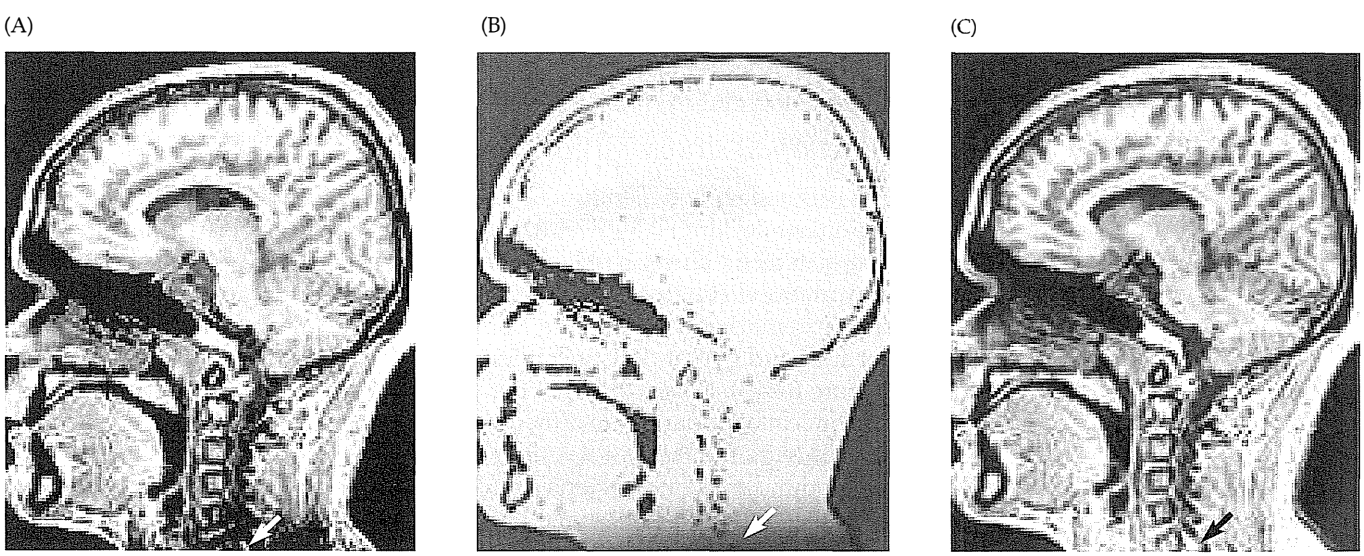

Figure 8.23 Bias field estimation and correction. There is a decrease in MR signal at the bottom (indicated by arrows) of this structural image (A). To correct for this signal loss, the relative intensity of the magnetic field is estimated (B), and a correction factor is applied to the original image. The low-signal region is corrected in the resulting image (C).

segmentation The process of partitioning an image into constituent parts, typically types of tissue (e.g., gray matter, white matter) or topographical divisions (e.g., different structural regions like Brodmann areas).

normalization The transformation of MRI data from an individual subject to match the spatial properties of a standardized image, such as an averaged brain derived from a sample of many individuals.

Bias field estimation and correction can substantially improve aspects of analysis that are dependent upon image uniformity. For segmentation algorithms to be accurate, different tissue types need to have similar values throughout the brain. Large bias field differences can cause discrepancies in gray/white contrast in different locations. Intensity values can be normalized throughout the brain by estimating and correcting for such inhomogeneities, thus improving the accuracy of segmentation.

Functional–Structural Coregistration and Normalization

The spatial and temporal corrections described in the previous sections ensure that each voxel contains data from a single brain region, as sampled at regular intervals throughout the time series. Such corrections are sufficient for analyses of the functional data from a single subject. Yet in most experiments, researchers want to understand how activation corresponds to the underlying neuroanatomy. Unfortunately, functional data typically are of low resolution and of little anatomical contrast, and they have geometric and intensity distortions, as we discussed above. Because of these limitations, we must often map our functional data onto high-resolution and high-contrast structural images. To facilitate this mapping, coregistration algorithms link the functional images to high-resolution structural images from the same subject.

Even if brain activity can be well localized within a subject through coregistration, there remains the problem of comparing activation between individuals, whether in the same study or in different studies. Some subjects have very large brains, while others have very small brains, and there is wide variation in shape, orientation, and gyral anatomy. For intersubject comparisons to be feasible, images of each subject's brain must be transformed so that they are the same size and shape as all of the others. This process is called normalization. Coregistration and normalization are important preprocessing steps for most fMRI studies, especially those that use voxel-based (i.e., not anatomical region-of-interest) analyses.

Functional–structural coregistration

The differences between functional and structural images of the same brain region are striking. A typical functional image appears as a relatively undifferentiated and blurry blob, with only the ventricles and the barest outlines of gray matter distinguishable (Figure 8.24A). High-resolution structural images appear remarkably detailed by comparison, with clear outlines of the different sulci and gyri and distinct boundaries between the gray and white matter (Figure 8.24B). This additional detail provides several advantages. Whereas anatomical boundaries are difficult, if not impossible, to identify on functional images (e.g., the Sylvian fissure is difficult to find in the functional image), such boundaries and regions of interest can be easily located on structural images. Because the size, shape, and sulcal patterns of the brain are much more distinct on structural images, it is beneficial to use information from structural images to guide the normalization of functional images. As mentioned above, the computational processes that map two types of images (e.g., functional and structural) on to each other are known as coregistration.

One may question the necessity of functional–structural coregistration, because both types of image are typically acquired in the same scanner ses-

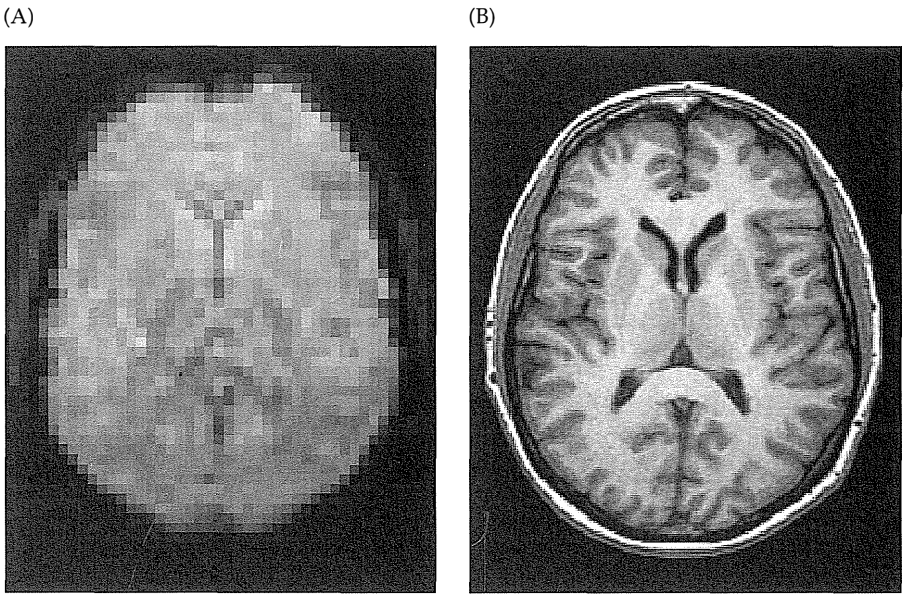

Figure 8.24 Comparison of functional and structural images. Functional (A) and structural (B) images have very different properties. Features that are readily visible on a structural image may be difficult to see or entirely absent on a lower-resolution, lower-contrast functional image of the same slice.

sion. Yet, in many cases the two types of image are acquired at different locations, either because different slices were wanted for each, or because the subject moved slightly between their acquisitions. A rigid-body transformation may be conducted for coregistration in which a cost function is minimized. However, because structural and functional images often have different, sometimes even opposite, contrasts, some cost functions, such as the sum of squared differences, are not appropriate. Cost functions based on mutual information, for example, can overcome this problem. Moreover, some pulse sequences used to acquire functional images may introduce subtle geometric distortions; for example, echo-planar functional images may be slightly stretched along one axis relative to a high-resolution structural image obtained from the same subject in the same session. If present, these distortions cannot be corrected by the six-parameter rigid-body transformation that we use for motion correction. If the distortion is linear, such that all voxels are similarly stretched along one or more axes, then a nine-parameter linear transformation can be used. In this transformation, three additional parameters are introduced to account for scaling differences along the x-, y-, or z-axes. If the distortion is more complex, with regions of greater and lesser stretching, then more-complex warping algorithms must be employed.

Spatial normalization

The human brain has remarkably variable morphology. The average adult brain is approximately 1300 cubic centimeters (cc) in volume, with values ranging from 1100 cc to 1500 cc (Figure 8.25). Thus, two subjects in the same fMRI experiment may differ in overall brain size by 30% or more. This difference is proportionally much smaller than the range in total body mass, which normally varies by about a factor of two or three in the adult population. There is also substantial variation in the shape of the adult human brain. For example, some people have brains that are longer and thinner than others. The differences may be especially pronounced in particular regions. The organization

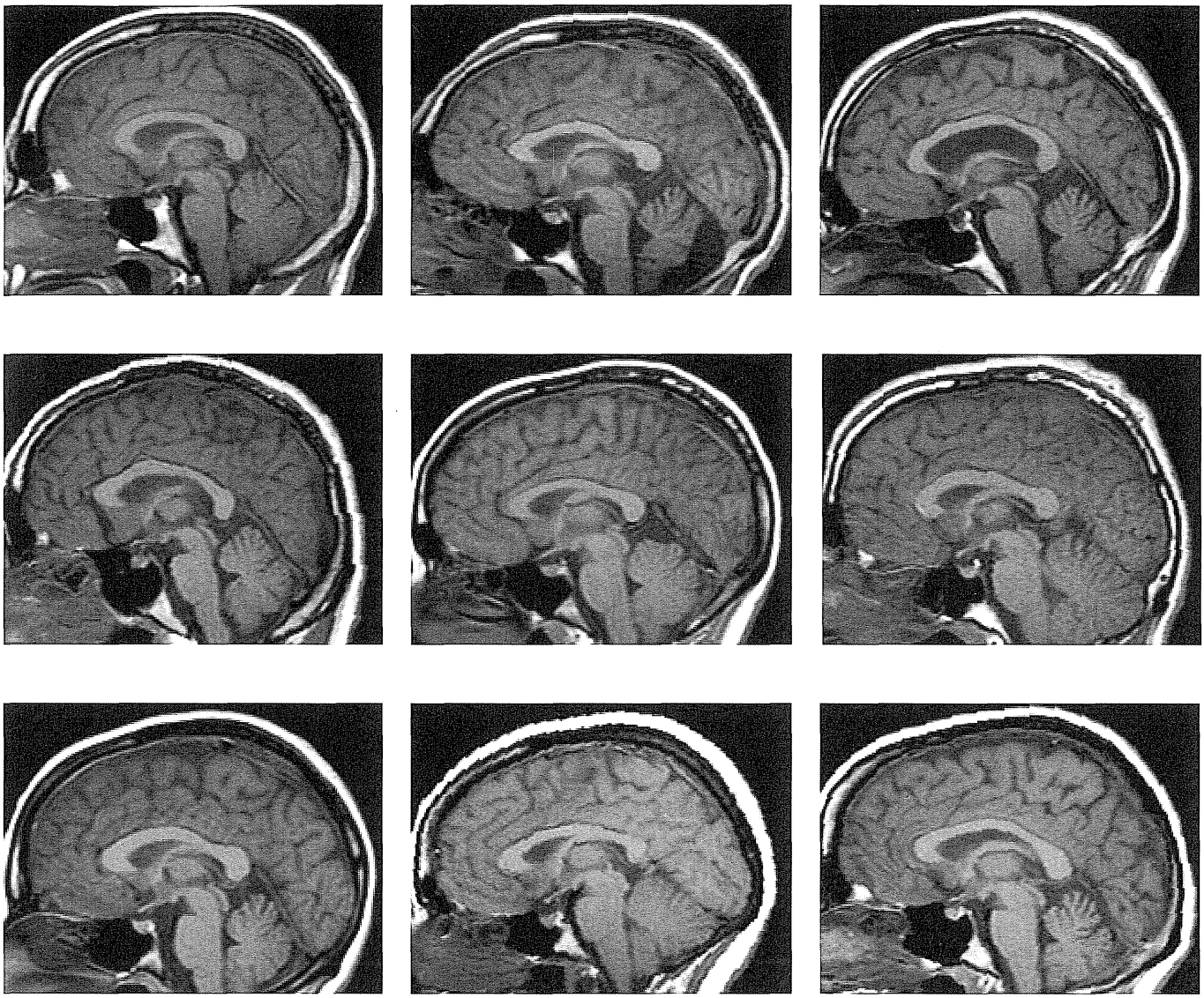

Figure 8.25 Examples of the variability in size and shape of the adult human brain. Each image provides a midsagittal view of the brain of a neurologically normal adult. Note the considerable variability in overall size, in relative height and width, and in the organization of internal structures. This variability poses problems for comparing areas of activation across subjects.

of gyri and sulci is sufficiently variable that even major landmarks, like the calcarine sulcus that divides the primary visual cortex, can have different positions and orientations in different individuals.

Normalization is a form of coregistration, except that here the image volumes to be compared differ in shape fundamentally rather than as a result of image distortion. The goal of normalization is to compensate for these shape differences by mathematically stretching, squeezing, and warping the images of each brain so that they are the same as those of every other brain. The concept of normalization should be familiar to anyone who has watched as computerized morphing programs transform one person's face into another's. Most

fMRI analysis packages include modules that normalize data into a common space. Although these programs are largely automated, researchers should always check the output of automated steps, as errors in normalization will propagate throughout the rest of the analyses.

Normalization of data within a study allows for the combination of data from different individuals. Furthermore, if data from two different studies have been normalized in the same fashion, then the areas of activity found in each study can be compared. For this reason, many journals encourage the reporting of experimental data as coordinates within a common normalization scheme, or stereotaxic space. The most widely used stereotaxic space is Talairach space, which was created by the French physician Jean Talairach and colleagues, and is based on a simple stereotaxic framework derived from measurements on a single brain, that of an elderly woman. The origin of the space is set at the midpoint of the anterior commissure, with the x- and y- axes defined by the horizontal plane connecting the anterior and posterior commissures (Figure 8.26). While the standardization provided by this framework has been extraordinarily important for neuroscience, the use of a single brain presents many problems, notably that the brain used was unrepresentative of the population at large. A better approach has come from recent attempts at creating probabilistic spaces using combined data from hundreds of individual scans. A commonly used-space was created by the researchers at the Montreal Neurological Institute, and was based on the anatomies of more than one hundred individuals. The template for MNI space has been scaled to match landmarks within the well-established Talairach atlas. Most normalization algorithms are based on such probabilistic templates. See the article by Chau and McIntosh in the Chapter References for an interesting comparison of these template spaces.

To warp a given brain to a template, normalization algorithms determine the overall size of the brain, as well as its gross anatomical features. Some algorithms also require the identification of key landmarks in the brain, such as major sulci; this may be done automatically, or require user input. Some researchers

stereotaxic space A precise mapping system (e.g., of the brain) using 3-D coordinates.

Talairach space A commonly used space for normalization of fMRI data; its coordinates are based on measurements from a single post-mortem human brain, as published in an atlas by Talairach and Tournoux.

MNI space A commonly used space for normalization of fMRI data; its coordinates are derived from an average of MRI structural images from more than one hundred individuals.

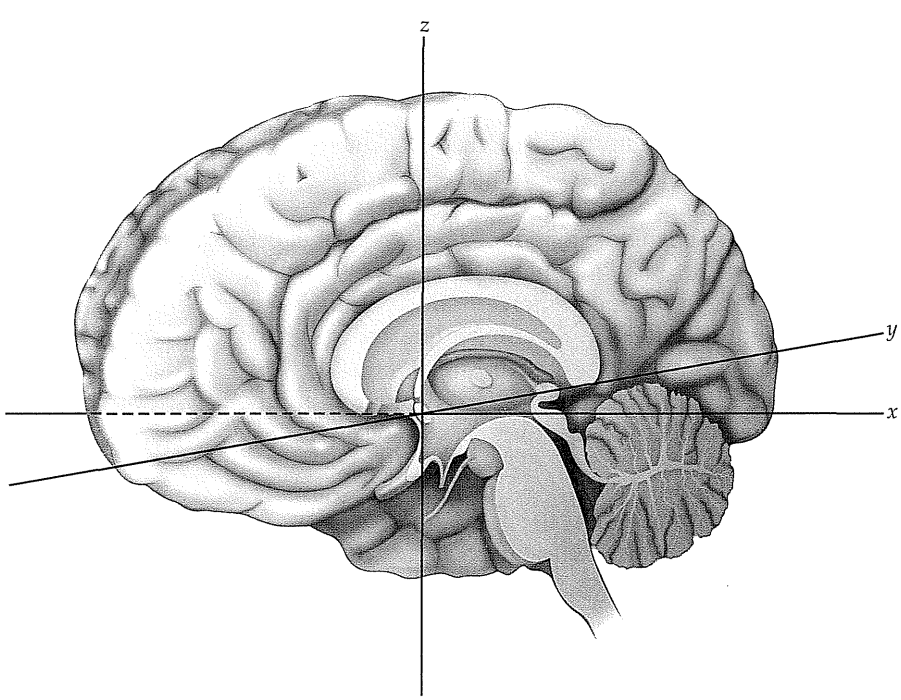

Figure 8.26 Typical coordinate axes for fMRI data. The most common axes for fMRI data define the x-axis as left to right and the y-axis by connecting the anterior and posterior commissures. The z-axis is perpendicular to the plane created by the other two lines.

cytoarchitecture The organization of the brain on the basis of cell structure.

filter Within the context of fMRI, an algorithm for removing temporal or spatial frequency components of data.

advocate surface-based normalization approaches. In these, the cerebral cortex, which is effectively just a large ~5 mm-thick sheet folded into a complex topography, is unfolded and blown up into a balloon shape. Surface-based approaches can have significant advantages in separating activations that are near to each other in volume space but not near each other in neural space (e.g., activation from voxels on opposite sides of a sulcus), especially if functional SNR is high.

Even if normalization algorithms were able to transform the images of two brains into the same stereotaxic framework, this would not mean that the brains would have activation in exactly the same voxels. Remember that normalization is based on gross morphological features of brains. These gross features do not necessarily indicate functional divisions between brain areas. More predictive of brain function are the regional cellular properties, or cytoarchitecture, which are usually not visible in MR images. Just as sulci and gyri are highly variable between individuals, so too are the boundaries between cytoarchitectonically distinct regions. For an example of the quantification of individual differences in the cytoarchitectonic organization of the human brain, see the work of Rajkowska and Goldman-Rakic in the Chapter References.

Normalization is a powerful technique that enables the testing of complex hypotheses with improved statistical power, and its positive impact on functional neuroimaging cannot be overstated. However, there are some caveats. Variability in brain features across individuals introduces theoretical constraints on normalization. Nearly all normalization approaches are based on subject samples drawn from the standard population of fMRI participants: young, typically college-age adults who are healthy and neurologically normal. Many other groups systematically differ from this population in the properties of their brains. The brains of elderly individuals may have atrophy, manifested as sulcal widening and enlarged ventricles. Young children may have differently-shaped brains, due to delayed maturation of some regions (e.g., the frontal cortex), and their images my have different contrast properties associated with reduced neuronal myelination. Male and female brains also differ in subtle ways. Thus, normalizing functional results between different subject groups may mask important group differences.

Variability in brain features across individuals also introduces practical constraints on normalization. Many patient groups have a specific local pathology associated with their disorder, while patients with tumors may have brains that are apparently normal in most regions but have severe distortions in the lesion area. Since most normalization approaches attempt to minimize the differences between the subject's brain and some template, abnormal features may reduce the accuracy of the matching process. Some normalization approaches have been developed for non-typical subject populations, but this remains an area of considerable interest. By its very nature, normalization emphasizes that which is common among individuals and de-emphasizes that which is unique. Small but meaningful variations among individuals' functional neuroanatomy may be lost through this process. Investigators interested in individual differences may wish to consider alternatives to normalization, such as subject-based region-of-interest analyses.

Temporal and Spatial Filtering

Filters are used to remove or retain different frequency components that are present in a composite signal. Filters can operate on 1-D temporal data, such as a voxel's time course of intensity changes, and on 2- or 3-D spatial data, such as adjacent voxels in a BOLD-contrast image volume. In neuroimaging, filters

are used to remove uninteresting variation in the data that can be safely attributed to noise sources, while preserving signals of interest. Thus, filtering can be used to increase functional SNR. Moreover, by reducing the dimensionality of the data, filters can reduce the problem of multiple statistical comparisons. In this section, we will explore both uses of filters in fMRI preprocessing.

Nyquist frequency The highest frequency that can be identified in a digitally sampled signal; it is defined as one-half of the sampling rate.

task frequency The rate of presentation of a periodic experimental task.

Temporal filtering

The use of temporal filters can substantially improve the quality of fMRI data by improving functional SNR. To describe how temporal filters work, we will begin by reintroducing the concept of the frequency spectrum of a signal. Consider a time series of data recorded from a single voxel, which describes the behavior of the voxel in the time domain. The same data can be converted, using a Fourier transform, to the frequency domain. The frequency range that is present in a sampled signal depends on its sampling rate, which is given by the TR for fMRI data. The maximum frequency that can be identified, or the Nyquist frequency, is equal to one-half of the sampling rate. For example, if the sampling rate is 0.5 Hz (TR of 2000 ms), any frequencies in the underlying signal higher than 0.25 Hz would not be present in the sampled data. Instead, power at those frequencies would be aliased, or artifactually present at other frequency values. Because of the Nyquist limitation, we must sample the brain at twice the rate of any phenomenon of interest.

Thought Question

Based on what you learned in earlier chapters, what disadvantages are there for collecting images at very high temporal resolution (short TR)?

In the example shown in Figure 8.27, there is considerable power at about 0.025 Hz, which approximately corresponds to the task frequency. These two

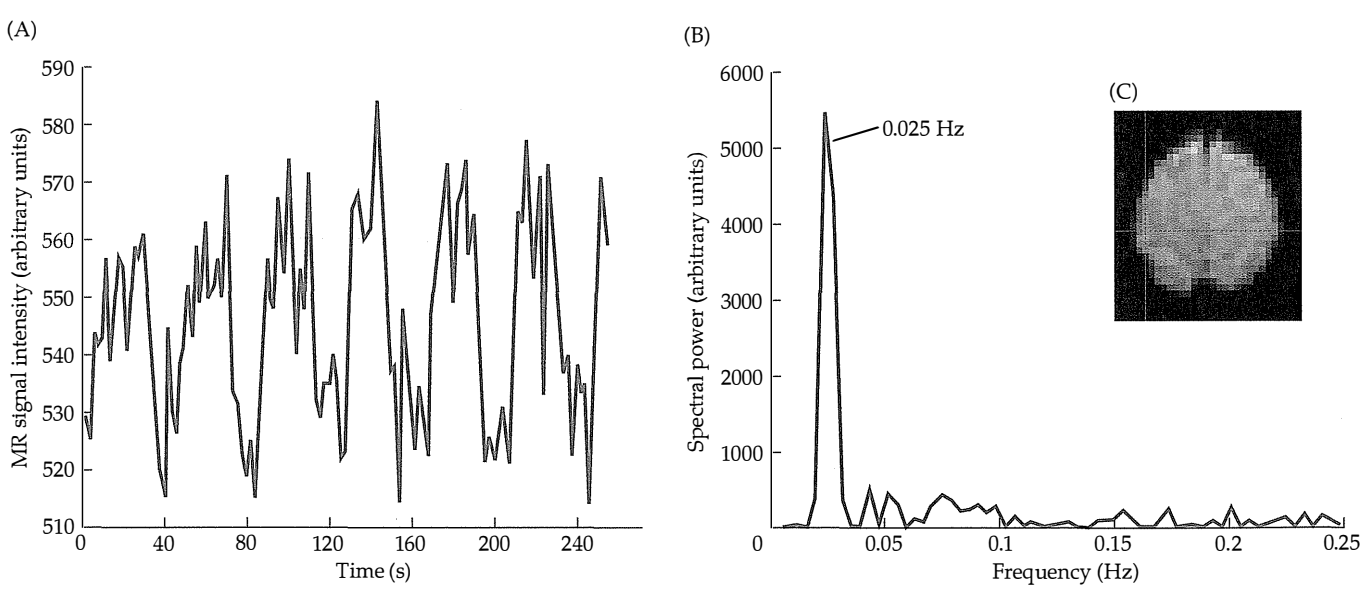

Figure 8.27 Comparison of the time and frequency domains for a single voxel. Shown are the raw time course (A) and power spectrum (B) from a single active voxel in the motor cortex (C). In this task, the subject alternated between squeezing his hands for 20 s and resting for 20 s. Visible in the power spectrum is the considerable power at the task frequency. (Note that the time course was normalized to a mean of zero before the power spectrum was calculated.)

graphs show exactly the same data, only transformed from one domain to another. In our analyses, we want to keep information about changes in the data that occur at the task frequency, but minimize changes in the data that occur at other frequencies. That is, we wish to reduce the contribution of noise from other frequency ranges. Suppose that we knew, based on physiological measurement that a subject breathed every 4 seconds (0.25 Hz), on average, during this run (see Figure 8.8 for an example). Since we are not interested in breathing, we would like to remove the effects of breathing from the data. But how? To reduce the influence of breathing, we construct a temporal filter that selectively attenuates frequencies around 0.25 Hz but leaves other frequencies essentially intact. This is called a band-stop filter, since it attenuates a range or band of frequencies. A low-pass filter leaves low frequencies intact while attenuating high frequencies, and a high-pass filter stops only low frequencies.

The choice of filter depends on what sort of variability should be eliminated. Typical heart rates during an fMRI experiment vary, but are often between 1.0 and 1.5 Hz. The rate of respiration is slower, about 0.2 to 0.3 Hz. For comparison, a typical experimental design might present alternating blocks of 12 s of task and 12 s of rest, for a total presentation rate of 0.04 Hz. A low-pass filter that excluded frequencies above 0.2 Hz could remove physiological oscillations without significantly reducing the ability to detect the task effect of interest. However, if the experiment used a fast event-related design in which stimuli were presented more rapidly (i.e., every few seconds), the task and respiration would be at similar frequencies, and such filtering would be extremely difficult. Changes of very low frequency are also observed in fMRI experiments, such as those related to scanner drift. These changes often take the form of near linear increases or decreases in absolute signal over the course of a several-minute experimental run. Such very slow changes can be extremely problematic for fMRI experiments, especially those using long-interval blocked designs. High-pass filtering of the data can remove slow drift-like trends. It is important to recognize that none of these factors, whether task, physiology, or drift, contributes to only a single frequency. For example, if the time course is not sufficiently well sampled, a high-frequency factor like heart rate could be aliased to a lower frequency, perhaps within the task range. All these factors provide energy at many frequencies, and as a result, temporal filtering should be done with caution.

An additional temporal consideration for fMRI analysis is the presence of temporal autocorrelation. That is, in all fMRI data series, the amplitude of the BOLD signal at past time points could be used to predict its amplitude at future time points. These regularities, if unaccounted for, can reduce the validity of the statistical models used for fMRI analyses. To minimize the effects of temporal autocorrelation, fMRI analysis packages use prewhitening algorithms that effectively eliminate that portion of the BOLD signal that is predicted by the previous time points. If successful, the residual signal (which can be used for fMRI analyses) becomes white noise, such that each time point is unrelated to its predecessors. This can greatly improve the ability to identify task-related signal changes. While prewhitening can be highly valuable for fMRI data, its effectiveness depends on the ability to accurately estimate the degree of autocorrelation, and researchers have developed multiple methods for this estimation. An alternative approach, precoloring, involves the introduction of specific autocorrelations into the dataset. Although precoloring is generally less effective than prewhitening, it can be more successful when the temporal autocorrelation cannot be well estimated.

prewhitening The application of filters to remove autocorrelations in a time series of data; in fMRI, prewhitening is typically applied before data analysis to remove task-unrelated noise.

precoloring The introduction of autocorrelations to a time series of data so that the time series will have known statistical properties; this is less commonly used than prewhitening in fMRI data analysis.

Spatial filtering

In many fMRI analyses, low-pass spatial filters are employed to reduce the high-frequency spatial components and "smooth" the images. The most common spatial smoothing technique is the introduction of a Gaussian filter. A Gaussian filter has the shape of a normal (or "bell-curve") distribution. When a Gaussian spatial filter is applied, it effectively spreads the intensity at each voxel in the image over nearby voxels. The width of the filter refers to the distance of its effect: a narrow filter spreads data over only a few voxels, while a wide filter spreads data over many voxels. Spatial filter width for fMRI data is generally expressed in millimeters at half of the maximum value (full-width-half-maximum, or FWHM).

What are the advantages of spatially filtering fMRI data? The foremost advantage can be understood in terms of the principle of matched filters, which indicates that using a filter of the same frequency as the signal of interest maximizes SNR. This is similar to the concept of the band-stop filter for temporal data described in the previous section. In fMRI images, the width of the signal of interest can be understood in a literal sense: the typical spatial extent of regions of activity. If there were no spatial correlation in fMRI data, so that one could not predict whether a voxel is active based on whether its neighbors are active, then spatial filtering would reduce SNR. However, all fMRI data have spatial correlation, due both to functional similarities between adjacent brain regions and to blurring introduced by the vascular system. The cerebral cortex itself has a depth of about 5 mm, so activation of even a single cortical column can result in two or three active voxels, depending on their size. Additional spatial correlation is introduced when comparing subjects. Because all subjects' brains differ in shape and size, and potentially in functional organization, areas of activation are rarely represented in exactly the same voxels. Instead, combining data from many subjects distributes activation across a range of voxels. By using a filter that matches the expected spatial correlation of the data, one can increase SNR considerably with a minimal loss of spatial resolution. These advantages of spatial smoothing may become more important as field strength increases. As discussed earlier in the chapter, at high field strengths (e.g., greater than 3.0 T) most noise is physiological rather than thermal. Recent research using a 7.0-T scanner suggests that collecting high-resolution data and then smoothing to a desired lower resolution improves functional SNR, compared with collecting data at the lower resolution directly.

A second advantage of spatial filtering lies in improving the validity of statistical techniques. During the analysis of any fMRI dataset, there will be an enormous number of statistical tests. In a typical functional imaging volume, there may be more than 100,000 voxels, each of which is evaluated for significant differences in signal. If the threshold for significance is set at $\alpha < 0.05$, as is frequently done for psychological or medical experiments, then there should be more than 5000 voxels that show significance due to chance alone. This is known as the multiple comparison problem, and is discussed in detail in Chapter 10. But if the data are spatially correlated, then there may be many fewer local maxima that exhibit significant activation (Figure 8.28). In addition to its effects on false-positive rates, smoothing provides the additional benefit of improving the validity of experimental tests by making parameter errors more normal. Any derived parameter, such as the significance value measured at a single voxel, can be considered to be a combination of its true value along with some error. Many common statistical tests assume that error in measurement is normally distributed. Smoothing increases the normality

spatial smoothing The blurring of fMRI data across adjacent voxels to improve the validity of statistical testing and maximize functional SNR, at a cost of spatial resolution.

matched filters The principle that a filter of the same frequency as the signal of interest provides the maximal signal-to-noise ratio.

multiple comparison problem The increase in the number of false-positive results (i.e., Type I errors) with increasing number of statistical tests. It is of particular consequence for voxel-wise fMRI analyses, which may have many thousands of statistical tests.

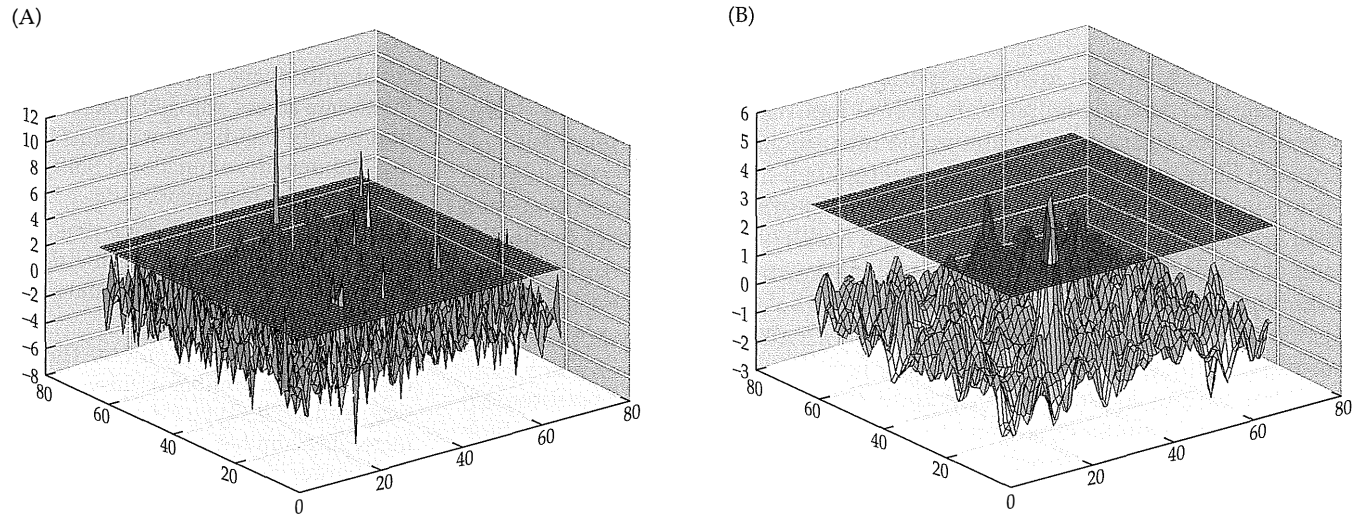

Figure 8.28 Reduction of false-positive rate by spatial smoothing. Shown in these graphs is signal intensity (on the vertical axis) for each of 64 by 64 voxels in a randomly generated dataset. For this simulation, we added an active region that was 4 by 3 voxels in size. Since there are approximately 4000 voxels in this dataset, a very large number may pass a threshold for significance (e.g., alpha of 0.01), as shown in (A). Spatial smoothing will average data over adjacent voxels, reducing the likelihood that a cluster of voxels will pass the same threshold. As shown in (B), only the active cluster passes the significance threshold after smoothing (note the difference in the *z*-axis scale between the graphs).

of data, because averaging of multiple observations tends toward the normal distribution, regardless of the properties of the individual observations (i.e., due to the Central Limit Theorem). Therefore, smoothing can have a positive effect on fMRI statistical analyses.

These advantages of spatial filtering can be particularly valuable for areas of the brain with low functional SNR. Parrish and colleagues conducted a set of simulations to determine the approximate SNR values needed to detect a BOLD signal change of a given amplitude, and to see how detection power changes with spatial filtering. They then applied those calculations to an fMRI time series measured for a clinical patient with a vascular malformation near the boundary between the parietal and occipital lobes. Then they repeated their analysis using a 6-mm Gaussian filter. Detection power increased considerably throughout the brain. Where before there was reduced functional SNR near the malformation and the inferior frontal lobe, now there was sufficient power to detect a response through nearly all of the brain. Note that spatial filtering provides an increase in SNR at a cost of reduced spatial resolution.

The primary disadvantages of spatial filtering result from the imperfect match between filter width and activation extent. If the filter used is too large, then meaningful activations could be attenuated below the threshold for significance. This is especially problematic when targeting very small brain regions, such as structures within the midbrain, where only a single voxel may be significantly active. If the filter used is too small, then it will have little positive effect on SNR, while reducing spatial resolution. Typical filter widths for fMRI are about 6 to 10 mm FWHM (i.e., about two to three voxels), although greater or lesser smoothing may be needed, depending on the noise level of the data. It is important to emphasize that spatial smoothing is beneficial for voxel-wise

analyses but has little effect on region-of-interest (ROI) analyses (see Chapter 10). In ROI approaches, the experimenter constructs bounded functional regions for subsequent analysis. The edges of these regions are considered to be meaningful, so their blurring may introduce unwanted variability into the data.

Summary

The core challenge of fMRI analyses is the detection of relatively small task-related variability, or signal, within large non-task-related variability, or noise. Three quantities are important: raw signal-to-noise ratio (raw SNR), contrast-to-noise ratio (CNR), and functional signal-to-noise ratio (functional SNR). Raw SNR depends on the magnitude of signal measured by the scanner compared with thermal noise. CNR depends on the intensity difference between two tissues of interest compared with the variability in intensity within one tissue. Functional SNR determines our ability to detect signal changes associated with experimental effects of interest, and is critical for many aspects of fMRI. While raw SNR scales linearly with the strength of the magnetic field, functional SNR scales less than linearly with field strength due to several sources of noise. Thermal and system variability in scanner hardware contribute to all types of MRI imaging but are much less important than physiological variability for fMRI, especially at high field strengths.

The steps used for minimizing the contributions of non-task-related variability are collectively known as preprocessing. Initial quality assurance tests are important for preventing and diagnosing data problems. Temporal and spatial preprocessing steps correct for variability due to differences in the timing of slice acquisition and in the spatial position of voxels, respectively. The most insidious cause of spatial error is head motion, which can introduce severe artifacts into the analyses, if not prevented or corrected. Spatial errors resulting from inhomogeneities in the static magnetic field or radiofrequency coil can be corrected through mapping or estimation of the resulting distortion field. To improve spatial localization of activity, images may be transformed both by functional–structural coregistration and by normalization. Functional MRI coregistration matches functional data to higher-resolution structural images, enabling the better anatomical localization of activity within a subject. Normalization mathematically warps subjects' brains to a standard stereotaxic framework, allowing for better comparisons between individuals within a study, as well as allowing the reporting of data derived from common coordinates, for comparisons between studies. Functional resolution can be improved by the judicious use of temporal and spatial filtering. Temporal filtering can remove selected noise components, such as those introduced by physiological processes, and can correct for low-frequency scanner drift. Spatial filtering can increase functional SNR, reduce apparent noise, and increase the validity of comparisons between subjects. However, improperly applied filters can significantly reduce the quality of the data.

REFER TO THE
fMRI
COMPANION WEBSITE AT
www.sinauer.com/fmri2e
for study questions and Web links.

Suggested Readings

Jezzard, P., Matthews, P. M., and Smith, S. M. (eds.) (2003). *Functional MRI: An Introduction to Methods.* Oxford University Press, Oxford. *A wide-ranging book that contains several chapters on preprocessing steps in fMRI.*

*Kruger, G., and Glover, G. H. (2001). Physiological noise in oxygenation-sensitive

magnetic resonance imaging. *Magn. Reson. Med.*, 46: 631–637. *Provides a clear description of different components of physiological noise.*

*Ress, D., Glover, G. H., Liu, J., and Wandell, B. (2007). Laminar profiles of functional activity in the human brain. *NeuroImage*, 34: 74–84. *An impressive demonstration of differences in BOLD responsivity as a function of the depth from the cortical surface, which corresponds to different layers of neurons.*

*Smith, S. M., Beckmann, C. F., Ramnani, N., Woolrich, M. W., Bannister, P. R., Jenkinson, M., Matthews, P. M., and McGonigle, D. J. (2005). Variability in fMRI: a re-examination of inter-session differences. *Human Brain Mapping*, 24: 248–257. *An interesting reanalysis of an earlier study that clarifies the relative magnitude of intra- and inter-subject variability in fMRI experiments.*

*Talairach, J., and Tournoux, P. (1988). *Co-Planar Stereotaxic Atlas of the Human Brain.* Thieme, New York. *This atlas has become extraordinarily influential as a reference for brain anatomy and function.*

*Indicates a reference that is a suggested reading in the field and is also cited in this chapter.

Chapter References

Aguirre, G. K., Zarahn, E., and D'Esposito, M. (1998). The variability of human, BOLD hemodynamic responses. *NeuroImage*, 8: 360–369.

Ashburner, J., and Friston, K. (1997). Multimodal image coregistration and partitioning—a unified framework. *NeuroImage*, 6(3): 209–217.

Blamire, A. M., Ogawa, S., Ugurbil, K., Rothman, D., McCarthy, G., Ellermann, J. M., Hyder, F., Rattner, Z., and Shulman, R. G. (1992). Dynamic mapping of the human visual cortext by high-speed magnetic resonance imaging. *Proc. Natl. Acad. Sci. U.S.A.*, 89(22): 11069–11073.

Bodurka, J., Ye, F., Petridou, N., Murphy, K., and Bandettini, P. A. (2007). Mapping the MRI voxel volume in which thermal noise matches physiological noise—implications for fMRI. *NeuroImage*, 34: 542–549.

Buxton, R. B. (2002). *Introduction to Functional Magnetic Resonance Imaging: Principles and Techniques.* Cambridge University Press, New York.

Chau, W., and McIntosh, A. R. (2005). The Talairach coordinate of a point in the MNI space: how to interpret it. *NeuroImage*, 25: 408–416.

Della-Maggiore, V., and Chau, W. (2002). An empirical comparison of SPM preprocessing parameters to the analysis of fMRI data. *NeuroImage*, 17(1): 19–28.

Edelstein, W. A., Glover, G. H., Hardy, C. J., and Redington, R. W. (1986). The intrinsic signal-to-noise ratio in NMR imaging. *Magn. Reson. Med.*, 3: 604–618.

Freire, L., and Mangin, J. F. (2001). Motion correction algorithms may create spurious brain activations in the absence of subject motion. *NeuroImage*, 14: 709–722.

Gati, J. S., Menon, R. S., Ugurbil, K., and Rutt, B. K. (1997). Experimental determination of the BOLD field strength dependence in vessels and tissue. *Magn. Reson. Med.*, 38: 296–302.

Guillemaud, R., and Brady, M. (1997). Estimating the bias field of MR images. *IEEE Trans. Med. Imaging*, 16(3): 238–251.

Handwerker, D. A., Ollinger, J. M., and D'Esposito, M. (2004). Variation of BOLD hemodynamic responses across subjects and brain regions and their effects on statistical analyses. *NeuroImage*, 21: 1639–1651.

Hu, X., Le, T. H., Parrish, T., and Erhard, P. (1995). Retrospective estimation and correction of physiological fluctuation in functional MRI. *Magn. Reson. Med.*, 34: 201–212.

Johnstone, T., Ores Walsh, K. S., Greischar, L. L., Alexander, A. L., Fox, A. S., Davidson, R. J., and Oakes, T. R. (2006). Motion correction and the use of motion covariates in multiple-subject fMRI analysis. *Hum. Brain Mapp.*, 27: 779–788.

Krasnow, B., Tamm, L., Greicius, M. D., Yang, T. T., Glover, G. H., Reiss, A. L., and Menon, V. (2003). Comparison of fMRI activation at 3 and 1.5 T during perceptual, cognitive, and affective processing. *NeuroImage*, 18: 813–826.

Kruger, G., Kastrup, A., and Glover, G. H. (2001). Neuroimaging at 1.5 T and 3.0 T: Comparison of oxygenation-sensitive magnetic resonance imaging. *Magn. Reson. Med.*, 45: 595–604.

Kwong, K. K., Belliveau, J. W., Chesler, D. A., Goldberg, I. E., Weisskoff, R. M., Poncelete, B. P., Kennedy, D. N., Hoppel, B. E., Cohen, M. S., Turner, R., et al. (1992). Dynamic magnetic resonance imaging of human brain activity during primary sensory stimulation. *Proc. Natl. Acad. Sci. U.S.A.*, 89(12): 5675–5679.

McGonigle, D. J., Howseman, A. M., Athwal, B. S., Friston, K. J., Frackowiak, R. S., and Holmes, A. P. (2000). Variability in fMRI: An examination of intersession differences. *NeuroImage*, 11: 708–734.

Miller, M. B., Van Horn, J. D., Wolford, G. L., Handy, T. C., Valsangkar-Smyth, M., Inati, S., Grafton, S., and Gazzaniga, M. S. (2002). Extensive individual differences in brain activations associated with episodic retrieval are reliable over time. *J. Cogn Neurosci.* 14: 1200–1214.

Oakes, T. R., Johnstone, T., Ores Walsh, K. S., Greischar, L. L., Alexander, A. L., Fox, A. S., and Davidson, R. J. (2005). Comparison of fMRI motion correction software tools. *NeuroImage.* 28: 529–543.

Ogawa, S., Kim, S.-G., Ugurbil, K., and Menon, R. S. (1998). On the characteristics of fMRI in the brain. *Ann. Rev. Biophys. Biomol. Struct.*, 27: 447–474.

Ogawa, S., Menon, R. S., Tank, D. W., Kim, S.-G., Merkle, H., Ellerman, J. M., and Ugurbil, K. (1993). Functional brain mapping by blood oxygenation level-dependent contrast magnetic resonance imaging. A comparison of signal characteristics with a biophysical model. *Biophys. J.*, 64: 803–812.

Parrish, T. B., Gitelman, D. R., LaBar, K. S., and Mesulam, M. M. (2000). Impact of signal-to-noise on functional MRI. *Magn. Reson. Med.*, 44: 925–932.

Peters, A. M., Brookes, M. J., Hoogenraad, F. G., Gowland, P. A., Francis, S. T., Morris, P. G., and Bowtell, R. (2007). T_2* measurements in human brain at 1.5, 3 and 7 T. *J. Magn. Reson. Imaging*, 25: 748–753.

Raj, D., Anderson, A. W., and Gore, J. C. (2001). Respiratory effects in human functional magnetic resonance imaging due to bulk susceptibility changes. *Phys. Med. Biol.*, 46: 3331–3340.

Rajkowska, G., and Goldman-Rakic, P. S. (1995). Cytoarchitectonic definition of prefrontal areas in the normal human cortex: II. Variability in locations of areas 9 and 46 and relationship to the Talairach Coordinate System. *Cereb. Cortex*, 5: 323–337.

Savoy, R. L. (2005). Experimental design in brain activation MRI: cautionary tales. *Brain Res. Bull.* 67: 361–367.

Saad, Z. S., Ropella, K. M., DeYoe, E. A., and Bandettini, P. A. (2003). The spatial extent of the BOLD response. *NeuroImage*, 19: 132–144.

Thomason, M. E., Foland, L. C., and Glover, G. H. (2007). Calibration of BOLD fMRI using breath holding reduces group variance during a cognitive task. *Hum. Brain Mapp.*, 28: 59–68.

Triantafyllou, C., Hoge, R. D., and Wald, L. L. (2006). Effect of spatial smoothing on physiological noise in high-resolution fMRI. *NeuroImage*, 32: 551–557.

Turner, R., Jezzard, P., Wen, H., Kwong, K. K., Le Bihan, D., Zeffiro, T., and Balaban, R. S. (1993). Functional mapping of the human visual cortex at 4 and 1.5 Tesla using deoxygenation contrast EPI. *Magn. Reson. Med.*, 29: 277–279.

Wang, J., Alsop, D. C., Li, L., Listerud, J., Gonzalez-At, J. B., Schnall, M. D., and Detre, J. A. (2002). Comparison of quantitative perfusion imaging using arterial spin labeling at 1.5 and 4.0 Tesla. *Magn. Reson. Med.*, 48: 242–254.

Yacoub, E., Shmuel, A., Logothetis, N., and Ugurbil, K. (2007). Robust detection of ocular dominance columns in humans using Hahn Spin Echo BOLD functional MRI at 7 Tesla. *NeuroImage*, 37: 1161–1177.

Yang, Y., Wen, H., Mattay, V. S., Balaban, R. S., Frank, J. A., and Duyn, J. H. (1999). Comparison of 3D BOLD functional MRI with spiral acquisition at 1.5 and 4.0 T. *NeuroImage*, 9: 446–451.

Chapter 9

Experimental Design

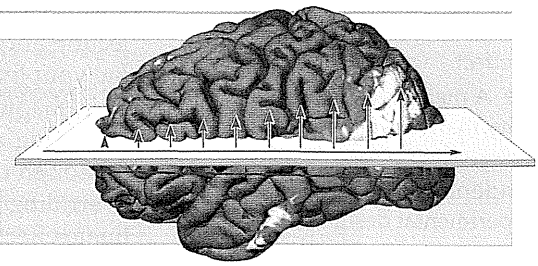

All scientific research begins with a question. For cognitive neuroscience research, that question may be as broad as "In what brain regions is increased activation associated with successful retrieval from memory?" or as focused as "Does the functional connectivity between the frontopolar and anterior temporal cortices modulate the retrieval of an autobiographical memory?" From the experimental question, a researcher derives a research hypothesis, which is a statement about how a given manipulation should change some measurement. Hypotheses, like research questions, may be very general or very specific. An example of a general hypothesis in fMRI research would be the statement "Activation in the frontal cortex will be reduced in depressed individuals." More specific hypotheses link fMRI data to other measurements; for example, "The activation in the middle frontal gyrus evoked by an n-back working memory task will decline proportionally to the degree of depression as measured by the Beck Depression Inventory." The key characteristic of a hypothesis is that it is falsifiable, that is, an experiment could be conducted that could disprove it. More specific hypotheses can be tested more easily and are thus more informative.

To test a hypothesis, a scientist designs an experiment. Experiments, in the technical sense of the word, first manipulate some aspect of the world and then measure the outcome of that manipulation. The canonical example of an experiment is Galileo's test of the effect of mass on acceleration due to gravity. Galileo speculated that an object's acceleration due to gravity does not depend on its mass. To test this hypothesis, he dropped two balls of different mass from a great height and found that they fell at the same rate. In this experiment, Galileo manipulated the mass of the objects being dropped and measured the relative time needed for them to fall a given distance. In modern fMRI experiments, scientists often manipulate some aspect of a stimulus, such as whether a picture is of a face or an object, or whether a word is easy or difficult to remember, and then measure the change in BOLD signal within the brain. The way in which a scientist sets up the manipulations and measurements in an experiment is known as experimental design.

All well-designed experiments share several characteristics: they test specific hypotheses, they rule out alternative explanations for the data, and they

functional connectivity A pattern of functional relationships among regions, inferred from common changes in activation over time, that may reflect direct or indirect links between those regions.

research hypothesis A proposition about the nature of the world that makes predictions about the results of an experiment. For a hypothesis to be well formed, there must be some experiment whose outcome could prove it to be false.

experiment The controlled test of a hypothesis. Experiments manipulate one or more independent variables, measure one or more dependent variables, and evaluate those measurements using tests of statistical significance.

experimental design The organization of an experiment to allow effective testing of the research hypothesis.

efficiency The power of an experimental design to test a research hypothesis. Highly efficient designs can reject the null hypothesis even when the experimental manipulation has only a small effect.

variable A measured or manipulated quantity that varies within an experiment.

independent variables (IVs) Aspects of the experimental design that are intentionally manipulated by the experimenter and that are hypothesized to cause changes in the dependent variables.

conditions (or levels) Different values of the independent variable(s).

dependent variables (DVs) Quantities that are measured by the experimenter in order to evaluate the effects of the independent variables.

minimize the cost of running the experiment. Advance planning to ensure good experimental design is especially important for fMRI experiments, given the significant resources they require in direct scanner costs and in the time spent by the experimenters, research assistants, and/or technologists in collecting and analyzing the data. If your experiment is inadequate for answering your hypotheses, all of that investment in time and money may be wasted. This chapter discusses the basic principles of experimental design for fMRI, returning at the end to a comprehensive discussion of design efficiency. Although designs differ in their advantages and disadvantages, there is one overriding principle: the best experimental design is the one that lets you investigate effectively *your* particular research question.

Basic Principles of Experimental Design

The fundamental element of an experiment is the variable, of which there are two types. Independent variables (IVs) are aspects of the experimental design that are manipulated by the researcher. The choice of IV depends on the hypothesis to be tested. In Galileo's experiment, the IV was mass, and there were two levels of mass (light and heavy). Different types of fMRI studies use different IVs. In a study of visual perception, one could use the variable *stimulus category* by showing subjects different types of objects (e.g., faces, houses, tools). A study of attention might manipulate whether or not subjects pay attention to a given object, so that one condition could be *attended* and the other *unattended.* And in a study of long-term memory, one could train subjects using a list of words one week before putting them in the scanner, and then compare *remembered* words with *novel* words that were not previously learned. The different values of an IV are often called conditions or levels.

Dependent variables (DVs) reflect the data measured by the experimenter. Different dependent variables provide different evidence for or against a hypothesis. Galileo compared how rapidly two objects fell; his dependent variable was relative time. Most fMRI studies use BOLD signal change as the primary dependent variable, although a few studies use other measures, as described in Chapter 12. It is important to recognize that a single hypothesis can be evaluated using multiple dependent variables. For example, a common experiment in physics teaching laboratories is to repeat Galileo's experiment while taking photographs of the falling objects at regular time intervals using a strobe-light system, as shown in Figure 9.1. The photographs provide information about the dependent variable, distance, from which velocity can be calculated. Analogously, a single hypothesis about the brain could be tested using fMRI, event-related potentials (ERP), magnetoencephalography (MEG), or lesion studies. Different neuroscience techniques provide different dependent measures, which can together provide converging evidence for a hypothesis.

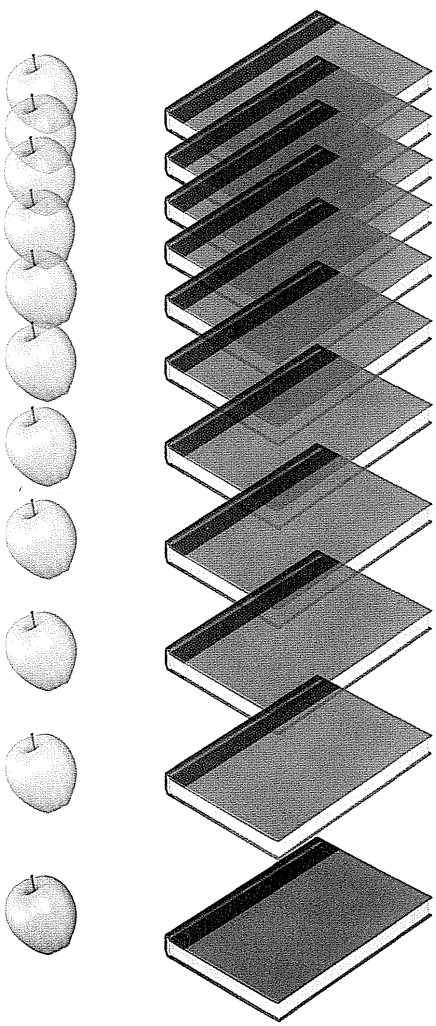

Figure 9.1 A simple experiment. By dropping two objects of different masses and photographing their positions at multiple time points, an experimenter can verify that the independent variable, mass, has no effect on the dependent variable, distance traveled over time.

categorical variable A variable that can take one of several discrete values.

Thought Question

The idea of converging evidence is a very important one in science. Why does the collection of data using different techniques (and thus different dependent variables) improve our ability to test research hypotheses?

Note that behavioral measures like response time and error rate can be considered as either DVs or IVs, depending on the context. In a psychological experiment, researchers collect behavioral data in order to examine the effects of the experimental manipulations, for example, when examining whether attention (IV) decreases response time (DV). However, if one is interested in the effects of errors (IV) on BOLD signal (DV), the behavioral data may become the manipulated factor. In the remainder of this text, we will define independent variables as those aspects of the experiment that serve as factors in an analysis, and dependent variables as those aspects that serve as data for the analysis.

Experimental variables, whether independent or dependent, may be categorical or continuous. A **categorical variable** can have one of a number of discrete values (Figure 9.2A). For example, if you want to map the hand regions of the motor cortex, you may set up an experiment in which the subject squeezes with either the left hand or the right hand. The IV in this experiment is *hand*, which obviously has only two values. But imagine that you are interested in measuring how activation in the motor cortex (DV) changes with the

(A) (B) (C)

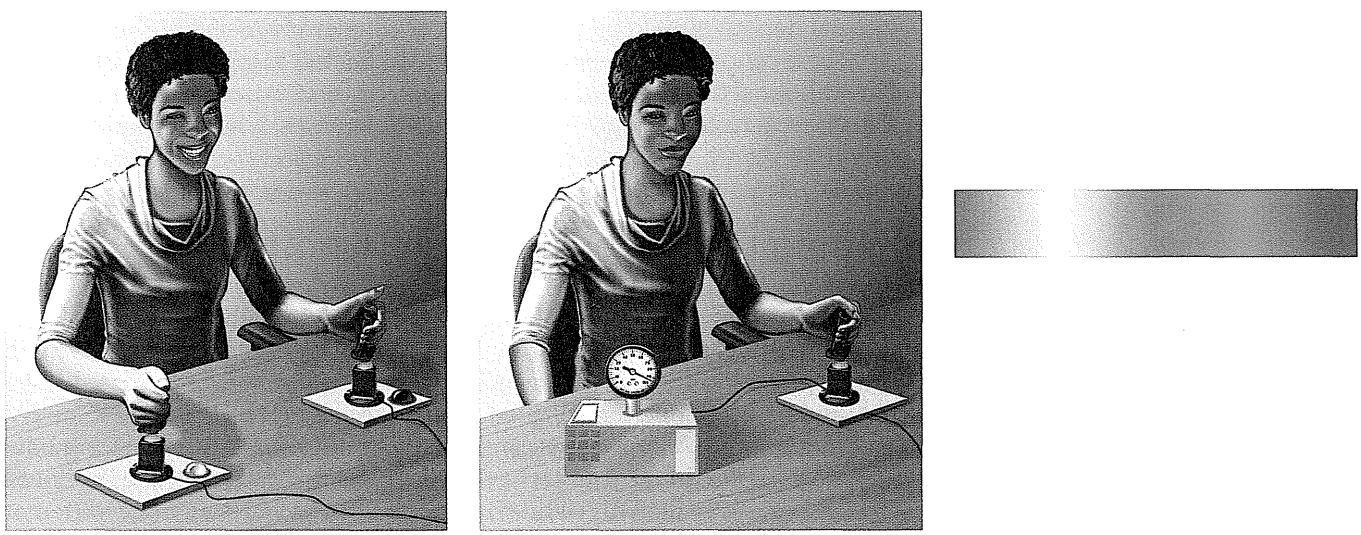

Figure 9.2 Categorical versus continuous variables. (A) A categorical variable is one that can take two or more discrete values. Thus, whether the subject squeezes her left hand or right hand is a categorical variable. (B) A continuous variable can take any of an infinite number of values, limited only by the precision of the measurement. How much force the subject exerts when squeezing her hand could be measured as a continuous variable. (C) Some continuous variables can be converted into categorical variables. Color, for example, is a continuous variable since it results from the frequency of visible light, which can take any of a range of values. However, we have names for discrete color categories in the continuous spectrum.

continuous variable A variable that can take any value within a range.

between-subjects A manipulation in which different conditions are assigned to different subject groups.

within-subjects A manipulation in which each subject participates in all experimental conditions.

pressure of squeezing (IV). Subjects could squeeze a sensor that measures how much force is exerted. In this experiment, force would be a continuous variable, because it could take any value within a range (Figure 9.2B). Categorical independent variables have been more commonly used in fMRI experiments, as they allow the use of treatment/control analyses, which are described in the next section. However, using continuous variables can in principle be much more powerful, and some experimental questions require them. Sometimes fMRI researchers discretize (i.e., convert from continuous to discrete) a continuous variable into a limited number of categories (Figure 9.2C), such as when classifying response times, usually measured in milliseconds, into the categories of "fast" or "slow." Changing continuous measures into categorical variables simplifies many types of analyses, but at the cost of eliminating a potentially important source of variability in the data. As fMRI analyses have grown more sophisticated (see the following two chapters), the use of continuous variables has become increasingly prevalent.

An important distinction can also be made between two types of manipulations. In a between-subjects manipulation, different subject groups reflect different values of the IV. Note that the group difference may be some intrinsic qualifier, like males versus females or drug abusers versus abstainers, or it may be assigned by an experimental manipulation. In fMRI studies, between-subjects experiments are most common in examinations of the effects of a drug or disease state. To study the effects of schizophrenia on executive processing in the frontal lobe, a researcher could run two groups of subjects, one with the disorder and one without. Designs that have different groups of subjects do different tasks are used less commonly, because differences in the groups' characteristics such as in age, gender, or education, could confound the results. For this reason, most fMRI studies use within-subjects manipulations, where each subject participates in all experimental conditions. As a rule of thumb, experimental designs should be within-subjects whenever possible.

These concepts apply not just to fMRI studies but to any research program. For additional discussion of the general principles of experimental design, we refer the interested student to the Chapter References, where several comprehensive texts are listed.

Setting Up a Good Research Hypothesis

Underlying any experimental design is a research hypothesis, which has the following basic structure: "Manipulating the independent variable (IV) will cause changes in the measurement (DV)." The hypothesis is validated if we manipulate the IV and the DV changes as expected, but it is falsified if the DV does not change. A hypothesis can be made more precise by specifying how IVs and DVs should relate to each other. For instance, "*Increasing* the IV should cause a *decrease* in the DV." While hypotheses can be stated in many different ways, they all have this same underlying structure of cause and effect.

In fMRI studies, there are three distinct levels of research hypotheses, representing three different types of questions that can be asked (Figure 9.3). At the most specific level are hypotheses about *hemodynamic* activation in the brain. Such hypotheses reflect questions about the BOLD effect itself, without making inferences about its causes. Many of the studies of refractory effects discussed in Chapter 7 fall into this category, such as the 2002 study by Birn and colleagues that investigated changes in the linearity of the hemodynamic response in different brain regions. A second class of hypotheses addresses

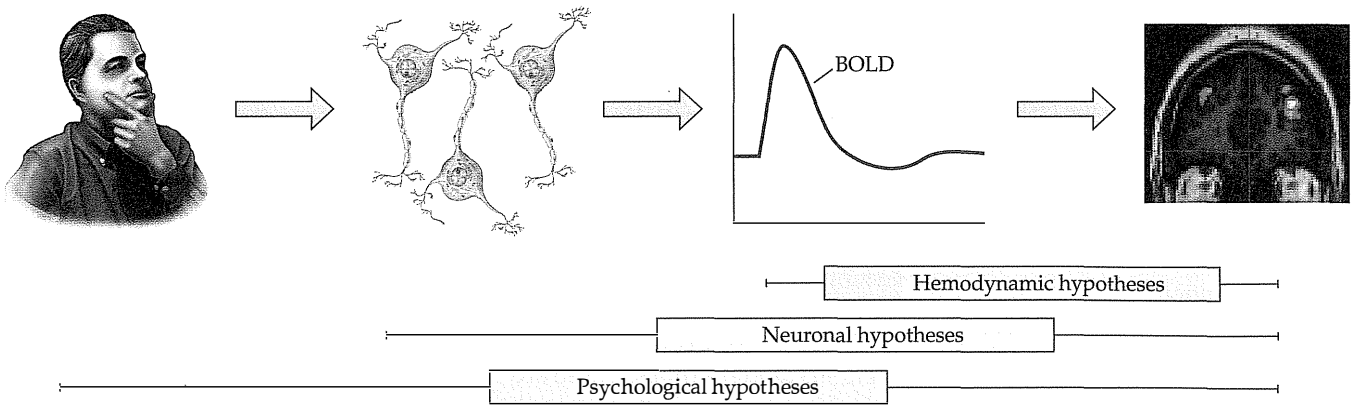

Figure 9.3 Constructing research hypotheses. Hypotheses are statements about the relationships between independent and dependent variables. For fMRI experiments, there are three types of research hypotheses. The most basic are hemodynamic hypotheses, statements about hemodynamic activation measured by fMRI. More complex are neuronal hypotheses, which make claims about how underlying neuronal activity should affect fMRI data. Finally, psychological hypotheses attempt to relate some aspect of cognition to observed fMRI results. Psychological hypotheses are the most challenging to construct, but they can have the greatest influence on the study of the brain.

questions about *neuronal* activity. Since fMRI does not measure neuronal activity directly, researchers must estimate that activity by transforming the measured BOLD signal. An example of a neuronal hypothesis for fMRI would be: "Neuronal activity within the superior temporal sulcus increases when viewing a video of a walking person." Note that although the fMRI measurement is still the BOLD signal, the manipulation is restricted to a specific class of stimuli and the inference relates to the neuronal activity itself. The third type of fMRI hypothesis is the *psychological* hypothesis. We can use fMRI to answer questions about psychological processes like attention, memory, or perception. One important hypothesis that has been studied using fMRI is: "Encoding of items into memory and retrieval of items from memory are associated with activation in different hemispheres." Note that this hypothesis relies on very general concepts (encoding and retrieval) that are not uniquely defined. Researchers can (and do) disagree over what those terms mean.

Psychological hypotheses can be the most difficult to construct, but they are often the most influential. Consider a hypothesis about the organization of the visual system that was advanced by Ungerleider and Mishkin in 1982. They suggested that visual information might be processed in two distinct pathways, a ventral occipitotemporal pathway that processes object features ("what") and a dorsal occipitoparietal pathway that processes spatial properties ("where"). From this simple statement have come literally hundreds of neuroimaging and electrophysiological studies, along with extensions of the initial hypothesis to include dorsal and ventral divisions in the frontal lobe and even debates over exactly what sorts of spatial/object information are represented. This particular hypothesis has become sufficiently well supported that it forms the basis of a **theory**, a generalizable set of rules that shapes thinking on a topic, in this case the visual system. It is important to recognize that this influential idea began with a simple and falsifiable hypothesis. Psychological hypotheses are limited by how well we can define the concepts of inter-

theory An organized set of ideas that guides thinking on a topic and that can be used to generate a variety of experimental hypotheses.

experimental condition A condition that contains the stimulus or task that is most relevant to the research hypothesis. Also called the task condition.

control condition A condition that provides a standard to which the experimental condition(s) can be compared. Also called the baseline condition or nontask condition.

epiphenomenal A secondary consequence of a causal chain of processes, but playing no causal role in the process of interest.

est. The "what/where" hypothesis depends on our intuitive understanding of the differences between spatial information and object information. Some researchers have suggested that spatial information includes how objects can be manipulated spatially, and thus the dorsal stream represents "how" information, not "where" information. The resulting debate has spawned new hypotheses about the organization of the visual system, changing the very terms used by the scientific community.

To test hypotheses, scientists set up experiments. Given the hypothesis "Manipulating the IV will cause changes in the DV," the experiment must contain at least two values of the IV and must be able to measure changes in the DV. The simplest way to set up an experiment is to have two conditions that occur at different times. These are usually separated into an **experimental condition** and a **control condition**, which differ only in the effect of interest. The experimental condition is sometimes called the task condition, and the control condition is sometimes called the baseline condition or non-task condition. In Chapter 7 we discussed the first BOLD fMRI experiment, which was reported by Kwong and colleagues in 1992. They hypothesized that manipulating the amount of visual stimulation would change the BOLD activation level in the primary visual cortex. Their experimental condition consisted of bright flashing lights that the subjects watched using LED goggles, while their control condition was darkness. When different levels of BOLD activation in the visual cortex were measured between conditions, they attributed that difference to the IV of light stimulation.

Are fMRI data correlational?

A frequent criticism of fMRI data is that they are correlational, or **epiphenomenal**, implying that one cannot use them to make causal inferences and thus cannot conduct tests of experimental hypotheses (Figure 9.4A and B). This criticism is derived from the nature of the BOLD signal. As outlined in Chapter 6,

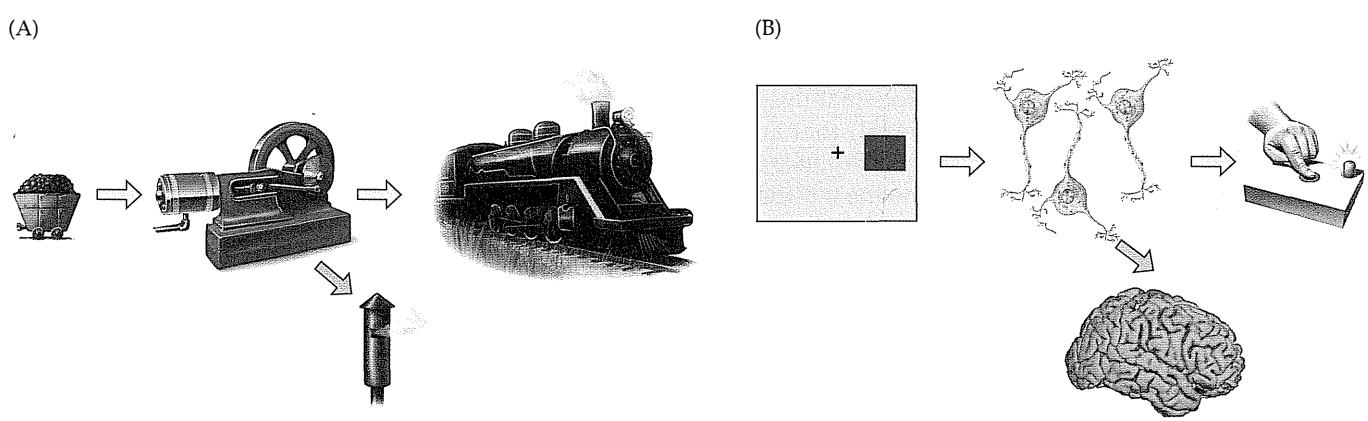

Figure 9.4 Causal chains and epiphenomena. A phenomenon can be part of a causal chain of events, or it can be a secondary consequence (epiphenomenon). (A) Feeding coal to a steam engine provides power that allows the train to move. The engine also emits steam as a by-product, which can be released via a whistle. Thus, the whistling noise is an epiphenomenon or a secondary consequence of the use of coal to power a steam engine. (B) Analogously, when you see a stimulus during an fMRI experiment, it causes your neurons to fire, which in turn evokes a behavioral response like pressing a button with your index finger. The neurons require oxygen to support their metabolism, and that supply of oxygen can be measured using fMRI. Note that even were the fMRI BOLD response epiphenomenal, like in this simplified model, it still could be used as an index of the neuronal activity.

current theories of brain function assume that information processing results from neuronal activity. Of primary importance are axonal action potentials and dendritic field potentials, but other aspects, including synaptic changes and neurotransmission, are also critical. So, when a physiologist implants an electrode into the brain and measures changes in a neuron's electrical potential, she assumes that such changes reflect some form of information processing, although the associated mental operations may be unknown. Hemodynamic changes, in contrast, do not necessarily reflect information processing. Remember from Chapter 7 that early studies showed that BOLD contrast could be evoked by physiological manipulations, such as CO_2 inspiration. These manipulations influenced the magnitude of the BOLD signal, presumably with little to no impact on computations in the brain.

What does it mean for the BOLD signal to be epiphenomenal, that is, merely correlated with neuronal activity? From a strong hypothesis-testing perspective, one could use fMRI data to test hemodynamic hypotheses, as described in the previous section, but not neuronal or psychological hypotheses. But nearly all fMRI studies investigate psychological questions! Fortunately for fMRI researchers, the correlational objection rests on an overly strict definition of hypothesis testing. All hypotheses are based on the principle that the experimental manipulation *causes* changes in the dependent variable. However, the chain of causation does not have to be fully elaborated. Consider a typical study evaluating the effect of a drug. To examine whether the drug has a beneficial effect, a researcher gives it to one group of subjects, while another group of subjects receives a placebo. If the experimental group does better than the control group on some measure, such as lower incidence of cancer or increased performance on a memory test, then the beneficial-effect hypothesis is supported. Such a result does not mean that the drug is a direct cause of the dependent measure; it could influence other factors (e.g., mood) that in turn cause the effect. Nor does it mean that no other manipulation could cause the effect. From this example, it is easy to recognize that all experiments, save perhaps those of low-level physics phenomena, have implicit causal structure.

In summary, *correlational* is not equivalent to *meaningless.* As critics correctly note, the mechanisms of BOLD activation are still not completely understood. But the inability to completely explain how neuronal activity leads to BOLD signal does not call into question that the two are related. Consider a simple analogy. You are standing next to a train track, waiting for a train. Within a few minutes, you hear the train's whistle far in the distance. Not being an engineer, you do not know what causes the whistling sound. Nor do you know whether the whistle is needed for the train to move, or is completely unnecessary and epiphenomenal. Despite your profound lack of knowledge about the mechanism behind the whistle, you are certain about one fact: when you hear a whistle, it means that a train is coming.

Just as the whistle serves as a reliable predictor of the train, BOLD fMRI data serve as a reliable predictor of neuronal activity. We return to this issue in Chapter 14 by considering how to combine fMRI data with information derived from other techniques.

Confounding factors

If an experiment has only two conditions, experimental and control, it is critical that they be as similar as possible. If the conditions differ in only one property, then any change in the dependent variable can be confidently attributed to the change in that property. This process is known as subtraction, since one

subtraction In experimental design, the direct comparison of two conditions that are assumed to differ only in one property, the independent variable.

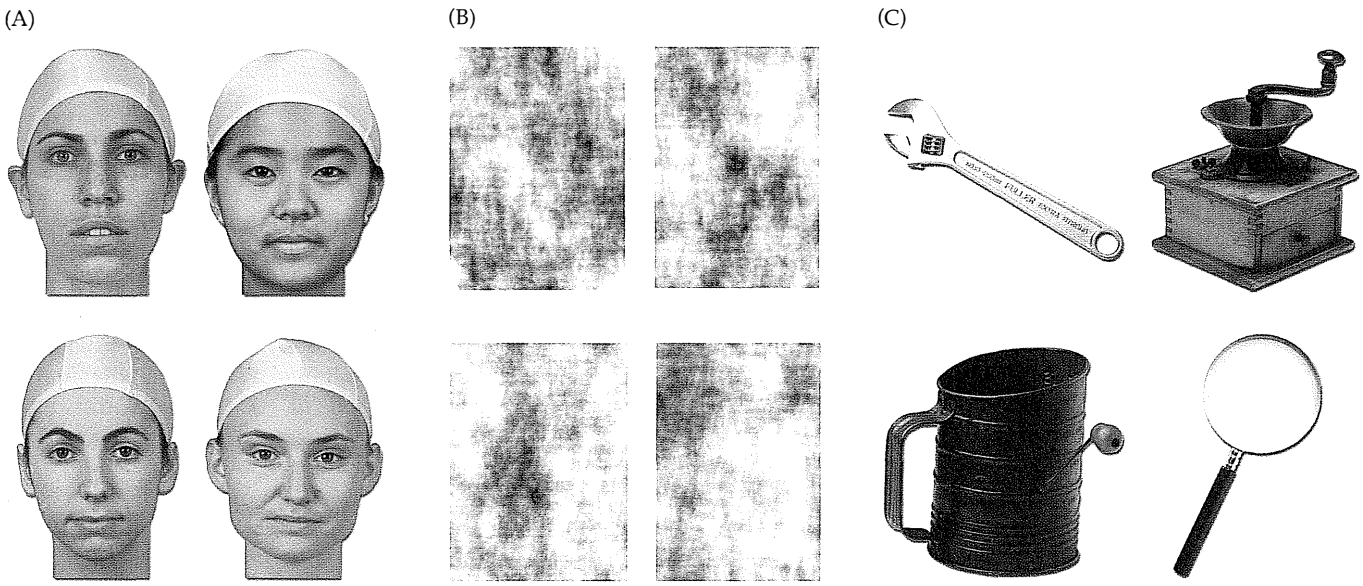

Figure 9.5 Selecting appropriate control stimuli. To study brain regions associated with face processing, you would want to manipulate the face-like characteristics of the stimuli in the experimental and control conditions. In the experimental condition, you could present a series of faces (A). However, many different control conditions are possible. (B) One option would be to present faces that have been transformed so that low-level visual properties are kept constant but the faces are no longer visible. Shown are images of faces that have been Fourier transformed, phase-scrambled, and inverse Fourier transformed. The same spatial frequency components are present, but they no longer form a face. (C) Another option is to present a series of simple objects in the control condition. The objects are visually interesting, like the faces, and have smaller parts that are nameable.

can subtract the value of the dependent variable in the control condition from its value in the experimental condition to quantify the effect of the manipulation. But if the conditions differ in more than one way, then there could be multiple explanations for experimental effects. Any factor that varies with the IV in an experiment is known as a **confounding factor**. Perhaps the most important aspect of experimental design, but the most difficult to master, is selecting good experimental and control conditions in order to minimize confounding factors.

confounding factor Any property that co-varies with the independent variable within the experiment but could be distinguished from the independent variable using a different experimental design.

FMRI studies with psychological hypotheses are particularly susceptible to confounding factors, since the concepts they address are often difficult to define. To understand why, consider the hypothesis that face perception relies on the fusiform gyrus within the inferior temporal lobe. The experimental condition seems obvious: present photographs of human faces (Figure 9.5A). But what is the appropriate control condition? One option would be to simply show nothing, making the design analogous to the Kwong study described above. The experimental and control conditions would thus differ in the intended IV, in that the experimental condition would present faces while the control condition would not, but they would also differ in other factors. In this case, confounding factors would include brightness, presence of edges, nameability, and visual interest, among many. Another possible control condition would be to present faces that have been transformed in some way, so that parameters like brightness and spatial frequency composition are similar between the two conditions (Figure 9.5B). Yet face perception means more than just processing of the physical properties that make up the face. It also refers to seeing an image as a face as opposed to some other type of object. This psy-

chological interpretation suggests another possible control condition, the presentation of random objects of generally similar complexity to the faces (Figure 9.5C). Such a comparison would identify areas of the brain that respond more to the faces than to the other similar objects.

An even more insidious type of confounding factor in fMRI studies is the hidden causal factor. According to the oft-repeated mantra, "Correlation does not imply causation." Just because event A occurs at the same time as event B does not mean that A causes B or that B causes A. Failure to heed this warning can lead to the confirmation of bad hypotheses. A classic example can be found in the link between ice cream consumption and violent crime: both are highest in summer months and lowest in winter months. Does this mean that eating ice cream causes crime, or vice versa? Of course not. Both variables are influenced by a third factor: temperature. This example will seem remedial to many students, but its basic logic holds in more complex fMRI studies. Suppose that you are studying the effects of alcohol on motor cortex function. Your subjects watch a computer screen on which the letters "L" and "R" flash in a random sequence, and they squeeze their left or right hands in response to the corresponding letters. You find that the BOLD signal in the motor cortex is reduced in subjects who drank alcohol compared with those who drank water. What do you conclude? One possibility, that alcohol reduces neuronal activity in the motor cortex, seems reasonable from the data. However, other interpretations should be considered. For example, the subjects may make many more mistakes under the influence of alcohol and squeeze their hands at the wrong times or not at all. The reduced BOLD activation may thus result from poor behavioral performance, not directly from the alcohol. Note that you cannot identify which factor, alcohol or behavioral performance, causes the reduced response with this single experiment. Additional experiments would be necessary to determine the true cause of the effect.

Confounding factors can be minimized if they are not correlated, within your experiment, with the independent variables of interest. The most basic approach to ensuring that this is the case is simple randomization. For example, making your experimental trials occur in a random order can eliminate many sorts of confounding factors related to response preparation, stimulus expectation, and task-switching. Note that, as is discussed in Box 9.2 at the end of this chapter, recent research has identified methods of randomization that take into account properties of the BOLD hemodynamic response to identify optimal sequences for trial presentation. When factors cannot be made completely random, or when randomizing might actually introduce a confounding factor (e.g., because of small numbers of subjects or events), scientists often try to ensure that a potential confounding factor is equally present for all conditions. This is called counterbalancing. If your experiment is comprised of three runs with different task instructions, the effects of practice or fatigue could be important. For some tasks, subjects may get better over time (i.e., practice effects), and thus their performance may be better in later runs. For other tasks, subjects might tire over time (i.e., fatigue effects), and their performance may worsen as the experiment goes on. To ameliorate these problems, you could counterbalance the order of runs across your subject groups: some are given the tasks in the order 1-2-3, others in the order 2-3-1, and the remainder in the order 3-1-2. By introducing randomization or counterbalancing into your design, you can increase the chances that confounding factors influence all conditions similarly.

A good way to identify confounding factors is to participate in your own experiments as a pilot subject. You may recognize an unexpected confound-

randomization A process for removing confounding factors by ensuring that they vary randomly with respect to the independent variable.

counterbalancing A process for removing confounding factors by ensuring that they have equal influence on the different conditions of the independent variable, usually by matching values across conditions.

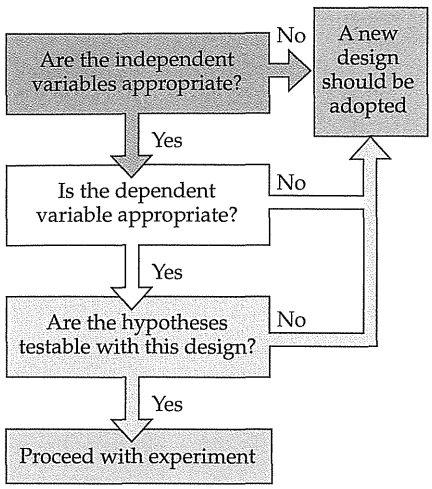

Figure 9.6 Questions to ask yourself when designing or evaluating a research study. These questions are critical for any study, regardless of whether it uses fMRI.

ing factor when you adopt a different strategy than expected, or when you find that the task is too easy or too difficult. Although one cannot always predict all the possible confounding factors, the costs of fMRI experiments in time and money provide ample incentive for good experimental design. The best designs enable the researcher to efficiently answer the questions of interest while requiring a minimum number of experimental subjects and expermental trials per subject.

All of the concepts discussed so far in this chapter are applicable to all areas of science, not just to fMRI experiments. Regardless of the topic, method, or discipline, researchers should always question their choices of independent variables, dependent variables, and hypotheses (Figure 9.6). Thoughtful experimental design is the cornerstone of the scientific method.

Good Practices in fMRI Experimental Design

Before discussing specific types of fMRI experimental design, we want to introduce some guidelines that are relevant to all fMRI studies. As emphasized throughout this textbook, it is very easy to conduct an uninteresting, underpowered, or uninterpretable fMRI study—and the most common cause of problems is poor experimental design. Conversely, attention to experimental design at the outset of a research project will maximize the chances of success. We advocate six basic (and non-exhaustive) rules for fMRI experimental design:

1. **Evoke the cognitive (or motor, perceptual, mnemonic, etc.) processes of interest.** This first rule may seem trivial, but it reflects a very real problem in fMRI research. It is very simple, especially for novice investigators, to create a seemingly well-designed fMRI task that fails to generate the very cognitive processes in which they are most interested. When designing an experiment, the first question you should ask is "What will my subjects be doing during this task?"

2. **Collect as much data as possible from each subject.** Ensure that, when your subjects are in the scanner, time is spent on the key task conditions, not wasted on nonessential aspects of the experiment. Without knowing the size of the effect that your manipulation will evoke, it is difficult to answer the question "How many trials do I need?" That said, collecting more data always gives you a better chance of obtaining interpretable results.

3. Moreover, if your design involves the integration of data across subjects, as is the case for most fMRI research, then **collect data from as many subjects as possible**. This is especially critical for comparisons between groups of subjects (e.g., younger vs. older adults), for which both intra- and inter-subject variability can compromise results.

4. **Choose your stimulus conditions and the timing of their presentation to evoke maximal changes in the cognitive processes of interest, over time.** Usually, this involves clumping stimuli so that there are some periods with continual engagement of the processes of interest, and other periods with no engagement of the processes of interest. Doing this increases the efficiency of experiments involving the detection of activated regions.

5. **Organize the timing of experimental stimuli so that successively elicited processes of interest are minimally correlated with each other,**

over time. This often requires using a variable interval between successive events, especially when those events occur relatively rapidly or as part of a complex task. Doing this increases the efficiency of experiments involving estimations of the time course of activation.

6. **Where possible, obtain measurements of your subjects' behavior that can be related to the fMRI activation.** This allows researchers to test more specific hypotheses about brain function, compared with simple comparisons of experimental conditions. Depending on the research question, these measurements could be obtained during the fMRI session itself (e.g., task performance), they could be part of a parallel behavioral experiment (e.g., subsequent memory effects), or they could be collected as independent assessments of some trait (e.g., intersubject variability).

Good experimental design is probably the most critical aspect of fMRI research. In the following sections we introduce some broad approaches to designing fMRI studies. But the topic of experimental design extends far beyond the scope of this single chapter. For a more extensive consideration of this subject, we refer the reader to the excellent articles by Henson, Liu, Poldrack, and Wager (cited at the end of the chapter).

Blocked Designs

The simplest way to evaluate the effect of the independent variable on the dependent variable is to compare an experimental condition (in which the IV is present) to a control condition (in which it is absent or at a lower level), using the logic of subtraction described in the previous section. For example, imagine that you want to investigate whether listening to music improves studying for examinations. Your subjects listen to a list of 20 words read one at a time. For some subjects, during the first ten words there is music playing in the background, while during the last ten words the room is quiet. To counterbalance the order of presentation, other subjects listen to music during the last ten words but not the first ten. In this experiment, the trials from each condition are grouped together in time to form blocks, as shown in Figure 9.7A. As a general definition, the independent variable is kept at a constant level throughout a block, and transitions between blocks represent changes in the level of the independent variable. Here there are two blocks, music and quiet, combined within a single blocked design. The basic analysis of any blocked-design experiment, whether fMRI or not, involves comparing the dependent measure in each block condition. For example, your subjects might remember, on average, eight of the words that they heard while music was playing but only six of the words that they heard when it was quiet. Unsurprisingly, such blocked designs, which are simple to create and straightforward to analyze, dominated the early years of fMRI (see Chapter 7).

To understand why blocked designs were first used, one must consider the context in which these early experiments took place. In the early 1990s, the magnitude of the BOLD change caused by neuronal activity was still unknown, and thus researchers adopted long block intervals to ensure that sufficient neuronal activity would be generated to evoke a measurable BOLD response. In addition, long task blocks had been necessary for PET imaging, which measures the total number of emission events following injection of a radioactive tracer (see Box 7.1). In a typical PET experiment using O^{15} to measure blood

block A time interval that contains trials from one condition.

blocked design The separation of experimental conditions into distinct blocks, so that each condition is presented for an extended period of time.

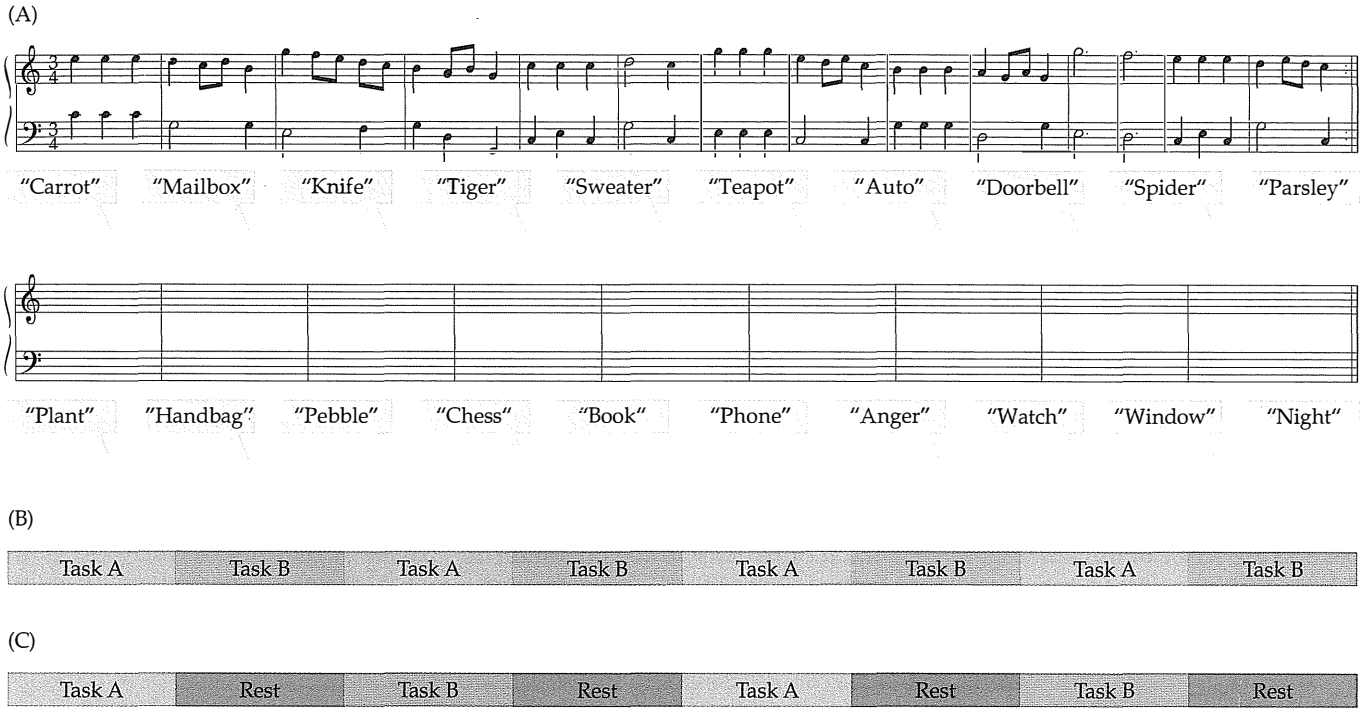

Figure 9.7 Basic principles of blocked designs. In a blocked fMRI design, the experimental tasks are separated into long-interval blocks. (A) A simple blocked design, in which subjects read a list of words presented one at a time. During the first block of ten stimuli, the subjects hear music playing, while during the second block of ten stimuli, no music is heard. Note that although each of these blocks contains multiple individual stimuli, in most blocked-design analyses it is assumed that the cognitive processes of interest are constant throughout the block. The most common blocked design alternates between two conditions (B), allowing identification of the difference in fMRI activation between them. For some research questions, a rest or baseline condition is introduced between the two blocks (C) so that activation that is independent of both conditions can be measured.

flow, a tracer would be injected and then the subject would perform one condition of the task for 60 to 90 s. Then there would be a second injection of the tracer, followed by 60 to 90 s of a second condition. A similar blocked approach was naturally adopted for the first fMRI studies, based on the idea of comparing steady-state activation in one task to steady-state activation in another. Even now, when much more is known about the construction and analysis of complex task designs, the simple blocked design remains an important part of fMRI.

Setting up a blocked design

The first issue to consider when creating a blocked design is the research question itself. Some experiments require long task blocks because the process of interest cannot be modulated over short intervals. If one is interested in studying vigilance or sustained attention, one could compare 30 s blocks in which subjects are concentrating on a task with 30 s blocks in which the subjects are not concentrating. Since active concentration may take some time to engage and disengage, using a blocked design will improve the subjects' ability to per-

form the task. Conversely, some experiments cannot use blocked designs due to the transience of the neuronal activity. Detection of infrequent targets, as in the common "oddball" or "n-back" paradigms, provides a good example. Imagine that you are watching a series of letters flashing rapidly on a computer screen. Your task is to press a button whenever you see an "X," which only appears five percent of the time. The oddball "X" cannot be presented repeatedly within a block, as that would change how subjects process it. An event-related or mixed design would instead be necessary.

Assuming that a blocked design is practical for an experiment, the researcher must next choose the experimental conditions and determine the timing of the blocks. The former requirement relates to the IV, in that conditions must be selected that maximally influence the desired IV without introducing confounding factors. The latter requirement relates to the DV, since the properties of the hemodynamic response determine the length of the blocks and whether there should be spacing between them. The choice of conditions for the different blocks relates in an important way to the goals of the experiment. Imagine that you are interested in whether or not nouns and verbs are processed in different areas of the brain. One obvious design would involve two conditions, nouns and verbs, each consisting of a series of words presented one at a time. Each condition could be presented for 30 s, and the conditions could alternate for the duration of the experiment. This **alternating design** (Figure 9.7B) is optimal for determining which voxels show differential activation as a function of the independent variable (i.e., the difference between the conditions). However, it does not provide any information about voxels that are active in both conditions or about the response to a single condition in isolation. To gain information about the independent responses to each condition requires additional **control blocks** (Figure 9.7C). Control blocks in which the subject does nothing, such as watching a blank screen where there is nothing to read, are also called **null-task blocks**. (Note that even null-task blocks may engage robust cognitive processing, as considered in Box 9.1.) Additional conditions require additional time, however, and should not be added unnecessarily. Therefore, whenever you choose which conditions to include in a blocked design, you should begin by evaluating whether a simple alternating design would be sufficient for answering your research questions.

After deciding on your experimental conditions, you should next consider the timing of your task blocks. Functional MRI experiments generally involve blocks ranging from about 10 s to about 1 minute. (Note that the use of very short blocks, especially when presented in randomized order, effectively changes the design to event-related.) Within that large range, the experimenter has considerable flexibility in the choice of timing parameters. Most important to consider is the effect of block length on the experimental task. Are there time constraints that preclude very short or very long blocks? In many working memory experiments, for example, subjects must rehearse a changing set of items over time. If the block is too short or too long, such a task may be too easy or too difficult. As for many psychology experiments, fatigue effects (and to a lesser extent, practice effects) should be considered. Very demanding tasks may be difficult to sustain over extended periods of time, and subjects may do worse at the end of a long block than at the beginning. In general, block length should be chosen so that the same mental processes are evoked throughout.

For most purposes, block length should be kept constant for all of the conditions. Remember that in an alternating design, the primary statistical analy-

alternating design A blocked design in which two conditions are presented one after another for the duration of the experimental run.

control block A time interval that contains trials of the control condition.

null-task block A control block in which there are no task requirements for the subject. Also called a baseline block or nontask block.

BOX 9.1 Baseline Activation in fMRI

The basic assumption of blocked designs is that block-related changes in BOLD signal result from differences between the experimental conditions. In the usual subtractive approach, there are two conditions: task and control. The task condition is assumed to consist of all of the neural processes present in the control condition, along with additional processes of interest. Consider the results from the following early fMRI experiment, as reported by Binder and colleagues in 1999. During task blocks, subjects listened to sequences consisting of low and high tones and pressed a button if a given sequence included two high tones (e.g., L-L-H-L-H). In control blocks, the subjects lay still in the scanner with their eyes closed. Each block lasted 24 s. Not surprisingly, the tone task evoked more fMRI BOLD activation than control blocks within the auditory, prefrontal, parietal, and motor cortices, among many other regions. These areas reflect regions that are associated with perception, decision, and response aspects of the task. The authors then looked for brain regions that were less active during the task blocks than during the rest blocks. Surprisingly, a set of specific regions (now called the **default network**) showed increased activation during rest, a finding since confirmed by many studies using both fMRI and PET. These results collectively suggest that the assumptions of the subtractive method may be flawed. Some aspects of cognition may actually be inhibited during performance of psychological experiments, such that cognitive processes present in the control condition may not be present during the task condition. In the last few years, interpreting **deactivations**, or decreases in hemodynamic activation, has become an area of considerable interest.

What does it mean for fMRI activation to decrease during an experimental task? In answering this question, it is critical to recognize that blocked designs only provide information about the relative difference between two conditions, not about absolute levels of activation. Without a clear baseline to which both conditions can be compared, several different types of changes in absolute activation could result in similar changes in relative activation (Figure 1). Gusnard and Raichle, in a comprehensive review of many research studies published in 2001, suggest that the appropriate baseline condition for functional neuroimaging should be defined using the **oxygen extraction fraction** (OEF), which is largely stable across the brain (Figure 2). Even though some areas of the brain have greater blood flow than others, and some areas have higher oxygen requirements than others, the proportion of oxygen that is extracted when the subjects are resting with their eyes closed is spatially uniform, with only a few exceptions. Remember from Chapter 7 that the OEF decreases as part of the BOLD response,

default network A set of brain regions whose activation tends to decrease during the performance of active, engaging tasks, but to increase during conditions of resting and reflection.

deactivations Decreases in BOLD activation during task blocks compared with nontask blocks.

oxygen extraction fraction (OEF) The proportion of available oxygen that is removed from the blood.

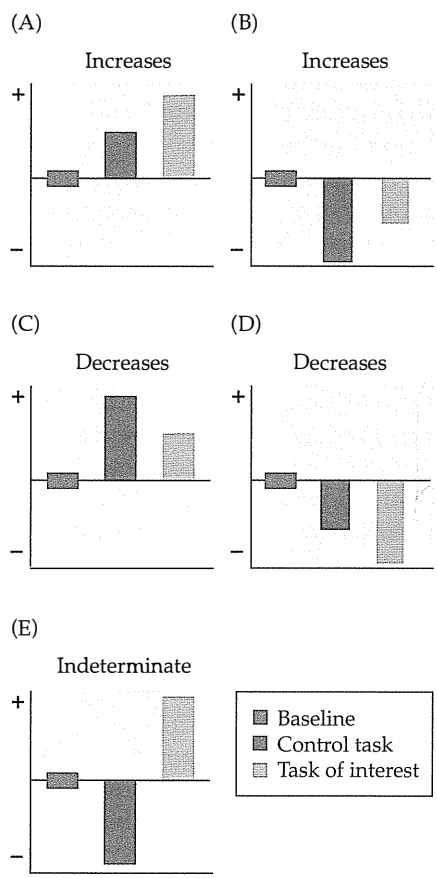

Figure 1 Possible origins of increases and decreases observed in fMRI. When experimental and control tasks are compared using a blocked design, there are several possible causes of observed increases or decreases in hemodynamic activation. First, an increase in activation during the experimental task could be observed when both tasks are either above baseline (A) or below baseline (B). Likewise, decreases in activation during the experimental task could be observed when both are above baseline (C) or below baseline (D). Note that in (A) and (C), both tasks have a positive effect compared with baseline, while in (B) and (D), both tasks have a negative effect compared with baseline. If one task is above baseline and the other below (E), comparisons of the tasks with each other would yield a large effect, but the effect in relation to baseline would be indeterminate. (After Gusnard and Raichle, 2001.)

BOX 9.1 *(continued)*

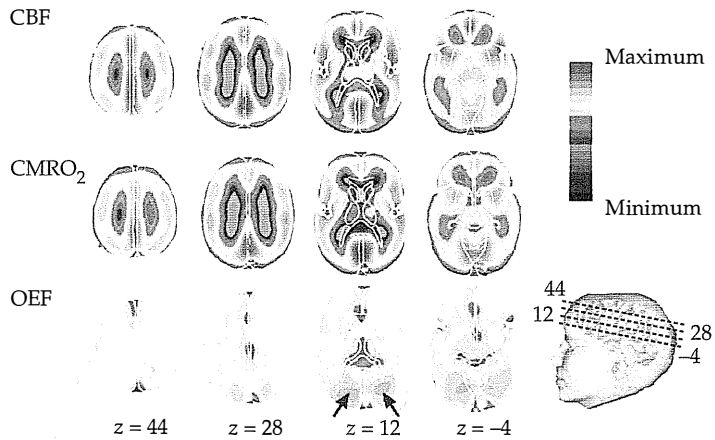

Figure 2 The oxygen extraction fraction (OEF) as a possible baseline for brain activity. Gusnard and Raichle suggest that the OEF, the proportion of available oxygen that is extracted from the blood, is highly stable across the brain and represents a good baseline for brain activity. Shown are four axial slices reflecting data from an experiment with 19 adult subjects. Also shown here are relative cerebral blood flow (CBF) and cerebral metabolic rate for oxygen ($CMRO_2$); the ratio between these quantities gives the OEF. The arrows indicate the only regions of increased oxygen extraction relative to the remainder of the brain. These are in the visual cortex and likely reflect the fact that the subjects in this data set had their eyes closed. The baseline for these regions may reflect open eyes and normal visual stimulation. (From Gusnard and Raichle, 2001.)

due to an overcompensatory increase in blood flow. Decreases from the baseline OEF indicate increased neuronal activity, whereas increases indicate decreased neuronal activity. Thus, a deactivation observed in an fMRI experiment might reflect a counterintuitive increase in metabolic activation within that region during a resting or inactive state, compared with during the performance of some active task. (However, see the recent article by Morcom and Fletcher for some important caveats for this and related conclusions.)

Across a wide range of fMRI studies, there has been remarkable consistency in the regions that evince deactivations during experimental tasks (or activations during non-task periods). These regions include the medial prefrontal cortex along the medial frontal gyrus, the posterior cingulate or precuneus, the lateral parietal cortex along the angular gyrus, and parts of the temporal lobe. Moreover, these regions exhibit a high degree of functional connectivity, such that moment-to-moment fluctuations in the activation of one region predict similar fluctuations in the other regions. Grecius and colleagues, in a 2003 article, collected fMRI data while subjects were lying in the scanner but performing no experimental task (i.e., a null-task session). They found that changes in the activation of the posterior cingulate are mirrored by similar changes in the medial prefrontal cortex and in the lateral parietal cortex, even in the absence of any external stimulus. Moreover, the activation of the posterior cingulate cortex was inversely correlated with activations in regions of the lateral prefrontal cortex associated with the goal-directed control of behavior. More recently, researchers have tracked changes in the functional connectivity among these regions between different stages of human development. A 2008 study by Fair and colleagues demonstrated that young children have reduced functional connectivity, particularly between the medial prefrontal and medial parietal cortex, compared with adult subjects. Functional connectivity between these same regions also declines in older adults, as shown in an elegant 2007 study by Andrews-Hanna and colleagues. Notably, this decline was greatest in individuals who also showed the highest levels of degeneration in connecting white-matter tracts, as measured using diffusion tensor imaging (see Box 5.1). This suggested that intact fiber connections between these regions are necessary for their functional connectivity.

What functions might this seemingly arbitrary set of regions serve? One possibility is that they may play important roles in the monitoring of external stimuli. Both the medial and lateral parietal cortices have been implicated in spatial and attentional processes. However, neuroimaging and single-unit studies indicate that these regions are not associated with attention to expected stimuli. Instead, they seem to be more associated with peripheral or unexpected events, consistent with the idea that they are part of a generalized monitoring system. The ventromedial frontal cortex, in contrast, is typically associated with emotional processing, including assessments of the likely reward consequences of future actions. Together, these sorts of monitoring processes can be considered examples of "self-

(continued on next page)

BOX 9.1 *(continued)*

directed", "stimulus-independent", or "introspective" thought (see the References for several articles discussing these ideas).

To experience self-directed thought, close your eyes and relax for at least 10 s. If you are like most people, you will feel an initial sense of withdrawal from the world around you, followed by a growing sensitivity to external stimuli. You will notice sounds that had previously been outside your awareness. You will become sensitive to heretofore unnoticed muscle tension or joint pain. In short, the baseline state of brain activation is very different from that evoked by a demanding task, like reading this book. This difference was recognized by William James, who described introspection as follows: "When I try to remember or reflect, the movements [in the mind] in question, instead of being directed toward the periphery, seem to come from the periphery inwards and feel like a sort of withdrawal from the outside world." (1890, p. 300)

Here, James emphasizes the essential difference between active and reflective states. The former is goal-directed, aimed at changing the surrounding environment or one's place in it. The latter is self-directed and passive, seeking information about the environment. James also notes his awareness of particular body motions during introspection, and how those physical movements might relate to the movement of thoughts. As in much of James's writing, his well-reasoned reflections anticipate the present discussion of baseline brain activation by more than a century. Rest or baseline conditions are not absent of mental processes. Instead, they contain particular types of processes associated with reflection, daydreaming, self-assessment, bodily attention, and emotion. Recent work by Mason and colleagues, for example, links stimulus-independent thought (e.g., mind-wandering) to activation of default network regions (Figure 3). When designing an fMRI experiment, you must account for

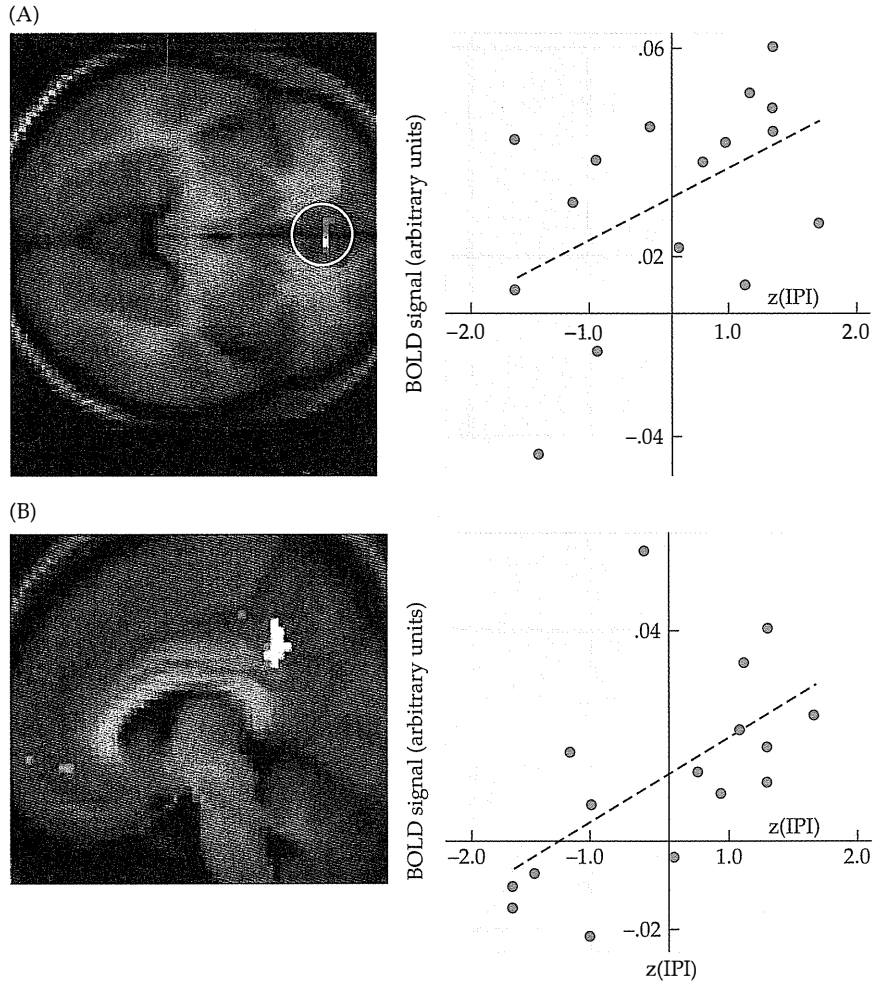

Figure 3 One of the potential interpretations of increased activation during non-task-related conditions is that it reflects "stimulus-independent thought," such as daydreaming and mind-wandering. To test this interpretation, Mason and colleagues trained subjects on working-memory tasks. On blocks of stimuli that were well-practiced, subjects became more likely to think non-task-related thoughts, compared to novel blocks of stimuli that required focused attention. The researchers compared fMRI activation during practiced and novel blocks. Shown circled at left are regions with greater activation during practiced blocks; these included the medial frontal cortex (A) and the posterior cingulate cortex (B). As shown on the scatterplots to the right, those subjects who were more likely to engage in mind-wandering (*x*-axes; *z*-scores on an independent daydreaming scale) exhibited the greatest activation in each of these regions (*y*-axes). The researchers conclude that these regions play an important role in stimulus-independent thought. (From Mason et al., 2007.)

BOX 9.1 *(continued)*

reflective processes in your choice of experimental and control conditions. If the control condition has no explicit task requirements, subjects will naturally begin thinking about how they are doing in the experiment, what they will have for dinner, which friends they will see this evening, or even a dull pain in their lower back that they only now are beginning to notice. For this reason, rest or null-task conditions are not recommended, as the sole control condition. Instead, conditions should be chosen so that subjects are always performing some active task or attending to a changing environment. For example, if the experimental condition consists of judging the familiarity of remembered words, consider a control condition where subjects read words and indicate whether they are presented in capital or lowercase letters. Both conditions require attention and decision processes, thus precluding activation in the baseline system, but only the former invokes memory processes. Another suggested procedure is to explicitly include a null-task condition within your design to provide a baseline. By doing so, you can evaluate whether relative differences between your conditions reflect differential increases above baseline or an effect for one condition but not the other (see Figure 1). Understanding the effect of baseline processing on fMRI data is important for any researcher, but it is especially critical for those who use blocked designs.

As a final point of consideration, several theorists have argued that the pervasive co-activation of default-network regions may reflect something much more fundamental than conscious but undirected thought. They point to phenomena like the presence of functional connectivity between these regions in patients under general anesthesia, along with the sorts of broad lifespan changes in that connectivity described earlier in the box. The sorts of fundamental processes that these regions might support remains mysterious, but there have been some speculations. These regions may form predictions about future mental operations, coming online when immediate task demands cease. They may increase the sensitivity of other brain regions to external stimuli, effectively turning up the gain on stimulus-response links elsewhere in the brain. Or, they may act to consolidate representations of past events, whether at the level of overt memories or learned behaviors. Whether one of these or another property accurately describes the collective function of these regions will remain an important topic for future cognitive neuroscience research.

sis evaluates differences between the two conditions. Even if one condition is labeled as the task and the other is called baseline, they are equally important for the statistical comparison. Statistical comparisons between two conditions are determined by the magnitude of the difference between the conditions compared with the variability within conditions, as seen in Figure 9.8. Since the standard deviation of a fMRI time course decreases with the square root of the number of time points (e.g., in a block), the overall standard deviation will be largest when one block is very long and the other very short (i.e., when the former has low variability, but the latter very high variability), while it will be smallest when the blocks are of equal length (e.g., both with intermediate variability). So, for optimal statistical power, the blocks in an alternating design should generally be of equal length. However, if more than two conditions are used, then unequal block lengths or block numbers may be beneficial. If a primary comparison is something like the combination of condition 1 and condition 2 versus condition 3, then it may be worth making condition three twice as long as the others. This often occurs in designs that use a null-task block along with two experimental conditions (i.e., 1-3-2-3-1-3-2-3-, etc). Also, if additional analyses will examine responses to individual events within an experimental block, as with the mixed designs described later in this chapter, then that block may be lengthened relative to a control block.

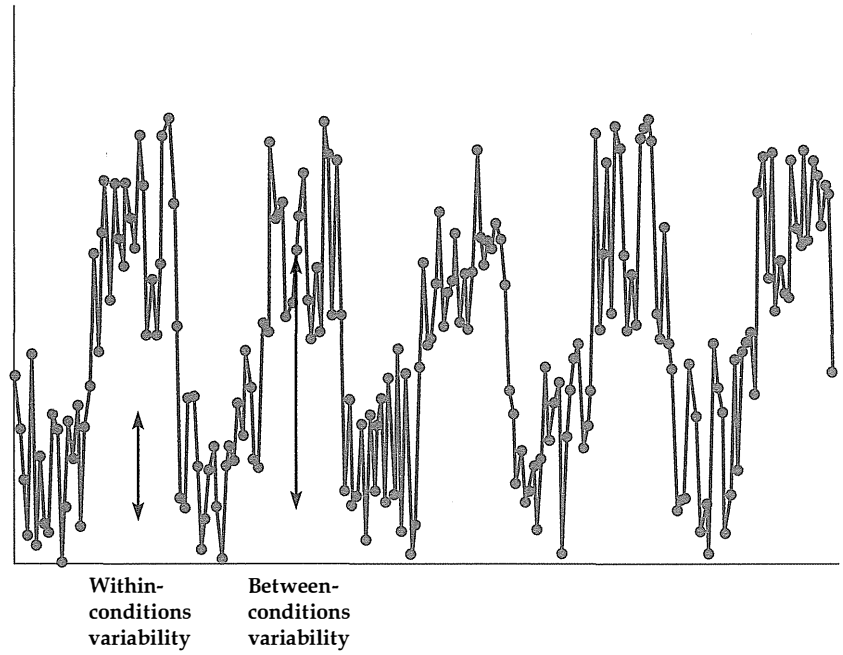

Figure 9.8 Within-conditions and between-conditions variability in blocked fMRI data. The goal of experimental design is to maximize the variability in the data that is due to the experimental manipulation (i.e., the between-conditions variability) while minimizing other sources of data variability (i.e., within-conditions variability). If the former is large compared with the latter, effects of interest can be identified.

Advantages and disadvantages of blocked designs

Though simple, blocked designs can be extremely powerful. For evaluating the strengths and weaknesses of an experimental design in fMRI, we consider two factors: detection, or knowing which voxels are active, and estimation, or knowing the time course of an active voxel. These factors correspond roughly to spatial and temporal resolution. Detection power depends on the total variance in BOLD signal introduced by the experimental design, while estimation efficiency depends on the randomness of stimulus presentation. A central principle of fMRI experiments is that a design that is good at detection may not be good at estimation, or vice versa. (We return to these issues in the extensive Box 9.2 later in this chapter.)

Blocked designs are very good for detecting significant fMRI activation. The detection power of a blocked design is determined by the balance between two factors. First, the difference in BOLD signal between conditions should be as large as possible. Figure 9.9 shows a simulation of how the measured BOLD activation changes as the length of the blocks changes from very long (40 s) to very short (2 s). With long block lengths, a very large response is evoked during the task blocks and the response returns to baseline during the nontask blocks. Thus, there is maximal variability between the blocks. If the block length is sufficiently short (i.e., less than about 10 s) then the hemodynamic response cannot return to baseline during the nontask blocks, and the BOLD amplitude will be reduced. This reduces the total variability in the data, which in turn reduces the experimental power. Reducing the block lengths to extremely short durations, such as only a few seconds, would lead to almost no difference in BOLD signal between task and nontask conditions. In summary, the use of long block intervals provides for maximal BOLD amplitude changes between conditions.

Second, the signal to noise ratio should be maximized at the task frequency. (Note that the task frequency is simply the inverse of the total task period; for example, if your experiment alternated a 20 s task block with a 20 s rest block,

detection Determination of whether or not activation within a given voxel changes in response to the experimental manipulation.

estimation Measurement of the pattern of change over time within an active voxel in response to the experimental manipulation.

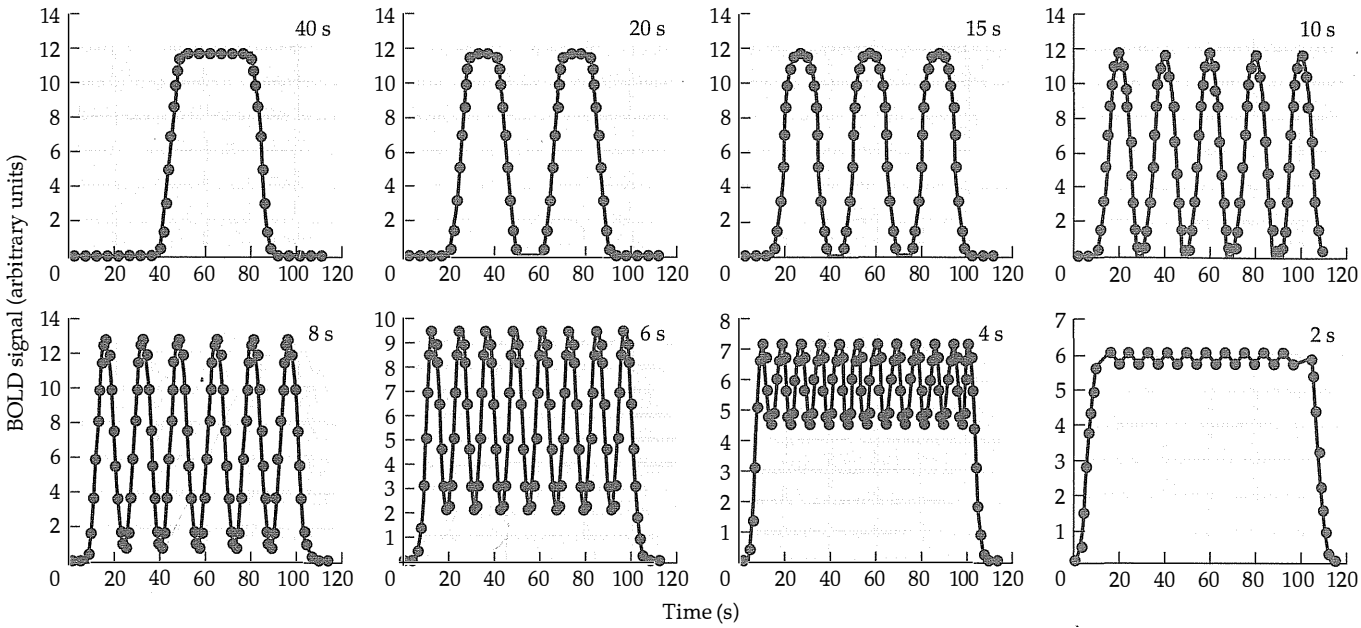

Figure 9.9 Effects of block interval on the fMRI hemodynamic response (BOLD signal). These charts show simulated fMRI hemodynamic responses of voxels active only during the task block of an alternating on/off design. The duration of each block is shown in the upper right corner of each graph. Note that as the block duration shortens below the length of the fMRI hemodynamic response (about 10 s), the response does not return to baseline. At very short block durations, there will be little or no difference between fMRI signal during active and inactive blocks. Note that the scales of the *y*-axes are reduced for block lengths of six seconds or less.

your task frequency would be 1/40 Hz.) The noise in a BOLD time course has its highest power at low frequencies and lowest power at high frequencies. For example, at very low frequencies, there can be significant scanner drift due to problems with the scanner hardware. If your design has very long (e.g., 180 s) blocks, it will be difficult to know whether signal changes from one block to the next result from the experimental manipulation or from low-frequency noise. As the block length is reduced, the task frequency increases and thus the design is more immune to low-frequency noise.

Together, these factors indicate that the noise at the task frequency will be greatest with relatively long block lengths and smallest with relatively short block lengths. As a rough guideline, block lengths of approximately the duration of the hemodynamic response (i.e., 10 s to 15 s) provide large signal changes while reducing noise at the task frequency to an acceptable level. However, depending on the spectrum of the noise, detection power may increase at even shorter block intervals of 6 s to 8 s (see the 1996 article by McCarthy and colleagues for an example). Longer blocks are often required for experiments that test cognitive processes like memory and attention, since it is difficult to ensure that those processes begin promptly. If design constraints necessitate the use of very short block periods, those blocks should be treated like single events and their order should be randomized. This procedure is described in the section on event-related designs.

While their detection power can be very good, blocked designs are relatively insensitive to the shape of the hemodynamic response. We can under-

scanner drift Slow changes in voxel intensity over time.

superposition A principle of linear systems that states that the total response to a set of inputs is equivalent to the summation of the independent responses to the inputs.

stand this insensitivity by returning to the idea of **superposition**, which was introduced in Chapter 7. Setting aside refractory effects for the moment, the hemodynamic response to two identical stimuli presented in succession is equal to the sum of the individual responses. As more and more stimuli are presented in succession, each contributes to the total hemodynamic response. With block lengths of about 10 s or more (i.e., longer than the duration of the hemodynamic response to a single stimulus), every time point within the block contains contributions from multiple stimuli, with each contribution at a different phase. The combined hemodynamic response thus rises rapidly at the onset of the task, then remains at a plateau until the end of the block.

Since the plateau value represents contributions from all phases of the hemodynamic response, the particular shape of the response does not matter. The yellow lines in each part of Figure 9.10 show four hypothetical hemodynamic responses, each with a different shape. The other colors show how the BOLD signal would change as more events are presented successively within a block. All four hypothetical responses have the same total signal amplitude, as measured by the areas under the curves. Consider the standard hemodynamic response shown in Figure 9.10A. As the length of the response block is

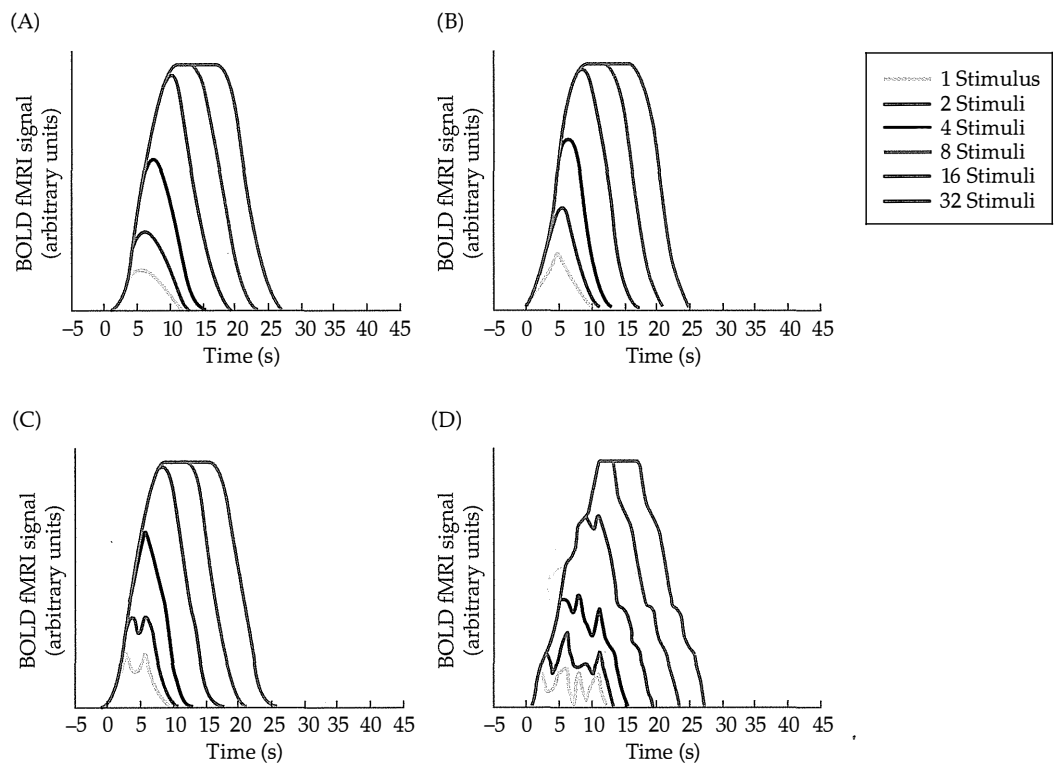

Figure 9.10 Insensitivity of blocked designs to the shape of the hemodynamic response. Each set of curves shows the simulated fMRI signal measured from blocks of 1, 2, 4, 8, 16, or 32 one-second stimuli. In (A), the base hemodynamic response shown in yellow has a standard form. As the number of stimuli in the blocks increases to 16 or more, the hemodynamic response reaches a plateau. Now consider the triangular waveform shown in (B). It is narrower than that in (A), so the response is different for small numbers of stimuli. But as more stimuli are averaged, the response approaches that of (A). Similar results can be seen for (C) and (D), which have very differently shaped hemodynamic responses. In fact, the hemodynamic response in (D) consists of the numerical values of the response in (A), but scrambled in a random order. So, if a single stimulus were present in the block, the BOLD data would look nothing like the standard hemodynamic response. Yet as increasing numbers of stimuli are averaged, the combined response will approach that of (A).

increased from two to 32 events, with each event being one second in duration and separated by two seconds, there is a consistent and smooth increase in overall signal amplitude, reaching a plateau at block lengths of about 12 s or longer. Now suppose that the hemodynamic response has a simple triangular form (Figure 9.10B). Obviously, this form differs considerably from that of the canonical hemodynamic response. But as the length of the block increases, the total hemodynamic response in panel B becomes more and more similar to that in panel A. As can be seen in the subsequent panels, the insensitivity of blocked designs to hemodynamic shape would hold if the hemodynamic response had two peaks (Figure 9.10C) and even if its values were completely randomized over the response duration (Figure 9.10D). For the same reasons, designs that use long stimulus blocks are also relatively insensitive to changes in the timing of the hemodynamic response; they would only identify effects associated with the onset of the first stimulus in the block.

Insensitivity to the shape and timing of the hemodynamic response has both advantages and disadvantages. The primary advantage is that it makes experimental analyses extraordinarily simple. When blocked, any hemodynamic response can be robustly modeled using a smoothed trapezoidal shape consisting of a rise, a plateau, and a fall. To evaluate the effect of the IV, the magnitude of the BOLD response during the task period can be compared with the response during a baseline period. If there is no effect, the random differences in activation between the blocks would follow the *t*-distribution, so the magnitude of the *t*-statistic reveals the significance of the effect. Other analyses are also possible, including power spectrum analyses, correlations, and explicit modeling of block waveforms (see Chapter 10). Balancing this advantage is a loss of estimation power. Imagine that you ran an experiment and recorded the data from the 32-stimuli-curve in Figure 9.10A. You would be unable to estimate whether the hemodynamic response looked like those in panels A, B, or C, because they all resulted in nearly identical data. In fact, with sufficient noise, even the random hemodynamic response in panel D would be impossible to distinguish from the others.

Thought Question

Imagine that you recreated Figure 9.10 using a sample hemodynamic response that is delayed by a few seconds. How would the amplitude and latency of the BOLD signal measured from that block be changed?

In summary, blocked designs are simple and powerful. They are easy to create and can be easily explained to others. If the experimental and task conditions are chosen carefully, then the analysis is very straightforward. Blocked designs are good at detecting voxels with significant activation, and they can identify a wide-range of task-related changes, regardless of any variation in the timing and shape of the BOLD signal. However, because the experimental condition is extended in time, it may evoke highly heterogeneous neuronal activity, making some tasks inappropriate for blocked designs. Blocked designs are also not useful for estimating the time course of activation in active voxels.

Event-Related Designs

event-related design The presentation of discrete, short-duration events whose timing and order may be randomized.

The second major type of experimental design in fMRI is the event-related design. The central assumption of an event-related design is that the neural

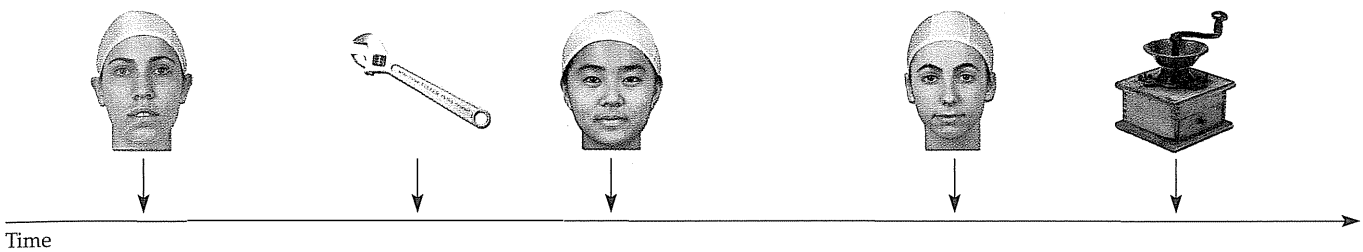

Figure 9.11 Schematic diagram of an event-related fMRI design. The basic idea underlying event-related fMRI designs is that the processes of interest can be evoked transiently by brief presentations of individual stimuli. Here, the relative timing of a series of stimuli is shown by their positions along the axis. The activation in response to the face stimuli can be compared with the activation in response to the object stimuli.

activity of interest will occur for short and discrete intervals, as when a brief flash of light evokes transient activity in the visual cortex. Stimuli that generate such short bursts of neural activity are known as events; in many experiments, a single trial may comprise more than one event. For example, an experiment looking at selective attention may use trials with two events: an initial attention-directing cue followed by a target. In most event-related designs, different conditions of the IV are associated with different events, as in the situation shown in Figure 9.11. Each event is separated in time from the previous event, with an interstimulus interval, or ISI, that can range from about 2 s to 20 s depending on the goals of the experiment. This differs from typical blocked designs, which may present many stimuli consecutively within a task block. Also unlike blocked designs, the different conditions are usually presented in a random order rather than an alternating pattern. Event-related designs have sometimes been called single-trial designs, to emphasize that stimuli are presented one at a time rather than within a block of trials. However, as data collection and analysis procedures have improved, analyses of changes in BOLD signal following only one stimulus presentation have become possible, and thus the label *single-trial* should be reserved for such experiments.

Event-related designs were rarely used in the early years of fMRI. Most research involved long-interval blocked designs, with the notable exception of the 1992 study by Blamire and colleagues discussed in Chapter 7. Furthermore, even the few studies that involved measurement of the BOLD response to short-duration stimuli did not include the additional analyses (i.e., trial averaging, latency measurements) that event-related designs afford. Within a few years, however, fMRI researchers began to use design ideas from electrophysiology in addition to the concepts drawn from PET. Since the first recordings of electrical activity in the human brain by Hans Berger in the 1920s, researchers had known of tonic changes in the electroencephalogram (EEG) associated with different states of arousal or alertness. These changes were identified by comparing the EEG pattern during one state (e.g., deep sleep) with the pattern during another state (e.g., waking). By the late 1950s and early 1960s, researchers began investigating whether signals associated with specific sensory or cognitive events could be identified within the continuous EEG. By synchronizing or time-locking the EEG signal to the onset of a stimulus and signal averaging across many trials, they could extract small electrical changes known as event-related potentials, or ERPs, from the continuous EEG. Some ERPs, particularly those with short latencies (e.g., <100 ms), were associated with sensory pro-

event A single instance of the experimental manipulation. Also known as a trial.

interstimulus interval (ISI) The separation in time between successive stimuli. Usually refers to the time between the end of one stimulus and the onset of the next, with the term "stimulus-onset asynchrony" (SOA) used to define the time between successive onsets.

electroencephalogram (EEG) The measurement of the electrical potential of the brain, usually through electrodes placed on the surface of the scalp.

time-locking Synchronization of analyses to events of interest, usually for the extraction of epochs.

signal averaging The combination of data from multiple instances of the same manipulation in order to improve functional SNR.

event-related potentials (ERPs) Small electrical changes in the brain that are associated with sensory or cognitive events.

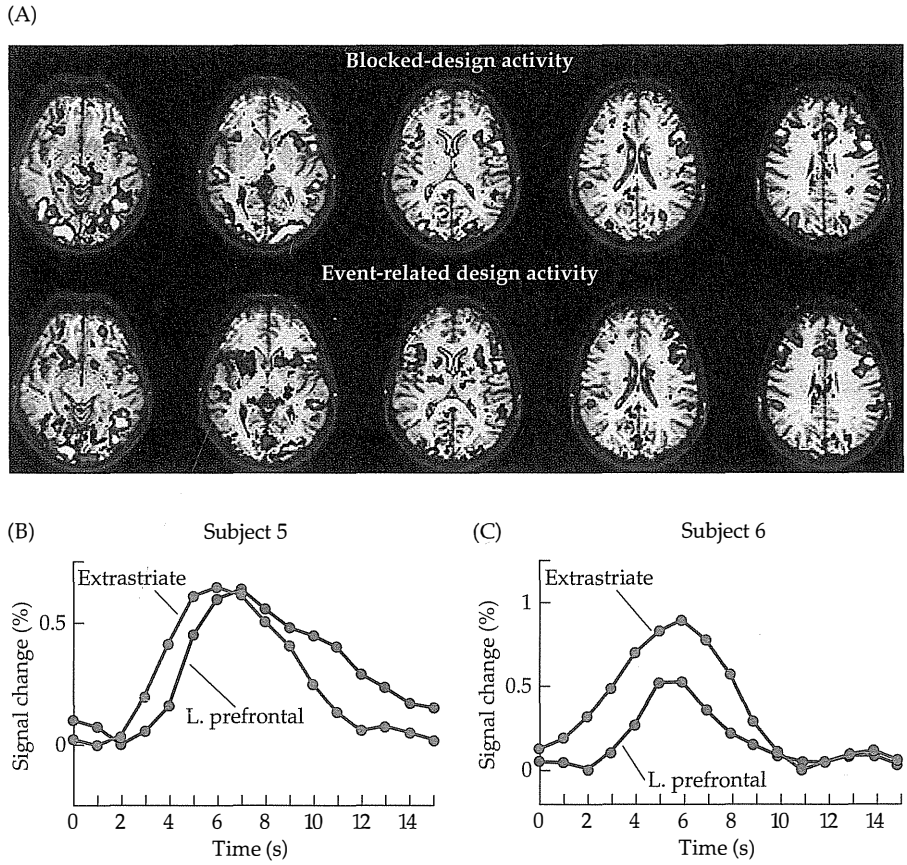

Figure 9.12 Results from one of the first comparisons of blocked and event-related designs. Subjects were shown word stems (e.g., "ora-") and then generated complete words (e.g., "orange"). The researchers compared blocked and event-related versions of the same design and found generally similar patterns of activation (A), although more activation was observed in the blocked designs. Of additional interest was the suggestion that the event-related design could be used to identify latency differences between brain regions. Parts (B) and (C) each show plots of the responses over time in two regions of the brain, the extrastriate cortex (blue line) and the left prefrontal cortex (red line), from two of their subjects. In Subject 5 (B) the response in the prefrontal cortex was slightly delayed compared with the response in the extrastriate region, although this result was not as clear in Subject 6 (C). (A from Buckner et al., 1996; B, C after Buckner et al., 1996.)

cessing. Others were associated with cognitive events. For example, when subjects must respond to the appearance of an unexpected stimulus, there arises a systematic positive ERP deflection (now known as the P300) about 300 ms following the stimulus onset. These key concepts, namely time-locking and signal averaging, were critical aspects of early event-related studies.

One of the first event-related studies, conducted by Buckner and colleagues, compared blocked and event-related versions of a word-generation task. Their results were encouraging; with both approaches they identified similar sets of activated regions in the visual, motor, and left prefrontal cortices (Figure 9.12A), although the amplitude of the activation was generally smaller in response to the events (<1%) than to the blocks (2–3%). Moreover, there was a suggestion that the relative timing of the hemodynamic response could be used to identify timing differences between regions (Figure 9.12B and C). In another very early event-related experiment, McCarthy and colleagues examined brain regions associated with the detection of an unexpected and infrequent stimulus. By its nature, this could not be studied within a blocked design, because blocking the stimuli would render them neither unexpected nor infrequent. The authors found that detection of an infrequent target evoked BOLD activation in the dorsolateral prefrontal cortex, chiefly in the right hemisphere, and in the lateral parietal cortex bilaterally (Figure 9.13A–D). Furthermore, they extracted segments from the fMRI time series that were time-locked to the presentation of the events of interest; these are known as epochs, and the result of averaging all the epochs from one condition is an averaged epoch.

epoch A time segment extracted from a larger series of images, usually corresponding to the period in time surrounding an event of interest.

averaged epoch The result of averaging a large number of epochs that are time-locked to similar events.

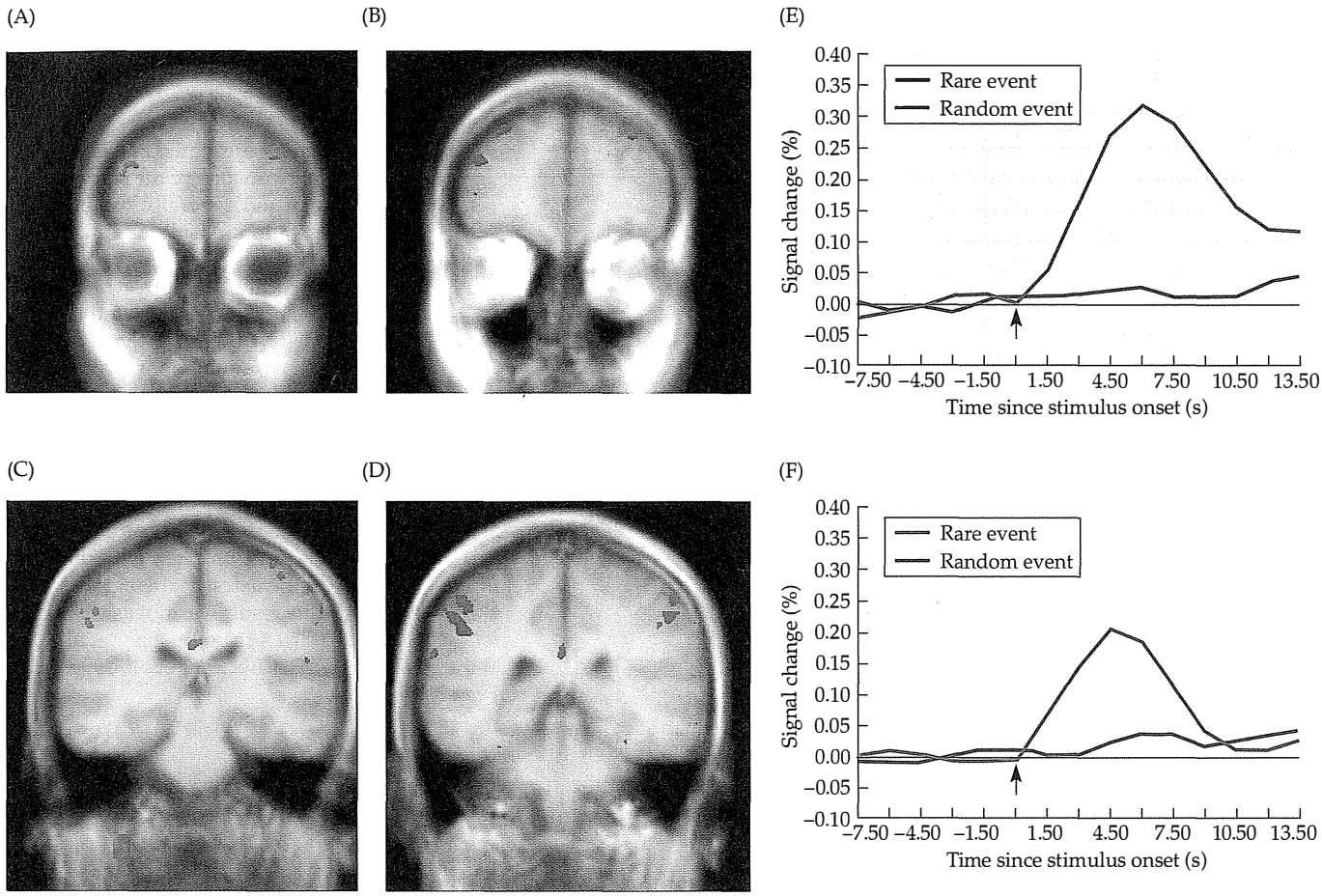

Figure 9.13 An early use of event-related fMRI to study detection of rare stimuli. Subjects watched a series of letters, most of which were "O"s, and pressed a button whenever a rare "X" target was presented. Data were collected from four coronal slices, two within the frontal lobe and two within the parietal lobe. The target stimuli evoked transient activation in the dorsolateral prefrontal cortex (A and B) and in the lateral parietal cortex (C and D), as indicated by the red color overlaid upon activated voxels. Shown are the event-related responses evoked by these target stimuli in the prefrontal (E) and parietal (F) cortices. (A–D from McCarthy et al., 1997; E, F after McCarthy et al., 1997.)

Plotted in Figure 9.13 E and F are averaged epochs containing the target-evoked hemodynamic responses, which exhibit a shape similar to that introduced in Chapter 7.

Principles of event-related fMRI

The first event-related experiments provided a new way to think about fMRI data. When stimuli were presented in a blocked design, the resulting BOLD signal was considered to reflect *steady-state* brain activation at any moment in time. Event-related studies, in contrast, measured transient changes in brain activation associated with discrete stimuli. The pattern of changes *over time* became critical for experimental analyses. For this reason, high temporal resolution is more important for event-related studies than for blocked studies.

Often in event-related studies, successive images are acquired with TRs of 1 s to 2 s, in order to sample the hemodynamic response at a sufficiently fast rate. Estimation of the time course of the hemodynamic response is often very good, especially when events are presented in relative isolation or when sophisticated strategies are applied to separate the responses to closely spaced events.

From the linear systems framework that was introduced in Chapter 7, one can consider stimulus events as impulses, each of which evokes a hemodynamic response. As first demonstrated by Boynton and colleagues in 1996, the amplitude and timing of a hemodynamic response depend on both the intensity and the duration of the evoking stimulus. To the extent that the linear assumption holds (i.e., that the BOLD responses to successive stimuli do not interact), it is possible in principle to present events very rapidly and extract the hemodynamic response associated with individual events. Dale and Buckner investigated this issue in a 1997 study. They hypothesized that signal averaging could be applied to event-related designs even if the events were presented only a few seconds apart, despite the much slower (10–15 s) rise and fall of the hemodynamic response. The stimuli were flashing checkerboards of one-second duration presented to either the left visual field or the right visual field (remember that a visual stimulus presented to the left evokes activation in the right visual cortex, and vice versa). Importantly, the order of presentation of the stimuli was randomized, not alternated, because alternation at such short interstimulus intervals would have removed any effects (see Figure 9.9, for example).

linear system A system that obeys the principles of scaling and superposition.

impulse A single input to a system. Impulses are assumed to be of infinitely short duration.

periodic event-related design An experimental design in which events of interest occur at regular intervals.

Thought Question

How would the assumptions of event-related fMRI be violated if the neuronal activity in response to an event was not an impulse but instead had a long duration (e.g., 5 s)? How would the hemodynamic response change?

Figure 9.14 shows data from one of their experiments. At interstimulus intervals of only 2 s, robust activation for each trial type could be detected in the contralateral primary visual cortex. In fact, the observed activation was more easily detected at shorter intervals than at longer intervals. This seems counterintuitive, but remember that experimental power depends on the amount of data that is averaged. In the 2-s condition, there were many more trials per experimental run than in the longer-interval conditions. When more trials are presented in rapid succession, the total variance in the BOLD signal increases, resulting in more experimental power. Dale and Buckner demonstrated that, provided the events of interest are presented in a random order, areas of BOLD activation can be detected even using very short interstimulus intervals.

Now, does this study imply that short intervals are best for event-related studies? Not necessarily, because these results focused on the detection of areas of activation, not estimation of the time course of the hemodynamic response. For accurate time-course estimation, many researchers have used periodic event-related designs that presented the events of interest at regular intervals. Slow (more than 15 s ISI) periodic designs are conceptually very simple, and their analysis is straightforward. Each event evokes a complete hemodynamic response, and events can be combined through selective averaging. Slow periodic designs are inefficient, however, due to their low frequency of events over time. Fast periodic designs would seemingly be more efficient, following the

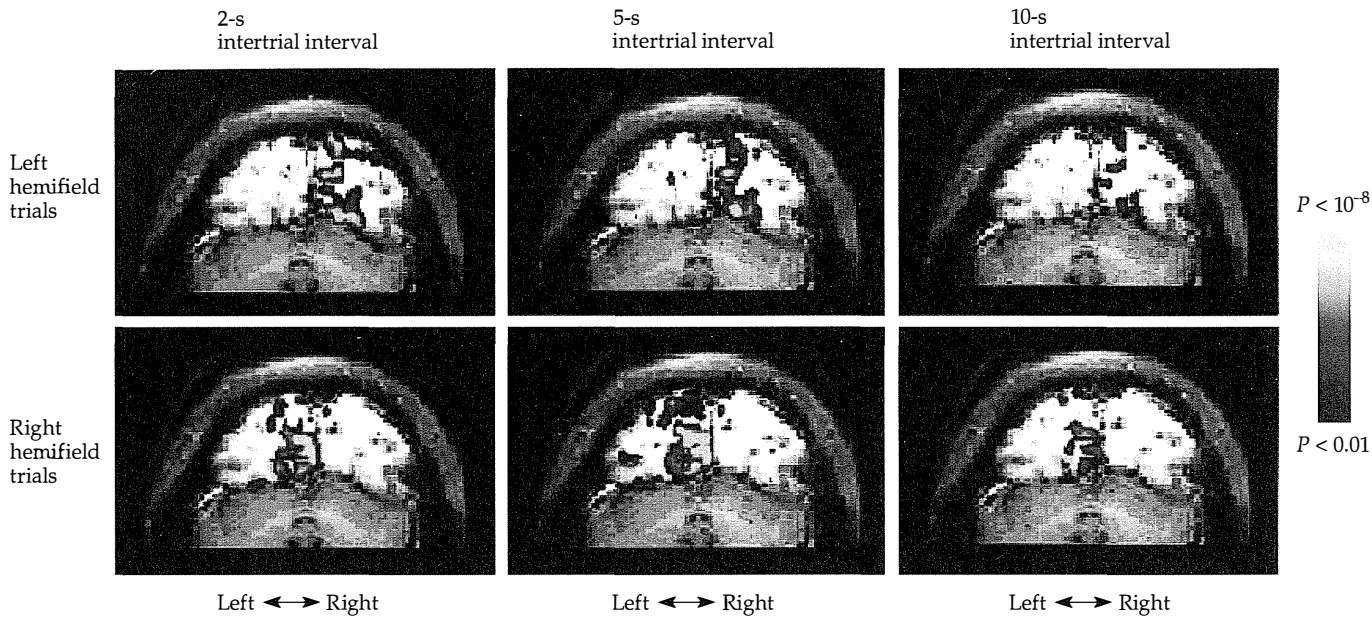

Figure 9.14 Rapid event-related fMRI with randomized stimulus presentation. Functional MRI activation associated with different stimulus types can be extracted from very rapid event-related designs, provided that the order of the stimuli is randomized. In this experiment, flickering visual checkerboard stimuli were randomly presented to either the left or right visual field with 2-, 5- or 10-second inter-trial intervals. Increased activation in the correct hemisphere (i.e., left visual cortex for stimuli presented to the right hemifield) was observed at all intervals, as shown here for a single subject. The bar scale at right indicates the significance values associated with each color on the images. Interestingly, the lowest significance values and smallest spatial extent of activation were found at the longest inter-trial interval, due to the much reduced number of experimental trials that were presented there compared to the shorter-interval conditions. (From Dale and Buckner, 1997.)

logic of the previous paragraph, but in fact may be even less practical. In 2000, Bandettini and Cox attempted to determine the best interstimulus interval for periodic presentation of a short-duration (2-s) stimulus. They found that at intermediate intervals of 10–12 s, substantial stimulus-related variability was present in the data, as shown in Figure 9.15A and B. However, as they shortened the interstimulus interval, the effects of the individual trials became less and less apparent. At the shortest interval tested, 2 s, there was an increase in BOLD activation at the beginning of the run but a plateau thereafter, precluding analysis of any individual trials.

Thus, a short-interval periodic design will cause the BOLD signal to saturate to some maximum value, so that the identification of stimulus-related effects is not possible, making the experiment essentially worthless. Many researchers now use experimental designs that involve short, but variable, intervals between successive stimuli, either by jittering the time interval between successive stimuli or by randomizing the order of different events. Based on data from a number of published studies, some using simulations and others empirical trials, there is now good evidence that the best experimental designs use variable interstimulus intervals in which successive events of the same type occur, on average, every 4 s to 6 s. (Note that this mean inter-

jittering Randomizing the intervals between successive stimulus events over some range.

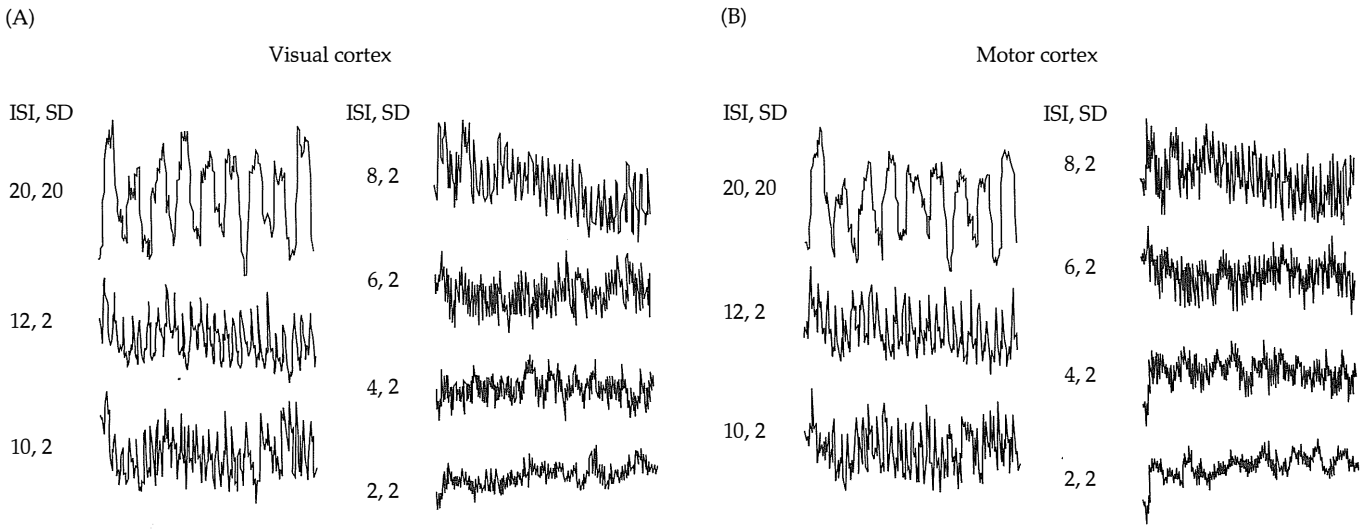

Figure 9.15 Effects of interstimulus interval on event-related fMRI activation. As the interval between successive events decreases, the overlap between consecutive hemodynamic responses reduces the variability in the BOLD signal. Subjects performed a finger tapping task while watching a flashing visual stimulus. Activations within regions of interest in the visual cortex (A) and motor cortex (B) were measured under a number of different experimental conditions. When there was a long interstimulus interval (ISI) of 20 s and a long stimulus duration (SD) of 20 s, mimicking a blocked design, there was clear alternating activation in both regions. However, for short-duration events of 2 s, periodic activation was present at long ISIs of 10 s to 12 s but not at short ISIs. (From Bandettini and Cox, 2000.)

val is sufficiently long to allow near-full recovery from the refractory effects described in Chapter 7.) Box 9.2 describes the key concepts of optimal experimental design in much greater detail.

We emphasize that the timing constraints described here apply to the interval between successive *events* and not necessarily to the interval between successive *stimuli.* Imagine an experiment that presented two types of stimuli, words and nonword letter strings. If you knew that a given brain region responded to the words but not the non-words, you could embed the words in a rapidly presented series of nonwords and the words would still evoke a large hemodynamic response. For that brain region, only the words would serve as events. However, for another brain region that responds equally to both words and nonwords, both types of stimuli would serve as events and BOLD activation would be at a steady state throughout the experiment. This logic is identical to that used in the study by McCarthy and colleagues described in the last section, and bears similarities to the fMRI-adaptation paradigms described in Chapter 8.

Advantages of event-related designs

Event-related designs have become increasingly common, now representing the lion's share of all fMRI research. This popularity has resulted from several advantages, as outlined here, combined with the increasing flexibility of fMRI analysis programs for handling the statistical models resulting from very complex designs.

BOX 9.2 Efficient fMRI Experimental Design

We have emphasized throughout this chapter that different types of designs have distinct advantages and disadvantages. Given the wide variety of questions that can be asked using fMRI, there is no way to create the perfect experimental design. However, there are many, many ways to create an imperfect, inefficient, or just plain bad experimental design.

What makes an experimental design efficient or *in*efficient? Recall that the overall goal of experimental design is to allow the researcher to test some research hypothesis. Most such hypotheses, if well-formed, involve differentiating between two or more experimental conditions. The efficiency of a design depends on its ability to distinguish between those conditions in terms of their levels of activation; efficient designs allow conditions to be differentiated using a relatively small fMRI dataset, whereas an inefficient design would require much more data to reach the same conclusion. One common problem of inefficient experimental designs is a high degree of correlation between the processes of interest. Correlation could arise because processes frequently co-occur (e.g., whenever Event A happens, Event B happens as well) or because distinct processes follow one another too closely in time (e.g., a cue to direct attention always occurs 100 ms before the target stimulus). Designs will also be inefficient if they are poor at evoking the processes of interest (and thus do not generate maximal BOLD signal changes). This can be particularly problematic when complex processes, or subjective states like aggression, regret, or decision making, are being studied. If subjects fail to take the task seriously, or engage in processing not anticipated by the experimenter, then an otherwise good design may become worthless. Finally, a design could be inefficient simply because it is poorly matched to the research hypothesis; a canonical example would be using a pure blocked design, but attempting to estimate the shape and timing of the hemodynamic response evoked by each stimulus within the blocks. Note that the same blocked design might be very efficient for answering a different sort of research question.

Two critical concepts are worth reemphasizing: efficiency depends on the specific experimental hypothesis, and it is measured by the amount of data that would be required to test that hypothesis. These concepts guide researchers who study how to create more efficient experimental designs. Broadly considered, these researchers ask the question, "Given a particular sort of hypothesis to be tested, how should I present experimental stimuli to maximize the size of my effects?" Key factors that have been studied include the ideal interval between successive experimental stimuli (whether events or blocks), whether that interval should be fixed or variable, and whether and how to randomize the order of stimuli. We will consider each of these factors in turn. For clarity, our examples will describe designs involving a single stimulus type (e.g., "what activation is evoked by the presentation of a face?") rather than two or more stimulus types (e.g., "what differential activation is evoked by faces vs. houses?"). Note, however, that the logic of the following argument holds for all types of designs.

The fMRI activation evoked by a single stimulus can persist for 15 s or more, considering the rise, fall, and undershoot of the BOLD hemodynamic response. Blocked designs take advantage of this sluggishness by effectively integrating activation across a number of successive stimuli. If the duration of the blocks is too short—less than about the duration of the hemodynamic response—then the differences between conditions will not be maximized. Remember that too-long blocks also have a disadvantage: if the blocks alternate at a relatively low frequency, then there will be greater noise at the frequency of alternation. For this reason, the optimal block length in an fMRI experiment is often around 20 s. A natural inference is that similar constraints apply to event-related designs. Many early researchers spaced successive events widely, with intervals of about 20 s, so that the response evoked by one stimulus does not overlap with the response evoked by another stimulus. For regularly-spaced events (i.e., periodic designs), intervals longer than about 15 s are indeed necessary for estimating the full shape of the hemodynamic response (see Figures 9.9 and 9.15 for examples). Yet, as shown by Dale in a 1999 article, this advantage completely disappears if the interval between successive stimuli (of the same type) is variable. For example, a periodic design with a fixed interstimulus interval of 4 s is extremely inefficient, because the BOLD signal quickly rises to its maximum value and remains high for the duration of the experiment. However, if the same stimuli are presented with interstimulus intervals that vary around a mean of 4 s, the ability to detect a significant BOLD effect (and even to estimate the shape of the hemodynamic response) increases remarkably! Subsequent work has revealed that the most efficient experimental designs are often event-related with very short, but highly variable, intervals between successive stimuli (see Figure 1).

BOX 9.2 *(continued)*

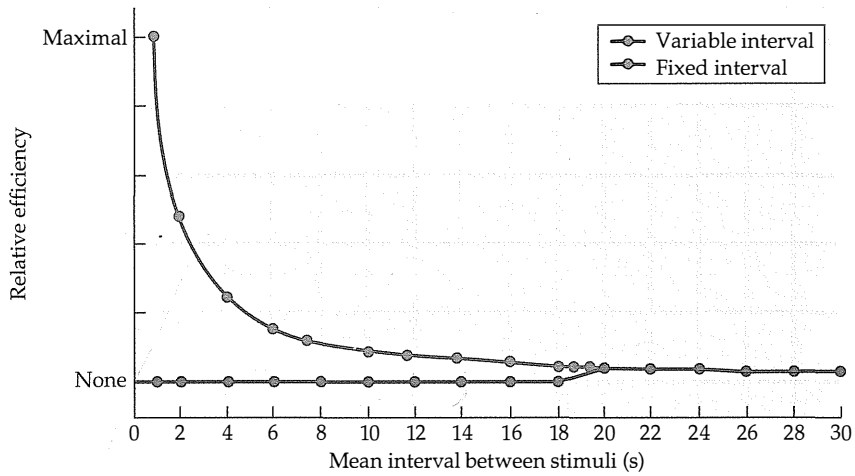

Figure 1 Efficiency of variable-interval and fixed-interval event-related designs. At relatively long intervals between stimuli (i.e., those greater than the typical width of the hemodynamic response), whether that interval is variable or fixed makes relatively little difference—both are relatively inefficient. However, at shorter intervals there is a marked increase in the efficiency of designs that incorporate variable intervals between successive stimuli. In contrast, if intervals between successive stimuli are short, the efficiency of a fixed-interval design (i.e., a periodic design) declines to zero. Designs that use fixed, but short, intervals have essentially no power, as is also shown in Figure 9.15. (After Dale, 1999.)

Why does using a variable, short interstimulus interval so dramatically increase the efficiency of fMRI experimental designs? The answer can be found by considering the properties of the time course of activation evoked by these designs. (We describe these properties conceptually in this section and refer those interested in the underlying mathematics to the papers by Dale, Liu, Wager, and their colleagues listed in the Chapter References.) When a few events occur in rapid succession, the combined hemodynamic response will increase to a near-maximal value. But, when events fail to occur for some time, the hemodynamic response will return to near-baseline levels. Thus, activated voxels will undergo large changes in amplitude over time, and the design has relatively good efficiency for research hypotheses involving the detection of those voxels. Moreover, variable intervals can have a second useful property: successive time points are relatively uncorrelated. Sometimes consecutive events will immediately follow each other, sometimes there will be a short gap between events, and sometimes there will be a long gap. To the extent that the presentation of one stimulus does not predict the occurrence of the next stimulus, this design has a maximal ability to estimate the shape of the hemodynamic response evoked by those events. Thus, introducing variable intervals between successive events can maximize estimation efficiency while maintaining very good detection efficiency. Another advantage of variable intervals is that they minimize the subjects' ability to predict when (and what) events will occur. This can reduce psychological processes associated with anticipation and expectation, while also preventing subjects from using simple strategies to perform the experimental tasks.

So far, we have emphasized the value of an efficient experimental design, while glossing over exactly *how* to construct one! Several approaches have been used in published research. Most common is simple randomization. If there are two event types that could occur with equal probability in a random sequence, the same event could occur several times in a row, or one event could not occur at all in a sequence of many stimuli. This results in a distribution of intervals that approximates that of an exponential decrease. One can also jitter the relative time between successive stimuli, as is necessary for short-interval designs with only one stimulus type, by determining the interstimulus interval using random draws from some distribution of possible intervals (e.g., a uniform distribution comprising integral values between 1 s and 7 s). Another approach is to have the statistical properties of the experimental design actually change over time. In a **semirandom design** (Figure 2), stimuli are sometimes likely to occur and sometimes unlikely to occur. For example, imagine that your event is a flashing checkerboard presented for 500 ms, and you are sampling the brain at a

semirandom design A type of event-related design in which the probability that an event will occur within a given time interval changes systematically over the course of the experiment.

(continued on next page)

BOX 9.2 *(continued)*

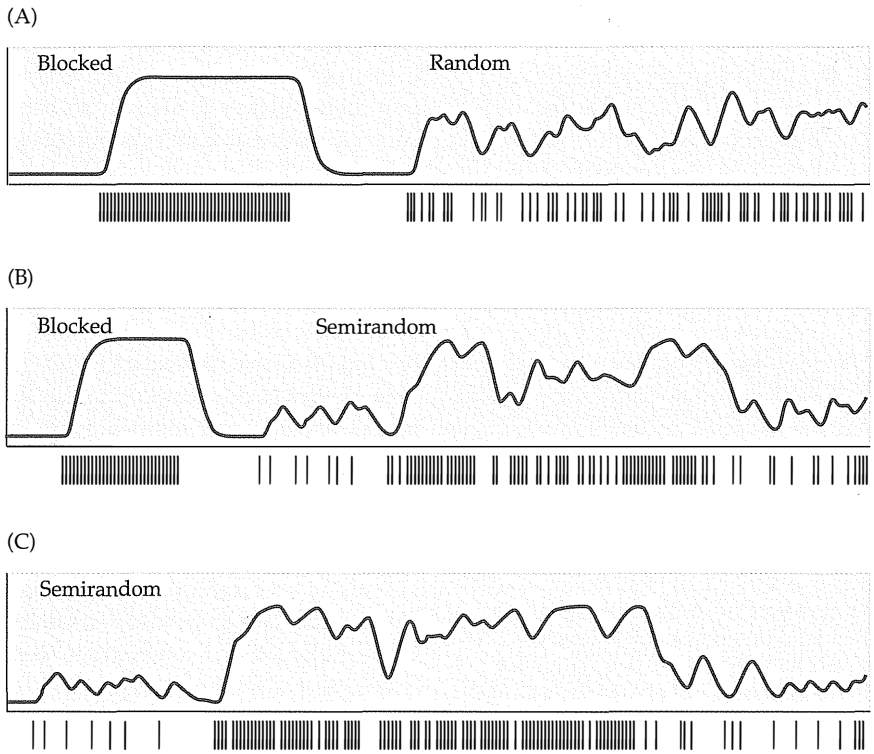

Figure 2 Semirandom designs combine features of blocked and event-related designs. The vertical lines below each graph represent the timing of each single stimulus, such as a flash of a visual checkerboard, and the graphed curves reflect the expected hemodynamic response. The semirandom design contains large-scale structure, in that some time intervals have high event-probability and some have low event-probability, with small-scale randomness. (A) and (B) combine a blocked epoch with random and semirandom periods, respectively, while (C) is a completely semirandom design. Note that these three designs have equal estimation efficiencies and detection powers. (After Liu et al., 2001.)

TR of 1000 ms. You can set up your experiment so that in the first 30 s block, each TR has a 25% chance of containing an event; in the next 60 s block, each TR has a 75% chance; and in the final 30 s, each TR has a 25% chance. The resulting design would look similar to Figure 2C. Although composed of individual events, semirandom designs are similar to blocked designs in that some time periods contain many events while others contain very few; this clustering increases the total variability in the BOLD signal. Work by Liu and colleagues has shown that, consistent with the conceptual predictions in the previous paragraph, semirandom designs can have detection power that are almost as good as those of blocked designs while also having optimal estimation powers.

By their nature, the properties of randomized experimental designs are... random. A random process might generate a sequence that has the virtues described in this box (i.e., event clustering, lack of temporal correlations), or it might not. As a simplified example, suppose that your experiment involved two stimulus types, here labeled "0" and "1," that were equally likely to occur over ten equally-spaced trials. A random process like a series of coin flips could generate any of 2^{10} possible sequences (e.g., 1010011011, 1111111000, or 0101010101) that vary considerably in their efficiency. Typical fMRI experiments contain tens if not hundreds of events, and the intervals between those events are rarely completely constrained by the cognitive demands of the task. Given such a multitude of possible stimulus orders and timings, the odds of simple randomization providing an experimental design that is near-optimal are vanishingly small. Efficiency can be improved significantly by generating many different random designs and then selecting the best alternative (i.e., performing a random search), but even this is unlikely to provide a near-optimal design, especially given the complexity of most fMRI experiments.

Researchers have therefore focused on developing algorithms that can quickly evaluate parameters of possible designs to identify the most efficient. Some researchers have used the tools of mathematics to generate rules for counterbalancing the order of events, leading to designs that are very good at estimating the hemodynamic response evoked by each stimulus class (e.g., the work of

BOX 9.2 *(continued)*

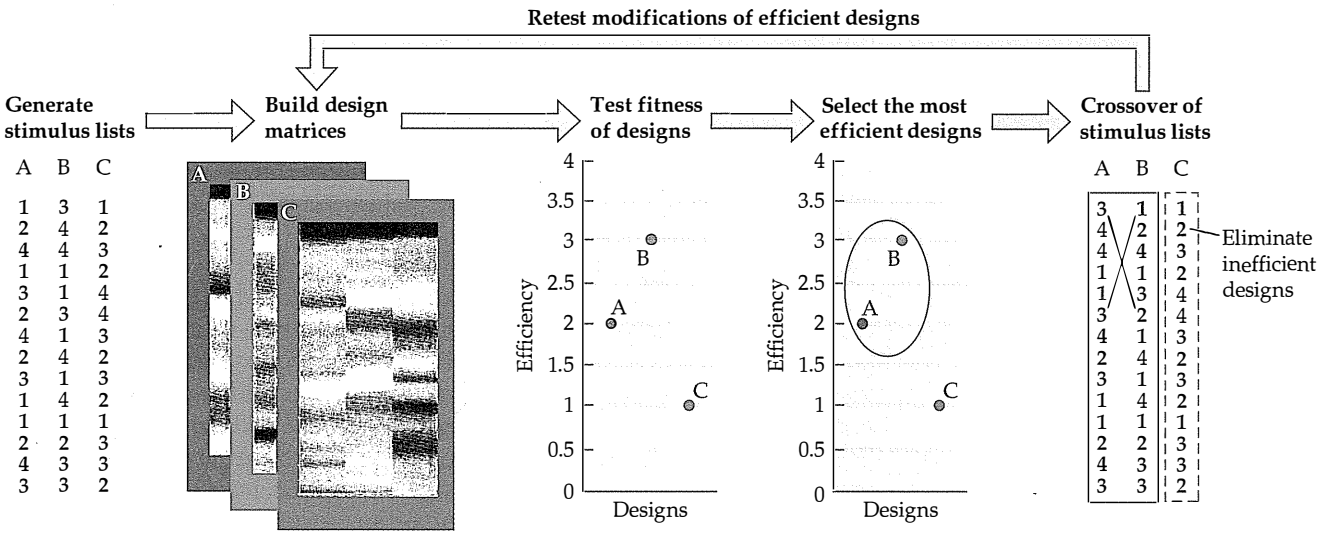

Figure 3 Selecting an efficient design using genetic algorithms. Because simple randomization of experimental stimuli may not result in an optimal design, researchers have investigated methods for finding those design parameters (e.g., the relative timing of events) that lead to the most efficient experimental designs. One promising approach uses techniques inspired by genetic models. The key concepts include initial generation of random stimulus lists (here shown for a design with four stimulus types), construction and testing of the associated statistical models, selection of the most efficient designs, and recombination of elements in those designs. By iterating over many generations of designs, this approach can be shown to converge on near-optimal designs much more rapidly than random searches. (After Wager & Nichols, 2003.)

Buracas and Boynton and of Aguirre cited in the Chapter References). One particularly exciting approach, developed by Wager and Nichols, is the use of genetic algorithms. Like their biological namesakes, genetic algorithms evaluate the relative fitness (i.e., design efficiency) of each design, which consists of many smaller units (i.e., the timing of events). Then, some aspects of the relatively good designs are combined (i.e., some events are swapped), while some elements of the designs undergo mutation (i.e., they change randomly), and then the new designs are tested for their levels of efficiency (Figure 3). Note that the least efficient designs are discarded, and thus options that are unlikely to lead to optimal designs are not explored. This process iterates until it reaches some criterion, such as obtaining a sufficiently good design, or reaching some time limit for searching. Simulations by these authors, using genetic algorithms, resulted in the rapid identification of designs that were near-optimal for specific criteria (e.g., that maximized estimation efficiency while retaining good detection power). Moreover, these designs were demonstrably better than those obtained by randomization or even random searches.

It is important to emphasize that, just as no single experimental design is appropriate for all research hypotheses, no approach for optimizing experimental designs is without specific limitations. Consider two tasks, one involving the passive viewing of discrete visual stimuli (e.g., 500 ms checkerboards), and the other involving making decisions about complex moral dilemmas. Algorithmic criteria that lead to an optimal design in the former case may select a very poor design for the latter case, simply because of the influence of time pressure on the way people evaluate complex decision scenarios. Returning to our cardinal rule for fMRI design, the most important thing to consider is whether the experimental design evokes the mental processes—and thus the neuronal activity and, in turn, the BOLD signal—that you intended.

trial sorting The post hoc assignment of events to conditions, often based on behavioral data.

subsequent memory An approach to fMRI analyses that sorts experimental stimuli based on whether they were remembered or forgotten in a later testing session; this allows identification of brain regions whose activation predicts successful encoding of stimulus properties into memory.

Estimations of the shape and timing of the hemodynamic response are generally much better for event-related designs than for blocked designs. Estimation is important for many types of research questions. By characterizing the precise timing and waveform of the hemodynamic response, researchers can make inferences about the relative timing of neuronal activity, about distinct processes within separate parts of a trial, about functional connectivity between regions, and about sustained activation within a region. Conversely, blocked designs generally have superior detection power because events are concentrated within the task blocks, whereas simple event-related designs evoke smaller overall changes in the BOLD signal. More complex event-related designs, however, can be optimized so that they can have very good detection power without sacrificing estimation efficiency (see Box 9.2), ameliorating the major disadvantage of event-related designs.

Even so, decisions about experimental design cannot be made solely on the basis of the relative importance of detection versus estimation. The major goal of fMRI research is understanding brain function, and so experiments should be designed so that specific functions can be readily individuated (e.g., separated in time). In this regard, event-related designs provide a degree of flexibility not present in most blocked designs, as the same events can be analyzed in different ways depending on the goals of the experiment. A researcher interested in how the presentation of an image affects its perception might present two types of images (e.g., faces and objects) in two orientations (e.g., right side up and upside down), with the images presented one at a time and in random order. These stimuli could be considered as one type of event, visual stimuli; two types of events, faces or objects; or even four distinct types.

Note that this flexibility means that researchers can even choose their events based on experimental data, often known as trial sorting. Like many of the characteristics of event-related fMRI analyses, the basic concepts of trial sorting are derived from earlier electrophysiological studies. Trials are often sorted based on subject responses, like accuracy or response time. For example, some brain structures, such as the anterior cingulate gyrus, are more active during trials in which the subject makes an error than during trials when the subject does not make errors. These differences may reflect cognitive processes like recognizing the mistake, adjusting response plans to prevent future errors, or reflecting on the cause of an error. Trials can even be sorted by their long-term consequences. In experiments using the subsequent memory paradigm, subjects are presented with a large series of items (e.g., pictures of unfamiliar scenes) while within the fMRI scanner. Usually, but not always, they perform some task unrelated to memory (e.g., judging whether the scene is indoor or outdoor). At some later time, subjects complete a memory test that includes these items and others that were not actually presented. Then, the researchers sort the original stimuli into categories of "remembered" and "forgotten," to identify brain regions associated with successful encoding of information into memory. The first such studies were reported in 1998 by Brewer and colleagues and by Wagner and colleagues, and since then, researchers have used this approach to map out the contributions of many regions to memory. For example, in a 2006 study by Adcock and colleagues, subjects were presented with a reward cue (e.g., $5 or 10¢) before each item to be remembered, so that the subjects knew how much money they could win if they successfully remembered that item. They found that for those items that were later remembered, there was increased activation in brain regions associated with evaluation of rewards (e.g., the striatum and the ventral tegmental area within the midbrain), along with increased correlations between those regions and the hippocampus. Conversely, memory impairments resulting from prior sleep deprivation,

as reported by Yoo and colleagues in 2007, are associated with reduced subsequent memory effects in the hippocampus, along with changes in the functional connectivity of that region.

Because of these advantages in flexibility, a large and increasing proportion of fMRI experiments have adopted event-related designs. But as we indicated earlier, event-related designs generally have lower detection power than similar blocked designs, resulting in part from their sensitivity to the shape of the hemodynamic response. If the wrong model for the fMRI hemodynamic response is used, then significant activations may be missed. Nevertheless, for a wide range of experimental tasks, event-related designs provide the best combination of flexibility and experimental power.

mixed design A design that contains features of both blocked and event-related approaches.

state-related processes Changes in the brain that are assumed to reflect distinct modes, or states, of function. State-related processes are more easily measured with blocked designs.

Mixed Designs

Some fMRI experiments combine the basic elements of blocked and event-related approaches. Within a **mixed design**, stimuli are presented in discrete and regular blocks, but within each block are multiple types of events. This is illustrated in Figure 9.16. An important difference between mixed designs and the other types of designs is that mixed designs allow analysis of IVs that change on different time scales. The task blocks, which may last for 20–30 s or more, are associated with sustained changes in task strategy, attention, or other cognitive processes. A subject may be attending to the left side of the visual display during one block and then attending to the right side for the next block. The different blocks induce different cognitive states in the subject, and thus blocked analyses can measure **state-related processes**. This differs conceptually from the semirandom designs described in Box 9.2, in that mixed designs assume that the grouping of events into a task block will cause the subject to adopt and maintain a particular cognitive state, whereas the individual stimuli in a semirandom design are assumed to evoke a particular cognitive process repeatedly (i.e., no underlying cognitive state emerges). Thus, mixed designs are appropriate when one wants to examine sustained brain activation, while optimized event-related designs are preferred for detection of transient brain activation.

As in an event-related design, the stimuli presented rapidly within the block will evoke separable short-term changes in the brain. For example, a subject may have been directed to watch a visual display on which stimuli will appear repeatedly on both the left and right sides, but to attend specifically to the left side on some blocks and to the right side on other blocks. Different events will evoke different processes; for example, an object presented on the attended left

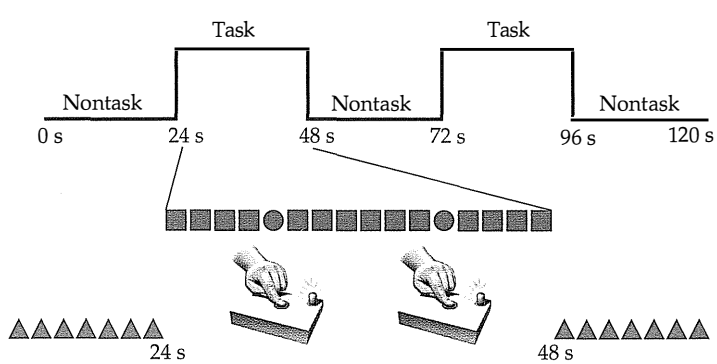

Figure 9.16 An example of a mixed fMRI design. In a mixed design, events of interest are clustered within extended blocks. Here, the task blocks involved an "oddball" paradigm in which subjects pressed buttons to the occurrence of infrequent target circles and ignored the non-target squares. Each circle was thus an event that evoked item-related cognitive processes. The task blocks alternated with non-task blocks (red triangles) that required no responses. Thus, the difference between the task and non-task blocks reflected state-related processes. (After Huettel et al., 2004.)

item-related processes Changes in the brain that are assumed to be caused by the properties of individual stimuli, or items. Item-related processes are more easily measured with event-related designs.

will lead to different changes in brain activation than an object presented on the unattended right. The individual events within a mixed design's blocks reflect item-related processes. Note that state- and item-related processes are not necessarily related within a task; for example, the brain structures responsible for attending to the left or right are not the same as those responsible for pressing buttons in response to targets. Mixed designs are thus extremely powerful for research questions that involve both a long-term cognitive process and short-term implementations of cognitive processes during individual trials.

Thought Question

Mixed designs can also be used to study transient processes that occur at the onset or end of a block. What sorts of cognitive processes are likely to occur at the beginning and end of a task block?

One of the first studies to demonstrate the power of mixed designs was reported in 2001 by Donaldson and colleagues, who wanted to differentiate between brain regions associated with attempted memory retrieval and regions associated with retrieval success. Their experiment consisted of long (105 s) task blocks that each contained 42 events of three types, presented in random order: words that had been studied in a prior practice session, words that had not been studied previously, and fixation events in which no word was presented. Sustained increases in activation during the task blocks were observed in the prefrontal and insular cortices, whereas event-related activation was found in a more diverse set of regions that included the visual cortex, the thalamus, and other parts of the prefrontal cortex. Only by using this sort of mixed design could the authors separate brain systems that underlie state- and item-related aspects of their task. As another example, a 2006 study by Dosenbach and colleagues used mixed designs in experiments involving ten different fMRI tasks and 183 subjects. Their interest was in characterizing brain regions that exhibited both increased activation at the onset of a task block and sustained activation throughout the block, regardless of the particular task that was being performed. Two regions, the anterior insula and anterior cingulate cortex, met these conditions, while also responding specifically to error trials. The authors' conclusion, that these regions constitute a system for establishing and maintaining task sets, could not have been reached without using a mixed design.

It is important to recognize, as noted by Donaldson and colleagues in their article, that state-related activation does not necessarily result in increased activation during one block type compared with another block type. Changes in a cognitive state could instead have modulatory effects on event-related activation, so that the hemodynamic responses to individual events within the block increase in amplitude. Consider a design in which task blocks involve attention to stimuli while nontask blocks do not. Within a region associated with the control of attention, there might be increased, steady-state activation throughout the task block. But in a region whose activation is influenced by attention, there might be no state-related effects, but instead larger hemodynamic responses to events within attended blocks than within unattended blocks. Mixed designs thus have great utility for many types of cognitive questions, but require analysis strategies targeted to the expected activation of interest.

Summary

The important issues in fMRI experimental design are the creation of a research hypothesis, the choice of experimental conditions to test that hypothesis, and the presentation of stimuli that manipulate the experimental conditions over time. When selecting conditions for an experiment, it is important to avoid confounding factors, or variables that unintentionally co-vary with the independent variable of interest. There are three main types of fMRI experimental designs: blocked, event-related, and mixed designs. In a blocked design, each condition is presented continuously for an extended period (one block) and the different blocks of conditions are usually alternated. Some blocked-design studies incorporate a baseline period without an experimental task, to account for specific brain regions that are often more active in baseline conditions. Event-related designs present stimuli one at a time rather than together in a block. Long-interval periodic event-related designs are useful when a prestimulus baseline is necessary but otherwise have poor experimental power. More desirable are event-related designs that use variable but short intervals between successive events of interest to optimize experimental power. Mixed designs combine blocked and event-related analyses and are used to distinguish between long-term sustained activation and short-term transient activation.

There is no perfect experimental design for all fMRI studies. The fundamental rule when designing your study is that you should choose the design that best suits your experimental question. Even a seemingly optimal event-related design could be useless if it does not evoke the cognitive processes of interest, just as a blocked design cannot be used if the conditions cannot be separated into different blocks. When designing a research study, the most important factor to consider is the simplest: which design will allow my experimental manipulation to evoke measurable differences in BOLD activation?

REFER TO THE
fMRI
COMPANION WEBSITE AT
www.sinauer.com/fmri2e
for study questions and Web links.

Suggested Readings

*Buckner, R. L., Bandettini, P. A., O'Craven, K. M., Savoy, R. L., Petersen, S. E., Raichle, M. E., and Rosen, B. R. (1996). Detection of cortical activation during averaged single trials of a cognitive task using functional magnetic resonance imaging. *Proc. Natl. Acad. Sci. U.S.A.*, 93: 14878–14883. *This early study anticipates the later power of event-related fMRI analyses.*

*Henson, R. N. (2006). Efficient experimental design for fMRI. In: *Statistical Parametric Mapping: The analysis of functional brain images.* (Friston, K., Ashburner, J., Kiebel, S., Nichols, T., and Penny, W., eds), Elsevier, London. pp. 193–210. *Provides an overview of the general principles underlying good experimental design in fMRI research.*

Keppel, G. (1991). *Design and Analysis: A Researcher's Handbook.* Prentice-Hall, Englewood Cliffs, NJ. *A classic, readable textbook on experimental design.*

*Poldrack, R. A., Fletcher, P. C., Henson, R. N., Worsley, K. J., Brett, M, and Nichols, T. E. (2008). Guidelines for reporting an fMRI study. *NeuroImage*, 40: 409–414. *This short review provides a set of recommendations for authors of scientific articles using fMRI, so that they can effectively and completely explain their experimental design and analysis steps to readers.*

Raichle, M. E., and Snyder, A. Z. (2007). A default mode of brain function: a brief history of an evolving idea. *NeuroImage*, 37: 1083–1090. *This commentary provides an updated overview of the evidence supporting the existence of a "default network" of brain regions whose activation increases during non-task conditions; companion commentaries in the same journal issue provide alternative perspectives on this topic.*

* Wager, T. D., and Nichols, T. E. (2003). Optimization of experimental design in fMRI: a general framework using a genetic algorithm. *NeuroImage*, 18: 293–309. *This article combines simulation and experimental work to demonstrate the effectiveness of genetic algorithms for identifying optimal parameters and stimulus presentations for fast event-related fMRI designs.*

*Indicates a reference that is a suggested reading in the field and is also cited in this chapter.

Chapter References

Adcock, R. A., Thangavel, A., Whitfield-Gabrieli, S., Knutson, B., and Gabrieli, J. D. (2006). Reward-motivated learning: mesolimbic activation precedes memory formation. *Neuron*, 50: 507–517.

Andrews-Hanna, J. R., Snyder, A. Z., Vincent, J. L., Lustig, C., Head, D., Raichle, M. E., and Buckner, R. L. (2007). Disruption of large-scale brain systems in advanced aging. *Neuron*, 56: 924–935.

Bandettini, P. A., and Cox, R. W. (2000). Event-related fMRI contrast when using constant interstimulus interval: Theory and experiment. *Magn. Reson. Med.*, 43(4): 540–548.

Binder, J. R., Frost, J. A., Hammeke, T. A., Bellgowan, P. S., Rao, S. M., and Cox, R. W. (1999). Conceptual processing during the conscious resting state. A functional MRI study. *J. Cogn. Neurosci.*, 11(1): 80–95.

Birn, R. M., Cox, R. W., and Bandettini, P. A. (2002). Detection versus estimation in event-related fMRI: Choosing the optimal stimulus timing. *NeuroImage*, 15: 252–264.

Blamire, A. M., Ogawa, S., Ugurbil, K., Rothman, D., McCarthy, G., Ellermann, J. M., Hyder, F., Rattner, Z., and Shulman, R. G. (1992). Dynamic mapping of the human visual cortex by high-speed magnetic resonance imaging. *Proc. Natl. Acad. Sci. U.S.A.*, 89: 11069–11073.

Boynton, G. M., Engel, S. A., Glover, G. H., and Heeger, D. J. (1996). Linear systems analysis of functional magnetic resonance imaging in human V1. *J. Neurosci.*, 16: 4207–4221.

Brewer, J. B., Zhao, Z., Desmond, J. E., Glover, G. H., and Gabrieli, J. D. (1998). Making memories: Brain activity that predicts how well visual experience will be remembered. *Science*, 281: 1185–1187.

Buracas, G. T., and Boynton, G. M. (2002) Efficient design of event-related fMRI experiments using M-sequences. *NeuroImage*, 16: 801–813.

Dale, A. M. (1999). Optimal experimental design for event-related fMRI. *Hum. Brain Mapping*, 8: 109–114.

Dale, A. M., and Buckner, R. L. (1997). Selective averaging of rapidly presented individual trials using fMRI. *Hum. Brain Mapping*, 5: 329–340.

Donaldson, D. I., Petersen, S. E., Ollinger, J. M., and Buckner, R. L. (2001). Dissociating state and item components of recognition memory using fMRI. *NeuroImage*, 13: 129–142.

Dosenbach, N. U., Visscher, K. M., Palmer, E. D., Miezin, F. M., Wenger, K.K., Kang, H. C., Burgund, E. D., Grimes, A. L., Schlaggar, B. L., and Petersen, S. E. (2006). A core system for the implementation of task sets. *Neuron*, 50: 799–812.

Fair, D. A., Cohen, A. L., Dosenbach, N. U., Church, J. A., Miezin, F. M., Barch, D. M., Raichle, M. E., Petersen, S. E., and Schlaggar, B. L. (2008). The maturing architecture of the brain's default network. *Proc. Natl. Acad. Sci. U.S.A.*, 105: 4028–4032.

Greicius, M. D., Krasnow, B., Reiss, A. L., and Menon, V. (2003). Functional connectivity in the resting brain: a network analysis of the default mode hypothesis. *Proc. Natl. Acad. Sci. U.S.A.*, 100: 253–258.

Gusnard, D. A., and Raichle, M. E. (2001). Searching for a baseline: Functional imaging and the resting human brain. *Nat. Rev. Neurosci.*, 2(10): 685–694.

Huettel, S. A., Misiurek, J., Jurkowski, A., and McCarthy, G. (2004). Dynamic and strategic aspects of executive processing. *Brain Research*, 1000: 78–84.

James, W. (1890). *The Principles of Psychology*. Dover, New York.

Liu, T. T., Frank, L. R., Wong, E. C., and Buxton, R. B. (2001). Detection power, estimation efficiency, and predictability in event-related fMRI. *NeuroImage*, 13: 759–773.

Liu, T. T. (2004). Efficiency, power, and entropy in event-related fMRI with multiple trial types: Part II: Design of experiments. *NeuroImage*, 21: 401–413.

Mason, M. F., Norton, M. I., Van Horn, J. D., Wegner, D. M., Grafton, S. T., and Macrae, C. N, (2007). Wandering minds: the default network and stimulus-independent thought. *Science*, 315: 393–395.

McCarthy, G., Luby, M., Gore, J., and Goldman-Rakic, P. (1997). Infrequent events transiently activate human prefrontal and parietal cortex as measured by functional MRI. *J. Neurophysiol.*, 77: 1630–1634.

McCarthy, G., Puce, A., Luby, M., Belger, A., and Allison, T. (1996). Magnetic resonance imaging studies of functional brain activation: Analysis and interpretation. *Electroencephalogr. Clin. Neurophysiol. Suppl.*, 47: 15–31.

Mechelli, A., Price, C. J., Henson, R. N., and Friston, K. J. (2003). Estimating efficiency a priori: a comparison of blocked and randomized designs. *NeuroImage*, 18: 798–805.

Morcom, A. M., and Fletcher, P. C. (2007). Does the brain have a baseline? Why we should be resisting a rest. *NeuroImage*, 37: 1073–1082.

Raichle, M. E., MacLeod, A. M., Snyder, A. Z., Powers, W. J., Gusnard, D. A., and Shulman, G. L. (2001). A default mode of brain function. *Proc. Natl. Acad. Sci. U.S.A.*, 98: 676–682.

Sutton, S., Braren, M., Zubin, J., and John, E. R. (1965). Evoked-potential correlates of stimulus uncertainty. *Science*, 150: 1187–1188.

Ungerleider, L. G., and Mishkin, M. (1982). Two cortical visual systems. In *Analysis of Visual Behavior* (D. J. Ingle, M. A. Goodale, and R. J. W. Mansfield, eds.), pp. 549–586. MIT Press, Cambridge, MA.

Visscher, K. M., Miezin, F. M., Kelly, J. E., Buckner, R. L., Donaldson, D. I., McAvoy, M. P., Bhalodia, V. M., and Petersen, S. E. (2003). Mixed blocked/event-related designs separate transient and sustained activity in fMRI. *NeuroImage*, 19: 1694–1708.

Wagner, A. D., Schacter, D. L., Rotte, M., Koutstaal, W., Maril, A., Dale, A. M., Rosen, B. R., and Buckner, R. L. (1998). Building memories: remembering and forgetting of verbal experiences as predicted by brain activity. *Science*, 281: 1188–1191.

Yoo, S. S., Hu, P. T., Gujar, N., Jolesz, F. A., and Walker, M. P. (2007). A deficit in the ability to form new human memories without sleep. *Nat. Neurosci.*, 10: 385–392.

Chapter 10

Statistical Analysis: Basic Analyses

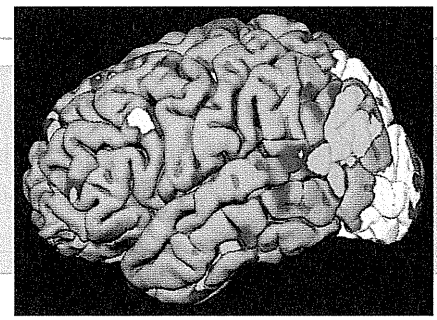

You have just completed data collection for the first subject of your first fMRI experiment. After careful consideration, you decided to use a simple two-condition blocked design. During task blocks, a series of famous names (e.g., Bill Clinton, David Beckham) flashed across the screen, while during non-task blocks, the names were of people unknown to the subject. You hypothesized that the task condition would be associated with greater activation in the fusiform gyrus, which is critical for face processing, because subjects would imagine the faces that go with the famous names. So, to evaluate this hypothesis, you calculated that the mean activation in the fusiform gyrus was 500 units during the famous-names blocks and 498 units during the unknown-names blocks. As you stare at these numbers, you realize that your hypothesis remains unanswered. The averages are numerically different, to be sure, but is the difference meaningful?

This example illustrates the use of **descriptive statistics**, or summaries of a data set. Any set of numbers can be described using statistics such as the mean, median, or standard deviation. But regardless of the experiment, the recorded data from a single subject do not provide a complete and unerring description of the world. Instead, the data represent just a single **sample**, or one set of observations out of the many that might have occurred in the experiment. If our subject had performed the task differently, or if we had selected a different subject, our data could have been very different. It is possible that the numerical differences between blocks, that we measured in this subject, were due to random variation, and would disappear if we used the subject in the same experiment a second time. As experimenters, we want to do more than just describe our observations; we want to make inferences about the underlying processes involved. Stated another way, we do not want to know merely whether the fMRI activation in the task block was greater than that in the non-task block within the particular set of data we recorded. Instead, we want to know whether the difference between conditions would be replicated in repeated observations from the same subject, from the same group of subjects, or from the population as a whole. To make such judgments, we must use **inferential statistics** that provide estimates of our certainty in the experimental hypothesis.

Recall from Chapter 9 that experiments should be designed to test a **research hypothesis**, often symbolized as H_1, that states a possible relationship

descriptive statistics Statistics that summarize the sample data but do not allow inferences about the larger population.

sample (1) A set of observations drawn from a larger population of potential observations. (2) An object to be imaged using magnetic resonance.

inferential statistics Statistics that make inferences about the characteristics of a population based on data obtained from a smaller sample.

research hypothesis A proposition about the nature of the world that makes predictions about the results of an experiment. For a hypothesis to be well formed, there must be some experiment whose outcome could prove it to be false.

null hypothesis The proposition that the experimental manipulation will have no effect on the experimental data. Most statistical analyses evaluate the probability that the null hypothesis is true, i.e., that the observed data reflect chance processes.

significance testing The process of evaluating whether the null hypothesis is true. Also known as hypothesis testing.

hypothesis-driven analysis The evaluation of data based on statistical tests of the validity of a null hypothesis.

between independent and dependent variables. Often only one hypothesis is stated, however, all experiments are designed to discriminate between two possible hypotheses, the research hypothesis and another, **null hypothesis** (H_0), which usually states that the manipulation has no effect. For the example described above, the null hypothesis (H_0) would be "Reading famous versus unknown names has no effect on fMRI activation in the fusiform gyrus." All well-formed hypotheses must be falsifiable, such that either the research or the null hypothesis, but not both, must be true. This can be seen by examining the typical mathematical form of the hypotheses:

$$H_1 : \text{Condition}_1 \neq \text{Condition}_2$$
$$H_0 : \text{Condition}_1 = \text{Condition}_2$$

Since the null hypothesis assumes that the independent variable has no effect, it predicts that the observed values of the dependent variable will be similarly distributed between the conditions. In the blocked design in our example above, the null hypothesis could assert that data obtained in the two conditions were drawn from the same distribution (i.e., some baseline level of activation + random, normally distributed noise), such that any differences between the blocks were caused by random fluctuations in the MR signal. For example, if the mean fMRI response during different non-task blocks ranged from 450 to 550 units, a value of 500 in a task block would be consistent with the null hypothesis. But if typical values for non-task blocks were from 497.95 to 498.05 units, then a task value of 500 would be unlikely to be due to chance, and we could reject the null hypothesis. The process of evaluating whether the observed data reflect experimental manipulations or chance processes is known as **significance testing**.

In the following sections, we explore a number of different approaches to the statistical evaluation of fMRI data. All of these **hypothesis-driven analysis** approaches differ in their assumptions and goals, but they share some common features. First, they express significance as the probability that the results could occur under the null hypothesis. The color maps that form the basis of many figures in fMRI manuscripts almost always express this probability, often with brighter, more-intense colors indicating a very low probability that the experimental effects are due to chance (Figure 10.1). Second, voxels whose probabil-

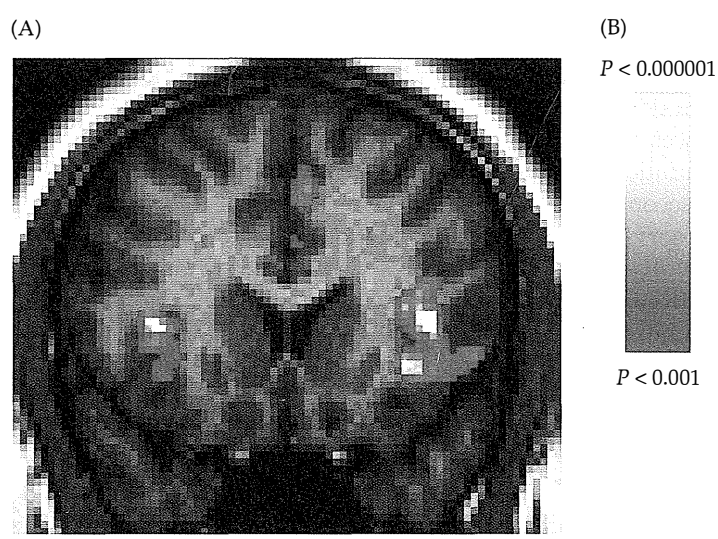

Figure 10.1 Statistical maps of fMRI data. Functional MRI data are usually displayed using a background anatomical MRI image with an overlaid statistical map (A). In the statistical map, voxels whose activation levels pass some threshold value are shown in color, with the intensity of the color corresponding to the degree of significance (B). More extreme significance values (lower probabilities) are usually shown in brighter colors. It is important to recognize that the colors represent the output of some statistical test, not absolute data values.

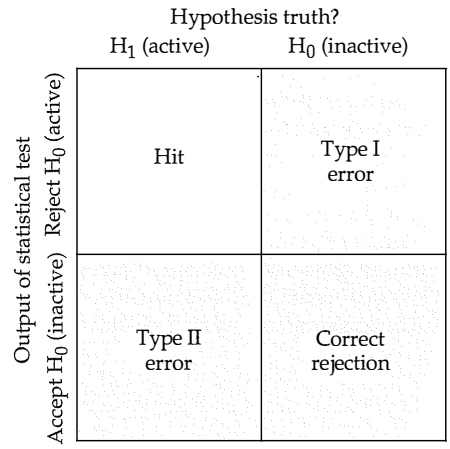

Figure 10.2 Types of experimental errors. When testing research hypotheses, there are four possible outcomes. The experimenter may reject the null hypothesis when it should be rejected; this is sometimes called a "hit," and in fMRI it corresponds to successfully identifying an active voxel. Rejecting the null hypothesis when it is in fact true is known as a Type I error, and in fMRI, this corresponds with labeling a voxel as active when it is not. Accepting the null hypothesis when it is in fact false is a Type II error; in fMRI, this is labeling a voxel as inactive when it is active. Type II errors are common in fMRI. Finally, accepting the null hypothesis when it is indeed true is called a "correct rejection."

ity levels are below a threshold probability, known as an alpha value, are labeled as significant and shown on the activation maps, while voxels whose probability levels are above the threshold are labeled as nonsignificant and not highlighted in color. The alpha value provides the probability of a Type I error, or deciding that the null hypothesis is false when it is really true (Figure 10.2). In terms of fMRI analyses, a Type I error means that a voxel was labeled as active when it was not (i.e., a false positive). Since fMRI studies may involve statistical tests on thousands of voxels, it can be challenging to decide on an appropriate alpha value. Third, the approaches to significance testing outlined in this chapter are generally conservative, in that they tend to exclude inactive voxels but do not detect all active voxels. This results in high rates of Type II error, or accepting the null hypothesis when it should be rejected (i.e., a false negative).

Just as no single experimental design is appropriate for all research questions, no single analysis approach can be used for all experiments. The correct analysis method for any given experiment depends on the experimental design, the hypotheses to be tested, and the type of error to be minimized. Therefore, in this chapter we discuss a number of different approaches to fMRI data analysis. We begin with simple analyses such as *t* and correlation tests and progress to the commonly used general linear model, which encompasses those simpler tests. We discuss the key issues that are specific to fMRI studies, including choosing an appropriate alpha value based on the number of voxels tested, and combining data from multiple subjects. We also describe a different approach to fMRI data processing called region-of-interest analysis, which has considerable power in elucidating the properties of anatomical and functional regions. Throughout, we emphasize the theory behind the different approaches to analysis, so that readers can make informed selections for their experiments. For equations and guidelines on implementing particular tests, we refer the reader to the statistical references listed at the end of this chapter. Note that we will consider a number of more advanced techniques, many of which adopt a different data-driven approach for fMRI data analysis, in the following Chapter 11.

Basic Statistical Tests

The simplest and oldest of all statistical tests can be used on the data shown in Figure 10.3. The data are the BOLD changes in a motor cortex voxel, associated with brief hand movements made in response to the periodic presentation of a 3 s duration stimulus. Following every presentation of the stimulus, there was an increase in signal that lasted for about 10 s. How do we know whether this voxel exhibits task-related activation? In this case, we can use the venerable interocular trauma test, which can be stated succinctly: the comparison is significant if the data, when plotted, hit you between the eyes. In the

alpha value An a priori probability (e.g., 0.001) chosen as the threshold for statistical significance. If the probability that the data would be obtained under the null hypothesis is less than the alpha value, the data are considered to be statistically significant.

Type I error Rejecting the null hypothesis when it is in fact true. Also known as a false positive.

Type II error Accepting the null hypothesis when it is in fact false. Also known as an incorrect rejection or false negative.

interocular trauma test An intuitive test of significance based on highly visible effects of the experimental manipulation. It states that data are significant if, when plotted, they hit you between the eyes.

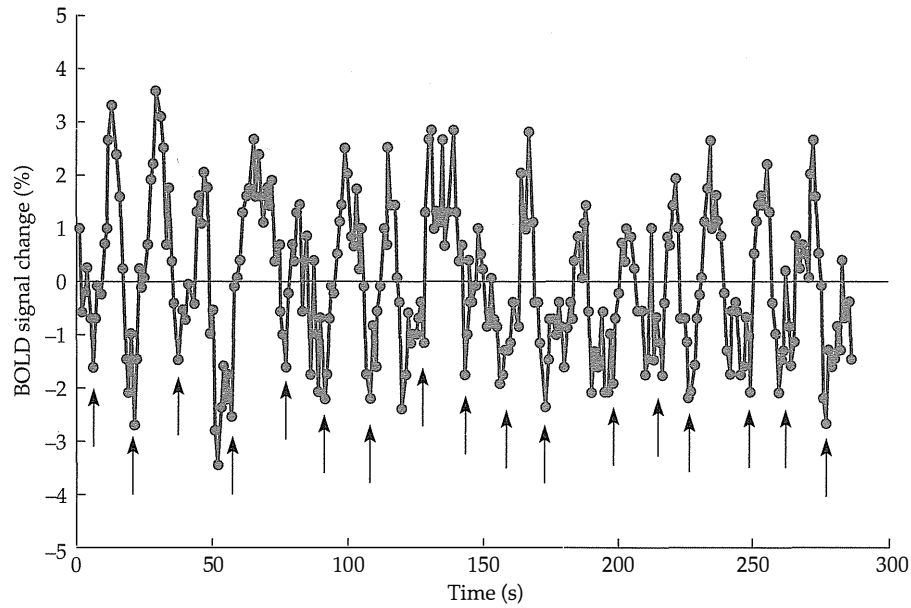

Figure 10.3 Use of the interocular trauma test for statistical significance. For some data, the effect of the experimental manipulation can be readily ascertained just by looking at the data. In this voxel, each time a brief visual stimulus was presented (arrows), there were significant increases in activation. From looking at these data, it is obvious that stimulus presentation elicited an effect. Most fMRI data, however, are not so easily analyzed!

plotted data, the effect of the independent variable is obvious, because every time the stimulus was presented there was a very large change in the dependent variable. If only all fMRI data were so simple to analyze! As discussed in Chapter 8, the SNR in most fMRI experiments is quite low, so effects are rarely so easy to spot in the raw data. Researchers must instead use formal significance testing to evaluate whether the experimental manipulation has any effect.

In this section, we describe some simple forms of statistical analysis and how they can be applied to fMRI data. But recognize that, with minor exceptions, these types of analyses are no longer common in fMRI research. They have been replaced by the more powerful and flexible regression approaches described in the following section. Nevertheless, they provide a good introduction to the two core concepts of fMRI data analysis: assessing whether two or more independent variables have significantly different effects on the BOLD signal, and creating models for the expected effects of independent variables.

Contrasting experimental conditions: the t*-test*

In a standard two-condition blocked design, the null hypothesis is simple: the difference between the conditions has no effect on the fMRI data. As described in the introduction to this chapter, a simpleminded way to compare the conditions would be to calculate the difference between the means of the data produced under each condition (i.e., 500 units versus 498 units). This comparison follows the logic of subtraction advanced in the previous chapter. However, a difference between condition means, by itself, is uninformative. It is necessary to evaluate whether that difference is large compared with some measure of the variability in the data, such as the standard deviation.

So, under the null hypothesis, any difference between the mean of the fMRI data recorded in Condition 1 and the mean of the data recorded in Condition 2 is due to random chance. The *t*-distribution describes the expected difference between two random samples drawn from the same distribution (Figure 10.4). The mean of the *t*-distribution is zero, since the two samples should on average have the same mean value, and the standard deviation of the *t*-distri-

subtraction In experimental design, the direct comparison of two conditions that are assumed to differ only in one property, the independent variable.

standard deviation A commonly used measure of the variability within a sample of data points.

distribution The pattern of variation of a variable under some conditions. For example, the normal distribution has a characteristic bell shape.

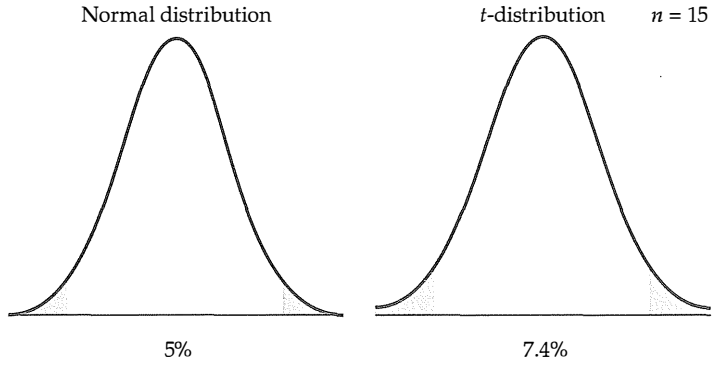

Figure 10.4 The normal distribution and the Student's t-distribution. The normal distribution is a bell-shaped curve that describes the variability in many random processes, and is the distribution of data from a large number of independent events. Many variables are distributed normally. The Student's t-distribution is a distribution of the means of samples drawn from a larger population, which may or may not be normally distributed. The t-distribution resembles the normal distribution at larger sample sizes ($n > 30$), but with fewer degrees of freedom, it is narrower near the center and has more of its values near the tails (shaded areas, percentages indicated below).

bution (i.e., the standard error of the mean) is the sample standard deviation divided by the square root of the sample size. Note that the t-distribution looks generally similar to the normal distribution, but has more extreme values, especially at small sample sizes. When the sample size is very large, however, the shape of the t-distribution approaches the shape of the normal distribution.

To conduct a t-test (Equation 10.1 and Figure 10.5), the researcher calculates the means for all data points in the two conditions (and) and divides their difference by the shared standard error (σ_{xy}):

$$t = \frac{\bar{x} - \bar{y}}{\sigma_{xy}} = \frac{\bar{x} - \bar{y}}{\sqrt{\sigma_x^2 + \sigma_y^2}} \tag{10.1}$$

The resulting t-statistic can then be converted to a probability value based on the degrees of freedom (df), or the number of unconstrained data points. For many statistical tests, the number of degrees of freedom within a sample is equal to the number of data points minus one. As an example, for a sample of 20 data points with a known mean value, there are 19 degrees of freedom, since if you know 19 of the data points and the mean, you can calculate the twentieth data point. Once the probability of the t-test has been determined using a statistical table or calculator, the researcher compares that probability with the alpha value for the experiment. For example, imagine that 25 time points were collected for each condition, and that the difference between the means is seven units, and the shared standard error is two units. The resulting t-statistic has

t-test A test for statistical significance based on the Student's t-distribution. The t-test typically evaluates whether the mean values of two sets of observations are sufficiently different to preclude their being drawn from the same distribution.

standard error A commonly used estimate of the likely discrepancy between a measured value and a true value, often calculated from a measure of variability in the data (i.e., the standard deviation) and the number of data points in the sample.

degrees of freedom (df) The number of independent observations within a data set. For many statistical tests, there are $n - 1$ degrees of freedom associated with n data points.

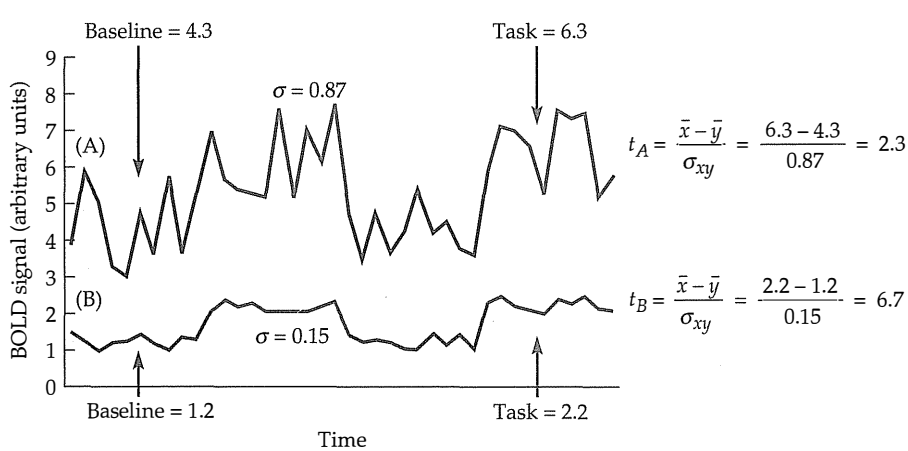

Figure 10.5 Conducting a t-test. The t-test compares the size of an effect (e.g., the difference between blocks) with the variability in the data (i.e., the shared standard error of that difference). Shown here are two simulated fMRI time courses. In plot A, the effect of the experimental manipulation is 2 units in amplitude, but the variability is relatively high, so the t-statistic is about 2.3. In plot B, the manipulation only has a 1-unit effect, but the variability is much smaller, and the resulting t-statistic (6.7) is much higher.

contrast (1) The intensity difference between different quantities being measured by an imaging system. It also can refer to the physical quantity being measured (e.g., T_1 contrast). (2) A statistical comparison of the activation evoked by two (or more) experimental conditions, in order to test a research hypothesis.

a value of 3.5. The researcher wants to evaluate this statistic against the experiment's alpha value, which has been set at 0.01. With 48 degrees of freedom (i.e., 24 from each group), we can calculate that there is less than a 0.001 chance that the data in these conditions were drawn from the same distribution. This probability is lower than the threshold alpha value, and thus the null hypothesis can be rejected.

Here we introduce the first of the core concepts for fMRI data analysis: experimental contrast. This very important term refers to a comparison between the activation levels evoked by two independent variables (or two levels of the same independent variable). The concept of experimental contrast has broad similarities to the idea of image contrast introduced in Chapter 1, where the term was used to describe differences between two forms of tissue in anatomical imaging. In a deep sense, the fundamental goal of fMRI analyses is to evaluate whether an experimental manipulation evoked a meaningful change in activation; in other words, whether a contrast between two conditions was statistically significant.

A primary challenge in adapting the logic of a *t*-test to fMRI lies in deciding which time points should be assigned to which experimental conditions. This problem is illustrated in Figure 10.6. Consider a standard alternating blocked-design fMRI study with two conditions, each of 20 s duration. If you repeated this design two times and collected fMRI data with a 1 s TR, then you would have a total of 80 time points in the dataset. Which time points should be assigned to condition A and which should be assigned to condition B? An obvious first option would be to assign the first 20 points to A, the next 20 to B, and so forth. But remember from Chapter 7 that the BOLD fMRI response lags behind neuronal activity. Therefore, a better approach would account for this lag by delaying the onset of all blocks (e.g., by about 6 s). But even this approach is imperfect. Because changes in the BOLD response are not instantaneous, there will be transition periods at the onset of each block where the measured fMRI signal will be changing from low to high or from high to low. By excluding these highly variable transition periods and sampling only the

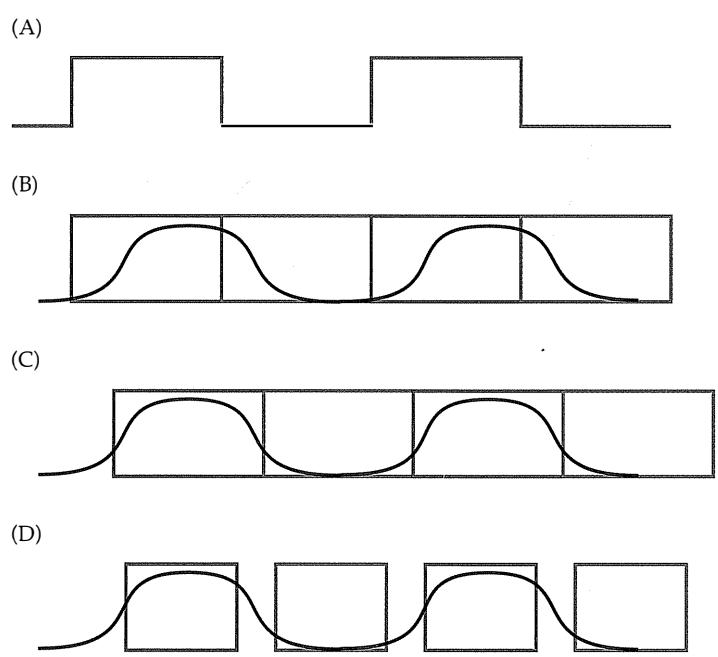

Figure 10.6 Assigning time points in a blocked design to conditions within a *t*-test. Consider the simple alternating blocked design shown in (A); red, task; blue, non-task. If we convolve this design with a hemodynamic response, we get the time course of activation shown by the black line in (B). Because of the hemodynamic latency, the predicted amplitude of the BOLD signal does correspond well to the timing of the original experimental design. By introducing a lag to the time points corresponding to conditions in the *t*-test (C), we can better fit the true timing of activation, although the transition periods between the blocks can introduce noise into the analyses. Excluding the block transitions (D) can further distinguish experimental conditions.

latter parts of each block, the researcher can select time points where the BOLD response has reached a steady state, maximizing the power of the *t*-test.

The *t*-test is used with the assumption that the data are drawn from normal distributions with equal variability, however, one of the strengths of the *t*-test for fMRI is that it is relatively insensitive to violations of this assumption. Even in a short fMRI session, there will be at least a few tens of time points collected per voxel, and in many sessions, hundreds of data points are collected per voxel for each condition. At these sample sizes, deviations from normality have no meaningful effect on the outcome of the test. Likewise, with large samples, the conditions may have very different numbers of time points or have different variability without compromising the outcome of the *t*-test. However, although the *t*-test may be statistically valid for fMRI data, several potential concerns do exist. Any systematic difference between the experimental conditions, whether associated with meaningful BOLD activation or with uninteresting artifacts like scanner drift or head motion, could result in a significant *t*-test (Figure 10.7). This is particularly a problem in blocked studies that have only a few cycles of the task and non-task conditions. The *t*-test is also inappropriate for answering questions about the timing of activation, since it combines data from all time points within a condition. Note also that while the *t*-test evaluates differences between the means of two distributions, it is insensitive to differences in their variability or shape. To find such differences, a Kolmogorov–Smirnov (K–S) test can be used.

While this discussion has focused on blocked designs, *t*-tests are also useful for some analyses of event-related designs. Remember that the basic role of the *t*-test is to identify a significant difference between the means of two samples of data. If a research question focuses on specific data points within an event-related design, then a *t*-test may be appropriate. Event-related designs may compare the magnitude of fMRI activation at a given time point between two different experimental conditions. For example, in a study published in

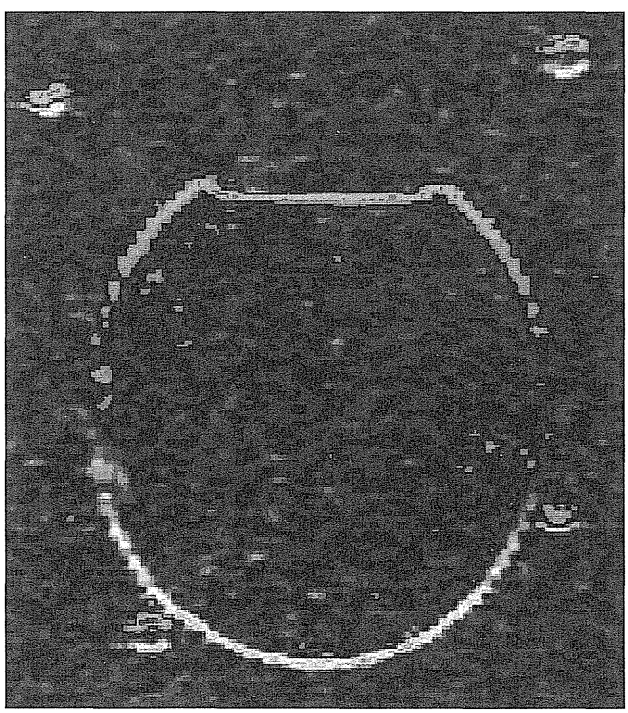

Figure 10.7 Effects of scanner drift on *t*-tests. Shown here is an activation map of a phantom, with positively significant voxels shown in the green-to-yellow color range and negatively significant voxels shown in the blue-to-pink color range. The position of the phantom "moved" slightly along the frequency-encoding direction (top to bottom) due to slow changes in the center frequency of the scanner over time. Even though there was no true activation, this motion within the images was significant according to the *t*-test.

2006 Cantlon and colleagues presented subjects with a series of visual patterns, most of which had the same number of elements, all with the same shape. In deviant trials, the pattern changed to a different number of elements (e.g., 32 instead of 16) or to elements with a different shape (e.g., squares instead of circular dots). The authors calculated the mean signal change over a pre-stimulus baseline in each voxel, for each time point from 3 s before to 12 s after every trial. A set of *t*-tests were used to evaluate whether activation in each voxel at the expected peak of the hemodynamic response (4.5–7 s after each event) was significantly greater after deviants with a number change versus deviants with a shape change. (Note that another set of between-subjects *t*-tests were used to determine whether the distribution of significance values in each voxel differed from chance expectation. This will be discussed in the section on Inter-subject Analyses later in this chapter.)

In summary, regardless of the experimental design, if the research question can be answered by evaluating whether or not two samples have statistically different means, then a *t*-test may be appropriate. Yet, univariate statistical tests such as the *t*-test have significant weaknesses. Because they are used to compare samples that differ in only one independent variable they are not appropriate when the experiment involves multiple variables. These types of test are best used when data points can be classified into distinct categories (e.g., activated versus not activated); conversely, they are difficult to apply to complex event-related designs. And, because these tests compare the relative magnitude of activation between conditions, they cannot be used to determine whether a given event type evoked a pattern of activation that was consistent with a predicted shape for the fMRI hemodynamic response. In the next section we consider a type of analysis that overcomes some of these limitations (while introducing new limitations of its own).

Comparing experimental and predicted responses: correlation analyses

While the *t*-test can be applied to many fMRI studies, it cannot be used to analyze the shape of the hemodynamic response. Indeed, when excluding transitions between task blocks, information about the shape of the response is explicitly removed. Nevertheless, the fMRI signal does contain important timing information. As discussed in Chapter 7, the fMRI hemodynamic response takes about 5 s to rise to its maximum after the onset of brief neuronal activity. Following the cessation of neuronal activity, the hemodynamic response falls over a period of 5 to 10 s and then stabilizes at a below-baseline level for an extended interval. The consistency of this pattern in the hemodynamic response allows us to predict the change in fMRI activation that should be evoked in an active voxel. Using a correlation analysis, we can quantify how well the observed data match a canonical hemodynamic response, thus identifying voxels in which the fMRI time course reflects underlying neuronal activity. Correlation analyses were first reported in fMRI by Bandettini and colleagues in 1993 and have since been an important part of fMRI analyses. In early fMRI studies, correlation tests were used to identify voxels with significant levels of activation. Now, the idea of correlation forms the core of regression analyses.

correlation analysis A type of statistical test that evaluates the strength of the relation between two variables. For fMRI studies, correlation analyses typically evaluate the correspondence between a predicted hemodynamic response and the observed data.

Conducting a correlation analysis on fMRI data is very simple. First, identify an epoch from your experimental data that should contain some task-related signal change, and predict the hemodynamic response that should be observed during that epoch. Second, calculate the covariance between the

experimental data (here, x) and the predicted hemodynamic response (here, y), which is indicated by the numerator in the right term of Equation 10.2:

$$r = \frac{1}{n-1} * \frac{\sum (x-\bar{x})(y-\bar{y})}{\sigma_x \sigma_y} \tag{10.2}$$

In essence, that numerator takes each observation (e.g., each time point), compares its experimental and predicted values to their mean values, and then sums the product over every observation. A positive covariance indicates that when the experimental data were large, the predicted data tended to be large; likewise, when one was small, the other was small. But if the covariance is negative, the values of the experimental data tended to be small while the values of the predicted data were large, or vice versa.

The third step in conducting the correlation analysis is to normalize the covariance by dividing it by the product of the standard deviations of the two epochs ($\sigma_x \sigma_y$). The resulting correlation coefficient, or r-value, can range from +1.0 to –1.0, or from perfect positive correlation to perfect negative correlation. A correlation of 0 indicates that the experimental data are not related to the predicted data. As with the t-test discussed in the previous section, the significance of the correlation coefficient can be evaluated using statistical tables based on the degrees of freedom; a correlation of 0.5 is more likely to be significant when based on 1000 data points than when based on 10. This basic correlation analysis is then repeated for every voxel in the brain to create the map of significant activation.

We now introduce the second of the core concepts for fMRI data analysis: building a model of the predicted fMRI response. In the language of statistics, a model is a collection of independent variables that together predict the likely outcome of the dependent variable. Each independent variable is called a regressor (also known as a predictor variable or a model factor). A basic fMRI correlation analysis is equivalent to a model with one regressor: a canonical hemodynamic response. If a voxel's data match the predicted values of the regressor, as determined by the significance of the correlation coefficient, then that voxel is considered to be activated by the experimental manipulation (Figure 10.8).

Given the differences between correlation and t-tests, it may surprise you that when they are applied to the same data set, they give identical results. Remember that the t-test evaluates whether data derived from one condition

correlation coefficient (r-value) A number between –1 and 1 that expresses the strength of the correlation between two variables.

model A collection of independent variables (and the relationships between those variables) that serve to predict a dependent variable.

regressor A hypothesized time course of BOLD activation caused by the manipulations of an independent variable or by another known source of variability.

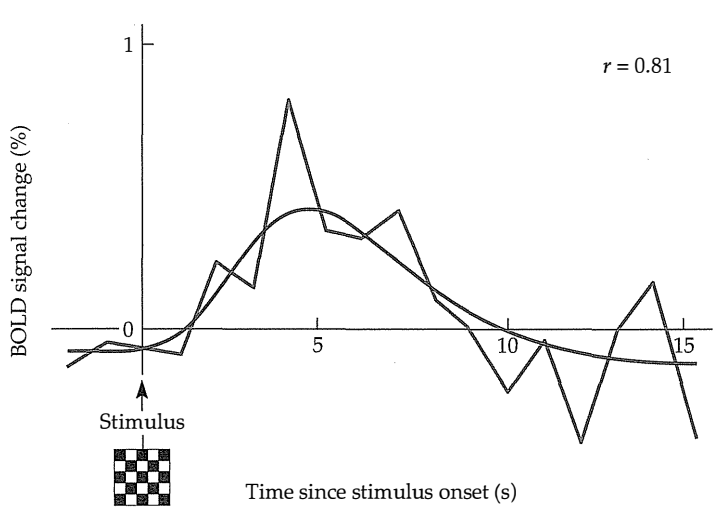

Figure 10.8 Correlation analyses match experimental data with a hypothesized hemodynamic response. Shown in blue is a hypothetical mean hemodynamic waveform, as would be obtained from averaging many trials of the same event (e.g., a flash of a visual checkerboard). The red curve indicates the hypothesized BOLD hemodynamic response. The correlation between these two time-courses can be calculated as $r = 0.81$, which would reflect a highly significant correlation. While few current fMRI studies use such literal correlations, the concept of comparing observed data to a predicted waveform underlies nearly all fMRI analyses.

differ from data obtained during another condition. Exactly the same test could be conducted by correlating the experimental data with a predicted data set that follows a boxcar waveform (i.e., in task blocks the predicted response would be 1, while in non-task blocks the response would be 0). This similarity is often seen in graphical representations of experimental designs, in which the different conditions are plotted as different values along the y-axis, and can be demonstrated using any sample data set and Equations 10.1 and 10.2. For any value of r, there is a corresponding value of t, given the degrees of freedom in the data. Note also that both tests measure signal change divided by non-signal variability, with the t-test using the difference between means and the correlation test using the more general measure of covariation. Thus, the power of the correlation coefficient (like the t-test) rests on having maximal variability in the signal of interest compared with noise. Furthermore, if the values of either the experimental or predicted data are distributed in a highly non-normal fashion, then the correlation statistic may not be meaningful. This may occur in fMRI studies if there are very long pre-stimulus or post-stimulus baseline periods, so that most data points in the prediction epoch are near zero.

Correlation analyses have often been used in conjunction with signal averaging. Averaging across stimulus epochs improves the estimate of the time course of activation in a voxel or region, increasing the power of a correlation test for detecting significant voxels. And, collecting epochs from different times within an experiment can minimize some potential sources of variability in the hemodynamic response (e.g., low-frequency drift, practice or fatigue effects). Signal averaging can also inform the choice of the predicted hemodynamic response. Using some canonical function may seem attractive, however, recall from Chapter 8 that the characteristics of the hemodynamic response may differ between subjects, brain regions, and stimuli. Such differences can reduce the significance of correlation tests. One way of overcoming this problem is to generate a unique hemodynamic response for each subject, based on averaged data collected during a screening run, using a task that targets some region of interest.

Correlation analyses have significant limitations. Identifying discrete epochs can be challenging if events of interest overlap or follow closely in time. Conversely, if events are widely spaced, some of the fMRI data will make minimal contributions to the analyses. Another problem is inherent in the correlation statistic, which depends only on the covariance between two variables. Suppose that you compare responses to two types of stimuli (e.g., upright and inverted faces) that evoke activation in the same brain region, but with one (e.g., upright faces) generating twice the activation amplitude as the other. The time course of activation evoked by each of these stimuli could be the same, making them each highly correlated with a predicted hemodynamic response. To test whether these two stimuli evoked different levels of activation, you would need to use a statistic that compares the amplitude of the evoked activation *between* two conditions, such as the t-test described in the previous section. And, for experimental designs that involve events or blocks that occur with a regular frequency, analysis methods that directly measure those frequency changes can be much more sensitive (see Box 10.1).

We emphasize that the techniques described so far, the t-test and correlation analyses, have complementary strengths. The former allows us to evaluate contrasts between experimental conditions, whereas the latter allows us to create models for expected fMRI activation. Both of these strengths are manifest in regression modeling, which now forms the basis for nearly all fMRI data analysis.

BOX 10.1 Identifying Task-Related Periodicity: Fourier Analyses

As discussed in Chapter 9, a blocked-design fMRI task presents stimulus conditions at regular intervals. As a consequence, the MR signal within an active voxel regularly rises during task blocks and falls during non-task blocks. The periodic nature of this signal change can be quantified using a **Fourier transform.** The Fourier transform expresses a temporally (or spatially) varying signal as the linear sum of a series of sine waves of different frequencies, amplitudes, and phases. A plot of the magnitude of each sine-wave component necessary to recreate the original signal is called a power spectrum. Thus, the power spectrum itself is another way of representing the original data. In the language of signal processing, the raw fMRI time series data are in the **time domain,** meaning that they show the relative intensity of the signal at each time point. The power spectrum represents the same data in the **frequency domain,** indicating the intensity of the signal at each component frequency. If a task-related signal rises and falls at a known frequency, then a peak will

(continued on next page)

Figure 1 Use of a Fourier analysis to calculate frequency and phase information from the BOLD signal. This patient, who had an arteriovenous malformation (AVM) in the left hemisphere (right side of image at center), participated in blocked-design motor squeeze tasks that began either with a left-hand squeeze or a right-hand squeeze. Data from primary motor cortex in each hemisphere are shown in the graphs, with the left hemisphere data shown on the right side of the figure. The raw data are shown in the upper graphs, the power spectra are shown in the middle graphs, and the phase at the task frequency (peak in spectra) is shown at bottom. Note that although both hemispheres had peaks at about the same frequencies, the phases were different, allowing dissociation of right-hand and left-hand activation.

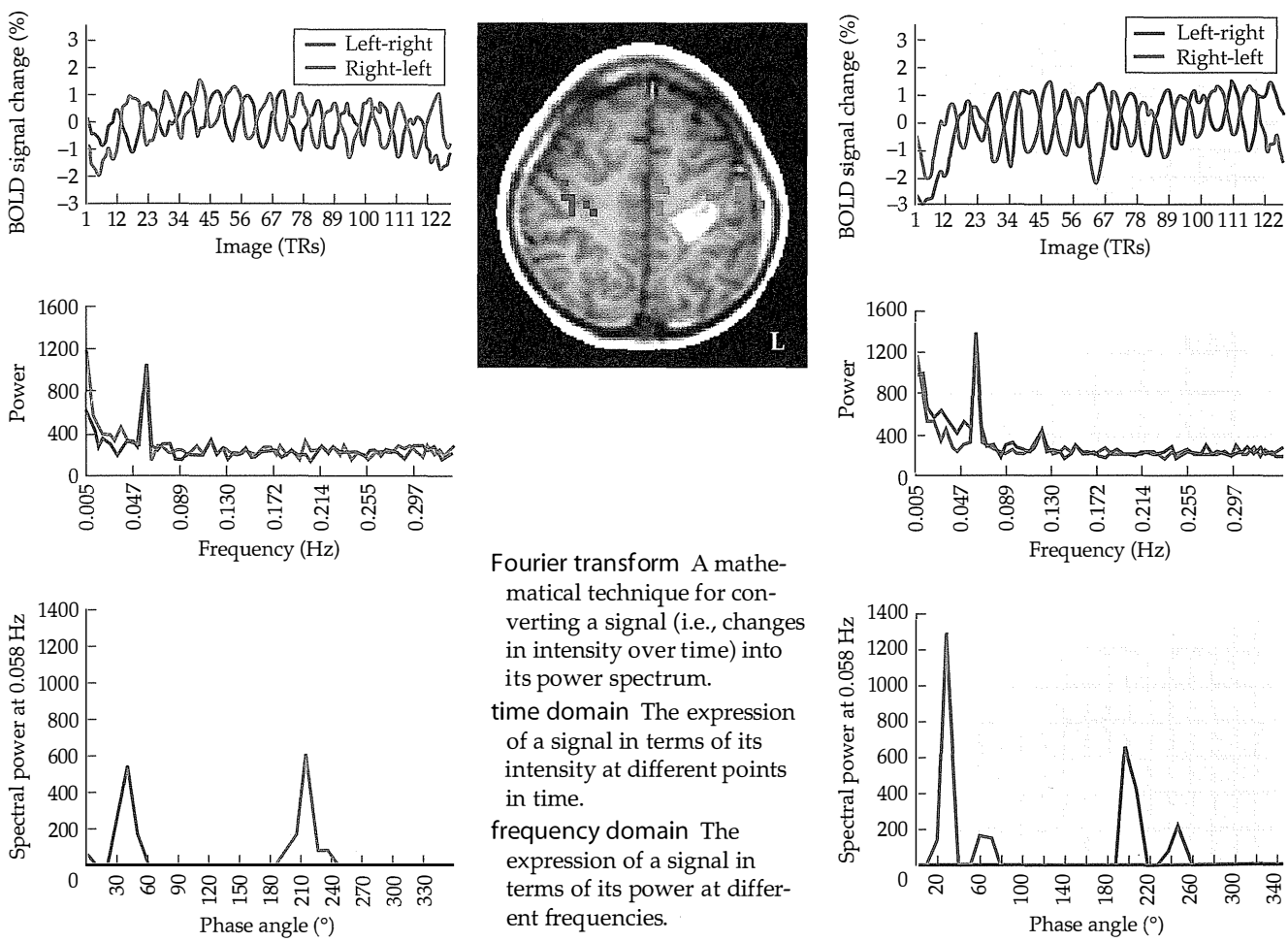

Fourier transform A mathematical technique for converting a signal (i.e., changes in intensity over time) into its power spectrum.

time domain The expression of a signal in terms of its intensity at different points in time.

frequency domain The expression of a signal in terms of its power at different frequencies.

BOX 10.1 *(continued)*

occur at that frequency in the power spectrum. We discussed in Chapter 8 the use of the Fourier transform to remove unwanted variability from the data, and here we extend that discussion to consider its use for statistical analysis of task-related variability.

In practice, the frequencies that can be measured by a Fourier analysis depend on how often the BOLD time series is sampled. The basic rule of sampling, the Nyquist sampling theorem, states that to accurately measure a given frequency, you must sample at a minimum of twice that frequency. Thus, the Fourier transform of n time points sampled at a given TR contains $n/2$ frequencies ranging from 0 Hz to $1/(2 \times \text{TR})$ Hz, which are represented along the x-axis of the power spectrum. The first frequency component, at 0 Hz, represents the mean intensity of the signal and is often called the DC component, after the electrical term for direct current (i.e., a constant-voltage power source). Since fMRI time courses are generally represented in arbitrary units with positive values proportional to the amount of current through the receiver coil, the DC component is generally positive and very large. Also present in almost all fMRI data, even from very stable scanners, is substantial low-frequency power associated with scanner drift, among other factors (see Chapter 8). There are also slow physiological changes due to vascular oscillations, although such effects are incompletely understood. Because of this power at low frequencies, very long block lengths are not ideal for fMRI.

Figure 2 The use of overlapping blocks with different frequencies. If several different classes of stimuli are presented at different frequencies, a Fourier transform can be used to separate activation associated with each. Here, faces are presented most frequently, animals are presented at an intermediate frequency, and objects are presented least frequently. Each is presented individually in an alternating blocked design, with scrambled objects as the control condition. Note that what subjects see changes at different points in the task, as shown in the sample visual displays at the top of the figure. Some of the time, all three categories will be present, while at other times, only one or two of the categories will be visible.

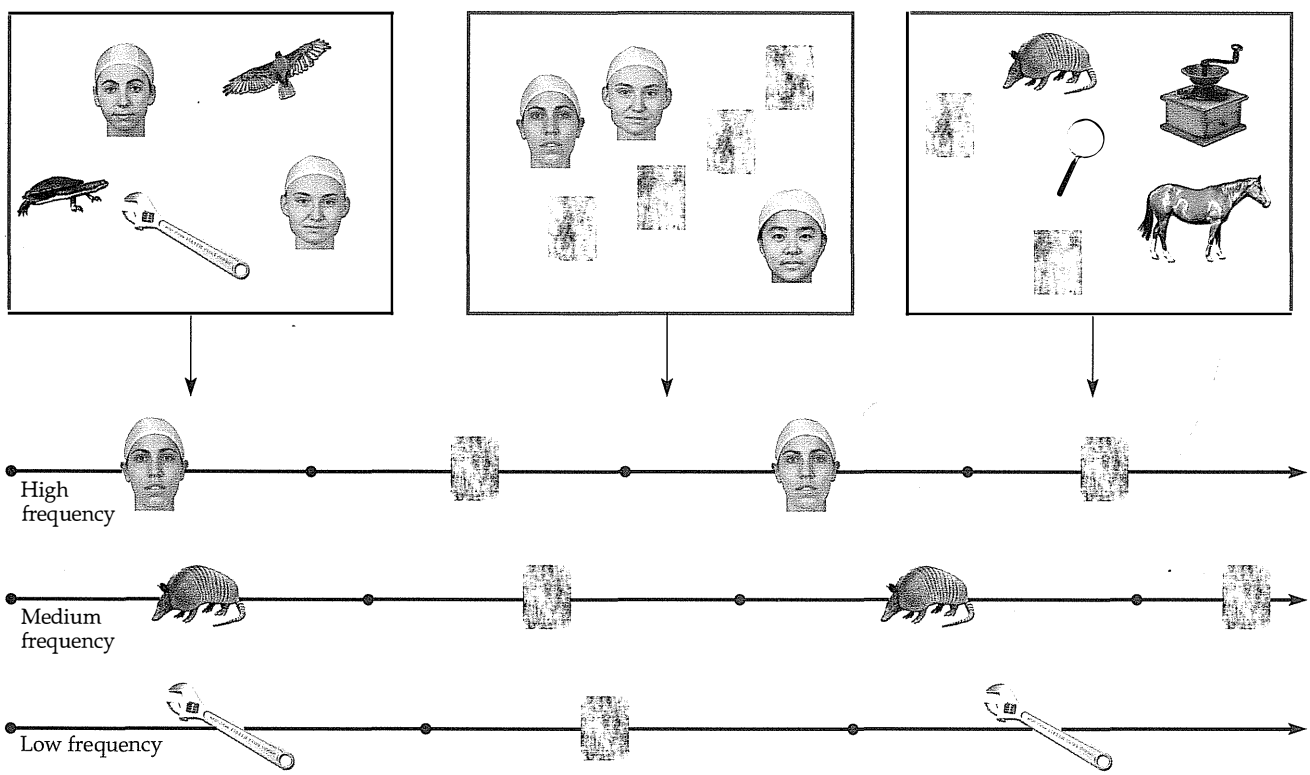

Regression Analyses

Nearly all fMRI data analyses share a single goal: model testing. Based on the timing and duration of events—or, more specifically, the timing and duration of the evoked neuronal activity—researchers generate a predicted hemodynamic response, guided by the concepts of scaling and superposition introduced in Chapter 7. These models contain predicted time courses for the entire session, rather than for individual epochs as described above for correlation analyses. And, they typically contain several distinct predictions (i.e., regressors) that correspond to different hypothesized processes (e.g., visual processing, retrieval from memory, and motor responses). The relative contribution of each of these regressors to the measured data, within each voxel, is then statistically evaluated using a technique known as multiple regression.

The core idea of regression is that the value of the observed data (y) can be attributed to two sources: a model comprising a linear combination of several regressors (x_i), each with a variable weighting (β_i); and residual noise in the data, or error in the measurements (ε). The basic formula for a regression analysis is given in Equation 10.3:

$$y = \beta_0 + \beta_1 x_1 + \beta_2 x_2 + \cdots + \beta_n x_n + \varepsilon \tag{10.3}$$

By convention, the Greek letter beta represents the parameter weight (β_i), or how much each regression factor contributes to the overall data. The term β_0 reflects the total contribution of all factors that are held constant throughout the experiment. For fMRI data, this would include the baseline signal intensity (i.e., mean T_2^* signal given the pulse sequence parameters) in each voxel, as well as any evoked activation that is constant throughout the experiment. Researchers sometimes colloquially refer to the parameter weights, which are calculated during regression analyses, as "beta values" or "betas." The symbol β should not be confused with the roman letter B, which is used to indicate magnetic field strength (or a magnetic field vector, **B**).

Regression models like that in Equation 10.3 have only one known quantity: the experimental data (y). The regressors (x_i) represent hypothesized factors that may or may not contribute to the data. Given the data and a specified set of regressors, the researcher can identify a combination of parameter weights that minimizes the error term. To evaluate the statistical significance of a regressor, the amount of variability it explains (when multiplied by its best-fitting parameter weight) is compared with the amount of variability explained by the error term. This statistical approach, when applied to data sets with many dependent variables, is known as the general linear model (GLM).

The general linear model: an overview

In fMRI experiments, the simple equation given above for the general linear model (Equation 10.3) is replaced by a set of matrices (Figure 10.9). The fMRI data (y) are represented as a two-dimensional data matrix consisting of n time points by V voxels. Note that the spatial structure of the fMRI data is not used in the general linear model, since the values of the parameter weights and error term are calculated independently for each voxel. Instead, all voxels in the imaging volume are arranged along one dimension, for ease of calculation. The design matrix, which specifies the linear model to be evaluated, consists of M regressors, each n time points in length. In some notation systems, the design

multiple regression A family of statistical approaches that evaluate the relative contributions of several independent variables to a dependent variable.

residual The variability in the data that remains unexplained after accounting for the model factors.

parameter weights For most fMRI analyses, quantities that reflect the relative contributions of the different model factors to the observed data within a given voxel.

general linear model (GLM) A class of statistical tests that assume that the experimental data are composed of the linear combination of different model factors, along with uncorrelated noise.

data matrix A representation of the measured fMRI data in two-dimensional form (i.e., voxels by time points).

design matrix In fMRI implementations of the general linear model, the specification of how the model factors change over time.

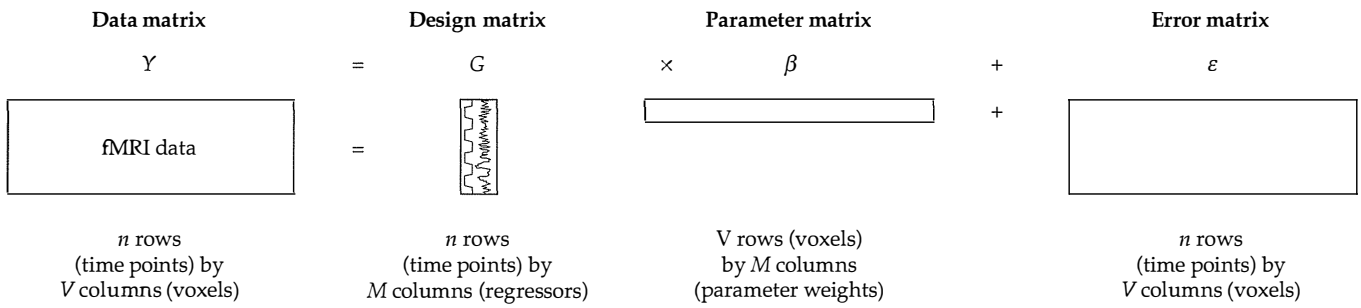

Figure 10.9 Basic principles of the general linear model in fMRI. The general linear model attempts to find the set of experimental parameters (β) for a design matrix (G) that best accounts for the original data (Y), by minimizing the unexplained error (ε).

matrix is denoted as G. The parameter matrix contains M parameter weights and V voxels, such that each cell indicates the β-value for a given voxel. Finally, the error matrix expresses the residual error for each voxel, and thus is an n-by-V matrix. Of these four matrices, the data are obtained experimentally, the design matrix is constructed by the experimenter based on the hypothesized effects of the experimental manipulations, and the parameter weights and residual error are calculated during the analysis.

The general linear model is elegant in its simplicity. After the data are obtained and the design matrix has been established, only one question must be answered: what values for the parameter matrix lead to the smallest values in the error matrix? To understand this process, consider a simple experiment in which the subject squeezes her hand every 20 s, while fMRI data are recorded over 60 time points with a TR of 1 s. You hypothesize that voxels associated with motor processing should show three distinct hemodynamic responses, one following each of the three hand squeezes. The design matrix would thus contain a single column with 60 values. The highest values would occur at around 4–6 s after each hand squeeze (i.e., at the peak of the hemodynamic response) and the lowest values would occur immediately before each hand squeeze (i.e., following the cessation of the hemodynamic response).

Your next task is to evaluate how much this hypothetical time course contributed to the real data, compared with variability outside of the model. Since fMRI data consist of many time points, the residual errors for a given voxel must be combined from all time points into a single value. A formula for combining many error values into one summary statistic is known as a cost function. In the general linear model, the standard cost function is the least-squares error, or the sum of all squared residuals (thus introducing greater penalties for very large errors). Choosing the least-squares error as a cost function allows the general linear model to be solved using a small set of matrix operations (see the statistical references cited at the end of the chapter for details). In this example, the parameter matrix consists of a single parameter (β_1) for each of the V voxels. Note that the parameter only provides an estimate of the relative signal amplitude evoked by the experimental manipulation (i.e., the size of the response in that voxel). To obtain a statistic, the value of the parameter must be divided by the residual error. Under the null hypothesis, this quantity should follow a statistical distribution called the F distribution, and so its significance can be evaluated as a function of the available degrees of freedom (which depend on both the number of time points and the number of regressors).

You may have noticed that both the general linear model and a correlation analysis calculate significance based on how well the experimental data fit a prediction. If that prediction contains only one regressor based on the convolution of events with a hemodynamic response, then the correlation analysis and the general linear model will provide similar statistics. The t-test can

parameter matrix A matrix that describes the relative contributions of each model to the observed data for each voxel.

error matrix That component of the fMRI data that is unexplained by the design matrix, when fit by the parameter matrix.

cost function A quantity that determines the amount of residual error in a comparison.

least-squares error A commonly used cost function, the sum of the squared residuals.

TABLE 10.1 Some of the Major Statistical Packages Available for the Analysis of fMRI Data

Package	Availability	Web site
AFNI	Freely available	afni.nimh.nih.gov/afni/
Brain Voyager	Commercial	www.brainvoyager.com
FSL	Freely available	www.fmrib.ox.ac.uk/fsl/
SPM	Freely available	www.fil.ion.ucl.ac.uk/spm/
VoxBo	Freely available	www.voxbo.org

also be incorporated into the general linear model, by using a regressor with only two discrete levels, one for each of two conditions within a blocked design. Even the Fourier transform can be expressed using a general linear model, although the necessary design matrix would be very complex, because it would need to contain a large number of independent frequency components.

The general linear model provides the theoretical framework that underlies most fMRI data analysis, regardless of the experimental design. All major fMRI statistical packages include routines for data analysis using the general linear model, although the specific implementation routine depends on the package (Table 10.1). However, each shares the same basic set of simple algorithms and assumptions. In short, the general linear model assumes that the raw data can be modeled as the sum of separate factors, each of which may vary independently across voxels, along with additive Gaussian noise that is also independently distributed across voxels. In the following sections, we evaluate the implications of these assumptions for constructing and testing models for fMRI data.

Constructing a design matrix: regressors of interest

Everything that fMRI researchers do to ensure data quality (e.g., pulse sequence selection, training subjects, preprocessing) can be viewed as efforts to minimize values in the error matrix (ε). Similarly, the primary purpose of fMRI experimental design is to facilitate the creation of the best possible design matrix (G). Why is the design matrix so important? The maps generated by fMRI experiments reflect the outcomes of statistical tests of a researcher's experimental hypotheses. If the hypotheses are poorly modeled within the design matrix (i.e., if the model mistakenly assigns a process of interest onto incorrect time points, or fails to include important contributors to the data) then those statistical tests will be underpowered, and the results will be incomplete or even misleading. It is no exaggeration to state that the greatest challenge in fMRI data analysis—indeed, in all fMRI experimentation—lies in creating the design matrix.

The regressors in the design matrix represent the hypothesized contributors to the fMRI time course. In the general linear model, regressors associated with specific hypotheses are known as experimental regressors, of which there are two types. Covariates are factors that can take any of a continuous range of values, where the value of the factor represents the amount of some known quantity. Indicators are factors that have integral values that indicate a qualitative level. Within fMRI design matrices, the most common experimental regressors are covariates that predict hemodynamic responses using the lin-

experimental regressors Model factors that are associated with specific experimental hypotheses.

covariates Regressors that can take any of a continuous range of values.

indicators Regressors that have integral values to indicate a qualitative level.

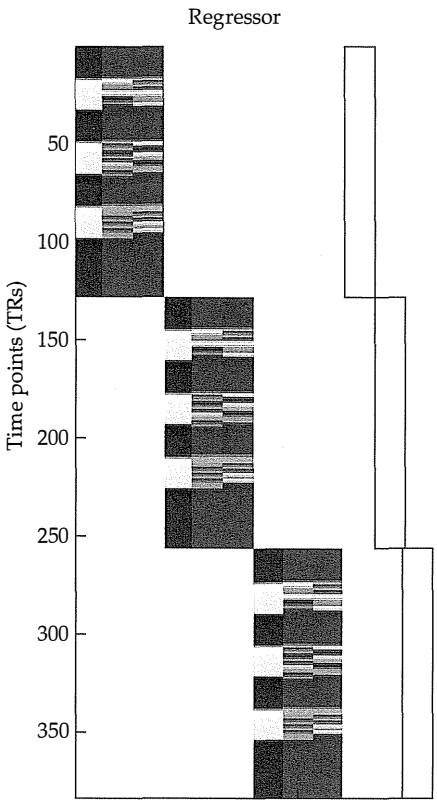

Figure 10.10 A design matrix for the general linear model, here shown for a mixed blocked/event-related design. The set of regressors that attempts to explain the experimental data using the general linear model is known as the design matrix. Here, three regressors represent different cognitive processes, each shown as a different column, within each of three runs. The first represents a blocked effect, while the second and third represent event-related effects associated with two different stimulus categories. The value of each regressor at each point in time is scaled using a dark–light color map. Black indicates that the regressor has its smallest values at that time point, while white indicates the greatest values. The three columns at far right reflect constant values included to remove the mean signal change for each run. Note that each run consists of roughly 130 brain images.

ear systems convolution (see Figure 7.27). That is, the researcher identifies periods of neuronal activity following experimental events (e.g., each time a fearful face is presented, there should be 1 s of activity associated with the perception of fear), and then convolves that neuronal activity with a canonical hemodynamic response, to generate a regressor. Indicators are relatively rare in fMRI design matrices, at least when modeling single-session data. Even hypotheses that involve discrete changes such as switching between states (e.g., mood levels) are generally better modeled using covariates, given the convolution with the fMRI hemodynamic response. However, indicators are critical for comparisons of fMRI data between sessions, as is necessary for both within-group (e.g., on versus off medication) and between-group (e.g., younger versus older adults) comparisons. Covariates and indicators are mathematically equivalent within the general linear model, however the latter have a restricted set of values, while the former can vary freely.

For our first example of a design matrix, consider the mixed blocked/event-related designs discussed at the end of Chapter 9. One such design might include task blocks consisting of two irregularly-spaced trial types, A and B, and non-task blocks where the subject rests. A design matrix describing these data could include one regressor for the blocked task versus rest factor, along with two more regressors representing the individual trial types (Figure 10.10). Graphical depictions of fMRI design matrices, like Figure 10.10, often show each regressor as a separate column whose value at each point in time is scaled using a dark–light color map. Black indicates that the regressor has its smallest values at that time point, while white indicates the greatest values. Each of the regressors should represent a prediction about how hemodynamic activation would change should a voxel be associated with that factor. So, the blocked regressor would have alternating periods of low and high activation with smooth transitions between them. The event-related regressors would have short-duration hemodynamic responses that are time-locked to the different trial types. Note that the analysis software subtracts the mean value from each regressor so that the variance associated with the mean signal intensity is not assigned to any experimental condition. Also, the regressors are usually constructed by convolving a hemodynamic response with high temporal precision (e.g., to a small fraction of a second), then down-sampling to the TR of the recorded data.

So far, the construction of a design matrix may seem straightforward and simple. But not all design matrices generate meaningful statistical tests. The most common problems arise from imperfect separation of the regressors. If two (or more) regressors are correlated with each other (i.e., they are collinear regressors), then variance explained by one such regressor may become confused with variance associated with another. Instead, all regressors in the model

collinear regressors Model factors that are highly correlated with one another. The inclusion of collinear regressors reduces the validity of general linear model analyses.

should be independent of, or orthogonal to, all other regressors. Given that fMRI regressors express predicted hemodynamic amplitude over time, for two regressors to be orthogonal, the hemodynamic activation they model must occur with distinct temporal patterns or with unrelated amplitudes. This restriction has important consequences for choosing regressors. If using a blocked design (e.g., alternating 30 s of task with 30 s of baseline), one could choose to include separate task and baseline regressors. Unfortunately, because these two regressors are perfectly negatively correlated with each other (i.e., when the task has maximal value, the baseline value is minimal), they will explain exactly the same variance in the experimental data. Considered another way: one could not, in principle, distinguish between a voxel whose response to task blocks was increasingly negative and a voxel whose response to baseline blocks was increasingly positive (see Box 9.1). Only one such regressor is required, as shown in the left column of Figure 10.10, to account for both sorts of block effects. In short, the more orthogonal your regressors, the better your chances (i.e., the smaller the difference in BOLD signal required) of identifying effects.

orthogonal A property of two variables (or vectors, sets of variables) such that they are completely uncorrelated with each other.

orthogonalize To remove correlation between two variables. In the context of fMRI data analysis, orthogonalizing one regressor (with regard to one or more other regressors) changes that regressor so that it is no longer correlated with the other regressor(s).

The best way to ensure a well-formed design matrix is to run a well-designed experiment. Indeed, the goals of efficient fMRI design (see Box 9.2) are to maximize variability within a regressor and to minimize correlations between regressors. However, some research hypotheses may preclude perfect orthogonality. For example, experiments investigating attentional effects on target processing may require the presentation of two stimuli in rapid succession: a first cue indicating the likely upcoming location of a second, target stimulus. For ideal fMRI experimental design, two stimulus categories should not have any temporal contingency, but the very nature of this task requires that the cue precede the target (potentially, by a short interval). When the experimental design does not adequately separate two regressors, researchers can orthogonalize one regressor with respect to one or more other regressors in the design matrix (Figure 10.11). In doing so, the analysis program will change that regressor so that it no longer correlates with (one or more) other regressors in the model. A researcher interested in target effects might orthogonalize the target regressor with respect to the cue regressor, to identify aspects of fMRI activation unique to the cue stimuli. Orthogonalization should not be thought of as a panacea for poor experimental design, but as a method for clarifying the effects attributable to a specific regressor.

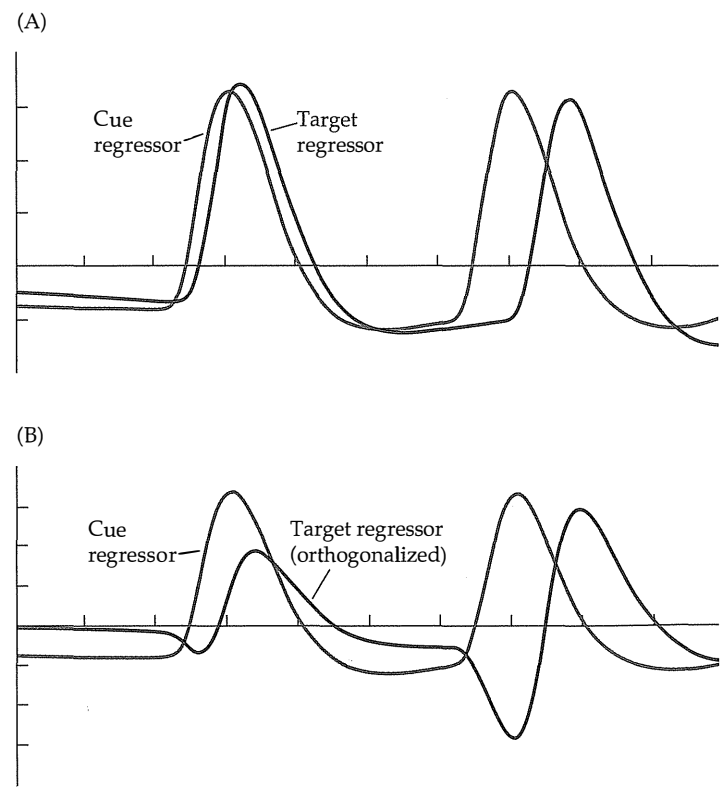

Figure 10.11 Orthogonalization of a regressor. (A) The two regressors represent hypothesized effects of an initial attentional cue (blue) and a subsequent target (red). Note that the two regressors are highly correlated over time, which prevents the regression analyses from identifying independent effects associated with each. (B) Orthogonalizing the target regressor with respect to the cue regressor changes the former's shape, leaving only that part of the signal that would reflect unique contributions from the target stimuli. Orthogonalization improves the interpretability of results when model regressors are not independent.

parametric effect A manipulation of some independent variable so that it takes a number of levels, to evoke regular changes (e.g., a linear increase) in the dependent variable.

An increasing proportion of fMRI experiments go beyond simple subtractive logic (i.e., comparing two conditions that differ in one factor) to include parametric effects. As the name implies, a parametric design incorporates multiple levels of some independent variable. Within the fMRI literature, common parameters include task difficulty, monetary reward, or the intensity of a perceptual stimulus. The parameter may be built into the task (e.g., using easy-, medium-, and hard-task blocks) or measured based on the subjects' behavior (e.g., response time in each trial). There are two ways to model parametric effects in a design matrix. One is to introduce a separate regressor for each level of the parameter (Figure 10.12A). This can work well if there are only a few levels and if the design efficiently separates those levels in time. This approach has the major advantage of allowing an estimation of the activation associated with each level, making it robust to non-linear changes in activation amplitude. However, it may not be appropriate for non-categorical parameters (e.g., response time). A second approach is to use two regressors, one for the main process and one for how that process changes parametrically (Figure 10.12B). In a 2008 study, Knutson and colleagues investigated brain mechanisms that might underlie the "endowment effect," which describes the tendency to over-value goods that you own. During a key part of each trial, they presented subjects with a potential prize (e.g., a digital camera) with an associated price (e.g., $25). They modeled the pricing phase of the trial, in part, with two regressors: a main-effect regressor (for overall decision-making processes) whose amplitude was constant throughout all trials, and a parametric regressor (for relative price) whose amplitude depended on the price of the goods. In designs like this one, the main effect and parametric regressors should be orthogonal with each other.

Note that in this latter approach, the regressor for the parametric effects is scaled so that the lowest values reflect negative signal changes and the highest values reflect positive signal changes. This may seem counterintuitive, given that we do not necessarily expect deactivation in voxels of interest (e.g., while evaluating prices). Remember, however, that the goal of multiple regression is

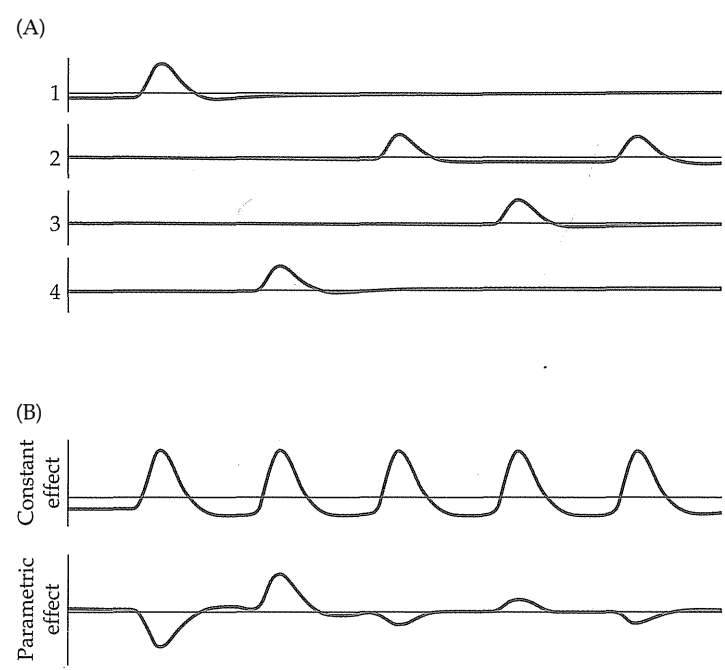

Figure 10.12 Creating models for parametric analyses. When an independent variable can take any of several levels along a continuum, researchers frequently set up their design matrix so that they can identify parametric changes on that variable. (A) One approach is to construct separate regressors for each level of the independent variable, here arranged from the lowest (1) to the highest (4) value. Subsequent contrasts between these regressors can reveal the effects of this variable. (B) Alternatively, two regressors can be used: one modeling a constant effect on every trial, and another modeling a variable effect across trials, depending on the parameter value.

to identify unique contributions of each of our regressors to the observed data, and thus regressors should be uncorrelated. If a voxel exhibited minimal activation, or even no activation, to the lowest levels of the parameter but maximal activation to the highest level of the parameter, then this two-regressor model could account for that activation, regardless of any main effect across trials.

nuisance regressors Model factors that are associated with known sources of variability that are not related to the experimental hypotheses.

Constructing a design matrix: nuisance regressors

In addition to the regressors of interest, the design matrix often includes additional regressors associated with known non-experimental sources of variability. These are known as nuisance regressors. Suppose that the MR scanner on which this study is conducted has a known linear drift (i.e., an increase in raw signal intensity over time) during experimental sessions. A savvy researcher could introduce an additional regressor into the design matrix to account for this drift. Or, if the subject's respiration was measured during the session, the design matrix could include a regressor for artifacts associated with breathing. Of course, these factors have nothing to do with the experimental hypotheses, in that the experiment was not designed to test scanner drift or subject respiration. So why are they included in the design matrix?

Nuisance factors serve two related purposes in experimental analyses. First, they can reduce the amount of residual variation included in the error term. If the intensity of a voxel were to drift by a few percentage points through the course of a run, the overall variability in the voxel would be very large, compared with the BOLD effect of interest. But if a linear regressor were added to the design matrix, much of that intensity drift would be assigned to that regressor rather than to the error term, increasing the significance of the results. Second, assigning known variability to nuisance factors improves the validity of the general linear model. The model assumes that residuals are independent and identically distributed as Gaussian noise, which may not be the case if a regular source of variation is excluded from the design matrix. It is therefore critical to include all anticipated changes in the BOLD signal, whether of interest or not. However, the unnecessary inclusion of extra factors is not recommended. Each additional column in the design matrix reduces the number of degrees of freedom available. In the limiting case, one could reproduce perfectly any set of n time points with a combination of $n - 1$ different model factors. Since the significance of any individual factor is evaluated as a function of the number of available degrees of freedom, it is in the researcher's interest for the number of factors to be as small as possible. In practice, the inclusion of a limited number of nuisance factors makes statistical testing more conservative, due to the reduced number of degrees of freedom, but can improve the validity of the general linear model.

No consensus exists about which nuisance regressors should be included in design matrices. The most commonly added nuisance regressors are head motion parameters, typically six regressors comprising three directions of translation and three axes of rotation. The value of each regressor at each point in time reflects the accumulated movement along that direction or around that axis, typically normalized to a range from –1 to +1. Within the design matrix, other regressors are then orthogonalized with respect to these parameters, so that variation in the data attributable to motion (e.g., an increase in activation along the edge of the brain each time a stimulus was presented) will be assigned to the nuisance, not task, regressors (Figure 10.13). Based on a 2006 comparison of analyses with and without motion parameters, Johnstone and colleagues

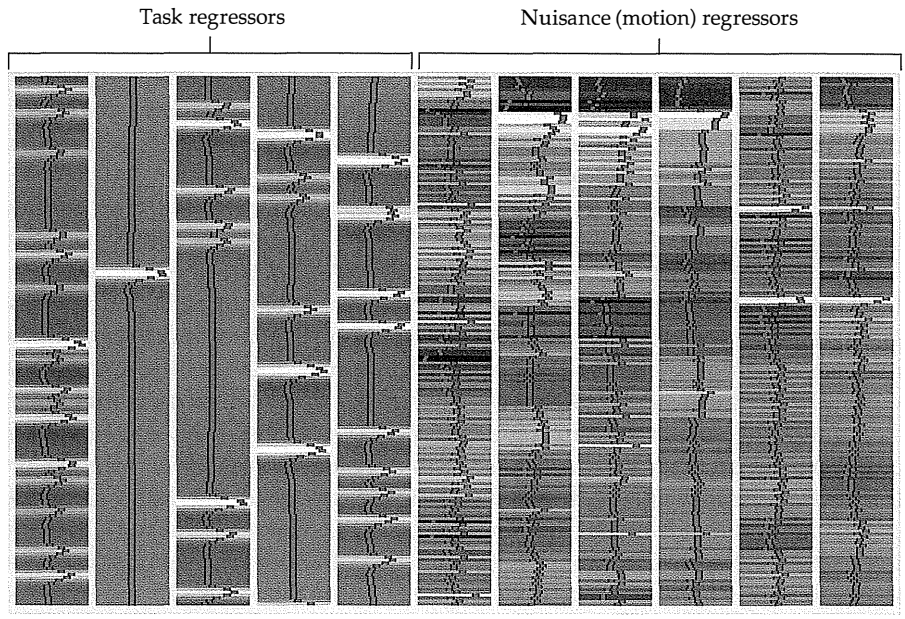

Figure 10.13 A design matrix including nuisance regressors to account for head motion. By including motion parameters as nuisance regressors, design matrices can account for an increased proportion of variance in the experimental data. Usually, researchers include six regressors corresponding to three directions of translation and three axes of rotation; the value at each time point indicates the actual net translation or rotation. Shown here is a hypothetical event-related design with five regressors of interest and six nuisance (motion) regressors. For clarity here, the red lines indicate the regressor values at each point in time, with more positive values going to the right.

concluded that including motion parameters in the design matrix generally improved the detection of real activation, especially for analyses of event-related designs. But, because blocked conditions may evoke regular task-related movement, including motion parameters greatly reduced the sensitivity of the analyses. Other researchers argue against including motion regressors in the design matrix, advocating instead for the removal of motion effects during preprocessing.

Some researchers may include regressors for physiological parameters such as heart rate or respiration, if those are recorded during the experiment. Because of their oscillatory nature, these physiological changes can cause regular fluctuations in the BOLD signal, potentially obscuring task-related activation. Recent work was done by Lund and colleagues and by Birn and colleagues to investigate the effects of including physiological data as nuisance regressors. Note that because of the relatively coarse temporal resolution of most fMRI studies (e.g., with typical TRs of 1–2 s), rapid physiological changes like heart rate will be under-sampled. To account for this problem, both groups modeled each type of physiological noise with a set of sine and cosine regressors corresponding to the major frequencies in the physiological data, rather than with a single regressor. (For additional details, see also the work of Glover and colleagues cited in the Chapter References.) Both groups reported that the inclusion of the nuisance regressors improved the detection of true activation, in multiple independent simulations and experiments.

Analysis programs differ in how they combine data from different runs within an experimental session. Some programs treat each run separately, conducting basic contrasts within each run as a first-level analysis, and then combining the data from multiple runs (and subjects) in higher-level analyses. Other programs combine all runs for each subject into the same design matrix. If the runs are combined, then the design matrix should include, for each run, a nuisance regressor with a constant value, as shown in the right-most columns of Figure 10.10. These regressors capture variance associated with differences in mean signal intensity

across runs. Alternatively, all runs can be normalized to the same mean signal intensity during preprocessing, obviating the need for these regressors.

Modeling neuronal activity

So far, we have emphasized that the regressors of interest in an fMRI design matrix represent predictions about hemodynamic changes in the brain, usually associated with the experimental manipulations. As a straightforward way of creating these regressors, a researcher can identify the onset of each stimulus in the experiment, and then convolve those onset times with a canonical hemodynamic response. Yet, this simple approach can lead to misleading results. Consider a simple experiment in which subjects see a picture of an object, and then must retrieve a specific, elaborated memory of a past event associated with that object. The pictures are presented for 2 s each with interstimulus intervals ranging between 20 and 30 s. After creating regressors using the simple stimulus-convolution approach, the researcher is surprised that visual cortical areas are active but memory-related areas are not. What could cause such a result? Imagine that you are the subject in this experiment, and you have been instructed to remember a detailed episode from your past, based on the picture on the screen. The first picture is a balloon. Now, recall a particular event in your life associated with balloons. If you are like most people, it took you between 5 and 15 s (or even longer, depending on the complexity of the memory) to recall and re-experience the particular event. Neurons associated with the retrieval of that memory would have a correspondingly extended period of activity, leading to hemodynamic changes that could span 20 s or more. To detect memory-related activation, the design matrix must accurately model the duration of neuronal processing, not just stimulus presentation (Figure 10.14).

This example illustrates the importance of thinking about the regressors in a design matrix as predictions of the BOLD time course, evoked by hypothesized neuronal activity. Before creating your design matrix for an experiment, you should think carefully about the separate types of brain processes that are evoked in your experiment, along with their timing and duration. In tasks

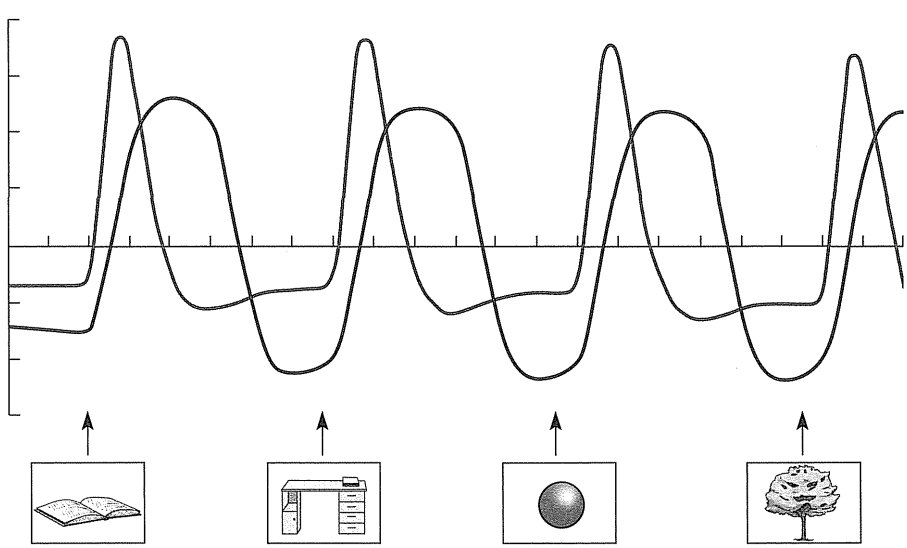

Figure 10.14 Effects of event duration on predictions for the hemodynamic time-course. Because regressors in a design matrix represent predicted hemodynamic time-courses, those regressors can vary dramatically depending on the researcher's hypothesis about the underlying neuronal activity. Suppose that your experiment involves the generation of memories based on pictures of objects, each viewed for 2 s, with 30 s intervals between successive stimuli. If you hypothesized that neuronal activity would only last for 2 s (i.e., the stimulus duration), you would obtain the regressor shown in blue. This might be appropriate for basic aspects of the task like visual processing, but would not be appropriate for slower processes like the generation of a memory. Such processes would evoke sustained neuronal activity that might last 10 s or more, resulting in a regressor like that shown in red.

where several processes are likely to be evoked sequentially, researchers often identify different phases of the task. These phases may be explicit, such as when a visually presented word must be remembered over a delay interval, followed by a cue that requires a decision about what word was presented. The resulting design matrix could have a separate regressor for each process. Or the phases may be implicit, established by the experimenter based on an expectation of what the subjects will do in the task. If the task is to remember a complex display of shapes presented for 10 s, the researcher might distinguish between two phases: a beginning encoding phase (2 s), when the subjects study the display; and a rehearsal phase (8 s), during which time the subjects commit particular aspects of the display to memory. In summary, no fMRI statistical analysis can be valid when the statistical test, here determined by the predictions of BOLD activation in the design matrix, does not reflect the actual changes in the brain associated with the experimental manipulations.

Modeling hemodynamic convolution

Most researchers create design matrices by convolving predicted neuronal activity with a standard hemodynamic response, as provided by their fMRI analysis packages. The hemodynamic response takes the stereotyped form introduced in Chapter 7 (see Figure 7.11), with a rise to a peak around 5 s after stimulus onset, followed by a return to baseline and subsequent undershoot at around 12–15 s. (Note that while analysis packages differ slightly in their default hemodynamic response, all share the same essential features.) The use of a single standard hemodynamic response greatly simplifies analyses. However, it can also constrain statistical models, particularly if its timing or shape differs from that observed during an experiment. Researchers have therefore explored a number of approaches for improving the generalizability of their design matrices.

All analysis packages allow the researcher to select from a broad range of hemodynamic response functions. But, what function should you choose? Most common are mathematical distributions that can be described with a small set of parameters (Figure 10.15A). Gamma and Poisson functions can roughly match the rise and fall of the hemodynamic response if appropriate parameters are selected. Some analysis packages use a mixture of two Gamma functions: a faster, larger function to model the initial rise and fall, and a slower, smaller function to model the subsequent undershoot. As introduced in Chapter 8, subject-specific hemodynamic response functions can be derived from a simple experiment (e.g., a finger-tapping task to evoke activation in the motor cortex) and then applied throughout the brain in subsequent analyses.

Regardless of the functional form chosen, the regressors in the model often differ slightly from the observed data. Such differences could arise from imperfect estimation of the timing of neuronal activity or from variability in the evoked hemodynamic response. To model small differences in hemodynamic onset, or in the shape of the hemodynamic response, the design matrix can include additional regressors known as **temporal derivatives** and **dispersion derivatives**. When one adds a temporal derivative to a signal, the combination will be a time-shifted version of the original signal. Similarly, including temporal derivatives in a fMRI design matrix makes the analysis robust to small mismatches between the timing of the regressors and the observed BOLD signal. The dispersion derivative can correct for small mismatches in the width of the hemodynamic response. Note that when temporal and/or dispersion derivatives are included, they are generally calculated independently for each

temporal derivative A regressor that, when added to a model, improves the robustness of that model to small variations in the timing of the hemodynamic response.

dispersion derivative A regressor that, when added to a model, improves the robustness of that model to small variations in the width of the hemodynamic response.

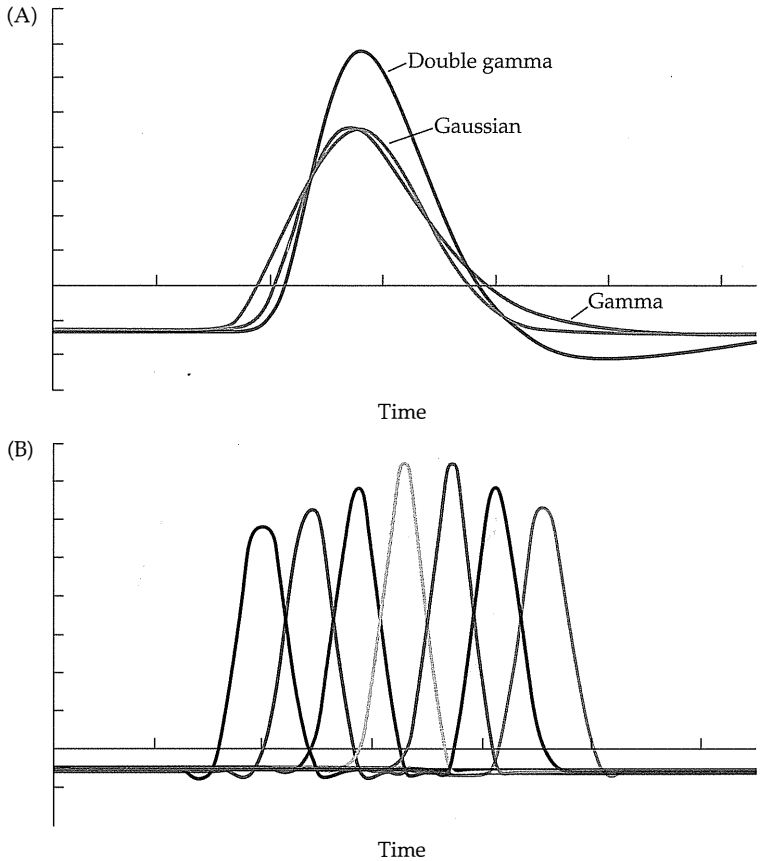

Figure 10.15 Possible functions underlying the BOLD hemodynamic response. (A) The hemodynamic response evoked by a single, short-duration event can be approximated using any of several functions, including simple Gaussian and Gamma functions. The combined effects of the hemodynamic rise, fall, and undershoot can be modeled using two Gamma functions, one subtracted from the other (red line). (B) Another approach is to use a set of basis functions, or a series of separate regressors (shown here as overlapping waveforms) that can be added together to obtain the measured hemodynamic response. A major advantage of using basis functions is that they can more flexibly model almost any evoked response, even if it differs from the canonical hemodynamic shape.

regressor of interest. This reduces the degrees of freedom, and thus increases the threshold for significance, in the regression model. Researchers differ in how they use these derivatives when calculating the parameter amplitudes (i.e., calculating β from just the regressor of interest, or from the combination of that regressor and its derivatives). Some laboratories regularly incorporate these derivatives into their analyses, while others do not.

An increasingly popular approach is to replace a single hemodynamic response function with a small number of **basis functions**, such as low-frequency sine and cosine waveforms or gamma functions. Since a wide range of hemodynamic responses can be modeled using a combination of multiple basis functions, this approach can be used to detect voxels whose time courses of activation are not standard, such as those with wider responses or with later peaks. Particularly promising are techniques that use **finite impulse response (FIR)** functions, which model each time unit with a separate basis function (Figure 10.15B). In principle, FIR modeling can be used to identify task-related changes in the BOLD signal regardless of the shape and timing of the evoked hemodynamic response. A researcher who lacks a strong hypothesis about the likely hemodynamic response might be well-served by using FIR or another set of basis functions, rather than a canonical response function. However, using basis functions increases the complexity of the design matrix, which in turn increases the challenge for detecting and interpreting significant results.

Finally, a frequent source of confusion when thinking about the use of the general linear model in fMRI is the idea of linearity itself. Remember from Chapter 8 that the BOLD response does not obey the assumptions of linearity

basis functions A set of functions whose linear combination can take on a wide range of functional forms. In fMRI analyses, researchers often replace a single hemodynamic response function with basis functions, to improve the flexibility of their design matrices.

finite impulse response (FIR) A signal processing approach that treats each time unit with a separate function (i.e., an impulse); this has the major advantage of making no assumptions about the shape of the observed response function.

at short interstimulus intervals. So, how can it be analyzed using the general linear model? This confusion derives from a misunderstanding of the type of linearity under consideration. The hemodynamic response is nonlinear with respect to stimulus presentation, because the combined response to two stimuli in succession is less than the sum of the responses to the two stimuli if presented independently. But, stimulus presentation is not itself important in the general linear model. What is important is that the overall BOLD time course, however it is modeled, adds linearly with other sources of variability in the data. So, refractory effects in the BOLD response can be incorporated directly into the experimental design matrix without compromising the validity of the model. One way to do this is to adjust the columns of the design matrix directly by including interaction effects. Another method, identified by Friston and colleagues in 1998, is to use Volterra kernels, which allow one to model the influence of a stimulus on subsequent stimuli, by specifying a second column in the design matrix. Without such corrections, the design matrix may not accurately capture the desired BOLD time course.

Contrasts

When analyzing fMRI data, researchers want to evaluate hypotheses about brain function. Because fMRI provides no information about absolute levels of activation, only about changes in activation over time, most research hypotheses involve comparison of activation between two conditions. For example, when identifying brain regions that support the perception of biological motion, the experiment might involve testing whether activation increases when subjects view a biological stimulus (e.g., a person walking) compared with a similar non-biological stimulus (e.g., a machine with moving levers and gears). As introduced in the discussion of *t*-tests, the statistical evaluation of whether the experimental manipulation evokes a significant change in activation is called a contrast.

Using the general linear model, an fMRI researcher constructs a design matrix consisting of a set of regressors, and then determines how strongly each of those regressors matches changes in the measured BOLD signal. Regressors that explain much of the BOLD signal have high-magnitude parameter weights (i.e., large β values), whereas regressors that explain little of the BOLD signal have parameter weights near zero. To test an experimental hypothesis, the researcher evaluates whether the experimental manipulation caused a significant change in those parameter weights. The form of the hypothesis determines the form of the contrast, or which parameter weights contribute to the test statistic. We consider three types of hypotheses in the following examples.

The simplest type of contrast evaluates whether a single regressor causes significant changes in the BOLD signal. Suppose that your experiment uses an event-related design with the randomized presentation of three types of visual stimulus: biological motion (e.g., a person walking), non-biological motion (e.g., a machine moving), and perceptual control (e.g., a rotating shape). Each of these stimuli is presented as a short movie of 2 s duration with 8 s intervals between consecutive stimuli. You set up each of these as a separate regressor in your design matrix (Figure 10.16A), using the approaches described in the previous sections. If you want to identify voxels whose activation increased in response to the biological motion stimulus, you would use the set of contrast weights (+1 0 0), as shown on the top row in Figure 10.16B. Conversely, to identify voxels whose activation decreased in response to biological motion, you would use the contrast weights (–1 0 0). Effectively, these contrasts use the

contrast weights A vector that expresses the predictions of a research hypothesis for the different regressors in a design matrix. When multiplied by the parameter weights from a fMRI regression analysis, the result can be evaluated for statistical significance.

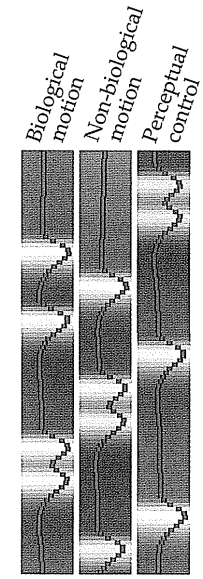

(A)

					F-test
(B)	Contrasts (main effects)	+1	0	0	Y
		−1	0	0	N
		0	+1	0	Y
		0	0	+1	Y
(C)	Contrasts (between conditions)	+1	−1	0	N
		+2	−1	−1	N

Figure 10.16 Setting up experimental contrasts. (A) In this hypothetical example, the experimental task consisted of three types of events that occurred in a random order, with a relatively long interstimulus interval, over the course of a single run. The hypothesized BOLD timecourse associated with each event type has been modeled in this design matrix by convolving a standard hemodynamic response function with brief neuronal activity at the onset of each event. (B) The positive main effects associated with each event type (i.e., what voxels increased in activation to those events?) can be specified by a positive value for that event regressor, leaving the other regressors at zero. Negative main effects (i.e., decreases in activation) can be specified by a negative value for that regressor. An *F*-test can be used to combine across multiple main effects (i.e., those rows included as "Y" here), identifying voxels that showed significant changes in activation across any of the conditions. (C) More critical for most fMRI studies are contrasts between conditions. These involve comparing the relative amplitude of activation between two or more regressors; the example here shows both a direct contrast between two conditions (+1 −1 0) and a contrast between one condition and the other two (+2 −1 −1).

parameter weight from the biological motion condition, but ignore the other conditions. The statistical software then multiplies the parameter weights by your chosen contrast weights, scales the resulting quantity by the residual error, and then evaluates (usually with a *t*-test) that scaled value against a null hypothesis of zero. Note that these single-condition contrasts, often referred to as main effects of a condition, can lack experimental control. Significant increases in one condition could arise from any of a host of factors, from visual stimulation to arousal. Thus, researchers often compare two or more regressors, following the subtractive logic described in the previous chapter.

If you want to test the (better controlled) hypothesis that biological motion evokes increased activation compared with non-biological motion, you would use the contrast weights (+1 −1 0), as shown in Figure 10.16C. This contrast provides a value for the difference between the biological motion and non-biological motion parameters, and then uses that value in the following statistical tests. Note that you could use other sets of contrast weights, depending on your hypothesis. To evaluate whether biological motion evokes greater activation than both other forms of motion, you would use the contrast weights (+2 −1 −1). Although statistical tests can incorporate any combination of weights (e.g., +1 −4 +3), researchers generally adopt relatively simple contrasts that reflect well-defined hypotheses. Note that contrasts between conditions generally use weights that sum to zero, reflecting the null hypothesis that the experimental manipulation had no effect. Also, contrasts are inherently directional, in that the contrast weights (+1 −1 0) are used to identify voxels with greater activation in response to the first stimulus type than to the second, whereas (−1 +1 0) is used to identify voxels with greater activation in response to the second stimulus type than the first. Researchers often include contrasts in both directions when testing hypotheses of particular interest.

Finally, research hypotheses sometimes involve combining over several different contrasts. Suppose you want to identify voxels that exhibit significant increases in activation in response to any of your three motion conditions. After setting up three of the single-condition contrasts described above, you could next enter all three contrasts into a single *F*-test (see Figure 10.16). The *F*-test evaluates whether any contrast or any combination of contrasts explains a significant amount of the variability in the measured data. Unlike *t*-tests, *F*-tests are non-directional: they do not indicate the direction of any of the contrasts. Nor do they provide information about which contrasts drive significance, only that

F-test A statistical test that evaluates differences among a set of distributions. For fMRI studies, *F*-tests can evaluate whether any of a set of contrasts exhibited a significant effect.

homoscedastic Having the property that the distributions of noise are similar for all experimental conditions.

heteroscedastic Having the property that the distributions of noise are different across experimental conditions.

a significant difference exists among the conditions. Researchers most commonly use F-tests to identify voxels that show some modulation in response to the experimental task, in advance of more targeted contrasts.

Assumptions of the general linear model

Provided that the design matrix is appropriate for testing the experimental hypotheses, several other conditions must be met for the general linear model to be appropriate. One assumption that has been the source of considerable debate is the use of the same design matrix throughout the brain. Although each voxel will have a different set of parameter weights, the model used to calculate those weights is identical. But we know that the properties of the hemodynamic response, especially its latency, may differ across brain regions. A model factor that is correct for one region may thus be incorrect for another, reducing the amount of variation explained by the model and increasing the residual error. The use of multiple basis functions provides some flexibility compared with using a single canonical hemodynamic response, but complicates the interpretation of the results. One way of overcoming the problem of regional variability is to combine a general linear model approach with region-of-interest analyses, as discussed later in this chapter.

Another assumption is that noise varies with a normal distribution that has similar properties at all *time points*. In other words, the contributions from noise do not vary over time, and thus are independent of the experimental task. That is, the data should be homoscedastic. If there is greater noise in one condition than another, the data are heteroscedastic. The general linear model assumes the former, however this assumption may not always be valid. Noise levels may be higher during BOLD activation than during rest, although whether such changes are due to hemodynamic variability or to variability in neuronal processing remains unknown. However, the contributions of noise may differ dramatically across *voxels*. A voxel that contains a major blood vessel or that is near the edge of the brain may have much higher noise levels than most others in the brain.

Another assumption is that that all voxels represent independent statistical tests, even though adjacent voxels tend to have very similar properties. In fact, introducing correlation between adjacent voxels through spatial smoothing is a common step during preprocessing. While the general linear model framework cannot account for spatial correlation, the significance values it generates can be adjusted at later stages of the analyses, as discussed later in this chapter, in the section on cluster-thresholding. Likewise, the model assumes that each time point is independent of all others, in that the residuals should be similarly distributed throughout. Scanner drift, thermal variation, head motion, and many other factors can cause the overall MR signal to change dramatically over time, influencing the amplitude of the residual error. Therefore, it is critical to attempt to remove such unwanted variability before it reaches the error term, either during preprocessing or by including appropriate nuisance factors.

In summary, the general linear model has become the dominant statistical framework for fMRI analyses. It subsumes other tests, like the t-test and correlation analyses, that represent special cases of this framework with simplified assumptions. The power of the general linear model comes from its flexibility. By incorporating into the design matrix appropriate regressors of interest, and excluding unwanted variability through nuisance regressors, a researcher may test nearly any experimental hypothesis. However, researchers must carefully construct their design matrices and select their contrasts, or their analysis may result in incorrect conclusions.

Corrections for Multiple Comparisons

A typical fMRI data set may contain about 20,000 voxels within the brain and several times that number outside of the brain. Imagine that you first target a single voxel within the gray matter adjacent to the right calcarine sulcus. Using data from a simple event-related visual task, you calculate a t-statistic of 2.4 based on the voxel's correlation with a task-related regressor in the general linear model. The chance that such an extreme t-statistic could occur under the null hypothesis, based on the degrees of freedom in the test, is only about 1 in 50 ($P = 0.02$), less than your alpha value of 0.05. Given such a low probability, you confidently reject the null hypothesis for that voxel. Flush with the excitement of a significant result, you decide to analyze the remaining voxels. You run all of the voxels through the correlation test, calculate a t-value for each, and compare those t-values with your alpha value. Now you find that about a thousand voxels, distributed in seemingly random fashion across the brain, pass your significance threshold (Figure 10.17). Even worse, a few thousand voxels outside the brain appear to be active! You stare at the computer screen in disbelief. Why have so many voxels produced significant results?

multiple comparison problem The increase in the number of false-positive results (i.e., Type I errors) with increasing number of statistical tests. It is of particular consequence for voxel-wise fMRI analyses, which may have many thousands of statistical tests.

This example illustrates one of the central problems of fMRI data analysis, that of **multiple comparisons**. Stated succinctly, the greater the number of statistical tests conducted, the greater the chance of a false-positive result. To illustrate this point, we created a random data set of roughly similar size to an fMRI imaging volume ($64 \times 64 \times 34 = 140{,}000$ voxels), where the intensity of each voxel at each of 40 time points was distributed as Gaussian noise. We then conducted a t-test on a hypothetical blocked design, comparing an arbitrarily labeled task block to another arbitrarily labeled non-task block (20 time points each). Both conditions consisted of random data, so any difference between them was due solely to chance. At an alpha value of 0.05, there were about 6800 active voxels; at an alpha of 0.01, there were about 11,400 active voxels; and at an alpha of 0.001, there were still 155 active voxels. All of these voxels are false positives, since there was no signal present in the original data. In any data set with random noise, the number of false-positive results for n statistical tests is simply $n \times \alpha$. The probability of having no false-positive results is given by Equation 10.4:

$$p(\text{no Type I error}) = (1-\alpha)^N \tag{10.4}$$

Note that for the alpha values that are typically used in social science experiments (e.g., 0.05, 0.01), this probability approaches zero for even small fMRI data sets. If you analyzed only a single slice of 4096 voxels at $a < 0.01$, the prob-

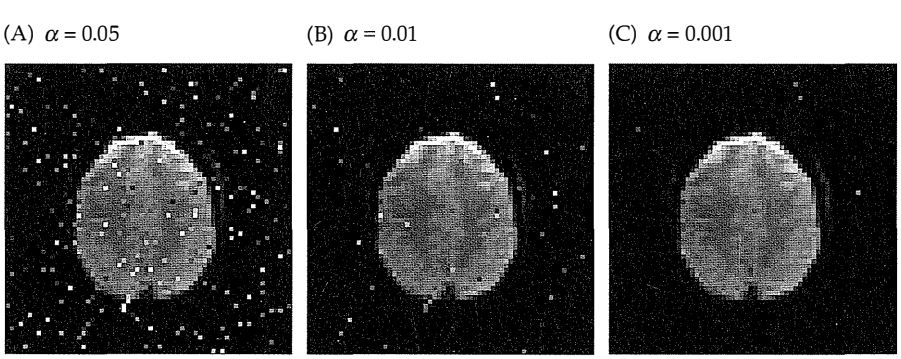

Figure 10.17 The problem of multiple comparisons. We simulated the effects of different alpha values ($\alpha = 0.05$, 0.01, and 0.001) on the number of activated voxels, using random data. The imaging volume consisted of 34 slices, each with matrix size of 64 by 64, resulting in a total of about 140,000 voxels. Note that since the data were random, any activation was due merely to chance. (A) At an alpha threshold of 0.05, there were more than 6800 active voxels, representing 4.9% of the total brain. (B) When the threshold was reduced to 0.01, there were 1397 active voxels (1.0% of the brain). (C) At a 0.001 threshold, there were still 155 active voxels (0.1%) throughout the brain. Shown in each panel are single slices, with only those voxels passing the appropriate significance threshold highlighted in color.

familywise error rate (FWER) The probability of making at least one Type I error, given the total number of statistical tests.

Bonferroni correction A stringent form of familywise error rate correction for multiple comparisons in which the alpha value is decreased proportionally to the number of independent statistical tests.

ability of having no false positives is 1.3×10^{-18}, or one quintillion to one. Stated differently, without correction for multiple comparisons, you are certain to make at least one Type I error of labeling a voxel as active when it is not.

Calculating the significance threshold

To overcome the problem of multiple comparisons, fMRI researchers always reduce the desired alpha value, so that voxels are less likely to pass the significance threshold by chance. The alpha value they select depends primarily on two factors: the types of error they want to avoid and the number of independent tests in the data. In this section, we focus on the first factor. Our examples make the simplifying assumption that the number of independent tests corresponds to the number of voxels. However, the spatial correlations within real fMRI data reduce the true number of independent statistical tests. We describe, in the following section, approaches for estimating the number of independent tests, replacing the idea of voxel-based thresholding with that of cluster-based thresholding.

The most common approach for the correction of multiple comparisons involves minimizing the number of false positive results (i.e., Type I errors), or controlling for **familywise error rate (FWER)**. A stringent method for controlling the FWER is **Bonferroni correction**, which holds constant the overall probability of a false positive, given the number of statistical tests conducted. To implement Bonferroni correction, the alpha value is decreased proportionally to the number of independent statistical tests (here, V voxels), as seen in Equation 10.5:

$$\alpha_{\text{bon}} = \frac{\alpha}{V} \tag{10.5}$$

Suppose that you decide on a target alpha value of 0.01. Even if your imaging volume included only 4096 voxels (i.e., a single slice), applying Bonferroni correction would reduce the alpha value from 0.01 to 0.000002. You would now have only a 1% chance of any Type I error. But, while Bonferroni correction effectively minimizes the chances of a Type I error, it also dramatically increases the probability of a Type II error, or failing to detect voxels with real activation (Figure 10.18). For many research questions, especially those that are exploratory or have clinical relevance, an increased rate of Type II errors may be unacceptable. Imagine that you have conducted an fMRI study to identify the cortex necessary for language processing in a patient about to undergo neuro-

Figure 10.18 Effects of Bonferroni correction on fMRI data. Shown are data from a single subject at three different levels of significance. At the lowest P value of 0.05, there is substantial activation, including some clear regions of activation and scattered noise. At an intermediate P value of 0.001, the activation is much reduced. After Bonferroni correction to an adjusted P value of 0.05 (unadjusted $P = 0.000001$), the most active regions are still present, but many of the other potentially meaningful regions of activation are lost.

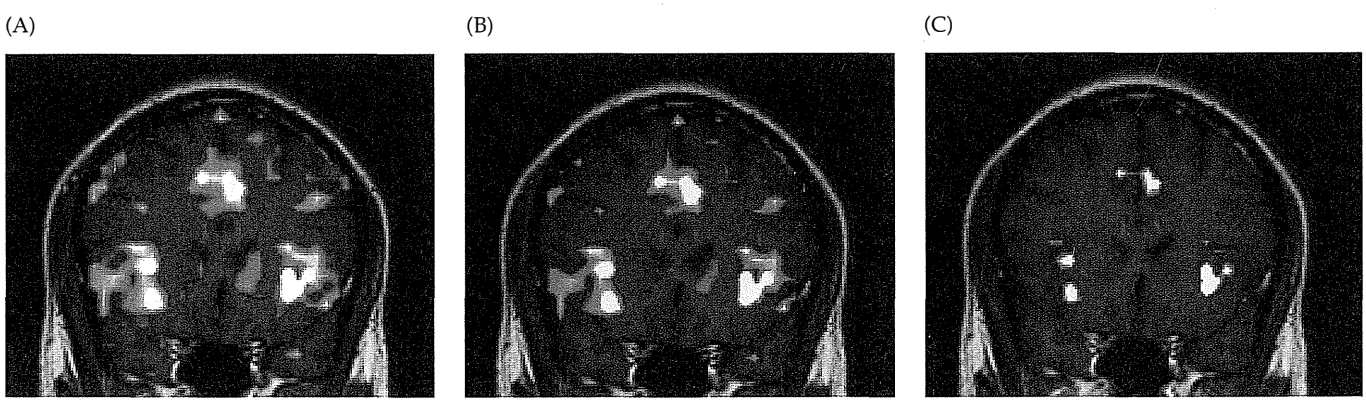

$P < 0.05$ (uncorrected) $P < 0.001$ (uncorrected) $P < 0.05$ (Bonferroni corrected)

surgery. A very conservative threshold might result in the identification of some active voxels, but there is a risk that other truly active voxels with lower significance values will be missed. In such a situation, Type II errors could lead to the removal of functional tissue and thus would have serious negative consequences for the patient.

An alternative and increasingly popular approach controls a different quantity, the false discovery rate (FDR). As its name implies, the false discovery rate describes the proportion of positive results (i.e., discoveries) that are actually false positives. For example, suppose that you choose a voxelwise false discovery rate of 0.05, calculate the necessary alpha value, and then observe 200 significant voxels using a given set of contrast weights. Based on your FDR criterion, you should expect that about 10 of those voxels are false positives. Now, suppose that you observed 400 active voxels using a different set of contrast weights within the same experiment. About 20 of those voxels would be expected to be false positives. In comparison, FWER correction would predict the same number of false positive results, regardless of the number of significant voxels. Because the alpha value used in FDR correction depends on the distribution of significance values, it is calculated using an iterated approach, as introduced to fMRI in 2002 by Genovese and colleagues.

First, an algorithm ranks the statistical tests (e.g., V voxels) according to their uncorrected probability of significance, from smallest probability (p_1; most likely to be significant) to greatest probability (p_V; least likely to be significant), as shown in Equation 10.6.

$$p_1 \leq p_2 \leq \cdots \leq p_v \tag{10.6}$$

Then, beginning with the voxel with the smallest probability (p_1), the algorithm identifies the voxel whose probability index (p_i) is greater than the voxel's ranking in the list (i) divided by the total number of tests (V), as corrected by the desired FDR (q). This is shown in Equation 10.7. All voxels ranked from p_1 to p_i are labeled as significant.

$$p_i \leq \frac{iq}{V} \tag{10.7}$$

Controlling the FDR rather than the FWER provides two primary advantages for fMRI research. First, FDR uses less-stringent correction (i.e., a greater alpha value) than FWER, especially if there are many activated voxels. If there were only one activated voxel ($i = 1$), then that voxel would have to pass full Bonferroni correction. But, as more and more voxels become activated, then the ranking term (i) increases in Equation 10.7, driving down the threshold for significance. Many researchers find the gain in experimental power to be worth the additional chance of Type I errors. Second, whereas FWER correction controls the proportion of false *tests*, FDR controls the proportion of false *claims*. In fMRI studies, which typically have data sets with many tests, each with a low probability of significance, researchers may care more about the rate of errors among their claims (e.g., activation clusters in a table) than among their statistical tests (e.g., voxels).

If researchers are testing hypotheses about targeted anatomical regions, they may only examine data from a small portion of the brain (e.g., the hippocampus), thus restricting their analyses to perhaps a few hundred or a few thousand voxels. Such small-volume correction leads to a much less severe correction factor (i.e., a smaller denominator in Equations 10.5 or 10.7) than full-brain correction. Small-volume correction should only be done before analyses, based on strong *a priori* hypotheses. Furthermore, because it ignores most voxels in the brain, it

false discovery rate (FDR) The probability of having at least one false positive result, given the set of reported positive results.

small-volume correction The restriction of analyses to specific regions-of-interest, defined *a priori*, to reduce the total number of statistical tests and thus allow for a more liberal significance threshold.

can readily to lead to the false impressions that activation is specific to a particular brain region, rather than distributed throughout the brain.

Finally, permutation approaches estimate the distribution of significance values that would be obtained by chance. These approaches permute (i.e., randomize the order of) the condition labels associated with the events within the design matrix. This approach falls into the class of "resampling" methods in the statistical literature. Suppose that your experiment consisted of 100 presentations of real words and 100 presentations of pseudo-words (e.g., "drelp"), in some random sequence. A permutation test takes those 200 events and randomly reassigns them to conditions, so half of the real words get included in the pseudo-word regressor, and vice versa. Because these regressors no longer systematically differ in their associated neural processes, any differences between them should be due to chance. The analyses are repeated many times, following each of a large number of permutations (e.g., > 100), recording the maximum significance value observed in any voxel (or any cluster). The distribution of maximum significance values then guides selection of the alpha value for the real analysis, such that, through the choice of a sufficiently high threshold, a false positive is unlikely to occur due to chance. Though computationally intensive, permutation approaches have the advantage of estimating false positives from the data set itself, and thus they can account for idiosyncratic features of particular data sets. However, some characteristics of fMRI data sets, notably their temporal autocorrelation, could violate assumptions of independent resampling in many designs (i.e., the exchangeability of labels). For such cases, researchers have proposed techniques for preprocessing the data to minimize effects of temporal autocorrelation. For details about permutation approaches, including their strengths and limitations, see the articles by Nichols and Hayasaka in the Chapter References.

Thresholding based on clusters of activation

Another approach to the correction of multiple comparisons is to use information about the sizes of any active clusters. If only a single isolated voxel passed a significance threshold, then that voxel's activation may result from mere chance. It is less likely, however, that a group of contiguous voxels will all be active by chance. This can be seen by careful examination of the data from Figure 10.17A. While many voxels in this figure are active due to chance, very few clusters of two or more adjacent voxels are present. Using cluster-size thresholding, which was first introduced in separate 1995 studies by Xiong and colleagues and Forman and colleagues, a researcher adopts a relatively liberal alpha value (e.g., $P < 0.01$) for voxelwise comparisons, and then increases the conservatism of the test by only counting clusters as significant if they are as large as some threshold. The cluster size to use as the threshold in a given experiment depends on several factors, including the desired alpha value and the number of independent tests in the imaging volume, and software analysis packages often suggest appropriate thresholds for a given data set.

Cluster-size thresholding works because as cluster size C increases, the number of such clusters (n_C) increases much more slowly than the probability that a given cluster is active. In a single slice of 4096 voxels (64×64), there are approximately 16,000 distinct clusters of two contiguous voxels and approximately 55,000 clusters of three contiguous voxels. (In three-dimensional data, several times as many clusters are present for each cluster size.) If the alpha value for the cluster (α_C) is set to 0.001, the expected number of false-positive voxels is 4096×0.001, or about 4. For the same alpha value, the joint probabil-

permutation In the context of significance testing, approaches that involve resampling the original data to directly determine the size of an effect that might be observed with a given alpha level.

cluster-size thresholding The adoption of a minimum size, in voxels, for a cluster of active voxels to be labeled as significant.

ity of two given voxels being active is just 0.001×0.001, which comes out to one in one million. Thus, the expected number of false-positive clusters of two contiguous voxels is $16{,}000 \times 0.000001$, or 0.016. Finally, the joint probability of any three voxels being active is $0.001 \times 0.001 \times 0.001$, which comes out to one in one billion. So, the expected number of false-positive clusters of three contiguous voxels is about $55{,}000 \times 0.000000001$, resulting in an expectation of 0.000055 false-positive clusters.

In summary, the likelihood of a false-positive result decreases with increasing cluster size. The effects of cluster-size thresholding on the false-positive rate are indicated in Equation 10.8 (compare to Equation 10.4), where n_c is the number of clusters in the data:

$$p = (\text{no clusterwise Type 1 error}) = (1 - \alpha_C)^{n_c} \tag{10.8}$$

By reducing the alpha value used in an experiment, cluster-size thresholding will often reduce the number of Type II errors, or misses of true activation. However, it makes several assumptions that, if violated, introduce potentially severe disadvantages. First, by definition, thresholding assumes that all areas of significant activation extend over a large number of voxels. This precludes small but meaningful activations. If your cluster-size threshold is six voxels, then detecting an active brain region of only four voxels in size becomes extremely unlikely. Some statistical programs use both the number of above-threshold voxels (as in the examples above) and the significance values of those voxels, to make better inferences about small but significant clusters of activation. Second, it assumes that activation foci are generally convex, or spherical, when calculating probabilities. If an active region has a very non-spherical shape, as when running linearly along the edge of a gyrus, then cluster size analyses may not be appropriate. Third, and most importantly, the above logic assumes that activation in adjacent voxels is uncorrelated, so that the probability of n voxels all being active is given by a^n. This assumption fails for fMRI data because of spatial correlation; significant voxels tend to cluster together, even if their significance results from noise processes. In the following section, we consider approaches that estimate this spatial correlation to improve calculation of correction factors.

Estimating the number of independent tests

When correcting for multiple comparisons, whether using FWER or FDR or some other approach, the adjusted alpha value derives from the number of independent statistical tests. For fMRI studies, this number could come from the number of voxels in the brain; if there are 20,000 voxels, there might be 20,000 tests. Yet, for many reasons, significance values tend to be highly correlated across adjacent voxels (see Figure 11.16 for an example). Inherent limitations in MRI data collection and image reconstruction allow signal to bleed across adjacent voxels (and even slices). Many sources of noise, notably head motion, systematically change the intensity of all voxels within a brain region. Activation itself often spans large regions, especially when generated by large vessels. Preprocessing steps, such as head motion correction and spatial normalization, introduce uncertainty regarding the contents of a voxel. And, in addition to all of these implicit factors, researchers usually apply explicit spatial smoothing before data analysis! Given these many sources of inter-voxel dependence in fMRI data, correction based on the number of voxels greatly overestimates the number of independent spatial units, resulting in a much too conservative alpha value. To determine a more accurate correction factor,

random field theory A branch of mathematics that deals with the properties of smooth, spatially extended data. Using random field theory, researchers can better calculate the number of independent tests within fMRI analyses.

smoothness The degree to which the time courses of nearby voxels are temporally correlated.

resolution elements (or resels) The independent statistical tests within an fMRI volume.

expected Euler characteristic The number of clusters of significant activation expected due to chance, as estimated from the number of independent statistical tests (i.e., resels).

voxelwise analyses Evaluations of hypotheses about the functional properties of individual voxels (or small clusters of voxels), often throughout the entire brain.

techniques have been proposed that modify the denominator in formulae like Equation 10.5, based on the degree of correlation between activated voxels.

To determine a better correction factor, Worsley and colleagues applied (Gaussian) random field theory to fMRI data. Random field theory is used to estimate the number of independent statistical tests needed, based on the spatial correlation, or smoothness, of the experimental data (see Figure 8.28). Although smoothness depends heavily on the properties of the Gaussian filter used in preprocessing, intrinsic correlations also matter, and thus smoothness is typically estimated computationally by the statistical program used for the analysis. Based on the smoothness, which can be expressed in voxels or millimeters, the number of independent tests in a data set can be calculated. If a data set consisting of x by y by z voxels had smoothness of V voxels, the number of independent comparisons (R) would be given by:

$$R = (x \times y \times z)/V^3 \tag{10.9}$$

The independent comparisons are sometimes known as resolution elements or resels. With even small to moderate amounts of smoothness in the data, the number of resels will be much less than the original number of voxels. At a smoothness of three voxels, there would be 1/27 as many resels as voxels. From the number of resels (with minor adjustments based on the shape of the brain volume), one can estimate how many clusters of activation should be found by chance at a given statistical threshold. The number of such clusters is known as the expected Euler characteristic. Note that for smooth random fields, like preprocessed fMRI data, the effect of threshold has a complex effect on the expected Euler characteristic. At very low statistical thresholds, only slightly above chance, there will be very few clusters. However, these clusters will be very large and interconnected since much of the brain will be labeled as active. At medium thresholds (i.e., at thresholds of about $P \approx 0.15$ for typical studies), there will be a very large number of smaller clusters labeled as active merely by chance. But as the threshold increases, the number of small clusters identified by chance should decrease. Here we have discussed smoothness and the resulting calculations of expected clusters of activation as something constant over the entire brain, however smoothness could differ from region to region. Recent work by Hayasaka and colleagues demonstrates that accounting for such regional differences can improve detection power.

Using random field theory, fMRI statistical software determines the statistical threshold whose expected Euler characteristic corresponds to the desired alpha value (e.g., 0.05). That is, given the number of resels in the data, at what threshold would there be only a 0.05 probability of an expected Euler characteristic of 1 (or greater), were there no true activation? For smoothed data, this threshold will always be much less conservative than that obtained through Bonferroni correction, leading to fewer Type II errors, and only a minimal risk of additional false positives. Nearly all fMRI research now uses some variant of random field theory to determine thresholds for statistical significance.

Region-of-Interest Analyses

Most fMRI studies involve statistical tests on individual voxels or clusters of voxels, often throughout an imaging volume that encompasses the entire brain. Such voxelwise analyses are appropriate for a wide range of research hypothe-

ses, especially those aimed at understanding particular cognitive processes. Yet some hypotheses require a more targeted analysis approach. If you are interested in a particular brain region, you may form your hypothesis about that region, rather than the entire brain. For example, you might ask, "Is the caudate nucleus active during recall of a word from memory?" In this example, the caudate nucleus becomes a region of interest, whose identity is based on anatomical criteria (Figure 10.19). In a deep sense, the basic question addressed by a voxelwise analysis, "What brain regions evince a particular pattern of fMRI activation?" is the inverse of the question posed by a **region-of-interest (ROI) analysis**, namely "What pattern of activation occurs in a particular brain region?"

region-of-interest (ROI) analysis Evaluations of hypotheses about the functional properties of brain regions (i.e., aggregated over a pre-determined set of voxels), often chosen to reflect *a priori* anatomical distinctions within the brain.

anatomical ROI Region of interest that is chosen based on anatomical criteria.

For most studies, the establishment of a ROI is based on *a priori* expectations about the likely involvement of that brain region in a task. For example, a researcher studying motor function might draw an ROI that encompasses the precentral gyrus, which contains the primary motor cortex. The ROI is considered to be a homogenous and indivisible unit, at least for the purposes of the ROI analysis. Usually, ROIs are drawn on structural T_1 or T_2 images collected at the beginning of a scanner session. The structural images are used for two reasons: they typically have higher resolution, often four times that of the functional images in each spatial dimension; and they have much greater tissue contrast. The ROIs are then coregistered to the functional data. In most ROI approaches, the researcher draws the edges of a particular brain area, such as the sulci that demarcate a gyrus of interest, and then selects all circumscribed voxels. If **anatomical ROIs** are chosen beforehand and are drawn without consultation with functional activation maps, then they can provide an unbiased estimate of activation within a given brain area.

Anatomical ROI analyses have several advantages over voxelwise methods. First, because there are always many fewer ROIs than voxels, the total number of statistical comparisons is greatly reduced, ameliorating the need for correction for multiple comparisons. For example, in a study of the motor cortex, a researcher might draw just two ROIs, to encompass the primary motor cortex in each hemisphere. Second, each ROI combines data from many voxels, so there will be a corresponding increase in the SNR, to the extent that the ROI is functionally homogenous. This spatial signal averaging complements the temporal signal averaging common to voxelwise and ROI analyses. Another advantage is that ROI approaches allow the identification of brain topography, as reflected in changes in activation levels across spatial locations

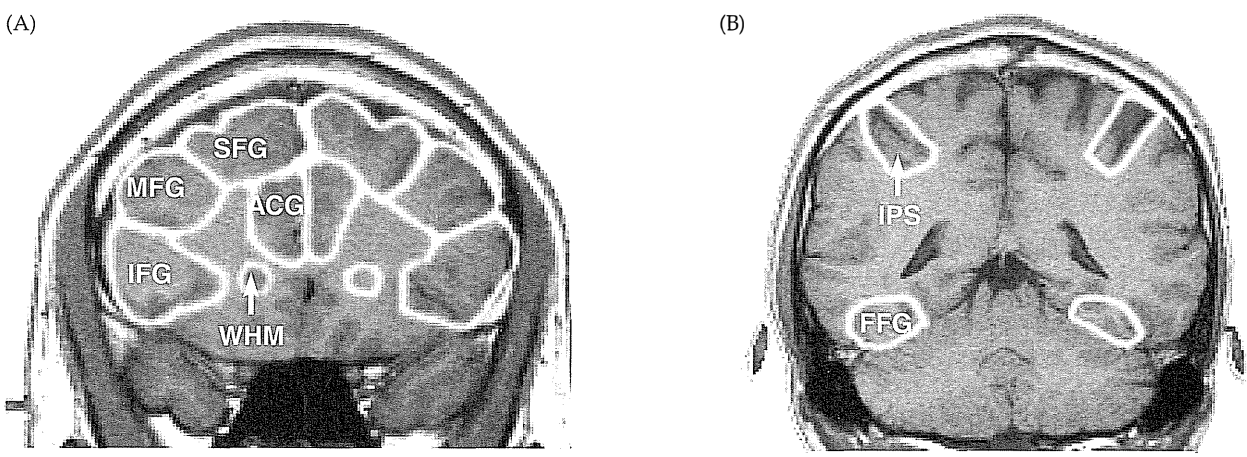

Figure 10.19 Region-of-interest analysis. Region-of-interest (ROI) analyses divide the brain into sections based on anatomical or functional criteria. (A) Shown on a coronal slice of the brain are locations of the inferior (IFG), middle (MFG), and superior (SFG) frontal gyri, the anterior cingulate gyrus (ACG), and a white-matter control region (WHM). (B) Shown on a coronal slice of the brain are locations of the intraparietal sulcus (IPS) and the fusiform gyrus (FFG). These ROIs were drawn based on anatomical criteria. (From Jha and McCarthy, 2000.)

within the brain. Comparisons between ROIs, whether in different regions of the same slice or in the same region across slices, can be used to create simple and easily understood parametric activation maps. Finally, ROI approaches ameliorate many of the problems of comparing data between subjects. When brain regions are drawn on a subject-specific basis, they match spatial locations across the subject sample, thus eliminating inaccuracies introduced when normalizing an individual's anatomy to a reference brain.

While anatomical ROI analyses provide important information about the functional properties of particular brain regions, they introduce a new problem: the potential mismatching of anatomical and functional regions of the brain. The idea that anatomically distinct regions of the brain are likely to have different functional properties is not new. An early and influential map of the brain was created by the German physician and neurobiologist Korbinian Brodmann, who divided the human cerebral cortex into nearly 50 anatomically distinct regions, known as Brodmann areas (see Box 6.2, Figure 4). Brodmann's areas were defined by their cytoarchitecture—differences in the size, types, and distribution of neurons within a brain region—and do not necessarily correspond to specific gyri or sulci. Functional MRI, at least at the spatial resolution typical of human studies, provides no information about cytoarchitectural features of the brain; thus, Brodmann areas cannot be directly determined for a particular MRI subject. However, even with perfect anatomical mapping, there would remain the problem of linking anatomical regions to functional divisions within the brain. For example, a complex task like the visual recognition of objects relies on defined occipitotemporal and occipitoparietal pathways that cross many anatomical regions. This problem can be partially overcome by drawing several ROIs that encompass different anatomical components of a functional network. Conversely, a single anatomical region may contain multiple functional regions. If only a small subdivision of the anatomical ROI is activated by your task, then your functional SNR may be reduced by the inclusion of many inactive voxels. Even finely mapped anatomical ROIs may not reflect true functional divisions within the brain.

Another powerful approach is to create functional ROIs, which include only voxels that were activated by a particular stimulus. For example, in many studies of face processing in the fusiform gyrus, Kanwisher and colleagues used a screening task, also known as a localizer task, to identify voxels that are differentially activated by faces compared with other complex visual stimuli. These face-activated voxels then comprised a functional "face area" ROI that the researchers used to evaluate the effects of other experimental manipulations (e.g., identity changes, selective attention) on face processing. Creating functional ROIs is critical when the boundaries of a (functionally significant) brain region cannot be readily identified by anatomical landmarks (e.g., the frontal pole, the temporoparietal junction). For an extended discussion of the value and limitations of this approach, we refer interested readers to the 2006 articles by Friston and by Kanwisher and their colleagues.

Both practical and theoretical problems prevent the universal use of ROI approaches. Simply put, creating anatomical ROIs can be extremely challenging. There are some automated programs that partition the brain into anatomical regions based on segmentation algorithms and templates of typical brain structure. Though much progress has been made, variation among subjects in the size, shape, and local organization of the brain impedes the development universally valid, but fully automated programs. Conversely, drawing anatomical ROIs manually on the structural MRI images requires substantial training, well-defined landmarks, and considerable labor. The subjective nature of ROI

Brodmann areas Divisions of the brain based on the influential cytoarchitectonic criteria of Korbinian Brodmann.

cytoarchitecture The organization of the brain on the basis of cell structure.

functional ROI A region of interest that is chosen based on functional criteria, such as the output of an independent voxelwise analysis.

localizer task An simple experimental paradigm designed to identify a set of voxels based on a known functional property, in preparation for subsequent analyses of that region in different paradigms.

drawing means that statistical evaluations are necessary to confirm that ROIs drawn by different people correspond with each other accurately. Therefore, ROI creation programs that combine the best features of automated and by-hand drawing are of great interest. These programs require the user to identify anatomical landmarks, such as major sulci, and the programs partition the brain into ROIs based on those landmarks. This combination provides a good compromise between accuracy and speed of creation.

Due to the variability in function within any anatomical region, ROI approaches to fMRI analysis should be combined with voxelwise approaches whenever possible. One potential combined approach is to use the anatomical ROI as a grouping factor. An investigator can then count and compare, for each experimental condition, the voxels identified in a voxelwise analysis within that ROI. The investigator can also remove data for the active voxels within the ROI and then examine the average time course of BOLD intensity in the remaining voxels. This approach can be used to search for voxels that may have a different pattern of activation than those identified using the general linear model. Finally, information about the differential timecourses of voxels within an ROI may lead to novel conclusions about local functions within a brain region, as will be discussed in Chapter 11.

Intersubject Analyses

So far, we have focused on the issue of identifying areas of activation within a single subject's brain. Yet nearly all fMRI studies involve multiple subjects, usually at least 15 per experiment. Often many more subjects are included, in experiments involving across-group comparisons. How can one use all of this data to better test experimental hypotheses? Combining data from multiple subjects presents several challenges. It is difficult to match anatomical locations between subjects, given the wide variability in shape and size of the adult human brain. Most experiments overcome this challenge by normalizing all subjects' data to a common stereotaxic space, as introduced in Chapter 8, either during preprocessing or following each subject's analysis. In conjunction with spatial smoothing, normalization greatly reduces anatomical differences between subjects, at a cost of functional resolution. Less common, but very useful, are ROI analyses for identifying particular brain regions based on each subject's anatomy, as described in the preceding section. Even if one is confident that the same brain region is identified in all subjects, whether by normalization or ROI, a theoretical problem remains: that of how to combine data from that region in multiple subjects, into a single statistical test.

There are two common approaches for intersubject analyses. For simplicity of exposition, we will consider how each approach affects the analysis of a single experiment with eight subjects who participated in two blocks with ten data points in each. However, the basic concepts discussed here apply to any number of subjects, to any number of data points in any design, and to any statistical test. The first, and most obvious, analysis approach involves combining all data points from all subjects into a single analysis. The 80 data points in the task condition and the 80 data points in the control condition could be compared using a t-test with 158 degrees of freedom. These approaches are known as fixed-effects analyses (Figure 10.20A), because they assume that the experimental effect is fixed, or constant across subjects, apart from the influence of random noise. Applied to fMRI data, fixed-effects models assume that the experimental manipulation has the same effect on BOLD signal in every

fixed-effects analyses Intersubject analyses that assume that the effect of the experimental manipulation is fixed across subjects, with differences between subjects caused by random noise.

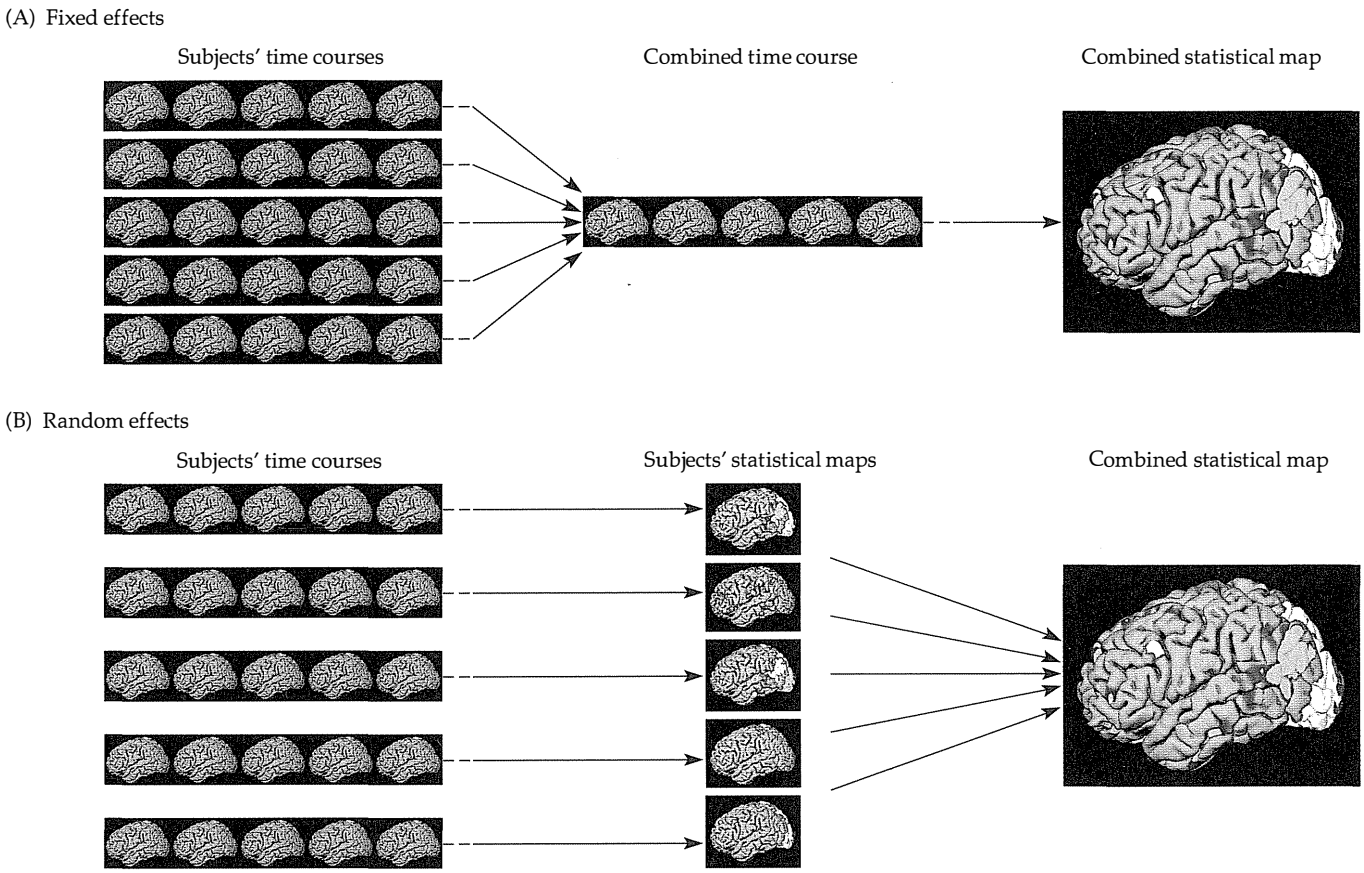

Figure 10.20 Conceptual outline of fixed- and random-effects analyses. (A) In a fixed-effects analysis, the experimental effect is assumed to be constant (i.e., fixed) across the subject population, so the experimental manipulation has the same effect on all subjects. The data are from all subjects are combined and then undergo testing for significance. (B) In a random-effects analysis, the experimental effect is considered to vary between subjects. A statistical map is created for each subject, and then the output of those statistical tests is subjected to a further level of analysis. The advantage of random-effects analyses is that they allow researchers to make inferences about the populations from which the subjects were drawn.

random-effects analysis Intersubject analysis that treats the effect of the experimental manipulation as variable across subjects, so that it could have a different effect on different subjects.

subject. (Note that, in the present section, the terms "fixed" and "random" refer solely to the subject factor. Other factors in the model are usually fixed, but might be random, depending on the experimental hypotheses.)

Though popular, fixed-effects analyses have an important disadvantage: they restrict statistical inferences to the particular sample of subjects used in the study. Suppose that in two of your subjects you measure a very large effect, while in the other six there is no effect at all. After averaging across the subjects, you compare your conditions by *t*-test and find that they differ significantly. You immediately recognize that this significant result seems inconsistent with the data, given that there was no effect in 75% of your subjects. This contradiction results from the sensitivity of fixed-effects models to extreme results from individual subjects. Under the assumption that the experimental manipulation affects all subjects similarly, the best estimate for its true effect is the mean of the data from all subjects. But, if the manipulation does not affect all subjects similarly, then the mean value might be misleading.

In order to make inferences about the population from which subjects are drawn, analyses must include information about the distribution of the effect across subjects. Each subject can be considered as one of many possible subjects who could have participated in the experiment. The experimental manipulation could have a different effect on each of these potential subjects; that is, some could have a large BOLD response, while others could have a small BOLD response. Most fMRI studies use a multi-stage random-effects analysis (Figure 10.20B). Since the combination of data from multiple subjects almost always treats independent variables as having *fixed* effects at earlier stages of

analysis, random-effects analyses (at the intersubject level) can also be considered as *mixed*-effects analyses, if information about the variability at the subject level is carried up to the intersubject level.

For clarity of presentation, we will describe a three-level analysis that progresses from runs to subjects to the sample; some fMRI analysis software combines the first two of these levels into one step. In the first-level analysis, the researcher calculates summary statistics (e.g., parameter estimates for regressors of interest) for the data from each run from each subject, independently. Then, in the second-level analysis, these statistics are combined from all runs performed with each subject, using a fixed-effect analysis. If a voxelwise approach is used, this creates a statistical map of the contrasts of interest for each subject. In the third-level analysis, the distribution of data from all the subjects is itself tested for significance. As a rough approximation, this can be done using a *t*-test that evaluates whether the subjects' summary statistics are drawn from a distribution with a mean of zero. More powerful statistical approaches incorporate variances from earlier levels to better estimate the true significance of the effects. If this third-level statistical test is significant at the established alpha value, then the researchers can conclude that the experimental manipulation would have an effect on the population from which the subjects were drawn. Note that the subject population for many fMRI studies may itself be unrepresentative, in that subjects tend to be college-age, intelligent, physically healthy, and neurologically normal. The use of random-effects analyses does not allow extension of results to those individuals who are not within the subject population (e.g., the elderly, children, or patient groups).

Thought Question

Given the limitation of random-effects analyses discussed here, what sorts of experiments are necessary for fMRI results to be applicable to a wide range of subject groups? What problems with subject selection and experimental design would researchers encounter?

In summary, fixed-effects analyses allow inferences about the group of subjects who were used in a particular study, while random-effects analyses allow inferences about the population from which the subjects were drawn. Random-effects analyses can be conducted with minimal additional computation, and most statistical packages now include them within standard analysis procedures. While studies using fixed-effects models are still published, many journal reviewers and granting agencies have recognized the importance of random-effects models, and evaluate manuscripts and grants accordingly. Thus, random-effects analyses are strongly recommended for fMRI studies.

Group and parametric effects

Often, fMRI researchers want to go beyond the identification of significant activation to describe how some subject characteristics influence the amplitude of that activation. Between-group comparisons involve testing different groups, such as males and females, to look for differences in some key characteristic. This approach is particularly important for fMRI studies of clinical populations. To better understand the brain dysfunction that contributes to depression, researchers might compare a patient group consisting of individuals with major depression with a control group consisting of individuals without any

depressive symptoms. Similarly, to understand age-related changes in frontal lobe function, researchers might compare a group of 20–30 year old individuals with a group of 65–75 year olds. Between-session comparisons involve testing the same individuals in multiple sessions that differ only in the independent variable (e.g., before and after drug therapy). Both types of comparison require the use of different statistical tests than those used for single-group analyses. Remember that single-group analyses evaluate whether an independent variable caused systematic changes in the BOLD signal (i.e., the parameter effects or contrast values were unlikely to have occurred by chance). Between-group comparisons evaluate whether two groups of individuals were influenced differently by the independent variable (i.e., the group differences in their parameter effect were unlikely to have occurred by chance), usually through simple statistics like a two-sample *t*-test. Because between-session comparisons include two or more similar tests per subject, intersubject variability can be accounted for using a paired *t*-test.

Group comparisons can lead to valuable new results, but do require careful planning. As for any other between-subjects research, the primary challenge of fMRI group comparisons is matching the groups with regard to factors other than the independent variable of interest. For example, depressed and non-depressed individuals could differ in many factors (e.g., current job status, number of close friends, medication history) in addition to the depression itself. As introduced in Chapter 8, groups may differ in the amount of noise in the BOLD signal, through task-unrelated factors like increased head motion. Furthermore, the effects observed in between-group studies are generally small, given that they are usually modulations of some other effect. Session comparisons limit inter-individual variability, and thus provide greater experimental power. However, repeating an experiment over multiple sessions can introduce unwanted practice effects, confounding differences in brain function with changes in task difficulty or subject strategy. In general, sample sizes for group comparisons need to be much larger than for standard single-group studies, or Type II errors will be likely.

Another approach for understanding differences between groups is to use some parametric trait (e.g., extraversion, depression score, age) as a covariate in the across-subjects analyses. This approach is used to test hypotheses of the form: in what brain regions does the differential activation identified by contrast X vary with trait Y? In a study published in 2007, Spitzer and colleagues investigated the relationship between the neural response to social punishment and the personality trait of selfish opportunism, also known as "Machiavellianism." Each subject played an economic game in which they could divide up a pot of money between himself and an opponent outside of the scanner. In some trials, the opponent could sacrifice some of his own money to take money away from the subject (i.e., as punishment), if the division seemed unfair. The authors found that the lateral orbitofrontal cortex exhibited increased activation when there was the potential for punishment, compared with control trials when the opponent could not respond (Figure 10.21). Notably, the magnitude of this activation correlated well with the subjects' Machiavellianism scores, as measured by an independent personality test, suggesting that the Machiavellian trait may reflect (or lead to) increased sensitivity to social punishments. Parametric across-subjects tests can illustrate novel and compelling relationships between brain and behavior. Researchers must be careful, when reporting their findings, not to overstate the meaning of their results by mapping complex traits onto single brain regions. Moreover, the direction of causality (i.e., from trait to process to brain

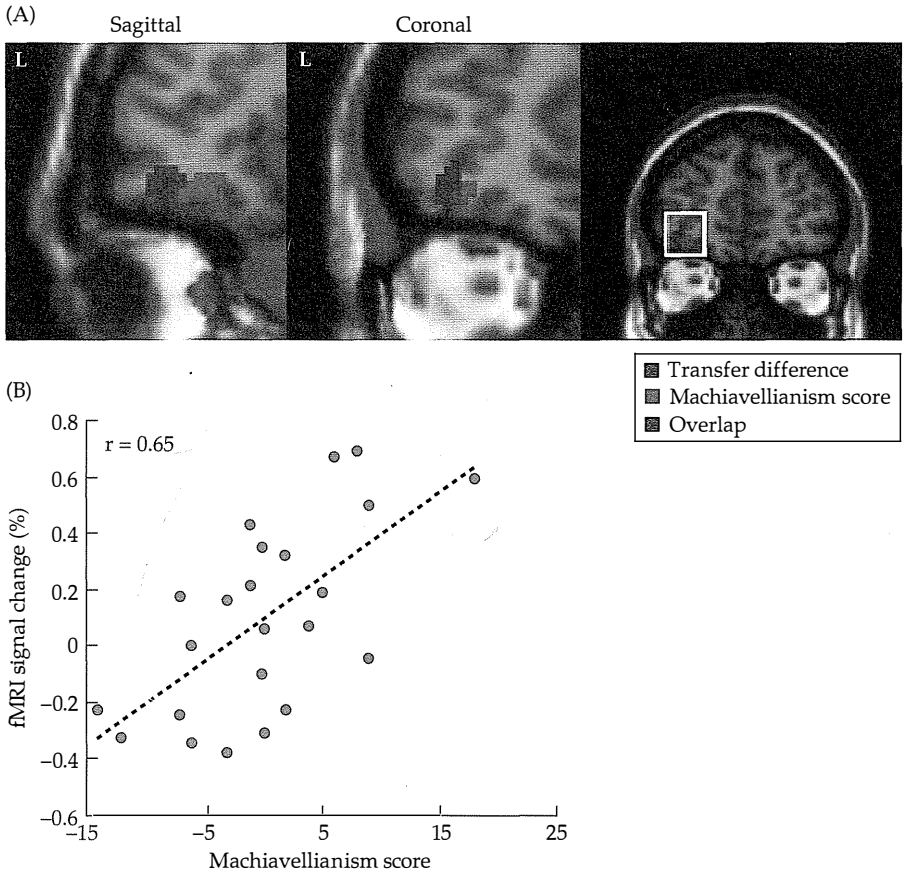

Figure 10.21 Relating fMRI activation to individual differences in a psychological trait. To understand the brain mechanisms that might underlie compliance with social norms, Spitzer and colleagues measured fMRI activation while subjects (in the scanner) divided up a pot of money between themselves and an opponent (outside the scanner). Some of the time, the opponent could take money away from the fMRI subject if the division was unfair (i.e., punishing him or her if too little money was transferred). (A) The authors measured activation in the orbitofrontal cortex (locations shown on the figure), in trials in which punishment was possible, compared with trials in which punishment was not possible. They found that activation was highly correlated with both a subject's generosity (i.e., their mean transfer difference) and with the subject's Machiavellianism score (a psychological scale of self-interested opportunism). (B) Those subjects who were the most Machiavellian, according to the independent psychological scale, tended to have the greatest activation in the orbitofrontal region, potentially linking this brain structure to this trait.

differences, or from brain differences to process to trait) can rarely be gleaned from fMRI data.

Displaying Statistical Results

The goal of most fMRI statistical tests, regardless of their complexity, is to evaluate the probability that the response in each voxel is consistent with the null hypothesis. When statistical tests from all voxels in the brain are combined, the result is a statistical map, or statistical parameter map, of brain activation (see also Figure 10.1). The statistical map is usually color-coded according to the probability value for each voxel. For example, if the (corrected) alpha value for an experiment was set at 0.01, a voxel with a near alpha probability value of 0.009 might be displayed in dark red, while a voxel with an extremely low probability value of 0.000001 might be shown in bright yellow. The association between probability values (or other statistic) and the colors that label them is known as a color map. In general, researchers use darker colors to indicate low significance levels and brighter colors to indicate high significance levels. The statistical map is usually displayed on top of a base image that illustrates brain anatomy. It is important not to confuse the properties of the base anatomical image with those of the overlaid statistical map. The former is usually of high resolution and has contrast dependent on a physical property of the brain (e.g., T_1), while the latter is a calculated statistical map reflecting the correspondence of the data to an experimental hypothesis. Note that although

statistical map (or statistical parameter map) In fMRI, the labeling of all voxels within the image according to the outcome of a statistical test.

color map The association between numerical values of a parameter and a set of colors.

base image The image on which a statistical map is displayed, often a high-resolution anatomical image.

radiological convention The practice of displaying images of the brain so that the left side of the image is the right side of the brain and vice versa, as if one were facing the subject.

neurological convention The practice of displaying images of the brain so that the left and right sides of the image correspond to the same sides of the brain, as if one were behind the subject.

the vast majority of color maps display statistical significance, other properties, such as percent signal change or latency, can also be displayed; see Figure 7.25 for an example.

There are many options for displaying fMRI data, each with advantages and disadvantages. Most commonly shown are single anatomical slices with overlaid color maps (Figure 10.22A). While these are relatively simple to create and interpret, readers may find it challenging to identify specific anatomical regions (i.e., which gyrus or sulcus is active). Depending on the area of interest, one slice orientation may be better than another. Gyri and sulci that run from left to right (e.g., the central sulcus) are difficult to identify in coronal slices, while those running from front to back (e.g., most frontal gyri) are harder to interpret in axial slices. Another limitation of single-slice displays is the choice of slices to include. Rarely will all the collected slices be displayed in a single poster, manuscript, or lecture slide, due to their sheer number. Instead, the researcher will display selected slices that illustrate the major activation locations found in the study. When showing single slices in research articles, it is critical to explicitly label the left and right hemispheres, due to the axial symmetry of the human brain. Historically, MRI data have been displayed in radiological convention, such that the left side of the image corresponds with the right side of the brain and vice versa. This convention results from the way in which radiologists typically interact with patients, who are generally facing them or lying in scanners with their feet toward them. Displaying fMRI data in normal or neurological convention (i.e., based on a surgeon looking from the head to the feet) has become increasingly common in recent years.

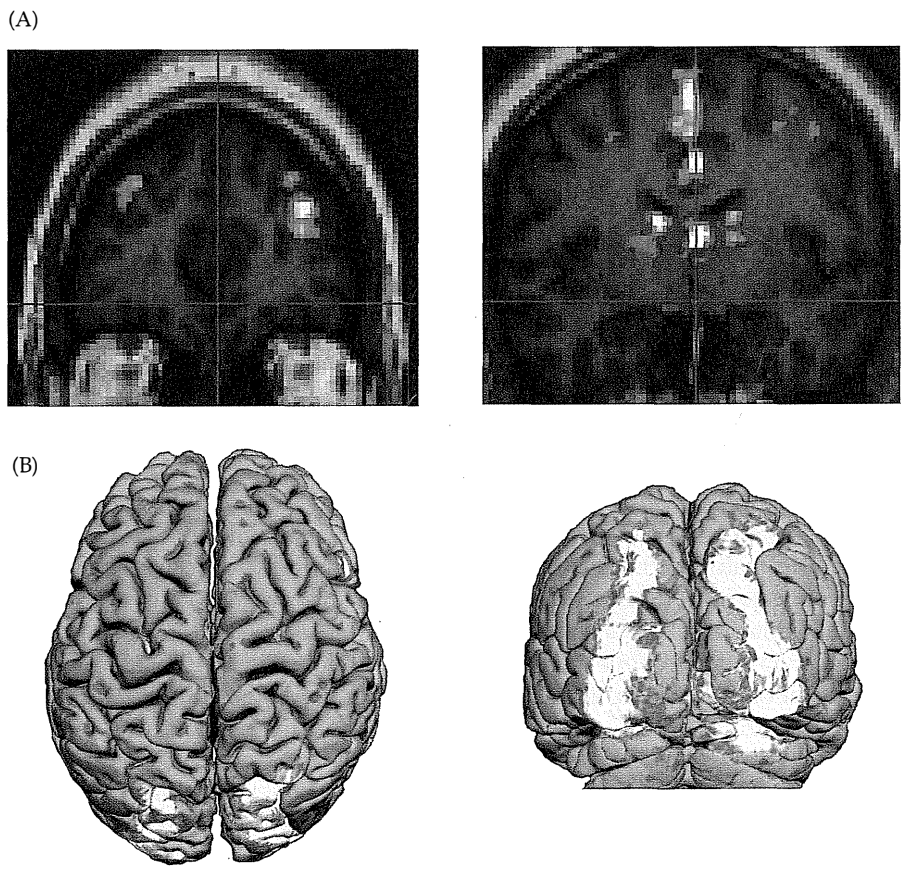

Figure 10.22 Two- and three-dimensional representations of fMRI data. Statistical maps of fMRI data are typically shown either as two-dimensional slices (A) or as three-dimensional rendered brains (B). (B from Huettel et al., 2001, created using FreeSurfer, CorTechs/Martinos Imaging Center, Boston, MA.)

While statistical maps are often calculated and displayed as two-dimensional slices, they can also be displayed in three-dimensional perspective (Figure 10.22B). Such displays are often called **rendered images**. The major advantage of three-dimensional rendering is that one can easily identify the locations of brain activation, especially with regard to prominent gyri and sulci. Such images are also more easily interpreted by naïve viewers who are more familiar with the general shape and external structure of the brain than with specific internal features. Hidden, however, are internal structures, such as the basal ganglia and thalamus, as well as internal cortical regions like the hippocampus, cingulate, and insula. In published figures, researchers often cut away a corner or side of the brain to reveal these and other deeper structures. It is also more difficult to show both hemispheres simultaneously in a single image, so authors often include more than one rendered image within a single figure. To overcome the problems introduced by the opacity of rendered images, some analysis programs generate transparent or semitransparent images, sometimes called **glass-brain views** (Figure 10.23A). These project all foci of activation onto an outline of the brain, allowing the researcher to see all of the activations at once. As with any projective display technique, a single glass-brain view is considerably underdetermined, in that many possible sets of activations could lead to the displayed image. For this reason, three orthogonal projections of the data are displayed. In addition, most programs also generate a set of three anatomical or reference slices that correspond with the glass-brain views, so that researchers can more easily localize activations (Figure 10.23B). Even experienced fMRI scientists can find complex glass-brain figures difficult to interpret, making them inappropriate for many purposes. They can, however, clearly show the specificity (or absence) of activation in a given contrast.

Rendering a brain image can be very computationally intensive, especially if the analysis program generates a smooth high-resolution surface based on an anatomical image. Many researchers, therefore, use simple two-dimensional

rendered image A display of MRI data in three-dimensional perspective.

glass-brain view A two-dimensional projection of fMRI data, as if the brain were made transparent and only the activations were visible.

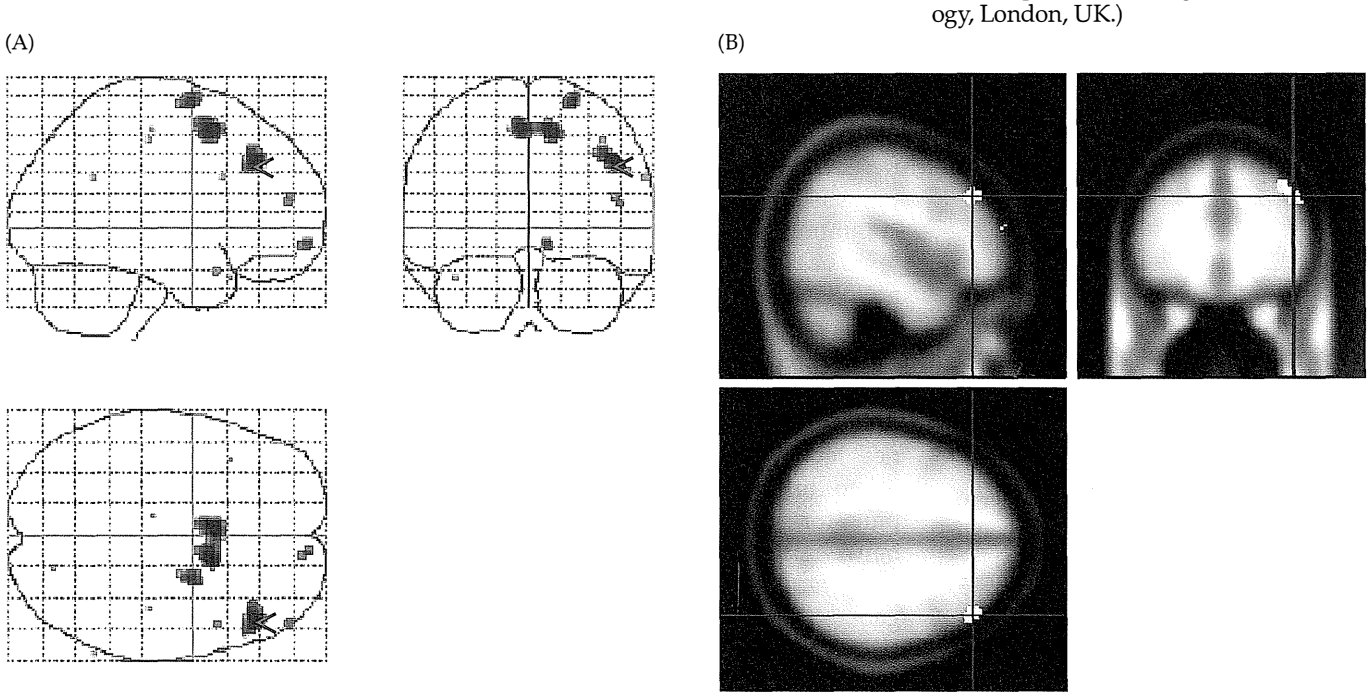

Figure 10.23 Glass-brain views of fMRI data. One common way to visualize fMRI data is to use a "glass-brain" view (A), which shows three orthogonal projections of the original data. The red arrow (<) in each view shows the same brain location. All activations are visible in each orientation, although it can be difficult to identify their anatomical locations. For this reason, although glass-brain views are useful when working with the data, other views may be preferable for a final display. Use of projection views in conjunction with anatomical or reference slices (B) makes identification of activation foci much easier. (Images created using SPM; Wellcome Department of Cognitive Neurology, London, UK.)

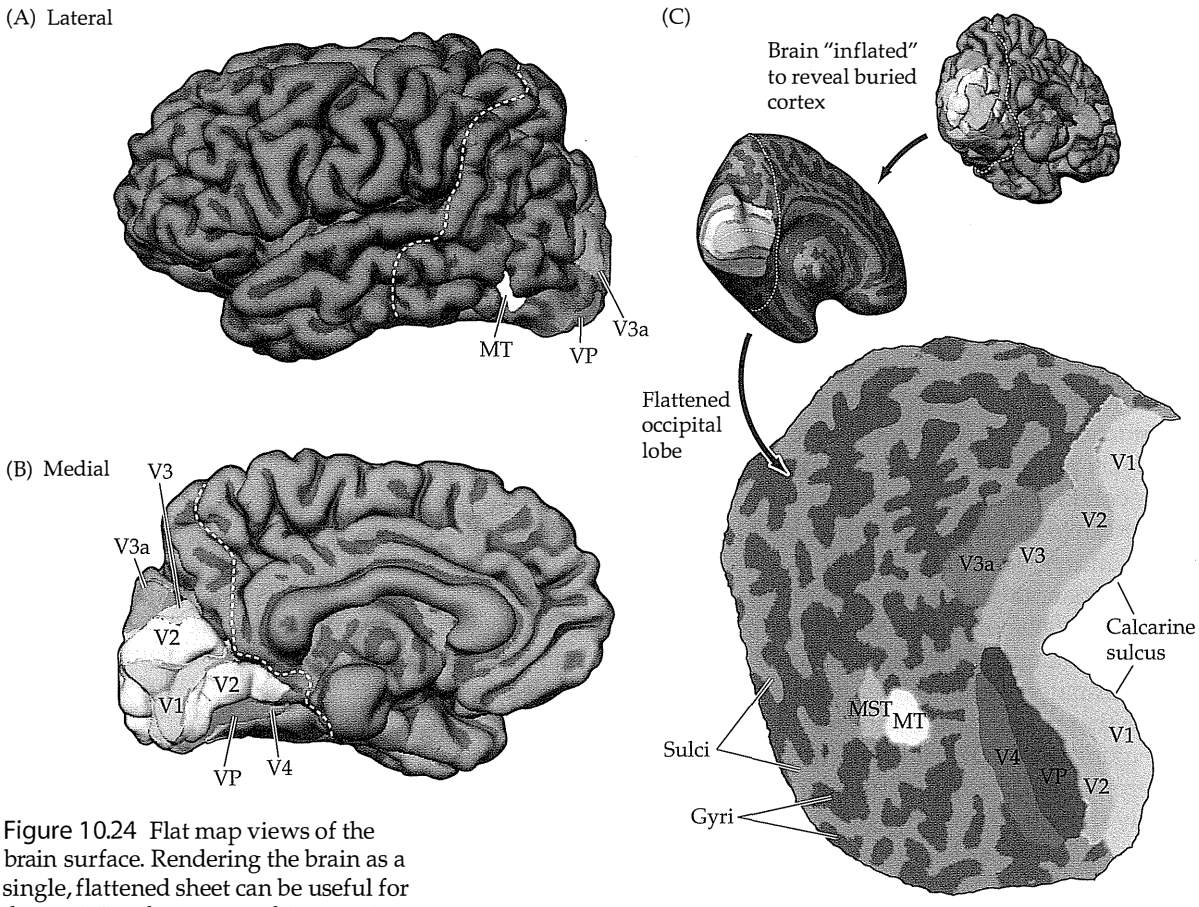

Figure 10.24 Flat map views of the brain surface. Rendering the brain as a single, flattened sheet can be useful for determining the topographic organization of the cortex. The most common use of flattened views is for retinotopic mapping of the visual cortex. After identifying areas of activation, as shown here on lateral (A) and medial (B) views of the visual cortex, researchers inflate, cut, and flatten the cortical surface (C) to show the spatial distribution of active regions. (After Sereno et al., 1995.)

or glass-brain displays when working with data from an experiment, and only create the high-quality rendered images when making final figures for a manuscript. Besides standard surface views, several other types of rendered images are available. To illustrate activation that lies within deep cortical sulci, the outer cortical layer can be removed or de-emphasized. For applications where precise distinctions between adjacent brain regions must be made, researchers may display fMRI data on inflated brains or flat maps (Figure 10.24). This is most common for retinotopic mapping of the visual system. Remember that the cortex is basically a single folded sheet about 5 mm in depth. As its name implies, an inflated brain recovers this structure by expanding the cortical surface like a balloon while maintaining its basic shape. A flat map is obtained by cutting the inflated surface at different points and then laying out the cortical sheet in two dimensions. Since no changes in depth are visible in these techniques, the original gyral and sulcal patterns are marked using different colors or brightness levels. When a three-dimensional object like the brain is transformed into a two-dimensional map, there are by necessity some local distortions. Compare, for example, world globes and world maps; the latter either have cuts between adjacent areas (i.e., Goode's interrupted map) or distortions in size (i.e., Mercator projections). Similarly, distortion is a significant problem in the generation of flat maps of the brain.

inflated brain A transformation of the cortical sheet into a balloon-like structure, removing gyral and sulcal folds so that activation can be more easily viewed.

flat map An unfolded and flattened representation of the cortical sheet to allow viewing of topographic changes over cortical space. Flat maps are most commonly used in fMRI to illustrate the organization of the visual cortex.

Summary

Since fMRI studies rely on the detection of a weak signal in the presence of substantial noise, careful statistical analysis is necessary. Most fMRI analyses are based on hypothesis testing. The researcher sets up two hypotheses, an experimental hypothesis with some prediction about the data and a null hypothesis based on random chance. The probability that the data could have occurred under the null hypothesis is compared with a threshold alpha value, and if the alpha value is exceeded, then the result is declared significant. Two types of errors are possible in hypothesis testing. Type I errors occur when a non-significant result is declared significant (a false positive), while Type II errors occur when a significant result is missed (a false negative). Functional MRI analyses typically attempt to exclude Type I errors, but as a result they lead to many Type II errors. Significantly active voxels are displayed on statistical maps, usually with the degree of significance indicated using a color scale.

Nearly all statistical tests used for hypothesis testing in fMRI experiments are variants of the general linear model, which treats the data as a linear summation of independent regressors (i.e., condition effects). When using the general linear model to analyze fMRI data, an experimenter creates a design matrix that contains regressors of interest as well as other known, but uninteresting, sources of variability in the data (nuisance regressors). Based on this design matrix, statistical software is used to determine how a given regressor predicts changes in the BOLD signal (parameter estimates) and whether some regressors lead to larger changes than others (contrast effects). Regardless of the analysis approach used, a central problem for fMRI studies is the vast number of statistical tests they require, which leads to false positive results. Standard corrections like the Bonferroni method are too strict and may eliminate true activations. One approach is to use information about spatial properties of activation, either through Gaussian random field theory or cluster-size thresholds. Another approach is to reduce the number of tests by using region-of-interest analyses, which allow targeted studies of particular anatomical areas. Finally, for all statistical analyses, data should be combined from multiple subjects to increase experimental power. Random-effects analyses enable researchers to make inferences about the populations from which the subjects were drawn, and are therefore preferred over traditional fixed-effects analyses.

REFER TO THE
fMRI
COMPANION WEBSITE AT
www.sinauer.com/fmri2e
for study questions and Web links.

Suggested Readings

*Brodmann, K. (1909). *Vergleichende Lokalisationslehre der Grosshirnrinde in ihren Prinzipien dargestellt auf Grund des Zellenbaues.* Barth, Leipzig, Germany. *A remarkably detailed collection of anatomical studies of human and animal cortices. An English-language translation by L. J. Garey from Imperial College Press is now available.*

Friston, K. J., Holmes, A. P., Worsley, K. J., Poline, J. P., Frith, C. D., and Frackowiak, R. S. J. (1995). Statistical parametric maps in functional imaging: A general linear approach. *Hum. Brain Mapping*, 5: 189–210. *Describes the use of the general linear model for analysis of PET and fMRI data; forms the basis for the popular statistical parametric mapping (SPM) approach to data analysis.*

Hill, T. and Lewicki, P. (2007). STATISTICS Methods and Applications. StatSoft, Tulsa, OK. *Provides a comprehensive and accessible overview to a wide range of statistical concepts. Also available at* www.statsoft.com/textbook/stathome.html.

Smith, S. M., Jenkinson, M., Woolrich, M. W., Beckmann, C. F., Behrens, T. E., Johansen-Berg, H., Bannister, P. R., De Luca, M., Drobnjak, I., Flitney, D. E., Niazy, R. K., Saunders, J., Vickers, J., Zhang, Y., De Stefano, N., Brady, J. M., and Matthews, P. M. (2004). *Advances in functional and structural MR image analysis and implementation as FSL. NeuroImage,* 23: S208–19. *This paper introduces the core concepts from the popular FMRIB Software Library (FSL) for the analysis of fMRI data.*

*Worsley, K. J., Marrett, S., Neelin, P., Vandal, A. C., Friston, K. J., and Evans, A. C. (1995). A unified statistical approach for determining significant signals in images of cerebral activation. *Hum. Brain Mapping,* 4: 58–73. *This paper establishes the mathematical underpinnings for spatial comparisons of functional brain images.*

*Indicates a reference that is a suggested reading in the field and is also cited in this chapter.

Chapter References

Aguirre, G. K., Zarahn, E., and D'Esposito, M. (1998a). A critique of the use of the Kolmogorov–Smirnov (KS) statistic for the analysis of BOLD fMRI data. *Magn. Reson. Med.,* 39: 500–505.

Aguirre, G. K., Zarahn, E., and D'Esposito, M. (1998b). The variability of human, BOLD hemodynamic responses. *NeuroImage,* 8: 360–369.

Bandettini, P. A., Jesmanowicz, A., Wong, E. C., and Hyde, J. S. (1993). Processing strategies for time-course data sets in functional MRI of the human brain. *Magn. Reson. Med.,* 30: 161–173.

Birn, R.M., Diamond, J.B., Smith, M.A., Bandettini, P.A. (2006). Separating respiratory-variation-related fluctuations from neuronal-activity-related fluctuations in fMRI. *NeuroImage,* 31: 1536–48.

Cantlon, J. F., Brannon, E. M., Carter, E. J., and Pelphrey, K. A. (2006). Functional imaging of numerical processing in adults and 4-y-old children. *PLoS Biology,* 4: e125.

Calhoun, V. D., Stevens, M. C., Pearlson, G. D., and Kiehl, K. A. (2004). fMRI analysis with the general linear model: removal of latency-induced amplitude bias by incorporation of hemodynamic derivative terms. *NeuroImage,* 22: 252–257.

Cordes, D., Haughton, V., Carew, J. D., Arfanakis, K., and Maravilla, K. (2002). Hierarchical clustering to measure connectivity in fMRI resting-state data. *J. Magn. Reson. Imaging,* 20: 305–317.

Cox, R. W. (1996). AFNI: Software for analysis and visualization of functional magnetic resonance neuroimages. *Comput. Biomed. Res.,* 29: 162–173.

Devlin, J. T. and Poldrack, R. A. (2007). In praise of tedious anatomy. *NeuroImage,* 37: 1033–41.

Forman, S. D., Cohen, J. D., Fitzgerald, M., Eddy, W. F., Mintun, M. A., and Noll, D. C. (1995). Improved assessment of significant activation in functional magnetic resonance imaging (fMRI): Use of a cluster-size threshold. *Magn. Reson. Med.,* 33: 636–647.

Freedman, D., Pisani, R., and Purves, R. (1997). *Statistics.* Norton, New York.

Friston, K. J., Josephs, O., Rees, G., and Turner, R. (1998). Nonlinear event-related responses in fMRI. *Magn. Reson. Med.,* 39(1): 41–52.

Friston, K. J., Rotshtein, P., Geng, J. J., Sterzer, P., and Henson, R. N. (2006). A critique of functional localisers. *NeuroImage,* 30: 1077–87.

Friston, K. J., Fletcher, P., Josephs, O., Holmes, A., Rugg, M. D., and Turner, R. (1998). Event-related fMRI: characterizing differential responses. *NeuroImage,* 7 30–40.

Genovese, C. R., Lazar, N. A., and Nichols, T. (2002). Thresholding of statistical maps in functional neuroimaging using the false discovery rate. *NeuroImage,* 15: 870–878.

Glover, G. H., Li, T. Q., and Ress, D. (2000). Image-based method for retrospective correction of physiological motion effects in fMRI: RETROICOR. *Magn. Reson. Med.,* 44: 162–167.

Hayasaka, S. and Nichols, T. E. (2003). Validating cluster size inference: random field and permutation methods. *NeuroImage*, 20: 2343–2356.

Hayasaka, S., Peiffer, A. M., Hugenschmidt, C. E., and Laurienti, P. J. (2007). Power and sample size calculation for neuroimaging studies by non-central random field theory. *NeuroImage*, 37: 721–730.

Hays, W. L. (1994). *Statistics* (5th ed.). Harcourt College, Fort Worth, TX.

Huettel, S. A., Güzeldere, G., and McCarthy, G. (2001). Dissociating the neural mechanisms of visual attention in change detection using functional MRI. *J. Cogn. Neurosci.*, 13(7): 1006–1018.

Jha, A. P., and McCarthy, G. (2000). The influence of memory load upon delay-interval activity in a working-memory task: An event-related functional MRI study. *J. Cogn. Neurosci.*, 12(Suppl. 2): 90–105.

Johnstone, T., Ores Walsh, K. S., Greischar, L. L., Alexander, A. L., Fox, A. S., Davidson, R. J., and Oakes, T. R. (2006). Motion correction and the use of motion covariates in multiple-subject fMRI analysis. *Hum. Brain Mapping*, 27: 779–788.

Kanwisher, N., McDermott, J., and Chun, M. (1997). The fusiform face area: A module in human extrastriate cortex specialized for the perception of faces. *J. Neurosc.*, 17: 4302–4311.

Knutson, B., Rick, S., Wimmer, G. E., Prelec, D., and Loewenstein, G. (2007). Neural predictors of purchases, *Neuron*, 53: 147–156.

Logan, B. R. and Rowe, D. B. (2004). An evaluation of thresholding techniques in fMRI analysis. *NeuroImage*, 22: 95–108.

Lund, T. E., Madsen, K. H., Sidaros, K., Luo, W. L., and Nichols, T. E. (2006). Non-white noise in fMRI: does modelling have an impact? *NeuroImage*, 29: 54–66.

Nichols, T. and Hayasaka, S. (2003). Controlling the familywise error rate in functional neuroimaging: a comparative review. *Stat. Methods Med. Res.*, 12: 419–446.

Saxe, R., Brett, M., and Kanwisher, N. (2006). Divide and conquer: a defense of functional localizers. *NeuroImage*, 30: 1088–1096; discussion 1097–1099.

Schlosser, M. J., Luby, M., Spencer, D. D., Awad, I. A., and McCarthy, G. (1999). Comparative localization of auditory comprehension by using functional magnetic resonance imaging and cortical stimulation. *J. Neurosurg.*, 91: 626–635.

Sereno, M. I., Dale, A. M., Reppas, J. B., Kwong, K. K., Belliveau, J. W., Brady, T. J., Rosen, B. R., Tootell, R.B. (1995). Borders of multiple visual areas in humans revealed by functional magnetic resonance imaging. *Science*, 268: 889–893.

Spitzer, M., Fischbacher, U., Herrnberger, B., Gron, G., and Fehr, E. (2007). The neural signature of social norm compliance. *Neuron*, 56: 185–196.

Xiong, J., Gao, J., Lancaster, J. L., and Fox, P. T. (1995). Clustered pixels analysis for functional MRI activation studies of the human brain. *Hum. Brain Mapping*, 3: 287–301.

Chapter 11

Statistical Analysis II: Advanced Approaches

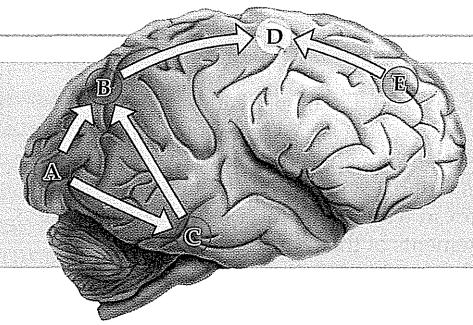

In Chapter 10 we introduced the core analysis methods that are used in the vast majority of fMRI studies. Most of those methods use variants of the general linear model to test specific hypotheses about brain function. These hypothesis-driven analyses have accounted for much of the growth of fMRI over the past decade, but they cannot address some potentially important research questions. In this chapter, we outline important and novel techniques for fMRI data analysis that go well beyond multiple regression. These techniques borrow technical concepts from many fields, including statistics and mathematics, economics and other social sciences, engineering, and computer science.

In general, the techniques described in this chapter are used to achieve one of two goals: exploration or prediction. Some techniques explore fMRI data in search of systematic variation, without necessarily adopting an a priori model for that variation. These data-driven analyses often use mathematical algorithms that partition the four-dimensional fMRI time series into a set of components that may reflect distinct aspects of brain functioning. Data-driven analyses may identify regularities that are clearly task-related (Figure 11.1), or they may discover task-unrelated variability that can be eliminated during preprocessing. These analyses are not subject to some of the problems that compromise hypothesis-driven analyses: poorly chosen models, unknown timing of neuronal activity, and variability in the hemodynamic response. Yet, they present many technical and interpretative challenges. Other techniques reverse the traditional direction of fMRI analyses, in that they use fMRI data to predict variations in behavior, perception, or cognition. Researchers now use fMRI to predict many aspects of thought and behavior, including susceptibility to psychiatric disorders, personality traits, complex economic decisions, and even conscious awareness of stimuli.

Some techniques do not fit neatly into one of these two categories. For example, we will also consider techniques for measuring the connectivity between brain regions; these share both exploration and prediction as goals. Yet, all of these techniques differ (sometimes dramatically!) from the simpler regression approaches considered in Chapter 10. In many ways, these new analysis techniques represent the future of BOLD fMRI, more than technological advances in fMRI technology.

hypothesis-driven analysis The evaluation of data based on statistical tests of the validity of a null hypothesis.

multiple regression A family of statistical approaches that evaluate the relative contributions of several independent variables to a dependent variable.

data-driven analysis Exploration of the intrinsic structure of data.

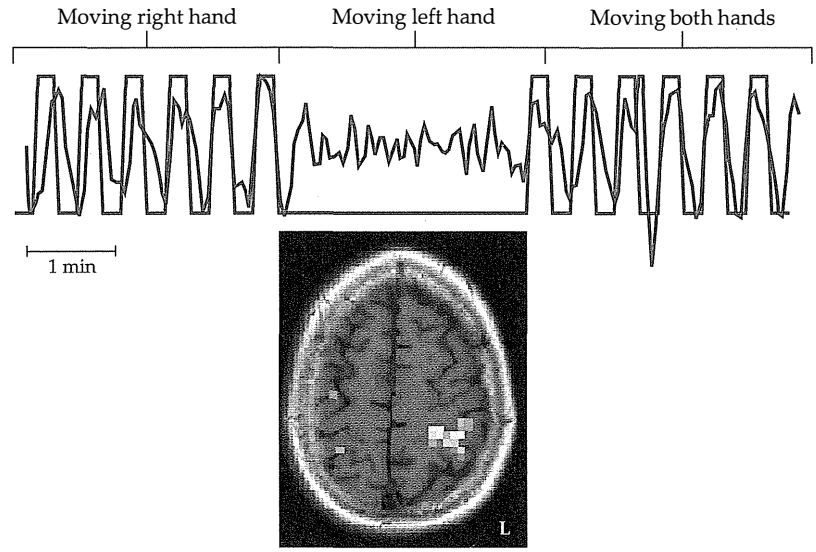

Figure 11.1 Data-driven analyses identify regular variation in fMRI data. This subject participated in a motor movement task with three phases: rotating the right hand at the wrist, rotating the left hand at the wrist, and rotating both hands simultaneously. The blocks of hand movement are shown in blue. By looking only at the raw fMRI data, using a technique called independent components analysis (ICA), the researchers found a set of voxels in the left motor cortex in which activation was evoked by all movements of the right hand. Note that these voxels were identified only by examination of the data themselves, not by hypothesis testing. (Data courtesy of Dr. Martin McKeown, University of British Columbia.)

Data Exploration Approaches

We here consider several techniques that allow researchers to explore their data for potentially meaningful variation. All parse the fMRI time series into sets of common features, or components, that consist of groups of voxels and their temporal properties. Importantly, their algorithms attempt to identify activation that is common to a group of voxels, rather than compare the activation of individual voxels with a hypothesized time course. The components are evaluated based on how much of the variation in the fMRI data they explain. These techniques vary both in the algorithms that they use to parse the time series data and, more importantly, in the rules they use to decide which features are meaningful. Some are completely model-free, in that they extract features without any regard to the underlying experimental paradigm. Others use some information about the task to shape how the components are extracted. These techniques can also differ somewhat in their goals; some are used to identify interesting forms of variability in order to suggest future analyses, while others are used to test simple hypotheses. We will discuss these approaches primarily in the context of identifying important aspects of brain function, however, some of these approaches are now also being used to identify uninteresting and non-task-related variability (e.g., for preprocessing).

Thought Question

Why might researchers use a combination of hypothesis-driven and data-driven analysis approaches?

component In the context of data-driven analyses, a feature of a data set that represents some aspect of its intrinsic structure.

Principal components analysis (PCA)

The major challenge of fMRI research, as outlined in previous chapters, lies in the detection of relatively small task-related variations against a large back-

ground of non-task-related processes, some representing random noise and others corresponding to unwanted regularities (e.g., breathing). This challenge can be overcome, at least theoretically, by the steps of preprocessing and data analysis: filtering the time series at noise frequencies, smoothing data across voxels, and averaging data from multiple events and sessions. But these steps, especially temporal filtering, require some knowledge of the properties of the noise compared with our signal of interest. What if one does not know the properties of the noise? Or, even more problematic, what if one does not know the properties of the signal? When faced with complex data sets like that of fMRI that contain several underlying components, including both task-related effects and different sources of noise, researchers often apply algorithms for data reduction. As the name implies, data reduction takes a complex, high-dimensional data set and transforms it into a simpler representation that retains most of the variation in the data.

A common technique for data reduction is principal components analysis (PCA). Considered broadly, PCA first identifies the component that accounts for the most variability in a dataset, then identifies a second component that accounts for the largest proportion of the remaining variability, and repeats until the desired number of components have been extracted. Any remaining variation in the data is discarded. (A related technique called factor analysis differs from PCA in that it only includes variation that is shared by all components, or factors, rather than including all variation in the dataset.) Because PCA is iterative, defining each component in relation to the previous components, the components are orthogonal to each other. For four-dimensional data sets like those obtained in fMRI studies, the components extracted by PCA can consist of eigenimages, or spatial patterns whose variations over time are expressed by their eigenvectors. The variance explained by each component is called its eigenvalue; larger eigenvalues mean that more variance is explained. It can be difficult to decide which components to retain and which to discard—that is, to define the set of components that accounts for the original data but does not include unwanted or spurious variability. One oft-used rule (the Kaiser Criterion) is to retain components that have eigenvalues greater than 1, which means that they explain at least as much variance as a variable from the original dataset. Another more graphical approach involves plotting the eigenvalue for each component, which will result in a curve known as a scree plot that resembles a decreasing exponential function. Then, the researchers discard all components beyond where the curve flattens out.

In theory, when researchers apply PCA to fMRI data, the output will consist of a set of components that represent regular activation patterns across voxels. If those components reflect interpretable consequences of an experimental task, then PCA can be used to map out functional systems that are distributed in different parts of the brain, which would be inaccessible when using normal hypothesis-based methods. However, PCA has many limitations. If the task-related signal constitutes only a minor portion of the experimental data, PCA is likely to misrepresent the pattern and timing of task activation. Furthermore, there are not always clear statistics for evaluating the significance of components. The best applications of PCA have involved combining it with other analysis techniques. For example, see the 2007 study by Ecker and colleagues, who initially identified subregions of visual cortex using standard hypothesis-driven techniques, and then used PCA to explore the functional connectivity among those regions.

data reduction The simplification of a data set by reducing its variability, such as by eliminating irrelevant, redundant, or non-predictive variables.

principal components analysis (PCA) A common technique for data reduction that simplifies high-dimensional data into a smaller set of components that retains most of the variability in the original data.

orthogonal A property of two variables (or vectors, sets of variables) such that they are completely uncorrelated with each other.

eigenimage Spatial maps, as generated by a principal components analysis, that reflect orthogonal components of a complex image (or time series of images).

eigenvector Following principal components analysis, a set of values that describes a component of the intrinsic variability in a dataset.

eigenvalue A mathematical description of the amount of variability in a dataset that is accounted for by a given component.

Independent components analysis (ICA)

independent components analysis (ICA) An important class of data-driven analyses that identify stationary sets of voxels whose activations vary together over time and are maximally distinguishable from other sets.

Most of the variance in any fMRI dataset will be uninteresting, given the small amplitude of the BOLD signal compared with sources of noise (see Chapter 8). Thus, the first few components extracted by PCA may all reflect noise, and because of the requirement of orthogonality, each of those components influences what is extracted subsequently. A relatively new statistical approach that overcomes this limitation is independent components analysis (ICA), which was introduced to fMRI in 1998 by McKeown and colleagues. An ICA analysis assumes that fMRI data consist of a set of spatially overlapping components, each with an independent spatial pattern and different time course (i.e., they contribute differently at different points in time; see Figure 11.2). The term "independent" means that the algorithm minimizes the overlap between the components; however, unlike PCA, the components do not need to be orthogonal with each other. Effectively, each ICA component is independent of all other components.

The ICA algorithm takes as its input the four-dimensional fMRI data set (i.e., the changes in intensity over time in all voxels) and extracts a set of spatiotemporal patterns such that the differences between the patterns are maxi-

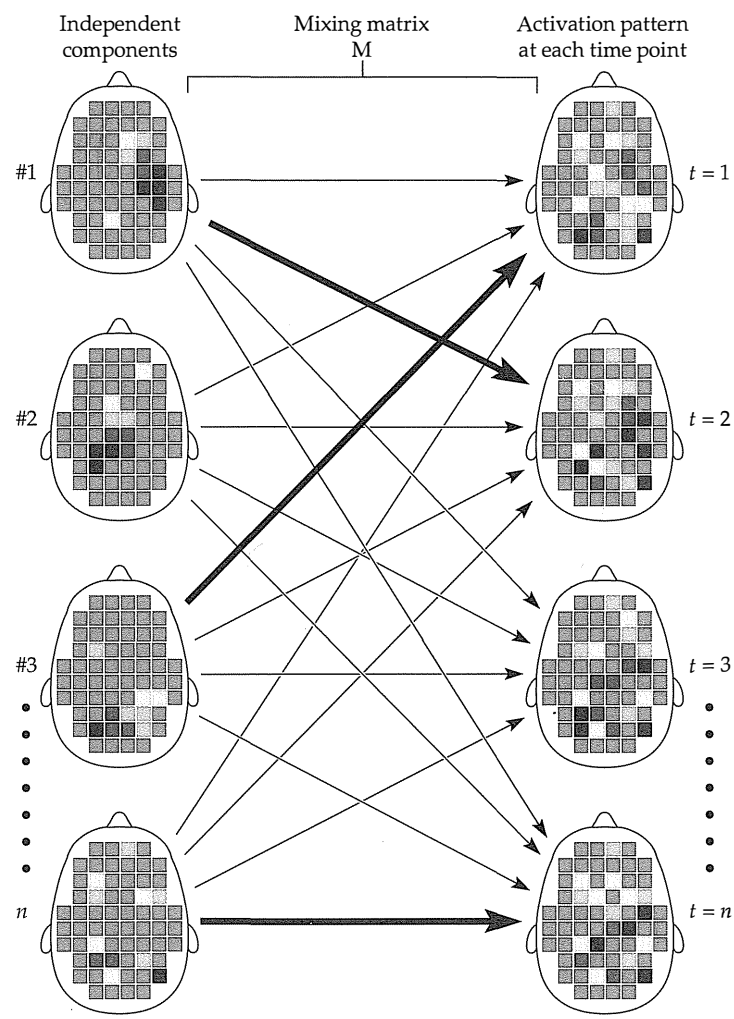

Figure 11.2 The goal of fMRI independent components analysis (ICA) is to identify a set of spatially overlapping patterns of brain activation (i.e., components) that can be mixed together to reconstitute the original fMRI time series. In this schematic example, thicker lines indicate when specific components contributed relatively heavily to specific time points.

mized. Each component describes the changes in activation within a defined set of voxels, but the activation of those voxels can change dramatically over time. For example, the voxels identified within one component could be activated in a task-related manner during some blocks, but not during others. A given voxel can be a member of more than one component, and its overall time course of activation will be split among those components, which may reflect both task-related activation and sources of noise (Figure 11.3). The most common ICA technique is **spatial ICA**, which emphasizes spatial independence by minimizing redundancy in the spatial maps of the components. However, researchers can also conduct **temporal ICA**, which minimizes redundancy in

spatial ICA A form of independent component analysis that generates components that have minimal spatial redundancy.

temporal ICA A form of independent component analysis that generates components that have minimal temporal redundancy.

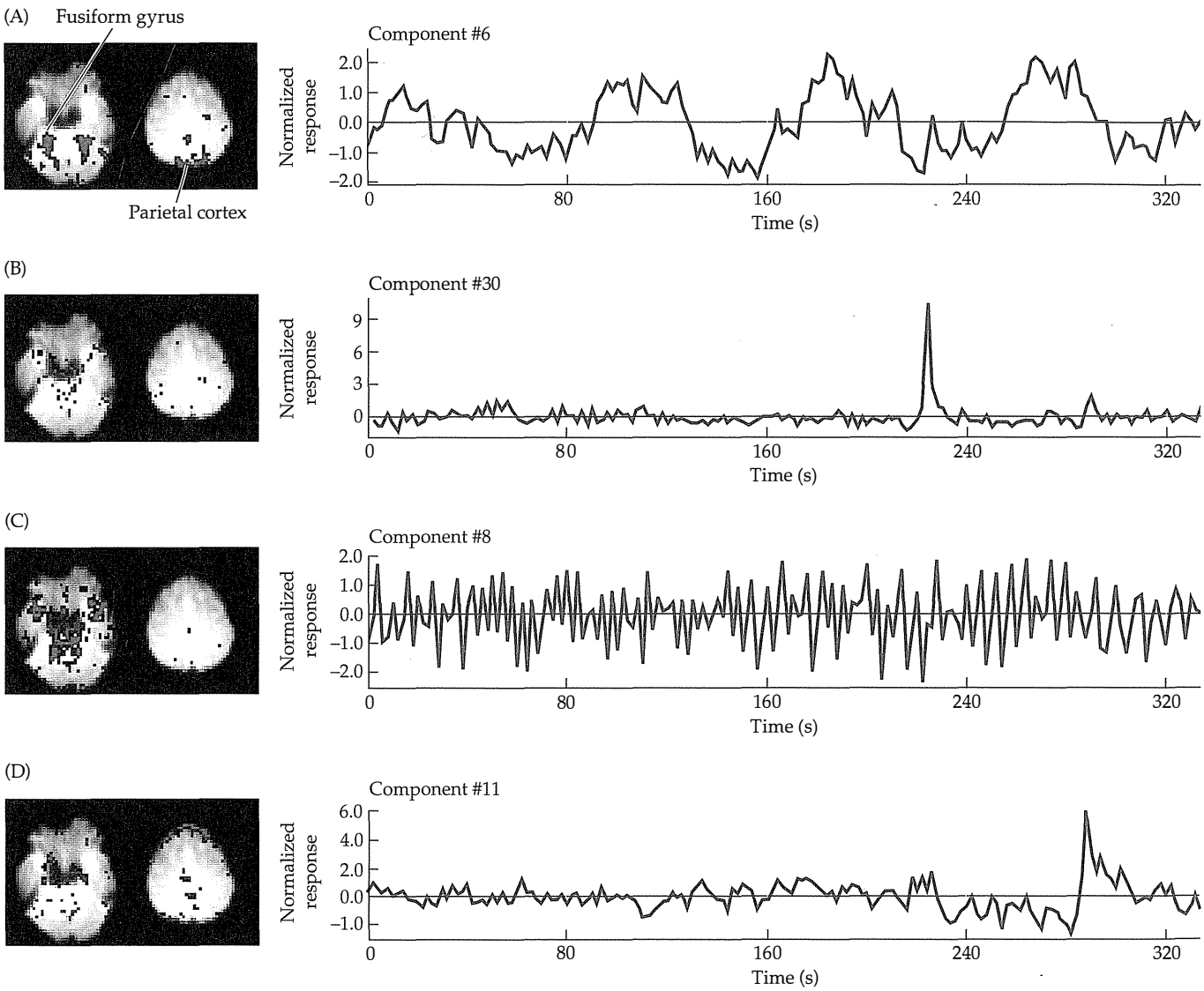

Figure 11.3 Extracting task-related and non-task-related components using ICA. In this session, the subject viewed photographs of faces and of photographs of houses in alternating 40 s blocks. A series of components, four of which are shown here, were extracted using ICA. (A) Within voxels in the fusiform gyrus and the dorsal parietal cortex, there was a task-related modulation of activation. Other components identified by ICA were associated with non-task-related variability, such as a transient scanner artifact (B), high-frequency physiological noise around vessels in the base of the brain (C), and head motion (D), which was evident as characteristic changes in activation along the edge of the brain.

the time courses of the components. Calhoun and colleagues demonstrated in 2001 that the choice between spatial or temporal ICA can have dramatic effects on the results, particularly if the underlying processes are correlated. For example, if the original data contain multiple components with a great degree of spatial overlap, then an ICA approach that attempts to maximize spatial independence may be invalid.

The application of ICA to fMRI data can result in the identification of sets of voxels with similar BOLD signal fluctuations over time, even if those voxels are distributed in different parts of the brain, and even if those voxels are influenced by different sources of noise. For example, in 2005 Beckmann and colleagues applied ICA to data collected while subjects were resting quietly in the scanner (see also Box 9.1). They found several independent components that tended to have similar spatial patterns in different subjects (Figure 11.4), suggesting that those components may reflect functional networks in the brain. By comparing the patterns of activation with prior fMRI work involving active tasks, the authors could identify components associated with vision, audition, executive control, self-directed thought, and other processes. Note that each of these components had a different time course in every subject, because each individual engaged in these processes at different times. Yet, the ICA algorithm could separate those components without any prior input of information about when the processes occurred. Another use of ICA is to identify and remove components whose temporal or spatial properties suggest that they reflect task-unrelated noise. As shown in a 2008 article by Tohka and colleagues, relatively simple and automated decision rules can identify ICA components that are likely to be noise-related. Then, the task-related components can be combined into a new, cleaner time series that is used in standard analyses.

As it is commonly formulated, ICA separates components blindly. No assumptions are made about BOLD signal change or task properties. Nor can standard statistical methods be used for evaluating the significance of any single component. Thus, a major challenge for data analysis using ICA lies in matching components to mental processes (and resulting hemodynamics) evoked by an experimental task. Several approaches combine data-driven ICA with hypothesis-driven statistics to overcome these limitations. A hybrid ICA technique introduced by McKeown in 2000 first uses spatial ICA to identify a set of components and then uses regression analyses to draw conclusions about the task-relatedness of each component. This allows researchers to identify meaningful stimulus-evoked changes, while also exploring their data for potentially unanticipated effects. See the 2004 article by Beckmann and Smith for a discussion of alternative approaches to ICA significance testing. In recent years, the major fMRI analysis packages have begun to incorporate ICA algorithms (e.g., the MELODIC module within FSL), making ICA broadly available to the research community. Despite its limitations, ICA can provide valuable insights into fMRI data, and we recommend that researchers explore its uses for their own studies.

Partial least squares (PLS)

partial least squares (PLS) An approach to analyzing functional neuroimaging data that is used to identify components whose amplitude is influenced by an experimental manipulation.

Another important method for data-driven fMRI analysis is partial least squares (PLS). This approach was developed in 1996 by McIntosh and colleagues for data collected using positron emission tomography (PET), and was subsequently extended for use with complex fMRI designs in 2004 by the same researchers. Like PCA and ICA, PLS identifies core features that contribute to variability in the fMRI signal. But unlike those techniques, it does not blindly identify components. By incorporating task information at an early stage, it

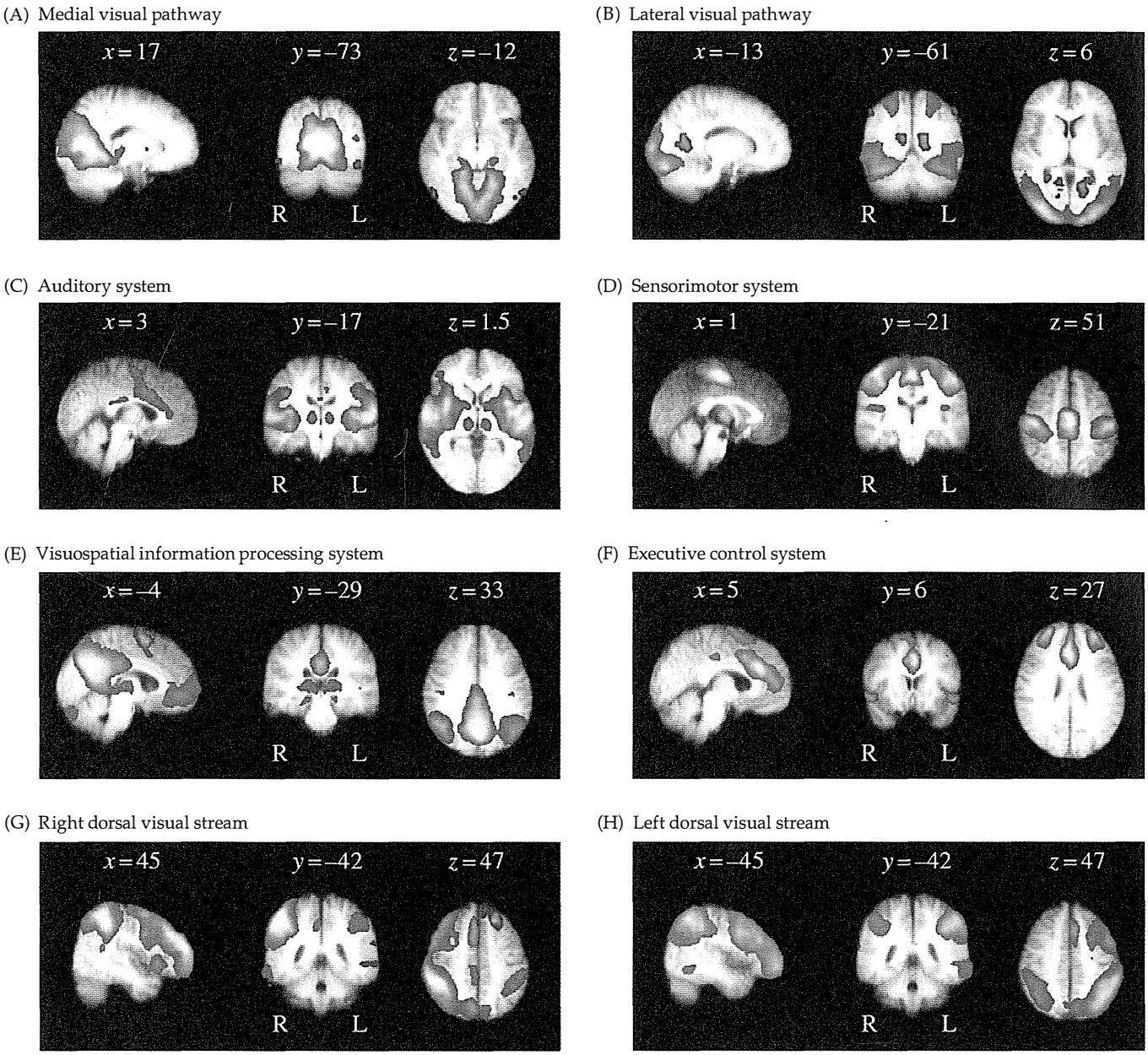

Figure 11.4 Using ICA to identify brain networks showing high resting-state connectivity. By applying data-driven analyses to fMRI data collected while the subjects were resting quietly, researchers could separate distinct networks whose activation tended to fluctuate similarly over time. The likely functions of these networks can be inferred based on prior work using active tasks and hypothesis-driven analyses. Shown here is a set of eight distinct brain networks, all of which were spatially consistent between subjects. Roughly characterized, these networks correspond to the following types of processing. (Adapted from Beckmann et al., 2005.)

identifies components whose amplitudes change between conditions, and can thus be attributed to the experimental manipulation. It uses a mathematical approach called singular value decomposition, which has conceptual similarities to the approach used in PCA, to identify a series of orthogonal compo-

latent variable A variable whose value is not directly measured, but is inferred based on the values of other variables.

permutation In the context of significance testing, approaches that involve resampling the original data to determine the size of an effect that might be observed with a given alpha level.

hyperscanning The simultaneous collection of fMRI data from two or more subjects who are interacting in an experimental paradigm.

nents. (Note that in principle, one could use ICA or some other more-complex approach instead.) Each component, typically labeled a **latent variable**, contains two vectors: a set of weights applied to different experimental conditions, and a set of voxels whose activation levels were maximally influenced by those condition weights. This output differs significantly from PCA or ICA, in that the separation of components is based on these task-related condition weights, not on potentially task-unrelated aspects of the voxel time courses. When applying PLS to event-related fMRI studies, researchers can identify epochs surrounding the events of interest that reveal differences in the hemodynamic response.

In many ways, PLS combines the strengths (and some weaknesses) of data-driven and hypothesis-driven analyses. Unlike regression approaches that use cluster-threshold correction, PLS can readily identify spatially diffuse but systematic patterns of activation. It can be particularly useful for evaluating how those patterns change with an experimental manipulation, thus providing measures of both differences and similarities between conditions. Behavioral variables, like response time or accuracy, can easily be included in the analyses. Once identified, components can be evaluated statistically using **permutation** tests. This involves randomizing the assignment of conditions among the events (or blocks) and then repeating the analysis; conducting many such tests generates a distribution of significance values under the null hypothesis, to which the measured significance value can be compared. Thus, PLS provides a rigorous method for evaluating whether specific voxels are influenced by the experimental task. Nevertheless, it shares some limitations with the regression approaches described in the previous chapter. Any errors in the labeling of the experimental conditions will propagate throughout the analysis, leading to results that are difficult to interpret. This and other problems can be minimized by using PLS in conjunction with other approaches. For example, one can follow a traditional regression approach, and use a PLS analysis to target a particular comparison of interest.

Between-Subjects Correlations: Hyperscanning

In fMRI, data are collected from one individual at a time. Many recent studies have involved interactions between individuals: physical actions like tickling and touch, perception of others' actions, and even competition in multiplayer games. Yet such fMRI data provide information about individuals who are engaging in these social interactions, not about the interactions themselves. Recent work involving a technique called **hyperscanning** (Figure 11.5) overcomes this limitation by collecting fMRI data from two or more subjects, each in separate scanners, while they interact with each other.

Hyperscanning introduces some technical challenges to fMRI studies. To improve comparisons between individuals, the scanner hardware and pulse sequences are generally kept as similar to each other as possible. Most importantly, both the data collection and stimulus presentation must be tightly synchronized between the scanners; otherwise, little will be gained over individual scanning sessions. A research group led by Read Montague has developed software protocols that coordinate scanning over the internet. Using these protocols, two subjects might lie in scanners thousands of miles apart, and compete with each other in an economic game! Upon first consideration, this might seem more a technical triumph than a novel analysis technique. Most researchers interested in social interactions place one subject in the fMRI scan-

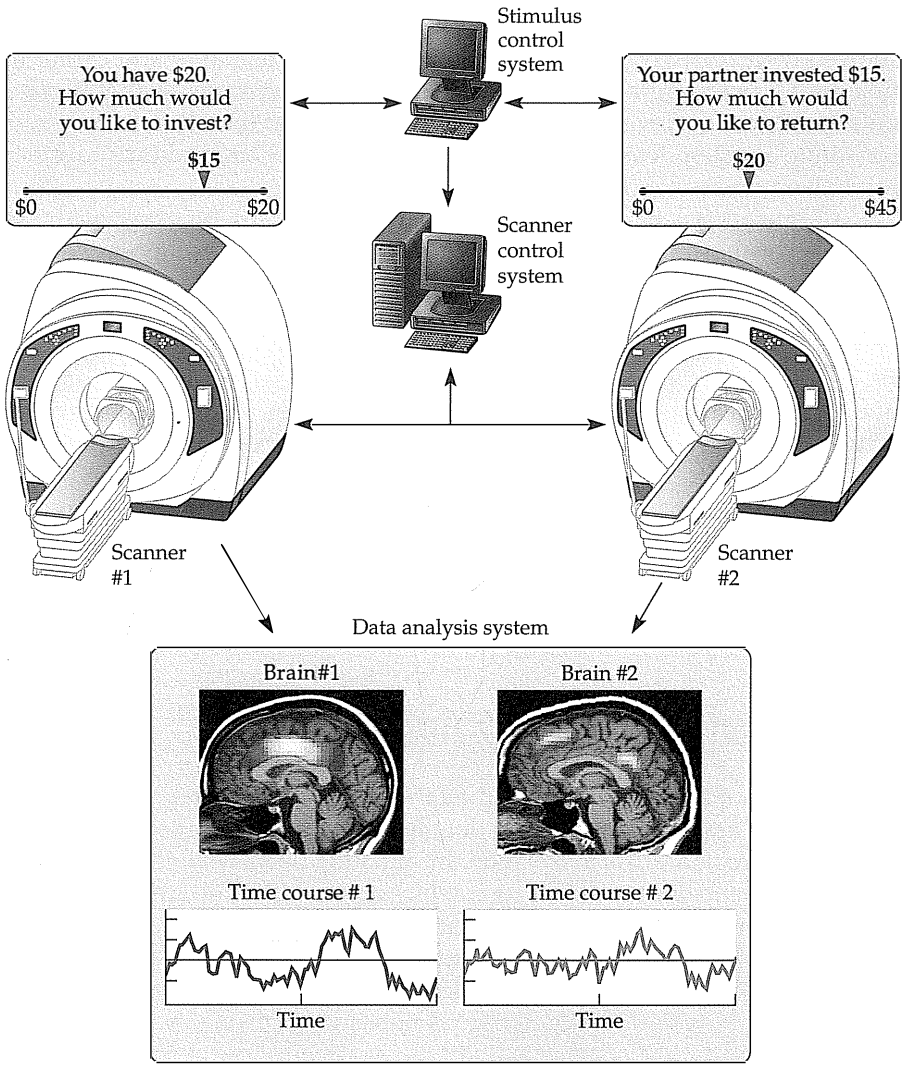

Figure 11.5 Hyperscanning fMRI. An intriguing approach to studying the neural basis of social interactions involves the collection of fMRI data from two (or more) subjects simultaneously, while they interact with each other (e.g., in an economic game, as in this schematic figure). Hyperscanning requires coordination of the experimental stimuli, so that the actions of one subject can influence the other, and of the fMRI scanners, so that the fMRI data from the two subjects can be compared. The chief advantage of hyperscanning fMRI is that it allows researchers to directly relate the activation in one person's brain to the activation in another person's brain, potentially identifying coordinated activation that might be difficult to find using standard techniques.

ner and one or more other participants at computers outside the scanner room. Thus, the participants interact normally (e.g., play a game together) while only one person's brain is being scanned. Even if two people were in scanners simultaneously, standard analysis methods would not provide novel information; there would merely be twice as many subjects in the sample.

For hyperscanning to provide a meaningful advance over traditional single-subject scanning, a different approach to data analysis is required. Specifically, researchers use activation in one individual's brain as a predictor of activation in another individual's brain. The first large-scale hyperscanning study was reported by King-Casas and colleagues in 2005. They were interested in the development of trust during repeated interactions. Their task involved a two-player game in which one individual (the investor) could send money to the second individual (the trustee). Any money so given was multiplied, whereupon the trustee could choose to return any amount, or nothing at all, back to the investor. Because participants did not know each other's identity, an investor would only be expected to send money if he or she trusted the trustee to return it. The authors found that activation in the trustee's caudate nucleus, a structure important for learning and reward evaluation, predicted the subsequent intention to return money. Over trials, as the players repeatedly

showed their trustworthiness, this activation shifted to earlier and earlier in time, and was accompanied by a parallel increase in activation within the cingulate cortex of the investor. The researchers concluded that these two regions constitute a system for evaluating the intentions of others, and thus together mark the progress of social interactions over time.

All interactions between individuals in a hyperscanning experiment are mediated by the intervening behavior; there are, of course, no direct influences between the two brains. Thus, in principle, any conclusion that could be drawn from hyperscanning fMRI could also be reached by scanning individuals one at a time. However, there are practical advantages to using hyperscanning. Because the subjects are participating in a common social setting, many aspects of the experimental task can be matched. Moreover, using one person's brain activation as a predictor of another's activation may result in the identification of temporal regularities that were not expected. In essence, if sufficient technical resources are available (i.e., two or more research scanners) hyperscanning might be used to spark new ideas about the neural mechanisms of social interactions. See Box 11.1 for another approach to combining data from different subjects: using correlation techniques to understand shared aspects of cognition when different people process the same complex visual stimulus.

Functional Connectivity Approaches

Most studies of brain function build on the concept of **localization of function**, that different brain regions support different forms of information processing. Yet no brain region exists in isolation. Information flows between regions via the action potentials carried by axons, which are bundled into large **fiber tracts**. For more than a century, neuroanatomists have mapped the anatomical connections between brain regions, in an attempt to understand the **structural connectivity** of the brain. Generally, this research has involved dissection and axon staining in brains of dead humans and non-human primates. While much remains to be discovered, the study of the anatomical connections between brain regions has provided a cornerstone for neuroscience research.

Despite the value of this anatomical research, knowledge of structural connections between brain regions can only provide a limited picture of information flow in the brain. Descriptions of **functional connectivity**, or how the activity of one brain region influences activity in another brain region, are also needed. Many researchers interested in functional connectivity have adopted fMRI techniques, because of their utility for measuring changes in activation throughout the entire brain. Studies of functional connectivity typically involve standard methods of fMRI data collection, but with relatively high temporal resolution. However, different methods for data analysis and statistical inference are used in functional connectivity studies compared with other types of fMRI research. As we will discuss in the following sections, functional connectivity analyses can extend either hypothesis- or data-driven analyses to draw more specific inferences about the direction and timing of information flow across brain regions.

localization of function The idea that the brain may have distinct regions that support particular mental processes.

fiber tracts Bundles of axons that convey signals, in the form of action potentials, from one brain region to another.

structural connectivity A pattern of structural connections between regions based on known axonal projections.

functional connectivity A pattern of functional relationships among regions, inferred from common changes in activation over time, that may reflect direct or indirect links between those regions.

From coactivation to connectivity: a conceptual overview

Functional MRI holds significant promise for elucidating the functional relationships between brain regions because of its spatial coverage. Most fMRI studies involve the collection of data from the entire brain every few seconds,

BOX 11.1 Intersubject Correlations in Free Viewing

Most fMRI studies treat their participants as independent entities, each performing the same task. Standard hypothesis-driven analyses combine data from different subjects to emphasize common effects and minimize subject-specific effects, thus improving the power of their statistical inferences. Consider, however, an alternative perspective on combining data from different subjects: if a group of individuals all show the same activation, regardless of the experimental hypothesis, then that shared activation likely reflects common mental processing. Here, we introduce the idea of looking for **intersubject correlations**, or common patterns of activation across subjects. Like other data-driven approaches to fMRI analysis, this involves looking for regular patterns in the data and then interpreting those regularities based on knowledge of the experimental paradigm. But unlike the approaches discussed elsewhere in the chapter, those regular patterns will be between subjects rather than within individual subjects.

An elegant example of intersubject correlations was reported by Hasson and colleagues in 2004. The authors were interested in understanding the brain processes that underlie perception in open-ended, natural settings, such as when people freely perceive and attend to distinct parts of the complex, changing world. This goal poses challenges for conventional hypothesis-driven analyses, given that the freedom of subjects to process visual stimuli idiosyncratically makes it difficult to identify what processes are ongoing at any one time. So, they hypothesized that complex perception, such as that engaged in while watching a movie, contains many processes that are common across individuals, and that those processes should be reflected in similarly common patterns of activation.

They showed five subjects a thirty-minute excerpt from a classic western movie, Sergio Leone's "The Good, the Bad and the Ugly." Subjects were not instructed to perform any particular task while watching the movie, but to view it normally and describe the plot at the end of the experiment. Then, the researchers simply collected a time series of fMRI data, using standard protocols for data collection, while their subjects watched the movie. After applying standard preprocessing steps, including normalization of all subjects to the same stereotaxic space, the authors then identified voxels whose time courses were significantly correlated between different pairs of subjects (ten unique pairings). They found significant across-subject correlations in about 30% of the cortical surface, including many parts of the visual cortex and the visual processing streams, as well as in regions within the frontal cortex (Figure 1). For a control condition, the au-

intersubject correlations Functional MRI time courses that are shared by different individuals while performing the same experimental tasks or experiencing the same stimuli.

(continued on next page)

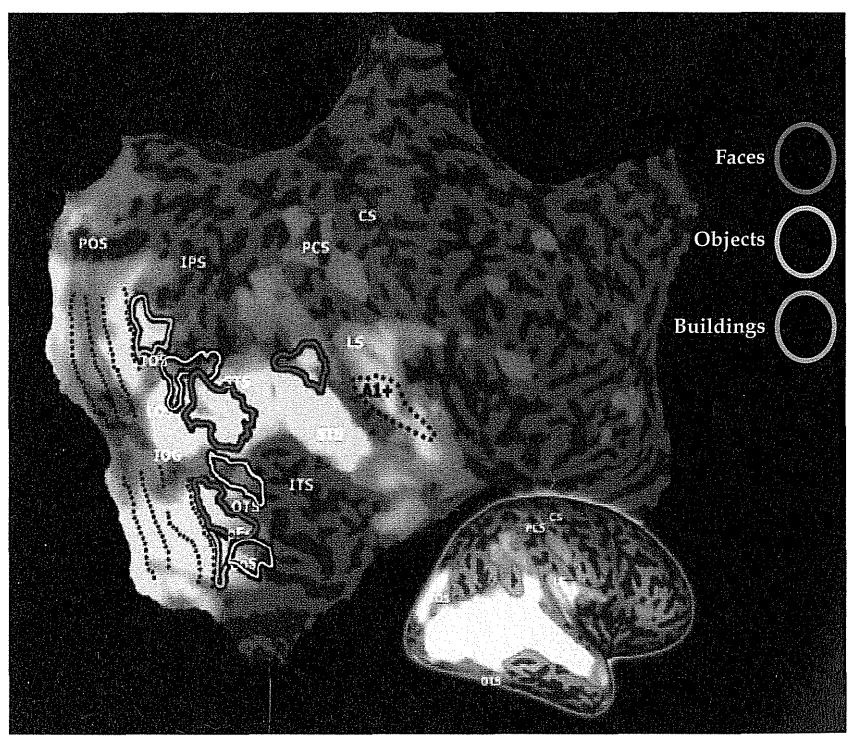

Figure 1 Regions exhibiting a common pattern of activation in subjects watching the same movie. While in the scanner, subjects watched an extended clip from the movie "The Good, the Bad and the Ugly." The common visual experience caused multiple brain regions to exhibit changes in activation that were roughly synchronized between subjects. As shown in this figure, these included regions associated with the visual processing of different stimulus types. (After Hasson et al., 2004.)

BOX 11.1 *(continued)*

thors repeated the experiment with a separate group of subjects who were lying in the scanner with their eyes closed. This resulted in only chance correlations between subjects.

Further analyses revealed that these intersubject correlations resulted from two different effects. First, activation throughout much of the brain, including most visual regions, rose and fell in a similar pattern across all subjects. To interpret this activation, the authors used a reverse correlation approach: they identified time points when this collection of regions showed maximum activation and then evaluated what was happening in the movie at those times. (This process is conceptually similar to the reverse-inference approach that will be discussed in Chapter 14.) They found that this non-spatially-selective component tended to have highest amplitude during the most surprising and evocative points in the movie (e.g., gunshots, explosions, or unexpected plot twists), and thus it could reflect a broad increase in arousal. Second, there were spatially-selective intersubject correlations that had a unique time course in each of several brain regions. To interpret these activations, the researchers again looked back at the movie. As shown in Figure 2, common activation in the fusiform cortex tended to increase in response to movie scenes that involved a close view of a face, while activation in the anterior collateral sulcus (adjacent to the parahippocampal gyrus) tended to increase in response to scenes that contained views of environments or buildings. While these regularities may seem straightforward given the known functionality of those regions, the authors also found some more subtle functional effects. For example, a region in the anterior parietal lobe exhibited regular increases in activation in response to a wide range of scenes. By looking for common elements in the movie, the authors concluded that this activation was probably evoked by on-camera hand movements. This basic technique has since been applied to other sorts of complex stimuli; for an example with auditory speech

Figure 2 After identifying brain regions that exhibited significant correlations between subjects, the researchers then examined the movie to identify content that resulted in those correlations. In the region of the fusiform gyrus shown at right, they found that the largest amplitude responses were reliably evoked by scenes that contained a close-up view of a face. (Adapted from Hasson and colleagues, 2004.)

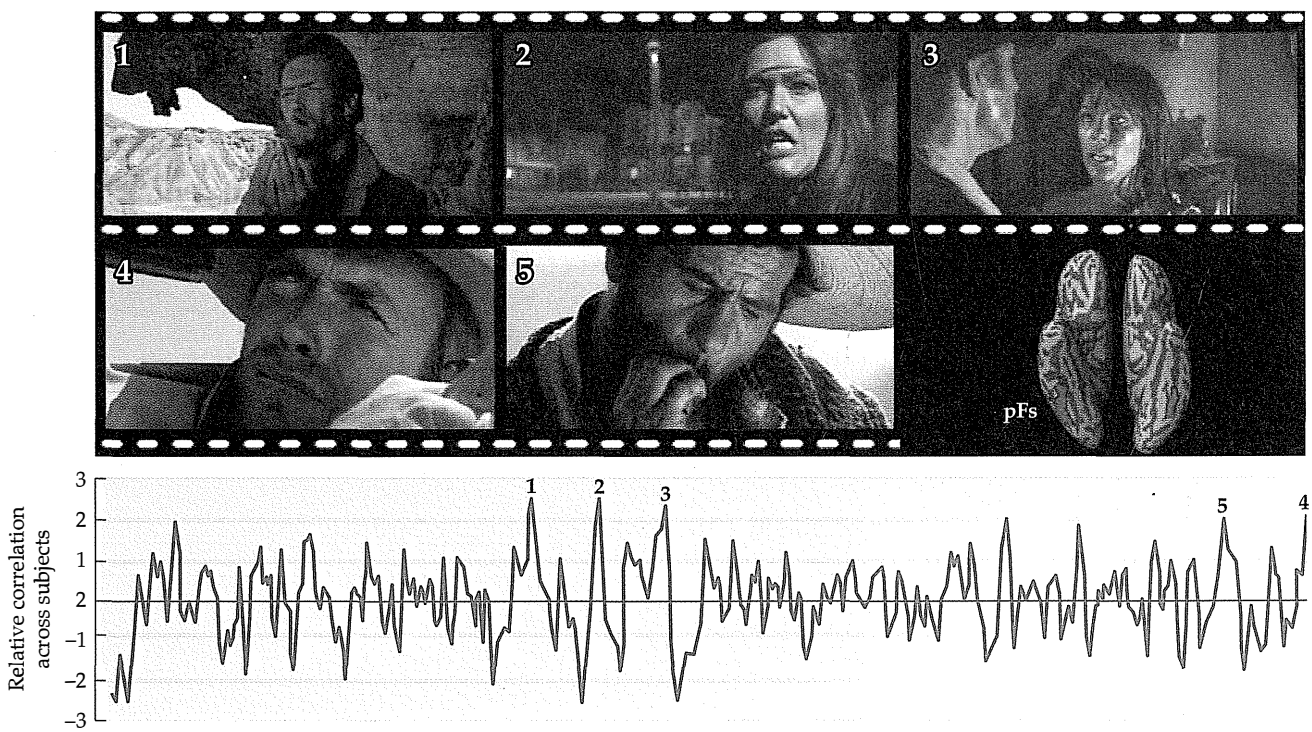

BOX 11.1 *(continued)*

stimuli, see the 2008 article by Wilson and colleagues.

A complementary approach was introduced in a series of studies by Bartels and Zeki, who also investigated natural viewing conditions, but using hypothesis-driven rather than data-driven analyses. In a 2005 study, these authors investigated interactions between brain regions while subjects passively viewed and listened to an extended movie clip—the James Bond movie "Tomorrow Never Dies"—interspersed with infrequent periods of darkness. They first used ICA to identify sets of brain regions whose activation moved together over time, and then examined the functional correlations between those regions to estimate the relative strengths of their connectivity. They found, as expected based on known anatomical structure, that the correlations between homologous pairs of regions in the two hemispheres (e.g., left and right area V3) were generally greater than between non-homologous regions. Interestingly, the non-homologous regions were actually more correlated while the display was blank. This suggests that during movie viewing these non-homologous regions contributed to different aspects of perception, while during the blank screen sessions their joint activation was driven by non-specific arousal processes. Note that this latter approach does not seek common changes in the raw fMRI time courses across subjects, as investigated by Hasson and colleagues, but instead looks for common patterns of connectivity.

reverse inference Reasoning from the outcome of a dependent variable to infer the state of an independent variable (or an intervening unobservable variable).

providing complete spatial coverage at moderate temporal resolution. Advanced pulse sequences now allow the collection of more than 20 slices per second, enabling sampling of the entire brain at roughly 1 Hz. Electrophysiological techniques may provide more complete characterizations of single brain regions, because they sample post-synaptic potentials at 1000 Hz or faster or can be used to identify individual action potentials. However, the spatial coverage available with fMRI provides some advantages for describing functional relationships between regions.

The simplest type of relationship between regions is **coactivation**, in which two or more distinct brain regions show simultaneous activity during an experimental task (Figure 11.6A). A classic example of coactivation can be seen in motor tasks: squeezing your left hand will result in activity in the precentral gyrus in the right hemisphere and the cerebellum in the left hemisphere. Hypothesis-driven fMRI analyses are designed to identify brain regions that show significant activity in response to some experimental manipulation, so by their very nature they provide coactivation data. It is common for fMRI researchers to report that a given experimental task evoked concurrent activity in multiple brain regions (e.g., that a working memory task evoked activity in the prefrontal and parietal cortices), and to infer from this that these regions are part of a single functional system.

However, while coactivation tells us that two brain regions are related, it tells us nothing about the form of that relationship. Consider the simple task of encoding a set of three faces into working memory. Subjects performing this task will show coactivation in the dorsolateral prefrontal cortex, superior parietal cortex, and fusiform gyrus. What can we conclude from this? One possibility is that top-down influences from the prefrontal cortex guide activity in the other regions. Another possibility is that visual processing in the temporal and parietal lobes may lead to prefrontal activity in a bottom-up fashion. Or, activity in all three regions may be triggered by signals from yet another source. Because of the inherent causal uncer-

coactivation The simultaneous activation of two or more brain regions within a single experimental task. Coactivation of brain regions does not imply that the regions are functionally connected.

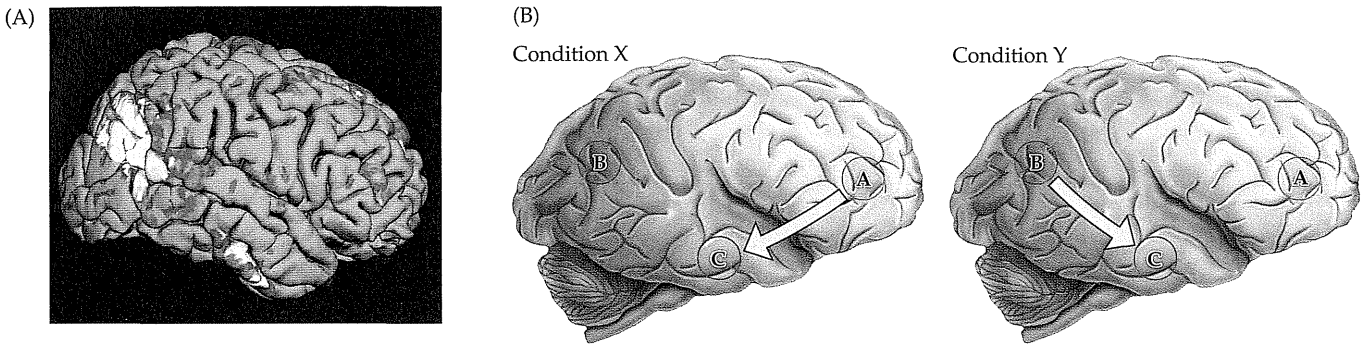

Figure 11.6 From coactivation to connectivity. (A) Any complex experimental task will evoke activity in several brain regions simultaneously. The regions indicated in this color map had significantly greater activity during a rest condition than during a visual search task with similar perceptual characteristics. Even though these regions are coactive, they do not necessarily serve the same function. (B) By looking at patterns of coactivation during different experimental conditions, we can make inferences about connectivity (i.e., the influence of one brain region on another). If one condition activates areas A and C, and another condition activates areas B and C, then we can begin to make inferences about the connectivity between these three regions. (A from Huettel et al., 2001.)

tainty in any single map of the brain, fMRI research has often been dismissed as merely descriptive (i.e., describing patterns of coactivation) rather than mechanistic (i.e., explaining how the brain accomplishes a complex behavior). Patterns of coactive regions are often erroneously summarized as networks of brain activity. This misuses the term "network," which should be restricted to descriptions of structural and functional connectivity that include the causal flow of information. For descriptions of simple associations among regions (i.e., with unknown connectivity and causality), a more appropriate term is system.

Nevertheless, fMRI *can* be used to build more sophisticated models of connectivity. Some aspects of connectivity can be deduced by measuring the covariance in activities among regions during different experimental conditions. Consider a simple example that consists of three brain regions, A, B, and C, and two experimental conditions, X and Y (Figure 11.6B). Under condition X, brain regions A and C are coactivated, but B is not active. Under condition Y, brain regions B and C are coactivated, but A is not active. These results indicate a double dissociation between regions A and B, since one manipulation has an effect on A but not B, and another on B but not A. From this it can be inferred that these regions have different functional properties. Furthermore, the results for region C provide information about connectivity. The observed pattern of associations and dissociations supports the hypothesis that regions A and B are both functionally related to C but not to each other. Because activation at C does not always predict activation of A or B, the data suggest (but do not prove) directionality. This conclusion would be strengthened if there was a measurable delay between activation in A or B and activation in C. However, the differences in the latency of hemodynamic timing throughout the brain either could reduce the impact of such results or could make such a delay undetectable. Of course, this example simplifies typical fMRI data, which often have a much more complex set of interrelationships.

network A description of the relationships among a set of brain regions, including their connectivity and causal relationships.

system A set of regions that are linked by coactivation, but for which the connectivity and causal relationships remain unknown.

double dissociation The demonstration that two experimental manipulations have different effects on two dependent variables. One manipulation affects the first variable but not the second, and the other manipulation affects the second but not the first.

Thought Question

Many scientists believe that the demonstration of a double dissociation is a necessary step for establishing a clear relationship between independent and dependent variables. Given what you know so far, what do double dissociations tell you that single dissociations do not?

Ideally, we would like models of connectivity to include information about unidirectional connections (i.e., A influences B) as well as feedback connections (i.e., A influences B, which leads to changes in A itself). In order to restrict

the number of possible functional connections within a model, researchers incorporate information about the anatomical connections between brain regions. Although most connections between brain regions are clearly bidirectional, there are a number of relatively unidirectional pathways or loops, especially between cortical and subcortical regions. The connection between the prefrontal cortex and the basal ganglia is one such pathway; the prefrontal cortex has heavy projections to the basal ganglia but receives little direct input in return. Instead, the basal ganglia project to the thalamus, which itself projects back to the prefrontal cortex. By incorporating information about these pathways into models of brain function, researchers can create models that are detailed and directional networks, rather than simple coactive systems.

resting-state connectivity The functional connectivity of a given brain region, when measured while the participant is not performing any coordinated, purposeful task.

Resting-state connectivity

The most straightforward evidence that two (or more) regions share functional connectivity comes from studies of resting-state connectivity. These studies are used to identify synchronous BOLD changes in multiple brain regions while subjects lie in the MRI scanner but do not perform any experimental task. These changes are thought to represent certain intrinsic operations of the brain, or to reflect stimulus-independent processing, rather than the effects of external stimuli. While resting-state connectivity can be found in any aspect of the BOLD signal, it is often evident in periodic and very slow changes in activation (e.g., 0.01 to 0.1 Hz). This was first demonstrated in the sensorimotor cortex by Biswal and colleagues in 1995 (Figure 11.7).

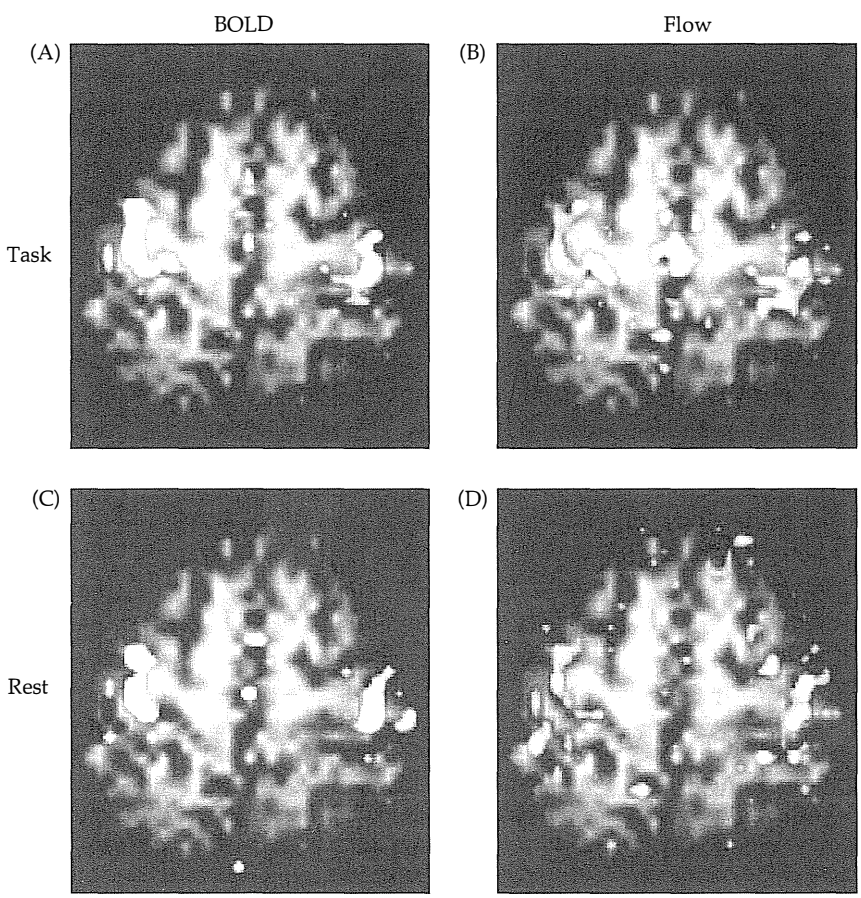

Figure 11.7 Similar patterns of resting-state and task-related functional connectivity. Functional MRI data using BOLD-sensitive (A) and blood-flow-sensitive (B) imaging were collected while the subject performed a bilateral finger tapping task. Significant activity in the motor cortex was found using both techniques. Resting-state data were also collected using each type of imaging. Low-frequency oscillations that signal functional connectivity between regions were identified. The BOLD resting data clearly indicated that the hand areas of the motor cortex were functionally connected (C), matching the activation data, while the flow resting data exhibited much less functional connectivity (D). (From Biswal et al., 1997.)

seed voxel A voxel chosen as a starting point for a connectivity analysis.

default network A set of brain regions whose activation tends to decrease during the performance of active, engaging tasks, but to increase during conditions of resting and reflection.

To identify low-frequency oscillations in the BOLD signal, researchers typically instruct subjects to relax without falling asleep, and then record fMRI data using normal pulse sequences. Because many other physiological processes can cause signal oscillations (e.g., respiratory and cardiac pulsations), it is important to separate oscillations that are potentially associated with neuronal activity from those associated with physiological fluctuations. One effective method is to sample at a very high temporal resolution, fast enough to identify cardiac pulsations (and slower respiration) without aliasing artifacts. Then, physiological variability can be identified and removed. Thereafter, broad patterns of common activation can be identified using data exploration techniques like PCA or ICA. Alternatively, a researcher can identify a seed voxel in a specific region of interest (ROI), and then examine what other regions exhibit similar fluctuations in activation over time. Using this approach, researchers have found coherent activation in sets of regions involved in visual, auditory, memory, and attentional processes, among others. In general, regions that are coactivated during active tasks also show resting-state connectivity. This suggests that brain regions with similar functionality tend to express similar patterns of spontaneous BOLD activation (and presumably neural activity, as well).

Studies of resting-state connectivity can provide insight into the properties of the so-called default network. Imagine that you are a subject in one of these studies. As you enter the scanner, the experimenter instructs you to close your eyes and relax, asking you to remain still without thinking about anything in particular. Perfect adherence to these instructions is, of course, impossible. One cannot shut off active thought in the same way that one closes a running faucet; indeed, the very act of remembering the task instructions violates them. You will spontaneously engage in all sorts of cognition, from remembering recent events to daydreaming about the future, and these thoughts lead to systematic and coordinated activation throughout the brain. However, not all aspects of resting-state connectivity can be attributed to ongoing complex cognitive processes. For example, in a 2007 study, Vincent and colleagues scanned anaesthetized monkeys and demonstrated robust resting-state connectivity in various brain systems. These and related findings indicate that coherent low-frequency fluctuations in the BOLD signal may reflect some general property of brain function.

Combining resting-state and task-related connectivity within the same study can strengthen conclusions about the relationships between brain regions. An early example of this type of study was published by Hampson and colleagues in 2002. They collected separate data sets from the same subjects in two types of run: resting and task. In the resting runs, nothing was presented and no response was required. The task runs consisted of a blocked design in which the subjects listened to either a reading of a story, or silence. The authors used an iterative comparison method that generated connectivity hypotheses based on one data set and tested those hypotheses using the other data set. The basic approach is shown in Figure 11.8. First, the authors used a standard blocked analysis on the task data set to create a task-related activity map. As expected, they found significant activity in Broca's area and Wernicke's area. This resulted in the hypothesis that these two regions are functionally related. To test this hypothesis, they used Broca's area as the seed for a connectivity analysis. The voxel time courses from the resting data set were low-pass filtered and then tested for correlation with the mean activity from Broca's area. Strong connectivity was found between Broca's area (in the left hemisphere) and the corresponding anatomical region in the right hemisphere, while weaker connectivity was noted both with Wernicke's area and a region in the left pre-

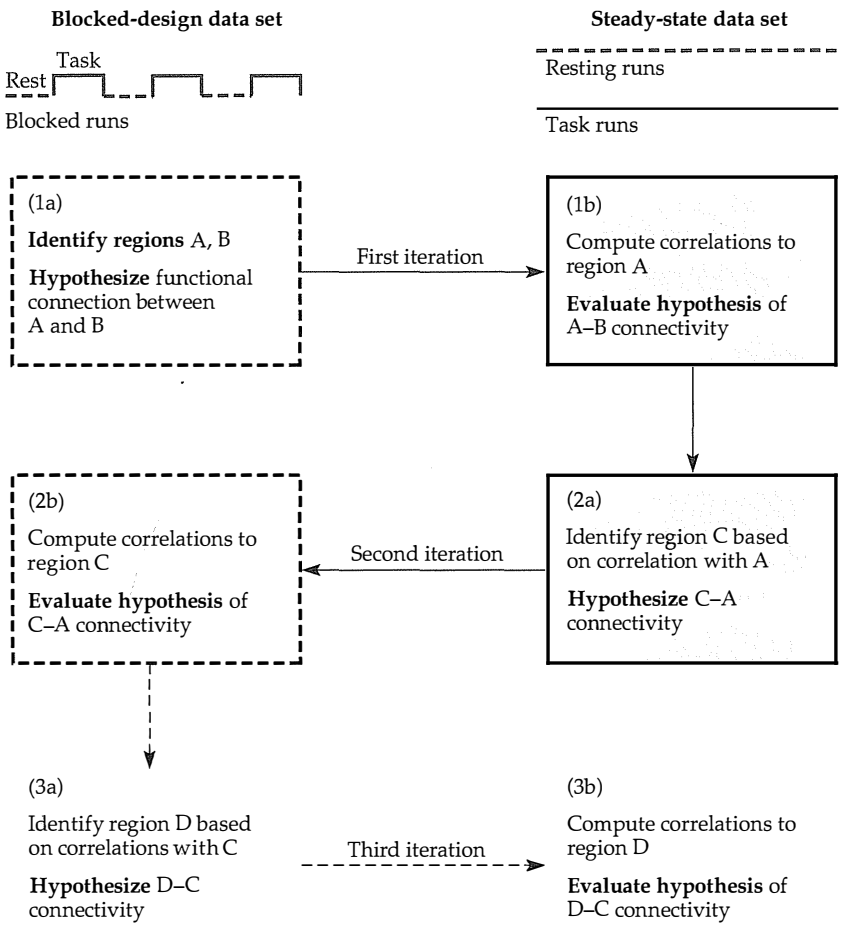

Figure 11.8 Combining resting-state and task-related connectivity. A central challenge of any data analysis approach is to combine hypothesis testing with hypothesis formation, since using the same data for both purposes can introduce bias. One way to overcome this problem is to collect two data sets from the same subjects, such as a blocked-design language comprehension task and a steady-state null task. Working back and forth between these data sets, researchers can identify regions of activity during the task and evaluate hypotheses about their connectivity with other regions. (After Hampson et al., 2002.)

motor cortex. In the second iteration of their analysis, the authors defined a new ROI in the left premotor cortex, based on this connectivity map. The hypothesis that Broca's area and the left premotor cortex are functionally connected was then tested, using both the auditory and silence conditions of the task data set independently. Both conditions revealed significant correlations between these regions. Note that this iterative approach, in which one data set generates hypotheses to be tested with the other data set, could in principle be extended to additional brain regions (e.g., steps 3a and 3b in Figure 11.8).

Psychophysiological interactions

Another approach for combining fMRI and behavioral data involves the identification of psychophysiological interactions (PPI), in a method developed by Friston and colleagues in 1997. The core concept of PPI is that mental processes, whether evoked by a stimulus condition or by the subject's behavior, modulate the influence of one brain region over another. Like other connectivity approaches, PPI uses the time course of activation in one seed region to predict changes in activation in another region. However, the process for identifying PPI sets this method apart from other techniques. First, PPI estimates the neuronal activity in the seed region that would have generated its measured fMRI time course. Second, that estimate is multiplied by the task timing, resulting in a prediction of neuronal activity associated with the experimental manipulation.

psychophysiological interaction (PPI)
A statistical approach for identifying the effect of an experimental manipulation on the functional connectivity between two brain regions.

This new prediction is then convolved with the fMRI hemodynamic response to generate the predicted PPI BOLD time course, which is then used as a regressor in the analysis design matrix to identify activation in other brain regions. The interactions identified by this approach are named "psychophysiological" because the approach is intended to model interactions between cognitive processes and physiological changes in the connectivity between brain regions.

An intriguing recent example of the power of PPI was reported by Bingel and colleagues in 2007. They were interested in the power of painful stimuli to quickly capture attention away from important tasks. One possible explanation for this effect was that painful stimuli engage the same brain systems as other sorts of distractors. For example, previous work from the same authors had shown that cognitive distraction, achieved by requiring subjects to remember letters presented at the center of a display, attenuated visual cortex activation in response to task-irrelevant background images. Another possibility, which they adopted as their research hypothesis, was that painful stimuli could evoke a similar effect (i.e., attenuating visual cortex activation), but through a different neural pathway. In their fMRI sessions, the authors tested both painful and cognitive distraction using PPI methods. To create painful distractions they shone infrared laser light onto the hands of their fMRI subjects. The associated pain evoked activation in the insular, cingulate, and somatosensory cortices. And, as expected, a difficult cognitive distraction task increased activation in prefrontal and parietal cortices. They focused their PPI analyses on one region related to pain (the anterior cingulate cortex) and one region related to cognitive difficulty (the parietal cortex), and examined whether these regions' activation predicted condition-specific effects in the visual cortex (i.e., decreased activation to passive viewing of low-contrast, compared to high-contrast, background images). As shown in Figure 11.9, their research hypothesis was confirmed: the cingulate cortex activity exerted a pain-related modulation on the lateral visual cortex, whereas the parietal cortex exerted a cognitive-difficulty-related modulation on the same region. Thus, by using PPI, the authors demonstrated that both pain and cognitive difficulty could attenuate visual cortex processing, but via different neural pathways.

Inferring causality from fMRI data

One well-recognized limitation of fMRI research is its difficulty with assigning causality, or determining that a particular pattern of fMRI activation led to a particular behavior or mental state. In Chapter 9, we raised this issue by discussing the idea that fMRI data are epiphenomenal, meaning that they do not reflect information processing itself, and thus cannot be used to produce models of brain function. While this fundamental objection can be overcome by considering that fMRI data provide a valuable index of the underlying information processing, more subtle causal problems remain. Suppose that we observe fMRI activation in two regions, A and B. How can we determine whether activation in region A caused changes in region B, activation in Region B caused changes in Region A, or that both were influenced by some other region? Determining how regions interact is necessary for understanding the flow of information throughout the brain, which in turn allows researchers to construct more biologically plausible models of brain function.

The limited temporal resolution of fMRI data poses many challenges for causal modeling. Nearly all connections between brain regions are bidirectional, such that the flow of information in one direction may be shortly followed by a flow of information in the other direction, and this back-and-forth

causality The judgment that one event led to another. For fMRI data, measures of causality attempt to determine whether changes in the activation of one brain region led to changes in the activation in another region.

epiphenomenal A secondary consequence of a causal chain of processes, but playing no causal role in the process of interest.

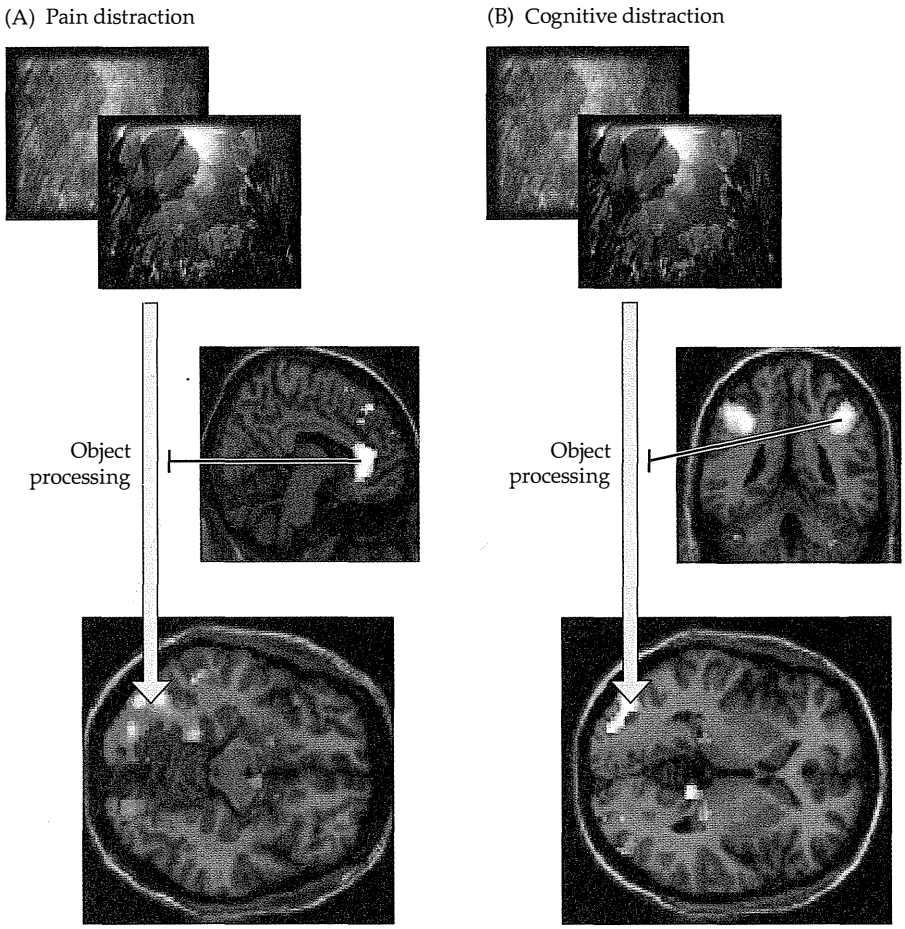

Figure 11.9 Identification of a psychophysiological interaction (PPI). Researchers hypothesized that processing in the visual cortex could be modulated by input from either of two regions, depending on the task context. (A) Using a PPI analysis, they found that the magnitude of pain-related activation in the anterior cingulate cortex modulated the influence of image contrast on the lateral occipital cortex, a region important for processing complex visual scenes. (B) Under conditions of cognitive distraction, however, the magnitude of working-memory-related activation in the parietal cortex now modulated the image-contrast effects in the visual cortex. Thus, PPI can distinguish modulatory contributions from distinct regions, which change according to task conditions. (After Bingel et al., 2007.)

signaling may occur repeatedly in the repetition time between consecutive image acquisitions. Collecting data with a relatively short TR greatly improves the robustness of causal analyses. Moreover, fMRI does not measure neuronal activity directly, but instead measures a hemodynamic marker of that activity. Thus, any small time differences in activation between regions may simply reflect differences in the timing of hemodynamic responses in those regions (see Chapter 7). Likewise, there exists strong evidence that integrative activity constitutes a major contributor to the BOLD signal, through the metabolic demands associated with restoring dendritic membrane potentials. Therefore, some BOLD signal changes could, at least in principle, represent feedback from downstream regions rather than signaling output, completely skewing assignments of causality. These and related caveats indicate that sophisticated approaches are needed for inferring causality using fMRI data.

A powerful technique for investigating relationships among regions activated in an fMRI study is structural equation modeling (SEM), which identifies the combination of connections between variables that can best account for the observed data. An SEM model consists of a set of nodes, each representing a single measured or latent variable from the data set, and a set of paths between those variables (Figure 11.10). By including both direct and indirect paths between variables, the model can evaluate whether one variable mediates the covariation between two other variables. (Note that when the model includes only measured data and no inferred or latent variables, the approach is a sub-

structural equation modeling (SEM) A statistical approach for testing a model of the relationships among a set of independent and dependent variables.

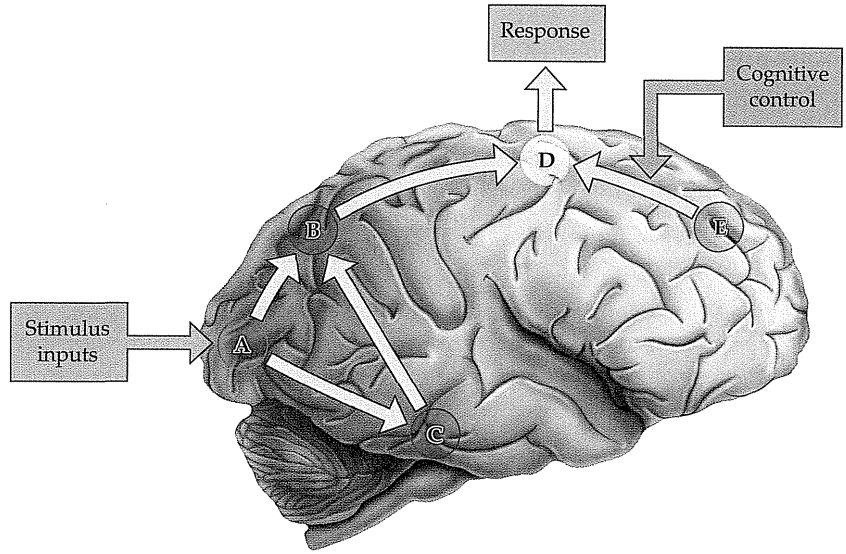

Figure 11.10 A conceptual illustration of fMRI structural equation modeling (SEM). The researchers establish a model of functional connections among a set of brain regions, often based on prior knowledge of the structural relationships between the regions. As in the hypothetical example shown, the model can involve both direct (A to B) or indirect (A to C to B) connections between regions. External stimuli or cognitive states can be shown to directly influence the activation of a region (e.g., stimulus inputs influence activation in A) or the connectivity between regions (e.g., increased cognitive control leads to a greater influence between E and D). Note that although the connections are shown as directional for clarity of this example, standard SEM models do not include information about directionality.

set of SEM called path analysis.) When setting up an SEM model, researchers often postulate connections between brain regions that are suggested by known anatomy, so that the pathways in the model reflect connecting pathways between brain regions. The first use of SEM in fMRI was published in 1997 by Buchel and Friston, who studied the effects of attention on processing in the visual cortex. They found that attention increased the connectivity between the extrastriate visual areas and the posterior parietal cortex. The prefrontal cortex was one potential source of this attentional control effect. More recent studies have used SEM both to evaluate models of connectivity between regions and to measure the effects of other factors on that connectivity. SEM can be used to elucidate many types of relationships between brain regions, and can be used to rule out hypothesized models for interactions. However, it has an important limitation: it does not include information about the relative timing of activation. Instead, it considers interactions between variables (e.g., brain regions) to occur instantaneously, with changes in those variables (e.g., activation in a region) determined by the values of other variables and the strengths of the connecting paths. In other words, in fMRI applications of SEM, possible causal relationships between brain regions are established beforehand within the model, not determined from the data.

To accommodate information about the relative timing of activation, researchers have adapted methods from time series modeling, specifically the idea of Granger causality. This approach, introduced by the Nobel laureate Clive Granger, has been enormously influential in economics and other social sciences. To understand Granger causality, consider two time series A and B, which could represent the BOLD signal measured in two brain regions. Time series A can be said to exert a Granger causal influence on time series B, only if knowledge of the past history of A improves predictions of the future values of B even when the past history of B (and of other variables) is included in the predictive model (Figure 11.11). From the perspective of fMRI, this would mean that knowledge of the activation in one source region (e.g., the left auditory cortex) would allow us to predict changes in the activation in another target region (e.g., Broca's area) at a future time point, with better accuracy than if looking at past activation in the target region alone. In essence, Granger causality quantifies how much, if any, unique information carried by the past history of one variable can be used to predict another variable. Note that

Granger causality A form of time series analysis that quantifies the information gained by using the past history of one variable to improve predictions of future values of another variable.

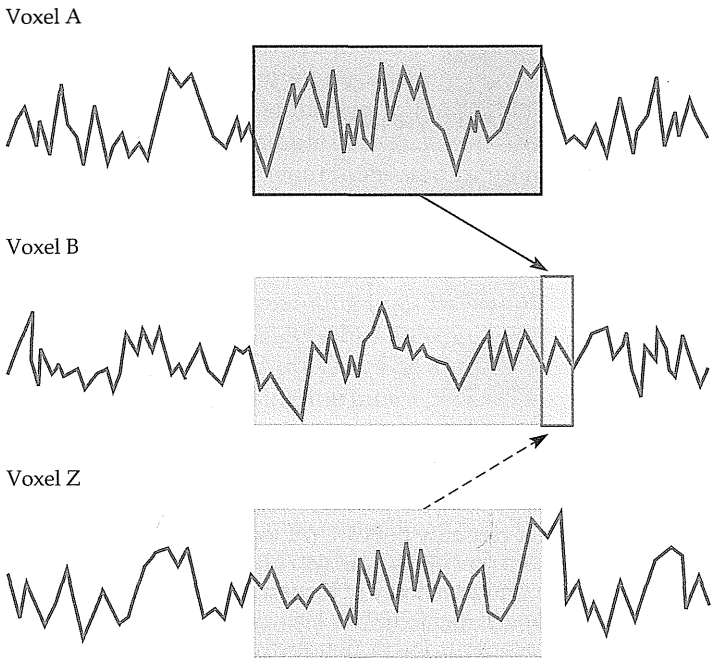

Figure 11.11 A schematic illustration of Granger causality. Consider three voxels (A, B, and Z), whose hypothetical time courses are illustrated in this figure. To infer that one voxel (A) exerts a Granger causal influence on another (B), the following conditions must apply: Knowledge about the past history of A (e.g., red block) should improve predictions about future values of B (blue block), compared to what could be predicted from the past history of B (green block) or from another reference time course (e.g., Z, gray block).

Granger causality is not a measure of true, physical causality. Because it makes the seemingly reasonable assumption that causes precede effects, in fMRI data the sluggishness of the BOLD time course could lead to apparent causal reversals. Moreover, if two time courses are highly redundant, a model that fails to account for possible intervening variables could lead to spurious conclusions. Even with these caveats noted, Granger causality does provide a useful mathematical framework for inferring influences between regions.

A data-driven implementation of Granger causality for fMRI was reported by Roebroeck and colleagues in 2005 (Figure 11.12). First they simulated a causal link between two brain regions, such that changes in the amplitudes of local field potentials in Region A altered the amplitudes of local field potentials in Region B. Through a number of simulations they tested delays of between 0 to 100 ms and variable levels of causal influence. They then convolved these simulated patterns of neuronal activity with a BOLD response function, to generate possible time courses of fMRI activation in those two regions. Their simulations demonstrated that neuronal delays as short as 50 ms could, in principle, be identified within fMRI data sampled at TRs of 500–1000 ms. (As noted above, the lower temporal resolution of fMRI data compared with the actual neuronal signals can lead to misidentification of the direction of causality. Thus, the authors argue that researchers should statistically compare both directions of causality: whether A to B causality is likely to be greater than B to A causality.) They next examined real fMRI data collected at a TR of 1 s while subjects performed a visual processing task that involved viewing photographs of faces and houses. Using a region of the fusiform gyrus known to be face-selective as their reference location, they found evidence for strong causal inputs from the early visual cortex and strong causal outputs to the parietal cortex. Thus, their Granger causality technique could recover known organization within the visual processing stream, even though images were only sampled at 1 s. For comparison, electrophysiological data indicate that the neuronal signals in these regions differ by only about 100 ms in their timing.

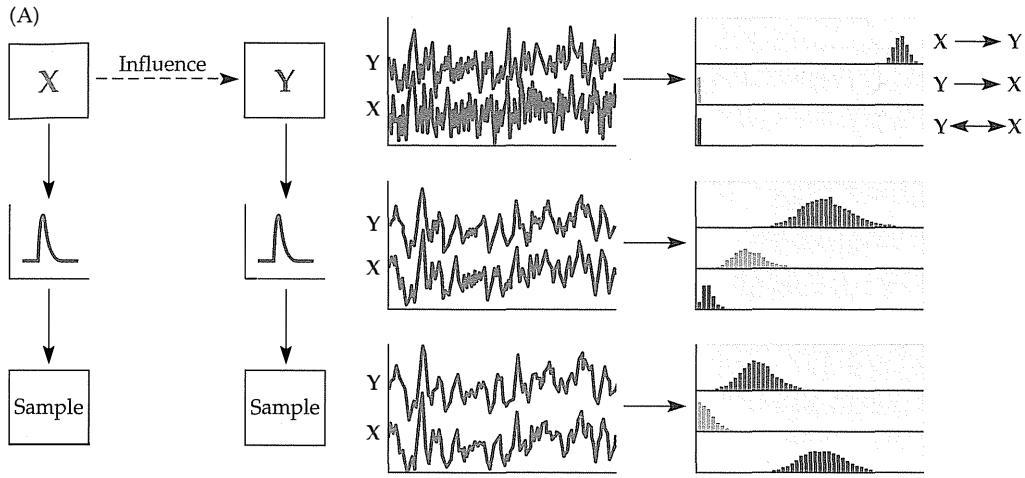

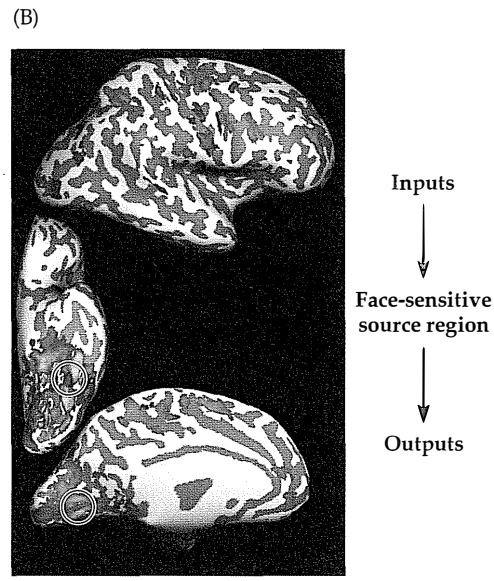

Figure 11.12 Using Granger causality in fMRI. (A, top row) Shown are simulated changes in the local field potentials from two brain regions with a causal relationship. Changes in the activity of Region X are assumed to cause changes in the activity of Region Y at 0–100 ms latency, without any reciprocal effects on X, or any simultaneous interactions between them. The distributions at right show the relative influence measures between the two regions, along with the bidirectional simultaneous influence. A distribution that is shifted to the right means that a casual relationship between the regions can be readily identified. Convolving the neuronal signals with a canonical BOLD hemodynamic response makes it more difficult to identify the direction of causal influence (A, middle row), and the course sampling of the fMRI data (i.e., at TR of 100–1000 ms) further accentuated the effects of simultaneous information between the two time series (A, bottom row). Across the simulations, the authors show that fMRI data sampled at a TR of about 500 ms can, in principle, detect causal effects between neuronal populations that have less than 100 ms latency. (B) Output from a Granger causality analysis for one subject. As a seed region, the authors used voxels from a face-sensitive region in the fusiform gyrus (red, circled). Regions shown in green exert causal influence on the seed region, whereas regions shown in blue receive causal influences from the seed region. (After Roebroeck et al., 2005.)

Another approach to understanding connectivity between brain regions is dynamic causal modeling (DCM), which was introduced by Friston and colleagues in 2003. Researchers using this method create a model of the functional connections between brain regions, and then evaluate how that connectivity changes as a result of experimental manipulations. Thus, they attempt to infer not just connectivity itself, but task-related changes in connectivity. In principle, knowledge about how experimental manipulations perturb the connectivity between brain regions can lead to better inferences about causality. The key idea of DCM is that experimental stimuli (or task conditions) can change the brain in either of two ways: by modulating a brain region directly (e.g., auditory input evokes activation in the auditory cortex) or by changing connectivity between two regions (e.g., effects on attention). To use DCM, researchers set up a model of relevant brain regions and their hypothesized interactions, and then use the observed fMRI data to evaluate the plausibility of that model. The neuronal activity in each of those brain regions is estimated as a deconvolution of the observed BOLD signal, and the interactions between

dynamic causal modeling (DCM) A statistical approach for testing models of the connectivity between brain regions, based on hypotheses about how experimental manipulations alter activation and connectivity between regions.

regions are inferred according to changes in the neuronal activity, not the BOLD signal itself. In 2008 Marreiros and colleagues extended the DCM approach to include multiple neuronal populations within each brain region, in order to better accommodate limitations in the spatial resolution of fMRI data.

An interesting example of the use of DCM was reported in 2008 by Kasess and colleagues. They were interested in motor imagery, or how individuals visualize physical movements. For example, basketball coaches will often tell players to visualize the sequence of movements before shooting a free throw under pressure. Prior neuroimaging work had clearly shown that brain regions involved with motor planning (e.g., the supplementary motor area, SMA) are activated by motor imagery, but the involvement of the primary motor cortex (M1), if any, remained unclear. The authors limited their imaging volume to four slices encompassing the motor cortex, and used high-speed fMRI with a TR of 300 ms. Their subjects participated in two tasks. In the motor execution task, subjects actually pressed a series of buttons when they heard an auditory cue, whereas in the motor imagery task, the same subjects only imagined pressing the buttons following the auditory cue. The authors tested a set of models of connectivity between the M1 and the SMA, including potential task-related influences on that connectivity. The best-performing model (Figure 11.13) indicated that imagery not only reduces activation in the SMA but also suppresses the connection between the SMA and the M1. This result demonstrates how DCM can extend the conclusions of fMRI studies beyond just activation of different regions, so that researchers can draw conclusions about how one region might suppress or enhance activation in another.

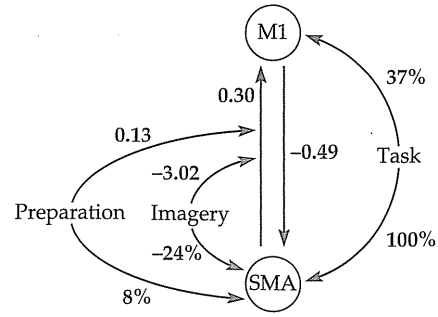

Figure 11.13 An example dynamic causal model (DCM) of fMRI data. Using high-temporal resolution fMRI, the researchers tested a variety of models for the interactions between the primary motor cortex (M1) and the supplementary motor area (SMA) during motor imagery and motor movements. The best-performing model, shown here, revealed that the normal feed-forward connections from SMA to M1 are suppressed under motor imagery. In contrast, an active motor task increases activation in both regions directly, and motor preparation evoked minimal changes on these regions and their connectivity. Enhancing effects are shown in red, while suppressing effects are shown in green. Note that direct task effects on brain regions are shown relative to the largest influence (of task on SMA), whereas indirect task effects on connectivity are characterized according to their relative strength and direction. (After Kasess et al., 2008.)

Combining fMRI and DTI

Functional connectivity analyses can be applied to any set of regions, regardless of whether those regions are really connected anatomically. Yet signals from one region to another travel via axons, which are typically organized into large-scale fiber tracts. Activation across broad regions might also reflect widespread changes in brain chemistry (e.g., neurotransmitter concentrations), which generally occur on a slower time scale than the scale typical for fMRI. Decades of neuroanatomical research have resulted in the mapping of the major fiber tracts, and provided a general wiring diagram of the human brain. All neurologically normal individuals share the same fiber tracts; for example, the left and right hemispheres always connect via the corpus callosum, while the frontal and anterior temporal lobes always connect via the uncinate fasciculus. However, the integrity of these tracts (e.g., the myelination of the constituent axons) does vary between individuals. Researchers can collect information about both the location and the integrity of fiber tracts via diffusion tensor imaging (DTI), which was introduced in Chapter 5. Like all other forms of MRI, DTI is non-invasive, and thus it allows researchers to measure properties of fiber tracts in normal human subjects.

By itself, DTI provides no information about brain function—it only provides information about brain structure. DTI data must be combined with other data to draw inferences about function. In one type of approach, DTI can be used to identify the existence and locations of fiber tracts that connect regions activated in an fMRI study. However, this approach has many limitations. Suppose you collect fMRI and DTI data from the same subjects. Your fMRI data show that both the lateral prefrontal cortex and the basal ganglia are activated by your task, and your DTI data reveal a fiber tract connecting these activated regions. What can you infer from these results? Even though the combined

diffusion tensor imaging (DTI) A collection of images that provide information about the magnitude and direction of molecular diffusion. It is often used to create maps of fractional anisotropy.

fractional anisotropy (FA) The preference for molecules to diffuse in an anisotropic manner. An FA value of 1 indicates that diffusion occurs along a single preferred axis, while a value of 0 indicates that diffusion is similar in all directions.

data suggest that some functional connections exist between these regions, you cannot determine whether information flows from the prefrontal cortex to the basal ganglia, or in the other direction, or in both directions. Nor could you tell whether any such connections are direct, or occur via intervening synapses. Thus, while DTI can show *that* a connection exists between two regions, it does not necessarily demonstrate that the identified connection contributes to information processing. In another type of approach, the integrity of specific fiber tracts, as assessed through DTI measures like fractional anisotropy, can be used to predict behavioral performance. For example, Madden and colleagues reported in 2004 that older adults who have reduced fractional anisotropy in the anterior limb of the internal capsule, a fiber tract connecting the prefrontal cortex and thalamus, tend to have slower performance on a visual search task. This approach has conceptual similarities to studies of brain lesions (see Chapter 13), in that it relates structural differences between individuals' brains to functional differences in their behavior.

An elegant example of the power of combining DTI with fMRI data was published in 2007 by Andrews-Hanna and colleagues. Prior neuroscience research, initially from postmortem brain measurements and more recently from DTI, had demonstrated that normal aging was associated with degeneration of white matter throughout the brain. Under what is commonly called the "disconnection hypothesis", this degeneration could reduce the efficacy of information flow between brain regions, leading to the broad and gradual decline in cognitive abilities observed with aging. To test this hypothesis, the researchers collected fMRI and DTI data from large samples of younger (18–40 y) and older adults (60–93 y). Their fMRI analyses evaluated the functional connectivity between the medial prefrontal cortex and medial parietal cortex, two of the central nodes within the default network (see Box 9.1). Consistent with prior research, these regions exhibited a high degree of functional connectivity in the younger adults; their time courses of activation were strongly correlated. This correlation was essentially absent in older adults (Figure 11.14A and B). For comparison, functional connectivity between other sets of regions (e.g., the left and right visual cortices) was the same in younger and older adults. Given these results, the authors tested whether the individuals who had the least functional connectivity also had the lowest fractional anisotropy in the white matter tract connecting these regions. This prediction was validated among the older adults (Figure 11.14C), even after controlling for the overall effects of age upon fractional anisotropy. To link these neural effects back to behavior, the authors demonstrated that those older adults with relatively well preserved functional connectivity between the medial prefrontal and medial parietal cortices tended to score better on a range of cognitive tests (Figure 11.14D). This study provides an excellent example of how fMRI, DTI, and behavioral data can be combined to support a simple conclusion: that age-related changes in the structural connections between regions alter their functional relationships, which in turn leads to broad deficits in cognitive function.

In summary, fMRI provides sufficient spatial and temporal resolution to identify connectivity between brain regions. Simple correlation approaches can be used to reveal regions that are functionally related, even in data sets collected in the absence of an experimental task. More complex hypothesis testing and modeling approaches allow estimation of the relative strength and directionality of the relationships between regions. DTI data can introduce anatomical constraints or suggest ROIs for connectivity models. The success of connectivity mapping rests on a simple principle: that complex behaviors and cognition depend on the computational contributions of a welter of differ-

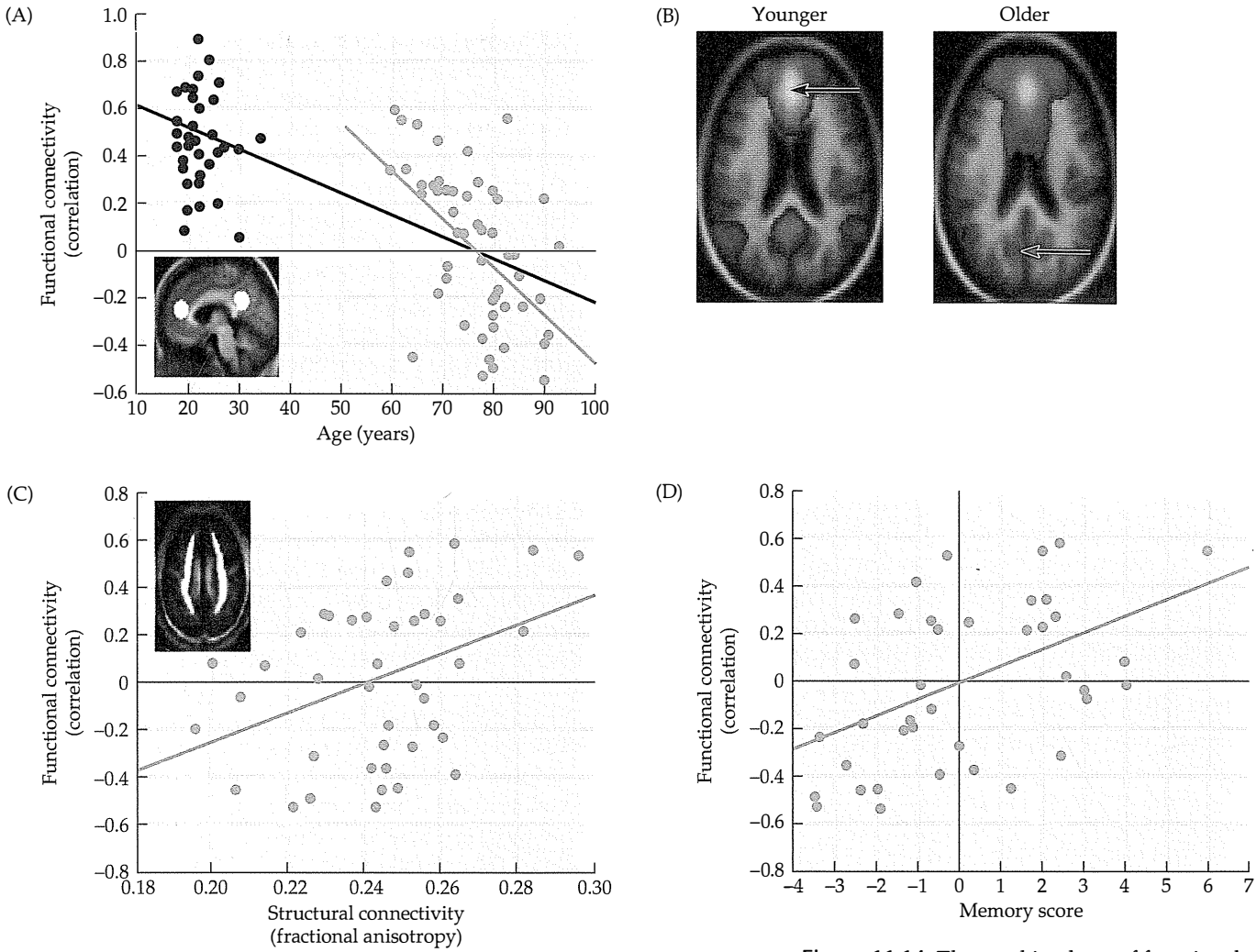

Figure 11.14 The combined use of functional and structural connectivity to understand age-related cognitive decline. (A) Compared with older adults, younger adults tend to have higher functional connectivity between the medial prefrontal and parietal cortices (regions highlighted on inset brain). Note that an age-related decline in functional connectivity is evident within the older adult sample (green line). (B) The pattern of functional connectivity from a seed voxel in the medial prefrontal cortex (approximate location indicated by black arrow). No significant functional connectivity to the medial parietal cortex (blue arrow) is evident in the older adults. (C) Among older adults, the degree of structural connectivity between these two regions (path shown on inset; values shown on x-axis) predicts the measured functional connectivity. (D) Those functional connectivity values in turn predict older adults' scores on tests of memory (shown) and other cognitive processes. (After Andrews-Hanna et al., 2007.)

ent anatomical regions. Even though each brain region projects to many others, considerable specialization remains. In 2002, Toni and colleagues introduced the idea that each region has a unique "connectional fingerprint" that represents its pattern of connectivity with other regions. We believe that this concept is a useful one, because it emphasizes that neuroscience analysis approaches benefit from anatomical considerations. Although all voxels may be treated similarly by standard fMRI analysis methods, they have different anatomical (and functional) connections. Connectivity mapping has the potential to elucidate these different properties of regions, thereby greatly improving the inferences that can be made from fMRI data.

Prediction Approaches

Suppose that you are a marketing researcher for a consumer electronics company in the year 2020. You assemble a focus group of individuals and bring them to your laboratory, which happens to contain an MRI

scanner. You place each person in your scanner and show them images and descriptions of the latest technological gadgets, while you measure activation evoked by each product. From this activation, and your prior knowledge of the brain regions associated with decision making, you attempt to identify which products (and ways of presenting those products) are likely to be successful in a competitive retail environment. While this example may seem fanciful at best—and fraught with ethical implications at worst (see Chapter 14 for additional discussions)—many fMRI researchers now use similar approaches for decidedly more scientific goals.

Prediction approaches reverse the typical direction of inference in fMRI research. The regression analyses described in the previous chapter explicitly treat task events as independent variables (i.e., forming regressors in a design matrix) and the observed fMRI data as dependent variables. In contrast, prediction approaches treat the fMRI data as independent variables that can predict some aspect of behavior, such as subjective experiences (e.g., looking at attractive versus unattractive images), subsequent memory (e.g., whether a word would be remembered at a memory test two weeks later), and simple purchasing decisions (e.g., whether to buy a new iPod). A variety of prediction approaches have been developed. Some studies label events according to subjects' behavior, not just the stimulus properties. Because these can be analyzed using the regression methods described in the previous chapter, we only briefly describe those approaches here. Others modify the general linear model to include some continuous, behaviorally defined predictor, either across subjects or across trials. Still others attempt to make inferences about the interactions between activation and some behavioral factor, integrating the connectivity methods described above with behavioral methods. And, some approaches use novel computational methods that use the joint changes in activation across sets of voxels to make their predictions.

Remember that none of these approaches provides clear information about causal relationships between brain regions, given the constraint due to the low temporal resolution of fMRI. In many ways, the distinction between "hypothesis testing" approaches and "prediction" approaches is more conceptual than methodological. However, that conceptual difference has important consequences for experimental practice. For example, some studies that attempt to predict behavior from fMRI data use a blinding approach: they create and test a model on part of the fMRI data (e.g., 3 of 4 experimental runs), and then validate that model on completely novel data (e.g., the final run). Whether or not a model is valid depends, in a very literal sense, on whether it can be generalized to new data. In a broad sense, we as fMRI researchers want to be able to predict the functional consequences of brain activation, not merely interpret the activation we observe. However, extreme caution should be taken in making these predictions; see Box 11.2 for examples in which the inaccurate prediction of functional properties could have life-changing effects.

Predicting variation among individuals

In the first fMRI studies, like that of Kwong and colleagues discussed in Chapter 7, each participant's data were analyzed individually—in effect, treating each individual as a separate experiment. These studies largely used very robust sensory or motor paradigms, which tend to evoke robust activation in every individual. However, as fMRI research began to address new cognitive phenomena, researchers began combining data from samples of participants. By doing so, the researchers increased their power for detecting effects that were common within the subject sample. In recent years, more and more studies have

BOX 11.2 Real-Time fMRI

Most fMRI analyses require substantial computational time. The preprocessing steps outlined in Chapter 8 involve complex signal processing algorithms, from the rigid-body spatial alignment required for motion correction to the temporal filtering used to remove task-unrelated variability. The multiple-regression analysis approaches described in Chapter 10 involve simple matrix operations, but even relatively simple computations can introduce substantial delay when repeated for many thousands of voxels, hundreds of time points, and dozens of subjects. Important analysis steps like correction for multiple comparisons involve additional, subject-specific computations. And, the data-driven approaches described in this chapter vary from relatively simple to remarkably complex. For most research fMRI studies using standard methods, the impressive power of modern computing hardware overcomes these challenges. For example, using a parallel-processing cluster, as is now available within many centers, an entire large-sample fMRI study can be analyzed within several hours. But for some applications, even this seemingly short delay can be unacceptable—those applications require real-time analyses. In this section, we consider two important applications of real-time fMRI: diagnostic scanning for pre-surgical planning and functional biofeedback.

Mapping function for pre-surgical planning

One common application of fMRI is the identification of functional areas that need to be preserved during neurosurgery. For many patients with brain tumors, vascular malformations, intractable epilepsy, or other types of pathology, surgical removal of the diseased portion of the brain provides the best clinical outcome. However, surgery may not be appropriate for all subjects, and the amount of tissue to be removed may depend on its functional properties. If tissue removal would result in damage to brain regions essential for language, memory, or primary sensory or motor processing, it could have a devastating effect on the patient's subsequent quality of life. For example, damage to the left temporal lobe may render someone unable to comprehend speech. Thus, when deciding on the course of treatment for a given patient, neurosurgeons want to be able to evaluate the likely consequences of removing a particular brain region. Cortical mapping plays an important role in this evaluation process.

Since the 1950s, cortical mapping has typically been done during the surgery itself by temporarily probing selected brain regions using direct electrical stimulation of the cerebral cortex (see Chapter 13). This process involves placing an electrode on different parts of the exposed cortical surface. By sending a small electrical current between two adjacent electrodes, the surgeon can inhibit or excite local neuronal activity. In most cases, direct stimulation impairs the function of a brain region; for example, stimulation of language areas may render patients temporarily unable to speak. In other cases, stimulation may actually cause the patient to hear sounds or see colors, motion, or shapes, if the electrodes are placed near primary sensory areas. Although direct electrical stimulation is widely used, it has some disadvantages. The procedure is highly invasive and time-consuming, the patient must be awakened during surgery, the range of functions that can be investigated is limited, and the only cortical areas that can be measured are those near the exposed surface of the brain.

To overcome these disadvantages, a number of hospitals have begun investigating the use of fMRI for cortical mapping in surgical patients (Figure 1). The advantages of fMRI are straightforward.

(continued on next page)

(A)

(B)

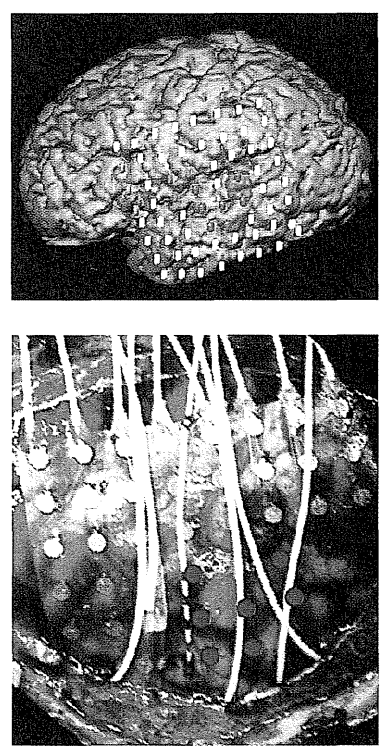

Figure 1 Cortical mapping of function. This patient was undergoing cortical mapping in preparation for neurosurgery. The subject underwent both fMRI (A) and direct electrical stimulation (B). On the reconstruction of the patient's brain in (A), the locations of the electrodes in the grid in (B) are shown as white spots. The electrodes are highlighted according to the effects that direct stimulation had on different tasks: orange, speech arrest; green, induced mouth or face movements; and blue, deficits in auditory comprehension and object naming. The locus of fMRI activity during a language comprehension task is shown on the brain surface in red. Note the overlap, although incomplete, between the fMRI and electrophysiological data.

BOX 11.2 *(continued)*

It can be used to map functions anywhere in the brain, including deep-brain structures difficult to reach using electrodes. It is noninvasive and can be conducted in advance of surgery to aid in surgical planning. Furthermore, a wide range of cognitive, motor, and perceptual functions can be tested. Combining functional and conventional anatomical MRI in the same scanning session can provide maps of important functional areas superimposed on high-resolution images that show detailed anatomical structure and sites of tissue pathology. Multiple brain functions can usually be mapped within a 30- to 40-minute scanning session, providing neurosurgeons with important information to aid in planning the surgical approach. Functional MRI can also be used in conjunction with traditional electrophysiological approaches, by guiding the placement of electrodes for subsequent testing during the operation.

Despite its obvious potential, diagnostic fMRI has not yet been used widely, primarily because its analysis and interpretation is technically demanding.

real-time analyses A set of computational steps designed for the rapid analysis of fMRI data, so that statistical tests can be conducted immediately following the acquisition of images.

pre-surgical planning The use of fMRI or another neuroscience technique to map particular functions in a single individual, in order to guide clinical decisions about the potential course and consequences of neurosurgery in that individual.

biofeedback Providing an explicit indicator of some physiological process, such as the beating of the heart or activation within a particular brain region, so that an individual can attempt to regulate that activation or guide behavior.

Whereas most fMRI research involves pooling results from many subjects, as described in the previous section, diagnostic fMRI must produce interpretable activation maps in a particular individual. It is critical that each scan produce high-quality MR images with good functional resolution. An important factor in achieving reliable diagnostic fMRI capabilities has been the development of real-time analysis methods. In real-time analysis, the fMRI data are reconstructed, preprocessed (if needed), and statistically analyzed immediately following the acquisition of each image. Thus, the desired functional maps are available at the conclusion of the scanning session. Real-time analyses can also be very useful for standard fMRI experiments, because they provide a way to monitor the quality of the results. If the subject moves his head excessively or is unable to perform the experimental task, real-time analyses can catch the problem during the session so that it can be corrected. Real-time generation of statistical maps can also make scanning more efficient by allowing each scan to run only as long as is necessary to reach a satisfactory confidence level. For clinical cortical mapping, the ability to assess task performance and activation map quality while the patient is still in the scanner is crucial. Finally, the goals of significance testing may differ dramatically between experimental and clinical fMRI analyses, since experimental analyses always aim to minimize false positive results, while clinical analyses may instead aim to avoid false negative results.

fMRI Biofeedback

Research into biofeedback, or providing data that allows people to influence their own bodily states, has a long and somewhat checkered history. Traditional uses of biofeedback involved relaxation or stress relief: in a typical paradigm, the participant wears sensors that monitor sympathetic nervous system responses (e.g., changes in heart rate or skin conductance) and is shown the output of those sensors on a computer monitor. The subject's task involves minimizing the responses in those sensors through conscious strategies that might involve self-distraction, emotional regulation, or cognitive control.

Modern fMRI biofeedback uses information about the subject's own fMRI activation to influence the presentation of experimental stimuli. By its very nature, biofeedback requires extremely rapid real-time analyses. Whereas the typical goal of pre-surgical planning is to generate a map of activation at the end of each run, studies involving fMRI biofeedback must derive measures of activation that are updated immediately after the collection of each volume. Early studies of fMRI biofeedback indicated that such rapid analyses were possible, with some constraints. In one particularly clever example reported in 2007 by Weiskopf and colleagues, participants in two scanners played a game of "Brain Pong." Like in the old Pong video game, each participant moved a virtual paddle up and down on a computer monitor, attempting to bounce a ball past their opponent's paddle. But in this game, they moved the paddle not with a joystick but by increasing or decreasing activation in a region of interest within the brain!

What effects might biofeedback have on fMRI participants? Some evidence comes from a 2004 article by DeCharms and colleagues, who trained participants to imagine moving their right hands during 30 s imagery blocks, which were separated by 30 s non-task blocks. (To ensure that the participants made no muscle movements during the imagery blocks, the researchers recorded electromyographic signals from the

BOX 11.2 *(continued)*

right hand.) At the end of each task block, the participant was given either accurate or inaccurate feedback about the level of activation in the left motor cortex relative to a target level. As the experiment progressed, subjects given accurate biofeedback both improved the SNR and increased the spatial extent of activation in the motor cortex. Conversely, subjects who were provided with inaccurate biofeedback could not increase the specificity of the BOLD signal over time. Additional, highly intriguing recent evidence comes from a 2007 paper by Bray and colleagues, who rewarded subjects if they were able to successfully activate a particular region of the somatosensory cortex. Over the course of the experiment, subjects learned by trial-and-error which region to activate and were progressively more specific in their activation. Together, these results suggest that subjects can adaptively use information supplied via biofeedback to up- (or down-) regulate specific brain regions, even without prior knowledge of the functions or identities of those regions.

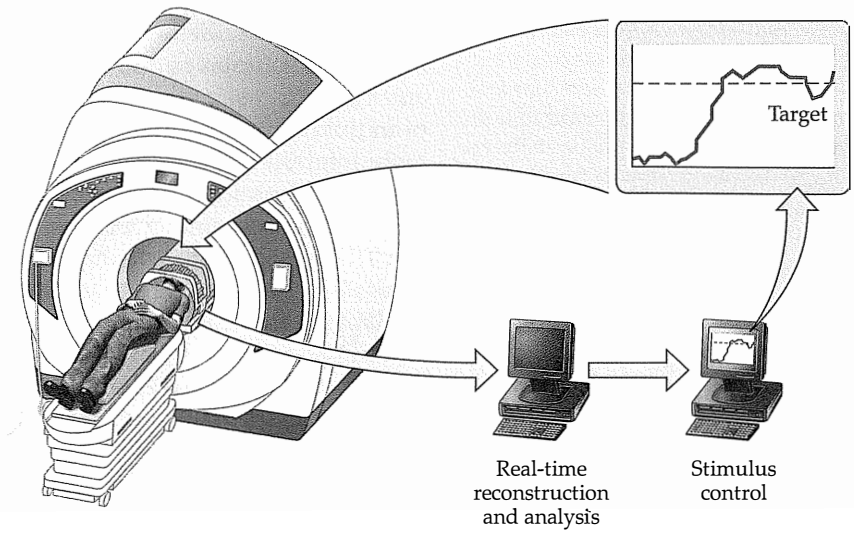

Figure 2 Biofeedback in fMRI research. For some experimental questions, researchers show fMRI subjects measurements of the activation in a particular brain region. Following training, participants can use this information to exert conscious control over the intensity of that activation, raising it or lowering it based on experimental instructions. This approach may become useful for treatment of clinical disorders involving dysregulatory deficits, such as chronic pain.

At this point in time, research into fMRI biofeedback remains at a relatively early stage. Most studies have simply supported the concept rather than provided novel information about brain function. Yet, several potentially exciting applications have already arisen. Perhaps most promising are the therapeutic applications, which apply the power and neural specificity of fMRI to the types of problems (e.g., chronic pain) addressed by other forms of biofeedback. In a 2005 study, De Charms and colleagues evaluated whether biofeedback about activation in the anterior cingulate cortex (ACC), a region thought to be critical for the regulation of emotional and painful stimuli, could ameliorate the experience of pain. Their participants included both chronic pain sufferers and control groups of individuals without chronic pain. During 60 s task blocks, subjects were instructed to increase or decrease the BOLD signal in the ACC, whose activation was represented by a virtual fire whose intensity indicated the level of activation. Individuals who were provided accurate biofeedback successfully controlled activation in the ACC over the course of training. But those subjects given inaccurate feedback were unsuccessful in regulating ACC activation. Most strikingly, those chronic pain patients who exhibited the best control over the ACC also expressed the greatest reduction in their pain levels.

Biofeedback research using fMRI still faces several limitations. For analyses to be completed in real-time, the experiments must use relatively straightforward designs and analysis methods. Typical are blocked-design studies in which the subject attempts to increase or decrease activation in a given region during an extended (>30 s) block. For comparison, rapid event-related designs are difficult to analyze in real time, both because of lower SNR and because successive events may generate overlapping time courses of activation. Using a pre-selected ROI can speed biofeedback training. As shown by Laconte and colleagues in a 2007 paper, researchers can use complex analysis approaches like pattern classification, if a training pattern is established earlier in the experimental session. Then, during the testing runs, each time point can be quickly compared with that training pattern for classification. Also, despite the promise of fMRI biofeedback, it lacks the obvious advantages of electrophysiological approaches, which can be conducted using less expensive and more portable equipment. Nevertheless, we expect that new approaches to fMRI biofeedback will lead to exciting new results, some of which will have important clinical consequences.

taken a different tack by examining effects that vary between subjects, thus seeking individual differences in brain function. At least three interrelated factors have contributed to the increased emphasis on variation among individuals. First, there has been a steady increase in the number of subjects per study. Whereas early studies often included ten or fewer subjects, many current studies contain samples of more than 20 individuals. Second, the standardization and validation of analysis approaches has made it easier to conduct analyses of individual differences. And third, fMRI researchers have become increasingly interested in new research areas in which individual variation is paramount, such as studies of personality traits, interpersonal attitudes, and decision preferences, among many others.

The most common method for analyzing individual differences involves correlations between fMRI data and behavioral data collected outside the scanner. For example, a researcher might give every subject a questionnaire that assesses some personality trait, like extraversion. The subjects' scores on that questionnaire are then entered into the across-subject analyses as a covariate (see Box 9.1, Figure 3, and Figure 10.21 for examples). In effect, the resulting significance tests identify voxels whose activation in one condition (or difference in activation between conditions) varies in proportion with subjects' trait scores. Other, more complex analysis methods are also possible. If a set of ROIs were implicated in a particular cognitive process (e.g., making risk-averse decisions), their amplitudes of activation might be combined to predict individual differences in behavior (e.g., an individual's overall level of risk aversion). Or, a data-reduction approach like PLS could be used to identify patterns of activation whose amplitude varies systematically between subjects. In principle, any statistical analysis of brain activation, from the simple approaches introduced previously to the advanced approaches outlined in this chapter, could serve to predict or measure individual differences. This sort of correlation approach has become a common tool for fMRI studies. Yet it is has an important limitation. If a behavioral measure has high variability or systematic bias, or simply does not map onto the hypothesized ROI, then null or misleading results will be obtained.

So far, we have talked about prediction in a relatively abstract sense: researchers identify two sets of variables, one reflecting measures of behavior and the other reflecting measures of brain function, and then evaluate how well knowledge about one of those sets (brain data) lets us predict the other (behavioral data). However, researchers now use fMRI to make much more explicit predictions. Consider the possibility of using some aspect of fMRI activation as a biomarker for a psychiatric disorder, such as schizophrenia. If we already know that someone has schizophrenia, then scanning them might seem to provide little new information about their clinical status. But suppose that we scan subjects after they have been diagnosed with that disorder, but before they undergo a particular treatment regimen. Information about their brain function, such as activation in the prefrontal cortex associated with executive function, might predict their subsequent improvement following therapy. If so, then researchers and clinicians could work together to best match treatment options to individuals. Even more promising are studies of asymptomatic individuals who are nonetheless at high risk for a disease. For example, the risk of schizophrenia increases dramatically in young adults who have a close relative with that disorder. By conducting prospective studies in these high-risk individuals, researchers may become better able to predict who will develop the disease, allowing for targeted early interventions that could delay, ameliorate, or prevent development of the disease.

individual differences Measures of variation among individuals within a population.

biomarker A phenotypic feature, whether physical, physiological, or behavioral, that provides a robust predictor of some experimentally or clinically important outcome.

Predicting variation in behavior

Behavior changes dramatically over time. Even when completing the same simple task over and over again (e.g., "press a button when you see a shape appear"), the same person will respond quickly on some trials and slowly on others. When someone studies a random set of words in advance of a memory test, some of the words will be remembered while others will be forgotten. Most fMRI studies account for such variability in behavior by varying how events are coded via the timing and amplitude of regressors in the design matrix. For example, researchers studying the subsequent memory effect might present a set of words during the scanning session, then test each subject's memory of those words in a behavioral testing session that could be hours, days, or even weeks later. When analyzing the fMRI data, the researchers create separate regressors for remembered and forgotten words. Similarly, a researcher interested in executive function might code each stimulus according to response time, resulting in regressors for various event durations across trials. (Introducing response time as a regressor in a design matrix can also be useful for minimizing unwanted effects of decision difficulty.) Coding events according to behavior has been particularly important in decision-making research, for which the key experimental conditions are often the choices made by the subject.

subsequent memory An approach to fMRI analyses that sorts experimental stimuli based on whether they were remembered or forgotten in a later testing session; this allows identification of brain regions whose activation predicts successful encoding of stimulus properties into memory.

logistic regression A subset of regression analysis that uses a set of independent variables to predict a binary outcome variable.

Often, researchers want to understand how different aspects of brain function (e.g., activation in different brain regions) predict variability in behavior. A particularly powerful approach has been to combine information about brain function and behavior in a logistic regression model. As introduced in Chapter 10, regression analyses use information from multiple independent variables to predict values of one or more dependent variables. Unlike standard regression analyses that use continuous dependent variables, logistic regression uses a categorical dependent variable. That is, it attempts to predict whether or not some outcome will occur, or to identify the state of some binary process. When using a logistic regression analysis, researchers typically identify a set of variables that might influence the subjects' behavior. Some of these variables might reflect brain activation, such as activation in each of several regions or even the level of functional connectivity between them, while other variables will reflect aspects of behavior, such as choices made during the previous trial, or the overall decision bias of the subject. Including behavioral data in the logistic regression model minimizes the chances of spurious brain-behavior relationships; i.e., claiming that a brain region predicts a particular behavior, when instead that region's activation was itself driven by other aspects of behavior.

A notable example of this approach was published in 2005 by Kuhnen and Knutson. They were interested in how different brain regions might interact to shape choices between risky and safe options in a simple investment game (Figure 11.15A). The subjects made a series of choices between three shapes: two symbolized risky stocks that could either win or lose $10, while one represented the safe bond that was guaranteed to win $1. For each block of 20 trials, one of the stocks was twice as likely to win money as to lose money, whereas the other was twice as likely to lose money as to win money. Initially, the subject did not know which stock was the good one. But over trials, as subjects gained information about the reward histories of each stock, they could make educated guesses in an attempt to earn more money. The optimal strategy, therefore, was to first pick the safe bond and then later, once enough information accumulated, switch over to choosing the presumably good stock. Yet people often made mistakes. They sometimes made risk-seeking mistakes by

(A)

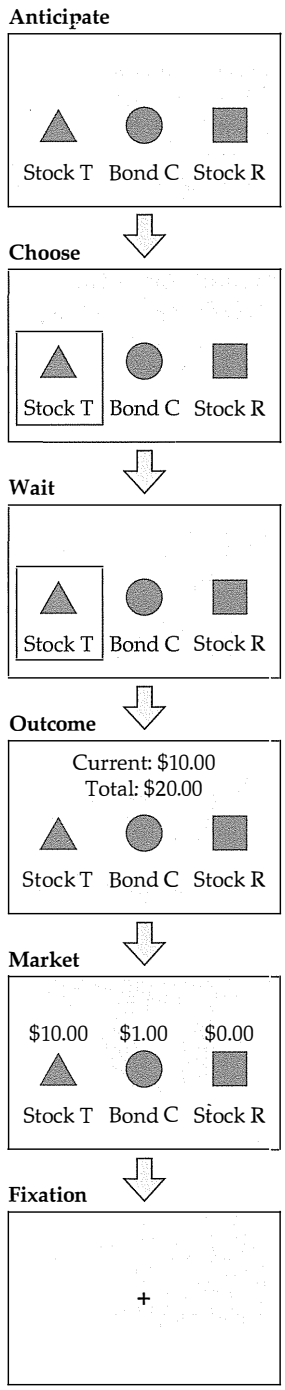

(B)

	Previous choice was a stock	Previous choice was a bond	
Risk-aversion mistakes	**Coef**	**Coef**	**All Data Coef**
NAcc	0.30	−0.58**	−0.20
Medial PFC	−0.12	−0.14	−0.16
Insula	1.10***	0.10	0.50**
$RelEarnings_{t-1}$	0.05***	−0.05***	−0.04***
$Outcome_{t-1}$	0.05**	—	0.05**
$Uncertainty_t$	3.93**	11.61***	11.71***
$CumEarnings_{t-1}$	0.02	0.02	0.03***
Constant	−2.36***	−2.48***	−3.31***

Figure 11.15 Using logistic regression to predict individual decisions from fMRI data. (A) Subjects played a simple stock-picking game (see text for details). (B) The researchers incorporated the trial-by-trial activation in each of three ROIs—the left nucleus accumbens (NAcc), the medial prefrontal cortex (PFC), and the insula—as predictor variables within a logistic regression model. Also included were a set of behavioral variables: the relative earnings of the chosen stock compared with the unchosen stock in the previous trial ($RelEarnings_{t-1}$), the earnings in the previous trial ($Outcome_{t-1}$), the subject's estimated uncertainty about which stock was better ($Uncertainty_t$), and the cumulative earnings so far in the experiment ($CumEarnings_{t-1}$), here divided by 10 for clarity. They found that increased activation in the insular cortex increased the chance of a risk-averse mistake following the previous choice of a stock, whereas increased activation in the nucleus accumbens decreased the chance of such a mistake following the choice of a bond. Each cell of the logistic regression matrix at right indicates the associated regression coefficient (Coef), or the degree to which that behavioral variable predicted choices. Asterisks indicate significance values: **, $p < 0.05$; ***, $p < 0.01$. (After Kuhnen and Knutson, 2005.)

choosing one of the stocks even before there was good information about which stock was likely to make money. They also made risk-averse mistakes by choosing the bond even though they had enough information to gamble on the good stock. The authors attempted to predict these mistakes in decision-making using a logistic regression that contained both behavioral information and measures of fMRI activation in key brain regions. As shown in Figure 11.15B, increased activation in the insula predicted that the subject would make a risk-averse mistake following a risky choice, whereas increased activation in the nucleus accumbens (i.e., part of the ventral striatum) decreased the chance of a risk-averse mistake following a safe choice. Most critically, these brain regions were significant predictors of behavior even though information about behavior itself was included in the model.

Pattern classification using machine learning algorithms

Anyone who has examined raw fMRI data has been struck by how nearby and even adjacent voxels may exhibit wildly different time courses (Figure 11.16), which may lead to large differences in significance values following statistical

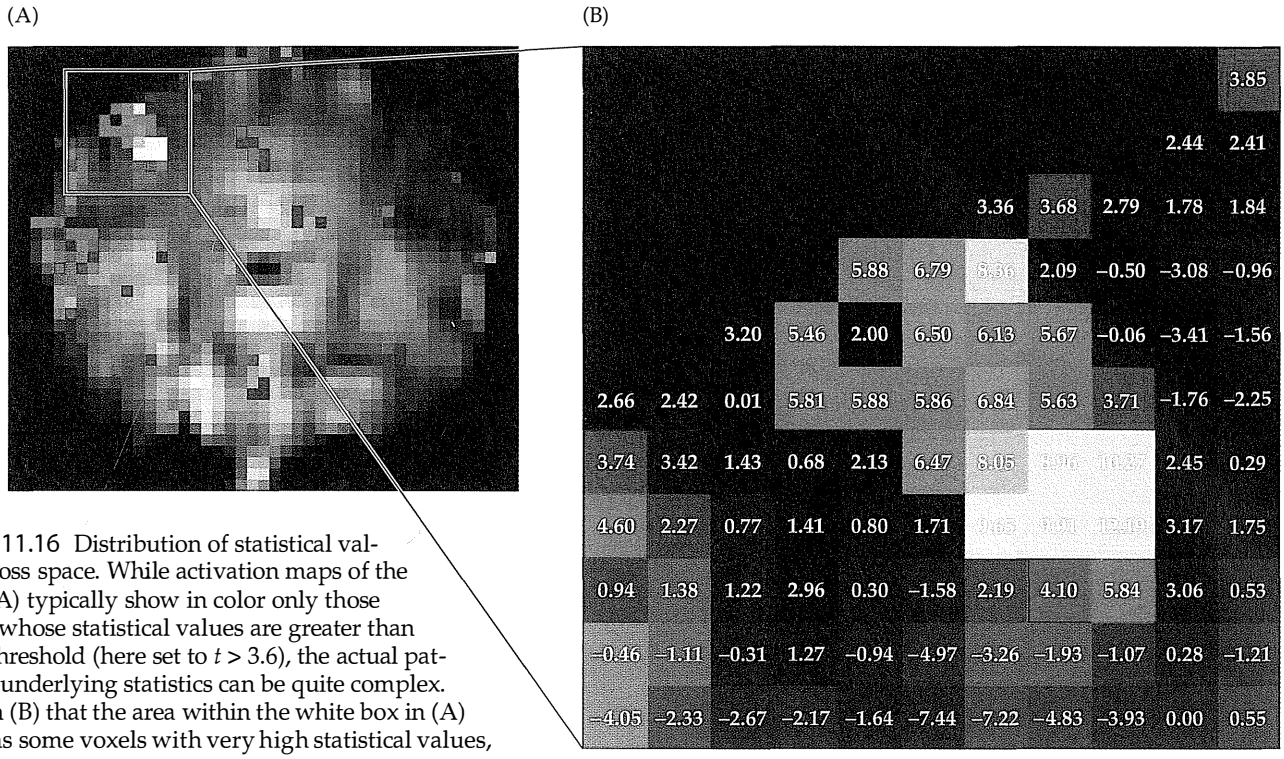

Figure 11.16 Distribution of statistical values across space. While activation maps of the brain (A) typically show in color only those voxels whose statistical values are greater than some threshold (here set to $t > 3.6$), the actual pattern of underlying statistics can be quite complex. Note in (B) that the area within the white box in (A) contains some voxels with very high statistical values, along with others that are only slightly above the threshold. In fact, some voxels that are designated as inactive, and thus not shown on the color map, have significance values quite near the threshold. Other nearby voxels even exhibit negative significance values.

analyses. Standard fMRI preprocessing and analysis steps ignore inter-voxel differences. Indeed, researchers typically apply spatial smoothing and require clusters of activation, both of which suppress differences between nearby voxels. Yet, we know from more than a half-century of basic neuroscience research that the cortex exhibits substantial local organization, often at a spatial scale of several millimeters or smaller (e.g., ocular dominance columns in the visual cortex). How can researchers use information from individual voxels to draw inferences about the function of a region?

Approaches to solving this problem have largely been based on **pattern classification** algorithms, building on research from the subfield of **machine learning** within computer science. Machine learning uses known items from a data set to create rules that can efficiently categorize new items. Suppose that you wanted to create a computer program that could categorize an animal as either a dog or a cat, based on its visual appearance. You show the program some representative dogs (e.g., greyhound, terrier, retriever) and some representative cats (e.g., siamese, persian, calico). From those examples, the program extracts some general rules for categorization, such as "large, long-legged animals with extended snouts are dogs." These rules should be broad enough to generalize to new examples of the category (e.g., "beagles"), but specific enough to exclude items that are not in that category. Moreover, the algorithm used to create the rules should be computationally tractable. Generally, no classification rule will be both simple and able to classify new items perfectly. For example, some types of dog are small, short-legged, and flat-snouted (e.g.,

pattern classification An attempt to separate individual examplars into different categories by constructing a set of decision rules based on some combination of their features.

machine learning A subdiscipline within computer science that develops algorithmic rules for relating input data to desirable outputs.

multi-voxel pattern classification An approach for pattern classification in fMRI research that uses as its input data the relative changes in activation across a set of voxels.

pugs). Therefore, the main challenge of pattern classification is to identify rules that can be generalized to new examples yet are simple and efficient.

For fMRI studies, researchers generally use **multi-voxel pattern classification**: they predict event categories from various patterns of activation across voxels, rather than from the overall increase or decrease in activation of a large brain region. Although there are several types of pattern classification algorithms used on fMRI data, all involve three main steps (Figure 11.17). First, a

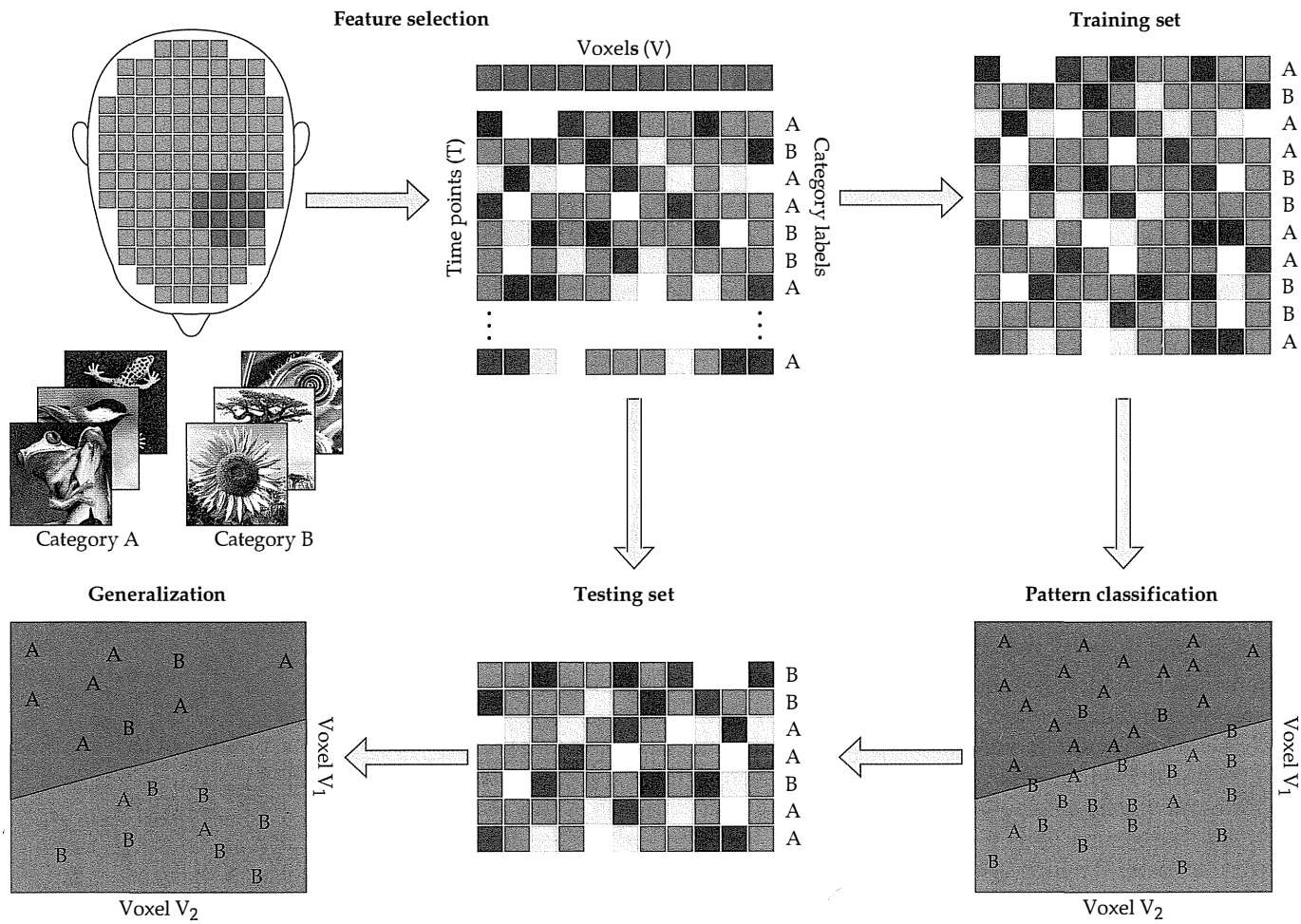

Figure 11.17 A conceptual overview of multi-voxel pattern classification of fMRI data. In this example, the researchers want to identify voxels whose activation predicts whether the subject is looking at photographs of animals or plants. At the first stage, feature selection, the researchers identify a subset of voxels for subsequent analyses. A typical feature set consists of the activation intensity for each voxel on each trial. The feature set splits into a training set, from which the pattern classifier will be derived, and a testing set that provides a novel test of the generalization of the classifier. Shown here is a simplified example of pattern classification using two features (i.e., two voxels) and two trial categories (A and B). The activation values of those two voxels on each trial are shown as a two-dimensional plot. Note that fMRI pattern classification involves many more dimensions, and thus a much higher-dimensional space. In the common technique of support vector machines, the pattern classification algorithm attempts to identify the surface that maximally distinguishes the two categories. Here, a linear classifier optimally separates the two stimulus categories. Once a classifier has been identified, it is tested on the novel training set, to ensure that the classification rule can be generalized to untested data.

subset of the fMRI data is extracted in a process called feature selection. In most cases, this involves identifying a subset of V voxels (e.g., all voxels within a predetermined ROI, or voxels within a particular searchlight) and identifying the BOLD amplitude in each voxel at each of T time points. Usually, those time points reflect the stimulus events or behaviors to be sorted, taking into account the delay in the hemodynamic response, for example by selecting a time point 4–6 s following the presentation of a stimulus. In some cases, researchers have used pattern classification to study processes that occur in advance of the subject making a decision, in which case the time points would be earlier than the corresponding behavioral events. This first step reduces the fMRI data to a set of vectors ($N_1 \ldots N_V$), each corresponding to the pattern of activation associated with one example from a category. Researchers often subtract the mean (or global) signal for the whole region from each vector, so that only relative changes in activation across voxels contribute to the classification algorithm.

Thought Question

Why might local patterns of fMRI activation across voxels within a region be more sensitive for detecting cognitive processes than the global change in activation from that entire region?

Second, the researchers partition their data into a training set and a testing set. For example, if the experiment consisted of 50 presentations of male faces and 50 presentations of female faces, the training set might contain 25 faces from each category and the testing set might contain the remaining 25 faces from each category. The vectors from the training set are then entered into a pattern classification algorithm, most commonly (for fMRI studies) using support vector machines (SVMs). Considered generally, an SVM takes the vectors within each of two categories A and B (each vector representing a set of points in a V-dimensional space), and attempts to find the surface that maximally distinguishes the two categories within that space. A linear SVM approach uses a hyperplane to distinguish the categories; that is, it finds the combination of voxel weights that best predicts whether a time point belongs to Category A or Category B. A non-linear SVM looks for the complex curved surface that best distinguishes the categories; in effect, it can use the joint movement of pairs or groups of voxels (e.g., increased activation in one voxel at the same time as decreased activation in another) to improve its predictions. The set of voxel weights, whether linear or non-linear, is known as a pattern classifier, and the points that lie along the pattern classifier boundary are called support vectors, hence the name for the technique.

Third, the researchers evaluate whether their pattern classifier can be generalized to new data. Several approaches can be used. One involves splitting the data, as described in the above example, with the success of the classifier defined primarily by its performance on a completely novel testing set. Another approach involves the iterated use of several training sets. For example, researchers could separate their data into five parts, use the first four in a training set for their pattern classifier, and then test the classifier using the fifth part. Then, they could use a different four-fifths of their data to generate a second classifier, and test the new classifier on the remaining one-fifth. By repeating this approach five times, and thus using each fifth of the data once as a testing set, the researchers can calculate the average predictive performance of classifiers using the input voxels. This is known as cross-validation. Further,

feature selection An initial step in pattern classification that involves the determination of which input variables should be included in the classification algorithm.

searchlight An approach to feature selection in the pattern classification of fMRI data. As its name implies, a searchlight reflects a geometrically defined ROI (e.g., a sphere of 5-voxel radius) that can be moved throughout the brain.

training set In pattern classification analysis, that part of the data set used to develop the classification algorithm.

testing set In pattern classification analysis, a novel part of the data set used to evaluate the robustness of the classification algorithm.

support vector machine (SVM) A class of algorithm used in pattern classification that attempts to identify the combination of features in the original data set that can most effectively differentiate between two categories.

cross-validation In pattern classification analysis, an approach to evaluating the effectiveness of classification using a given feature set. It involves the iterated generation and testing of classifiers based on different parts of the same training set.

researchers can combine these techniques by first using cross-validation to identify sets of voxels whose activation best distinguishes categories, followed by testing an optimized classifier on an as-yet-unexamined testing set.

Because pattern classification relies on relative changes in intensity in individual voxels, rather than changes in the overall activation of a large region, some aspects of data analysis in pattern classification differ from standard approaches. Notably, researchers do not typically apply spatial smoothing during preprocessing. As discussed in Chapter 8, smoothing spreads information from one voxel across its neighboring voxels, which can improve some aspects of fMRI analyses, such as reducing the number of independent comparisons and minimizing voxel-dependent noise. However, introducing spatial blurring makes individual voxels less predictive. Pattern classification can be improved at the initial, feature-selection stage by excluding some voxels beforehand, so that they do not contribute to the classifier. Features can be based on anatomical criteria (e.g., selecting specific ROIs), functional criteria (e.g., using only activated voxels from another statistical test), or statistical criteria (e.g., removing high variability voxels). Pattern classification studies typically involve analyses at the single-subject level, largely because the fine spatial patterns that distinguish different processes may differ across subjects. The brains of two subjects may share gross functional similarities, such as increased activation in the lateral occipital cortex in response to visual stimuli, and thus may lead to similar outcomes using standard analysis methods. However, the responses of individual voxels to different stimulus categories might differ dramatically. So, researchers usually evaluate whether a given spatial location (e.g., voxels in the primary visual cortex) can be used for pattern classification in each of their subjects. It is less common to derive a spatial pattern in one or more subjects and extend that pattern to novel subjects. See the 2005 paper by Davatzikos and colleagues in the chapter references for a rare example.

Capabilities and challenges of fMRI pattern classification

Pattern classification analyses provide several advantages over the regression-based approaches described in Chapter 10. By evaluating changes in the activation of individual voxels, pattern classification incorporates information that is typically discarded or smoothed over. This can greatly improve the sensitivity for detecting small but meaningful changes in fMRI activation. Some task-related effects are detectible using pattern classification, but completely undetectable using standard techniques. Suppose that a process causes opposing changes in two neighboring voxels, such that one increases in activation when the other decreases in activation. A pattern classification approach could detect that those joint movements were task-related, whereas standard analysis techniques would see only minimal changes in overall activation. However, the value of pattern classification extends much farther than simply increasing the sensitivity of analyses. The most powerful applications of this approach address questions about processes that are distributed throughout brain regions. Here we highlight some exciting applications of pattern classification, many of which represent the very cutting edge of fMRI research.

Unquestionably, fMRI pattern classification has had the greatest impact on studies of the neural basis of perception, specifically visual perception. Extensive prior research, mostly using electrophysiological recordings from other species, has demonstrated that our visual perceptions result from the combined output of a hierarchy of neurons, each only processing a small portion of the visual world. While many of the details of visual system function-

ing remain to be discovered, there exists strong evidence for both large- and small-scale organization. Different regions of the cortex process distinct visual features: neurons in the primary visual cortex respond to simple lines and edges, whereas neurons farther along the visual processing pathway respond to objects from specific categories. At least within the early visual regions, individual neurons are arranged spatially according to their input, specifically according to the arrangement of the parts of the retina (and thus the visual field) to which they are most sensitive.

Given how much is already known about the visual system, primarily from electrophysiological research, what can fMRI pattern classification contribute? One potential answer comes from a consideration of the advantages of fMRI. Because fMRI can be conducted in human subjects who are performing any of a wide range of experimental tasks, researchers can use it to study how different visual regions contribute to complex processes: increasing attention, improving the encoding of stimuli into memory, or even imagining a particular object. For example, a 2005 article by Kamitani and Tong used pattern classification to identify voxels whose activation was sensitive to the orientation of a visual stimulus. They found that the pattern of activation in early visual cortical regions reliably distinguished line gratings in two different orientations (e.g., 45° versus 135°), as would be expected based on prior electrophysiological studies. They then showed subjects a complex grid pattern that contained line gratings of both orientations, and asked the subjects to monitor one of the two gratings for infrequent changes in its line width. They found that selective attention to one orientation systematically modulated the voxel pattern associated with the passive viewing of that orientation. Conversely, they could reliably predict to which orientation the subject was attending by analyzing activation in specific, local patterns within the visual cortex. This study, along with many others, demonstrates how pattern classification can allow researchers both to identify category-specific patterns of fMRI activation and to evaluate how those patterns are modulated by different cognitive processes.

Another important application for pattern classification has been the perception of object categories. There has been substantial debate about whether higher visual regions that process complex stimulus properties, like object identity and category, contain some internal topographic organization. Cox and Savoy reported an early example of object categorization in 2003. Their subjects viewed examples of ten different object categories, ranging from the commonplace (e.g., "chairs") to the whimsical (e.g., "garden gnomes"). Different examples of each category were presented within 20 s blocks, and the mean activation during that block was calculated for all voxels within the visual cortex ROIs. Even in their most conservative analysis, one that restricted the feature set to voxels within object-selective regions and that used independent sets of blocks for their training and testing sets, their pattern classifier could correctly identify what object category was being shown about 30–50% of the time. These values are much greater than the chance level of 10%.

It is important to recognize that this study by Cox and Savoy and similar studies show *that* voxels contain independent information about perception; they do not suggest what form that information might take. Kay and colleagues found one way of bridging this gap in an elegant study published in 2008. First they showed each of their two subjects nearly two thousand different photographs of natural scenes while measuring activation in the visual cortex. From the resulting activation maps, they estimated each voxel's sensitivity to different spatial locations and line orientations; in effect, this was an attempt to infer the properties of the neurons within that voxel. They next

recorded fMRI activation while the same subjects viewed 120 new images, each shown 15 times. By comparing the activation pattern during each trial with the predicted activation pattern for each of the 120 images, the authors could predict what image the subject was viewing, based only on the brain activation. Remarkably, their predictions were accurate for 92% and 72% of the images in their two subjects, demonstrating that fMRI could be used to predict the contents of visual experience, based on a priori models of the functional properties of individual voxels.

While studies of visual perception have led the growth of fMRI pattern classification, recent experiments in other topic areas have provided striking examples of its power. One application of fMRI that has attracted considerable and wide-ranging attention is its potential for anticipating our thoughts and actions before they occur. While this may seem impossible, or at best the speculations of bad science fiction, there has been a long history of research into neural signals that precede conscious awareness, following largely from the work of the physiologist Benjamin Libet. In a 2008 article, Soon and colleagues investigated whether fMRI pattern classification could be used to detect subjects' intentions to engage in an action, even before they were consciously aware of those intentions. Subjects viewed a continually changing series of letters, each presented for 500 ms (Figure 11.18A). At any point in time, the subject could decide to press either the left or right button, whereupon a screen popped up

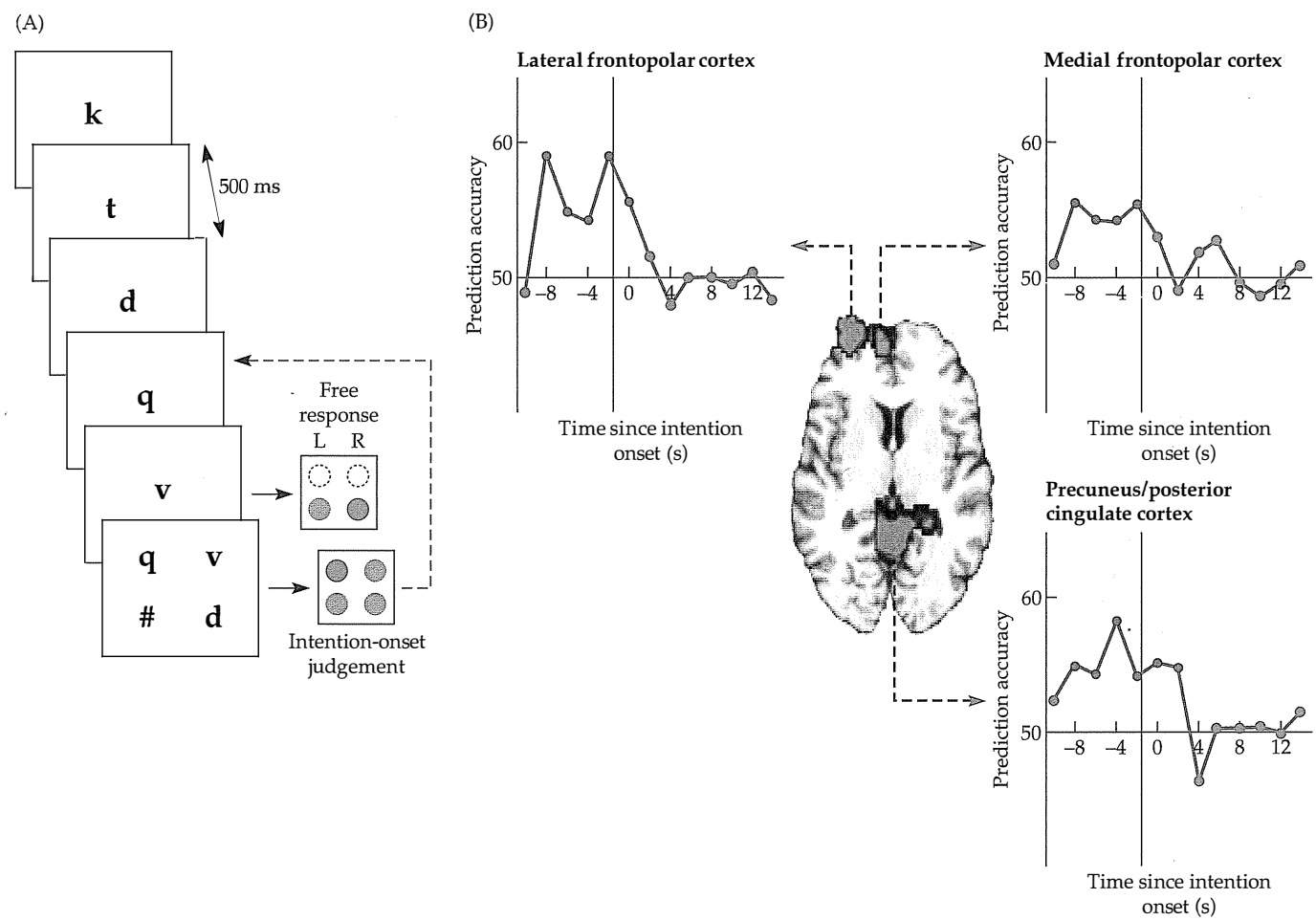

Figure 11.18 Using fMRI pattern classification to reveal brain regions that predict later conscious decisions. (A) Participants viewed a rapidly changing series of letters, each shown for 500 ms. Whenever the subject desired, he or she could press either the left or right button on a keypad. After that decision, a feedback screen popped up with letters and symbols, and the subject simply indicated which letter had been visible when the decision was made (mean onset time for awareness indicated by the vertical line). (B) The researchers examined time points prior to the reported onset of the decision using pattern classification. In a striking result, activation in the anterior part of the prefrontal cortex (i.e., lateral frontopolar cortex) and in the medial parietal cortex (i.e., posterior cingulate cortex) predicted the subsequent decision as much as 7 s in advance. Red circles indicate time points with significant predictive power. (After Soon et al., 2008.)

and the subject indicated which letter had been visible when they made their decision. As might be expected, subjects typically reported that their conscious decision occurred less than a second before they actually pressed the button. However, the authors found that activation in an anterior region of the prefrontal cortex (Figure 11.18B) could predict which button would be pressed as much as 7 s before the conscious decision! Given the delay of the hemodynamic response, this region carries information about the nature of an upcoming decision as much as 10 s in advance. While these results fall far short of reading someone's mind (see Chapter 14 for associated ethical issues), they lead to some intriguing possibilities for future research; for example, an in-scanner video game that uses real-time pattern classification analyses to counter subjects' moves before they occur.

Although powerful, pattern classification approaches will not replace traditional fMRI analyses, at least in the near term. Because of the size of fMRI datasets, pattern classification is a computationally intensive process. Identifying an optimal classifier can require many hours of computer time, and testing that classifier for significance may require many repetitions of the analysis using a permutation approach. Furthermore, even if local patterns are identified, the processes they support may remain obscure, especially if no clear spatial topography exists. Local information may itself be present in several regions. For example, in a 2007 study Hampton and O'Doherty identified a set of three regions that together predicted subjects' decisions in a reward-learning task. This sort of result cannot by itself distinguish the specific contributions of individual regions, however, it provides a starting point for research using other analysis approaches (e.g., functional connectivity methods). Finally, pattern classification remains an inherently within-subject technique: the specific patterns identified within one subject are unlikely to generalize to other subjects, given the differences in functional organization in different brains. Despite these limitations, we expect that pattern classification will become a popular and even mainstream approach in future fMRI research.

Summary

Until recently, most fMRI studies have used hypothesis-driven approaches for data analysis: the researcher creates a hypothesis about task-related changes in the BOLD signal and then tests how well each voxel matches that hypothesis. However, in recent years, researchers have implemented a variety of data-driven approaches that are used to identify intrinsic variation within an fMRI data set, and then relate that variation to function. Some techniques such as PCA or ICA attempt to separate spatial or temporal patterns within the fMRI timecourse; these can be useful for exploring complex data sets or for removing unwanted variability during preprocessing. Functional connectivity algorithms describe the interrelationships between spatially distant brain regions, which may range from simple correlations between regions to causal influences of one region upon other. Data about the functional connections between regions can be combined with the results of standard fMRI analyses, or with structural information obtained using DTI, to obtain more complete descriptions of functional networks. Finally, researchers now frequently use data about brain function to predict subjects' behavior or traits. A particularly important approach is fMRI pattern classification, which uses information about the relative changes in intensity across a set of voxels to predict a perceptual or cognitive state. Researchers have used pattern classification to investigate topics as diverse as how objects are

REFER TO THE
fMRI
COMPANION WEBSITE AT
www.sinauer.com/fmri2e
for study questions and Web links.

processed in the visual cortex and how decisions arise within the prefrontal cortex. Many data-driven approaches share common limitations—they are often computationally intensive and require complex approaches to determine statistical significance—yet they constitute some of the most exciting new directions for fMRI research.

Suggested Readings

*Andrews-Hanna, J. R., Snyder, A. Z., Vincent, J. L., Lustig, C., Head, D., Raichle, M. E., and Buckner, R. L. (2007). Disruption of large-scale brain systems in advanced aging. *Neuron*, 56: 924–935. *This article provides a compelling example of combining standard fMRI analyses, DTI mapping of fiber tracts, and functional connectivity analyses for understanding the cognitive changes that accompany aging.*

deCharms, R. C. (2008). Applications of real-time fMRI. *Nat. Rev. Neurosci.*, 9: 720–729. *This review article describes the major challenges of real-time fMRI, with an emphasis on its use in biofeedback.*

*Friston, K. J., Harrison, L., and Penny, W. (2003). Dynamic causal modelling. *NeuroImage*, 19, 1273–1302. *This article describes an important method for investigating task-related changes in functional connectivity.*

*Kay, K. N., Naselaris, T., Prenger, R. J., and Gallant, J. L. (2008). Identifying natural images from human brain activity. *Nature*, 452: 352–355. *This recent article describes an elegant study that uses an fMRI-generated model of visual cortex to predict the contents of novel images being viewed by participants.*

*Kuhnen, C. M., and Knutson, B. (2005). The neural basis of financial risk taking. *Neuron*, 47: 763–770. *This article illustrates how logistic regression analyses can use activation patterns in regions of interest to predict trial-by-trial mistakes in economic decision-making.*

Norman, K. A., Polyn, S. M., Detre, G. J., and Haxby, J. V. (2006). Beyond mind-reading: multi-voxel pattern analysis of fMRI data. *Trends Cogn. Sci.*, 10: 424–430. *This review article outlines the core concepts of fMRI pattern classification, as well as some key applications.*

*Soon, C. S., Brass, M., Heinze, H. J., and Haynes, J. D. (2008). Unconscious determinants of free decisions in the human brain. *Nat. Neurosci.*, 11: 543–545. *This remarkable study shows that fMRI pattern classification can predict participants' free choices at least 7 s before subjects report the awareness to make those choices.*

*Indicates a reference that is a suggested reading in the field and is also cited in this chapter.

Chapter References

Andersen, A. H., Gash, D. M., and Avison, M. J. (1999). Principal component analysis of the dynamic response measured by fMRI: a generalized linear systems framework. *J. Magn. Reson. Imaging*, 17: 795–815.

Bartels, A., and Zeki, S. (2004). Functional brain mapping during free viewing of natural scenes. *Hum. Brain Mapp.*, 21: 75–85.

Bartels, A., and Zeki, S. (2005). Brain dynamics during natural viewing conditions—a new guide for mapping connectivity in vivo. *NeuroImage*, 24: 339–349.

Baumgartner, R., Ryner, L., Richter, W., Summers, R., Jarmasz, M., and Somorjai, R. (2000). Comparison of two exploratory data analysis methods for fMRI: fuzzy clustering vs. principal component analysis. *J. Magn. Reson. Imaging*, 18: 89–94.

Beckmann, C. F., and Smith, S. M. (2004). Probabilistic independent component analysis for functional magnetic resonance imaging. *I. E. E. E. Trans. Med. Imaging*, 23: 137–152.

Beckmann, C. F., DeLuca, M., Devlin, J. T., and Smith, S. M. (2005). Investigations into resting-state connectivity using independent component analysis. *Philos. Trans. R. Soc. Lond. B. Biol. Sci.*, 360: 1001–1013.

Bingel, U., Rose, M., Glascher, J., and Buchel, C. (2007). fMRI reveals how pain modulates visual object processing in the ventral visual stream. *Neuron*, 55: 157–167.

Bray, S., Shimojo, S., and O'Doherty, J. P. (2007). Direct instrumental conditioning of neural activity using functional magnetic resonance imaging-derived reward feedback. *J. Neurosci.*, 27: 7498–7507.

Calhoun, V. D., Adali, T., Pearlson, G. D., and Pekar, J. J. (2001). Spatial and temporal independent component analysis of functional MRI data containing a pair of task-related waveforms. *Hum. Brain Mapp.*, 13: 43–53.

Cox, D. D., and Savoy, R. L. (2003). Functional magnetic resonance imaging (fMRI) "brain reading": detecting and classifying distributed patterns of fMRI activity in human visual cortex. *NeuroImage*, 19: 261–270.

Cox, R. W., Jesmanowicz, A., and Hyde, J. S. (1995). Real-time functional magnetic resonance imaging. *Magn. Reson. Med.*, 33: 230–236.

Davatzikos, C., Ruparel, K., Fan, Y., Shen, D. G., Acharyya, M., Loughead, J. W., Gur, R. C., and Langleben, D. D. (2005). Classifying spatial patterns of brain activity with machine learning methods: application to lie detection. *NeuroImage*, 28: 663–668.

deCharms, R. C., Christoff, K., Glover, G. H., Pauly, J. M., Whitfield, S., and Gabrieli, J. D. (2004). Learned regulation of spatially localized brain activation using real-time fMRI. *NeuroImage*, 21: 436–443.

deCharms, R. C., Maeda, F., Glover, G. H., Ludlow, D., Pauly, J. M., Soneji, D., Gabrieli, J. D., and Mackey, S. C. (2005). Control over brain activation and pain learned by using real-time functional MRI. *Proc. Natl. Acad. Sci. U. S. A.*, 102: 18626–18631.

Ecker, C., Reynaud, E., Williams, S. C., and Brammer, M. J. (2007). Detecting functional nodes in large-scale cortical networks with functional magnetic resonance imaging: a principal component analysis of the human visual system. *Hum. Brain Mapp.*, 28: 817–834.

Fair, D. A., Schlaggar, B. L., Cohen, A. L., Miezin, F. M., Dosenbach, N. U., Wenger, K. K., Fox, M. D., Snyder, A. Z., Raichle, M. E., and Petersen, S. E. (2007). A method for using blocked and event-related fMRI data to study "resting state" functional connectivity. *NeuroImage*, 35: 396–405.

Fox, M. D., and Raichle, M. E. (2007). Spontaneous fluctuations in brain activity observed with functional magnetic resonance imaging. *Nat. Rev. Neurosci.*, 8: 700–711.

Friston, K. J., Buechel, C., Fink, G. R., Morris, J., Rolls, E., and Dolan, R. J. (1997). Psychophysiological and modulatory interactions in neuroimaging. *NeuroImage*, 6: 218–229.

Greicius, M. D., Krasnow, B., Reiss, A. L., and Menon, V. (2003). Functional connectivity in the resting brain: a network analysis of the default mode hypothesis. *Proc. Natl. Acad. Sci. U. S. A.*, 100: 253–258.

Hampton, A. N., and O'Doherty, J. P. (2007). Decoding the neural substrates of reward-related decision making with functional MRI. *Proc. Natl. Acad. Sci. U. S. A.*,104: 1377–1382.

Hasson, U., Furman, O., Clark, D., Dudai, Y., and Davachi, L. (2008). Enhanced intersubject correlations during movie viewing correlate with successful episodic encoding. *Neuron*, 57: 452–462.

Hasson, U., Nir, Y., Levy, I., Fuhrmann, G., and Malach, R. (2004). Intersubject synchronization of cortical activity during natural vision. *Science*, 303: 1634–1640.

Haynes, J. D., and Rees, G. (2005). Predicting the orientation of invisible stimuli from activity in human primary visual cortex. *Nature Neurosci.* 8: 686–691.

Huettel, S. A., Güzeldere, G., and McCarthy, G. (2001). Dissociating the neural mechanisms of visual attention in change detection using functional MRI. *J Cogn Neurosci.*, 13: 1006–1018.

Kamitani, Y., and Tong, F. (2005). Decoding the visual and subjective contents of the human brain. *Nature Neurosci.* 8: 679–685.

Kasess, C. H., Windischberger, C., Cunnington, R., Lanzenberger, R., Pezawas, L., and Moser, E. (2008). The suppressive influence of SMA on M1 in motor imagery revealed by fMRI and dynamic causal modeling. *NeuroImage* 40: 828–837.

Kim, J., and Horwitz, B. (2008). Investigating the neural basis for fMRI-based functional connectivity in a blocked design: application to interregional correlations and psycho-physiological interactions. *J. Magn. Reson. Imaging*, 26: 583–593.

King-Casas, B., Tomlin, D., Anen, C., Camerer, C. F., Quartz, S. R., and Montague, P. R. (2005). Getting to know you: reputation and trust in a two-person economic exchange. *Science*, 308: 78–83.

Kriegeskorte, N., Goebel, R., and Bandettini, P. (2006). Information-based functional brain mapping. *Proc. Natl. Acad. Sci. U. S. A.*, 103: 3863–3868.

Kwong, K. K., Belliveau, J. W., Chesler, D. A., Goldberg, I. E., Weisskoff, R. M., Poncelet, B. P., Kennedy, D. N., Hoppel, B. E., Cohen, M. S., and Turner, R. (1992). Dynamic magnetic resonance imaging of human brain activity during primary sensory stimulation. *Proc. Natl. Acad. Sci. U. S. A.*, 89: 5675–5679.

LaConte, S. M., Peltier, S. J., and Hu, X. P. (2007). Real-time fMRI using brain-state classification. *Hum. Brain. Mapp.*, 28: 1033–1044.

Libet, B., Gleason, C. A., Wright, E. W., and Pearl, D. K. (1983). Time of conscious intention to act in relation to onset of cerebral activity (readiness-potential). The unconscious initiation of a freely voluntary act. *Brain*, 106: 623–642.

Madden, D. J., Whiting, W. L., Huettel, S. A., White, L. E., MacFall, J. R., and Provenzale, J. M. (2004). Diffusion tensor imaging of adult age differences in cerebral white matter: relation to response time. *NeuroImage*, 21: 1174–1181.

Marreiros, A. C., Kiebel, S. J., and Friston, K. J. (2008). Dynamic causal modelling for fMRI: a two-state model. *NeuroImage*, 39: 269–278.

McIntosh, A. R., Bookstein, F. L., Haxby, J. V., and Grady, C. L. (1996). Spatial pattern analysis of functional brain images using partial least squares. *NeuroImage*, 3: 143–157.

McIntosh, A. R., Chau, W. K., and Protzner, A. B. (2004). Spatiotemporal analysis of event-related fMRI data using partial least squares. *NeuroImage*, 23: 764–775.

McKeown, M. J., Makeig, S., Brown, G. G., Jung, T. P., Kindermann, S. S., Bell, A. J., and Sejnowski, T. J. (1998). Analysis of fMRI data by blind separation into independent spatial components. *Hum. Brain Mapp.*, 6: 160–188.

Montague, P. R., Berns, G. S., Cohen, J. D., McClure, S. M., Pagnoni, G., Dhamala, M., Wiest, M. C., Karpov, I., King, R. D., Apple, N., and Fisher, R. E. (2002). Hyperscanning: simultaneous fMRI during linked social interactions. *NeuroImage*, 16: 1159–1164.

Pessoa, L., and Padmala, S. (2007). Decoding near-threshold perception of fear from distributed single-trial brain activation. *Cereb. Cortex*, 17: 691–701.

Roebroeck, A., Formisano, E., and Goebel, R. (2005). Mapping directed influence over the brain using Granger causality and fMRI. *NeuroImage*, 25: 230–242.

Tohka, J., Foerde, K., Aron, A. R., Tom, S. M., Toga, A. W., and Poldrack, R. A. (2008). Automatic independent component labeling for artifact removal in fMRI. *NeuroImage*, 39: 1227–1245.

Toni, I., Rowe, J., Stephan, K. E., and Passingham, R. E. (2002). Changes of cortico-striatal effective connectivity during visuomotor learning. *Cereb. Cortex*, 12: 1040–1047.

Vincent, J. L., Patel, G. H., Fox, M. D., Snyder, A. Z., Baker, J. T., Van Essen, D. C., Zempel, J. M., Snyder, L. H., Corbetta, M., and Raichle, M. E. (2007). Intrinsic functional architecture in the anaesthetized monkey brain. *Nature*, 447: 83–86.

Voyvodic, J. T. (1999). Real-time fMRI paradigm control, physiology, and behavior combined with near real-time statistical analysis. *NeuroImage*, 10: 91–106.

Weiskopf, N., Sitaram, R., Josephs, O., Veit, R., Scharnowski, F., Goebel, R., Birbaumer, N., Deichmann, R., and Mathiak, K. (2007). Real-time functional magnetic resonance imaging: methods and applications. *J. Magn. Reson. Imaging*, 25: 989–1003.

Wilson, S. M., Molnar-Szakacs, I., and Iacoboni, M. (2008). Beyond superior temporal cortex: intersubject correlations in narrative speech comprehension. *Cereb. Cortex*, 18: 230–242.

Chapter 12

Advanced fMRI Methods

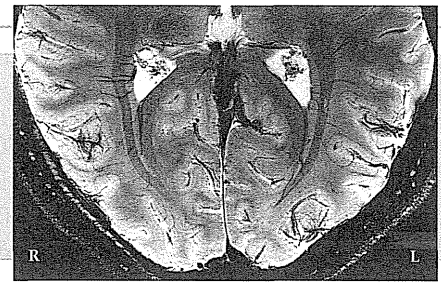

Functional MRI methods have evolved dramatically since the 1990s. Many early fMRI studies collected data from only one or two slices through the brain, at rates as slow as one image every ten seconds. Using these simple methods, researchers demonstrated that fMRI could be used to identify the functional properties of specific brain locations, such as the activation of the occipital lobe during a visual stimulation task. This early research was used largely to find evidence for existing concepts, rather than to obtain novel findings. But by the early 2000s, there was an explosion of interest in applying fMRI to truly new topics, such as prospective memory, decision making, and consciousness. Fast event-related designs combined with advanced pulse sequences enabled the estimation of rapid hemodynamic changes, while new statistical approaches facilitated the analysis of patterns of activation throughout the brain. When we published the first edition of this textbook in 2004, the breathless pace of advancement could be seen in the cutting-edge methods of that time: parallel imaging, compensation for susceptibility artifacts, examination of functional connectivity, and new non-BOLD contrasts.

The pace of advancement in fMRI methods continues to accelerate. The advanced fMRI methods listed above are now commonplace—witness their inclusion in earlier chapters, alongside more traditional approaches. On the horizon are new methods for fMRI data collection. Some of these methods promise better spatial and temporal resolution, through a combination of stronger magnetic fields, denser receiver arrays, and faster imaging sequences. Continued advances allow researchers to see fine structures and probe transient events, leading to new applications for fMRI. Potentially more important, however, are innovative forms of MR contrast that generate specific and quantitative measurements of brain function and structure. Given the scope of these many recent approaches, our current edition contains a dramatically revised set of advanced methods, providing a strong testament to the rapid progress of fMRI research.

The methods discussed in this chapter provide only partial snapshots of the promising research approaches being developed today. Given the sheer number of laboratories that are currently pushing the bounds of fMRI, we cannot document all advances. Instead, we point readers toward likely and exciting directions of future progress, with the goal of stimulating innovative

thoughts about the future directions of fMRI. Not only do many important research questions remain unanswered, but we still do not know what limits (if any) restrict the questions that can be asked. We look forward with great anticipation to new, unforeseen methods that will shape the course of fMRI research.

Improved Spatial Resolution

Compared with other noninvasive neuroimaging methods, MRI has clear advantages in its attainable level of spatial resolution. In recent years, the pursuit of even higher spatial resolution, with concomitant increases in the accuracy of functional localization, has driven many of the advances in the design of new imaging hardware and pulse sequences. The most visible advance has been the continual increases in MRI field strength, both in standard and cutting-edge scanners. Whereas most institutions used 1.5-T scanners throughout the 1990s and early 2000s, new MRI facilities typically install higher-field scanners of 3.0-T field strength. Similarly, ultra-high magnetic fields (i.e., 7.0 T or greater) were once restricted to small-bore scanners such as those used for imaging small animals. However, because of the many demonstrations of increased sensitivity, which can lead to improved spatial resolution, there has been growing interest in using such high field strengths for human research. Large 7.0-T scanners were previously found in only a few leading research centers, but now close to 30 human research laboratories worldwide possess ultra-high-field scanners. Some of these whole-body scanners have field strengths greater than 9.0 T. In the following sections, we highlight some potential applications of ultra-high-field scanning that will likely be used in future fMRI research.

MR microscopy

The use of very strong magnetic fields has a long history in animal MRI research. Hereafter, we will refer to studies that attempt to resolve image details with sizes on the order of tens of micrometers as ultra-high-resolution MRI or MR microscopy. Ultra-high-resolution MRI has become an important tool for understanding brain anatomy. In recent years, spatial resolution of structures that are several tens of micrometers (μm) in size has been regularly achieved. This level of resolution is similar to that obtained from traditional light-microscopic techniques. A sample ultra-high-resolution image, shown in Figure 12.1, was collected with voxels of 43 μm in size. Future improvements in spatial resolution may lead to voxel sizes as small as a few micrometers. If attainable, images with that level of resolution would allow the imaging of single neurons and their connecting fibers.

Imagine the possibility of imaging a single neuron! To understand the challenge of such a task, consider that a typical fMRI voxel has dimensions of about 4 mm on each side, and is roughly similar in size to the word "the" in this book. Millions of neurons exist within that single voxel. The cell body, or soma, of a neuron may be only a few tens of micrometers in diameter, while its axon may stretch only a few millimeters. Despite the challenges posed by such a small scale, there have been some promising results in anatomical MRI. In 1999, Dodd and colleagues sought to create images of T cells, which are important components of the immune system. A single T cell is approximately 5 μm in diameter, or one two-hundredth of a millimeter. To scan these cells directly would require a resolution of about 2 μm, so that the cell would stretch over

ultra-high-resolution MRI The acquisition of MR images with voxel sizes in the order of tens of micrometers. Applications of ultra-high-resolution MRI to animal tissues are known as MR microscopy.

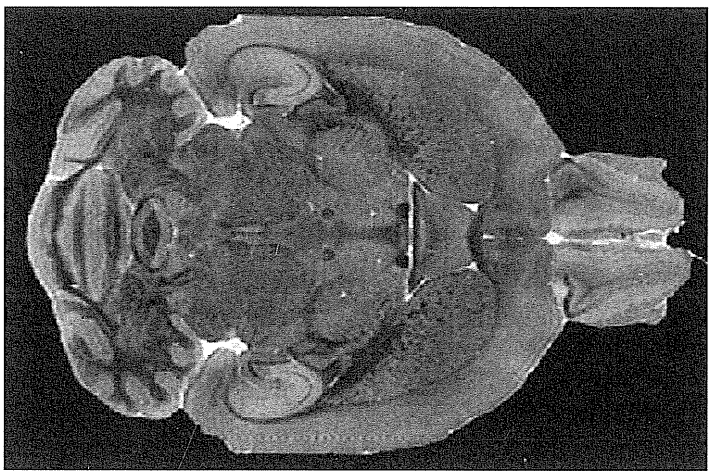

Figure 12.1 An ultra-high-resolution MR microscopy image. This image of a living mouse's brain consists of cubic voxels with only 43 μm on each side. To appreciate the spatial resolution of this image, consider that approximately one million of its voxels would fit within a single 4 mm × 4 mm × 5 mm human fMRI voxel. (Courtesy of Dr. G. Allan Johnson, Center for In-vivo Microscopy, Duke University.)

several voxels. This resolution cannot be obtained using typical MR contrasts (e.g., T_1 differences between tissues). However, when these researchers introduced highly paramagnetic iron oxide into the cells, the iron generated large regions of susceptibility-induced signal loss that they could measure on T_2*-sensitive images. The magnetic susceptibility effects leading to these images share a similar mechanisms to that of BOLD contrast, as described in Chapter 7, but at a much smaller scale. Using a small-bore scanner at 4.7 T, Dodd and colleagues collected images with extremely high resolution (voxel dimensions of about 25 μm on each side), and the positions of the T cells became visible. More recently, this basic approach has been extended to live animals. Using micron-sized particles of iron oxide, Shapiro and colleagues created images of hepatocytes, cells in the liver that are important for a variety of metabolic processes. The tiny iron oxide particles distorted the local T_2* signal, making single cells visible on MRI images with spatial resolution of about 100 μm (Figure 12.2).

Figure 12.2 Labeling single cells using MRI. (A) In an image taken of a living mouse, the liver (horizontal structure at center) appears as relatively undifferentiated tissue broken up by brighter blood vessels. (B) For a different experimental session, the researchers injected another mouse with hepatocytes (i.e., cells important for processing proteins and carbohydrates) that had been labeled using iron oxide. When they scanned the mouse a month later, the T_2* images showed individual hepatocytes as dark discs throughout the liver. This provided one of the first examples of using MRI to detect single cells in living animals. Subsequent in vitro imaging of tissue samples revealed that no hepatocytes were visible in samples from the control mouse (C; liver boundary shown as a dashed line), but hepatocytes were clearly visible in samples from the experimental mouse (D). (After Shapiro et al., 2006.)

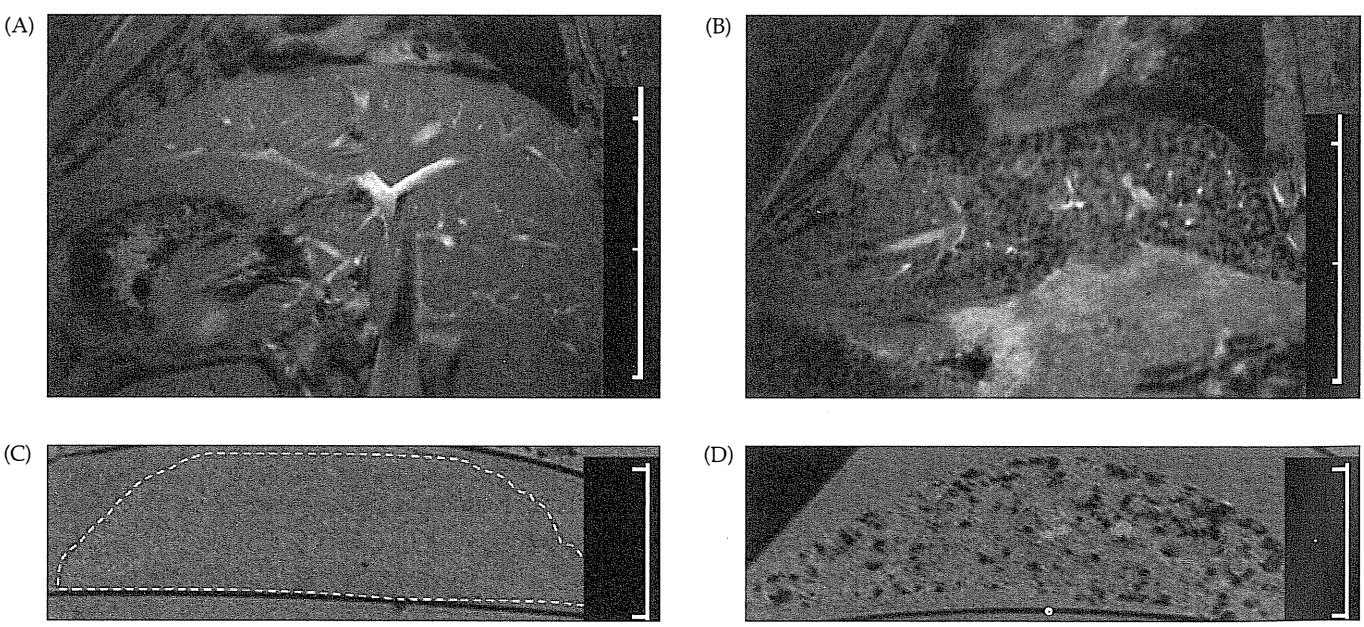

magnet diameter The diameter of the electromagnetic coil that generates the strong static field used in MRI.

effective bore size The clearance within the bore of the MRI scanner that limits the maximum size of the sample that can be scanned.

volumetric Relating to the measurement of volume.

morphometric Relating to the measurement of shape.

The ability to image single cells in vivo may lead to many exciting applications, such as tracking stem cells, monitoring cellular divisions during development, and detecting amyloid plaques in early Alzheimer's disease. Given the pace of change in imaging hardware, as well as the availability of innovative contrast agents, researchers may achieve single-cell imaging in the human brain within the foreseeable future. However, many limitations remain. Chief among them is that the use of exogenous contrast agents like iron oxide does not allow the imaging of structures within cells, as can be done with electron microscopes, but instead provides information about the locations of cells. In addition, most of the iron oxide-based contrast agents are limited to non-human studies by their potential toxicity.

Ultra-high-field MRI scanners with bore sizes large enough to accommodate humans are extremely expensive and difficult to maintain, and are thus uncommon. Typical small-bore scanners for rodent imaging may have field strengths of 7.0 T or greater, but magnet diameters of only 8 to 30 cm. For comparison, typical whole-body MRI scanners have magnet diameters of 90 to 100 cm. Once outfitted with other imaging hardware, the effective bore sizes for small-animal scanners may only be 4 to 20 cm, while human scanners have effective bore sizes of about 60 cm. It is difficult to maintain the stability of extremely strong magnetic fields over large distances. Furthermore, using the small voxel sizes available with ultra-high-field scanners poses its own set of challenges. Since the total MR signal measured from a voxel is roughly proportional to its volume, the amplitude of the signal used to collect ultra-high spatial resolution images is much lower than the amplitude for images at normal spatial scales. Voxel volume decreases with the cube of spatial resolution, such that a voxel of 0.5 mm per side has only one eighth the volume of one that is 1 mm per side. A 25 μm voxel, like that obtained by Dodd and colleagues, has only one sixty-four thousandth of the volume of a 1 mm voxel. Thus, acquisition of sufficient MR signal to generate an acceptable raw SNR using that voxel size would require an extremely long scan time, which may not be tolerable for human participants. For example, images of the sort shown in Figure 12.1 may require more than 24 hours of collection time, and even relatively rapid acquisition methods may require a few hours. As a result, collecting ultra-high-resolution MRI images in vivo will exacerbate problems associated with physiological changes over time.

Thought Question

Based on what you learned in Chapter 8 about the sources of noise in MRI, what problems would you encounter when attempting ultra-high-resolution MRI in vivo?

Ultra-high-resolution scanning is simpler and less expensive with animal subjects for several reasons, such as reduced cost and increased homogeneity of the static field, smaller size and greater strength of the gradient fields, and the ability to scan an anesthetized or restrained subject for a long scanning duration. Nevertheless, the trend is toward ultra-high-resolution scanning in humans as well. One important future consequence of high-resolution human scanning will be the increased precision of volumetric and morphometric techniques to measure properties of size and shape. Based on the tissue contrasts used for the MR images (e.g., T_1), researchers can outline a given brain structure in different samples (e.g., normal vs. schizophrenic humans, knockout vs.

wild-type mice) and then investigate changes in brain anatomy associated with the group difference. The results can be readily stored in a database, such as that established by the Biomedical Informatics Research Network, so that other investigators can compare their data with a standardized set. Because the MRI data are collected electronically, they are more easily analyzed and disseminated than data from traditional microscopic slides. Improved spatial resolution will also have direct advantages for fMRI research. Remember that the BOLD hemodynamic response is evoked by neuronal activity that may be organized on a sub-millimeter scale. This spatially restricted neuronal activity, rather than the more widespread vascular response, controls the flow of information in the brain. Therefore, improvements in the resolution of MRI down to the cellular level may have significant consequences for functional studies.

parallel imaging or **(multiple-channel imaging)** The use of multiple receiver channels to acquire data following a single excitation pulse.

phased array A method for arranging multiple surface detector coils to improve spatial coverage while maintaining high sensitivity.

Parallel imaging

If the pursuit of higher magnetic fields has been the engine advancing MRI technology, the development of **multiple-channel acquisition**, or **parallel imaging**, using coil arrays has provided the high-octane fuel. Just a few years ago, nearly all MRI scanners used single coils for excitation and reception. An advanced new direction for MRI is the use of several reception coils combined in parallel into a **phased array**. Now, most new MRI scanners can combine data from at least eight independent receiver channels, which facilitates faster and higher-resolution imaging. The use of multiple-channel acquisition provides two advantages. One is that it increases the spatial resolution and raw SNR without increasing acquisition time; the other is that it reduces the duration of the readout window, and thus minimizes spatial distortion, without compromising SNR.

To see an example of increasing spatial resolution using multiple-channel acquisition, consider the schematic reception system shown in Figure 12.3A. Here, the four receiver coils simultaneously but independently cover the four quadrants of the imaging volume, each with a matrix size of $n \times n$ (e.g., 128×128). An image that contains the entire sample, with a matrix size of $2n \times 2n$ (e.g., 256×256), can be obtained by simply combining all four images, as illustrated in Figure 12.3B. Note here that the imaging matrix dimensions are doubled, without any increase in imaging time. Such an

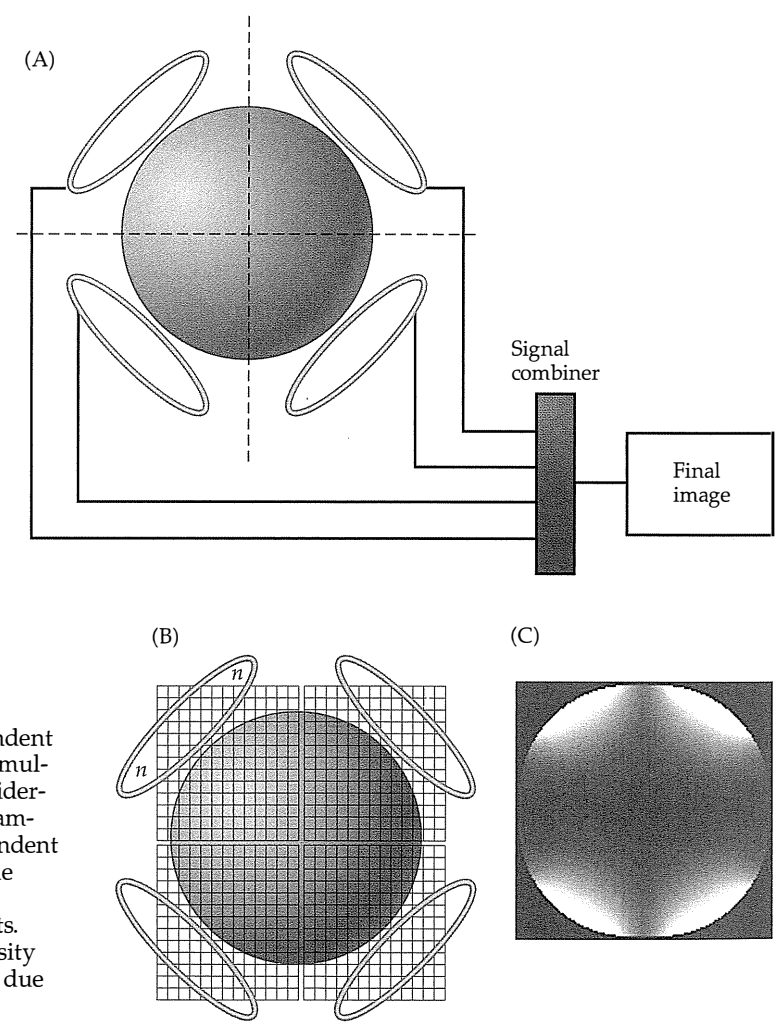

Figure 12.3 Multiple-channel acquisition with independent fields of view. By using more than one reception coil simultaneously (A), spatial resolution can be improved considerably without increasing imaging time. The simplest example is shown in (B), where each coil samples an independent quadrant of the object (i.e., a reduced field of view). The final image of the uniform spherical phantom (C) is obtained by simply combining the individual quadrants. Note that the final image has non-uniform signal intensity and will suffer from aliasing artifacts (not shown here) due to the sensitivity of each coil to the other quadrants.

implementation is conceptually straightforward; however, each image usually contains signal from other quadrants, due to wrapping of the images because of spatial subsampling. In addition, the signal intensity of the final image (Figure 12.3C) varies severely in space, depending on the voxel position with respect to the individual surface coils. For fMRI, this could result in differences in the functional SNR across the brain.

Multiple-channel imaging can also be used to increase spatial resolution via the collection of data from coils with overlapping fields of view. During the imaging session, all channels acquire data with a greater field-of-view in *k*-space (i.e., a higher resolution) than will be used for the final image. To keep the time of data acquisition short, the *k*-space data are subsampled for individual coils (Figure 12.4A), resulting in the four severely wrapped images shown in Figure 12.4B. Each voxel in these images contains signal from four overlapping images of the brain. However, we can remove the overlap with a straightforward algorithm. The intensity of any given voxel in each of these four images, I_1 to I_4, reflects a combination of the sensitivity S_{ij} of each coil i at that location j (Figure 12.4C), and the actual intensity values for that voxel in each of the images (ρ_1 through ρ_4):

$$I_1 = S_{11}\rho_1 + S_{12}\,\rho_2 + S_{13}\,\rho_3 + S_{14}\,\rho_4$$

$$I_2 = S_{21}\rho_1 + S_{22}\,\rho_2 + S_{23}\,\rho_3 + S_{24}\,\rho_4$$

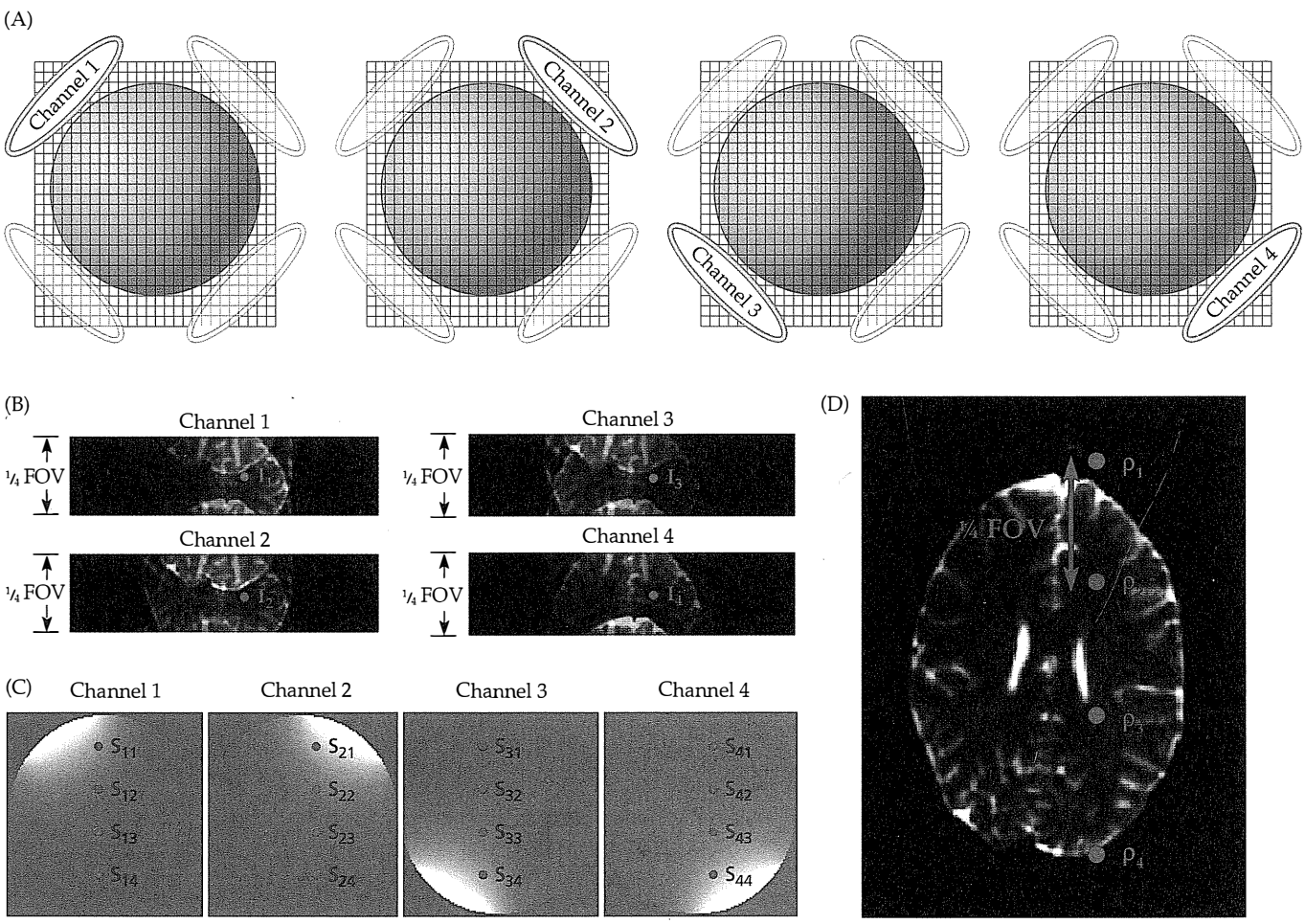

Figure 12.4 Multiple-channel acquisition with overlapping fields of view. (A) If four receiver coils are each used to sample the entire object, the resulting images (B) will contain overlapping sections of the original image, weighted by the differential sensitivities of the coils across space. A given point in each of these four images (I_1 through I_4) contains information from each of several equally spaced voxels in the sample ($\rho 1$ through $\rho 4$). Each of these images has one-quarter of the field of view (FOV) of the desired image. Field maps are obtained for individual coils to determine their spatial sensitivities (C), which are measured at points S_{ij} for each coil i and spatial location j. This information can be used during the reconstruction process to produce a final unfolded image with improved spatial resolution (D).

$$I_3 = S_{31}\rho_1 + S_{32}\,\rho_2 + S_{33}\,\rho_3 + S_{34}\,\rho_4$$

$$I_4 = S_{41}\rho_1 + S_{42}\,\rho_2 + S_{43}\,\rho_3 + S_{44}\,\rho_4$$

Note that by incorporating field maps from individual coils, either in phantoms or in the same subject, we can explicitly measure S_{ij}, the sensitivity of coil i at location j. Because I_1 to I_4 is known from the collected images and all S_{ij} values can be identified from the field maps, we can solve for the actual voxel values and obtain a final unfolded image with high spatial resolution (Figure 12.4D).

The relationship between the number of coils and the matrix size can be expressed more generally in the following way. Assuming that the number of receiver coils is M, the number of sampling points for each coil is P, and the number of voxels desired in the final reconstructed image is n^2, we must use enough coils so that $M \times P > n^2$. Thus, as M coils are used, the matrix size could increase by a factor of up to $\sqrt{M}$ for a given acquisition time in 2D imaging. This has been demonstrated experimentally by Sodickson and colleagues, and also by Pruessmann and colleagues. In addition to increasing spatial resolution, multiple-channel acquisition can also be used to increase the raw SNR. When multiple coils are targeted at the same brain region, images from individual channels can be combined to increase the magnitude of the signal.

massive coil array A method for arranging a large number of surface detector coils to improve spatial coverage while maintaining high sensitivity.

Parallel imaging with massive coil arrays

Cutting-edge techniques now involve much denser sets of receivers, arranged in massive coil arrays. When coupled with ultra-high magnetic fields, massive coil arrays can provide further improvements in sensitivity and efficiency, pushing human MRI to an unprecedented level of spatial resolution. As their name implies, massive coil arrays involve many small, overlapping wire loops, each connected to a separate input channel on the scanner. For human brain imaging, each of these loops rests over a different part of the scalp. Shown in Figure 12.5A is a 32-channel array used for human brain imaging within a 7.0-T scanner. Massive coil arrays provide two key advantages for structural and functional MRI. First, they can drastically increase the speed of image acquisition, as will be discussed more extensively in the following section. Second, they improve the quality of reception at ultra-high field strengths. As static field strength increases, the capacitance (i.e., ability to store electric charge) of the

Figure 12.5 Massively parallel imaging. (A) Shown is a 32-channel massively parallel array that is used within a 7.0-T MRI scanner. At left is the volume coil used for excitation, at center are the preamplifiers for each of the 32 individual channels, and at right is the parallel coil array used for reception, which is mounted on a cap to surround a human head. The array consists of a set of overlapping wire loops visible on the sides of the cap. (B) Using this array, researchers can collect structural MRI data at ultra-high-resolution (i.e., in-plane voxel sizes of 200 mm). Shown here is a T_2-weighted axial image through the occipital cortex that reveals remarkable detail in both the white and gray matter. (Images courtesy of Dr. Lawrence Wald, Massachusetts General Hospital.)

(A)

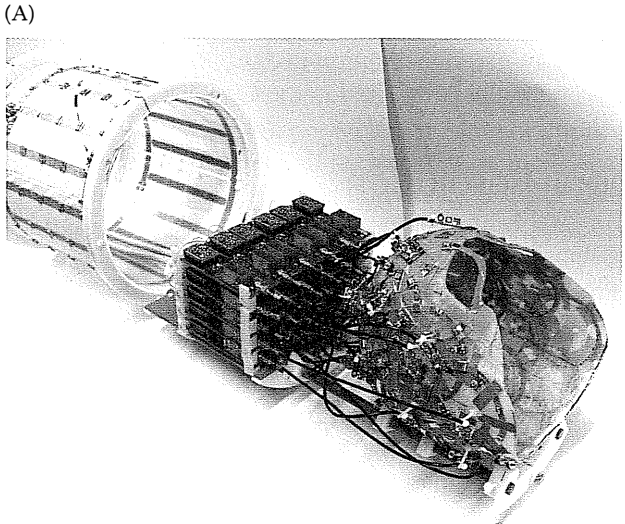

(B)

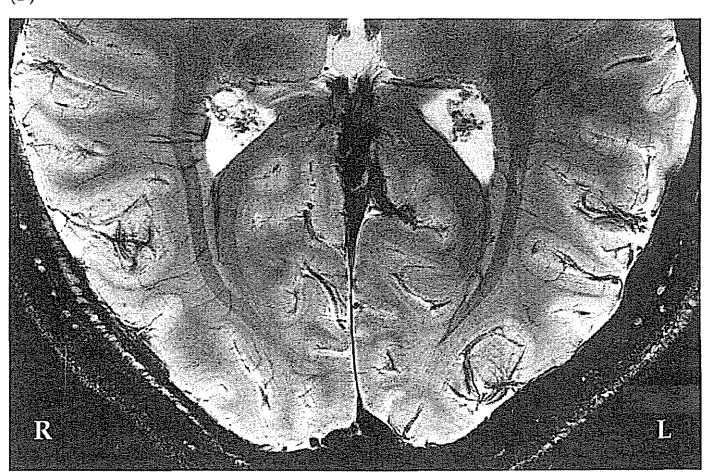

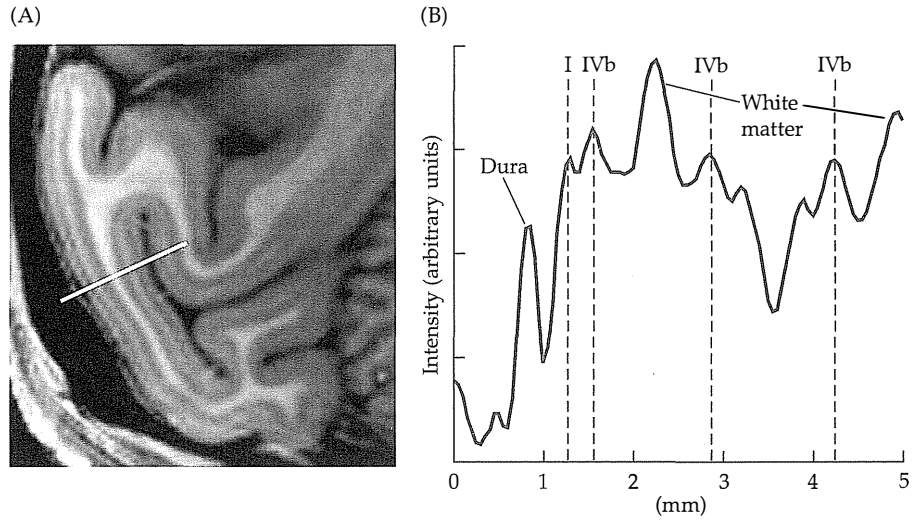

Figure 12.6 Using massively parallel imaging to distinguish cortical layers. (A) This ultra-high-resolution 7.0-T MRI image, collected using an apparatus similar to that shown in Figure 12.5, shows the distinct cortical layers within a monkey brain. (B) A plot of relative intensity along the solid line crossing the cortex in (A). Note the intensity peaks that correspond to individual cortical layers (labeled via Roman numerals), in particular the increased intensity found in layer IV. (Data courtesy of Dr. Lawrence Wald, Massachusetts General Hospital.)

human head approximates that of the circuits within the volume head coil (see Chapter 2). As a result, slight changes in head position or size can dramatically affect the mutual coupling between the head and the coil, in turn altering the resonance frequency of the head coil. Changes in the resonance frequency will lead to off-resonance excitation and poor reception, reducing the measured MR signal. Because of these problems, ensuring the homogeneity of the volume coil has been a challenge for ultra-high-field MRI. Massive coil arrays minimize these problems by requiring much smaller capacitors, solving the mutual inductance problem and improving SNR. These coils also share, with single surface coils, the advantage of increased sensitivity to nearby brain regions (e.g., the cortex under the coils), at the cost of decreased sensitivity to deep structures.

Researchers using massive coil arrays have created spectacular images of human brain structures. Figure 12.5B shows an axial brain image with 200 μm voxels, which was collected at 7.0 T. This exquisite image depicts anatomical details (e.g., blood vessels and fiber tracts) with the sort of clarity typically associated with histological slides viewed under a microscope. For studies of brain function, high resolution MRI may become most useful for focusing in on local cortical structures. Recall that the gray matter around the surface of the cortex contains multiple layers, each with characteristic cell types (see Box 6.2). These layers are distinguishable on high-resolution MR images (Figure 12.6), and this will potentially facilitate the localization of task-evoked BOLD signal to one or more of these layers. For an example of the use of a single targeted surface coil to resolve gray-matter activation with millimeter resolution, see the 2007 study by Ress and colleagues, cited in the Chapter References.

electroencephalogram/electroencephalography (EEG) The measurement of the electrical potential of the brain, usually through electrodes placed on the surface of the scalp.

magnetoencephalography (MEG) A noninvasive functional neuroimaging technique that measures very small changes in magnetic fields caused by the electrical activity of neurons, with potentially high spatial and temporal resolution.

Improved Temporal Resolution

A weakness of fMRI is its slow sampling rate. In comparison with electrophysiological techniques like electroencephalography (EEG) and magnetoencephalography (MEG), which detect changes in the brain with roughly millisecond resolution, fMRI samples the brain approximately once per second, or even less frequently. Temporal resolution in fMRI is limited by three factors (see Chapter 8 for an extended discussion). First, although individual slices can be acquired within a few tens of milliseconds, 20 or more slices are required in order to sample the entire brain with reasonable spatial resolution. Thus, the

time between successive acquisitions of the entire brain is much longer than the acquisition time for a single slice. Second, the net magnetization of voxels recovers slowly between successive excitations. Even if one wanted to repeatedly sample a single slice as rapidly as possible, the functional SNR in that slice decreases dramatically at very short repetition times. Third, BOLD contrast does not measure neuronal activity directly, but instead measures the hemodynamic response associated with that activity. The delay between neuronal activity and its hemodynamic expression reduces temporal resolution. Unless these limitations are overcome, a number of important research questions will remain outside the purview of fMRI.

Here we introduce some of the major advances in pulse sequence development and experimental design that have contributed to improved temporal resolution. Improvements in MR scanners, notably the development of more efficient gradient systems, have also led to faster image acquisition rates and improved temporal resolution. However, further advances in hardware development will likely have only a limited impact on temporal resolution, due to the intrinsic limitations of BOLD fMRI. We will describe some approaches to overcoming those limitations in the final part of this chapter.

Multiple-channel acquisition

Recall that the use of multiple detector coils can improve spatial resolution without increasing imaging time. Similarly, multiple-channel acquisition can improve temporal resolution without sacrificing spatial resolution or spatial coverage. One approach involves collecting independent information from each coil. If a single coil is sufficient for acquiring an $n \times n$ image (i.e., signal from $n \times n$ different voxels), four independent coils could collect that same image, each acquiring $n/2 \times n/2$ data points. Since each coil only acquires one-quarter of the original data, the image can be collected in one-quarter of the time.

Alternatively, scanners can collect redundant information (i.e., signal from the same voxels) using a set of overlapping coils. This allows *k*-space to be sampled less densely, and thus images can be collected more rapidly, based on the parallel-imaging principles introduced earlier in this chapter. Specialized reconstruction algorithms are used to resolve the otherwise aliased image (due to under-sampling), using maps of magnetic field sensitivity collected by each of the multiple coils. In general, if there are M receiver coils each sampling P points, the requirement for redundancy means that there must be more samples than voxels in the image: $M \times P > n^2$. Thus, temporal resolution improves in proportion with the number of receiver coils used, that is, by a factor of up to M. This improvement is in image acquisition time only, and does not affect the recovery of the net magnetization or the delay introduced by the hemodynamic response. These latter factors mean that improvements in temporal resolution will not always lead to concomitant increases in functional resolution, at least for BOLD fMRI. Note that the addition of coils has different effects on spatial and temporal resolution. Because spatial resolution is measured in squared units within a slice (mm^2), it increases in proportion with the change in the square root of the number of coils. But temporal resolution is measured in linear units (s), and it improves linearly with the number of coils.

Partial k-*space imaging*

In Chapter 5 we introduced popular fMRI pulse sequences, notably gradient-echo echo-planar imaging (EPI) and gradient-echo spiral imaging. These pulse

partial *k*-space imaging A technique for reducing data acquisition time (and thus increasing temporal resolution) by collecting only part of the *k*-space data following each excitation and filling the uncollected portions of *k*-space with estimated data.

keyhole imaging A partial *k*-space imaging technique in which only the center of *k*-space is collected following each excitation, in order to maximize raw SNR while minimizing acquisition time.

conjugate mirroring A partial *k*-space imaging technique in which data collected from one half of *k*-space is used to estimate data from the other half.

sequences rely on very rapid changes in magnetic gradients to enable collection of data in *k*-space, and thus the speed of data acquisition can be increased by using more powerful magnetic gradients. However, all MRI scanning must fall within safety limits, specifically the limits of human tolerance to changes in magnetic field strength over time (dB/dt) and to absorption of radiofrequency energy (e.g., specific absorption rate, SAR). As fMRI approaches these safety limits, researchers must find other methods to improve temporal resolution, and one approach is to change how *k*-space data are collected. One key area of development is partial *k*-space imaging, in which *k*-space is incompletely sampled during each acquisition. This shortens the data acquisition window, allowing images to be collected more rapidly.

A partial *k*-space pulse sequence allows the collection of data from some *k*-space points but not others. Since points near the center of *k*-space contain most of the MR signal, they are usually sampled while points near the periphery are omitted. One simple approach to ensure that the reconstructed image has the desired matrix size is to fill the missing peripheral *k*-space points with zero values. Because this zero-filling approach does not sample the parts of *k*-space associated with higher spatial frequencies, the resulting images will lose fine detail and will appear blurred (see Figure 4.20 for an analogous effect). Note that the blurring caused by zero filling in *k*-space is equivalent to a sinc interpolation in image space. For most applications, sampling the center of *k*-space and zero-filling the remainder of the matrix does not provide acceptable results.

Other forms of partial *k*-space imaging use more effective methods for assigning values to non-sampled locations in *k*-space. One frequently used method is known as keyhole imaging (Figure 12.7A). Only the center portion of *k*-space is sampled during each trial, while peripheral regions are filled in with previously acquired data. This eliminates the blurring effects that occur with zero-filling, although there is no real gain in high-spatial-frequency functional information. Another approach, conjugate mirroring, samples only part of *k*-space during each trial, filling in the missing regions using data from the opposite region of *k*-space (Figure 12.7B). Recall that *k*-space possesses radial symmetry, meaning that every spatial frequency corresponds to two points (e.g., one in the upper left and another in the lower right). Standard pulse sequences sample both points, typically one before and the other after the center of *k*-space is sampled. Conjugate mirroring sequences sample only one of these points and then estimate the other. However, points near the center of

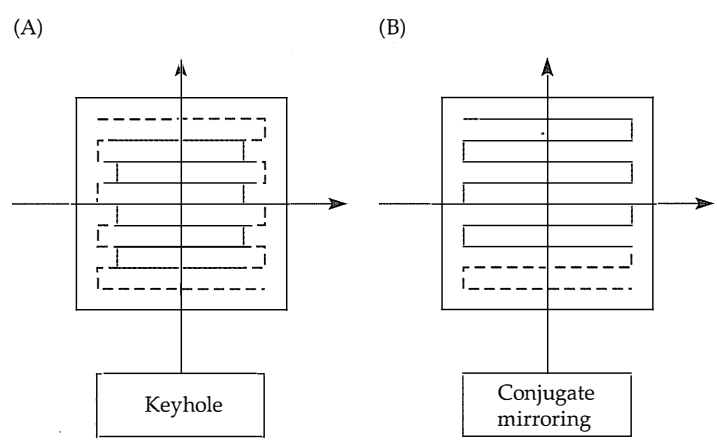

Figure 12.7 Reducing imaging acquisition time through partial *k*-space imaging. Shown are two common methods for reducing *k*-space coverage to gain increased temporal resolution while maintaining the same imaging matrix and spatial resolution. (A) A keyhole pattern, where the center of *k*-space (shown in orange) is acquired for each image while the periphery of *k*-space (in blue) is filled with previously acquired data. The use of previously acquired data avoids the blurring effect induced by zero-filling methods. (B) A conjugate mirroring technique, in which data are acquired from one half of *k*-space (in orange) and mirrored onto the other half (in blue). Note that in the conjugate mirroring technique, data are acquired from slightly more than half of *k*-space to ensure that the center is well represented, in order to maximize raw SNR.

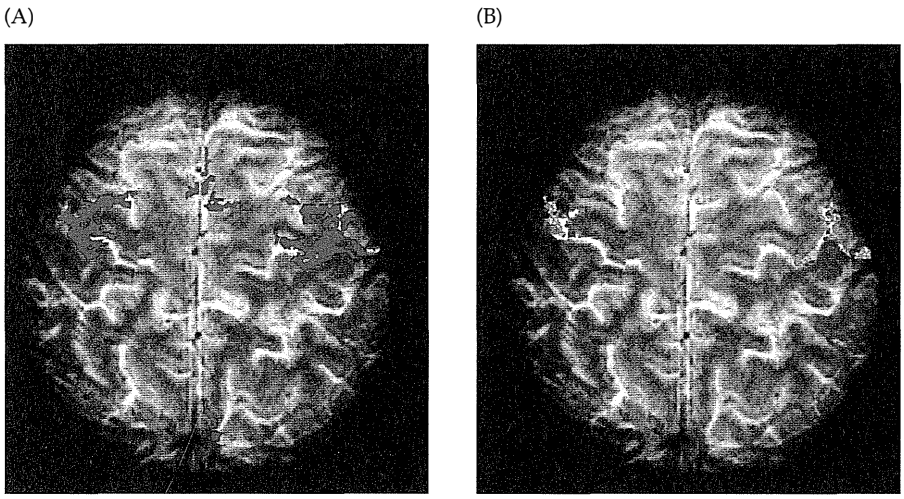

Figure 12.8 Fast partial *k*-space fMRI with cubic millimeter resolution. Use of a partial *k*-space acquisition strategy can greatly improve the speed of image acquisition. (A) is at $1 \times 1 \times 10$ mm resolution, while (B) is at $1 \times 1 \times 1$ mm resolution. These single-shot images were collected at roughly the same speed as normal fMRI images, despite having much higher resolution. The subject participated in a bimanual finger tapping task. (Courtesy of Dr. Andrzej Jesmanowicz and Dr. James S. Hyde, Medical College of Wisconsin.)

k-space are still sampled twice, to maximize the raw SNR. Both of these approaches allow the collection of fMRI images at very high temporal resolution with excellent spatial resolution. In one example of conjugate mirroring at 3.0 T, researchers were able to collect isotropic slices through the human brain with a spatial resolution of 1 mm^3, at an acquisition rate of a few tens of milliseconds per slice (Figure 12.8).

Thought Question

What might be a disadvantage of conjugate mirroring? As a hint, consider what factors contribute to the raw MR signal measured at each point in *k*-space. Why would it be better to collect two samples of the *k*-space data than just one sample?

Because both keyhole and conjugate mirroring techniques fully sample the center of *k*-space, most of the MR signal (and thus raw SNR) is preserved. But when one is attempting to measure BOLD signal changes within a small region, the raw SNR may not be the most important factor. For many research questions, identifying changes in function within small brain regions may be more important than identifying large swaths of activation across the brain. To map small functional regions, researchers may need information from peripheral regions of *k*-space that correspond to high-spatial-frequency components. A method known as outer *k*-space (OK) imaging has been proposed by Glover and colleagues to preserve potentially important changes in functional activity (Figure 12.9). Outer *k*-space imaging can be thought of as the complement of the keyhole technique described in the last paragraph, in that the former samples only the peripheral portions of *k*-space while the latter samples only the center of *k*-space.

Partial sampling of *k*-space is analogous to the idea of filtering introduced in Chapter 8 for signals in the time domain. If only part of *k*-space is sampled, then spatial frequencies outside the sampling range are effectively filtered. Thus, keyhole imaging is analogous to a low-pass spatial filter, while outer *k*-space imaging is analogous to a high-pass filter. Recall from Chapter 8 that the correct filter to use for a given signal depends on the frequency of that sig-

outer *k*-space (OK) imaging A partial *k*-space imaging technique in which only the periphery of *k*-space is collected following each excitation, in order to ensure that high-spatial-frequency components of the MR signal are present.

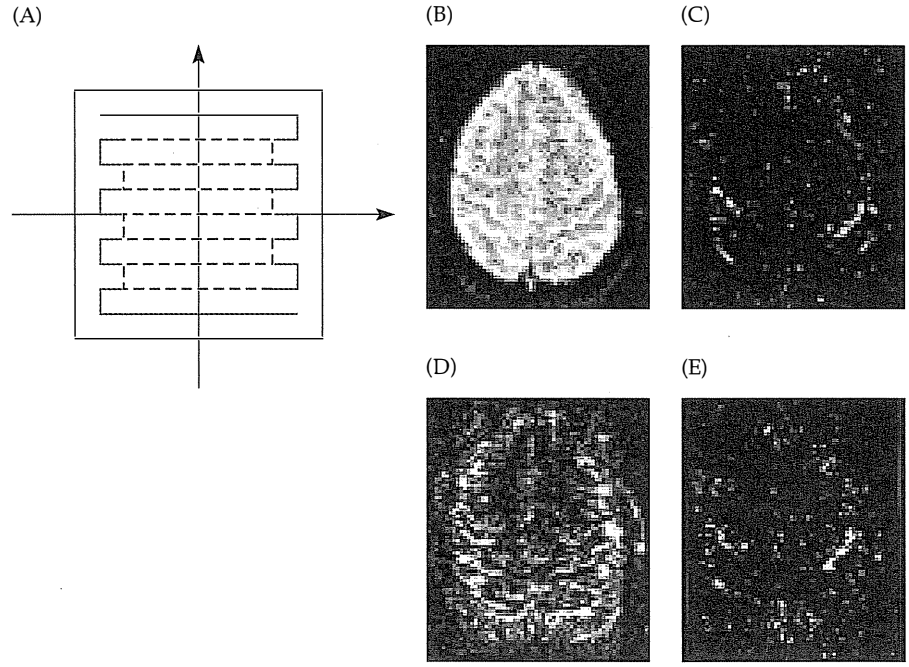

Figure 12.9 Rapid fMRI using outer k-space imaging. (A) Outer k-space imaging records data from the periphery of k-space (orange) while filling the center of k-space with previously acquired data (blue). The potential value of this technique for fMRI is that the peripheral points may contribute more to high spatial frequency effects, such as small BOLD activations. A standard EPI image from a time series of volumes is shown in (B), and the BOLD significance map from that time series is shown in (C). For comparison, (D) shows an EPI image acquired using outer k-space filling, with its significance map shown in (E). The two types of EPI images are substantially different from each other, since the image in (D) completely lacks low spatial frequencies, however, the two activation maps are similar. (Data courtesy of Dr. Gary Glover, Stanford University.)

nal, according to the principle of matched filters. If the spatial pattern of activation is known, then an optimal k-space trajectory can be constructed that fully maintains the spatial integrity of the activation, while maximizing temporal resolution.

Efficient k-*space trajectories*

Echo-planar imaging is the most popular fast imaging method for fMRI, but it does not use the scanner gradients optimally. Traditional EPI implementations alternate between the x- and y-gradients to traverse a stepwise path through k-space (see Figure 5.30). Because the amplitude of the gradient determines the velocity of the k-space trajectory, turning on only one gradient at any given time limits the speed at which k-space data can be acquired. To overcome this limitation and increase the speed of slice acquisition, pulse sequences have been developed that use both the x- and y-gradients simultaneously. In a standard EPI sequence, turning on the x-gradient allows the collection of a single horizontal line of k-space in time t. However, if both the x- and y-gradients are turned on, a single diagonal line of k-space can be collected in time $t/\sqrt{2}$; thus an overall improvement of $1/\sqrt{2}$ in temporal resolution can be achieved. This method, which was originally proposed and demonstrated by Wong back in 1992, is illustrated in Figure 12.10.

Another approach for data acquisition using both gradients at the same time is spiral imaging, which was also introduced in Chapter 5. Some spiral imaging techniques employ a spiral-out trajectory, which always starts from the center of k-space (Figure 12.11A). In spiral-out imaging, the center of k-space is sampled before any gradient is applied, and therefore the center cannot be missed due to gradient problems. Furthermore, because the gradients are very weak in the center, these sequences minimize image artifacts associated with blood flow. However, spiral-out imaging also has disadvantages, chiefly the necessity for a time gap between excitation and the beginning of

matched filters The principle that a filter of the same frequency as the signal of interest provides the maximal signal-to-noise ratio.

spiral imaging A technique for fast image acquisition that uses sinusoidally changing gradients to trace a corkscrew trajectory through k-space.

spiral-out trajectory A corkscrew path that begins at the center of k-space and ends at the periphery. It is the most common form of spiral imaging.

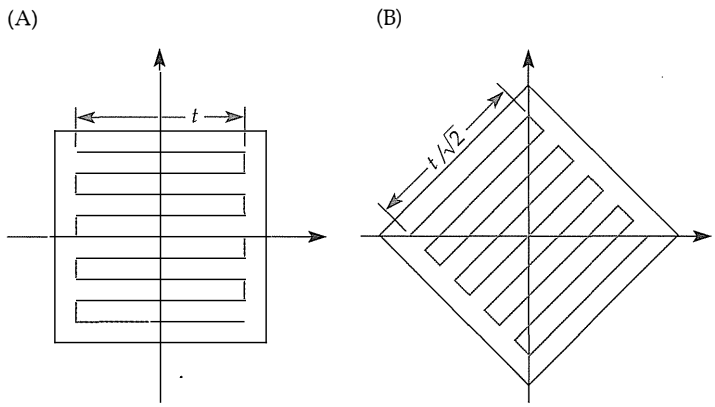

Figure 12.10 Simultaneous use of x- and y-gradients to speed image acquisition. A typical EPI path through k-space uses the x-gradient to collect one line of k-space in time t (A). By using both the x- and y-gradients concurrently to traverse a diagonal path through k-space, one line of k-space can be collected in time $t/\sqrt{2}$, increasing the speed of data acquisition by a similar factor (B). This effectively increases temporal resolution without sacrificing spatial resolution.

data acquisition (i.e., the TE) to ensure sufficient T_2* sensitivity. As a result, the total imaging time for spiral-out acquisition is the sum of the TE (often about 30 to 40 ms) and the length of the readout window (which could be an additional 30 ms or more). And, because spiral sequences do not trace out a grid within k-space, the reconstruction process requires interpolation that can introduce mild blurring in the images.

Figure 12.11 Spiral imaging sequences. Spiral sequences trace spiral paths through k-space, allowing more-efficient use of the gradients and more-rapid data acquisition. In the conventional spiral-out sequence (A), the gradients are turned on at time TE, but in the spiral-in technique (B), the gradients are turned on earlier so that the center of k-space is reached at time TE. The spiral-in sequence can thus be used to acquire data more rapidly than the spiral-out sequence.

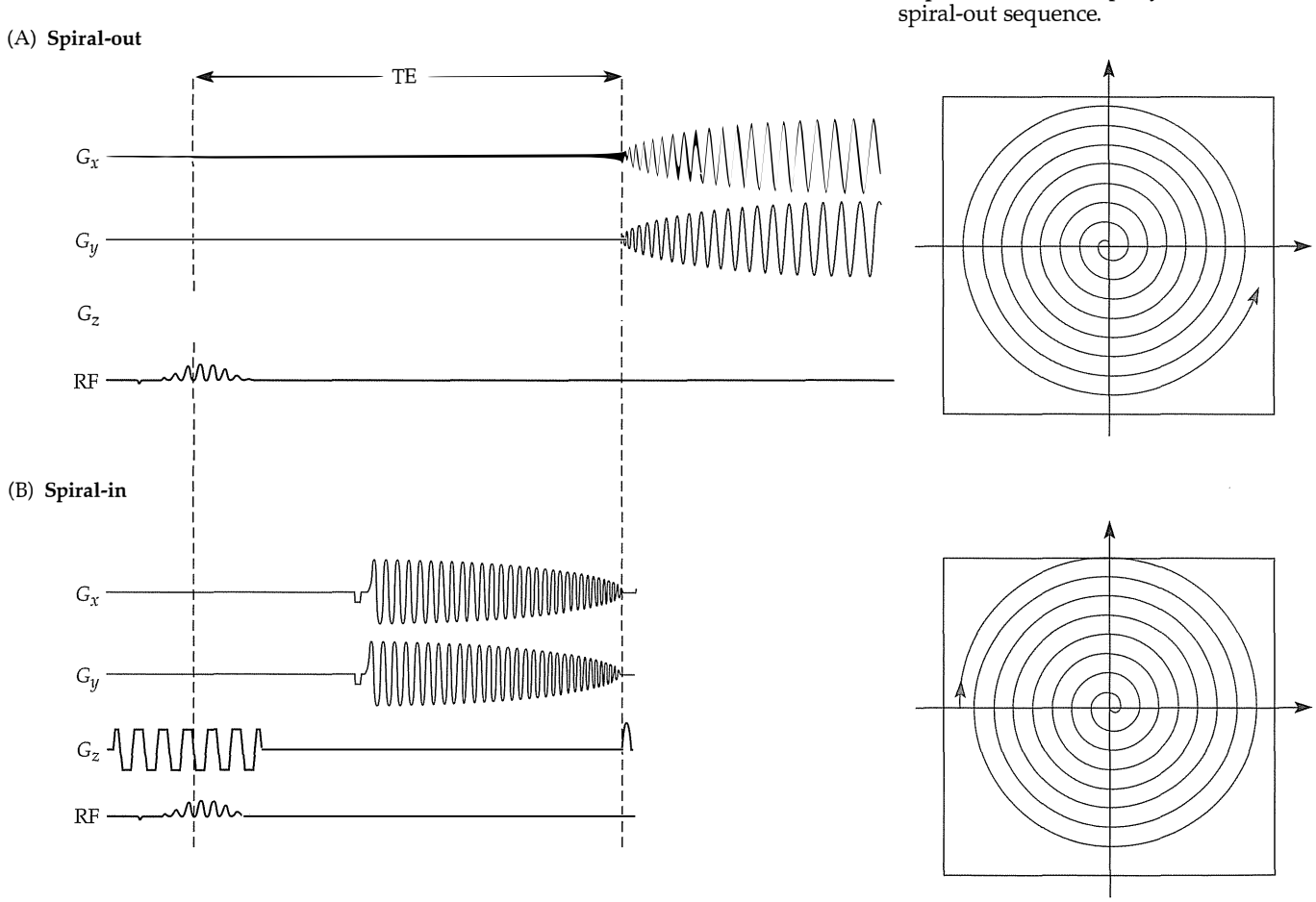

spiral-in trajectory A corkscrew path that begins at the periphery of *k*-space and ends at the center. Spiral-in imaging has the advantage that data acquisition can begin before time TE and thus the total time needed to collect an image is reduced.

spiral-in-and-out trajectory A corkscrew path that begins at the periphery of *k*-space, progresses through the center, and then returns to the periphery. Spiral-in-and-out imaging samples each location in *k*-space multiple times, potentially improving the SNR and spatial fidelity of the images.

interleaved stimulus presentation The presentation of events of interest at different points within a TR over trials (e.g., one-quarter, one-half, and three-quarters of TR in addition to TR onset), increasing the effective sampling rate of an experiment at the expense of fewer trials per condition.

How could the acquisition time for spiral imaging be further improved? One effective strategy, demonstrated by Glover and Law in 2001 and by Guo and Song in 2003, is to acquire data during the time gap before TE. A spiral-in trajectory begins data acquisition in the periphery of *k*-space immediately following excitation and completes data acquisition in the center of *k*-space at time TE (Figure 12.11B). This ensures sufficient T_2* weighting while minimizing the time between successive excitation pulses. Thus, the rate of slice acquisition can be improved by up to a factor of two. A typical spiral-in pulse sequence with a 64 × 64 matrix allows acquisition of approximately 24 slices each second (with a TE of 30 ms). Using such a sequence, it is possible to acquire data from the entire brain with a temporal resolution of approximately 1 s. As its name implies, a spiral-in-and-out trajectory begins in the periphery of *k*-space, progresses inward using a spiral-in pattern, and then progresses outward using a spiral-out pattern. This trajectory requires the same amount of time for data acquisition as a spiral-out trajectory (i.e., the spiral-in component occurs during what would otherwise be unused time). The use of pulse sequences with spiral-in-and-out patterns can improve signal recovery in brain regions that experience susceptibility artifacts, however using the gradients continously throughout a longer data acquisition interval can pose challenges for the scanner hardware (e.g., heating). As spiral imaging techniques become more established, we expect that they will surpass echo-planar trajectories in their popularity for fMRI studies.

Improved experimental designs

It is important to recognize that temporal resolution cannot be increased indefinitely, even with further advances in the rate of image acquisition. The T_1 and T_2* properties of brain tissues restrict the maximum SNR that can be achieved at a given temporal resolution, just as the net magnetization of a voxel restricts the maximum SNR that can be achieved at a given spatial resolution. That is, as TR decreases, the raw SNR also decreases. At very short TRs (e.g., below 200 ms), the resulting decrease in functional SNR may preclude the detection of BOLD signal changes. Therefore, it is critical to optimize experimental designs so that temporal resolution can be maximized.

The technique known as interleaved stimulus presentation can improve the effective sampling rate for a given TR (see Chapter 7). By jittering the time of stimulus presentation within the TR, one can sample hemodynamic time courses with different delays relative to the stimulus onset in different trials. These multiple samples can be combined into a single time course, with the effective sampling rate reduced from the actual TR by a factor equal to the number of interleaved steps. For example, with an actual TR of 2000 ms and 10 jittering steps, one could sample at an effective rate of 200 ms. The primary disadvantage of interleaved stimulus presentation is that the duration of data acquisition increases with the gain in temporal resolution. To increase the effective sampling rate by a factor of ten while maintaining the same number of samples per condition, the experiment length must likewise be increased by a factor of ten.

Because of the uncertainty associated with the relationship between the fMRI hemodynamic response and neuronal activity, the detection of millisecond-level differences in the timing of neuronal activity is challenging for fMRI studies. However, a number of researchers have investigated whether the clever manipulation of experimental paradigms will allow the probing of very fast neuronal events. In a study with rats as subjects, Ogawa and colleagues devel-

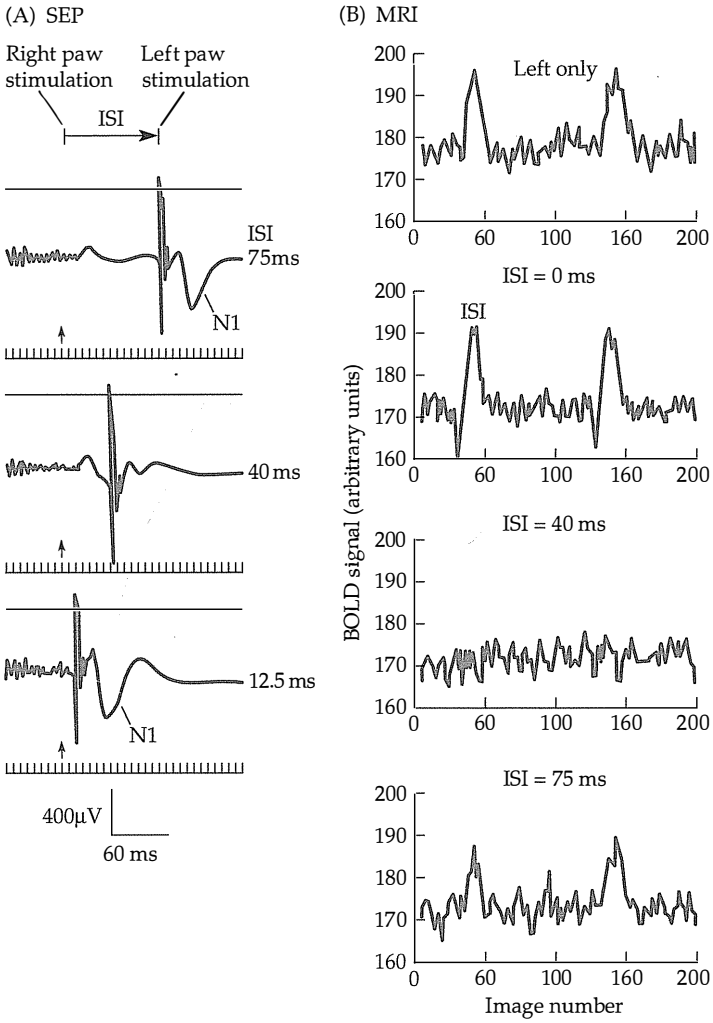

Figure 12.12 Using neural interactions to improve the temporal resolution of fMRI. In this experiment, researchers investigated the electrophysiological and BOLD responses to bilateral stimulation of the rat forepaws in the somatosensory cortex. The graphs in (A) show the electrophysiological responses in the right somatosensory cortex. Normally, a somatosensory evoked potential (SEP; N1) is present following stimulation of the left forepaw (e.g., in the 12.5- and 75-ms interstimulus interval [ISI] conditions). But when the right stimulation precedes the left by about 40 ms, then there is suppression of the electrical activity. Importantly, that suppression is also present in the BOLD response (B), suggesting that fMRI suppression designs may be used to resolve very small differences in event timing, in the order of tens of milliseconds. (After Ogawa et al., 2000.)

oped a technique that induces either excitatory or inhibitory neural interactions, by presenting consecutive stimuli separated by very short intervals, in the order of tens of milliseconds. By applying consecutive forepaw stimulations with variable interstimulus intervals, the research team was able to detect the inhibition due to neuronal refractoriness in the response to the second stimulus (Figure 12.12). Such an inhibition effect is subsequently manifested in the BOLD signal. This manipulation provides improved temporal resolution for neuronal events without physically increasing the sampling interval, since neuronal *interactions* on the order of milliseconds can lead to very different hemodynamic responses. Similar effects have been used to make spatial judgments about brain regions in fMRI-adaptation paradigms (see Chapter 7).

Improved Functional Resolution through New Contrast Mechanisms

As we have already discussed, advances in imaging hardware do promise further improvements in spatial and temporal resolution, however, new technologies cannot overcome some fundamental limitations of BOLD fMRI. Nearly

all current fMRI studies derive contrast from an indirect marker of neuronal activity: deoxygenated hemoglobin. Thus, the organization of the vascular system constrains the temporal and spatial specificity of BOLD fMRI measurements. To overcome this problem, a number of laboratories have developed innovative imaging techniques that directly measure other, more direct markers of neuronal activity. Some approaches utilize MRI signals that are based on metabolic properties such as changes in cell pH, increases or decreases in temperature, or the presence of flow of ions. Other approaches create images based on gene expression. And, a class of very promising techniques creates images sensitive to neuronal activity itself! The novel contrasts we discuss here reflect only some of the many possible new approaches. We are hopeful that as the field progresses, these and other new approaches will complement, and perhaps even replace, traditional BOLD fMRI.

Temperature-dependent contrast

No biomarker can be more readily appreciated than body temperature. All of us have experienced the biological effects of temperature change, such as when a fever saps our energy and leaves us unable to function effectively. Mechanisms for regulating body temperature developed early in evolution and, in humans, take many forms: cellular, vascular, muscular, and behavioral. Specific brain regions, including the hypothalamus, regulate thermal balance for the entire body. The brain is critically important for all aspects of life, and its temperature is very tightly regulated. Even small local temperature changes in the brain can lead to significant pathologies. Furthermore, abnormal brain temperature can signal pathological conditions such as traumatic brain injury. Improvements in the mapping of brain temperature, may have consequences both for functional and clinical neuroimaging.

Increases in brain temperature arise mainly from metabolic processes, notably oxygen metabolism, while decreases in brain temperature reflect the removal of warm blood via the venous system. During steady-state (i.e., resting) conditions, the balance between heat production and removal leads to a constant brain temperature. Increases in neuronal activity generate increased oxygen metabolism and blood flow, perturbing this equilibrium over short time periods. Because blood flow increases more than oxygen consumption (which enables BOLD contrast) brain temperature typically decreases following neuronal activity. But, because increases in blood flow lag increases in metabolism by a few seconds, there may be transient increases in temperature associated with the increased oxygen metabolism. Evidence from animal experiments has revealed transient, activity-related changes in temperature as small as 0.01°C and as large as 0.2°C. Moreover, temperature changes can in turn influence neuronal and metabolic activity, whether by altering the rate of chemical reactions, altering the affinity of hemoglobin for oxygen, or changing the response properties of individual neurons. At present, no consensus exists about the precise relationships between the changes in neuronal activity, temperature, blood flow, oxygen metabolism, and temperature. Even so, the possibility of mapping brain temperature has sparked exciting new research.

temperature-sensitive contrast agent
A compound that, when injected into an organism, influences the MR signal differently depending on the local tissue temperature.

Temperature mapping, like many other physiological measurements, is technically challenging because the targeted changes can be very small. Most approaches so far have used contrast based on exogenously applied agents. Trubel and colleagues developed a temperature-sensitive contrast agent, specifically a thulium compound whose resonance frequency varies according to tem-

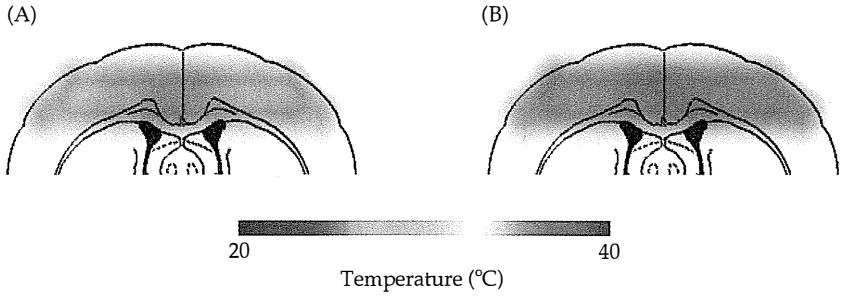

Figure 12.13 In vivo temperature mapping with a thulium compound in an anesthetized rat. The researchers used a compound that has four temperature-sensitive proton groups, each with a different resonance frequency. As temperature increases, two of those groups exhibit decreases in resonance frequencies and the other two exhibit increases in resonance frequencies. When this compound is introduced into a rat brain, researchers can create MR-based maps of temperature in vivo. Compared with conditions of normal neuronal activity (A), there is a significant increase in temperature (about 1–2°C) following bicuculline-induced seizure (B). (Data courtesy of Drs. Daniel Coman and Fahmeed Hyder, Yale University.)

perature. Using a chemical-shift imaging sequence at ultra-high field strengths, they created temperature-sensitive images of a rat brain. Introduced in Chapter 5, chemical shift imaging relies on differences in electron shielding around hydrogen nuclei, depending on their chemical environment. As shown in Figure 12.13, under conditions of excessive neuronal firing (i.e., an induced seizure), there was a global increase in temperature of about 1–2°C.

Future studies may generate temperature maps based on endogenous contrast mechanisms, albeit with greatly reduced sensitivity. One potential mechanism builds on the concept, introduced in Chapter 3, that net magnetization depends on temperature. As temperature increases, spins are more likely to move between the high and low energy states, decreasing the net magnetization. Recall that the intensity of a proton density image is directly proportional to the net magnetization within that voxel. Thus, in principle, proton density contrast could be used to generate temperature-dependent maps of brain function. Another possibility relies on the increase in molecular motion caused by temperature increases. This effect could allow, again in principle, estimation of temperature based on the rate of water diffusion, using the diffusion imaging techniques introduced in Chapter 5. However, the most promising method to date for generating endogenous temperature-dependent contrast is still based on chemical shifts. Water molecules normally form hydrogen bonds that minimize electron shielding effects. However, as temperature increases, these hydrogen bonds become more likely to break, increasing electron shielding and lowering the resonance frequency of those protons. Such changes in resonance frequency can be readily identified in maps of the phases of the MR signal. Moreover, the electron shielding effect has a linear dependence on temperature throughout virtually the entire range of physiological conditions. For these reasons, resonance-frequency-based phase mapping is the method of choice for in vivo temperature imaging.

We note that even though these endogenous contrast methods hold much promise, they can only detect changes in temperature, not absolute values. Exogenous contrast agents can be introduced in a controlled fashion, so that quantitative information is available about their prevalence in a given brain region. Therefore, exogenous agents have the important advantage that they allow the researcher to measure absolute temperature levels.

pH-dependent contrast

Cellular homeostasis requires the regulation of acid-base concentrations and, thus, the pH value. Important regulatory mechanisms involve the transport and exchange of common ions across membranes, including Na^+/H^+ exchange, Na^+-driven Cl^-/HCO_3^- exchange, Na^+-HCO_3^- cotransport, and passive Cl^-/HCO_3^- exchange. The control of pH in both the intracellular and extracellular fluids is

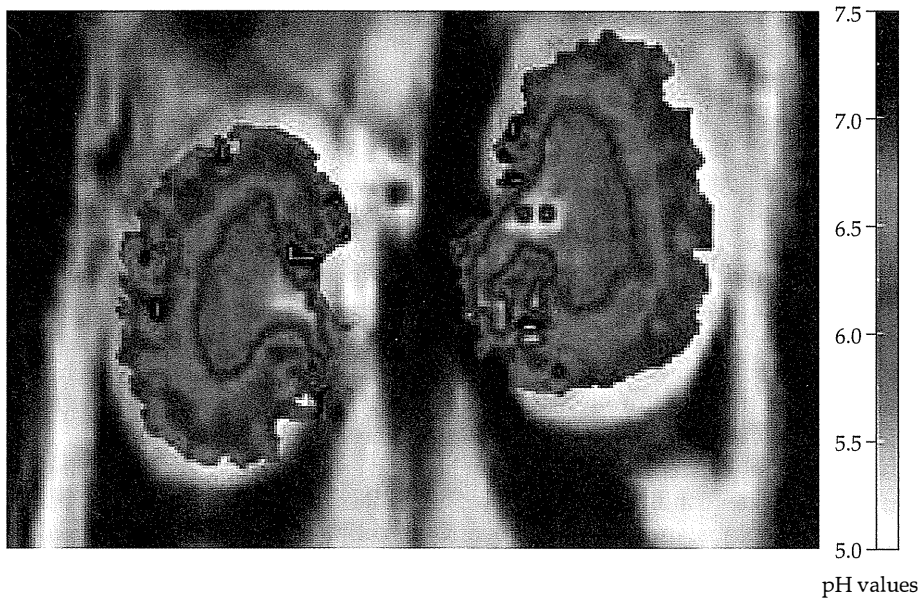

Figure 12.14 Contrast-enhanced pH-sensitive MRI imaging. Shown are images of rat kidneys that reveal a systematic pH gradient across those organs. (Image courtesy of Dr. A. Dean Sherry, University of Texas Southwestern Medical Center.)

especially important for effective neural function. The electrical activity of neurons evokes pH changes both inside and outside the cell. These changes occur within a few microseconds, can last as long as several minutes, and can be as large as several tenths of a pH unit. Brain metabolism can also lead to significant intracellular and extracellular pH changes across wide regions.

Because of the ubiquity and importance of neural pH changes, methods for mapping the spatial distribution of tissue pH would have considerable relevance to basic and clinical neuroscience. As for temperature imaging, robust maps of pH can be created using exogenous pH-sensitive contrast agents such as the synthetic agent $GdDOTP^{5-}$. An exogenous pH-sensitive contrast agent developed by Sherry and colleagues was used to obtain pH distributions within the kidneys of a live rat (Figure 12.14). The major problem with using these contrast agents in humans is their toxicity, which precludes their use for purely research purposes. Moreover, contrast agents that work in other parts of the body may not be useful for neural imaging, if they cannot pass the blood-brain barrier. Nevertheless, the initial success in animal models suggests that pH imaging in humans may become a useful diagnostic tool.

Endogenous contrast mechanisms will be necessary for the development of pH-dependent imaging in human neuroscience research. Most potential endogenous signals lack sufficient sensitivity and specificity for in vivo pH mapping. One encouraging possibility comes from studies of the exchange between hydrogen atoms in water and the amide hydrogen atoms in cellular proteins and peptides. As outlined in a 2003 paper by Zhou and colleagues, the MR signal intensities of the amide protons depend on these hydrogen exchange rates, which are sensitive to pH. Shown in Figure 12.15 is an example of pH imaging during focal ischemia (i.e., reduced blood flow) in the rat brain. While a conventional T_2-weighted image revealed no significant signal differences between the area of the lesion and the rest of the brain, the pH map derived from the amide-proton-transfer contrast clearly delineated the region of focal ischemia, in good agreement with a stained tissue sample. Advanced versions of this approach may be used to detect pH changes associated with the electrical activity of neurons.

pH-sensitive contrast agent A compound that, when injected into an organism, influences the MR signal differently depending on the pH of the local environment.

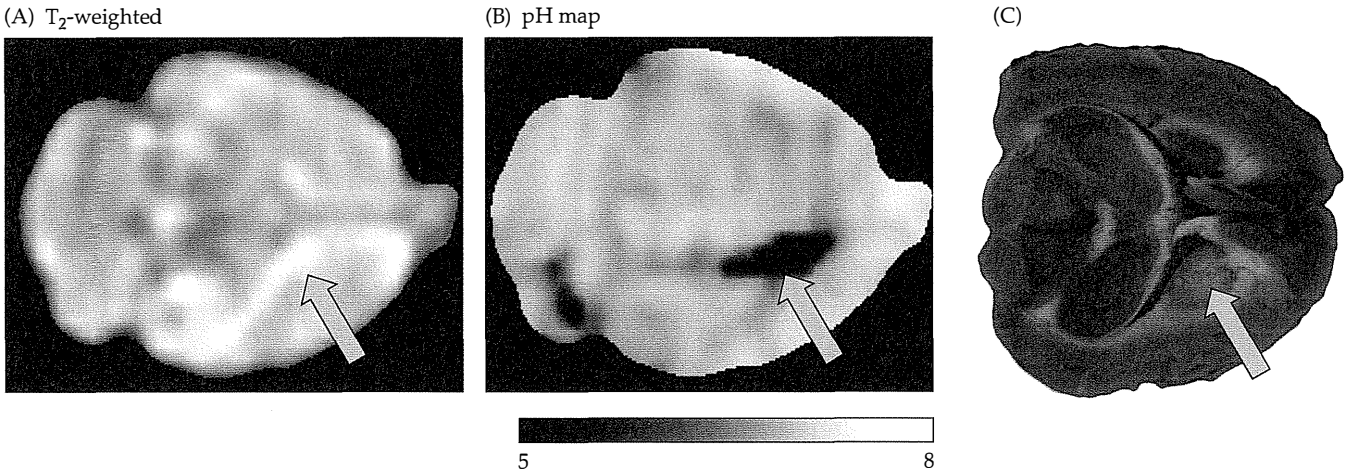

Figure 12.15 Using pH-sensitive imaging to identify focal neural ischemia. (A) The area of restricted blood flow is difficult to identify in this conventional T_2-weighted image of a rat brain. (B) However, in a pH-sensitive image the ischemic tissue stands out clearly as darkened voxels. (C) For reference, staining the tissue (using the ischemia identifier TTC) revealed the location of damage, here evident as the lighter color compared with the normal tissue on the opposite side. (Images courtesy of Drs. Jinyuan Zhou and Peter van Zijl, Johns Hopkins Medical School.)

Ion-gated contrast

Information flow in the nervous system relies on continual changes in the electrical potential of neurons, which is regulated by the flow of ions such as Na^+, K^+, and Ca^{2+} through ion gates in their membranes. In particular, Ca^{2+} ions play an important role as messengers in a wide range of cellular signaling pathways, making them an ideal candidate for ion-specific contrast mechanisms. However, these biologically relevant ions have very small concentrations (e.g., in the μM range) in vivo. Therefore, exogenous contrast agents, whose characteristics can be controlled or activated by ion targets, are used. These agents are likely to provide exciting new information about brain function at the systems level.

In an example of this work, a team led by A. Janasoff has been developing new calcium-sensitive contrast agents to improve the sensitivity of MRI calcium detection. In a recent article by Atanasijevic and colleagues, they reported on the use of superparamagnetic iron oxide (SPIO) nanoparticles that, when aggregated, greatly increase the T_2 relaxation rates of nearby protons. In fact, in vitro measurements suggest that a concentration of only 1 nM of the SPIO agent would be necessary for a 20% decrease in the MRI signal—a truly remarkable sensitivity. To confirm this, the authors utilized well-studied interactions between the calcium-binding protein calmodulin (CaM) and a target peptide sequence known as M13. Binding between these proteins is reversible, dependent on the Ca^{2+} concentration, and thus provides an opportunity for measuring Ca^{2+} concentrations in real time. The authors bound both CaM and M13 separately to the SPIO nanoparticles. They predicted that the presence of Ca^{2+} would cause aggregation of the two proteins and thus cause aggregation of the SPIO particles, leading to a marked change in the T_2 contrast. Indeed, in the presence of Ca^{2+} (in a $CaCl_2$ solution), significant aggregation of the nanoparticles was observed, while no aggregation effect was seen in the absence of free Ca^{2+} (Figure 12.16A). This aggregation increased the T_2 values (Figure 12.16B) and signal (Figure 12.16C) of the surrounding proton pool. These contrast changes were detectable at particle concentrations near 1 nM and CaM concentrations below 1 μM.

Extending these results to studies of human brain function will still require much work. For these specific agents to provide functional MRI contrast, they must penetrate the blood brain barrier and be non-toxic. Nevertheless, the direct imaging of ion flow would have great advantages for studying neuronal

calcium-sensitive contrast agent A compound that, when injected into an organism, influences the MR signal differently depending on the local concentrations of calcium ions. Such agents could lead to maps of neuronal signaling.

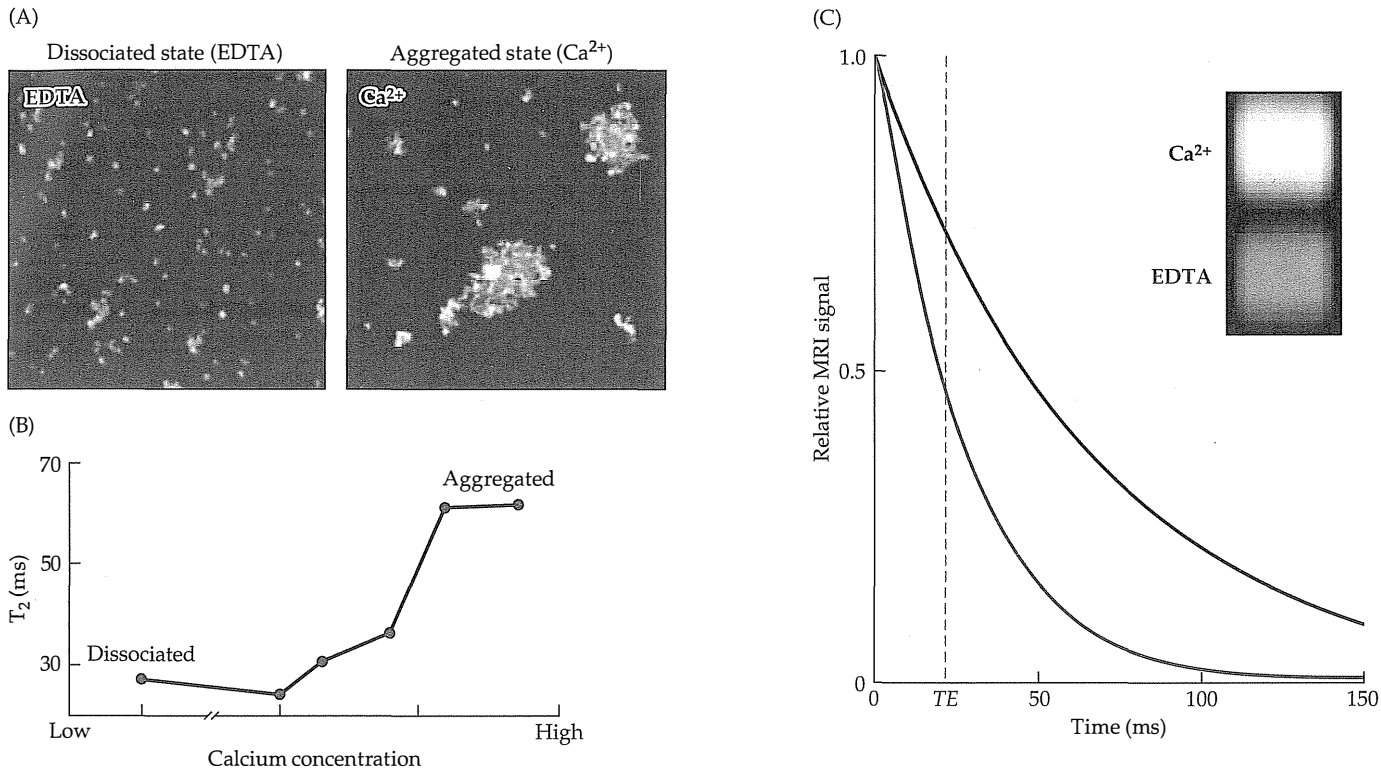

Figure 12.16 MRI contrast agents for calcium-dependent imaging. (A) Researchers have created iron-oxide-containing nanoparticles that aggregate in the presence of free calcium (at right), but not in the presence of the calcium chelator EDTA (left), as shown in these atomic-force micrographs. (B) The aggregation of these nanoparticles increases the T_2 constant in vitro. (C) The MR signal decays exponentially, however signal from tissues containing sufficient levels of calcium would decay more slowly (red curve) than signal from tissues without free calcium (green curve), leading to a brightening of the MR image (inset). This principle could allow the MR-based tracking of calcium concentrations that reflect neuronal activity. (After Atanasijevic et al., 2006.)

activity. Therefore, the development of calcium-sensitive contrast agents has attracted substantial interest from neuroscience laboratories.

Neuronal magnetic field contrast

The ultimate goal of functional MRI is to move beyond indirect measures of brain function, whether large-scale BOLD hemodynamics or local ion flows, to direct measurements of neuronal firing. This quest dates back more than two decades to work by Joy and Henkleman, who caused small electric currents in muscles and measured those currents using MRI. More recently, studies in customized phantoms (e.g., a gel or liquid medium embedded with current-carrying wires) offer direct evidence for the possibility of imaging neuroelectric activities in vivo. These studies demonstrated that minute electric currents, equivalent in magnitude to neuroelectric currents, altered the resonance frequencies of nearby spins through their effects on the local magnetic field. Bodurka and colleagues showed that images sensitive to the phase of the MR signal can be used to detect small phase offsets near the sources of these tiny currents, resulting in visible magnetic field changes as small as 2×10^{-10} T (200 pT) and as brief as 40 ms. For comparison, the evoked magnetic fields measured on the scalp (i.e., ~2–4 cm away from the current source) by MEG are in the order of 10^{-12} (spontaneous) to 10^{-13} (evoked) T. Extrapolation of the MEG results to sources of these currents within the brain suggests that the peak local magnetic field changes may be in the order of 10^{-10} T, and the changes may last for less than 100 ms. Thus, studies in phantoms demonstrate that direct neuronal imaging is possible, at least in principle.

Yet, many steps lie between principle and practice. A recent report from Petridou and colleagues demonstrated that changes in neuronal magnetic fields can indeed be detected, at least in vitro. The authors prepared tissue cultures

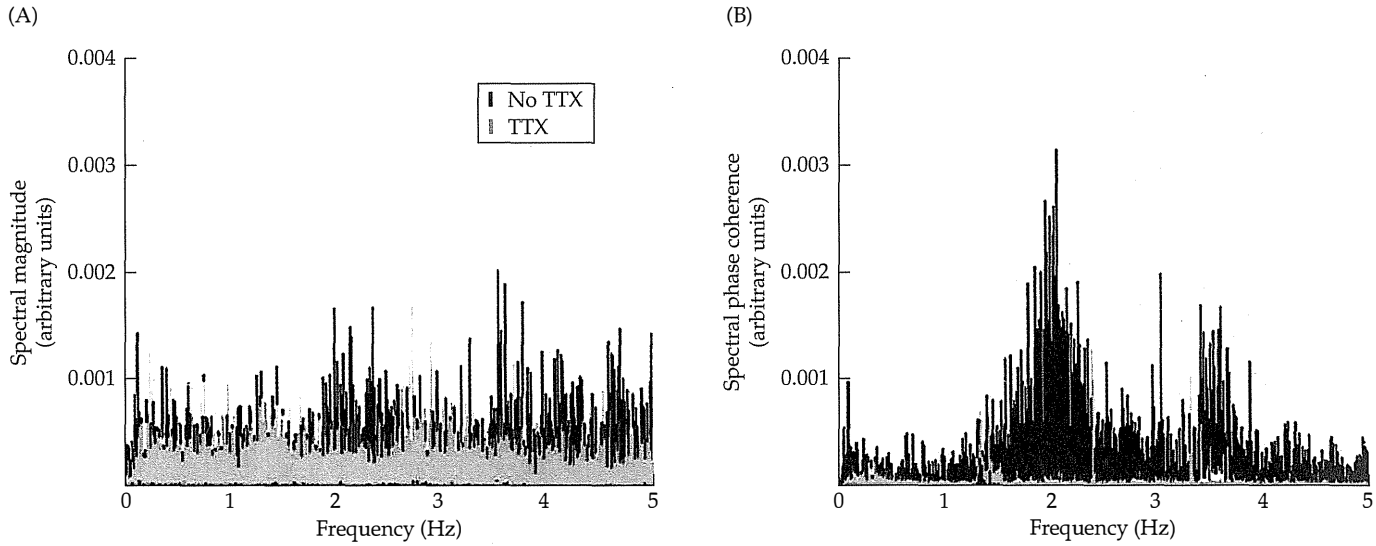

Figure 12.17 Neuronal-activity-related changes specific to MR phase coherence. Researchers administered the neurotoxin TTX, which blocks action potentials, to slices of a rat brain in vitro. (A) The resulting MR magnitude time series had relatively normal spectral power over the range of frequencies available to be measured (TTX: green lines; normal tissue: black lines). However, the phase coherence of the MR signal (B) was essentially abolished by TTX administration. These results illustrate that phase information contained in the MRI signal can, in principle, detect changes in neuroelectric activity. (After Petridou et al., 2006.)

containing slices from the somatosensory cortex and the basal ganglia of newborn rats. These organotypic cultures maintain core features of intact brain tissue, such as the layered organization of the cortex and the parallel orientation of pyramidal neurons, and they generate spontaneous neuronal activity in the presence of appropriate nutrients. The researchers used MRI to measure activity in these tissues under normal conditions and in the presence of tetrodotoxin, which shuts down action potentials by blocking sodium channels. As shown in Figure 12.17, the MR phase spectrum changed dramatically after the administration of tetrodotoxin, demonstrating that MRI phase images can detect, at least globally, changes in the magnetic field caused by neuronal activities.

The exact mechanism for these effects remains unclear. One potential indicator comes from the fact that the signal changes were greater for MR phase than for MR magnitude. Because the MR signal increases with a coherent precession of protons but decays when precession is heterogeneous, these effects are consistent with a synchronized activity that resulted in homogeneous magnetic field changes, and in turn caused shifts in the phase of the MR signal.

Lorentz effect contrast

Another approach to direct measurement of neuronal activity relies on the physical displacement of neurons within the magnetic field. When an ion is in motion, it experiences a physical displacement proportional to the strength of the magnetic field it experiences. This is known as the Lorentz force, and its application to functional MRI has become known as Lorentz effect imaging. The earliest studies of Lorentz effect imaging by Song and colleagues involved a phantom containing a wire that could carry charges of different magnitudes. When the phantom was placed in the strong field of an MRI scanner, a current passing through the wire caused it to displace very slightly. The authors showed that the movement of the wire could be detected using MRI and that gradient pulses amplified the associated signal loss. All conductors, not just wires, experience the Lorentz effect. Later, the same group demonstrated that ionic currents in nerves can be detected in vivo with MRI. Following stimulation of the median nerve (in the forearm), they applied synchronized oscillatory gradients calibrated to the expected speed of signal propagation. They

Lorentz force The force on a moving charge within a magnetic field. Lorentz forces cause spatial displacements in ions and conductors if they are placed in strong magnetic fields.

Lorentz effect imaging (LEI) A technique for direct visualization of ionic electrical activity using MRI.

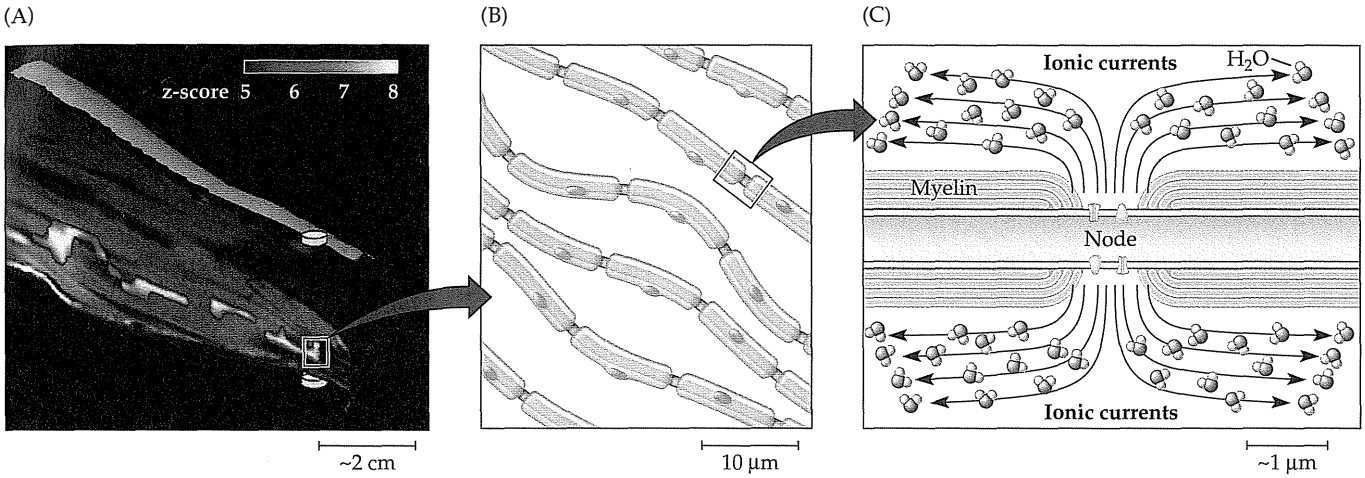

Figure 12.18 A conceptual overview of using MRI to directly measure the conduction of signals within nerves. (A) Recent studies have demonstrated that specialized MRI pulse sequences can detect ionic currents. Here, the median nerve within the forearm was stimulated following a mild electric shock to the wrist (from leads shown as small cylinders). By using gradients whose oscillation was synchronized to the speed of nerve conduction, the researchers could map the electrical signal traveling down that nerve's axon (highlighted in color). (B) Most axons consist of long fibers covered in myelin sheaths that facilitate the rapid propagation of action potentials. (C) At gaps in the myelin (called Nodes of Ranvier), movements of ions across membrane channels lead to ionic currents in the surrounding medium. These currents' influence on the properties of surrounding water molecules can potentially give rise to an ionic Lorentz effect that could be measured with MRI. (A after Truong and Song, 2006.)

identified rapid, localized changes in the MRI signal that corresponded with nerve conduction (Figure 12.18A and B). While the exact mechanism underlying these changes remains under active investigation, the authors attributed this result to the ionic Lorentz effect (Figure 12.18C).

Applying Lorentz effect imaging to the human brain introduces yet more levels of complexity. Neural conduction, whether in axons or in dendrites, generates a range of ionic currents that form loops along the conducting path. Moreover, because of the strength of the volume current during neuronal activity, the Lorentz effect on neurons may be amplified by the surrounding water molecules. A recent study by Truong and colleagues investigated the Lorentz effect in ionic solutions. They found that ionic flows change trajectories during conduction under a magnetic field (Figure 12.19A). By synchronizing the gradient oscillation with the timing of the ionic conduction, the authors could identify an amplification of the Lorentz effect in surrounding water molecules that was detectable by MRI (Figure 12.19B). Although these and similar approaches have a long way to go before they can be used to trace neuronal activity in the human brain, we fully expect that continual advances will shape the course of fMRI research, potentially leading to the replacement of BOLD contrast.

REFER TO THE
fMRI
COMPANION WEBSITE AT
www.sinauer.com/fmri2e
for study questions and Web links.

Summary

Nearly all current fMRI studies share the same constraints. They sample the brain with a spatial resolution of a few millimeters and a temporal resolution of a few seconds. The resulting images are sensitive to BOLD contrast, which is an indirect measure of neuronal activity. Though a large array of research questions can be answered despite these limitations, advances in the spatial and temporal resolution of fMRI will greatly expand its applicability. Many of the advances so far have been driven by hardware improvements, notably by increasing the strength of the static and gradient fields and by using more advanced parallel receiver coil arrangements, which have pushed the spatial resolution to an unprecedented level. However, further improvements will need to come from a better understanding of important biomarkers and novel contrasts in the brain, that can be used to specifically detect neuronal and physiological changes during brain activity. Potential new forms of contrast may be sensitive to brain temperature, pH,

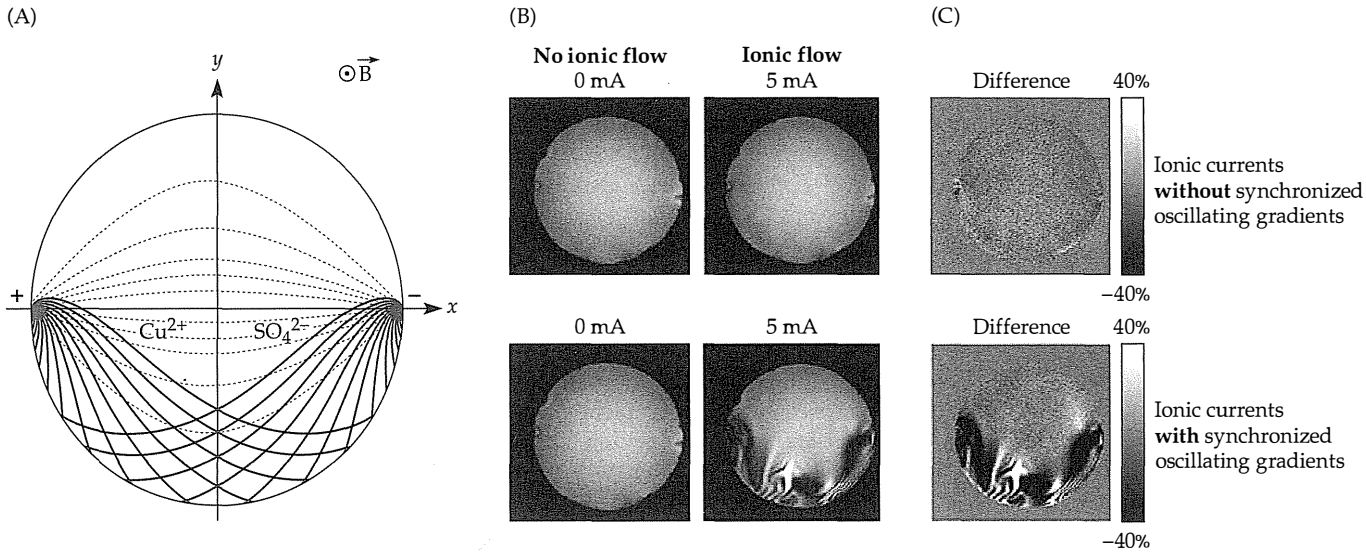

Figure 12.19 Measuring ionic current flows with MRI. (A) Shown is a schematic diagram indicating ionic flows within a spherical phantom containing positive (Cu^{2+}) and negative (SO_4^{2-}) ions, when a current is created between the cathode (+) and anode (–) poles of that phantom. In the absence of any strong magnetic field, the ions will flow in smooth, symmetrical paths (dashed lines) through the middle of the phantom. However, if the phantom is subjected to a strong magnetic field, here shown as coming up out of the page plane, the ionic flows will deviate systematically toward one edge of the phantom (solid lines). (B) When no current is applied, and thus no ionic flows are present (top row), then the phantom appears homogenous in MR intensity. Application of a 5 mA current (bottom row) causes ionic flows that can be detected as distortions within the phantom, as predicted by the schematic diagram of likely paths of flow. (C) Shown are images of the difference between ionic flow (5 mA) and no ionic flow (0 mA) conditions. Note that these distortions are only evident when the pulse sequence uses synchronized oscillating gradients calibrated to the timing of ionic flow. (After Truong et al., 2008.)

or changes in ion concentrations. Most tantalizing of all are demonstrations of direct imaging of the magnetic field changes or electrical currents associated with neuronal activity. Although many of these approaches are still in the very early stages of development, we expect them to provide important new information about brain function in coming years.

Suggested Readings

*Glover, G. H., and Law, C. S. (2001). Spiral-in/out BOLD fMRI for increased SNR and reduced susceptibility artifacts. *Magn. Reson. Med.*, 46(3): 515–522. *The first demonstration of simultaneous image acquisition using both spiral-in and spiral-out trajectories to recover susceptibility-induced signal losses with high temporal efficiency.*

Johnson, G. A., Cofer, G. P., Gewalt, S. L., and Hedlund, L. W. (2002). Morphologic phenotyping with MR microscopy: the visible mouse. *Radiology*, 222: 789–793. *This manuscript discusses advances in MR microscopy and their applications.*

*Truong, T. K. and Song, A. W. (2006). Finding neuroelectric activity under magnetic-field oscillations (NAMO) with magnetic resonance imaging in vivo. *Proc. Natl. Acad. Sci. U. S. A.*, 103(33): 12598–12601. *This experiment demonstrates that the transmission of an action potential, here in peripheral nerves, can be mapped using MRI.*

*Ress, D., Glover, G. H., Liu, J., and Wandell, B. (2007). Laminar profiles of functional activity in the human brain. *NeuroImage* 34: 74–84. *An interesting recent example of how fMRI can be used to differentiate activation associated with distinct layers within the cortex.*

*Indicates a reference that is a suggested reading in the field and is also cited in this chapter.

Chapter References

Atanasijevic, T., Shusteff, M., Fam, P., and Jasanoff, A. (2006). Calcium-sensitive MRI contrast agents based on superparamagnetic iron oxide nanoparticles and calmodulin, *Proc. Natl. Acad. Sci. U. S. A.*, 103(40): 14707–14712.

Biswal, B., Yetkin, F. Z., Haughton, V. M., and Hyde, J. S. (1995). Functional connectivity in the motor cortex of resting human brain using echo-planar MRI. *Magn. Reson. Med.*, 34(4): 537–541.

Bodurka, J., and Bandettini, P. A. (2002). Toward direct mapping of neuronal activity: MRI detection of ultraweak, transient magnetic field changes. *Magn. Reson. Med.*, 47: 1052–1058.

Bodurka, J., Jesmanowicz, A., Hyde, J. S., Xu, H., Estkowski, L., and Li, S.-J. (1999). Current-induced magnetic resonance phase imaging. *J. Magn. Reson.*, 137(1): 265–271.

Chesler, M. (2003). Regulation and Modulation of pH in the Brain. *Physiol. Rev.* 83: 1183–1221.

Cohen, D. (1968). Magnetoencephalography: evidence of magnetic fields produced by alpha-rhythm currents. *Science*, 161: 784–786.

Dodd, S. J., Williams, M., Suhan, J. P., Williams, D. S., Koretsky, A. P., and Ho, C. (1999). Detection of single mammalian cells by high-resolution magnetic resonance imaging. *Biophys. J.*, 76: 103–109.

Hamalainen, M., Hari, R., Ilmoniemi, R. J., Knuutila, J., and Lounasmaa, O.V. (1993). Magnetoencephalography—theory, instrumentation, and applications to noninvasive studies of the working human brain. *Rev. Mod. Phys.*, 65: 413–497.

Joy, M., Scott, G., and Henkelman, M. (1989). In vivo detection of applied electric currents by magnetic resonance imaging. *J. Magn. Reson. Imaging*, 7(1): 89–94.

Ogawa, S., Lee, T. M., Stepnoski, R., Chen, W., Zhu, X. H., and Ugurbil, K. (2000). An approach to probe neural systems interaction by functional MRI at neural time scale down to milliseconds. *Proc. Natl. Acad. Sci. U. S. A.*, 97: 11026–11031.

Pruessmann, K. P., Weiger, M., Scheidegger, M. B., and Boesiger, P. (1999). SENSE: sensitivity encoding for fast MRI. *Magn. Reson. Med.*, 42: 952–962.

Raghunand, N., Howison, C., Sherry, A. D., Zhang, S., and Gillies, R. J. (2003). Renal & Systemic pH Imaging by Contrast-Enhanced MRI. *Magn. Reson. Med.*, 49: 249–257.

Rieke, V. and Butts-Pauly, K. (2008). MR thermometry. *J. Magn. Reson. Imaging*, 27(2): 376–390.

Romani, G. L. Fundamentals on neuromagnetism. In: Williamson, S. (ed.) (1989). *Advances in biomagnetics.* Plenum Press, New York, pp. 33–46.

Petridou, N., Planz, D., Silva, A. C., Loew, M., Bodurka, J, and Bandettini, P. A., (2006). Direct magnetic resonance detection of neuronal electrical activity. *Proc. Natl. Acad. Sci. U. S. A.*, 103(43): 16015–16020.

Shapiro, E., Sharer, K., Skrtic, S., and Koretsky, A. (2006). In vivo detection of single cells by MRI. *Magn. Reson. Med.*, 55: 242–249.

Sodickson, D. K., and Manning, W. J. (1997) Simultaneous acquisition of spatial harmonics (SMASH): fast imaging with radiofrequency coil arrays. *Magn. Reson. Med.*, 38: 591–603.

Song, A. W., and Takahashi, A. M. (2001). Lorentz effect imaging. *J. Magn. Reson. Imaging*, 19(6): 763–767.

Truong, T. K., Avram, A., Song, A. W. 2008. Lorentz effect imaging of ionic currents in solution, *J. Magn. Reson.*, 191(1): 93–99.

Trubel, H. K., Maceijewski, P. K., Farber, J. H., and Hyder, F. (2003). Brain temperature measured by 1H-NMR in conjunction with a lanthanide complex. *J. Appl. Physiol.*, 94(4): 1641–1649.

Vincent, J. L., Patel, G. H., Fox, M. D., Snyder, A. Z., Baker, J. T., van Essen, D. C., Zempel, J. M., Snyder, L. H., Corbetta, M., and Raichle, M. E. (2007). Intrinsic functional architecture in the anaesthetized monkey brain. *Nature*, 447(7140): 83–86.

Yablonskiy, D. A., Ackerman, J., and Raichle, M. E. (2000). Coupling between changes in human brain temperature and oxidative metabolism during prolonged visual stimulation. *Proc. Natl. Acad. Sci. U. S. A.*, 97(13): 7603–7608.

Zhou, J., Payen, J. F., Wilson, D. A., Traystman, R. J., and Van Zijl, P. (2003). Using the amide proton signals of intracellular proteins and peptides to detect pH effects in MRI. *Nat. Med.* 9(8): 1085–1090.

Chapter 13

Combining fMRI with other Techniques

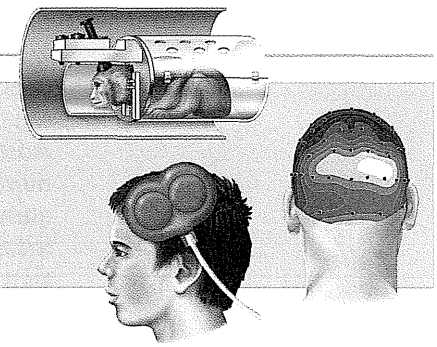

In this chapter we will consider more broadly the relationships between fMRI and other methods used to study brain function. We adopt the perspective of a neuroscientist whose interest lies not in the technical intricacies of specific methods but rather in using those methods to understand brain function. No single technique yet available (even one as multifaceted and powerful as fMRI) can fully elucidate the perceptual, motor, and cognitive processes within the brain. All techniques have weaknesses that limit the scope of their interpretative power. Indeed, one important motive for this book has been to clarify the limitations and challenges of fMRI as it is currently practiced. To overcome the weakness of individual techniques, students of brain function should employ converging operations in their research programs. That is, they should bring corroborating and complementary evidence from multiple techniques to answer a single research question. We will first consider the discipline of cognitive neuroscience generally, and functional brain mapping in particular. Then, we will describe the main techniques that have been used in concert with fMRI. Roughly considered, these techniques fall into one of two classes: manipulation techniques that change how the brain functions, and measurement techniques that observe brain function as it occurs. Throughout, we will emphasize that no matter how advanced the methods, it is ultimately the precision of the research question that determines the rate of scientific progress.

Cognitive Neuroscience

Cognitive neuroscience seeks to understand how complex behavior is produced by the functional repertoire of the brain. Like cognitive science, it studies mental processes that mediate between sensory input and expressed behavior. Like neuroscience, it seeks mechanistic explanations for behavior in the activity of neurons and in the context of evolution. Given these disciplines of origin, one straightforward strategy for cognitive neuroscientists would be to use fMRI and other neuroimaging techniques to identify the brain regions associated with the mental processes identified by cognitive science. Once the

converging operations The use of two or more techniques to provide complementary evidence used to test an experimental hypothesis or scientific theory.

region that supports a given process is identified, its underlying neural circuitry can be studied in greater detail (perhaps using molecular, neurophysiological, or computational methods). If only brain mapping were so easy!

While the strategy introduced in the previous paragraph is purposefully oversimplified, it captures much of the logic used by many cognitive neuroscience studies. Is there anything unreasonable about this simple approach? A first problem concerns the questionable biological reality of the postulated mental processes, or constructs, to be studied. Many cognitive scientists are attracted to functional neuroimaging precisely because it seems to provide the means to validate abstract psychological constructs. That is, if an experimental manipulation alters a postulated construct and changes brain activity, then the construct is assumed to exist. However, there is rarely any direct evidence that a psychological construct exists as a biological entity. Indeed, a model of a cognitive process may have considerable explanatory power even though none of its parts correspond to real brain regions or measurable patterns of brain activity.

The history of science is replete with psychological constructs that were once dominant but have been discredited and forgotten. Imagine that fMRI were available in Gall's time. Would it have made sense to conduct an fMRI experiment to search for neural activity associated with approbativeness, a phrenological faculty associated with one's personal vanity? Or imagine that fMRI were available in Vienna in 1920. Would it have made sense to conduct an fMRI experiment to search for the neural locus of the id? Imagine that fMRI is available in your laboratory now. Does it make sense to conduct an fMRI study to search for the neural substrate of working memory, or altruism, or emotional intelligence? At one time or another, a wide array of constructs have been used to explain complex behavior. Some are no longer credible, others are hotly debated, while others still have widespread currency.

A second potential problem results from assuming that a unitary psychological concept must be realized by a unitary biological entity. One might conclude, on the basis of a blob of active voxels found using fMRI or a new component identified using electrophysiology, that a construct as abstract and multifaceted as emotional intelligence is actually a discrete brain process controlled by a particular part of the cortex. Yet this is unlikely to be the case. Complex constructs probably emerge from the coordinated activity of more basic functions, and the mapping of any complex construct to a single, discrete anatomical focus seems improbable.

Third, the course of neural activity need not be isomorphic with the presumed behavior of the construct. Does increased attention have to be manifest as an increased BOLD signal? Or could attention decrease BOLD activation in a brain region? Does maintaining a memory over a 20-s period require neurons to continually fire for 20 seconds? While many fMRI statistical analyses assume isomorphism between stimuli and the measures of brain function they evoke, this assumption may be wrong under many circumstances.

Fourth, the very nature of most physiological methods in cognitive neuroscience ensures that researchers find evidence for localization of function. All of the many techniques discussed in this chapter provide data about spatially differentiated functions. A cognitive function that was equally distributed throughout the brain would be nearly invisible to the physiological techniques described in this book. In recent years, the advent of functional connectivity techniques in fMRI—along with the simultaneous development of multielectrode recording approaches in non-human electrophysiology—has begun to provide information about larger networks of brain function. Even so, it is not

construct An abstract concept that explains behavior but which itself is not directly observable. Attention is an example of a psychological construct.

isomorphic Having an identical form. A physiological measurement that is isomorphic with a psychological construct would vary over time consistently with the postulated changes in the construct.

localization of function The idea that the brain may have distinct regions that support particular mental processes.

functional connectivity A pattern of functional relationships among regions, inferred from common changes in activation over time, that may reflect direct or indirect links between those regions.

surprising that most cognitive neuroscience studies conclude that some psychological construct is localized to a small set of spatially discrete regions.

Finally, investigators often implicitly assume that, within some limits, functions are localized in the same brain regions of different individuals. In many fMRI studies, great effort is expended to normalize each individual's brain anatomy to a common standardized brain space or atlas (see Chapter 8). Normalization improves the statistical reliability of the inferences we draw from imaging data, while reassuring scientists who are suspicious of single observations. Similar methods have been devised to standardize electrophysiological and lesion data into common coordinate systems. While normalization methods have been extraordinarily useful for many research questions, they are not appropriate for brain functions that are located in different regions in different individuals. For example, the hemispheric laterality of language can vary with handedness or as a result of early brain injury. If a subject group contained some left-handed and some right-handed individuals, a group statistical analysis might reveal bilateral activation even though each subject had a highly lateralized pattern. Therefore, when studying questions related to language function, investigators often attempt to minimize suspected differences in brain organization by selecting only right-handed subjects.

Strategies for research in cognitive neuroscience

In contrast to the idealized strategy discussed earlier in this chapter, the real practice of cognitive neuroscience is messy and incremental. A research hypothesis may be initiated by a concept from psychology, such as the distinction between short-term and long-term memory. Or, the idea may come from a neurological observation, for example, that bilateral lesions of the medial temporal lobe lead to a permanent disability to create new memories. Following the initial hypothesis is a cycle of testing, refinements of the hypothesis, and more testing.

Physiological data, and in particular fMRI, can play an important role in this iterative process, by breaking down complex behavior into functional components. One strategy is to assume that activation at different anatomical loci or at different temporal latencies reflects different cognitive processes. Following this logic, if you run the perfect experiment to isolate your favorite psychological construct, and you reliably identify several discrete foci of activity, then you conclude that your construct must have several components. You can then perform additional experiments to try to dissociate these components on the basis of psychological manipulations. A related strategy reverses the emphasis. You can test a wide range of experimental manipulations to see which alter the activity of a single brain region. To what stimuli is this area sensitive? Does its activity change with learning? Must a stimulus be attended to for activity to be evoked, or is activity evoked automatically? How does activity change if the subject is given extensive training with the stimuli?

By continually testing and revising hypotheses about brain function, cognitive neuroscientists can help transform an ill-defined psychological construct into a clear theory whose components are associated with specific brain structures. Conversely, psychological concepts can shape the course of cognitive neuroscience by indicating important areas for research. In the following sections, we describe the various techniques used by cognitive neuroscientists to test their hypotheses. Within each section, we describe the technique, its applications, and its integration with fMRI research. We hope to convey how converging studies using these seemingly disparate techniques provide the best opportunity for advances in our understanding of brain function.

Manipulating Brain Function

Some research techniques are direct: they quantify changes in the world caused by an experimental manipulation. For example, if you are interested in the effects of an induced magnetic field on the voltage across a wire, you can collect data using a voltmeter attached to electrodes on the wire. Similarly, you can place electrodes directly on the brain surface to measure voltage changes associated with neuronal activity. Other methods are indirect and collect data about something correlated with, but not necessarily caused by, the process of interest. Most brain imaging methods, including fMRI, provide indirect measures of neuronal activity. If the correlation between the measured process and the process of interest is high and reliable, then an indirect method can be very valuable. However, if these processes are only weakly correlated, or can be dissociated by other (often unknown) processes, then the value of an indirect technique is diminished.

For research questions about psychological constructs, all techniques for measuring brain activity are indirect (see Figures 9.3 and 9.4). Even when neuronal activity is measured directly using certain electrophysiological techniques, it does not necessarily reflect the psychological construct of interest. For this reason, neuroimaging and electrophysiological techniques are commonly criticized as revealing correlations, not causes. That is, while they can demonstrate an association between a brain region and a psychological construct, they cannot establish that the brain region is necessary for the construct. As an example: If an investigator demonstrates with fMRI that the performance of a working memory task activates a specific region of the dorsolateral prefrontal cortex, would the removal of that region of the cortex (or, less drastically, the elimination of its activation) impair working memory? To answer questions about necessity, cognitive neuroscientists must manipulate the brain in some way and then assess the effects of that manipulation on behavior.

direct cortical stimulation Applying small currents directly to brain tissue to excite or disrupt neural activity. Direct cortical stimulation is usually conducted in humans to localize critical brain regions in the context of neurosurgery.

microstimulation Applying currents through microelectrodes to stimulate activity in a small number of neurons.

transcranial magnetic stimulation (TMS) A technique for temporarily stimulating a brain region to disrupt its function. TMS uses an electromagnetic coil placed close to the scalp; when current passes through the coil, it generates a magnetic field in the nearby brain tissue, producing localized electrical currents.

equipotentiality The concept that a function is so widely distributed within the brain that it depends on the activity of the brain as a whole. Equipotentiality is the antithesis of localization of function.

Direct cortical stimulation

An extremely important technique for establishing the necessity of a brain region for a cognitive construct is cortical stimulation, or the application of an electrical current to evoke neuronal activity. Three primary stimulation techniques are in use today. In direct cortical stimulation, electrical current is introduced using relatively large electrodes that are placed on the surface of the brain, directly into the brain tissue, or even on the surface of the scalp. Many modern animal studies use microstimulation techniques that activate only a small number of neurons. For studies in volunteer human subjects, the introduction of a focal magnetic field from outside the skull, through a process known as transcranial magnetic stimulation (TMS), evokes activity in neurons within a large brain region.

The first scientific studies of direct cortical stimulation were reported in the 1870s, during a period of transition in neuroscience. Before this time, the dominant concept of brain organization had been the idea of equipotentiality, that cognitive functions were equally distributed throughout the cortex. This idea had been based largely on the work of the French physiologist Pierre Flourens, who created lesions in the brains of rabbits and pigeons and then observed their behavior. Lesions in subcortical structures caused specific behavioral deficits (e.g., lesions in the medulla impaired respiration), but damage to the cortex was never functionally specific. Based on these results and those from other laboratories using other species, Flourens became a vocal opponent of the idea of local-

ization of function in the cortex—and of its advocates (e.g., Gall; see Chapter 1). However, there was already significant experimental evidence in favor of cortical localization, notably Broca's 1861 observation of aphasia (i.e., an inability to speak) caused by a circumscribed left frontal lesion. Within this changing climate, the German physiologists Gustav Fritsch and Eduard Hitzig reported that direct cortical stimulation of anterior regions of the cortex in dogs caused muscular movements on the contralateral side. Stimulation of other brain regions produced no such movement. Their results precipitated an explosion of interest in cortical stimulation, and researchers such as the British scientist David Ferrier soon mapped large regions of the sensory and motor cortices. By the 1876 publication of Ferrier's influential book *The Function of the Brain*, evidence against equipotentiality had become overwhelming.

Today, direct cortical stimulation is most frequently used to map areas of critical function (e.g., language, motor abilities) in patients awaiting or undergoing neurosurgery. Based on the functions of brain regions located near the surgical target, neurosurgeons may change the path taken through the brain surface in order to leave critical areas intact while removing a deep tumor, or they may remove more or less tissue during a resection. This minimizes the chance that the patient will suffer from motor, language, or other deficits as a result of the surgery. An early pioneer of this approach was the American-born neurosurgeon Wilder Penfield, who helped found the Montreal Neurological Institute. During the 1940s and 1950s, Penfield and his colleagues methodically mapped the human brain in patients undergoing surgery while awake. In addition to the sensory and motor cortices, Penfield studied brain regions involved in language processing and memory. Within the discipline of neurosurgery, direct cortical stimulation remains the standard procedure for functional brain mapping.

In the modern practice of direct cortical stimulation, a pair of stimulating electrodes is placed on the surface of the cortex (Figure 13.1A). One electrode, designated the anode, provides the source of electrical current, while the second electrode, designated the cathode, provides the sink to which the current will flow. The stimulation usually consists of weak (1 to 10 μA) current pulses, rapidly presented (e.g., 50 Hz), each of 100 to 500 μs duration. During stimulation, brain tissue in the current path between the anode and the cathode is depolarized. Stimulation mapping is often conducted during the surgery itself. The surgeon moves the electrodes to different locations on the exposed cortical surface, tests the effect of stimulation on the function(s) of interest, and then places numbered sterile paper tickets on the cortex, as markers of function (Figure 13.1B). If sensory or language functions are being tested, the patient needs to be awake and cooperative during that part of the procedure. Some

anode A source of positive charge or ions, and an attractor of free electrons.

cathode An attractor for positive charge or ions, and a source of free electrons.

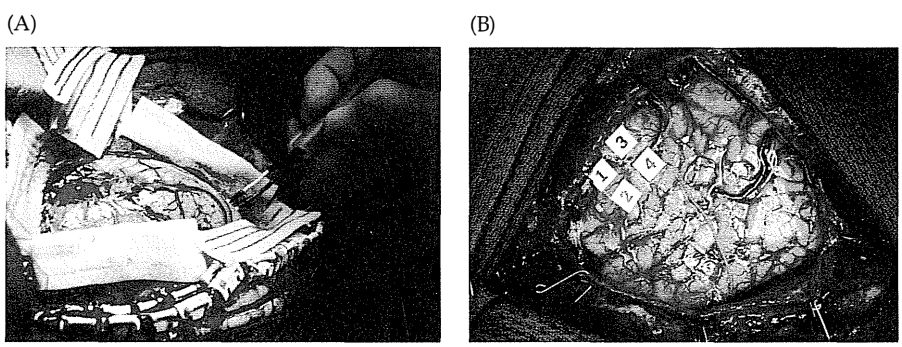

Figure 13.1 Direct cortical stimulation. In some neurosurgical procedures, it is important to localize particular functional brain regions that might be located near the planned excision. In direct cortical stimulation performed during surgery, a surgeon places a pair of stimulating electrodes on the surface of the brain while testing the patient for language comprehension, speech, sensation, or movement. In (A), the surgeon's gloved hand can be seen holding the cathode and anode above the brain's surface. In (B), functional areas of the brain are marked by sterile tickets that indicate what function was evoked or interrupted at that site. (Courtesy of Dr. Dennis D. Spencer, Yale University; photographs by Joseph Jasiorkowski.)

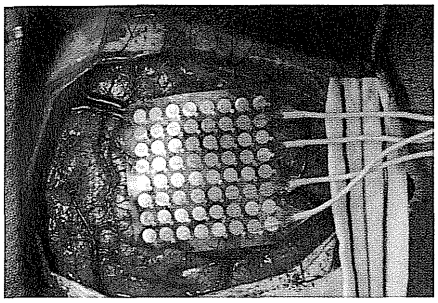

Figure 13.2 An eight by eight grid of electrodes embedded in a sylastic grid and placed on the exposed cortical surface of the human brain. (Courtesy of Dr. Dennis D. Spencer, Yale University; photograph by Joseph Jasiorkowski.)

muscular twitches evoked by stimulation can be observed with patients who are under light anesthesia.

In patients with some forms of epilepsy, grids of electrodes are sometimes implanted subdurally over a period of days or weeks (Figure 13.2). The grids are typically constructed of a flexible sylastic sheet into which small electrodes are embedded. A typical grid may consist of an 8 by 8 array of electrodes, each separated by 1 cm and therefore covering a 49 cm^2 area of cortex. By recording the frequency and locations of seizures within this grid, the patient's doctors can determine whether a particular surgical excision would reduce seizure frequency or eliminate the seizures entirely. In these circumstances, direct cortical stimulation mapping is sometimes performed using these electrode grids. Electrical current is systematically introduced between adjacent pairs of electrodes while the subject is engaged in a language, motor, or perceptual task. Since patients are conscious, alert, and comfortable during these extraoperative stimulation studies, much useful information has been obtained about higher cognitive function from these procedures.

Functional consequences of direct cortical stimulation

The consequences of direct cortical stimulation differ for different brain regions. Stimulation in some locations evokes a positive response; for example, stimulation of the hand region of the primary motor cortex might evoke flexion of the fingers in the contralateral hand, while stimulation of the mouth region may cause the lips to twitch or the tongue to move. Positive responses provide particularly strong evidence for the causal role of a brain region in an action or percept. In other regions, stimulation might cause a negative response: it inhibits activity. Stimulation of a small region of the left inferior frontal region (i.e., Broca's area) can cause speech arrest, even though patients can still move their mouths and tongues on command. After the stimulation ends, patients report that they knew what they wanted to say but were unable to say it. During stimulation of Wernicke's area in the posterior temporal cortex, patients remain able to speak but they may not be able to understand the speech of others, carry out spoken commands, or complete simple sentences. Or, stimulation may have no effects at all. This may occur because the current density was too weak to depolarize nearby neurons, in which case increasing the current may yield a response. It may also result from a failure to test the specific process supported by that region. For example, as described in the following paragraph, stimulation of some regions of the fusiform gyrus in the temporal lobe produces an inability to recognize familiar faces while preserving the ability to name familiar objects. An investigator who never presented images of faces during stimulation might mistakenly conclude that the fusiform gyrus was functionally silent.

Sometimes both positive and negative effects can be obtained by stimulation at the same site. Stimulation of the supplementary motor area can evoke both simple and complex coordinated motor actions. It can also disrupt ongoing motor activity that requires bimanual coordination, such as twiddling one's thumbs. A striking example of both positive and negative effects of stimulation comes from a 1999 study by Puce and colleagues, who stimulated electrode sites on intracranial grids within the fusiform gyrus. Before stimulation, the researchers showed the subjects photographs of familiar and famous faces of people the subjects were able to identify. The faces, but not other stimulus categories, evoked large changes in electrical potential in electrodes within the fusiform gyrus. The investigators then stimulated those electrodes. Several of

the subjects became prosopagnosic during the duration of the stimulation; that is, they could no longer recognize the faces, although they could recognize common objects. When the stimulation ended, they could once again recognize the faces. While the disruption of face recognition by stimulation was a noteworthy finding, there was the possibility that the effect was not specific to faces. Perhaps the disruption would also have occurred for any object that had a specific ellipsoidal shape, had bilateral symmetry, or was in the general category of living things. However, in two of the subjects, stimulation evoked a vivid hallucination of a face. This remarkable positive effect of stimulation provided strong evidence that the observed disruption was specific to faces.

homotopic The cortex in one cerebral hemisphere that corresponds to the same region in the other hemisphere.

While direct cortical stimulation is a potentially powerful technique, it has several limitations. First, it is invasive and may precipitate a seizure, particularly in patients who suffer from epilepsy. This risk means that direct cortical stimulation can only be performed as part of a clinical procedure. Second, at high electrical currents that are sufficient to depolarize neurons, the current may spread from the stimulating electrodes and excite brain regions some distance away. This can introduce uncertainty in the interpretation of the localization results. For this reason, the cathode and anode are usually kept in close proximity, and the investigator gradually increases the stimulating current so that the threshold at which a stimulation effect is first observed can be monitored. Third, positive or negative effects of stimulation do not necessarily indicate that the surgical removal of the stimulated region will cause corresponding deficits. For example, a 1986 stimulation study by Luders and colleagues found that stimulation of part of the left fusiform gyrus can lead to an inability to speak or understand language. Despite these striking deficits, surgical removal of this region does not typically cause the same severe and lasting language deficits that follow removal of Wernicke's or Broca's areas. Why does damage to some brain areas lead to functional deficits, while damage to others results only in mild or transient deficits? As we will consider in the discussion of lesion studies later in the chapter, this may reflect the ability of the brain to reorganize some functions following damage, perhaps by engaging homotopic regions in the opposite hemisphere.

Several studies have directly compared cortical stimulation with fMRI. In 1999, Schlosser and colleagues tested patients who were about to undergo surgery in the language-dominant temporal lobe. To help guide the neurosurgeon, localization of temporal lobe language regions was attempted preoperatively using a blocked-design fMRI study in which native English-speaking subjects passively listened to speech that alternated between familiar (English) and unfamiliar (Turkish) languages. The same speaker was used throughout, and basic auditory properties were controlled between the two conditions. Greater activation was observed in response to the English speech in the lateral temporal (i.e., Wernicke's area) and inferior frontal (i.e., Broca's area) cortices in the language-dominant hemisphere of most subjects tested. Direct cortical stimulation was also used to localize the lateral temporal language region in some subjects. At electrode locations near the locations of fMRI activity, cortical stimulation interfered with auditory comprehension, object naming, or speech production tasks in nearly all subjects. Stimulation therefore validated the results obtained from the fMRI task. However, while the correspondence between temporal lobe language areas identified by fMRI and by direct cortical stimulation was generally good, differences were noted in the spatial extent of activation using these different methods.

As noted in Chapter 7, the spatial extent of fMRI activation may overestimate the area in which neuronal activation occurs, and so these methods may

single-pulse TMS The delivery of a single TMS stimulation pulse, in order to disrupt some ongoing brain process.

repetitive TMS (rTMS) The delivery of an extended series of closely spaced TMS stimulation pulses, in order to effect long-lasting changes in brain function.

identify different boundaries of a functional region. Because the spatial limits of the activation may influence the extent of a surgical resection, methods for real-time fMRI analysis may require different approaches than are typical for research studies (see Box 11.2). Nevertheless, the results of Schlosser and colleagues suggest that information from direct cortical stimulation may complement evidence obtained by fMRI studies.

Transcranial magnetic stimulation (TMS)

So far in this chapter we have discussed invasive methods for direct cortical stimulation that involve opening the skull to place electrodes against the brain. An alternative and less-invasive method, transcranial magnetic stimulation, was introduced in the 1980s. In TMS studies, an electrical coil is placed on the outside of the skull and rapidly charged with current (Figure 13.3A). This generates a strong magnetic field (as large as several Tesla) that lasts less than a millisecond. This field extends through the skull and into the brain (Figure 13.3B), where it produces an electrical current in local axons by electromagnetic induction. The configuration of the coil influences the focality of the field and, thus, the spread of the electrical current. One popular coil design has the shape of a figure eight, for which the field is maximal near the midway point between the coils.

Researchers use TMS in either of two ways: to deliver a single brief electrical pulse to the brain (single-pulse TMS), or to deliver a series of pulses over a period of minutes (repetitive TMS, or rTMS). Note that we consider intermediate approaches involving short bursts of pulses over a few seconds to be within the general category of single-pulse TMS, given that they share conceptual underpinnings. These two approaches differ in their effects on brain function. Single-pulse TMS first evokes a brief (~10 ms) burst of neuronal activity, perhaps reflecting evoked activation in local neural circuits, then leads to a longer interval (~200 ms) of relatively suppressed neuronal activity. Single-pulse TMS thus causes a very transient disruption of an ongoing process. Repetitive TMS can cause long-term effects (e.g., lasting for many minutes) on the excitability of neurons within the affected region. The neurons may become either more or less excitable, depending on the pattern of pulses delivered. Moreover, rTMS may lead to indirect changes in brain physiology, such as long-term increases in blood flow to a stimulated region. Because of the breadth of its effects, rTMS has been evaluated as a potential treatment for chronic neurological and psychiatric conditions. Despite some early promising results in

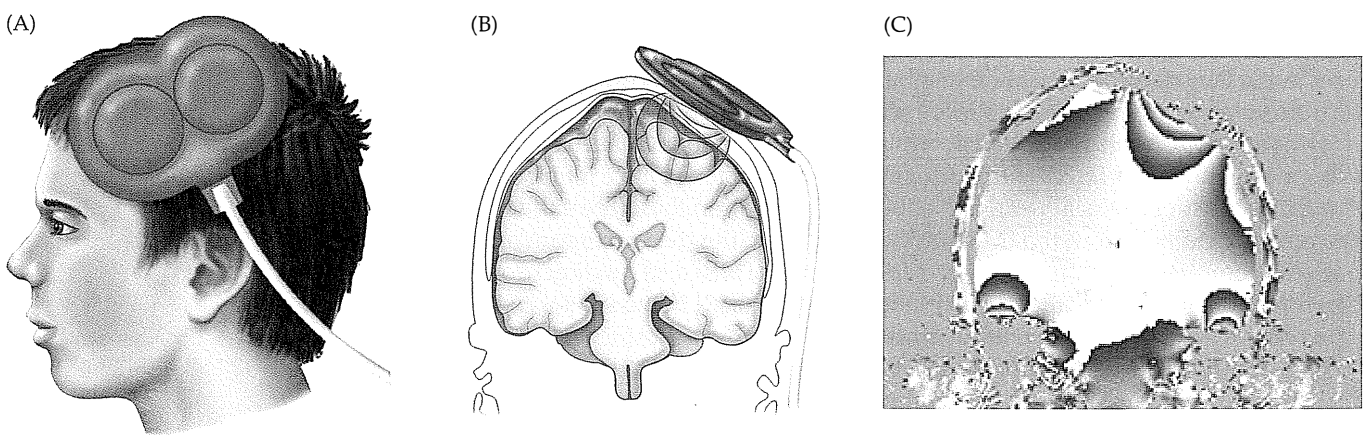

Figure 13.3 Transcranial magnetic stimulation (TMS). In TMS, an electromagnetic coil is placed on the surface of the skull (A). Rapidly reversing the flow of a very strong current within the coil induces a changing magnetic field in the brain (B), which in turn evokes electric currents in neurons. The magnetic field lines associated with a TMS pulse can be seen in the upper right of this coronal MRI phase map (C). (C from Drs. Daryl Bohning and Mark George, Medical University of South Carolina.)

the treatment of several disorders (e.g., depression), the clinical efficacy of rTMS remains a subject of vigorous debate in the literature. For a recent and thoughtful summary, see the 2007 review article by Ridding and Rothwell cited in the chapter references.

Thought question

How might the physiological changes evoked by TMS mirror those evoked by rapidly changing gradients during MRI?

As currently practiced, TMS is considered a safe and noninvasive method and has been used in more than 2000 published studies of both healthy volunteers and patients. Indeed, one of the authors of this textbook was a volunteer subject in one of the first studies performed to test the safety of the single-pulse TMS method. It should be noted, however, that prior to the establishment of safe operating limits and procedures, rTMS evoked seizures in a small number of presumably normal subjects who had no prior history of epileptic activity. Also, due to the spread of the current, the actual brain regions stimulated are much more extensive than in the direct cortical stimulation studies discussed earlier (see Figure 13.3C).

TMS has been used in a large number of creative studies of brain function. By manipulating the latency at which a pulse is applied to a given brain region, researchers can interrupt processing at different points in time. For example, in 2003, Mottaghy and colleagues used single-pulse TMS to study verbal working memory in a "two-back" task (i.e., subjects viewed a series of letters and pressed a button when the current letter matched one from two trials ago). The delay between the task stimulus and the delivery of the TMS was varied over a range of 140 to 500 ms. The authors found that working memory processes were impaired by shorter-latency TMS delivered to the parietal cortex and by longer-latency TMS delivered to the frontal cortex. This suggested that the flow of information was from parietal to frontal sites. Within the frontal lobe, TMS delivered to the right hemisphere caused disruption with shorter delays than stimulation in the left frontal region, suggesting a flow of information from the right to the left hemispheres. However, delivery of TMS did not disrupt a simple control task that did not have a working memory component, which indicated that the effects of TMS in these regions were specific to working memory processes and specific to particular intervals in time. TMS can also be used to examine relatively long-distance influences between brain regions. As shown in a 2006 study by Ruff and colleagues, TMS applied to the frontal eye fields (i.e., regions of the frontal lobes that support eye movements and visual attention) modulated activation in the early regions of the visual cortex, which in turn changed the quality of visual perceptions.

One of the most promising uses of TMS has been to determine whether regions activated in fMRI studies are essential for task performance. For example, in 2002 Rushworth and colleagues used fMRI to identify regions of the frontal lobe that were activated during two forms of task switching. In the response-switching condition, subjects switched between rules for selecting a response, while in the visual-switching condition, subjects switched between rules for selecting a stimulus. For each trial in each condition, the subject either kept or switched the rule from the previous trial. Although the two conditions evoked fMRI activity in somewhat different sets of brain regions, both activated the pre-supplementary motor area (pre-SMA) region of the medial frontal cortex. The authors thus hypothesized that this region plays an important role

in task switching. To test this hypothesis, the authors later stimulated the pre-SMA using rTMS. This disrupted both tasks, but only in trials when the subject switched from the previous task rule. When the TMS stimulator was moved over the motor cortex adjacent to the region of fMRI activity, stimulation had no effect on the task. Together with the fMRI results, these TMS data provide important converging evidence that the pre-SMA is a critical brain region in task switching, and furthermore, that its role is limited to actual task switches. While combined or parallel use of TMS and fMRI is still relatively rare, such studies provide important complementary information about the timing of brain function and causal influences on brain function.

Brain lesions

One of the earliest and most productive approaches for studying brain function was the observation of behavioral or cognitive changes associated with brain lesions. Shortly after Broca's 1861 discovery, many other effects of brain lesions were reported. In 1868, Dr. John Harlow described his observations of Phineas Gage, a railroad foreman in Cavendish, Vermont, who in 1848 suffered a horrible accident in which an explosive charge blasted an iron tamping rod through his left cheekbone and out of the top of his head. Gage not only survived the accident, and was able to walk and speak within minutes, but lived for another 12 years. However, according to later reports, Gage suffered from a dramatic change in personality: he became profane, irresponsible, and showed little regard for others. (A 2002 book by MacMillan paints a somewhat more complex picture of these personality changes.) Gage's was one of the first cases in which a profound alteration of personality was linked to a lesion within a specific brain region. Around that same time, early researchers such as the German neurologist Hermann Munk created controlled, experimental lesions in animals to make important discoveries about the organization of the cerebral cortex. Other scientists, like David Ferrier, used both lesion and cortical stimulation to study brain function in animals.

Lesion studies in both humans and animals remain central to cognitive neuroscience research. Like cortical stimulation experiments, which create transient and reversible impairments, lesion studies provide information about the necessity of a brain region for a particular function. However, lesion studies have several obvious limitations. Studies in humans depend primarily on naturally occurring lesions, such as those produced by strokes, which can be large and extend across many functional brain regions. This variability makes it impossible for investigators to assemble a group of patients with identical lesions. Furthermore, natural lesions often involve damage to white-matter pathways, thus impairing functions that are supported by distant brain regions that were undamaged but became disconnected. Some types of lesion can be studied in groups of patients with similar damage, as may occur with well-defined surgical lesions. An example is patients who have received temporal lobectomies to relieve intractable epileptic seizures. However, such patients may have suffered for many years from preexisting neurological disorders, and often continue to take powerful drugs that may alter normal brain function.

Lesion studies can also have interpretive difficulties. Unlike the positive results sometimes observed with direct cortical stimulation, lesions do not *produce* complex behaviors. Thus, the loss of function following a brain lesion does not guarantee that the damaged brain tissue was the locus for that particular function. For example, a large lesion in the primary visual cortex would impair not only basic visual perception but also many higher-order functions like object

recognition, reading, and eye gaze perception. It would be absurd to suggest that all of these visually based functions reside in the primary visual cortex, yet this region is clearly essential for every one of them. For this reason, investigators who employ the lesion approach systematically compare the effects of lesions in different brain regions on performance in various experimental tasks, in order to identify patterns of association and dissociation between brain regions.

To this end, several groups around the world have established large databases, or registries, of individuals who have brain lesions and who have been studied while performing large numbers of different tasks. For a broad overview of the registry approach, see the 2008 review article by Fellows and colleagues cited in the chapter references. One example is the Cognitive Neuroscience Patient Registry developed by Antonio and Hanna Damasio and their many collaborators at the University of Iowa. Another is the patient registry developed by Robert Knight and his colleagues at the University of California, Berkeley. These and similar registries contain both contact information and quantitative reconstructions of lesions (using structural MRI data) for large numbers of individuals with brain damage. By identifying individuals who share a particular form of damage (Figure 13.4) and testing those people using a spectrum of behavioral tasks, researchers can evaluate whether damage to particular regions contributes to changes in one or more aspects of behavior.

registry A patient database. A registry might include information about the locations of brain lesions in a large population of individuals who might then be asked to participate in experimental studies.

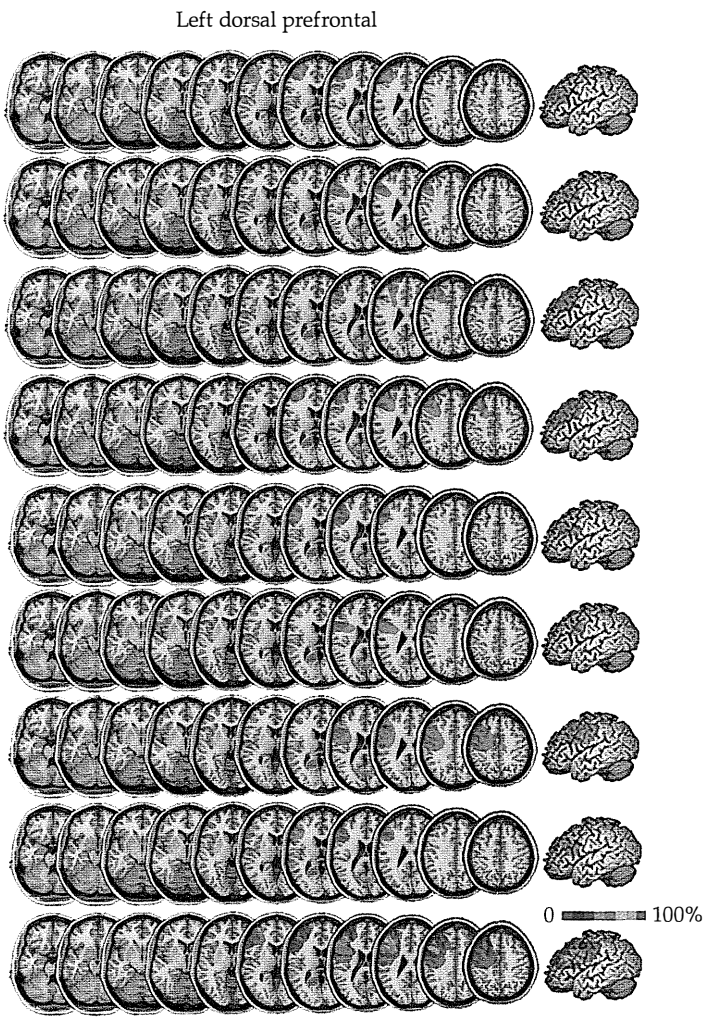

Figure 13.4 Lesion maps from a patient registry. Shown are lesions in the left dorsal prefrontal cortex of eight subjects (top eight rows). The lesions are indicated by red shading on a stack of axial MRI slices and on a surface reconstruction (at right). The bottom row shows a color-coded summary that indicates the degree of lesion overlap in this sample. (Courtesy of Dr. Robert Knight, University of California, Berkeley.)

double dissociation The demonstration that two experimental manipulations have different effects on two dependent variables. One manipulation affects the first variable but not the second, and the other manipulation affects the second but not the first.

single dissociation The demonstration that an experimental manipulation has an effect on one variable but not on a second variable.

plasticity The change in the normal functional properties of brain tissue following injury or experience.

Lesion studies have considerable value for the dissection of complex tasks into their components. In 1955, Teuber introduced the concept of the double dissociation (see Chapter 11 for a discussion of its applications to fMRI). By demonstrating that a lesion in brain structure A impairs function X but not function Y, a researcher establishes a single dissociation between the functions. But with the additional result that a lesion in structure B disrupts function Y but not function X, the researcher has established a double dissociation, and can make more specific inferences about brain function. Consider the following example. An investigator creates a model for face processing based on the hypothesis that separate processes exist for retrieving face identity and for judging emotional facial expression. Then, that investigator shows that a group of lesion patients have impaired face recognition but normal ability to judge emotional expressions. Although this result is consistent with the model, it could also merely reflect that face recognition is more difficult, and thus more easily disrupted. More conclusive support for the model would come from a second demonstration showing that damage to a different brain region impairs judgments of emotional expressions but not face recognition. The book by Shallice, listed in the suggested readings, provides additional discussion of lesion interpretation in the context of neuropsychological theory, including caveats concerning double dissociation.

Combined lesion and fMRI studies

Evidence from lesion studies can greatly extend the interpretive power of fMRI. When a process both evokes fMRI activity in a brain region and is disrupted when that region is lesioned, researchers can more readily conclude that the process relies on that brain region for its execution. The benefits of converging lesion and fMRI studies are thus similar to those of combined direct cortical stimulation and fMRI studies, as discussed earlier.

Many studies that have combined lesion analysis and fMRI in a single individual were designed to investigate the influence of a developmental lesion on a well-localized function, such as language processing in the left hemisphere. For example, in 2002, Staudt and colleagues found that individuals who had suffered perinatal left-hemisphere lesions exhibited language-related activation in the right hemisphere. From these fMRI results, the authors argued that early damage to left-hemisphere regions that support language would result in the recruitment of homotopic regions in the undamaged right hemisphere. Another example comes from the 1997 work of Schlosser and colleagues, who studied a 19-year-old patient with a large arteriovenous malformation in her right frontal and rostral parietal lobes. Since childhood, she had poor motor control but preserved sensation in the left side of her body (i.e., hemiparesis). During an fMRI session her left and right hands were alternately stroked with a brush. Strong activation was obtained in response to both types of stimulation, but stroking the left hand activated the primary sensory region of the *ipsilateral* left hemisphere (Figure 13.5). That is, her brain was reorganized so that sensations from both sides of the body were (at least partially) represented in the same hemisphere. These fMRI studies provide strong evidence for the functional plasticity of the human cortex in response to early brain injury. Note that acute lesions, such as from surgery, may lead to dramatic and permanent changes in function. An intriguing recent example comes from a 2006 study by Gaillard and colleagues, who found that the surgical removal of a word-selective region in a patient's ventral visual cortex not only altered the fMRI response to words but also led to a comprehensive reading deficit.

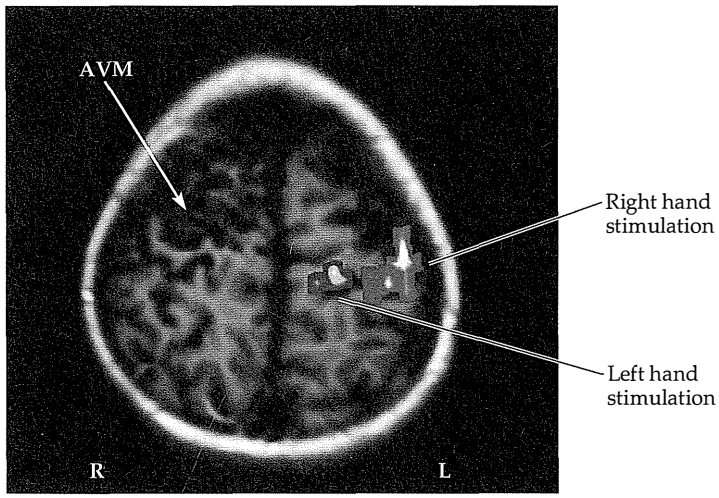

Figure 13.5 Evidence for functional plasticity from combined lesion/fMRI studies. Shown are the patterns of fMRI activations evoked by stroking the right hand (red) and left hand (blue) in a patient with a large arteriovenous malformation (AVM) in the right hemisphere. Note that the response to the left hand occurs in the left, or ipsilesional, hemisphere. (From Schlosser et al., 1997.)

Combined fMRI and lesion methods have also been used to study recovery of function in individuals who acquired lesions in adulthood from stroke or other brain injury. Using fMRI, TMS, and magnetoencephalography, in 1998 Rossini and colleagues investigated changes in the brain of a poststroke patient who had recovered significant motor function. Their results suggested that the sensorimotor cortex in the affected hemisphere was enlarged, and shifted posteriorly, compared to the other hemisphere. In a similar study conducted in 1997, Cramer and colleagues used fMRI to study 10 patients who had recovered good motor function following stroke. When the patients performed a finger tapping task, activity in the sensorimotor cortex of the unaffected hemisphere was *increased* relative to controls. Increased activation was also found in the SMA and cerebellum. These results suggest that recovery of motor function after stroke involves the increased participation of homotopic regions of the unaffected hemisphere and midline motor regions. While some activation was observed in the affected hemisphere of the stroke patients, it was restricted to the periphery of the damaged region. Because of its spatial resolution and noninvasiveness, fMRI can be used both to complement lesion studies in order to understand brain organization and to supplement lesion data in order to investigate functional changes associated with the lesions.

Thought question

What properties of fMRI may make it a poor choice for assessing function in patients with vascular lesions?

Probabilistic brain atlases

Up to this point, we have discussed two sources of structural damage to the brain: surgical excision of brain tissue, and focal lesions that make existing tissue nonviable. However, there are many other ways in which brain structure could change. Some diseases that affect the brain (e.g., Alzheimer's disease and schizophrenia) do not cause frank and focal lesions. Rather, regions within the brain of an afflicted individual may degenerate over the course of the illness. As with lesions due to stroke or surgery, volume loss in particular regions

recovery of function The improvement in a previously impaired ability over time, due to functional or structural changes within the brain.

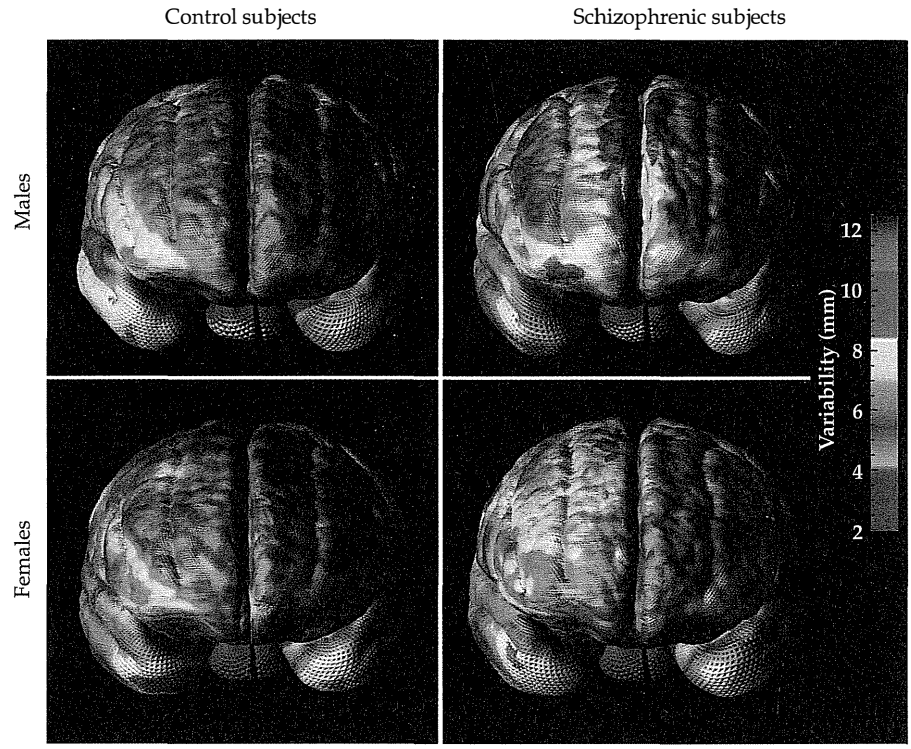

Figure 13.6 Variability in brain anatomy. These brain diagrams are overlaid with maps of variability in brain anatomy in the cortex of control and schizophrenic subjects (both males and females). Areas of high variability amongst individuals are shown in red-purple, while areas of low variability are shown in blue. Increased variability is observed in the frontal cortex for both male and female schizophrenics. (Courtesy of Drs. Katherine Narr and Arthur Toga, Laboratory of Neuroimaging, University of California, Los Angeles.)

may impair specific cognitive functions, and thus fMRI studies in these patient groups may be valuable as a prognostic indicator. Other aspects of brain structure, such as white matter integrity measured using DTI (see Chapters 5 and 11), or cortical thickness measured by anatomical MRI, may change during normal development. For example, the trajectory of change in cortical thickness can predict subsequent intelligence in children, as shown in a 2006 study by Shaw and colleagues.

New image processing techniques take advantage of large MRI databases and advanced computational methods to determine how variation in the structural properties of particular regions might predict disease states or brain function in individuals. Recall that in Chapter 8 we discussed how preprocessing fMRI data often involves the warping of the brains from individual subjects into a stereotaxic space to simplify statistical analyses across subjects. The degree to which a brain must be warped to match a normalized space might itself be of interest, because it provides a quantitative measure of regional brain variability. Investigators are using similar approaches to study structural differences between diseased and normal brains. Figure 13.6 illustrates the variability that can be found in brains of schizophrenic individuals compared with healthy control individuals. Note that the brains of the schizophrenic individuals show greater variability (red-purple colors) in several regions of the frontal lobes, including the midline. This finding corroborates results from many fMRI studies demonstrating that schizophrenic subjects show abnormal BOLD activation patterns in the prefrontal cortex, while performing a variety of tasks. Readers interested in learning more about the use of probabilistic brain atlases to study human disease are referred to the article by Toga and colleagues in the suggested readings.

Brain imaging and genomics

For a growing number of neurological and psychiatric disorders, researchers are discovering genetic variations, or polymorphisms, that are associated with increased risks of individuals developing those conditions. As researchers have begun to investigate the effects of these polymorphisms on brain function, a new field has emerged that has been named by Hariri and Weinberger as imaging genomics.

polymorphism A common variation in a gene or segment of DNA.

imaging genomics A new field that investigates the effect of genetic variation on brain structure and function.

An early and notable study conducted by Bookheimer and colleagues in 2000 used fMRI to investigate memory processes in people with and without genetic risk factors for dementia. Thirty individuals were tested, all of whom were neurologically normal and had memory scores within the normal ranges for their ages. However, 16 of the individuals carried the epsilon 4 allele of the apolipoprotein E gene (*APOE-4*), which is associated with an increased risk of developing Alzheimer's disease. The remaining 14 individuals carried the epsilon 3 allele (*APOE-3*) and thus were not at increased risk. In an fMRI experiment that involved retrieval of items from memory, the *APOE-4* group showed increased activation of the hippocampus, the parietal cortex, and the prefrontal cortex, compared with the levels of activation in the same regions in the *APOE-3* group. These structures have been implicated as important to memory in many other experiments. When a subgroup of subjects participated in memory tests two years later, the decline in their memory performance was predicted by the degree of increased activation. That is, *APOE-4* individuals who had increased fMRI activity in these regions were more likely to develop memory impairments. These results suggest that fMRI can be used to detect subtle patterns of damage that may result in later functional deficits, even before the functional impairments can be detected clinically. This study also points to the interesting possibility that increased fMRI activation may indicate compensatory processes that offset the functional consequences of the incipient disease.

More recent work has emphasized the potential role of particular neurotransmitter systems that may mediate diverse cognitive functions. As summarized in a 2006 review by Hariri and colleagues, there has been substantial interest in variation among individuals in the genes that control the synaptic reuptake of the neurotransmitter serotonin. A common paradigm involves scanning two groups of subjects using fMRI: those who possess alleles associated with higher synaptic concentrations of serotonin, and those who possess alleles associated with lower synaptic concentrations of serotonin. These different alleles have also been associated with phenotypic differences in traits like anxiety—high serotonin concentration predicts greater anxiety. Thus, many experiments have used stimuli that might evoke strong social or emotional responses (e.g., photographs of faces with different emotional expressions). In a number of studies, individuals with genetic variations that predict high synaptic concentrations of serotonin exhibited increased activation in the amygdala when shown photographs of emotional faces. This perhaps reflects the increased reactivity of that brain region to salient environmental cues in these individuals.

In summary, information about brain structure provided by stimulation, lesion, or TMS studies complements information about brain function provided by fMRI. Inferences made using one technique are improved by converging studies using other techniques. Questions about causality that are raised by fMRI results can be answered using lesion studies, just as fMRI can answer questions about large-scale systems and recovery of function that are

raised by lesion data. Furthermore, fMRI can assess the functional consequences of individual differences in brain structure and genes. Therefore, techniques that examine the consequences of changes in neuronal activity will continue to be critical for research programs in cognitive neuroscience.

Measuring Brain Function

The first direct measurements of nervous system activity were obtained in 1848 by the German physiologist Emil Du Bois-Reymond, who discovered that nerves in a frog exhibit action potentials. Shortly afterwards, Hermann von Helmholtz used action potentials to measure the speed of conduction along the frog's nerve. It is a scientific irony that Du Bois-Reymond and Helmholtz were both students of the physiologist Johannes Müller, who held the vitalist belief that activity of the nervous system was epiphenomenal and thus could not be measured experimentally. These early studies did much to explain neural transmission in peripheral nerves and muscle fibers. However, it was not until 1875 that the first electrical recordings of brain activity were published by the physician Richard Caton of Liverpool. Strongly influenced by the studies of his contemporary David Ferrier, Caton wanted to measure electrical potential changes in the cortex. Because these electrical changes were extremely weak, he used a reflecting galvanometer that had a mirror attached to its coils. As the voltage changed in the cortex of the animal subject, the position of the mirror moved very slightly, causing a visible change in the position of a reflected beam of light. This primitive amplification method made it possible to observe the very small voltage changes associated with brain activity. A half century later, the Austrian psychiatrist Hans Berger extended Caton's work by measuring continuous changes in voltage on the scalp over time. The technique that he developed became known as electroencephalography, and its measurement became known as the electroencephalogram (EEG).

Many different electrophysiological methods exist for studying different facets of neuronal electrical activity, or electrogenesis (Box 13.1). At one extreme, these methods can measure changes in ion flow across isolated patches of a single neuron's membrane, while at the other extreme, they can measure the synchronized activity of millions of neurons. We will begin our examination of direct measures of neuronal activity with a discussion of the recording of action potentials from individual neurons, a technique known as single-cell or single-unit recording. We will then discuss the recording of summated field potentials associated with postsynaptic activity. Field potentials can be measured in different ways at different scales, using both intracranial electrodes and scalp electrodes. We will conclude this section of the chapter with a consideration of magnetoencephalography (MEG), a technique that records the magnetic fields associated with neuronal activity.

action potential A wave of depolarization that travels down a neuronal axon.

electroencephalogram/electroencephalogram (EEG) The measurement of the electrical potential of the brain, usually through electrodes placed on the surface of the scalp.

electrogenesis The generation of electrical electrophysiological phenomena by a living organism.

single-unit recording Collection of data about the electrophysiological activity (e.g., action potentials) of a single neuron.

field potentials Changes in electrical potential over space associated with postsynaptic neuronal activity.

magnetoencephalography (MEG) A noninvasive functional neuroimaging technique that measures very small changes in magnetic fields caused by the electrical activity of neurons, with potentially high spatial and temporal resolution.

Single-unit recording

The most direct measures of neuronal electrical activity characterize action potentials. The primitive methods used by Du Bois-Reymond to record the action potential in 1848 were greatly advanced by the introduction of the microelectrode in the first half of the twentieth century. Microelectrodes are placed either inside a neuron or next to the neuron's cell body in the extracellular space. Studies measuring the rate of action potentials using microelectrodes, a technique known as single-unit recording, have generated some of the most important discoveries in all of neuroscience.

BOX 13.1 Electrogenesis

In Chapter 6, we described the sequence of events associated with the depolarization of a small segment of the neuronal membrane. That discussion was in the context of the resulting demands for metabolites, the supply of which form the basis of the fMRI BOLD signal. Here we consider the electrophysiological consequences of membrane depolarization. Recall that the movement of ions through membrane channels supports information processing through the integrative and signaling activity of neurons. In this context, integrative activity refers to the total pattern of excitatory postsynaptic potentials (EPSPs) and inhibitory postsynaptic potentials (IPSPs) on the neuron's dendritic arbors and cell body. EPSPs and IPSPs vary in magnitude and duration depending on the strength and timing of the synaptic input. If the pattern of EPSPs and IPSPs can be considered a computation performed on a pattern of synaptic input, then the action potential is the output of this computation. Unlike postsynaptic potentials, action potentials are all-or-none; if the summation of EPSPs and IPSPs at the axon hillock surpasses a threshold, a self-propagating action potential will be triggered. But if the threshold is not surpassed, no action potential will occur. Because the action potential carries information to other interconnected neurons, we refer to action potentials as the signaling component of information processing in the brain.

What do we mean by *electro*physiological? What properties of ions, membranes, and channels involve electricity? Atoms normally have as many negatively charged electrons as they have positively charged protons, and thus they are electrically neutral, having no net charge. However, if an atom gains or loses one or more electrons, it becomes an electrically charged ion. Na^+ is a positively charged sodium ion because it has lost an electron, while Cl^- is a negatively charged chlorine ion because it has gained an electron. Due to the selective permeability of a neuron's membrane and the action of ionic pumps, there is an unequal distribution of ions across the neuronal membrane and thus an unequal distribution of charge. An electrode placed inside a neuron at rest would record a large potential difference compared with an electrode outside the neuron, with the interior of the membrane about –70 mV relative to the outside.

Let's consider the sequence of events associated with the depolarization of a small patch of a neuron's membrane. First, there is an inward positive current caused by the inflow of positive sodium ions, creating a relative deficit in positive charge in the surrounding extracellular space. The depolarized patch of membrane thus becomes a current sink and attracts positively charged ions (Figure 1). The inrushing positive charge flows within the neuron and away from the depolarized membrane, creating an intracellular accumulation of positive charge. This, in turn, causes an outward positive current from the unexcited portions of the neuronal membrane. This outward flow constitutes a current source, from which the positive ions flow back through the extracellular space toward the sink. To conserve charge, the efflux from the

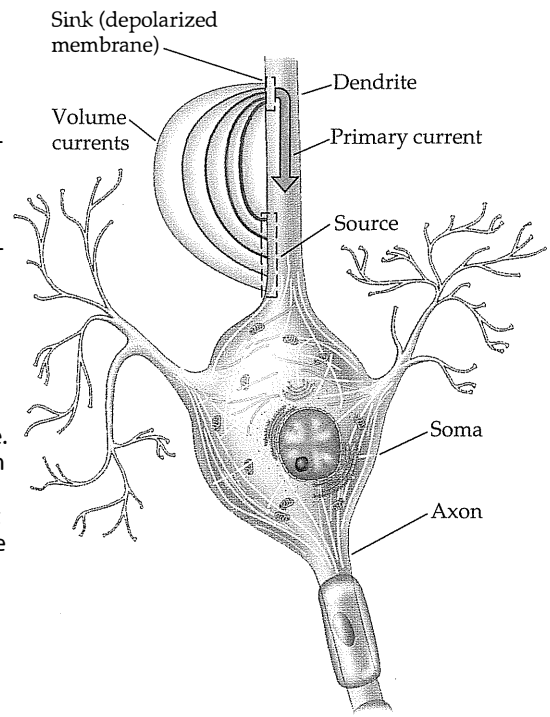

Figure 1 Current flow in a depolarized neuron. The patch of depolarization caused by synaptic activity becomes a current sink where current enters the neuron in the form of positively charged Na^+ ions. The buildup of positive charge within the neuron causes a current flow within the neuron called the primary current. To conserve charge, positive current flow exits the unexcited portions of the neuron's membrane, creating a current source. In the extracellular space, return or volume currents flow back toward the sink. Although most dense nearest the neuron, these volume currents extend throughout the brain. When viewed from a distance, the close apposition of the current source and sink approximates a current dipole.

ion A charged atom.

pump A transport system that moves ions across a cell membrane against their concentration gradient.

current sink An attractor of positive ions. A depolarized patch of neuronal membrane is a current sink because positively charged ions will flow toward it.

current source A source of positive ions.

(continued on next page)

BOX 13.1 *(continued)*

source is equal to the influx at the sink. The strong current flow within the restricted intracellular space of the neuron is called the **primary current**, while the relatively weak return flow through the much larger extracellular conductive medium (or **volume conductor**) is called the **volume current**. While the primary current is confined to the intracellular space of the neuron, the volume currents extend throughout the conductive medium that contains the neuron.

The charge at the current source generates an electric field that is directed radially outward and whose strength decays with the inverse square of the distance from the source. That is, doubling the distance from the current source increases the area occupied by the electric field by a factor of four, and thus the intensity of the electric field is only one-fourth as strong. The charge at the current sink generates an electrical field that is directed radially inward.

Because the distance along the neuron between the source and sink is very small, we can idealize this close apposition of positive and negative point sources as a **current dipole**. The electrical field produced by a dipole is simply the vector sums of the outward- and inward-oriented radial electric fields of the current source and sink. The electric field generated by the current dipole can be represented by a set of flux lines through the volume conductor that connect the point charges (Figure 2).

A potential difference can be measured in volts (or, more typically for brain electrophysiology, microvolts) between locations in the electric field. Isopotential lines, along which the voltage is con-

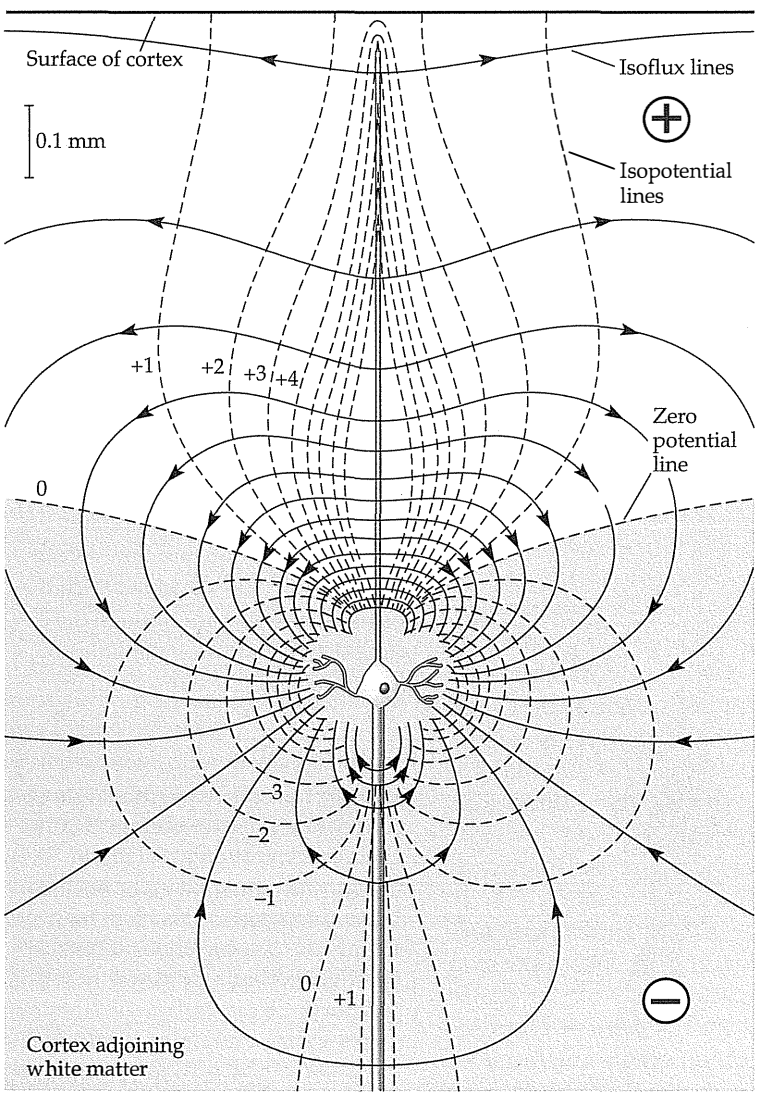

primary current The current flow within a neuron caused by the inflow of ions through ionic channels opened by synaptic activity.

volume conductor A continuously conductive medium. The brain, meninges, skull, and scalp constitute a volume conductor throughout which currents created by ionic flow can be measured.

volume current The return current through the extracellular medium that balances the primary current within a neuron.

current dipole A positive and negative point charge separated by an infinitesimal distance. A current dipole is used as a simple and convenient model for the electromagnetic fields produced by an activated neuron.

Figure 2 The extracellular electric field in the brain associated with neuronal activity. Shown is a representation of the consequences of the depolarization of the soma of a pyramidal cell. The volume currents are shown as solid isoflux lines, while the isopotential lines are dashed. The zero potential line occurs where the flux lines begin to bend inward toward the sink. Positive potentials are measured above the zero potential line and negative potentials are measured below. Note that the field weakens with increasing distance from the neuron. (After Cruetzfeldt, 1974.)

BOX 13.1 *(continued)*

stant, are perpendicular to the electric field lines. Because the charges at the source and sink are equal and opposite, the zero potential line is located at the point where the outward-directed field from the source begins to bend inward to the sink. The isopotential lines on the outward-directed side of the field measure positive voltages, while the isopotential lines on the inward-directed side of the field measure negative voltages. In the case of a depolarized neuron, the electric field produced by the source and sink can be measured by electrodes at different points in the extracellular space. For example, if depolarization occurred in the apical dendrites, then an electrode near the dendrites would record a negative potential relative to an electrode near the soma. If the soma were depolarized, as shown in Figure 2, the reverse would occur. The dipole is a convenient model for a depolarized neuron. Indeed, when observed from a distance, the fields generated by the coordinated activity of a larger assemblage of neurons can be modeled as though they were produced by a single equivalent dipole. This forms the basis for several of the techniques described later in this chapter.

In principle, the volume currents associated with neuronal depolarization can be detected anywhere within the volume conductor. Indeed, because the conductive medium around a neuron includes the entire brain and skull, neuronal activity can be detected with electrodes placed on the scalp.

apical dendrites The dendrites that are distant from the neuronal cell body. For typical pyramidal cells in the cortex, the apical dendrites extend to the superficial layers of cortex, while the cell bodies are located in deeper layers.

equivalent dipole A simplifying model that represents the electromagnetic field produced by a population of neurons as though it were produced by a single dipole.

The value of single-unit recording was powerfully demonstrated in studies initiated in the late 1950s by David Hubel and Torsten Wiesel, who were working at that time in the laboratory of Steven Kuffler at Johns Hopkins University. Using single-cell recording, Kuffler had previously demonstrated that retinal ganglion cells had a "center-surround" organization. That is, these cells increased their activity when a light was flashed in the center of a receptive field and decreased their activity when a light was flashed in the periphery of their receptive field. Hubel and Wiesel extended those studies into the visual cortex (Figure 13.7). By presenting more-complex stimuli, such as lines and edges, Hubel and Wiesel discovered that some cells in the primary visual cortex had receptive fields very different from those of retinal ganglion cells. Simple cells had a more rectangular receptive field that consisted of a central rectangular region with an excitatory response and rectangular regions above and below with an inhibitory response—as if these cells reflected the total output of a line of ganglion cells—and their rate of firing varied with the orientation of a visible line or edge. A similar approach was used to identify a second population of complex cells, which responded best to lines of a particular orientation, regardless of their position within the receptive field. Later studies built on this work to describe many important properties of the visual cortex, including its columnar arrangement and its changes during development. For these fundamental discoveries, Hubel and Wiesel received the Nobel Prize in Physiology or Medicine in 1981.

A more recent example of the value of single-unit recording in cognitive neuroscience comes from the work of Patricia Goldman-Rakic and her colleagues, who explored the properties of neurons in the monkey's prefrontal cortex during an oculomotor delayed response task. Monkeys were required to remember the location of a visual target that was briefly presented in the periph-

receptive field The part of the visual field that, when stimulated, will result in an increase in firing of a particular neuron.

simple cell A neuron in the visual cortex that responds with increased firing to a stimulus with a preferred orientation in its receptive field, and with decreased firing to a stimulus in the region surrounding its receptive field.

complex cell A neuron in the visual cortex with a larger receptive field than a simple cell and that responds to a stimulus with preferred orientation anywhere within its receptive field.

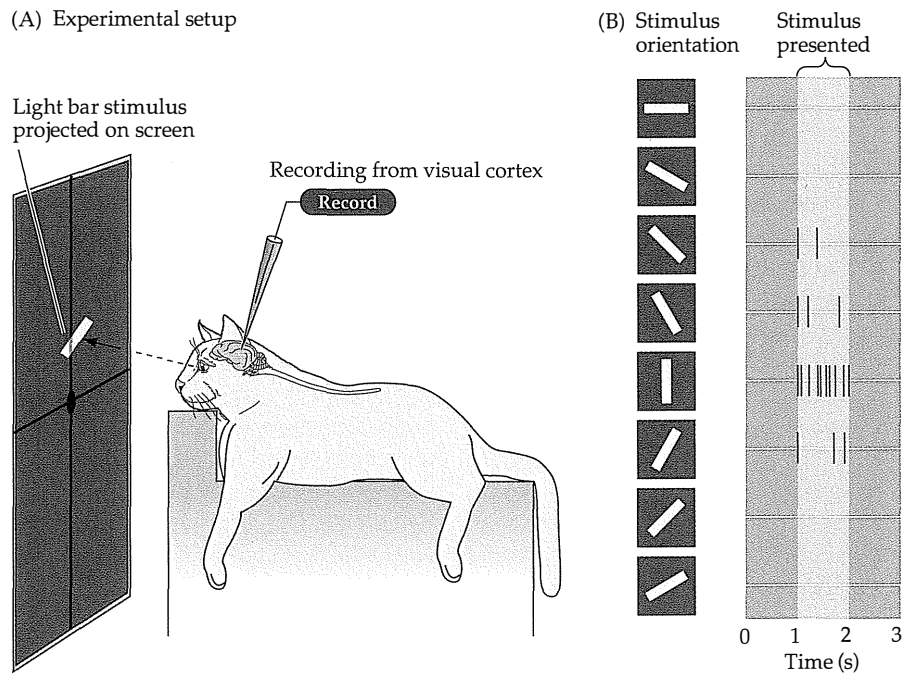

Figure 13.7 Single-unit recording. This figure illustrates the recording of a simple cell from the visual cortex of the cat. (A) The cat views a slit of light, whose orientation is systematically varied. (B) The single-unit discharge is shown for each orientation. The preferred vertical orientation is indicated by the abrupt burst of action potentials for this stimulus. Some degree of generalization can be seen by the response of the cell to slightly off-vertical orientations.

ery of their visual field and to make an eye movement to the remembered location at the end of a delay period (Figure 13.8). Shown in the figure are eight panels, each corresponding to a particular location of a visual target within space. Within each panel are a series of rows, or rasters, in which a black dot indicates the occurrence of an action potential. Each of the rasters corresponds to one trial of the delayed response task. At the bottom of each panel is a histogram that indicates the number of times the neuron fired at a particular time during the task across all trials. The spatial specificity of this neuron was striking, in that significant firing was only observed when the target was presented at the lower-left location. Even more remarkable was the fact that the neuron fired reliably throughout the delay interval, when the stimulus had disappeared and the monkey maintained the target location in memory. Because there was little to no neuronal activity in the other seven locations, Chafee and Goldman-Rakic suggested that this neuron was coding one specific location in visual space, and was not responding in a general way to the delay interval. Other neurons in the same small region of cortex responded selectively to the other visual target locations. Due to the spatial selectivity of these neurons (like the primary visual cortex neurons discussed in the previous paragraph), the researchers concluded that these neurons had memory fields, or locations in visual space about which they preferentially maintained information. The clarity of these and similar results have led to many fMRI studies of the neural basis of working memory, and interested readers are directed to the reviews by Miller and Cohen and by Curtis and D'Esposito in the Chapter References.

Limitations of single-unit recording

raster A depiction of the firing rate of action potentials by a neuron in which time is represented along the horizontal axis and a dot indicates the occurrence of an action potential.

Both the spatial and temporal resolution of single-unit recording are several orders of magnitude more precise than the resolution that can be obtained using fMRI. As can be appreciated from the above examples, single-unit recording can identify adjacent neurons that differ in their response properties (e.g.,

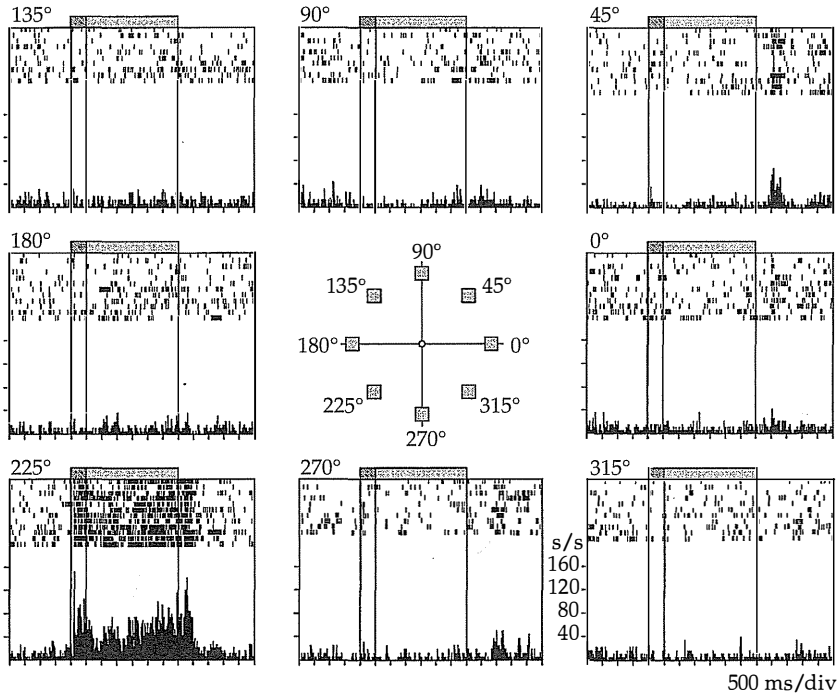

Figure 13.8 Single-unit recording in an oculomotor delayed response task. Monkeys were trained to fixate on a cross at the center of a display while a target stimulus was illuminated for 500 ms at one of eight peripheral locations. Following the disappearance of the stimulus, the monkey maintained fixation for an additional 3 s delay period. At the conclusion of the delay period, the fixation cross disappeared and the monkey moved its eyes to the remembered location of the visual target and, if correct, received a juice reward. Plotted in the surrounding panels are the single-unit responses from one neuron in the principal sulcus in the prefrontal cortex, showing that neuron's response to memory stimuli from each of eight spatial locations (as illustrated by the center map). Within each of these eight panels, the first pair of vertical lines demarcates the interval during which the visual cue was presented. The last vertical line indicates the end of the delay period. The rasters at the top of each panel indicate individual trials, while the bottom histogram indicates the firing rate over time (in spikes per second). (From Chafee and Goldman-Rakic, 1998.)

having different memory fields or responding to different aspects of a complex stimulus). In particular, the temporal resolution of single-unit recording is exquisite: each action potential of a neuron can be recorded as it occurs. Given these advantages, it is unsurprising that single-unit recording has made many outstanding contributions to neuroscience.

However, while the strengths of the single-unit recording technique far outweigh its weaknesses, the latter are still notable. Most significant is the fact that single-unit recording is an invasive technique that requires the brain to be penetrated by the recording electrode. Although single-unit recordings have been made on a limited basis in humans undergoing neurosurgery, this technique is primarily restricted to animals. A second limitation is that single-unit recording does not establish a causal relationship between the firing pattern of a neuron and the presumed underlying process. Thus, while it appears that the neuron represented in Figure 13.8 is coding one spatial location during working memory, the result demonstrates only a correlation. Would the removal of that single neuron render the animal incapable of remembering that specific spatial location? It is unlikely that working memory would be so dependent on a single neuron among the billions that constitute the monkey's brain. Also, the challenges of identifying active neurons and tracking them over time limit most studies to collecting data from only a few tens of neurons, each of which was identified based on some criteria (e.g., changing firing rate in response to some experimental manipulation). Many other neurons within the same region might not respond to the particular stimuli used in an experiment, but could nevertheless support some important function.

One way to establish a causal relationship between a brain region and a cognitive construct under study is to disable the brain region and observe whether the process of interest can proceed without the participation of the neurons in that region. Techniques for disabling brain activity were discussed

earlier in this chapter and include permanent or temporary brain lesions and transcranial magnetic stimulation. For example, many lesion studies in monkeys have firmly established that damage to the prefrontal cortex, whether permanent (e.g., caused by surgical lesions) or reversible (e.g., caused by local cooling or chemical agents), produces a selective deficit in working memory performance. Thus, the integration of converging data from single-unit recordings and lesion studies makes a much stronger case that these neurons play causal roles in working memory processes than the case made by either technique alone.

A second way to establish a causal relationship is to artificially control the firing of a neuron and observe its effect on behavior. Such an approach has been taken by Newsome and colleagues, who have used microstimulation to alter the output of neurons in the motion-sensitive visual cortex (MT/V5) in monkeys. Such neurons fire more frequently when a stimulus moves in one direction, which is often referred to as the "preferred direction" of the neuron, and thus their firing rate predicts the motion judgments expressed by the monkey. In a seminal 1994 study, Salzman and colleagues trained monkeys to perform a psychophysical task in which rewards were given for correctly indicating the direction of movement of a field of flickering dots. On most trials, dots with random motion were added to dilute the proportion of dots moving in a coordinated direction, making the task much more difficult. Yet, when electrical microstimulation was applied to neurons with the correct preferred direction, the monkeys' performance improved. These data demonstrated that increased neuronal firing provides a code for direction preference that can cause monkeys to make particular judgments in a behavioral task.

Finally, while single-unit studies are difficult to conduct simultaneously with neuroimaging techniques like fMRI, research using both techniques can be conducted in parallel or in series. Some research programs now begin with exploratory fMRI studies that are followed by confirmatory single-unit studies. Others use human fMRI experiments to test hypotheses that were generated using single-unit recording. In addition, there has been increased interest in using fMRI in non-human primates as a potential bridge between these two techniques (see the discussion at the end of this chapter).

Properties of electrical field potentials

The term "field potential" refers to the summation of extracellular excitatory and inhibitory postsynaptic potentials. We shall use the shorthand PSP to refer collectively to excitatory postsynaptic potentials (EPSPs) and inhibitory postsynaptic potentials (IPSPs). Because the electrical activity of the neuron changes rapidly based on the strength and pattern of synaptic inputs, field potentials change rapidly to reflect this input. Thus, measurements of field potentials describe the underlying integrative neuronal activity with high temporal fidelity. Field potentials can be recorded by electrodes located anywhere within a conductive volume. Intracranial electrodes touch the cortical surface or penetrate deep structures within the brain, whereas extracranial electrodes rest on the surface of the intact scalp. Either type of electrode measures PSPs using similar principles, but the relative proximity of an electrode to the neuronal activity influences its sensitivity and spatial resolution.

Field potentials measured at these various spatial scales have provided useful complementary information for fMRI studies. However, it is the prospect of integrating scalp-recorded field potentials with fMRI measurements that has excited the greatest interest. It would be highly advantageous to combine

PSP Any postsynaptic potential, excitatory or inhibitory, that results from synaptic activity.

excitatory postsynaptic potential (EPSP) A depolarization of the postsynaptic cell membrane.

inhibitory postsynaptic potential (IPSP) A hyperpolarization of the postsynaptic cell membrane.

information about the sequence of neural events obtained using field potential recording with information about the location of neural activity provided by fMRI. This combination could potentially provide an unparalleled description of the spatiotemporal activity of neurons during cognitive tasks. Despite this promise, technical and theoretical limitations have slowed progress in achieving a fusion of these techniques.

Four facts about postsynaptic potentials are most critical for the following discussion. First, unlike the very brief (less than 1 ms) duration of a typical action potential, individual PSPs can be tens of milliseconds in duration. Second, hundreds or even thousands of synapses may make contact with the dendrites and soma of a single neuron, and PSPs can occur at many nearby synapses simultaneously. Third, as explained in Box 13.1, the volume current associated with an individual PSP extends into the extracellular space with a strength that diminishes rapidly with increasing distance from the source and sink. Fourth, the volume currents associated with individual PSPs combine in the extracellular space. Thus, the signal recorded by an electrode reflects the sum of *all* of the PSPs produced at every synapse of every neuron in the brain, weighted according to their distance from the electrode.

However, the contribution of an individual PSP to a field potential is strongly influenced by the geometry and timing of its activity, such that an electrode will be much more sensitive to some aspects of activity than others. If all active neurons in a region have the same orientation and spatial arrangement, the extracellular volume currents they generate will combine to form a strong field. However, imagine that the neurons are geometrically rearranged so that alternating neurons are physically reversed in orientation. The activity of adjacent neurons would now have opposite polarity, and the resulting extracellular fields would be largely cancelled out. Cancellation could also occur if the dipoles had completely random orientations. The timing of the synaptic input to a population of neurons also affects the resulting extracellular field potential. If the synaptic input occurs at one time, as when activity is evoked by a sensory stimulus, then greater summation will occur than if the input is not synchronous. Thus, field potential recording is biased toward fields produced by synchronous inputs on regularly arranged neurons, such as those caused by simultaneous sensory input to a layer of pyramidal cells in the cortex. This synchronous activity often leads to oscillations in electrode voltage that are visible as regular waves in EEG recordings. These have been labeled according to their frequency bands (e.g., relaxation leads to activity in the Alpha band of about 10 Hz, while alert thinking leads to activity in the Beta band of 12–30 Hz).

Localizing the neural generators of field potentials

If an electrode placed anywhere in the brain will record the sum of all EPSPs and IPSPs of all synapses in the brain at any instant, how can field potential recording be used to localize active neurons? The answer is complex and relies on different biophysical concepts than those discussed for fMRI. Remember that field potentials are measured as the difference in voltage (or electrical potential) between pairs of electrodes. For intracranial electrode recordings, one electrode might be placed inside the brain while the second electrode might placed outside of the brain (e.g., on the scalp, chin, or earlobe). This external electrode is sometimes called the reference electrode, because it is relatively inactive compared with the electrode in the brain. In another arrangement, both electrodes may be placed inside the brain and the difference in their activity may be of interest. Regardless of the arrangement, the basic principles of

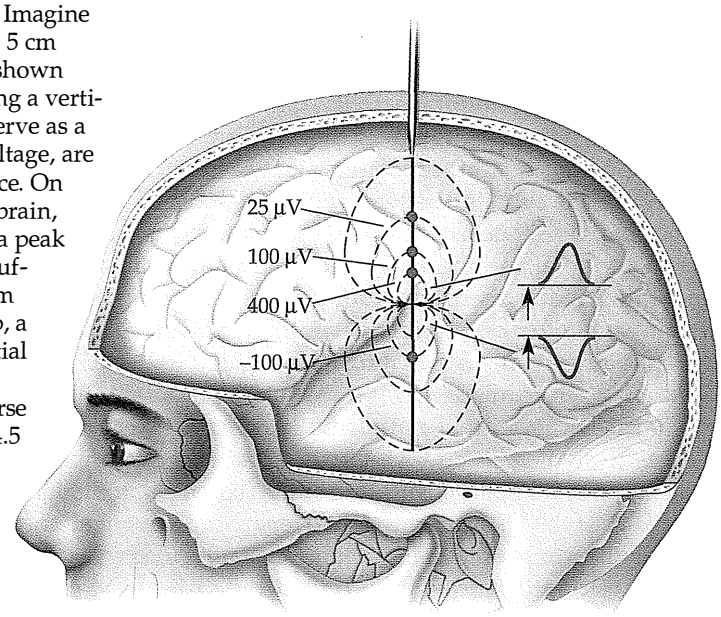

Figure 13.9 Localization of the generator of a field potential. Imagine that a stimulus evokes activity in a single ideal dipole located 5 cm below the skull's surface (isopotential, but not flux, lines are shown here). To locate the dipole, researchers lower an electrode along a vertical trajectory. A second electrode is placed on the earlobe to serve as a reference, and all measurements of potential difference, or voltage, are made between the electrode within the brain and this reference. On the first measurement, the electrode is lowered 4 cm into the brain, the stimulus is presented, and a waveform is measured with a peak potential difference of 100 μV. This single measurement is insufficient to localize the dipole. If the electrode is next raised 2 cm upward from this starting location so that it is now 2 cm deep, a potential difference of 25 μV is measured. Because the potential difference is smaller, the researchers conclude that they have moved the electrode farther away from the dipole. They reverse direction and move the electrode down 2.5 cm, to a position 4.5 cm into the brain. They now record a potential difference of 400 μV. By plotting their voltage measurements by distance, they recognize that the measurements follow an inverse square relationship and that the dipole must be located 5 cm deep. If the researchers lower their electrode past the zero isopotential line, an abrupt change in polarity occurs (indicated by the plots in green).

field potential measurement are the same. Because the volume currents associated with PSPs extend throughout the conductive medium (i.e., brain, fluid, and scalp), the magnitude of the measured potential difference between two electrodes depends on the location of the dipole generator.

Although an electrode inside the brain might record a potential difference relative to a distant electrode outside the brain, there is no localizing information in that single measurement. From a single electrode pair, a nearby dipole generating a weak field cannot be distinguished from a distant dipole generating a very strong field. To localize the neuronal generator, one must make several measurements of the field to estimate its shape (Figure 13.9). The approach of localizing active neural tissue by mapping its electric field works well as long as there is only one spatially focal population of active neurons (i.e., one equivalent dipole). If several distinct populations of neurons are active (i.e., multiple equivalent dipoles), their electric fields overlap and their locations cannot be determined with certainty from the combined field. This is known as the **inverse problem** (Figure 13.10). However, due to the quadratic decay of electric field strength with distance, a given dipole will have very different effects on nearby electrodes but will contribute similarly (and weakly) to distant electrodes. Thus, to make inferences about the locations of the dipoles generating an electrical field, we need to sample that field using a large number of electrodes. Data collected using fMRI can play an important role in this process by identifying candidate areas of brain activation that may be possible sources of neuronal activity.

inverse problem The mathematical impossibility of determining the distribution of electrical sources within an object based on the measurement of electrical or magnetic fields at the surface of the object.

Intracranially recorded field potentials

At any instant, there are immeasurable numbers of current dipoles within the brain. The spontaneous fluctuation of field potentials caused by these dipoles gives rise to the electroencephalogram, or EEG, signal. However, most EEG activity will be unrelated to the processing of the particular sensory or cognitive events of interest and can therefore be considered as physiological noise.

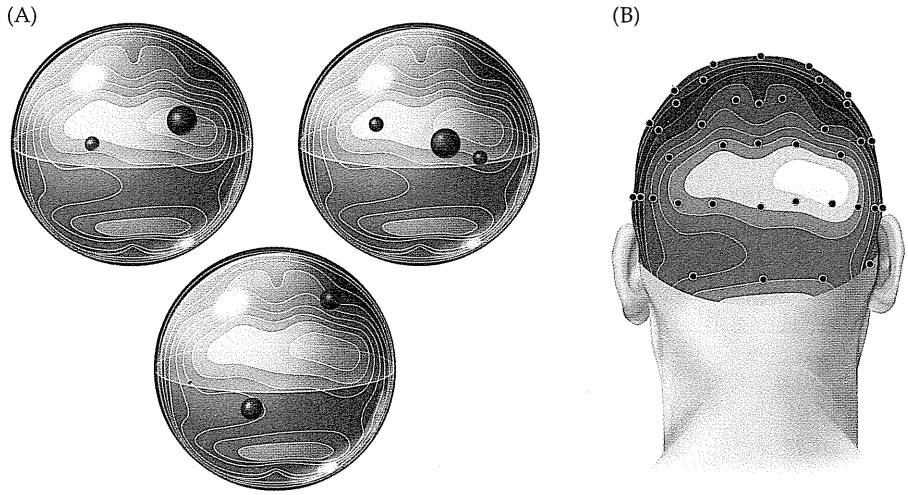

Figure 13.10 The inverse problem in ERP source localization. Scalp-recorded electrophysiological techniques (EEG, ERP) have difficulty mapping patterns of activity across the brain, due to the inverse problem (A). Three distributions of sources within a sphere are indicated. Because the brain is highly conductive, each source contributes to the total activity measured at surface electrodes. Although the activation sources differ in location, number, and intensity, they all could evoke the same electrical activity measured on the surface. Procedures for localizing sources of activity, known as electrical dipole modeling, rely on assumptions about the number and location of those sources. (B) A typical scalp voltage map recorded in an ERP experiment of visual attention. Combined fMRI and ERP studies can be used to improve inferences about the sources of the ERP generators. (ERP data courtesy of Dr. Joseph Hopfinger, University of North Carolina, Chapel Hill.)

This noise can be reduced by averaging many trials, which eliminates local field fluctuations that are not synchronized to the event of interest, leaving only the field potentials that are associated with the synchronizing event. The discussions in these sections focus on signal-averaged field potentials that are time-locked to a stimulus, or evoked potentials.

Evoked potential recordings have been used in many seminal studies of the sensory and motor organization of the brain. In the late 1930s, Clinton Woolsey and colleagues measured evoked potentials from electrodes placed on the surface of the sensory cortex (of cats and monkeys) to delineate its somatotopic organization. Although intracranial evoked potential mapping in animals has gradually given way to single-unit studies, it is still used in human studies today, usually in the context of epilepsy seizure monitoring or localization of function during neurosurgery. Intracranial recording has exceptional spatial and temporal resolution and thus can localize and record the timing of synaptic events associated with different populations of neurons (see Box 13.2 for an example). Using the techniques developed earlier by Allison and Wood, a 1997 study by Puce and colleagues compared evoked potential and fMRI techniques for localizing the hand region of the somatosensory cortex. The correspondence of localization by both techniques was quite good, suggesting that fMRI methods performed before surgery may provide similar information to cortical surface evoked potential studies performed during surgery. This conclusion was similar to that described earlier in the chapter for comparisons of direct cortical stimulation and fMRI. However, the coarse temporal resolution of the fMRI data meant that it could not be used to distinguish between separate populations of neurons within the somatosensory cortex, or determine the timing of synaptic events.

While the earliest field potential recordings using intracranial electrodes in humans investigated basic sensory processes, this technique has also been used to investigate human perception and cognition. When the eliciting event is considered to be a perceptual or cognitive event and not a simple sensory stimulus, the term event-related potential (ERP) is often applied. The deflections in the signal-averaged ERP waveform are known as ERP components, and they often have stereotypic latencies and distributions of voltage across electrode locations. One of the earliest ERP examples was reported by Sutton and colleagues in 1965, who presented subjects with simple auditory and visual stimuli that were either expected or unexpected based on cues presented shortly beforehand. When the

evoked potential A field potential that occurs in response to a sensory stimulus.

event-related potentials (ERPs) Small electrical changes in the brain that are associated with sensory or cognitive events.

ERP component A stereotypic feature of an ERP waveform, such as a peak or trough at a particular latency, that has a presumed functional significance.

BOX 13.2 Localization of Function Using Field Potential Recordings

Because the volume currents associated with synaptic activity extend throughout the surrounding conductive medium, field potentials can be recorded deep inside the brain, on the surface of the cortex, or on the surface of the skull. However, because the volume currents are denser nearer to the active neurons, the spatial resolution of field potential measurement is greatest at nearby locations. In this box, we demonstrate how field potentials evoked by brief somatosensory stimulation to the median nerve at the wrist are manifest at different recording scales, including an array of penetrating electrodes in the monkey somatosensory cortex (Figure 1A), a surface array of electrodes on the human somatosensory cortex (Figure 1B), and an array of electrodes on the intact scalp of a human (Figure 1C).

Shown in the upper left panel of Figure 1A is a sagittal view of the central sulcus. The primary motor cortex (Brodmann area 4) is on the precentral bank of the central sulcus, while the primary sensory cortex is located on the posterior bank of the central sulcus (area 3b) and the crown of the postcentral gyrus (area 1). The neurons in area 3b are oriented tangentially, or horizontally, to the cortical surface, with their apical dendrites oriented anteriorly in the direction of area 4. The neurons in area 1 are oriented radially, or vertically, with their apical dendrites oriented upwards toward the crown of the postcentral gyrus. The dots in this panel indicate locations from which field potential measurements were made. The color contour maps indicate the distribution of voltages at seven different time points after the stimulus was presented.

At 9 ms after a brief stimulation to the median nerve of the arm, the cell bodies of the area 3b somatosensory neurons have already become depolar-

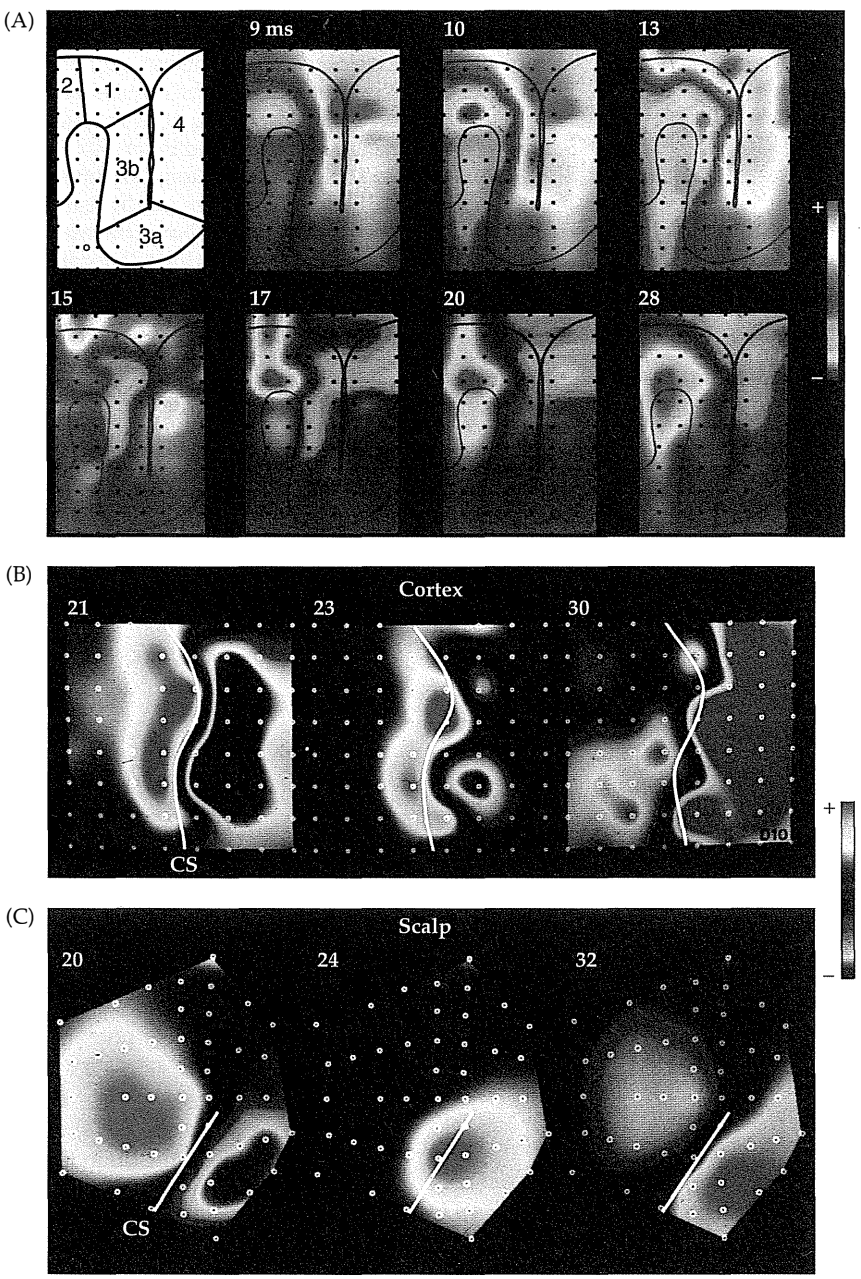

Figure 1 A comparison of field potential recordings made intracranially in the monkey (A), intracranially in the human (B), and on the surface of the human scalp (C). Anterior brain regions are shown to the right in (A) and to the left in (B) and (C). For reference the central sulcus (CS) is shown as a white line in parts (B) and (C).

BOX 13.2 *(continued)*

ized (cool colors) while the apical dendrites become polarized (hot colors). The tangential orientation of this dipolar field is made obvious by the close horizontal apposition of the red and purple blobs. By 13 ms, the cell bodies in the area 1 somatosensory neurons become depolarized. This creates a vertically oriented dipole, with positive voltages recorded directly above the crown of the postcentral gyrus and negative voltages recorded below. This radial dipole begins to fade by 17 ms. However, at 17 ms, the activation of the area 3b neurons now extends to the apical dendrites. The sink–source relationship between the apical dendrites and the soma now reverses, and the polarity of the field reverses. The reversal of the field can be appreciated by comparing the positions of the hot and cool colors at 10 and 20 ms.

This same sequence of events can be observed in field potential recordings from the cortical surface, as shown in Figure 1B. These recordings were made with electrode arrays similar to that shown in Figure 13.2. Unlike the monkey electrodes, which penetrate the brain in columns, these electrodes in the human brain are lying on the surface. The anterior brain is to the left in each panel. Because of the larger size of the human body, the initial depolarization of the cell bodies of the somatosensory neurons in area 3b occurs with a latency of about 20 ms, at which time a positive current flows from the source in the apical dendrites to the sink in the cell body. This is recorded as a positive evoked potential (called a P20) at the level of the apical dendrites and anterior electrode locations. A negative evoked potential (N20) is simultaneously recorded at the level of the soma and at posterior electrode locations. The neurons in area 1 are activated about 5 ms later, at which time a positive evoked potential (P25) is recorded directly above their apical dendrites. This occurs somewhat medially to the main axis of the area 3b dipole. And, as in the monkey, the field generated by the 3b neurons reverses polarity, as is evident at 30 ms. Finally, the same sequence of events can be recorded with electrodes placed on the scalp surface, as indicated in Figure 1C.

These cortical and scalp recordings demonstrate some facts about localizing neurons from field potential maps. As in our simple example in Figure 1, the actual location of the area 3b neurons is marked by the isopotential line. Because these neurons are oriented horizontally, the largest positive and negative fields are located to the anterior and posterior, respectively, of the active neurons. Thus, it is the shape of the field and not its maximum amplitude that is used to localize the area 3b neurons. This situation is different for the radially oriented area 1 neurons. As their associated dipolar field is oriented vertically, the neurons are located directly below the maximum field potential. Thus, the shape and orientation of the dipolar fields are important in localizing the active neurons.

subjects experienced an unexpected stimulus, there was a systematic positive deflection in the EEG waveform that peaked about 300 ms following stimulus presentation. That has since been labeled the P300 (or P3) response. In subsequent years, there have been literally thousands of electrophysiological studies investigating the properties of this component. More recently, fMRI researchers using similar paradigms have identified regions of the prefrontal and parietal cortex, among others, whose activations increase in response to unexpected events. As shown in a 2004 study by Bledowski and colleagues, distinct sets of brain regions may support different aspects of the P300 response: regions of the parietal and temporal cortex may contribute to P300s evoked by task-irrelevant events, whereas regions of the prefrontal and insular cortex may contribute to P300s evoked by unexpected events that require immediate action.

Higher perceptual processes have been investigated by Allison and colleagues, who measured ERPs from intracranial electrodes within the areas of the ventral occipitotemporal lobe associated with complex vision. In their studies, patients were shown pictures of many different types of objects, including faces, flowers, words, and scrambled objects that maintained their low-level visual properties but were unrecognizable. Faces, but not other stimulus categories, evoked focal ERPs from the surface of the fusiform gyrus (Figure 13.11). Direct

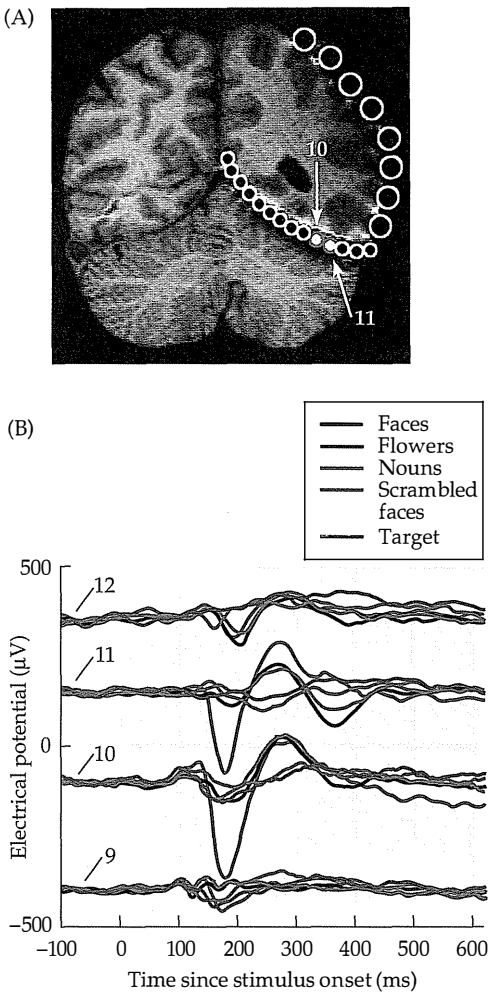

Figure 13.11 Intracranial recording of field potentials. (A) A coronal MR image that illustrates the locations of subdural electrodes in a single patient. The electrodes were contained within a sylastic strip with an interelectrode distance of 5 mm that crossed the surface of the fusiform gyrus (at electrodes 10 and 11). (B) Changes in signal-averaged field potentials over time, for electrodes 9, 10, 11 and 12. Signal-averaged field potentials are superimposed for several stimulus categories. Large focal negative field potentials with a latency of about 200 ms were evoked by the faces (red line) but not by the other stimulus categories. These face-specific ERPs were largest in the fusiform gyrus. Note, however, that electrodes only 5 mm distant from either side of these two electrodes did not record face-specific potentials.

cortical stimulation of the same region produced transient prosopagnosia and face hallucinations in some patients. In 1997, Puce and colleagues compared the location of this face-specific region to that identified by fMRI. The study was conducted by performing both procedures in each of two patients, although not simultaneously. Good correspondence was obtained between the location of the face-specific ERPs and fMRI activation by faces. So, if we know that fMRI and ERP activity are both present in a brain region, how can we know which of the sequence of field potentials measured in that location contribute to the BOLD signal? Note that electrodes within the fusiform gyrus revealed several sorts of field potentials. Early in processing is observed a face-specific potential, known as the N200, that reflects a negative change in polarity about 200 ms after stimulus onset. This early response may share some neural generators with a component known as the N170 that is measured using scalp-related ERPs. There are also later and long-lasting face-specific changes in the ERP signal that occur after about 600 to 800 ms; the onset of this activity can be seen in Figure 13.11B for Electrode 10. One possible interpretation for these two forms of activity is that the early potential reflects the initial perceptual processing of the face, while the later potential represents recurrent or feedback influences from higher brain regions. Under this idea, different functional processes are not separated in space but are separated in time.

To evaluate whether this model of fusiform function is correct, one must manipulate some aspect of the stimulus that would affect one functional process but not the other. For example, recognition of a face may be supported by completely different brain regions, but the results of that distant processing may modulate the activation of the fusiform gyrus. So, an experimenter could manipulate such things as the identities of presented faces, attention to face identity, or memory of face identity. If the fMRI activation in the fusiform gyrus reflects the later potential, then variation in face identity may cause changes in the BOLD signal and in the later evoked potential, but not in the N200. Because a psychological construct may be associated with some aspects of neural activity (e.g., BOLD signal change) but not others (e.g., the N200), converging operations are critical. For example, a researcher who observes an fMRI response in the fusiform gyrus to judgments of face identity might infer that this response reflects neuronal activity at the time of the most prominent face-specific ERP, that is, at 200 ms. Thus, fMRI data considered in isolation may lead to the premature conclusion that judgments of face identity occur early in time within the fusiform gyrus. Although hypothetical, this example reflects current debates concerning the sequence of events associated with face processing in the brain, including the effects of directed attention, face memory, and emotional face expression. Since great care must be taken in interpreting the timing of events when only fMRI evidence is available, intracranial electrode recordings can provide an important complementary source of information.

Scalp-recorded field potentials

Because the skull and scalp are conductive, the field potentials generated in the brain can also be recorded from arrays of electrodes placed on the scalp. Unlike intracranial field potential studies, which can only be conducted within a limited clinical context, extracranial (or scalp-recorded)

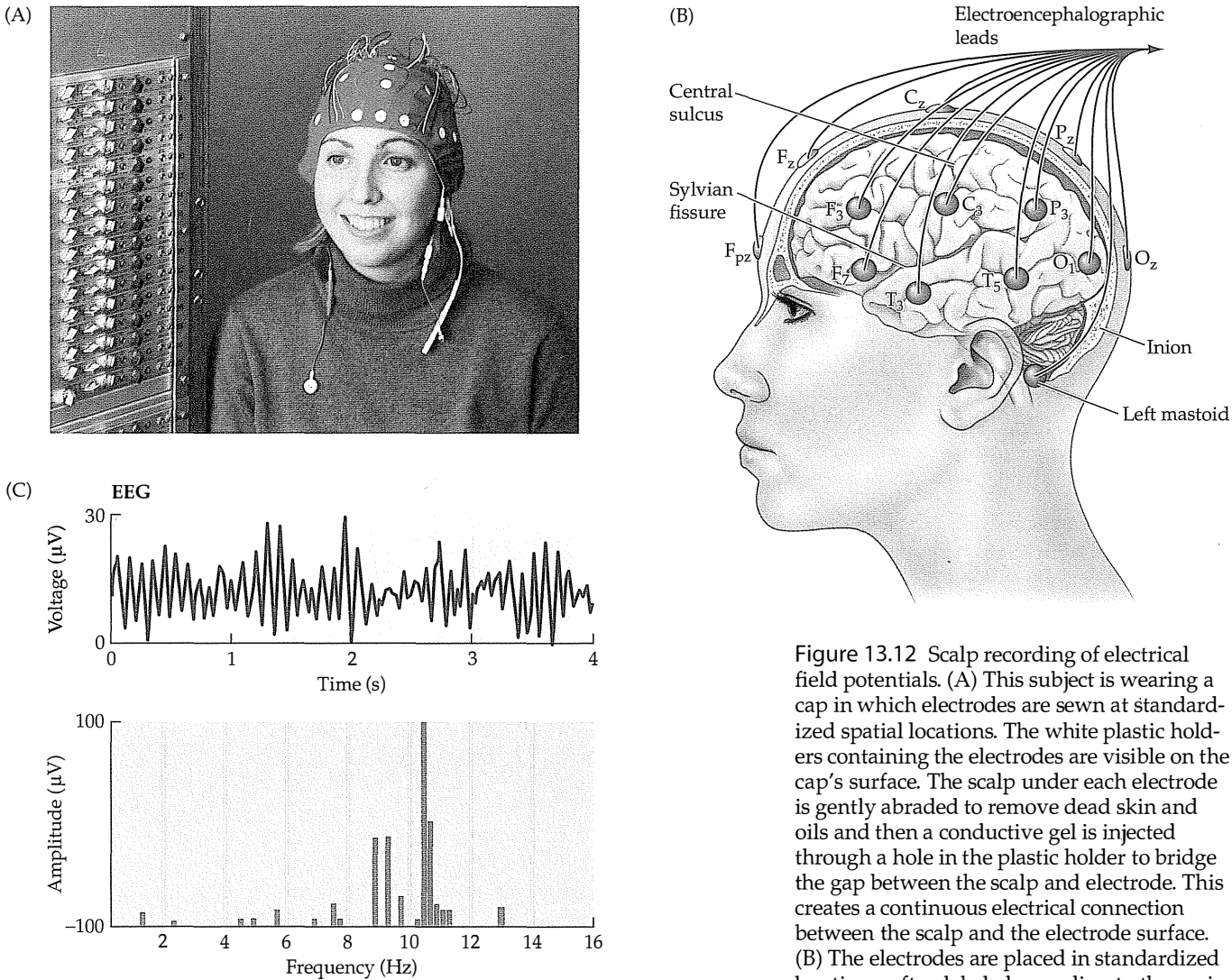

Figure 13.12 Scalp recording of electrical field potentials. (A) This subject is wearing a cap in which electrodes are sewn at standardized spatial locations. The white plastic holders containing the electrodes are visible on the cap's surface. The scalp under each electrode is gently abraded to remove dead skin and oils and then a conductive gel is injected through a hole in the plastic holder to bridge the gap between the scalp and electrode. This creates a continuous electrical connection between the scalp and the electrode surface. (B) The electrodes are placed in standardized locations, often labeled according to the position on the skull. Typical electrode location names are shown here. The potential difference between each electrode and a reference (here, on the left mastoid, behind the ear) is recorded and amplified by a factor of tens of thousands by a bank of amplifiers, as shown on the left in A. (C) The resulting time-varying signal is known as the electroencephalogram, or EEG. Shown is typical ongoing EEG activity in a normal subject who is awake with eyes closed. The regular 10-Hz oscillatory activity, shown as a function of time in the top panel and as a function of frequency in the lower panel, is within what is known as the alpha EEG frequency band. For many cognitive experiments, the EEG signal is recorded by a computer and signal-averaged with respect to stimulus or response events. The resulting averages are called scalp-recorded evoked potentials or event-related potentials (ERPs).

field potential studies are conducted with normal volunteer subjects in hundreds of laboratories around the world. The electrodes are placed at standard locations on the scalp surface, either one at a time using adhesives or via a stretch cap with electrodes at standard locations (Figure 13.12). A typical electrode cap might include 64 electrodes, although some may have 128 or more.

Researchers are interested in identifying ERP components that are associated with various aspects of language comprehension, memory, executive processing, attention, face perception, and dozens of other processes. Based on these components, researchers have developed process models that take advantage of the high temporal resolution of ERPs to predict the sequences of functional operations that occur during complex behaviors. As we noted in our introduction to cognitive neuroscience earlier in this chapter, these process models may have considerable value for understanding cognition, even if information is lacking about where these operations occur within the brain. This makes ERP recording a valuable tool for cognitive neuroscience research.

BOX 13.3 Combining fMRI and EEG/ERP techniques

All methods for noninvasively measuring brain activity in humans, including fMRI, have advantages and disadvantages. As noted throughout this textbook, a strength of fMRI is its excellent spatial resolution, which allows the identification of activated regions with better than a one-centimeter resolution. Yet, fMRI only provides temporal resolution on the order of seconds. Since many aspects of neuronal activity occur much more rapidly, on the order of a few tens of milliseconds, fMRI data contains relatively limited information about the sequences of the underlying neuronal events (see Chapter 7 for examples). In contrast, electrical recording techniques such as the measurement of event-related potentials (ERPs) or examining changes in the power frequency of the electroencephalogram (EEG), can resolve changes in evoked brain activity with millisecond precision, but give only coarse information about the spatial distribution of that activity. Because fMRI and ERP/EEG techniques have largely complementary strengths and limitations, combining these methods may provide a more comprehensive picture of brain function (see Figure 1 for an example).

There are two primary approaches for combining these techniques: parallel EEG-fMRI and simultaneous EEG-fMRI. Parallel studies generally involve the collection of data sequentially, using both methods in the same subjects performing the same tasks, usually in an event-related design. For an example, see the 2005 article by Busse and colleagues cited in the references. Most studies use relatively rapid event-related designs, so that there is sufficient power to identify effects associated with each event type. This can introduce problematic overlap between the neural responses evoked by successive stimuli, both because of the sluggishness of the hemodynamic response and the latency of some ERP components. To mitigate the response overlap, researchers typically randomize stimuli and use algorithms that can extract the response associated with one event within a rapid sequence. Note that similar sorts of procedures underlie fast event-related fMRI analyses more generally. The fMRI data provide information about the locations of activation that can improve the spatial inferences drawn from EEG data. In most such studies, the clusters of significant fMRI activation define a set of possible sources for the observed ERP effects. These a priori constraints substantially increase the likelihood that the source analysis algorithms will converge on an accurate solution. While parallel EEG-fMRI studies have made many advances, they have intrinsic limitations. They assume that the extracted brain activity recorded in the separate sessions reflects reasonably similar cognitive processes. Furthermore, they only allow researchers to draw conclusions about average activity observed during performance of a task, but not about trial-to-trial variation in activity.

Potentially more powerful is the simultaneous collection of ERP/EEG and fMRI data. This provides the ability to compare directly the fMRI activation and ERP activity evoked by each event—greatly increasing the power of comparisons between these different types of data. The primary disadvantages of simultaneous EEG-fMRI studies are technical. All electrodes and wires must be MR compatible and the electrode cap must be comfortable enough (and small enough) for extended wear in the confined space of the MR scanner. Placing electrodes on the surface of the scalp can cause artifacts in the MR images. And, the rapidly changing currents in the MR gradient coils induce electric currents in the ERP recording hardware, which in turn cause large and problematic artifacts in the recorded electrophysiological signal. One approach for minimizing these artifacts is clustered (or sparse) acquisition. This involves collecting the fMRI data dur-

forward solution The direct calculation of the electric and magnetic fields that would occur at an array of sensors based on a given distribution of dipoles with known orientations and magnitudes.

Given the topic of this textbook, our discussion of scalp ERPs is motivated by their potential for complementing fMRI studies. See Box 13.3 for an extended discussion of the technical and conceptual challenges of combining these techniques. If we know the precise spatial configuration and strength of the equivalent dipoles active at a particular instant, then it is possible to compute the exact scalp distribution of potential that would result. This mathematically tractable process is known as the **forward solution**. Furthermore, the temporal sequence of neuronal events, even those separated by mere milliseconds, changes the scalp distribution of the electric fields in predictable ways. If fMRI can tell us the exact location of all brain regions activated by a stimulus, if we

BOX 13.3 *(continued)*

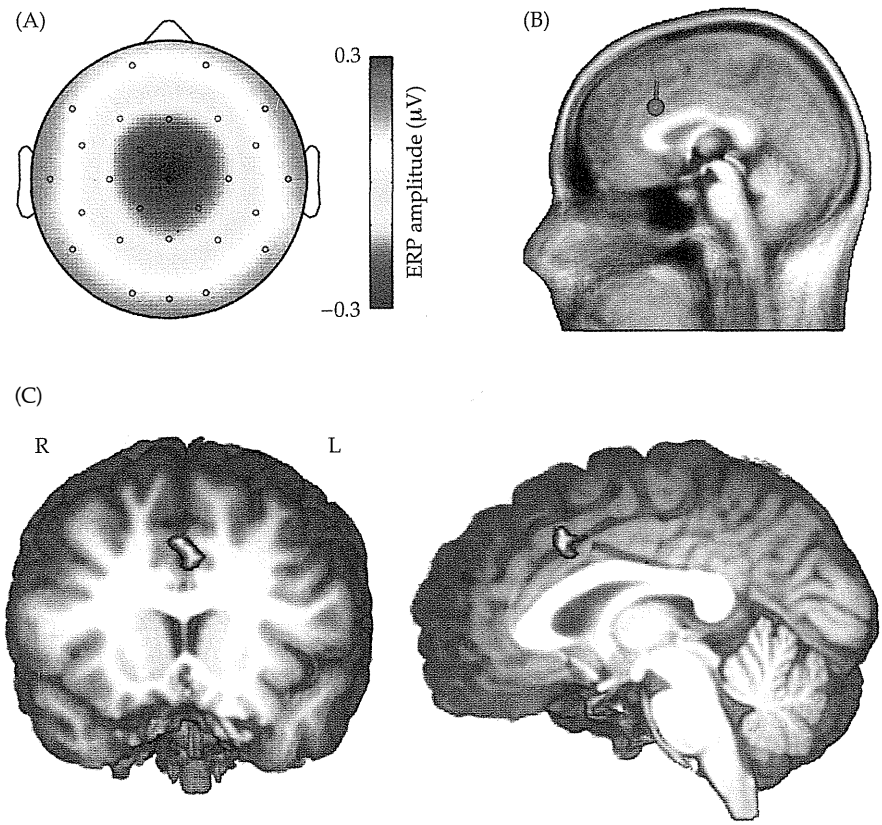

Figure 1 Simultaneous acquisition of fMRI and ERP data in a cognitive experiment. Subjects performed a response incompatibility task in which they had to respond with a left or right button press according to the direction of an arrow in the middle of a screen. In half of the trials, that arrow was preceded 80 ms earlier by an arrow cue pointing in the same direction (compatible condition), while in the other half of the trials, the arrow cue pointed in the opposite direction (incompatible condition). (A) Compared with correct responses, errors on incompatible trials evoked a centrally located ERP component whose peak occurred shortly after the button press. (B) The estimated source generator of the ERP was the anterior cingulate gyrus (red circle; tail indicates dipole direction). (C) The authors then used the amplitude of the ERP response on each trial to predict the amplitude of the fMRI hemodynamic response. They found a significant correlation with voxels in the anterior cingulate gyrus (shown in two views), thus providing strong and converging evidence that this region was associated with task performance. (After Debener et al., 2005.)

ing part of the TR, which is typically made somewhat longer, leaving an open period when the gradients are not changing and the electrophysiological data can be acquired without artifacts. Alternatively, filtering algorithms can estimate and remove the artifactual activity. Another challenge comes from the effects of physiological noise: pulsations associated with blood flow can cause movement of the EEG electrodes inside the magnetic field of the scanner. Although these technical complexities of the simultaneous-recording approach have thus far limited its application and thus its impact, these difficulties are steadily being overcome. Accordingly, the simultaneous-recording approach is becoming more practical and will undoubtedly make major contributions to the field of cognitive neuroscience.

know the orientation of the active neurons in those regions, *and* if we know the precise time course of activity in those regions, then we should be able to calculate the resulting scalp electric fields using forward solution techniques.

While this would be an impressive technical feat, its successful implementation depends on us already knowing everything about the spatiotemporal sequence of neuronal activity. What if you measured the electric field at the scalp? Could you then calculate the spatial configuration of neural generators and the temporal sequence of their activation? This reverse operation, computing the spatial configuration of dipoles from knowledge of the scalp distribution of voltage, is known as the inverse problem, introduced previously. If

the inverse problem could be solved, the need for localizing techniques like fMRI would be greatly reduced, as scalp-recorded ERP studies would provide complete information about both temporal and spatial properties of neuronal activity. If we know for certain that only one dipole is active, we can solve for its location from an adequate sample of its potential distribution on the scalp. However, in the more likely event that many dipoles are simultaneously active, this approach will not work, because different configurations of dipoles can create the same distribution of voltage at the scalp. Thus, the inverse problem has no unique solution.

The inverse problem applies to all field potential recording, not just scalp ERPs. However, in intracranial recording we can move our electrode so close to the active neurons that the contributions from distant dipoles are negligible – making it appear as if only one equivalent dipole is active at each electrode. For scalp recording, all electrodes on the scalp are, in essence, distant from all dipoles in the brain. This problem is compounded by the presence of the skull, which has a much higher electrical resistance than the brain and greatly reduces the spatial resolution of scalp-recorded ERPs. Even though no algorithm can provide a unique solution to the inverse problem, many powerful techniques have been developed to create approximate solutions by incorporating simplifying assumptions. Readers interested in additional details on this topic are directed to the paper by Baillet and colleagues listed in the suggested readings.

What if the spatial configuration of dipoles was known in advance? Under such conditions it would be possible to use the scalp ERP data to estimate the temporal changes in the strength of those dipoles and thus generate a time course of activity for each brain region. It has been asserted that fMRI activations may be used to provide the locations of the dipole generators, and thus scalp-recorded ERPs could provide information about the dipole time courses. In 1998, the validity of this approach was tested by Liu and colleagues using Monte Carlo simulations. Their modeling attempted to account for two potential problems in combining fMRI and electrophysiological measurement: that some active neural generators would not be represented by an fMRI activation, and that an fMRI activation might not be associated with neural activity. The results of their simulations were encouraging, and the authors suggested that fMRI might be useful for seeding models of dipole structure.

Magnetoencephalography

In the prior section on field potentials, we explained how electrophysiological methods could be used to localize neuronal activity by measuring electrical field potentials. A current flowing through space gives rise to both an electric field and a magnetic field. The neuroscience technique for measuring these magnetic fields is magnetoencephalography, or MEG. The magnetic signals produced by neuronal activity are extremely weak, on the order of 100 femtoTesla or fT (an fT is 10^{-15} Tesla). To record these weak fields, MEG scanners use very sensitive coils known as superconducting quantum interference devices, or SQUIDs, that detect magnetic flux. In early studies, a single SQUID sensor attached to a gantry was moved systematically over the skull to make sequential measurements of the magnetic flux. In modern MEG systems, hundreds of sensors are housed in a helmetlike device and measurements are made simultaneously (Figure 13.13).

evoked magnetic fields (EMFs) A change in the MEG signal that occurs in response to a particular stimulus. An EMF is the magnetic equivalent of an evoked potential or event-related potential in EEG.

Despite the difference in instrumentation, MEG studies are very similar in practice to scalp-recorded electric field potential studies (i.e., both EEG and ERPs). Just as ERPs can be obtained by time-locked averaging of the EEG waveform, **evoked magnetic fields**, or **EMFs**, can be identified by time-locked averaging of the MEG waveform. Moreover, MEG recording has a significant advan-

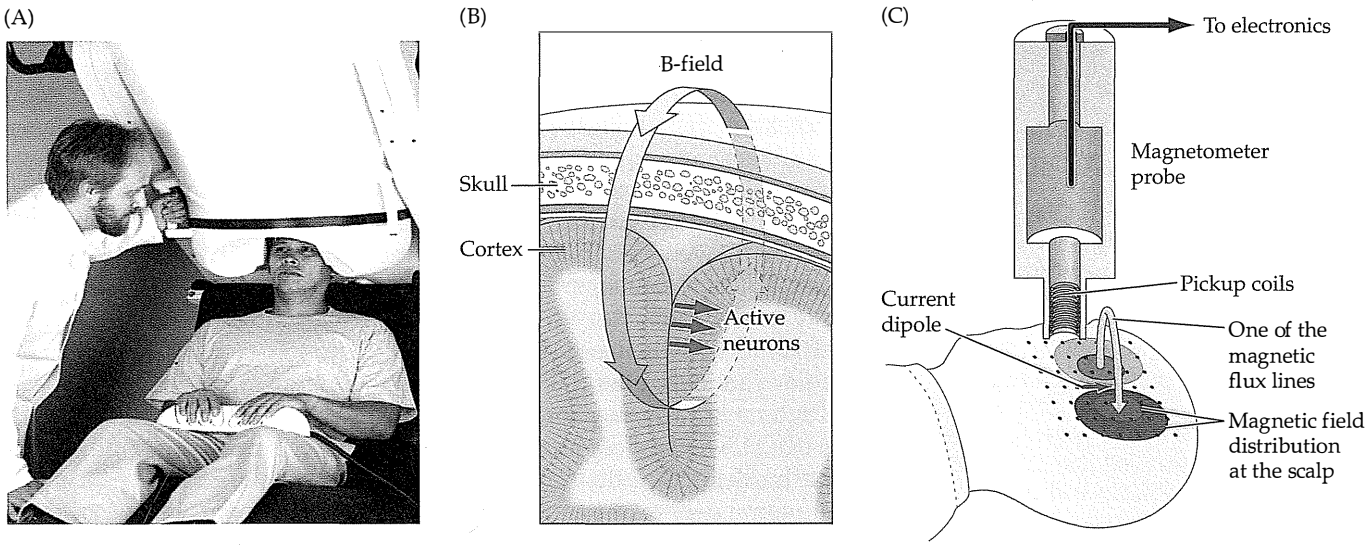

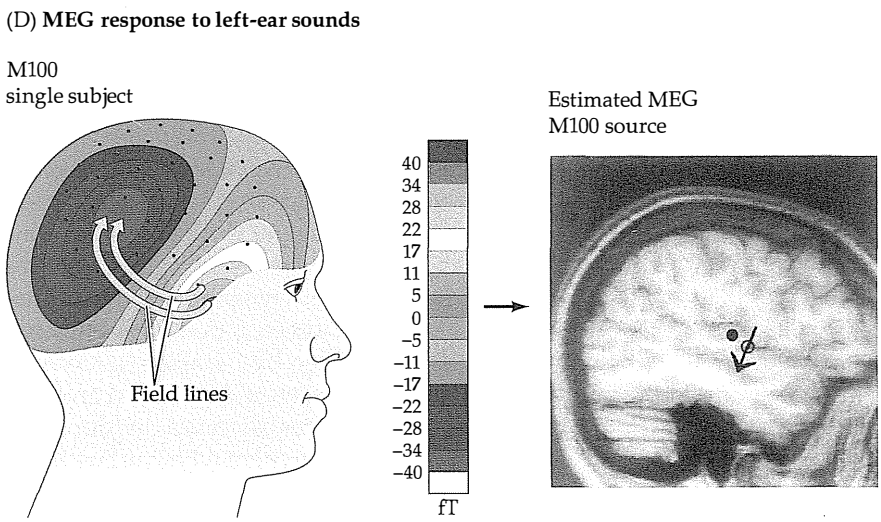

Figure 13.13 Magnetoencephalography (MEG). (A) Shown is a modern MEG system with 248 MEG sensors plus additional channels for noise reduction and simultaneous EEG recording. The sensors are located in the helmet close to the subject's head. The SQUID sensor devices require cryogens contained in the large thermos-like dewar to maintain superconductivity. (B) Just as an electrical current in a wire creates a circular magnetic field, dendritic currents in the cortex produce circular magnetic fields that can penetrate the scalp. The fields most easily measured are generated by neurons in the sulci, because those fields penetrate the scalp and can be detected by a magnetometer outside the skull. Conversely, fields generated by neurons in gyri tend to be parallel to the scalp and thus are more difficult to detect. (C) By placing these magnetometer sensors adjacent to the scalp, the highly sensitive detector coils can identify the changing magnetic flux from active neurons that penetrates the skull. (D) Distribution of the magnetic fields over the head of a normal subject, showing the changes in field strength evoked by an auditory stimulus around 100 ms after its presentation (i.e., the M100 component). The MR image in the right panel shows the estimated location of the source neurons derived by dipole source analysis. (A, courtesy of Dr. Ken Squires, 4D Neuroimaging; D after Woldorff et al., 1999.)

tage compared with scalp-recorded ERPs; because magnetic fields are unimpeded by the high resistance of the skull, they can be measured with higher spatial resolution than electric fields. In that sense, MEG and EMF measurements are more similar to direct cortical recordings than to scalp recordings, although MEG is not immune to the inverse problem.

Unlike electrophysiological methods that depend on volume currents, MEG depends mainly on the primary current that extends along the long axis of the neuron and is very sensitive to the neuron's orientation. In a spherical medium, like that approximated by the skull, the magnetic fields generated by a radially oriented dipole cannot be detected outside of the head. Thus, if the primary current does not have a component that is tangential to the surface of the skull, it cannot be detected by MEG. This can be both an advantage and a disadvantage. It is an advantage in that radially oriented neuronal populations can be ignored in modeling the generators of magnetic fields, and thus the models are simpler. It is a disadvantage in that MEG does not provide a complete description of neuronal activity (e.g., it is largely insensitive to activity in neurons at the top of gyri). For this reason, MEG and EEG measurements are often obtained simultaneously.

Similar strategies have been advanced for combining EMF and fMRI studies as have been developed for combining ERP and fMRI. For example, a 1999 study by Ahlfors and colleagues combined fMRI with MEG to examine the neural response to a sudden change in perceived motion. They used fMRI to identify several regions within the visual cortex: the primary (V1) and secondary (V2) visual cortices, and a motion sensitive area (MT+). The fMRI-derived location of the MT+ activation matched that of the peak EMF response during a time range of 130 to 170 ms and again at about 260 ms. In contrast, EMF responses from V1 and V2 were very small, with peak activities at about 200 to 260 ms. As these activations were longer in latency than the initial activity for area MT+, they may reflect feedback from other areas. This latter conclusion, based on the EMFs, is important, because fMRI data alone suggest that activity in V1 and V2 may be early in the anatomical sequence of motion processing.

To date, relatively few studies combine measurements of EMFs or ERPs with fMRI. However, despite the significant obstacles related to ambiguities in dipole modeling solutions, the addition of fMRI data to constrain the modeling of neural generators and to infer their time courses of activation holds much promise. The temporal ordering of neuronal activity in a widespread pattern of fMRI activations would be a tremendous leap forward in the modeling of complex sensory, motor, and cognitive tasks.

Using fMRI with non-human primates

The fMRI studies described so far in this book have been restricted to human subjects. Yet in principle, other animals could serve as research subjects. Within the past few years, a handful of laboratories have begun fMRI studies of non-human primates, primarily monkeys (e.g., the rhesus macaque, *Macaca mulatta*). Although fMRI is not necessary for the in vivo study of the animal brain, given the power of intracranial electrophysiology, it does provide some important advantages (see the commentary written by Paradiso in 1999 for additional discussion). First, and most importantly, it can link human and animal research. In all fields of science, technical advances can cause divisions that are based on methodology rather than topic. Researchers who conduct electrophysiological studies of decision making in monkeys may communicate with other monkey electrophysiologists but not with researchers using human neuroimaging. Studies using fMRI in monkeys can bridge the gap between human fMRI and monkey electrophysiology, allowing their results to be more easily integrated. This may be particularly important for topics like vision, whose basic neural organization was established primarily using animal electrophysiology.

Second, the use of fMRI in animals provides information that can compensate for the limitations of other techniques. In many ways, intracranial electrophysiology is considered to provide the clearest evidence for the function of a brain region, in that implanted electrodes can provide direct information about neuronal activity. However, each electrode records activity from only a small brain region (in some cases a single neuron), and therefore a breadth of spatial coverage is sacrificed. Using fMRI to guide subsequent electrode placement could substantially improve the efficiency of electrophysiological research. And, since fMRI does not require surgery (e.g., to implant electrodes), it may have some ethical advantages for some forms of exploratory research.

Third, animal fMRI studies can inform human fMRI work, even though both brain anatomy and cognitive function differ between species. More data can be collected in animal fMRI studies than is typical in human research, given

that the same animal could participate in a large number of experimental sessions. Thus, functional SNR could potentially be much higher in animal fMRI, benefiting studies with more experimental conditions or with parametric changes in an independent variable. Using fMRI in monkeys also provides an opportunity to introduce other concurrent manipulations, such as simultaneous electrophysiological recording, use of contrast agents, or evaluation of drug effects. While these manipulations may not be practical in human volunteers, they may be conducted under the guidelines for acceptable care and use of laboratory animals.

The first studies using fMRI in nonhuman primates were published in 1998 by two groups who simultaneously conducted very similar experiments. Stefanacci and colleagues recorded fMRI BOLD data from the visual cortex of a rhesus monkey during a passive viewing task. The animal lay in a prone (or "sphinx") position within a specially designed apparatus, which was itself contained within a local gradient coil inside a standard clinical 1.5-T MRI scanner (Figure 13.14). The animal's head was fixed into place using a head post, so that it could look down the scanner bore at a display screen. A mock scanner was used over a period of a month to familiarize the monkey with the confinement and noise levels of the scanner. During the scanning sessions, the monkey watched a video movie that was presented in a 16 s on/16 s off blocked design. The monkey also periodically received a squirt of juice as a reward for staying still during the session. Using scanning procedures similar to those

Figure 13.14 Collecting fMRI data in the monkey. Using fMRI with nonhuman animals poses problems, particularly when they are awake and performing a task. This figure shows one of the first successful fMRI experiments with monkeys. A rhesus macaque monkey was placed in a special primate chair that was turned sideways to fit into the bore of a standard human 1.5-T scanner (top). The animal watched a movie presented in a blocked on/off design. Significant BOLD activity was found in the temporal (A) and occipital (B) lobes. Researchers noted that there were substantial problems with head motion, due in part to the use of scanning and restraint hardware that were not designed specifically for monkeys. (From Stefanacci et al., 1998.)

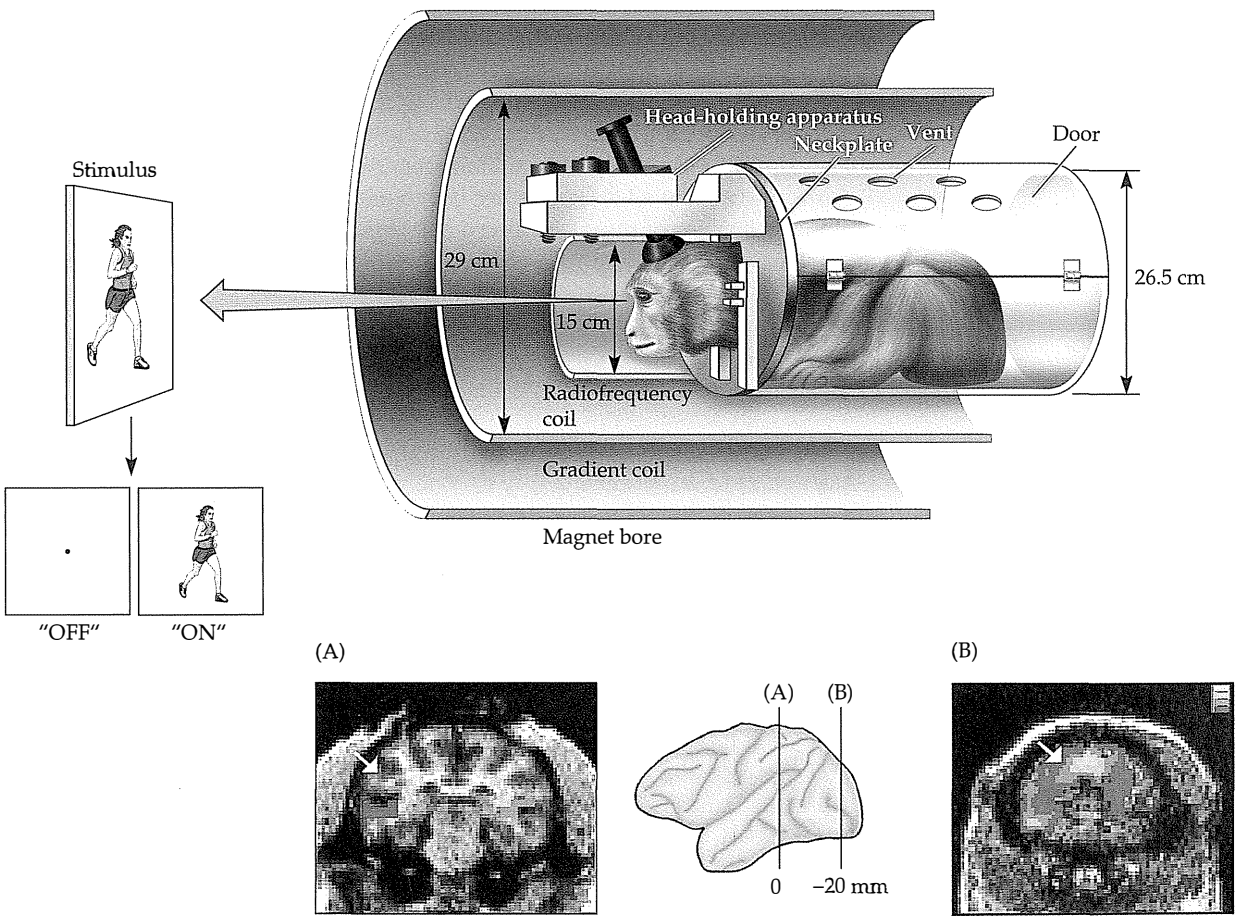

used in human studies, the authors found significant activation in occipital visual regions, as well as in higher visual regions within the superior temporal gyrus. Another study by Dubowitz and colleagues used a similar apparatus and visual stimulation paradigm. Their results mirrored those of Stefanacci and colleagues, in that they were able to identify regions of significant activity in the visual cortex.

Though highly exploratory, these early studies demonstrated the feasibility of collecting BOLD fMRI data in monkeys. Subsequent studies from these groups and others have replicated the results, while suggesting topics for future research. One area that holds particular promise is the use of exogenous contrast agents to increase SNR. Recall from Chapter 7 that injection of a highly paramagnetic substance into the bloodstream causes susceptibility-related signal loss on T_2*-weighted images. Because the magnitude of this signal loss depends on the total amount of the contrast agent that is present in a voxel, it serves as an index of local cerebral blood volume. While exogenous contrast agents are not practical for most human fMRI studies given the noninvasiveness of standard BOLD measurement, they may offer significant advantages for studies in nonhuman animals. As an example, a 2002 study by Leite and colleagues demonstrated that the use of an exogenous contrast agent (monocrystalline iron oxide nanoparticles, or MIONs) increased functional sensitivity by a factor of two to three over BOLD contrast, depending on the experimental design.

Another important research area is the use of animal fMRI models to improve understanding of the basic principles of BOLD fMRI. In a series of experiments, Logothetis and colleagues have investigated the relationship between hemodynamic and electrophysiological measures of brain activity, using concurrent fMRI and ERP/EEG measurements. We have discussed the results of these studies in detail in Chapter 7, but one of their technical advances is illustrated here, namely a custom vertical-bore MRI scanner designed specifically for use with monkeys (Figure 13.15). Several other institutions have installed monkey-specific scanners in recent years.

Although nearly all fMRI studies in monkeys have explored basic sensory functioning, studies of more-advanced cognitive processes are also possible. In

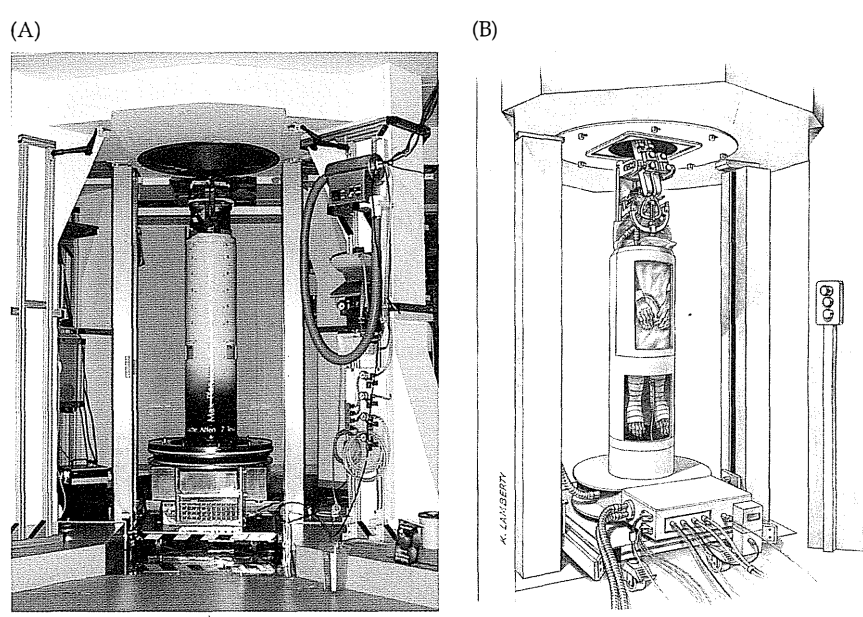

Figure 13.15 A custom MRI scanner for monkey studies. (A) Through the creation of hardware specific for studies of nonhuman animals, the quality of fMRI data can be greatly improved. Logothetis and colleagues have created a custom scanner that allows the animal to remain upright with the head restrained (B). (Courtesy of Dr. Nikos Logothetis, Max Planck Institute, Tübingen, Germany.)

a very interesting study of executive function published in 2002, Nakahara and colleagues investigated the brain regions involved in shifting between response sets. An important hallmark of human prefrontal cortex damage is an inability to shift from one mode of responding to another, as demonstrated by behavioral impairments in the Wisconsin Card Sorting Test. In order to study set shifting in monkeys, Nakahara and colleagues developed a modified version of this test that two macaque monkeys (*Macaca fuscata*) performed within a standard clinical scanner. The authors found significant activity in response to category shifts in the monkeys' inferior prefrontal cortex, as well as in the intraparietal sulcus, posterior cingulate, precuneus, and insula. They then compared these regions of activity with those from an identical fMRI experiment conducted in humans (Figure 13.16). The authors found that the humans also showed significant activity in the inferior prefrontal cortex, in a region with similar cytoarchitectonic properties as those identified in monkeys. Future studies of this type will be critical for comparing maps of brain function between species.

The use of fMRI in nonhuman animals has considerable potential, but it also presents a new set of challenges. In a sense, it combines all of the problems of fMRI with all of the problems of animal studies. One difficulty that must be overcome is subject motivation. Human fMRI subjects may be motivated by several factors: the desire to help the experimenter, a sense of purpose in helping to advance science, or the thought of the payment they will receive upon completion of the study. In contrast, animal subjects are more motivated by the direct rewards given for experimental compliance, such as squirts of juice. Though juice is a good reward system for behavioral studies, it is not ideal for fMRI. Swallowing a sip of juice requires the contraction of muscles in the jaw and throat, which in turn causes both distortions in the local magnetic field and head motion. Even with a periodic reward, an animal may have difficulty remaining still. For example, in the study by Stefanacci and colleagues, a number of the experimental runs were severely corrupted by large head motions.

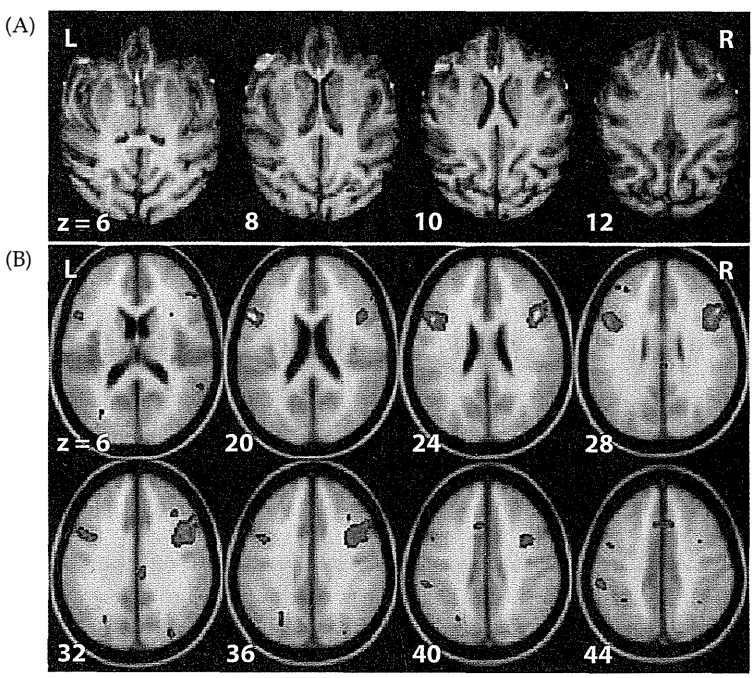

Figure 13.16 Comparison of fMRI data from monkeys and humans. A potentially exciting use of fMRI in monkeys is the direct comparison with human data. Data were collected from both macaque monkeys (A) and humans (B) in a variant of the Wisconsin Card Sorting Test (height of slices, z, shown in mm). In both species, there was significant activity in the bilateral inferior frontal cortex in response to stimuli that required a shift from one response set to another. This result suggests that these regions may be functionally homologous between the species. Note that the brain images are shown at different scales; the human brain has more than ten times the volume of the macaque brain. (After Nakahara et al., 2002.)

The authors noted that this head motion may have been exacerbated by the limitations of using a clinical MRI scanner with a primate chair inserted within the bore, so dedicated monkey scanners have the potential to minimize such problems.

Finally, we note that animal models themselves have limitations. Monkeys are similar to humans in overall brain organization, but they are expensive to maintain and test, and relatively few institutions have large colonies. A less expensive option is to use rodents, as is typical for behavioral neuroscientific studies. Rats are cheap, common, and perform many tasks well, but they have extremely small brains (about 2 cc). Most genetic manipulations have been performed in mice, making them good candidates for studies of the effects of specific genes on brain function, but their brains are smaller still (about 0.4 cc). To emphasize the problem of scale involved with imaging a rodent brain, consider that with a voxel size typical for human studies, only about 30 voxels would be needed to contain the entire brain of a rat, and only about 6 would be needed for the brain of a mouse. Yet despite these limitations, several fMRI studies in rodents have been conducted using ultra-high-field scanners. These studies have generated exquisite maps of sensory cortices, as exemplified by an image of the olfactory bulb of a rat produced by Xu and colleagues. Thus, fMRI studies of nonhuman primates and other animals are likely to become increasingly important, both for improving our understanding of brain function and for clarifying the basic physiological mechanisms of fMRI.

Summary

REFER TO THE
fMRI
COMPANION WEBSITE AT
www.sinauer.com/fmri2e
for study questions and Web links.

The field of cognitive neuroscience is growing rapidly and accruing a broad range of experimental observations. In part, this reflects the vitality of a young field that has only recently gained access to new and powerful techniques like fMRI. However, the continued maturation of cognitive neuroscience will require more than observations—it will require new theoretical frameworks based on convergent data from many methods. Two classes of techniques are used by cognitive neuroscientists. The first class includes approaches that manipulate brain function, such as direct cortical stimulation, TMS, genetics, and lesion studies. These techniques can guide inferences about the necessity of a brain region for a given cognitive process, providing important complementary evidence for fMRI studies. The second class includes approaches that measure brain function, notably electrophysiological studies of single-unit activity, local electrical field potentials, and local magnetic field changes (along with neuroimaging techniques like PET and fMRI). These electrophysiological approaches provide better temporal resolution than fMRI but have problems with localization of neuronal generators. Combined fMRI and electrophysiological studies thus show promise for improving functional resolution, although many technical challenges remain. Researchers should choose their experimental strategies, including techniques and experimental designs, according to their research questions. This interdisciplinary approach is the future of cognitive neuroscience, and indeed of all of science.

Suggested Readings

Allison, T., Wood, C. C., and McCarthy, G. (1986). The central nervous system. In *Psychophysiology: Systems, Processes and Applications: A Handbook* (E. Donchin, S. Porges, and M. Coles, eds.), pages 5–25. Guilford Press, New York. *An introduction*

to the physiology of field potentials with a philosophical consideration of their use in localizing sensory, motor, and cognitive function.

*Baillet, S., Mosher, J. C., and Leahy, R. M. (2001). Electromagnetic brain mapping. *IEEE Signal Processing Magazine*, November: 14–30. *A very accessible review of the use of mathematical techniques to localize neuronal generators of electrical and magnetic fields.*

Brazier, M. A. B. (1988). *A History of Neurophysiology in the 19th Century.* Raven Press, New York. *A fascinating history of the use and development of electrophysiological methods in neuroscience.*

Hämäläinen, M., Hari, R., Ilmoniemi, R., Knuutila, J., and Lounasmaa, O. (1993). Magnetoencephalography. Theory, instrumentation and applications to the noninvasive study of human brain function. *Rev. Modern Phys.*, 65: 413–497. *An excellent and comprehensive review of MEG, including neurophysiology, instrumentation, and modeling.*

*Hariri, A. R., Drabant, E. M., and Weinberger, D. R. (2006). Imaging genetics: perspectives from studies of genetically driven variation in serotonin function and corticolimbic affective processing. *Biol. Psychiatry*, 59: 888–897. *An overview of the combination of genomic and functional neuroimaging data, with an emphasis on recent studies of the role of serotonin in the processing of emotional information.*

*Shallice, T. (1988). *From Neuropsychology to Mental Structure.* Cambridge University Press, Cambridge. *A classic text that considers at length the interpretative issues associated with lesion studies in humans.*

* Toga, A. W., Thompson, P. M., Mega, M. S., Narr, K. L., and Blanton, R. E. (2001). Probabilistic approaches for atlasing normal and disease-specific brain variability. *Anat. Embryol.*, 204(4): 267–282. *An interesting review of the use of probabilistic brain atlases to identify disease-related changes in brain morphometry.*

*Indicates a reference that is a suggested reading in the field and is also cited in this chapter.

Chapter References

Ahlfors, S. P., Simpson, G. V., Dale, A. M., Belliveau, J. W., Liu, A. K., Korvenoja, A., Virtanen, J., Huotilainen, M., Tootell, R. B., Aronen, H. J., and Ilmoniemi, R. J. (1999). Spatiotemporal activity of a cortical network for processing visual motion revealed by MEG and fMRI. *J. Neurophysiol.*, 82(5): 2545–2555.

Allison, T. (1982). Scalp and cortical recordings of initial somatosensory cortex activity to median nerve stimulation in man. *Ann. N.Y. Acad. Sci.*, 388: 671–678.

Allison, T., McCarthy, G., Wood, C. C. and Jones, S. J. (1991). Potentials evoked in human and monkey cerebral cortex by stimulation of the median nerve. *Brain*, 114: 2465–2503.

Allison, T., McCarthy, G., Wood, C. C., Williamson, P. D. and Spencer, D. D. (1989). Human cortical evoked potentials by stimulation of the median nerve. I. Cytoarchitectonic areas generating short-latency activity. *J. Neurophysiol.*, 62: 694–710.

Allison, T., Puce, A., Spencer, D. D., and McCarthy, G. (1999). Electrophysiological studies of human face perception. I: Potentials generated in occipitotemporal cortex by face and non-face stimuli. *Cereb. Cortex*, 9(5): 415–430.

Belger, A., Puce, A., Krystal, J. H., Gore, J. C., Goldman-Rakic, P. S., and McCarthy, G. (1998). Dissociation of mnemonic and perceptual processes during spatial and non-spatial working memory using fMRI. *Hum. Brain Mapping*, 6: 14–32.

Berger, H. (1929). Über das Elektroenkephalogram des Menschen. *Arch. Psychiatr. Nervenkr.*, 87: 527–570.

Bledowski, C., Prvulovic, D., Hoechstetter, K., Scherg, M., Wibral, M., Goebel, R., and Linden, D. E. (2004). Localizing P300 generators in visual target and distractor processing: a combined event-related potential and functional magnetic resonance imaging study. *J. Neurosci.*, 24: 9353–9360.

Bohning, D. E., Pecheny, A. P., Epstein, C. M., Speer, A. M., Vincent, D. J., Dannels, W., and George, M. S. (1997). Mapping transcranial magnetic stimulation (TMS) fields in vivo with MRI. *NeuroReport*, 8(11): 2535–2538.

Bookheimer, S. Y., Strojwas, M. H., Cohen, M. S., Saunders, A. M., Pericak-Vance, M. A., Mozziotta, J. C., and Small, G. W. (2000). Patterns of brain activation in people at risk for Alzheimer's disease. *N. Engl. J. Med.*, 343(7): 450–456.

Broca, P. (1861). Remarques sur le siége de la faculté du langage articulé, suivies d'une observation d'aphemie (perte de la parole). *Bulletins de la société anatomique de Paris*, année 36, 2ème serie, tome 6: 330–357.

Busse, L., Roberts, K. C., Crist, R. E., Weissman, D. H., and Woldorff, M. G. (2005). The spread of attention across modalities and space in a multisensory object. *Proc. Natl. Acad. Sci. U. S. A.*, 102: 18751–18756.

Caton, R. (1875). The electric currents of the brain. *Br. Med. J.*, 2: 278.

Chafee, M. V., and Goldman-Rakic, P. S. (1998). Matching patterns of activity in primate prefrontal area 8a and parietal area 7ip neurons during a spatial working memory task. *J. Neurophysiol.*, 79: 2919–2940.

Cohen, D. (1972). Magnetoencephalography: Evidence of magnetic fields produced by alpha rhythm currents. *Science*, 161: 664–666.

Cramer, S. C., Nelles, G., Benson, R. R., Kaplan, J. D., Parker, R. A., Kwong, K. K., Kennedy, D. N., Finklestein, S. P., and Rosen, B. R. (1997). A functional MRI study of subjects recovered from hemiparetic stroke. *Stroke*, 28: 2518–2527.

Cruetzfeldt, O. (1974). The neuronal generation of the EEG. In *Handbook of Electroencephalography and Clinical Neurophysiology*, Vol. 2, Part C (A. Remond, ed.). Elsevier, Amsterdam.

Curtis, C. E., and D'Esposito, M. D. (2003). Persistent activity in the prefrontal cortex during working memory. *Trends Cognitive Sci.*, 7(9): 415–423.

Dale, A. M., Liu, A. K., Fischl, B. R., Buckner, R. L., Belliveau, J. W., Lewine, J. D., and Halgren, E. (2000). Dynamic statistical parametric mapping: Combining fMRI and MEG for high-resolution imaging of cortical activity. *Neuron*, 26(1): 55–67.

Debener, S., Ullsperger, M., Siegel, M., and Engel, A. K. (2006). Single-trial EEG-fMRI reveals the dynamics of cognitive function. *Trends Cogn. Sci.*, 10: 558–563.

Debener, S., Ullsperger, M., Siegel, M., Fiehler, K., von Cramon, D. Y., and Engel, A. K. (2005). Trial-by-trial coupling of concurrent electroencephalogram and functional magnetic resonance imaging identifies the dynamics of performance monitoring. *J. Neurosci.*, 25: 11730–11737.

Di Russo, F., Martinez, A., and Hillyard, S. A. (2003). Source analysis of event-related cortical activity during visuo-spatial attention. *Cereb. Cortex*, 13(5): 486–499.

Du Bois-Reymond, E. (1848). *Untersuchungen über thierische Elektricität, Erster Band.* Georg Reimer, Berlin.

Fellows, L. K., Stark, M., Berg, A., and Chatterjee, A. (2008). Patient registries in cognitive neuroscience research: advantages, challenges, and practical advice. *J. Cogn. Neurosci.*, 20: 1107–1113.

Ferrier, D. (1876). *The Functions of the Brain.* Smith, Elder, London.

Flourens, M.-J.-P. (1824). *Recherches expérimentales sur les propriétés et les fonctions du système nerveux, dans les animaux vertébrés.* Crevot, Paris.

Fritsch, G., and Hitzig, E. (1870). Über die elektrische Erregbarkeit des Grosshirns. *Archiv für Anatomie, Physiologie, und wissenschaftliche Medicin.*, 37: 300–332.

Funahashi, S., Bruce, C. J., and Goldman-Rakic, P. S. (1989). Mnemonic coding of visual space in the monkey's dorsolateral prefrontal cortex. *J. Neurophysiol.*, 61: 331–349.

Gaillard, R., Naccache, L., Pinel, P., Clemenceau, S., Volle, E., Hasboun, D., Dupont, S., Baulac, M., Dehaene, S., Adam, C., and Cohen, L. (2006). Direct intracranial, FMRI, and lesion evidence for the causal role of left inferotemporal cortex in reading. *Neuron*, 50: 191–204.

Haaland, K. Y., Harrington, D. L., and Knight, R. T. (2000). Neural representations of skilled movement. *Brain*, 123: 2306–2313.

Hariri, A. R., and Weinberger, D. R. (2003). Imaging genomics. *Br. Med. Bull.*, 65: 259–270.

Hariri, A. R., Mattay, V. S., Tessitore, A., Kolachana, B., Fera, F., Goldman, D., Egan, M. F., and Weinberger, D. R. (2002). Serotonin transporter genetic variation and the response of the human amygdala. *Science*, 297: 400–403.

Hubel, D. H., and Wiesel, T. N. (1959). Receptive fields of single neurons in the cat's striate cortex. *J. Physiol.*, 148: 574–591.

Hubel, D. H., and Wiesel, T. N. (1962). Receptive fields, binocular interaction and functional architecture in the cat's visual cortex. *J. Physiol.*, 160: 106–154.

Keck, M. E., Welt, T., Muller, M. B., Erhardt, A., Ohl, F., Toschi, N., Holsboer, F., and Sillaber, I. (2002). Repetitive transcranial magnetic stimulation increases the release of dopamine in the mesolimbic and mesostriatal system. *Neuropharmacology*, 43(1): 101–109.

Kuffler, S. W. (1953). Discharge patterns and functional organization of mammalian retina. *J. Neurophysiol.*, 16: 37–68.

Liu, A. K., Belliveau, J. W., and Dale, A. M. (1998). Spatiotemporal imaging of human brain activity using functional MRI constrained magnetoencephalography data: Monte Carlo simulations. *Proc. Natl. Acad. Sci. U.S.A.*, 95(15): 8945–8950.

MacMillan, M. (2000). *An odd kind of fame: Stories of Phineas Gage.* MIT Press, Cambridge, Massachusetts.

Marshall, W. H., Woolsey, C. N., and Bard, P. (1937). Cortical representation of tactile sensibility as indicated by cortical potentials. *Science*, 85: 388–390.

Miller, E. K., and Cohen, J. D. (2001). An integrative theory of prefrontal cortex function. *Annu. Rev. Neurosci.*, 24: 167–202.

Mottaghy, F. M., Gangitano, M., Krause, B. J., and Pascual-Leone, A. (2003). Chronometry of parietal and prefrontal activations in verbal working memory revealed by transcranial magnetic stimulation. *NeuroImage*, 18(3): 565–575.

Pascual-Leone, A., Valls-Sole, J., Brasil-Neto, J. P., Cohen, L. G., and Hallett, M. (1992). Seizure induction and transcranial magnetic stimulation. *Lancet*, 339(8799): 997.

Penfield, W. (1950). *The Cerebral Cortex of Man: A Clinical Study of Localization of Function.* Macmillan, New York.

Puce, A., Allison, T., and McCarthy, G. (1999). Electrophysiological studies of human face perception III. Effects of top-down processing on face-specific potentials. *Cereb. Cortex*, 9: 445–458.

Puce, A., Allison, T., Spencer, S. S., Spencer, D. D., and McCarthy, G. (1997). A comparison of cortical activation evoked by faces measured by intracranial field potentials and functional MRI: Two case studies. *Hum. Brain Mapping*, 5: 298–305.

Puce, A., Constable, R. T., Luby, M. L., McCarthy, G., Nobre, A. C., Spencer, D. D., Gore, J. C., and Allison, T. (1995). Functional magnetic resonance imaging of sensory and motor cortex: Comparison with electrophysiological localization. *J. Neurosurg.*, 83(2): 262–270.

Ridding, M. C., and Rothwell, J. C. (2007). Is there a future for therapeutic use of transcranial magnetic stimulation? *Nat. Rev. Neurosci.*, 8: 559–567.

Ritter, P., and Villringer, A. (2006). Simultaneous EEG-fMRI. *Neurosci. Biobehav. Rev.*, 30: 823–838.

Rossini, P. M., Caltagirone, C., Castriota-Scanderbeg, A., Cicinelli, P., Del Gratta, C., Demartin, M., Pizzella, V., Traversa, R., and Romani, G. L. (1998). Hand motor cortical area reorganization in stroke: A study with fMRI, MEG and TCS maps. *NeuroReport*, 9(9): 2141–2146.

Ruff, C. C., Blankenburg, F., Bjoertomt, O., Bestmann, S., Freeman, E., Haynes, J. D., Rees, G., Josephs, O., Deichmann, R., and Driver, J. (2006). Concurrent TMS-fMRI and psychophysics reveal frontal influences on human retinotopic visual cortex. *Curr. Biol.* 16: 1479–1488.

Rushworth, M. F., Hadland, K. A., Paus, T., and Sipila, P. K. (2002). Role of the human medial frontal cortex in task switching: A combined fMRI and TMS study. *J. Neurophysiol.*, 87(5): 2577–2592.

Salzman, C. D., Britten, K. H., and Newsome, W. T. (1990). Cortical microstimulation influences perceptual judgments of motion direction. *Nature*, 346(6280): 174–177.

Schlosser, M. J., Luby, M., Spencer, D. D., Awad, I. A., and McCarthy, G. (1999). Comparative localization of auditory comprehension using functional MRI and cortical stimulation. *J. Neurosurg.*, 91: 626–635.

Schlosser, M. J., McCarthy, G., Fulbright, R. K., Awad, I. A., and Gore, J. C. (1997). Cerebral vascular malformations adjacent to sensorimotor and visual cortex: Functional magnetic resonance imaging studies before and after therapeutic intervention. *Stroke,* 28: 1130–1137.

Shaw, P., Greenstein, D., Lerch, J., Clasen, L., Lenroot, R., Gogtay, N., Evans, A., Rapoport, J., and Giedd, J. (2006). Intellectual ability and cortical development in children and adolescents. *Nature,* 440: 676–679.

Staudt, M., Lidzba, K., Grodd, W., Wildgruber, D., Erb, M., and Krageloh-Mann, I. (2002). Right-hemispheric organization of language following early left-sided brain lesions: Functional MRI topography. *NeuroImage,* 16(4): 954–967.

Stefanacci, L., Reber, P., Costanza, J., Wong, E., Buxton, R., Zola, S., Squire, L., and Albright T. (1998). fMRI of monkey visual cortex. *Neuron,* 20: 1051–1057.

Sutton, S., Braren, M., Zubin, J., and John, E. R. (1965). Evoked-potential correlates of stimulus uncertainty. *Science,* 150: 1187–1188.

Talairach, J., and Tournoux, P. (1998). *Co-planar Stereotaxic Atlas of the Human Brain.* Thieme Medical Publishers Inc., New York.

Teuber, H. L. (1955). Physiological psychology. *Annu. Rev. Psychol.,* 9: 267–296.

Wernicke, K. (1874). *Der aphasische Symptomencomplex. Eine psychologische Studie auf anatomischer Basis.* Breslau, Germany.

Woldorff, M. G., Tempelmann, C., Fell, J., Tegeler, C., Gaschler-Markefski, B., Hinrichs, H., Heinz, H. J., and Scheich, H. (1999). Lateralized auditory spatial perception and the contralaterality of cortical processing as studied with functional magnetic resonance imaging and magnetoencephalography. *Hum. Brain Mapp.,* 7: 49–66.

Wood, C. C., Spencer, D. D., Allison, T., McCarthy, G., Williamson, P. D., and Goff, W. R. (1988). Localization of human sensorimotor cortex during surgery by cortical surface recording of somatosensory evoked potentials. *J. Neurosurg.,* 68(1): 99–111.

Woolsey, C. N., Erickson, T. C., and Gilson, W. E. (1979). Localization in somatic sensory and motor areas of human cerebral cortex as determined by direct recording of evoked potentials and electrical stimulation. *J. Neurosurg.,* 51(4): 476–506.

Chapter 14

The Future of fMRI: Practical and Ethical Issues

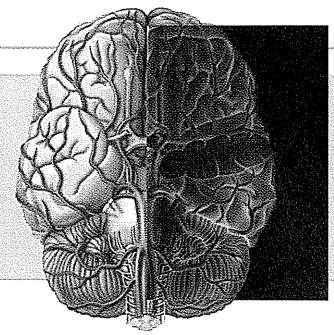

Introduction

On November 11, 2007, the *New York Times* published an article that examined how uncommitted voters responded to images of candidates for the United States President. Although the 2008 presidential election was still a year away, the character of the campaign had already taken shape. The top candidates were already well known to the electorate through debates and advertisements. The core issues—the Iraq war, the economy, and health care—were central in the minds of voters. Moreover, immeasurable reams of newsprint had already been dedicated to analyses of voter attitudes and behavior. Against this noisy background, a single article (even in as prestigious a news outlet as the *New York Times*) would barely be noticed. Yet, this story was an immediate hit. It became the most-emailed article from the *Times*, while engendering immediate celebrations and rebuttals from many other news sources. In speculating why the article—labeled as an opinion/editorial piece—became so controversial, one should begin with its title: "This is Your Brain on Politics."

Authored by neuroscientists, political scientists, and applied fMRI researchers, the article described an fMRI experiment in which 20 potential voters viewed images and videos of leading candidates. (The details of the design were not provided in the Times article, but they are not critical for this brief summary.) Based on the patterns of activation evoked by different candidates, the authors made inferences about the emotional and cognitive attitudes that could drive voting behavior; for example, "Videos of McCain and Obama indicated a notable lack of any powerful reactions, positive or negative," "Rudy Giuliani versus Fred Thompson: the latter evokes more empathy," and "Emotions about Hillary Clinton are mixed." In support of this last conclusion, voters who reported disliking Clinton showed increased activation in the anterior cingulate cortex, a region often associated with behavioral conflict. Accompanying the article was a multimedia slide show that displayed attractively rendered three-dimensional brains, with the functional associations of the activated regions helpfully labeled (e.g., "conflict").

Rarely has a single news story so clearly highlighted both the promise and limitations of fMRI. Imagine a similar story that made inferences from polling data, or from a survey of a small, single-interest group. Would it be newsworthy that Hillary Clinton, one of the more polarizing figures of recent U.S. pol-

itics, evokes mixed emotions? Or that one candidate evokes more empathy than another? The story generated such excitement not because of its conclusions, but because of its use of fMRI to reach those conclusions. As other fMRI research receives similar or even greater attention in the popular press, the detractors of the technique have become increasingly vocal. Eminent scientists from many fields have lamented the undue emphasis on fMRI research, believing that the claims of the popular press, and even of some researchers, are often overstated. (An interesting parallel can be seen in research involving genetic engineering, which has raised a similar mix of exuberance and caution.)

In this chapter, we consider a range of issues related to the practice of fMRI: What can and should researchers say about fMRI data? What restrictions should be placed on the sorts of people to be scanned or the sorts of topics to be studied? What constraints should guide how researchers interact with their participants? What commercial applications should arise from cutting-edge fMRI research? These are complex, important questions without simple answers. Indeed, they often lead fMRI researchers to disagree with each other. Three days after the publication of the New York Times article referenced above, a letter to the editor was published with much less fanfare. In it, an international group of fMRI researchers indicated their serious concerns with using fMRI to study political advertising, and with the presentation of that work in the Times. Tellingly, there was little news coverage of this cautionary letter.

Interpreting and Presenting fMRI Data

We first examine how fMRI findings are disseminated by news reporters, science writers, and the researchers themselves. As fMRI becomes an increasingly common and important technique, its applications to problems of real-world interest have caught the attention of the news media and the public at large (Figure 14.1). Journalists, bioethicists, and fMRI researchers have grown concerned with the challenges in describing complex research to a popular audience. How does one encapsulate, within a few short paragraphs, all of the complex physics, physiology, experimental design, and statistics that underlie even the most basic fMRI study? It is a challenge for textbook authors to describe these topics clearly, and much more so for journalists writing articles for nonscientific audiences. We briefly outline some key challenges and principles in this section. Interested readers may refer to the resources listed at the end of the chapter for further discussion of these topics.

Our examples hereafter are largely hypothetical, for two reasons. First, many authors of legitimately groundbreaking scientific research have been chagrined by the coverage of that work in the popular media. The scientists themselves can unintentionally mislead journalists or the public at large. A quotation that seems reasonable to a scientist in the context of an extended interview may, in isolation, lead a lay audience to inappropriate conclusions. Second, if we focus on the details of specific articles, we run the risk of obscuring broader themes. Instead, we have created hypothetical examples that reflect the spirit of specific real news articles, while changing the details. Given the diversity of fMRI research and the explosion of new research during the writing of this book, some of these invented experiments may now have counterparts in the peer-reviewed literature, perhaps even with accompanying news stories! But unless we have explicitly indicated otherwise, such parallels are coincidental. We invite the reader to search through any current news database to find real-world examples of the types of media coverage outlined here.

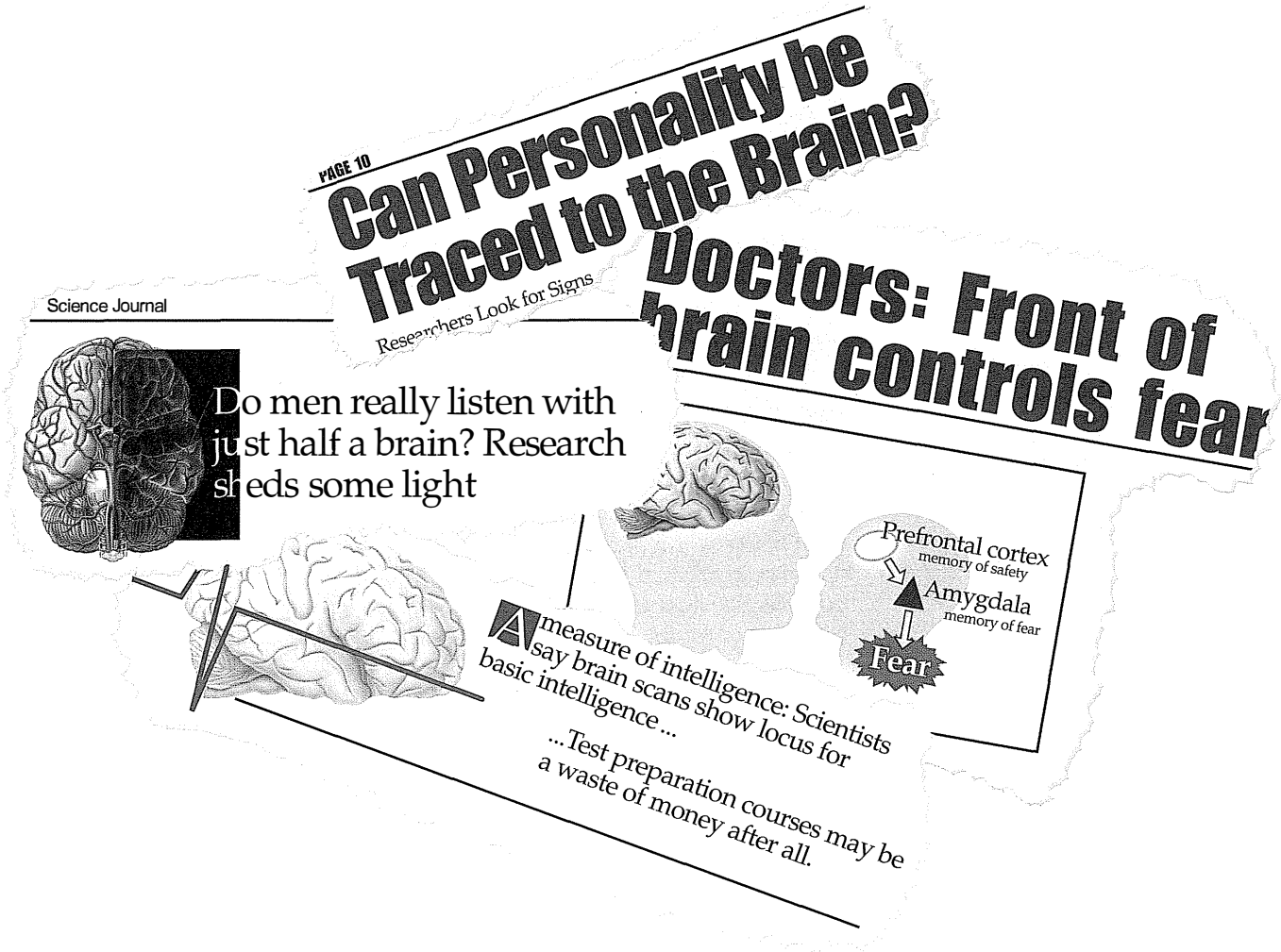

Figure 14.1 Functional MRI studies have elicited substantial media coverage, for better or worse. While this has led to increased public interest in neuroimaging, as well as increased recognition of the influence of the brain on behavior, many stories emphasize sensationalism over accuracy. Media reports of fMRI studies share some common properties. Anatomical regions are often generalized, because the intended audience knows neither the anatomy nor the jargon used to describe it (e.g., the frontopolar cortex vs. the prefrontal cortex). Complex concepts like personality, intelligence, and emotion are linked to specific areas, even when the research study describes activation in terms of brain systems. The study's results are applied to common behavior, for example, how one can become a better parent or stock market investor. And there is often a focus on studies of individual differences or social psychology that tap into common stereotypes about behavior.

Coverage of fMRI research in the popular media

Throughout this book, we have emphasized fMRI's *flexibility*, how it can be used to study a remarkable range of mental and behavioral phenomena. This breadth can be illustrated in a set of examples, all collected from a single day's search for popular news articles that discuss fMRI experiments (Table 14.1). These articles constitute a small, but surprisingly representative, sample of how media outlets report fMRI research. Several common themes emerge in this sample, as well as in wider surveys of news coverage: medical advances that presage cures for clinical conditions, the identification of the biological basis for some difference amongst individuals, and the validation or invalidation of some popularly held belief.

TABLE 14.1 Headlines describing fMRI research, from a single day's news

Woman Convicted of Child Abuse Hopes fMRI Can Prove Her Innocence (Wired News)
Searching for God in the Brain (*Scientific American*)
Neuroscientist Uses Brain Scan to See Lies Form (NPR)
Why Teens Are Such Impulsive Risk-Takers (*Science Daily*)
Research Cracks Door of Hope on Alzheimer's (*Ashland City Times*, TN)
Digital Thought Police (*Popular Mechanics*)
An MRI into the Minds of US Voters (*Daily Texan*, Austin TX)
Brain Circuits that Control Hunger Identified (*Science Daily*)
Built for Optimism (*Wall Street Journal*)
Women Risk Risky Sex at Worst Time (Web MD)

The first of these themes, medical advances, represents the simplest and most benign form of news coverage. Many such articles describe a newly published study that identifies differences in fMRI activation between two groups of subjects (e.g., drug addicts and non-addicts) during the performance of some task (e.g., decision-making). Others describe basic science research that has implications for clinical practice. As for other articles about medical discoveries, the translation of a complex fMRI study into a short-format article poses some limitations. The details of the methods are simplified, the results are distilled into some simple take-home message, and the potential for future discoveries is often exaggerated. The lead author on the study usually provides a supporting quotation which often takes a stereotyped form: one or two sentences describing the basic results, followed by a concluding sentence about the study's importance to the general public. Despite these caveats, articles about the medical implications of fMRI studies are critical for the dissemination of the best research results to a popular audience.

More problematic are stories that veer into the domain of individual differences. Perhaps nothing attracts readers more than articles about "what makes us who we are," whether those differences involve gender, age, personality, intelligence, or attitudes. While behavioral studies are critical for understanding how individuals differ, in recent years fMRI research has provided new information about the underlying mechanisms controlling those differences. Consider a hypothetical example: an fMRI study finds that creative visual artists exhibit increased activation in the anterior prefrontal cortex, compared with non-artists. Popular accounts of this finding could conceivably emphasize the researchers' discovery of the "seat of creativity" in the brain, as localized to the prefrontal cortex. This conclusion would be incomplete at best, downright misleading at worst. Yet, it would make for a very compelling news story.

Thought Question

If you were writing an article for a non-scientific audience, how would you introduce fMRI's capabilities and limitations?

individual differences Measures of variation among individuals within a population.

Why are stories about the basis of individual brain differences so attractive? One possibility, suggested by Racine and colleagues in a thoughtful review of fMRI media coverage, is that brain activation becomes a measurable proxy for deeper aspects of the self. In the spirit of nineteenth-century

phrenology, news stories about individual differences simplify complex concepts (e.g., personality traits like creativity) to the functioning of a single chunk of brain tissue. Racine and colleagues label this concept neuroessentialism, reflecting the idea that the essence of the self is captured in the brain. At its logical extreme, this concept is completely defensible: any behavioral differences between individuals must reflect concomitant neural differences. Yet, neuroessentialism fails at a practical level, in that fMRI data (even in the best studies) cannot capture individual differences with the precision implied by news reports. For example, creativity is such a broad concept that it would be difficult to equate it to any pattern of brain activation, much less the data from a single fMRI study.

The third category of common news coverage is the presentation of fMRI data as conclusive evidence for or against a popularly held belief. Stories of this type emphasize that fMRI provides new scientific proof that this belief is true or false. In another hypothetical example, suppose that fMRI data indicated that playing video games evoked activation in the brain's reward circuitry, just like drugs of abuse. Would this prove that video games are addictive, as an article in the popular press might imply? The observation of a given pattern of brain activation does not imply specific cognitive processes, as we consider in more detail in Box 14.1. Nevertheless, the presence of fMRI data can make a belief seem more valid. This phenomenon has been labeled neurorealism by Racine and colleagues, reflecting a sense that fMRI data provide definitive and objective proof about a belief—in contrast to studies of behavior or psychology that might seem to provide more subjective information.

Not even the most ardent advocates of fMRI research would support a strong neurorealist viewpoint. As argued throughout this book, fMRI is one technique among many available to the scientist. If used improperly, it can lead to inconclusive or erroneous conclusions (like any other technique). Perhaps because fMRI research carries an air of technical mystery—unlike surveys or laboratory measures of behavior—it seems more scientific to a lay audience. The images it creates can seem like snapshots of the brain at work, especially when one glosses over the enormous conceptual gap between those images and the underlying experimental design. In any case, neurorealistic language is endemic to descriptions of fMRI studies in the popular media. Later in this chapter, we provide rough guidelines for how this and other problems can be minimized, if not avoided entirely, when describing fMRI research.

neuroessentialism The intuition that neuroscience data are isomorphic with the subjective self.

neurorealism The tendency to consider a behavioral or mental phenomenon to be more real based on the presence of neuroscience data.

Core principles for presenting fMRI research

The discussion so far paints a pessimistic and discouraging picture of fMRI news coverage. These problems are hardly unique to reports about fMRI research. Whether discussing neuroscience or genetics, developmental psychology or particle physics, science journalists have the unenviable challenge of repackaging dense and complex concepts for lay audiences. This is an extraordinarily difficult task, but it is essential for funding, as well as publicizing, research. When submitting grant applications to the U.S. National Institutes of Health (NIH), fMRI researchers write short abstracts of their proposals for the public record. These abstracts not only describe the proposal's basic science, but also discuss the potential consequences of the research for improving health outcomes. Being able to describe the importance of one's research to a lay audience is thus important for a variety of reasons.

On a more positive note, there is much good science writing, even about fMRI research. The best articles describe new discoveries in an intriguing and

BOX 14.1 Reverse Inference

Most fMRI experiments are designed to test hypotheses of a specific form: does our experimental manipulation alter brain functioning? In most cases, experimenters manipulate some independent variable (IV), such as working memory load, noise in a visual display, or the difficulty of a decision-making task. They then use statistical tests (see Chapter 10) to evaluate whether changes in the IV predict changes in a dependent variable (DV), which is typically the magnitude of the BOLD signal. A significant relationship between the IV and the DV leads to the inference that the manipulation caused the observed brain changes, and thus that the brain region showing the changes is involved in the underlying mental processes (Figure 1).

Rarely, however, is any experiment so well designed that only a single mental process is evoked by a task manipulation. Experiments on perception, for example, often use discrete classes of visual stimuli like faces or houses. These classes differ in their visual characteristics, but they also may differ in other properties, such as the memories or emotions they generate. Suppose that a hypothetical experiment shows that face stimuli, compared with houses, evoke increased fMRI activation in the amygdala, a brain region previously shown to be central for emotional processing. Should the researchers assume that there was a greater emotional response to the faces? On the surface, this seems reasonable: if the amygdala is associated with emotion and we observe amygdala activation, then can't we assume that emotional processing was present in the task? Despite their pervasiveness in the fMRI literature, assumptions of this type contain a serious and often damaging logical error.

Reasoning from brain activation to mental process is a form of **reverse inference**, in that it takes a dependent variable, the fMRI activation, and infers the state of an independent variable, the generating cognitive process. This problem is not unique to fMRI; consider the challenge of diagnosing a psychiatric condition based on behavioral data. Yet, as discussed throughout this chapter, the tendency to think of fMRI activation as "pictures of the mind" has led to the frequent use of reverse inference among scientists and journalists alike. For an extended discussion of this problem, refer to the article by Russell Poldrack in the suggested readings.

The challenge of reverse inference can be distilled to a single concept, **selectivity**, which is a property of an outcome (i.e., of a DV). An outcome is highly selective if it only occurs as a result of one manipulation, whereas an outcome has low selectivity if it could result from any of a number of manipulations. As shown in Figure 2, reverse inference may be justifiable under conditions of high selectivity, with respect to the links between mental processes and brain activation, and between task manipulation and mental processes.

Figure 1 As described throughout this textbook, fMRI research involves making a chain of inferences: from experimental stimuli (A), to associated cognitive processes (B), to changes in the activity of neurons (C), to metabolic changes in the BOLD signal (D), and finally to statistical maps of activation (E). Usually, inference goes from left to right along this chain; for example, "because our experimental conditions differ in the demand for working memory, the observed contrast in prefrontal cortex activation must reflect the role of that region in maintaining information in working memory." More problematic, though, is reversing the direction of inference, or drawing conclusions about what cognitive processes are involved in a task, based on the observed pattern of activation (blue arrow).

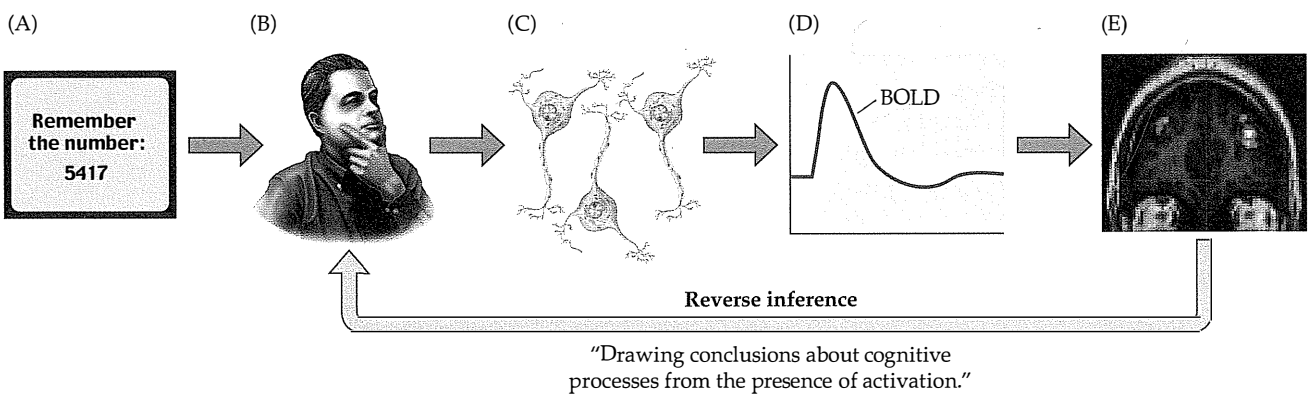

BOX 14.1 *(continued)*

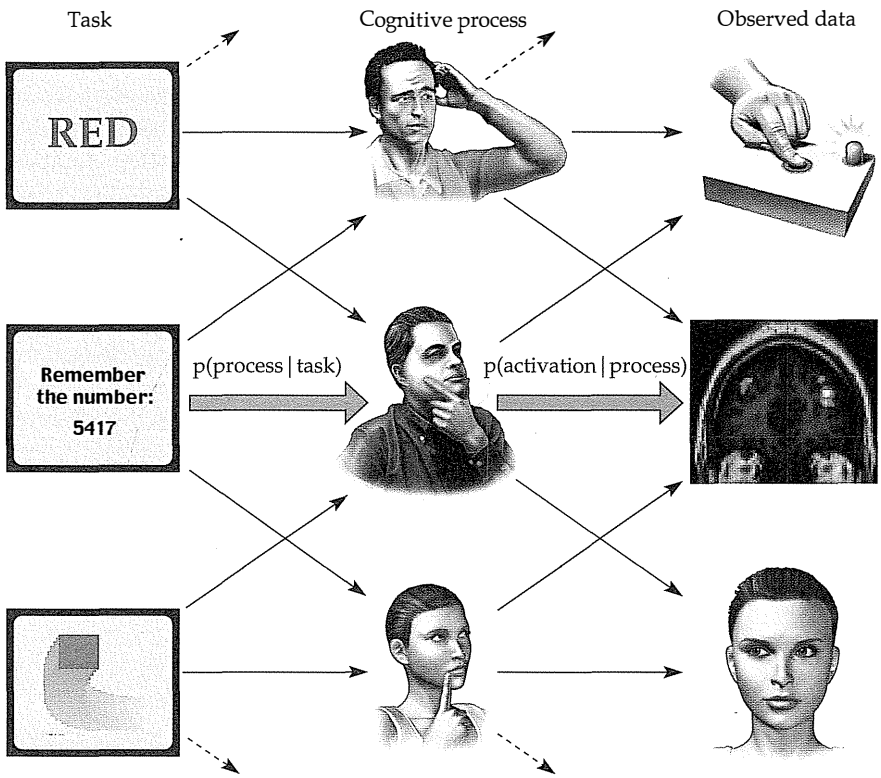

Figure 2 The complexity of inferential relationships in fMRI research. Shown in the middle row is a simplified version of Figure 1 that indicates the typical direction of forward inference in fMRI research. Yet, at each step in the process, there are additional possible explanations for the observed data. For example, a given cognitive process (say, selection of an appropriate response) could have been evoked by many tasks besides the one actually used in the experiment (left column). Likewise, activation in a given region could often have been evoked by multiple cognitive processes (middle column), just as a given cognitive process could lead to multiple types of observed data (right column). Reverse inference, or reasoning from activation to process or task, is only justifiable when both the regions of activation and the cognitive processes of interest have a great deal of specificity; that is, when the thick arrows (i.e., inferences of interest) have much higher probability than all other arrows (i.e., other potential inferences).

It is important to recognize that the mere presence of activation is unlikely to justify reverse inference. Few, if any, brain regions are only activated by a single function, much less by a single stimulus. Perhaps the best examples of a region that is activated by a single class of stimuli are the primary sensory cortices, but even those are activated not only by perceived stimuli but also by imagery, attention, and other mental processes. By contrast, activation of parts of the lateral frontal lobe has been observed in a remarkable variety of tasks, from memory to decision making. Nevertheless, one should not simply abandon the idea of reverse inference in those latter areas, given that a primary goal of cognitive neuroscience is to discover new relationships between cognition and the brain.

How, then, can one improve the selectivity of an experiment?

Two potential answers are evident when considering Figure 2. The first possibility lies in improving the relationship between the task manipulation and the mental process of interest. Simple subtractive designs are relatively unconstrained because the two conditions may differ on many features. More powerful are complex designs that vary some parameter in a continuous fashion. A researcher who wants to use reverse inference for emotional content could create a paradigm in which both the positivity and arousal of the emotional stimuli vary continuously (i.e., from positive to negative, or from least to most arousing). Observing that a region's activation increases as stimuli become more positive, but does not change according to how arousing they are, would strengthen the relationship between mental process and task manipulation. Another approach lies in using better-defined fMRI measures. Selectivity can be improved by moving beyond simple activation of a single region to include patterns of activation within one or more regions, changes in activation over time, or even measures of causality or functional connectivity.

reverse inference Reasoning from the outcome of a dependent variable to infer the state of an independent variable (or an intervening unobservable variable).

selectivity The tendency for a manipulation to lead to one outcome. Perfect selectivity is sometimes referred to as "specificity."

converging operations The use of two or more techniques to provide complementary evidence used to test an experimental hypothesis or scientific theory.

accessible manner, emphasizing the novelty without downplaying the limitations. (For examples, see *American Scientist* or *Nature News and Views*.) Even dry and factual summaries, if accurate, serve an important purpose by emphasizing that fMRI research provides important new information that may lead to improved medical outcomes. In short, science writing can be both accurate and accessible.

We describe here some core principles that should shape the presentation of fMRI data in the popular media. These guidelines are not exhaustive, nor are they completely inflexible. In some cases, they may be interpreted loosely or even ignored, depending on the goals of the presenter. But we believe that they constitute a reasonable set of guidelines for researchers and journalists alike.

First, give no special status to fMRI results, compared with those of other scientific methods. In many cases, knowledge about brain function will be critical for unlocking longstanding psychological puzzles; a better understanding of mechanism will lead to better models for behavior and cognition. However, images of an active brain have little value without concomitant knowledge about behavior or physiology. Researchers have been increasingly creative in relating BOLD data to behavioral data, which can lead to new and specific inferences about brain function. Understanding brain function will require converging operations, combining data from multiple sources to support a single conclusion (Figure 14.2). To return to one of our earlier examples, fMRI data about the effects

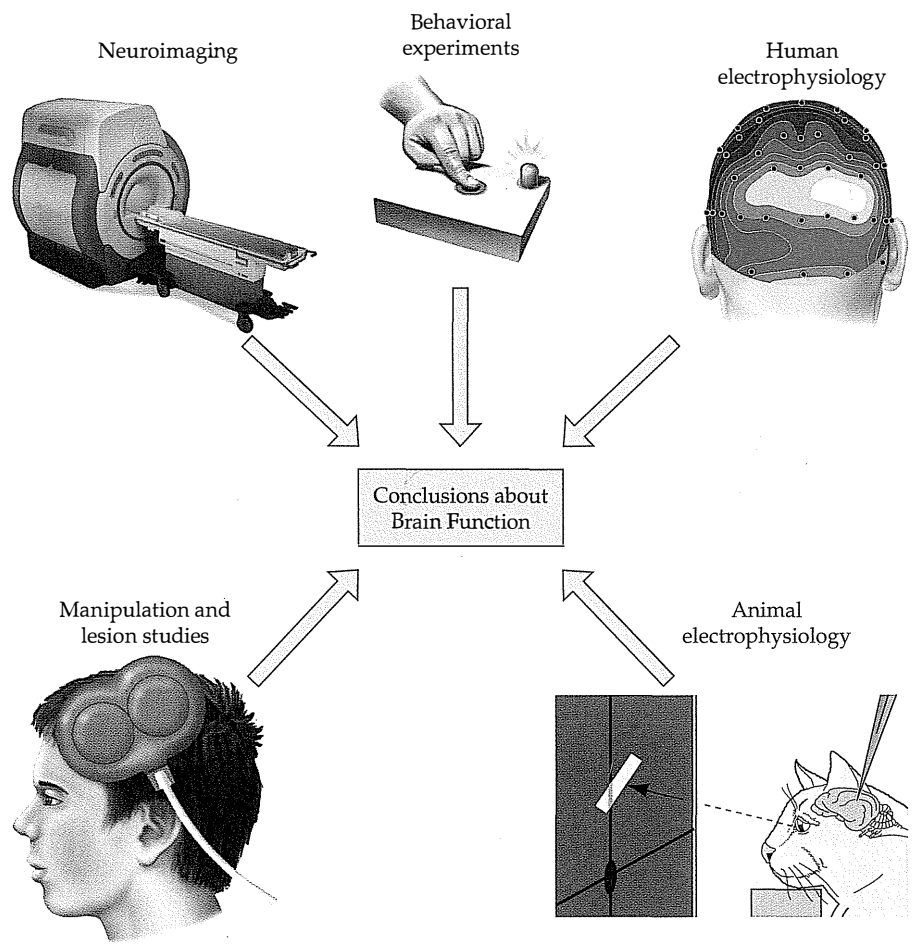

Figure 14.2 Converging operations. To improve the validity and breadth of conclusions about brain function, researchers should use multiple methods to address a single question. If different methods, each with particular strengths and limitations, converge on a single answer, the researcher can be more confident that the results are meaningful.

of videogame playing on reward systems are critical, not because they validate or refute the idea of gaming addiction, but because they provide information that can be used to develop new, more-refined behavioral measures.

Second, emphasize the deep rather than the superficial limitations of the research. Most scientific news articles temper their positive conclusions with brief notes about limitations. For fMRI studies, small sample sizes, the indirect measure of brain hemodynamics, and the need for more research before drawing firm conclusions, are often mentioned. These vague statements do little to help the audience evaluate the research. Small samples can be highly valid if representative, and hemodynamic measures, though indirect, provide a useful index of neuronal function. The deep limitations of fMRI studies come neither from the physics nor the physiology; they arise from the experimental design. Researchers should convey the strengths and weaknesses of their designs, emphasizing why they made specific design choices. They might also describe what sorts of future experimental designs will be sparked by the study. Journalists should question those design choices, especially when very broad conclusions about complex real-world phenomena are being drawn from simple experiments.

Third, avoid the seductive trap of generalizing from brain to mind. When done well, fMRI experiments provide important information about how mental or behavioral processes are represented in the brain. In many cases, knowledge about brain function is valuable in itself. For example, if a specific neural dysfunction can be associated with a particular disorder (e.g., hypofrontality in schizophrenia), this may be critical for guiding treatment, even if the mental consequences of that dysfunction are difficult to interpret. But if you reverse the direction of inference (as outlined in Box 14.1), you run the risk of misleading a lay readership.

Fourth, do not subvert the peer review system. One of the bedrock principles of modern science is peer review, which means that discoveries must be vetted by other experts in the field before they can be published in the scientific literature (Figure 14.3). In ideal cases, peer review allows a set of unbiased experts to evaluate the rigor and validity of a study's methods and conclusions. Even

peer review The practice of vetting scientific research by experts in the discipline. Most journals and funding agencies use a peer review system to determine what research can be published or funded.

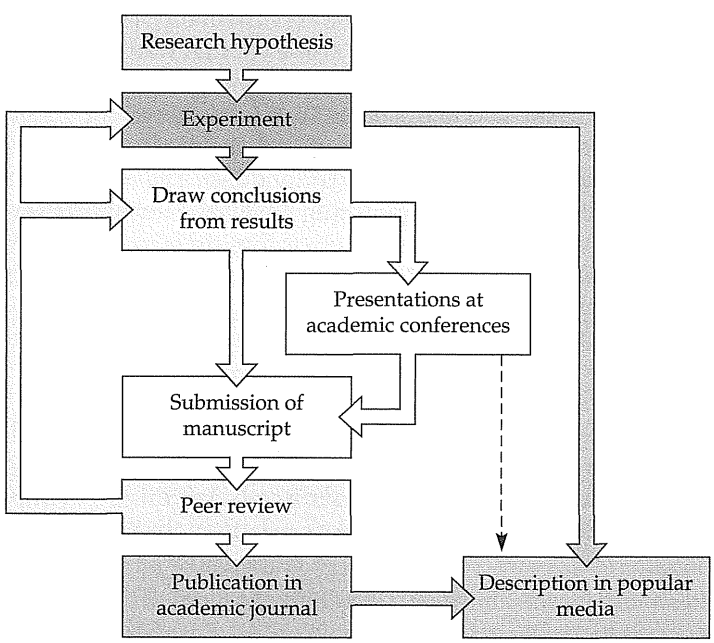

Figure 14.3 A schematic overview of the scientific process. Research begins with an hypothesis that is tested by an experiment, which in turn leads to a set of conclusions. The core element of scientific research is peer review, or the evaluation of the rigor and validity of the researchers' methods and conclusions, usually by a small set of independent experts in the field. Exciting new results are often reported in the popular media following peer review and publication in an academic journal. When researchers present their results directly to the media (red arrow) there is a substantial risk that the results will be misrepresented or overstated. Some academic conferences provide information to the media about selected high-impact findings, as indicated by the dashed line. These early reports can provide an important service to the public, but researchers should nevertheless be cautious about making claims that have not yet passed peer review.

given its practical weaknesses (reviewer bias or laziness; the possibility of fraud or mistakes) peer review remains a nearly universal standard for scientific research. When a finding is trumpeted in the popular press without prior peer review, there is an extraordinary risk that its conclusions are not justified by the results. For this reason many top journals will not publish research that has already been publicized widely. As a better way to disseminate scientific research, many researchers now deposit published articles into public-access archives. This practice is even required by some funding agencies.

Fifth and finally, collaborate with journalists to ensure the accuracy and balance of articles about your work. When discussing cutting-edge work, scientists must think of themselves as both advocates and teachers. How can I convey my excitement about this research without overstating its importance? What background information does the journalist need to know in order to present my research accurately? It is rare for a journalist, even one with a degree in a related field, to have much background knowledge about a study. Thus, fMRI researchers should work closely with journalists to educate them about both the strengths and limitations of the research technique. For most academic scientists, a good resource is the local university news office, which typically contains experienced science writers. Interacting with science writers is often useful in helping researchers understand how the general public will interpret their findings.

We are fortunate that discoveries based on fMRI research have received consistent and positive news coverage over the past few years. It is the responsibility of all fMRI researchers to interact with journalists and the media in a responsible and ethical manner, both to promote their own research and to maximize the public understanding of science.

Conducting fMRI Research

All medical research with human subjects, including experiments using fMRI, must be conducted in accordance with ethical principles designed to protect those subjects' rights. An early and important articulation of these principles was the Nuremberg Code, which was written as part of the trials of Nazi war criminals following World War II. At that time, the Nuremberg Military Tribunal recognized that some of the most heinous crimes of that war were committed in the name of science. Some horrors included intentionally administering infectious disease agents, subjecting prisoners to extreme conditions (e.g., extreme altitude or extended immersion in sea water), and conducting anatomical and musculoskeletal experiments on healthy individuals. The Nuremberg Code provided standards for judging and punishing the Nazi crimes and principles for ensuring that research would be conducted more ethically in the future. The regulations established by the Nuremberg Code include:

- Subjects must give voluntary and informed consent to participate in research.
- An individual may withdraw from the study voluntarily.
- Experimental procedures must minimize the risks to the subjects.
- Risks to participants may never exceed the potential humanitarian benefits (e.g., increased knowledge about a medical disorder). If these benefits could be obtained by other means that incur less risk, then the study cannot be conducted.
- The researchers should be scientifically competent and knowledgeable about the ethical conduct of research.

subject An individual who participates in a research study. Some journals and scientific societies prefer the term "participant," to emphasize the voluntary nature of research.

Nuremberg Code A set of principles for the ethical conduct of research involving human subjects that was developed following the trials of Nazi war criminals in the 1940s.

informed consent The process in which a potential subject voluntarily agrees to participate in a research study, after learning about the procedures, risks, and benefits of the study.

More recently, these ideas have been distilled into three core principles. The emphasis on individual rights and voluntary participation has come to be known as the principle of respect for persons. In many cases, individuals who cannot make an informed, voluntary decision to participate in a study must themselves receive direct benefit from the research. The emphasis on minimizing risks to participants and maximizing benefits to participants or society is known as the principle of beneficence. Furthermore, both risks and benefits must be distributed as fairly as possible throughout society, under the principle of justice. These three principles, which were established in 1978 by the U.S. National Commission for the Protection of Human Subjects, remain the cornerstones of modern scientific research involving human subjects. In the following sections, we discuss how these ethical principles guide the way fMRI research is conducted.

Proposing and approving fMRI research

Before researchers can begin any experiment involving human participants, including experiments using fMRI, they must obtain outside approval for their research procedures. To do so, they document their experimental plans so that a board of impartial reviewers can assess the risks and benefits of the research. Within U.S. institutions, these are called Institutional Review Boards (IRBs). The examples we present in this section are drawn from U.S. research, however, similar guidelines are in place for research conducted in other countries.

Each IRB is charged with ensuring that research conducted at its institution adheres to the core ethical principles described above, and to legal and regulatory guidelines. The IRB membership must consist of individuals with diverse backgrounds, from scientists who provide expertise about the experimental techniques to community members who are otherwise unaffiliated with the institution. Community members serve a critical oversight role, in that their perspectives on the risks and benefits of research may differ dramatically from those of academic scientists. When research is conducted on individuals who may be unable to provide voluntary and informed consent (e.g., prisoners, children, or mentally disabled persons), then the IRB must include at least one individual with particular expertise with (and concern for) those subjects.

Each IRB reviews all research conducted at its institution, including research by individuals who have positions at that institution, but do their research elsewhere. This local oversight frees researchers from having to report to a national review board. But, it also means that each IRB must be largely independent from the institution and from the scientists it oversees, so that it can evaluate research in a fair and unbiased manner. In addition to its role in approving and reviewing experimental procedures, the IRB also oversees the ethical training of scientists at its institution. Often this training takes the form of workshops or online training material that scientists must complete (and renew annually) before being certified to conduct research.

To have their experimental procedures reviewed, scientists submit a research protocol to the IRB. For fMRI studies, the protocol typically contains information about the potential subjects and how they will be recruited, the scanner and pulse sequences to be used, and the experimental paradigms to be followed. The protocol must contain sufficient information to allow the IRB to evaluate the research according to the core principles described above. A consent form, which must be signed by each research subject before participating in the study, is also necessary (see Figure 14.4 for an example). For fMRI research, the consent form usually describes what will happen during the

respect for persons The principle that individuals should be treated as autonomous decision makers who should be given the opportunity to make informed decisions about their participation in research studies. Individuals with an impaired capacity for autonomous decision making must be granted additional protection.

beneficence The principle that research protocols should maximize the potential benefits of research while minimizing the costs to any individual subject.

justice In the context of research involving human subjects, the principle that the costs of research are distributed broadly and fairly across society.

Institutional Review Board (IRB) An independent group of individuals who evaluate the ethical practice of research conducted at their institution. Researchers who wish to conduct research with human subjects must have the approval of their IRB.

research protocol A document describing the procedures of a research study, in a form that can be evaluated by the local Institutional Review Board.

consent form A document that describes the procedures, risks, and benefits of a research study in clear language, so that potential subjects can make an informed decision about participating.

Figure 14.4 An example of a consent form. Consent forms provide information to potential research participants, so that they can make an informed decision about whether to participate in the study. Consent forms typically explain the procedures of the research and describe any risks or benefits. They must be written in a clear, jargon-free manner.

DUKE UNIVERSITY HEALTH SYSTEM

Consent Form to Participate in Research on the Functional Neuroimaging of Executive and Cognitive Processing

IRB #:

We are asking you to take part in a research study in the Brain Imaging and Analysis Center at Duke University Medical Center in which magnetic resonance pictures of your brain will be taken. In order to decide whether or not you wish to be a part of this research study, you should know enough about its risks and benefits to make an informed judgment. This consent form gives you detailed information about the research study that a member of the research team will discuss with you. This discussion should go over all aspects of this research: its purpose, the procedures that will be performed, any risks of the procedures, and possible benefits. Once you understand the study, you will be asked if you wish to participate and, if so, you will be asked to sign this form. This study is being sponsored by a grant from the National Institutes of Health.

Description of Procedures:

Pictures of your brain will be taken using magnetic resonance imaging (MRI). MRI uses strong magnetic fields and radio waves to make pictures. Special pictures will be taken that provide information about the areas of the brain that become active when you see or hear particular kinds of stimuli and make simple judgments about them. You will see videos that may include faces, objects such as cars or furniture, words, numbers, colored patterns, shapes, dots, or abstract designs. You may also listen to spoken words in English or to other non-speech sounds. You may be given information about other people's decisions and asked to use that information in your decisions. Also, you may have the opportunity to play games in which you can win money for yourself, for another individual, or for a charitable organization. You might be asked to choose a charity for which you would like to earn money from a list of eligible charities. The study staff will tell you exactly what stimuli you will receive during this study. In addition, the study staff may ask you to push a button or to move your hand or foot when particular stimuli appear.

During the study, you will lie on your back on a narrow bed that will be pushed into the MRI machine. The MRI technician will provide padding for your head and knees to make you more comfortable. If you are uncomfortable or feel pain because of lying down, tell the technician immediately. The technician will position your head inside a head tube, and the platform will be pushed into the MRI machine. You will hear a loud noise while the machine is collecting pictures. You will be able to communicate with the technician during the study using a microphone and speaker in the MRI machine. It is expected that the MRI portion of this study will take 1-2 hours. Depending upon the specific experiment, one or two additional testing sessions outside of the MRI machine may be required. Each session will last approximately 1-2 hours. These sessions will be conducted in a computer laboratory or in a scanner simulator, and they will involve practicing the experimental task and answering questions about your attitudes and preferences regarding different types of decisions. The scanner simulator looks and sounds like an MRI scanner, however it does not have a magnetic field.

Risks and Inconveniences:

There are no known long-term health risks from exposure to the magnetic fields and radio waves used to make these MRI brain pictures. However, it is not assured that harmful effects will not be recognized in the future. Strong magnetic fields pose safety risks because they attract metals such as iron, and radio waves can interfere with medical devices such as pacemakers. It can be dangerous for people that have medical devices, metal objects, or metal debris in their bodies to go into a MRI machine. This includes certain dyes found in some tattoos. It is also dangerous to bring loose metal objects into the room containing the MRI machine, because those objects may be pulled towards the magnet and could injure

Page 1 of 4 Subject's Initials

experiment, how the MRI scanner works, the safety issues associated with fMRI (see Chapter 2), procedures for ensuring confidentiality (see the following section), and the rights of research participants. Consent forms must be written in clear, jargon-free language; a common standard is that someone with only an eighth-grade reading level must be able to read the form and give informed consent. The consent form does not represent a contract to participate in the study; the subject always has the right to withdraw from the study at any time. In most cases, the consent form should describe the research goals and practices in a complete and accurate manner. However, some experiments involve deception, in that information about the nature of the task is omitted from the consent form (and from the instructions given to the subjects). Deception is used deliberately in some fMRI experiments, such as those examining social interactions (e.g., research on peer pressure) or memory (e.g., research on implicit encoding into memory). Because of the importance of informed consent, the use of deception must be well justified by the researchers.

deception The use of experimental procedures that intentionally mislead subjects.

Thought Question

Should researchers be allowed to deceive their subjects at all? What are the advantages of deception? What are the costs?

Once these forms (along with any others required by the institution) are submitted to the IRB, a review committee within the IRB will evaluate the proposal. Depending on the committee's review, the proposal may be rejected, returned to the investigator with suggestions for revisions, or approved. The U.S. Food and Drug Administration (FDA), which oversees safety issues associated with medical devices, has classified most MRI scanners (when used within guidelines for operating limits) as devices involving "nonsignificant risk" to human subjects. This classification means that in the U.S., research involving fMRI is subject to fewer regulations and restrictions than research involving devices that are judged to pose significant risks to subjects. Furthermore, it means that the institutional IRB panel has sufficient authority to approve research involving fMRI without soliciting FDA approval, which may be required for studies involving "significant risk" drugs or devices.

Scientists sometimes describe their local IRBs in adversarial terms. Like other institutions, IRBs can be bureaucratic and unwieldy. They may be slow, inefficient, and capricious in their decision-making. Yet they are critical for ensuring the rights of research subjects and the responsible practice of science. A better way to think about the IRB is as a research partner. Rather than blindly submitting protocols and then complaining about rejections, researchers need to work closely with IRB staff and review panels throughout the process. The expertise of IRB members can be very helpful in ensuring that subjects are informed, and that correct procedures are followed. Adhering to good ethical practices not only ensures compliance with regulations, it can also greatly improve the quality of the data. Furthermore, as a condition of publication, journals require that research be conducted under an IRB-approved protocol.

Ensuring the confidentiality of fMRI data

Nearly all uses of fMRI involve research: the collection of data as part of an experiment, and the testing of hypotheses using samples of subjects drawn from larger populations. Yet fMRI research shares many features with clinical MRI practice. Researchers may collect their data on the same scanner as used for clinical patients. Research sessions may include some of the same pulse sequences and the collection of some of the same types of images (especially anatomical) as those in clinical sessions. Some fMRI studies involve drug administration, or test subjects who have psychiatric disorders. If an fMRI subject has a neurological abnormality, such as a brain tumor or cyst, that abnormality may be visible on the anatomical images (see Box 14.2). Thus, even though an fMRI study may have a purely research-oriented goal, some of the data collected during the study may be medical.

One example of how medical regulations can influence fMRI research in the U.S. is the Health Insurance Portability and Accountability Act (HIPAA). This act was passed in 1996 by the U.S. Congress, and codified as a Privacy Rule by the U.S. Department of Health and Human Services in 2000. A central goal of HIPAA was to streamline the transfer of healthcare-related information through the standardization of language, resulting in a reduction in paperwork. This

research The accumulation of data, whether by observation or experimentation, to develop general knowledge.

Health Insurance Portability and Accountability Act (HIPAA) An act passed by the U.S. Congress that requires specific procedures for ensuring the privacy of health information.

BOX 14.2 Incidental Findings in fMRI Research

The anatomical MR images used in this book are, in almost all cases, from neurologically normal young adults who have volunteered to participate in research fMRI scans (for examples, see Figure 8.25). Even though individuals in this population are generally healthy, asymptomatic, and high-functioning, some of them have structural brain abnormalities that are visible on their anatomical MR images (Figure 1). When identified as part of a research MRI experiment, such unexpected abnormalities are known as **incidental findings**.

The rate of incidental findings can be surprisingly high, even in healthy populations. Several large-sample studies have found that about one to two percent of asymptomatic volunteer subjects have incidental findings noted by reviewing radiologists, although relatively few of these require medical intervention. In particular populations, such as older adults, this rate may be even higher. For example, a 2007 study by Vernooij and colleagues examined the MR images of two thousand older individuals who had volunteered for research scans. Fully 7% of all participants had asymptomatic brain infarcts (i.e., stroke damage), another 1.8% had small aneurysms, and another 1.6% had some form of tumor. Notably, only two of these incidental findings required operative treatment.

incidental finding The discovery of an abnormality, usually on a structural MR image, in an asymptomatic individual who was scanned for non-medical reasons.

Figure 1 Examples of incidental findings observed in brain MRIs from asymptomatic individuals. In each image, the arrow or arrows indicate the abnormalities: (A) aneurysm of the anterior communicating artery, (B) tonsillar herniation, (C) a vestibular schwannoma, (D) a large meningioma, (E) a large sudural hematoma, and (F) a trigeminal schwannoma. (From Vernooij et al., 2007.)

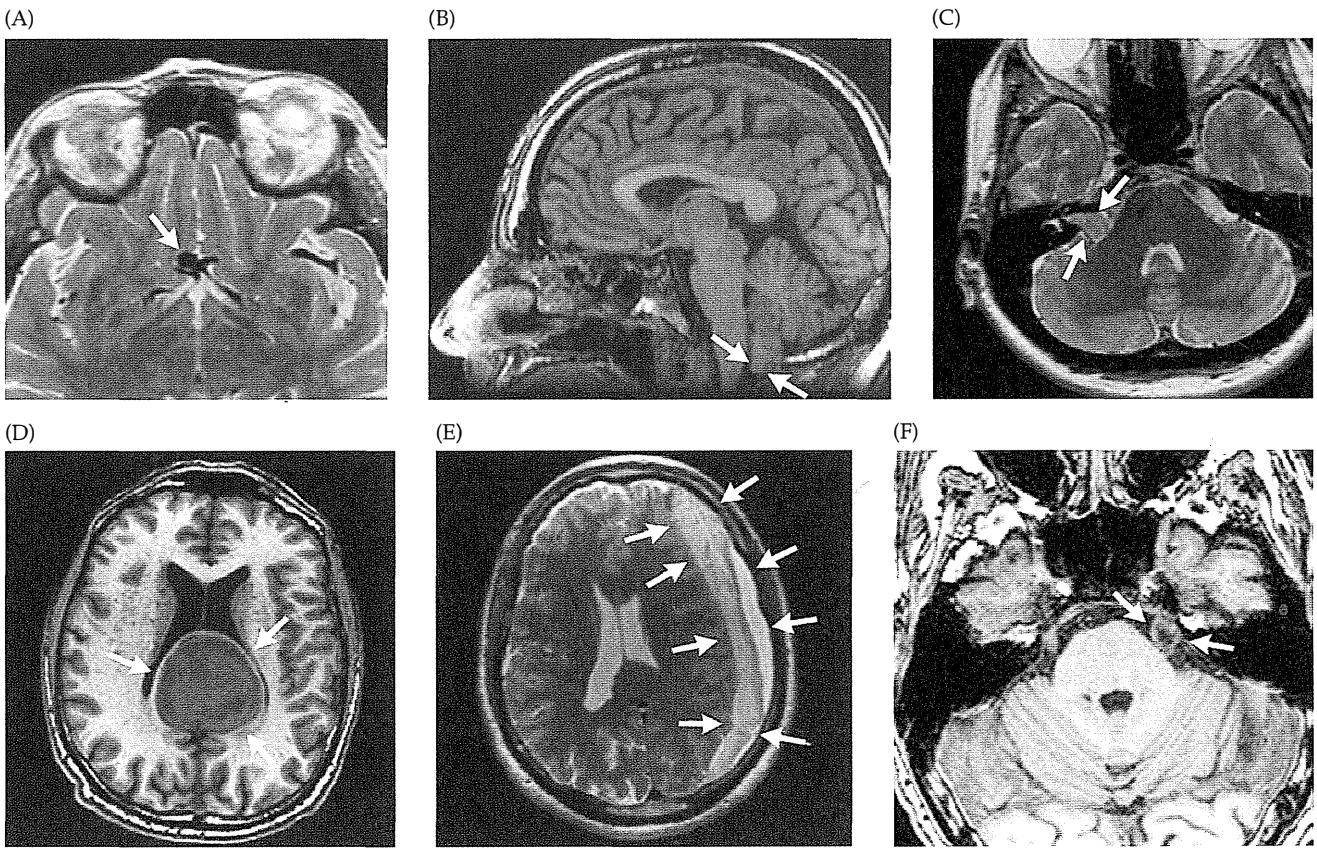

BOX 14.2 *(continued)*

Given that a single MRI center may scan hundreds or even thousands of subjects per year, incidental findings are a regular (albeit infrequent) part of fMRI research. Yet, there are no standard and universally accepted procedures for dealing with them. In this box, we consider four ethical issues associated with incidental findings: what sorts of anatomical scans should be collected, who should review those scans, what the subjects should be told about their incidental findings (and when they should be told), and who should bear the costs of these procedures? These questions are matters of active debate among fMRI researchers, policy makers, and bioethicists, and thus there are no simple answers. We are hopeful, that this box will spark discussions about this very important topic.

As discussed in earlier chapters, most fMRI sessions include the collection of a single set of high-resolution anatomical images (usually, but not always, with T_1 contrast) that facilitate the normalization of the functional data to a standardized stereotaxic space. These images, though valuable for mapping gross gyral and sulcal anatomy, are not sufficient for clinical diagnosis. Some types of damage, for example, lead to a substantial signal increase on T_2-weighted images, reflecting an excess of intracellular or extracellular fluid. These include many tumors, stroke infarcts, and hemorrhaging, all of which may be difficult to identify on the images typically collected during fMRI studies. To maximize the chances of catching incidental findings, researchers would need to add new anatomical sequences to the fMRI protocol, which adds time (e.g., an additional 10–15 minutes) and thus increases costs. Few institutions now require researchers to collect a full set of clinical-quality anatomical images for neurologically normal subjects, although such scans are often collected when the volunteer subjects must be evaluated for potential pathologies (e.g., when studying brain function in very old individuals). However, it is possible that future ethical standards, perhaps combined with new spatial normalization and segmentation approaches, will require the collection of multiple types of anatomical images as standard practice.

Possible Procedures for Incidental Findings

Incidental findings are, by their very nature, unexpected and unlikely. Therefore, a key question is who should review images to check for potential abnormalities. When an individual with relevant medical training is part of the research team, as is often the case when a study uses volunteers who are likely to have damage or degeneration (e.g., older adults or recovering trauma patients), then that person usually reviews the images. However, most fMRI studies are led by scientists who lack formal medical training and who therefore are not certified to diagnose problems or to recommend courses of treatment.

Institutions vary in their procedures for such studies. One survey reported that about one-third of all MRI institutions have a neuroradiologist examine the anatomical images of every subject, another one-half only refer images with suspected abnormalities to a neuroradiologist, and the remainder do not review images when collected under standard research protocols.

To some bioethicists and policy makers, the ethically justifiable course of action seems obvious: we should, of course, have a trained physician look at all of our MRI scans! Yet, even this conservative approach raises a host of practical and ethical concerns. Neuroradiologists are expensive and rare in a typical research environment. Many fMRI centers, such as those affiliated with non-medical institutions like psychology departments, do not have on-site medical personnel. Having anatomical images read by a neuroradiologist would add hundreds of dollars to the costs of scans, which could make an already expensive technique cost-prohibitive.

Minor logistical concerns include authorship and subject confidentiality. Should a physician who reviews anatomical images for incidental findings be included as a collaborator on the project (and, potentially, a co-author on manuscripts)? If not, then procedures must be in place to ensure the confidentiality of the images during review. Regular review by trained professionals can engender unwanted expectations in research subjects. Some individuals may choose to participate in the study because of a desire for a free medical test. Giving this impression to participants could be considered an undue inducement to participate, while also changing the nature of the subject pool and impairing data quality. Moreover, unless the anatomical images really do constitute a full clinical set, even the most expert neuroradiologist could not certify that the individual has no abnormalities, even if there were no incidental findings apparent on the collected scans.

Given these concerns, some institutions have adopted an opposite policy: because fMRI subjects are volunteering for a non-clinical experiment, researchers should not evaluate their scans for any medical condition. Clinical care is neither implied nor expected, giving this approach the advantages of simplicity

(continued on next page)

BOX 14.2 *(continued)*

and consistency. Imagine, however, that you are a new graduate student working in an fMRI laboratory with this policy. While examining the anatomical images from your first fMRI study, you come across an image that looks very odd to your untrained eye. One of the lateral ventricles is grossly misshapen, compressing the adjacent cerebral hemisphere. You have no medical training and thus have no principled way of evaluating the images for pathology. Yet, you have now seen enough MR images to have a rough sense that this seems unusual. What should you do? Should you ignore your suspicions, given that you are just a student, not a physician? A reasonable person could argue that because the scans were non-clinical in nature, any apparent abnormalities should indeed be ignored, especially since false alarms are likely to be common and costly (as discussed below). But what if the participant had reported being generally healthy, save for some recent minor headaches? This fact seemed innocuous at the time of scan, but now seems worrisome in the context of the anatomical images. Should you still ignore the possible incidental finding?

Recognizing both the costs of implementing clinical procedures for non-clinical fMRI scanning, and the potential consequences of neglecting rare but serious incidental findings, the majority of centers have adopted an intermediate policy. Scans are initially evaluated by the non-medically-trained researchers as part of their normal review of data quality. If those researchers see something that appears abnormal, they then refer those images to a designated neuroradiologist, who can recommend a diagnostic follow-up exam if needed. If an abnormality is identified during the scanning session itself, additional anatomical images can be collected immediately, so that the neuroradiologist can make a more informed diagnosis. In principle, this procedure does risk missing some brain abnormalities that could have been identified if clinical-quality images were evaluated by trained personnel. However, it greatly reduces both the costs and logistical challenges, which is a tradeoff that may be acceptable for research studies.

In making decisions about the procedures for incidental findings, one must consider the expectations of the research participants. Most participants are largely naïve about MR scanning; just as they expect fMRI to be able to read their thoughts, they expect that a clean structural MR image means that they have no abnormalities. A recent poll found that 97% of the participants in a set of fMRI studies expected to be notified if there was anything abnormal about their brains. As these subjects may implicitly recognize, any policy that does not tell subjects about a life-threatening medical problem would be ethically dubious. However, knowledge about incidental findings, especially if benign, can have negative consequences. Suppose that some weeks following your participation in a fMRI experiment, you were told that something abnormal was observed in your anatomical images. You contact your primary care physician, who refers you to a specialist, who schedules a clinical MRI, which finally reveals a common and benign condition (e.g., a cyst or slight structural defect). During that extended process, you may have suffered through weeks of uncertainty and stress. When considering this issue, Mamourian raises the analogy of prospective whole-body CT or MRI

goal required new approaches for organizing private health information (e.g., establishing online databases for medical research), raising potential privacy and confidentiality concerns. Thus, regulations within HIPAA also prohibit the unauthorized sharing of information among medical providers, insurers, and employers. For example, a corporation cannot request the medical records of its employees in order to make firing or promotion decisions. Conversely, HIPAA also specifies the rights of individuals to request information about their medical records, including what organizations have had access to what information at what times. Because fMRI data may contain private health information, studies using fMRI in the United States must comply with the HIPAA regulations. Analogous regulations govern research in other countries, including Canada (the Personal Information Protection and Electronic Documents Act) and the European Union (the Directive on Data Privacy).

BOX 14.2 *(continued)*

screening. Few people would argue that asymptomatic individuals should get such screenings, given the resources required and the risk of false positives. And in the absence of symptoms, the significance of many incidental findings would be difficult to interpret. Can we justify large-scale screening of asymptomatic people who happen to enroll in fMRI studies?

Topics for Future Consideration

How best to deal with incidental findings will remain a topic of debate for years to come. It is possible, perhaps even likely, that no consensus will emerge. Instead, individual institutions may adopt policies that reflect their local attitudes (and biases). Of growing importance will be questions of resource allocation: who will bear the costs of increased attention to incidental findings? The seemingly innocuous requirement for an additional ten-minute anatomical scan within every fMRI session would add many millions of dollars in scanner time charges within the United States alone. The increased costs of scanning would have immediate negative consequences for scientific productivity. Referring all fMRI scans to neuroradiologists would be even more expensive, especially if costs were borne by individual investigators. Institutions going that route may build the cost of reading the anatomical images into the standard hourly scanner charges, thus saving money through economies of scale.

While it may seem callous to weigh these financial costs against the real benefits of identifying potentially life-threatening medical conditions, one should never lose sight of the fact that such cost-benefit tradeoffs are endemic to modern society. Individuals at all levels of medical care, from policy makers to physicians, face choices about whether medical care is justified, given its costs. In this case, do the benefits gained from comprehensive screening for incidental findings justify the scientific and monetary costs? Considering only the clinical benefits, it is hard to argue that screening asymptomatic young adults is an effective use of health care resources. But, considered within the context of fMRI research, there are credible arguments that such screening is not only justified but also expected. Only through broad discussions between ethicists and MRI researchers will these issues be resolved.

Thus far we have considered only incidental findings observed on anatomical scans. What about the functional images? Should those be evaluated for markers of disorders? This seems like a remote and abstract possibility, given the rudimentary nature of most fMRI measurements, but consider a very simple case. Suppose that you are conducting a study that compares individuals with schizophrenia with psychiatrically normal controls. You discover that schizophrenic participants have greatly reduced activation in one particular brain region compared with nearly all of the control subjects. However, one control subject's data lie squarely within the range of the patient group. Should that fact be communicated to the subject? This type of scenario, while fiction today, will soon be reality as researchers show that fMRI has diagnostic validity for some disorders. Like other technologies, as fMRI becomes increasingly powerful, the ethical issues it raises become increasingly important.

The regulations guiding data confidentiality are complex, context-dependent, and sometimes difficult to interpret. Yet they have substantial implications for fMRI research. Some journals have required authors to deposit their data into approved, publicly accessible databases. To ensure the privacy of their research subjects, the investigators must remove any information that might link the data to particular individuals. This process is called **de-identification**. For fMRI data, potential links could include the subjects' names, dates of birth, contact information, and scanner session numbers. Depending on the quality of the anatomical images, the skull and facial physiognomy might also link subjects to their data (particularly if there is other information that identifies what individuals might have been used as subjects in the study). Thus, the skull and facial features are sometimes removed before structural images are made publicly accessible (Figure 14.5).

de-identification Removal of information that may link research data or medical information to a particular individual.

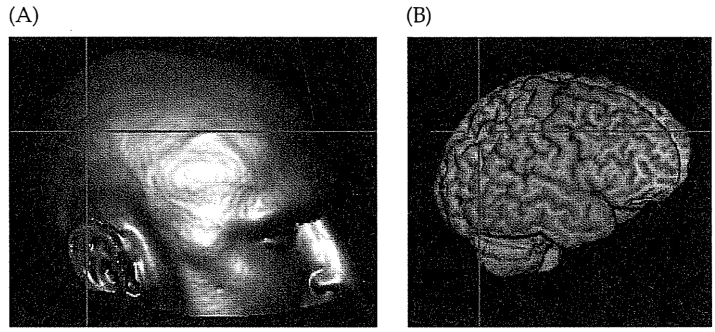

Figure 14.5 Skull stripping to remove facial features. (A) Because the imaging volume extends to include the skull, it is possible to render an image that shows some aspects of facial physiognomy. Even so, the rendered skull is often not readily identifiable, especially if there is no other information about whose data it might represent. (B) To eliminate any concerns about facial information, the skull is sometimes stripped from the anatomical image before fMRI data are deposited in any publicly accessible repository. (Images from MRIcron, courtesy of Dr. Chris Rorden.)

Thought Question

How can fMRI researchers balance the need to keep medical information confidential with the desire to share fMRI data with their peers? Do the benefits of confidentiality outweigh the costs?

The need to ensure confidentiality can raise obstacles for fMRI researchers. Without the subjects' approval, some data cannot be shared with scientists outside the IRB protocol, even other scientists at the same institution. For this reason, some researchers include data-sharing language in the consent form, so that subjects can approve the conditions under which their data will be distributed (e.g., to a database in de-identified form). Furthermore, confidentiality issues increase in relevance as basic fMRI research intersects with clinical applications. Research that combines fMRI with genetic measurements or with drug manipulations has the power to identify specific biomarkers associated with certain disorders or personality traits (e.g., an fMRI response in the amygdala may predict whether someone suffers from anxiety). In such cases, a pattern of fMRI activation, or even the raw BOLD time course itself, may represent medically relevant information. As a general rule, fMRI data should be de-identified at early stages of analysis, both as a legal necessity and as good scientific practice.

Safe conduct of fMRI studies

Above all else, fMRI researchers must minimize the risks associated with the MR environment. The hardware used for fMRI generates very strong static magnetic fields, weaker but rapidly varying gradient fields, and periodic bursts of radiofrequency energy. Each of these components is associated with safety risks that range from relatively benign (e.g., heating associated with the absorption of radiofrequency energy) to potentially life-threatening (e.g., projectile motion within the static magnetic field). The dangers associated with specific MRI hardware components were covered in Chapter 2, along with the practices used in many MRI centers for minimizing the risks to subjects.

Creating safety procedures that work for a large research MRI center with many diverse uses raises a host of ethical (and practical) concerns. As fMRI becomes increasingly popular, it has attracted researchers from a wide variety of backgrounds; not just physics, neuroscience, and psychology, but such areas as linguistics, education, and economics. Furthermore, there has been a dramatic increase in the number of individuals doing fMRI research. At a

large institution, there may be more than one hundred faculty, staff, and students involved with fMRI research in some form. Typically, the MRI center will require everyone who works at the scanners to complete some level of safety training. This may range from a very simple test for those just needing entrance to the MR console room, to a complex hands-on training session for those who set up subjects in the scanner. If the researcher will be controlling the scanner itself, then a more extensive set of training sessions are usually required.

redundant safeguards The use of multiple independent procedures that could each identify potential problems or unsafe situations.

Thought Question

Should students be allowed to control the scanner console by themselves? Or, should scanner control be reserved for certified MRI technologists? How should an MRI center balance the need for student training with the desire to minimize risk to research subjects?

Despite the many safety precautions taken, you will hear stories about narrowly averted accidents if you spend any time in an MRI center, even a highly regarded one. Most often-recalled are stories about trained individuals, including physicians and scientists, who attempted to enter the MR scanner room while still wearing their pagers, carrying metal clipboards, or talking on cellular phones. Another typical story is about the patient who reports no abnormalities on the screening form, only to reveal at the last moment before entering the scanner that he or she has a pacemaker, aneurysm clip, or other implanted device. Although some of these stories may be exaggerated, they contain core elements that are of real concern. Trained people sometimes forget to remove potential projectiles, while research participants sometimes neglect to mention implanted metal, or conditions that would disqualify them from participation. Such situations pose the most difficult challenges for the safe conduct of fMRI studies, in that they typically involve absentminded errors rather than poor decisions or malice. Thus, the simple training of researchers cannot ensure the safety of research subjects by itself.

A powerful concept for thinking about the safe conduct of fMRI research is that of redundant safeguards, or having multiple independent procedures for identifying and correcting potential problems. The value of redundancy can be clearly seen when screening subjects. One good policy is to conduct safety screening at three separate times (Figure 14.6). When a potential subject first contacts the laboratory about being in a session, the researcher should ask ques-

Figure 14.6 A hierarchical approach to safety screening. To minimize the chances of unsafe scanning, safety screening should occur at each of three stages: (A) an initial phone call that screens for significant concerns; (B) a comprehensive screening, including completion of a safety form, on the day of scanning; and (C) a final check for worn or carried metal immediately before entering the scanner.

(A) Initial phone screening

(B) Onsite interview

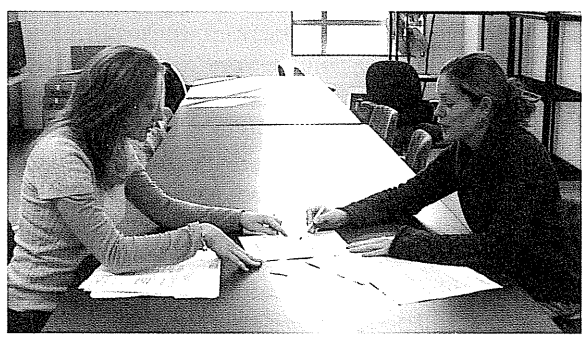

(C) Scanner access

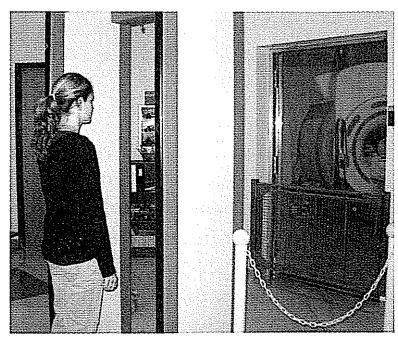

tions about implanted metal, medical devices, and any other conditions, such as a past eye injury involving metal, that would exclude the individual from participation in any fMRI study. Eligible participants are also told at that time not to bring any metal to the scanning session. Then, when the subject comes to the MRI center on the day of the session, he or she fills out an MRI safety form that asks detailed questions about a wide variety of problems and conditions. Note that this information is only collected *after* informed consent is obtained, because comprehensive private health information is requested. And finally, before the subject enters the scanner itself, one of the research team should ask questions about implanted or worn metal, such as: "Do you have any metal in your body?" "Are you wearing anything with metal?" "Do you have any items in your pockets or in your hair?" By asking subjects about metal (and other safety hazards) multiple times in different contexts, the laboratory increases the chances of identifying potential problems before they cause harm to the subject.

The procedures described above are redundant over time, in that they are repeated at different stages during an experiment. There is also value in having procedures that are redundant across individuals. All members of a research team, from the most senior faculty advisor to a beginning graduate student, must adhere to good safety practices. Students and others should be ready to challenge unsafe practices, even if the offender is a senior faculty member or physician. No one, no matter how experienced, should object to being asked about safety procedures. Moreover, fMRI researchers should not depend on technologists (or other staff members) for the safety of their subjects. More than one individual should read the completed safety forms, ask about worn or carried metal, verify that earplugs are correctly fitted, and check on the subject's overall well-being. When safety becomes the responsibility of only one person, then the risk of errors increases.

Pregnancy testing in fMRI research

Structural MRI provides very high resolution and multiple tissue contrasts, while also allowing large field-of-view images in any plane, giving it some significant advantages over other non-invasive imaging methods. Because of these advantages, MRI has become an increasingly prevalent technique for scanning pregnant women. For evaluating certain conditions in the fetus, such as congenital brain or spine defects, MRI can provide information with contrast and resolution not obtainable using any other technique. Furthermore, MRI has become a critical component of the standard of care for many non-pregnancy-related conditions (such as tumors), so that pregnant women with those conditions are scanned in order to guide the course of treatment. In such cases, it is clear that the diagnostic advantages of MRI provide substantial (in some cases, life-saving) benefits to these patients.

In fMRI research a very different standard, one that weighs the potential harms against the minimal benefits accrued to participants, is used in determining whether individuals can participate as subjects. As we stressed in Chapter 2, the magnetic fields and radiofrequency energy used in standard fMRI scanning have no known deleterious biological effects. Even so, one cannot rule out potential unknown risks to the developing fetus. Therefore nearly all fMRI centers prohibit research scans on pregnant women. This restriction has considerable relevance for research studies, because many potential fMRI subjects are adolescent or adult women of childbearing age. Some fMRI centers allow women to certify that they are not pregnant, while others require a neg-

unknown risks Possible negative outcomes that, though not anticipated based on the best available science, nevertheless influence research or clinical procedures. Most fMRI centers do not scan pregnant women because of potential unknown risks to the developing fetus.

ative urine (or rarely, blood) pregnancy test before participation. These differences in requirements do not reflect differences in the actual risks associated with fMRI scanning at different institutions, but they reflect variations in how local institutional review boards weigh unknown risks.

Applying fMRI to New and Controversial Topics

Most applications of fMRI are not controversial. A few arbitrarily chosen examples of such applications are: studying memory encoding in the medial temporal lobe, mapping attention effects in the secondary visual cortex, and evaluating the effects of practice on motor processing in the cerebellum. In all these cases, researchers tested well-defined hypotheses about specific brain regions, and as a result, gained new knowledge about brain function. Other applications have less traditional goals. Some fMRI researchers work with educators to evaluate the effectiveness of different curricula, with the goal of improving teaching methods in elementary schools. Others collaborate with marketing scientists to understand the brain mechanisms underlying purchasing decisions. Still others have partnered with industry to develop new methods for assessing psychiatric and neurological disorders, evaluating treatments for addiction, and tracking neural problems during development.

Not all fMRI applications, either existing or potential, are so obviously salutary. In recent years there have been numerous studies relating fMRI data to traits and attitudes, even in the absence of overt behavior. One could readily imagine using fMRI to identify markers of intelligence, political preferences, sexual orientation, and even religious beliefs. Even seemingly benign areas of research (e.g., romantic love) could have unexpected consequences: are you really in love if your brain doesn't show an expected pattern of activation? Some research topics are patently controversial. Suppose that researchers identify a pattern of fMRI data, say increased activation in the amygdala, that correlates with racist attitudes in subjects presented with images of individuals of different races. Should a person be judged as "racist" based on his or her brain responses to such images, even in the absence of any actions (or even, potentially, any thoughts) to the contrary? These examples seem controversial because they suggest the possibility of using fMRI to gain hidden information that could contradict overt behavioral measurements. Similar concerns have arisen in other domains of science, notably human genetics, and there is as yet little consensus on how to balance scientific inquiry with societal consequences. (Note that the examples in this section are hardly abstract; many of these topics are already areas of active fMRI research.)

Non-traditional applications of fMRI can evoke a range of emotional responses, from praise to suspicion. All these applications are clearly within the purview of science; shouldn't we learn about the motivators for our purchases or the underpinnings of our lies? And all have been studied for many years using traditional techniques, such as standardized testing by educators or the use of focus groups by market researchers. But when fMRI is added to the research program, new ethical concerns arise. In this section, we discuss how fMRI should be applied to real-world problems. As examples we use two general classes of applications, here labeled "reading minds" and "identifying traits." Our goal is not to criticize current efforts in these areas; on the contrary, we believe that these represent some of the most cutting-edge topics for fMRI research. Nevertheless, we do want to emphasize some ethical pitfalls that could derail these promising research efforts.

Reading minds

On the cover of the November 2007 issue of *Popular Mechanics*, there was a photograph of a man lying in an MRI scanner (Figure 14.7). A targeting reticle was overlaid on the photograph, as if the man were being observed through the sight of a gun, and the adjacent headline blared, "Digital Thought Police." The accompanying article grabbed readers' attention through a series of provocative claims: "How Brain Scans Could Invade Your Private Life," "What if employers want to use this technology as part of a standard job interview?," and even "Boosters say a nearly foolproof lie detector based on brain scanning is just around the corner." Perhaps even more revealing were the comments posted online by magazine readers. Many were cautious, recognizing the limitations of fMRI. Others were fearful of fMRI's capabilities, worrying about the ethical implications of an accurate lie detector. Most disturbingly, a substantial portion of the commentators were worried about scientists using fMRI to read minds (to steal ideas or ferret out impure thoughts) or even to control people against their will. It is tempting to dismiss such ideas as the opinions of uneducated crackpots. Consider, however, that these comments came largely from people who have computer access, live in a society with constant exposure to advanced technology, and read a magazine devoted to applications of science to daily life.

It is easy to think of an fMRI scanner as a mind-reading device. One of the authors of this textbook still remembers his nervousness as an fMRI subject many years ago; he wondered what the experimenter could tell about his thinking. We hope that by now, every reader of this book has been disabused of this notion. Stated baldly, fMRI is far too limited a technique to read the contents of consciousness in anything other than the coarsest sense. Even the best examples of data-driven fMRI analyses, introduced in Chapter 11, provide insight

mind reading The ability to construct a comprehensive description of the contents of consciousness. This is currently far beyond the capacity of any neuroscience technique.

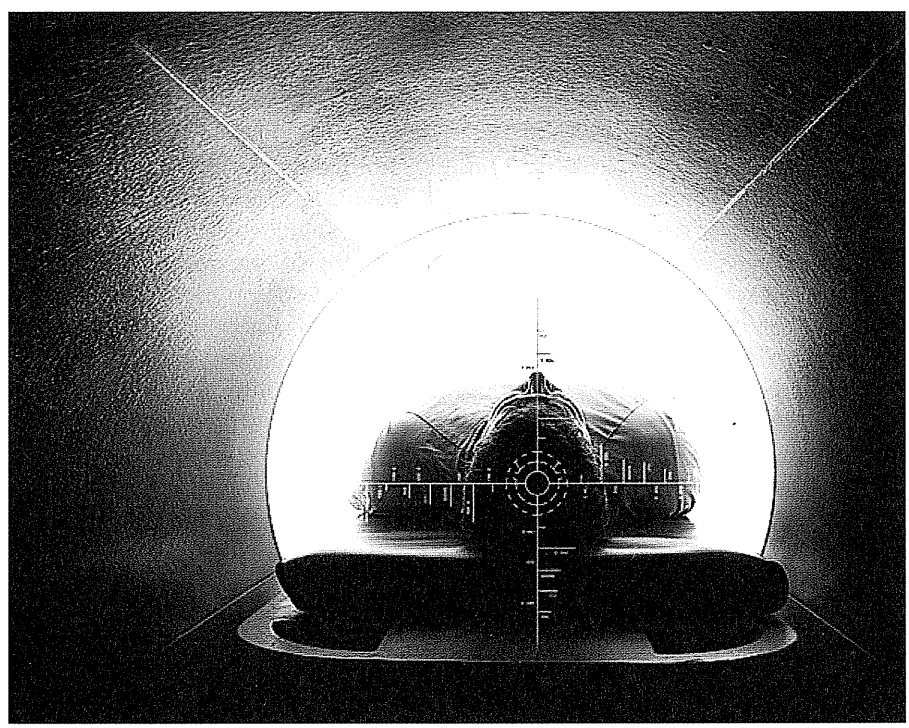

Figure 14.7 An example of the representation of fMRI in the mass media. (From Wise, 2007.)

into only the most restricted aspects of mental life: Does the subject see a vertical or horizontal line? Is the subject adding numbers or subtracting them? But even such thoughts can have considerable importance. The guilt or innocence of an accused murderer could rest on the credibility of a single alibi witness. Suppose that fMRI could be used to determine one simple fact: whether or not a witness is telling the truth. This one application would revolutionize the legal system, even if the rest of the mind remained inaccessible.

Lie detection using physiological measurements has a long and controversial history. The best-known instrument is the polygraph, which first measures several physiological responses (e.g., blood pressure, skin conductance, respiratory rate) to known truths and falsehoods, and then uses those responses to evaluate statements of unknown veracity. The polygraph, which has been around for nearly a century, occupies a nearly mystical place in popular culture. Nevertheless, its effectiveness remains highly questionable, with accuracy in real-world settings often little better than chance. The uses and misuses of polygraph technology are well beyond the scope of this chapter. We refer readers to the 2002 report of the National Academy of Sciences for a detailed consideration.

polygraph A device that measures multiple physiological indicators to judge whether an individual is lying. Despite their pervasiveness, polygraphs have proven to have minimal validity for detecting lies in real-world settings.

The use of fMRI could have several advantages over polygraphs. A complex pattern of brain activation might be more difficult to fake—while also being more sensitive—than simple peripheral nervous system responses. And in principle, the fMRI data could be examined in a blinded manner. By contrast, the polygraph examination is usually conducted by a specialist whose judgment shapes both the flow of questions and the interpretation of the answers. Over the past decade, many researchers have evaluated the capability of fMRI data to detect lies. Studies by Daniel Langleben and colleagues have shown that intentionally deceptive responses led to increased activation within the superior medial prefrontal cortex, among other regions, and that activation in this region discriminated lies from truth with approximately 80% accuracy (Figure 14.8). Other groups have reported similar accuracy based on activa-

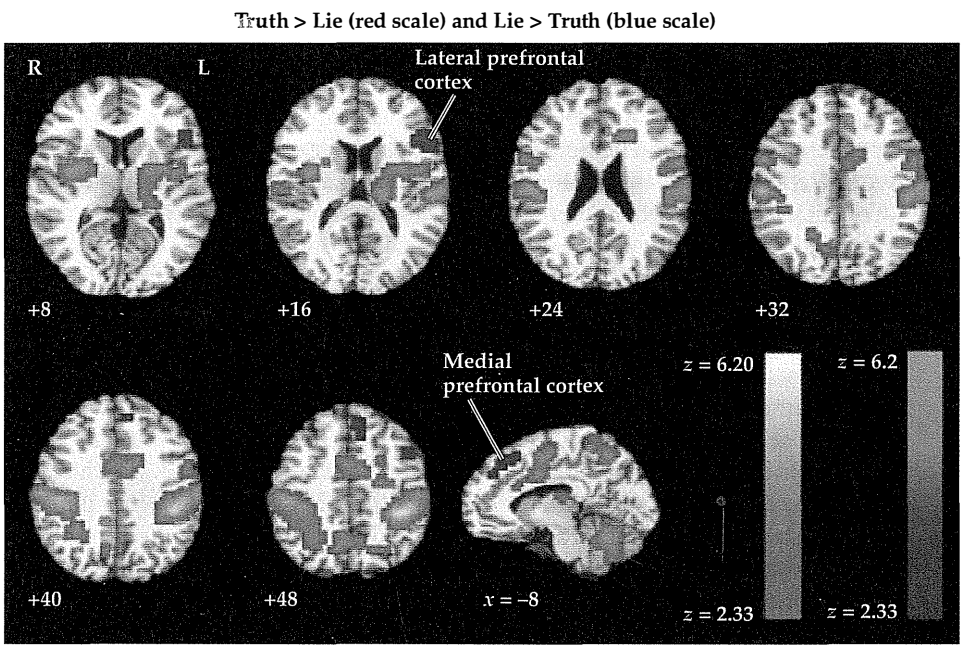

Figure 14.8 The use of fMRI to detect deception. Studies from several laboratories have shown that fMRI can be used to detect intentional deception, at least under conditions amenable to laboratory testing. In this example, from the work of Daniel Langleben and colleagues, subjects were shown a playing card and then variously asked to lie or tell the truth about the identity of that card. Activation measured using fMRI reliably differentiated these actions; for example, lying evoked greater activation than truth-telling in the lateral and medial prefrontal cortices. The *z*-coordinates for the slices are shown at the bottom, and the significance values indicated via the colormaps are shown at the right. (After Langleben et al., 2005.)

tion in different sets of regions. Even more accurate results have been obtained by using more advanced techniques derived from machine learning, such as those that have been applied to other "mind-reading" tasks like perceptual discrimination. In all these cases, however, the deception involved laboratory instructions—not the sort of real-world, high-consequence decisions that would be important for legal or hiring decisions.

As we mentioned earlier, the use of fMRI for lie detection has generated considerable controversy. Evidence for this comes from the fact that review articles that comment on fMRI lie detection are several times as numerous as the peer-reviewed research articles themselves. This controversy has, in part, been targeted at several companies who propose commercialization of fMRI lie detection. One of those companies holds a patent for "Functional brain imaging for detecting and assessing deception and concealed recognition, and cognitive/emotional response to information," which was granted to the fMRI researcher Langleben and the University of Pennsylvania in 2005. As is typically the case for early patents in a field, this patent is very broad, in that it intends to cover all uses of fMRI and all analysis methods for detecting deception. However, it makes reference to the specific example of the prefrontal cortex activation, which was demonstrated in the early studies. Although there is little evidence so far that these early ventures will lead to long-term success, there could be an enormous market for an effective fMRI lie-detection technique.

Thought Question

Should scientists and corporations be able to patent the use of fMRI for specific applications, like lie detection? How could such patents change the course of future research, whether positively or negatively?

Both the hype and fear associated with real-world lie detection by fMRI are based on a limited understanding of fMRI's capabilities. Testing so far has been generally restricted to healthy young adults who lie about relatively minor events (i.e., the identity of a playing card or an action taken only recently in a laboratory). The neural predictors of lie detection may differ dramatically depending on the type of lie or the presence of a neurological condition. To compromise the results of a test, a subject need only move his or her head at opportune times. But a lie detector, like many other products, does not have to work well to be profitable; potential consumers just need to believe that it works. (Coincidentally, this phenomenon is also responsible for the success of the polygraph, in several senses.) Belief in the power of a complex technique like fMRI is relatively easy to manipulate; the complexity and mystery of the MRI scanner makes it difficult for the lay public to evaluate its capabilities. To the average non-scientist, it may seem only a small step to using fMRI to guide decisions about others' character— from the mundane to malevolent. Those developing and commercializing these new applications must take steps to educate the public, not only about the strengths of fMRI but also about its limitations.

Another issue to consider is that of intellectual property. As mentioned above, both U.S. and international patents have been granted for the use of fMRI to detect deception. Broadly considered, patents are intended to protect inventions against late-coming competitors, so that inventors can reap the commercial benefits of their discoveries. One challenge for patent courts is the need to balance the protection of intellectual property against the right for fair com-

intellectual property The protected legal status given to an idea, product, or invention so that its owner has exclusive rights for its use, commercial or otherwise.

petition. Putting aside the specific example of lie detection, what sorts of fMRI discoveries should be patentable? Suppose that a researcher discovers that the amygdala is more active in dyslexic individuals than in non-dyslexics, to use a hypothetical example. Would this discovery allow the researcher to patent that experimental design as a test for dyslexia? Could that researcher patent the use of fMRI *itself*, even when using algorithms developed by other researchers, to test for dyslexia? If intellectual property rights are interpreted too narrowly, then many potentially valuable commercial applications of fMRI may be missed. But too broad an interpretation may have a chilling effect on research itself. Scientists who use fMRI should be willing to play major roles in future debates about these issues.

trait A psychological term used to define an intrinsic, and perhaps stable over time, feature of one's nature.

Identifying traits

There has been growing interest in the use of fMRI to study differences between individuals. In psychological terms, enduring aspects of our personalities and minds that have broad effects on our behavior are called **traits**. Note that the term "individual differences," introduced earlier, is broader and less rigorous, in that it could reflect any measured variation between individuals, including variation in their responses to a single experiment. Some of the interest in using fMRI to measure traits comes from the lay sense that neuroimaging data are more scientific than behavioral measurements (i.e., the idea of neurorealism, advanced earlier in the chapter). This idea is not only incorrect, it damages the reputation of neuroimaging and its practitioners. Other interest in studying traits comes from the new field of **imaging genomics**, which was introduced in Chapter 13. Functional neuroimaging can provide important intermediary links between genes and traits, by showing that a given genetic polymorphism alters the functioning of a particular brain system, which in turn influences a behavioral trait. Finally, many fMRI researchers have begun examining individual differences as a standard part of their research programs. By showing that activation in a brain region directly predicts some individual difference, whether behavior in an experiment or a more-robust trait, the researchers can make a much stronger case for the links between brain function and the underlying cognitive processes.

For these latter reasons, measurements of individual differences now pervade the fMRI literature. Researchers have identified neural correlates of neuroticism, risk-taking, memory span, racial attitudes, altruism, reasoning ability, and many, many other behavioral measures (see Figure 14.9 for examples). Some of these differences in brain function may reflect traits, while others may be specific to particular experimental tasks. There are two primary challenges with using fMRI data to identify traits. First, the sample sizes in fMRI experiments are generally much smaller than in behavioral experiments. Behavioral studies that use factor analyses to glean traits from questionnaires (or similar instruments) typically enroll hundreds of subjects, ideally with broad demographic characteristics. Even though the average number of subjects in fMRI experiments has increased over recent years, sample sizes of more than 30 subjects are still relatively uncommon. Subjects in fMRI studies still tend to be drawn from samples of convenience, usually healthy and educated young adults. Second, fMRI experiments almost always use a single experimental task to manipulate brain function. A reliable individual difference may be identified in the activation associated with that task, but a researcher cannot justifiably conclude that the same activation pattern would occur in response to other tasks. Only if it were expressed in a range of scenarios could an individual difference be considered to be a general trait.

imaging genomics A new field that investigates the effect of genetic variation on brain structure and function.

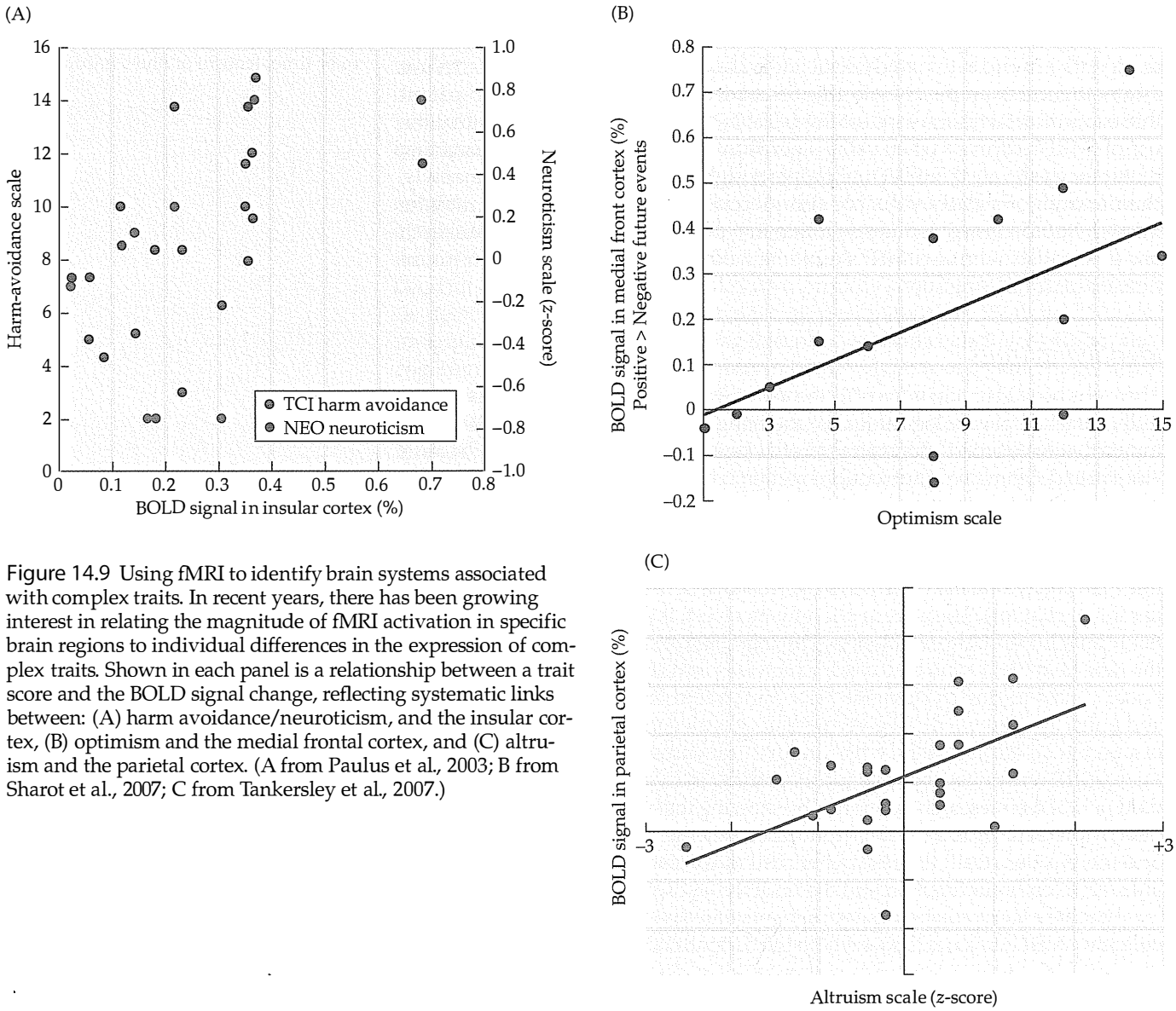

Figure 14.9 Using fMRI to identify brain systems associated with complex traits. In recent years, there has been growing interest in relating the magnitude of fMRI activation in specific brain regions to individual differences in the expression of complex traits. Shown in each panel is a relationship between a trait score and the BOLD signal change, reflecting systematic links between: (A) harm avoidance/neuroticism, and the insular cortex, (B) optimism and the medial frontal cortex, and (C) altruism and the parietal cortex. (A from Paulus et al., 2003; B from Sharot et al., 2007; C from Tankersley et al., 2007.)

Thought Question

Suppose that fMRI researchers were able to demonstrate, through compelling evidence from numerous studies, that a particular pattern of brain activation was a reliable marker of some personality characteristic (e.g., honesty, aggressiveness). Do you think that corporations or government agencies should be allowed to use fMRI testing to screen potential employees? If not, how would fMRI screening differ from existing personality and aptitude testing?

These limitations, while recognized by many researchers, have not deterred enthusiasm for commercial applications of fMRI. One possibility, which will surely become reality in the near future, is the use of fMRI to screen individ-

uals to evaluate their suitability for a job. While fMRI sessions are expensive, costing hundreds of dollars per scan, their costs pale before the consequences of mistakes in hiring. Consider just one possibly controversial but realistic example: the evaluation of potential soldiers enlisting in the U.S. military. A substantial fraction (approximately 13% in recent years) of individuals who enlist in the U.S. military drop out before completing their basic training, at a cost of approximately $50,000 per recruit. For fMRI screening to be cost-effective, it would need to reduce the attrition rate by about 3% (i.e., through identifying medical or psychological indicators that an individual would drop out). Corporations likewise spend tens of thousands of dollars on recruiting for mid- and higher-level positions. We emphasize these costs not because we believe that fMRI *should* be used to screen individuals for desirable traits. We do so, instead, because the societal costs of poor personnel decisions are so large that fMRI, even with its attendant expense, *has the potential* to be used for such screening. As fMRI researchers develop increasingly robust paradigms to predict particular behavioral traits, the field may progress to the point where fMRI could be used—whether justifiably or not—to directly predict desirable outcomes from patterns of brain activation.

The initial public reaction to such uses of fMRI will undoubtedly be vehemently negative, largely due to the mistrust of complex technologies (witness the comments about "mind control" described in the previous section). But after the initial outrage fades, policy makers will be left with difficult ethical choices. Our society values privacy, as exemplified in the HIPAA legislation within the U.S., but we also want our institutions (e.g., corporations and military) to operate efficiently. An fMRI procedure that predicted susceptibility to post-traumatic stress disorder (PTSD) could be used to effectively exclude some individuals from certain categories of military service. Such a test would improve the effectiveness of the military, greatly reduce medical costs, and minimize those individuals' chances of a debilitating disorder. Those real benefits would have to be weighed against the potential harms, including the loss of privacy and the abuse of technology. Simple instruments, from intelligence tests to lie detectors, can be wielded bluntly and harmfully, to deny educational resources to the non-gifted or to preclude employment to the non-trustworthy. Given the complexity of fMRI, its potential for misuse is far greater.

The Future of fMRI Research (and your role in it)

When we published the First Edition of this textbook in 2004, fMRI research was restricted primarily to the field of cognitive neuroscience. Relatively few directors of fMRI laboratories had begun their research careers using that technique. Most practitioners had come from other fields, notably electrophysiology, psychiatry, or experimental psychology. The idea of a linguistics or economics department getting its own MRI scanner would have seemed ludicrous to many university presidents. On a more positive note, funding agencies such as the U.S. National Institutes of Health were at that time supporting grants using fMRI at very high rates. (One member of a review panel commented that, "every application seems to have a set of fMRI experiments.")

Functional MRI is now a mature research technique. An entire generation of academics has grown up reading fMRI papers and conducting fMRI experiments, and many members of that generation are now leading their own laboratories and conducting cutting-edge research. Research using fMRI has engendered a level of collaboration unprecedented in the neurosciences (and

TABLE 14.2 Advice for new researchers

1. Look at your data, always.
2. Understand the principles underlying your research methods.
3. Choose your methods based on your research questions, not the reverse.
4. Collaborate broadly across disciplines.

perhaps even in the biological sciences), in that it touches on nearly all disciplines in the social sciences and even many in the humanities. Economists are indeed arguing about the results of fMRI experiments, while legal scholars and ethicists are debating many of the issues raised in this chapter. These sorts of collaborations will only increase, especially as the results of fMRI studies provide new insights into the mechanisms underlying human thought and behavior. These are truly remarkable times to be a scientist.

Nevertheless, some cautionary notes are again necessary (as summarized in Table 14.2). From the many studies described in this book, it is clear that neuroimaging in general, and fMRI in particular, provides an extraordinarily powerful and flexible tool for answering questions about brain function. Technological developments will continue to improve the spatial and temporal resolution of fMRI, further extending its interpretive reach. However, even though the emphasis of this book has been on a particular technique, we stress that science should be driven not by techniques but by questions. No method is valuable unless it can answer interesting and important questions. Therefore, although experimental techniques should be mastered, just as a craftsman should become expert with his or her tools, they should not define a scientist's research program. All techniques have limitations, and the conscientious researcher should use multiple approaches to address scientific questions, so that the limitations of particular approaches do not affect the quality of the overall conclusions. For this reason, we advocate that researchers employ a multimodal, converging operations approach that combines different techniques.

The most remarkable aspect of fMRI, and one that never fails to amaze us, is its accessibility. Undergraduate students with no prior neuroscience experience can, within a single day, use fMRI to create a functional map of the motor cortex (or some other region) in a healthy subject. This accessibility has resulted from the development of comprehensive analysis programs, some of which can take raw data from the scanner and, with a minimum of input from the user, generate beautiful three-dimensional maps of function. It is tempting for those new to the technique to assume that it is unnecessary to understand the workings of such programs. Indeed, one can use the technique of fMRI without understanding its physical and biological foundations, making those foundations seem unnecessary for (or even impediments to) scientific progress. We believe that as these attitudes have become increasingly common, they almost invariably lead to research errors, false claims, or misrepresentations of fMRI's strengths and limitations.

We advocate a far different and more data-centric attitude. All scientists should understand the processes that generate their data, by examining both the techniques and the experimental designs. For fMRI in particular, the processes that generate the data are not trivial, but their understanding greatly

facilitates effective experimental design. Even though it is now very easy to acquire fMRI data, the tremendous resources required to perform fMRI research should not be squandered on trivial questions or bad experiments. With this last point in mind, new researchers should remember that skepticism is a valued part of science, and it should be applied as liberally to one's own results as to those of others. Furthermore, one should not blindly trust data analysis packages, because each statistical approach, like any other aspect of research, has strengths and weaknesses. Always evaluate whether your approach is the right one for your experimental question, and constantly check the quality of your data and procedures. The power of fMRI allows researchers to not only address important questions, but also to make spectacular mistakes.

Finally, we encourage new investigators to seek out colleagues from other disciplines. Many of the largest questions about mind, brain, and behavior touch on many disciplines. Like many other fMRI researchers, we collaborate with psychologists, psychiatrists, physicists, radiologists, and neurobiologists. We also collaborate with economists, decision scientists, and even philosophers. Functional MRI could contribute answers to questions asked in each of these fields, and conversely, each of these fields provides important concepts that could shape the thinking of fMRI researchers. Within the field of neuroscience itself, the integration of fMRI with other neuroscientific approaches has led to new ways of thinking about brain function, many of which could not have arisen from fMRI research alone.

Even after many years in the field, we still marvel at these connections between techniques, scientists, and disciplines. One should never take for granted the remarkable ability of fMRI to look inside another person's brain. We are hopeful that many of you reading this textbook will experience a similar sense of wonder.

Summary

The very success of fMRI for measuring brain function has raised a number of ethical problems. The most visible among these is the challenge of conveying fMRI results to the broader public. Several errors are common, including the overstatement of results, a failure to discuss limitations, and the tendency to treat fMRI data as uncritical proof of controversial claims. Even experienced fMRI researchers are not immune to the misrepresentation of results. A particularly common problem lies in generalizing from brain activation to cognitive process, in the form of reasoning known as reverse inference. The nature of the data collected in fMRI studies can lead to ethical concerns. Researchers must ensure that fMRI data are collected in a safe manner that ensures the privacy and other rights of the research subjects. How to handle incidental findings in fMRI research remains a point of debate among scientists and other members of the community. Other ethical problems lie in the application of fMRI data to new and controversial domains, such as inferring intentionality or measuring personality traits. Future fMRI research should not avoid these topics, but should be guided by accurate information about fMRI's real strengths and limitations. As fMRI has matured as a technique, it has had increasing influence upon a wide range of disciplines. Thus, its ethical issues are no longer of interest to just a handful of researchers; they have deep importance for science and society.

REFER TO THE
fMRI
COMPANION WEBSITE AT
www.sinauer.com/fmri2e
for study questions and Web links.

Suggested Readings

Farah, M. J. (2005). Neuroethics: the practical and the philosophical. *Trends Cogn. Sci.*, 9: 34–40. *This review provides a broad and engaging overview of the ethical issues posed by neuroscience research.*

Gazzaniga, M. S. (2005). *The Ethical Brain.* Dana Press, New York. *This collection of short essays covers a broad range of issues in neuroethics, including the role of neuroscience in determining morality, legal questions associated with personal responsibility, and the use of neuroimaging to detect deception.*

National Institutes of Health. *Regulations and Ethical Guidelines.* (http://ohsr.od.nih.gov/guidelines/index.html). *This website contains the text of the major international agreements on the ethical conduct of research involving human participants.*

*Poldrack, R. A. (2006). Can cognitive processes be inferred from neuroimaging data? *Trends Cogn. Sci.*, 10: 59–63. *This article considers the practice of reverse inference in fMRI research, emphasizing both its logical errors and its theoretical implications.*

*Racine, E., Bar-Ilan, O., and Illes, J. (2005). fMRI in the public eye. *Nat. Rev. Neurosci.*, 6: 159–164. *An interesting theoretical review of media coverage of fMRI research, including a discussion of common problems in how fMRI is presented to the public.*

*Indicates a reference that is a suggested reading in the field and is also cited in this chapter.

Chapter References

Aron, A. and 16 others. (2007). Politics and the Brain. *New York Times* (Letter), November 14, 2007.

Iacoboni, M., Freedman, J., Kaplan, J., Freedman, T., Knapp, B., and Fitzgerald, K. (2007). This Is Your Brain on Politics. *New York Times* (Opinion/Editorial), November 11, 2007.

Illes, J., Kirschen, M. P., Edwards, E., Stanford, L. R., Bandettini, P., Cho, M. K., Ford, P. J., Glover, G. H., Kulynych, J., Macklin, R., Michael, D. B., and Wolf, S. M. (2006). Ethics. Incidental findings in brain imaging research. *Science*, 311: 783–784.

Katzman, G. L., Dagher, P. A., and Patronas, N. J. (1999). Incidental findings on brain magnetic resonance imaging from 1000 asymptomatic volunteers. *N. Engl. J. Med.*, 282: 36–39.

Kozel F. A., Johnson, K. A., Mu, Q., Grenesko, E. L., Laken, S. J., and George, M. S. (2005). Detecting deception using functional magnetic resonance imaging. *Biol. Psychiatry*, 58: 605–613.

Langleben, D. D., Loughead, J. W., Bilker, W. B., Ruparel, K., Childress, A. R,. Busch, S. I., and Gur, R.C. (2005). Telling truth from lie in individual subjects with fast event-related fMRI. *Hum. Brain Mapp.*, 26: 262–272.

Langleben D. D., Schroeder, L., Maldjian, J. A., Gur, R. C., McDonald, S., Ragland, J. D., O'Brien, C. P., and Childress, A. R. (2002). Brain activity during simulated deception: an event-related functional magnetic resonance study. *NeuroImage*, 15: 727–732.

Mamourian, A. (2004). Incidental findings on research functional MR images: Should we look? *Am. J. Neuroradiol.*, 25: 520–522.

National Research Council of the National Academies (2003). *The Polygraph and Lie Detection.* Washington, D.C.: The National Academies Press.

Nature Editorial (2006). Lure of lie detectors spooks ethicists. *Nature*, 441: 918–919.

Paulus, M. P., Rogalsky, C., Simmons, A., Feinstein, J. S., and Stein, M.B. (2003). Increased activation in the right insula during risk-taking decision making is related to harm avoidance and neuroticism. *NeuroImage*, 19: 1439–1448.

Illes, J., Kirschen, M. P., Karetsky, K., Kelly, M., Saha, A., Desmond, J. E., Raffin, T. A., Glover, G. H., and Atlas, S. W. (2004). Discovery and disclosure of incidental findings in neuroimaging research. *J. Magn. Reson. Imaging*, 20: 743–747.

Sawyer-Glover, A. M. and Shellock, F. G. (2000). Pre-MRI procedure screening: rec-

ommendations and safety considerations for biomedical implants and devices. *J. Magn. Reson. Imaging*, 12: 92–106.

Sharot, T., Riccardi, A. M., Raio, C. M., and Phelps, E. A. (2007). Neural mechanisms mediating optimism bias. *Nature*, 450: 102–105.

Tankersley, D., Stowe, C. J., and Huettel, S. A. (2007). Altruism is associated with an increased neural response to agency. *Nat. Neurosci.*, 10: 150–151.

Trials of War Criminals before the Nuremberg Military Tribunals under Control Council Law No. 10, Vol. 2, pp. 181–182. U.S. Government Printing Office, 1949, Washington, D.C.

Vernooij, M. W., Ikram, M. A., Tanghe, H. L., Vincent, A. J., Hofman, A., Krestin, G. P., Niessen, W. J., Breteler, M. M., and van der Lugt, A. (2007). Incidental findings on brain MRI in the general population. *N. Engl. J. Med.*, 357: 1821–1828.

Wise, J. (2007). Thought Police: How Brain Scans Could Invade Your Private Life. *Pop. Mech.*, 184 (11): 64–70.

Yue, N. C., Longstreth, W. T., Jr., Elster, A. D., Jungreis, C. A., O'Leary, D. H., and Poirier, V. C. (1997). Clinically serious abnormalities found incidentally at MR imaging of the brain: data from the Cardiovascular Health Study. *Radiology*, 202: 41–46.

Glossary

180-degree excitation pulse A quantity of electromagnetic energy that, when applied to a spin system during MR excitation, results in a flipping of the usual net magnetization, such that there are now more nuclei in the high-energy state than in the low-energy state.

90-degree excitation pulse A quantity of electromagnetic energy that, when applied to a spin system during MR excitation, results in equal numbers of nuclei in the low- and high-energy states.

A

action potential A wave of depolarization that travels down a neuronal axon.

adaptation A change in the response to a stimulus following its repeated presentation.

adenosine triphosphate (ATP) A nucleotide containing three phosphate groups that is the primary energy source for cells in the human body.

aerobic glycolysis The process, consisting of glycolysis, the TCA cycle, and the electron transport chain, that breaks down glucose in the presence of oxygen, resulting in a gain of 36 ATP molecules.

aliasing The sampling of a signal at a rate insufficient to resolve the highest frequencies that are present. The energy at those frequencies becomes artifactually expressed at lower frequencies, distorting the measured signal.

alpha value An a priori probability (e.g., 0.001) chosen as the threshold for statistical significance. If the probability that the data would be obtained under the null hypothesis is less than the alpha value, the data are considered to be statistically significant.

alternating design A blocked design in which two conditions are presented one after another for the duration of the experimental run.

anaerobic glycolysis The conversion of glucose to lactate in the absence of oxygen.

anatomical ROI Region of interest that is chosen based on anatomical criteria.

angular momentum (J) A quantity given by multiplying the mass of a spinning body by its angular velocity.

anisotropic Having different properties in different directions; often referenced in the context of anisotropic diffusion, where molecules tend to diffuse along one axis but not others.

anode A source of positive charge or ions, and an attractor of free electrons.

antiparallel state The high-energy state in which an atomic spin precesses around an axis that is antiparallel (i.e., opposite) to that of the main magnetic field.

apical dendrites The dendrites that are distant from the neuronal cell body. For typical pyramidal cells in the cortex, the apical dendrites extend to the superficial layers of cortex, while the cell bodies are located in deeper layers.

apparent diffusion coefficient (ADC) The quantification of diffusivity assuming isotropic diffusion.

arachnoid The middle membrane covering the brain; its name comes from its weblike appearance.

arterial spin labeling (ASL) A family of perfusion imaging techniques that measure blood flow by labeling spins with excitation pulses and then waiting for the labeled spins to enter the imaging plane before data acquisition.

arteries Blood vessels that carry oxygenated blood from the heart to the rest of the body.

arterioles Small arteries.

ascending/descending slice acquisition The collection of data in consecutive order, so that slices are acquired sequentially from one end of the imaging volume to the other.

astrocyte A type of glial cell that regulates the extracellular environment.

autoradiography An invasive imaging technique that labels molecules using radioactive isotopes and then measures the concentration of those molecules by exposing slices of tissue to photographic emulsions.

averaged epoch The result of averaging a large number of epochs that are time-locked to similar events.

axial A horizontal view of the brain (along the x–y plane in MRI).

axon hillock A region of the cell body located at the emergence of the axon. Changes in its electrical potential lead to the generation of action potentials.

axon A neuronal process that transmits an electrical impulse from the cell body to the synapse, performing a primarily signaling function.

B

b factor The degree of diffusion weighting applied within a pulse sequence.

B The sum of all magnetic fields experienced by a spin.

B_0 The strong static magnetic field generated by an MRI scanner.

B_{1eff} The effective magnetic field experienced by a spin system during excitation.

balloon model A model of the interaction between changes in blood volume and changes in blood flow associated with neuronal activity.

basal ganglia A set of nuclei in the forebrain that includes the caudate, putamen, and globus pallidus.

base image The image on which a statistical map is displayed, often a high-resolution anatomical image.

basis functions A set of functions whose linear combination can take on a wide range of functional forms. In fMRI analyses, researchers often replace a single hemodynamic response function with basis functions, to improve the flexibility of their design matrices.

beneficence The principle that research protocols should maximize the potential benefits of research while minimizing the costs to any individual subject.

between-subjects A manipulation in which different conditions are assigned to different subject groups.

bias field estimation A technique for estimating inhomogeneities in the magnetic field based on intensity variations in collected images.

biofeedback Providing an explicit indicator of some physiological process, such as the beating of the heart or activation within a particular brain region, so that an individual can attempt to regulate that activation or guide behavior.

biomarker A phenotypic feature, whether physical, physiological, or behavioral, that provides a robust predictor of some experimentally or clinically important outcome.

Bloch equation An equation that describes how the net magnetization of a spin system changes over time in the presence of a time-varying magnetic field.

block A time interval that contains trials from one condition.

blocked design The separation of experimental conditions into distinct blocks, so that each condition is presented for an extended period of time.

blood-oxygenation-level-dependent (BOLD) contrast The difference in signal on T_2*-weighted images as a function of the amount of deoxygenated hemoglobin.

bolus A quantity of a substance that is introduced into a system and then progresses through that system over time.

Bonferroni correction A stringent form of familywise error rate correction for multiple comparisons in which the alpha value is decreased proportionally to the number of independent statistical tests.

brain stem The midbrain, pons, and medulla.

Brodmann areas Divisions of the brain based on the influential cytoarchitectonic criteria of Korbinian Brodmann.

C

calcium-sensitive contrast agent A compound that, when injected into an organism, influences the MR signal differently depending on the local concentrations of calcium ions. Such agents could lead to maps of neuronal signaling.

capillaries Small and thin-walled blood vessels. The extraction of oxygen and glucose from the blood and the removal of waste carbon dioxide occur in the capillaries.

capillary recruitment The idea that increased blood flow through the capillary bed results in perfusion of previously unperfused capillaries.

categorical variable A variable that can take one of several discrete values.

cathode An attractor for positive charge or ions, and a source of free electrons.

caudal Toward the back of the brain.

causality The judgment that one event led to another. For fMRI data, measures of causality attempt to determine whether changes in the activation of one brain region led to changes in the activation in another region.

central nervous system (CNS) The brain and spinal cord.

central sulcus A deep fissure that separates the frontal and parietal lobes of the brain.

cerebellum A large cortical structure at the caudal base of the brain that plays an important role in motor function.

cerebrospinal fluid (CSF) A colorless liquid that surrounds the brain and spinal cord and fills the ventricles within the brain.

cerebrum The two hemispheres forming the major part of the brain.

chemical shift imaging A technique for measuring the concentration of particular chemicals, based on subtle differences in the resonance of the protons they contain.

circle of Willis The interconnection between the basilar artery and the carotid arteries at the base of the cranial vault.

cluster-size thresholding The adoption of a minimum size, in voxels, for a cluster of active voxels to be labeled as significant.

coactivation The simultaneous activation of two or more brain regions within a single experimental task. Coactivation of brain regions does not imply that the regions are functionally connected.

collinear regressors Model factors that are highly correlated with one another. The inclusion of collinear regressors reduces the validity of general linear model analyses.

color map The association between numerical values of a parameter and a set of colors.

complex cell A neuron in the visual cortex with a larger receptive field than a simple cell and that responds to a stimulus with preferred orientation anywhere within its receptive field.

component In the context of data-driven analyses, a feature of a data set that represents some aspect of its intrinsic structure.

concentration gradient A difference in the density of a substance across space. Substances diffuse along concentration gradients from areas of high concentration to areas of low concentration.

conditions (or levels) Different values of the independent variable(s).

confounding factor Any property that co-varies with the independent variable within the experiment but could be distinguished from the independent variable using a different experimental design.

conjugate mirroring A partial *k*-space imaging technique in which data collected from one half of *k*-space is used to estimate data from the other half.

consent form A document that describes the procedures, risks, and benefits of a research study in clear language, so that potential subjects can make an informed decision about participating.

construct An abstract concept that explains behavior but which itself is not directly observable. Attention is an example of a psychological construct.

continuous ASL A type of perfusion imaging that uses a second transmitter coil to label spins within an upstream artery while collecting images.

continuous variable A variable that can take any value within a range.

contrast (1) The intensity difference between different quantities being measured by an imaging system. It also can refer to the physical quantity being measured (e.g., T_1 contrast). (2) A statistical comparison of the activation evoked by two (or more) experimental conditions, in order to test a research hypothesis.

contrast agent A substance injected into the body to increase image contrast.

contrast weights A vector that expresses the predictions of a research hypothesis for the different regressors in a design matrix. When multiplied by the parameter weights from a fMRI regression analysis, the result can be evaluated for statistical significance.

contrast-to-noise ratio (CNR) The magnitude of the intensity difference between different quantities divided by the variability in their measurements.

control block A time interval that contains trials of the control condition.

control condition A condition that provides a standard to which the experimental condition(s) can be compared. Also called the baseline condition or nontask condition.

converging operations The use of two or more techniques to provide complementary evidence used to test an experimental hypothesis or scientific theory.

coregistration The spatial alignment of two images or image volumes.

coronal A frontal view of the brain (along the *x*–*z* plane in MRI).

corpus callosum The large white-matter bundle that is the primary connection between the cerebral hemispheres. The anterior portion is known as the genu and the posterior portion is known as the splenium.

correlation analysis A type of statistical test that evaluates the strength of the relation between two variables. For fMRI studies, correlation analyses typically evaluate the correspondence between a predicted hemodynamic response and the observed data.

correlation coefficient (r-value) A number between –1 and 1 that expresses the strength of the correlation between two variables.

cortex (neocortex) The thin wrapping of cell bodies around the outer surface of the brain.

cost function A quantity that determines the amount of residual error in a comparison.

counterbalancing A process for removing confounding factors by ensuring that they have equal influence on the different conditions of the independent variable, usually by matching values across conditions.

covariates Regressors that can take any of a continuous range of values.

cross product The vector product of two vectors. Its direction is perpendicular to the plane defined by those vectors and its magnitude is given by multiplying their product times the sine of the angle between them.

cross-validation In pattern classification analysis, an approach to evaluating the effectiveness of classification using a given feature set. It involves the iterated generation and testing of classifiers based on different parts of the same training set.

cryogens Cooling agents used to reduce the temperature of the electromagnetic coils in an MRI scanner.

current dipole A positive and negative point charge separated by an infinitesimal distance. A current dipole is used as a simple and convenient model for the electromagnetic fields produced by an activated neuron.

current sink An attractor of positive ions. A depolarized patch of neuronal membrane is a current sink because positively charged ions will flow toward it.

current source A source of positive ions.

cytoarchitecture The organization of the brain on the basis of cell structure.

D

data matrix A representation of the measured fMRI data in two-dimensional form (i.e., voxels by time points).

data reduction The simplification of a data set by reducing its variability, such as by eliminating irrelevant, redundant, or non-predictive variables.

data-driven analysis Exploration of the intrinsic structure of data.

dB/dt The change in magnetic field strength (dB) over time (dt).

deactivations Decreases in BOLD activation during task blocks compared with nontask blocks.

deception The use of experimental procedures that intentionally mislead subjects.

default network A set of brain regions whose activation tends to decrease during the performance of active, engaging tasks, but to increase during conditions of resting and reflection.

degrees of freedom (df) The number of independent observations within a data set. For many statistical tests, there are $n - 1$ degrees of freedom associated with n data points.

de-identification Removal of information that may link research data or medical information to a particular individual.

dendrite A neuronal process that receives signals from other cells, performing a primarily integrative function.

deoxygenated hemoglobin (dHb) Hemoglobin without attached oxygen; it is paramagnetic.

dependent variables (DVs) Quantities that are measured by the experimenter in order to evaluate the effects of the independent variables.

descriptive statistics Statistics that summarize the sample data but do not allow inferences about the larger population.

design matrix In fMRI implementations of the general linear model, the specification of how the model factors change over time.

detection Determination of whether activation of a given voxel changes in response to the experimental manipulation.

detector coil An electromagnetic coil that measures energy emitted back to the environment after its initial absorption by the sample.

diamagnetic Having the property of a weak repulsion from a magnetic field.

diffusion The random motion of molecules through a medium over time.

diffusion tensor imaging (DTI) A collection of images that provide information about the magnitude and direction of molecular diffusion. It is often used to create maps of fractional anisotropy.

diffusion weighting The application of magnetic gradients to cause changes in the MR signal that are dependent on the amplitude and/or direction of diffusion.

direct cortical stimulation Applying small currents directly to brain tissue to excite or disrupt neural activity. Direct cortical stimulation is usually conducted in humans to localize critical brain regions in the context of neurosurgery.

dispersion derivative A regressor that, when added to a model, improves the robustness of that model to small variations in the width of the hemodynamic response.

distribution The pattern of variation of a variable under some conditions. For example, the normal distribution has a characteristic bell shape.

dopamine An important neurotransmitter that is part of the family known as biogenic amines. Dopamine is produced within cells in the brainstem that project broadly to the striatum and cortex (especially the frontal lobe).

dorsal Toward the top of the brain.

dot product The scalar product of two vectors. It is created by summing the products along each dimension.

double dissociation The demonstration that two experimental manipulations have different effects on two dependent variables. One manipulation affects the first variable but not the second, and the other manipulation affects the second but not the first.

dura The outermost membrane covering the brain; its name comes from its thickness and toughness.

dynamic causal modeling (DCM) A statistical approach for testing models of the connectivity between brain regions, based on hypotheses about how experimental manipulations alter activation and connectivity between regions.

E

echo time (TE) The time interval between an excitation pulse and data acquisition (defined as the collection of data from the center of k-space), usually expressed in milliseconds.

echo-planar imaging (EPI) A technique that allows collection of an entire two-dimensional image by changing spatial gradients rapidly following a single electromagnetic pulse from a transmitter coil.

effect size The numerical difference between means divided by the standard deviation.

effective bore size The clearance within the bore of the MRI scanner that limits the maximum size of the sample that can be scanned.

efficiency The power of an experimental design to test a research hypothesis. Highly efficient designs can reject the null hypothesis even when the experimental manipulation has only a small effect.

eigenimage Spatial maps, as generated by a principal components analysis, that reflect orthogonal components of a complex image (or time series of images).

eigenvalue A mathematical description of the amount of variability in a dataset that is accounted for by a given component.

eigenvector Following principal components analysis, a set of values that describes a component of the intrinsic variability in a dataset.

electroencephalogram/electroencephalography (EEG) The measurement of the electrical potential of the brain, usually through electrodes placed on the surface of the scalp.

electrogenesis The generation of electrical electrophysiological phenomena by a living organism.

electromotive force (emf) A difference in electrical potential that can be used to drive a current through a circuit. The MR signal is the electromotive force caused by the changing magnetic field across the detector coil.

electron transport chain The third step in aerobic glycolysis; it generates an additional 34 ATP molecules.

endogenous contrast Contrast that depends on an intrinsic property of biological tissue.

epiphenomenal A secondary consequence of a causal chain of processes, but playing no causal role in the process of interest.

epoch A time segment extracted from a larger series of images, usually corresponding to the period in time surrounding an event of interest.

equipotentiality The concept that a function is so widely distributed within the brain that it depends on the activity of the brain as a whole. Equipotentiality is the antithesis of localization of function.

equivalent dipole A simplifying model that represents the electromagnetic field produced by a population of neurons as though it were produced by a single dipole.

ERP component A stereotypic feature of an ERP waveform, such as a peak or trough at a particular latency, that has a presumed functional significance.

error matrix That component of the fMRI data that is unexplained by the design matrix, when fit by the parameter matrix.

estimation Measurement of the pattern of change over time within an active voxel in response to the experimental manipulation.

event A single instance of the experimental manipulation. Also known as a trial.

event-related design The presentation of discrete, short-duration events whose timing and order may be randomized.

event-related potentials (ERPs) Small electrical changes in the brain that are associated with sensory or cognitive events.

evoked magnetic fields (EMFs) A change in the MEG signal that occurs in response to a particular stimulus. An EMF is the magnetic equivalent of an evoked potential or event-related potential in EEG.

evoked potential A field potential that occurs in response to a sensory stimulus.

excitation The process of sending electromagnetic energy to a sample at its resonant frequency (also called transmission). The application of an excitation pulse to a spin system causes some of the spins to change from a low-energy state to a high-energy state.

excitatory postsynaptic potential (EPSP) A depolarization of the postsynaptic cell membrane.

exogenous contrast Contrast that requires the injection of a foreign substance into the body.

expected Euler characteristic The number of clusters of significant activation expected due to chance, as estimated from the number of independent statistical tests (i.e., resels).

experiment The controlled test of a hypothesis. Experiments manipulate one or more independent variables, measure one or more dependent variables, and evaluate those measurements using tests of statistical significance.

experimental condition A condition that contains the stimulus or task that is most relevant to the research hypothesis. Also called the task condition.

experimental design The organization of an experiment to allow effective testing of the research hypothesis.

experimental regressors Model factors that are associated with specific experimental hypotheses.

F

false discovery rate (FDR) The probability of having at least one false positive result, given the set of reported positive results.

familywise error rate (FWER) The probability of making at least one Type I error, given the total number of statistical tests.

feature selection An initial step in pattern classification that involves the determination of which input variables should be included in the classification algorithm.

fiber tracts Bundles of axons that convey signals, in the form of action potentials, from one brain region to another.

field map An image of the intensity of the magnetic field across space.

field of view (FOV) The total extent of an image along a spatial dimension.

field potentials Changes in electrical potential over space associated with postsynaptic neuronal activity.

field strength The magnitude of the static magnetic field generated by a scanner, typically expressed in units of Tesla.

field uniformity In the context of MRI, a uniform magnetic field is one that has a constant strength throughout a wide region near the center of the scanner bore.

filling *k*-space The process of collecting samples from throughout *k*-space in order to collect data sufficient for image formation.

filter Within the context of fMRI, an algorithm for removing temporal or spatial frequency components of data.

finite impulse response (FIR) A signal processing approach that treats each time unit with a separate function (i.e., an impulse); this has the major advantage of making no assumptions about the shape of the observed response function.

fixed-effects analyses Intersubject analyses that assume that the effect of the experimental manipulation is fixed across subjects, with differences between subjects caused by random noise.

flat map An unfolded and flattened representation of the cortical sheet to allow viewing of topographic changes over cortical space. Flat maps are most commonly used in fMRI to illustrate the organization of the visual cortex.

flip angle The change in the precession angle of the net magnetization following excitation.

flux A measure of the strength of a magnetic field over an area of space.

fMRI-adaptation Reduction in the BOLD response to the repeated presentation of a set of stimuli that differ in some attribute, indicating that the brain region being studied is insensitive (as measured by fMRI) to the stimulus attribute being varied.

forward solution The direct calculation of the electric and magnetic fields that would occur at an array of sensors based on a given distribution of dipoles with known orientations and magnitudes.

Fourier transform A mathematical technique for converting a signal (i.e., changes in intensity over time) into its power spectrum.

fractional anisotropy (FA) The preference for molecules to diffuse in an anisotropic manner. An FA value of 1 indicates that diffusion occurs along a single preferred axis, while a value of 0 indicates that diffusion is similar in all directions.

frequency domain The expression of a signal in terms of its power at different frequencies.

frequency-encoding gradient A gradient that is applied during the data acquisition period, so that the spin precession frequencies change over space.

frontal lobe The most anterior lobe of the cerebrum; it is important for executive processing, motor control, memory, and many other functions.

***F*-test** A statistical test that evaluates differences among a set of distributions. For fMRI studies, *F*-tests can evaluate whether any of a set of contrasts exhibited a significant effect.

functional connectivity A pattern of functional relationships among regions, inferred from common changes in activation over time, that may reflect direct or indirect links between those regions.

functional contrast A type of contrast that provides information about a physiological correlate of brain function, such as changes in blood oxygenation.

functional magnetic resonance imaging (fMRI) A neuroimaging technique that uses standard MRI scanners to investigate changes in brain function over time.

functional neuroimaging A class of research techniques that create images of the functional organization of the brain. Common functional neuroimaging techniques include fMRI, PET, and optical imaging.

functional resolution The ability to map measured physiological variation to underlying mental processes.

functional ROI A region of interest that is chosen based on functional criteria, such as the output of an independent voxelwise analysis.

functional signal-to-noise ratio (functional SNR) The ratio between the intensity of a signal associated with changes in brain function and the variability in the data due to all sources of noise. Functional SNR is sometimes called dynamic CNR or functional CNR.

G

γ-aminobutyric acid (GABA) One of the most important inhibitory neurotransmitters.

general linear model (GLM) A class of statistical tests that assume that the experimental data are composed of the linear combination of different model factors, along with uncorrelated noise.

glass-brain view A two-dimensional projection of fMRI data, as if the brain were made transparent and only the activations were visible.

glial cells (glia) Brain cells that support the activities of neurons but are not primarily involved with information transmission.

glucose A sugar made by the human body whose stored energy is used to produce ATP.

glutamate One of the most important excitatory neurotransmitters.

glycolysis The process of breaking down glucose into other compounds to produce ATP.

gradient coils Electromagnetic coils that create controlled spatial variation in the strength of the magnetic field.

gradient-echo (GRE) imaging One of the two primary types of pulse sequences used in MRI; it uses gradients to generate the MR signal changes that are measured at data acquisition.

Granger causality A form of time series analysis that quantifies the information gained by using the past history of one variable to improve predictions of future values of another variable.

gyri Rises in the cortical surface.

gyromagnetic ratio (γ) The ratio between the charge and mass of a spin. The gyromagnetic ratio is a constant for a given type of nucleus.

H

Health Insurance Portability and Accountability Act (HIPAA) An act passed by the U.S. Congress that requires specific procedures for ensuring the privacy of health information.

hemifield One half of a visual display, usually referring to the left or right half.

hemodynamic response (HDR) The change in MR signal on T_2* images following local neuronal activity. The hemodynamic response results from a decrease in the amount of deoxygenated hemoglobin present within a voxel.

hemodynamic Having to do with changes in blood flow or other blood properties.

heteroscedastic Having the property that the distributions of noise are different across experimental conditions.

homogeneity Uniformity over space and time.

homoscedastic Having the property that the distributions of noise are similar for all experimental conditions.

homotopic The cortex in one cerebral hemisphere that corresponds to the same region in the other hemisphere.

hyperscanning The simultaneous collection of fMRI data from two or more subjects who are interacting in an experimental paradigm.

hypothalamus A brain nucleus that supports homeostatic functions, including the regulation of food and water intake.

hypothesis-driven analysis The evaluation of data based on statistical tests of the validity of a null hypothesis.

I

image reconstruction The process by which the raw MR signal, as acquired in *k*-space form, is converted into spatially informative images.

image A visual description of how one or more quantities vary over space.

imaging genomics A new field that investigates the effect of genetic variation on brain structure and function.

imaging plane The plane in which changes in MR signal are recorded during perfusion imaging.

impulse A single input to a system. Impulses are assumed to be of infinitely short duration.

incidental finding The discovery of an abnormality, usually on a structural MR image, in an asymptomatic individual who was scanned for non-medical reasons.

independent components analysis (ICA) An important class of data-driven analyses that identify stationary sets of voxels whose activations vary together over time and are maximally distinguishable from other sets.

independent variables (IVs) Aspects of the experimental design that are intentionally manipulated by the experi-

indicators Regressors that have integral values to indicate a qualitative level.

individual differences Measures of variation among individuals within a population.

inferential statistics Statistics that make inferences about the characteristics of a population based on data obtained from a smaller sample.

inflated brain A transformation of the cortical sheet into a balloon-like structure, removing gyral and sulcal folds so that activation can be more easily viewed.

informed consent The process in which a potential subject voluntarily agrees to participate in a research study, after learning about the procedures, risks, and benefits of the study.

inhibitory postsynaptic potential (IPSP) A hyperpolarization of the postsynaptic cell membrane.

initial dip The short-term decrease in MR signal immediately following the onset of neuronal activity, before the main positive component of the hemodynamic response. The initial dip may result from initial oxygen extraction before the later overcompensatory response.

Institutional Review Board (IRB) An independent group of individuals who evaluate the ethical practice of research conducted at their institution. Researchers who wish to conduct research with human subjects must have the approval of their IRB.

insula The "island" cortex hidden inside the anterior part of the Sylvian fissure; it is important for emotional processing and for the chemical senses.

integrative activity The collection of inputs from other neurons through dendritic or somatic connections.

intellectual property The protected legal status given to an idea, product, or invention so that its owner has exclusive rights for its use, commercial or otherwise.

interleaved slice acquisition The collection of data in an alternating order, so that data are first acquired from the odd-numbered slices and then from the even-numbered slices, to minimize the influence of excitation pulses upon adjacent slices.

interleaved stimulus presentation The presentation of events of interest at different points within a TR over trials (e.g., one-quarter, one-half, and three-quarters of TR in addition to TR onset), increasing the effective sampling rate of an experiment at the expense of fewer trials per condition.

interocular trauma test An intuitive test of significance based on highly visible effects of the experimental manipulation. It states that data are significant if, when plotted, they hit you between the eyes.

interstimulus interval (ISI) The separation in time between successive stimuli. Usually refers to the time between the end of one stimulus and the onset of the next, with the term "stimulus-onset asynchrony" (SOA) used to define the time between successive onsets.

intersubject correlations Functional MRI time courses that are shared by different individuals while performing the same experimental tasks or experiencing the same stimuli.

intersubject variability Variability in fMRI data across a set of subjects; it includes the factors associated with intrasubject variability, along with between-subjects differences in task performance and physiology.

inverse problem The mathematical impossibility of determining the distribution of electrical sources within an object based on the measurement of electrical or magnetic fields at the surface of the object.

inversion recovery A technique for increasing T_1 contrast by adding a 180° inversion pulse before a standard pulse sequence.

ion channel A pore in the membrane of a cell that allows passage of particular ions under certain conditions.

ion A charged atom.

ionizing radiation Electromagnetic radiation that has sufficient energy to separate electrons from electrically neutral atoms, turning them into ions.

isomorphic Having an identical form. A physiological measurement that is isomorphic with a psychological construct would vary over time consistently with the postulated changes in the construct.

isotropic Having similar properties in all directions.

item-related processes Changes in the brain that are assumed to be caused by the properties of individual stimuli, or items. Item-related processes are more easily measured with event-related designs.

J

jittering Randomizing the intervals between successive stimulus events over some range.

justice In the context of research involving human subjects, the principle that the costs of research are distributed broadly and fairly across society.

K

keyhole imaging A partial *k*-space imaging technique in which only the center of *k*-space is collected following each excitation, in order to maximize raw SNR while minimizing acquisition time.

***k*-space trajectory** A path through *k*-space. Different pulse sequences adopt different *k*-space trajectories.

***k*-space** A notation scheme used to describe MRI data acquisition. The use of *k*-space provides mathematical and conceptual advantages for describing the acquired MR signal in image form.

L

labeling plane The plane in which initial excitation pulses are applied during perfusion imaging.

laboratory frame The normal reference frame that is aligned with the magnetic field of the scanner.

large-vessel effects Signal changes in veins that drain a functionally active region but are distant from the neuronal activity of interest.

Larmor frequency The resonant frequency of a spin within a magnetic field of a given strength. It defines the frequency of electromagnetic radiation needed during excitation to make spins change to a high-energy state, as well as the frequency emitted by spins when they return to the low-energy state.

latent variable A variable whose value is not directly measured, but is inferred based on the values of other variables.

lateral Toward the side of the brain.

least-squares error A commonly used cost function, the sum of the squared residuals.

linear system A system that obeys the principles of scaling and superposition.

localization of function The idea that the brain may have distinct regions that support particular mental processes.

localizer task An simple experimental paradigm designed to identify a set of voxels based on a known functional property, in preparation for subsequent analyses of that region in different paradigms.

logistic regression A subset of regression analysis that uses a set of independent variables to predict a binary outcome variable.

longitudinal relaxation (or spin–lattice relaxation) The recovery of the net magnetization along the longitudinal direction as spins return to the parallel state.

longitudinal Parallel to the main magnetic field, or the z-direction, of the scanner (i.e., into the bore).

Lorentz effect imaging (LEI) A technique for direct visualization of ionic electrical activity using MRI.

Lorentz force The force on a moving charge within a magnetic field. Lorentz forces cause spatial displacements in ions and conductors if they are placed in strong magnetic fields.

M

machine learning A subdiscipline within computer science that develops algorithmic rules for relating input data to desirable outputs.

magnet diameter The diameter of the electromagnetic coil that generates the strong static field used in MRI.

magnetic field mapping The collection of explicit information about the strength of the magnetic field at different spatial locations.

magnetic moment (μ) The torque (i.e., turning force) exerted on a magnet, moving electrical charge, or current-carrying coil when it is placed in a magnetic field.

magnetic resonance angiography (MRA) The creation of images of the vascular system using MRI.

magnetic resonance The absorption of energy from a magnetic field that oscillates at a particular frequency.

magnetic susceptibility The intensity of magnetization of a substance when placed within a magnetic field.

magnetization transfer An MR imaging technique that uses an off-resonance excitation pulse to saturate the MR signal from large molecules; the subsequent influence of that pulse upon free protons in water indicates the concentration of those large molecules.

magnetoencephalography (MEG) A noninvasive functional neuroimaging technique that measures very small changes in magnetic fields caused by the electrical activity of neurons, with potentially high spatial and temporal resolution.

massive coil array A method for arranging a large number of surface detector coils to improve spatial coverage while maintaining high sensitivity.

matched filters The principle that a filter of the same frequency as the signal of interest provides the maximal signal-to-noise ratio.

medial Toward the middle of the brain.

medulla oblongata A continuation of the spinal cord at the base of the brain that is important for the control of basic physiological functions.

microstimulation Applying currents through microelectrodes to stimulate activity in a small number of neurons.

midbrain A section of the brain rostral to the pons; it includes a number of important nuclei.

mind reading The ability to construct a comprehensive description of the contents of consciousness. This is currently far beyond the capacity of any neuroscience technique.

mixed design A design that contains features of both blocked and event-related approaches.

MNI space A commonly used space for normalization of fMRI data; its coordinates are derived from an average of MRI structural images from several hundred individuals.

mock scanner A device that simulates a real MRI scanner, usually by reproducing the scanner bore, the bed that the subjects lie on, and the sounds made during scanning.

model A collection of independent variables (and the relationships between those variables) that serve to predict a dependent variable.

morphometric Relating to the measurement of shape.

motion contrasts Contrast mechanisms that are sensitive to the movement of spins through space (e.g., diffusion, perfusion).

MR signal equation A single equation that describes the MR signal as a function of the properties of the object being imaged under a spatially varying magnetic field.

MR signal The current measured in a detector coil following excitation and reception.

multiple comparison problem The increase in the number of false-positive results (i.e., Type I errors) with increasing number of statistical tests. It is of particular consequence for voxel-wise fMRI analyses, which may have many thousands of statistical tests.

multiple regression A family of statistical approaches that evaluate the relative contributions of several independent variables to a dependent variable.

multi-voxel pattern classification An apprcach for pattern classification in fMRI research that uses as its input data the relative changes in activation across a set of voxels.

mutual information In the context of MRI, the amount of information about one image that is provided by knowledge of another image.

myelin A fatty substance that forms sheaths surrounding axons that serve to speed the transmission of action potentials.

N

net magnetization (M) The sum of the magnetic moments of all spins within a spin system.

network A description of the relationships among a set of brain regions, including their connectivity and causal relationships.

neuroessentialism The intuition that neuroscience data are isomorphic with the subjective self.

neurological convention The practice of displaying images of the brain so that the left and right sides of the image correspond to the same sides of the brain, as if one were behind the subject.

neuron A cell that is the basic information-processing unit of the nervous system.

neurorealism The tendency to consider a behavioral or mental phenomenon to be more real based on the presence of neuroscience data.

neurotransmitters Chemicals released by presynaptic neurons that travel across the synaptic cleft to influence receptors on postsynaptic neurons.

NMR property A label for atomic nuclei that have both a magnetic moment and angular momentum, which together allow them to exhibit nuclear magnetic resonance effects.

noise Non-meaningful changes in some quantity. There are many sources of noise in fMRI studies, and some changes may be classified as either noise or signal, depending on the goals of the study.

nonlinearity The property whereby the combined response to two or more events is not equivalent to the summation of the responses to the individual events in isolation.

normalization The transformation of MRI data from an individual subject to match the spatial properties of a standardized image, such as an averaged brain derived from a sample of many individuals.

nuclear induction The initial term for nuclear magnetic resonance effects, as labeled by Bloch and colleagues.

nuclear magnetic resonance (NMR) The measurable changes in magnetic properties of atomic nuclei induced by the application of an oscillating magnetic field at the resonant frequency of the nuclei.

nuisance regressors Model factors that are associated with known sources of variability that are not related to the experimental hypotheses.

null hypothesis The proposition that the experimental manipulation will have no effect on the experimental data. Most statistical analyses evaluate the probability that the null hypothesis is true, i.e., that the observed data reflect chance processes.

null-task block A control block in which there are no task requirements for the subject. Also called a baseline block or nontask block.

Nuremberg Code A set of principles for the ethical conduct of research involving human subjects that was developed following the trials of Nazi war criminals in the 1940s.

nutation The spiraling change in the precession angle of the net magnetization during an excitation pulse.

Nyquist frequency The highest frequency that can be identified in a digitally sampled signal; it is defined as one-half of the sampling rate.

O

occipital lobe The most posterior lobe of the brain; it is primarily associated with visual processing.

ocular dominance The degree to which a given neuron in the visual cortex responds more to stimuli presented to one eye than to stimuli presented to the other eye.

off-resonance excitation The presentation of an excitation pulse at a frequency other than the resonant frequency of the sample, resulting in reduced efficiency.

oligodendrocyte A type of glial cell that constructs the myelin sheaths around axons.

on-resonance excitation The presentation of an excitation pulse at the resonant frequency of the sample, resulting in maximum efficiency.

orthogonal A property of two variables (or vectors, sets of variables) such that they are completely uncorrelated with each other.

orthogonalize To remove correlation between two variables. In the context of fMRI data analysis, orthogonalizing one regressor (with regard to one or more other regressors) changes that regressor so that it is no longer correlated with the other regressor(s).

oscillating magnetic field A magnetic field whose intensity changes over time. Most such fields used in MRI oscillate at the frequency range of radio waves (megahertz, or MHz) and as such they are often called radiofrequency fields.

outer *k*-space (OK) imaging A partial *k*-space imaging technique in which only the periphery of *k*-space is collected following each excitation, in order to ensure that high-spatial-frequency components of the MR signal are present.

oxygen extraction fraction (OEF) The proportion of available oxygen that is removed from the blood.

oxygenated hemoglobin (Hb) Hemoglobin with attached oxygen; it is diamagnetic.

P

parallel imaging or (**multiple-channel imaging**) The use of multiple receiver channels to acquire data following a single excitation pulse.

parallel state The low-energy state in which an atomic spin precesses around an axis that is parallel to that of the main magnetic field.

paramagnetic Having the property of being attracted to a magnetic field, though with less concentration of magnetic flux than ferromagnetic objects.

parameter matrix A matrix that describes the relative contributions of each model to the observed data for each voxel.

parameter weights For most fMRI analyses, quantities that reflect the relative contributions of the different model factors to the observed data within a given voxel.

parametric effect A manipulation of some independent variable so that it takes a number of levels, to evoke regular changes (e.g., a linear increase) in the dependent variable.

parietal lobe The lobe on the posterior and dorsal surfaces of the cerebrum; it is important for spatial processing, cognitive processing, and many other functions.

partial *k*-space imaging A technique for reducing data acquisition time (and thus increasing temporal resolution) by collecting only part of the *k*-space data following each excitation and filling the uncollected portions of *k*-space with estimated data.

partial least squares (PLS) An approach to analyzing functional neuroimaging data that is used to identify components whose amplitude is influenced by an experimental manipulation.

partial volume effects The combination, within a single voxel, of signal contributions from two or more distinct tissue types or functional regions.

pattern classification An attempt to separate individual examplars into different categories by constructing a set of decision rules based on some combination of their features.

peak The maximal amplitude of the hemodynamic response, occurring typically about 4 to 6 s following a short-duration event.

peer review The practice of vetting scientific research by experts in the discipline. Most journals and funding agencies use a peer review system to determine what research can be published or funded.

perfusion Blood flow through tissue.

periodic event-related design An experimental design in which events of interest occur at regular intervals.

permutation In the context of significance testing, approaches that involve resampling the original data to determine the size of an effect that might be observed with a given alpha level.

phantom An object used for testing MR systems. Most phantoms are filled with liquids or gels with known properties, so that problems with the scanner system can be readily identified.

phase Accumulated change in angle.

phased array A method for arranging multiple surface detector coils to improve spatial coverage while maintaining high sensitivity.

phase-encoding gradient A gradient that is applied before the data acquisition period, so that spins can accumulate differential phase offsets over space.

phrenologists Adherents to the belief that bumps and indentations on the skull provided information about the magnitude of some trait supported by the underlying brain region.

pH-sensitive contrast agent A compound that, when injected into an organism, influences the MR signal differently depending on the pH of the local environment.

physiological noise Fluctuations in MR signal intensity over space and time due to physiological activity of the human body. Sources of physiological noise include motion, respiration, cardiac activity, and metabolic reactions.

pia The innermost membrane covering the brain; it closely adheres to the brain's contours.

pixel A two-dimensional picture element.

plasticity The change in the normal functional properties of brain tissue following injury or experience.

polygraph A device that measures multiple physiological indicators to judge whether an individual is lying. Despite their pervasiveness, polygraphs have proven to have minimal validity for detecting lies in real-world settings.

polymorphism A common variation in a gene or segment of DNA.

pons Part of the brain stem; it serves as a relay system for motor and sensory nerves.

positron emission tomography (PET) A functional neuroimaging technique that creates images based on the movement of injected radioactive material.

power spectrum A representation of the strength of different frequency components within a signal. The Fourier transform converts a signal (i.e., changes in intensity over time) into its power spectrum.

power The probability of detecting an effect of the experimental manipulation.

precession The gyroscopic motion of a spinning object, in which the axis of the spin itself rotates around a central axis, like a spinning top.

precoloring The introduction of autocorrelations to a time series of data so that the time series will have known statistical properties; this is less commonly used than prewhitening in fMRI data analysis.

preprocessing Computational procedures that are applied to fMRI data following image reconstruction but before statistical analysis. Preprocessing steps are intended to reduce the variability in the data that is not associated with the experimental task, and to prepare the data for statistical testing.

pre-surgical planning The use of fMRI or another neuroscience technique to map particular functions in a single individual, in order to guide clinical decisions about the potential course and consequences of neurosurgery in that individual.

prewhitening The application of filters to remove autocorrelations in a time series of data; in fMRI, prewhitening is typically applied before data analysis to remove task-unrelated noise.

primary current The current flow within a neuron caused by the inflow of ions through ionic channels opened by synaptic activity.

principal components analysis (PCA) A common technique for data reduction that simplifies high-dimensional data into a smaller set of components that retains most of the variability in the original data.

principle of reciprocity The rule stating that the quality of an electromagnetic coil for transmission is equivalent to its quality for reception (i.e., if it can generate a homogeneous magnetic field at excitation, it can also receive signals uniformly).

projectile effect The movement of an untethered ferromagnetic object through the air toward the bore of the MRI scanner.

proton-density imaging The creation of MR images that are sensitive to the number of protons present within each voxel.

PSP Any postsynaptic potential, excitatory or inhibitory, that results from synaptic activity.

psychophysiological interaction (PPI) A statistical approach for identifying the effect of an experimental manipulation on the functional connectivity between two brain regions.

pulse sequence A series of changing magnetic field gradients and oscillating electromagnetic fields that allows the

MRI scanner to create images sensitive to a particular physical property.

pulsed ASL A type of perfusion imaging that uses a single coil both to label spins in one plane and to record MR signal in another plane, separated by a brief delay period.

pump A transport system that moves ions across a cell membrane against their concentration gradients.

Q

quality assurance (QA) A set of procedures designed to identify problems with fMRI data so that they do not compromise experimental analyses.

R

radiofrequency coils Electromagnetic coils used to generate and receive energy at the sample's resonant frequency, which for field strengths typical to MRI is in the radiofrequency range.

radiological convention The practice of displaying images of the brain so that the left side of the image is the right side of the brain and vice versa, as if one were facing the subject.

random field theory A branch of mathematics that deals with the properties of smooth, spatially extended data. Using random field theory, researchers can better calculate the number of independent tests within fMRI analyses.

random-effects analysis Intersubject analysis that treats the effect of the experimental manipulation as variable across subjects, so that it could have a different effect on different subjects.

randomization A process for removing confounding factors by ensuring that they vary randomly with respect to the independent variable.

raster A depiction of the firing rate of action potentials by a neuron in which time is represented along the horizontal axis and a dot indicates the occurrence of an action potential.

raw signal-to-noise ratio (raw SNR) The ratio between the MR signal intensity associated with a sample (e.g., the brain) and the thermal noise that is measured outside the sample.

reaction time The time required for someone to make a simple motor response to the presentation of a visual stimulus. Note that this is distinct from response time, which applies to situations in which someone must choose between two or more possible responses.

real-time analyses A set of computational steps designed for the rapid analysis of fMRI data, so that statistical tests can be conducted immediately following the acquisition of images.

reception The process of receiving electromagnetic energy emitted by a sample at its resonant frequency (also called detection). As nuclei return to a low-energy state following the cessation of the excitation pulse, they emit energy that can be measured by a receiver coil.

receptive field The part of the visual field that, when stimulated, will result in an increase in firing of a particular neuron.

recovery of function The improvement in a previously impaired ability over time, due to functional or structural changes within the brain.

redundant safeguards The use of multiple independent procedures that could each identify potential problems or unsafe situations.

reference volume A target image volume to which other image volumes are to be aligned.

refocusing pulse A 180°-electromagnetic pulse that compensates for the gradual loss of phase coherence following initial excitation.

refractory effects Changes in the amplitude and timing of a response based on the characteristics of preceding responses.

refractory period A time period following the presentation of a stimulus during which subsequent stimuli evoke a reduced response. For BOLD fMRI, the refractory periods for many types of stimuli last approximately 6 s.

region-of-interest (ROI) analyses Evaluations of hypotheses about the functional properties of brain regions (i.e., aggregated over a pre-determined set of voxels), often chosen to reflect a priori anatomical distinctions within the brain.

registry A patient database. A registry might include information about the locations of brain lesions in a large population of individuals who might then be asked to participate in experimental studies.

regressor A hypothesized time course of BOLD activation caused by the manipulations of an independent variable or by another known source of variability.

relaxation A change in net magnetization over time.

rendered image A display of MRI data in three-dimensional perspective.

repetition time (TR) The time interval between successive excitation pulses, usually expressed in seconds.

repetitive TMS (rTMS) The delivery of an extended series of closely spaced TMS stimulation pulses, in order to effect long-lasting changes in brain function.

research hypothesis A proposition about the nature of the world that makes predictions about the results of an experiment. For a hypothesis to be well formed, there must be some experiment whose outcome could prove it to be false.

research protocol A document describing the procedures of a research study, in a form that can be evaluated by the local Institutional Review Board.

research The accumulation of data, whether by observation or experimentation, to develop general knowledge.

residual The variability in the data that remains unexplained after accounting for the model factors.

resistance vessels Arterioles that control the flow of blood through the capillary bed.

resolution elements (or resels) The independent statistical tests within an fMRI volume.

resonant frequency The frequency of oscillation that provides maximum energy transfer to the system.

respect for persons The principle that individuals should be treated as autonomous decision makers who should be given the opportunity to make informed decisions about their participation in research studies. Individuals with an impaired capacity for autonomous decision making must be granted additional protection.

response time The time required for someone to execute a choice between two or more possible responses. Note that this is distinct from reaction time, which applies to situations when only one possible response is present.

resting-state connectivity The functional connectivity of a given brain region, when measured while the participant is not performing any coordinated, purposeful task.

reverse inference Reasoning from the outcome of a dependent variable to infer the state of an independent variable (or an intervening unobservable variable).

right-hand rule A method used to determine the direction of a magnetic moment generated by a moving charge or electrical current. If the fingers of the right hand are curled around the direction of spin, then the magnetic moment will be in the direction indicated by the thumb.

rigid-body transformation A spatial transformation that does not change the size or shape of an object; it has three translational parameters and three rotational parameters.

rostral Toward the front of the brain.

rotating frame A reference frame that rotates at the Larmor frequency of the spin of interest. The rotating frame is adopted to simplify mathematical descriptions of the effects of excitation.

rotation The turning of an object around an axis in space (in the absence of translation).

run An uninterrupted presentation of an experimental task, usually lasting 5 to 10 minutes for fMRI studies. It also refers to the set of functional images collected during that task presentation.

S

sagittal A side view of the brain (along the y–z plane in MRI).

sample (1) A set of observations drawn from a larger population of potential observations. (2) An object to be imaged using magnetic resonance.

sampling rate The frequency in time with which a measurement is made.

scalar A quantity that has magnitude but not direction. Scalars are italicized in this text.

scaling A principle of linear systems that states that the magnitude of the system output must be proportional to the system input.

scanner drift Slow changes in voxel intensity over time.

searchlight An approach to feature selection in the pattern classification of fMRI data. As its name implies, a searchlight reflects a geometrically defined ROI (e.g., a sphere of 5-voxel radius) that can be moved throughout the brain.

seed voxel A voxel chosen as a starting point for a connectivity analysis.

segmentation The process of partitioning an image into constituent parts, typically types of tissue (e.g., gray matter, white matter) or topographical divisions (e.g., different structural regions like Brodmann areas).

selectivity The tendency for a manipulation to lead to one outcome. Perfect selectivity is sometimes referred to as "specificity."

semirandom design A type of event-related design in which the probability that an event will occur within a given time interval changes systematically over the course of the experiment.

session A single visit to the scanner by a subject. For fMRI studies, each session usually includes both structural and functional scans.

shimming coils Electromagnetic coils that compensate for inhomogeneities in the static magnetic field.

signal averaging The combination of data from multiple instances of the same manipulation in order to improve functional SNR.

signal Meaningful changes in some quantity. For fMRI, an important class of signals includes changes in intensity associated with the BOLD response across a series of T_2^* images.

signaling activity The transmission of the outcome of an integrative process from one neuron to another.

signal-to-noise ratio (SNR) The relative strength of a signal compared with other sources of variability in the data.

significance testing The process of evaluating whether the null hypothesis is true. Also known as hypothesis testing.

simple cell A neuron in the visual cortex that responds with increased firing to a stimulus with a preferred orientation in its receptive field, and with decreased firing to a stimulus in the region surrounding its receptive field.

single dissociation The demonstration that an experimental manipulation has an effect on one variable but not on a second variable.

single-pulse TMS The delivery of a single TMS stimulation pulse, in order to disrupt some ongoing brain process.

single-unit recording Collection of data about the electrophysiological activity (e.g., action potentials) of a single neuron.

sinuses The term sinus has two primary meanings in neuroanatomy: (1) long venous channels formed by meningeal coverings that form the primary draining system for the brain, and (2) air-filled cavities in the skull.

slice A single slab of an imaging volume. The thickness of the slice is defined by the strength of the gradient and the bandwidth of the electromagnetic pulse used to select it.

slice selection The combined use of a spatial magnetic field gradient and an electromagnetic pulse to excite spins within a slice.

small-volume correction The restriction of analyses to specific regions-of-interest, defined a priori, to reduce the total number of statistical tests and thus allow for a more liberal significance threshold.

smoothness The degree to which the time courses of nearby voxels are temporally correlated.

sodium–potassium pump A transport system that removes three sodium ions from within a cell while bringing two potassium ions into the cell.

soma The body of the cell; it contains cytoplasm, the cell nucleus, and organelles.

spatial extent The number of active voxels within a cluster of activity (i.e., the size of the active region).

spatial frequency The frequency with which some pattern occurs over space.

spatial gradient (G) A magnetic field whose strength varies systematically over space. Note that since a given spatial location only experiences one magnetic field, which represents the sum of all fields present, spatial gradients in MRI act to change the effective strength of the main magnetic field over space.

spatial ICA A form of independent component analysis that generates components that have minimal spatial redundancy.

spatial interpolation The estimation of the intensity of an image at a spatial location that was not originally sampled, using data from nearby locations.

spatial resolution The ability to distinguish changes in an image (or map) across different spatial locations.

spatial smoothing The blurring of fMRI data across adjacent voxels to improve the validity of statistical testing and maximize functional SNR, at a cost of spatial resolution.

specific absorption rate (SAR) A quantity that describes how much electromagnetic energy is absorbed by the body over time.

speed–accuracy trade-off The improvement in the speed of a response at the expense of accuracy, or vice versa, within an experimental task.

spin system A collection of atomic nuclei that possess the NMR property within a spatial location.

spin-echo (SE) imaging One of the two primary types of pulse sequences used in MRI; it uses a second 180° electromagnetic pulse to generate the MR signal changes that are measured at data acquisition.

spins Atomic nuclei that possess the NMR property; that is, they have both a magnetic moment and angular momentum.

spiral imaging A technique for fast image acquisition that uses sinusoidally changing gradients to trace a corkscrew trajectory through *k*-space.

spiral-out trajectory A corkscrew path that begins at the center of *k*-space and ends at the periphery. It is the most common form of spiral imaging.

standard deviation A commonly used measure of the variability within a sample of data points.

standard error A commonly used estimate of the likely discrepancy between a measured value and a true value, often calculated from a measure of variability in the data (i.e., the standard deviation) and the number of data points in the sample.

state-related processes Changes in the brain that are assumed to reflect distinct modes, or states, of function. State-related processes are more easily measured with blocked designs.

static contrasts Contrast mechanisms that are sensitive to the type, number, relaxation properties, and local environment of spins (e.g., T_1, T_2, proton density).

static magnetic field The strong magnetic field at the center of the MRI scanner whose strength does not change over time. The strength of the static magnetic field is expressed in Tesla (T).

statistical map (or statistical parameter map) In fMRI, the labeling of all voxels within the image according to the outcome of a statistical test.

stereotaxic space A precise mapping system (e.g., of the brain) using 3-D coordinates.

structural connectivity A pattern of structural connections between regions based on known axonal projections.

structural equation modeling (SEM) A statistical approach for testing a model of the relationships among a set of independent and dependent variables.

subject An individual who participates in a research study. Some journals and scientific societies prefer the term "participant," to emphasize the voluntary nature of research.

subsequent memory An approach to fMRI analyses that sorts experimental stimuli based on whether they were remembered or forgotten in a later testing session; this allows identification of brain regions whose activation predicts successful encoding of stimulus properties into memory.

subtraction In experimental design, the direct comparison of two conditions that are assumed to differ only in one property, the independent variable.

sulci Troughs in the cortical surface.

superconducting electromagnets A set of wires made of metal alloys that have no resistance to electricity at very low temperatures. By cooling the electromagnet to near absolute zero, a strong magnetic field can be generated with minimal electrical power requirements.

superposition A principle of linear systems that states that the total response to a set of inputs is equivalent to the summation of the independent responses to the inputs.

support vector machine (SVM) A class of algorithm used in pattern classification that attempts to identify the combination of features in the original data set that can most effectively differentiate between two categories.

surface coil A radiofrequency coil that is placed on the surface of the head, very close to the location of interest. Surface coils have excellent sensitivity to the signal from nearby regions but poor sensitivity to signal from distant regions.

susceptibility artifacts Signal losses on T_2*-dependent images due to magnetic field inhomogeneities in regions where air and tissue are adjacent.

Sylvian fissure The deep sulcus separating the temporal lobe from the frontal and parietal lobes.

synapse A junction between neurons where the presynaptic process of an axon is apposed to the postsynaptic process of a dendrite or cell body.

synaptic cleft A gap between presynaptic and postsynaptic membranes.

system noise Fluctuations in MR signal intensity over space or time that are caused by imperfect functioning of the scanner hardware.

system A set of regions that are linked by coactivation, but for which the connectivity and causal relationships remain unknown.

T

T_1 (recovery) The time constant that describes the recovery of the longitudinal component of net magnetization over time.

T_1-weighted (T_1-dependent) Images that provide information about the relative T_1 values of tissue; also known as T_1 images.

T_2 (decay) The time constant that describes the decay of the transverse component of net magnetization due to accumulated phase differences caused by spin–spin interactions.

T_2* (decay) The time constant that describes the decay of the transverse component of net magnetization due to both accumulated phase differences and local magnetic field inhomogeneities. T_2* is always shorter than T_2. BOLD-contrast fMRI relies on T_2* contrast.

T_2* blurring Distortions in T_2* images that result from having a data acquisition window that is sufficiently long that significant T_2* decay occurs over that interval.

T_2*-weighted (T_2*-dependent) Images that provide information about the relative T_2* values of tissue. T_2*-weighted images are commonly used for BOLD-contrast fMRI.

T_2-weighted (T_2-dependent) Images that provide information about the relative T_2 values of tissue; also known simply as T_2 images.

Talairach space A commonly used space for normalization of fMRI data; its coordinates are based on measurements from a single post-mortem human brain, as published in an atlas by Talairach and Tournoux.

task frequency The rate of presentation of a periodic experimental task.

TCA cycle The second step in aerobic glycolysis; it involves the oxidation of pyruvate.

temperature-sensitive contrast agent A compound that, when injected into an organism, influences the MR signal differently depending on the local tissue temperature.

temporal derivative A regressor that, when added to a model, improves the robustness of that model to small variations in the timing of the hemodynamic response.

temporal ICA A form of independent component analysis that generates components that have minimal temporal redundancy.

temporal interpolation The estimation of the value of a signal at a time point that was not originally collected, using data from nearby time points.

temporal lobe The lobe on the ventral surface of the cerebrum; it is important for auditory and visual processing, language, memory, and many other functions.

temporal resolution The ability to distinguish changes in a signal (or map) across time.

tensor A collection of vector fields governed by three principal axes.

testing set In pattern classification analysis, a novel part of the data set used to evaluate the robustness of the classification algorithm.

thalamus A brain nucleus that is important for many aspects of perception and cognition; it is highly interconnected with many regions of the cerebral cortex.

theory An organized set of ideas that guides thinking on a topic and that can be used to generate a variety of experimental hypotheses.

thermal noise Fluctuations in MR signal intensity over space or time that are caused by the thermal motion of electrons within the sample or scanner hardware.

time course The change in MR signal over a series of fMRI images.

time domain The expression of a signal in terms of its intensity at different points in time.

time series A large number of fMRI images collected at different points in time.

time-locking Synchronization of analyses to events of interest, usually for the extraction of epochs.

torque A force that induces rotational motion.

torsion A rotation (twisting) of an object. Even if the motion of an object is restricted so that it cannot translate, a strong magnetic field will still exert a torque that may cause it to rotate so that it becomes aligned with the magnetic field.

tractography The identification and measurement, often using diffusion tensor imaging, of white matter tracts that connect distant brain regions.

training set In pattern classification analysis, that part of the data set used to develop the classification algorithm.

transcranial magnetic stimulation (TMS) A technique for temporarily stimulating a brain region to disrupt its function. TMS uses an electromagnetic coil placed close to the scalp; when current passes through the coil, it generates a magnetic field in the nearby brain tissue, producing localized electric currents.

translation The movement of an object along an axis in space (in the absence of rotation).

transmitter coil An electromagnetic coil that generates an oscillating magnetic field at the resonant frequency of atomic nuclei within a sample.

transverse Perpendicular to the main magnetic field of the scanner, in the x–y plane.

transverse relaxation (or spin–spin relaxation) The loss of net magnetization within the transverse plane due to the loss of phase coherence of the spins.

trial sorting The post hoc assignment of events to conditions, often based on behavioral data.

trial A single instance of the experimental manipulation.

***t*-test** A test for statistical significance based on the Student's t-distribution. The t-test typically evaluates whether the mean values of two sets of observations are sufficiently different to preclude their being drawn from the same distribution.

Type I error Rejecting the null hypothesis when it is in fact true. Also known as a false positive.

Type II error Accepting the null hypothesis when it is in fact false. Also known as an incorrect rejection or false negative.

U

ultra-high-resolution MRI The acquisition of MR images with voxel sizes in the order of tens of micrometers. Applications of ultra-high-resolution MRI to animal tissues are known as MR microscopy.

undershoot The decrease in MR signal amplitude below baseline due to the combination of reduced blood flow and increased blood volume.

unknown risks Possible negative outcomes that, though not anticipated based on the best available science, nevertheless influence research or clinical procedures. Most fMRI centers do not scan pregnant women because of potential unknown risks to the developing fetus.

V

variable A measured or manipulated quantity that varies within an experiment.

vasoactive substances Substances that change the diameter of blood vessels.

vector A quantity with both magnitude and direction. Vectors are in boldface in this text.

veins Blood vessels that carry blood from the body to the heart. Blood in the veins (except for the pulmonary vein) is partially deoxygenated.

velocity-encoded phase contrast (VENC-PC) MRA A type of MR angiography that uses gradient fields to induce phase differences associated with vascular flow so that the flow velocity of vessels can be measured.

ventral Toward the bottom of the brain.

ventricles Fluid-filled cavities within the brain.

venules Small veins.

volume coil A radiofrequency coil that surrounds the entire sample, with roughly similar sensitivity throughout.

volume conductor A continuously conductive medium. The brain, meninges, skull, and scalp constitute a volume conductor throughout which currents created by ionic flow can be measured.

volume current The return current through the extracellular medium that balances the primary current within a neuron.

volume A single image of the brain, itself consisting of multiple slices and voxels.

volumetric Relating to the measurement of volume.

voxel A three-dimensional volume element.

voxelwise analyses Evaluations of hypotheses about the functional properties of individual voxels (or small clusters of voxels), often throughout the entire brain.

voxelwise analysis The evaluation of statistical tests at the level of individual voxels.

W

within-subjects A manipulation in which each subject participates in all experimental conditions.

Index

acetylcholine, 9
Achieva scanner, *32*
acoustic noise, 54
action potentials, 165, 459
active gradient-shielding, 202
active state, 308
adaptation, 235
adenosine, 175
adenosine triphosphate (ATP), 163, 166–168
aerobic glycolysis, 166
AFNI, *345*
aging, cognitive decline and, 400, *401*
algorithms, 322–323
aliasing, 259
alpha values, 333, 357–358, 361
alternating design, 305, 309
γ-aminobutyric acid (GABA), 163
amygdala, 184, *189*
anaerobic glycolysis, 166–167
anatomical ROIs, 363–365
angiography, 135
  See also MR angiography
angular momentum (J)
  defined, 59
  nuclei and, 69
  overview, 75
  of a proton, 70–71
  spin precession and, 72, 73
animal studies, 476–480
anisotropic diffusion, 139
anode, 447
anterior cerebral arteries, *171*, 172, *173*
anterior cingulate cortex, 326, 394, 405, 485
anterior collateral sulcus, 388
anterior commissure, *183*, *189*
anterior inferior cerebellar artery, *171*
anterior insula, 326
anterior parietal lobe, 388
anterior temporal lobe, *188*
antiparallel state, 61–62, 71, 74–75, 76–77
aorta, 170
aortic arch, 171–172
aphasia, 447
apical dendrites, 461
APOE-3 gene, 457
apparent diffusion coefficient, 139, 142, *143*
arachnoid, 182
arousal, measuring, 43
arterial spin labeling, 144–146
arteries, 170
  See also blood vessels; brain vascular system
arterioles, 170, *180*, 181
ascending/descending slice acquisition, 270
astrocytes, 177–178, 182
autoradiography, 196
averaged epochs, 315–316
axial view, 188
axon hillock, *161*, 164–165
axons, 160, *161*

B_{1eff}, 80–81, 82
b factor, 139
balloon model, 211
band-stop filters, 286
basal ganglia, 184, 391, 439
basal vein, *173*
base image, 369
baseline activation, 306–309
baseline condition, 298
basilar artery, *171*, 172, *173*
basis functions, 353
behavior, predicting variation in, 407–408
beneficence, 495
Berger, Hans, 314, 458
Berns, Gregory, 7
beta values, 343
betas, 343
between-subjects correlations, 384–386
between-subjects manipulation, 296
bias field, 279, 280
bias field estimation, 279–280
biofeedback, 404–405
biomarkers, 406
Biot, Jean-Baptiste, 34
birdcage coil, 37
bite bars, 274
Bloch, Felix, 17, 18
Bloch equation, 87, 100–101, 144
blocked designs
  advantages and disadvantages, 310–313
  baseline activation, 306–309
  compared to event-related designs, 315
  defined, 303
  Fourier analyses, 341–342
  optimal block length, 320
  overview, 247, 303–304
  refractor effects and, 233–234
  setting up, 304–305, 309
  t-tests and, 336–337
blocks, 303
blood flow
  control of, 175–179
  coupling glucose metabolism to, 196, 198–200
  effects on capillaries, 179–181
  factors affecting, 174–175
  perfusion-weighted contrast and, 142–146
  rates of, 175
blood-oxygenated-level dependent (BOLD) contrast
  ADC maps and, *143*
  compared to perfusion contrast, *146*
  concept of, 159–160
  correlational data criticism, 298–299
  coupling glucose metabolism to blood flow, 196, 198–200
  discovery of, 194–196
  hemodynamic hypotheses and, 296, *297*
  linearity and, 353–354
  neuronal hypotheses and, 297
  refractory effects, 229–230, 233–236
  resting-state connectivity and, 391–392
  scanner field strength and, 251
  schematic of, *195*
  variability affecting, 243–244
  See also BOLD fMRI
blood oxygenation
  fMRI studies and, 4, 5
  See also hemoglobin
blood pressure, 49
blood vessels
  issues of spatial specificity and, 252–253
  MR angiography, 135–138
  overview, 170–171
  See also brain vascular system
body temperature, 434–435
Bohr relation, 74
BOLD fMRI
  blocked designs, 303, 310–313
  event-related designs, 316–319
  growth of, 201–207
  history of, 193–200
  neuronal activity and, 209–210
  spatial resolution, 214–220
  temporal resolution, 220–229

See also blood-oxygenated-level dependent contrast
BOLD refractory effects, 229–230, 233–236
Boltzmann's constant, 76
bolus, 204
Bonferroni correction, 358
bore size
effective, 422
gradient coil strength and, 39–40
brain
anatomy, 182–189
connectivity and, 386
coordinate axes, *283*
energy budget, 167–168
energy consumption, 165–168
functional plasticity, 454, *455*
temperature, 434–435
variability in size and volume, 281, *282*
brain function manipulation
brain imaging and genomics, 457
brain lesions, 425–454
direct cortical stimulation, 446–450
probabilistic brain atlases, 455–456
research techniques, 446
transcranial magnetic stimulation, 450–452
brain function measurement
field potentials, 464–474
historical overview, 458
magnetoencephalography, 474–476
single-unit recording, 458, 461–464
brain lesion studies
combined with fMRI, 454–455
overview, 452–454
brain mapping
atlases, 455–456
early history of, 2–3
fMRI-generated, *12*
lesion maps, *453*
brain metabolism
measurement techniques and, 5
PET and, 4, 5
"Brain Pong," 404
brain stem, 184, *188*
brain studies
on brain chemistry, 9
functional, 1–3
using lesions, 452–455
brain tumors, *141*
brain vascular system
anatomy of, 171–172, *173*
blood flow, 174–181 (*see also* blood flow)
blood flow rates, 170
brain function and blood flow question, 168–169
microcirculation, 172–174
Brain Voyager, *345*
Broca, Paul, 8, 447
Broca's area, 8, 392, 393
Brodmann, Korbinian, 185, 364
Brodmann area 1, 468, 469
Brodmann area 4, 468
Brodmann area 3b, 468–469
Brodmann areas, 185, *186*, 364
bulk magnetization. *See* net magnetization

calcarine cortex, 204
calcarine sulcus, *174*, *187*
calcium ions
ion-gated contrast and, 437–438
vasodilation and, 177–178
calcium-sensitive contrast agents, 437
callosomarginal artery, *173*
calmodulin, 437
capillaries, 170–171, 179–181
capillary recruitment, 181
categorical variable, 295–296
cathode, 447
Caton, Richard, 458
caudal, 182
caudate nucleus, 184, *189*, 385
causal chains, 298–299
causality, inferring from fMRI data, 394–399
central nervous system, 182–189
central sulcus, 186, *187*, 468–469
cerebellum, 182, *183*, *186*, *187*, *188*
cerebral blood flow, 196, 198, 199
cerebral cortex, *12*, 185, 284
cerebral hemispheres, 185, 186
cerebral metabolic rate for glucose, 198, 199
cerebral metabolic rate for oxygen, 198
cerebral metabolism, 165–168
cerebrospinal fluid (CSF), *123*, 127, 182–183
cerebrum, 184, 185
Chadwick, James, 15
chemical contrast, 132–133
chemical shift imaging, 132–133, 435
choline, *133*
chronic pain, 405
cingulate cortex, 7, 386
cingulate gyrus, *183*, *187*, *189*
circle of Willis, *171*, 172
cisterns, 182
citric acid cycle. *See* tricarboxylic acid cycle
claustrophobia, 53–54
clinical cortical mapping, 403–404
Clinton, Hillary, 485
cluster-size thresholding, 360–361
clustered acquisition, 472–473
CNR. *See* contrast-to-noise ratio
coactivation, 389–390
cochlear implants, 52
cognitive decline, age-related, 400, *401*
cognitive neuroscience, 443–445
Cognitive Neuroscience Patient Registry, 453
coil sensitivity, 38
colliculi, *183*, *188*
collinear regressors, 346
color map, 369–370
common carotid artery, *171*, 172
compasses, 32
complementarity, 13–14
complex cells, 461
components, in data-driven analyses, 378
computer hardware, in MRI scanners, 41
computerized tomography (CT), 21, 202, *203*
concentration gradients, 162
conditions, 294
confounding factors, 299–302
conjugate mirroring, 427–428
connectivity, 386
See also functional connectivity analyses
connectivity mapping, 399–401
conscious decisions, prediction of, 414–415
consent forms, 45–46, 495–496
constructs, 444
continuous ASL, 144, 145
continuous variables, 296
contrast
concept overview, 9–11
defined, 123
experimental, 336
overview of, 248
contrast agents, 204–205, 422, 434, 437, 478
contrast-to-noise ratio (CNR), 10, 11, 245, 248
contrast weights, 354–355
contrasts, 354–356
control blocks, 305
control condition, 298
control system, 43
converging operations, 443, 492
coordinate axes, for the brain, *283*
coregistration, 276–277
functional-structural, 280–281
coronal view, 188–189
corpus callosum, 1, *183*, 187, *189*
correlation analyses, 338–340, 344
correlation coefficient, 339
correlational data issue, 298–299
correlations, 446
cortex, 1, 160, 185–189
cortical mapping, real-time, 403–404
cortical thickness, 456
Coryell, Charles, 193
cost function, 276, 344
counterbalancing, 301
covariates, 345, 346
creatine, *133*
cross product, 68
cross-slice excitation, 108
cross-validation, 411–412
cryogens, 35
CT. *See* computerized tomography
current dipole, 460
current sink, 459
current source, 459
cytoarchitectonic mapping, 185
cytoarchitecture, 185, 284, 364

da Vinci, Leonardo, 2
Damadian, Raymond, 19, 22, 202
Damasio, Antonio and Hanna, 453
data analysis
early fMRI and, 207
fundamental problems in, 243
overview, 247
See also data-driven analyses; MR signal analysis; statistical analyses; *specific approaches*
data-driven analyses
independent components analysis, 380–382, *383*
overview, 377
partial least squares, 382–384
principal components analysis, 378–379
data matrix, 343, *344*
data reduction, 379
databases, for brain lesions, 453
de-identification, 501, 502
deactivations, 306, 307
deception, 496
decisions, prediction of, 414–415
default network, 306, 392
degrees of freedom, 335
dementia, 457
dendrites, 160, *161*
deoxygenated hemoglobin (dHb), 11, 193–200
dependent variable (DV), 294–295, 298, 490
Descartes, Rene, 1, 2
descriptive statistics, 331
design matrix
assumptions of the general linear model and, 356
construction, 345–349

modeling neuronal activity, 351–352
nuisance regressors, 349–351
overview, 343, 344
detection, 247, 310
detector coil, 18
diagnostic fMRI, 403–404
diamagnetism, 193
diencephalon, 184
diffusion, 138
diffusion spectrum imaging, 140–141
diffusion tensor imaging, 140–142, 399–401
diffusion-weighted contrast, 138–142
diffusion weighting, 139, 142, 211, 218–219
dipoles
current, 460
equivalent, 461
neuronal generators and, 466
scalp-recorded field potentials and, 473–474
direct cortical stimulation
compared to fMRI, 449–450
functional consequences, 448–449
limitations, 449
overview, 446–448
"disconnection hypothesis," 400
diseases, brain studies and, 455–456
dispersion derivatives, 352–353
distortions, correction, 277–280
distribution, 334
dopamine, 176
dorsal, 182
dorsomedial nucleus, 184
dot product, 68
double dissociation, 390, 454
"double-saddle," 39
dread, neural basis, 7
drug studies, 9
Du Bois-Reymond, Emil, 458
Duke University, 202
dura, 182
dynamic causal modeling, 398–399
dynamic CNR, 248

echo-planar imaging (EPI)
active-gradient shielding and, 202
artifacts and, 148, *149*, *150*, 151
current use of, 207
k-space and, 430, *431*
overview, 19, 147–148
signal recovery and distortion correction, 152–154, *155*
echo time (TE)
defined, 123
MR angiography and, 136
physiological noise and, 261
proton-density contrast and, 123–124
T_1 contrast and, 126
T_2 contrast and, 129
T_2^* contrast and, 132
edge effects, head motion and, 271–272
EEG. *See* electroencephalography
effect size, 248
effective bore size, 422
efficiency, 294
efficient *k*-space trajectories, 430–432
eigenimages, 379
eigenvalue, 379
eigenvectors, 379
electric currents, gradient magnetic field effects and, 50–52
electrical field potentials. *See* field potentials
electrode studies, of neurons, 5, 8
electrodes, in direct cortical stimulation, 447
electroencephalography (EEG)
combined with fMRI, 472–473
event-related potentials and, 314
field potentials and, 466–467
limitations, 159
MEG and, 475
origin of, 458
overview, 8, *471*
resolution qualities, *14*
synchronous waves, 465
electrogenesis, 458, 459–461
electromagnets, 33–35
electromotive force, 83
electron shielding effect, 435
electron transport chain, 166, *167*
electrophysiological measures, 209–210, 216, *217*
endogenous contrast
defined, 121
MR angiography and, 136
perfusion imaging and, 144–146
"endowment effect," 348
energy minimization, 61
entorhinal cortex, 187–188
epilepsy, 448
epiphenomenal data issue, 298–299
epiphenomenon, 394
EPISTAR, *144*, 145–146
epochs, 211, 315–316
equipotentiality, 446
equivalent dipole, 461
ERP components, 467, 469, 471
ERPs. *See* event-related potentials
error matrix, 344
estimation, 247, 310
ethics, in conducting fMRI research, 494–495
European Union, 44
event-related designs
advantages of, 319, 324–325
central assumption of, 313–314
compared to blocked designs, 315
defined, 313
overview, 247
principles of, 316–319
refractor effects and, 234
t-tests and, 337–338
event-related potentials (ERPs)
combined with fMRI, 472–473
intracranially recorded field potentials and, 467, 469–470
overview, 314–315
resolution qualities, *14*
scalp-recorded field potentials and, 471–474
events, 314
evoked magnetic fields, 474–476
evoked potentials, 467
excitation
defined, 35, 67
overview, 35–36
of a spin system, 64–65
See also spin excitation
excitation field, 277, 278–279
excitation pulse
MR signal and, 100
slice selection, 106–108
spin excitation, 78–82, *83*
excitatory neurotransmitters, 163
excitatory postsynaptic potential (EPSP)
action potential and, 459
BOLD changes and, 216
brain energy consumption and, 167–168
defined, 163
neuronal information processing and, 165
See also electrophysiological measures; postsynaptic potentials
exogenous contrast
defined, 121
functional studies and, 204–205
MR angiography and, 136
perfusion MRI and, 143–144
exogenous contrast agents, 204–205, 478
expected Euler characteristic, 362
experimental condition, 298
experimental contrast, 336
experimental control system, 43
experimental design
blocked designs (*see* blocked designs)
characteristics of, 293–294
defined, 293
efficiency in, 320–323
event-related (*see* event-related designs)
goals of, 345, 347
good practices in, 302–303
mixed designs, 247, 325–326, 346
outline of, 45–48
overview of, 247
principles of, 294–296
research hypothesis, 296–302
experimental power, 250
experimental regressors, 345
experiments, 293
external carotid artery, *171*, 172
external magnetic field
spin precession, 71–73
spins in, 60–62, 71–74
extracranial field potentials, 470–474
eye movements, 43–44

F distribution, 344
F-test, 355–356
face recognition, 469–470
factor analysis, 379
FAIR, *144*, 146
false discovery rate, 359
false-positive results. *See* Type I errors
falx, 172
familywise error rate, 358, 359
Faraday, Michael, 193
fast imaging sequences, 147–154
feature selection, 411
Ferrier, David, 447, 452, 458
fiber tracts, 386
field homogeneity, 34
field inhomogeneities, 277–280
field maps, 278
field of view, 115–116, 117, 214
field potentials
defined, 458, 464
intracranially recorded, 466–467, 469–470
localization of function using, 468–469
localizing neural generators of, 465–466
properties of, 464–465
field strength
effects on fMRI data, 250–254
Larmor frequency and, 97, 100
MRI and, 34–35
raw signal-to-noise ratio and, 251–252
signal-to-noise ratio and, 63

spatial properties of activation and, 252–254
ultra-high, 420
field uniformity, 34
filling *k*-space, 112
filters
spatial filtering, 287–289
temporal filtering, 285–286
uses of, 284–285
finite impulse response, 353
fixed-effects analyses, 365–366, 367
flat maps, 372
flip angle, 82, 222
Flourens, Pierre, 446
fluoro-2-deoxy-D-glucose (FDG), 197
flux, 61
flux lines, 60–61
fMRI. *See* functional magnetic resonance imaging
fMRI adaptation, 235–237
fMRI data
acquisition, 246–247
analysis (*see* data analysis; statistical analyses)
combining with diffusion tensor imaging, 399–401
confidentiality, 497, 500–502
effects of field strength on, 250–254
inferring causality from, 394–399
interpreting and presenting, 486–494
noise and (*see* noise)
preprocessing, 244–245
variability across subjects and sessions, 264–266
variability affecting, 243–244
fMRI research
confidentiality of data, 500–502
converging operations, 443
ethical principles, 494–495
future of, 511–513
growth in, *24*
incidental findings, 498–501
non-traditional applications, 505–511
popular media coverage, 485–486, 487–489
pregnancy testing in, 504–505
principles for presenting, 489, 492–494
proposing and approving, 495–497
protocol, 495
reverse inference, 490–491
safe conduct of, 502–504
scientific research process, *493*
FONAR Corporation, 20, 22, 23, 202
Food and Drug Administration (FDA), 497
foramen lacerum, 172
foramen magnum, *171*, 172, 182
forebrain, 184
forward Fourier transforms, 110
forward solution, 472–473
Fourier transforms, 110, *113*, 341–342, 345
fractional anisotropy, 140, 142, 400
frequency domain, 341
frequency encoding gradient, 93–95, 110, 112–113
Fritsch, Gustav, 447
frontal lobe, 1, *183*, 186, 187, 451
FSL, *345*
Function of the Brain, The (Ferrier), 447
functional CNR, 248
functional connectivity, 293, 307, 386, 444
functional connectivity analyses
combining fMRI and diffusion tensor imaging, 399–401
conceptual overview, 386, 389–391
inferring causality from fMRI data, 394–399
psychophysiological interactions, 393–394, *395*
resting-state connectivity, 391–393
functional contrast, 11
functional magnetic resonance imaging (fMRI)
animal studies and, 476–480
data analysis (*see* data analysis; statistical analyses)
defined, 3
early studies, 203–207
experimental design (*see* experimental design)
functional contrast, 11
goal of, 246
history of, 15–24
as a measurement technique, 5, 8
overview, 3–4
physiological monitoring, 43–44
uses of, 6–7
See also fMRI data; fMRI research
functional neuroimaging, 4
functional plasticity, 454, *455*
functional resolution
concept overview, 14–15
ion-gated contrast, 437–438
Lorentz effect contrast, 439–440, *441*
neuronal magnetic field contrast, 438–439
pH-dependent contrast, 435–436
temperature-dependent contrast, 434–435
functional ROIs, 364
functional signal-to-noise ratio, 248–250, 432
functional-structural coregistration, 280–281
fusiform cortex, 388
fusiform gyrus, 236–237, 250, 448–449, 470

gadolinium, 136
gadolinium diethylenetriaminepentaacetic acid (Gd-DTPA), 204
Gage, Phineas, 452
Galileo, 293
Gall, Franz Joseph, 2
Gamma function, 352, *353*
gamma radiation, 197–198
γ-aminobutyric acid (GABA), 163
Gaussian filter, 287, 288
Gaussian theory, 362
General Electric, 202
Sigma series scanner, *32*
1.5-T scanners, 23
general linear model (GLM)
assumptions of, 356
contrasts, 354–356
design matrix construction, 345–349
modeling neuronal activity, 351–352
nuisance regressors, 349–351
overview, 343–345
genetic algorithms, 323
genomics, brain imaging and, 457, 509
genu of the corpus callosum, *187*
glass-brain views, 371
glial cells (glia), 161, 182
GLM. *See* general linear model
globus pallidus, 184
glucose, 166
glucose metabolism, coupling with blood flow, 196, 198–200
glutamate, 163, 168
glycolysis, 166, *167*
Golay pair, 39
Goldman-Rakic, Patricia, 461–462
Gorter, Cornelis, 16
gradient coils, 38–41, 207
gradient-echo echo-planar imaging, 427–428
gradient-echo imaging, 112, 125, 152–153
gradient-echo sequences, 112, 132
gradient-echo spiral imaging, 427–428
gradient fields
in MR image formation, 90–91
MR signal equation and, 106
nonlinearities and, 118–120
safety risks, 50–52
Granger, Clive, 396
Granger causality, 396–397, *398*
graphic user interface, *42*
gray matter, *123*, 167
great cerebral vein of Galen, *173*
group effects, 367–368
G_x. *See* frequency encoding gradient
gyri, 185
gyromagnetic ratio (γ), 71, 74, 75, 81, 97
G_z, 91, 92–93

Harlow, John, 452
HDR. *See* hemodynamic response
head motion
correction, 276–277
effects of, 271–274
prevention, 274–276
head motion parameters, 349–350
head restraints, 274–275
Health Insurance Portability and Accountability Act (HIPAA), 497, 500
Helmholtz, Hermann von, 458
Helmholtz pairs, 34, *40*
hemifields, 226
hemodynamic, 160
hemodynamic convolution, 352–354
hemodynamic hypotheses, 296, *297*
hemodynamic response (HDR)
blocked designs and, 311–313
correlation analysis, 338–340
effects of slice acquisition on, *270*
initial dip, 208, 211–214
linearity of, 229–237
overview, 208, 211
temporal resolution, 220–229
hemodynamic response functions, 352–353
hemoglobin
deoxygenated, 11, 193–200
magnetic properties, 193–196
oxygenated, 193–200
See also blood oxygenation
heteroscedastic noise, 356
hidden causal factors, 301
high angular resolution diffusion imaging, 141
high-pass filters, 286
high-temperature approximation, 76
hindbrain, 182
hippocampus, 184, 187–188, 325, 457
Hitzig, Eduard, 447
homoscedastic noise, 356
homotopy, 449
homunculus, 186
Hubel, David, 461

hydrogen atoms. *See* protons
hypercapnia, 181
hyperscanning, 384–386
hypocapnia, 181
hypothalamus, 184
hypotheses, 293, 331–332
See also research hypotheses
hypothesis-driven analyses, 332–333, 377

image formation, 89
image space, 113–117
images, 19, 89
imaging genomics, 457, 509
imaging plane, 144
implanted medical devices, 50, 52
impulses, 230, 317
incidental findings, 498–501
independent comparisons, 362
independent components analysis, 380–382, *383*
independent variable (IV), 294–295, 298, 490
indicators, 345, 346
individual differences, 402, 406, 488
"Indomitable," 20, *21*, 251
inferential statistics, 331
inferior colliculi, 184
inferior frontal gyrus, *186*
inferior frontal lobe, 8, *188*
inferior fronto-occiptal tract, *141*
inferior longitudinal fasciculus, *141*
inferior prefrontal cortex, 479
inferior sagittal sinus, 172, *173*
inferior temporal lobe, *188*
inflated brains, 372
informed consent, 494
inhibitory neurotransmitters, 163
inhibitory postsynaptic potential (IPSP)
action potential and, 459
BOLD changes and, 216
brain energy consumption and, 167–168
defined, 163
neuronal information processing and, 165
See also electrophysiological measures; postsynaptic potentials
initial dip, 208, 211–214
Institutional Review Boards (IRBs), 495, 497
insula, 186, 187, *189*, 408
insular cortex, 7
integrating activity, 161
intellectual property, 508–509
inter-session variability, 265–266
interleaved slice acquisition, 108, 270
interleaved stimulus presentation, 222–223, 432
internal capsule, *189*, 400
internal carotid arteries, 171, 172, *173*
internal cerebral vein, *173*
internal jugular veins, 172, *173*
interocular trauma test, 333, *334*
interpolation techniques, 270–271
interstimulus interval, 314, 318, *319*
intersubject analyses, 365–369
intersubject correlations, 387–389
intersubject variability, 22–23, 262
intracortical arteries, 174
intrasubject variability, 262
intrinsic noise, 256–258
introspective thought, 308
inverse Fourier transforms, 110
inverse problem, 466, *467*, 473–474
inversion recovery, 127, *128*
ion channels, 162–163
ion-gated contrast, 437–438
ion pumps, 162, 163, 165, 459
ionizing radiation, 197–198
ions, 162
iron oxide, 422
isomorphy, 444
isopotential lines, 460–461
isotropic diffusion, 139
isotropic spatial resolution, 214
item-related processes, 326

James, William, 169, 308
jittering, 228, 318
job screening, 511
jugular foramen, 172
jugular veins, 172
justice, 495

k-space
in 3-D imaging, 117
converting to image space, 114–117
echo-planar imaging and, 147, 148, *149*
image space and, 113–114, *115*
in two-dimensional spatial encoding, 109–113
k-space trajectories, 110
Kaiser Criterion, 379
keyhole imaging, 428, 429
Knight, Robert, 453
Krebs cycle. *See* tricarboxylic acid cycle
Kuffler, Steven, 461

labeling coil, 144
labeling plane, 144
laboratory frame, 78, *79*
lactate, 167
Langleben, Daniel, 507
large-vessel effects, 217–218
Larmor frequency
defined, 61, 74
factors determining, 97
magnetic field strength and, 97, 100
net magnetization of bulk matter and, 77
during the reception period, 65
latent variable, 384
lateral, 182
lateral geniculate nucleus, 184
lateral occipital complex, 236–237
lateral occipital lobe, 236
lateral orbitofrontal cortex, 368, *369*
lateral parietal cortex, 307
lateral prefrontal cortex, 307
lateral ventricle, *189*
lateral visual cortex, 394
Lauterbur, Paul, 19–20, 22, 93
least-squares error, 344
Leborgne (patient), 8
left fusiform gyrus, 449
left premotor cortex, 392–393
left vertebral artery, *171*
lesion studies, 8–9
levels, 294
Libet, Benjamin, 414
lie detection, 507–508
limbic lobe, 186
linear gradient coils, 38–39
linear system
challenges to, 233–235
defined, 229
evidence for BOLD rough linearity, 231–233
fMRI-adaptation and, 235–237
properties of, 230–231
refractory effects and, 229–230
stimulus events and, 317
linearity, BOLD response and, 353–354
liquid nitrogen, 35
local shims, 153, *154*
localization of function, 1, 386, 444
localizer task, 364
locus coeruleus, 178
lodestones, 32
logistic regression, 407–408
longitudinal magnetization, 100–101, 106, *122*
longitudinal recovery, 66
longitudinal relaxation, 66, 85–86
longitudinal vector component, 63
Lorentz effect imaging, 439–440, *441*
Lorentz forces, 54, 439
low-pass filters, 286

M13, 437
macaque monkeys *(Macaca fuscata)*, 479
Machiavellianism, 368, *369*
machine learning algorithms, 408–412
macromolecular contrast, 133–135
magnet diameter, 422
magnetic field(s)
discovery of, 32
Earth's, 3
flux lines, 60–61
spins and, 100
strength (*see* field strength)
See also gradient fields; static magnetic fields; *specific kinds*
magnetic field compensation. *See* shimming
magnetic field map/mapping, 154, *155*, 278
magnetic flux (Φ), 83, 84
magnetic moment (μ)
defined, 59
described, 69–70
Pauli's concept of, 15
spin precession and, 72, 73
spin state of protons and, 74
magnetic resonance (MR)
in bulk matter, 17–18
cardinal principle of, 75
concept of, 17
early studies of, 15–17
first images, 18–21
magnetic resonance imaging (MRI)
artifacts in images, *268*
contrast-to-noise, *11*
growth of, 21, 23–24, 202–203
overview of, 3–4
spatial resolution, 12–13, 420–426
See also MR image formation; MRI safety; MRI scanners
magnetic susceptibility, 193
magnetization transfer, 134–135
magnetoencephalography (MEG), 8, *14*, 159, 458, 474–476
magnetohydrodynamic processes, 49
MAGNETOM Avanto Scanner, *32*
magnets, 32
See also electromagnets
main effects of a condition, 355
manipulation techniques, 4–5, 8–9
Mansfield, Peter, 19–20, 22, 44, 147, 202
mask restraining systems, *274*, 275

massive coil arrays, 425–426
matched filters, 287
matrix size, 214
maximum torque, 59, 69–70, 72
Maxwell pair, 38, *39*, *40*
mean transit time, 143
measurement techniques, 4–5, 8–9
media, coverage of fMRI research, 485–486, 487–489
medial, 182
medial frontal gyrus, 307
medial geniculate nucleus, 184
medial parietal cortex, 307, 400
medial prefrontal cortex, 307, 400
medial temporal lobe, 188
medulla oblongata, 182, 184, *187*
MEG. *See* magnetoencephalography
membrane depolarization, 459–461
memory impairments, 324–325
memory retrieval, 326
meninges, 182
mesencephalon, 182
metencephalon, 182
mice, 480
microelectrodes, 458
microstimulation, 446, 464
midbrain, 182, 184, *187*
middle cerebral arteries, *171*, 172, *173*
middle frontal gyrus, *186*
middle temporal gyrus, *186*
mind reading, 506–509
Minkoff, Larry, 20, *21*
mixed-effects analysis, 367
mixed experimental designs, 247, 325–326, 346
MNI space, 283
mock scanners, 53
model factor, 339
model testing, 343
models, in statistics, 339
monkey studies, 476–480
monocrystalline iron oxide nanoparticles, 478
Montreal Neurological Institute, 283
morphometric techniques, 422
Mosso, Angelo, 169
motion contrasts
  defined, 121
  diffusion-weighted, 138–142
  MR angiography, 135–138
  perfusion-weighted, 142–146
motion parameters, 349–350
motion-sensitive visual cortex, 464
motor cortex, 235
MR angiography, 135–138
MR image formation
  conceptual path overview, 90–91, 96–97
  converting from *k*-space to image space, 114–117
  frequency encoding, 93–95, 110, 112–113
  image space and *k*-space, 113–114, *115*
  phase encoding, 93, 95–96, 110, 112
  signal analysis, 97, 100–106
  slice selection, 91–93, 106–109
  spatial encoding, 98–99
  3-D imaging, 117–120
  two-dimensional spatial encoding, 109–113
MR microscopy, 420–423
MR signal
  defined, 35
  equation for, 105–106, 110
  signal-to-noise ratio and, 84
MR signal analysis
  longitudinal magnetization, 100–101
  MR signal equation, 105–106
  overview of, 97, 100–101
  transverse magnetization, 101–105
MR signal generation
  angular momentum, 70–71
  Bloch equation, 87
  conceptual path overview, *58*, *67*
  energy difference between parallel and antiparallel states, 74–75
  excitation and reception, 64–65, 77–84
  magnetic moment, 69–70
  nuclear spins, 59–60, 69
  quantitative path overview, *58*
  relaxation mechanisms, 65–67, 85–87
  spin system magnetization, 62–64, 75–77
  spins in an external magnetic field, 60–62, 71–74
MRI. *See* magnetic resonance imaging
MRI safety
  acoustic noise, 54
  claustrophobia, 53–54
  gradient magnetic field effects, 50–52
  public policy and, 44
  radiofrequency field effects, 52–53
  static magnetic fields, 44, 48–49
  translation and torsion, 49–50
MRI scanners
  1.5-T, 23–24
  components overview, 31
  computer hardware and software, 41–42
  examples, *32*
  experimental control system, 43
  FDA approval, 497
  gradient coils, 38–41
  monkey-specific, 478
  physiological monitoring equipment, 43–44
  radiofrequency coils, 35–38
  schematic organization, *33*
  shimming coils, 41
  static magnetic field, 32–35
Müller, Johannes, 458
multi-voxel pattern classification, 410–412
multiple-channel acquisition, 423–425, 427
multiple comparison problem
  cluster-size thresholding, 360–361
  defined, 287
  estimating the number of independent tests, 361–362
  overview, 357–358
  significance threshold, 358–360
multiple regressions, 343, 348–349, 377
multiple sclerosis, 140
Munk, Hermann, 452
mutual information, 276
myelencephalon, 182
myelin, *161*, 182
myelination, 134–135

"n-back" paradigm, 305
N20 potential, 469
N170 potential, 470
N200 potential, 470
NAA, *133*
nausea, 49
neocortex, 160, 185
net magnetization (M)
  B_{1eff} and, 80, 81
  defined, 60
  dependence on temperature, 435
  described, 76–77
  flip angle, 82
  gyroscopic rotation, 81
  nutation, 81
  precession, 97, 100
  properties of, 62–64
  relaxation and, 86
  signal reception and, 84, *85*
  spin excitation and, 78, 79, 81–82
  vector and axis projections, 100, *101*
networks
  of brain activity, 390
  default, 392
neuroanatomy, 182–189
neuroelectric currents, 438
neuroessentialism, 489
neurological convention, 370
neuronal hypotheses, 297
neuronal magnetic field contrast, 438–439
neuronal membranes, 162
neurons
  BOLD fMRI and, 209–210
  described, 160–162
  electrode studies, 5, 8
  electrogenesis, 459–461
  ion channels, 162–163
  modeling activity of, 351–352
  neurovascular coupling, 176–178
neurorealism, 489
neurotransmitters, 9, 163, *164*
neurovascular coupling, 176–178
neutrons, 59
New York Times, 485, 486
news media, coverage of fMRI research, 485–486, 487–489
90-degree excitation pulse, 65
nitric oxide, 175
NMDA (N-methyl-D-aspartate), 163
Nobel Prize in Physics, 17, 18
Nobel Prize in Physiology or Medicine, 22–23, 89, 147, 461
noise
  acoustic, 54
  assumptions of the general linear model and, 356
  behavioral and cognitive variability in task performance, 262–263, 266–267
  causes of, 255–256
  definitions of, 245, 248
  inter-session variability, 265–266
  intersubject variability, 264–265
  mapped across the brain, *257*
  motion and physiological noise, 259–262
  non-task related neural variability, 262
  system, 258–259
  thermal, 256–258
non-human primate studies, 476–480
non-task condition, 298
nonlinearities, 233
noradrenaline, 178
normalization, 220, 280, 281–284, 444
nuclear induction, 18
nuclear magnetic resonance, 16–21
  See also magnetic resonance imaging
nuclear magnetic resonance property, 59, *60*, 69
nuclear spins, 59–60, 69, 75
nucleus accumbens, 408
nuisance regressors, 349–351
null hypothesis, 332

null-task blocks, 305
Nuremberg Code, 494
nutation, 81
Nyquist frequency, 285
Nyquist sampling theorem, 342

object categorization studies, 413
occipital lobe, *12*, *183*, 186, 187, *188*
occipital sinus, *173*
ocular dominance, 219
ocular dominance columns, *252*
"oddball" paradigm, 305, *325*
Oersted, Hans, 33
off-resonance excitation, 80, 82, *83*, 108
olfactory nerve, *188*
oligodendrocytes, 182
on-resonance excitation, 79, *83*
180-degree excitation pulse, 65
1.5-T scanners, 23–24
opacity, 10
optic chiasm, *188*
optical imaging, 159
orbitofrontal cortex, 368, *369*
orientation columns, 213
orthogonality, 347, 379
orthogonalize, 347
oscillating magnetic fields, 16–17
outer *k*-space imaging, 429–430
Owen, Adrian, 6
oxygen extraction fraction, 306–307
oxygen-to-glucose index, 196
oxygenated hemoglobin (Hb), 193–200

P3 potential, 469
P20 potential, 469
P25 potential, 469
P300 potential, 469
pacemakers, 52
"pain matrix," 7
parahippocampal cortex, 6
parahippocampal gyrus, 187–188
parallel EEG/ERP-fMRI, 472
parallel imaging, 423–425, 425–426
parallel state, 61–62, 71, 74–75, 76–77
paramagnetism, 193
parameter matrix, 343–344
parameter weight, 343
parametric across-subjects tests, 368–369
parametric effects, 348
parietal cortex, 6, 394, 457
parietal lobe, *12*, *183*, 186, 187
parieto-occipital sulcus, *183*
Parkinson's disease, 184
partial *k*-space imaging, 427–430
partial least squares, 382–384
partial volume effects, 215–216, 252
pattern classification
  limitations, 415
  prediction of conscious decisions, 414–415
  using machine learning algorithms, 408–412
  visual perception studies, 412–414
pattern classifier, 411
Pauli, Wolfgang, 15
Pauling, Linus, 193
peer review, 493–494
Penfield, Wilder, 447
perfusion, 142–143
perfusion MRI, 143–146
perfusion-weighted contrast, 142–146
pericallosal artery, *173*
pericytes, 176
perinatal left-hemisphere lesions, 454
periodic event-related designs, 317–319
permanent magnets, 32
permutation, 360
permutation tests, 384
"persistent vegetative state," 6
PET. *See* positron emission tomography
pH-dependent contrast, 435–436
phantoms, 268, *269*
phase encoding gradient, 93, 95–96, 110, 112
phased arrays, 36, 37–38, 423
Philips company, 23
  Achieva scanner, *32*
phosphenes, 49
phrenology, 1–2
physiological monitoring, 43–44
physiological noise, 259–262
physiological parameters, 350
pia, 182
pineal gland, 1, 184
pixels, 11–12
Planck's constant, 74
plasticity, functional, 454, *455*
Poisson function, 352
polygraphs, 507
polymorphisms, 457
pons, 182, 184, *187*, *188*
popular media, coverage of fMRI research, 485–486, 487–489
positron emission tomography (PET)
  blocked designs and, 303–304
  described, 4, 197–198
  functional contrast, 11
  measurement of brain metabolism, 4, 5
  resolution qualities, *14*
postcentral gyrus, 186–187, *187*, 468, 469
posterior cerebral arteries, *171*, 172, *173*
posterior cingulate cortex, 307
posterior commissure, *189*
posterior communicating arteries, *171*
posterior fossa, 182
posterior fusiform gyrus, 236
posterior inferior cerebellar artery, *171*
posterior parietal cortex, 237
postsynaptic potential (PSP), 464, 465
potassium ions, 175
power, experimental, 250
power spectrum, 255, *256*
pre-supplementary motor area, 451–452
pre-surgical planning, 403–404
precentral gyrus, 186, *187*
precession
  defined, 61
  of net magnetization, 77, 97, 100
  of protons, 61–62, 71–74
precession frequency, 61, 71–74
precoloring, 286
precuneus. *See* posterior cingulate cortex
prediction approaches
  overview, 401–402
  pattern classification, 408–415
  predicting variability in behavior, 407–408
  predicting variation among individuals, 402, 406
prediction of conscious decisions, 414–415
predictor variable, 339
prefrontal cortex, 391, 415, 457
pregnancy, fMRI research and, 504–505
preprocessing
  distortion correction, 277–280
  goals, 267
  head motion correction, 276–277
  head motion prevention, 274–276
  head motion problems, 271–274
  quality assurance, 267–269
  slice acquisition time correction, 269–271
preprocessing algorithms, 244–245
prewhitening, 286
primary current, 460
primary motor cortex (M1), 186, 227, 399, 468
primary sensory cortex, 235, 468–469
primary visual cortex (V1), *12*, 227, 235, 394, 476
primate studies, 476–480
principal components analysis, 378–379
principle of reciprocity, 84
Principles of Psychology (James), 169
Privacy Rule, 497, 500
probabilistic brain atlases, 455–456
projectile effects, 44, 50, *51*
proton-density contrast, 123–125, *126*
proton-density imaging, 123–125, *126*
protons
  angular momentum, 70–71
  magnetic moment, 69–70
  mass, 71
  parallel and antiparallel states, 61–62, 71
  precession, 61–62, 71–74
  spin, 59–60, 69
psychological constructs, 444
psychological hypotheses
  characteristics of, 297–298
  confounding factors and, 300–301
psychophysiological interactions, 393–394, *395*
pulse sequence, 3
  defined, 92
  frequency encoding, 94–95
  phase encoding, 95–96
  slice selection and, 92–93
pulsed ASL, 144, 145–146
pumps, ionic, 162, 163, 165, 459
pupil dilation, 43
Purcell, Edward, 17, 18
putamen, 184, *189*, 220
pyramidal cells, 182, 185

Q-value, 38
quality assurance, 267–269
quantum mechanics, 75

r-value, 339
Rabi, Isidor, 16, 17
radiofrequency coils
  arrangements, 36–38
  in MRI scanners, 35–38
  sensitivity, 38
  system noise and, 258–259
radiofrequency excitation pulse, 64–65, 91, 92–93
radiofrequency field effects, 52–53
radiofrequency fields, 35
radiofrequency heating, 52–53
radiofrequency noise, 268
radiological convention, 370
random-effects analysis, 366–367
random field theory, 362
randomization, 301, 321
rasters, 462
rats, 480
raw signal-to-noise ratio, 245, 251–252

reaction time, 223, 262
reading minds, 506–509
readout period, 94–95
real-time analyses, 403–405
receiver coils, 83
reception
defined, 35, 65
the MR signal and, 67, 83–84, *85*
overview, 35–36, 83–84
receptive field, 461
reciprocity, principle of, 84
recovery of function, 455
red nucleus, 184
redundant safeguards, 503–504
reference electrode, 465
reference volume, 276
reflecting galvanometer, 458
reflective state, 308
refocusing pulse, 125
refractory effects, 229–230, 233–236
refractory period, 233
region-of-interest (ROI) analyses, 220, 247, 289, 362–365
registries, for brain lesions, 453
regression analyses
contrasts, 354–356
design matrix construction, 345–349
general linear model, 356 (*see* general linear model)
modeling hemodynamic convolution, 352–354
modeling neuronal activity, 351–352
nuisance regressors, 349–351
overview, 343
regressors
contrast and, 354
defined, 339
in the design matrix, 345–349
nuisance, 349–351
relative blood flow, 143
relative blood volume, 143
relaxation, 65–67, 85–87
rendered images, 371
repetition time (TR)
defined, 122
interleaved stimulus presentation and, 432
MR angiography and, 136
proton-density contrast and, 123–124
T_1 contrast and, 126
T_2 contrast and, 129
T_2* contrast and, 132
repetitive TMS, 450–451
"resampling" methods, 360
research hypotheses
confounding factors, 299–302
correlational data criticism, 298–299
defined, 293, 331–332
levels of, 296–298
testing, 298
research protocol, 495
resels, 362
residual error, 344
resistance vessels, 175
resolution, 11–15
resolution elements, 362
resonance, 78
resonance frequency, 17, 134
respect for persons, 495
response time, 262, *263*
resting-state connectivity, 391–393
reticular formation, 184
retinal ganglion cells, 461
reverse inference, 388, 389, 490–491
rhesus monkey, 477–478
right-hand rule, 59
right vertebral artery, *171*
rigid-body transformation, 276
rodent studies, 480
ROI analyses. *See* region-of-interest analyses
rostral, 182
rotating frame, 79, 80
rotating magnetic field, *78*
rotations, 276
rTMS, 450–451
runs, 246

safeguards, redundant, 503–504
safety screening, 503–504
sagittal view, 182
samples, 331
sampling rate, 13
Savart, Félix, 34
scalars, 68
scaling, of a linear system, 230
scalp-recorded field potentials, 470–474
scanner drift, 258, 311, *337*
scanners. *See* MRI scanners
schizophrenia, 234–235, 406, 456
scientific research process, *493*
searchlight, 411
secondary visual cortex, 476
seed voxel, 392
segmentation, 125, 280
seizures, 448
rTMS evoked, 450–451
selectivity, 490
"self-directed" thought, 308
selfish opportunism, 368, *369*
semi-random design, 321–322
sensitivity factor, 38
sensorimotor cortex, 455
sensory gating, 234–235
serotonin, 9, 457
sessions, 246
issues of variability between, 265–266
shimming, 153, *154*, 278
shimming coils, 31, 41, 278
Siemens company, 23
MAGNETOM Avanto Scanner, *32*
Sigma series scanner, *32*
signal, 245, 248
signal averaging, 314–315, 340
signal-to-noise ratio (SNR)
defined, 245
field strength and, 63, 84
temporal resolution and, 432
signaling activity, 161
significance testing, 332
significance threshold, 358–360
similarity measure, 276
simple cells, 461
simple randomization, 321
simultaneous EEG/ERP-fMRI, 472–473
sinc interpolation, 271
sinc-modulated electromagnetic pulse, 108
single dissociation, 454
single-loop inductor-capacitor circuit, 36–37, 38
single-pulse TMS, 450, 451
single-trial designs, 314
single-unit recording
limitations, 462–464
overview, 458, 461–462
singular value decomposition, 383–384
sinuses, vascular, 172, *173*
skin electrical conductance, 43
slice acquisition time correction, 269–271
slice selection, 91–93, 106–109
slice thickness, 214
slices, 246
small volume correction, 359–360
smoothing, 220, 287–289
smoothness, of data, 362
SNR. *See* signal-to-noise ratio
sodium-potassium pump, 162, 163, 165, 168
software, for MRI scanners, 41–42
solenoids, 34
soma, 160, *161*
somatosensory cortex, 7, 439
sparse acquisition, 472–473
spatial correlation, 362
spatial encoding, 98–99
two-dimensional, 109–113
spatial extent, 252, 253–254
spatial filtering, 287–289
spatial gradient (G), 19, 92, 100
spatial ICA, 381
spatial interpolation, 277
spatial noise, 255–256
spatial normalization, 281–284
spatial resolution
concept overview, 11–13, 14
defined, 11
determining, 219–220
MR microscopy, 420–423
parallel imaging, 423–425
parallel imaging with massive coil arrays, 425–426
partial volume effects, 215–216
the vascular system and, 216–219
voxel size and, 214–216
spatial smoothing, 220, 287–289
spatial specificity, 252–253, 254
spatial variability, 265
specific absorption rate, 52–53
speed-accuracy trade-off, 263
spin, 15
spin-echo imaging, 125, 131, 218, 219
spin-echo pulse sequences, 127, 131, 153–154
spin excitation, 78–82, *83*
spin frequency, 15–16
spin nutation, 81
spin phase, *111*
spin precession, 61–62, 71–74
spin precession frequencies
phase encoding and, 95–96
slice selection and, 91, 92
spatial gradient G and, 100
spin systems
defined, 59
excitation, 64–65
magnetization, 62–64, 75–77
relaxation, 85–87
spinal cord, 182
spin–lattice relaxation, 66, 86
spins
defined, 59
in external magnetic fields, 60–62, 71–74
nuclear, 59–60, 69, 75
quantum behavior, 75
static magnetic field B and, 100
spiral imaging, 148–151, 152–154, 430
spiral-in-and-out trajectory, 432

spiral-in trajectory, 432
spiral-out imaging, 430–431
spiral-out trajectory, 430
splenium of the corpus callosum, *187*
SPM, *345*
Spurzheim, Johann, 2
standard deviation, 334
standard error, 335
state-related processes, 325
static contrasts
  chemical, 132–133
  defined, 121
  macromolecular, 133–135
  overview, 122–123
  proton-density, 123–125, *126*
  T_1 contrast, 126–127, *128*
  T_2 contrast, 129–131
  T_2* contrast, 131–132
static magnetic field (B_0)
  correction of distortions, 278
  defined, 15–16
  early magnetic resonance studies, 15–16, 17
  inhomogeneities and, 118, 277
  in MR image formation, 90–91
  MR signal and, 100
  in MRI scanners, 31, 32–35
  net magnetization and, 100
  oscillating magnetic fields and, 17
  safety concerns, 44, 48–49
  spin precession and, 72, 73
  symbol for, 61
  Tesla units, 3
  the work to flip spin states and, 74
statistical analyses
  advanced approaches, 377
  basic tests, 333–340
  between-subjects correlations, 384–386
  corrections for multiple comparisons, 357–362
  correlation analysis, 338–340
  data-driven analyses, 377, 378–384
  descriptive, 331
  displaying results, 369–372
  early fMRI data analysis and, 207
  Fourier analyses, 341–342
  functional connectivity approaches, 386, 389–391
  inferential, 331
  intersubject analyses, 365–369
  intersubject correlations, 387–389
  prediction approaches, 401–615
  region-of-interest analyses, 362–365
  regression analyses (*See* regression analyses)
  software packages, *345*
  t-test, 334–338
statistical maps, 369–372
statistical packages, *345*
statistical parameter map, 369–372
stellate cells, 182, 185
stereotaxic space, 283
stimulus duration, temporal resolution and, 225–229
"stimulus-independent" thought, 308
stimulus timing, temporal resolution and, 225–229
straight sinus, 172, *173*
strokes, 455
structural connectivity, 386
structural equation modeling, 395–396
structural MRI, 246
subclavian arteries, *171*, 172
subclavian vein, 172
subjects, 494
  experimental, 246
  head motion prevention, 274–276
subsequent memory, 324–325, 407
substantia nigra, 184
subtraction, 299–300, 334
sulci, 185
superconducting electromagnets, 35
superconducting quantum interference devices, 474
superior cerebellar artery, *173*
superior colliculi, 184
superior frontal gyrus, *186*
superior fronto-occiptal tract, *141*
superior longitudinal fasciculus, *141*
superior parietal lobe, 225
superior sagittal sinus, 172, *173*, 182
superior temporal gyrus, *186*
superior vena cava, 172
superparamagnetic iron oxide nanoparticles, 437
superposition, 230–231, 312
supplementary motor area (SMA), 6, 227, 235, 399
support vector machines, 411
support vectors, 411
surface coils, 36–37, 278–279
susceptibility artifacts
  corrections, 152–154, *155*
  defined, 131
  echo-planar imaging and, 148, *149*
  high-field fMRI and, 254, *255*
  spin-echo imaging and, 131
  spiral imaging and, 151
Swedenborg, Emanuel, 1
Sylvian fissure, *186*, 187, *189*
synapses, 161–162, 163, *164*
synaptic cleft, 161
system noise, 258–259
systems, of brain activity, 390

T_2* blurring, 215
T_1 contrast, 10, 126–127, *128*
T_2 contrast, 10, 129–131
T_2* contrast, 131–132
T_1-contrast images, 10, *11*, 102
T_2-contrast images, 10–11, 104
T_2 decay, 66, 86
T_2* decay, 66, 87
T_1-dependent images, 126
T_2-dependent images, 129
T_2*-dependent images, 131
T_1 recovery, 86, 102
T_1 relaxation, 66–67, 92
T_2 relaxation, 66–67, 92
T_1 time constant
  field strength and, 254
  MR signal and, 122–123
  MR signal relaxation and, 66–67, 86
T_2 time constant
  MR signal and, 122–123
  MR signal relaxation and, 66–67, 86
  T_2* and, 131
T_2* time constant, 66, 87
  blood oxygenation and, 194, 195
  field strength and, 254
T_1-weighted images, 126
T_2-weighted images, 129
T_2*-weighted images, 131
T cells, 420–421
Talairach, Jean, 283
Talairach space, 283
task blocks, 325–326
task condition, 298, 306
task frequency, 285–286
TE. *See* echo time
"technique space," 13–14
telencephalon, 184
temperature, net magnetization and, 63
temperature-dependent contrast, 434–435
temperature-sensitive contrast agent, 434
temporal autocorrelation, 286
temporal derivatives, 352–353
temporal filtering, 285–286
temporal ICA, 381–382
temporal interpolation, 270–271
temporal lobe, *189*
  baseline activation and, 307
  described, 187
  localization of language regions, 449
  susceptibility artifacts and, 254
temporal noise, 255–256
temporal resolution
  defined, 13
  determining, 223–225
  effects of stimulus duration and timing, 225–229
  efficient *k*-space trajectories, 430–432
  factors limiting, 426–427
  improved experimental designs, 432–433
  multiple-channel acquisition, 427
  overview, 220–223
  partial *k*-space imaging, 427–430
  in single-unit recording, 463
  "technique space" and, 13–14
temporal variability, 265
tensor, 139
tentorium, 182
Tesla, 3
testing set, 411
tetrodotoxin, 439
thalamus, *183*, 184, *187*, *189*, 391
theory, 297
thermal noise, 256–258
3-D imaging, 117–120
three-dimensional rendering, 371
thresholding, 360–361
thulium, 434
time course, 211
time domain, 341
time-locking, 314–315
time-of-flight MRA, 136–137
time series, 246
TMS. *See* transcranial magnetic stimulation
torque, 59, 69–70, 72, 79
torsion, 50, 61
TR. *See* repetition time
tractography, 140, 142
training set, 411
trait identification, 509–511
transcranial magnetic stimulation (TMS), 8, *14*, 446, 450–452
translations, 50, *51*, 276
transmitter coil, 18
transverse decay, 66
transverse gradients, 38–39
transverse magnetization, 101–105, 122
transverse relaxation, 66, 85–87, 131
transverse sinus, 172, *173*

transverse vector component, 63
trial sorting, 324
trials, 247
tricarboxylic acid cycle, 166, 167
t-test
correlation analysis and, 339–340
described, 334–338
general linear model and, 344–345
2-D Bessel sinc function, 113
2-D Fourier transforms, 110
two-dimensional spatial encoding, 109–113
Type I errors, 287, *288*, 333, 357, 358
Type II errors, 333, 361

ultra-high-field scanners, 420
ultra-high magnetic fields, 420
ultra-high resolution MRI, 420–423
uncinate fasciculus, *141*
undershoot, 211
University of California, Berkeley, 453
University of Iowa, 453
unknown risks, 504
U.S. Department of Health and Human Services, 497
U.S. Food and Drug Administration, 497
U.S. National Commission for the Protection of Human Subjects, 495

V5, 235
vacuum-pack head restraint, *274*, 275
variables
categorical, 295–296
continuous, 296
defined, 294
dependent and independent, 294–295
Varian Associates Company, 18, 23, 202
vascular dementia, 140
vascular system
spatial specificity of BOLD fMRI and, 216–219
vessels, 170–171
See also blood vessels; brain vascular system
vasoactive substances, 175
vectors, 68
veins, 171, 217–218
See also blood vessels; brain vascular system
velocity-encoded phase contrast MRA, 137–138
venogram, *132*
ventral, 182
ventral frontal lobe, *153*
ventral lateral nucleus, 184
ventral lobe, 254, *255*
ventral occipitotemporal lobe, 469–470
ventral postero-lateral nucleus, 184
ventral striatum, *12*
ventral temporal lobe, *153*
ventricles, 182
ventromedial frontal cortex, 307
venules, 171, 181
vertebral/basilar arteries, 171, 172
vertical-bore MRI scanners, 478
vertigo, 49
visual perception studies, pattern classification and, 412–414
visual system, *142*
Volterra kernels, 354
volume coils, 36, 37, 278
volume conductor, 460
volume current, 460
volumes, of data, 246
volumetric techniques, 422
VoxBo, *345*
voxel size, spatial resolution and, 214–216
voxels
defined, 12
dimensions, 214
in the hierarchy of data acquisition, 246
partial volume effect and, 252
resolution and, 12–13
spatial smoothing, 356
time and frequency domains, *285*
voxelwise analyses, 247, 362–363, 365

waveforms, constructing complex forms, *111*
Wernicke's area, 392
white matter, *184*
age-related degeneration, 400, *401*
time constants T_1 and T_2, *123*
Wiesel, Torsten, 461
Willis, Thomas, 172
Wisconsin Card Sorting Test, 479
within-subjects manipulation, 296
Woolsey, Clinton, 467

x-gradients, 38–39, *40*, *91*
X-rays, in computerized tomography, 21

y-gradients, 38–39, *40*, *91*

z-gradients, 38, *40*, 91, 92–93
z-shim gradient, 153
Zeeman effect, 63
zero crossing, 127, *128*